10th International Conference on Modulated Semiconductor Structures

MSS10

23 -27 July, 2001

Johannes Kepler University Linz, Austria

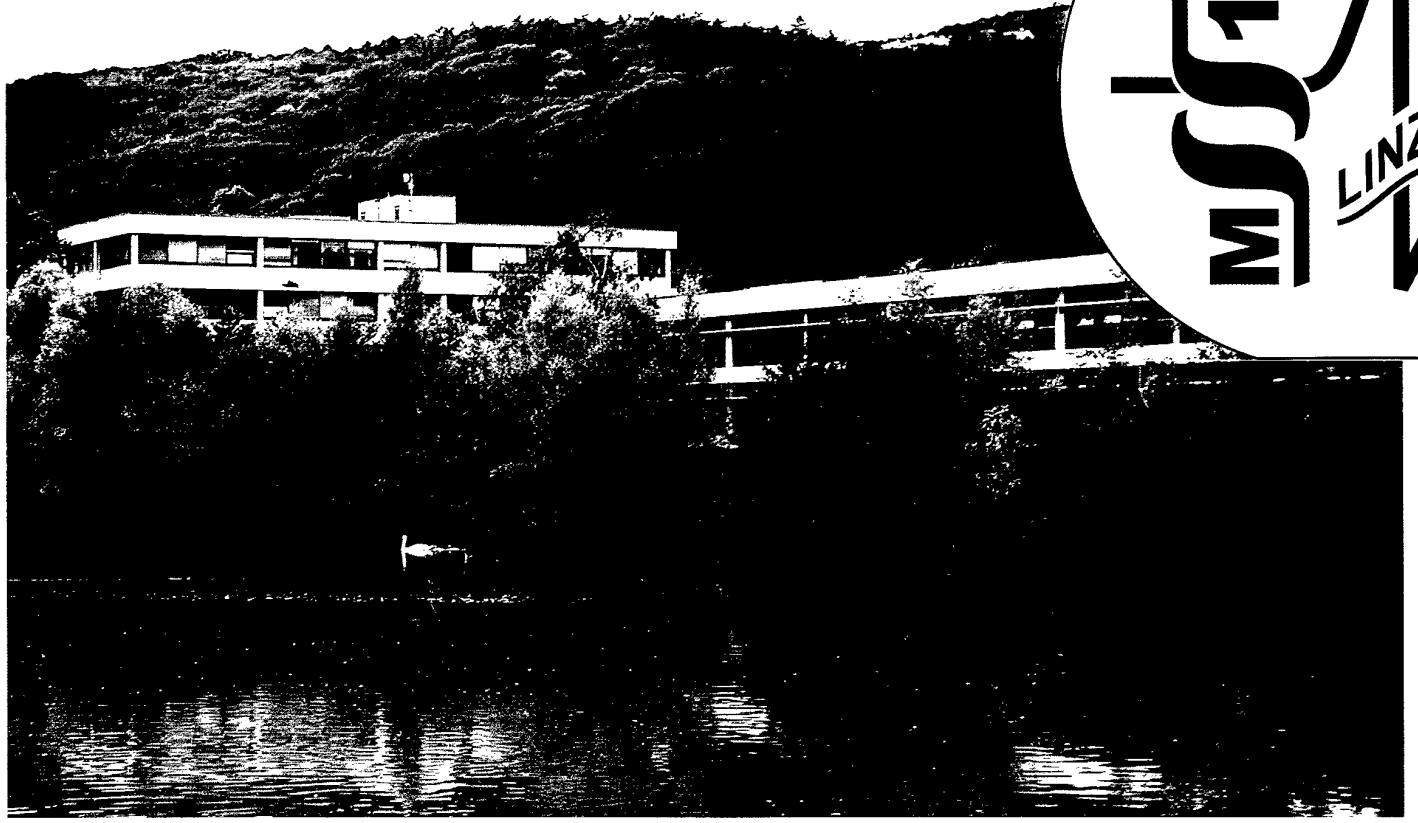

20010827 061

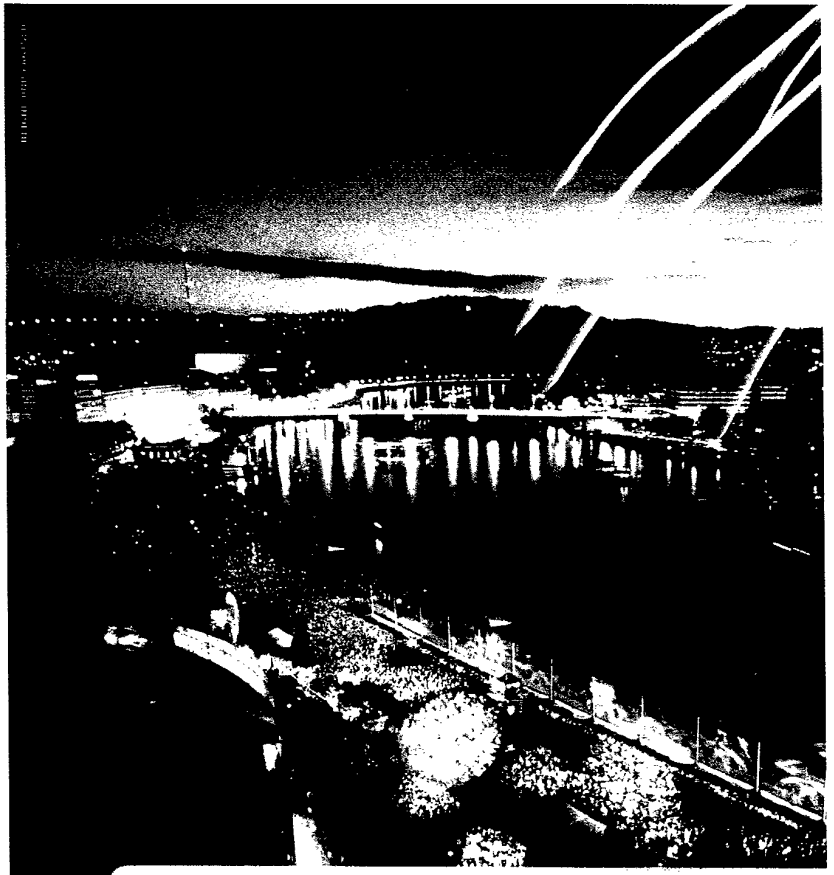

ESG und SBL heißen jetzt **Linz AG.**

Energie, Wärme, Sauberkeit, Mobilität. 365 Tage im Jahr. 24 Stunden am Tag. Dafür gibt es jetzt einen neuen Namen: LINZ AG – der neue Name von ESG + SBL. Auch im Internet unter www.linzag.at

LINZ AG

www.linzag.at

Immer bestens versorgt.

X-ray diffraction for today and tomorrow

The inevitability of change has long been recognized - and the pace of change is accelerating at an ever increasing rate. This is true in the laboratory domain as in every other aspect of modern life. What you require from your X-ray diffractometer could be a world apart from your expectations today.

The Philips X'Pert PRO diffractometer system is an X-ray diffraction system with a virtually limitless capacity to adapt to changing circumstances. The PreFIX (Pre-aligned, Fast-Interchangeable X-Ray optics) system enables instruments to be reconfigured in a few minutes to handle different types of analysis.

A totally open design architecture guarantees full freedom to accommodate further advances in years to come.

The X'Pert PRO MRD is designed for materials research:

- Rocking curves
- Reciprocal space maps
- Reflectometry
- (Thin film) phase analysis
- Stress and texture
- In-plane diffraction

Philips Analytical
Lelyweg 1,
7602 EA Almelo
The Netherlands
Tel: +31 546 534 444
Fax: +31 546 534 592

www.analytical.philips.com

Let's make things better.

PHILIPS

10th International Conference on Modulated Semiconductor Structures

MSS10

ABSTRACT BOOKLET

DISTRIBUTION STATEMENT A
Approved for Public Release
Distribution Unlimited

23 - 27 July 2001

Johannes Kepler University Linz, Austria

ORGANIZING COMMITTEE

Conference Chairman: G. Bauer (Univ. Linz)

G. Brunthaler (Univ. Linz)
W. Heiss (Univ. Linz)
W. Jantsch (Univ. Linz)
G. Leising (AT&S Leoben)
F. Schäffler (Univ. Linz)
G. Springholz (Univ. Linz)
H. Heinrich (Univ. Linz)
K. Hingerl (Univ. Linz)
H. Krenn (Univ. Graz)
L. Palmetshofer (Univ. Linz)
H. Sitter (Univ. Linz)
K. Unterrainer (TU Vienna)

ADVISORY COMMITTEE

Honorary Members

L. Esaki (ISTEP, Tokyo)
A. Madhukar (USC, Los Angeles)
F. Grunthaner (JPL, Pasadena)

Members

F. Capasso (Bell Labs, Lucent)
C. Hamaguchi (Osaka Univ)
J.P. Kotthaus (Univ. Munich)
N. Miura (Univ. Tokyo)
V. Shchukin (Ioffe Inst., TU Berlin)
L. Viña (Univ. Madrid)
L. Eaves (Univ. Nottingham)
E. Kapon (Univ. Lausanne)
D. Loss (Univ. Basel)
K. Ploog (PDI, Berlin)
Y. Shiraki (Univ. Tokyo)

PROGRAM COMMITTEE

G. Abstreiter (TU Munich)
G. Bauer (Univ. Linz)
S. Forrest (Princeton Univ.)
E. Gornik (TU Vienna)
J. Meyer (NRL Washington)
H. Ohno (Tokoku Univ.)
M. Skolnick (Univ. Sheffield)
Y. Arakawa (Univ. Tokyo)
T. Dietl (IFPAN, Warsaw)
J.M. Gerard (CNET Bagneux)
M. Heiblum (Weizmann Inst.)
E. Molinari (Univ. Modena)
P. Petroff (UC, Santa Barbara)

CONFERENCE VENUE

Johannes Kepler Universität Linz
Kepler Building, HS 1
Altenberger Str. 69
A-4040 Linz / Austria

CONTACT ADDRESS

Institute for Semiconductor Physics
Johannes Kepler University Linz
Altenberger Str. 69
A-4040 Linz /Austria
Tel: +43 732 2468 9600
FAX: +43 732 2468 8650
e-mail: mss10@hlphys.uni-linz.ac.at
http://www.hlphys.uni-linz.ac.at/mss10.htm

SOCIAL PROGRAM

Reception of the Mayor of Linz

The mayor of the city of Linz will hold a reception in the renowned **Ars Electronica Center, Linz,** on **Sunday July 22, 2001**. The event will commence with a guided tour through the Ars Electronica Center and then proceed to the reception in the cafeteria of the center. To accommodate the large number of participants two groups will be formed, with the respective guided tours starting at 18:00 and 19:30 hours. The Ars Electronica Center is located next to the New City Hall of Linz on the north side of the main bridge *(Nibelungen-Brücke).* It can easily be reached by public transportation from the Johannes Kepler University (tram line 1, see local plan). We recommend that participants come to the on-site registration desk in the Kepler Building on the campus of the Johannes Kepler University before the reception to pick up their badge and free ticket for public transportation. The registration desk will be opened on Sunday, July 22, 2001, at 15:00 hours (3:00 pm).

Conference Excursion

The conference excursion will take place on Wednesday, July 25, 2001.
Three different destinations will be offered. Participants are requested to sign up for one of these at the registration desk. Scheduled destinations are:

1. Boat tour on the beautifully located lake **Traunsee,** with spectacular view of the **alpine peaks** surrounding the lake.
2. Guided tour through the monastery of **Melk,** which is located on the river **Danube** next to one of the most beautiful river landscapes in Europe, the **Wachau.**
3. Guided tour "In Memoriam of Austrian Composer **Anton Bruckner**" to locations in **Linz, Ansfelden** and **St. Florian.**

Departure by bus will be at 12:15 hours from the parking lot in front of the Cafeteria of the Johannes Kepler University. Lunch boxes and soft drinks will be distributed on the buses.

Conference Dinner

Following the excursion on Wednesday, July 25, 2001, the conference dinner will be held in the marble hall of the baroque monastery of **St Florian.** For those interested an organ concert will be conducted on the famous Bruckner organ in the Basilica of the monastery. The Conference Dinner is **not included** in the conference fees. Tickets for the Conference Dinner are available through on-line registration, and at the on-site registration desk.

EXHIBITIONS

There will be an exhibition of **scientific equipment** and books in the lobby next to the main lecture hall (HS 1) of the Kepler Building.

The ETH Zürich has organized an exhibition on ***Wolfgang Pauli and Modern Physics***. This exhibition is on tour at the Johannes Kepler University throughout spring 2001, and it has been extended to make it available to the attendants of MSS 10. The Wolfgang Pauli Exhibition is also located in the Kepler Building. Admission is free.

FINAL PROGRAM

CONFERENCE PROGRAM

Sunday, July 22

Registration *(University Campus)* — *15:00*

Reception of the Mayor of Linz *(ARS Electronica Center, City Center)* — *18:00 and 19:30*

Monday, July 23

Morning Session — *Monday 8:30 – 12:35*

Opening 8:30 - 8:40 — **G. Bauer**

Single Dot Spectroscopy I — **Chairperson: J. Kotthaus**

MoM1 8:40 - 9:10 (invited)
Optically detected single electron charging in a quantum dot
A. Zrenner, F. Findeis, M. Baier, M. Bichler, G. Abstreiter, U. Hohenester and E. Molinari - *Walter Schottky Institut, Technische Universität München*

MoM2 9:10 - 9:25
Enhancement of the exciton-phonon coupling in single InAs/GaAs quantum dots
A. Lemaitre, A. D. Ashmore, J. J. Finley, D. J. Mowbray, M. S. Skolnick, M. Hopkinson and T. F. Krauss - *Department of Physics and Astronomy, University of Sheffield*

MoM3 9:25 - 9:40
The influence of carrier diffusion on the formation of charged excitons in InAs/GaAs quantum dots
K. F. Karlsson , E. S. Moskalenko, P. O. Holtz, B. Monemar and W. V. Schoenfeld - *Dept. of Physics and Measurement Technology, Linköping University*

MoM4 9:40 - 9:55
Photoluminescence up-conversion of single InAs/GaAs quantum dots
G. Cassabois, C. Kammerer, C. Voisin, C. Delalande, Ph. Roussignol and J. M. Gerard - *LPMC, Ecole Normale Supérieure*

MoM5 9:55 - 10:10
Quantum dots as sensitive probes of their environment
Y. Ducommun, A. Hartmann and E. Kapon - *Swiss Federal Institute of Technology (EPFL), Department of Physics*

MoM6 10:10 - 10:25
Probing the dynamic response of a single Quantum Dot
R.H. Blick, H. Qin, D.W. van der Weide and K. Eberl - *LMU Muenchen CeNS*

Coffee Break (10:25 – 10:50)

Transport — **Chairperson: C. Hamaguchi**

MoM7 10:50 - 11:05
Magneto-tunneling spectroscopy in multiple gated self-assembled quantum dots
R J A Hill, P C Main, A Patane, B Gustafson, L Eaves, M Henini, S Tarucha and D G Austing - *School of Physics and Astronomy, University of Nottingham,*

MoM8 11:05 - 11:20
Magnetically induced non-zero angular momentum in a few electrons silicon quantum dot
L. P. Rokhinson, L. J. Guo, S. Y. Chou and D. C. Tsui - *Department of Electrical Engineering, Princeton University*

MoM9 11:20 - 11:35
Internal degrees of freedom of three dimensional quantum dots
S. Lindemann, T. Heinzel, K. Ensslin, K. Maranowski and A. C. Gossard - *ETH Zürich*

MoM10 11:35 - 11:50
Anisotropy in the conductance of high mobility modulation-doped quantum wells on GaAs(001) substrates
K.- J. Friedland, R. Hey, H. Kostial, Y. Hirayama and K. H. Ploog - *Paul-Drude-Institut fuer Festkoerperelektronik*

MoM11 11:50 - 12:05
High-Mobility Electrons in Modulation-Doped AlAs Quantum Wells
E. P. De Poortere, Y. Shkolnikov, E. Tutuc, S. J. Papadakis and M. Shayegan - *Department of Electrical Engineering, Princeton University*

MoM12 12:05 - 12:20
Spin alignment of electrons in PbTe/(Pb,Eu)Te nanostructures
G. Grabecki, J. Wróbel, T. Dietl, E. Papis, E. Kaminska, A. Piotrowska, G. Springholz and G. Bauer - *Institute of Physics, Polish Academy of Sciences*

MoM13 12:20 - 12:35
Optics with Electrons: Fabry-Pérot Resonances and Anti-Reflection Coating for Ballistic Electrons in Finite Superlattices
C. Pacher, G. Strasser, E. Gornik, F. Elsholz, A. Wacker, G. Kießlich and E. Schöll - *Institute for Solid-State Electronics, Vienna University of Technology*

Lunch Break (12:35 – 13:50)

Afternoon Session — *Monday 13:50 – 15:50*

Fast and Ultrafast Carrier Dynamics — **Chairperson: N. Miura**

MoA1 13:50 - 14:20 (invited)
Microscopich carrier dynamics in quantum wells modulated by high frequency lateral fields
P.V. Santos, F. Alsina, S.K. Zhang, R. Hey, A. García-Cristóbal and A. Cantarero - *Paul-Drude-Institut für Festkörperelektronik*

MoA2 14:20 - 14:35
Investigation of nano electromechanical systems using surface acoustic waves
F. W. Beil, A. Hörner, R.H. Blick and A. Wixforth - *Center for NanoScience and Sektion Physik der Ludwigs-Maximilians-Universität*

MoA3 14:35 - 14:50
Ultrafast coherent nonlinear dynamics of intersubband excitations in a quasi-two-dimensional electron gas
M. Woerner, R. A. Kaindl, F. Eickemeyer, K. Reimann, T. Elsaesser, R. Hey and K. Ploog - *Max-Born-Institut für Nichtlineare Optik und Kurzzeitspektroskopie*

MoA4 14:50 - 15:05
Wannier-Stark localization in InAs/(GaIn)Sb supperlattice diodes
L. Bürkle, F. Fuchs, W. Pletschen and J. Schmitz - *Fraunhofer-Institut für Angewandte Festkörperphysik*

MoA5 15:05 - 15:20
Search for gain in a superlattice
H.Willenberg, S.Blaser, D.Hofstetter, M.Beck, G.H.Döhler and J.Faist - *Physics Institute, University of Neuchâtel*

MoA6 15:20 - 15:35
Breakdown of optical selection rules in a highly-biased quantum well
T. Imai, M. Morifuji, C. Hamaguchi, P. Vogl, G. Bohm, G. Trankle and G. Weimann - *Department of Electronic Engineering, Osaka University*

MoA7 15:35 - 15:50
Damping of a Bloch oscillation by Zener tunneling
D. Meinhold, B.Rosam, F.Loeser, V.G.Lyssenko, J.Zhang, F.Rossi, K.Koehler and K.Leo - *Institut fuer Angewandte Photophysik, Universitaet Dresden*

Coffee Break (15:50 – 16:10)

Poster Session I — *Monday 16:10 – 18:00*

*For detailed information see section on **Poster Presentations I***

Break (18:00 – 19:00)

Evening Session — *Monday 19:00 – 20:30*

Rump Session: Molecular Electronics — Chairperson: G. Leising

MoE1 19:00 – 19:30 (invited)
Semiconductor heterojunctions in polymer semiconductor diodes
R. Friend – *Cavendish Laboratory, Cambridge*

MoE2 19:30 – 20:00 (invited)
2D electron physics in organic molecular crystals
B. Batlogg – *ETH Hönggerberg*

MoE3 20:00 - 20:30 (invited)
Nanotechnology approaches to self-organized biomolecular electronic devices
R. Cingolani - *University of Lecce*

Tuesday, July 24

Morning Session — *Tuesday 8:30 – 12:25*

Microcavities and Photonics — Chairperson: M. Skolnick

TuM1 8:30 - 9:00 (invited)
Polariton Scattering and Condensation in Semiconductor Microcavities
J. J. Baumberg - *Dept. of Physics and Astronomy, University of Southampton*

TuM2 9:00 - 9:15
Time resolved stimulated emission in excitonic semiconductor microcavities
J. Bloch, B. Sermage, C. Jacquot, P. Senellart and V. Thierry-Mieg - *LPN-CNRS*

TuM3 9:15 - 9:30
Enhancement of exciton exchange energy splitting by the confined electric field in photonic wires
G. Dasbach, A.A. Dremin, M. Bayer, N.A. Gippius, V. D. Kulakovskii and A. Forchel - *Technische Physik, Universität Würzburg*

TuM4 9:30 - 9:45
Enhanced Rabi Splitting in a Superlattice-Microcavity System
J. H. Dickerson, E. E. Mendez, S. Manotas, F. Agulló-Rueda, C. Pecharromán and A. A. Allerman - *Department of Physics and Astronomy SUNY at Stony Brook*

TuM5 9:45 - 10:00
Strong Coupling of CdS Quantum Dots to Confined Photonic Modes in ZnSe-based Microcavities
T. Tawara, I. Suemune and H. Kumano - *Research Institute for Electronic Science, Hokkaido University*

TuM6 10:00 - 10:15
Optical Double Resonance of Electronic Raman Scattering in a AlAs-AlGaAs Microcavity
T. Kipp, L. Rolf, C. Schüller, D. Endler, Ch. Heyn and D. Heitmann - *Institut für Angewandte Physik und Zentrum für Mikrostrukturforschung, Universität Hamburg*

Coffee Break (10:15 – 10:40)

Single Dot Spectroscopy II — Chairperson: E. Kapon

TuM7 10:40 - 10:55
Coherence properties of single self-organized quantum dots
T. Flissikowski, A. Hundt and F. Henneberger - *Institut für Physik, Humboldt-Universität zu Berlin*

TuM8 10:55 - 11:10
Artificial atoms and molecules of charge carriers in positively and negatively charged quantum dots
D.V. Regelman, D.Gershoni, E. Ehrenfreund, W.V. Schoenfeld and P.M. Petroff - *Physics Department, Technion - Israel Institute of Technology*

TuM9 11:10 - 11:25
Optical spectroscopy of single quantum dot molecules under applied electric field
Itay Shtrichman, Brian D. Gerardot, Claus Metzner, Winston V. Schoenfeld and Pierre M. Petroff - *Materials Department , University of California, Santa Barbara*

TuM10 11:25 - 11:40
Fine structure of neutral and charged excitons: A sensitive tool for probing the symmetry of self-assembled dots
M. Bayer, G. Ortner , A. Forchel, P. Hawrylak and S. Fafard - *Technische Physik, Universität Würzburg*

TuM11 11:40 - 11:55
Optical Properties of Single Charge Tunable InGaAs Quantum Dots
A.D.Ashmore, J.J.Finley, R. Oulton, P.W.Fry, A. Lemaitre, D. J. Mowbray, M. S. Skolnick, M. Hopkinson, P. D. Buckle and P. A. Maksym - *Department of Physics and Astronomy, Sheffield*

Optical Properties of Nanostructures I — Chairperson: E. Gornik

TuM12 11:55 - 12.10
Giant permanent dipole moments of excitons in semiconductor nanostructures
C. Schulhauser, D. Haft, R. J. Warburton, K. Karrai, W. Schoenfeld, J. M. Garcia and P. M. Petroff - *Department of Physics, Heriot-Watt University*

TuM13 12:10 - 12:25
Magnetic properties of excitons in charge-tunable quantum rings
D. Haft, C. Schulhauser, A. O. Govorov, R. J. Warburton, K. Karrai, W. Schoenfeld, J. M. Garcia and P. M. Petroff - *Sektion Physik der LMU*

Lunch Break (12:25 – 13:40)

Afternoon Session — *Tuesday 13:40 – 17:15*

Optical Properties of Nanostructures II — Chairperson: Y. Arakawa

TuA1 13:40 - 14:10 (invited)
Infrared magneto-spectroscopy of polaron states in InAs/GaAs self-assembled quantum dots
S. Hameau, J.N. Isaia, E. Deleporte, Y. Guldner, O. Verzelen, R. Ferreira, G. Bastard, J. Zeman and J.M. Gérard - *Ecole Normale Supérieure - LPMC*

TuA2 14:10 - 14:25
Morphological and optical anisotropy of self-assembled quantum dots probed by magneto-tunnelling and photoluminescence-polarisation spectroscopy
A. Patané, L. Eaves, A. Levin, P. C. Main, M. Henini, E.E. Vdovin, Yu. V. Dubrovskii and Yu. N. Khanin - *School of Physics and Astronomy, University of Nottingham,*

TuA3 14:25 - 14:40
Quantum interference effect in photoionization spectra of self-assembled InAs quantum dots
K. Hirakawa, Ph. Lelong, K. Hirotani, S. -W. Lee, S. Fujimoto and H. Sakaki - *Institute of Industrial Science, University of Tokyo*

TuA4 14:40 - 14:55
2D-1D crossover from quantum well to quantum wire behaviour in GaAs V-groove structures
R. Roshan, N.I. Cade, M.Hauert, A..C.Maciel, J.F.Ryan, A.Schwarz, T.Schapers and H.Lüth - *Condensed Matter Physics, University of Oxford*

TuA5 14:55 - 15:10
Quantum mechanical repulsion of exciton levels in a disordered quantum well evidenced by near-field spectroscopy
F. Intonti, V. Emiliani, C. Lienau, T. Elsaesser, V. Savona, E. Runge, R. Zimmermann, R. Nötzel and K. H. Ploog - *Max-Born-Institut für Nichtlineare Optik und Kurzzeitspektroskopie*

TuA6 15:10 - 15:25
Directional phonon-assisted cascading of photoexcited carriers in stepped $In_X(Al_{0.17}Ga_{0.83})_{1-X}As/Al_{0.17}Ga_{0.83}As$ multiple quantum wells
S. Machida, M. Matsuo, K. Fujiwara, J.R. Jensen and J.M. Hvam - *Kyushu Institute of Technology, Dept of Electrical Engineering*

TuA7 15:25 - 15:40
Heterostructures Interface Effects on the Far-Infrared Magneto-Optical Spectra of InAs/GaSb Quantum Wells
G. Comanescu, R.J. Wagner, B.D. McCombe, B.V. Shanabrook, B.R. Bennett, S.K. Singh, J.G. Tischler and B.A. Weinstein - *Department of physics, State University of New York at Buffalo*

Coffee Break (15:40 – 16:00)

THz Emission **Chairperson: G. Abstreiter**

TuA8 16:00 - 16:15
Magnetic field enhancement of terahertz emission from III-V semiconductors
A Corchia, M B Johnston, R McLaughlin, D D Arnone, E H Linfield, A G Davies and M Pepper - *Semiconductor Physics Group Cavendish Laboratory, Cambridge*

TuA9 16:15 - 16:30
Terahertz-Quantum Cascade Emitters
J. Ulrich, R. Zobl, W. Schrenk, G. Strasser and K. Unterrainer - *Institut für Festkörperelektronik, Technische Universität Wien*

Towards Quantum Communication **Chairperson: E. Molinari**

TuA10 16:30 - 16:45
Tailoring photon emission statistics of a single quantum box for quantum communications.
E. Moreau, J.M. Gérard, I. Robert and I. Abram - *CNRS/Laboratoire Photonique et Nanostructures*

TuA11 16:45 - 17:00
Entangled states of electron-hole complex in a single InAs/GaAs coupled quantum dot molecule in a magnetic field
M. Korkusinski, P. Hawrylak, M. Bayer, G. Ortner, A. Larionov, V. B. Timofeev, A. Forchel, S. Fafard and Z. Wasilewski - *Institute for Microstructural Sciences National Research Council of Canada*

TuA12 17:00 - 17:15
Spintronics and Quantum Computing in Semiconductors
D. Loss - *Department of Physics and Astronomy, Basel*

Break (17:15 – 17:30)

Poster Session II ***Tuesday 17:30 – 19:30***

For detailed information see section on ***Poster Presentations II***

Wednesday, July 25

Morning Session ***Wednesday 8:30 – 12:00***

Novel Materials **Chairperson: L. Eaves**

WeM1 8:30 - 9:00 (invited)
Parallel synthesis and high throughput characterization of ZnO based alloy films, heterostructures and devices
M. Kawasaki - *Department of Innovative and Engineered Materials, Tokyo Institute of Technology*

WeM2 9:00 - 9:30 (invited)
How to make GaN-Electronics Work: Physics and Technology
U.K. Mishra - *University of California, Santa Barbara*

WeM3 9:30 - 10:00 (invited)
Optical Gain in Silicon Nanocrystals
F. Priolo , G. Franzò, F. Iacona, E. Ceretta Moreira, D. Pacifici and A. Irrera - *INFM and University of Catania*

WeM4 10:00 - 10:30 (invited)
Semiconductor nanotubes and nanopipelines
O. G. Schmidt - *Max-Planck-Institut für Festkörperforschung, Stuttgart*

Coffee Break (10:30 – 11:00)

Novel Modulated Structures **Chairperson: B. Batlogg**

WeM5 11:00 - 11:15
Coupled quantum dots in single-wall carbon nanotubes
K. Ishibashi, M. Suzuki, T. Ida and Y. Aoyagi - *Semiconductors Laboratory, The Institute of Physical and Chemical Research (RIKEN)*

WeM6 11:15 - 11:30
Coherent Inter- and Intramolecular Phonons in Quasi-1D Organic Crystals
T.W. Canzler, T. Hasche, R. Scholz and K.Leo - *TU-Dresden, IAPP*

WeM7 11:30 - 11:45
Tuning of optical gain in soluble thiophene-based oligomers
M.Anni, G.Gigli, M. Zavelani-Rossi, C. Gadermaier, G. Lanzani, G.Barbarella, L. Favaretto and R.Cingolani - *Istituto Nazionale di Fisica della Materia (INFM), Dipartimento di Ingegneria dell'Innovazione, Università degli Studi di Lecce*

WeM8 11:45 - 12:00
Electronic Properties and Conductivity of Guanine Assemblies
E. Molinari, R. Di Felice, A. Calzolari and A. Garbesi - *INFM & Physics Dept, University of Modena and Reggio*

Conference Excursion *departure:* ***12:15***

Conference Banquet

Organ Concert *– Bruckner Organ, Basilica of St. Florian*
Dinner *– Marble Hall of the Monastery of St. Florian* ***19:30 - 22:30***

Thursday, July 26

Morning session — *Thursday 8:30 – 12:15*

Quantum Cascade Structures I — **Chairperson: M. Helm**

ThM1 8:30 - 9:00 (invited)
Recent results in quantum cascade lasers and intersubband transitions in GaN/AlGaN multiple quantum wells
C. Gmachl, H. M. Ng, S. V. Frolov, R. Paiella, R. Martini, H. Y. Hwang, D. L. Sivco, F. Capasso, A. Y. Cho and H. C. Liu - *Bell Laboratories, Lucent Technologies*

ThM2 9:00 - 9:15
Intervalley scattering in GaAs-AlAs quantum cascade lasers
L.R.Wilson, D.A.Carder, M.J.Steer, J.W.Cockburn, M.Hopkinson, C.K.Chia, G.Hill and R.Airey - *University of Sheffield*

ThM3 9:15 - 9:30
High performance single mode GaAs quantum cascade lasers
W. Schrenk, E. Gornik, H. Page, C. Sirtori, V. Ortiz and G. Strasser, *Institut fuer Festkoerperelektronik TU Wien*

ThM4 9:30 - 9:45
Optimized large optical cavity design for 10.8 μm (Al)GaAs Quantum Cascade Laser
Nicolaus Ulbrich, Giuseppe Scarpa, Alfred Sigl, Max Bichler , Dieter Schuh, Markus-Christian Amann and Gerhard Abstreiter - *Walter Schottky Institute, Technical University of Munich*

ThM5 9:45 - 10:00
Far-Infrared Quantum Cascade Lasers at lambda > 20 um.
R. Colombelli, F. Capasso , C. Gmachl, A. L. Hutchinson, D. L. Sivco, A. Tredicucci, M. C. Wanke, A. M. Sergent and A. Y. Cho - *Bell-Labs, Lucent Technologies*

ThM6 10:00 - 10:15
Cyclotron and intersubband emission of InGaAs/AlGaAs quantum cascade structure in the quantum regime
Stéphane Blaser, Michel Rochat, Mattias Beck and Jérôme Faist - *Institut de Physique, Université de Neuchâtel*

Coffee Break (10:15 – 10:30)

Quantum Cascade Structures II — **Chairperson: E. Ehrenfreund**

ThM7 10:30 - 11:00 (invited)
Intersubband quantum cascades in the Si /SiGe material system
L. Diehl, G. Dehlinger, H. Sigg, U. Gennser, D. Grützmacher, E. Müller, J. Faist and K. Ensslin - *Laboratoire de Photonique et de Nanostructures - CNRS*

ThM8 11:00 - 11:15
Ultrafast intersubband scattering of holes in p-type modulation-doped $Si_{1-x}Ge_x$/Si multiple quantum wells
M. Woerner, R. A. Kaindl, M. Wurm, K. Reimann, T. Elsaesser, C. Miesner, K. Brunner and G. Abstreiter - *Max-Born-Institut für Nichtlineare Optik und Kurzzeitspektroskopie*

Devices — **Chairperson: P. Petroff**

ThM9 11:15 - 11:30
Ultra-short channel transistors fabricated by cleaved-edge overgrowth
F. Ertl, T. Asperger, R. A. Deutschmann, M. Bichler and G. Abstreiter - *Walter Schottky Institut, Technische Universität München*

ThM10 11:30 - 11:45
GaAs and InGaAs Single Electron Hexagonal Nanowire Circuits Based on Binary Decision Diagram Logic Architecture
S. Kasai and H. Hasegawa - *Research Center for Interface Quantum Electronics and Graduate School of Electronics and Information Engineering, Hokkaido University*

ThM11 11:45 - 12:00
Voltage-switchable Bragg reflector for planar optical waveguides
W. R. Frank, A. O. Govorov, W. Wegscheider, K. Karrai and J. P. Kotthaus - *CeNS und Sektion Physik, Ludwig-Maximilians-Universität München*

ThM12 12:00 - 12:15
Room Temperature Single-Hole Silicon Memory
N.T. Bagraev, A.D. Bouravleuv, L.E. Klyachkin, A.M. Malyarenko and S.A. Rykov - *Ioffe Physico-Technical Institute, St.Petersburg*

Lunch Break (12:15 – 13:15)

Afternoon session — *Thursday 13:15 – 15:15*

Nanostructure Growth and Fabrication — **Chairperson: Y. Shiraki**

ThA1 13:15 - 13:45 (invited)
Heteorepitaxy of dissimilar materials: Effect of interface structure on strain and defect formation
A. Trampert - *Paul-Drude-Institut fuer Festkoerperelektronik*

ThA2 13:45 - 14:00
Axially modulated quantum wires
B. Dwir, K. Leifer and E. Kapon - *Institute for Micro- and Optoelectronics, Physics Dept., Swiss Federal Institute of Technology (EPFL)*

ThA3 14:00 - 14:15
Fabrication and characterization of III-V nanowhiskers
B. J. Ohlsson, M. Bjork, M. H. Magnusson, A. Persson, L. R. Wallenberg and L. Samuelson - *Department of Solid State Physics, University of Lund*

ThA4 14:15 - 14:30
Spatially Site-Controlled InAs Quantum Dot Lattices
S. Kohmoto, H. Nakamura, S. Nishikawa and K. Asakawa - *The Femtosecond Technology Research Association (FESTA)*

ThA5 14:30 - 14:45
Effect of phosphorus on Ge/Si(001) island formation
T. I. Kamins, G. Medeiros-Ribeiro, D. A. A. Ohlberg and R. Stanley Williams - *Hewlett-Packard Laboratories*

ThA6 14:45 - 15:00
Silicon/Silicon(sub)oxide heterostructures grown by Molecular Beam Epitaxy
A. Sticht, M. Markmann, K.Brunner, G. Zandler and G. Abstreiter - *Walter Schottky Institut, TU München*

ThA7 15:00 - 15:15
Optical and electrical properties of Fe/GaAs (001) hybrid structures grown by molecular beam epitaxy
Y. Chye, V. Huard, M. White and P. Petroff - *Department of Electrical and Computer Engineering, University of California, Santa Barbara*

Coffee Break (15:15 – 16:00)

Poster Session III — *Thursday 16:00 – 18:00*

For detailed information see section on ***Poster Presentations III***

Break (18:00 – 19:00)

Evening Session — *Thursday 19:00 – 21:00*

Rump Session: Spintronics — Chairperson: H.Ohno

ThE1 19:00 - 19:30 (invited)
Manipulation and storage of quantum information with semiconductor spintronics
I. Malajovich, E. Johnston-Halperin, R.L. Kawakami, J.J. Berry, N. Samarth and D.D. Awschalom - *Department of Physics, University of California Santa Barbara*

ThE2 19:30 - 20:00 (invited)
Ferromagnetism in II-VI based semiconductor structures
J. Cibert, D. Ferrand, S. Tatarenko, A. Wasiela, P. Kossacki and T. Dietl - *Laboratoire de Spectrométrie Physique, CNRS / Université Joseph Fourier Grenoble*

ThE3 20:00 - 20:30 (invited)
III-V based magnetic heterostructures for spintronics
M. Tanaka - *Department of Electronic Engineering, University of Tokyo*

ThE4 20:30 - 21:00 (invited)
Spin injection and spin accumulation in mesoscopic two-dimensional electron gas and metal spin valves.
B.J. van Wees - *Department of Applied Physics and Materials Science Centre, University of Groningen*

Friday, July 27

Morning session — *Friday 8:30 – 12:00*

Spin Electronics and Magnetic Heterostructures — Chairperson: T. Dietl

FrM1 8:30 - 8:45
Spin lifetimes and g-factor tuning in Si/SiGe quantum wells
N. Sandersfeld, M.Mühlberger, W. Jantsch, Z. Wilamowski and F. Schäffler - *Inst. f. Halbleiter- und Festkörperphysik, Johannes Kepler Universität Linz*

FrM2 8:45 - 9:00
Electrical Spininjection using II-VI Dilute Magnetic Semiconductors as Spin Aligners
L.W. Molenkamp, G. Schmidt, P. Grabs, C. Gould and G. Richter - *Physikalisches Institut (EP3), Universität Würzburg*

FrM3 9:00 - 9:15
Spin polarization dynamics in n-doped InAs/GaAs quantum dots
S. Cortez, A.Jbeli, X.Marie, O. Krebs, R. Ferreira, T.Amand, P. Voisin and J-M. Gérard - *Laboratoire de Physique de la Matière Condensée de l'Ecole Normale Supérieure*

FrM4 9:15 - 9:30
Photoluminescence spectroscopy on single CdSe quantum dots in a semimagnetic ZnMnSe matrix
H. Schömig, M.K. Welsch, S. Zaitsev, G. Bacher, V.D. Kulakovskii, A. Forchel, S. Lee, M. Dobrowolska and J.K. Furdyna - *Physikalisches Institu , Universität Würzburg*

FrM5 9:30 - 9:45
Photo-carrier induced magnetism in (In,Mn)As/GaSb magnetic alloy semiconductor heterostructures
H. Munekata, A. Oiwa and T. Slupinski - *Kanagawa Academy of Science and Technology*

FrM6 9:45 - 10:00
Valence-band alignment at (Ga,Mn)As/GaAs heterointerface
Y.Ohno, I.Arata and H.Ohno - *Laboratory for Electronic Intelligent Systems, Research Institute of Electrical Communication, Tohoku University*

FrM7 10:00 - 10:15
Non-linear spin transport in magnetic semiconductor multiple quantum wells
David Sanchez, A. H. MacDonald and Gloria Platero - *Departamento de Teoria de la Materia Condensada, Instituto de Ciencia de Materiales de Madrid (CSIC)*

Coffee Break (10:15 – 10:30)

Cavities and Single Photon Sources — Chairperson: A.Madhukar

FrM8 10:30 - 11:00 (invited)
A quantum dot single-photon source
C. Becher, A. Kiraz, P. Michler, W. V. Schoenfeld, P.M. Petroff, L. Zhang, E. Hu and A. Imamoglu - *Institut für Experimentalphysik, Universität Innsbruck*

FrM9 11:00 - 11:15
Single-mode single photon source based on isolated InAs quantum boxes in micropillars
E. Moreau, J.M. Gérard, I. Robert, I. Abram, L. Manin and V. Thierry-Mieg - *CNRS/Laboratoire Photonique et Nanostructures*

FrM10 11:15 - 11:30
Coherent dynamics of microcavity polaritons in the nonlinear regime
A. Huynh, J. Tignon, Ph. Roussignol, C. Delalande, R. André, R. Romestain and D. Le Si Dang - *Ecole Normale Supérieure, LPMC*

FrM11 11:30 - 12:00 (invited)
CQED experiments with InAs quantum dots
B. Gayral - *ECE Department, University of California at Santa Barbara*

Lunch Break (12:00 – 13:30)

Afternoon Session — *Friday 13:30 – 15:00*

Quantum Dot and Wire Lasers — Chairperson: A.C. Gossard

FrA1 13:30 - 14:00 (invited)
Carrier dynamics and device characteristics of quantum dot lasers and microcavity light emitters
D.G. Deppe, C. Cao, O.B. Shchekin, Z. Zou, H. Chen, T.F. Boggess, L. Zhang and K. Gundogdu - *The University of Texas at Austin, Microelectronics Research*

FrA2 14:00 – 14:15
Mid-infrared surface-emitting PbSe/PbEuTe quantum dot lasers
G. Springholz, T. Schwarzl, W. Heiss, M. Aigle, H. Pascher, T. Fromherz, G. Bauer
Institut für Halbleiter- und Festkörperphysik, Universität Linz

FrA3 14:15 - 14:30
Optical emission in a V-groove Quantum Wire Laser diode under high magnetic fields
L. Sirigu, H. Weman, F. Karlsson, D. Y. Oberli, A. Rudra and E. Kapon - *Department of Physics, Swiss Federal Institute of Technology-EPFL*

FrA4 10:30 – 15:00 (invited)
Quantum dots for VCSEL applications at λ=μm
N. Ledentsov, D. Bimberg V.M. Ustinov, Zh.I. Alferov, J.A. Lott - *Technische Universität Berlin*

Closing*.....*15:00

Poster Presentations I — *Monday 16:00 – 18:00*

AI Si/SiGe based structures

MoP1
Phonons in self-assembled Ge/Si structures
A.G.Milekhin - *Institute of Semiconductor Physics, Russian Academy of Sciences*

MoP2
Hole transport of SiGe channels on step-bunched vicinal Si surfaces
R. Neumann, K. Brunner and G. Abstreiter - *Walter Schottky Institut, TU München*

MoP3
The surface morphology of single $Si_{1-x}Ge_x$ layers grown on vicinal Si(001): step bunching and strain-effects
C. Schelling, M. Mühlberger, G. Springholz and F. Schäffler - *Institut für Halbleiter- und Festkörperphysik, Johannes Kepler Universität Linz*

MoP4
Chemically vapor deposited Si nanowires nucleated by self-assembled Ti islands on patterned and unpatterned Si substrates
T. I. Kamins, R. Stanley Williams, T. Hesjedal and J. S. Harris - *Hewlett-Packard Laboratories*

MoP6
LEPECVD - a novel process for high-speed heterostructure SiGe FET's
M. Kummer, C. Soltmann, E. Müller, C. Rosenblad, T. Hackbarth, M. Zeuner, G. Höck and H. von Känel - *Institut für Festkörperphysik, ETH Zürich*

MoP7
Morphology of virtual SiGe substrates grown at very low temperatures
C. Teichert, C. Hofer, K. Lyutovich, M. Bauer and E. Kasper - *Institute of Physics, University of Leoben*

MoP8
Strain and composition profile of uncapped SiGe islands
J. Stangl, M.Meduna, A. Daniel, V. Holy, T. Roch, G. Bauer, O.G. Schmidt and K. Eberl - *Inst. für Halbleiter- und Festkörperphysik, Johannes kepler Universität Linz*

MoP9
Shape evolution of Ge domes on Si(001) during first stages of Si capping
A. Rastelli, M. Kummer and H. von Kaenel - *Universita' degli Studi di Pavia, Dipartimento di Fisica "A. Volta"*

MoP10
Photoluminescence of Si-based heterostructures and quantum dots
E. Ribeiro, E.F. da Silva Jr, V.N. Freire, V. Lemos, Y. Ikoma, F. Watanabe and T. Motooka, *Departamento de Fisica Cidade Universitaria, Recife -Pe, Brazil*

MoP11
Unimodal dome-shaped islands of Ge-on-Si(001) by step-wise growth in UHV-CVD
Vilma Zela, Ines Pietzonka, Torsten Sass, Claes Thelander and Werner Seifert - *Lund University Solid State Physics*

MoP12
Ge quantum dots in Si: self-assembly, ordering and level spectroscopy
K. Brunner, D. Bougeard, C. Miesner, M. Herbst, C. Schramm, G. Abstreiter, A. Vörckel and H. Kurz - *Walter Schottky Institute, Technical University Munich*

MoP13
Optical properties of ordered Ge islands
L.Vescan and T. Stoica - *Institut für Schichten und Grenzflächen, Forschungszentrum Jülich GmbH*

MoP14
Intersubband transitions in boron doped self-assembled Ge quantum dots
W. Mac, T. Fromherz, C. Miesner, K. Brunner, G. Bauer and G. Abstreiter - *Institut für Halbleiter- und Festkörperphysik, Universität Linz*

MoP15
Many-particle effects in excitonic transitions in type-II Ge/Si quantum dots
A.I. Yakimov, N.P. Stepina, A.V. Dvurechenskii, A.I. Nikiforov and A.V. Nenashev - *Institute of Semiconductor Physics, Novosibirsk*

MoP16
Influence of the Si-Ge Interface on Phononless Radiative Recombination in Ge Hut Clusters Grown on Si (001)
M.W. Dashiell, U. Denker, O.G. Schmidt and K. Eberl - *Max-Planck-Institut fur Festkoerperforschung, Stuttgart*

MoP17
Improvement in photoluminescence efficiency of $Si_{1-x}Ge_x$ alloy nanocrystals embedded in SiO2 matrices by P doping
K. Toshikiyo, M. Tokunaga, S. Takeoka, M. Fujii and S. Hayashi - *Graduate School of Science and Technology, Kobe University*

MoP18
Excitation of Nd3+and Tm3+ by the energy transfer from Si nanocrystals
K. Watanabe, H. Tamaoka, M. Fujii and S. Hayashi - *Graduate School of Science and Technology, Kobe University*

MoP19
Gated wires and interferometers based on Si/SiGe heterostructures
O.Estibals, Z.D.Kvon, J.C.Portal, A.Y.Plotnikov, J.L.Gauffier, N.J.Woods, J.Zhang and J.J.Harris - *Institute for Semiconductor Physics, Novosibirsk*

MoP20
Fabrication of Si/SiGe quantum point contacts by electron-beam lithography and shallow wet-chemical etching
U. Wieser, U. Kunze, K. Ismail and J. O. Chu - *Ruhr-Universität Bochum*

MoP21
Si-based light emission from Ge-implanted SiO_2 layers: Electric and optoelectronic properties
L. Rebohle , T. Gebel , J. von Borany, W. Skorupa and M. Helm - *Forschungszentrum Rossendorf e.V., Institut für Ionenstrahlphysik und Materialforschung*

MoP22
Fabrication of strain-balanced $Si_{0.73}Ge_{0.27}$/Si distributed Bragg reflectors on Si substrates for optical device applications
K. Kawaguchi, S. Koh, Y. Shiraki and J. Zhang - *RCAST, The University of Tokyo*

MoP23
The advantages of p-type and design methodologies for SiGe far-infrared (Terahertz) quantum well infrared photodetectors (QWIPs)
M. A. Gadir, P. Harrison and R. A. Soref - *School of Electronic and Electrical Engineering, University of Leeds*

MoP24
Light emission from erbium doped nanostructures embedded in silicon microcavities
N.T. Bagraev, A.D. Bouravleuv, W. Gehlhoff, L.E. Klyachkin, A.M. Malyarenko, M.M. Mezdrogina, V.V. Romanov and A.P. Skvortsov - *A.F.Ioffe Physico-Technical Institute, St. Petersburg*

MoP25
Reflection and transmission of light in the photonic-band-gap range of triangular lattice of Si nanopillars with the 500 nm period
Vladimir V. Poborchii, Tetsuya Tada and Toshihiko Kanayama - *JRCAT (Joint Research Center for Atom Technology), Tsukuba*

MoP26
Determination of the Rashba Field in modulation doped Si/SiGe Quantum Wells from Conduction Electron Spin Resonance
Z. Wilamowski and W. Jantsch - *Institut für Halbleiter- und Festkörperphysik, Johannes Kepler Universität*

BI Characterization and Fabrication of Nanosturctures

MoP27
Influence of capping conditions on structural properties of CdSe quantum dot structures
T. Passow, K. Leonardi, H. Heinke, T. Schmidt, J. Falta, A. Stockmann, H. Selke and D. Hommel - *Institut für Festkörperphysik, Universität Bremen*

MoP28
(Ga Mn)As: As incorporation in the host lattice depending on the substrate temperature and the Mn content
G.M. Schott, A.Bader, C.Schuhmacher and W. Faschinger - *Physikalisches Institut, Universität Würzburg*

MoP29
Fabrication and characterization of III-V semiconductor superlattices with sinusoidal compositional modulation
X. Liu, Y. Sasaki, J. K. Furdyna, P.M. Reimer and S. Lee - *Department of Physics, University of Notre Dame*

MoP30
X-ray scattering on InP/InGaP quantum dot multilayers
M. Schmidbauer, F. Hatami, P. Schäfer, M. Hanke, T. Panzner, W.T. Masselink and R. Köhler - *Humboldt-Universität zu Berlin, Institut für Physik, AG Röntgenbeugung*

MoP31
Finite size effects in the vertical and lateral ordering of self-organized PbSe quantum dot superlattices
R. Lechner, A. Raab, G. Springholz, M. Pinczolits, V. Holy, P. Mayer, G. Bauer, H. Kang and L. Salamanca-Riba, *Institut für Halbleiterphysik, Universität Linz*

MoP32
Atomistic Simulation of Strain Relaxation in $In_xGa_{1-x}As/GaAs$ Quantum Dots with Nonuniform Composition
M. A. Migliorato, A. G. Cullis, M. Fearn and J. H. Jefferson - *Department of Electronic and Electrical Engineering, The University of Sheffield*

MoP33
Structure and ordering of GaN quantum dot multilayer investigated by x-ray grazing incidence techniques
V. Chamard, T. H. Metzger, E. Bellet-Amalric, B. Daudin, C. Adelmann, H. Mariette and G. Mula - *European Radiation Synchrotron Facility*

MoP34
Two-wave X-ray optical diagnostics of Ge_xSi_{1-x}/Si modulation-doped heterostructures
A.G. Touryanski, I.V. Pirshin, M. M. Rzaev, F. Schäffler and M. Mühlberger - *Lebedev Institute, Moscow*

MoP35
Fabrication of height-controlled InAs quantum dots on GaAs surfaces by in-situ $AsBr_3$ etching and molecular beam epitaxy
T. Yang, S. Kohmoto, H. Nakamura and K. Asakawa - *The Femtosecond Technology Research Association (FESTA)*

MoP36
Direct fabrication of parallel quantum dots with an atomic force microscope
U. F. Keyser, M. Paesler, U. Zeitler, R. J. Haug and K. Eberl - *Institut für Festkörperphysik, Universität Hannover*

MoP37
Quantitative determination of the charge on surface steps by high-resolution local scanning-tunneling spectroscopy
M. Kemerink, T.C.G. Reusch, D.M. Bruls, P.M. Koenraad, H.W.M. Salemink and J.H. Wolter - *Physics Department, Eindhoven University of Technology*

MoP38
Characterization of GaAs Crystalline Nano-Rod Grown by Molecular Beam Epitaxy
H. G. Lee and T. W. Kang - *Quantum-functional Semiconductor Research Center and Department Physics, Dongguk Unversity*

MoP39
In situ structuring during MBE regrowth with shadow masks
T. Schallenberg, C. Schumacher and W. Faschinger - *Experimentelle Physik III, Universität Würzburg*

MoP40
Carrier Confinement of a InGaAs QW Induced by a Periodical Stressor Layer
J. Grenzer, U. Zeimer, U. Pietsch, S. Gramlich, F. Bugge, V. Smirnitzki, Ch. Lienau, S. Grigorian, M. Weyers and G. Tränkle - *Universität Potsdam, Institut für Physik/Strukturanalyse*

MoP41
Highly efficient two-photon absorbing Material for application in three-dimensional Micro and Nanostructuring
A. Hohenau, C. Cagran, U. Scherf and G. Leising - *Institut für Nanostrukturierte Materialien und Photonik, Joanneum Research*

MoP42
Nano-scale dislocation patterning in PbTe on PbSe (100) heteroepitaxy studied by UHV scanning tunneling microscopy
K. Wiesauer and G. Springholz - Institut für Halbleiterphysik, *Johannes Kepler Universit, Linz*

MoP43
Heteroepitaxial PbTe-on Si pn-junction IR-sensors: Correlations between material and device properties
H. Zogg, K. Alchalabi and D. Zimin - *Thin Film Physics Group, ETH-Technopark*

MoP44
Absorption and Photoluminescence in $PbTe/Pb_{1-x}Eu_xTe$ quantum wells
E. Abramof, E.A. de Andrada e Silva, I.I. Zasavitskii, S.O. Ferreira, P. Motisuke, P.H.O. Rappl and A.Y. Ueta - *Laboratório Associado de Sensores e Materiais - LAS, Instituto Nacional de Pesquisas Espaciais - INPE*

MoP45
Nano-scale metallic and superconducting circuits in semiconducting superlattices
N.Ya. Fogel , E.A. Pashitskii, A.V. Danilov, Yu.Bomze, R.I. Shekhter and M. Jonson - *Solid State Institute, Technion - Israel Institute of Technology*

MoP46
Fabrication and elastic properties of InAs freestanding structures based on InAs/GaAs(111)A heteroepitaxial systems
H. Yamaguchi, R. Dreyfus, S. Miyashita and Y. Hirayama - *NTT Basic Research Laboratories*

CI Transport

MoP47
Etching temperature dependent mobilities up to 190.000 cm^2/Vs at chlorine etched and regrown interfaces
S. Beyer, S. Löhr, Ch. Heyn, D. Heitmann and W. Hansen - *Institut für Angewandte Physik und Zentrum für Mikrostrukturforschung, Universität Hamburg,*

MoE48
Much enhanced electron mobility in a pseudomorphic $In_{0.74}Ga_{0.26}As/In_{0.46}AlAs$ QW-HEMT structure with (411)A super-flat interfaces grown by MBE
T. Kitada, T. Aoki, I. Watanabe, K. Kanzaki, S. Shimomura and S. Hiyamizu - *Graduate School of Engineering Science, Osaka University*

MoP49
Study of free GaAs surfaces using a back-gated undoped GaAs/AlGaAs heterostructure
A. Kawaharazuka, T. Saku, C. A. Kikuchi, Y. Horikoshi and Y. Hirayama - *Waseda University*

MoP50
Edge-channel transport through quantum wires with a magnetic quantum dot
H.-S. Sim, G. Ihm, N. Kim, S. J. Lee and K. J. Chang - *Department of Physics, Korea Advanced Institute of Science and Technology*

MoP51
Transport in quantum dot-arrays
N. Mori, T. Ishida, Y. Takamura and C. Hamaguchi - *Department of Electronic Engineering, Osaka University*

MoP52
Local spectroscopy of mesoscopic systems with scanning probe techniques
T. Ihn, J. Rychen, T. Vancura, T. Cilento, R. Held, K. Ensslin, W. Wegscheider and M. Bichler - *Laboratorium für Festkoerperphysik, ETH Zuerich*

MoP53
Spin-resolved transport in single electron tunneling
J. Könemann, P. König and R. J. Haug - *Institut für Festkörperhysik, Universität Hannover*

MoP54
Intersubband scattering in serially connected quantum wires
B. Dwir, D. Kaufman, E. Kapon and A. Palevski - *Institute for Micro- and Optoelectronics, Physics Dept., Swiss Federal Institute of Technology (EPFL)*

MoP55
Hund's Rule and Addition Energy Spectra of Cylindrical Quantum Dots
P. Matagné, J.P Leburton, D.G. Austind and S. Tarucha - *Computational Electronic Group, Beckman Institute, University of Illinois*

MoP56
The Evolution of Fractal Patterns during a Classical-Quantum Transition
A.P. Micolich, R.P. Taylor, A.G. Davies, J.P. Bird, A.Ehlert, T.M. Fromhold, R. Newbury, L.D. Macks, W.R. Tribe and H. Linke - *Materials Science Institute, Physics Department, University of Oregon*

MoP57
Low temperature transport in dual-gated SETs fabricated by selective are metalorganic vapor phase epitaxy
J. Motohisa, W.G. wan der Wiel, J.M. Elzerman, S. De Franceschi, F. Nakajima, Y. Ogasawara, T. Fukui and L.P. Kouwenhoven - *Research Center for Interface Quantum Electronics, Hokkaido University*

MoP58
T - dependent Resistivity Anomaly in Doped AlAs/GaAs Lateral Superlattices: Evidence for Fermi-Liquid Behaviour
P. Denk and J. - L. Pelouard - *Lehrstuhl für angewandte Physik, Universität München*

MoP59
Exclusion of quantum coherence as the origin of the metallic state in Si-MOS structures
G. Brunthaler, A. Prinz, G.Pillwein, T.Berer, G. Bauer and V.M. Pudalov - *Johannes Kepler University, Institut für Halbleiterphysik*

MoP60
Random 1D structures as filters for electrical and optical signals
A. Krokhin, F. Izrailev, U. Kuhl, H.-J. Stöckmann and S. Ulloa - *Instituto de Fisica, Universidad Autonoma de Puebla*

MoP61
Electrical Rectification in Channelling by Magnetic Edge States
D. N. Lawton, A. Nogaret, M. V. Makarenko, O. V. Kibis and M. Henini, S.J.Bending, J.C.Portal, D.K. Maude- *Department of Physics, University of Bath*

MoP62
Two-way current switch using Coulomb blockade in GaAs quantum dots fabricated by selective area MOVPE
F. Nakajima, Y. Ogasawara, J. Motohisa and T. Fukui - *Research Center for Interface Quantum Electronics (RCIQE), Hokkaido University*

MoP63
Transient high-field transport and electro-optical properties of AlGaAs-grading-structures
L. Robledo, M. Eckardt, A. Schwanhäußer, G. Döhler, H. Lutz and A. Seilmeier - *Institut für Technische Physik 1, Erlangen*

MoP64
Dynamical transport of photoexcited carriers between shallow and deep quantum wells embedded in a GaAs/AlAs superlattice
A. Satake, T. Ikemoto, K. Fujiwara, L. Schrottke, R. Hey and T. Grahn - *Department of Electrical Engineering, Kyushu Institute of Technology*

MoP65
Hot-carrier dynamics in semiconductor-based quantum-cascade lasers: a Monte Carlo study
R. C. Iotti and F. Rossi - *Dipartimento di Fisica, Politecnico di Torino*

MoP66
Magnetotransport through AFM-defined Antidot Arrays
A. Dorn, A. Fuhrer, T. Heinzel, K. Ensslin, W. Wegscheider and M. Bichler - *ETH Zürich*

MoP67
Comparison of experimental and calculated resistance in p-SiGe over a wide temperature range
V. Senz, T. Ihn, T. Heinzel, K. Ensslin, G. Dehlinger, D. Gruetzmacher, U. Gennser, E.H. Hwang and S. das Sarma - *Solid State Physics Laboratory HPF E13, ETH Zürich*

MoP68
An Ultra-narrow Electron Injector for Ballistic Electron Spectroscopy
M. Kast, C. Pacher, M. Coquelin, G. Fasching, G. Strasser and E. Gornik - *Institut für Festkörperelektronik, TU-Wien*

MoP69
Magnetoresistance of a modulated two-dimensional electron gas in parallel magnetic field
A. Nauen, U. Zeitler, A. G. M. Jansen, R. J. Haug, M. Dilger and K. Eberl - *Inst. f. Festkörperphysik, Abt. Nanostrukturen, Uni Hannover,*

MoP70
Strained relaxation in high-mobility InAs inserted-channel hetrostructures with metamorphic buffer.
S. Mendach, C. M. Hu, Ch. Heyn, S. Schnüll, H. P. Oepen, R. Anton and W. Hansen - *Institut für Angewandte Physik und Mikrostrukturforschung, Uni Hamburg*

MoP71
Magnetoresistance of vertical transport in InAs/GaSb superlattices
V. J. Hales, R. J. Nicholas and N. J. Mason - *University of Oxford*

MoP72
Current modulated light reflectance spectroscopy with submicron spatial resolution in semiconductor heterostructures
O. A. Ryabushkin and E. I. Lonskaya - *Institute of Radio Engineering and Electronics Russian Academy of Sciences*

MoP73
Negative magnetoresistance of SiGe quantum wells doped with boron
R. Zobl, E. Gornik, I. V. Altukhov, N. G. Zhdanova and M. S. Kagan - *Institute of Radioengineering and Electronics, Russian Academy of Sciences*

MoP74
Spin orientation of electrons by lateral electric field in 2D system without inversion symmetry
A. V. Chaplik, M. V. Entin and L. I. Magarill - *Institute of Semiconductor Physics, Siberian Branch of Russian Academy of Sciences*

MoP75
In-plane magnetic field induced spin polarization and transition to insulating behavior in two-dimensional hole systems
E. Tutuc, E.P. De Poortere, S.J. Papadakis and M. Shayegan - *Department of Electrical Engineering, Princeton University*

MoP76
Transport of a two-dimensional electrons in the lattice of diffusive and thermalizing scatterers.
Z.D.Kvon, O.Estibals, A.Y.Plotnikov, J.C.Portal and A.I.Toropov - *Institute of Semiconductor Physics, Novosibirsk*

MoP77
Magnetic field induced breakdown of the current-voltage characteristics in SeGe-heterostructures containing quantum dots
K.-M. Haendel, C. Lenz, U. Denker, O. G. Schmidt, K. Eberl and R. J. Haug - *Universität Hannover, Institut für Festkörperphysik*

DI Organic Semiconductor Structures

MoP78
Random lasing from weakly scattering media; spectrum universality in DOO-PPV pol ymer films
M.E. Raikh, R.C. Polson and Z.V. Vardeny - *Physics Department, University of Utah*

MoP79
White light from blue: white emitting organic LEDs based on spin coated blends of blue emitting molecules.
M. Mazzeo, J. Thompson, R. I. R. Blyth, M. Anni, G. Gigli, R. Cingolani and G. Barbarella - *Dip. di Ingegneria dell'Innovazione, Universita' di Lecce*

MoP80
Measuring the potential distribution inside soft organic semiconductors with a scanning-tunneling microscope
M. Kemerink, P. Offermans, J.K.J. van Duren, R.A.J. Janssen, P.M. Koenraad, H.W.M. Salemink and J.H. Wolter - *Physics Department, Eindhoven University of Technology*

MoP81
Selfabsorption effects in a LEC with low Stokes shift
F.P. Wenzl, P.Pachler, D.Somitsch, P.Knoll, U.Scherf, C.Schmitt, R.Güntner and G.Leising - *TU Graz*

MoP82
Device characterization of conjugated Polymer/Fullerene bulk hetero-junction solar cells
G. Matt, T. Muters, T. Fromherz, D. Vanderzande, N. S. Saricifci and C. J. Brabec - *Linz Institute for Organic Solar Cells (LIOS), Johannes Kepler Univ.*

MoP83
Superlattice model to describe inter-molecular wavefunction overlap in polydiacetylene crystalline films
H. Munekata and T. Kondo - *Imaging Science and Engineering Laboratory, Tokyo Institute of Technology*

MoP84
Organic-template induced structural phase transition of GeS_2 and $GeSe_2$ in organic-inorganic hybrid superstructures
P.J. Klar, L. Chen, M. Güngerich, W. Heimbrodt, N. Oberender, D. Kempe and M. Fröba - *Department of Physics and Materials Science Center, Philipps-University of Marburg*

MoP85
Epitaxial growth of para-sexiphenyl films on mica characterised with X-ray diffraction pole figure technique
Harald Plank, Roland Resel, Jozef Keckes, Andrei Andreev, Helmut Sitter, Sabine Purger, Annette Thierry and Bernard Lotz - *Institute of Solid State Physics, Graz University of Technology*

MoP87
Topology effects on local electronic properties and on the conductance of molecular structures
A. Latge, D. C. Marcucci and M. V. Tovar Costa - *Instituto de Fisica, Univerdidad Federal Fluminense*

Poster Presentations II — *Tuesday 17:30 – 19:30*

AII GaN based structures

TuP1
Characterization of intrinsic and doped GaN layers and nanocolumns
J. Sánchez-Páramo, J.M. Calleja, E. Calleja, M.A. Sánchez-García and U. Jahn - *Materials Physics Department, Science Faculty , UAM (Universidad Autónoma de Madrid)*

TuP2
Evidence for type I band alignment in GaNAs/GaAs quantum structures from optical spectroscopies
I.A.Buyanova, G.Pozina, P.N.Hai, W.M.Chen, H.P.Xin and C.W.Tu - *Department of Physics and Measurement Technology, Linkoping University*

TuP3
N incorporation in GaInNAs materials grown by MBE
W. Li, M. Pessa, J. Likonen, J. Riikonen, J. Toivonen and H. Lipsanen - *Optoelectronics Reaserch Center, Tampere University of Technology*

TuP4
The effective mass and conduction band states of GaAsN/GaAs quantum wells.
C. Skierbiszewski, S. P. Lepkowski, P. Perlin, T. Suski and W. Jantsch - *High Pressure Research Center, Polish Academy of Sciences*

TuP5
Effect of hydrogen on the electronic properties of $In_xGa_{1-x}As_{1-y}N_y$
M. Bissiri, V. Gaspari, A. Polimeni, G. Baldassarri H. v. H., F. Ranalli, N. Nucara, M. Geddo, M. Capizzi, M. Fischer and M. Reinhardt - *Department of Physics, University of Rome "La Sapienza"*

TuP6
Phase separation and gap bowing in zinc-blende InGaN, InAlN, BGaN, and BAlN alloy layers
L. M. R. Scolfaro, J. R. Leite, L. K. Teles, J. Furthmüller, F. Bechstedt, T. Frey, D. J. As and K. Lischka - *Instituto de Fisica - Universidade de São Paulo, DFMM*

TuP7
Quantum dot photoluminescence from cubic GaN/InGaN/GaN heterostructures
K. Lischka, O. Husberg, A. Khartchenko, D.J. As, O.C. Noriega, A. Tabata, L.M.R. Scolfaro and J.R. Leite - *University of Paderborn*

TuP8
The effects of adjacent dislocations on the electronic and optical properties of GaN/AlN quantum dots
A.D. Andreev, J.R. Downes and E. P. O'Reilly - *Physics Department, University of Surrey*

TuP9
AlN/GaN Short-Period Superlattices with Monolayer AlN for Optical-Device Applications
A. Ishida, M. Kitano, T. Ose, H. Nagasawa, K. Ishino, Y. Inoue and H. Fujiyasu - *Department of Electrical and Electronic Engineering, Shizuoka University*

TuP10
Gain Characteristics of Ideal Dilute Nitride Quantum Well Lasers
S. Tomic and E.P. O'Reilly - *Department of Physics, University of Surrey*

TuP11
Strong graded interface related piezoelectric polarization weakening effects on exciton confinement in single $In_xGa_{1-x}N$/GaN quantum wells
Ewerton Wagner Santos Caetano, Valder Nogueira Freire and Gil de Aquino Farias - *Departamento de Física, Universidade Federal do Ceará*

TuP12
Gate voltage dependence of subband structure in a two-dimensional electron gas in AlGaN/GaN heterostructures
K.Tsubaki, N.Maeda, T. Saitoh, T.Nishida and N.Kobayashi - *NTT Basic Research Labs*

BII Quantum Communication and Computing

TuP13
Quantum gates using tunneling electron spins of a quantum-dot-chain
S. Muto, H. Sasakura, S. Adachi, Y. Kajiwara and K. Shiramine - *Applied Physics Department, Hokkaido University*

TuP14
Quantum Information Processing with Semiconductor Macroatoms
Irene D'Amico, Eliana Biolatti, Ehoud Pazy, Paolo Zanardi and Fausto Rossi - *Institute for Scientific Interchange (ISI)*

TuP15
Intrinsic dipole-dipole excitonic coupling in GaN quantum dots:application to quantum information processing
S.De Rinaldis, R.Rinaldi, R.Cingolani, I.D'Amico, E.Biolatti and F.Rossi - *INFM-Dipartimento di Ingegneria dell'Innovazione, ISUFI-Istituto Superiore Universitario per la Formazione Interdisciplinare,Universita' di Lecce*

TuP16
Designing heterostructures with predefined value of light-hole g factor for coherent solid-state quantum receiver
A. A. Kiselev, K. W. Kim and E. Yablonovitch - *Department of Electrical and Computer Engineering, North Carolina State University*

CII Cavities, Microcavities and Photonics

TuP18
Colloidally Synthesized Photonic Crystals Impregnated with Semiconductor Nanocrystals
Nikolai Gaponik, Andrei Susha, Alexander Eychmüller and Andrey Rogach - *Institute of Physical Chemistry, University of Hamburg*

TuP19
Above-room-temperature operation of IV-VI microcavitiy lasers
T. Schwarzl, W. Heiss, G. Springholz, K. Biermann, K. Reimann - *Insitut für Halbleiter- und Festkörperphysik, Universität Linz*

TuP20
Branching ratio of an incident light at the multi-branch region of photonic bands
T. Minami and K. Cho - *Graduate School of Engineering Science, Osaka University*

TuP21
Finite size effects on superlattice phonons studied by coupled microcavity enhanced Raman scattering
M. Trigo, R. G. Pregliasco, A. Fainstein, B. Jusserand and V. Thierry-Mieg - *Centro Atomico Bariloche (CNEA)*

TuP22
Modified spontaneous emission properties of CdS quantum dots embedded in novel three-dimensional microcavities
H. Kumano, A. Ueta and I. Suemune - *Research Institute for Electronic Science, Hokkaido University, Japan*

TuP23
Dressing the electronic states of quantum dots in pillar microcavities
G. Panzarini, L.C. Andreani, U. Hohenester and E. Molinari - *dip.to di Fisica, universita' di Modena e Reggio Emilia*

TuP24
Formation of air-bridge type two-dimensional photonic crystals having air hole array grown by selective area metal-organic vapor phase epitaxy
M. Akabori, J. Motohisa and T. Fukui - *RCIQE, Hokkaido University*

TuP25
Photoreflectance and photoluminescence characterisation of InGaAs/AlAsSb quantum wells grown by molecular beam epitaxy
T. Mozume and N. Georgiev - *FESTA Laboratories, Femtosecond Technology Research Association,*

TuP26
Room temperature lasing of quantum wire VCSELs by optical pumping grown on the (775)B GaAs substrates by MBE
Y. Ohno, H. Kanamori, S. Shimomura and S. Hiyamizu - *Department of Physics, Graduate School of Engineering Science, Osaka University*

TuP27
Organic microcavities based on thermally evaporated TeOx-LiF Dielectric Mirrors
M. Anni , G. Gigli, S. Patanè, A. Arena, M. Allegrini and R. Cingolani - *Istituto Nazionale di Fisica della Materia (INFM), Dipartimento di Ingegneria dell'Innovazione, Università degli Studi di Lecce*

TuP28
Parametric polariton oscillation: Temperature dependence and Non-linear polarization properties
A. I. Tartakovskii, D. N. Krizhanovskii, V. D. Kulakovskii, M. S. Skolnick and J. S. Roberts - *Department of Physics & Astronomy, University of Sheffield*

TuP29
Impact of exciton localisation on cavity polaritons
V. D. Kulakovskii, A. I. Tartakovskii, D. N. Krizhanovskii, M. S. Skolnick and J. S. Roberts - *Department of Physics & Astronomy, University of Sheffield*

TuP30
Manifestations of quantum chaos in spectra of 2D photonic crystals
L. Gumen, J. Arriaga and A. Krokhin - *Instituto de Fisica, Universidad Autonoma de Puebla*

TuP31
Radiative width of collective modes in a resonant Bragg reflector:the validity limit of super-radiant mode
T.Ikawa and K.Cho - *Department of Material Physics, Graduate School of Engineering Science, Osaka University*

TuP32
Coupling of GaAs/AlGaAs quantum well photoluminescence to metal surface plasmons excited by grating couplers
N. Sawaki, T. Ohashi and M. Yamaguchi - *Department of Electronics, Nagoya University*

TuP33
Time-resolved imaging by using micro-PL measurement and sum frequency mixing
Y. Nagamune and M. Ogura - *Electrotechnical Laboratory, Tsukuba-shi, Ibaraki*

TuP34
Intersubband plasmon polaritons in MQW structures and their manifestation in TIR spectra
M. Zaluzny and W. Zietkowski - *Instituute of Physics, M. Curie Sklodowska, University, Lublin*

DII Tunneling and Carrier Dynamics

TuP35
Miniband magneto-transport in GaAs-AlAs island superlattices
A. Patane', A. Ignatov, E. Schomburg, L. Eaves, A. Levin, R. Scheuerer, P.C. Main, K. F. Renk, V. M. Ustinov and A. E. Zhukov - *School of Physics and Astronomy, University of Nottingham,*

TuP36
Ultra Fast Decay of Enhanced Degenerate Four Wave Mixing of Multiple GaAs Thin Layers
H. Ishihara - *Department of Physical Science, Graduate School of Engineering Science, Osaka University*

TuP37
Investigation of intersubband relaxation dynamics by pump-probe spectroscopy and application to ultrafast all-optical modulation scheme
Takashi Asano, Shin Yoshizawa and Susumu Noda - *Dept. of Electron. Sci. & Eng., Kyoto Univ.*

TuP39
Temperature-induced breakdown of stationary electric field domains in superlattices
David Sanchez, Luis L. Bonilla and Gloria Platero - *Departamento de Teoria de la Materia Condensada, Instituto de Ciencia de Materiales de Madrid (CSIC).*

TuP40
High field electron transport in GaAs/$Al_xGa_{1-x}As$ p-i-n-i-p-structures investigated by ultrafast absorption changes
H. Lutz, A. Schwanhäußer, M. Eckardt, G. Döhler, L. Robledo and A. Seilmeier - *Experimentalphysik 3, Universität Bayreuth*

TuP41
Intensity-independent, highly polarization- or wavelength sensitive opto-electronic switches
P. Kiesel, M. Müller, T. Kippenberg, J. Spieler, S. Malzer and G.H. Döhler - *Uni Erlangen, Institute for Technical Physics*

TuP42
Resonant-tunneling effect in a periodically modulated electrical field
S.A.Vitusevich, A.Förster, A.E.Belyaev, D.I.Sheka, H.Lüth, N.Klein, S.V.Danylyuk and R.V.Konakova - *Institut für Schichten und Grenzflächen (ISG), Forschungszentrum Jülich*

TuP43
Spontaneous Spin Splitting Observed in Resonant Tunneling Diode with a Narrow Band Gap Asymmetric Quantum Well
T. Kikutani, S. Gozu, Y. Sato and S. Yamada - *Center for New Materials, Japan Advanced Institute of Science and Technology (JAIST)*

TuP44
Nano-scale Schottky contacts: Ultrafast drift-diffusion dynamics studied in the optical near-field
M. Achermann, U. Siegner, L.-E. Wernersson and U. Keller - *ETH Zurich*

EII Quantum Dots, Quantum Wires I: Growth, Optical Properties

TuP45
Two modes of Ga diffusion into InAs self-assembled quantum dots suggested by ion channeling
N. Matsumura, T. Haga, S. Muto, Y. Nakata and N. Yokoyama - *Department of Applied Physics, Hokkaido University*

TuP46
Monte Carlo Simulation of Self-Organized Quantum Dot Structures: Crossover from Kinetics to Thermodynamics
R. Kunert, M. Meixner, E. Schöll, V. A. Shchukin and D. Bimberg - *Institut fût Theoretische Physik, Technische Universität Berlin*

TuP47
Density and size control of self-assembled InAs quantum dots
I. Kamiya, Ichiro Tanaka and H. Sakaki - *Systems Engineering, Wakayama University*

TuP48
InGaAs islands formed on shallow patterned GaAs (100) substrates by molecular-beam epitaxy
Q. Gong, R. Noetzel, H.-P. Schoenherr and K. H. Ploog - *COBRA Inter-University Research Institute, Eindhoven Univeristy of Technology*

TuP49
Formation of GaSb/GaAs Quantum Dots in MOCVD growth
L. Müller-Kirsch, R. Heitz, U. W. Pohl, I. Häusler, H. Kirmse, W. Neumann and D. Bimberg - *Institut für Festkörperphysik, Technische Universität Berlin,*

TuP50
Photoconductive response of InAs/GaAs quantum dot stacks
S. Hofer, H. Hirner, R. Bratschitsch, G. Strasser and K. Unterrainer - *Institut für Festkörperelektronik, Technische Universität Wien*

TuP51
Piezoelectric effects in ultrahigh quality AlGaAs/GaAs single quantum wire
X-Q Liu, X.-L Wang, M. Ogura, T. Guillet, V. Voliotis and R. Grousson - *Electron Devices Division, Electrotechnical Laboratory, Japan*

TuP52
Raman study of self-assembled InAs quantum dots embedded in AlAs: influence of growth temperature
D. A. Tenne, A. K. Bakarov, A. I. Toropov and D. R. T. Zahn - *Department of Physics, The Pennsylvania State University*

TuP53
Transition from spatially indirect to direct recombination in stacked layers of self-assembled InP quantum dots
J. Maes, M. Hayne, Y. M. Manz, O. G. Schmidt, K. Eberl and V. V. Moshchalkov - *Laboratorium voor Vaste-Stoffysica en Magnetisme, Katholieke Universiteit Leuven*

TuP54
Electronic struckture of Self-Assembled InAs Quantum Dots
C. Bock, K. H. Schmidt, U. Kunze, V. V. Khorenko, S. Malzer and G. Döhler - *Ruhr-Universität Bochum*

TuP55
Photoluminescence of quasi-zero-dimensional InGaAsP quantum dots
K.Ozasa and Y.Aoyagi - *Semiconductors lab., RIKEN*

TuP56
Band Offset of InAs Self-assembled Dots on GaAs
D. Rakoczy, G. Strasser and J. Smoliner - *Institut für Festkörperelektronik, TU-Wien*

TuP57
Tailoring and controlling electron-hole states in single and coupled semiconductor quantum dots
Ulrich Hohenester, Filippo Troiani and Elisa Molinari - *Institut fuer Theoretische Physik, Karl-Franzens-Universitaet Graz*

TuP58
Exchange coupling and polarization relaxation in self-assembled quantum dots
R. Ferreira - *Laboratoire de Physique de la Matiere Condensee - ENS*

TuP59
Spatial and dynamic effects on the capacitance of self-organized semiconductor quantum dot structures
R. Wetzler, A. Rack, A. Wacker, E. Schöll, C.M.A. Kapteyn, R. Heitz and D. Bimberg - *Institut für Theoretische Physik, Technische Universität Berlin*

TuP60
Polarization of the interband optical dipole in InAs/GaAs self-organized quantum dots
S. Cortez, O. Krebs, P. Voisin and J-M. Gérard - *Laboratoire de Physique de la Matière Condensée de l'Ecole Normale Supérieure*

TuP61
Photoconductive spectra in InAs/InAlAs/InP quantum dot structures
S.E. Schacham, G. Bahir, E. Finkman, W. Sheng, J.P. Leburton -- *Dept. of Electrical Engineering, Technion, Israel*

TuP62
Manipulating single quantum dot states in a lateral electric field
J. Seufert, M. Obert, M. Rambach, G. Bacher, N. A. Gippius, A. Forchel, T. Passow, K. Leonardi and D. Hommel - *Technische Physik, Universität Würzburg*

TuP63
Photoluminescence linewidth narrowing of InAs/GaAs self-assembled quantum dots
S. Kiravittaya, Y. Nakamura and O. G. Schmidt - *Max-Planck-Institut fuer Festkoerperforschung*

TuP64
Polarization anisotropy of photoluminescence from multilayer InAs/GaAs quantum dots
J. Humlicek, D. Munzar, K. Navratil, M. Lorenc, J. Oswald, J. Pangrac and E. Hulicius - *Institute of Condensed Matter Physics, Masaryk University Brno*

TuP65
Tuned exciton kinetics in self-organized InGaAs/GaAs quantum dots
H. Born, R. Heitz, A. Hoffmann and D. Bimberg - *Institut für Festkörperphysik, Technische Universität Berlin*

TuP66
Electronic properties of InAs/GaAs quantum dot stacks
A. Schliwa, O. Stier, R. Heitz, M. Grundmann and D. Bimberg - *Institut f. Festkörperphysik, TU Berlin*

TuP67
Electron and hole localization in coupled InP/InGaP self-assembled quantum dots
M. Tadic, F. M. Peeters, B. Partoens and K. Janssens - *Departement Natuurkunde, Universiteit Antwerpen*

TuP68
Coherent propagation in multistacked layers of quantum dots
Giovanna Panzarini, Ulrich Hohenester and Elisa Molinari - *Dip. di Fisica, Universita' di Modena e Reggio Emilia*

TuP69
Tunable Mid-IR Emission using a Novel Quantum Dot-Quantum Well Coupled System
R. A. Child, R. J. Nicholas, N. J. Mason and E. Alphandery - *Clarendon Laboratory, Department of Physics, University of Oxford*

TuP70
Pauli-blocking absorption experiments on self-assembled quantum dots
F. Bickel, D. Haft, R. J. Warburton, K. Karrai, W. Schoenfeld, J. M. Garcia and P. M. Petroff - *Center for NanoScience and Sektion Physik, Ludwig-Maximilians-Universität München*

TuP71
Photocurrent spectroscopy of modulation doped InAs self-assembled quantum dots
P. Hawrylak, M. Korkusinski, J. Kyriakidis, H.C. Liu, R. Dudek, S. Fafard and Z. Wasilewski - *Institute for Microstructural Sciences, National Research Council of Canada*

TuP72
Time-resolved photoluminescence near Fermi level in a field-induced quantum dot lattice
K. Hammura, S. Nomura and Y. Aoyagi - *RIKEN, Saitama, Japan*

TuP73
Interdot Energy Transfer in a System of Coupled InAs/GaAs Quantum Dots
Yu. I. Mazur, J. W. Tomm, G. G. Tarasov, H. Kissel, C. Walther, Z. Ya. Zhuchenko and W. T. Masselink - *Humboldt university Berlin, Department of Physics, FET*

TuP74
Size-Selective Optically Excited Capacitance Transient Spectroscopy of InAs/GaAs Quantum Dots
C. M. A. Kapteyn, J. Ehehalt, R. Heitz, D. Bimberg, G. E. Cirlin, V. M. Ustinov and N. N. Ledentsov - *Institut für Festkörperphysik, PN 5-2, Technische Universität Berlin*

TuP75
Observation of dip structures in PLE spectra of a highly excited single self-assembled quantum dot
S. Kako, T. Sugimoto, Y. Toda, S. Ishida, M. Nishioka and Y. Arakawa - *Research Center for Advanced Science and Technology, University of Tokyo*

TuP76
Very large subband separation in GaAs/AlGaAs V-groove quantum wires
T. Otterburg, F. Lelarge, D.Y. Oberli, A. Rudra and E. Kapon - *Swiss Federal Institute of Technology Lausanne (EPFL),*

TuP77
Growth of InGaAs Ridge Quantum Wires and Dots for Quantum LSIs by Atomic Hydrogen-Assisted Selective MBE Growth on InP Substrates
Tsutomu Muranaka, Seiya Kasai, Chao Jiang and Hideki Hasegawa - *Reseach Center for Interface Quantum Electronics, Hokkaido University*

TuP78
Carrier Recombination Processes in Disordered Quantum Wire Superlattice
A. Sasaki, R. Okanishi, X. Q. Liu, X. L. Wang and M. Ogura - *Dpt. of Electronics, Osaka Electro-Communication Univ.*

TuP79
High peak-to-valley ratio in resonant tunnelling through stacked InAs quantum dots
T. Bryllert, M. Borgstrom, T. Sass, B. Gustafson, L-E. Wernersson, W. Seifert and L. Samuelson - *Lund University, Solid State Physics*

TuP80
Influence of the size of self-assembled InAs/AlAs quantum dots on photoluminescence and resonant tunneling
K. Pierz, Z. Ma, I. Hapke-Wurst, U. F. Keyser, U. Zeitler and R. J. Haug - *Physikalisch-Technische Bundesanstalt, Braunschweig*

TuP81
Resonant tunneling through a single self-assembled InAs quantum dots in a micro-RTD structure
I. Kamiya, I. Tanaka, K. Tanaka and H. Sakaki - *Non-Equilibrium Laboratory, Mitsubishi Chemical Corporation*

TuP82
Anomalous diamagnetic shift of excitons in II-VI quantum dots and in indirect short period supperlattices
N. Miura, T. Yasuhira, K. Uchida, E. Kurtz, C. Klingshirn, H. Nakashima, F. Issiki and Y. Shiraki - *Institute for Solid State Physics, University of Tokyo*

TuP83
Interplay of surface charges and excitons localized in CdSe/ZnSe quantum dots
V. Türck, S. Rodt, R. Heitz, O. Stier, M. Straßburg, U. W. Pohl and D. Bimberg - *Institut für Festkörperphysik, Technische Universität Berlin*

TuP84
Excitons, biexcitons and charged excitons in CdTe single quantum dots
L. Besombes, K. Kheng, L. Marsal and H. Mariette - *Département de Recherche Fondamentale sur la Matière Condensée / SP2M, CEA Grenoble*

Poster Presentations III — *Thursday 16:00 – 18:00*

AIII Quantum Dots and Wires II

ThP1
Growth simulation of GaAs/AlGaAs quantum dot grown in tetrahedral-shaped recesses on GaAs (111)B substrate
T.Tsujikawa, M.Ogura and H.Yaguchi - *Osaka National Research Institute, AIST*

ThP2
State-filling and renormalization in charged InGaAs/GaAs quantum dots
R. Heitz, F. Guffarth, C. M. A. Kapteyn, F. Heinrichsdorff and D. Bimberg - *Institut für Festkörperphysik, TU Berlin*

ThP3
A combined investigation of lateral and vertical Stark effect in InAs self-assembled quantum dots in waveguide structures
O. Wolst, M. Schardt, S. Malzer and G. H. Döhler - *Uni Erlangen, Institute for technical Physics*

ThP4
Optical properties of wetting layers in stacked InAs/GaAs quantum dot structures: strain effects and electronic coupling
Q.T. Winzer, R. Goldhahn, G. Gobsch, H. Heidemeyer, O.G. Schmidt, K. Eberl - *Institut für Physik, TU Ilmenau, Germany*

ThP5
Level bleaching in a single quantum dot observed by photocurrent-spectroscopy
Evelin Beham, Artur Zrenner, Frank Findeis, Martin Baier, Max Bichler and Gerhard Abstreiter - *Walter Schottky Institut, Technische Universität München*

ThP6
Determination of Binding Energies of Electron and Hole Bound States in Self-Assembled InAs Quantum Dots
S. Fujimoto, S. -W. Lee, K. Hirotani and K. Hirakawa - *Institute of Industrial Science, University of Tokyo*

ThP7
Electronic structure of quantum-dot molecules and solids
G.W. Bryant, W. Jaskolski – *National Institute of Standards and Technology, Gaithersburg*

ThP8
Binding energies of excitonic complexes in square and T-shaped quantum wires
Takuma Tsuchiya - *Japan Advanced Institute of Science and Technology (JAIST)*

ThP9
Excitons in quantum ring structures in a magnetic field: Persistent currents
A. O. Govorov, A. V. Kalameitsev, R. J. Warburton and K. Karrai - *Ohio University, Department of Physics and Astronomy*

ThP10
STM-induced luminescence of individual InGaAs quantum dots: evidence for charged excitons
T. K. Johal, G. Pagliara, R. Rinaldi, M. Lomascolo, A. Passaseo and R. Cingolani - *INFM-Unita di Lecce, Department of Innovative Engineering, Universityof Lecce*

ThP11
A quantum dot infrared photodetector with lateral carrier transport
L. Chu, A. Zrenner, D. Bougeard, M. Bichler and G. Abstreiter - *Walter-Schottky-Institut, Technische Universität München*

ThP12
Quantum dot micro-LEDs for the study of single-dot electro-luminescence, fabricated by focused ion beam
M.Vitzethum, R. Schmidt, P. Kiesel, P. Schafmeister, D. Reuter, J. Koch, A.D. Wieck and G.H. Döhler *Institut für Technische Physik I, Universität Erlangen-Nürnberg*

ThP13
Lifetime of Photoexcited Carriers in Modulation-Doped Quantum Dot Infrared Photodetectors
S. -W. Lee and K. Hirakawa - *IIS, University of Tokyo*

ThP14
Theoretical analysis of electron transport in quantum dot structures
V. Ryzhii, I. Khmyrova, M. Willander and V. Mitin - *Computer Solid State Physics Laboratroy, University of Aizu*

ThP15
Spin-Dependent Single-Hole Tunneling in Self-Assembled Silicon Quantum Rings
N.T. Bagraev, A.D. Bouravleuv, W. Gehlhoff, V.K. Ivanov, L.E. Klyachkin, A.M. Malyarenko, S.A. Rykov and I.A. Shelykh - *A.F.Ioffe Physico-Technical Institute, St. Petersburg*

ThP16
Surface morphology evolution of 1.3 μm wavelength $In_{0.5}Ga_{0.5}As$/GaAs island structures grown by molecular beam epitaxy
Z.C. Niu, X.D. Wang, Z.H. Miao and S.L. Feng - *Inst. of Semiconductors, Beijing*

ThP17
Polaron couplings in quantum dot molecules
O. Verzelen, R. Ferreira and G. Bastard - *Laboratoire de Physique de la Matiere Condensee ENS*

ThP19
On the spin injection in ZnMnSe/ZnCdSe heterostructures
I.A. Buyanova, W.M. Chen, B. Monemar, A.A. Toropov, Y. Terent'ev, S.V. Sorokin, A.V. Lebedev, S.V. Ivanov and P.S. Kop'ev - *Dept of Physics and Measurement Technology, Linkoping University*

BIII Spintronics and Magnetic Heterostructures

ThP20
Rashba spin-splitting energies probed by anti-weak-localization analyses in symmetric and asymmetric InAlAs/InGaAs/InAlAs quantum wells
T. Koga, J. Nitta, T. Akazaki and H. Takayanagi - *NTT Basic Research Laboratories*

ThP21
Correlation between exciton-decay and localization in digital magnetic heterostructures
W. Heiss, G. Prechtl, S. Mackowski and E. Janik - *Abteilung für Festkörperphysik, Universität Linz*

ThP22
Micro-luminescence study of hybrid ferromagnet/diluted magnetic semiconductor quantum structures
G. Cywinski, M. Czeczott, J. Wrobel, K. Fronc, S. Mackowski, T. Wojtowicz and J. Kossut - *Institute of Physics, PAN, Warsaw*

ThP23
Model for ballistic spin-transport in ferromagnet/2-dimensional electron gas/ferromagnet structures
Th. Schäpers, J. Nitta, H. B. Heersche and H. Takayanagi - *Institut fuer Schichten und Grenzflaechen (ISG-1), Forschungszentrum Juelich*

ThP24
Exchange interactions in CdMnTe/CdMgTe quantum wells under high magnetic fields and high pressure
T. Yasuhira, K. Uchida, Y. H. Matsuda, N. Miura, S. Kuroda and K. Takita - *Institute for Solid State Physics, University of Tokyo*

ThP25
Effective spin diffusion across hugely lattice mismatched heterointerfaces
M. Ghali, J. Kossut, E. Janik, K. Reginski, L. Klopotowski, S. Mackowski, G. Cywinski and P. Dluzewski - *SL3.1, Institute of Physics, PAS, Warsaw*

ThP27
Correlation of magnetism and doping in the magnetic semiconductor (Ga,Mn)As with Mn(Ga)As clusters
Th. Hartmann, M. Lampalzer, P.J. Klar, K. Volz, W. Stolz, W. Heimbrodt, H.-A. Krug von Nidda and A. Loidl - *Department of Physics and Materials Science Centre, Philipps University of Marburg*

ThP28
Spin interference and Fabry-Pérot resonances in ferromagnet-semiconductor-ferromagnet devices
T. Matsuyama, C.-M. Hu, D. Grundler, G. Meier, D. Heitmann and U. Merkt - *Institut für Angewandte Physik, und Zentrum für Mikrostrukturforschung, Universität Hamburg*

ThP29
Molecular beam epitaxy of CdMnSe on InAs: a new material system for spin injection
G. Richter, P. Grabs, R. Fiederling, P. Bach, G. Schmidt, L. W. Molenkamp, W. Weigand, T. Gleim, C. Heske and E. Umbach - *Physikalisches Institut (EP3), Universität Würzburg*

ThP30
Growth characteristics and magnetic properties of MnAs/AlAs/MnAs trilayer heterostructures grown on vicinal GaAs(111)B substrates
S. Sugahara and M. Tanaka - *Dept. of Electronic Engineering, The University of Tokyo*

ThP31
Micro-Raman scattering study of $Ga_{1-x}Mn_xAs$
W. Limmer, M. Glunk, W. Schoch, A. Köder, R. Kling, R. Sauer and A. Waag - *Abteilung Halbleiterphysik, Universität Ulm,*

ThP32
Epitaxy and characterization of GaMn(N)As for spin electronics
A. Waag, A. Köder, R. Kling, W. Schoch, W. Limmer and R. Sauer - *Abteilung Halbleiterphysik, Universität Ulm*

ThP33
Scaling of ferromagnet/semiconductor contacts for the study of spin-dependent collection
A. Bournel, P. Dollfus and P. Hesto - *Institut d'Electronique Fondamentale, UMR CNRS 8622*

ThP34
Magneto-Optical Properties of GaAs Based Semiconductor Magneto Photonic Crystals
H. Shimizu and M. Tanaka - *M. Tanaka Lab., Dept. of Electronic Engineering, The Univ. of Tokyo*

ThP35
T-shaped ballistic structure with adjustable spin-orbit effect: Spin filtering and directional multiplexing
A. A. Kiselev and K. W. Kim - *Department of Electrical and Computer Engineering, North Carolina State University*

ThP36
Conversion of spin into directed electric current in quantum wells
S. D. Ganichev, E. L. Ivchenko, S. N. Danilov, W. Wegscheider, D. Weiss, J. Eroms and W. Prettl - *Institut für Experimentelle und Angewandte Physik, Universität Regensburg*

ThP37
Spin-orbit interaction in an InAlAs/InAs heterostructure
Kanji Yoh, S.Abe, T. Doi, Y. Katano, H. Ohno, K. Sueoka and K. Mukasa - *RCIQE, Hokkaido University*

ThP38
Microstructure and electronic characterization of self-assembled ErAs nanoparticles in InGaAs
M. Hanson, D.C. Driscoll, C. Gallinat and A.C. Gossard - *Materials Department, University of California at Santa Barbara*

ThP39
Spin polarization spectra of strained superlattices
A. D. Andreev and A. V. Subashiev - *Experimental Physics Department , St.-Petersburg State Technical University*

CIII Device Structures

ThP40
The performance of hybrid-molecular devices with current CMOS technology as a reference point
R. Stadler and M. Forshaw - *Department of Physics and Astronomy, University College London*

ThP41
High Thermoelectric Figure of Merit ZT in PbTe and Bi_2Te_3 Based Superlattice Structures Reducing the Thermal Conductivity
H. Beyer, J. Nurnus, H. Böttner, A. Lambrecht, E. Wagner and G. Bauer - *Fraunhofer Institut Physikalische Messtechnik, Freiburg*

ThP42
Electron-phonon coupling in n++SOI film probed using Si-Al NIS junctions
M. Prunnila, J. Ahopelto, A. Savin, P. Kivinen, J. Pekola and A. Manninen - *VTT Microelectronics Centre, ESPOO, Finland*

ThP43
Investigation of Self-Aligned p++-GaAs/n-InGaP Hetero-Junction Field-Effect Transistors
W.-S. Lour, M.-K. Tsai, K.-C. Chen, S.-W. Tan, Y.-W. Wu and Y.-J. Yang - *Department of Electrical Engineering, National Taiwan-Ocean Univ.*

ThP44
Fabrication of two dimensional in-plane gate transistors by active focussed ion beam doping
D. Reuter, C. Meier, A. Seekamp and A. D. Wieck - *Lehrstuhl für Angewandte Festkörperphysik, Ruhr-Universität Bochum*

ThP45
Novel Electrical Properties of Three-Terminal Ballistic Junctions and Demonstration of Their Applications in Nanoelectronics
H. Q. Xu, I. Shorubalko, I. Maximov, D. Nilsson, W. Seifert, P. Omling and L. Samuelson - *Solid State Physics, Lund University*

ThP46
Double-dot-like charge transport through a small size silicon single electron transistor
B. H. Choi, Y. S. Yu, S. H. Son, S. W. Hwang, D. Ahn, D. H. Kim and B. G. Park - *School of Electrical Engineering, Korea University, Seoul*

ThP47
The Fully Quantized Transistor
B. Gustafson, D. Csontos, L.-E. Wernersson, M. Suhara, H.Q. Xu and L. Samuelson - *Div. of Solid State Physics, Lund University*

ThP48
Switching characteristics and demonstration of logic functions in modulation doped GaAs/AlGaAs nanoelectronic devices
L. Worschech, S. Reitzenstein, F. Fischer, M. Keßelring and A. Forchel - *Wuerzburg University*

ThP49
The Transient Signal Response of Deep Submicron $Si/Si_{0.77}Ge_{0.23}$ MODFETs
A. Yangthaisong, G.C. Crow and R.A. Abram - *Department of Physics, University of Durham*

ThP50
First principles calculations of the dark current in QWIPs
N. E. I. Etteh and P. Harrison - *School of Electronic and Electrical Engineering, University of Leeds*

ThP51
Effect of doping profile on the potential performance of buried channel SiGeC/Si heterostructure MOS devices
E. Cassan, P. Dollfus and S. Galdin - *IEF - UMR CNRS 8622*

ThP52
Multilevel logic element based on the long period GaAs/AlGaAs superlattice.
Yu.A.Mityagin, Yu.A.Efimov, V.N.Murzin and A.A.Pishchulin - *Lebedev Physical Institute, Moscow*

DIII Intersubband, THz Spectroscopy, QW and QC-lasers

ThP54
Photoluminescence study of GaAs/AlGaAs micro-tube with uniaxially strained quantum wells
K. Kubota, P. Vaccaro, N. Ohtani, Y. Hirose, M. Hosoda and T. Aida - *ATR Adaptive Communications Research Laboratories, Kyoto*

ThP55
Quantum-confined impurities as single-electron quantum dots: Free-electron laser studies and application to Terahertz emitters
M. P. Halsall, P. Harrison, J.-P. R. Wells and I. V. Bradley - *School of Electronic and Electrical Engineering, University of Leeds*

ThP56
Theoretical Analysis of THz photon-assisted tunneling and optical gain in resonant tunneling diodes
M.Asada and N.Sashinaka - *Dept. Electrical and Electronic Eng., Tokyo Institute of Technology*

ThP57
Intersubband relaxation dynamics in semiconductor quantum structures
R. Bratschitsch, T. Müller, G. Strasser and K. Unterrainer - *Institut für Festkörperelektronik, Technische Universität Wien*

ThP58
Localized and resonant acceptor states in strained $Ge/Ge_{1-x}Si_x$ multiple quantum well heterostructures
V.Ya.Aleshkin, V.I.Gavrilenko, I.V.Erofeeva, D.V.Kozlov and O.A.Kuznetsov - *Institute for Physics of Microstructures of Russian Academy of Sciences*

ThP59
Stimulated emission of teraherz acoustic phonons as a result of action of nonequilibrium phonon flux upon the localized exciton ensemble
E. E. Onishchenko, V. S. Bagaev and V. V. Zaitsev - *P.N.Lebedev Physical Institute RAS, Moscow*

ThP60
Physics and Application of Terahertz Phase Modulation
R. Kersting, R. Bratschitsch, G. Strasser and K. Unterrainer - *Physics Department, Rensselaer Polytechnic Institute*

ThP61
InGaAs/InAlAs superlattice detector for THz radiation
E.Schomburg, M.Krätschmer, A.Vollnhals, F.Klappenberger, R.Scheuerer, K.F.Renk, V.Ustinov, A.Zhukov and A.Kovsh - *Institut für Angewandte Physik, Universität Regensburg*

ThP62
Stable and unstable homoepitaxy of GaAs at low substrate temperatures
G. Apostolopoulos, J. Herfort, N. Boukos, A. Travlos and K. H. Ploog - *Paul-Drude-Institut für Festkörperelektronik*

ThP63
Segregation effects on the optical properties of (InAs)/(GaSb) superlattices
R. Magri and A. Zunger - *Dipartimento di Fisica, Universita' di Modena e Reggio Emila,*

ThP64
Two-dimensional electron gas at $Ga_{0.5}In_{0.5}P/GaAs$ heterointerface spontaneously induced by ordering
K. Yamashita, T. Kita, Y. Wang, K. Murase, C. Geng, F. Scholz and H. Schweizer - *Department of Electrical and Electronics Engineering, Faculty of Engineering, Kobe Univeersity*

ThP65
Electron transport and optical properties of InGaAs QWs with quasi-periodic (L~30nm) interface corrugation grown on vicinal (111)B GaAs
T. Noda, Y. Nagamune, Y. Nakamura and H. Sakaki - *Institute of Industrial Science, University of Tokyo*

ThP66
Extremely flat growth-interrupted InAlAs surface grown on (411)A-oriented InP substrate
I. Watanabe, T. KItada, K. Kanzaki, D. Kawaura, M. Yamamoto, S. Shimomura and S. Hiyamizu - *Graduate School of Engineering Science, Osaka University*

ThP67
Direct experimental verification of the q-dependence of the electron-LO-phonon interaction
D. S. Kainth, M. N. Khalid and H. P. Hughes - *Department of Physics, University of Cambridge*

ThP68
Wavevector dispersion of excitations of the two-dimensional electron gas from light scattering using a grating coupler
C. Kristukat, A.R. Goñi, P. Grambow, K. Eberl and C. Thomsen - *Institut f. Festkoerperphysik, Technische Universitaet Berlin*

ThP69
Effect of an electric field on electronic excitations in double quantum well systems
U. Haboeck, A.R. Goñi, K. Eberl and C. Thomsen - *Institut f. Festkoerperphysik, Technische Universitaet Berlin*

ThP70
Linewidth broadening of excitonic luminescence from quantum wells in pulsed magnetic fields
A. Polimeni, A. Patané, R. K. Hayden, L. Eaves, M. Henini, P. C. Main, K. Uchida, N. Miura, D. Sherwood and M. Fromhold - *Department of Physics, University of Rome "La Sapienza"*

ThP71
Excitonic Instabilities in Semiconductor Superlattices
D. C. Marinescu and J. J. Quinn - *Department of Physics, Clemson University*

ThP72
The influence of intrersubband transitions on the resonant and extended electronic states in GaAs/AlGaAs asymmetric quantum wells
R. Beserman, M. Levy, D. Krapf, A. Sa'ar, V. Thierry-Mieg and R. Planel - *Solid State Institute and Physics Department, Technion, Israel Institute of Technology*

ThP73
Intersubband terahertz electro-luminescence from GaAs?AlGaAs quantum cascade structures
S S Dhillon, D D Arnone, A G Davies, E H Linfield, R Harrell and D A Ritchie - *Semiconductor Physics Group, Cavendish Laboratory*

ThP74
Resonant States and THz Lasing in SiGe Quantum Well Structures delta-doped with Boron
M.S. Kagan and I.N.Yassievich - *Ioffe Physico-Technical Institute, St.Petersburg*

ThP75
Mid infrared range injection laser, based on intersubband carrier transitions and resonant Auger processes in type II quantum wells
L.E. Vorobjev, V.L. Zerova, D.A. Firsov and G.G. Zegrya - *Ioffe Institute, St.Petersburg*

ThP76
Quantum transport calculations for quantum cascade laser structures
S.-C. Lee and A. Wacker - *Institut fuer Theoretische Physik, Technische Universitaet Berlin*

ThP77
Gain Optimization in Optically Pumped Unipolar Quantum Well Lasers
S. Tomic, V. Milanovic and Z. Ikonic - *Department of Physics, University of Surrey*

ThP78
Optical and electrical investigation of population properties for quantum cascade structures
L. Schrottke, R. Hey, H.-Y. Hao and H. T. Grahn - *Paul Drude Institute for Solid State Electronics*

ThP79
Capture and confinement of light and carriers in graded index quantum well laser structures
G. Aichmayr, H. P. van der Meulen, L. Vina, J. M. Calleja, F. Schaefer, J. P. Reithmaier and A. Forchel
Universidad Autonoma Madrid, Depto. Fisica de Materiales C-IV 506b

ORAL PRESENTATIONS

Optically detected single electron charging in a quantum dot

A. Zrenner[1], F. Findeis[1], M. Baier[1], M. Bichler[1], G. Abstreiter[1], U. Hohenester[2], and E. Molinari[2]

[1]Walter Schottky Institut, Technische Universität München, Am Coulombwall, D-85748 Garching, Germany
[2]Istituto Nazionale per la Fisica della Materia (INFM) and Dipartimento di Fisica Università di Modena e Reggio Emilia, Via Campi 213/A, 41100 Modena, Italy

Discrete numbers of electrons have been introduced in InGaAs self-assembled quantum dots by means of electric field tuneable diode structures. The optical excitations of such self-assembled artificial ions have been studied by magneto-photoluminescence spectroscopy. Optical access to single quantum dots has thereby been realised via electron-beam written shadow masks. Detailed spectroscopic studies have been performed as a function of bias voltage (electron number) and magnetic field under the condition of non-resonant optical excitation. In our experiments we have considered two structures with different tunneling interaction between quantum dot and n-doped electron reservoir.

In photoluminescence experiments we observe the fully resolved emissions of the neutral (X^0), single charged (X^{1-}) and double charged exciton (X^{2-}). The corresponding few particle interaction energies are directly obtained from our optical spectra and are compared to theoretical model calculations. Our experimental data are found in good agreement with the calculations for situations where the spatial extent of the hole wave functions is smaller as compared to the electron wave functions. The ratio of both is identified as the leading term which controls the magnitude of the X^{1-} binding energy.

The bias dependent switching behaviour between the X^0, X^{1-}, and X^{2-} PL lines is found to be dependent on the tunneling probability between quantum dot and n-doped electron reservoir. It can be explained in terms of carrier statistics in the optical excitation process and single electron tunneling.

The application of magnetic field to charged exciton complexes opens an interesting field of spin physics in quantum dots. At high magnetic fields one Zeeman component of the single charged exciton is found to be quenched, which is attributed to the competing effects of tunneling and spin-flip processes for p-shell electrons. The observation of spin dependent tunneling from singlet and triplet states nicely demonstrates that spin related phenomena can be considerably enhanced in quantum dots.

Corresponding author: Artur Zrenner, Walter Schottky Institut, Technische Universität München, Am Coulombwall, D-85748 Garching, Germany.
phone: +49 89 289 12772, Fax: +49 89 3206620
email: artur.zrenner@wsi.tum.de

Enhancement of the exciton-phonon coupling in single InAs/GaAs quantum dots

A. Lemaître[1], A. D. Ashmore[1], J. J. Finley[1], D. J. Mowbray[1], M. S. Skolnick[1], M. Hopkinson[2], T. F. Krauss[3],

[1] Department of Physics and Astronomy, University of Sheffield, Sheffield, S3 7RH, U.K.
[2] Dept of Electronic and Electrical Engineering, University of Sheffield, Sheffield, U.K.
[3] Department of Physics and Astronomy, University of St Andrews, St Andrews, U.K.

Exciton–LO phonon coupling in InAs/GaAs quantum dots was investigated via single dot spectroscopy. A very pronounced asymmetry in the strength of the exciton–LO phonon coupling has been found between emission and absorption (via PLE) spectra. The results demonstrate that, as expected, the intrinsic coupling is weak in these highly confined systems. The strong overlap of the electron and hole wavefunctions reduces the polar character of the exciton, thus leading to a very weak interaction with LO-phonons [1]. Nevertheless we show that strong coupling can occur, through i) resonant mixing with the excited excitonic states or ii) mediated by charged defects close to the dots, which perturb the electron-hole charge distribution in the dots.

Excitonic complexes were first identified through their PL signature (Fig. 1a), measured at 10 K [2]. When exciting above the wetting layer (WL) band-gap, the spectra in the excitonic ground state (GS) region show 3 peaks corresponding to the recombination of the single exciton (X), biexciton (2X) and a charged exciton (X*). Under resonant excitation, PL spectra reveal a series of new peaks (X_1, X_2, X_3) emerging within 2 meV below the X line. They arise from the recombination of single exciton perturbed by charged defects in/around the dot. These defects induce a Stark shift of the X_n lines and also polarise the electron-hole charge distribution in the dot, thus enhancing the dipole moment.

We then investigated the coupling of the X and X_n to LO-phonons from the intensity of the phonon replicas in emission and absorption (PLE). In PLE (Fig. 1b), two broad features are observed ~ 31 and ~ 62 meV above the detection energy for all X and X_n complexes. Their energies correspond closely to typical LO-phonon energies. These features arise from phonon-assisted absorption when a photon is absorbed into the state $|\mathrm{GS} + n\mathrm{LO}\rangle$ followed by creation of an exciton in the ground state $|\mathrm{GS}\rangle$ and the simultaneous emission of n phonons. This process is enhanced by resonant mixing with excited excitonic states, which lie close to the phonon features as shown in Fig. 1c. In emission the counterpart process, phonon-assisted emission of a photon from the state $|\mathrm{GS} - 1\mathrm{LO}\rangle$, was not observed since there are no excitonic states below the zero-phonon line with which to mix resonantly. The strength of the coupling is also different for the two types of excitonic species X and X_n. In PLE, for X, the phonon features are very weak compared to the signal measured for excitation energies greater than the WL bandgap. In contrast, the phonon features associated with X_n show intensities comparable to excitation at the WL energy. This indicates that the perturbed X_n are more likely to couple to phonons than X. This enhancement arises from the coupling of LO-phonons to the enhanced dipole moment of the exciton induced by the charged defects.

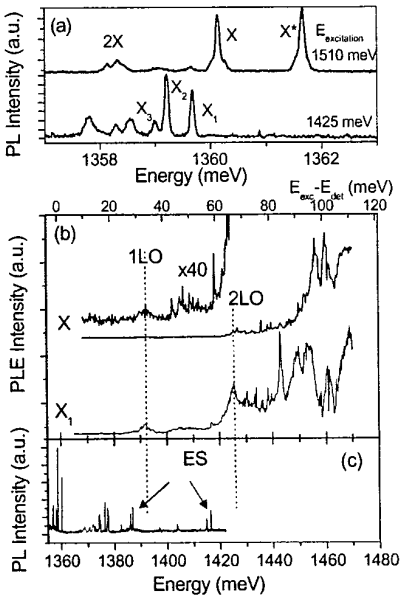

Figure 1: a) PL spectra in the ground-state region for excitation energies above and below the wetting layer bandgap (1460 meV). b) PLE spectra for detection at the energies of the X and X_1 lines. c) High power PL spectrum showing the emission from excited states.

References

[1] S. Schmitt-Rink, D. A. B. Miller, and D. S. Chemla, Phys. Rev. B **35**, 8113 (1987).
[2] J. J. Finley *et al.*, Phys. Rev. B **63**, 073307 (2001).

Corresponding author: Aristide Lemaître, Department of Physics and Astronomy, University of Sheffield, Sheffield, S3 7RH, U.K.
phone: +44 114 222 3522, Fax: +44 114 272 8079,
email: a.lemaitre@sheffield.ac.uk

The influence of carrier diffusion on the formation of charged excitons in InAs/GaAs quantum dots

K. F. Karlsson[1], E. S. Moskalenko[1,2], P. O. Holtz[1], B. Monemar[1], W. V. Schoenfeld[3], J. M. Garcia[3], P. M. Petroff[3],

[1]Department of Physics and Measurement Technology, Linköping University, S-581 83 Linköping Sweden
[2]A.F.Ioffe Physical-Technical Institute, Russian Academy of Sciences, 194021, Polytechnicheskaya 26, St.Petersburg, Russia
[3]Materials Department, University of California, Santa Barbara, California 93106

Charged- and multi-exciton complexes in quantum dots (QDs) have attracted strong attention because the QD behavior is very sensitive to the exact number of confined carriers. In the present study we demonstrate a new method to create and study negatively charged excitons in single QDs in low-dot-density samples.

In the MBE grown samples studied, lens-shaped QDs are formed from about 1.7 InAs monolayers deposition by the Stranski-Krastanow technique. A sample region with a very low dot density, was chosen for our study, where the interdot spacing was estimated to be about 10 μm, well exceeding the resolving power of the PL-setup used.

Several QDs have been studied and most of them show an analogous behavior. In the PL spectra of a selected QD, the ground state emission exhibit a dramatic dependence on the excitation energy (ω_{photon}) in the case of above barrier band gap excitation and low excitation power (P_{ex}) (Fig. 1). In addition to the recombination of the single exciton in the ground state (denoted X in Fig. 1), two new lines X^- and X^{--} of comparable intensity to X are present at certain excitation energies (Fig. 1b). These novel lines are interpreted as the recombination of excitons with one (two) extra electrons present in the QD, i.e. negatively charged excitons. With this interpretation, the experimentally evaluated binding energies of X^- and X^{--} are in very good agreement with the theoretically predicted values as proposed by Ref. 1.

The appearance of charged excitons at some excitation energies can be explained in terms of an effective diffusivity of the photo-generated carriers [2], which in turn affects the capture probability of the QD. The excess kinetic energy of the carriers, defined as the difference between the excitation energy and the barrier band gap, can essentially be released either by fast emission of LO-phonons or by much slower emission of acoustic phonos. Hence, if the excess kinetic energy exactly fits with an integer number of LO-phonon energies the carriers quickly become motionless at the band edge, resulting in a lower diffusivity. On the contrary, if the excess kinetic energy does not fit with an integer number of LO-phonon energies, it takes much longer time to completely release the excess energy, resulting in a higher diffusivity. Carriers with higher diffusivity can move in a larger spatial region and are thus more likely to pass in the vicinity of the QD to become trapped. We propose that at certain excitation energies the electrons have higher diffusivity than the heavy-holes resulting in a population of QDs which on average have electrons in excess, i.e. negatively charged excitons can be formed. The observed counter-phase oscillation of the X and X^{--} intensity versus the excitation energy, with a periodicity that exactly corresponds to the electron's part of the excess kinetic energy of the LO-phonon energy, as shown in the of Fig. 2, supports this proposal.

An alternative way to increase the diffusivity of the carriers, in particular for electrons, is to increase the crystal temperature, T. When the excitation energy is chosen in such a way that solely the line X is present in the PL spectrum at T = 4 K, an increase of the temperature initiates the appearance of X^- and X^{--} (Fig. 3a). Analogously, when the excitation energy is chosen to give X, X^- and X^{--} of comparable intensity at T = 4 K, the X line is totally quenched as the temperature is increased to T = 35 K, while the intensity of the X^{--} line is increased (Fig. 3b). To exclude the possibility that the temperature activates localized electrons that become trapped by the QD, the excitation energy is tuned to the low-energy tail of the wetting layer. In this case, only localized (immobile) carriers are created without any excess energy to diffuse. (See Fig. 3c.) As expected, only the X line is detected at both low and high temperatures, indicating no essential contribution from thermally activated electrons.

The possibility to create charged excitons by optical means, without any for the purpose specially fabricated sample, can be used as an effective tool for further studies of charged exciton complexes.

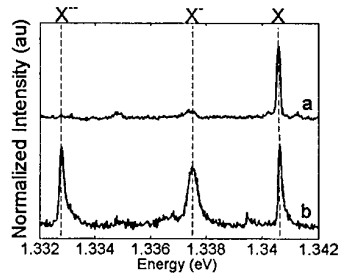

Fig. 1. PL spectra of the ground state emission of a single QD at T = 4 K: (a) ω_{photon} = 1.684 eV, P_{ex} = 8 nW and (b) ω_{photon} = 1.536 eV, P_{ex} = 3.2 nW

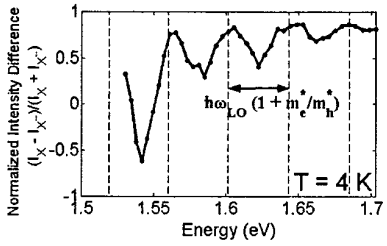

Fig. 2. The differential intensity of X and X^{--} versus the excitation energy, which reflects the periodicity of the competition between these excitons. The dashed lines correspond to excitation energies at which the electron's part of the excess kinetic energy is an integer number of LO-phonon energies, with the GaAs band gap as a reference energy.

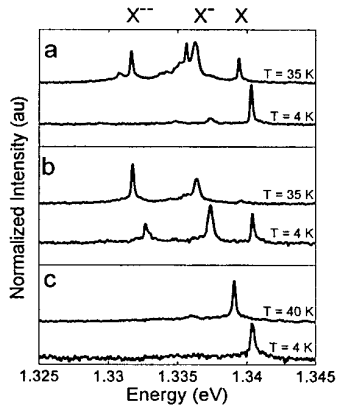

Fig. 3. PL spectra the QD showing the temperature dependence at different excitation energies (a) ω_{photon} = 1.686 eV and P_{ex} = 5 nW, (b) ω_{photon} = 1.557 eV and P_{ex} = 5 nW and (c) ω_{photon} = 1.433 eV and P_{ex} = 30 μW

References

[1] R.J.Warburton, et al., Phys.Rev.B 58 16221 (1998), [2] J.P.Wolfe, et al., Sci. Technol. 7, B240 (1992)

Photoluminescence up-conversion of single InAs/GaAs quantum dots

G. Cassabois[1], C. Kammerer[1], C. Voisin[1], C. Delalande[1], Ph. Roussignol[1], J.M. Gérard[2],

[1]Laboratoire de Physique de la Matière Condensée de l'Ecole Normale Supérieure, 24, rue Lhomond 75231 Paris Cedex 05, France
[2]France Telecom R&D, 196 Avenue Henri Ravera 92220 Bagneux, France

Photoluminescence (PL) up-conversion is a striking feature in optical spectroscopy because of its unusual nature, namely the observation of a photoluminescence signal at energies higher than the excitation energy. In the last few years, PL up-conversion has attracted much attention because of its observation in semiconductor heterojunctions or nanostructures with a high efficiency under cw-excitation [1-4]. Auger processes [1] or two-step two-photon absorption [2] have been proposed to explain this phenomenon. Whatever the mechanisms that up-convert the carriers, the intermediate states which are resonant with the excitation energy and allow this efficient PL up-conversion, are deep states that paradoxically act as non-radiative centers for conventional PL. Previous studies on self-assembled quantum dots (QD) samples reported the observation of an up-converted PL signal arising either from the GaAs substrate [4] or from the InP QDs embedded in a heterojunction where electrons are injected [3].

Here we report the observation of an efficient PL up-conversion for single quantum dots. MicroPL measurements on mesa structures of a self-assembled InAs/GaAs QDs sample reveal the existence of a strong PL up-conversion arising from single QDs and also from the InAs wetting layer (WL). Typical spectra recorded at 10 K under cw-excitation by a Ti:Sa laser are shown in Fig. 1. For curve (a), the laser was tuned above the WL transition energy at 1.428 eV. The PL spectrum shows a strong emission at 1.42 eV corresponding to carrier recombination in the WL and narrow lines below 1.4 eV corresponding to single QDs transitions (approximately 10 under the laser spot). For curve (b), the laser is tuned below the WL transition energy at 1.345 eV with an excitation density 30 times larger. Surprisingly, the PL spectrum (shifted for clarity) is unchanged. We have performed power dependent measurements which show a nearly quadratic dependence of the up-converted PL intensity from the QDs. Excitation spectroscopy of the up-converted PL signal has also been performed. The up-converted photoluminescence excitation spectra exhibit identical features for the WL and the single QDs, i.e. a band tail probably coming from the deep states localized at the rough interfaces of the WL quantum well.

This first observation of PL up-conversion of single self-assembled QDs demonstrates the influence on the QD properties of the deep electronic states located at the vicinity of the QDs. These non-radiative centers may play a key role for the population relaxation as well as for the coherence relaxation, two issues of fundamental interest for QDs based lasers and quantum information devices, respectively.

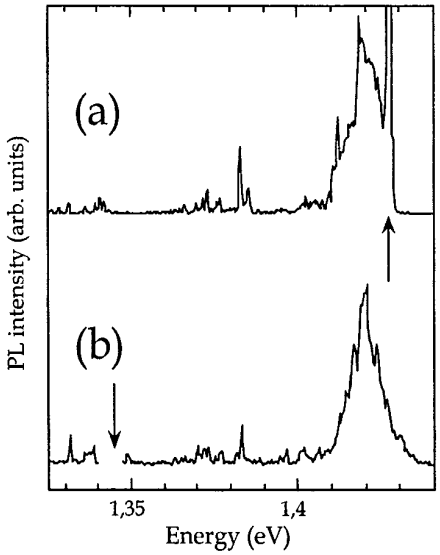

Fig. 1 : Photoluminescence of single InAs/GaAs quantum dots at 10 K. The excitation energy (indicated by the arrow) is 1.428 eV for curve (a) and 1.345 eV for curve (b). The incident power is 6.5 μW for curve (a) and 200 μW for curve (b).

References

*[1] W. Seidel, A. Titkov, J. P. Andre, P. Voisin, and M. Voos, Phys. Rev. Lett. **73**, 2356 (1994).*
*[2] R. Hellmann, A. Euteneuer, S. G. Hense, J. Feldmann, P. Thomas, E. O. Göbel, D. R. Yakovlev, A. Waag, and G. Landwehr, Phys. Rev. B **51**, 18053 (1995).*
*[3] I. V. Ignatiev, I. E. Kozin, H. W. Ren, S. Sugou, and Y. Masumoto, Phys. Rev. B **60**, R14001 (1999).*
[4] P. P. Paskov, P. O. Holtz, B. Monemar, J. M. Garcia, W. V. Schoenfeld, and P. M. Petroff, Appl. Phys. Lett. 77, 812 (2000).

Corresponding author: Guillaume Cassabois, Laboratoire de Physique de la Matière Condensée de l'Ecole Normale Supérieure, 24 rue Lhomond 75231 Paris Cedex 05, France,
phone: +33.1.44.32.25.56, Fax : +33.1.44.32.38.40,
email : Guillaume.Cassabois@lpmc.ens.fr

Quantum dots as sensitive probes of their environment

Y. Ducommun[1], A. Hartmann[1], E. Kapon[1]

[1]Department of Physics, Swiss Federal Institute of Technology Lausanne (EPFL), CH-1015 Lausanne, Switzerland

Even though semiconductor quantum dots (QDs) are often described as "artificial atoms" due to their predicted discrete density of states, the fact that QDs are embedded in a (potentially) inhomogeneous semiconductor matrix imposes the consideration of possible interactions of QD carriers with the solid-state environment for understanding their electronic properties [1,2]. In particular, spatial or temporal fluctuations in the QD solid-state environment can be undesirable sources of inhomogeneous broadening of the atomic-like density of states. In order to exploit the advantages of the three-dimensional confinement in future QD-based optoelectronic devices, a good understanding of the QD-environment interactions is therefore of fundamental importance.

Here, we summarize some properties of single QDs in the presence of a n- or p-type shallow impurity background. The QDs are fabricated using epitaxial growth of $GaAs/Al_xGa_{1-x}As$ heterostructures on substrates patterned with inverted pyramids. A post-growth processing step results in sharp upright standing pyramids, each containing a QD at its tip (see Fig. 1a). The type of the residual impurity background in the $Al_xGa_{1-x}As$ barrier is determined by the OMCVD growth conditions, namely, the V/III ratio: p-type for V/III ~ 500, n-type for V/III ~ 1000. The estimated impurity concentration is about 10^{17} cm^{-3}, as measured on reference, planar samples. Individual QDs are optically probed using a micro-photoluminescence (μPL) setup.

Under above-barrier band-gap excitation, the evolution of the single-QD μPL power dependence is very different for samples with p- and n-type background, especially in the low excitation power (LP) limit, where multi-excitonic occupation of the QD can be excluded (compare Fig. 1b, c).

For **n-type samples**, we show that the PL fine structure is reproducible from QD to QD, and is due to *intrinsic* QD multi-particle interactions between carriers transferred by the surrounding impurities [2]. A photo-depletion mechanism induced by the above-barrier optical excitation efficiently controls the number of excess electrons in the QD. Recombination of charged excitons can be identified in the μPL spectra of single QDs (see labels next to the corresponding peaks in Fig. 1b). By comparing different structurally identical QDs, we demonstrate that the dynamics of these charged multi-particle states is strongly dependent on the exact distribution of donors around each dot. In addition, the comparison between above- and below-barrier band-gap excitation μPL spectra of a given QD allows the identification of a p-type minority doping in our n-type structures. Our analysis gives us the number and type of all the impurities in the surroundings of the dot (typically more than six for majority n-type and less than two for minority p-type). Here, *extrinsic* QD-impurity interactions mainly act as a perturbation on the QD energy levels, by causing a ~ 1 meV broadening of the emission lines in the extremely low excitation power regime (see bottom spectra in Fig. 1b).

For **p-type samples**, the single-QD PL fine structure is very different (see Fig. 1c). First, it is not reproducible from QD to QD, even within the same sample. Second, the emission lines are broad (~ 1 – 5 meV) throughout the low excitation power limit. In fact, we will show that the dynamics of hole transfer from the acceptors to the QD is too slow to result in excess QD hole occupation under continuous above-barrier band-gap excitation, thus excluding *intrinsic* multi-particle interactions as an explanation of the observed μPL evolution. Here, the PL fine structure is dominated by *extrinsic* QD-impurity interactions due to long-timescale fluctuations in the impurities charge state configuration.

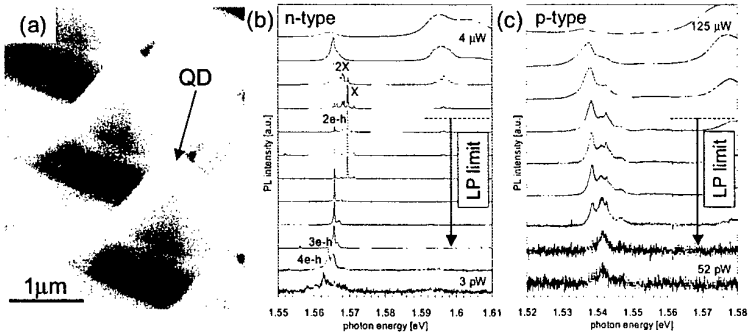

Fig. 1: (a) Scanning electron microscope image of an array of sharp pyramids, each containing a GaAs QD at the tip. (b) and (c) Series of single-QD μPL spectra as a function of above-barrier excitation power, for a sample with n-type (b) or p-type (c) residual background doping in the AlGaAs barrier.

In summary, our results demonstrate that the optical properties of semiconductor QDs are modified in a yet uncontrolled manner by the presence of a shallow impurity background. Furthermore, the *type* of the residual doping strongly influence the resulting single-QD PL fine structure. Here, the timescale of the environment fluctuations is expected to play a significant role [3]. Such environmental effects should also impact the performance of future QD-based devices. Indeed, a good structural uniformity is not sufficient to preserve the narrow optical spectrum of, e.g., an ensemble of QDs. In addition, very low impurity concentration in the QDs environment is required.

References

[1] S. A. Empedocles and M. G. Bawendi, Science **278**, 2114 (1997).
[2] A. Hartmann *et al.*, Phys. Rev. Lett. **84**, 5648 (2000).
[3] Y. Ducommun *et al.*, to be submitted.

Corresponding author: Yann Ducommun, Department of Physics, Swiss Federal Institute of Technology Lausanne (EPFL), CH-1015 Lausanne, Switzerland.
Phone: +41 21 693 54 92, Fax: +41 21 693 54 80
email: yann.ducommun@epfl.ch

Probing the dynamic response of a single Quantum Dot

R.H. Blick[1], H. Qin[1], D.W. van der Weide[2], and K. Eberl[3]

[1]Center for NanoScience, Ludwig-Maximilians-Universität, Geschwister Scholl Platz 1, 80539 München, Germany
[2]Department of Electrical and Computer Engineering, University of Wisconsin, 1415 Engineering Dr, Madison, WI 53706, USA
[2]Max-Planck-Institut für Festkörperforschung, Heisenbergstr. 1, 70569 Stuttgart, Germany

Structured semiconductor quantum dots allow direct studies of the dynamics of few electron systems.. Microwave spectroscopy on quantum dots has been limited to measuring the induced photocurrent in response to radiation, which has demonstrated photon-assisted tunneling (PAT) through single and coupled dots [1]. In this work a single quantum dot is realized in the two-dimensional electron gas of an $Al_xGa_{1-x}As/GaAs$ heterostructure, containing roughly 30 electrons that are strongly coupled to the leads. Conventional transport study shows strong elastic cotunneling in the Coulomb blockade (CB) regime and inelastic tunneling in the single-electron tunneling (SET) regime.

Here we present photoconductance measurements on a single laterally gated quantum dot in the few electron limit using a wideband, i.e. pulsed, millimeter-wave spectrometer. The quantum dot is first characterized by conventional transport spectroscopy [2], which is then compared to the photoconductance spectra. By down converting the millimeter wave signal coherently via a beat note between two microwave sources, the amplitude and phase of the photoconductance can be determined. The spectrometer allows us to observe excited states of the quantum dot and trace these states at non-zero bias. It enables us to reveal the variation of the quantum dot's capacitance [3]. Finally, since we detect harmonics with a lock-in amplifier, we can perform broadband spectroscopy on the dot system without changing the heat load in contrast to conventional tuned sources, such as Gunn diodes.

The spectrometer itself consists of two nonlinear transmission lines (NLTLs), generating trains of short pulses with harmonic frequency contents up to 400 GHz. In contrast to an earlier version of the spectrometer [4] we now have integrated both NLTLs in a single brass box, which is mounted directly on top of a cylindrical wave guide (lower cut-off at 80 GHz) of the sample holder in a dilution refrigerator. This allows us to probe complex photoconductance in the 80 – 400 GHz range. A top view is shown in Fig. 1(a): The NLTLs are fed with two synthesizers connected on the left and right ports. The output of the two sources is then added by a power combiner and sent to a bow-tie antenna. The combiner and antenna circuit are defined by evaporating gold (Au) onto a silicon (Si) substrate. The impedance of the whole circuit is matched to the 50 Ω antenna. The superimposed radiation of the NLTLs is finally radiated into the cylindrical waveguide through a silicon hemisphere attached to the antenna on the back side of the circuit [see Fig. 1(b)]. A close-up of one of the NLTLs is given in Fig. 1(c). The meander shaped coplanar wave guide is intersected by voltage tunable Schottky diodes, leading to the pulse-forming response of the transmission line. Although the output power of the sources is low to minimize heating, we observe a well-pronounced photoconductance signal.

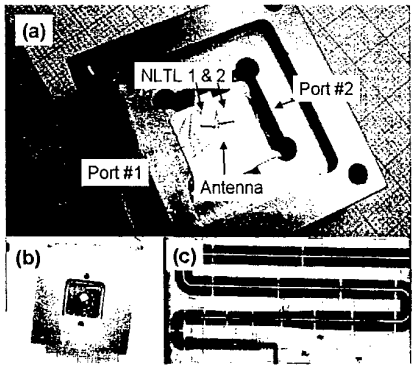

Fig. 1:(a) Top view of the heterodyne spectrometer circuit: The circuit is in the center of a brass box with two SMA ports feeding the two NLTLs. (b) View of the silicon hemisphere on the back side of the box, emitting the radiation. (c) Magnification of one of the meander-shaped transmission lines – the intersections are the position of the Schottky diodes.

We like to acknowledge support by the Deutsche Forschungsgemeinschaft through SFB 348, BMBF (Quantenstrukturbauelemente) and the Defense Advanced Research Projects Agency (Ultrafast Electronics Program); DvdW acknowledges support from NSF and ONR. H.Q. acknowledges support by the Volkswagen foundation.

References

[1] R.H. Blick, *Microwave Spectroscopy on Quantum Dots*, Handbook of Nanostructured Materials and Nanotechnology, Volume **2**, Chapter 6, 307 (2000).
[2] H. Qin et al., Phys. Rev. B **63**, 35320 (2001); cond-mat/0003170.
[3] H. Qin et al., submitted (2001).
[4] R.H. Blick et al., Phys. Rev. Lett. **81**, 689 (1998).

Corresponding author: Robert H. Blick, Center for NanoScience, Ludwig-Maximilians-Universität, Geschwister Scholl Platz 1, 80539 München, Germany.
phone: +49 89 2180 3733, Fax: +49 89 2180 5831
email: robert.blick@physik.uni-muenchen.de

Magneto-tunnelling spectroscopy in multiple gated self-assembled quantum dots

R J A Hill[1], P C Main[1], A Patane[1], B Gustafson[1]
L Eaves[1], M Henini[1], S Tarucha[2] and D G Austing[3]

[1] *School of Physics and Astronomy, University of Nottingham, Nottingham NG7 2RD, UK*
[2] *Dept. of Physics, University of Tokyo, Tokyo 113-8654, Japan*
[3] *NTT Basic Research Laboratories, Atsugi, Kanagawa 243-0198, Japan*

We have recently employed a multiple-gating technology to probe a planar ensemble of InAs "self-assembled" dots (QDs) embedded within an (AlGa)As tunnel barrier [1]. Our structure is a small (~1μm) diameter vertical transistor device that incorporates four independent lateral gates in addition to the usual source (s) and drain (d) contacts (see Figure 1). An applied gate voltage, V_g, changes the electrostatic potential profile within the (AlGa)As barrier layer containing the QDs (see Figure 2a). The effect of V_g on an individual QD is to adjust its potential energy by an amount dependent on its proximity to the gates. This allows us to use V_g to address a particular dot. As shown in Figure 2b, the sharp resonant peaks in conductance, $G(V_{sd})$, due to tunnelling through individual QDs, are shifted at different rates with varying V_g.

We also investigate the effect of a magnetic field, **B**, applied parallel to the barrier plane. At a fixed V_g and source-drain voltage, V_{sd}, the amplitude of each resonance peak is affected by both the magnitude and direction of **B** (see Figure 2c). This provides information about the spatial character of the wave function of the QDs [2]. The special feature of the wavefunction mapping technique in these new gated structures is that we can use the gate voltage variation to assign the resonance peaks to distinct dots. For example, the resonant peaks labelled α and β in Figure 2b have almost identical dependences on V_g which lead us to believe that they are due to tunnelling through quantum states of the *same* dot. In particular, the angular variation and form of the G(B) curves indicate that α and β correspond respectively to the ground and first-excited state of the dot. The gate addressing technique therefore provides a means of identifying and measuring the energy levels and configurations of states in a single quantum dot.

We also discuss the role of QD charging on the transport properties of these small gated mesas. We used structures grown on differently oriented substrates and/or having a different composition of the barrier matrix material surrounding the dots. We find that the barrier matrix plays a major role in determining the amplitude of the resonant current features, due to the effect of the dot charging on the potential profile of the device.

References

[1] D.G. Austing et al., Appl. Phys. Lett. 75, 671 (1999)
[2] E.E. Vdovin et al., Science 290, 124 (2000)

Corresponding author: Richard Hill
School of Physics and Astronomy, University of Nottingham, NG7 2RD, UK
phone: +44-115-9515151-8334 fax: +44-115-9515180
e-mail: ppxrjah@nottingham.ac.uk

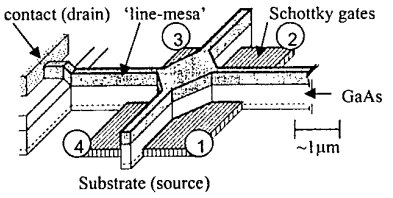

Fig.1. Schematic of our device. The current flows vertically (on this diagram) through the central square of the cross. The metalised surface of the line-mesa provides the connection between the central square and the top contact.

----- Barrier layer containing QDs

Fig.2b. Grey-scale plot showing conductance as a function of source-drain voltage (V_{sd}) and gate voltage (V_g). Conductance peaks due to resonant tunnelling through individual dots are shown by the bright lines.

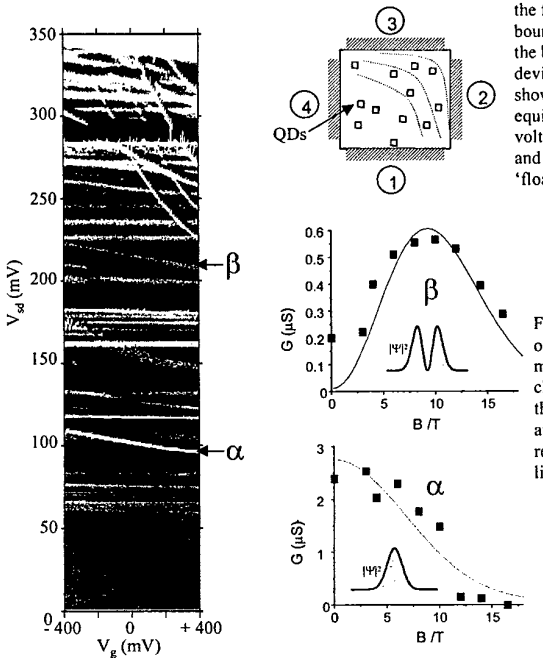

Fig.2a. Schematic showing the four lateral gates bounding a section through the barrier layer of the device. The dashed lines show schematically the equipotentials when a voltage is applied to gates 2 and 3 while 1 and 4 are left 'floating'.

Fig.2c. The conductance, G of peaks α and β exhibit magnetic field dependences characteristic of tunnelling through a QD ground state and 1st-excited state respectively. Continuous lines are guides to the eye.

Magnetically induced non-zero angular momentum in a few electrons silicon quantum dot

L. P. Rokhinson[1], L. J. Guo[2], S. Y. Chou[1], D. C. Tsui[1]
[1]*Department of Electrical Engineering, Princeton University, Princeton, NJ 08544, USA*
[2]*Department of Electrical Engineering and Computer Science, University of Michigan, Ann Arbor, MI 48109 USA*

Most of single electron tunneling experiments are performed on two-dimensional quantum dots with weak and smooth confining potential created electrostatically by gates. In such dots, the magnetic field B dependence of energy levels is dominated by orbital effects even at low B. High field redistribution of the electron density is related to the formation of gaps in the otherwise continuous filling of angular momentum states. Recently, it has become possible to investigate quantum dots in a different regime of very small size, strong confinement, and strong local disorder. This regime is realized in three-dimensional Si dots with confining potential provided by a sharp Si/SiO_2 interface *[1]*. The lack of rotational symmetry mixes states with different angular momenta, eliminating the linear in B term of the orbital energy, and the parabolic B^2 term is suppressed by strong confinement. Thus, in this extreme quantum limit the B dependence of the energy levels is expected to be simple and to consist of linear Zeeman shifts. Indeed, earlier we demonstrated that the shifts of CB peak positions are dominated by the Zeeman effect *[2]* and spin configuration of the dot can be readily extracted.

In this work we focus on small fluctuations in the peak position, which appears at high B and low T in a Si quantum dot with a few electrons, $N \sim 4$ - 6. The fluctuations have a very distinct saw-tooth pattern: as a function of B, fast linear shifts in the peak position are interrupted by abrupt jumps in the opposite direction, see Fig. 1. As a result, in some intervals of the gate voltage the occupancy of the ground state oscillates between N and $N-1$ several times as B changes. We provide experimental evidence that the linear segments of the fluctuations are due to the formation of states with non-zero angular momentum. We speculate that high B suppresses the mixing of states with different angular momenta. The abrupt jumps of peak positions are most likely due to magnetically induced localization of charges and their redistribution inside the dot.

References

[1] E. Leobandung, L.J. Guo, Y. Wang, and S.Y. Chou, Appl. Phys. Lett. **67**, 938 (1995)
[2] L.P. Rokhinson, L.J. Guo, S.Y. Chou, and D.C. Tsui, Phys. Rev. B **63**, 035321 (2001)

Corresponding author: Leonid Rokhinson, Department of Electrical Engineering, Princeton University, Princeton, NJ 08544, USA
phone: +1-609-258-2152, Fax: +1-609-258-6279
email: leonid@ee.princeton.edu

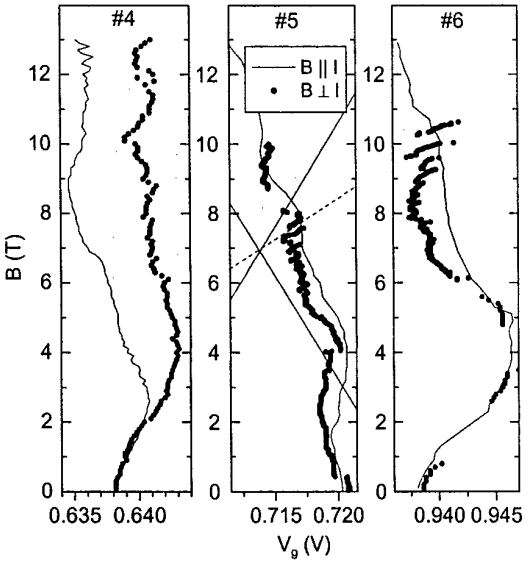

Fig. 1: Positions of the Coulomb blockade peaks 4, 5, and 6 are shown as a function of in-plane (solid line) or perpendicular (dots) magnetic filed. In the shaded regions jumps in peak positions are observed for $B_\perp$. Straight lines have slopes $\frac{1}{2}g\mu^*$ (solid) and $\frac{1}{2}\hbar\omega_c / B$ (dashed).

Internal degrees of freedom of three dimensional quantum dots

S. Lindemann[1], T. Heinzel[1], K. Ensslin[1], K. Maranowski[2] and A. C. Gossard[2]

[1] Solid State Physics Laboratory, ETH Zurich, 8093Zurich, Switzerland
[2]Materials Department, UCSB, Ca 93106, USA

Semiconductor based quantum dots (QD) are usually fabricated on two-dimensional electron gases (2DEG). Here we start from a quasi-three dimensional electron gas embedded in a parabolic potential. The parabolic quantum well is grown by molecular beam epitaxy by grading the Al content of a wide quantum well [1] thus that several subbands can be occupied. Via a gate voltage applied to the back of the quantum well the subband occupancy as well as the two-dimensional electron density can be tuned.
Here we present results on a quantum dot which is defined by conventional split gate electrodes on top of a GaAlAs heterostructure containing a parabolic quantum well. By tuning a single split gate pair conductance quantization is observed. [2] When the entire gate geometry consisting of the usual two split gate pairs as well as two plunger gates is tuned, high quality Coulomb peaks arise in the conductance through the quantum dot. The two-dimensional carrier density and with it the occupancy of the quantum dot can also be tuned by the back gate voltage. For very negative back gate voltages only one electrical subband in growth direction is populated and the Coulomb peaks basically reproduce the behavior of SETs fabricated on two-dimensional electron gases. With increasing areal density, however, the Coulomb peaks start to fluctuate in position as well as in amplitude if several consecutive plunger gate sweeps with otherwise identical parameters are compared. The magnitude of the fluctuations increases with density.
Fluctuations in Coulomb peak positions are usually attributed to background charge re-arrangements. Fluctuations from the surrounding substrate are expected to lead to a negligible contribution to the fluctuations since we can drive the quantum dot into a non-fluctuating regime with negative back gate voltages. While we can not completely rule out that certain impurities suddenly become occupied or unoccupied for a given back gate voltage it seems very unlikely that this is the dominant process because the magnitude of the fluctuations can be tuned relatively precisely with back gate voltage and magnetic field. They start roughly where the second subband in the dot becomes populated..
The electron density in the dot can be determined from magneto Coulomb oscillations. We find that the areal electron density suddenly increases more strongly with back gate voltage once the second subband in growth direction becomes populated in the dot. This is most likely related to the complicated three dimensional self-consistent potential and how it evolves under changing split gate and back gate voltages. We find experimentally, that the lateral dot size actually decreases as the two-dimensional density in the system is increased with a more positive back gate voltage. This can be explained by measuring the capacitances between the various top gates involved relative to the quantum dot as well as the backgate capacitance. The additional degree of freedom, which is not present in quantum dots fabricated on standard 2DEGs, leads to an electrostatic confinement, which is strongly coupled for all spatial directions.
For two-dimensional systems it is well known that the density of states of a higher subband can have a mobility edge extending below the actual subband bottom. For electrons in the lower subband additional intersubband scattering can arise even if the upper subband is not yet populated with mobile carriers. We tentatively ascribe the increased fluctuations of the Coulomb peaks with increasing carrier density to a charging of these localized states below the second subband edge. This is consistent with the observation that these fluctuations are reduced for large magnetic fields driving the quantum dot into the quantum Hall regime.
We conclude that the three-dimensional nature of our quantum dot leads to an additional degree of freedom which may strongly influence the self-consistent potential as well as the details of the charging process.

References

[1] for a review see A. C. Gossard, IEEE J. Quant. Electron. **22**, 1649 (1986)
[2] G. Salis, T. Heinzel, K. Ensslin, O. J. Homan, W. Bächtold, K. Maranowski, and A. C. Gossard, Phys. Rev. B **60**, 7756 (1999)

Corresponding author: Klaus Ensslin, Solid State Physics Laboratory, ETH Zurich,
8093 Zurich, Switzerland
phone: +41-1-633 2209, Fax: +41-1-633 1146
email: ensslin@solid.phys.ethz.ch

Anisotropy in the conductance of high mobility modulation-doped quantum wells on GaAs(001) substrates

K.- J. Friedland[1], R. Hey[1], H. Kostial[1], Y. Hirayama[2] and K. H. Ploog[1]

[1]Paul-Drude-Institut für Festkörperelektronik, Hausvogteiplatz 5-7, 10117 Berlin, Germany
[2]NTT Basic Research Laboratories, 3-1, Morinosato Wakamiya, Atsugi 243, Japan

The surface morphology during growth by molecular-beam epitaxy has a distinct influence on the low-temperature electron transport properties of semiconductor heterostructures with high mobilities. In particular step bunching in the step flow growth mode may result in a corrugation and/or formation of anisotropic islands on the GaAs surface. A heterointerface formed by such a surface becomes therefore a source for anisotropy. This anisotropy is reflected by interface roughness scattering, which is one of the most effective mechanisms of low-temperature scattering in high-mobility modulation-doped structures, where the scattering from ionized impurities is suppressed [1]. Scattering from ionized impurities may be minimized in heterostructures by a large distance between the doping layer and the two-dimensional conducting channel, which results, however, in a low density of the two-dimensional electron gas (2DEG).

We investigate here the anisotropy of the conductance in modulation-doped single quantum wells (SQW), where the scattering from ionized impurities is suppressed by selective screening of the potential fluctuations caused by the ionized impurities in the doping layer [2]. The barriers of the SQW are formed by short-period AlAs/GaAs superlattices (SPSL). High mobility electrons in the SQW are provided by two single Si δ-doping layers in the GaAs part of the superlattice placed on both sides of the SQW. Additionally X-like conduction-band states are occupied in the AlAs sequence of the SPSL. Electrons in these states exhibit heavy mass and are located close to the doping layer and provide a high screening capability. They are localized at the minima of the fluctuating potential, thus smoothing the fluctuations of the scattering potential (FSP). As a result, the mobility of the electrons in the GaAs SQW can be increased considerably. Figure 1 shows the magneto-transport measurements of ρ_{xx} and ρ_{xy} for a 13 nm wide SQW at 0.3 K. Due to the screening of the FSP, the highest mobility amounts to $\mu = 280\ m^2/Vs$ at an electron density of $n = 9.4 \times 10^{15}\ m^{-2}$ in Hall-bar structures oriented along the $[1\bar{1}0]$ direction. The mobility does not depend on the spacer layer thickness, although the electron density changes from 0.7 up to $1.5 \times 10^{16}\ m^{-2}$, indicating the dominance of interface roughness scattering. In Hall-bar structures oriented along the perpendicular [110] direction, the mobility becomes 2-3 times lower with a large variation of the values over the wafer. AFM images of the layer surfaces show a distinct anisotropic island formation with clear hints to step bunching as being its origin. We will compare the dominant correlation lengths with the relevant scattering lengths of the electronic transport in order to prove the existing theories for anisotropic electron transport in high-mobility 2DEG. We will discuss the influence of the particular growth conditions, e.g., spatial inhomogeneity of the superlattice period arising from noncoincidence of the rotation frequency of the wafer during growth with the deposition rate for the corresponding sequences of the SPSL, in order to explain the large variation of transport anisotropy.

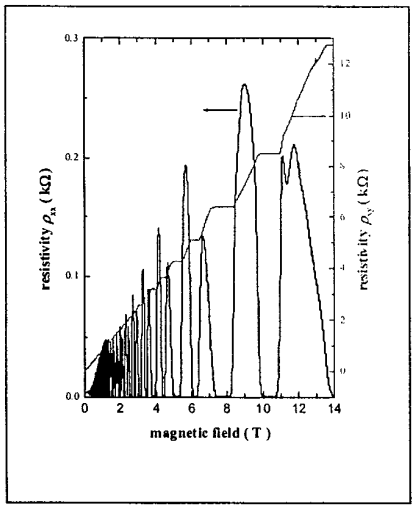

Fig. 1: Magnetic field dependence of ρ_{xx} and ρ_{xy} at T=0.3 K for a GaAs SQW, mobility $\mu = 280\ m^2/Vs$ and carrier density $n = 9.4 \times 10^{15}\ m^{-2}$.

Fig. 2: AFM image (5 μm × 5 μm) of a typical as-grown surface. Gray scale: 0-2 nm

References

[1] Y. Tokura, T. Saku, and Y. Horikoshi, Phys. Rev. B 53, 10528 (1996).

[2] K.- J. Friedland, R. Hey, H. Kostial, R. Klann, and K. Ploog, Phys. Rev. Lett. 77, 4616 (1996).

Corresponding author: K.- J. Friedland, Paul-Drude-Institut für Festkörperelektronik, Hausvogteiplatz 5-7, 10117 Berlin, Germany
phone: +49 30 20377349, Fax: +49 3020377515
email: kjf@pdi-berlin.de

High-Mobility Electrons in Modulation-Doped AlAs Quantum Wells

E. P. De Poortere, Y. Shkolnikov, E. Tutuc, S. J. Papadakis, M. Shayegan,

Department of Electrical Engineering, Princeton University,
Princeton, NJ 08544, USA

GaAs/AlGaAs heterojunctions are at the heart of some of the most successful electronic systems. They are widely used to explore the fundamental physical properties of interacting electron fluids, and also enjoy numerous practical applications. Less known is the fact that AlAs, a material traditionally used as a barrier in modulation-doped heterostructures, can also serve as the quantum well of a lattice-matched heterojunction [1-2]. Such is the case in modulation-doped $Al_{0.40}Ga_{0.60}As$/AlAs heterostructures, where electrons are trapped in the AlAs quantum well at the X point of the Brillouin zone. Due to the threefold symmetry of the X-point electron pockets in reciprocal space, valley degeneracy is also possible in AlAs. Other differences between electrons in GaAs and AlAs include the large and anisotropic effective mass (m_l = 1.1, m_t = 0.2) and larger g-factor (g = 2) of AlAs electrons.

We report here a significant improvement in the quality of two-dimensional (2D) electrons in AlAs quantum wells, confirmed by electron mobilities as high as 250,000 cm^2/Vs at 0.3 K. Carrier density ranges from 1.5 to 9.5 x 10^{11} cm^{-2}, and is tuned by illumination and gate biasing. These AlAs quantum wells, 110 *Å*- to 150 *Å*-thick, are bordered by $Al_{0.40}Ga_{0.60}As$ barriers and modulation-doped with Si on one side of the well only, in contrast to previously reported samples, which were doped on both sides of the well [1, 2]. Within the first Landau level, we observe magnetoresistance minima at filling fractions 2/3, 3/5, and 1/3, 2/5, 3/7. Measurements on our high-density AlAs samples show that electrons occupy multiple X-point valleys (Figs. 1, 2). In addition, these samples show fractional quantum Hall states at filling factors up to 11/3, as high a fraction as the highest quality GaAs samples show.

The quality of our samples has also allowed us to resolve a surprising phenomenon that takes place at magnetic phase transitions between quantum Hall Ising ferromagnets. We have shown that resistance spikes occur at these magnetic transitions, and are likely caused by dissipation at magnetic domain wall boundaries [3]. This effect has important implications for the study of itinerant-electron ferromagnetism, since it allows us to determine with good precision the change in the exchange energy of the electron system as it undergoes these magnetic transitions.

References

[1] T. P. Smith III et al., Phys. Rev. B **35**, 9349 (1987).
[2] T. S. Lay et al., Phys. Rev. B **62**, 3120 (1993) and references therein.
[3] E. P. De Poortere et al., Science **290**, 1546 (2000).

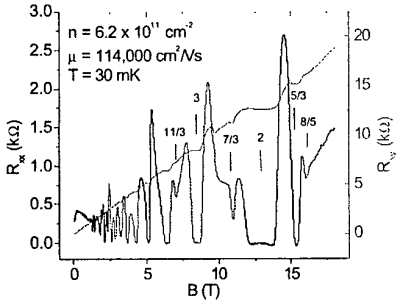

Fig. 1 Magnetoresistance of AlAs 2D electrons with valley degeneracy, showing fractional quantum Hall states up to the filling factor ν = 11/3.

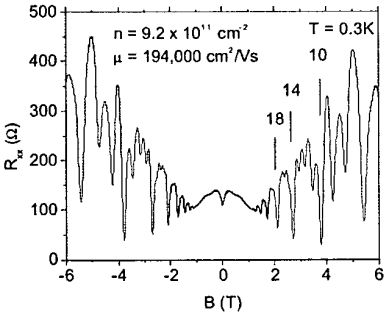

Fig. 2 Low-field magnetoresistance (R_{xx}) of an AlAs quantum well with valley degeneracy. Strong R_{xx} minima are seen every fourth integer Landau level filling.

Corresponding Author: Etienne De Poortere, Department of Electrical Engineering,
Princeton University, Princeton, NJ 08544, USA,
Tel: +1 (609) 258-5434, Fax: +1 (609) 258-1840,
email : poortere@ee.princeton.edu

Spin alignment of electrons in PbTe/(Pb,Eu)Te nanostructures

G. Grabecki[1], J. Wróbel[1], T. Dietl[1], E. Papis[2], E. Kamińska[2], A. Piotrowska[2], G. Springholz[3] and G. Bauer[3]

[1]Institute of Physics, Polish Academy of Sciences
al. Lotników 32/46, PL-02-668 Warszawa, Poland
[2]Institute of Electron Technology, al. Lotników 32/46, PL-02-668 Warszawa, Poland
[3]Institut für Halbleiter- und Festkörperphysik, Johannes Kepler Universität Linz,
Altenbergerstraße 69, A-4040 Linz, Austria

There is a growing amount of concepts suggesting potential functionalities of spin degrees of freedom and of spin-polarized currents. In this context, particularly useful are magnetic or narrow-gap semiconductors, in which Zeeman splitting can compete with the cyclotron energy. In this work, we report on the generation of electron current, which is carried by several electric subbands, and which is already entirely spin-polarized in a magnetic field below 1 T.

Our spin aligner consists of a submicron PbTe quantum point contact patterned by electron beam lithography of 50 nm PbTe quantum well. This well is embedded between Bi-doped $Pb_{0.92}Eu_{0.08}Te$ barriers grown by MBE onto 2.5 μm $Pb_{0.92}Eu_{0.08}Te$ undoped buffer layer and BaF_2 substrate. The initial electron concentration and mobility were typically $4\cdot 10^{12}$ cm^{-2} and 10^5 cm^2/Vs, respectively. Etched trenches, 1 μm deep, define the conducting channel and side gates. The gate bias is transferred under the channel by highly dislocated and p-type interfacial layer residing between the lattice mismatched substrate and the buffer. Such nanostructures can be tuned in a wide range of the carrier concentrations, and their properties are reproducible between subsequent cooling cycles.

Owing to an extremely large dielectric constant of PbTe ($\varepsilon_0 \approx 1350$), long-range Coulomb potentials are suppressed, so that the electron transport is ballistic. Accordingly, conductance quantization $G = i\times 2e^2/h$ is observed in two probe geometry, as the gate voltage is swept. Interestingly, only *plateaux* corresponding to i = 1, 3, 6, ... are resolved. This is caused by a relatively large thickness of the quantum well making the conductor cross-section to be elliptical. Theoretically predicted 1D sublevel distribution for such a case [1] is consistent with the orbital degeneracy we detect.

Due to a large spin splitting of the electrons in PbTe, $\frac{1}{2}g^*m^* \approx 0.7$, the spin-resolved steps start to appear already below 1 T. Moreover, the spin-splitting becomes larger than 1D quantization energy. This manifests itself as halving of the zero-field quantization *plateau* numbers: in the magnetic field range from 0.7 T to 1.3 T, we observe i = 0.5, 1.5, 3... This demonstrates that the initial sequence of 1D sublevels remains unchanged in this field range but the electron liquid becomes entirely spin-polarized, even if several 1D subbands is occupied. At higher fields, in which all orbital degeneracies are removed, the conductance steps acquire a constant height, $0.5\times 2e^2/h$.

[1] A.G. Scherbakov et al., *Phys. Rev. B* 53, 4054 (1996).

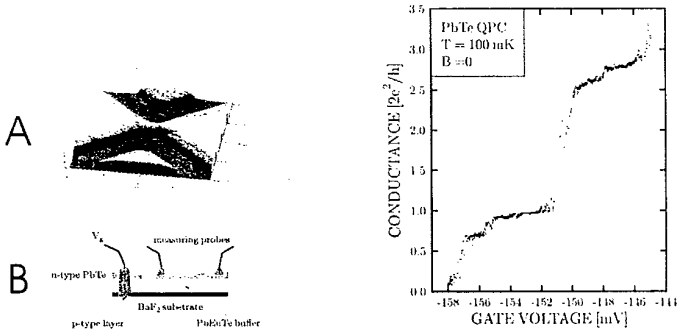

Fig. 1: A) Atomic force microscopy profile of a quantum point contact of PbTe/PbEuTe.

B) Schematic view of the device cross-section illustrating the gate contact to the defected p-type layer.

Fig. 2: Zero field conductance quantization of the PbTe/PbEuTe point contact. The transmission at plateau i = 1 is greater than 90%; a small step at i = 0.7 is not observed in all structures

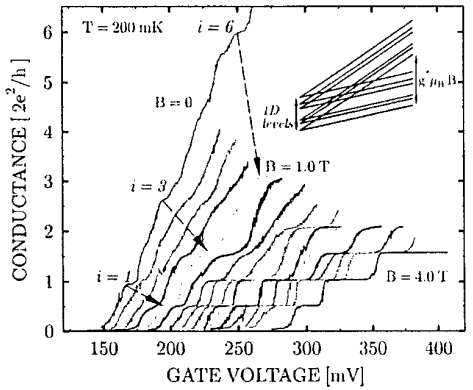

Fig. 3 : Conductance quantization at various magnetic fields between 0 to 4 T, shown with a step of 0.25 T. Inset depicts scheme of the lowest 1D subbands.

Corresponding author: Grzegorz Grabecki, Institute of Physics, Polish Academy of Sciences
al. Lotników 32/46, PL-02-668 Warszawa, Poland
phone: +48 22 843 53 24, Fax: +48 22 843 09 26
email: grabec@ifpan.edu.pl

Optics with Electrons: Fabry-Pérot Resonances and Anti-Reflection Coating for Ballistic Electrons in Finite Superlattices

C. Pacher[1], G. Strasser[1], E. Gornik[1], F. Elsholz[2], A. Wacker[2], G. Kießlich[2], E. Schöll[2]

[1] Institut für Festkörperelektronik und Mikrostrukturzentrum, Technische Universität Wien, 1040 Wien, Austria

[2] Institut für Theoretische Physik, Technische Universität Berlin, 10623 Berlin, Germany

An analogy between mesoscopic transport and classical optics is studied both theoretically and experimentally: The influence of a quantum mechanical anti-reflection coating for ballistic electron transport through short period superlattices is investigated. The transmission through an undoped superlattice consisting of five periods of $b = 2.5$ nm thick $Al_{0.3}Ga_{0.7}As$ barriers and $w = 6.5$ nm thick GaAs wells is compared with the transmission through an identical superlattice embedded between two additional barriers, which form the anti-reflection coating (ARC). As coherent transport dominates in short superlattices [1] the transmission $T(E)$ through the structures is calculated with the help of a simple transfer matrix formalism including nonparabolicity. In order to maximize the transmission $T(E)$ through the first miniband of the superlattice different parameters of the additional barriers are analyzed. The maximum transmission for an ARC in a distance which equals the superlattice well width w is found for $b' = b/2 = 1.25$ nm thick additional barriers. For these parameters an enhancement of the transmission through the first miniband by a factor of 3.1 is calculated (FIG. 1).

We derived an analytical expression for the transmission through finite superlattices with ARC, and give an interpretation of this formula, demonstrating the ARC with additional barrier widths b' to be the direct counterpart of a $\lambda/4$-layer in optics. Using an analytical expression for the transmission through finite superlattices, we show that the transmission resonances in the range of the minibands can be understood as Fabry-Pérot resonances which correspond to the wavelength commensurabilities of the *Bloch vector* q.

With the help of the well developed technology of three-terminal devices [2,3] we are able to prove this predictions experimentally. In a three-terminal device (FIG. 2) hot electrons are injected through a tunnel barrier. These hot electrons are tunable in their energy by means of an applied voltage between the emitter contact (E) and the base contact behind the barrier. After traversing a drift region the hot electrons hit the superlattice. In a third contact, the collector (C), the electrons, which were transmitted through the superlattice, are detected. From the ratio $\alpha = I_C/I_E$ of the measured currents at T=4.2K an energy-resolved spectrum $T(E)$ of the analyzed structure is obtained (FIG. 3). The measured positions of the minibands in both samples agree very well with our calculations. The enhancement of the transmission T_{SL}^{ARC}/T_{SL} in the first miniband is experimentally found to be 2.4. For the second miniband an enhancement of 76% is calculated, experimentally it is found to be 35%. Transmission resonances in the second miniband (the mentioned Fabry-Pérot resonances) are observed for the normal superlattice, whereas the transmission is smooth for the superlattice with ARC (FIG. 4), which is both in good agreement with the calculations. Applying a potential difference V_{BC} between the base and the collector contact the influence of an electric field across the superlattices is also studied (FIG. 3). For the first miniband the transmission does not depend on the direction of the applied electric field (pure ballistic transport, [1]), this behaviour changes for the second miniband (onset of diffusive transport, [1]). The reason is an additional scattering process in the (broader) second miniband: optical phonons.

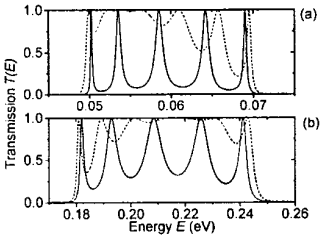

Figure 1: Calculated transmission T_{SL} (full line), T_{SL}^{ARC} (dashed line) versus energy through the first (a) and the second (b) miniband of the investigated superlattices.

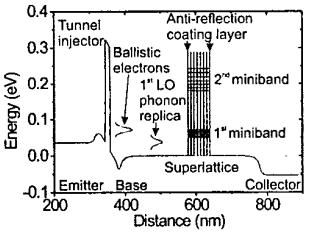

Figure 2: Schematic band structure (energy versus distance) of the three-terminal device with the superlattice with anti-reflection coating.

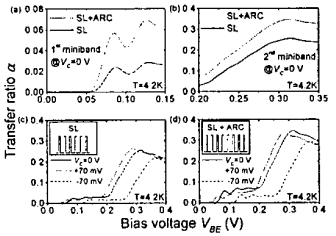

Figure 3: Measured transfer ratios α versus emitter-base voltage V_{BE}.

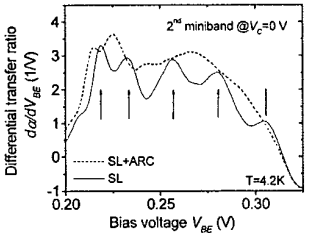

Figure 4: Differential transfer ratio versus emitter-base voltage V_{BE} in the range of the second miniband. Arrows mark the positions of the Fabry-Pérot resonances

References

[1] C. Rauch et al., Phys. Rev. Lett. **81**, 3495 (1998).
[2] M. Heiblum et al., Phys. Rev. Lett. **55**, 2200 (1985).
[3] C. Rauch et al., Appl. Phys. Lett. **70**, 649 (1997).

Corresponding author: Christoph Pacher, Institut für Festkörperelektronik,
phone: +43 1 58801 36229, Fax: +43 1 58801 36299,
email: christoph.pacher@tuwien.ac.at

Microscopic carrier dynamics in quantum wells modulated by high frequency lateral fields

P.V. Santos[1], F. Alsina[1], S.K. Zhang[1], R. Hey[1], A. García-Cristóbal[2], and A. Cantarero[2]

[1] Paul Drude Institute, Hausvogteiplatz 5–7, 10117 Berlin, Germany
[2] Materials Science Institute, University of Valencia, E-46100 Valencia, Spain

High frequency electric fields produced by metal gratings (MG's) and by surface acoustic waves (SAW's) provide an efficient way of inducing a dynamic lateral modulation of the electronic properties of quantum well (QW) structures. The type-II potential modulation induced by MG's and by the piezoelectric field of a SAW in GaAs is sufficiently strong to ionize photogenerated electron-hole pairs and to trap the electrons and holes in the maxima and minima of the electric potential [1]. In the case of SAW's, a second contribution to the modulation comes from the strain field, which leads to a weak (of a few meV's) lateral modulation of the band-gap.

In this contribution, we investigate the microscopic dynamics of photogenerated carriers in GaAs QW's under high frequency electric and acoustic lateral fields using spatially and time-resolved photoluminescence (PL). Since the modulation is both spatial and time dependent, this technique gives a deep insight into the mechanisms of the interaction between field and carriers. We show that the intensity, energy, and phase of PL pulses excited by pulsed illumination provide a direct mapping of the microscopic carrier distribution in the modulated potential and, in case of a SAW, of the band-gap modulation induced by the SAW strain field. Furthermore, we demonstrate that the interaction depends not only on the field amplitude, but also on the transport properties of the carriers.

The studies were performed on GaAs QW's with $Al_{0.3}Ga_{0.7}As$ barriers grown by molecular-beam epitaxy on GaAs (001). SAW's propagating along the x = [110] surface direction were generated by aluminum split-finger interdigital transducers [IDT's, cf. Fig. 1(a)] deposited on the sample surface and designed for operation at a wavelength $\lambda_{SAW} = 5.6$ μm (corresponding to a frequency $\omega_{SAW}/(2\pi) = 520$ MHz at 12 K). The PL measurements were carried out at 12 K using a confocal microscope with illumination and detection areas with a diameter of about 2 μm. The continuous radiation from a Ti:sapphire laser ($\lambda_L = 765$ nm) was employed as excitation source.

The induced modulation of the band-gap by the SAW strain field [cf. Fig. 1(b)] is expected to split the cw PL line into a doublet with energy separation corresponding to the peak-to-peak amplitude of the band-gap modulation $E_s = E_{g,max} - E_{g,min}$ [2]. Since E_s (of ≈ 1 meV for typical SAW powers) is comparable to the PL line width, it is normally not clearly observed in the cw PL spectrum [cf. Fig. 1(c)]. The effects of the band-gap modulation become apparent in time-resolved measurements. Figure 1(d) shows the time-resolved traces obtained for the three detection energies indicated by arrows in Fig. 1(c). The SAW field modulates the signals collected at the energies $E_{g,max}$ and $E_{g,min}$ at the fundamental frequency ω_{SAW}. The modulation phase for these two energies, stated in terms of the phase angle $\phi = (2\pi/\lambda_{SAW})x - \omega_{SAW}t$, are shifted by π with respect to each other, thus indicating that the emission takes place at time intervals delayed by half of the SAW period. For an intermediate energy (E_g), however, time-resolved traces display a strong modulation at the 2nd harmonic of the SAW frequency, owing to the fact that the detection energy matches the band-gap twice in a SAW cycle.

A further interesting point regards the relative intensities of the different components of the PL line. We demonstrate that these intensities are determined by the spatial distribution of the electron (n) and of the hole density (p) in the SAW potential, which are mainly controlled by the piezoelectric field and by the transport properties of the carriers. We have developed a model for the carrier distribution and for the recombination probability (assumed to be proportional to the np product) based on the solution of the drift-diffusion equations for electrons and holes in the dynamic SAW potential. The model shows that the highly mobile electrons have a sharp spatial distribution around the maxima of the piezoelectric potential, which also coincides with the positions where the band-gap is maximum. Due to the lower hole mobility, p has a much wider spatial distribution. As a consequence, the time dependence of the recombination probability and, therefore, of the PL amplitude, basically reflects the electron distribution under the detection spots. These results demonstrate the fundamental role of the carrier mobilities on the PL response under high frequency SAW's.

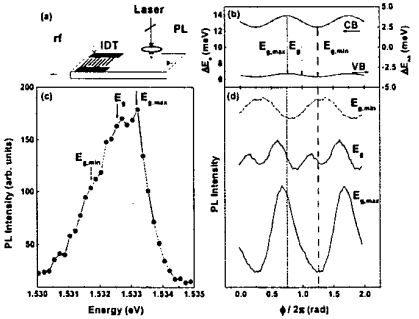

Figure 1: (a) Sample structure. (b) Calculated conduction (CB, ΔE_c) and valence band (VB, ΔE_{hh}) modulation induced by the SAW strain. (c) cw PL spectra of a 15 nm $GaAs/Al_{0.3}Ga_{0.7}As$ single QW under a surface acoustic wave with P_{rf} = 16 dBm. (d) Time-resolved PL detected at the three energies depicted by the vertical arrows in (b) and (c). The curves are shifted vertically for clarity.

References

[1] C. Rocke et. al., Phys. Rev. Lett. **78**, 4099 (1997).
[2] T. Sogawa et. al., Phys. Rev. B **63**, 121307 (2001).

Corresponding author: Paulo V. Santos, Paul-Drude-Institut für Festkörperelektronik, Hausvogteiplatz 5–7, 10117 Berlin, Germany.
phone: +49 30 20377 221, Fax: +49 30 20377 515,
email: santos@pdi-berlin.de

Investigation of nano electromechanical systems using surface acoustic waves

F.W. Beil, A. Hörner, R.H. Blick, A. Wixforth,

Center for NanoScience and Sektion Physik, Ludwig-Maximilians-Universität, Geschwister-Scholl-Platz 1, 80539 München, Germany.

In recent years nano electromechanical systems (NEMS) have attracted wide attention caused by their possible use as fast and sensitive tools for communications technologies and sensors [1]. In addition, NEMS can be regarded as 'quantum-mechanical' counterparts of macroscopic mechanical oscillators, when operated in the GHz range and at ultra low temperatures. Due to the smallness of our NEMS devices, which in this case consist of of freely suspended beam resonators [2] covered by a several nm thick metal layer (see Fig. 1), the eigenfrequencies range in the 100 MHz to 1 GHz regime. These frequencies coincide with those typically processed on surface acoustic wave (SAW) devices, which makes a mutual interaction feasible. SAWs are harmonic acoustic modes that are easily excited on piezoelectric crystals using planar structures like interdigital transducers (IDT) (see Fig. 2). SAWs are bound to the surface, within a layer of approximately one wavelength thickness and propagate at a velocity of about 3000 m/s. By adjusting the SAW-frequency to the eigenfrequency of the mechanical resonator it should be possible to couple to the resonances in the beam. To match the two frequencies, it is necessary to calculate the response of the mechanical resonator in advance using finite element calculations [3], as shown in Fig. 1 and than adjusting the frequency of the SAW by the period of the IDT. A typical setup is shown in Fig. 1, where the resonator is formed by a gold covered beam to permit the detection of the oscillation due to induced currents in a magnetic field while the IDTs allow the generation of SAWs that drive the eigenmode. By appropriate design of the IDTs (see Fig. 2) it is possible to focus the SAW on the beam thus reaching higher driving forces. This novel kind of excitation avoids ohmic losses due to the finite resistance of the conducting layer covering the beam, decreasing the quality factor of the resonators. Observing the excitation of the resonator by measuring the reflection loss of the SAW at the beam would totally supersede a metal layer covering the resonators eliminating the influences of the conductor on the elastic properties of the resonator.

We discuss first experimental results on the interaction of SAWs with NEMS on a GaAs substrate. We compare standard exciting means for micromechanical resonators to our new approach using SAW.

References

[1] A.N. Cleland and M.L. Roukes, Nature **392**, 160 (1998).
[2] A. Kraus, A. Erbe, R.H. Blick, Nanotechnology **11**, 165 (2000)
[3] SOLVIA, ver. 95.0 (1997)

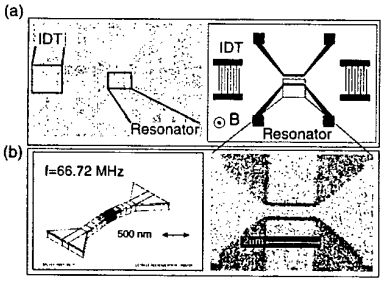

Figure 1: (a) Setup showing the resonator machined out of freely suspended GaAs covered by a 50 nm thick gold layer. Placed in a magnetic field the oscillations of the beam can be observed measuring induced currents. The two IDTs generate SAW at the eigenfrequency of the resonator thus exciting resonant oscillation of the beam (b) Scanning electron micrographs of a resonator together with the result of finite element simulations.

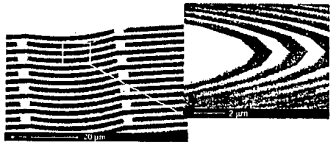

Figure 2: Scanning electron micrograph of a focusing IDT. The potential drop between two fingers induces a mechanical deformation of the material below due to the inverse piezoelectric effect. If the rf-signal matches the resonance condition $f = \frac{v_{SAW}}{\lambda}$, where λ is the period of the fingers, a coherent acoustic beam is generated. Due to the bending of the fingers the SAW is focused in one spot.

Corresponding author: F. W. Beil, Center for NanoScience and Sektion Physik, Ludwig-Maximilians-Universität, Geschwister-Scholl-Platz 1, 80539 München, Germany.
phone: +49 (0)89 2180 3586, Fax: +41 (0)89 2180 3182,
email: beil@informatik.uni-muenchen.de

Ultrafast coherent nonlinear dynamics of intersubband excitations in a quasi-two-dimensional electron gas

M. Woerner[1], R. A. Kaindl[1], F. Eickemeyer[1], K. Reimann[1], T. Elsaesser[1], R. Hey[2], K. Ploog[2]

[1]Max-Born-Institut f. Nichtlineare Optik und Kurzzeitspektroskopie, 12489 Berlin, Germany
[2]Paul-Drude-Institut für Festkörperelektronik, 10117 Berlin, Germany

Today, only little is known about the **coherent nonlinear** response of intersubband (IS) transitions in quantum wells (QWs). However, recent developments like controlled shaping [1] and time-resolved detection [2] of electric field transients in the mid-infrared (MIR) allow to investigate and directly manipulate coherent IS excitations. Furthermore, state-of-the-art n-type modulation-doped GaAs/AlGaAs multiple quantum wells (MQWs) are now that excellent that the linewidth of IS transitions is no longer governed by disorder-induced inhomogeneous broadening, but by the bandstructure and by **carrier-carrier interactions** [3]. Coherent IS polarizations provide particularly sensitive probes of these fundamental interactions. Most studies have investigated the energy position and the **inhomogeneous** broadening of IS lineshapes [4]. In contrast, the nature of **homogeneous** broadening is much less understood. Nonlinear optical techniques which can grasp the polarization dynamics provide the key to characterize these irreversible dephasing processes [3].

Here, we present two different techniques to characterize and manipulate the coherent nonlinear IS polarization of quantum wells with negligible disorder-induced inhomogeneous broadening. The sample consists of 51 GaAs QWs of 10-nm width separated by 20-nm thick $Al_{0.35}Ga_{0.65}As$ barriers (electron density $n_S = 5\times10^{10}$ cm^{-2}). The n=1 to n=2 IS absorption has a very small line width of 3.7 meV (FWHM). All experiments are performed at T = 15 K.

First we discuss time-integrated and time-resolved four-wave-mixing (FWM) experiments in the MIR to investigate IS dephasing [5]. MIR pulses of 100-fs duration are tuned resonant to the n=1 → n=2 transition at $\lambda \approx 12.4$ μm. The time-resolved FWM transients [Fig. 1(a)] exhibit peak positions which depend linearly on Δt_{12}. The slope [(Fig. 1(b)] is indicative of a free-induction decay of the macroscopic polarization and gives direct evidence for predominant **homogeneous** broadening of the IS absorption profile. From the decay of the time-integrated signals [Fig. 2(a)] one derives an IS dephasing time of $T_2 = 320$ fs, which fully accounts for the 3.7-meV linewidth. As discussed earlier [3], this irreversible dephasing is dominantly due to carrier-carrier scattering. Intensity-dependent measurements show that the dephasing rate is almost constant for excitation densities up to 30%. Thus our sample behaves almost like an ideal homogeneously-broadened two-level system.

In a second experiment, we demonstrate for the first time coherent nonlinear control of IS excitations in GaAs/AlGaAs QWs by extremely weak electric field-transients of sub-pJ energy. Near-infrared 17-fs pulses centered at 780 nm are amplitude- and phase-shaped in a programmable pulse shaper to generate tailored mid-infrared transients by phasematched difference-frequency mixing in a 0.5-mm-thick GaSe crystal [1]. The time-dependent electric field of such transients is measured directly by electro-optic sampling [2]. In the upper and middle panels of Figs. 1 (c) and (d), we compare electric field transients through an undoped reference sample of with pulses through the QW sample (note the **different** ordinate scales). The difference of these transients (lower panels) represent the re-emitted free-induction decay (FID) of the IS transition. With increasing amplitude of the exciting electric field, one finds a pronounced saturation of the emitted field. The amplitudes as a function of the

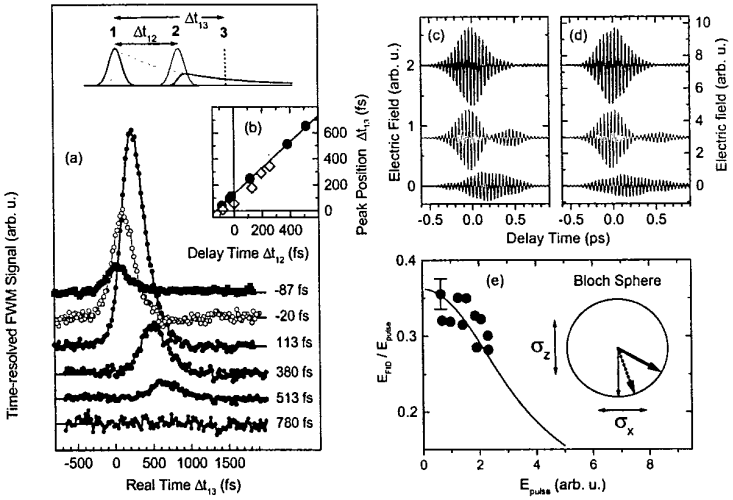

Fig. 1: (a) Time-resolved FWM transients detected using sum-frequency mixing with near-infrared pulses. Signals are shown as a function of time delay Δt_{13} between the near-infrared pulse 3 and the mid-infrared pulse 1, at various fixed delays Δt_{12} (see inset). (b) Peak positions of the transients for different Δt_{12} (dots), compared to a linear dependence $\Delta t_{13} = \Delta t_{12} + 130$ fs (solid line). Measured electric field transients and FID of the IS excitation for (c) low and (d) high fields. (e) Symbols: ratio between the field amplitudes of the re-emitted E_{FID} and the excitation E_{pulse} as a function of E_{pulse}. Solid line: model calculation using the Maxwell-Bloch equations. Inset: Bloch sphere.

incoming field are summarized in Fig. 1 (e). The observed nonlinearity corresponds to an excitation of 30% of (n=1) electrons to the (n=2) subband and is caused by extremely weak excitation pulses with energies of less than 1 pJ. Our experimental data are confirmed by model calculations using Maxwell-Bloch equations for an homogeneously-broadened two-level system. The observed saturation of the FID is due to a partial Rabi flop in the Bloch sphere of up to 60°.

References

[1] F. Eickemeyer et al., Opt. Lett. 25, 1472 (2000)
[2] Q. Wu and X.-C. Zhang, Appl. Phys. Lett. **71**, 1285 (1997).
[3] R. A. Kaindl et al., Phys. Rev. Lett. **80**, 3575 (1998).
[4] see, e.g., S. Graf et al., Phys. Rev. Lett. **84**, 2686 (2000) and references therein.
[5] R. A. Kaindl et al., Phys. Rev. B (in press, 15 April 2001)

Corresponding author: Michael Woerner, Max-Born-Institut für Nichtlineare Optik und Kurzzeitspektroskopie, Max-Born-Straße 2A, D-12489 Berlin, Germany.
phone: +49 30 6392 1470, Fax: +49 30 6392 1489
email: woerner@mbi-berlin.de

Wannier-Stark localization in InAs/(GaIn)Sb superlattice diodes

L. Bürkle, F. Fuchs, W. Pletschen, and J. Schmitz

Fraunhofer-Institut für Angewandte Festkörperphysik (IAF), Tullastrasse 72,
D-79108 Freiburg, Germany

In recent years antimonide-based heterostructures have attracted significant interest in particular in the field of optoelectronic devices operating in the mid and far infrared spectral range. In particular, InAs/(GaIn)Sb superlattices (SLs) are well suited for the fabrication of high performance photodetectors for the 8–12 µm wavelength region [1,2]. Such SLs show a broken gap type-II band alignment with the conduction band edge of InAs being lower in energy than the (GaIn)Sb valence band edge. For short-period SLs with sufficiently thin individual layers, confinement and strain effects result in an effective band gap which is tunable between zero and about 0.3 eV [3]. The thickness of the individual layers in the SLs used for IR photodiodes is typically on the order of 10 atomic monolayers (MLs), leading to strong electronic coupling between the adjacent wells. The electron wave function is centered in the InAs layers, but strongly delocalized with a miniband width typically exceeding 100 meV [4]. However, the type-II character of the system remains due to the localization of heavy hole (HH) states in the (GaIn)Sb layers.

When an electric field F is applied parallel to the growth direction of the SL, energy levels in adjacent quantum-wells are misaligned by an energy eFd_{SL}, where e is the electron charge and d_{SL} the SL period, and the coupling between wave functions of individual quantum-wells is reduced. As the electric field increases, the carriers in the SL become more and more localized and, thus, the 3D nature of the minibands is continuously reduced to quasi-2D Wannier-Stark states [5].

In our presentation, we give experimental evidence for the formation of localized Wannier-Stark states in the depletion region of low band gap ($E_g \approx 0.15$ eV) InAs/(GaIn)Sb SL infrared photodiodes [6]. In the photo current spectra of reverse biased photodiodes (Fig. 1) maxima are observed, which shift in spectral position when the strength of the electric field in the depletion region of the diode is varied. Taking into account the spatially indirect type-II nature of interband transitions in InAs/(GaIn)Sb SLs, the spectral positions of the observed maxima can be explained in the framework of localized Wannier-Stark states.

Besides photo current spectra, the current-voltage (I-V) characteristics of the diodes were investigated. In the reverse bias regime dominated by Zener tunneling the differential resistance of the diodes reveals an oscillatory behavior (Fig. 2). These oscillations are due to a resonant enhancement of the Zener tunneling current by Wannier-Stark states in the depletion region of the SL diode [7]. A model is presented which quantitatively describes the occurrence of the oscillations in the I-V curves. In addition, the influence of a magnetic field on the Wannier-Stark oscillations in the Zener current was investigated for magnetic fields oriented parallel and perpendicular to the built-in electric field of the SL diode. While the period of the oscillations in the I-V curves is conserved, the resonances are shifted, reflecting the energy shift introduced to the Wannier-Stark states by the magnetic field. This voltage shift exhibits a strong dependence on the magnetic field orientation.

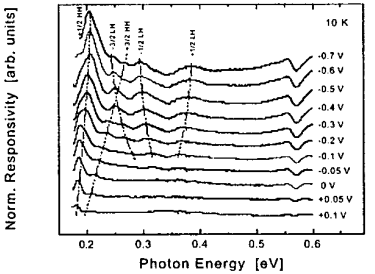

Fig. 1: Photo response of an InAs/(GaIn)Sb superlattice diode normalized to a reference spectrum taken at $U \approx U_{bi}$ as a function of an applied DC voltage

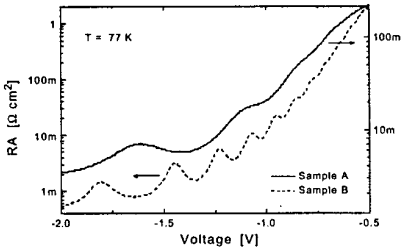

Fig. 2: Differential resistance as a function of applied voltage of two different InAs/(GaIn)Sb superlattice diodes measured at 77 K. Sample A and B differ both in doping and SL period. Oscillations in the Zener current can be clearly observed

References

[1] J. L. Johnson, L. A. Samoska, A. C. Gossard, J. L. Merz, M. D. Jack, G. R. Chapman, B. A. Baumgratz, K. Kosai, and S. M. Johnson, J. Appl. Phys. **80**, 1116 (1996).
[2] F. Fuchs, U. Weimar, W. Pletschen, J. Schmitz, E. Ahlswede, M. Walther, J. Wagner, and P. Koidl, Appl. Phys. Lett. **71**, 3251 (1997).
[3] D. L. Smith and C. Mailhiot, J. Appl. Phys. **62**, 2545 (1987).
[4] F. Fuchs, E. Ahlswede, U. Weimar, W. Pletschen, J. Schmitz, M. Hartung, B. Jager, and F. Szmulowicz, Appl. Phys. Lett. **73**, 3760 (1998).
[5] E. E. Mendez, F. Agulló-Rueda, and J. M. Hong, Phys. Rev. Lett. **60**, 2426 (1988).
[6] L. Bürkle, F. Fuchs, E. Ahlswede, W. Pletschen, and J. Schmitz, submitted to Phys. Rev. B.
[7] C. Hamaguchi, M. Yamaguchi, H. Nagasawa, M. Morifuji, A. DiCarlo, P. Vogl, G.Böhm, G. Tränkle, G. Weimann, Y. Nishikawa, and S. Muto, Jpn. J. Appl. Phys. **34**, 4519 (1995).

Corresponding author: Lutz Bürkle, Fraunhofer-Institut für Angewandte Festkörperphysik,
Tullastrasse 72, D-79108 Freiburg, Germany,
Phone: ++49 (761) 5159-637, Fax: ++49 (761) 5159-677,
Email: buerkle@iaf.fhg.de

Search for gain in a superlattice

H. Willenberg[1], S. Blaser[1], D. Hofstetter[1], M. Beck[1], G. H Döhler[2], J. Faist[1]

[1]Institut de Physique, Université de Neuchâtel, Switzerland
[2] Institut für Technische Physik I, Universität Erlangen-Nürnberg, Germany

Though Bloch oscillations in semiconductor superlattice were predicted in the early seventies [1], it took more than two decades for a direct experimental observation in four-wave mixing experiments [2]. The concept of a Bloch oscillator, in which these charge oscillations would be converted into a coherent, tunable THz emission, is still waiting for its realization.

The emission process of Bloch oscillations requires a quantitative description within the alternative Wannier-Stark picture. In this approach it must regarded as an amplified transition between the rungs of the Wannier-Stark ladder despite a missing population inversion. Also, experiments have not yet confirmed the dispersive gain due to Bloch oscillations that previous models [3-4] of the semi-classical motion in superlattice mini-bands predict. Though it has been clearly shown that a superlattice couples to terahertz photons [5], the rather large theoretical gain has not been observed so far.

We propose an experimental method to measure the Bloch gain that concentrates on its dispersive nature, which gives rise to absorption above and (stimulated) emission below the field-dependent Bloch frequency $\omega_B = eFd/\hbar$ (where e is the elementary charge, F the electric field, d the superlattice period and eFd is the Wannier-Stark spacing).

The superlattice is processed as a laser structure and embedded into a wave guide. In addition, the lower part of one facet is polished at a 45° angle. This way, the light can be coupled out of the structure either by the facet (after passing the wave guide) or by the 45° angle (as for a luminescence experiment) as shown in Fig. 1.

The comparison of the emission passing through the wave guide and luminescence signal from the 45° angle allows to identify gain and loss mechanisms in the wave guide. The "amplified" signal from the wave guide is expected to be red-shifted by δ in respect to the spontaneous emission between adjacent Wannier-Stark states at $\hbar\omega = eFd$, as the Bloch gain peaks below eFd.

In Fig. 2 the observed mid-infrared electroluminescence in the doped superlattice is shown, which originates from both inter-Wannier-Stark ladder and intra-Wannier-Stark ladder transitions. The $2 \rightarrow 1$ emission peak attributed to the transition between first excited and ground state within a quantum well (inter-ladder) is strongly suppressed in the wave guide and the $1' \rightarrow 1$ peak corresponding to the diagonal intra-ladder transition is indeed red-shifted.

However, in the present experiment a detailed investigation of the interplay of wave guide losses, re-absorption into the first excited state and the dispersive Bloch gain, allows an explanation of the observed shift without postulating gain: to stabilize the electrical field inside the device the superlattice has to be biased beyond the negative differential region. Thereby, the ground-state is brought close to resonance to the first excited state of the adjacent period, thus causing a pronounced re-absorption, which suppresses the high-energy flank of the diagonal transition and pushes the luminescence signal within the Wannier-Stark ladder towards lower energies.

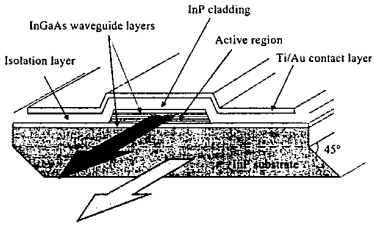

Figure 1: Scheme of one laser stripe with the polished 45° angle facet.

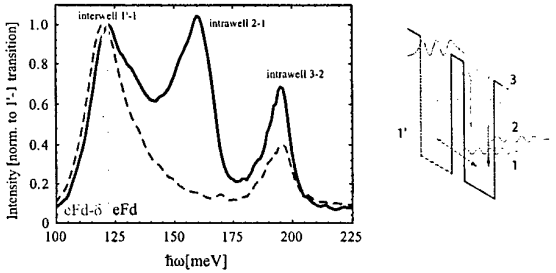

Figure 2: Electroluminescence spectra (normalized to the $1' \rightarrow 1$ diagonal transition = intra-Wannier-Stark ladder transition) for both signals coming from the facet (dashed curve) and from the 45° (solid curve) for a current of $I = 1.2\,\mathrm{A}$, at $T = 4\,\mathrm{K}$ (miniband width $\Delta = 9.8\,\mathrm{meV}$, period of $d = 11.2\,\mathrm{nm}$). The shift of the peak corresponding to the $1' \rightarrow 1$ transition is clearly resolved.

References

[1] L. Esaki, R. Tsu, (1970), IBM J. Res. Dev. **14**, 61.
[2] J. Feldmann, K. Leo, J. Shah, D.A.B. Miller, J.E. Cunnigham, T. Meier, G. von Plessen, A. Schulze, P. Thomas, S. Schmitt-Rink, (1992) Phys. Rev. B **46**, 7252.
[3] S.A. Ktitorov, G.S. Simin, V.Ya.Sindalovskii. (1972) Sov. Phys. Solid State **13**, 1872.
[4] A.A. Ignatov, Yu.A. Romanov. (1976) Phys. Stat. Sol.B **73**, 327.
[5] K. Unterrainer, B.J. Keay, M.C. Wanke, S.J. Allen, D. Leonard, G. Medeiros-Ribeiro, U. Bhattacharya, M.J.W. Rodwell. (1996), Phys. Rev. Lett.**76**, 2973.

Corresponding author: Harald Willenberg,
Institut de Physique, Université Neuchâtel,
Rue A.-L. Breguet 1, CH-2000 Neuchâtel, Switzerland,
phone: +41 32 7182947, Fax: +41 32 718 2901, email: harald@willenberg.de

Breakdown of optical selection rules in a highly-biased quantum well

T. Imai,[1] M. Morifuji,[1] C. Hamaguchi,[1] P. Vogl,[2] G. Böhm,[2] G. Tränkle,[2] and G. Weimann[2]
[1] Department of Electronic Engineering, Osaka University, Suita, Osaka 565-0871, Japan
[2] Walter Schottky Institute, Technical University of Munich, D-85748 Garching, Germany

Electronic states in a confined structure can be controlled by externally applied electric fields. In a single quantum well, applied voltage along the growth axis gives rise to red-shift of optical absorption (or recombination) energies. Accompanied with the red-shift, oscillator strength of allowed transitions decreases, whereas that of forbidden transitions increases because wavefunctions of electrons and holes are deformed toward opposite directions and thus overlap between these states changes. These effects are well known as quantum confined Stark effect. Although behavior of ground states in electric fields has been well investigated, that between higher states has not attracted much attention so far.

We have carried out electroreflectance measurements for a single quantum well embedded in a p-i-n diode, in order to investigate optical behavior of high-index states in high electric fields.

Figure 1 shows the electroreflectance spectra measured in applied voltages $+1.2 \sim -2.0$ [V]. Complicated spectra indicate that many kinds of optical transitions occur due to breakdown of the selection rule in high electric field. In the upper panel of Fig. 2, the open circles indicate transition energies plotted as functions of applied voltage with the size of the circles indicating the intensity. We note that +1.52 [V] corresponds to zero electric field. We see that all the signals show red-shift with increasing applied electric field accompanied with changes of intensity.

We carried out band line-up calculations base on the effective mass approximation in order to analyze these signals. In the upper panel of Fig. 2, the solid curves show calculated transition energies between ground heavy-hole state (hh1) and electronic states (el1, el2, and el3). The dotted curves show transition energies between light-hole state (lh1) and electronic states. We see good agreement between experimental and calculated transition energies.

Experimental signal intensity also shows good correspondence with calculation. In the lower panel of Fig. 2, we show calculated optical matrix elements between heavy-hole and electronic states as functions of applied voltage. The matrix element between the ground states (denoted as el1–hh1), which is allowed at zero field (+1.52 [V] as noted), decreases rapidly with increasing electric field. On the other hands, the intensity of transitions el2–hh1, which must be zero at zero field due to the selection rule, increases with increasing electric field, whereas it decreases in higher electric fields. Matrix element of transition el3–hh1 also shows similar behavior. Such changes of transition matrix elements are well understood by considering shapes of charge density and their deformation due to electric field. We see that the changes of transition intensities due to applied electric fields agree with experimental data.

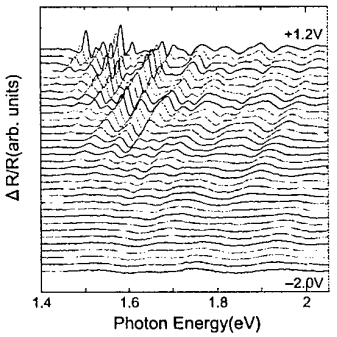

Figure 1: Electroreflectance spectra obtained from a quantum well embedded in the p-i-n diode.

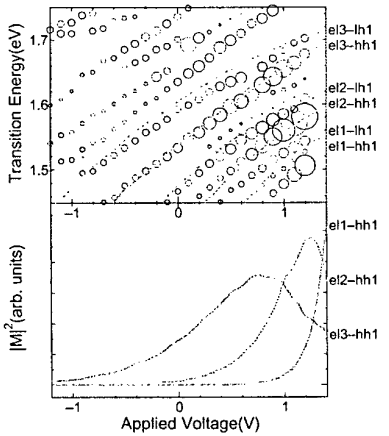

Figure 2: Upper panel: Experimental transition energies are plotted by open circles with the size indicating intensity. Calculated transition energies are plotted by curves. Lower panel: calculated matrix elements for transitions el1–hh1, el2–hh1, and el3–hh1 are plotted as functions of applied voltage.

Reference

[1] T. Kai, M. Morifuji, M. Yamaguchi and C. Hamaguchi, Semicond. Sci. & Technol. **9**, 1465 (1994).

Corresponding author: Masato Morifuji, Department of Electronic Engineering, Osaka University, Suita, Osaka 565-0871, Japan
phone: +81 6 6879 7766, fax: +81 6 6879 7753,
e-mail: morifuji@ele.eng.osaka-u.ac.jp

Damping of a Bloch oscillation by Zener tunneling

D. Meinhold[1], B. Rosam[1], F. Löser[1], V. G. Lyssenko[1], J. Zhang[2], F. Rossi[3] K. Köhler[4], and K. Leo[1]

[1] Institut für Angewandte Photophysik, Technische Universität Dresden, D-01069 Dresden, Germany
[2] Max-Planck-Institut für Physik komplexer Systeme D-01187 Dresden, Germany
[3] Instituto Nazionale per la Fisica della Materia (INFM) and Departimento di Fisica, Politecnico di Torino, 10129 Torino, Italy
[4] Fraunhofer-Institut für Angewandte Festkörperphysik, D-79108 Freiburg, Germany

There was a longstanding theoretical debate whether Bloch-oscillations (BO) or their energy-domain equivalent, the Wannier-Stark-ladder (WSL), exist, or whether they are suppressed by Zener-tunneling to higher bands. Both BO and WSL have recently been observed in semiconductor heterostructures, where coherence of the electronic ensemble was preserved longer than the Bloch-oscillation period. Surprisingly, the effect of *Zener tunneling*, a key high-field transport effect, was never observed or discussed in these publications.

Here, we present the first experimental study of the *temporal dynamics of Zener tunneling* [1]. To investigate this effect, we have designed a shallow 35 period 50/54 Å $GaAs/Al_{0.11}Ga_{0.89}As$ superlattice, which wells contain only one below-barrier electronic miniband. This structure is particularly suitable for a direct observation of the coupling of confined states to delocalized above-barrier states. By tuning the internal electric field, the coupling can be varied up to fields where confined and delocalized states energetically and spatially overlap.

By means of intraband polarization sensitive transient pump probe spectroscopy, we investigate the electric field induced changes in the dynamics of a *Bloch*-oscillating wavepacket. The exciting pump pulse was centered between hh_0 and hh_{-1}, creating a superposition of these states. The field-dependent *Bloch*-period is inversely proportional to the WSL spacing and was tuned from $900fs$ to $160fs$.

The upper right inset of figure 1 shows typical pump probe traces for three internal fields. The squares in the main plot show the decay times of the modulation. Surprisingly, at a threshold field of $24kV/cm$, we observe a sudden drop of the intraband decay time, accompanied by the observation of a *polarization revival* at around $1.8ps$. At this electric field, the confined WSL-states and delocalized above barrier states are in resonance and the BO wavepacket resonantly Zemer-tunnels into these delocalized states within a few BO periods. At this time, the electron density is spread over more than 10 wells. Nevertheless, coherence of the system is not completely lost and the initially created Wannier-Stark-wavepacket partially reconstitutes within the confinement. The observed inital drop in the ensemble coherence time is partly due to destructive polarization interference of the intraband polarization caused by the confined and the above barrier states. Beside the Bloch-beating, a beating of confined states with delocalized above barrier states is observed.

To model these experimental results qualitatively, we have calculated both the confined and the above barrier electronic states of a finite 35 well superlattice, subjected to an

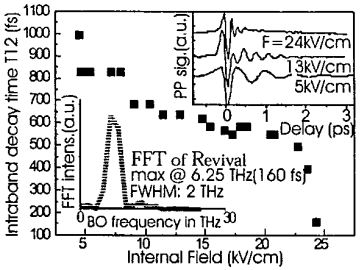

Figure 1: Experimental results: Damping of a *Bloch*-oscillating wavepacket due to coupling to continuum states. Upper right inset: Typical pump probe traces for different applied electric fields. Lower left inset: Fourier transform of trace for $24kV/cm$ from 1.5 to $2ps$. The measurements were performed at $10K$.

electric dc field. Our simulation shows that the initially confined electronic wavepacket travels out of the confinement to delocalized states and regroups after the revival time.

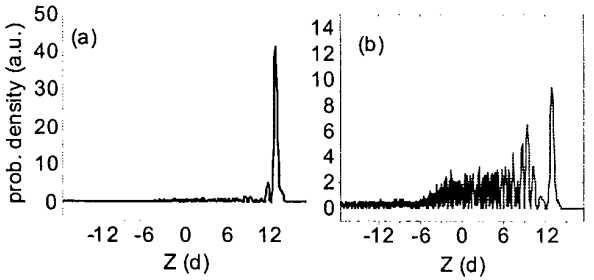

Figure 2: Theoretical results: For an electric field of $24kV/cm$, a) and b) show the square of the wavefunction amplitude of a confined state and an above barrier state, respectively, at spatial position of well 13. The energetic splitting of $1.7meV$ results in a beating period of $2.5ps$.

References

[1] B. Rosam, D. Meinhold, F. Löser, V. G. Lyssenko, S. Glutsch, F. Bechstedt, F. Rossi, K. Köhler, and K. Leo. Phys. Rev. Lett. **86**, 1307 (2001).

Corresponding author: Dirk Meinhold, Institut für Angewandte Photophysik, Technische Universität Dresden, D-01069 Dresden, Germany,
phone: +493514632464, fax: +493514637065,
email: meinhold@iapp.de, www.iapp.de

Semiconductor Heterojunctions in Polymer Semiconductor Diodes.

Richard Friend

University of Cambridge, Cavendish Laboratory, Madingley Road, Cambridge CB3 0HE, UK

Conjugated polymers now provide a class of processible, film-forming semiconductors and metals. We have worked on the development of the semiconductor physics of these materials by using them as the active components in a range of semiconductor devices. Polymer light-emitting diodes show particular promise, providing full colour range (red, green and blue), efficiency (above 20 lumen/W for green emitters). I will also discuss progress made on their application to displays, with integration with active-matrix TFT drive, and with patterned deposition using ink-jet printing techniques.

Polymer LED efficiency is considered to be controlled by ratio of singlet to triplet excitons formed by electron-hole capture, since the exchange energy for these strongly-bound excitons is large (> 0.7 eV), so that only singlet excitons can produce raditiative emission. The spin-independent ratio of 1:3 would limit efficiency to 25%, but several experiments now reported for polymers indicate a higher ratio, of nearer 50% singlets, and indicate therefore spin-dependent electron-hole capture.

Polymer-polymer heterojunctions can be exploited both in LEDs and also in polymer photovoltaic cells. An important approach which can be exploited with solution-processed polymers is the formation of de-mixed polymer blends formed with electron- and hole-accepting polymers, and we have recently studied the process of demixing in such systems. I will discuss conditions required for photo-induced charge transfer (as required for photovoltaic diode operation) or for energy transfer (as required for LEDs), and discuss the role played by interfaces between electrode and semiconducting polymer.

Polymer semiconductors can also be used in field-effect transistors, for which control of order is important if high field-effect mobilities are to be achieved, and I will discuss recent work in Cambridge in which mobilities up to 0.1 cm^2/Vs are measured. I will also present recent work on the use of ink-jet printing to fabricate all-polymer circuits.

Corresponding author: R. H. Friend, Cavendish Laboratory, Madingley Road, Cambridge CB3 0HE, UK, phone +44 1223 337218, fax. +44 1223 353397, e-mail rhf10@cam.ac.uk

"2D electron physics in organic molecular crystals"

Bertram Batlogg, ETH Zürich, Switzerland*

Organic molecular crystals of unprecedented quality offer new opportunities to study many-body physics in new parameter spaces and to explore potential applications. They are the basis for fabricating field-effect devices where the carrier concentration in the channel can be varied over a wide range. Through this electric field-induced charge carrier "doping", we transform acenes, fullerenes and other molecular crystals continuously from their highly insulating into the superconducting state. In the talk, we will discuss the various ground states that are encountered.

In particular we will first study the nature of the charge carriers in the dilute limit. Their low temperature mobility can reach very high values, in excess of 10^5 cm^2/Vs, and their mean free path several tens of micrometer. The electron-electron interaction is more than an order of magnitude more pronounced than in GaAs at comparable densities, leading to highly stable Quantum Hall states that can be observed up to relatively high temperatures. Of equal importance is the electron-lattice interaction, which leads to a drastic mass enhancement of the charge carriers upon increase of the temperature. Various experiments tell us about the interaction spectrum. At low temperatures, the mass is near that of free electrons and increases to 20-40 m_e at ambient temperature. Concomitant with the temperature-induced mass enhancement is a reduction of the effective bandwidth that becomes smaller than the thermal energy not far above room temperature. Consequently, the coherent band transport crosses over to an incoherent hopping motion of the charges. The low-temperature quasiparticles are thus the result of many-body interactions.

When the density of these charge carriers is increased a 2D metallic sheet is formed that can undergo a transition into the superconducting state. In the acenes, T_cs up to ~4K are observed. The most interesting application of this technique is on C_{60}, where the induced holes form a superconducting state below 52K. As the gate-field controls the carrier density in the channel one has the option of laterally patterning the superconducting carrier density. This has been used to create Josephson junctions with a controllable weak link.

Work done in collaboration with: J. Hendrik Schön and Christian Kloc, Bell Labs
* Also at Bell Labs, Lucent Technologies, Murray Hill, NJ

NANOTECHNOLOGY APPROACHES TO SELF-ORGANIZED BIOMOLECULAR ELECTRONIC DEVICES

Roberto Cingolani
INFM- University of Lecce, Italy

We discuss the problem of interconnecting biomolecules with metallic nanopatterns to fabricate planar electronic devices.
The self organization of biomolecules such as DNA basis (deoxi-guanosines) or metalloproteins (Azurin) is exploited to form solid state films which are deposited in planar two or three terminal devices.
The solid state biomolecular films exhibit a photocurrent experiments.

We show that the device operation is influenced primarily by the self organization length of the solid state biomolecular film and by the width of the metallic gap of the two terminal devices. Narrow gaps (below 60 nm) probe individual ordered clusters of self organized molecules and exhibit a clear diode characteristic, whose polarity is given by the intrinsic dipole of the molecular self assembled phase.

Wider gaps (>120 nm), are influenced by the disorder of the self assembled film, and show a clear metal/semiconductor/metal behavior, with photosensitivity as high as 1 W/A.

The issues of aging, scalability and device performances will be addressed at the end of the talk.

Polariton Scattering and Condensation in Semiconductor Microcavities

Jeremy J. Baumberg

Department of Physics & Astronomy and Electronics & Computer Science, University of Southampton, Southampton SO17 1BJ, UK
j.j.baumberg@soton.ac.uk

Technological advances in semiconductor light emitters in recent years have been primed by rapid developments in the field of wavelength scale structures such as LED's, VCSEL's and quantum microcavities. By highly controlled epitaxial growth it is possible to manipulate both electronic and photonic properties in the same structure. In semiconductor microcavities the exciton confined in the quantum well is strongly coupled to photon confined between highly reflective Bragg mirrors producing two new eigenstates of the system called polaritons. These new quasiparticles obey a completely new modified dispersion relation that allows for intense new *parametric* scattering processes to occur[1,2].

It has been shown that these new scattering processes are also possible under resonant *CW* excitation, despite the much weaker intensities achieved as compared to the pulsed excitation. This scattering mechanism is extremely efficient, is stimulated by final state occupation and provides a very efficient channel for polariton relaxation[1-5]. The resulting vertical-cavity optical parametric oscillator (or 'μOPO') has a lower threshold than any VCSEL, and emits beams at a variety of different angles. We will discuss the implications for building lasers based on these new scattering processes, and suggest that ultra-low thresholds can be achieved.

The macroscopic occupation of polaritons possessing a common phase provides a system which is the optical analogue of a condensate. We suggest a number of new phenomena that might be observed in this system, such as the Josephson effect. Such experiments presage coherent devices based on the vastly enhanced solid-state coherences possible from such quantum engineering.

References

[1] P.G. Savvidis *et al.*, Phys. Rev. Lett. **84**, 1547 (2000).
[2] C. Ciuti *et al.*, Phys. Rev. B **62**, R4825 (2000).
[3] R.M. Stevenson *et al*, Phys. Rev. Lett. **85**, 3680 (2000).
[4] P.G. Savvidis *et al.*, Phys.Rev.B **62**, R13278 (2000).
[5] J.J. Baumberg *et al.*, Phys. Rev. B **62**, R16247 (2000).

Time resolved stimulated emission in excitonic semiconductor microcavities.

J. Bloch, B. Sermage, C. Jacquot, P. Senellart and V. Thierry-Mieg

LPN-CNRS 196 Henri Ravera, BP 29, 92222 Bagneux Cedex

The possibility of obtaining stimulated processes in semiconductor microcavities presenting a strong coupling between QW excitons and the optical cavity mode has excited many laboratories[1-3] because the stimulation is due to polariton states occupation which are partly excitons and then matter.

People have observed stimulated emission in microcavities but the fact that the microcavity is still in the strong coupling regime is controversial. To elucidate this question, we have done two series of time and spectral luminescence measurement either with an excitation energy above the stop-band or with a resonant excitation energy. In both cases, the sample was at low temperature (10 K) and we have studied two III-V microcavities, one with a Rabi splitting of 3.6 meV and the other one with 12 meV.

In the first series of experiment, we excite on a reflectivity minimum above the stop band and we look with a streak camera to the time resolved spectrum of the emission at k=0 as a function of excitation power. In strong coupling regime and at low excitation, we observe a linear and a quadratic variation of the luminescence intensity. At higher excitation we observe a progressive decrease of the Rabi splitting which becomes zero well before the threshold of the stimulated emission (Fig. 1). This is due to the fact that we create a large population of exciton in the reservoir where the lifetime is large. This population lowers the exciton oscillator strength by phase space occupation. This decrease to zero of the Rabi splitting before lasing threshold has been observed on the two microcavities and for different detunings.

In the second series of experiments, we excite resonantly at the magic angle[3] with a pulse laser and we observe a strong stimulated emission with an excitation power dependence much more than quadratic (Fig. 2) and yet the microcavity is still in the strong coupling regime (no shift of the luminescence wavelength). The laser emission is delayed relative to the excitation pulse due to the time necessary to create a polariton population at k = 0.

[1] A. Imamoglu, R. J. Ram, S. Pau and Y. Yamamoto, Phys. Rev. A, 53, 4250 (1996).

[2] L.S. Dang, D. Heger, R. André, F. Bœuf and R. Romestain, Phys. Rev. Lett., 81, 3920 (1998).

[3] P.G. Savvidis, J.J. Baumberg, R. M. Stevenson, M. S. Skolnick, D. M. Whittaker and J. S. Roberts, Phys. Rev. Lett., 84, 1547 (2000).

a) 50 μW b) 100 μW c) 200 μW d) 500 μW

Fig. 1. Time resolved spectra of the luminescence from the first microcavity (R = 3.6 meV) at zero detuning for non resonant excitation and for increasing excitation powers. The overall time range (vertical axis oriented downside) is 2 ns and the overall spectral range (horizontal axis oriented right side) is 19 meV. One can observe the luminescence of the upper and lower branches at k = 0. The fact they get closer at short times mean that the Rabi splitting get smaller. On image d), the microcavity is close to threshold.

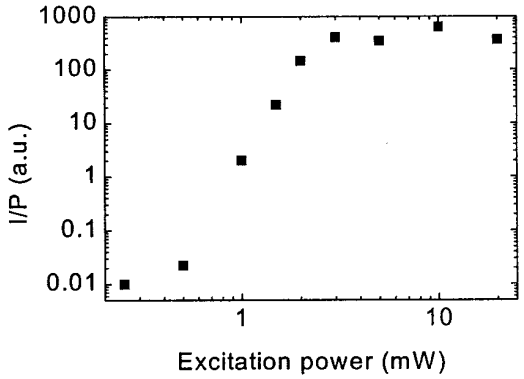

Fig. 2. Variation of the luminescence intensity at k = 0 divided by the excitation power for an excitation at the magic angle.

Enhancement of exciton exchange energy splitting by the confined electric field in photonic wires

G.Dasbach[1], A.A.Dremin[1,2], M. Bayer[1], N.A.Gippius[1,3], V. D. Kulakovskii[1,2], A. Forchel[1]

[1] Technische Physik, Universität Würzburg, Am Hubland, 97074 Würzburg, Germany
[2] Institute of Solid State Physics, RAS, 142432 Chernogolovka, Russia
[3] General Physics Institute, RAS, 117333 Moscow, Russia

Non-linear amplification processes in a semiconductor microcavity in the strong coupling regime have attracted considerable interest recently. Here we report pump-and-probe studies on photonic wires. We observe pronounced quantum beats in the differential cavity transmission with periods that decrease with increasing excitation power. The beats which are absent for a planar cavity appear over delay times of up to 60 ps indicating long living coherence in the system. From these observations we tentatively assign the beats to a coherent superposition of the bright excitons which are split due to the long ranged exchange interaction.

The photonic wire structures with widths of 3 μm were fabricated by lithography and etching from a planar microcavity. In the optical experiments the pump beam resonantly excited polaritons in the lower polariton branch only. The excitation with co-circularly polarized pump and probe pulses results in a narrowing and strong enhancement of the transmission peak of the lower polariton branch, independent of the pump angle. The amplification process can be identified as a 'hole burning' effect in the quantum well absorption, due to a filling of localized excitonic states. In the planar microcavity system we observe no amplification for anti-circular excitation, giving prove of the phase space filling argument mentioned above. In the photonic wires a breaking of theses strict polarization selection rules is observed and we find an increase of the differential transmission for co- as well as for anti-circular excitation.

In addition to the broken polarization selection rules the decay is superimposed by an oscillation, where the anti-circular signal is shifted by π with respect to the oscillation observed under co-circular excitation. Inline with the beating in the differential transmission we find an oscillation of the spectral position of the lower polariton branch, as can be seen in Fig. 1. The solid (open) symbols mark the spectral position of the lower polariton line for co-circular (anti-circular) excitation as function of the delay. The solid trace displays the averaged spectral position, which shows no oscillation and agrees with the behaviour typical for an unpatterned microcavity. The beats are observed even after 50 ps delay corresponding to long decoherence times in the system, which is a clear indication that spin degrees of localized excitons might be involved. We note that the energy splitting between the two coherently excited states depends on the pump excitation power: It decreases with decreasing excitation power from about 130 μeV for 20 mW excitation to 60 μeV for 5 mW, as determined from the data at short delays. For even lower excitation the beat period becomes longer than the decay time of the differential transmission so that the splitting can no longer be determined.

Due to the patterning of the cavity, the strain in lateral direction is partially released. The strain release results in an asymmetry of the localization potential for excitons. Such asymmetries result in a splitting of the optically active exciton doublet with the spin J=±1 into two singlets, $|+1\rangle \pm |-1\rangle$, by the long range electron-hole exchange interaction. This exchange splitting is the only splitting that we envisage as origin for the observed beatings. The state splitting for excitons that are only rather weakly localized in the present quantum well typically would hardly exceed $\sim$ 20 μeV leading to a beat periode of more than hundred ps.

The remarkable magnitude of the energy splitting and its power dependence observed here indicate an enhancement of the exciton exchange energy splitting by the confined electric field. Further, the long range exchange must increase with increasing cavity occupation. This suggestion is supported by the pump power density dependence of the energy splitting. Further, for high excitation powers the oscillation periode is not constant as function of delay but increases with increasing delay, i.e. with decreasing cavity occupation.

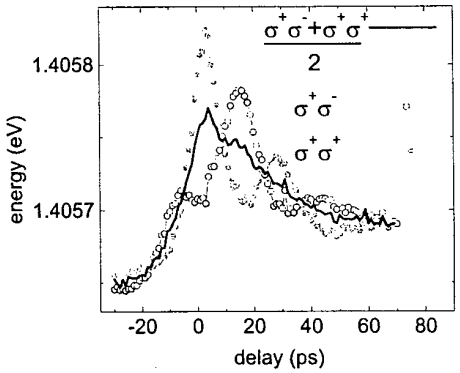

Figure 1: Spectral position of the lower polariton branch as function of delay for co-circular (solid symbols) and anti-circular (open symbols) excitation (P_{pump} = 23mW) conditions.

Corresponding author: Gregor Dasbach, Technische Physik, Universität Würzburg, Am Hubland, 97074 Würzburg, Germany.
phone: +49 931 888 5883, Fax: +49 931 888 5143,
email: dasbach@physik.uni-wuerzburg.de

Enhanced Rabi Splitting in a Superlattice-Microcavity System

J. H. Dickerson[1], E. E. Mendez[1], S. Manotas[2], F. Agulló-Rueda[2], C. Pecharromán[2], and A. A. Allerman[3]

[1]State University of New York at Stony Brook, Stony Brook, NY 11794-3800, USA
[2]Instituto de Ciencia de Materiales de Madrid, CSIC, Cantoblanco, 28049 Madrid, Spain
[3]Sandia National Laboratory, Albuquerque, NM 87185, USA

We have observed a large coupling between the photonic mode of a microcavity and Stark-localized excitons from a superlattice embedded in it. The coupling is significantly stronger than in comparable microcavities containing quantum wells at the antinodes only. This enhancement is explained by the large density of excitons in a superlattice combined with their large binding energy once they are localized by an electric field.

Strong photon-exciton coupling in a microcavity is manifested as a Rabi splitting in features of the optical spectra. Since the magnitude of that splitting is proportional to the square root of the product of the oscillator strength and the linear density of excitons, there have been many efforts to increase either of the two factors, e.g., by using II-VI compounds as base materials or by filling the entire cavity with a semiconductor in "bulk." The drawback of this latter approach, however, is that it trades a large excitonic density for a small binding energy and, correspondingly, a small oscillator strength.

We have overcome this limitation by filling the entire cavity with a narrow-barrier superlattice subjected to an electric field. The superlattice maximizes the density of quantum wells while the field enhances the exciton binding energy through Wannier-Stark localization of the superlattice states. The Rabi splitting was determined primarily from reflectivity measurements on various spots of the wafers or as a function of temperature. The microcavities consisted of two distributed Bragg reflector mirrors flanking a 30 period 84Å GaAs / 20Å $Al_{.25}Ga_{.75}As$ superlattice, which formed the active region of a 3λ/2 cavity. The mirrors were doped to form a *p-i-n* configuration that provided the internal electric field to induce Wannier-Stark localization in the superlattice.

Using this scheme we have found a distinct Rabi splitting of 8.5 meV at room temperature and of 9.5 meV at T = 238K, which represents almost a 50% increase of the splitting in a comparable optical structure in which quantum wells were placed exclusively at the antinodes. The observed enhancement of the Rabi splitting is consistent with a simple simulation of the reflectivity for a set of 30 GaAs absorbers (each 84Å thick and 20Å apart from each other) distributed throughout a cavity defined by two dielectric mirrors.

Corresponding author: Emilio Mendez, Department of Physics and Astronomy,
State University of New York at Stony Brook, Stony Brook, NY 11794-3800, USA
Phone: 1 631 632 8065, Fax: 1 631 632 8774
Email: emendez@notes.cc.sunysb.edu

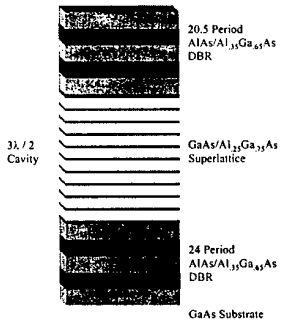

Figure 1: Two Distributed Bragg reflector mirrors, comprised of alternating λ/4 layers of 689Å AlAs and 602Å $Al_{.35}Ga_{.65}As$, defining a 3λ/2 cavity formed by an 84Å GaAs / 20Å $Al_{.25}Ga_{.75}As$ superlattice. The top mirror is p-doped, and the bottom mirror is n-doped.

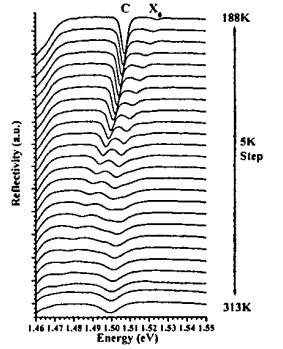

Figure 2: Reflectivity spectra of the microcavity across a range of temperatures from 188K to 313K. The spectra are shifted vertically in a cascade format for clarity. Two anticrossings are observable among the spectra: Δ_1 at 238K, and Δ_2 at 253K.

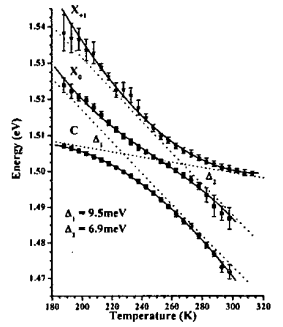

Figure 3: The energies of the reflectivity dips plotted as functions of temperature. The two rapidly changing modes correspond to 0 (main, X_0) and +1 (X_{+1}) heavy-hole exciton transitions of the Stark ladder; the more gradually changing mode corresponds to the cavity. The dotted lines indicate the temperature trends of the uncoupled cavity mode and the superlattice modes. The magnitudes of the Rabi splittings are Δ_1=9.5meV and Δ_2=6.9meV.

Strong Coupling of CdS Quantum Dots to Confined Photonic Modes in ZnSe-based Microcavities

T. Tawara, I. Suemune, and H. Kumano

Research Institute for Electronic Science, Hokkaido University, Kita-12, Nishi-6, Sapporo 060-0812, Japan

1. Introduction

Interaction of atoms with photonic fields in an optical cavity has attracted much attention to study and control radiative recombination processes [1,2]. Semiconductor optical cavities most extensively studied up to now is the microcavities based on distributed Bragg reflectors (DBRs) [3]. Two regimes of the interactions in the microcavities have been discussed, i.e., weak coupling and strong coupling regimes. The latter case shows especially interesting features such as Rabi vacuum-field splitting and exciton-polariton properties [4]. Quantum dots (QDs) are a kind of artificial atoms and it is an interesting issue whether the strong coupling regime can be observed by the interaction of QDs with photonic fields in a microcavity. Such a problem was dealt with theoretically for InAs QDs embedded in a pillar microcavity, but the conclusion was not favourable for the observation of the strong coupling [5]. Accordingly no experimental observations of strong coupling of QDs in microcavities have been reported so far to our knowledge.

In this paper, the possibility of the strong coupling regime is studied with CdS QDs embedded in ZnSe-based microcavities. CdS has the bulk exciton binding energy of ~30meV, which is much larger than 4.2meV of GaAs and 1.7meV of InAs, and therefore the larger oscillator strength than that of GaAs or InAs. This positive materials factor may open the door to observe the strong coupling of QDs with the photonic fields confined in a microcavity. The growth of ZnSe-based distributed Bragg reflectors (DBR) [6,7] and of monolithic microcavities based on the DBRs [8] has been studied so far for this purpose. The demonstration of the strong coupling regime with CdS QDs will be reported in this work.

2. Experiment

ZnSe-based microcavities were grown by metalorganic vapor-phase epitaxy on (001) GaAs substrates. The DBR consists of periodic layers of ZnSe and ZnSe (9.5Å)/MgS (32.0Å) superlattices each with a quarter-wavelegth thickness. Just 5 periods of the DBR exhibited the reflectivity of 92% [8]. A ZnSe wavelength (λ) cavity was formed with 4.5-periods bottom DBR and 4 periods top DBR and the clear cavity resonance mode was observed as shown in Fig. 1. CdS QDs were embedded at the antinode of the wavelength (λ) cavities. The effectively-2-monolayers-thick CdS was deposited, which resulted in the QDs with the average height of ~6nm, diameter of ~25nm, and the density of ~3×10^{9}cm^{-2}as shown in Fig. 2. The two cases of 5 stacks and 31 stacks of the CdS QDs embedded in the λ cavities were studied with photoluminescence (PL) spectrum as well as reflection spectrum measurements at ~20K.

3. Results and Discussions

In the case of the 5-stacks of the CdS QDs, the detuning-properties were reasonably explained with the weak coupling regime. On the other hand, the case of the 31-stacks of the CdS QDs embedded in theλcavity showed the splitting of the PL peaks around the peak expected for the luminescence from the QDs. The result is shown in Fig. 3, where the splitting systematically changes with the detuning energy measured from the cavity resonance mode. The results are summarized in Fig. 4 with open circles and it could be fitted with the absorption coefficient of 1×10^{5}cm^{-1} and the the radiative transition linewidth of 0.5meV for the CdS QDs as shown with the solid lines in Fig. 4. The successful observation of the Rabi splitting of ~3meV in the latter case will be due to the increase of the Rabi splitting with the increased number of the QD oscillators as well as the larger oscillator strength of CdS. This, to our knowledge, is the first observation of the strong coupling regime of QDs in microcavities.

References

[1] E. M. Purcell, Phys. Rev. 69, 681 (1946).
[2] D. Kleppner, Phys. Rev. Lett. 47, 233 (1981).
[3] C. Weisbuch, M. Nishioka, A. Ishikawa, and Y. Arakawa, Phys. Rev. Lett. 69, 3314 (1992).
[4] V. Savona, L. C. Andreani, P. Schwendimann, and A. Quattropani, Solid State Communications 93, 733 (1995).
[5] L. C. Andreani, G. Panzarini, and J.-M. Gerard, Phys. Rev. B 60, 13279 (1999).
[6] T. Tawara, M. Arita, K. Uesugi, and I. Suemune, J. Cryst. Growth 184/185, 777 (1998).
[7] T. Tawara, I. Suemune, S. Tanaka, J. Cryst. Growth 214/215, 1019 (2000).
[8] T. Tawara, H. Yoshida, T. Yogo, S. Tanaka, and I. Suemune, J. Cryst. Growth 221, 699 (2000).

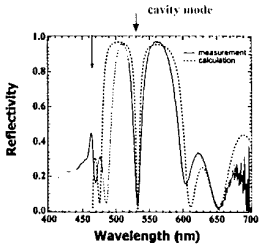

Fig.1 Reflection spectrum of a ZnSe-based microcavity.

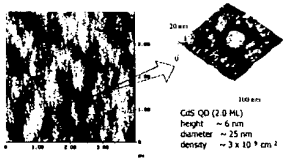

Fig.2 CdS quantum dots formed with deposition of 2-ML of CdS on ZnSe.

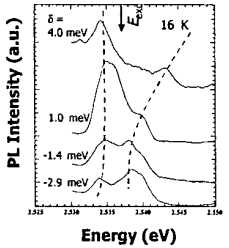

Fig.3 Splitting of the PL peaks observed from 31-stack of CdS quantum dots embeded in a microcavity.

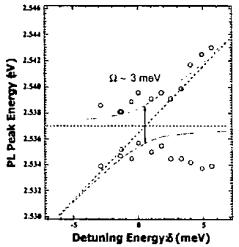

Fig.4 Summary of the PL peaks observed from the microcavity. Open circles are measured peak energies and the solid lines are fit with a model assuming the strong coupling.

Corresponding author: I. Suemune, Research Institute for Electronic Science, Hokkaido University, Kita-12, Nishi-6, Sapporo 060-0812, Japan
Phone:+81-11-706-2878, Fax: +81-11-706-4973 E-mail address: isuemune@es.hokudai.ac.jp

Optical Double Resonance of Electronic Raman Scattering in a AlAs-AlGaAs Microcavity

T. Kipp, L. Rolf, C. Schüller, D. Endler, Ch. Heyn, D. Heitmann,

Institut für Angewandte Physik und Zentrum für Mikrostrukturforschung,
Universität Hamburg, Jungiusstraße 11. D-20355 Hamburg, Germany

We report on Raman spectroscopy of modulation-doped quantum wells embedded inside a planar semiconductor microcavity. We have observed for the first time an optical double resonance in Raman experiments on *electronic* excitations of the two-dimensional electron system (2DES) inside the cavity. In double resonance, the Raman signals are enhanced by about three orders of magnitude compared to the single-resonance case.

The molecular-beam-epitaxy grown microcavity sample consists of a $Al_{0.2}Ga_{0.8}As$ λ cavity (spacer) with AlAs-$Al_{0.4}Ga_{0.6}As$ quarter-wave layers on both sides, which act as distributed Bragg reflectors. In the center of the spacer, there is a one-sided modulation-doped 30-nm-wide GaAs quantum well. The widths of the microcavity layers are chosen so that the cavity-mode energy is below the GaAs bandgap. This allows us to discriminate in the Raman experiments between optical resonances and electronic resonances of the quantum well. For simultaneous transmission and Raman experiments, the GaAs substrate was completely removed from the back side of the sample. By transmission experiments we monitor the cavity mode position.

We demonstrate that the Raman intensities of the scattering by the intersubband charge-density excitation (CDE) and the spin-density excitation (SDE) of the 2DES are enhanced when the incident laser energy is in resonance with the cavity mode, i.e., an optical single resonance. In these measurements we can definitely exclude an intrinsic *electronic* resonance of the quantum well, because the first excitonic transition in the quantum well occurs at an energy of 25 meV higher than the energy of the cavity mode.

The energy of the cavity mode increases with increasing angle of the incident light with respect to the growth axis. Therefore, by using specific angles for the incident and scattered light, both the exciting laser and the scattered photons can be tuned into resonance with a cavity mode, i.e., an optical double resonance is achieved. Double resonant Raman scattering has so far only been observed for optical phonons in undoped structures (Fainstein et al., PRL **75**, 3764 (1995)).

Our setup allowed to continuously tune the difference in the energies of the cavity modes for incident and scattered light of up to 30 meV. We were therefore able to detect both the CDE and SDE, which have energies of about 26.5 meV and 22 meV, respectively, under optical double resonant conditions. The experiment shows that these electronic intersubband excitations can be enhanced by about three orders of magnitude, compared to the single-resonance case, where only the laser photons are in resonance with the cavity. Moreover, since we are using a high-quality cavity with a cavity mode width smaller than the widths of the electronic excitations, we are able to selectively enhance different parts of the excitations.

We acknowledge financial support by the German Science foundation through SFB 508 and GrK's "Nanostructured Solids" and "Localized Fields".

Corresponding author: Christian Schüller,
Institut für Angewandte Physik und Zentrum für Mikrostrukturforschung,
Universität Hamburg, Jungiusstraße 11, D-20355 Hamburg, Germany.
phone: +49 40 42838-5308, Fax: +49 40 42838-6332,
email: schueller@physnet.uni-hamburg.de

Coherence properties of single self-organized quantum dots

T. Flissikowski, A. Hundt and F. Henneberger

Institut für Physik, Humboldt Universität zu Berlin,
Invalidenstraße 110, D-10115 Berlin

We report on the observation of quantum beats in the secondary emission from a single quantum dot (QD). These beats, associated with single-photon interference, carry direct information about the coherence of the electronic state behind the emission. The high-quality CdSe/ZnSe QD structures were grown by molecular beam epitaxy. Confocal spectroscopy in combination with sample texturing allows access to individual QDs. A typical PL line is depicted in Fig. 1. The 70 μeV width is resolution limited, demonstrating an exceedingly small homogeneous broadening of the ground-state exciton $|X_0\rangle$. No resolvable spectral line drift or blinking is observed within typical detection periods (up to 10 min). Even when extending the observation over several hours, the long-term line shift is below 150 μeV (see see inset Fig.1).

For QDs with symmetry below D_{2d}, $|X_0\rangle$ is split by the electron-hole exchange interaction in two levels with dipole moments oriented along the two non-equivalent in-plane QD axes. [1] Indeed many QDs with a higher degree of in-plane anisotropy than in Fig. 1 are found, where this splitting is directly manifested by a doublet character of the PL line. Variation of the energy splitting (40 μeV < $\Delta E_{ex} \leq$ 450 μeV) signifies considerable fluctuations of the QD symmetry. The doublet of the $|X_0\rangle$ exciton in conjunction with its radiative coupling to the total ground-state represents a V-type system, where quantum beats in the spontaneous emission may occur. [2] However, as the components are cross-polarized, interference is only possibly by projecting the polarizations on a common axis before detection. The set-up used for the measurements in Fig. 2 consists of two cross-aligned polarizers for excitation ($\vec{e}_0$) and detection ($\vec{e}_A$), where the angle φ_0 between $\vec{e}_0$ ($\vec{e}_A$) and the fundamental QD axes, oriented along [1,1,0] ([1, $\bar{1}$,0]), is tunable. For quasi-resonant phonon-assisted excitation, clear beating oscillations are observed (Fig. 2). The beating period of 322 ps corresponds to a fine structure splitting of $\Delta E_{ex} = \hbar(\omega_x - \omega_y)$ = 13 μeV, not resolvable in the spectral domain. The signal variation with angle φ_0 is in full accord with the polarization characteristics of the system. During relaxation of the primarily excited phonon-exciton complex, the dipole orientation is randomized, however without spoiling totally the coherence. Once the exciton has reached the groundstate no further decoherence occurs. [3] We conclude that the coherence time for the QD exciton is much longer than its life-time.

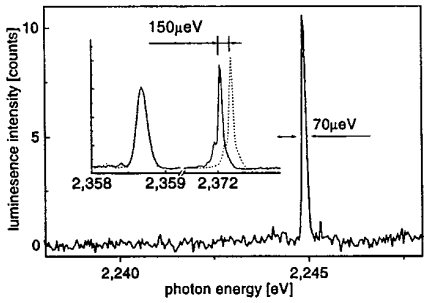

Fig. 1: PL spectra of a single CdSe/ZnSe QD from a 150x150nm island at T = 5 K. Inset: PL lines of two QDs under cw-excitation, right after starting the measurement (full line) and 5 h later (dotted line).

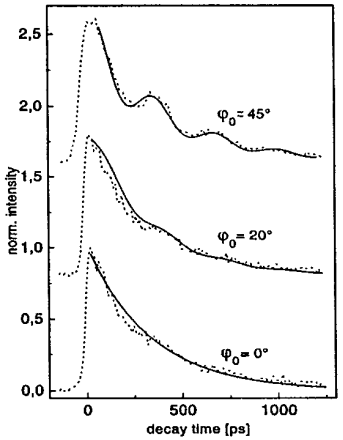

Fig. 2: PL transients of an single quantum dot for excitation at 1-LO phonon resonance for three polarization configuration. (dotted curves: experiment, full lines: fit)

References

[1] D. Gammon et al., Phys. Rev. Lett. **76**, 3005 (1996); V. D. Kulakovskii et al., Phys. Rev. Lett. **82**, 1780 (1999); J. Puls et al., Phys. Rev. B **60**, R16303 (1999).

[2] P. Meystre, M. Sargent III : Elements of Quantum Optics, Second Edition, Springer Berlin, 1991; V. Langer et al., Phys. Rev. Lett. **64**, 854 (1990)

[3] T. Flissikowski et al., accepted for publication in Phys. Rev. Lett.

Corresponding author: Fritz Henneberger, Institut f. Physik, Humboldt-Universität zu Berlin
Invalidenstraße 110, 10115 Berlin, Germany Tel.: +49 – 30 – 2093 7670,
FAX: +49 – 30 –2093 7886,E-mail: henne@physik.hu-berlin.de

Artificial atoms and molecules of charge carriers in positively and negatively charged quantum dots

D.V. Regelman[1], D.Gershoni[1], E. Ehrenfreund[1], W.V. Schoenfeld[2], P.M. Petroff[2]

[1]Physics Department, Technion - Israel Institute of Technology, Haifa, 32000, Israel
[2]Materials Department, University of California, Santa Barbara, CA 93106 USA

We report on the first observation of photoluminescence from both positive and negative charge states of a single semiconductor quantum dot.

For this purpose we designed a structure enabling optical injection of a controlled unequal number of negative electrons and positive holes into an isolated InGaAs quantum dot embedded in a GaAs/AlAs mixed type quantum well structure.[1] With the structure that we designed, using all optical means, we were able to switch between the discrete charged states -3, -2, -1, 0, +1 and +2 of single quantum dots. The carriers that we inject optically, form confined collective 'artificial atoms and molecules' states in the QD. Radiative e-h pair recombination takes place after such a collective few carrier state relaxes to its ground state.

We resolve spectrally and temporally the photoluminescence from the optically excited quantum dot and use it to determine the collective states from which it originated. In particular, we identify collective states, which contain charge of one type, coupled to few charges of the other type. These states can be viewed as the artificial analog of charged atoms such as H^-, H^{-2}, H^{-3}, and charged molecules such as H_2^+ and H_3^{+2}.[2]

We use careful comparison between the PL emission spectra for a single In(Ga)As/GaAs quantum dot in this mixed type structure (Fig 1b) and those of a single quantum dot in a GaAs layer (Fig. 1a). Using time-resolved spectroscopy and a comparison between cw and pulse-excited PL spectra [3] we were able to accurately determine the charge state of the single QDs at a given excitation intensity level.

We demonstrate that, unlike the case in negatively charged QDs, and unlike higher dimensionality charged collective states [4], our positively charged dots show an **increase** in their PL emission energy relative to the emission from charge-neutral dots. Thus, the emission due to radiative recombination of an e-h pair from a positively charged dot results in a PL blue shift.

Our model calculations reveal that this trend originates from the larger spatial localization of the hole-wavefunction with respect to that of the electron. We use our experimental results to estimate the size difference between the hole and electron envelope wavefunctions. With this estimation, our calculations agree well with the measured results.

Though the calculations are quite intense, they can be essentially summarized as follows: The energy associated with hole-hole repulsion is larger than the energy associated with electron-hole attraction, while the last one is larger than the energy associated with electron-electron repulsion.[5] Therefore, in the presently studied QDs, as already alluded to previously [6,7], excess electrons decrease (red shift) the recombination energy, while excess holes increase (blue shift) it.

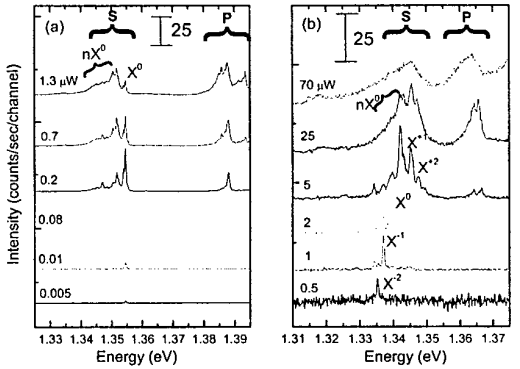

Fig 1 Steady state PL spectra of single quantum dots for increasing excitation intensities. (a) From a neutral dot (the control sample) and (b) from a charged dot (mixed type sample). The discrete PL line due to the recombination of neutral excitons (X^0, nX^0), negatively charged (X^{-1}) and positively charged X^{+1} excitons are marked in the figures.

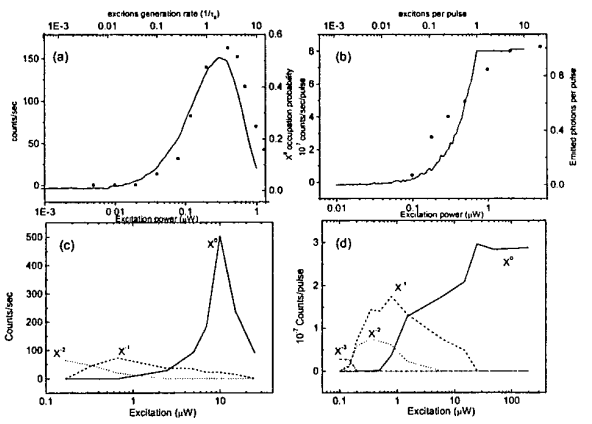

Fig.2:PL intensity of the various spectral lines as a function of excitation intensity. (a) The neutral X^0 line from the control sample at cw excitation. (b) Same as (a) at pulse excitation. The solid lines in the figures represent our rate equation model calculations. Note the typical difference between cw and pulsed excitation. Whereas in the first case the PL intensity goes through a clear maximum and then decreases with further increase of the excitation density, in the second case it saturates and remains constant. The negatively charged and the neutral PL lines from the mixed type dots for cw (c) and for pulse excitation (d). Note the clear difference between the PL lines from negatively charged states and those from neutral states. We use these differences for determining the origin of the various PL lines.

References

[1] W.V.Schoenfeld, T.Lundstrom, P.M.Petroff, D.Gershoni, *Appl. Phys. Lett.***70**, 2194 (1999)

[2] Verkade, J.G. "A pictorial approach to molecular bonding", (Springler-Verlag, New-York 1986)

[3] E. Dekel, et al Phys. Rev. B **62**, 11038,(2000).

[4] S. Glasber, G. Finkelstein, H. Shtrikman, I. Bar-Joseph, *Phys. Rev. B* **59**, R10425, (1999)

[5] Ph. Lelong, and G. Bastard *Solid State Commun.* **98**, 819-823 (1996).

[6] L. Landin, et al, *Science* **280**, 162-264 (1998).

[7] J. J. Finley, et al Phys. Rev. B **63**, 07307, (2001)

Corresponding author: David Gershoni, Physics Department, Technion, Haifa, 32000, Israel.
phone: +97248293693, Fax: +972 48235107
email: dg@physics.technion.ac.il

Optical spectroscopy of single quantum dot molecules under applied electric field

I. Shtrichman, B. D. Gerardot, C. Metzner, W. V. Schoenfeld, P. M. Petroff
Materials Department, University of California, Santa Barbara, CA. 93106, USA

Electronically coupled quantum dot pairs (QD molecules) have been proposed to operate as quantum gates, the basic building blocks for quantum computation schemes [1]. In recent years, several attempts have been made to experimentally realize such a system [2, 3]. The coupling between two QDs is highly sensitive to the relative energy levels of the dots. These energies are fixed for each QD by its dimensions and material composition. By varying an electric field between the two QDs, one can bring the electronic states of the dots into and out of resonance. In this work we study the coupling between adjacent quantum dots by measuring the photoluminescence (PL) spectra under applied external electric field. We compare the spectra of a single QD, a single QD molecule, and a single electronically uncoupled QD pair.

The three MBE grown samples contain an intrinsic layer embedded between two n-doped GaAs layers, which serve as the front and back electrodes of the device (n-i-n structure). The intrinsic GaAs layer contains either a single InAs QD layer or two vertically stacked strain coupled QD layers with different separation (45 or 150 Å). Two GaAs/AlAs superlattice barriers surround the intrinsic GaAs layer to reduce current flow through the device. The samples were not rotated during the InAs deposition, and therefore a gradient in the self-assembled QDs density was formed across the wafers.

We use a micro-PL setup with spatial resolution of 1 μm and the low QD density parts of the samples (~ 10^7 cm^{-2}) to optically isolate and study a single QD pair. A continues wave Ti:Sapphire laser, operating at an energy below the GaAs barrier, was used to excite the samples through the front semi-transparent metal gate. A short monochromator (0.19 m) combined with a CCD array was used to detect the luminescence.

In Fig. 1a we show the PL spectra from the high dot density part (~ 10^{10} cm^{-2}) of the 45 Å coupled QDs sample for different excitation intensities with no applied voltage. The spectra are vertically displaced for clarity, and their low energy part marks their zero intensity. We identify the two peaks, which dominate the spectrum at the lowest excitation powers, as the inhomogeneously broadened luminescence from the QD molecules ensemble. The first peak (QD1) has the same energy as in the single QD sample (not shown), and therefore we relate it to the seed, first grown layer of QDs that form the molecules. We relate the second peak (QD2) to the second, strain coupled layer of QDs. We attribute the separation of ~ 90 meV between the two dots ground states to: a) their unintentional size and composition differences, and b) the different strain field that they induce on each other. Several excited states of QD1 and QD2, separated by 40 meV and 25 meV, respectively, are observed in the spectra as the excitation power increases.

In Fig. 1b we display the integrated luminescence intensity of the different states, which are resolved using a multi-Gaussian fit to each spectrum, as a function of the excitation intensity. We find that the PL intensity of the QD1 ensemble ground state grows linearly with the excitation intensity over 6 orders of magnitude, in perfect agreement with the single QD sample. In contrast, the ground state of QD2 saturates at much lower powers. We conclude that this phenomenon is due to transfer of one type of carrier from a low level of QD2 to one of the high levels of QD1. In the PL spectra of the 150 Å strain-coupled QDs sample (not shown) we also identify the two different dots, which are separated by ~ 70 meV. In this case, however, the two dots in the pair behave exactly as two individual QDs, and no coupling between them is found.

In the micro-PL spectra of a single QD we observe, as the excitation intensity is raised, a number of sharp peaks in the spectra in agreement with previous works [4]. When varying the electric field at constant excitation intensity, we find that the peaks in the spectra change their relative intensities due to a change in the effective exciton capture rate into the dot. No shift in the positions of the peaks is observed with the applied field. The spectra from the 150 Å separated QDs pair strongly resemble the single QD results.

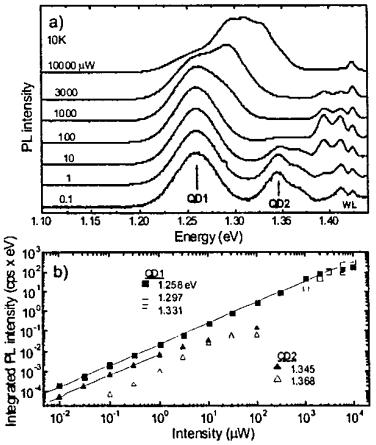

Fig. 1: a) PL spectra from the high dot density part of the 45 Å coupled QDs sample for different excitation intensities. The excitation energy is 1.96 eV. b) Integrated intensity of the PL peaks. The solid lines are linear fits to the data.

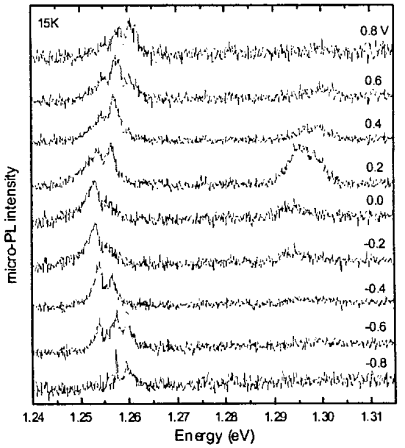

Fig. 2: Micro-PL spectra from a single 45 Å coupled QD molecule for different applied voltages. 1 V corresponds to an electric field of 3.8 mV/nm. The excitation energy is 1.47 eV.

This behavior is in contrast with the results from the 45 Å separated QDs molecule sample. In Fig. 2 we display micro-PL spectra of a single QD molecule for different applied voltages. In this case, 1 V corresponds to an electric field of 3.8 mV/nm (relative shift of 17 meV between the energy levels of the two dots). We note that several peaks appear and disappear around the ground state (~ 1.26 eV) of the lower energy dot (QD1) while varying the electric field. We suggest that this phenomenon is due to the charging of QD1 by carriers from the adjacent dot (QD2), as mentioned above, together with a change in the effective capture of carriers due to tunneling out of the dot.

We support our assumptions by a theoretical model, which accounts for both the kinetics and the many-body interactions in the QD molecule. In a first step, the phonon-assisted hopping rates between the discrete states of adjacent QDs are computed as a function of the level detuning. We then perform a Monte-Carlo simulation of the carrier kinetics, yielding the statistical probabilities of the various electron-hole complexes in the QD pair. Next, we calculate the quantum states and photon emission spectra of the most important complexes by a direct diagonalization of the many-body Hamiltonian (configuration interaction method). Finally, the time-integrated PL spectra are obtained by weighting the emission spectra with the dynamical occupation probabilities of the respective complexes.

[1] A. Berenco *et. al.*, Phys. Rev. Lett. **74**, 4083 (1995).
[2] G. Schedelbeck *et. al.*, Science **278**, 1792 (1997).
[3] M. Bayer *et. al.*, Science **291**, 451 (2001).
[4] E. Dekel *et. al.*, Phys. Rev. Lett. **80**, 4991 (1998).

Fine structure of neutral and charged excitons: A sensitive tool for probing the symmetry of self-assembled dots

M. Bayer[1], G. Ortner[1], A. Forchel[1], P. Hawrylak[2], S. Fafard[2]

[1] Technische Physik, Universität Würzburg, Am Hubland, 97074 Würzburg, Germany
[2] Institute for Microstructural Sciences, NRC, Ottawa O1A R6, Canada

Despite its enormous success for obtaining quantum dots of high optical quality, the self-assembled growth technique still raises questions about the symmetry of the fabricated dot structures. Here we will demonstrate, that the exciton fine structure represents an excellent tool to learn about the dot symmetry. From spectroscopy of single self-assembled quantum dots in magnetic field we find that the whole spectrum from perfect rotational to totally broken in-plane symmetry is found in the studied structures. Vice versa, these strong variations permit us to develop a comprehensive picture of the exciton fine structure pattern for strongly different symmetry scenarios. In particular, the influence of the short and the long range exchange can be studied in detail. Further, from the data we can uniquely distinguish between neutral and charged excitons, because for the latter ones the exchange interactions vanishes. The experimental data will be compared to a detailed theoretical analysis.

The fine structure of excitons has been studied by magneto-photoluminescence spectroscopy of self-assembled In(Ga)As/(Al)GaAs single quantum dots. Both strength and orientation of the magnetic field have been varied. Symmetry of the dot structures as well as its breaking cause characteristic features in the optical spectra, which are determined by the electron-hole exchange and the Zeeman interaction of the carriers. The symmetry breaking can be either dot inherent due to geometry asymmetries or it can be obtained by applying a magnetic field with an orientation different from the dot symmetry axis.

As an example, Fig. 1 shows the fine structure pattern observed for a neutral exciton in an InAs/GaAs quantum dot with strongly broken symmetry. Due to the symmetry breaking the exciton angular momentum is no longer a good quantum number so that bright and dark excitons mix. Therefore the nominally dark excitons can be observed already at zero magnetic field about 400 μeV below the bright exciton doublet. This exchange energy splitting is almost two orders of magnitude larger than that for InAs bulk demonstrating the drastic enhancement of Coulomb correlations in the studied strongly confined quantum dots. Both the bright and the dark exciton doublet show a further splitting due to both the short and the long range exchange which is caused by confinement potential asymmetries. For magnetic field in Faraday-configuration, the splitting of the emission features is enhanced due to the Zeeman interaction of the carrier spins. With increasing B, two of the split branches come into resonance and a pronounced anticrossing occurs, in contrast to quantum dots of high symmetry, for which these branches cross each other.

For InAs quantum dots embedded in an AlGaAs matrix we observe a class of quantum dots with a behavior quite similar to that described above. However, for these dots no exchange energy splitting between the bright and the dark doublet is observed. This can only be explained by the presence of an equilibrium charge in the quantum dots, so that the emission originates from charged excitons. In case of a negatively charged exciton in its ground state, for example, the hole spin interacts with a spin singlet state of two electrons. Therefore the exchange interaction goes to zero in strongly confined quantum dots. This demonstrates that the exchange interaction which couples the spins of electron and hole in a neutral exciton, can be switched off by adding an additional carrier.

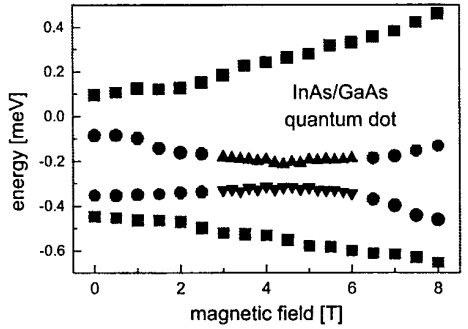

Figure 1: Exciton transition energies as function of magnetic field in an InAs/GaAs quantum dot with a strongly broken symmetry. Due to this symmetry breaking a pronounced anticrossing between a nominally bright and a nominally dark exciton occurs.

Corresponding author: Manfred Bayer, Technische Physik, Universität Würzburg, Am Hubland, 97074 Würzburg, Germany.
phone: +49 931 888 5883, Fax: +49 931 888 5143,
email: mbayer@physik.uni-wuerzburg.de

Optical Properties of Single Charge Tunable InGaAs Quantum Dots

A. D. Ashmore[1], J. J. Finley[1], R. Oulton[1], P. W. Fry[1], A. Lemaître[1], D. J. Mowbray[1], M. S. Skolnick[1], M. Hopkinson[2], P. D. Buckle[3], P. A. Maksym[4]

[1]Department of Physics and Astronomy, The University of Sheffield, Sheffield, S3 7RH, U.K.
[2]Department of Electronic and Electrical Engineering, The University of Sheffield, Sheffield, S1 3JD, U.K.
[3]DERA, St. Andrews Road, Malvern, Worcestershire, WR14 3PS, U.K.
[4]Department of Physics and Astronomy, The University of Leicester, Leicester, LE1 7RH, U.K.

We report the results of extensive magneto-optical investigations of neutral and negatively charged single and multi-excitonic states in single $In_{0.5}Ga_{0.5}As$ self-assembled quantum dots (QDs). The results obtained reveal important new information regarding the influence of Coulomb interaction and correlation effects on the optical properties of QDs. Magneto-optical measurements provide additional data concerning the evolution of the excitonic *g*-factor and diamagnetic shift as electrons are controllably added to the QD.

Incorporation of the QDs into the intrinsic region of a metal-semiconductor Schottky gated structure enables sequential electron charging of the QDs by varying the gate potential (V_g). Single dots are addressed using micro-photoluminescence (μPL) performed through sub-micro nano-apertures in the gate contact. Capacitance-voltage measurements reveal charging of up to two electron shells corresponding to a maximum of $N_e \approx 4$ spectator electrons occupying the QDs before charging of the underlying wetting layer occurs.

The evolution with V_g (N_e) of the ground state PL emission from a single dot at low optical excitation levels is presented in fig 1. For large negative V_g, the dot is uncharged and recombination from the charge neutral exciton (X^0) is observed (~40μeV FWHM). As V_g reduces, electrons are sequentially loaded into the dot and the form of the PL emission undergoes a series of pronounced transformations that reflect controlled modifications of the configuration and number of particles in the dot [1]. For charging with a single excess electron ($N_e = 1$), X^0 disappears and is replaced by the negatively charged exciton (X^-) 5.5±0.7meV to *lower* energy. By comparing the magnitude and sign of the $X^0 \rightarrow X^-$ energy shift with full many body calculations, we show that this observation indicates that the electron wavefunction is significantly more delocalised laterally in the QD than the hole. For $N_e = 2$, a clear emission doublet appears (X^{2-}) reflecting the two energetically distinct (singlet and triplet) final two-electron states [2]. However, after the next charging threshold ($N_e = 3$) an emission *singlet* (X^{3-}) emerges from the three electron final state. We show that this surprising observation, which indicates a pronounced departure from *Hunds-rule* like state filling, arises since the degeneracy of the p-levels is lifted overwhelming the attractive $p - p'$ exchange interactions in the five particle (4e + 1h) initial state. Indeed, for $N_e = 4$ (X^{4-}) an emission multiplet due to s-p electron exchange reappears as for X^{2-} [2]. At V_g~-0.3V the emission spectrum suddenly broadens and sharp features are no-longer observable as charging of the wetting layer occurs.

Stark shift spectroscopy of the X^{n-} lines reveals rich information regarding the form of the electron-hole wavefunctions. For X^{n-} ($0 \le n \le 3$) the observed Stark effect is weak revealing a small excitonic dipole ($|p|=0.5\pm0.2.10^{-29}$ Cm), consistent with the disc like form of the dots (size ~3 x ~25nm). However, the Stark shift observed for X^{4-} is significantly larger, possibly reflecting electron occupation of an excited state of the vertical (z) motion.

Magneto-optical investigations have also been performed in which we have investigated the excitonic *g*-factor and ΔE_{dia} for X^{n-} ($0 \le n \le 4$). We found only a weak systematic increase of the excitonic *g*-factor from 0.9 to 1.1 due to electron charging. In contrast, the quadratic component of ΔE_{dia} was found to be strongly sensitive to N_e, decreasing from 10 to 6±2μeV/T^2 for $X^0 \rightarrow X^{2-}$ before reducing suddenly to zero for X^{3-} and recovering to 12±2μeV/T^2 for X^{4-}. This highly unusual behaviour may indicate formation of an incompressible-like many particle configuration for X^{3-}.

At higher optical excitation levels, neutral and charged bi-exciton recombination is observed. In contrast to X^{n-}, the energy shift between $2X^0$ and $2X^-$ is very weak ($-0.8 \pm 0.2 meV$). This observation, which is reproduced by our many body calculations, arises due to the completely filled s-shell for the $2X^0$ initial state and is a direct optical manifestation of shell filling effects in quantum dots.

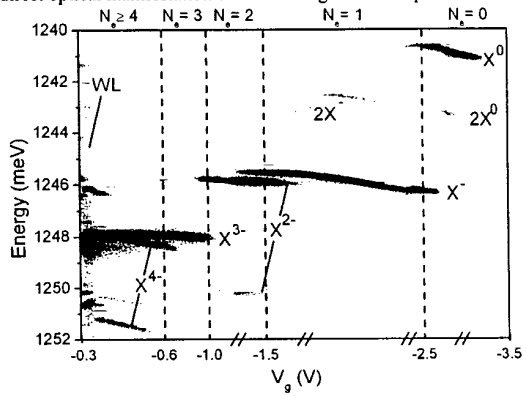

Figure. 1 : Low temperature (T=7K) single dot ground state (s-shell) PL emission as a function of gate potential. Vertical dashed lines denote charging thresholds.

References

[1] P. Hawrylak and A. Wojs, *Quantum Dots* (Springer Verlag, 1998)
[2] R. J. Warburton, *et al.* Nature, **405**, p296, (2000)

Corresponding author: Adam Ashmore, Department of Physics and Astronomy, The University of Sheffield, Sheffield, S3 7RH, U.K.
Phone: +44 (0)114 2223529, Fax +44 (0)114 2728079
Email: a.d.ashmore@sheffield.ac.uk

Giant permanent dipole moments of excitons in semiconductor nanostructures

C. Schulhauser[1], D. Haft[1], R. J. Warburton[1,2], K. Karrai[1], W. Schoenfeld[3], J. M. Garcia[3,4] and P. M. Petroff[3]

[1]*Center for NanoScience and Sektion Physik, Ludwig-Maximilians-Universität, Geschwister-Scholl-Platz 1, 80539 München, Germany*
[2]*Department of Physics, Heriot-Watt University, Edinburgh EH14 4AS, UK*
[3]*Materials Department and QUEST, University of California, Santa Barbara, California 93106, USA*
[4]*Instituto de Microelectrónica de Madrid, Isaac Newton 8, 28760 Tres Cantos, Madrid, Spain*

There are many open questions concerning the extent to which the electronic properties of semiconductor nanostructures can be tailored by self-assembly. We report here new and surprising results on the permanent electric dipole moment of excitons confined in quantum rings, nanostructures formed with a modified Stranski-Krastanow growth procedure.

The quantum rings are formed in an annealing step introduced during the growth of InAs nanostructures on GaAs. We grow initially InAs quantum dots, and then we deposit a few nanometres of GaAs and introduce a growth pause during which a remarkable shape transformation takes place: the dots become thinner in the growth direction, and more extended laterally, developing a pronounced ring-like structure. We have pioneered the charging of individual quantum dots with individual electrons, experiments which combine single-dot spectroscopy with our specially developed metal-insulator-semiconductor heterostructures [1]. In the present work we use the same structures in order to determine the dependence of the emission energy of individual quantum rings on the vertical electric field.

The two electrodes of our device are a highly doped back contact, 175 nm from the sample surface, and a semi-transparent gate electrode on the sample surface. The quantum rings are located between the two electrodes, 25 nm from the back contact. Application of a gate voltage changes the vertical electric field; it also leads to perfect Coulomb blockade which we can detect through the emission: whenever an electron tunnels from the back contact into a quantum ring, the emission makes a discrete jump in energy. To determine the Stark shift, we convert the gate voltage into electric field, taking into account the distance between the two electrodes and the Schottky barrier at the semiconductor surface. We also subtract the shifts on charging from the emission energy. We find that this converted energy has a smooth dependence on electric field, presumably because the charging energies do not depend on the exact electric field, being determined by intra-ring Coulomb interactions, and because the dots in the vertical direction are very strongly confined. We find that the curve of emission energy versus electric field for each quantum ring can be fitted precisely with a linear and a quadratic term. The linear term corresponds to the permanent electric dipole moment; the quadratic term to the polarizability. We find a number of surprising and unexpected effects.

First, the permanent dipole moment can be extremely large, up to 3 nm (expressing the dipole moment as the electronic charge multiplied by a length). This is almost an order of magnitude larger than the value reported by Fry *et al.* [2] for conventional InAs dots on GaAs. It is astonishing that the dipole moment can be comparable to the vertical height of the quantum rings. Furthermore, the permanent dipole moment is opposite in sign to that of conventional InAs quantum dots. Secondly, the permanent dipole moment varies enormously from quantum ring to quantum ring even though the fluctuations in emission energy from ring to ring are small. There is a clear trend on the emission energy: particularly low emission energy rings have small permanent dipole moments, with the permanent dipole moments increasing with increasing emission energy. Thirdly, we find a clear correlation without statistical fluctuations between the permanent electric dipole moment and the polarizability: there is an exact linear relationship between the two quantities.

The permanent dipole moment measures the separation between the centre-of-gravity of the electron and hole wave functions, a quantity which is a sensitive function of the strain and the indium distribution in the nanostructure. For InAs quantum dots, the strain field and the In-profile (the dots are In-rich at the top, In-poor at the bottom) both lead to permanent dipole moments but of opposite sign and the two effects tend to cancel. In our case, our results strongly imply that we have a highly modified indium profile, quite possibly reversed, allowing the strain and In-profile contributions to the permanent dipole moment to add. The huge difference in this parameter between quantum dots and quantum rings is clearly a consequence of the different growth procedure. During overgrowth, the GaAs cap destabilizes the In-rich tops of the dots, and this drives the profound changes in the structures.

The correspondence between the permanent dipole moment and the polarizability can be understood by assuming that the vertical confinement potential is harmonic and that there is a constant, ring-independent in-built electric field. We present a classical model to account for this in-built electric field.

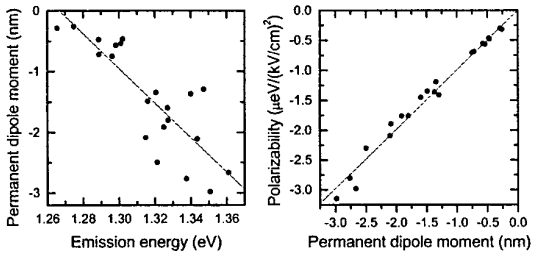

Left: the permanent dipole moment (expressed as the electron charge times a length) against emission energy for several quantum rings. Right: the polarizability against permanent dipole moment for the same quantum rings.

[1] R. J. Warburton *et al.*, Nautre **405**, 926 (2000).
[2] P. W. Fry *et al.*, Phys. Rev. Lett. **84**, 733 (2000).

Corresponding author : Richard Warburton, Department of Physics, Heriot-Watt University, Edinburgh EH14 4AS, UK.
Phone: 00 44 131 4518069; FAX 00 44 131 4513136; email: R.J.Warburton@hw.ac.uk

Magnetic properties of excitons in charge-tunable quantum rings

D. Haft[1], C. Schulhauser[1], A. O. Govorov[2], R. J. Warburton[1,3], K. Karrai[1], W. Schoenfeld[4], J. M. Garcia[4,5] and P. M. Petroff[4]

[1]*Center for NanoScience and Sektion Physik, Ludwig-Maximilians-Universität, Geschwister-Scholl-Platz 1, 80539 München, Germany*
[2]*Institute of Semiconductor Physics, Russian Academy of Sciences, Siberian Branch, 630090 Novosibirsk, Russia*
[3]*Department of Physics, Heriot-Watt University, Edinburgh EH14 4AS, UK*
[4]*Materials Department and QUEST, University of California, Santa Barbara, California 93106, USA*
[5]*Instituto de Microelectrónica de Madrid, Isaac Newton 8, 28760 Tres Cantos, Madrid, Spain*

The ability to detect optically the effect of single electron charging on a single semiconductor quantum dot was demonstrated for the first time by R. J. Warburton and co-workers [1]. The experimental results are spectacular: the optical emission from a single quantum dot changes its color whenever an electron is added. The emission originates from the radiative recombination of ground state excitons which can be prepared with a particular charge: neutral (X^0), singly charged (X^{-1}), doubly charged (X^{-2}), and so on, up to a limit determined by the confining potential. The changes to the optical spectra on charging reveal the importance of Coulomb interactions. These interactions should be sensitive to a magnetic field. A pertinent example is the prediction of an Aharonov-Bohm effect for an exciton confined in a quantum ring [2]. In this work, we present the first experimental investigations of the high magnetic field properties of neutral and charged excitons.

The samples consist of self-assembled InAs quantum rings grown on GaAs by molecular beam epitaxy. The growth of InAs quantum dots is interrupted during overgrowth with GaAs and this affects dramatically the morphology of the dots, leading to a ring-like shape [2]. The rings are embedded in a field-effect structure which allows electrons to tunnel from a reservoir (n-doped GaAs) situated 25 nm away from the ring layer. A semi-transparent metal film (the gate) evaporated on the sample surface allows us to control the number of electrons in a particular ring through a gate voltage. Single ring photoluminescence (PL) was obtained using a confocal microscope operating at liquid-He temperatures and in high magnetic fields. In order to improve the spatial selectivity, an opaque metal film was evaporated on the sample containing apertures of diameter 300 nm. We have gathered data on a large number of individual rings, and this has turned out to be crucial as the magneto-optical properties vary dramatically from one ring to the next, despite the small inhomogeneous broadening in the ensemble PL.

In a magnetic field B, the PL splits into two branches with a linear splitting due to the Zeeman effect. Both branches have a diamagnetic energy shift which is measured to be quadratic in B. The curvature associated with the diamagnetic shift (the diamagnetic curvature hereafter) is not only a measure of the spatial extent of the excitonic wave function but is also sensitive to Coulomb interactions. We have found three distinctive behaviors among all the investigated rings. In the first case (type I), the diamagnetic curvature is independent of the charge state of the exciton. Conversely, for other rings (type II) the diamagnetic curvature is reduced by up to a factor of two upon charging the exciton with one excess electron. Finally, for some other rings (type III) the diamagnetic curvature changes abruptly at a magnetic field of about 6 Tesla.

Type I behavior is observed for rings that tend to emit in the red-most part of the ensemble emission. The magneto-optics of these rings can be understood by treating the Coulomb interactions as perturbations to the single-particle structure, and this is entirely consistent with the deep confinement potential. On the other hand, the behavior of the type II rings cannot be explained within a Hartree picture. Type II rings tend to emit on the high-energy side of the ensemble emission where Coulomb interactions are relatively more important. These ideas cannot even qualitatively account for the behavior of the type III rings. We note that there is no obvious correlation with the emission energy for these rings. The abrupt change of diamagnetic curvature appears at magnetic fields where a single quantum flux threads the ring, and this suggests that we are observing a phase-related effect. The exact nature of this effect is an open issue at present; existing theory assumes that the rings are very thin in the radial direction which is not true in this case. It is an exciting possibility however that an Aharonov-Bohm effect survives for finite-thickness rings. We find type-III behavior in a minority of the rings. This might be because phase-related effects can be disrupted by some form of localizing potential. However, it might be the case that type I and type II rings also exhibit a change in diamagnetic curvature but at higher magnetic fields. Experiments are currently underway to resolve this point.

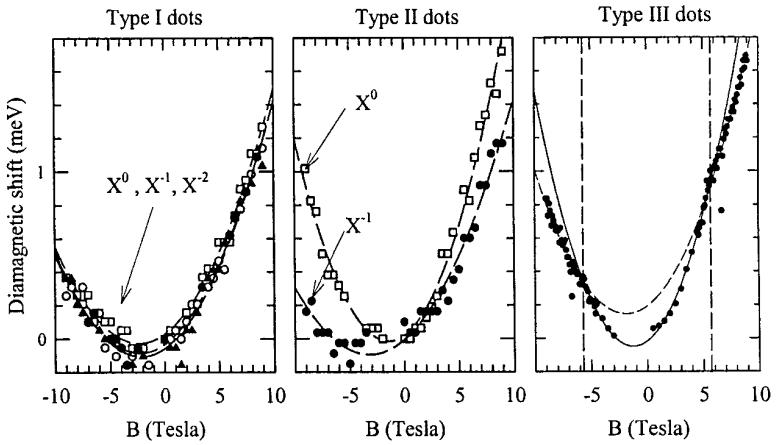

Diamagnetic shift of the exciton ground state for three quantum rings. Left: type I behavior (equal diamagnetic shifts for X^0, X^{-1} and X^{-2}). Center: type II behavior (diamagnetic shift a factor of two smaller for X^{-1} than for X^0). Right: type III behavior (an abrupt change at 6 T).

[1] R. J. Warburton *et al.*, Nature **405**, 926 (2000).
[2] R. A. Römer and M. E. Raikh, Phys. Rev. B **62**, 7045 (2000).
Corresponding author : Khaled Karrai, Sektion Physik der LMU, Geschwister-Scholl-Platz 1, 80539 München, Germany; phone 00 49 89 2180 3125; FAX 00 49 89 2180 3182; email: Khaled.Karrai@physik.uni-muenchen.de

Infrared magneto-spectroscopy of polaron states in InAs/GaAs self-assembled quantum dots

S.Hamcau[1], J.N.Isaia[1], E.Deleporte[1],Y.Guldner[1], O.Verzelen[1], R.Ferreira[1], G.Bastard[1], J.Zeman[2], J.M.Gérard[3],

[1] Laboratoire de Physique de la Matière Condensée, Ecole Normale Supérieure, 24 rue Lhomond, 75231 Paris Cedex 05, France

[2] Grenoble High Magnetic Field Laboratory, CNRS/MPI, 25 avenue des Martyrs, 38042 Grenoble Cedex 9, France

[3] CNRS - Laboratoire de Photonique et Nanostructures, 196 avenue Henri Ravera, B.P. 29, 92222 Bagneux Cedex, France

Electrons and LO phonons in semiconductor quantum dots are in strong coupling regime resulting from the interaction between the discrete electronic levels and the LO-phonon continuum of finite width [1,2]. This implies that electrons and LO-phonons form mixed modes, the polaron states, which would be everlasting if both their constituents, electrons and phonons, were stable excitations [3].

We have investigated, by FIR magnetotransmission experiments up to 28 Tesla at $T = 2\,\mathrm{K}$, this strong coupling regime in self-assembled InAs/GaAs quantum dots. The sample doping was adjusted in order to transfer on average one electron per dot and to populate only the dot ground state. We have studied, in three different samples with increasing lateral diameter of the quantum dots, the magneto-optical transitions between the ground and the first excited states which are s-like and p-like respectively because of the quasi-cylindrical symmetry of the dots. Because of the Zeeman splitting of the p-state, two transitions $s - p+$ and $s - p-$ can be excited in the range $200 - 800\,\mathrm{cm}^{-1}$ depending on the FIR radiation polarization. The experiments consist of monitoring, by means of the magnetic field, a resonant interaction between the discrete ($p\pm$, 0 LO-phonon) states and the continuum of either (s, 1 LO-phonon), ($p-$, 1 LO-phonon) or (s, 2 LO-phonons). The magnetic field dispersion of the transmission minima shows, in the whole field range from 0 to 28 Tesla, important deviations from the expected dispersion neglecting the electron-phonon interaction (Figure 1). In particular, it evidences huge anticrossings which correspond to the formation of 1 or 2 LO- phonons polarons.

In all cases, a purely electronic level model is unable to account for the experimental data and we have to consider magneto-optical transitions between polaron states. Indeed, we have calculated the coupling between the relevant mixed electron-lattice states using the Fröhlich hamiltonian, and obtained the energies of the polarons and of the dipolar electric optical transitions. An excellent agreement between the experiments and the calculations is obtained for the three samples demonstrating that the electrons and optical phonons experience a strong coupling regime, and that the magneto-optical transitions always occur between polaron states. This strong coupling regime raises interesting problems as in particular the question of the energy relaxation in these sytems, since the usual relaxation channel, the irreversible emission of LO phonons by electrons, does not exist in quantum dots [3].

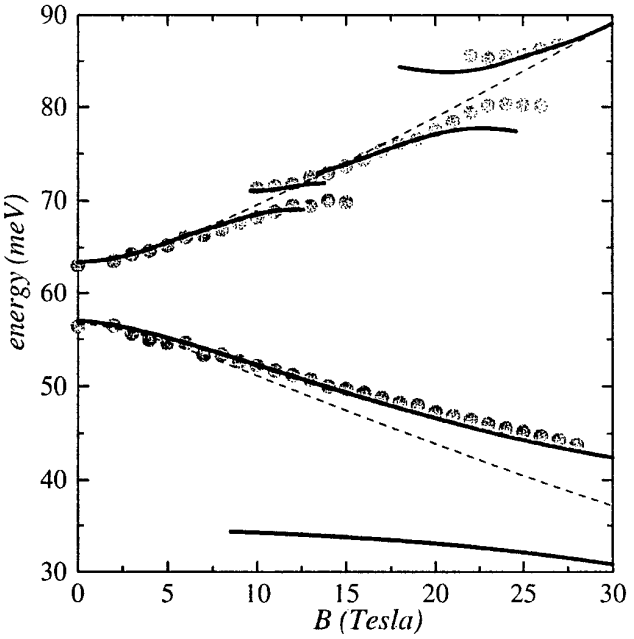

Figure 1: Magnetic field dispersion of the experimental transmission minima (full circles). The dashed lines are the calculated dispersions neglecting the electron-phonon interaction. The bold solid lines are the calculated dispersions taking into account the electron-phonon interaction.

References

[1] S.Hameau et al, Phys. Rev. Lett. **83**, 4152 (1999).
[2] T. Inoshita and H. Sakaki, Phys.Rev. **B56**, R4355 (1997).
[3] O. Verzelen, R. Ferreira, G. Bastard, Phys. Rev. **B62**, R4809 (2000)

Corresponding author: Emmanuelle Deleporte, Ecole Normale Supérieure, Laboratoire de Physique de la Matière Condensée, 24 rue Lhomond, 75231 Paris Cedex 05, France.
Phone: 33-01-44-32-34-49, Fax: 33-01-44-32-38-40
Email: Emmanuelle.Deleporte@lpmc.ens.fr

Morphological and optical anisotropy of self-assembled quantum dots probed by magneto-tunnelling and photoluminescence-polarisation spectroscopy

A. Patanè[1], L. Eaves[1], A. Levin[1], P.C. Main[1], M. Henini[1],
E. E. Vdovin[2], Yu.V. Dubrovskii[2], Yu.N. Khanin[2]

[1]*School of Physics and Astronomy, University of Nottingham, Nottingham NG7 2RD, UK*
[2]*Institute of Microelectronics Technology RAS, Chernogolovka, Russia*

Recently, we proposed a novel approach to probe the electron wave function in a quantum dot (QD) based on magneto-tunnelling spectroscopy (MTS) [1]. The technique exploits the effect of the classical Lorentz force on the motion of a electron tunnelling through a QD and can be regarded as the momentum ($\underline{k}$-) space analogue of STM imaging: electrons are imaged according to their wave-vector and the MTS images give the probability density in $\underline{k}$-space of the wave function of an electron confined inside a QD.

Here we use the MTS technique to probe the confined states of InAs self-assembled QDs grown on a (100)- and (311)B-oriented GaAs substrate. The MTS images in Fig. 1 indicate that the electron wave function of the QD has a biaxial symmetry in the growth plane, with axes corresponding quite closely to the main crystallographic directions in the (100) and (311)B plane. The in-plane anisotropy of the electron wave function is stronger for the (311)B QDs. Since the bare (311)B-oriented GaAs surface reconstructs by forming arrays of dimer rows [2], we believe that they may act as a template for the subsequent growth of the strained material, giving rise to the formation of elongated InAs islands.

We investigate the influence of the anisotropy of the QD shape on the photoluminescence (PL) polarisation properties of the dots. We show that the anisotropic shape of the dot also results in an anisotropy of the PL polarisation (see Fig. 2). An optical anisotropy can be induced by a non-homogeneous in-plane strain field and/or anisotropic confinement potential associated to the dot. Our data indicate that the polarisation anisotropy does not correlate directly with the dot confinement potential. It can be seen from Fig. 1 and 2 that for (311)B QDs the excess PL polarisation is parallel to the long axis in k-space of the electron wave function of the QD. Note that this is the direction of the short axis in real space. In contrast, the excess polarisation is at 45° to the long axis for the QDs grown on (100). By studying a set of InAs/GaAs heterostructures with variable InAs coverage and/or different growth conditions, we show that the larger dots, emitting at lower energies, are more polarised (see Fig. 3) and that the anisotropy of strain field associated to the dot gives the main contribution to the PL polarisation.

References

[1] E.E. Vdovin et al., Science 290, 124 (2000)
[2] J. Marquez et al., Phys. Rev. B 62, 9969 (2000)

Corresponding author: Dr Amalia Patanè
School of Physics and Astronomy, University of Nottingham, Nottingham NG7 2RD, UK
phone: +44-115-9515151-8334 fax: +44-115-9515180
e-mail: Amalia.Patane@nottingham.ac.uk

Fig. 1: Distribution in the plane (k_X, k_Y) of the square of the Fourier transform, $\Phi_{QD}(k_X, k_Y)$, of the probability density of the electron confined in the dot for the ground state of QDs grown on a (311)B- and (100)-oriented GaAs substrate. The arrows labelled p indicate the direction of preferential polarisation of the QD PL.

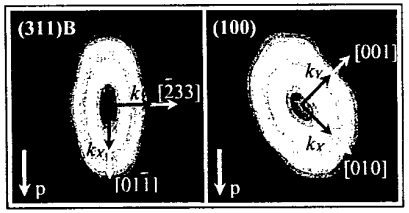

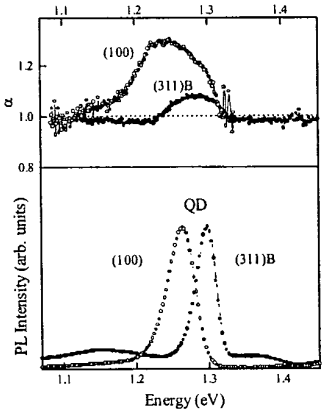

Fig. 2: Bottom: PL spectrum at 10K for the (311)B and (100) QDs whose MTS image is shown in Fig. 1. Top: PL polarisation spectra for (311)B and (100) QDs. The polarisation intensity, α, is defined as the ratio between the PL intensity polarised along two main crystallographic directions on the (311)B ([01$\bar{1}$] and [$\bar{2}$33]) and (100) ([01$\bar{1}$] and [011]) plane.

Fig. 3: Degree of polarisation (α) of the PL of InAs/GaAs quantum dots (QDs) and wetting layer (WL) vs the peak energy, $h\nu$, of the QD or WL PL band for (311)B samples.

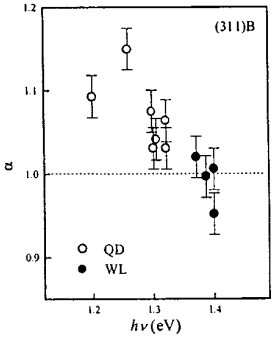

Quantum Interference Effect in Photoionization Spectra of Self-Assembled InAs Quantum Dots

K. Hirakawa*, Ph. Lelong, K. Hirotani, S.-W. Lee*, S. Fujimoto, and H. Sakaki
Institute of Industrial Science, University of Tokyo
4-6-1 Komaba, Meguro-ku, Tokyo 153-8505, Japan
**also with CREST, JST*

There are numerous reports on the zero-dimensional (0D) bound states formed in self-assembled InAs quantum dots (QDs) embedded in GaAs matrix and the understanding of their electronic structures are being gradually established. However, the electronic properties of the continuum states associated with QDs above the conduction band edge of GaAs has not been investigated, mostly because optical transition probabilities from the bound states in the QDs to the continuum are very small and almost undetectable by direct optical absorption measurements.

In this work, we have investigated the photoionization spectra of the s-bound states in the self-assembled InAs QDs by utilizing recently proposed QD infrared photodetector structure [1]. It is found that, although the photoionization spectra of large QDs (diameter~40 nm) have ordinary spectral shape known for 0D-3D transitions (sharp rize and gradual decay), the photoionization spectra of small QDs (diameter~18 nm) exhibit a sharp quenching. Theoretical calculation of the photoionization spectra of self-assembled QD system revealed that the observed quenching is due to the interference between the 2D-continuum states associated with the wetting layer and the 3D-continuum in the conduction band of GaAs.

The samples used in this work were high-sensitivity n-type modulation-doped QD infrared photodetectors (MD-QDIP), which utilize photoionization of QDs by mid infrared radiation. The size of the QDs was controlled by changing growth temperatures and As pressures. Figs. 1(a) and (b) show photoluminescence spectra of heavily doped large and small QD samples, respectively. At least 3 bound states are confined in the conduction band of large QDs, whereas only single PL peak is observed for small QDs.

The photocurrent spectra of the MD-QDIPs were measured in a normal incidence geometry by a Fourier transform spectrometer. Doping densities in the samples for infrared photocurrent measurements were set in a way such that only s-bound states in the QDs are occupied. Fig. 2 shows the photocurrent spectra of MD-QDIPs with QDs of different sizes. The photoionization spectra of large QDs (Fig. 2(a)) exhibit a broad peak, which rises at around 370 meV and gradually decays with increasing photon energy. (A large peak observed above 700 meV is due to deep levels in the substrate and not relevant here.) The observed spectral shape is consistent with an ordinary 0D-3D transition picture. On the contrary, as seen in Fig. 2(b), photoionization spectra of small QDs rise at around 120 meV and, surprisingly, shows a pronounced quenching at 300 meV. The photoionization thresholds observed for large and small QDs (370 meV and 120 meV, respectively) are in good agreement with the activation energy determined from dark current measurements on the identical samples.

In order to understand the origin of the observed peculiar quenching of the photoionization spectra of small QDs, we have performed theoretical calculation on the photoionization spectra of self-assembled QD system (lens-shaped QDs and wetting layer). It was found that the quenching of the photoionization spectra originates from the interference between the 2D-continuum states associated with the wetting layer and the 3D-continuum in the conduction band of GaAs. Furthermore, the observed dependence of the photoionization spectra on the QD size was also well reproduced.

Reference [1] S. –W. Lee, K. Hirakawa, and Y. Shimada, Appl. Phys. Lett. **75**, 1428 (1999).

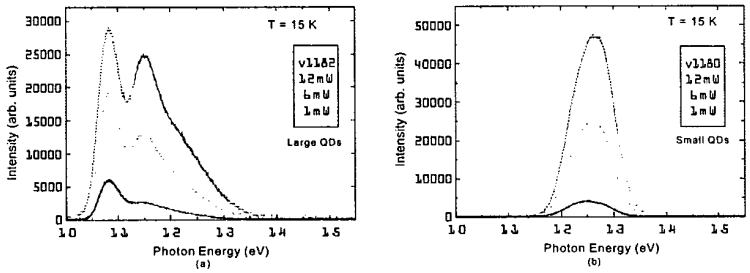

Fig. 1 Photoluminescence spectra of heavily doped MD-QDIP samples. (a) large QDs and (b) small QDs.

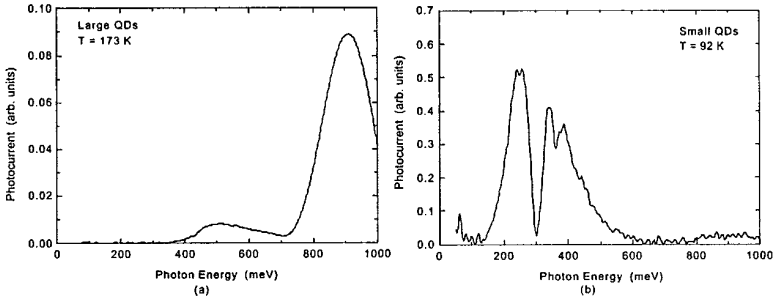

Fig. 2 Infrared photocurrent spectra measured for MD-QDIPS with QDs of different sizes; (a) large QDs and (b) small QDs.

Corresponding author:
K. Hirakawa
Institute of Industrial Science, University of Tokyo
4-6-1 Komaba, Meguro-ku, Tokyo 158-8505, Japan
Phone: +81-3-5452-6260, Fax: +81-3-5452-6262
Email: hirakawa@nano.iis.u-tokyo.ac.jp

2D-1D crossover from quantum well to quantum wire behaviour in GaAs v-groove structures

R. Roshan[1], N.I. Cade[1], M. Hauert[1], A.C. Maciel[1], J.F. Ryan[1]
A. Schwarz[2], T. Schäpers[2], H. Lüth[2]

[1] Clarendon Lab, Department of Physics, Oxford University , Oxford, OX1 3PU, UK
[2] ISI, Forschungszentrum Jülich, 52425 Jülich, Germany

The growth and fabrication of GaAs v-groove quantum wire (QWR) structures have so far produced devices with high optical quality and strong one-dimensional spatial confinement [1]. These structures are formed in $[01\bar{1}]$ oriented grooves with nominal [111]A sidewalls. The recent development of modulation-doped v-groove structures [2,3], and measurements of electron transport on these structures[3], have opened up the possibility of nanostructure device networks using v-groove wire interconnects. We have developed a method for electrically contacting wires which involves the fabrication of wide grooves with an aperture $> 20\mu$m at each end of the v-groove: as the wire grows in the v-groove, a contiguous 2D electron gas is formed in the (100) bottom quantum well (BQW) which grows on the bottom facet of the wide groove. However, the electrical properties of this structure depend strongly on the nature of the electronic states in the 2D-1D transitional region. In this paper we describe measurements of surface topography and scanning near-field photoluminescence (PL) of discrete structures in which the groove aperture is systematically narrowed. We obtain clear evidence of the formation of "corner" QWRs which coalesce to form single wires in grooves narrower than $\sim 5\mu$m.

The structure investigated here contains a series of nominally undoped grooves with apertures ranging from $1-16\mu$m. In each case a nominal 3nm GaAs QW is grown within AlGaAs barriers. Optical measurements were performed at 10K using a low-temperature scanning near-field optical microscope (LT-SNOM) [4]. Topographic information was obtained by measuring the shear force on the scanning fibre tip.

Topographic profiles of the different grooves are shown in Figure 1(a). At 3μm the grooves are clearly v-shaped, and a transition to u-shaped behaviour occurs at $\sim 4-6\mu$m where the bottom surface is clearly concave. At 7μm the bottom facet is flat, but at larger widths a w-shaped profile is observed as corner v-grooves develop and the bottom surface becomes convex. These measurements suggest the formation of complex quasi-1D/2D electronic states in the buried QW layer. Figure 1(b) shows SNOM PL spectra obtained from the 12μm groove as a function of position across the groove: $x = 0$ corresponds to the groove center, while $x = 3\mu$m corresponds to the corner (c.f. Fig.1(a)). The dominant feature at 1.694eV at the groove centre arises from the BQW: the estimated layer width is 2.5nm. The line-width is relatively large; at $x = 1.5\mu$m it is resolved into several discrete components which are indicative of monolayer interface fluctuations. In the corner of the groove the dominant feature is at 1.646eV; this arises from the side quantum well (SQW) whose width is estimated to be 2.8nm. When the probe is placed at 6μm (i.e. close to the edge of the groove on the top surface) we observe a strong PL signal at ~ 1.60eV. On the basis of previous measurements [3] we identify this signal as arising from the quasi-1D states formed in the corner v-groove. PL from wire is not observed when the tip is placed directly above the QWR (i.e. at $x = 3\mu$m) due to total internal reflection, but it is

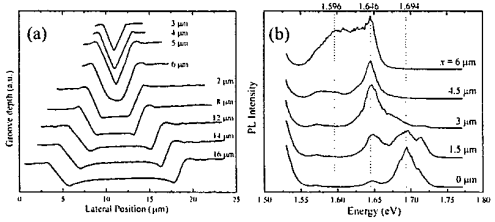

Figure 1: (a)Topographic cross-sections of different grooves; (b)PL spectra for different lateral positions of the SNOM tip within the 12μm groove

detected at the edge of the groove on the top surface [4]. These features are confirmed in Fig. 2 which shows simultaneous SNOM and topography measurements for 12 and 5μm grooves. The QWR signal in both cases is maximum when the structure is excited close to the extremities of the grooves on the top surface. The SQW signal in the 5μm structure essentially fills the groove, but in the 12μm structure the SQW signal is resolved into two components consistent with a fully-developed outer SQW and an incomplete inner SQW of the corner v-groove which develops into the BQW near the centre of the groove.

These data reveal that the transition from the QW to QWR in v-groove structures involves the formation of separate quasi-1D electronic states in weakly confined v-grooves which form at the corners, and which merge into a single QWR for apertures $< 5\mu$m. We will present simultaneous topographical, hot carrier luminescence and electrical transport measurements of structures in this cross-over region which will elucidate the spatial distribution of the current in the 2D-1D transition region in QWR contacts.

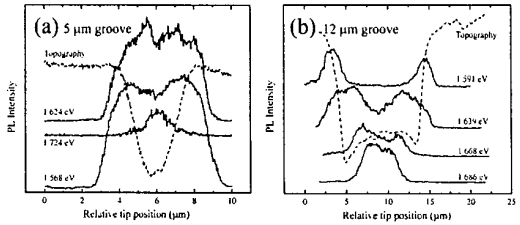

Figure 2: PL intensity at different energies as a function of SNOM tip position

References

[1] T.G. Kim, X-L. Wang, R. Kaji and M. Ogura, Physica **E7**, 508 (2000).
[2] A. Schwarz et al., Physica **E7**, 760 (2000).
[3] A.C. Maciel et al., Physica **B272**, 101 (1999).
[4] M. Hauert et al., Proc. ICPS 25 (2001) (to be published).

Corresponding author: Rakesh Roshan, Clarendon Laboratory, Oxford, UK.
Phone: +44 1865 272358, Fax: +44 1865 272400, Email: r.roshan1@physics.ox.ac.uk

Quantum mechanical repulsion of exciton levels in a disordered quantum well evidenced by near-field spectroscopy

Francesca Intonti[1], Valentina Emiliani[1], Christoph Lienau[1], Thomas Elasaesser[1], Vincenzo Savona[2], Erich Runge[2], Roland Zimmermann[2], Richard Nötzel[3], Klaus H. Ploog[3]

[1]Max-Born-Institut für Nichtlineare Optik und Kurzzeitspektroskopie, Max-Born-Str. 2A, 12489 Berlin, Germany
[2]Institut für Physik, Humboldt Universität, Hausvogteiplatz 5-7, 10117 Berlin, Germany
[3]Paul-Drude-Institut für Festkörperelektronik, Hausvogteiplatz 5-7, 10117 Berlin, Germany

Localized states play a key role for the optical and transport properties of disordered quantum systems, e.g., thin quantum wells. Here, exciton localization within a spatially fluctuating, interface-roughness induced disorder potential gives rise to pronounced inhomogeneous broadening of far-field optical spectra. In experiments with high spatial and spectral resolution the smooth, inhomogeneously broadened PL spectra break up into many narrow emission spikes from single localized excitons whose individual spectral widths are often determined by experimental resolution or by the natural line width [1-4]. So far, it has been difficult to infer from such single exciton spectra precise information about the underlying disorder potential or the nature of the excitonic wavefunctions.

In this paper we provide first clear experimental evidence that the non-negligible spatial overlap of excitonic wavefunctions in adjacent minima of this disorder potential gives rise to a level-repulsion of the excitonic eigenenergies. This quantum-mechanical hallmark of localization is revealed through a statistical analysis of the two-energy autocorrelation function of a set of several hundred near-field PL spectra. Through an accurate comparison to a quantum theory of the excitonic center-of-mass motion, we demonstrate that this autocorrelation function bears precise information about the average spatial correlation length of underlying disorder potential, giving the spatial and energetic correlations of excitons in disordered quantum systems [5].

As a model system, we investigate a 3 nm thick GaAs/AlGaAs quantum well grown on a GaAs (311)A substrate. The low temperature, high spatial and spectral resolution (150 nm and 100 μeV, respectively) near-field PL spectra are dominated by a set of spectrally sharp and intense emission lines. while the spatially averaged PL spectrum is characterized by a 15 meV broad structureless emission band (Fig. 1).

In Fig. 2, the two-energy-autocorrelation function $R_c(\Delta E)$ [6] derived from a set of over 400 individual near-field spectra is compared to that calculated within a quantum theoretical treatment of the exciton center-of-mass motion in a two-dimensional spatially correlated disordered potential. The self-correlation of the individual emission spikes gives rise to a narrow spike around ΔE=0. The quantum mechanical level repulsion manifests itself in a clear shoulder at ΔE =1-2 meV. This behavior is in excellent agreement with the theoretical simulation (solid line) and strikingly different from the classical limit (dotted line) which neglects level repulsion and is determined solely by the energy correlation of the potential itself. At larger ΔE, both experimental and calculated $R_c(\Delta E)$ follow the classical autocorrelation.

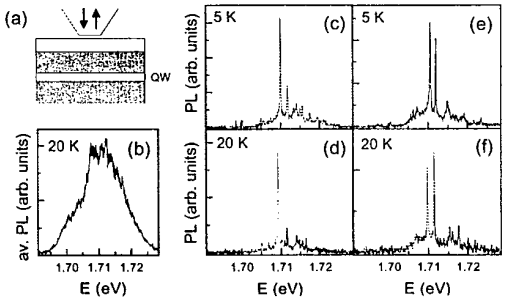

Fig. 1: (a) Schematic experimental setup. (b) averaged PL spectrum (T = 20 K). (c)-(f) Representative near-field PL spectra recorded at two different spatial position and two temperatures.

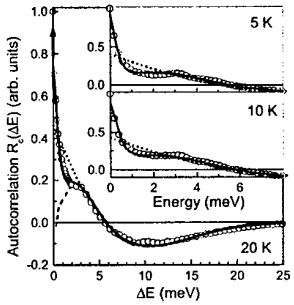

Fig. 2: Two-energy autocorrelation function R_c (ΔE) of a set of 400 near-field PL spectra (circles) at T = 20 K compared to the quantum-mechanical theoretical simulation (solid line). The dotted line shows the classical limit. The dashed line represents the raw numerical simulation without homogeneous line broadening - the δ-like self-correlation peak is denoted by the arrow at ΔE=0. Insets: Level repulsion region for T = 5 K and T = 10 K.

The agreement between experimental data and quantum-mechanical simulation allows to extract the statistical parameters of the underlying disorder potential, namely the disorder strength σ = 5 meV and the correlation length ξ = 17 nm. This opens the way to a systematic characterization of disordered systems by means of correlation techniques providing new insight into the growth correlated properties of semiconductor nanostructures.

References

[1] K. Brunner et al., Phys. Rev. Lett **73**, 1138 (1994).
[2] H.F. Hess et al., Science **264**, 1740 (1994).
[3] D. Gammon et al., Phys. Rev. Lett. **76**, 3005 (1996).
[4] F. Intonti et al., Phys. Rev. B, **63**, 075313 (2001)
[5] F. Intonti et al., submitted.
[6] V. Savona and R. Zimmermann, Phys. Rev. B. **60**, 4928 (1999).

Corresponding author: Francesca Intonti, Max-Born-Institut für Nichtlineare Optik und Kurzzeitspektroskopie, Max-Born-Str. 2A, D-12489 Berlin, Germany,
phone: +49 30 6392 1471, Fax: +49 30 6392 1489
email: intonti@mbi-berlin.de

Directional phonon-assisted cascading of photoexcited carriers in stepped $In_X(Al_{0.17}Ga_{0.83})_{1-X}As$/ $Al_{0.17}Ga_{0.83}As$ multiple quantum wells

S. Machida[1], M. Matsuo[1], K. Fujiwara[1], J.R.Jensen[2] and J.M. Hvam[2]

[1]Kyushu Institute of Technology, Tobata, Kitakyushu 804-8550, Japan
[2]Research Center COM, Technical University of Denmark, Building 349, DK-2800 Kgs. Lyngby, Denmark

Cascading flow and/or capture of injected or photoexcited carriers in composite quantum well (QW) heterostructures are crucial for devise applications such as those utilizing inter-subband and inter-well transitions [1-2]. In this paper, perpendicular motion of photoexcited electron and hole pairs assisted by phonon scattering is investigated in a novel step-graded staircase heterostructure consisting of strained $In_X(Al_{0.17}Ga_{0.83})_{1-X}As$ multiple quantum wells with similar widths but different five x (= 5.3, 8.8, 12, 15 and 18%, named QW1, 2, 3, 4 and 5, respectively) values (see Fig. 1) by cw and time-resolved photoluminescence (PL) experiments. Temperature (T) dependence of cw PL spectra of the sample reveals, as shown in Fig. 2, distinct five peaks corresponding to the QW layers, which evolve with T (from 14 K to 200 K). At a first glance it appears they change in a complex manner. However, we note that there exists a clear trend of the variations. That is, as T increases, the PL peaks decrease their relative intensities progressively from shorter wavelength sides after increasing the signal amplitude in the intermediate T range. For example, the QW3 PL peak shows the highest intensity at 50 K and then decreases monotonously above 60 K. A quantitative plot of the wavelength integrated PL intensities (shown in Fig. 3) indicates that there are some plateaus or even restorations of the PL signal in the temperature range that depends on the QW potential depth. These results mean that the photoexcited carriers directionally move from shallower to deeper QW's via phonon-assisted activation above the barrier band edge state. Once captured by the deeper well, they cannot go back to the shallower well, since more thermal activation energies are required to escape from that particular well at a given T. Thus, directional phonon-assisted cascading of photoexcited carriers is realized in the novel stepped QW heterostructure. PL dynamics (shown in Fig. 4 for the case of QW3) directly evidence the perpendicular flowing of photoexcited carriers and the capture by the deeper QW 4. A significant increase of the PL rise observed at 50 K (in Fig. 4) and faster PL decays of the neighboring QW2 (not shown) provide firm evidences for the carrier flow and capture proceeses. These results show that a design of stepped heterostructures can be used to tailor directional motion of carriers in quantum heterostructures.

References
[1] H.T. Grahn (Ed.), *Semiconductor Superlattices: Growth and Electronic Properties*, World Scientific, Singapore, 1995.
[2] H. Schneider, C. Schönbei, K. Schwarz and M. Walter, Physica E2, 28 (1998).

Corresponding author: Kenzo Fujiwara, Kyushu Institute of Technology, Tobata, Kitakyushu 804-8550, Japan, Phone: +81 93 884 3221, Fax: +81 93 884 0879,
email: fujiwara@ele.kyutech.ac.jp

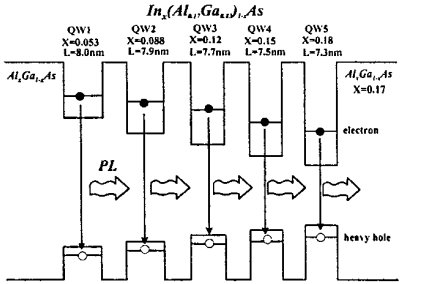

Fig. 1 Schematic potential diagram of step-graded staircase heterostructure consisting of strained $In_X(Al_{0.17}Ga_{0.83})_{1-X}As$ multiple quantum wells with similar widths but different five x (= 5.3, 8.8, 12, 15 and 18%, named QW1, 2, 3, 4 and 5, respectively) values.

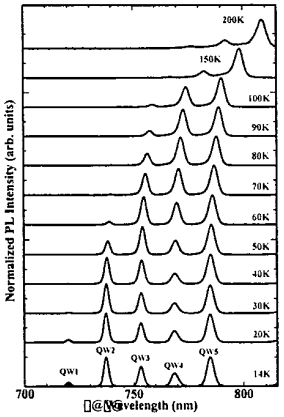

Fig. 2 Normalized PL spectra as a function of lattice temperature between 14 and 200 K.

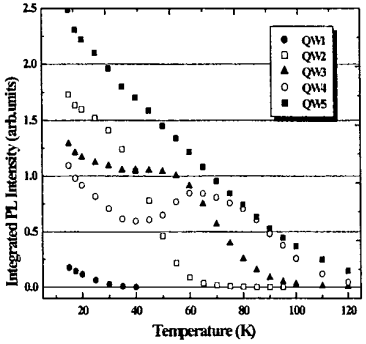

Fig. 3 Wavelength integrated PL intensities of the emission bands for QW1, QW2, QW3, QW4 and QW5 as a function lattice temperature.

Fig. 4 PL intensity of the QW3 emission band as a function of time at seven temperatures. Note that at 50 K the PL transient shows a significant increase of the rise, while the PL decay at 70 K is determined by the escape time of carriers to QW4.

Heterostructure Interface Effects on the Far-Infrared Magneto-Optical Spectra of InAs/Gasb Quantum Wells

G. Comanescu[1], R. J. Wagner[2], B. D. McCombe[1], B. V. Shanabrook[2], B. R. Bennett[2], S. K. Singh[1], J.G. Tischler[1,2] and B.A. Weinstein[1].

[1]University at Buffalo, The State University of New York, Buffalo, New York 14260
[2]Naval Research Laboratory, Washington, DC 20375

InAs/GaSb heterostructures have been of considerable recent interest because of the unusual Type-II, broken gap band alignment, which permits great flexibility in design of IR lasers and detectors [1]. This electronic configuration also gives rise to hybridization between valence band states in GaSb and conduction band states in InAs for appropriate values of momentum in the heterostructure plane (where the dispersion curves cross in the absence of coupling). A great deal of experimental work has been done to study these interesting properties as well as the effects of electron-electron and electron–hole interactions [2,3]. The strength of the hybridization across the InAs/GaSb interface is very sensitive to interface formation, InSb bonds or GaAs bonds. This can be roughly explained in terms of the large difference between the band gaps of GaAs and InSb [4]. Several experiments have explored the influence of the interface on such quantities as valence band offset, electron concentration and electron mobility [5,6]. The envelope function overlap integral between InAs conduction band and GaSb valence band is very sensitive to interface formation. Therefore the interface type should have significant effects on experimental quantities that depend strongly on overlap integral such as the hybridization bandgap. Cyclotron resonance experiments provide information about hybridization.

We report far-infrared (FIR) cyclotron resonance (CR) studies of two InAs/GaSb Type II heterostructures at 4.2 K in magnetic fields up to 15 T. Both samples consist of a single 30 nm InAs quantum well surrounded by GaSb barriers of 100 nm and 2000 nm. The only intended difference between the samples is the interface bonding between the InAs well and GaSb barrier, which was controlled during growth: GaAs (sample 1) or InSb (sample 2) bonds. Sample 1 shows spectra mostly governed by non-parabolicity effects for the two occupied electron subbands on the other hand, Sample 2 (InSb bonds) shows strong hybridization of the InAs conduction and GaSb valence band Landau levels [Fig.1]. The much larger hybridization effects in sample 2 are consistent with interface effects on bandstructure [Ref.4]:a monolayer of GaAs at the interface behaves like a barrier whereas a monolayer of InSb behaves like a well for electrons in InAs and GaSb. Thus the overlap integral, consequently the hybridization gap is much larger for the InSb interface (sample 2) than the GaAs interface (sample 1). In addition, the CR line widths in sample 2 are much narrower than the corresponding line widths in sample 1. The detailed dependencies will be discussed in the light of the known effects of bonding type on the interface properties. Unfortunately, the population of two subbands brings an additional complexity to our system. Shubinkov-de Haas measurements on both samples [Fig.2] provide electron and hole concentrations in reasonable agreement with the electron and hole concentrations obtained from the CR integrated absorption.

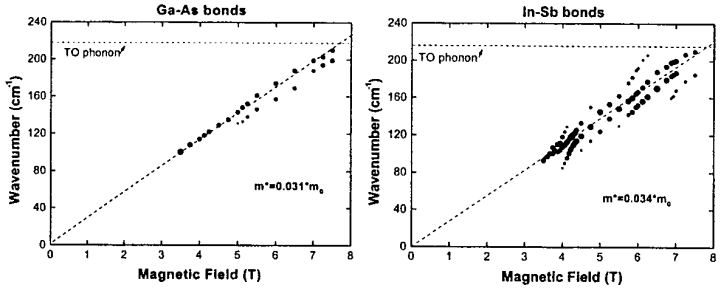

Fig. 1 Cyclotron resonance for: left-sample 1 (GaAs bonds); right-sample 2 (InSb bonds). Clear anti-level crossing is seen for sample 2. This is associated with conduction –valence landau level hybridization across the interface. This behavior is not observed in sample 1.

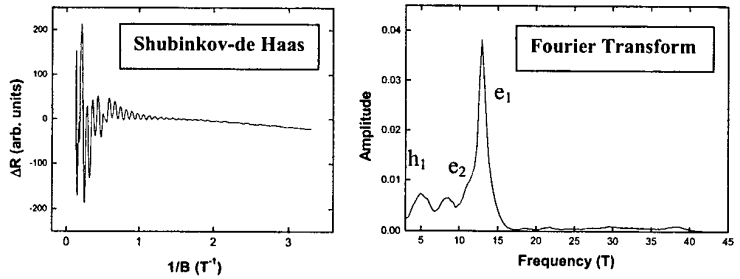

Fig. 2 Shubinkov-de Haas data for sample 1. Left panel – resistance oscillations vs. inverse magnetic field. Right panel – Fourier Transform of the data of the right panel. The multiple peaks are due to occupancy of two electron and one hole sub-band.

References

[1] I. Vurgaftman and J.R. Meyer , J. Appl. Phys. 86, 4734 (1999)
[2] J. Kono *et al.*, Phys. Rev. B 55, 1617 (1997) and references therein
[3] M.J. Yang *et al.*, Phys. Rev. Lett. 78, 4613 (1997)
[4] C. Priester *et al.*, Phys. Rev. B 49, 2919 (1994)
[5] J.R. Waterman *et al.*, Semicond. Sci. Technol. 8, S106 (1993)
[6] J.R. Meyer *et al.*, ICPS 1994

Corresponding author: Gelu Comanescu, State University of New York at Buffalo, Amherst Campus, Department of Physics, 239 Fronczak Hall, Buffalo NY,14260-1500
Phone: +01 716 645 2389, Fax: +01 716 645 2507,
Email: gc1@acsu.buffalo.edu; gc1@mccombe.physics.buffalo.edu

Magnetic field-induced enhancement of terahertz emission from III-V semiconductors

A. Corchia[1], M.B. Johnston[1], R. McLaughlin[1], D.D. Arnone[2], E.H. Linfield[1], A.G. Davies[1], M. Pepper[1,2]

[1]*Semiconductor Physics Group, Cavendish Laboratory, University of Cambridge, Madingley Road, Cambridge CB3 0HE, UK.*

[2]*Toshiba Research Europe Limited, Cambridge Research Laboratory, 260 Cambridge Science Park, Milton Road, Cambridge CB4 0WE, UK*

The terahertz (THz) frequency range, usually defined as 100GHz–10THz, represents a significant portion of the electro-magnetic spectrum for which compact, solid-state sources are still not available. Neither transit time devices (e.g. HEMTs and Gunn diodes) operating up to a few hundred GHz, or optical sources lying on the higher frequency side (e.g. infra-red lasers and LEDs) can efficiently span the 'THz gap'. Recently, the need for such sources has been significantly emphasised by the demonstration of promising biomedical applications of THz spectroscopy and imaging [1], which stand together with traditional and well-developed applications within solid-state physics.

Semiconductor surfaces have been widely used as THz emitters by exploiting bulk electro-optic rectification, a process in which a non-linear polarisation is induced by sub-picosecond laser pulses, resulting in emission of THz radiation. An alternative ultra-fast generation mechanism is surface field photoconduction, in which the intrinsic electric field at a semiconductor surface accelerates photogenerated carriers. Their coherent motion results in the cooperative emission of THz radiation. Recent results have shown that the THz power emitted from surfaces of InAs, GaAs and InSb after photoexcitation can be significantly enhanced by placing the semiconductor in a magnetic field [2,3]. Together with an enhancement in the emitted THz power, a change in the polarisation of the THz field has been observed, which is ascribed to the Lorentz force affecting the carrier trajectory. The maximum radiated power possible from such systems and the mechanisms by which a magnetic field can enhance emission have, however, been an issue of great debate.

We will address this issue by comparing detailed experimental results with simulations of THz emission from both InAs (see Figure 1) and GaAs surfaces in magnetic fields of up to 8T. Both semiconductors were excited by 1nJ pulses of 1.57eV photons from a mode-locked Ti-Sapphire laser, with emission measured both by an incoherent bolometer detection scheme and coherent electro-optic sampling. InAs and GaAs were chosen for this study since they exhibit fundamentally different surface field generation mechanisms. Emission from InAs is dominated by the difference in the mobilities of hot electrons and hot holes, whilst from GaAs the acceleration of cold electrons in the surface depletion field dominates. In both cases, however, our three-dimensional model of the carrier dynamics in the vicinity of the semiconductor surface successfully explains the behaviour of the measured THz power with magnetic field and its observed polarisation dependence.

Our results will demonstrate the key roles played by carrier-carrier scattering induced saturation of the THz power, and screening of internal electric fields. Both effects are magnetic field dependent and are critical in obtaining a full understanding of THz generation in a magnetic field – a point not fully appreciated in earlier studies.

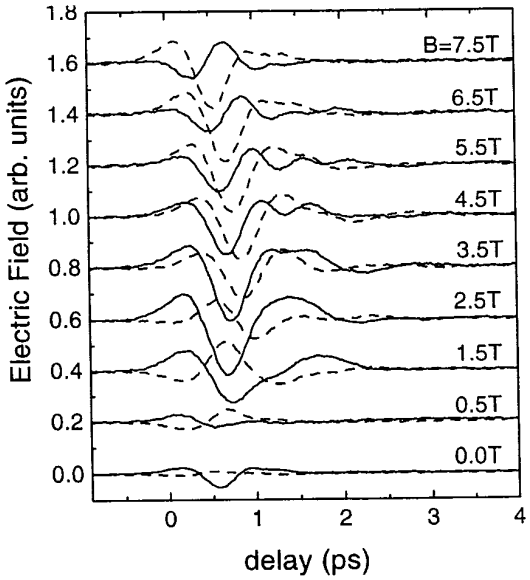

Fig.1: Experimentally observed radiated THz transient from the surface field of InAs. A 45° reflection geometry was used with the magnetic field parallel to the propagation of the emitted THz radiation. The transients at different magnetic fields are offset for clarity. *TM* polarisation transients are shown in solid lines, *TE* polarisations in dashed lines.

References:
[1] C.M. Ciesla, D.D. Arnone, A. Corchia, D. Crawley, C. Longbottom, E.H. Linfield, and M. Pepper, Proceedings of SPIE **3934**, 73 (2000).
[2] R. McLaughlin, A. Corchia, M.B. Johnston, Q. Chen, D.D. Arnone, G.A.C. Jones, E.H. Linfield, A.G. Davies, and M. Pepper, *Appl. Phy. Lett.* **76**, 2038 (2000).
[3] H. Ohtake, S. Ono, M. Sakai, Z. Liu, T. Tsukamoto, and N. Sarukara, *Appl. Phy. Lett.* **76**, 1398 (2000).

Corresponding Author: Edmund Linfield, Cavendish Laboratory, Madingley Road, Cambridge, CB3 0HE, UK,
Phone: +44 1223 337387, Fax: +44 1223 337271
email: ehl10@cam.ac.uk

Terahertz-Quantum Cascade Emitters

J. Ulrich, R. Zobl, W. Schrenk, G. Strasser, K. Unterrainer

Institut für Festkörperelektronik, Technische Universität Wien,
Floragasse 7, A-1040 Wien, Austria

The need of compact sources of coherent radiation in the frequency regime between 1 and 10 THz has stimulated the development of a terahertz (or far-infrared) quantum cascade (QC) laser [1-3]. A simple scaling of the successful concept of mid-infrared QC-lasers [4] is impracticable because resonant emission of longitudinal optical (LO) phonons (in GaAs at 8.7 THz, 36 meV) cannot be utilized likewise, and because waveguide losses caused by free carrier absorption become crucial at THz-frequencies.

Fast intersubband relaxation between subbands mediated by electron-electron scattering in combination with emission of LO-phonons from hot electrons counteracts population inversion [1]. We demonstrate that the relaxation rate is significantly reduced in a magnetic field applied perpendicular to the growth direction [5]. This effect manifests itself in an enhancement of the electroluminescence efficiency and in a reduction of the current. The electroluminescence intensity and the current show characteristic magneto-oscillations stemming from Landau-intersubband resonances. The periodicity of the oscillations allows to deduce the energy of the intersubband transition. The amplitude of the oscillations is a measure for the fraction of the current undergoing the transition designed for luminescence.

The above mentioned measurement techniques allow us to compare different band structure designs. Two similar samples with emission photon energies around 18 meV have been grown, one based on an intrawell transition, the other based on an interwell transition [6]. The interwell emission peak is slightly broader than the intrawell emission and exhibits a Stark-shift of 6 meV. The spontaneous emission efficiency of both samples reaches its maximum when the miniband is flat, that is, when the carrier injection into the initial subband of the transition is expected to be optimal. The intrawell and interwell transition have about the same efficiency. This means that the total relaxation rate is reduced by the same amount as the radiative transition rate when the initial and final subbands become spatially separated.

Incorporating thin AlAs barriers instead of $Al_{0.15}Ga_{0.85}As$ barriers leads to an improvement of the injection efficiency. Using a barrier height of 1000 meV in the band structure calculation, we get a good prediction of the transition energy and flat miniband voltage. The higher barriers suppress the fraction of the current not passing through the laser transition. This becomes obvious from a smaller overall current density, from a stronger oscillatory component in the current vs. magnetic field characteristics [see Fig 1], and from a higher electroluminescence efficiency [see Fig 2].

In conclusion, we suggest that a terahertz-quantum cascade laser should be based on an intrawell transition (because of the narrower emission line and the more stable emission frequency) in the AlAs/GaAs material system (because of the reduced dark current). Its operation could be facilitated by an in-plane quantization of the electron motion in a magnetic field, as we have demonstrated, or in quantum dots.

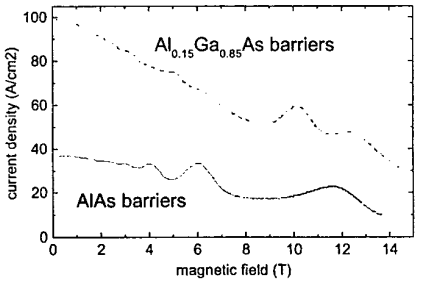

Fig. 1: Current density vs. magnetic field characteristics of two samples with different barrier materials.

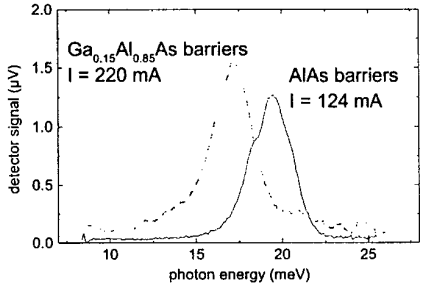

Fig. 2: Intersubband electroluminescence spectra of two samples with different barrier materials. The emission from the AlAs-barrier sample has about the same peak intensity at a significantly smaller current and there is less broadband background emission.

References

[1] M. Rochat, J. Faist, M. Beck, U. Oesterle, and M. Ilegems, Appl. Phys. Lett. 73, 3724 (1998).
[2] J. Ulrich, R. Zobl, N. Finger, K. Unterrainer, G. Strasser, and E. Gornik, Physica B 272, 216 (1999).
[3] B. S. Williams, B. Xu, Q. Hu, and M. R. Melloch, Appl. Phys. Lett. 75, 2927 (1999).
[4] J. Faist, F. Capasso, D. L. Sivco, C. Sirtori, A. L. Hutchinson, and A. Y. Cho, Science 264, 553 (1994).
[5] J. Ulrich, R. Zobl, K. Unterrainer, G. Strasser, and E. Gornik, Appl. Phys. Lett. 76, 19 (2000).
[6] J. Ulrich, R. Zobl, W. Schrenk, G. Strasser, K. Unterrainer, and E. Gornik, Appl. Phys. Lett. 77, 1928 (2000).

Corresponding author: Jochen Ulrich,
Institut für Festkörperelektronik, Technische Universität Wien,
Floragasse 7, A-1040 Wien, Austria
phone: +43-1-58801-36228, Fax: +43-1-58801-36299
email: Jochen.Ulrich@tuwien.ac.at

Tailoring photon emission statistics of a single quantum box for quantum communications.

E. Moreau, J.M. Gérard, I. Robert and I. Abram
CNRS/Laboratoire Photonique et Nanostructures, 196 av. Henri Ravera, 92220 Bagneux
Tel : 33 1 42317156 Fax : 33 1 42534930 jeanmichel.gerard@rd.francetelecom.fr

Quantum cryptography (QC) is intensively studied, as a possible way to improve confidentiality on communication channels. Various schemes have been proposed for QC, either based on single photon states or on pairs of photons in an entangled state. The development of solid-state sources able to generate such quantum states of light is recognized as a critical issue for the practical implementation of quantum cryptography (QC) in telecommunications systems. Among solid-state emitters, self-assembled quantum dots display major assets such as stability, high quantum efficiency, easy electrical or optical non-resonant pumping, and the possible use of the Purcell effect in optical microcavities for collecting efficiently emitted single photons into a single mode.

Unlike atoms or molecules however, a single QD can store more than one elementary excitation (i.e. several electron-hole pairs). Particular excitation or detection schemes should be used to avoid the generation of more than one photon. We report here a detailed study of the statistical properties of the emission from a single QD, for continuous wave or pulsed excitation, as a function of the excitation power ; these properties are studied by microphotoluminescence (including time resolved PL measurements on single QDs), and photon correlation spectroscopy.

We have proposed to implement the strong Coulomb interaction between trapped charge carriers in a QD [1]. If several electron-hole pairs are injected in a QD after a pulsed excitation, several photons are emitted during its sequential desexcitation, at different energies. A spectral selection can then be performed to collect the « last emitted » photon (X line) or the « two last emitted photons » (X line + XX line). The successful emission of single photon pulses with this approach has been recently evidenced by several groups [2] using photon correlation experiments.

Complementary information is obtained by studying by microphotoluminescence a single InAs QD at 8K for a pulsed non-resonant optical excitation. For a sufficiently strong excitation, the intensities of the exciton (X) and biexciton (XX) lines do not depend on the excitation power, and are equal within experimental accuracy. The saturation behavior confirms that during the sequential radiative desexcitation of a QD (into which several electron-hole pairs have been injected), a single photon at most is emitted within the X and XX lines. The saturation at the same intensity for X and XX lines reveals that non-radiative processes are negligible and that one photon per pulse is actually emitted into each lines by the QD. This result is essential for the generation of photon pairs using QDs.

The sequential desexcitation of a QD has been investigated by time-resolved spectroscopy and photon correlation spectroscopy : we compare the X and XX lifetimes, and demonstrate for the first time that XX photons are always emitted before X photons. This observation provides a firm support to the identification of the X and XX lines as being related to a single QD.

Finally, we compare the excitation power dependence of a single QD under pulsed and cw excitation. This comparison highlights the unique sensitivity of QDs to the excitation protocol, and shows their emission statistics can be tailored to a large extent. A quantitative fit of these dependences can be obtained by simple rate equation models, and allows to probe if a QD is neutral or contains already one electron (or one hole) when unexcited.

[1] J.M. Gérard et al, J Lightwave Technol, 17, 2089 (99)
[2] P. Michler et al, Science 290, 2282 (00) ; Santori et al, PRL fev 2001

Entangled states of electron-hole complex in a single InAs/GaAs coupled quantum dot molecule in a magnetic field

M. Korkusinski[1], P. Hawrylak [1], M. Bayer[2], G. Ortner[2], A. Larionov[2], V.B.Timofeev[2], A.Forchel[2], S. Fafard[1], Z. Wasilewski[1]

[1]Institute for Microstructural Sciences, National Research Council of Canada, Ottawa, K1A OR6, Canada

[2]Technische Physik, Wurzburg University, Am Hubland, D-97074, Wurzburg, Germany

An electron-hole complex in a pair of coupled quantum dots represents a simple example of a pair of entangled qubits [1]. The information carried by individual qubit is related to the quantum dot index (isospin). We present here new results of calculations and experiments on electron and valence hole states in a single pair of vertically stacked and electronically coupled InAs self-assembled quantum dots in a magnetic field. The effect of spin, valence band mixing, quantum dot radius, height, and quantum dot separation on the emission spectrum is investigated. The calculation starts with the calculation of strain. The strain enters the Bir-Pikus Hamiltonian and allows the determination of the effective band offset and the splitting of the light holes and the spin split-off band. The effective mass approximation and the k*p approach are employed to calculate the electron and the valence hole levels of coupled dots using the recursive Green function method and the adiabatic approximation. The single particle electron and hole levels are further used in the calculation of direct and exchange electron-hole scattering matrix elements, and of the exciton spectrum. The effect of quantum dot molecule asymmetry on electron and/or hole tunneling is treated perturbatively. The results of calculations are compared with results of photoluminescence measurements of the exciton fine structure in several coupled quantum dot molecules in a magnetic field up to 8 T. The fine structure is found to vary depending on the degree of quantum dot symmetry. In quantum molecules with high symmetry a spin-split doublet dominates the ground state exciton emission. In molecules of low symmetry, a splitting into excitonic manifold occurs. The splitting shows pronounced anti-crossing behavior as a function of the magnetic field. The fine structure of the exciton emission in a magnetic field carries information on tunneling of spin by electrons and by holes. Comparison of theory and experiment will be presented.

References

[1] M. Bayer, P. Hawrylak, K. Hinzer, S. Fafard, M. Korkusinski, Z. R. Wasilewski , O. Stern and A. Forchel , Science **291**, 451 (2001).

Corresponding author: Pawel Hawrylak, Institute for Microstructural Sciences, National Research Council of Canada, Ottawa, K1A OR6, Canada

phone: +001 613 993 9389, Fax: +001 613 993 9389

email: pawel.hawrylak@nrc.ca

Spintronics and Quantum Computing in Semiconductors

Daniel Loss
Department of Physics
University of Basel, Switzerland

If the states of electron spins in solids can be created, manipulated, and measured at the single-quantum level, an entirely new form of information processing, quantum computing and quantum communication, will be possible [1]. I review [2] our proposed spin-quantum dot architecture for a quantum computer, thereby indicating a variety of first generation nanostructures, as well as magnetic and electrical measurements which should be considered. I will discuss a spin filter and spin detection mechanism [3] at the single-spin level which can be used for read-in and read-out in conventional as well as in quantum computer gates. Addressing the feasibility of quantum communication with entangled electrons [4,5] I discuss electronic Einstein-Podolsky-Rosen pairs produced by an ``Andreev entangler"[6,7] and show that the spin entanglement of two electrons (in a Fermi sea) can be detected in transport and noise measurements in mesoscopic systems [4,5].

[1] D. Loss, D.P. DiVincenzo, Phys. Rev. A 57 (1998) 120; cond-mat/9701055.
[2] G. Burkard, H.A. Engel, D. Loss, Fortschr. Phys. 48, 9-11, 965 (2000).
[3] P. Recher, E. Sukhorukov, D. Loss, Phys. Rev. Lett. 85, 1962 (2000).
[4] H.A. Engel, D. Loss, to appear in Phys. Rev. Lett. (April '01); cond-mat/0011193.
[5] D. Loss, E. Sukhorukov, Phys. Rev. Lett. 84, 1035 (2000).
[6] G. Burkard, D. Loss, E. Sukhorukov, Phys. Rev. B 61, R16303 (2000).
[7] M.-S. Choi, C. Bruder, D. Loss, Phys. Rev. B 62, 13569 (2000);
[8] P. Recher, E.Sukhorukov, D. Loss,to appear in Phys. Rev. B (April, '01); cond-mat/0009452.

Parallel synthesis and high throughput characterization of ZnO based alloy films, heterostructures and devices

M. Kawasaki

Department of Innovative and Engineered Materials, Tokyo Institute of Technology
Yokohama, 226-8502, Japan
and
Combinatorial Materials Exploration and Technology (COMET),
National Institute for Research in Inorganic Materials
Tsukuba, 305-0044, Japan

As an oxide wide band gap semiconductor, ZnO has attracted considerable attention for the application in short wavelength light emitting devices and laser diodes, since we reported on room temperature ultraviolet lasing due to exciton recombination where exciton has quite large binding energy of 60meV being stable under dense excitation at room temperature [1]. Extensive research since then has revealed the followings; laser cavity can be naturally made with using grain boundaries in self-assembled honeycomb structures made of nano-scale hexagonal crystals as mirrors [2], band gap can be tuned between 3 and 4eV by alloying with CdO or MgO [3], superlattices such as (Mg, Zn)O/ZnO can be made to observe quantum-size effect [4], and single crystal wafer of $ScMgZnO_4$ can be used as a lattice matched substrate[5]. It is important to fabricate and characterize many superlattices having different layer thickness or barrier height for understanding the detailed physics of excitons in superlattices for realizing highly efficient multiple quantum well lasers. However this kind of research is time consuming and sometimes boring because semiconductor physics is well matured to be able to predict most of the experimental results.

To make these tasks ***EASY*** and ***FAST***, we are focusing our efforts on the adoption of ***COMBINATORIAL CHEMISTRY*** to the epitaxial thin films research [6]. Combinatorial methodology was first introduced to the field of new drag synthesis and related bio- and organic- science and technology and has been extended to the search for better catalysts [7]. Here, we present parallel synthesis and high throughput characterization techniques to explore ZnO based opt-electronics.

By modifying the conventional pulsed laser deposition system by scanning RHEED and computerized masking and target holder systems, we are now able to integrate on a single crystalline substrate about 10 specimens, which have variant doping concentration [8] and/or variant component-layer thickness in superlattices [9]. For integrating more specimens on a substrate, we can use composition-spread approach where doping concentration has continuous gradient on a substrate to yield in practically 100 samples integrated on a substrate [10]. For analyzing these specimens, we have developed several high throughput techniques including concurrent X-ray diffraction, scanning SQUID microscope, microwave microscope, concurrent measurement system for transport properties, and spectroscopic microscopy.

In this talk, we present several topics selected from our recent activities including

(1) Parallel synthesis of ZnO based superlattices[9]
(2) Optical properties and efficient stimulated emission above room temperature[11]
(3) Systematic studies of exiciton properties in superlattices[12]
(4) Diluted magnetic semiconductor [13]
(5) Electronic devices such as invisible transistors.

However, true goal of this combinatorial approach is to find out something new and surprising, which brings impact to the scientific and industrial communities. For this purpose, we are now extending the research to the fields that are unrevealed, yet. One of the serendipitous discoveries is invisible ferromagnet in an oxide diluted magnetic semiconductor, Co-doped TiO2 (anatase) by Matsumoto et al. [14]

This work is conducted under the collaboration with Y. Segawa, Z. K. Tang, H. Ohno, H. Koinuma, T. Hasegawa, T. Chikyow, Y. Matsumoto, T. Fukumura, M. Lippmaa and their research teams.

References

[1] P. Yu et al., Proc. of 23rd Int'l Conf. on Physics of Semiconductors, 1996, p. 1453; K. Z. Tang et al., Solid State Comum, 103, 459 (1997).
[2] Z. K. Tang et al., Appl. Phys. Lett., 72, 3270 (1998).
[3] A. Ohtomo, Appl. Phys. Lett., 72, 2466 (1998); T. Makino et al., Appl Phys. Lett. 78, 1237 (2001).
[4] A. Ohtomo, Appl. Phys. Lett., 75, 980 (1999).
[5] A. Ohtomo, Appl. Phys. Lett. 75, 2635 (1999).
[6] See http://oxide.rlem.titech.ac.jp/combi/ for our COMET project activities.
[7] As an example of reviews, B. Jandeleit et. al., Angew. Chem. Int. Ed., 38, 2494 (1999).
[8] Y. Matsumoto et. al., Jpn. J. Appl. Phys., 38, L603 (1999).
[9] A. Ohtomo et al., Proc. SPIE 3941, 70 (2000).
[10] T. Fukumura et. al., Appl. Phys. Lett., 77 3426 (2000).
[11] Ohtomo et. al., Appl. Phys. Lett., 77, 2204 (2000).
[12] T. Makino et al., Appl. Phys. Lett. 77, 975 (2000); Appl. Phys. Lett. 76, 3549 (2000); H. D. Sun, et al., Appl. Phys. Lett. 77, 4250 (2000); Appl. Phys. Lett., March 26 issue (2001).
[13] T. Fukumura et al., Appl.Phys. Lett., 75, 3366 (1999); Appl. Phys. Lett., 78, 958 (2001).
[14] Y. Matsumoto et. al., Science 291, 854 (2001).

Corresponding author: Masashi Kawasaki,
Department of Innovative and Engineered Materials, Tokyo Institute of Technology
Nagatsuta, Midori, Yokohama, 226-8502, Japan
phone: +81-45-924-5362, Fax: +81-45-924-5399
email: kawasaki@oxide.rlem.titech.ac.jp

How to make GaN-Electronics Work: Physics and Technology

Umesh K. Mishra
ECE Department
UCSB, Santa Barbara, CA. 93018
mishra@ece.ucsb.edu

Gallium Nitride based materials have established themselves as crucial to the opto-electronics industry filling the spectral gap from green to the UV for a variety of applications such as displays, lighting and potentially high density storage. The applications of GaN-based materials to electronics has however had a slower beginning because of existing solutions in applications of interest primarily in power electronics (for switching and power conditioning applications) and microwave sources and amplifiers for communications and RADAR. For Gallium Nitride to penetrate these markets, it has to provide either a compelling performance advantage or reduced cost or, as the electronics industry has taught us over and over again, preferably both.

The most promising insertion of GaN seems to be that of AlGaN/GaN HEMTs in the microwave arena. Here the growth of the AlGaN/GaN structure is performed either on Sapphire (Al_2O_3) or on semi-insulating SiC. The latter is preferred because of the high thermal conductivity of the substrate and the lack of oxygen as an unintentional dopant , a constant problem with Sapphire as the substrate. The two-dimensional electron gas (2DEG) in the channel can be induced either purely by the net positive polarization charge at the AlGaN/GaN interface or in combination with a donor (most commonly Si) in the AlGaN. It is our hypothesis that charge neutrality requires that the surface have a positive charge to balance the 2DEG concentration and this is provided by a deep surface donor. The disadvantage of this surface state is that the large time constants associated with charging and discharging the states leads to dispersion between the small signal and large signal characteristics of the HEMT. This problem is mitigated by surface passivation using SiN. The mechanism of the solution is not fully determined as yet. The mobility of the 2DEG has recently been theoretically analyzed and experimentally verified to be dominated by alloy scattering (once the epitaxial layer growth has been optimized to minimize interface roughness scattering). This has led to the development of AlN/GaN based HEMTs where the alloy scattering has been eliminated by the use of binary compounds. The 2 DEG sheet resistance in these structures is now below 180 ohms/sq., comparable with the AlInAs/GaInAs system. A combination of advanced underatnding of the physics and improved technologies has led to a power density of over 9.8 W/mm at X-band almost a factor of 10 over the conventional GaAs system

The development of HBTs in the AlGaN/GaN system will also discussed and issues of p-type doping highlighted.

Luminescence in Silicon Nanostructures and their Interaction with Erbium Ions

F. Priolo[(a)], G. Franzò[(a)], F. Iacona[(b)], E. Ceretta Moreira[(a)], D. Pacifici[(a)], A. Irrera[(a)], L. Dal Negro[(c)] and L. Pavesi[(c)]
[(a)]INFM and Dipartimento di Fisica, Università di Catania, Catania, Italy
[(b)]CNR-IMETEM, Catania, Italy
[(c)]INFM and Dipartimento di Fisica, Università di Trento, Trento, Italy

In the last decade quite a strong effort has been devoted towards the achievement of efficient light emission from silicon. Among the different approaches rare-earth doping and quantum confinement in Si nanostructures have shown great potentialities.
In the present work the luminescence properties of several different low dimensional silicon structures will be analyzed and compared. It will be shown that both Si ion implantation and chemical vapor deposition represent quite powerful tools to achieve nanometer sized Si structures embedded within SiO_2. Depending on the preparation conditions the dimensions can be properly varied. Moreover, nanocrystalline Si/SiO_2 superlattices can be formed with the Si nanocrystals (nc) being almost completely isolated among themselves. All of these structures present a strong room temperature optical emission, a weak luminescence temperature dependence and a clear blue shift of the luminescence with decreasing crystalline size. By measuring the risetime of the luminescence signal at different laser pump powers it has been possible to determine the Si nc excitation cross section σ_{NC}. It has been demonstrated that σ_{NC} for almost isolated Si nc is ~ 2×10^{-16} cm^2.
Moreover we will show that optical gain and stimulated emission can be achieved from Si nanocrystals when prepared under particular conditions. It is shown that emission spectra have a strong line narrowing under amplification conditions and optical gain is demonstrated also in a single pass configuration.
Finally the characteristics of Si nc embedded within Si/SiO_2 Fabry-Perot microcavities are investigated. It is shown that very narrow (up to $\Delta\lambda$~1.5 nm) and intense luminescence peaks can be obtained at different wavelengths between 700 and 900 nm by properly setting the cavity resonance (see Fig. 1). The luminescence intensity of the on-axis emission is over an order of magnitude above that of similar samples without a cavity and the overall luminescence is confined within a 30° cone from the sample normal.
A detailed investigation on the interaction mechanisms between Si nanocrystals and Er ions introduced by ion implantation will be also presented. When nanocrystals are doped with Er they absorb energy which is then preferentially transferred to the rare earth. Many points appear of extreme interest in this process. First of all the nanocrystals act as efficient sensitizers for Er which is excited much more efficiently than in pure SiO_2. Indeed, room temperature luminescence yields two orders of magnitude higher are observed for Er-doped SiO_2 in presence of nanocrystals than in pure SiO_2. Moreover, since Er is now embedded within a SiO_2 matrix, the non-radiative decay channels typically limiting Er luminescence in Si are absent. This further improves the luminescence yield which is almost temperature independent in the range 15-300 K. When Er is implanted in Si nc, the *nc*-related luminescence is quenched while the Er-related luminescence at 1.54 μm appears and increases with increasing Er dose. High resolution luminescence spectra of Er doped Si nc are identical to those of Er doped SiO_2, while they are very different from those of Er doped crystalline Si, suggesting that the emitting Er ions are located in the SiO_2 or at the Si nc/SiO_2 interface. The effective excitation cross section of Er ions through Si *nc* has been determined to be ~1.1×10^{-16} cm^2. This number resembles the excitation cross section of *nc* themselves demonstrating that the coupling is extremely strong.
Finally the characteristics of Er-doped Si nc embedded within Si/SiO_2 Fabry-Perot microcavities are investigated. It is shown that very narrow ($\Delta\lambda$~5 nm) and intense luminescence peaks can be obtained at around 1.54 μm for Er-doped Si nc by properly setting the cavity resonance. In analogy with the Si nc optical microcavity the luminescence intensity of the on-axis emission is over an order of magnitude above that of similar samples without a cavity and the overall luminescence is confined within a 30° cone from the sample normal.
These data will be presented and the future trends and applications discussed.

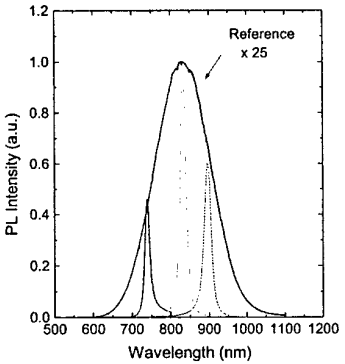

Fig. 1: Room temperature PL spectra for three different Si nanocrystals microcavities having resonances at 739, 830 and 897 nm. The PL spectrum of the same Si nanocrystals outside the cavity is also reported (multiplied by a factor of 25).

Corresponding author:
Francesco Priolo
INFM and Physics Department
University of Catania
Corso Italia 57
95129 Catania (Italy)
tel: +39-095-7195421
fax: +39-095-383023
e-mail: priolo@ct.infn.it

Semiconductor nanotubes and nanopipelines

O. G. Schmidt
Max-Planck-Institut für Festkörperforschung, Heisenbergstraße 1, 70569 Stuttgart, Germany

Recently, it was shown that nanotubes can be formed from thin solid films released from their substrate[1,2]. There are two methods for making these solid-state nanotubes[2], involving a 'general' (method I) and a 'specialized' (method II) procedure. Both rely on the release of thin layers from a substrate by selective etching. For the general method I, a thin solid film of almost arbitrary composition is detached from its substrate and folded back onto its own surface (see Fig. 1a). The resultant crease forms a nanotube. The specialized method II relies on inherently built-in strain within the thin solid film. Once the film is freed from the substrate, the layer rolls up by itself and forms a nanotube (see Fig. 1b).

A SiGe based nanotube, which has formed along the edge of the sample, is shown in Fig. 2. The tube is 20 μm long and has a diameter of 530 nm. It adopts a slight bend of the sample edge and its position is precisely defined by the etching time.

The huge potential that lies in this nanofabrication process is demonstrated by a spectacular multi-wall nanotube shown in figure 3. The tube consists of a 4 nm thick InGaAs epitaxial layer that has rolled up over a distance of 50 μm (Fig. 3a) on a GaAs (001) surface. The tube is 9 μm long (see Fig. 3b) and has a diameter of 500 nm. The nanotube's perimeter of about 1.6 μm suggests that the tube has performed about $n = 30$ rotations during the roll-up procedure. We can only speculate about this surprisingly large number of rotations. However, a zoom into the lower opening of the nanotube proofs that the tube has completed at minimum eight revolutions (see Fig. 3c). The inner tube walls are formed in a homogeneously circular fashion whereas some wrinkles are evident in the outer layers. Such multi-wall nanotubes might have fascinating new physical properties since the neighbouring layers are likely to bond together and form a perfect new single crystal. Nanotubes with a wide range of properties could be tailored since semiconductor epitaxy delivers unrivalled control over material composition, doping concentrations and layer thicknesses.

Further design freedom is achieved by combining different materials. We were able to combine semiconductor (SiGe), insulator (silicon dioxide), and a metal (titanium) layers into a single nanotube. The initial layer sequence is given in figure 4a by a cross-sectional transmission electron microscopy image. The semiconductor layer sequence allows for nanotube roll-up according to method II. The inherent forces causing the up-bending of the layers are strong enough to roll-in the insulator and the top-lying titanium film. The final result of the nanotube formation is depicted in figure 4b. The SEM image reveals a straight and homogeneous SiGe/SiO_x/Ti nanotube with a diameter of 310 nm.

Figure 5 shows an examples of how to accomplish more sophisticated nanotube structures. To create this nanopipeline system (by method I), we processed a curved nanoslit into the sample surface and the epi-layer was detached and folded back onto the sample surface parallel to this curvature. This special geometry causes the epilayer to produce distinct folds on the surface which are perpendicular to the main nanotube. Such self-formed creases could be used as inlet and outlet channels for fluid or gas supply into the main nanopipeline.

[1] V. Y. Prinz et al., Physica E 6, 828 (2000).
[2] O. G. Schmidt and K.Eberl, Nature 410, 168 (2001).

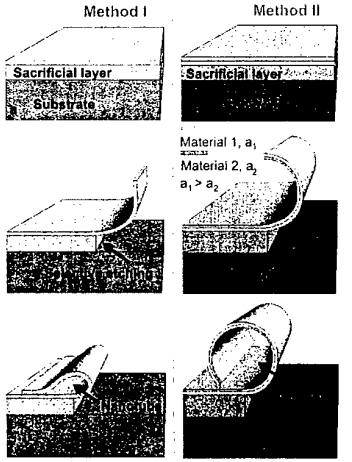

Fig. 1: Nanotube formation after (a) general method and (b) a specialised method involving a strained bilayer released from its substrate. In both cases a nanotube or nanopipeline forms.

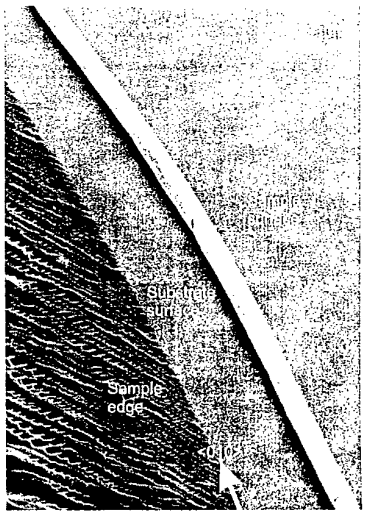

Fig. 2: SiGe nanotube formed along the [010] edge of a Si substrate.

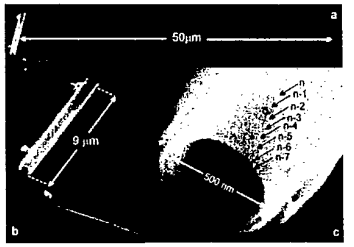

Fig. 3: InGaAs nanotube rolled up on a GaAs surface for at minimum 8 times.

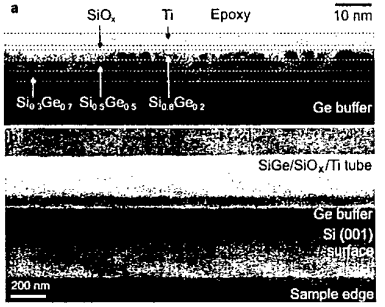

Fig. 4: Integration of a semiconductor (SiGe), an insulator (SiO2) and a metal (Ti) into a single nanotube.

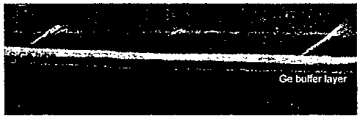

Fig. 5: Pipeline system with Inlet/Outlet channels. The system was fabricated using the general procedure described in Fig. 1a.

Coupled quantum dots in single-wall carbon nanotubes

K.Ishibashi[1], M.Suzuki[2], T.Ida[1] and Y.Aoyagi[1,3]

[1] Semiconductors Laboratory, The Institute of Physical and Chemical Research (RIKEN), 2-1, Hirosawa, Wako, Saitama 351-0198, Japan
[2] Department of Electrical and Electronics, Toyo University, 2100, Kujirai, Kawagoe, Saitama 350-8585, Japan
[3] Interdisciplinary Graduate School of Science and Technology, Tokyo Institute of Technology, 4259, Nagatsuda, Midoriku, Yokohama, Japan

Single-wall carbon nanotubes (SWNTs), because of their extremely small diameter of about 1nm, could be used for the building block of coupled quantum dot system with a size which is difficult to achieve with conventional lithography. We have established the process to fabricate electrical contacts to individual SWNTs, and realize the single quantum dot [1]. In this paper, we present our recent experimental results on the formation of coupled quantum dots by depositing a narrow SiO_2 layer on SWNTs in between the current contacts (Fig.1).

After the current contacts were fabricated on the individual SWNTs, the coulomb diamond measurement was carried out at 4.2K, and the result is shown in Fig.2(a). In this measurement, the I-V curves were measured with one gate voltage varied in step and the other unbiased (see Fig.1), and displayed with offsets. The regular and periodic appearance of the Coulomb diamond indicates the single quantum dot formation. The charging energy (e^2/C_Σ: C_Σ the self capacitance) and the spacing (ΔE) of zero-dimensional confined levels are about 10meV and 5.3meV, respectively. After the single quantum dot formation was confirmed, this sample was taken out of the cryostat, and the SiO_2 layer was deposited on the same SWNTs in between the current contacts using mark alignment technique in electron beam lithography and lift off. The result of the Coulomb diamond measurement after the SiO_2 deposition is shown in Fig.2(b). In this measurement, the same gate was varied as in the case of Fig.2(a). There are clear differences compared with the results in Fig.2(a). These are (1) widened Coulomb gap, (2) irregular Coulomb diamonds and (3) negative differential conductance (NDC).

Above experimental observations suggest the formation of coupled quantum dots. The deposited SiO_2 layer seems to have divided the single dot into two. The Coulomb blockade characteristics ((1) and (2)) may be explained by the stochastic Coulomb blockade which occurs in two-dot system with different self-capacitance. The widened Coulomb gap might be attributed to the reduced size of the dots. Taking into account the fact that NDC was not observed in the single dot before the deposition, the observed NDC is possibly due to the resonant tunneling between discrete levels in each dot. The detailed resonant mechanism is not clear yet, but we will also present the temperature and bias dependence of the Coulomb blockade oscillations which seem to show electrostatic coupling effect between the two dots.

References
[1] K.Ishibashi, T.Ida, M.Suzuki, K.Tsukagoshi and Y.Aoyagi: Jpn. J.Appl. Phys. 39 (2000) 7053

Corresponding author: Koji Ishibashi, Semiconductors Laboratory, The Institute of Physical and Chemical Research (RIKEN), 2-1, Hirosawa, Wako, Saitama 351-0198, Japan
Phone: +81-48-462-1111 Fax: +81-48-462-4659 E-mail: kishiba@postman.riken.go.jp

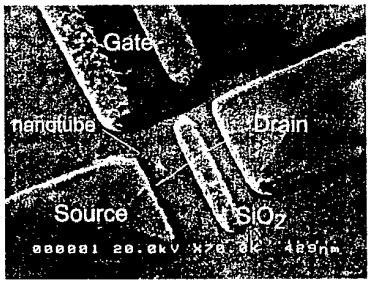

Fig.1: SEM micrograph of one of the completed devices

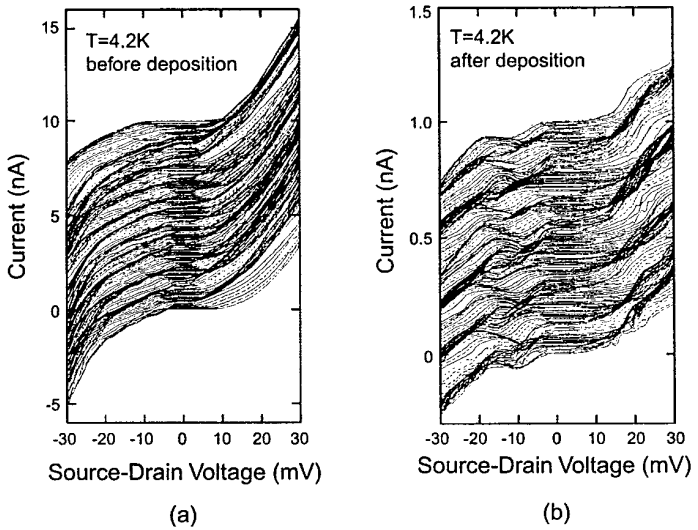

Fig.2: Coulomb diamond measurement
(a) before and (b) after the SiO_2 deposition

Coherent Inter- and Intramolecular Phonons in Quasi-1D Organic Crystals

T.W. Canzler[1], T. Hasche[1], R. Scholz[2] , K. Leo[1]

[1] Institut für Angewandte Photophysik, Technische Univesität Dresden, 01062 Dresden, Germany
[2] Institut für Physik, Technische Universität Chemnitz, 09107 Chemnitz, Germany

Organic thin films with semiconducting properties are very promising for device applications such as charge transport layers, organic LED, and solar cells. Particularly attractive for applications are molecules which form quasi-1D molecular crystals with strong orbital overlap between neighboring molecules: Here, the strong intermolecular interaction is expected to favor the generation and transport of charge carriers. However, the phonon properties of such 1D organic crystals, especially exciton self-trapping, might be critical for the realization of emission devices. Therefore, a detailed investigation of the exciton-phonon interaction is required.

We have time resolved the coherent motion of external and internal phonons in thin films of MePTCDI (N-N'-dimethylperylene-3,4,9,10-dicarboximide), employed as a model system for a quasi-1D organic molecular semiconductor [1]. We applied a femtosecond pump-probe technique, in which an 25 fs pump pulse excites the lowest energy exciton band of the sample and a time-delayed probe pulse measures the resulting transmission change as a function of pump-probe delay. The phonon modes coupled to the excitonic transition are impulsively excited, creating wave packets which oscillate at the characteristic phonon frequencies of the material. The time-resolved transmission change following impulsive excitation is given in Fig. 1. The most conspicuous feature is a strong modulation due to propagating phonon wave packets. The absolute Fourier Amplitude of a fit to the oscillating part is shown in Fig. 2. and reveals oscillations at eleven different frequencies.

We have performed calculations of the internal vibrations of an isolated MePTCDI molecule using density-functional tight-binding methods [2]. We assign the three highest energy oscillations to A_g–symmetric intramolecular phonons by comparing the experimental oscillation energies with these calculated internal phonon frequencies and with literature data from resonant Raman scattering. The six oscillations at lower energy are ascribed to librational lattice phonons. This interpretation is based on symmetry considerations and a comparison with literature data for experimental lattice phonon energies of β-perylene, which has the same crystal structure as MePTCDI. The two lowest energetic modes are assigned to B_g–symmetric intramolecular phonons. These modes are predicted by our calculation and symmetry considerations support this assignment. In addition, we will discuss the experimentally determined damping times of the external modes, which show a systematic decrease with increasing phonon energy.

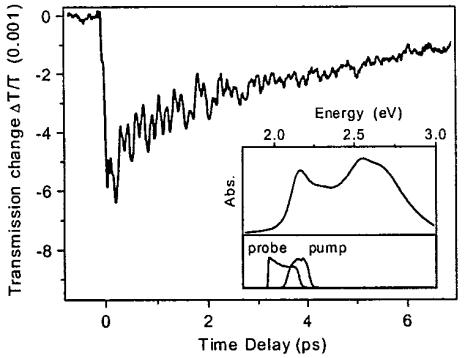

Fig. 1: Time-resolved differential transmission of the MePTCDI layer. Inset: Absorbance of the thin film sample and spectral shape of pump- and probe pulses.

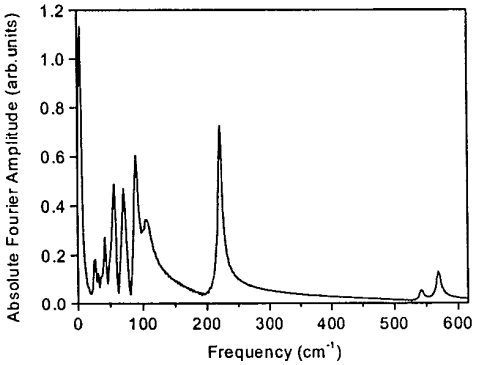

Fig. 2: Absolute of the complex Fourier amplitude of the fitted oscillatory contribution to the experimental signal. The three highest energetic modes stem from intramolecular A_g vibrations, the six modes between 33 and 105 cm^{-1} from librational lattice phonons and the two lowest energetic modes at 5 and 25 cm^{-1} are due to intramolecular B_g modes.

References

[1] T. Hasche, T.W. Canzler, R. Scholz, M. Hoffmann, K. Schmidt, Th. Frauenheim, and K. Leo, Phys. Rev. Lett., accepted for publication.
[2] R. Scholz et al., Phys. Rev. **B 61**, 13659 (2000).

Corresponding author: Tobias W. Canzler, Institut für Angewandte Photophysik, Technische Univesität Dresden, 01062 Dresden, Germany.
phone: +49 351 463 2464, Fax: +49 351 463 7065
email: canzler@iapp.de

Tuning of optical gain in soluble thiophene-based oligomers

M.Anni[1], G.Gigli[1], M. Zavelani-Rossi[2], C. Gadermaier[3], G. Lanzani[2], G.Barbarella[4], L. Favaretto[4], R.Cingolani[1]

[1]Istituto Nazionale Fisica della Materia (INFM), Dip. Ingegneria dell'Innovazione, Università di Lecce, Via per Arnesano, 73100 Lecce, ITALY
[2] Dip. Fisica, Politecnico di Milano, Piazza L. Da Vinci 32, 20133 Milano, ITALY
[3] Dip. Matematica e Fisica, Università di Sassari, Via Vienna 2, 07100 Sassari, ITALY
[4]Consiglio Nazionale delle Ricerche (CNR), ICOCEA, Area della Ricerca di Bologna, Via Gobetti 101, 40129 Bologna ITALY

Great attention has been paid in the last years to the research of good active material for solid state organic lasers. One of the main advantages of organic materials stands in cheap device technology, which exploits spin coating or direct printing on flexible plastic substrates over large areas, provided the materials are soluble. To date the study of optical amplification on thiophenes, characterized by a high chemical stability, is limited to single crystals of short insoluble molecules, not suitable for technological applications. However, recent results on the thienyl-SS-dioxide functionalization of thiophenes, have revealed their wide tunability [1], high chemical stability [2], increased electron affinity [3] and excellent solubility in common organic solvents, thus making the modified thiophenes appealing candidates for organic lasers and Light Emitting Diodes (LEDs).

In this work we report on the evidence of optical gain in spin coated films of soluble thiophene-S,S-dioxide oligomers. The molecular functionalization allows to obtain photoluminescence efficiency up to 70 % and tunable emission from blue to near infrared. We demonstrate through pump-probe measurements that the materials show optical gain with a maximum gain cross section of $9*10^{-18}$ cm^{-2}. The different functionalization pattern allows us to obtain tunable optical gain in the range from 490 nm to 680 nm. The gain lifetime is studied through time resolved pump and probe with 150 fs resolution.

The amplification and lasing properties of a prototype molecule of the family are studied. The PL spectrum shows an evident line narrowing for excitation density higher than 960 μJcm^{-2} which is attributed to Amplified Spontaneous Emission (ASE) assisted by wave-guiding in the film slab. The gain spectrum is about 20 nm broad, peaked at 616 nm and has a maximum value of 14.5 cm^{-1} for an excitation density of 1.53 mJ cm^{-2}. In order to describe the lasing properties of the molecule a resonant dielectric cavity is studied. The molecule shows single mode laser emission for pump energy higher than 4.3 mJ cm^{-2}. The broad gain spectrum allows to tune the wavelength of laser emission from 590 nm to 620 nm. These results are remarkable for future applications of thienyl-S,S-dioxide oligomers to optically pumped microcavity lasers. These molecules show full tunability among the visible and near infrared spectrum by using the same chemistry. Their high solubility in all common organic solvents together with the good film forming properties allows to use spin-coating for the device realization. Moreover their increased electron affinity, already exploited in the realization of efficient, stable, and low turn on voltage multicolor LEDs [4] makes these molecules interesting for electrically driven devices.

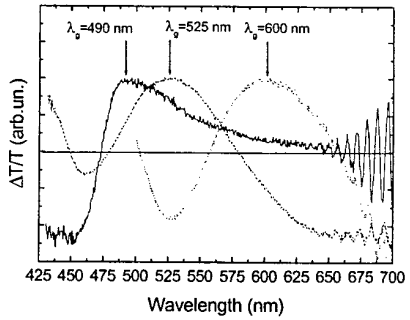

Fig.1: Differential transmission spectra of three molecule with different functionalization pattern. The tunable gain ($\Delta T>0$) in the range 490-680 nm is clearly visible.

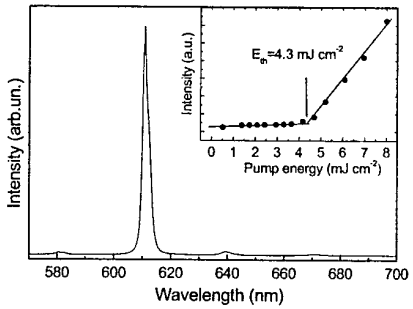

Fig.2: PL spectrum of the red emitting molecule over the lasing threshold. Inset: input-output characteristic of the laser, the threshold of lasing, as well as the linear dependence on the output intensity on the pump density are visible.

References

[1] M. Anni, G. Gigli, V. Paladini, R. Cingolani, G. Barbarella, L. Favaretto, G. Sotgiu, and M. Zambianchi, Appl. Phys. Lett. **77**, 2458 (2000).
[2] G. Barbarella, L. Favaretto, M. Zambianchi, O. Pudova, C. Arbizzani, A. Bongini, and M. Mastragostino, Adv. Mat. **10**, 551 (1998).
[3] G. Barbarella, L. Favaretto, G. Sotgiu, M. Zambianchi, V. Fattori, M. Cocchi, F. Cacialli, G. Gigli, and R. Cingolani, Adv. Mater. **11**, 1375 (1999).
[4] G. Gigli, O. Inganas, M. Anni, M. De Vittorio, G. Barbarella, L. Favaretto and R. Cingolani, Appl. Phys.Lett **78**, 1493 (2001).

Corresponding author: Marco Anni, Istituto Nazionale di Fisica della Materia, Univarsità degli Studi di Lecce,Dipartimento di Ingegneria dell'Innovazione. Via per Arnesano 73100 Lecce, Italy.
phone: +390832320231, Fax: +390832326351
email: marco.anni@unile.it

Electronic Properties and Conductivity of Guanine Assemblies

E. Molinari[1], R. Di Felice[1], A. Calzolari[1], A. Garbesi[2]

[1]INFM – Dipartimento di Fisica ,Università di Modena e Reggio Emilia, via Campi 213/A, 41100 Modena, Italy
[2]CNR ISOF, Area della Ricerca, via P. Godetti 101, 40129 Bologna, Italy

Because of their sequence-specific recognition properties, DNA molecules are attractive for the construction of nanometer scale electronics, where their self-assembling capability might be used to wire the electronic materials in a programmable way [1]. Moreover, there is currently a lively research effort to exploit double-stranded DNA molecules as conductors to fabricate molecular electronic devices. Indeed, a recent experiment has demonstrated conductivity in a poly(G)-poly(C) DNA sequence [2]. A semiconducting behavior was displayed by a metallic nanogate filled with a dried solution of a lipophilic derivative of 2'-deoxyguanosine [3]. Despite the evidence of charge migration in the mentioned solid-state experiments [2,3], as well as in solution-chemistry experiments [4], there is no unanimous agreement on the actual conductance and on the microscopic mechanisms that control electron or hole mobility in DNA-base assemblies.

We have addressed the above issues by performing DFT-GGA ab-initio calculations of the structural and ground state electronic properties of extended model structures whose building block is the guanine (G) base alone. These models are the simplest base pair aggregates characterized experimentally [3], and allow feasible theoretical simulations and direct comparison with experimental data.

We have considered stacked and hydrogen-bonded structures, including vertical stacking of G-quartets [5] and ribbons [6]. For stacked geometries, the stability is affected by the relative charge distribution of the π orbitals in adjacent guanine molecules. π –π coupling in some stacked columns induces dispersive energy bands, while no dispersion is identified in the planar ribbons along the connection of hydrogen bonds. The bandstructure and the calculated conductance of dispersive configurations may justify a contribution of Bloch-type band transport to the conduction of deoxyguanosine fibers, while in B-DNA-like configurations band transport is expected to be negligible, and other mechanisms for mobility must play a role.

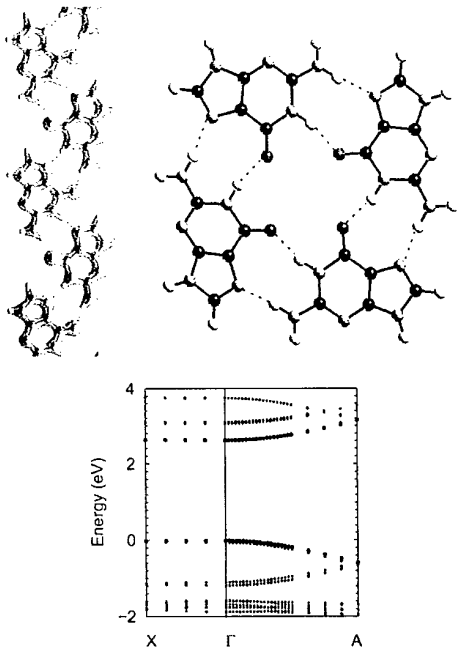

Fig. 1: Top view images of the structure of G ribbons (top left) and of G4 quartets (top right). The bottom panel shows the calculated bandstructure of a vertical periodic stack of eclipsed ribbons, along two mutually orthogonal reciprocal space directions. The dispersion of the HOMO and LUMO bands is negligible in the ΓA direction (along the ribbon), whereas it is finite in the ΓX direction (perpendicular to the plane of the ribbon).

References

[1] E. Braun, Y. Eichen, U. Sivan, and G. Bel-Yoseph, Nature 391, 775 (1998).
[2] D. Porath, A. Bezryadin, S. de Vries, and C. Dekker, Nature 403, 635 (2000).
[3] R. Rinaldi, E. Branca, R. Cingolani, R. Di Felice, E. Molinari, S. Masiero, G.P. Spada, G. Gottarelli, and A. Garbesi, submitted (2001).
[4] B. Giese, Acc. Chem. Res. 33, 631 (2000); D.B. Hall, R.E. Homlin, and J.K. Barton, Nature 382, 731 (1996).
[5] K. Phillips, Z. Dauter, A.I.H. Murchie, D.M.J. Lilley, and B. Luisi, J. Mol. Biol. 273, 171 (1997).
[6] G. Gottarelli, S. Masiero, E. Mezzina, S. Pieraccini, J.P. Rabe, P. Samorì, and G.P. Spada, Chem. Eur. J. A 6, 3241 (2000).

Corresponding author: Prof. Elisa Molinari, INFM – Dipartimento di Fisica ,Università di Modena e Reggio Emilia, via Campi 213/A, 41100 Modena, Italy.
Phone: +39 059 2055284, Fax: +39-059-374752
Email: molinari@unimo.it

Recent results in quantum cascade lasers and intersubband transitions in GaN/AlGaN multiple quantum wells

C. Gmachl,[1] H. M. Ng,[1] S. V. Frolov,[1] R. Paiella,[1] R. Martini,[1] H. Y. Hwang,[1] D. L. Sivco,[1] F. Capasso,[1] A. Y. Cho,[1] and H. C. Liu[2]

[1]Bell Laboratories, Lucent Technologies, 600 Mountain Ave., Murray Hill, NJ 07974, USA
[2]Institute for Microstructural Sciences, NRC, Ottawa, ON, K1A 0R6 Canada

Quantum cascade (QC) lasers have reached a considerable level of performance, such as emission wavelengths ranging from 3 to 24 μm, very high peak output power levels in the Watt range, and above room temperature operation [1]. As a result, new interest is directed towards the investigation and optimization of more complex device properties such as the lasers' high-speed properties.

Here we focus first on improved QC lasers fabricated with chalcogenide lateral waveguide claddings. Several-micrometer thick $Ge_{0.25}Se_{0.75}$ glass has been deposited by pulsed laser ablation onto the side walls of narrow, deep etched laser ridges. The intrinsically low mid-infrared attenuation of the chalcogenide material helped reduce the waveguide loss of the lasers significantly, by up to ~ 50 %, when compared to conventional ridge waveguides. This resulted in an improved overall laser performance, such as a reduction of the threshold current density, an increase in slope efficiency, and an improved temperature performance. [2] The thick chalcogenide cladding and burying layer also significantly reduced stray capacitance of the devices and improved their high-speed modulation properties, allowing easily for direct modulation up to 2 GHz. This has been exploited to demonstrate a first use of QC lasers in optical wireless communications such as a free-space television link over a distance of 70 meters. [3]

The lasers' high-speed capabilities have furthermore been exploited for their active and passive mode-locking. In both cases, pulses as short as a few (3-5) picoseconds with a repetition rate around 12 GHz, the round-trip frequency of the lasers have been measured. [4]

Fueled by this recent success of high-speed modulated mid-infrared QC lasers, optical devices based on intersubband (IS) transitions face a rising interest also in other wavelength ranges. The intrinsically ultrafast electron dynamics associated with IS-transitions warrants research into the latter for the communications wavelength range ($\lambda \sim 1.55$ μm). Few material systems, however, provide a sufficiently large band-discontinuity for the quantum wells (QWs) to accommodate the large subband spacing needed for such short wavelengths, Sb-based materials or group-III-nitrides presently being the best candidates. The rapid success of GaN-based interband light emitting diodes and lasers makes this material system particularly attractive. Here, we present our initial measurements of IS-transitions in the communications wavelength range, with peak absorption wavelengths as short as 1.4 μm. [5]

The wurtzite-type GaN/AlGaN MQW samples were grown by molecular beam epitaxy on c-axis sapphire substrate with GaN and AlGaN buffer layers of varying composition and thickness. In particular, a strained $Al_{0.65}Ga_{0.35}N$ buffer layer was used in combination with very high AlN mole fraction QW barriers, in order to alleviate problems associated with the otherwise giant strain. Two types of samples were grown, MQWs with single QWs and bulk-like barriers, and also single QWs with superlattice (SL)-type barriers. The latter use electron Bragg confinement from the SL to increase electron confinement in the upper subband(s) and henceforth allow the use of lower AlN mole fraction barriers. IS-absorption at wavelengths of 1.44, 1.41, and 1.52 μm are measured for 11, 12, and 13 Å wide GaN QWs, respectively.

Fig. 1, left, shows a transmission electron microscope image of the second type of structures, which use SL barriers. The active absorbing GaN QW was 16 Å wide and the SL barriers consisted of three 8 Å wide GaN QWs interleaved with 16 Å wide 65 % AlN mole-fraction barriers. All samples contained 15 nominally identical repetitions of that structure and a GaN buffer layer. Several more combinations of SLs and QWs were grown and tested, the shortest peak absorption wavelength obtained being 1.52 μm. In particular, the insertion of the SL QWs now allows modulation doping of the main QW. Fig. 1, right, shows the transmission spectrum with a peak absorption wavelength of 1.67 μm. For this particular sample we also measured the intersubband electron scattering time using conventional pump-probe technique. Using 1.55 μm as pump- and 1.70 μm as probe-wavelength, we obtain an electron scattering time of 370 fs. This result is encouraging for the implementations of IS-transitions in ultrafast optical components.

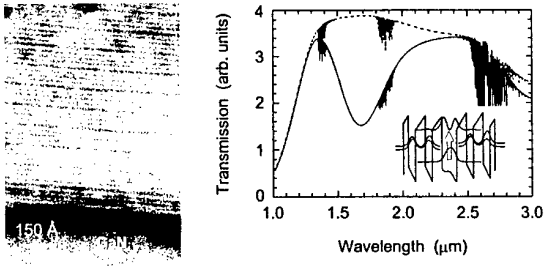

Fig. 1: *Left:* Transmission electron microscope image of a portion of a GaN MQW structure with superlattice barriers. Light gray layers indicate $Al_{0.65}Ga_{0.35}N$, dark gray layers GaN. *Right:* Transmission spectrum of this GaN/AlGaN MQW structure (solid line) and background spectrum (dashed line). The measurements have been taken in multiple pass geometry, in p-polarization, and the spectra have been matched in intensity. Inset: Energy diagram of a portion of the conduction band of the GaN/AlGaN MQW structure; the open arrow indicates the IS-absorption process.

References

[1] F. Capasso et al., IEEE J. Select. Topics Quantum Electron. 6, 931 (2000) and references therein.
[2] C. Gmachl et al., accepted for publication in IEEE Photon. Techn. Lett. (2001).
[3] R. Martini et al., Electron. Lett. 37, 191 (2001).
[4] R. Paiella et al., Science 290, 1739 (2000).
[5] C. Gmachl et al., Appl. Phys. Lett. 77, 3722 (2000).

Corresponding author: Claire Gmachl, Bell Laboratories, Lucent Technologies,
600 Mountain Ave., Murray Hill, NJ 07974, USA
phone: +1 908 582 6164, Fax: +1 908 582 7660
email: cg@lucent.com

Intervalley scattering in GaAs-AlAs quantum cascade lasers

L.R.Wilson[1], D.A.Carder[1], M.J.Steer[1], J.W.Cockburn[1], M.Hopkinson[2], C.K.Chia[2], G.Hill[2], R.Airey[2]

[1] Department of Physics and Astronomy, University of Sheffield, Sheffield S3 7RH, UK
[2] EPSRC III-V Semiconductor Central Facility, Department of Electronic and Electrical Engineering, University of Sheffield, Sheffield S1 3JD, UK

Significant advances in GaAs-based quantum cascade (QC) laser performance have been achieved in recent months. In particular, a reduced temperature sensitivity of device performance for QC lasers incorporating high, indirect bandgap ($1 \geq x \geq 0.4$) $Al_xGa_{1-x}As$ barriers relative to QC lasers with direct $Al_{0.33}Ga_{0.67}As$ barriers has been demonstrated. However, device operation is ultimately limited by negative differential resistance effects arising from intervalley (Γ-X) scattering. It is therefore essential to understand the role of intervalley scattering in determining QC laser performance in order to optimise device design.

Here we present the first study of the effects of Γ-X scattering in QC lasers. We show that for lasing to occur electron injection into the upper laser level must proceed via Γ states confined below the lowest X state in the injection barrier. We overcome the limit this places on the minimum operating wavelength ($\lambda \approx 8\mu m$) by utilising a novel injection barrier design to achieve lasing at $\lambda = 7.2\mu m$. In addition, we achieve excellent laser performance from a GaAs-AlAs QC laser incorporating InAs monolayers in the active regions. The InAs monolayers have a minimal effect on the upper laser level but decrease the confinement energy of the lower laser level. Thus a significantly reduced emission wavelength (8.2μm compared with 11.2μm) is achieved whilst maintaining very similar laser performance.

A series of 4 GaAs-AlAs QC lasers has been investigated in which the energy separation between the ground state of the injection region (E_{inj}) and the confined X state in the injection barriers (E_X) is varied. The samples contain 45 periods, with each period consisting of a 6-well bridging/injector region and 2-well active region. Fig. 1 shows the moduli squared of the relevant wavefunctions for a section of the conduction band profile of the longest emission wavelength ($\lambda \approx 9\mu m$) laser (sample A). Under operating conditions, the ground state of the bridging region (E_{inj}) and the E3 are energetically aligned and electrons are injected through the injection barrier into E3 at an energy below the lowest confined X state in the AlAs barrier (E_X). The laser transition occurs between levels E3 and E2. The active region well widths are reduced from sample A to sample C, increasing the E3 confinement energy and the calculated laser transition energy (E3-E2). In addition, the quantum well widths in the injector regions are reduced from sample A to C, increasing the confinement energy of E_{inj}. The injection barrier thickness (20Å) is constant for all samples and consequently the energy separation of E_X and E_{inj} is reduced from 24meV for sample A to 12meV for sample B. In sample C, E_X lies 27meV <u>below</u> E_{inj}.

Laser spectra measured under pulsed current operation just beyond threshold are displayed in Fig. 2. The transition wavelengths are in good agreement with calculations, with $\lambda = 9.0\mu m$ and 8.5μm measured for samples A and B, respectively. No laser emission was observed from sample C. This result clearly suggests that in sample C, where the X state lies below E_{inj}, electrons scatter from E_{inj} to E2 and E1, via E_X, thus reducing the injection efficiency into E3. This reduces the E3-E2 population inversion below the value required for lasing. The energetic crossover of E_{inj}(E3) with E_X therefore limits the shortest operating wavelength for GaAs-AlAs layers incorporating a single AlAs injection barrier to $\lambda \geq 8\mu m$. In order to overcome this limitation we have designed a sample (sample D) in which the injection "barrier" consists of two narrow (8Å) AlAs layers separated by a 6Å GaAs layer. As shown in Fig. 3, the use of thin AlAs barriers increases the confinement energy of the barrier X states such that E_X now lies above E_{inj} (E_X-E_{inj}=62meV). In contrast to sample C this novel approach results in laser emission, with the measured low temperature laser emission wavelength, $\lambda = 7.25\mu m$, (Fig. 2) agreeing well with the calculated transition wavelength ($\lambda = 7.1\mu m$). Sample D also exhibits a superior temperature performance (T_0=148K above T=120K) relative to samples A and B (T_0=120K). This is a result of the increased E_X-E_{inj} energy separation which reduces thermally activated leakage of electrons from the injector region through E_X.

In addition to our Γ-X scattering studies we have advanced the work of Ref. [1] in which InAs monolayer deposition in the active regions of a GaAs-$Al_{0.33}Ga_{0.67}As$ laser was used to significantly reduce the emission wavelength. We have now designed and tested GaAs-AlAs QC lasers incorporating InAs monolayers. A substantial improvement in laser performance has been achieved relative to Ref. [1] with the present devices emitting at $\lambda \approx 8.2\mu m$ ($\lambda \approx 11.2\mu m$ without InAs) and operating up to 250K with a high T_0=185K. The current-voltage characteristics indicate that energy level misalignment within the structure limits the maximum operating temperature, suggesting that with suitable minor design modifications room temperature operation should soon be possible.

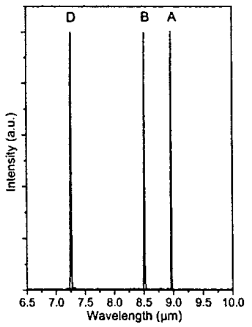

Fig. 2. Low temperature laser spectra measured for samples A, B and D.

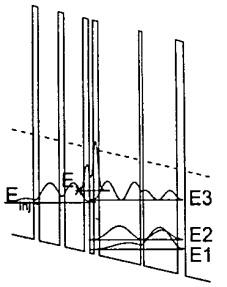

Fig. 3. Γ (solid) and X (dashed) conduction band profile for sample D.

Fig. 1. Γ (solid) and X (dashed) conduction band profile for sample A.

References

[1] L.R.Wilson, J.W.Cockburn, M.J.Steer, D.A.Carder, M.S.Skolnick, M.Hopkinson and G.Hill, Appl. Phys. Lett. **78**, 413 (2001).

Corresponding author: Luke Wilson, Department of Physics and Astronomy, University of Sheffield, Hicks Building, Hounsfield Road, Sheffield S3 7RH, UK.
phone: +44 114 2223599, Fax: +44 114 2728079
email: Luke.Wilson@Sheffield.ac.uk

High performance single mode GaAs quantum cascade lasers

W. Schrenk[1], E. Gornik[1], H. Page[2], C. Sirtori[2], V. Ortiz[2], G. Strasser[1]

[1]Solid State Electronics, TU Wien, Floragasse 7, A-4040 Vienna, Austria
[2]Laboratoire Central de Recherche, THALES-CSF,91404 Orsay, France

Quantum cascade laser (QCL) have proven to be a reliable coherent source in the mid-infrared regime. In this sophisticated multilayer structures intraband optical transitions are used for the generation of light. The wavelength of these lasers can be designed engineering electronic states by means of their quantum mechanical confinement. Since the first demonstration of quantum cascade lasers in the GaInAs/AlInAs/InP [1] and the GaAs/AlGaAs material system [2] continous progress in design and performance of quantum cascade lasers have been made. For a variety of applications like chemical sensing, single mode emission by distributed feedback can be achieved [3]. The emission wavelength is continuously tunable according to the temperature dependence of the effective refractive index. We fabricated GaAs-based first order DFB lasers to achieve single mode emission [4].

In this work we intent to present the latest results we achieved in the improvement of GaAs based QCLs. Starting from single mode DFBs we demonstrated second order surface emitting single mode quantum cascade lasers [5]. Very recently we reported about continuous-wave operation of first-order distributed feedback quantum cascade lasers at λ = 11.8 µm [6], based on inter-miniband transitions in a AlAs/GaAs superlattice. The active material consists of 40 periods of an AlAs/GaAs chirped superlattice. A plasmon enhanced waveguide is used for vertical optical confinement while lateral electrical and optical confinement is achieved by deep etched ridges. The Bragg grating is defined by contact lithography and etched into the surface of the top cladding layer, thus avoiding the need of regrowth. The whole grating region is covered with gold, resulting in a large contact area. The lasers, with as cleaved facets, are mounted (epilayer up) in a flow cryostat.

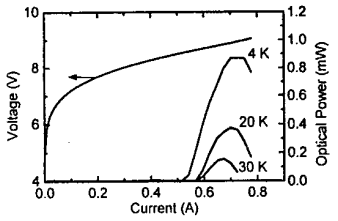

Fig. 1: Voltage and output power vs. current of an L = 0.665mm long and w = 30µm wide distributed feedback laser in continuous-wave operation for several heat sink temperatures.

The absolute power of the emitted light is measured with a calibrated thermopile detector (Fig. 1). The emission wavelength depends on the laser current, because of the electrical heating in the active material. We derive the effective temperature in the laser cavity from the emission wavelength. We use the measured dependence of the emission wavelength from the heat sink temperature in pulsed-mode operation (pulse repetition rate 5 kHz; pulse length 100 ns), where the effective temperature change within a pulse can be neglected and the average heat load is low.

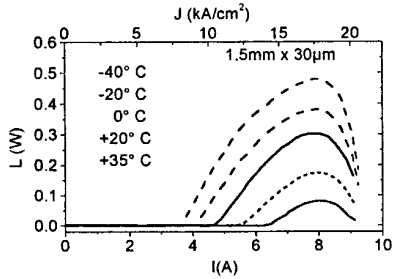

Fig. 2: Voltage and output power vs. current of an L = 1.5 mm long and w = 30µm wide distributed feedback laser in pulsed operation for several heat sink temperatures.

Additionally we want to report about pulsed single mode emission from a GaAs-based quantum cascade laser working at room temperature. This material consists of a GaAs/AlGaAs heterostructure with 45 % Aluminum in the barrier material and is the first GaAs- based QCL showing lasing at room temperature [7]. 36 periods of active material are embedded in plasmon enhanced waveguide and the Bragg grating is processed as described above. Single mode emission up to 65°C was achieved at an emission wavelength of $\lambda \approx 9.5$ µm, tunable with temperature. The absolute power of the emitted light (as-cleaved facets) for various temperatures is shown in Figure 2.

References

[1] J. Faist, F. Capasso, D. L. Sivco, C. Sirtori, A. L. Hutchinson, and A. Y. Cho, Science **264**, 553 (1994)
[2] C. Sirtori, P. Kruck, S. Barbieri, P. Collot, J. Nagle, M. Beck, J. Faist, and U. Oesterle, Appl. Phys. Lett., **73**, 3486 (1998).
[3] J. Faist, C. Gmachl, F. Capasso, C. Sirtori, D. L. Sivco, J. N. Baillargeon, and A. Y. Cho, Appl. Phys. Lett., **70**, 3486 (1998).
[4] W. Schrenk, N. Finger, S. Gianordoli, L. Hvozdara, G. Strasser, E. Gornik, Appl. Phys. Lett. **76**, 253 (2000).
[5] W. Schrenk, N. Finger, S. Gianordoli, L. Hvozdara, G. Strasser, and E. Gornik, Appl. Phys. Lett. **77**, 2086 (2000).
[6] W. Schrenk, N. Finger, S. Gianordoli, E. Gornik, and G. Strasser, Appl. Phys. Lett. **77**, 3328 (2000).
[7] H. Page, C. Becker, A. Robertson, G. Glastre, V. Ortiz, C. Sirtori, "300K Operation of a GaAs based Quantum Cascade Laser at $\lambda \approx 9$ µm", submitted to Appl. Phys. Lett.

Corresponding author: Gottfried Strasser, Institut für Festkörperelektronik, Technische Universität Wien, Floragasse 7, A-1040 Wien, Austria.
phone: +43 1 58801 362 18, Fax: +43 1 58801 362 99
email: gottfried.strasser@tuwien.ac.at

Optimized large optical cavity design for 10.8 µm (Al)GaAs Quantum Cascade Laser

N. Ulbrich[1], G. Scarpa, A. Sigl, M. Bichler, D. Schuh, M.-C. Amann and G. Abstreiter

[1]Walter Schottky Institute, Technical University of Munich, Am Coulombwall 3, D-85748 Garching, Germany

Quantum cascade lasers have shown tremendous performance improvements and technological progress since their first demonstration in the material system InGaAs/InAlAs lattice matched to InP[1]. The use of (Al)GaAs heterostructures as unipolar lasers has been successfully demonstrated about three years ago[2]. Despite significant improvements for both material systems, however, room-temperature continuous wave operation still represents the major challenge for further developments. In GaAs based quantum cascade lasers the use of GaAs cladding layers with appropriate doping profile imposes several advantages over AlGaAs as cladding material including comparatively lower absorption losses and the possibility to grow very thick cladding layers which is advantageous especially for long wavelength (λ>10 µm) lasers[3]. We believe, however, the waveguide losses α_w to be still one of the strongest limiting factors on the performance of GaAs based intersubband lasers, with α_w being predominantly controlled by free-carrier absorption.

We report on the development of an optimized design for a large optical cavity waveguide of a 10.8 µm (Al)GaAs quantum cascade laser presenting theoretical and experimental results on the reduction of free-carrier plasma absorption losses. The waveguide design of our reference sample, which is based on published values[4], is displayed in figure 1. Two 3.8 µm thick $n_{Si}=8\cdot10^{16}$ cm^{-3} doped GaAs layers are used as waveguide core which is sandwiched between two $n_{Si}=8\cdot10^{18}$ cm^{-3} doped GaAs layers as cladding material.

We have grown several samples with identical active regions emitting at 10.8 µm and different waveguides. The parameters that can be varied in order to optimize the waveguide design are: doping concentration and thickness of the heavily doped cladding layers and of the low doped separate-confinement GaAs layers, respectively. Here, we varied the doping concentration in order to maximize the figure of merit Γ_{AR}/α_w, where Γ_{AR} is the confinement factor of the mode in the active region. Table 1 contains the results of our calculations for our different samples. The calculated waveguide losses can be reduced from 28.2 cm^{-1} for our reference sample (sample A) to 21.7 cm^{-1} for sample D while maintaining approximately the same confinement factor Γ_{AR} in the active region which results in an increase of the figure of merit by 28 % from $1.14\cdot10^{-2}$ cm to $1.46\cdot10^{-2}$ cm. For our calculations we use the classical Drude model for the complex dielectric constant of semiconductors to calculate the mode profile and the absorption losses α_w of the waveguide with α_w being calculated taking into account only the free-carrier absorption coefficients of the four layers forming the waveguides.

Figure 2 shows a plot of the threshold current densities versus reciprocal cavity length for the four different samples. A good optical confinement with a low threshold current density could be achieved in sample D with a 3.8 µm thick core with a doping concentration of $n_{Si}=4\cdot10^{16}$ cm^{-3} and a highly doped 1.2 µm cladding with $n_{Si}=8\cdot10^{18}$ cm^{-3}. We have achieved a reduction of the threshold current density by 30 % to $J_{th}(inf)=3.41$ kA/cm^2 compared to our reference sample (4.84 kA/cm^2). The other 2 samples with a lower doping of the cladding layers ($n_{Si}=6\cdot10^{18}$) show higher current densities than the reference laser which we believe is due to a larger penetration of the optical mode into the metallic contacts. In conclusion we have grown several different waveguides for a 10.8 µm GaAs quantum cascade laser. By reducing the free-carrier absorption losses in the thick waveguide core we achieved a reduction of the threshold current density by 30 % compared to our reference.

	Γ_{AR}	α_W	Γ_A / α_W
Sample A	32.2 %	28.2 cm^{-1}	$1.14\cdot10^{-2}$ cm
Sample B	30.9 %	25.3 cm^{-1}	$1.22\cdot10^{-2}$ cm
Sample C	30.4 %	22.2 cm^{-1}	$1.37\cdot10^{-2}$ cm
Sample D	31.7 %	21.7 cm^{-1}	$1.46\cdot10^{-2}$ cm

Tab. 1: Confinement factor Γ_{AR}, waveguide lossses α_W and figure of merit Γ_A / α_W for different GaAs based quantum cascade lasers.

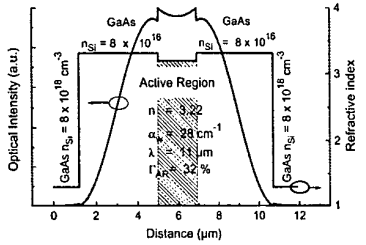

Fig. 1: Mode profile and refractive index profile of a large optical cavity (Al)GaAs quantum cascade laser.

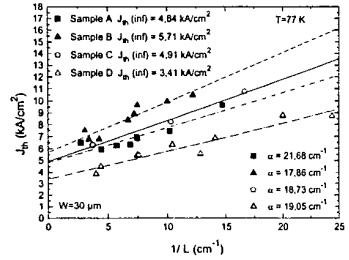

Fig. 2: Threshold current density vs. reciprocal cavity length for various doping profiles of our GaAs quantum cascade laser.

References

[1] J. Faist, F. Capasso, D. L. Sivco, C. Sirtori, A. L. Hutchinson, A. Y. Cho, Science **264**, 553 (1994)

[2] C. Sirtori, P. Kruck, S. Barbieri, P. Collot, J. Nagle, M. Beck , J. Faist, and U. Oesterle Appl. Phys. Lett. **73**, 3486 (1998)

[3] C. Sirtori, P. Kruck, S. Barbieri, H. Page, J. Nagle, M. Beck , J. Faist, and U. Oesterle Appl. Phys. Lett. **75**, 3911 (1999)

[4] P. Kruck, H. Page, C. Sirtori, S. Barbieri, M. Stellmacher and J. Nagle, Appl. Phys. Lett. **76**, 3340 (2000)

Corresponding author: Nicolaus Ulbrich, Walter Schottky Institute, Technical University of Munich, Am Coulombwall 3, D-85748 Garching, Germany
phone: +49 89 289 12776, Fax: +49 89 3206620
email: nicolaus.ulbrich@wsi.tu-muenchen.de

Far-Infrared Quantum Cascade Lasers at $\lambda > 20$ μm

Raffaele Colombelli, Federico Capasso, Claire Gmachl, Albert L. Hutchinson, Deborah L. Sivco, Alessandro Tredicucci, Michael C. Wanke, A. Michael Sergent, and Alfred Y. Cho

Bell Laboratories, Lucent Technologies, 600 Mountain Avenue, Murray Hill, NJ 07974

Quantum Cascade (QC) lasers have established themselves rapidly as tunable coherent sources in the mid-infrared (MIR) range of the electromagnetic spectrum [1]. The frontier of research has since expanded to further topics like new material systems, ultrahigh-speed operation and mode locking, and the exploration of new frequency ranges [2-5].
With regards to the latter, the extension to the far-infrared range (FIR) is of particular interest due to the lack of narrow-band, high-power, and compact sources in this wavelength range, but presents a formidable challenge related to physics issues and technical difficulties. At very long wavelengths, anomalies in the dielectric function forbid laser operation in proximity of the *reststrahlenband;* free carrier absorption becomes a dominant factor for the optical losses and *electron-electron* scattering can no longer be ignored as non-radiative recombination channel. Additionally, new types of waveguide concepts have to be adopted [6] in order to reduce the otherwise prohibitive large epitaxial layer thickness, enhance the optical confinement, and control the waveguide loss, and increased accuracy in the band-gap design becomes one of the key factors.

Here, we report the first QC lasers operating above 20 μm, in particular at 21.5 μm and 24 μm wavelength (see Fig. 1, insets). No other III-V semiconductor laser has operated previously at such long wavelength. Laser action, obtained up to a maximum temperature of 140 K and 130 K, respectively, and with a maximum output power of few mW (see Fig. 1), originates from interminiband transitions in appropriately "chirped" graded superlattices. We calculated very large optical dipole matrix elements of 4.6/4.8 nm and a lifetime of the upper laser state of ~ 0.7 ps.
The specific choice of the design wavelengths was guided by the presence of narrow gaps in the InGaAs two-phonon absorption spectrum. The absorption spectrum of any III-V semiconductor at frequencies just above the *reststrahlenband* consists of many intense absorption features related to two-phonon processes and van Hove singularities [7]. As these processes add optical loss to free-carrier absorption, it is important to avoid them to reduce the laser threshold.

The waveguide design consists of a surface-plasmon guide on top (a 300 nm thick gold layer) and of 1.5 μm of InGaAs n-doped to 7×10^{16} cm^{-3} on the bottom to enhance dielectric confinement; this results in a high confinement factor (Γ=0.88 and 0.76, respectively) and a calculated waveguide attenuation of α_w=40 cm^{-1}.

While the surface-plasmon waveguide solution provides very high performance for long wavelengths 17 – 24 μm QC lasers, it is obvious from calculations that in the quest for the realization of a QC laser at wavelengths on the lower energy side of the *reststrahlenband* ($\lambda > 50$ μm) the waveguide design must be further improved. For these reasons we designed and fabricated a laser at $\lambda = 21.5$ μm, in which the low-doped InGaAs layer below the cascade stack is replaced by a 750 nm thick highly doped n^{++}-InGaAs layer. The n^{++} doped semiconductor acts as bottom "metal" thus realizing a two-sided surface-plasmon waveguide, with an extremely high calculated confinement factor $\Gamma \sim 0.98$.

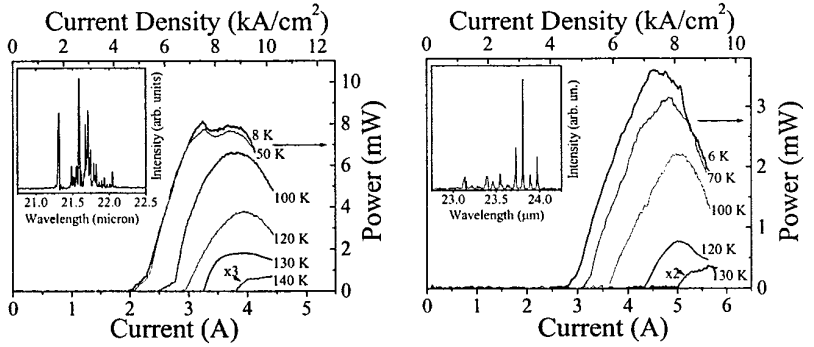

Fig. 1: L-I characteristics of the 21.5 μm (left) and 24 μm (right) wavelength lasers, for a 1.5 mm long, 31 μm and 36 μm wide device respectively, operated in pulse mode (50 ns pulse width, 5 KHz repetition rate). Insets: Pulsed (50 ns pulse width, 84 KHz repetition rate) emission spectra of the lasers. Devices are 36 μm wide and 750 μm long. The drive currents were 1.6 A and 1.75 A respectively. The spectra were measured in rapid scan using a Nicolet Fourier transform infrared spectrometer and a He-cooled Si-bolometer. The spectral resolution was set to 0.125 cm^{-1}.

The device exhibited a threshold current density of 7.1 kA/cm^2, approximately 1.7 times the threshold of the single-sided surface-plasmon, which were 4.1 kA/cm^2 and 4.6 kA/cm^2 for 21.5 μm and 24 μm wavelength, respectively. The discrepancy between the computed and measured longitudinal modes spacing indicates a stronger penetration of the mode into the n^{++} layer than expected, as the doping cannot be increased indefinitely. However, the result is encouraging since the waveguide loss of a double surface-plasmon waveguide will only decrease when we move to longer wavelengths. This is also the first functional "double-plasmon" QC laser, and provides the proof of principle for the suggested waveguide configuration for any submillimiter wavelength QC laser.

References

[1] F. Capasso, C. Gmachl, R. Paiella, A. Tredicucci, A. L. Hutchinson, D. L. Sivco, J. N. Baillargeon, A. Y. Cho, and H. C. Liu "New Frontiers In Quantum Cascade Lasers and Applications", *IEEE J. Select. Topics Quantum Electron.* **6**, pp. 931–947 (2000).
[2] C. Sirtori, P. Kruck, S. Barbieri, P. Collot, J. Nagle, M. Beck, J. Faist, and U. Oesterle, *Appl. Phys. Lett.* **73**, 3486-3488 (1998).
[3] C. Gmachl, H. M. Ng, and A. Y. Cho, *Appl. Phys. Lett.* **77**, 334 - 336 (2000).
[4] M. Rochat, J. Faist, M. Beck, U. Oesterle, and Marc Ilegems, *Appl. Phys. Lett.* **73**, 3724 (1998).
[5] R. Paiella, F. Capasso, C. Gmachl, D. L. Sivco, J. N. Baillargeon, A. L. Hutchinson, A. Y. Cho, and H. C. Liu, *Science* **290**, 1739 (2000).
[6] A. Tredicucci, C. Gmachl, F. Capasso, D. L. Sivco, A. L. Hutchinson, and A. Y. Cho, *Appl. Phys. Lett.* **76**, 2164 (2000), and references therein.
[7] E. S. Koteles, and W. R. Datars, *Solid State Comm.* **19**, 221 (1976).

Corresponding author: Raffaele Colombelli, Bell Laboratories, Lucent Technologies,
600 Mountain Avenue, room 7D-224, Murray Hill, NJ 07974
phone: +1 908 582 2731, Fax: +1 908 582 7660
email: colombel@physics.bell-labs.com

Cyclotron and intersubband emission of InGaAs/AlGaAs quantum cascade structures in the quantum regime

Stéphane Blaser, Michel Rochat, Mattias Beck, Jérôme Faist

Physics Institute, University of Neuchâtel, Rue A.-L. Breguet 1,CH-2000 Neuchâtel, Switzerland

Quantum cascade lasers based on intersubband transitions have been successfully demonstrated in the midinfrared. In contrast, the same quantum cascade technology have not yet been realized in the far-infrared (FIR). Nevertheless intersubband electroluminescence has been demonstrated by several groups [1].

It is well known that a magnetic field applied perpendicularely to the layers localizes the in-plane states into Landau levels. This added localization offers the possibility of simulating a quantum box structure: the intersubband emission should occur between Landau levels instead of subbands, efficiently quenching the non-radiative transitions like Auger scattering [2].

Magnetic field enhanced terahertz intersubband emission has been already observed in a GaAs/AlGaAs structure by Ulrich *et al.*, but only by a factor of two at 7.2 T [3]. The full quantum regime ($\hbar\omega_c > h\nu$) was not reached in these experiments. We present here measurements performed in high magnetic fields on a quantum cascade structure based on a vertical transition in AlInAs/InGaAs material. Both the cyclotron and intersubband emission were observed. Application of a magnetic field enhances the intersubband emission intensity by a factor of more than five at $B = 12$ T. Compared to GaAs/AlGaAs, the AlInAs/InGaAs material has a smaller effective mass ($m^* = 0.0427 \cdot m_0$), so the cyclotron energy is much larger (at 12 T, $\hbar\omega_c \sim 32$ meV and $h\nu \sim 15$ meV). So the lateral quantification due to the magnetic field is higher than the quantification in the layers direction. We are then in the quantum limit of the quantum box structure.

Fig. 1(a) shows spectra performed at a constant current of 40mA for different magnetic field between 0 and 9 T. We observe a substantial increase of the intensity of the intersubband emission by increasing the magnetic field on the sample. We observed also a second moving peak between 2 and 5.5 T. This peak is due to the cyclotron emission of the sample. Fig. 2 shows the transition energy of both intersubband and cyclotron emission vs. applied magnetic field up to 12 T. The positions of the cyclotron emission is in very good agreement with the theoretical values shown by the dashed curve. Fig. 1(b) shows the light intensity as a function of the magnetic field. We observe strong oscillations which we attribute to the magneto-intersubband resonances.

References

[1] M. Rochat, J. Faist, M. Beck, U. Oesterle, and M. Ilegems, Appl. Phys. Lett. **73**, 3724 (1998).

[2] S. Blaser, M. Rochat, M. Beck, J. Faist, and U. Oesterle, Phys. Rev. B **61**, 8369 (2000).

[3] J. Ulrich, K. Unterrainer, G. Strasser, and E. Gornik, Appl. Phys. Lett. **77**, 1928 (2000).

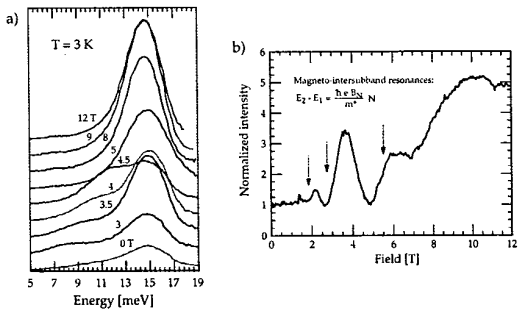

Figure 1: (a) Cyclotron and intersubband emission spectra at a constant current of 40mA for various magnetic fields. The spectra are plotted with arbitrary offsets. (b) Light intensity (normalized to the zero field value) vs. magnetic field for $I =$ 40mA. The arrows indicate the positions of the magneto-intersubband resonances with respect to the equation in insert.

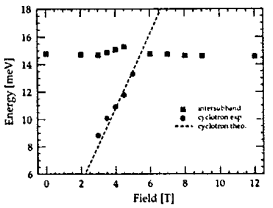

Figure 2: Transition energy vs. magnetic field for the intersubband emission (squares) and cyclotron emission, experimentally (circles) and theoretically (dashed curve).

Corresponding author: Stéphane Blaser, Physics Institute, University of Neuchâtel, Rue A.-L. Breguet 1,CH-2000 Neuchâtel, Switzerland.
phone: +41 32 718 2949, Fax: +41 32 718 2901,
email: stephane.blaser@unine.ch

Intersubband quantum cascades in the Si /SiGe material system.

L. Diehl,[1] G. Dehlinger,[1] H. Sigg,[1] U. Gennser,[2] D. Grützmacher,[1] E. Müller,[1]
J. Faist,[3] and K. Ensslin.[4]

[1] Paul Scherrer Institute, CH-5232 Villigen, Switzerland.
[2] LPS-CNRS, F-92220 Bagneux, France.
[3] Institute of Physics, University of Neuchâtel, CH-2000 Neuchâtel, Switzerland.
[4] Solid State Physics Laboratory, ETH Zürich, CH-8093 Zürich, Switzerland

The intersubband quantum cascade laser is today a versatile light source for the mid-infrared. Its principle may be of particular interest in conjunction with Si based materials, since it offers a path towards efficient light emission without the nature of the bandgap having any bearing on it. However, Si/SiGe heterostructures carry with them several material issues that have to be mastered, for example the high built-in strain. In addition, their valence band offset is highly dominant, so that vertical transport structures almost exclusively have been realized using hole conduction. This implies that in a Si/SiGe cascade structure a multiple series of heavy hole and light hole states must be controlled and the interaction between the different valence bands must be well understood.

We have recently reported the observation of intersubband electroluminescence from p-type Si/SiGe quantum cascade structures, centered at 120 - 130 meV with a width of approximately 20 meV [1]. The structures consist of 10 pseudomorphically grown, highly strained cascades. Here, evidence will be presented confirming that the electroluminescence peak arises from the intended transition between two heavy hole states in the main quantum well: measurements of confinement shifts, polarization dependence and differential absorption. The nonradiative lifetime is found to depend strongly on the design of the quantum well structure, and is shown to reach values comparable to that of an equivalent GaInAs/AlInAs laser structure. The role of confinement and phonon scattering to light hole states will be discussed.

In order to achieve a Si/SiGe quantum cascade laser complex questions still need to be addressed, such as the increase from 10 to 30-50 periods, the choice of lasing scheme, the implementation of an optical cavity, and the reduction of the free-carrier absorption in the samples. These issues will be considered in reference to work on SiGe strain relaxed buffer layer.

References

[1] G. Dehlinger, et al., Science 290, 2277 (2000).

Corresponding author: Ulf Gennser, Laboratoire de Photonique et de Nanostructures - CNRS,
196 Avenue Henri Ravera, BP 29, 92222 Bagneux Cedex, France.
phone: +33 (0)142317177, Fax: +33 (0)142317378
email: Ulf.Gennser@L2M.cnrs.fr

Ultrafast intersubband scattering of holes in p-type modulation-doped $Si_{1-x}Ge_x/Si$ multiple quantum wells

M. Woerner[1], R. A. Kaindl[1,2], M. Wurm[1], K. Reimann[1], T. Elsaesser[1], C. Miesner[3], K. Brunner[3], G. Abstreiter[3]

[1]Max-Born-Institut für Nichtlineare Optik und Kurzzeitspektroskopie, 12489 Berlin,Germany
[2]present address: Lawrence Berkeley National Laboratory, Berkeley, CA 94720, USA
[3]Walter-Schottky-Institut, Technische Universität München, 85748 Garching, Germany

Optical intersubband excitations in semiconductor nanostructures provide direct insight into the ultrafast dynamics of coherent optical polarizations and nonequilibrium carriers and play a key role for novel devices such as quantum cascade lasers. So far, most experiments have concentrated on intersubband excitations of quasi-two-dimensional electron plasmas [1]. In contrast, intersubband transitions of quasi-two-dimensional holes, which are highly relevant for device applications, have been much less explored. Very recently, first intersubband electroluminescence from $Si_{1-x}Ge_x/Si$ quantum cascade structures has been observed an important milestone on the road to the first silicon-based laser [2]. A crucial key parameter in such structures is the lifetime of heavy holes (HHs) in the various subbands which is - in contrast to electrons in conduction subbands - dominantly determined by hole-optical phonon scattering via the **optical deformation potential**. Here, we present the first time-resolved study of hole plasmas in quantum wells using direct intersubband excitation and probing of HHs in p-type modulation-doped $Si_{0.5}Ge_{0.5}/Si$ multiple quantum wells [3]. We demonstrate that an nonequilibrium population in the HH2 subband decays with a time constant of only **250 fs** predominantly via cascaded intersubband scattering processes involving the intermediate light-hole-split-off (LHSO1) subband. Subsequent thermalization of backscattered holes with unexcited carriers via intraband optical phonon and Coulomb scattering occurs on a timescale of several hundreds of femtoseconds depending on the excitation density. Thermalization results in an ultrafast heating of the HH1 distribution which subsequently cools down to lattice temperature on a 25-ps timescale.

In our femtosecond experiments we investigate high-quality p-type $Si_{1-x}Ge_x/Si$ multiple quantum wells grown by solid-source molecular beam epitaxy. The structure consists of ten periods of modulation-doped ($n = 1.2 \times 10^{12}$ cm^{-2}) $Si_{1-x}Ge_x$ quantum wells (4.4 nm wide, $x = 50\%$) separated by 18-nm Si barriers. Polarized absorption spectra reveal an intersubband line due to HH1-HH2 transitions, centered at 167 meV in accordance with the calculated subband energy difference. Mid-infrared pump and probe pulses of 150 fs duration are derived from the output of a 1-kHz optical parametric amplifier by difference frequency mixing in GaSe [4]. Broad pulse spectra allow to probe across the whole intersubband line by spectral selection after the sample. At low excitation densities [Figs. 1(a,b)], the transmission changes are dominated by redistribution of holes in the HH1 subband. The ≈1 ps rise and subsequent slow decay on a ≈25 ps time scale correspond to heating and cooling, respectively. In contrast, at high excitation [Fig. 1(c)] an additional fast component is observed, which is due to a nonequilibrium population in the HH2 band. We have extracted this nonequilibrium component by subtracting the heating dynamics in the HH1 band. The resulting transient [Fig 1(d)] essentially represents the population dynamics of the HH2 band. This suggests an intersubband relaxation time of $\tau_{IS} = 250$ fs. A microscopic analysis based on calculations of the valence band structure and scattering processes will be discussed. Such calculations yield an overall HH2 depopulation time of 225 fs, which is in good agreement with the measured IS scattering time. It is important to note that due to the symmetry of the deformation potential tensor the cascaded indirect process via the LHSO1 subband [arrow B in Fig. 1(d)] is about three times faster than direct HH2↔HH1 intersubband scattering (arrow A).

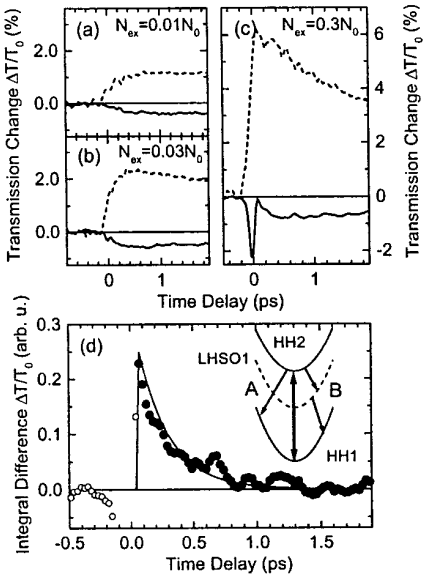

Fig. 1: (a)-(c) Time evolution of nonlinear transmission changes probed at the spectral position of strongest induced bleaching (dashed lines) or strongest enhanced absorption (solid lines). Results are shown for three different excitation densities N_{ex} / N_0 = (a) 0.01, (b) 0.03, and (c) 0.3. (d) Fast bleaching signal obtained from the data, as explained in the text. It reflects IS relaxation in the time-range of sequential pump-probe interaction (filled circles, $\Delta t > 70$ fs). Solid line: Single exponential decay with 250 fs. Inset: Optical excitation and IS scattering in the bandstructure.

References

[1] T. Elsaesser, M. Woerner, Phys. Reports **321**, 253 (1999).
[2] G. Dehlinger et al., Science **290**, 2277 (2000).
[3] R. A. Kaindl et al., Phys. Rev. Lett. **86**, 1122 (2001).
[4] R. A. Kaindl et al., J. Opt. Soc. Am. B **17**, 2086 (2000).

Corresponding author: Michael Woerner, Max-Born-Institut für Nichtlineare Optik und Kurzzeitspektroskopie, Max-Born-Straße 2A, D-12489 Berlin, Germany.
phone: +49 30 6392 1470, Fax: +49 30 6392 1489
email: woerner@mbi-berlin.de

Ultra-short channel transistors fabricated by cleaved-edge overgrowth

F. Ertl, T. Asperger, R. A. Deutschmann, M. Bichler, G. Abstreiter

Walter Schottky Institut, Technische Universität München,
Am Coulombwall 3, D-85748 Garching, Germany

We employ the cleaved-edge overgrowth (CEO) [1] technique to fabricate vertical transistors with channel lengths of only a few 10 nm. Our efforts are focused on testing the limits of scaling down the source-drain distance, of which we present our latest results.

Vertical transistor substrates are grown by GaAs/AlGaAs molecular beam epitaxy (MBE) on semi-insulating (001)-GaAs wafers. The substrates have a barrier sandwiched between 1 μm thick n^+-GaAs source/drain contacts and differ only in the type of the barrier, as shown in Fig. 1. All MBE layers can be deposited with atomic precision to define the geometric channel length L of the transistor by the barrier thickness. We evaluate different concepts to minimize leakage currents from source to drain: barriers with p^+-δ-doping (Fig. 1(a)) and simple or embedded hetero-barriers (Fig. 1(b)+1(c)) are used. The substrates are cleaved under ultra-high vacuum conditions and a QW thick GaAs electron channel, the AlAs gate barrier and the n^+-GaAs gate contact are deposited on the freshly exposed cleavage plane. Finally a mesa is etched on the specimen and ohmic contacts are processed.

All samples are characterized by measuring the I-V curves under gate voltage bias. In our setup the topmost contact is grounded and the source-drain voltage is applied to the bottom contact. The source-drain current is measured while simultaneously the voltage drop across the channel is recorded in 4-point-probe configuration.

Measurements of vertical transistors with a $6{\cdot}10^{12}$ 1/cm^2 p^+-δ-doped barrier are presented in Fig. 2. In these devices an effective channel length L_{Eff} results from electrostatic depletion in the contact regions flanking the p^+-δ-spike. The length of L_{Eff}=70 nm was obtained from capacitance measurements and confirmed by self-consistent calculations. I-V traces at 4.2 K (Fig. 2(a)) or at 300 K (Fig. 2(b)) from a sample with QW=40 nm channel thickness show typical subthreshold transistor behavior. For gate voltages below 0.7 V the transistor stays in the turned-off regime, above gate leakage becomes dominant. At low temperatures the device behavior is governed by punch-through of electrons: at positive drain voltage the effective channel barrier height is reduced and electrons are tunneling from source to drain. At high temperatures an additional thermally activated current appears across this barrier. Fig. 2 exhibits both contributions as the curves shift either with gate voltage or temperature.

Furthermore we study devices equipped with an $Al_{0.45}Ga_{0.55}As$ hetero-barrier, of which measurements at 4.2 K are plotted in Fig. 3. In this case the geometrical channel length is L=50 nm and results are shown for QW=20 nm (Fig. 3(a)) and QW=40 nm (Fig. 3(b)). Above a small positive gate voltage this device type shows turned-on transistor operation with an quasi-saturated region. The loss of the complete saturation is a typical short channel effect. Closer examination of the data reveals that the onset of the quasi-saturation shifts linearly to higher values with increasing gate voltage. When the channel thickness is raised, even though the channel cross section is increased, we observe an unexpected decrease in the average source–drain current. This behavior might be explained by additional series resistances stemming from the contact-channel coupling as the electron gas is located further away from the contacts at larger channel thicknesses.

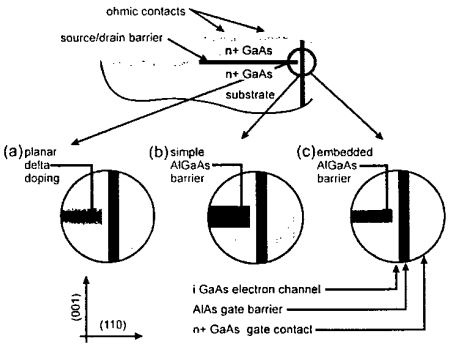

Fig. 1: Cross section of a vertical transistor fabricated by cleaved-edge overgrowth. In the (001)-direction a GaAs substrate is overgrown with two thick n^+-GaAs layers, which serve as source/drain contacts and are separated by a insulating barrier. Different kinds of barriers are under investigation: (a) GaAs with a p^+-δ-doping, (b) simple AlGaAs barrier and (c) GaAs embedded AlGaAs barrier. In the (110)-direction the gate structure is deposited consisting of a GaAs electron channel, AlAs gate barrier and n^+-GaAs gate contact. The geometrical length L of the vertical transistor is determined by the thickness of the (001)-barrier and the channel thickness QW by the (110)-quantum well formed between (001)-barrier and gate.

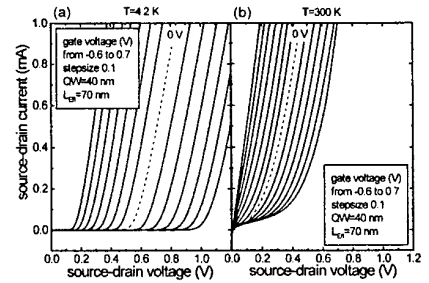

Fig. 2: Typical output characteristics of a vertical transistor device, which has a $6{\cdot}10^{12}$ 1/cm^2 p^+-δ-doped barrier. The electron channel length is L_{Eff}=70 nm and the thickness QW=40 nm. An effective length results from electrostatic depletion in the contact regions flanking the p^+-δ-spike. The device behavior is presented for temperatures of (a) T=4.2 K and (b) T=300 K. Within the applied gate voltage range the transistor stays turned-off and subthreshold operation is visible. Also punch-through behavior shows up in the shift of the curves with either gate voltage or temperature.

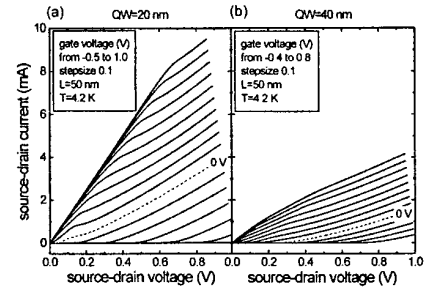

Fig. 3: Current-voltage relation of samples equipped with an $Al_{0.45}Ga_{0.55}As$ hetero-barrier. The devices are L=50 nm long and the temperature is fixed at T=4.2 K. Samples with different electron channel thicknesses (a) QW=20 nm and (b) QW=40 nm can be compared. Commonly both transistors show a quasi-saturated region, the onset of which increases linearly with the gate voltage. The loss of complete saturation represents a typical short channel effect. As the channel thickness is increased the average source-drain current decreases, although the channel cross section is enlarged.

References

[1] L.N. Pfeiffer, K.W. West, H.L. Stormer, J.P. Eisenstein, K.W. Baldwin, D. Gershoni, and J. Spector, Appl. Phys. Lett. **56**, 1697 (1990).

Corresponding author: Frank Ertl, Walter Schottky Institut, Technische Universität München, Am Coulombwall 3, D-85748 Garching, Germany,
phone: +49 89 28912778, fax: +49 89 3206620,
email: ertl@wsi.tum.de

GaAs and InGaAs Single Electron Hexagonal Nanowire Circuits Based on Binary Decision Diagram Logic Architecture

Seiya Kasai and Hideki Hasegawa
Research Center for Interface Quantum Electronics and Graduate School of Electronics and Information Engineering, Hokkaido University, N-13, W-8, Kita-ku, Sapporo 060-8628, Japan
Tel:+81-11-706-7176, Fax:+81-11-716-6004, E-mail: kasai@rciqe.hokudai.ac.jp

In spite of research on quantum devices over 25 years, no realistic prospect for quantum (Q-) LSIs exists at present. This is probably because no attempts were made to change the basic logic architecture from the Boolean logic gate architecture with AND/OR gates etc., where very uniform and robust devices such as Si CMOS devices are essentially required.

This paper investigates the feasibility of our novel approach[1] for single electron Q-LSIs based on the binary-decision-diagram (BDD) logic architecture, using arrays of GaAs and InGaAs single electron BDD node devices formed on hexagonal nanowire networks.

The function of the node device is to send a single electron (SE) coming into the entry branch either into 0- or 1-branch depending on a gate input as shown in **Fig.1**. Any logic function can be realized by connecting many such node devices. In contrast to the logic gate architecture, no direct output-to-input connection is necessary, thereby requiring no large voltage gain, no precise input-output voltage matching, no large fan-in and fan-out numbers and no large current drivability. It is a good architecture for quantum devices operating near the quantum limit of delay-power product. For hardware implementation, we paid attention to the basic three-fold branch symmetry of the node device, and used GaAs and InGaAs hexagonal nanowire networks controlled by nm-scale Schottky wrap gates (WPGs)[2] shown in **Figs.2(a)-(c)** were used. WPGs provide tight gate control, strong electron confinement and a simple lateral structure suitable for planar integration. The present Q-LSI structure is obviously applicable, in future, to molecular nanowire networks.

Previously, we demonstrated 3-WPG GaAs SE node devices shown in **Fig.3(a)**[1]. Here, however, small and uniform dot sizes were difficult to realize. In this study, we used a new SE node device shown in **Fig.3(b)** consisting of two 2-WPG single electron transistors (SETs). For GaAs devices such as shown in **Fig.3(c)**, several-100nm-wide nanowires made by EB lithography and wet etching were used. For InGaAs devices, several-10-nm-wide nanowires embedded in InAlAs barriers were grown on patterned InP substrates by selective MBE. Each branch of the fabricated GaAs and InGaAs node devices exhibited clear conductance oscillations as shown in **Figs.4(a)** and **(b)**. The behavior can be explained by single elctron transport through lateral resonant tunneling as shown in **Figs.5(a)** and **(b)** for a GaAs device. With these, clear path switching utilizing the first conductance peak was obtained.

As an example of integration, a GaAs honeycomb two-bit quantum adder without nanowire crossover was designed and fabricated as shown in **Fig.6(a)**. It showed a correct operation as partly shown in **Fig.6(b)**. Correct operation was seen at least up to 120 K by bias adjustments. This is because, with temperature increase, the circuits should show gradual transitions from the single electron quantum regime with a minimum possible delay-power product to a few electron quantum regime, and finally to the many electron classical regime. Therefore, wire size reduction should lead to room temperature operation in the single electron quantum regime. To realize this, we are growing submicron-pitch sub-10nm-wide InGaAs honeycomb nanowire networks such as shown in **Fig.7** by selective MBE. The results using such InGaAs networks will also be discussed.

[1] S. Kasai, Y. Amemiya and H. Hasegawa, Tech. Dig. 2000 IEDM (2000) 585.
[2] S. Kasai and H. Hasegawa, Jpn. J. Appl. Phys. **40** (2001) in press.

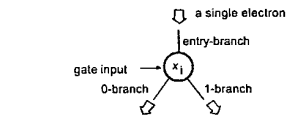

Fig.1 Single electron BDD node device

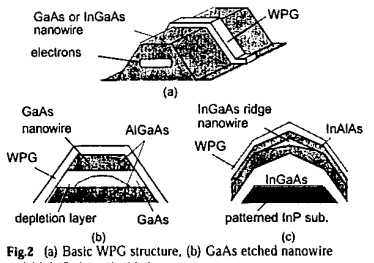

Fig.2 (a) Basic WPG structure, (b) GaAs etched nanowire and (c) InGaAs embedded nanowire.

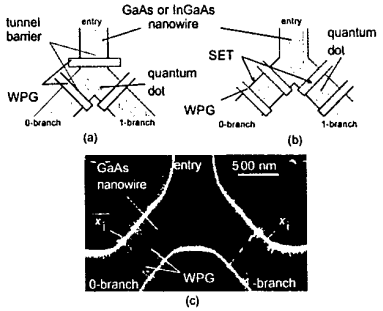

Fig.3 WPG quantum BDD node devices with (a) 3-WPGs with a QD, (b) 2-WPG SETs and (c) SEM image of a fabricated GaAs node device.

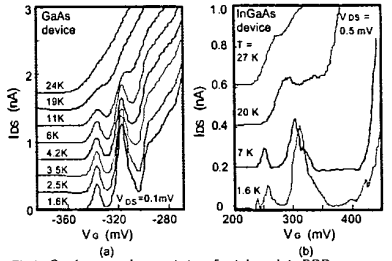

Fig.4 Conductance characteristics of exit branch in BDD node devices having (a) GaAs WPG SET and (b) InGaAs WPG SET.

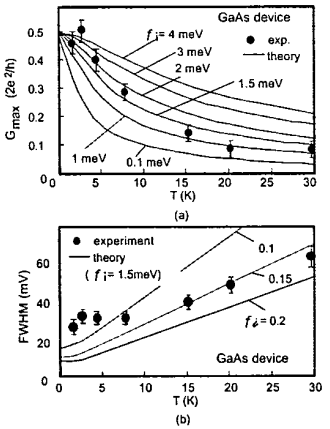

Fig.5 Temperature dependence of (a) conductance peak height and (b) FWHM in GaAs WPG SET.

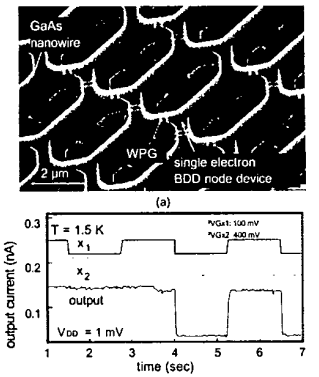

Fig.6 (a) Fabricated WPG BDD 2-bit adder utilizing GaAs nanowire array and (b) an example of input/output wave form.

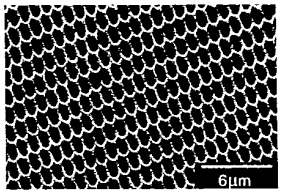

Fig.7 InGaAs nanowire honeycomb structure.

Voltage-switchable Bragg reflector for planar optical waveguides

W. R. Frank[1], A. O. Govorov[2], W. Wegscheider[3], K. Karrai[1], J. P. Kotthaus[1]

[1]Center for Nanoscience and Sektion Physik, Ludwig-Maximilians-Universität München, Geschwister-Scholl-Platz 1, 80539 Munich, Germany
[2]Institute for Semiconductor Physics, Russian Academy of Sciences, Siberian Branch, Lavrent'eva Av. 13, Novosibirsk 630090, Russia
[3]Institut für Angewandte und Experimentelle Physik, Universität Regensburg, 93040 Regensburg, Germany

Permanent, grating-induced Bragg reflectors (BRs) for planar optical waveguides (WGs) are commonly used in distributed feedback lasers. A switchable BR would be highly desirable for applications in optical communications for routing signals between different fiber inputs and outputs, and possibly also for novel semiconductor laser devices. We proposed in reference [1] a voltage-switchable BR based on the quantum confined Stark effect (QCSE): the device consists of a planar optical WG with a multiple quantum well (MQW) in its core in which a periodically modulated static electric field is induced by an interdigitated gate on the sample surface that is biased with respect to a back contact. The normal component of the electric field induces a periodic modulation of the refractive index in the quantum wells because of the QCSE. This index modulation causes photonic band gaps in the mode dispersion of the WG and thus acts as a BR. Here we present an experimental realization of this concept. Our sample consists of an $Al_xGa_{1-x}As$ heterostructure comprising a planar WG with twelve 10 nm wide GaAs quantum wells in its core surrounded by AlAs/GaAs superlattices serving as WG claddings. The interdigitated gate (IDT) is defined by e-beam lithography with a positive resist and RF sputtering of indium tin oxide with subsequent lift-off. This technology currently limits our gate grating period to 250 nm and hence the period of the BR to 500 nm. Since the wavelength of the TE_0 mode of our WG is approximately 250 nm we obtain a Bragg angle of roughly 15° and thus a deflection of the beam of 30°. In order to avoid a possible loss of the optical signal by total internal reflection at the sample edge, a 1.5 µm high, 800 µm diameter semi-circular mesa with vertical edges around the BR area is defined by anisotropic reactive ion etching in $SiCl_4$ prior to the preparation of the gates. Fig. 1 a) shows the design of the sample together with the experimental setup: Instead of using a tunable laser and coupling optics to feed light into the WG, we use the broad intrinsic room-temperature photoluminescence (PL) spectrum of the MQW as a built-in light source with wavelengths ideally matched to the optical properties of the WG [2]. The PL is excited with a 635 nm laser diode stabilized at 2 mW. The light traveling in all directions within the WG is directed to the BR area by a 10 µm wide etched rib defined together with the mesa. The PL light from the edge of the mesa is collected with a microscope objective and fed into an imaging spectrograph (f = 300 mm) allowing us to simultaneously record spectra from different heights of the mesa edge. The excitation laser is fixed relative to the sample and both can be rotated together around a surface normal through the center of the mesa which is also the intersection of the straight light path from the rib and the front of the BR area. Thus we can collect and analyze the edge PL from a wide angular range around the BR. During the angular scans, we probed various combinations of negative gate voltages at every angle ($V_{1/2} = V_0 \pm \Delta V$). Positive gate voltages cause leakage currents from the back contact to the gates across the quantum wells, destructing the BR effect permanently. Without gate voltages, we obtained in the angular direction for all wavelengths a bell-shaped PL pattern centered about the forward direction (0°). The edge PL spectrum ranged from about 850 to 890 nm with a maximum at about 868 nm. In order to assess the effect of the BR, we divided the PL spectra taken with non-zero gate voltages by the zero-voltage spectra. We found several distinct features (Fig 1 b): In the angular region behind the BR (-15° to 15° in Fig 1 b) the PL is clearly suppressed. This is caused mostly by the QCSE redshift of the average quantum well absorption, but partly also by the BR effect. In the angular region not covered by the BR (> 15°) the PL signal is essentially unchanged by the voltage applied to the gate electrodes. At 31.2°, a peak with a FHWM of approximately 2° is visible. The angular position and FWHM of this peak are independent of the applied gate voltages. The peak is weakly visible when the same voltage is applied to both gates ($\Delta V = 0$), giving the effect of a homogeneous gate, hence of a homogeneous index change at the front of the BR area, acting as a mirror. With increasing voltage difference ΔV, the peak position moves toward longer wavelengths and the peak height grows from 1.12 for $\Delta V = 0$ to 1.52 for ΔV = 6.25 V. This clearly demonstrates the dominance of the BR reflection by the periodic index modulation over the reflection by the homogeneous index change also induced by the gate voltages. The observed effects are also in good qualitative agreement with an extended theory based on reference [1]. In an optimized version, the voltage-switchable BR could serve as a useful device for optoelectronic applications.

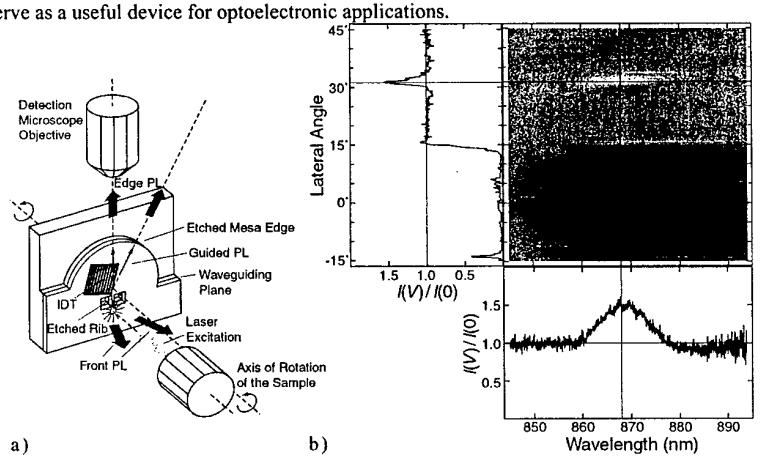

Fig. 1: a) Sketch of the sample and the experimental setup. The arrows in the sample plane mark the forward direction and the direction of the expected Bragg reflex, respectively. b) Edge PL intensity for gate voltages V_0 = - 10.0 V, ΔV = 6.25 V divided by the PL intensity for zero gate voltage. The sections are at 868 nm and 31.2°, respectively.

References

[1] A. O. Govorov, W. Hansen and J. P. Kotthaus, J. Appl. Phys. 80, 7151 (1996).
[2] D. Labilloy et al., Appl. Phys. Lett. 71, 738 (1997).

Corresponding author: Wolfgang R. Frank, CeNS and Sektion Physik, Ludwig-Maximilians-Universität München, Geschwister-Scholl-Platz 1, 80539 Munich, Germany.
phone: +49 89 2180 3773, Fax: +49 89 2180 3182
email: Wolfgang.Frank@physik.uni-muenchen.de

Room Temperature Single–Hole Silicon Memory

N.T. Bagraev, A.D. Bouravleuv, L.E. Klyachkin, A.M. Malyarenko, S.A. Rykov

[1]Atomic Physics Division, A. F. Ioffe Physico-Technical Institute,
Polytekhnicheskaya 26, 194021, St.Petersburg, Russia

Planar nano-technology is recently used to fabricate the semiconductor quantum wires that contain the systems of isolated quantum dots with capacitances small enough to study the charging effects of discrete electrons and holes. However, the principal limits of lithography resolution prohibit the preparation of nanometer-scale structures that are necessary to observe the operations of single-charge devices at room temperature. Nevertheless, room temperature single-electron phenomena have been found to emerge from studies of self-assembled semiconductor nanostructures. The actual pathways that are favourable to high temperature single-charging effects therewith were to replace the monolithic quantum dot on the multiple-tunnel junction (MTJ). Here we use the self-assembled nanostructures that consist of the MTJ series to demonstrate the room temperature operation of the single-hole memory cell performed, for the first time, on the basis of an impurity superlattice (Fig.1). The impurity superlattice of this art is made possible by utilizing the self-assembled quantum wells that are naturally formed by short-time diffusion of boron into the Si(100)-wafer.

Short-time diffusion of boron (900°C) has been performed from the gas phase into the n-type monocrystalline silicon (100) using controlled surface injection of self-interstitials and vacancies. The ultra-shallow p^+-n junctions obtained have been used as the FET structures with the p^+ hole channel, the depth of which is determined by SIMS as 10 nm. This p^+ hole channel has been found to consist of self-assembled longitudinal quantum wells (SLQW) divided by the δ-barriers heavily doped with boron thereby forming an impurity superlattice. The STM images allowed to identify the antidots that represent small self-interstitials clusters and penetrate through the impurity superlattice. The quantum wire (2.0nm×2.0nm) revealed by a special constriction inside the p^+-n junction has been shown to provide a basis to perform the operation of a single-charge electrometer, whereas the Coulomb blockade regime is created by the quantum dot that represents the MTJ (2.0×2.0×2.0nm) series placed between antidots (Fig.1a). In the framework of side-gated technique, the gate voltage has been applied by the system of the parallel quantum wires that cross the quantum wire of an electrometer (Fig.1b). The local tunnelling spectroscopy (LTS) measurements performed at 300K have exhibited the Coulomb blockade regime that is due to the presence of an isolated quantum dot inside the quantum wire of an electrometer (Fig.2). Besides, the Coulomb-blockade oscillations have been found to be controlable by recharging the storage dot near the side-gated channel that exhibit the single-hole memory effects as a hysteresis in the CV characteristics and the amplitude variation of the Coulomb oscillations as a function of the gate voltage (Fig.3).

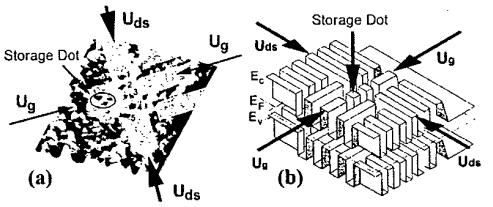

Fig. 1: (a) - STM image of the experimental single-hole memory device based on a self-assembled MTJ series; (b) – Three-dimensional diagram of the one-electron band scheme of the single-hole memory device based on a self-assembled MTJ series.

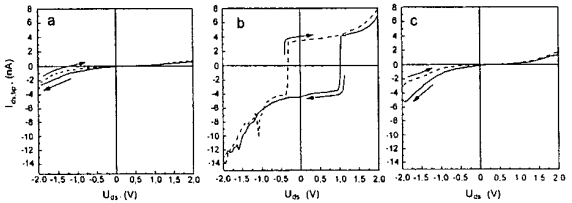

Fig. 2: Room temperature operation of the single-hole memory cell that is revealed by varying the gate voltage in the I_{ds} –V_{ds} characteristics of the single-hole transistor performed as an electrometer.
The $I_{ds}(V_{ds})$ dependence was measured using the LTS technique; the duration of scan was 10 ms.
(a) – U_g=4 mV; (b)- U_g=6 mV; (c) - U_g=8 mV

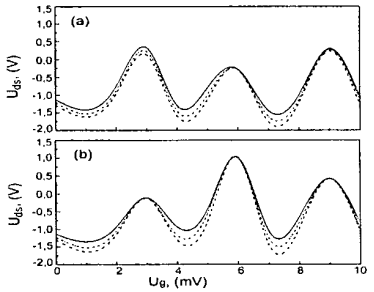

Fig. 3: Modulation dependence $V_{ds}(V_g)$ of a single-hole transistor that exhibits room temperature operation of the single-hole memory cell as the I_{ds} hysteresis during forward (a) and reverse (b) scan of the drain-source voltage
I_{ds}= -0.3 nA - solid line; I_{ds}= -0.6 nA - dashed line; I_{ds}= -0.9 nA - dashed with dots

Corresponding author: Prof.Dr.N.T.Bagraev, A.F.Ioffe Physico-Technical Institute,
194021, St.Petersburg, Russia.
phone: 007 (812) 2479315, Fax: 007 (812) 2471017
email: impurity.dipole@pop.ioffe.rssi.ru

Heteroepitaxy of dissimilar materials: Effect of interface structure on strain and defect formation

Achim Trampert

Paul-Drude-Institut für Festkörperelektronik, Hausvogteiplatz 5-7, D-10117 Berlin, Germany

Heteroepitaxial growth has been established as a powerful technique to create single crystalline thin films or artificial low-dimensional quantum systems. Beyond that, heteroepitaxy opens the possibility to combine crystalline materials that can be very different in symmetry, bonding and lattice constant, respectively. Thus, it is feasible to fabricate heterosystems with tailored magnetic, optical or electrical properties – as for example, it is the case for ferromagnetic-semiconducting hybrid structures.

In all these systems, the atomic arrangement at the interface is not only responsible for the specific epitaxial alignment, but also for the development of the resulting microstructure. Residual strains as well as extended defects in the epilayers affect the desired properties and thus strongly decide about the quality of the heterosystem's functionality.

In general, epitaxy describes a condition for which adjoining crystals have a definite orientation relationship with a low-energy interfacial structure being favored. In conventional heteroepitaxial growth, like (In,Ga)As on GaAs, the low-energy criterion is simply fulfilled by accommodating the small lattice mismatch through biaxial strain and lattice misfit dislocations at the interface between the structurally similar materials (semi-coherent interface). This concept of lattice accommodation, however, will fail in the case of *general* heteroepitaxy where the lattice mismatch can be arbitrary large and the crystal symmetry between film and substrate can be quite different. Low-energy interfaces are often discussed here in terms of geometric criteria based on structural coincidences between the adjoining crystal lattices [1]. Such an interface - if guaranteeing heteroepitaxy - should meet the following criteria: First, the accommodation of lattice planes occurs in such a way that long-range strain fields will be minimized and, second, local plastic relaxation processes generating interface-specific mismatch dislocations (not necessary equivalent to bulk dislocations) additionally reduce the interfacial energy. Complex extended defects distributions within the layers are mainly produced by misfit dislocation interaction and/or by the growth-dependent island coalescence during nucleation.

In the present talk, two extreme cases of heteroepitaxy of dissimilar materials will be discussed in order to verify the universality of the given criteria: The first case deals with the ferromagnetic MnAs - semiconducting GaAs system combining hexagonal and cubic crystal structures [2]. The second case is the GaN – $LiAlO_2$ system, where hexagonal nitrides are epitaxially grown on tetragonal oxide substrates in a unique orientation [3].

References

[1] A. Trampert, K. H. Ploog, Cryst. Res. Technol. 35, 793 (2000).
[2] A. Trampert *et al.*, will apear in Appl. Phys. Lett., issue of 23 April 2001.
[3] P. Waltereit *et al.*, Nature 406, 865 (2000).

Corresponding author: Achim Trampert, Paul-Drude-Institut für Festkörperelektronik, Hausvogteiplatz 5-7, 10117 Berlin, Germany. Phone: +4 9 30 20377 424, Fax: +49 30 20377 515, email: trampert@pdi-berlin.de

Axially modulated quantum wires

B. Dwir, K. Leifer, E. Kapon

Physics department, Swiss Federal Institute of Technology Lausanne (EPFL), CH-1015 Lausanne, Switzerland

Uniform quantum wire (QWR) structures, which confine electron and hole movement to one dimension, have been studied for several years and have shown a multitude of unique physical properties. However, axially modulated QWRs, where the confinement potential and even the dimensionality vary along the structure, have been not been studied experimentally, although theoretical predictions are promising of new and interesting phenomena [1]. By combining electron-beam lithography (EBL) and self-limited growth, we fabricated novel structures, where a single layer of GaAs in a heterostructure can change from quantum well (QW) to quantum wire on a sub-μm scale. Moreover, quantum-dot (QD) like, short (100-200 nm) thickened QWR sections can be produced in the structure.

Our GaAs substrate is patterned by EBL and wet etching to produce a sequence of wide and narrow V-groove along the [01$\bar{1}$] direction (Fig.1a). A GaAs/AlGaAs multi-layer structure is then grown, and the sample cleaved to yield a sequence of atomic force microscope (AFM) cross-sectional images [2] along the groove, Fig. 1c. One can observe that GaAs layers close to the substrate (layers 1-3) form a planar (QW) at the wide part (images A-C), which gradually changes to a QWR at the narrow part (images E,F). GaAs layers, which are grown after a thick buffer (layers 9,10), form a thick QWR only at the central part of the groove (image A), which changes immediately to a bent QW layer (images B-E) before returning to the self-limited QWR structure (image F).

These structural features were confirmed by detailed cross-sectional and top AFM imaging, as well as by optical spectroscopy. For this purpose, a heterostructure comprising 250 nm AlGaAs buffer, a thin (1.5 nm) GaAs layer and 50 nm AlGaAs cap was grown on a variable-width V-grooved substrate. This structure was characterized by photoluminescence (PL) and cathodoluminescence (CL) at low temperature. The PL spectra (Fig.2A) show clearly a QWR peak (#1, at 1.61 eV) from a uniform V-groove, while the wide parts of the V-groove produce extra PL peaks (#2,3), at about 1.56 eV and 1.59 eV. By using CL with spatial resolution of 250 nm (Fig. 2B) we could better establish the relation between structural and electronic features. The peaks at 1.55 and 1.565 eV are clearly produced at the center of the wide groove, while the peak at 1.585 eV comes from QWR sections close to the wide part. At 1.61 eV, the central part of the QWR luminesces. These results indicate that a short and thick (QD-like) QWR section is indeed formed at the center of the wide groove. Moreover, the QWR growth outside the wide part is also influenced by the existence of the wide part, since thickness variations (showing as variation in CL energy, from 1.59 to 1.61 eV) in the QWR seem to occur on a length scale of 2 μm.

The above analysis shows that these structures are indeed very versatile, since they allow us to design many types of novel, mixed-dimensionality heterostructures. Among these one could imagine the adiabatic (smooth) transition between quantum well and quantum wire, useful for electron transport measurements, or the confinement of electrons in a QD-like part of a QWR, for tunneling and Coulomb blockade devices.

References

[1] P. Exner, Phys. Lett. A **141**, 213 (1989), P. Exner and P. Seba, J. Math. Phys. **30**, 2574 (1989), J. Goldstone and R.L. Jaffe, Phys. Rev. B **45**, 14100 (1992), C. S. Lent, D. J. Kirkner, J. Appl. Phys. **67**, 6353 (1990).

[2] F. Reinhardt, B. Dwir and E. Kapon, Appl. Phys. Lett. **68**, 3168 (1996).

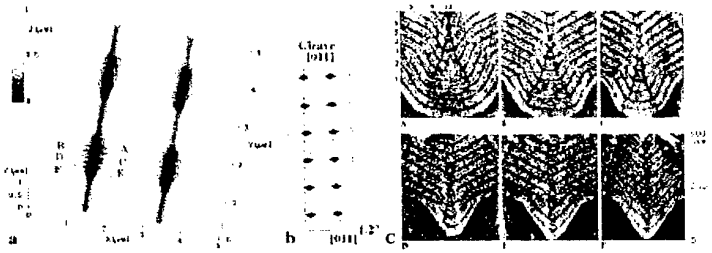

Fig. 1: a. AFM top image of the substrate with a variable-width V-groove array. b. Schematics showing the principle of cross-sectional AFM sequence, where the tilted grooves produce a sequence of shifted AFM images in one cleave. c. Cross-sectional AFM images of an AlGaAs / GaAs multilayer structure. Distance from the center of the wide region is : A. 0. B. 130 nm. C. 240 nm. D. 300 nm. E. 435 nm. F. 500 nm. The GaAs layers (dark) are numbered from 1 to 10.

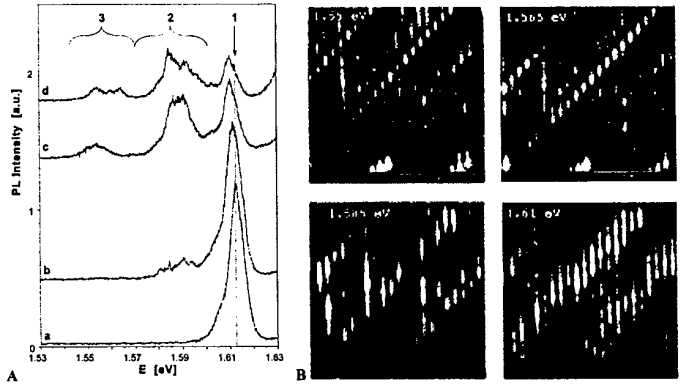

Fig. 2: A : PL spectra at T = 10K of : a. QWR grown in a straight narrow V-groove. b. Narrow part in a variable-width structure, at a distance of 2.5 μm from the wide part. c,d. Center of the wide part in similar structures. B : CL images (at detection energies corresponding to the peaks in A) of a variable-width QWR array with 10 μm between wide parts and 1 μm between grooves.

Corresponding author: Benjamin Dwir, IMO-DP, EPFL, CH-1015 Lausanne Switzerland
phone: +41 21 693 3755, Fax: +41 21 693 4525
email: benjamin.dwir@epfl.ch

Fabrication and characterization of III-V nanowhiskers

B. J. Ohlsson[1], M. Bjork[1], M. H. Magnusson[1], A. Persson[1], L. R. Wallenberg[2], and L. Samuelson[1].

[1]Department of Solid State Physics, Institute for Physics, University of Lund, Box 118, S-22100 Lund, Sweden
[2]Department of Inorganic Chemistry, Institute for Chemistry, University of Lund, Box 124, S-22100 Lund, Sweden

Nanowhiskers are highly interesting objects mainly because of the one-dimensional properties and the size, which leads to strong quantization effects and high mobilities. Applications can range from optoelectronics and high-speed electronics to field emitters and nanoprobes for SPM characterization. The whiskers are grown under quasi-liquid phase epitaxial conditions, generally referred to as vapor liquid solid (VLS) growth [1], and are seeded by Au aerosol particles.

We present results from experiments aimed towards synthesizing size-selected rod-shaped nanowhiskers. We have mainly investigated the GaAs and InAs materials systems, but some GaP and InP runs were made as well. The whiskers were grown by means of chemical beam epitaxy (CBE) on GaAs (111)B substrates. Since (111)B is the preferred growth direction for the whiskers, we get vertical whiskers. Under appropriate growth conditions, the whiskers grow rod-shaped, with a uniform diameter in contrast to MOCVD-grown whiskers, which tend to be tapered [2]. We attribute this improvement to the specific low-pressure conditions of CBE. Typical lengths are about 1 μm.

The size selectivity of the nanowhiskers was achieved by using size-selected Au aerosol particles as catalysts for the VLS growth. The Au particles were produced in a locally constructed aerosol facility [3] situated in a glove box with ultra-pure N_2 atmosphere. By these means, we can fabricate Au particles of any chosen size between 10 and 80 nm, with a narrow size distribution of ±5% of the mean particle diameter. The particles deposit at random positions on the substrate, but the surface coverage can be chosen at will, specifically, it is independently of the particle size.

In order to see whether it is possible to position the whiskers at specific places on the substrate, we have used AFM manipulation [4] to move the Au particles before whisker growth. In this way, we can follow the growth of individual nanowhiskers originating from specific catalytic particles. Results show that, after growth, some of the whiskers are displaced from the original positions of the Au particles. Whether this can be suppressed by appropriate growth conditions remains to be seen.

By electron beam lithography and AFM manipulation, it is possible to attach electrical contacts to individual nanowhiskers. Experiments show that it is possible to achieve ohmic contacts between InAs whiskers and Au electrodes. In addition, electron microscopy investigations as well as optical characterization of III/V nanowhiskers will be presented.

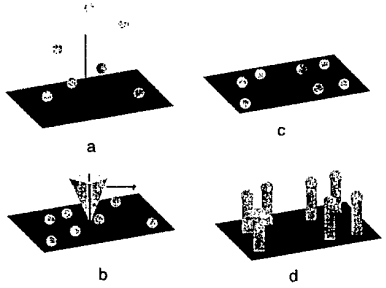

Fig. 1: Principal overview over the fabrication of nanowhiskers. a. Deposition of size selected Au particles on a GaAs substrate. b. Positioning of the Au particles by AFM manipulation. c. Alloying of the Au particles together with the substrate constituents. d One dimensional epitaxial growth of size selected nanowhiskers.

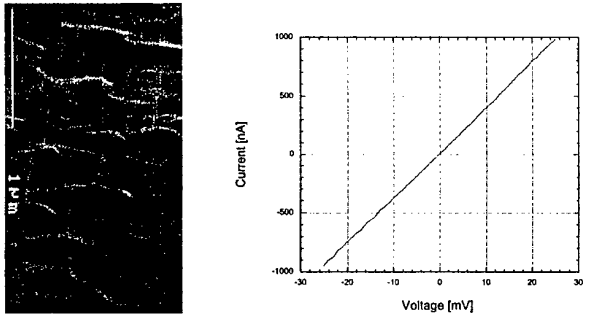

Fig. 2: a. 30 nm GaAs whiskers grown on a GaAs(111) B substrate. b. Current-voltage characteristics of a 70 nm InAs whisker

References

[1] R. S. Wagner and W. C. Ellis, Appl. Phys. Lett. 4, 89 (1964).
[2] K. Hiruma, M. Yazawa, K. Haraguchi, K. Ogawa, T. Katsuyama, M. Koguchi, and H. Kakibayashi, J. Appl. Phys. 74, 3164 (1993).
[3] M. H. Magnussson, K. Deppert, J-O. Malm, J-O Bovin, and L. Samuelson, J. Nanoparticles Res. 1: 243 (1999)
[4] T. Junno, K. Deppert, L. Montelius , L Samuelson
Appl. Phys. Lett. 66: 3627 (1995)

Corresponding author: Jonas Ohlsson, Department of Solid State Physics, Institute for Physics, University of Lund, Box 118, S-22100, Sweden
phone: +46 46 222 9586, Fax: +46 46 222 3631
email: jonas.ohlsson@ftf.lth.se

Spatially Site-Controlled InAs Quantum Dot Lattices

S. Kohmoto, H. Nakamura, S. Nishikawa, and K. Asakawa

The Femtosecond Technology Research Association (FESTA)
5 - 5 Tokodai, Tsukuba 300-2635, Japan

Multiple stacking of Stranski-Krastanov quantum dot (SKQD) layers leads to spatial ordering of QD positions, due to strain field propagation [1]. This technique is expected to improve QD size uniformity through gradual regularization of strain distributions with layer stacking [2]. In addition, it has the potential to produce novel QD structures, such as electrically-coupled QD ensembles and three-dimensional QD crystals [3].

In this study, to achieve such spatial ordering more efficiently and perfectly, we propose and demonstrate the use of a regular QD array, in place of the SKQDs commonly used, which form randomly on the substrates, as a starting layer of the multi-stacking. With this site-initiation approach, the optimal size uniformity of the QDs can be established at the earlier stacking stage and misalignment of QDs in the QD crystals can be reduced.

We fabricated the initial regular InAs QD array on GaAs(001) surfaces using an STM assisted site-control technique [4]. This allows arbitrary in-plane QD arrangement at nanometer precision. Multiple InAs SKQD layers were then grown with spacers for vertical alignment above the initial regular QD array via strain fields. This resulted in a spatially site-controlled InAs QD lattice.

An example of the arbitrary nanoscale SKQD lattices is shown in Fig. 1, in which the stacked InAs SKQDs array is configured to have a hexagonal-like unit cell with a lattice parameter of 50 - 60 nm. This configuration can achieve an area QD density around 4 x 10^{10} cm^{-2}. Figure 2 shows the STM images for the formation process of the spatially site-controlled InAs SKQD lattice. These are images of the identical surface region obtained by tip repositioning function in our STM system [4]. As confirmed by the positions of QDs in Figs. 2(a) and (d), the square lattice configuration in the lower SKQD layer is retained in the upper layer. The vertical pairing probability of QDs between two layers is almost 100%, while no QD is observed at interstitial positions. On the other hand, when the lattice configuration is not properly designed, strain field interference between adjacent sites arises, decreasing vertical pairing probability, as shown in Fig. 3. These results demonstrate that the spatial strain field can be well managed by this approach. Room temperature PL measurements revealed distinct emissions from the spatial SKQD lattice, as shown in Fig. 4, indicating good crystallographic quality despite the addition of an artificial STM process. Further improvements in the initial QD array and growth conditions will increase the promise of the site-initiated spatial ordering approach described here for producing uniform QDs and novel nanostructure systems.

This work was supported by the NEDO within the framework of the Femtosecond Technology Project.

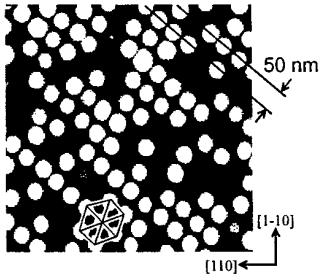

Fig. 1 (left). STM image of a hexagonal InAs SKQD array on a GaAs(001) spacer fabricated by spatial site control. Scan area: 600 nm x 600 nm.

Fig. 2 (below). STM images for the stacking process of the spatially site-controlled InAs SKQD lattice; (a) lower QDs, (b) spacer layer, (c) wetting layer, and (d) upper QDs. These are images of the same area obtained using the tip repositioning function [4]. Scan area: 1000 nm x 1200 nm.

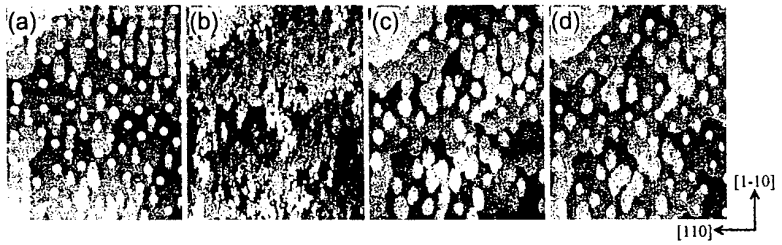

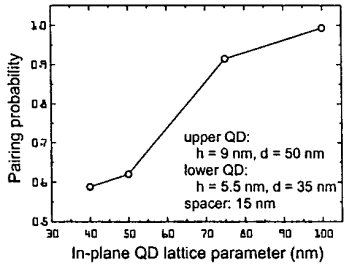

Fig. 3. Vertical pairing probability of QDs between two SKQD layers with <100> square lattices.

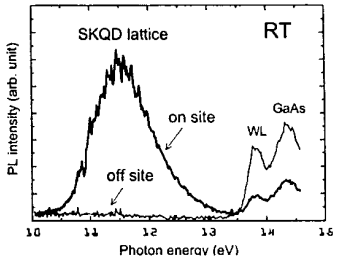

Fig. 4. Room temperature PL spectrum of a 5-layer stacked InAs SKQD lattice ("on site").

References

[1] Q. Xie, et al., Phys. Rev. Lett. **75**, 2542(1995). [2] J. Tersoff, et al., Phys. Rev. Lett. **76**, 1675(1996). [3] G. Springholz, et al., Science **282**, 734(1998). [4] S. Kohmoto, et al., Appl. Phys. Lett. **75**, 3488(1999); J. Electron. Mater. **29**, 525(2000).

Corresponding author: Shigeru Kohmoto, The Femtosecond Technology Research Association (FESTA), 5 - 5 Tokodai, Tsukuba 300-2635, Japan, phone: +81-298-47-5181, fax: +81-298-47-4417, e-mail: kohmoto@festa.or.jp

Effect of phosphorus on Ge/Si(001) island formation

T. I. Kamins[1], G. Medeiros-Ribeiro[2], D. A. A. Ohlberg[1], and R. Stanley Williams[1]

[1] Quantum Science Research, Hewlett-Packard Laboratories, Palo Alto CA 94304-1126, USA
[2] Laboratorio Nacional de Luz Sincrotron, Campinas SP 13083-970, Brazil

Self-assembled Ge islands on Si(001) have been extensive studied [1]. Similar results have been obtained for islands deposited by chemical vapor deposition (CVD) and for those deposited by physical vapor deposition in ultra-high vacuum. Above the wetting layer thickness, undoped layers can exhibit three types of islands depending on the amount of Ge deposited and the deposition conditions: {105} faceted pyramids for low coverages (~6 eq-ML); multi-faceted "domes" for intermediate coverages (~11 eq-ML); and large, defective islands ("super-domes") above about 15 eq-ML. Typical volumes for pyramids and domes are 5000 nm^3 and 1.5×10^4 nm^3, respectively.

When PH_3 is added to the CVD deposition environment, three very different types of islands form, as shown in Figure 1. For low coverages, very low precursor islands ("mounds") are seen. At somewhat higher coverages (~6 eq-ML), small "mini-domes" dominate, and at intermediate coverages (~11 eq-ML), large pyramids form. These "super-pyramids" are bounded by {311} facets near their tops and {111} facets near their bases. Each of these shapes has steeper facets and a smaller volume than the corresponding growth stage for pure Ge on Si(001). The volume of the three types of doped islands are 300-400 nm^3, ~6000 nm^3, and ~10^5 nm^3, respectively. The volume:area relation of the mini-domes approaches that of undoped domes, but the island size is smaller for the mini-domes. The islands (mini-domes) in a ~6 eq-ML doped layer have a maximum in the volume distribution (Figure 2), while the islands (pyramids) in an undoped layer of the same thickness do not.

We attribute the different behavior of undoped and doped structures to the modification of the surface energies of the bounding facets by the phosphorus at the surface of the Ge islands The effect of adsorbed species on the surface of Ge/Si(001) has been observed previously for other elements, such as Sb and In [2]; the doped islands are bounded on top by a (001) plane, with the importance of this plane varying for different dopants. For phosphorus, no (001) plane is visible at the top of the super-pyramids.

The presence of PH_3 during annealing retards coarsening (Figure 3). Although coarsening can be kinetically limited by adsorbed species, the shapes of the islands, as well as their volume distributions, are modified by changing the annealing ambient from H_2 to PH_3/H_2, again suggesting that the presence of phosphorus changes the surface energy of the islands, not just the dynamics of island formation and modification. When doped islands are annealed in H_2, the presence of phosphorus in the islands initially retards structural rearrangement. As the phosphorus leaves the islands by diffusion or evaporation, the island shapes change.

[1] R. Stanley Williams, *et al.*, Acc. Chem. Res. **32**, 425 (1999).
[2] D. J. Eaglesham, F. C. Unterwald, and D. C. Jacobson, Phys. Rev. Lett. **70**, 966 (1993).

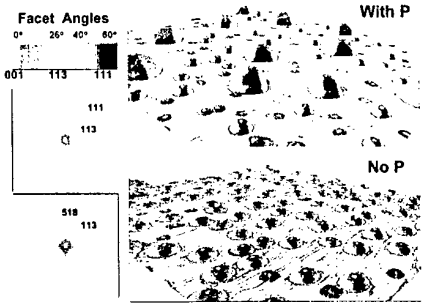

Figure 1: Perspective atomic-force micrographs of phosphorus-doped (top) and undoped (bottom) Ge islands on Si(001), along with corresponding representations of facet angles for Ge layers ~11 eq-ML thick. (1 μm × 1 μm surface area).

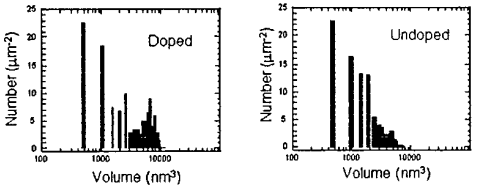

Figure 2: Distribution of island volumes for phosphorus-doped and undoped Ge islands in layers ~6 eq-ML thick.

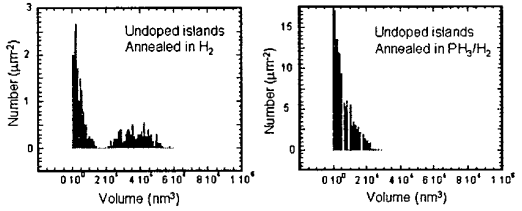

Figure 3: Distribution of island volumes after annealing undoped Ge islands in H_2 or in a PH_3/H_2 ambient for layers ~6 eq-ML thick.

Corresponding author: Ted Kamins, Principal Scientist, Quantum Science Research
Hewlett-Packard Labs, 1501 Page Mill Road, Palo Alto CA 94304-1126, USA
Telephone: 650-857-5470; FAX: 650-236-9885
e-mail: kamins@hpl.hp.com

Silicon/Silicon(sub)oxide heterostructures grown by Molecular Beam Epitaxy

A. Sticht , M. Markmann, K. Brunner, G. Zandler and G. Abstreiter

Walter Schottky Institut, TU München, Am Coulombwall, D-85748 Garching

For many future applications, like resonant tunneling diodes, quantum cascade lasers or optical emitters based on silicon, a suitable barrier material is needed. In principle, silicon dioxide (SiO_2) would be a good candidate because of its high band offsets and the good interface quality achievable for thermal oxides as used in MOS technology. However, its amorphous nature makes overgrowth with single crystalline silicon nearly impossible, thus preventing its use in more complex structures. In this work, we examine MBE-growth and the structural properties of very thin silicon (sub)oxide (SiO_x) layers embedded in silicon employing various types of measurements like RHEED, AFM and TEM and ellipsometry as well as their transport characteristics.

We apply two different methods for growing thin (sub)oxide layers embedded in silicon *in situ* in an MBE system. For layers about two nanometers wide, the wafer surface is exposed to molecular oxygen up to a background pressure of 10^{-6} mbar without any silicon flux. At nominal growth temperatures between 440°C and 500°C, these layers can be overgrown with single crystalline silicon. Fig. 1 shows a high resolution TEM picture taken from such a layer. The layer is continuous and about 2 nm wide, with some lateral inhomogenities. In the overgrown Si layer, dislocations can be seen which disappear after about 40nm overgrowth. *In-situ* reflection high energy electron diffraction (RHEED) measurements show patterns corresponding to three-dimensional growth during the early stages of overgrowth, while the typical pattern of a 2x1 reconstructed silicon surface reappears after about 50nm overgrowth.

In the second method, for fabrication of thicker SiO_x layers, a silicon flux of 0.1Å/s is maintained while introducing oxygen into the growth chamber. These layers were grown up to 300nm thickness. They were overgrown with polycrystalline silicon.

Both kinds of oxide layers exhibit a current blocking behavior at low temperatures and current increases at higher temperatures with activation energies of up to 300meV depending on the structural parameters. Figure 2 shows the temperature-dependent current-voltage characteristics of a thin SiO_X layer grown by the first method. Comparing a sample with one $SiO_{1.6}$ layer of 5nm width and a sample with two of these barrier layers 50nm apart from each other, indicates that a second barrier improves the current blocking behavior of the structure, rising the breakthrough voltage from about 0.5V to about 2V.

Current transport across these barriers generates very hot electrons as shown by Monte-Carlo-simulations (Fig. 3). These hot carriers can be used for efficient impact excitation of erbium in silicon, resulting in light emission at 1.54µm, an important wavelength for fiber communication. Figure 4 shows the normalized current-dependent electroluminescence of a n-Si/SiO_X/Si:Er:O/n-Si structure compared with the luminescence of a conventional pn diode in reverse bias. The structure with the suboxide layer exhibits a 5 times higher $\sigma\tau$ product, with σ the excitation cross section of the erbium and τ the lifetime of the excited state. Combining the pn diode with an additional suboxide layer leads to up to 14 times higher EL output. Periodic nin cascade structure with several SiO_x layers followed by erbium doped layers promise a significant increase of the active volume for light emission.

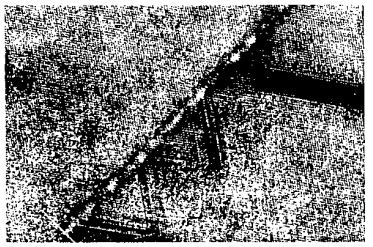

Fig. 1: High resolution TEM image of a 2nm wide suboxide layer embedded in single crystalline silicon. The white arrow indicates growth direction. The dislocations seen in the overgrown layer disappear after about 50nm.

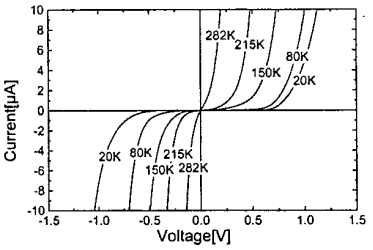

Fig. 2: Temperature dependent IV curves of a single oxide layer about 2nm wide embedded between highly n-doped single crystalline silicon layers. At low temperatures, current blocking behavior up to 0.5 V is observed.

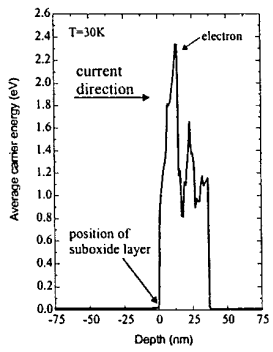

Fig. 3: Monte Carlo simulation of the hot electron energy distribution behind a suboxide barrier with 300meV barrier height at a current of 100mA.

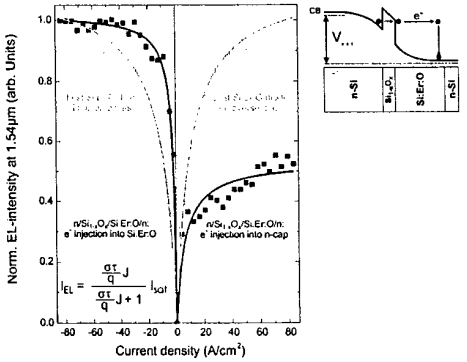

Fig. 4: Current-dependent EL intensity when exciting erbium through a suboxide barrier (black) compared to a conventional pn diode (grey). The faster rise of the black curve in reverse bias corresponds to a higher excitation efficency of the suboxide structure. The small figure on the right shows the schematic band structure.

Corresponding author:Andreas Sticht, Walter Schottky Institut, Technische Universität München, Am Coulombwall 3, D-85748 Garching, Germany,
phone: +49 89 28912778, fax: +49 89 3206620,
email: sticht@wsi.tum.de

Optical and electrical properties of Fe/GaAs (001) hybrid structures grown by molecular beam epitaxy.

Y. Chye, V. Huard, M. White, P. Petroff

Center for Spintronics and Quantum Computation
University of California
Santa Barbara, CA 93106
USA

Hybrid magnetic-semiconductor structures could have important applications in the field of spintronic devices. We report here on two new methods which dramatically improve the epitaxy of Fe thin films on GaAs (001) semi-insulating substrates using molecular beam epitaxy (MBE). The two growth methods are aimed at: a) suppressing the interdiffusion between Fe and GaAs or $Al_{1-x}Ga_xAs$ ($0<x<1$) hence preventing the formation of FeAs [1] and Fe_2GaAs precipitates; b) minimizing the trap concentration at the metal/semiconductor interface. With the first method, Fe films are deposited at −150°C on GaAs or $Al_{1-x}Ga_xAs$. This low temperature deposition is used to alleviate surface exchange reactions. The second method uses an ultra-thin (2ML) Al blocking layer deposited by MBE before deposition of the Fe film. This Al blocking layer is introduced to bind the surface As atoms and form an AlAs epitaxial layer at the Fe/GaAs interface. Therefore, this layer should act as a barrier to interdiffusion and surface exchange reactions.

The samples were grown in two separate MBE chambers. GaAs buffer layers and $GaAs/Al_{0.3}Ga_{0.7}As$ quantum well structures were deposited in one MBE chamber following the standard deposition procedures. An amorphous As capping layer was used for sample protection during the transfer between chambers. The second MBE chamber was used for the deposition of Al and Fe thin films after the As cap was desorbed at 400°C. The single-crystal nature and morphology of the surface were monitored by RHEED during deposition. After the Fe deposition, the samples were subsequently capped with a layer of amorphous Al.

The structural properties of the films were characterized by atomic force microscopy (AFM) and transmission electron microscopy (TEM). These characterizations, together with RHEED, show the Fe epitaxial growth on (001) GaAs, even for depositions at −150°C. The Fe film orientation relationships with the GaAs lattice were found for all films to be identical to those previously reported [2]. Figure 1 shows the hysteresis loops measured by superconducting quantum interference device (SQUID) magnetometry for a series of Fe thin films (100Å thick) under the following deposition conditions: (a) room temperature Fe (RT Fe), (b) low temperature Fe: −150°C (LT Fe), (c) RT Fe with a RT Al blocking layer (RT Al+Fe). (d) LT Fe with a LT Al blocking layer (LT Al+Fe). All films reveal an in-plane magnetic anisotropy with easy and hard axes along [110] and [1$\bar{1}$0], respectively. As seen, the easy axis hysteresis loop of the RT Fe sample shows a more gradual transition to the saturation magnetization when compared to the LT samples. This behavior is consistent with the presence of interface defects or precipitates that interact with the domain wall motion in the RT sample. LT deposition could reduce the defects by suppressing the Ga, As, and Fe interdiffusion during growth as suggested by the sharp transitions to saturation in the hysteresis loop. Figures 1(c) and (d) further support our explanation by showing that the RT Al+Fe and LT Al+Fe hysteresis loops are almost identical and have very sharp transitions. These results are consistent with the formation of an AlAs layer which prevents the As and/or Ga out-diffusion. The diamagnetic response observed in Figures 1(c) and (d) at higher applied magnetic fields is consistent with the formation of a two-dimensional electron gas at the AlAs and GaAs interface.

To further investigate the interface quality between Fe and GaAs, we deposited Fe films on a structure containing a GaAs quantum well (QW) located 20nm below the Fe layer. The n-doped ($5.10^{18}cm^{-3}$) $Al_{0.3}Ga_{0.7}As$ (20nm) /i-GaAs (5nm)/ p-doped ($5.10^{18}cm^{-3}$) $Al_{0.3}Ga_{0.7}As$ (20nm) quantum well was the same for the four deposition conditions. Figure 2 shows the photoluminescence (PL) intensities measured at 4°K. The measurements are normalized to the bulk-GaAs peak. The RT Fe film shows the weakest QW luminescence while the RT Al+Fe film is the strongest. The LT Fe and LT Al+Fe structures show a small luminescence degradation. Our measurements of the I-V characteristics on these samples indicate a Schottky rectifying behavior for the 4 samples with a mid-gap pinning of the Fermi level. These data along with the PL data suggest that the reactions of the Al blocking layer with the surface As atoms result in the formation of an ultra-thin AlAs layer. This AlAs blocking layer minimizes the role of interface traps leading to the better QW luminescence of the RT Fe+Al film. The poor luminescence of the RT Fe structure is ascribed to the presence of interface traps and FeAs precipitates. We believe that some of the epitaxial structures presented here could be promising candidates for spintronic applications.

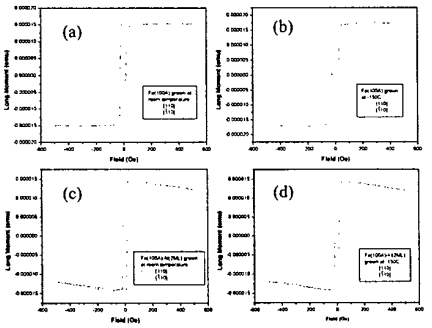

Figure 1: Hysteresis loops for (a) RT Fe, (b) LT Fe, (c) RT Al+Fe and (d) LT Al+Fe samples. In (c) and (d) the Al blocking layer was deposited at the same temperature as that of the Fe layer.

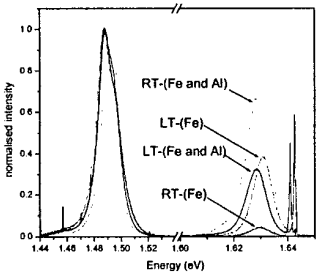

Figure 2: Photoluminescence spectra for a series of deposition conditions of the Al blocking layer and Fe films. The lines at 1.63eV and at 1.49eV correspond to the quantum well and GaAs buffer layer, respectively.

The authors would like to acknowledge J. English, A. Jackson, R. Kawakami, M. Hanson, H. Lee, E. Letts and J. Johnson for their technical assistance. This project is supported by the Center for Spintronics and Quantum Computation DARPA/ONR grant (#N00014-99-1-1096) and an NSF IGERT grant.

References

[1] G. A. Prinz and J. J. Krebs, Appl. Phys. Lett. **39**, 397 (1981).
[2] J. J. Krebs, B. T. Jonker, and G. A. Prinz, **61**, 2596 (1987); B. Lepine, C. Lallaizon, S. Ababou, A. Guivarc'h, S. Deputier, A. Filipe, F. Nguyen Van Dau, A. Schuhl, F. Abel, C. Cohen, J. of Crystal Growth, **201/202**, 702 (1999).

Corresponding author: Pierre Petroff, Materials Department, University of California, Santa Barbara CA 93106, USA
Phone: 805-893-8256, Fax: 805-893-8983
Email: petroff@engineering.ucsb.edu

Manipulation and storage of quantum information with semiconductor spintronics

I. Malajovich[1], E. Johnston-Halperin[1], R.L. Kawakami[1], J.J. Berry[2], N. Samarth[2], D.D. Awschalom[1]

[1]Department of Physics, University of California, Santa Barbara, CA 93106 USA
[2]Department of Physics, Pennsylvania State University, University Park, PA 16802 USA

There is a growing interest in the use of spin in semiconductor quantum structures as a medium for the manipulation and storage of classical and quantum information. Femtosecond-resolved optical experiments reveal a remarkable resistance of quantum spin states to environmental decoherence in a variety of semiconductors [1,2,3]. Optical pulses are used to create a superposition of the basis spin states defined by an applied magnetic field, and to follow the phase, amplitude, and location of the resulting electronic spin precession in bulk semiconductors, heterostructures, and quantum dots. The data show that spin lifetimes can exceed hundreds of nanoseconds and spin packets can be transported over a hundred microns in some of these systems.

Spatial imaging and dynamical magnetometry monitors decoherence and dephasing of itinerant spin information as it flows not only through semiconductors, but also across dissimilar material interfaces in engineered structures [2]. The interfaces appear surprisingly permeable to the flow of spin information over a broad range of temperatures, where regional boundaries may be used to control the resulting spin coherent phase. Moreover, recent measurements distinguish several parallel channels of interlayer spin coherent injection within semiconductor heterostructures. We observe relative increases in spin coherent injection of up to 500% in electrically-biased structures, and 4000% when p-n junctions are used to impose a built-in bias. The former results from a new 'persistent' spin conduction mode that appears upon bias, sourcing coherent spin transfer for at least 1-2 orders of magnitude longer than in unbiased structures (Figure 1). These experiments reveal promising new opportunities for multifunctional spintronic devices (such as spin transistors that combine memory and logic functions) wherein the amplitude and phase of the net spin current are controlled by *either* electrical or magnetic fields.

As the majority of studies to date have been performed in high quality semiconductor systems, a deeper understanding of the effect of defects on spin-coherence is clearly important for the development of spin-based electronics. In this context the III-V semiconductor GaN is intriguing in that it combines a high density of charged threading dislocations with high optical quality, allowing optical investigation of the effects of momentum scattering on coherent electronic spin states. Despite densities of charged threading dislocations of ~5×10^8 cm^{-2}, we observe electron spin coherence in n-type MOCVD-grown GaN epilayers (Figure 2) with spin lifetimes of ~ 20 ns at T = 5 K that persist to room temperature [3]. Further investigations in the vicinity of the metal-insulator transition reveal a dependence on both magnetic field and temperature qualitatively similar to previous studies in n-type GaAs, suggesting a common origin for spin relaxation in these systems.

A complementary approach to developing spintronic devices is based on generating novel magnetic materials, and is exemplified in recent work involving III-V ferromagnetic semiconductors (e.g., (Ga,Mn)As and (In,Mn)As). This approach has already led to the demonstration of zero-field spin injection in a hybrid structure involving both high quality semiconductor epilayers and ferromagnetic (Ga,Mn)As [4]. The integration of these two approaches—introducing coherent spins into ferromagnetic nanostructures—could lead to a new class of quantum magnetoelectronics based on the spin degree of freedom. In particular, some quantum computation schemes rely on the interaction of coherent spins with ferromagnetic materials to facilitate quantum logic operations. To investigate the nature of the carrier-mediated ferromagnetism in these materials, it is desirable to disentangle the electronic and magnetic interactions through alternative semiconductor growth techniques. We have grown (Ga,Mn)As as a digital ferromagnetic heterostructure (i.e. digital alloy) by alternately depositing GaAs and submonolayer MnAs using low-temperature molecular beam epitaxy [5]. Magnetic measurements indicate ferromagnetism in the digital structures. Further, by varying the spacing of the MnAs layers, we systematically investigate the length scale of the ferromagnetic interaction and find that the Curie temperature varies with the MnAs spacing with evidence for magnetic decoupling beyond 40 ML (11 nm) spacing. In fact, single layers of 0.5 ML MnAs embedded in a GaAs host are shown to be ferromagnetic. This growth technique therefore offers the opportunity for the separation of electronic and magnetic interactions suggested above, enabling future developments in magnetoelectronics and optoelectronics.

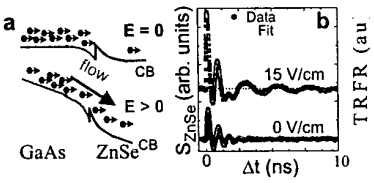

Fig. 1: (a) Schematic conduction band (CB) spin transfer for GaAs/ZnSe heterostructures with and without an applied electric field. (b) Time resolved Kerr rotation measurements at B = 75 mT and T = 5 K taken at different biases.

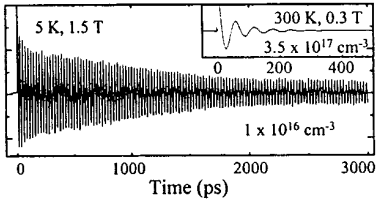

Fig. 2: Time resolved Faraday rotation (TRFR) of an MOCVD grown GaN epilayer with n = 1×10^{16} cm^{-3}. (Inset: TRFR at room temperature of epilayer with n = 3.5×10^{17} cm^{-3}.)

References

[1] D.D. Awschalom and J.M. Kikkawa, Physics Today 52, 33 (1999).
[2] I. Malajovich et al., Phys. Rev. Lett. 84, 1015 (2000).
[3] B. Beschoten et al., Phys. Rev. Rapid Commun. B63, 1212XX (2001).
[4] Y. Ohno et al., Nature 402, 790 (1999).
[5] R.L. Kawakami et al., Appl. Phys. Lett. 77, 2379 (2000)

Corresponding author: David D. Awschalom, Department of Physics, University of California, Santa Barbara, California 93106, USA.
phone: +1 805 893 2121, Fax: +1 805 893-4170
email: awsch@physics.ucsb.edu

Ferromagnetism in II-VI based semiconductor structures

J.Cibert[a], D.Ferrand[a], S.Tatarenko[a], A.Wasiela[a], P.Kossacki[b], T.Dietl[c],
(a) Laboratoire de Spectrométrie Physique, BP87, 38402 Saint Martin d'Hères cedex, France
(b) Institute of Experimental Physics, Warsaw University
(c) Institute of Physics, Polish Academy of Science, Warsaw

II-VI diluted magnetic semiconductors appear as model systems for the study of carrier induced ferromagnetism in zinc-blend semiconductors. The spins and the carriers can be introduced independently, so that a broad range of carrier concentrations and spin contents can be obtained as well in a 3D configuration and in 2D structures. In addition, the material properties have been accurately determined on nominally undoped samples.

Carrier induced ferromagnetism has been observed in modulation-doped $Cd_{1-x}Mn_xTe$ quantum wells [1,2] and in $Zn_{1-x}Mn_xTe$ layers [3] heavily doped p-type. The magnetic susceptibility, measured directly in the case of the thick layers, or through magneto-optical spectroscopy in the case of quantum wells, was found to diverge at low temperature in the doped samples, while the undoped samples exhibit an antiferromagnetic behaviour. Below the Curie-Weiss temperature, remanence is observed in the magnetization cycles of $Zn_{1-x}Mn_xTe$ layers, while a zero-field splitting of the photoluminescence line from the quantum wells is ascribed to the onset of a local spontaneous magnetization.

A simple mean-field model - or Zener model – has been used to explain the general features of the carrier induced interaction. Using this uniform limit of the RKKY model is justified in most semiconductor structures since the average Mn-Mn distance is definitely smaller than the Fermi wavelength, which gives the characteristic scale of the RKKY oscillations. The effect of the (antiferromagnetic) superexchange interaction between Mn ions is introduced using the parameters determined on undoped materials. This simple model surprisingly well accounts for the observed critical temperatures (figure). It also helps identifying characteristic features which - from the experimentalist's viewpoint - will have to be included in a more elaborated model. Some of them are well identified, through the mean field model, as crucial to understand the experimental results, and hence they will have to be kept in spite of the complication they can introduce. Other points on the contrary appear as discrepancies between the experimental data and the predictions of the mean field model.

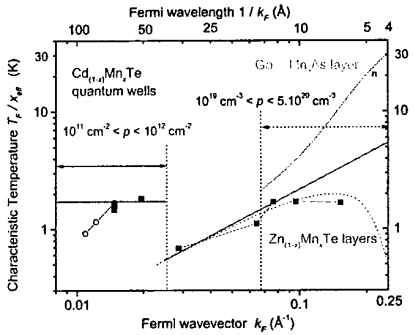

Fig. Normalised characteristic temperature measured in $Cd_{1-x}Mn_xTe$ quantum wells and in $Zn_{1-x}Mn_xTe$ and $Ga_{1-x}Mn_xAs$ layers (symbols) and calculated in the mean field model (solid lines) and in the RKKY model for 2% Mn (dotted line).

The values of the spin-carrier coupling constants readily explains that the spin-spin interaction is more efficiently induced by holes than by electrons (such as in ZnO heavily doped *n*-type). The model also strongly emphasises the importance of properly taking into account the detailed structure of the valence band which results from the effects of spin-orbit coupling. In a quantum well, confinement and strain result in a strong anisotropy of the hole wavefunctions (heavy holes), so that the carrier-induced spin-spin coupling takes the Ising form. In an unstrained thick layer, an isotropic, Heisenberg-like form is recovered, but the spin-orbit coupling reduces the strength of the spin-spin interaction. [3] Finally, in materials with a smaller spin-orbit coupling, larger spin-spin couplings are expected. [4]

A first extension of the mean field model consists in considering the spatial dependence of the interaction. In the $Zn_{1-x}Mn_xTe$ layers with the lower Mn content x and heavier p-type doping, the Fermi wavelength can no more be considered as large with respect to the Mn-Mn distance, hence the spatial dependence of the spin-spin interaction (i.e., the RKKY oscillations) must be taken into account; Accordingly a smaller critical temperature is calculated and actually is measured. The situation of the $Cd_{1-x}Mn_xTe$ quantum wells is more intriguing, since the q-dependence of the Pauli susceptibility of the 2D gas suggests the possibility of a more complicated ordered phase. [2]

Some effects which appear to be important for a complete understanding of the experimental results, are not easily incorporated in the mean-field model, so that more elaborated models are needed. In the $Zn_{1-x}Mn_xTe$ layers a spin-induced metal-insulator transition is clearly evidenced in the magnetoresistance data. A ferromagnetic behaviour is yet observed on samples on both sides of the transition, but disorder appears to decrease the value of the magnetization. The $Cd_{1-x}Mn_xTe$ quantum wells are probably less affected by disorder. Remote acceptors are less efficient to create electrostatic disorder, so that a 2D hole gas of good quality can be realised with large values of the Fermi wavelength; Thus, spin disorder is better averaged since a large number of Mn atoms are contained in a volume defined by the quantum well thickness and the Fermi wavelength. Moreover, confinement reduces the mixing of carrier wavefunctions. As a result, sharp photoluminescence lines allow us to demonstrate the enhanced Zeeman effect (i.e., the ferromagnetic susceptibility) up to the value of the valence band splitting where a complete polarization of the carriers is reached. However carrier-carrier interactions should be incorporated in the model, and disorder appears to control the transition from antiferromagnetic to ferromagnetic behaviour when the carrier concentration is changed in a sample.

References

[1] A.Haury, A.Wasiela, A.Arnoult, J.Cibert, T.Dietl, Y.Merle d'Aubigné, S.Tatarenko Phys. Rev. Lett. 79, 511 (1997).
[2] P. Kossacki, D. Ferrand, A. Arnoult, J. Cibert, S. Tatarenko, A. Wasiela, Y. Merle d'Aubigné, J-L. Staeheli, J-D. Ganiere, W. Bardyszewski, K. Swiatek, M. Sawicki, J. Wróbel, and T. Dietl, Physica E 6, 709 (2000).
[3] D. Ferrand, J. Cibert, A. Wasiela, C. Bourgognon, S. Tatarenko, G. Fishman, T. Andrearczyk, J. Jaroszynski, S. Kolesnik, T. Dietl, B. Barbara and D. Dufeu, Phys. Rev. B 63, 85201 (2001); cond- mat/ 0007502.
[4] T.Dietl, H.Ohno, F.Matsukura, J.Cibert, D.Ferrand; Science 287, 1019 (2000).

III-V based magnetic heterostructures for spintronics

Masaaki Tanaka

Department of Electronic Engineering, The University of Tokyo, 7-3-1 Hongo, Bunkyo-ku, Tokyo 113-8656, Japan; also CREST, Japan Science & Technology Corporation
Phone: +81-3-5841-6728, Fax: +81-3-5803-3975, Email: masaaki@ee.t.u-tokyo.ac.jp

Magnetic / III-V semiconductor hybrid materials, such as ferromagnet/semiconductor heterostructures, magnetic alloy semiconductors, and magnetic granular nanostructures embedded in semiconductors, can give rise to spin-dependent functions in semiconductor-based devices [1]. Here we present two examples of novel III-V based magnetic heterostructures for semiconductor-based "spintronic" devices. These are shown to have spin-related functions, large tunneling magneto-resistance (TMR) and large magneto-optical effect, which cannot be realized by conventional nonmagnetic materials and heterostructures.

First, we present very large TMR (>70%) in semiconductor magnetic tunnel junctions (MTJs) having (GaMn)As ferromagnetic electrodes separated by an ultrathin AlAs layer as a tunnel barrier. Trilayer heterostructures, $(Ga_{1-x}Mn_x)As(x=0.04$, 50nm)/AlAs(d nm)/$(Ga_{1-x}Mn_x)As$ (x=0.033, 50nm), were grown on p^+GaAs substrates by low-temperature molecular beam epitaxy (LTMBE) [2]. By using a shutter linearly moving in front of a substrate, a wedge-type AlAs barrier was grown to form tunnel junctions with the barrier thickness d ranging from 1.3nm to 3.0nm within a wafer. Mesa etched MTJs with 20 - 200 μm in diameter were fabricated, and showed clear TMR due to the change from parallel to anti-parallel magnetization (the spin-valve effect) of the two ferromagnetic (GaMn)As layers. We have obtained the TMR ratio up to 75 % at 8K for the junction with d=1.5 nm when the magnetic field was applied along the [100] axis in the film plane. For d>1.6nm, the TMR ratio was found to decrease with the barrier thickness. This behavior can be explained by calculations based on the tight-binding model assuming that the wavevector $\boldsymbol{k}_{//}$ of carriers is conserved in tunneling [3]. This means that Julliere's model [4], which is often used for analyzing TMR in conventional MTJs, is not valid in such epitaxial MTJs. Also, we have found that the TMR behavior strongly depends on the applied magnetic field direction, which is well explained by the cubic magneto-crystalline anisotropy of GaMnAs [5].

Unlike the conventional MTJs made of polycrystalline ferromagnetic metals and an amorphous tunnel barrier, the present MTJs are all-epitaxial monocrystalline semiconductor-based junctions, which have the following advantages: (1) MTJs made of all-semiconductor heterostructures can be integrated with semiconductor circuitry. (2) In principle, many parameters, such as the barrier height, barrier thickness, and Fermi energy of the electrodes, are controllable. (3) Introduction of quantum heterostructures, such as resonant tunneling structures, is easier than any other material system.

Second, we show that magneto-optical effect can be controllably enhanced at room temperature, in MBE-grown semiconductor based multilayer structures consisting of a magnetic layer and distributed Bragg reflectors (DBR). Here, the magnetic layer is GaAs which contains MnAs nanoscale clusters (hereafter GaAs:MnAs). GaAs:MnAs can be formed by annealing (GaMn)As alloy which was grown by low-temperature MBE [6]. During the annealing process at 500 - 750 °C, ferromagnetic MnAs nano-scale clusters are formed in a GaAs matrix without damaging the monocrystalline quality. This ferromagnet-semiconductor granular material GaAs:MnAs shows a super-paramagnetic behavior and has large magneto optical effect at room temperature. Multilayer structures consisting of DBR(the thickness of each layer is $\lambda/4n$) / GaAs:MnAs(thickness is $\lambda/2n$) / DBR(the thickness of each layer is $\lambda/4n$) were grown by MBE on GaAs substrates, where λ is the operation wavelength and n is the refractive index of each layer. Since this structure works as a magnetic microcavity, the lightwave of wavelength λ is localized in the centered magnetic layer, leading to the enhancement of magneto-optical Faraday effect. We have observed significant enhancement of Faraday effect by a factor of 6 - 7 at room temperature, under only 1- 2 kOe at the aimed wavelength of 0.98 μm [7-8]. We have also studied theoretical design and optimization of the magneto-optical performance in the SMPC structures and how to reduce the optical loss in the GaAs:MnAs magnetic layer [8-9].

This is a new class of semiconductor-based magneto-photonic crystal (SMPC), whose potential strengths are the following: (1) Consisting of all epitaxial III-V based materials, SMPC can be readily integrated with III-V based opto-electronic devices. (2) By choosing various III-V semiconductors and structural parameters, one has a lot of freedom in the design, and the operation wavelength can be tuned in a wide range (in principle from ultraviolet to infrared). (3) Room temperature operation at relatively low magnetic field is possible.

References

[1] M. Tanaka, J. Mater. Sci. & Eng. **B31**, 117 (1995); M. Tanaka, Physica **E2**, 372 (1998); M. Tanaka, J. Vac. Sci. & Technol. **B16**, 2267 (1998), ibid. **A18**, 1247 (2000).
[2] Y. Higo, H. Shimizu, and M. Tanaka, *presented at Int. Conf. on the Physics and Application of Spin-Related Phenomena in Semiconductors, paper-LN2, Sendai, September 2000,* to be published in Physica E.
[3] Y. Higo and M. Tanaka, submitted.
[4] M. Julliere, Phys. Lett. **54**A, 225 (1975).
[5] Y. Higo, H. Shimizu, and M. Tanaka, *presented at 8th MMM-Intermag, paper-BC2, San Antonio,* to be published in J. Appl. Phys.
[6] J. De Boeck, R. Oesterholt, A. Van Esch, H. Bender, C. Bruynseraede, C. Van Hoof, and G. Borghs, Appl. Phys. Lett. **68**, 2744 (1996).
[7] H. Shimizu, M. Miyamura, and M. Tanaka, J. Vac. Sci. & Technol. **B18**, 2063 (2000).
[8] H. Shimizu, M. Miyamura, and M. Tanaka, Appl. Phys. Lett. **78**, 1523 (2001).
[9] H. Shimizu and M. Tanaka, *presented at 8th MMM-Intermag, San Antonio, paper-FE4,* to be published in J. Appl. Phys.

Corresponding Author: Masaaki Tanaka, Department of Electronic Engineering, The University of Tokyo, 7-3-1 Hongo, Bunkyo-ku, Tokyo 113-8656, Japan
Phone: +81-3-5841-6728, Fax: +81-3-5803-3975, Email: masaaki@ee.t.u-tokyo.ac.jp

Spin injection and spin accumulation in mesoscopic two-dimensional electron gas and metal spin valves.

B.J. van Wees
Department of Applied Physics and Materials Science Centre
University of Groningen
9747 AG Groningen
The Netherlands

An exciting new direction in the field of spin-based electronics or "spintronics" is the possibility to generate, control and apply spin polarized currents and the associated phenomenon of spin accumulation. In this talk I will discuss our results on mesoscopic spin valve structures, where two ferromagnetic electrodes are coupled to either a two-dimensional electron gas present in an InAs quantum well, or to a non-magnetic metal.
In the semiconductor devices we have so far not been able to observe indications of spin polarized transport[1]. An explanation for this can be given in terms of "conductivity mismatch". However, in the full-metal devices we have observed clear evidence for spin injection and spin accumulation, both at 4.2K and at room temperature[2]. We have measured the spin signal in devices with electrode spacing ranging from 250 nm to 2 μm. From the analysis we obtain surprsingly large spin flip lengths in the Cu of 1 μm at 4.2K and 350 nm at RT. This opens up new possibilities to control the spin e.g. by means of controlled precession in an applied magnetic field. Furthermore I will show how the "conductivity mismatch" problem might be avoided, using magnetic tunnel junctions for injection and detection of spin polarized currents in a two-dimensional electron gas.

[1] A.T. Filip, B.H. Hoving, F.J. Jedema, and B.J. van Wees, Phys. Rev. B62, 9996 (2000)
[2] F.J. Jedema, A.T. Filip, and B.J. van Wees, Nature March 15 (2001), to be published

Spin lifetimes and g-factor tuning in Si/SiGe quantum wells

N. Sandersfeld[1], M.Mühlberger[1], W. Jantsch[1], Z. Wilamowski[1,2], F. Schäffler[1]

[1]Institut für Halbleiter- und Festkörperphysik, Johannes-Kepler-Universität Linz, A-4040 Linz, Austria
[2]Institute of Physics, Polish Academy of Sciences, Al Lotnikow 32/64, PL-0668 Warsaw, Poland

While electron spin is the most important parameter in magnetic storage devices, it has presently no relevance for commercial semiconductor devices. This is about to change, mainly due to the novel quantum computing concepts that emerged in recent years. If quantum computers can ever be realized in semiconductor materials with their superior miniaturization and integration technologies, spin will be of paramount importance.[i] Because for such applications spin coherence times have to be as long as possible, the choice of semiconductors is limited to materials with small spin-orbit interaction and a negligible amount of nuclear spins associated with the matrix and dopant atoms. Silicon is certainly a prime candidate, because it not only fulfills that precondition, but it also is the only material suited for ultra large scale integration.

Here we report on the spin properties of 2-dimensional electron gases (2DEG) in strained Si and SiGe channels of modulation-doped Si/SiGe quantum wells. In a standard microwave absorption experiment we measured the conduction electron spin resonance (CESR), and simultaneously the cyclotron resonance (CR) signal of the 2DEG. The latter yields a large background signal extending over a broad magnetic field range, whereas the former appears as a very narrow signal at a g-factor very close to 2 (Fig.1). In high-quality samples, which also show carrier mobilities in excess of 100,000 cm²/Vs at low temperatures, the CESR signal is as narrow as 30mG. By measuring the ESR signal as a function of incident microwave power the spin relaxation time was derived. We find longitudinal spin relaxation times of up to 30μs, and transversal spin relaxation times around 1μs. These time constants are 3 - 4 orders of magnitude longer than the corresponding spin life times in the best III-V materials reported so far.

A second precondition for quantum computing is the setting of a defined initial spin configuration. For this purpose, it was proposed in Ref. i to induce a spin flip operation in an ESR configuration. Spin flips in a quantum computer cell should then be switched on and off by a gate voltage, which tunes the Landé g-factor for the selected carrier. A rather complex Si/SiGe structure was proposed in Ref. i to facilitate this function.

We demonstrate with two experiments that a much simpler device structure can be employed for inducing a spin flip operation with an applied gate voltage. Fig. 2 shows the variation of the g factor as a function of composition in strained $Si_{1-x}Ge_x$ quantum wells with 0 x 10%. Although the conduction band remains Si-like in this rather narrow range of compositions, a clear variation of the g factor is observed. Given the experimental resonance widths indicated in Fig. 2, this x range is already sufficient to switch the spin resonance in a microwave cavity on and off. The only additional requirement would be a double-channel configuration with a Si and a $Si_{90}Ge_{10}$ channel next to each other, and a gate that can switch the carriers between these channels.

The feasibility of this concept is also demonstrated in Fig. 3, which shows the tuning of the g factor in a Si/SiGe MODFET as a function of the applied gate voltage for the ESR magnetic field in the plane of the 2DEG. Here the gate voltage shifts the electron wave function more and more into the $Si_{0.75}Ge_{0.25}$ barrier, which leads to a monotonous decrease of the g factor over a sufficiently large range.

[i] R. Vrijen, E.Jablonovitch et al., Phys. Rev. A **62**, 012306 (2000)

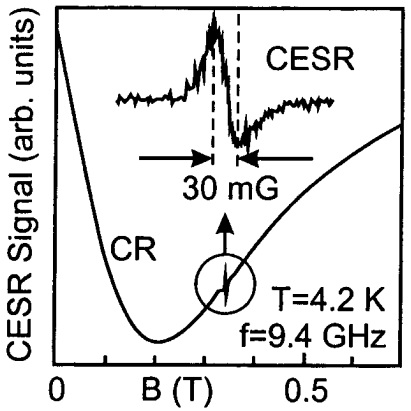

Fig. 1: First derivative of the microwave absorption signal with respect to magnetic field as a function of magnetic field obtained on the SiGe quantum well sample.

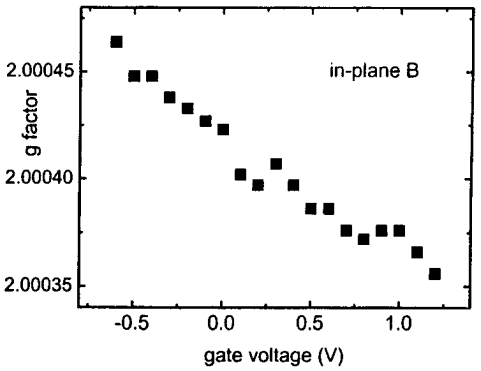

Fig. 3: Shift of the g-factor in a Si/SiG MODFET as a function of the applied gat voltage for the magnetic field of the ESF set-up in the plane of the 2DEG.

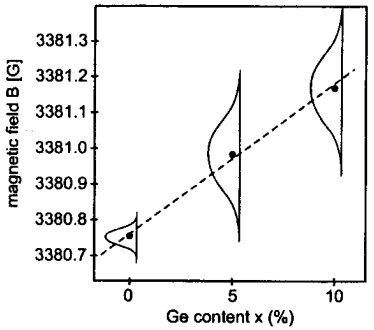

Fig. 2: Landé g factor versus compositio for strained $Si_{1-x}Ge_x$ quantum wells on relaxed $Si_{0.75}Ge_{0.25}$ buffer layer. Lin widths of the observed ESR signals ar indicated.

Corresponding Author: Friedrich Schäffler, Institut für Halbleiter- und Festkörperphysik, Johannes Kepler Universität, A-4040 Linz, Austria
phone: +43 732 2468 9606, fax: +43 732 2468 8650
e-mail: f.schaffler@hlphys.uni-linz.ac.at

Electrical Spininjection using II-VI Dilute Magnetic Semiconductors as Spin Aligners

L.W. Molenkamp, G. Schmidt, P. Grabs, C. Gould and G. Richter

Physikalisches Institut (EP3), Universität Würzburg, Am Hubland, D-97074 Würzburg, Germany

The surprising difficulties encountered by a large number of researchers in obtaining electrical injection of a spin-polarized current into a semiconductor from metallic ferromagnetic contacts can be understood from a simple model[1] that bears many similarities to those used to understand Giant Magnetoresistance (GMR) effects in metallic multilayers[2]. We will briefly discuss this model, the main outcome of which is that spin-injection into semiconductors can be inhibited by a large difference in resistance between the spin-injecting contact and the non-magnetic semiconductor.
The model indicates several ways out of this problem; we have chosen a rather direct route. Instead of ferromagnetic metals, we use II-VI Dilute Magnetic Semiconductors (DMSs) as spin injecting contacts. These contacts evidently have a comparable low conductivity as non-magnetic semiconductors. Moreover, II-VI DMSs, which typically contain up to ten % Mn, are paramagnets, but exhibit at low applied magnetic field a giant Zeeman splitting of the band edge states, which causes the charge-carriers (electrons in our case) to align their spin to the lower Zeeman level, yielding a strongly spin polarized current.
We have successfully implemented such spin-aligners for injecting a strongly (at least up to 90 %) spin-polarized current, and describe two types of experiments evidencing this effect. First, we have used spin-aligner as the top contact of III-V pin-diodes[3]. The electroluminescence of these diodes exhibits a strong degree of circular optical polarization, which can be used to directly determine the degree of spin-polarization of the injected current. Second[4], we present results on the magnetoresistance of a simple all electrical device, consisting of two DMS contacts on a non-magnetic semiconductor. These devices exhibit a novel, strongly positive magnetoresistance effect, which due to the injection of a spin-polarized current into the non-magnetic layer. This effect can be regarded as the paramagnetic analog of the GMR effect, and has potential for reading out the spin state in spintronic devices.

References

[1] G. Schmidt, D. Ferrand, L.W. Molenkamp, A.T. Filip, and B.J. van Wees, Phys. Rev. B62, R4790 (2000).
[2] T. Valet and A. Fert, Phys. Rev. B40, 7099 (1993).
[3] R. Fiederling, M. Keim, G. Reuscher, W. Ossau, G. Schmidt, A. Waag, and L.W. Molenkamp, Nature 402, 787 (1999).
[4] G. Schmidt, G. Richter, P. Grabs, D. Ferrand, L. W. Molenkamp, submitted.

Corresponding author: Laurens W. Molenkamp, Physikalisches Institut (EP 3), Universität Würzburg, Am Hubland, D-97074 Würzburg, Germany.
phone: +49 931 888 4925, Fax: +49 931 888 5142
email: laurens.molenkamp@physik.uni-wuerzburg.de

Spin polarization dynamics in n-doped InAs/GaAs quantum dots

S. Cortez[1], A.Jbeli[2], X.Marie[2], O. Krebs[1], R. Ferreira[1],

T.Amand[2], P. Voisin[1], J-M. Gérard[3]

[1]Laboratoire de Physique de la Matière Condensée de l'Ecole Normale Supérieure, 24 rue Lhomond, 75005 Paris, France
[2]Laboratoire de Physique de la Matière Condensée, INSA-CNRS, 135 Avenue de Rangueil, 31077 Toulouse Cedex, France
[3]Laboratoire de Photonique et Nanostructures, 196 Av. H. Ravera, F92220 Bagneux, France

Because of their atomic-like energy spectrum, self assembled quantum dots (QD's) appear as an ideal candidate for the experimental realization of an elementary quantum gate in the condensed matter [1]. Indeed, spin relaxation processes such as motional narrowing and band mixing become inefficient in such heterostructures. In non intentionally doped QD's, the electron-hole pair fine structure is strongly affected by the interplay between the exchange interaction and the reduced C_{2v} symmetry of the quantum dot. The exciton ground state is characterized by two linearly polarized eigenstates along [110] and [-110]. Recent time-resolved experiments [2] performed under strictly resonant excitation demonstrated the stability of the correlated electron-hole pair ground state polarization during the whole radiative lifetime of the exciton up to temperatures of 30 K. Under non resonant excitation conditions, the circular polarization of the exciton luminescence after a circularly polarized light excitation experiences a fast decay (hundreds of picoseconds) [3]. Hence, very little is known about the possibility of controlling the spin of a single electron in a quantum dot and its relaxation dynamics.

Here we report on the optical orientation dynamics of trions in n-doped quantum dots under non resonant excitation. The doping level of our sample corresponds to an average of one electron per dot. We studied both continuous wave and time resolved luminescence under circularly polarized excitation. The circular polarization of the luminescence was clearly measured at 10 K under excitation at 1.55eV, above the GaAs band gap, which implies a complete depolarization of the holes spin. In time resolved measurements, the circular polarization of the luminescence increased from +10% up to +25% during the radiative recombination time when exciting in the GaAs barrier. We interpret this as a consequence of the spin dependent energy relaxation due to Pauli blocking [3]. Surprisingly, the polarization is reversed when exciting in the wetting layer , and evolves from -15% up to -45% after 2 ns. Moreover, the temperature dependence of the optical orientation when exciting in the wetting layer proves to be drastically different from previous measurement in undoped samples under resonant linear excitation. At 75 K, the polarization of the luminescence is still strong (-10%) and doesn't decay during the radiative lifetime of the trion.

Although more experiments are necessary to understand properly the trion spin structure, we can already conclude that the electronic spin is maintained during the capture and the energy relaxation. The observed polarization arises from dots populated by two electron in both the ground state and first excited state with parallel spins. The fine structure of the trion seems to be essentially governed by the exchange interaction between the two electrons, which acts as an effective magnetic field on the system. These experimental data support the fact that the electron-electron exchange term is stronger than the electron-hole one within a given quantum dot.

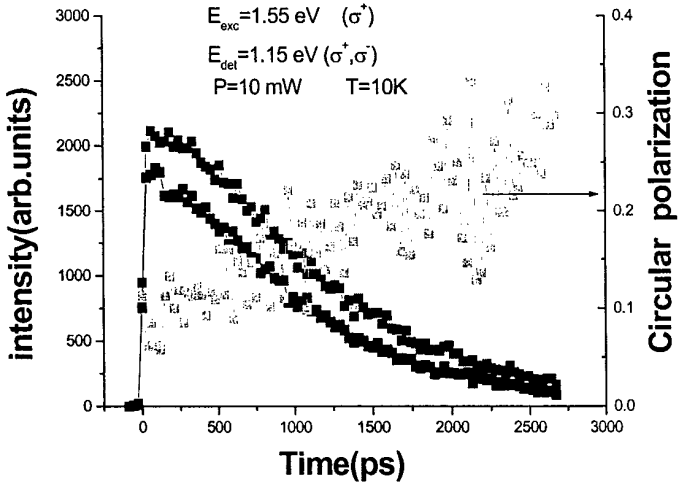

Fig. 1: Time dependant circularly polarized luminescence of n-doped QD's after an excitation in the GaAs barrier with a picosecond Ti:Sa laser pulse. The polarization increases from 10% up to 25% during the recombination lifetime.

References

[1] Daniel Loss and Eugene V. Sukhorukov , Phys. Rev. Lett. **84**, 1035 (2000)
[2] M.Paillard, X.Marie, P.Renucci, T.Amand, A.Jbeli and J.M.Gerard, Phys. Rev. Lett. **86**, 1634 (2001)
[3] M. Paillard, X. Marie, P. Renucci, T. Amand, V. Kalevich, K. Kavokin, V. Ustinov, Phys. Stat. Sol. (b), **221**, 71(2000)

Corresponding author: Cortez Sebastien, LPMC-ENS, 24 rue Lhomond
75005 Paris , France
phone: +33 1 44 32 33 81, Fax: +33 1 44 32 38 40
email: sebastien.cortez@lpmc.ens.fr

Photoluminescence spectroscopy on single CdSe quantum dots in a semimagnetic ZnMnSe matrix

H. Schömig[1], M.K. Welsch[1], S. Zaitsev[2], G. Bacher[1], V.D. Kulakovskii[2] and A. Forchel[1]
[1]Technische Physik, Universität Würzburg, Am Hubland, 97074 Würzburg, Germany
[2]Institute of Solid State Physics, RAS, 142432 Chernogolovka, Russia

S. Lee#, M. Dobrowolska, J.K. Furdyna
Department of Physics, University of Notre Dame, Notre Dame, IN 46556, USA

Quantum dots (QDs) represent the ultimate goal in the realisation of low-dimensional semiconductor structures. Among others, the self-organized growth of QDs proved to be an efficent technique applicable to various material systems like InAs/GaAs or CdSe/ZnSe. According to a proposal made by Loss [1] the spin states of a carrier confined in such structures could serve as a Q-Bit for quantum information processing and ferromagnetic and paramagnetic single dots are possible candidates for single Q-Bit and read-out operations, respectively. In this context a profound understanding of the interaction between individual charge carriers with their magnetic environment is of strong interest. Here we present for the first time photoluminescence studies on single CdSe QDs embedded in a semimagnetic ZnMnSe barrier. The strong exchange interaction between the spin of the carriers and the spins of magnetic ions results in effective g-factors of more than 100 and in the formation of a quasi-zero dimensional excitonic magnetic polaron (EMP), i.e. a small region where the Mn^{2+} spins are aligned in the carrier induced exchange field.

Up to now, efforts to incorporate manganese ions isoelectronically into the matrix of self-organized CdSe dots resulted in samples with low quantum efficiencies due to non-radiatiative recombination via internal Mn^{2+} states. We have grown self-assembled CdSe quantum dots embedded between $Zn_{0.75}Mn_{0.25}Se$ barriers by MBE on a (100) GaAs substrate, taking care to prepare samples where the CdSe QD transition is energetically below the transition between internal Mn^{2+} states (see Fig. 1). The selection of individual quantum dots was achieved using Al masks with apertures down to 100 nm in diameter, which were prepared by electron beam lithography and lift-off technique. For performing photoluminescence (PL) experiments the samples were mounted in a He bath cryostat. The UV lines of an Argon-ion laser (λ=350...364 nm) were used for excitation and the PL signal was detected by a liquid nitrogen cooled CCD camera. Magneto PL studies were carried out with a split-coil solenoid in Faraday configuration at T=2 K.

As can be seen in Fig. 1, the inhomogeneously broadened PL spectrum of a QD ensemble splits into individual lines, if the spatial resolution is increased. Surprisingly, these lines have a rather large linewidth of about 8 meV, which can be attributed to temporal fluctuations of the magnetisation within the exciton localization volume. This is supported by the fact, that a pronounced linewidth narrowing by about a factor of 3 is obtained, if the Mn^{2+} spins are aligned in an external magnetic field of about 8 T, in quite good agreement with theoretical calculations. Increasing the temperature results in a pronounced blueshift of the QD energy up to 30 K, where the total shift amounts to about 8 meV. In contrast, non-magnetic CdSe SQDs display a behaviour which is well-known from bulk semiconductors und described by Varshni's law. The observed difference can be explained by the formation of EMPs in semi-magnetic SQDs: At low temperatures, the Mn^{2+} (here about a few 100) become aligned in the quantum mechanical exchange field B_{MP} of the charge carriers. For increasing temperature the magnetic ordering inside the EMP is reduced and thus, the emission line shifts to higher energy (see inset of Fig. 1) [2]. In order to align the Mn^{2+} spins in a well-defined manner an external magnetic field B_{ext} was applied. As can be seen in Fig. 2, this results in a pronounced red shift of the PL energy due to the giant Zeeman effect. Remarkably both the low temperature measurements (T = 2 K) in a magnetic field and the temperatures series at B = 0 can be described by a Brillouin-like behavior. Thus, the Mn^{2+} spins behave like a paramagnetic system with a temperature $T+T_0$ exposed to an effective magnetic field $B_{ext}+B_{MP}$, where T_0 takes into account the antiferromagnetic interaction between neighboring Mn^{2+}- spins [3]. From the experimental data an internal exchange field B_{MP} = 2.6 T can be extracted.

In consequence we have shown, that both the energy and the linewidth of the recombining electron-hole pair in a magnetic SQD directly monitors the magnetization on a nanometer scale!

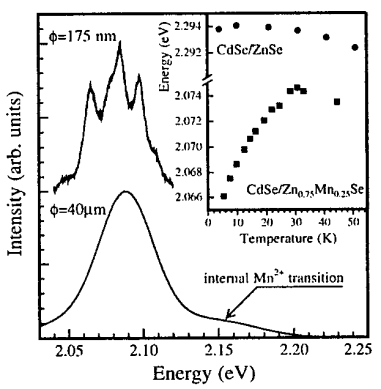

Fig. 1: PL spectra recorded with an aperture of 40 µm and 175 nm respectively. Inset: Temperature dependent emission energy of a single QD with and without magnetic matrix.

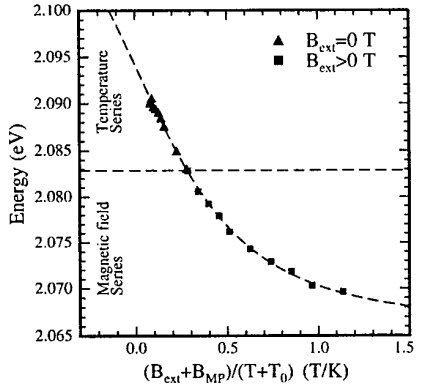

Fig. 2: Energy shift of a SQD emission line versus $(B_{ext}+B_{MP})/(T+T_0)$ for both a temperature and magnetic field series.

References

current address: Department of Electronic Materials Engineering, Kwangwoon University, Seoul, 139-701 Korea

[1] D. Loss, D.P. DiVincenzo, Phys. Rev. A **57**, 120 (1998)

[2] A.A. Maksimov, G. Bacher, A. MacDonald, V.D. Kulakovskii, A. Forchel, Ch. Becker, G. Landwehr, L.W. Molenkamp, Phys. Rev. B **62**, R7767 (2000)

[3] J.A. Gaj, R. Planel, G. Fishman, Solid State Com. **29**, 435 (1979)

Corresponding author: Herbert Schömig, Technische Physik, Universität Würzburg, am Hubland, D. –97074 Würzburg, Germany,
phone: +49-931-888-5104,fax: +49-931-888-5143,email:schoemig@physik.uni-wuerzburg.de

Photo-carrier induced magnetism in (In,Mn)As/GaSb magnetic alloy semiconductor heterostructures

H. Munekata[1)], A. Oiwa, and T. Slupinski
Kanagawa Academy of Science and Technology
KSP East 309, 3-2-1 Sakado, Takatsu-ku, Kawasaki 213-0012, Japan
[1)] *Imaging Science and Engineering Laboratory, Tokyo Institute of Technology*
4259 Nagatsuda, Midori-ku, Yokohama 226-8503, Japan

Ferromagnetism in III-V-based magnetic alloy semiconductors can be regarded a large-scale cooperative phenomenon, or phase transition, induced by the strong interaction between carrier spins and local magnetic moments. This may mean that the physical properties associated with this phenomenon can be controlled precisely as a function of carrier numbers and/or spin polarity. Up to now, inducement of ferromagnetic order has been found possible by both light illumination [1] and application of an electric field [2] in InMnAs-based heterostructures. A change in the magnetic coercive force by the light illumination has also been demonstrated recently with ferromagnetic *p*-type (In,Mn)As/GaSb heterostructures [3]. In order to understand these important effects quantitatively, we have studied both preparation and photo-carrier induced magnetism for (In,Mn)As/GaSb heterostructures in detail.

Various types of *p*-(In,Mn)As/GaSb heterostructures were prepared by molecular beam epitaxy on GaAs(100) substrates with Mn content x up to about $x = 0.2$ [4]. Sometimes, GaSb layers were doped with Te to control intentionally the built-in electric field across the (In,Mn)As/GaSb heterojunction. Substrate temperature T_s for the preparation of an (In,Mn)As layer was T_s = 190-240 °C. Curie temperature T_c of ferromagnetic *p*-(In,Mn)As depends on both growth condition and the amount of incorporated Mn. At the point of writing this abstract, T_c for $x = 0.12$ samples is 40 – 50 K with nominal hole concentration of $p = 2 - 6\times10^{19}$ cm^{-3}. There is a strong self-compensation effect for the incorporated acceptor Mn. Perpendicular magnetic anisotropy with a well-defined squared hysteresis loop has been observed for some of the samples. This is an indication for the confinement of tensile strain in the (In,Mn)As layer [5], and we call such samples as high quality samples. In any case, ferromagnetic order tends to become loose with decreasing the p value, say below 1×10^{19} cm^{-3}.

As shown schematically in Fig.1, when the heterostructure is irradiated with light, the light path through a very thin (In,Mn)As layer (E_g = 0.4 eV) and is absorbed predominantly in the relatively thick GaSb layer (E_g = 0.8 eV), yielding electrons and holes in the *non-magnetic* GaSb layer. Photo-generated holes are then transferred into the *magnetic* (In,Mn)As layer by the electric field across the interface, and stored there. In the (In,Mn)As layer, an increase in hole numbers enhances the strength of carrier-induced ferromagnetic interaction. Consequently, this results in an increase in magnetization, as well as the photoconductivity, even after the light is turned off. Persistent photoconductivity is noticeable up to around 175 K, whereas the enhanced magnetization eventually vanishes at around 40 K. The induced ferromagnetic interaction is not strong enough to overcome the thermal fluctuation.

Wavelength dependencies for both persistent photoconductivity and magnetization enhancement are shown respectively in Fig.2(a) and (b). The experiments have been carried out with the fixed excitation power of 0.1 mW/cm^2. While persistent photoconductivity is observable throughout the excitation wavelengths of 700 nm - 1.55 μm, the amount of change in magnetization decreases monotonically with increasing the wavelength and vanishes at the wavelength of 1.55 μm ($h\nu$ = 0.8 eV). The discrepancy in the wavelength dependence between the two behaviors suggests that holes generated in the GaSb layer are not transferred effectively in the (In,Mn)As layer, especially in case of the 1.55-μm excitation. One likely explanation is to assume another hole accumulation region in the GaSb side of the (In,Mn)As/GaSb interface. This hypothetical region, as shown also in Fig.1 by a black triangular area, could be anticipated by solving the self-consistent Poisson-Schrödinger equations. Systematically studying the experimental data, we estimate that about 30% of photo-generated holes can be transferred from GaSb to (In,Mn)As layers. More effective charge transfer is desired to realize the photo-enhanced magnetization at higher temperatures. A *p*-(In,Mn)As/n-GaSb:Te heterostructure will provide a stronger electric field across the junction and may be much suitable for the hole transfer process. We will discuss this point at the conference site.

Another important aspect of the carrier-induced magnetism is that the strength of the ferromagnetic exchange manifests itself in the magnetic characteristics. One such example is the reduction of coercive force by the light irradiation (Fig.3). The hysteresis loops shown in the figure clearly shows that the process of

magnetization reversal begins at a magnetic field lower than that in the dark. The numbers of holes that was accumulated in the (In,Mn)As layers during the light illumination were low 10^{18} cm^{-3}, being about 3% of the background hole concentration, whereas the coercive force is reduced for about 45%. The effect may lead us to realize the light-induced magnetization reversal.

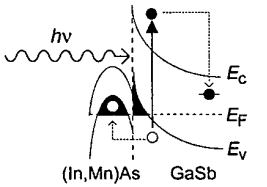

Fig. 1 : Schematic band diagram of *p*-(In,Mn)As/GaSb. E_F, E_C, and E_V represent Fermi level, conduction band edge, and valence band edge, respectively.

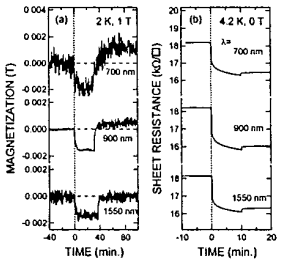

Fig. 2 : Changes in (a) magnetization at 2 K under the applied magnetic field of 1 T, and (b) sample resistance at 4 K during the light irradiation with various wavelengths.

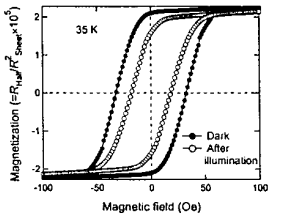

Fig. 3 : Magnetization hysteresis curves before (●) and after(○) light Illumination.

References

[1] H. Munekata, T. Abe, S. Koshihara, A. Oiwa, M. Hirasawa, S. Katsumoto, Y. Iye, C. Urano, and H. Takagi, *J. Appl. Phys.* **81**, 4862 (1997); S. Koshihara, A. Oiwa, M. Hirasawa, S. Katsumoto, Y. Iye, C. Urano, H. Takagi, and H. Munekata, *Phys. Rev. Lett.* **78**, 4617 (1997).
[2] H. Ohno, D. Chiba, F. Matsukura, T. Omiya, E. Abe, T. Dietl, Y. Ohno, and K. Ohtani, Nature **408**, 944 (2000).
[3] A. Oiwa, T. Slupinski, and H. Munekata, Appl. Phys. Lett. **78**, 518-520 (2001).
[4] T. Slupinski, A. Oiwa, and H. Munekata, 13th Intern'l Conf. on Crystal Growth (Jul. 30 – Aug. 4, 2001, Kyoto).
[5] H. Munekata, A. Zaslavsky, P. Fumagalli, and R.J. Gambino, *Appl. Phys. Lett.* **63**, 2929 (1993).

Corresponding author: H. Munekata, Kanagawa Academy of Science and Technology, KSP East 309, 3-2-1 Sakado, Takatsu-ku, Kawasaki 213-0012, Japan
Phone : +81-44-924-2044, Fax : +81-44-924-2039,
e-mail : hiro@isl.titech.ac.jp

Valence-band alignment at (Ga,Mn)As/GaAs heterointerface

Y. Ohno, I. Arata, F. Matsukura, and H. Ohno

Laboratory for Electronic Intelligent Systems, Research Institute of Electrical Communication, Tohoku University, 2-1-1 Katahira, Aoba-ku, Sendai 980-8577, Japan

Ferromagnetic semiconductor (Ga,Mn)As [1] is one of promising materials for making use of spin degree of freedom in future semiconductor "spintronics" devices. The origin of ferromagnetism for (Ga,Mn)As is considered to be hole-mediated exchange interaction between localized magnetic moments [2]. Thus p-type ferromagnetic (Ga,Mn)As can be utilized as hole spin polarizer or spin-polarized hole reservoir, when it is hybridized to conventional nonmagnetic semiconductor heterostructures.

Recently, spin injection into nonmagnetic semiconductor has been demonstrated by probing polarization of light emitted from (Ga,Mn)As/(In,Ga)As/n-GaAs *p-i-n* junction light emitting diodes [3]. In such systems, the band alignment at a (Ga,Mn)As/GaAs interface may play a crucial role in determining the degree of spin polarization of holes injected from (Ga,Mn)As into GaAs. However, the actual band structure in (Ga,Mn)As/GaAs heterostructures is not well understood.

In the present work, we investigated the valence band structure in (Ga,Mn)As/GaAs heterostructures by measuring current-voltage (*I-V*) characteristics of (Ga,Mn)As / GaAs / p-GaAs *p-i-p* diodes (see Fig. 1). We prepared several samples consisting of 200 nm-thick (Ga,Mn)As with different Mn concentration (1.4% ~ 5.1%) and 400 nm undoped GaAs grown on p-GaAs substrates. The *I-V* characteristics of such *p-i-p* structures exhibit somewhat rectifying feature (see Fig. 2). Under positive bias condition, where hole current flows from the top (Ga,Mn)As to p-GaAs substrate via a GaAs spacer, the current does not depend on the bias voltage so much, but strongly on the temperature. This suggests the existence of a potential barrier.

To evaluate the valence band offset at (Ga,Mn)As/GaAs interface, we employed a simple thermoionic emission model, which accounts for the *I-V* characteristics quite well. From the fitting parameters, we found an effective barrier height Δ to be 80~140 meV for samples with various Mn concentrations (see Fig. 3), and no clear Mn concentration dependence is observed. The existence of the potential barrier at the (Ga,Mn)As/GaAs interface may lead to unique temperature dependence of electroluminescence intensity as well as the current-voltage characteristics observed in (Ga,Mn)As/i-(In,Ga)As/n-GaAs *p-i-n* diode [4].

References

[1] H. Ohno, A. Shen, F. Matsukura, A. Oiwa, A. Endo, and Y. Iye, Appl. Phys. Lett. **69**, 363 (1996).
[2] T. Dietl, H. Ohno, F. Matsukura, J. Cibert, and D. Ferrand, Science **287**, 1019 (2000).
[3] Y. Ohno, D.K. Young, B. Beschoten, F. Matsukura, H. Ohno, and D.D. Awschalom, Nature **402**, 790 (1999).
[4] I. Arata, Y. Ohno, F. Matsukura, and H. Ohno, to be published in Physica E

Corresponding author: Yuzo OHNO
Laboratory for Electronic Intelligent Systems, Research Institute of Electrical Communication, Tohoku University, 2-1-1 Katahira, Aoba-ku, Sendai 980-8577, Japan
phone: +81-22-217-5555, Fax: +81-217-5555, e-mail: oono@riec.tohoku.ac.jp

Fig. 1: Cross sectional view of (Ga,Mn)As/i-GaAs/p-GaAs p-i-p diode structure.

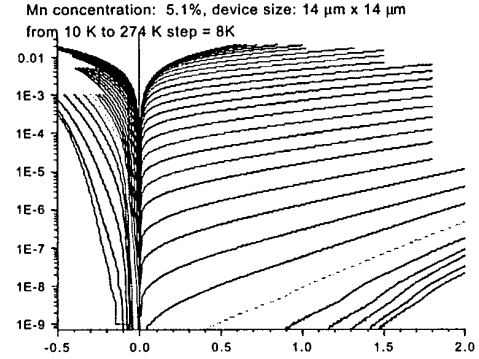

Fig. 2: Typical temperature dependence of the current-voltage characteristics of (Ga,Mn)As/i-GaAs/p-GaAs p-i-p diode. Mn concentration in (Ga,Mn)As is 5.1%. Hole current flows from top (Ga,Mn)As into bottom p-GaAs under a positive bias.

Fig. 3: Evaluated barrier height Δ at (Ga,Mn)As/GaAs interface (measured from the Fermi energy of (Ga,Mn)As) based on a thermoionic emission model.

Non-linear spin transport in magnetic semiconductor multiple quantum wells

David Sánchez[1], A. H. MacDonald[2,3], Gloria Platero[1],

[1] Instituto de Ciencia de Materiales de Madrid (CSIC), Cantoblanco, 28049 Madrid, Spain

[2] Department of Physics, Indiana University, Bloomington, Indiana 47405

[3] Department of Physics, University of Texas at Austin, Austin, Texas 78712

Novel physical properties and technological devices have emerged from the interplay between quantum localization and the explotation of spin transport [1]. Of special interest are II-VI magnetic semiconductor (MS) heterostructures due to the Zeeman tunability of confinement in magnetic barriers and magnetically coupled double quantum wells (QWs), the study of spin-dependent dynamics of polarized excitons in spin superlattices (SLs), the observation of optically-probed spin coherence, and the injection of highly polarized spin current in GaAs/AlGaAs light emitting diodes.

The recent fabrication of n-doped II-VI MS QWs and SLs has given rise to 2D electron gases ferromagnetically coupled with Mn^{+2} magnetic ions "digitally" incorporated into the sample [2]. The exchange interaction occurring between s-electrons in the conduction band and d-local moments results in large spin splittings. Actually, fully polarized exciton populations have been encountered at relatively low magnetic fields ($\sim$ 1 T).

In III-V non-magnetic weakly-coupled dc-biased SLs, the formation of electric field domains has been proven both theoretically and experimentally [3]. This results in the observation of a sawtooth-like I–V characteristics in the negative differential conductance region. Along each branch two approximately constant electric field regions develop, separated by a layer of accumulating electrons, allowing 2D-2D resonant tunneling between populated subbands. More degrees of freedom supplemented to the MQW system by means of either a magnetic field applied perperdicular to the interfaces or far-infrared irradiation whose phase is chosen different in consecutive barriers, have been proven to provide extra branches and enrich the physics involved. Hence the inclusion of the electronic spin in the study of perpendicular transport in MQWs is expected to play a crucial role in the physics of electric field domain formation.

Here we present a theoretical model for addressing quantum transport in biased ZnSe/(Zn,Cd,Mn)Se multiple quantum wells [4]. Non-, partly- and fully-polarized situations are taking into account within a self-consistent scheme. The main ingredients of our model are, namely: (i) a theory for the current between two spin-polarized 2DEGs; (ii) a continuity equation including not only transmission coefficients but also taking into account the spin relaxation in the case of non-equilibrium spin populations; (iii) a relationship between the up and down chemical potentials and their densities; and (iv) an application of a simple mean field theory to describe the Coulomb interaction. We see how the new features appearing in the I–V curve depend on the degree of spin splitting and how the spin bottleneck effect turns out to have a strong influence in the instability regions.

Furthermore, an interesting feature can be obtained by sweeping voltages up and down from distinct initial electric field profiles. In GaAs/AlGaAs superlattices it has been proven that multistable stationary states show up in this way. Our numerical results have been obtained in a 9-well ZnSe/ZnCdSe SL in which the central well has been doped with magnetic impurities. Fig. 1 shows the change in the magnetic well spin polarization as a function of voltage. Notice that the behaviour somewhat mimics that of a sawtooth-like I–V curve. Even *reversed* polarization can be observed for the (second subband)$\longrightarrow$(first subband) transition provided the spin-flip relaxation time is sufficiently large (a direct consequence of the spin bottleneck effect). Inset of Fig. 1 shows three different values of the spin polarization, P, which can be obtained from different initial biases. Sweeping up biases from very low voltages mean reaching the first value of P. If the sweeping direction is now reversed at around $V = 0.1$ V, the second value of P is achieved. Eventually the third value of P is obtained by sweeping down voltages from a initial high-field profile. Hence a *triple* stability between distinct permanent physical values of P is observed. We emphasize that this kind of hysteretic phenomena between magnetic states are driven by *electric* fields.

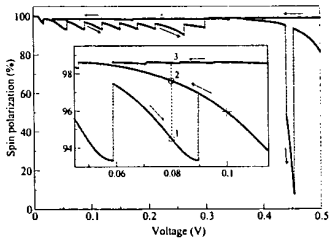

Figure 1: Multistability between distinct polarization states within a magnetic superlattice. Inset shows a blow-up with three different states reached at V = 0.08 meV.

References

[1] H. Ohno, Science **281**, 951 (1998).

[2] D.D. Awschalom and N. Samarth, J. Magn. Magn. Mat. **200**, 130 (1999).

[3] R. Aguado, G. Platero, M. Moscoso, and L.L. Bonilla, Phys. Rev. B **55**, R16053 (1997).

[4] D. Sánchez, A.H. MacDonald, and G. Platero (preprint).

Corresponding author: David Sánchez, Instituto de Ciencia de Materiales de Madrid (CSIC), Cantoblanco, 28049 Madrid, Spain.
Phone: +34 913349000 no. 168, fax: +34 913720623,
email: dsanchez@icmm.csic.es

A quantum dot single-photon source

C. Becher[1,3], A. Kiraz[1], P. Michler[1,4], W.V. Schoenfeld[2], P.M. Petroff[1,2], Lidong Zhang[1], E. Hu[1,2], and A. Imamoğlu[1]

[1] Department of Electrical and Computer Engineering, University of California, Santa Barbara, CA 93106, USA
[2] Materials Department, University of California, Santa Barbara, CA 93106, USA
[3] Institut für Experimentalphysik, Universität Innsbruck, A-6020 Innsbruck, Austria
[4] Institut für Festkörperphysik, Universität Bremen, D-28334 Bremen, Germany

Many applications in the emerging field of quantum information science [1] require deterministic single photon sources, also termed single photon turnstile device [2], emitting single photons on demand. We demonstrate a single photon source with nearly 100% efficiency based on pulsed laser excitation of a single self-assembled InAs quantum dot (QD) embedded in a high quality (Q) factor microcavity structure [3,4]. Regulation of the photon emission process of the QD exciton ground state (1X) transition is accomplished by a combination of two effects: Coulomb interactions creating an anharmonic multiexciton spectrum and a slow relaxation of highly excited QDs leading to vanishing re-excitation probability following the photon emission event at the 1X transition [5].

The microcavity samples were grown by molecular beam epitaxy and consisted of a 5 μm diameter GaAs disk, containing self-assembled InAs QDs (density $\leq 10^8\ cm^{-2}$), and a pedestal area (microdisk structure) [4]. The microdisks are mounted in a He gas flow cryostat. The experimental setup combines a diffraction-limited scanning optical microscope for spatially resolved photoluminescence spectroscopy and a Hanbury Brown and Twiss setup for photon correlation measurements. Optical pumping is performed with a mode-locked femtosecond ($\sim$ 250 fs) Ti:sapphire laser, operating at 750 nm and generating electron-hole pairs in the GaAs layers.

Figure 1 shows the measured unnormalized correlation function $G^{(2)}(\tau)$ for (A) the pulsed Ti:sapphire laser, and (B) the 1X transition of a QD that is far detuned from all modes of the microdisk resonator (T = 4 K). $G^{(2)}(\tau)$ of the pulsed Ti:sapphire laser exhibits peaks at integer multiples of the pulse repetition rate T_{rep}. The photon correlation of the QD 1X emission also shows peaks at multiples of T_{rep} , but the peak at $\tau = 0$ is no longer present, i.e., the probability of finding a second photon following the detection of the first photon at $\tau = 0$ vanishes. Absence of the peak at $\tau = 0$ provides strong evidence for an ideal single photon turnstile operation. As the QD 1X transition is driven in saturation and the recombination is predominantly radiative [6], every excitation pulse generates a single photon pulse. Carriers in the GaAs barrier and the wetting layer recombine much faster than the QD exciton (100-200 ps vs. 2.2 ns [6]) such that the probability of re-excitation of the QD and emission of a second photon is very small ($< 5 \cdot 10^{-3}$).

In addition, we achieve turnstile operation of a coupled QD-cavity system by temperature tuning the 1X transition of another QD into resonance with a cavity mode (Q $\sim$ 6500) [5,7]. Figure 2 shows the measured $G^{(2)}(\tau)$ for the 1X transition (A) out of resonance (T = 4 K), and (B) on resonance with the microdisk mode (T = 36 K). On resonance the FWHM of the photon correlation peaks is narrower due to the Purcell effect which causes

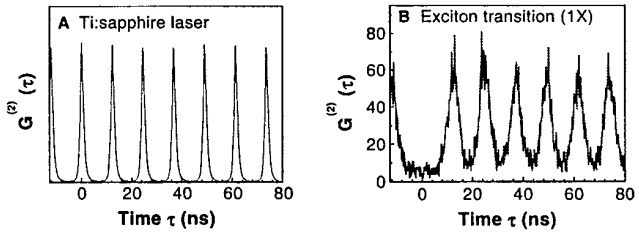

Figure 1: Measured unnormalized correlation function $G^{(2)}(\tau)$ of (A) a mode-locked Ti:sapphire laser (FWHM = 250 fs), and (B) a single QD excitonic ground state (1X) emission under pulsed excitation conditions (82 MHz).

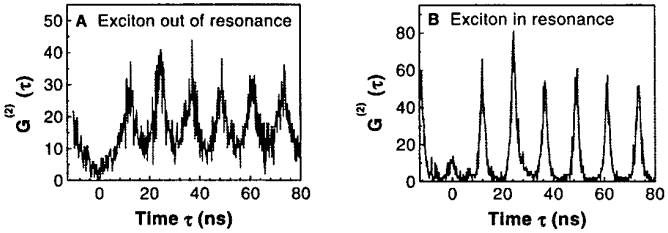

Figure 2: Measured unnormalized correlation function $G^{(2)}(\tau)$ of a single QD excitonic ground state emission (A) out of resonance, and (B) at resonance with a cavity mode ($Q \sim 6500$), under pulsed excitation conditions (82 MHz).

a reduction of the 1X transition lifetime and ensures that photons are primarily emitted into the cavity mode. We assume that the small peak at $\tau = 0$ observed in the resonance case is due to background emission into the mode.

References

[1] D. Bouwmeester, A. Ekert, and A. Zeilinger, *The physics of quantum information* (Springer, Berlin, 2000).
[2] A. Imamoğlu and Y. Yamamoto, Phys. Rev. Lett. **72**, 210 (1994).
[3] J.-M. Gérard and B. Gayral, IEEE J. Lightwave Technol. **17**, 2089 (1999).
[4] P. Michler et al., Appl. Phys. Lett. **77**, 184 (2000).
[5] P. Michler et al., Science **290**, 2282 (2000).
[6] C. Becher et al., Phys. Rev. B **63**, 121312(R) (2001).
[7] A. Kiraz et al., *submitted to Appl. Phys. Lett.*

Corresponding author: Christoph Becher, Institut für Experimentalphysik, Universität Innsbruck, Technikerstrasse 25, A-6020 Innsbruck, Austria.
phone: ++43 512 507 6332 , Fax: ++43 512 507 2952,
email: christoph.becher@uibk.ac.at

Single-mode single photon source based on isolated InAs quantum boxes in micropillars

E. Moreau, J.M. Gérard, I. Robert, I. Abram, L. Manin and V. Thierry-Mieg
CNRS/Laboratoire Photonique et Nanostructures, 196 av. Henri Ravera, 92220 Bagneux
Tel : 33 1 42317156 Fax : 33 1 42534930 jeanmichel.gerard@rd.francetelecom.fr

The development of efficient solid-state single-photon sources is an important prerequisit for a large scale implementation of secure telecommunication systems based on quantum crytography. Various solid-state emitters including molecules, F-centers, semiconductor nanocrystals and self-assembled quantum boxes (QBs) have recently demonstrated an ability to emit antibunched light. Though working at low temperature, QBs present some important assets in this context : QBs exhibit 1) a good stability (no photobleaching, no blinking), 2) a quantum efficiency very close to one, 3) a short radiative lifetime (1 ns), 4) a quasi-monochromatic emission (< 25 μeV at 4K), which allows to exploit CQED effects to tailor their emission properties, and 5) can be easily inserted inside semiconductor microcavities. We present the first **single-mode** solid-state single photon source, which is based on an isolated InAs QB in a pillar microcavity, as proposed few years ago [1].

GaAs/AlAs pillar microcavities containing a dilute array of InAs/GaAs QDs (~50 μm^{-2}) have been processed by e-beam lithography and reactive ion etching and studied by microphotoluminescence (μPL). For strong excitation conditions, each QB emits a broad emission line ; μPL spectra then reflect the density of modes of the micropillar. Cavity Q's of the order of 400-1000 are observed for 1μm diameter pillars, which corresponds to a Purcell factor of 6-15. For weak excitation powers on the opposite, the spectra consist of few (1-5) sharp emission lines within the fundamental mode energy range, which highlights the successful coupling of one or few QBs to this cavity mode.

In order to prepare single photons, these sources are pumped using a pulsed optical excitation by a Ti :sapphire laser (80 MHz repetition rate) and we select spectrally using a monochromator only one of the emission lines observed under weak excitation. This line corresponds to the emission of a given QB when it contains only one exciton (X line), as shown by the linear power dependence of its intensity. Due to the strong Coulomb interaction between trapped carriers, emission lines corresponding to a different filling of the QB occur at energies which are well separated spectrally, and not collected. Under such conditions, the deterministic emission of a single photon is expected as soon as more than one electron-hole pair is injected in the QB. Photon correlation experiments at 8K show that the probability for emitting two photons or more (non zero due to background residual light) is a factor of 6 smaller than for a coherent source. This demonstrates the generation of highly non-classical light, already close to the ideal single-photon emission regime, from isolated QBs in micropillars.

Time-resolved experiments confirm that such single QBs on resonance with one cavity mode also experience a strong Purcell effect (up to a fivefold enhancement of their spontaneous emission (SE) rate has been observed). Since the SE emission is selectively enhanced for the resonant cavity mode alone (not for leaky modes), the Purcell effect can be used to collect and prepare the single photons into a given quantum state (same spatial mode, same polarisation), which is essential in view of an application to quantum cryptography. We present polarisation-resolved μPL data obtained on elliptical micropillars with a non-degenerate fundamental mode. In this case, emitted single photons are linearly polarized along the long axis of the pillar cross section, with a linear polarisation rate as high as 95%.

We finally discuss the possible future performance of QB-based single photon sources, including their maximum bit rate and operating temperature.

[1] J.M. Gérard et al, J. Lightwave Technology, 17, 2089 (1999); Phys.Rev.Lett 81, 1110 (1998)

Coherent dynamics of microcavity polaritons in the nonlinear regime

A. Huynh[1], J. Tignon[1], Ph. Roussignol[1], C. Delalande[1],

R. André[2], R. Romestain[2], D. Le Si Dang[2]

[1]Laboratoire de Physique de la Matière Condensée, Ecole Normale Supérieure, 24, rue Lhomond, F-75005 Paris, France
[2]Laboratoire de Spectrométrie Physique, Université Joseph Fourier-Grenoble I, BP 87, F-38402 Saint Martin d'Hères, France

Semiconductor microcavities present a unique way to control light-matter coupling in solids. The strong exciton-photon coupling resulting in the polaritons eigenstates can be tailored by structure design and control of the optical excitation. Due to their excitonic part, polaritons are composite bosons. Coulomb interactions as well as phase space filling (Pauli blocking) can be responsible for polariton-polariton interactions. Interestingly, polaritons have a density of states strongly reduced as compared to bare excitons and could in principle exhibit collective bosonic behavior at excitation densities well below the excitonic saturation. Several authors have recently reported nonlinear emission from microcavities in the strong coupling regime, scattering stimulated by final state occupation [1]. The possibility of achieving a Bose-Einstein-like condensation [2] is the subject of a controversial debate. In this context, it is of primary importance to understand what is the nature of the nonlinear interaction involved in the polariton-polariton scattering process. Here, we present an experimental and theoretical study of four wave mixing in II-VI microcavities. We show how a fine analysis of the FWM signal allows to measure the relative weight of the Coulomb and Pauli blocking mediated interactions.

The experiment was carried out on a 2λ-$Cd_{0.40}Mg_{0.60}Te$ microcavity containing 6 CdTe quantum wells. The cavity is embedded between 17.5 (23) pairs of distributed Bragg reflectors $CdMg_{0.80}Te/CdMn_{0.25}Te$ on top (bottom). A slight wedge in the cavity allows to adjust the exciton-photon relative weight. Measurements where performed at 6 K and laser excitation was provided by 100-fs Ti:Sa laser pulses. Reflectivity measurements (Fig. 1(b)) reveal a 13.8 meV normal mode splitting at zero detuning and small polariton linewidths (below 1 meV) showing the high quality of the sample. We performed self-diffracted four-wave mixing (FWM) : two co-linearly polarized laser pulses, separated by a time delay $\Delta\tau$, are incident on the sample with wave vectors $\mathbf{k}_1$ and $\mathbf{k}_2$. The nonlinearities in the sample generate, in the $2\mathbf{k}_2$-$\mathbf{k}_1$ background-free direction, a signal which is detected in the reflection geometry. Figure 1(a) shows the time-integrated FWM intensity as a function of the time delay for increasing excitation intensities below the excitonic saturation threshold. Here, both polariton modes where coherently excited (see laser profile in Fig. 1(b)). The signal envelop grows exponentially at negative time delays and decays twice slower for positive delays. Oscillations result from quantum beatings between the strongly coupled modes. A careful examination shows that the oscillations contrast is reduced when increasing the excitation intensity, but also that this contrast reduction is even more pronounced for negative time delays than for positive time delays. At high intensity, the oscillations tend to vanish completely at negative time delays.

In order to analyze these results, we applied the *averaged polarization model* [3]. In this approximation, the coupled Bloch-Maxwell equations are solved. The effect of the microcavity is described by a damped oscillator at the cavity frequency, driven by the external electric field and coupled to the interband polarization. We compute the third order polarization in the FWM direction. Fig. 1(c) shows the FWM signal computed when the Coulomb interaction is canceled (bottom curve) and when the Pauli blocking is assumed to be negligible (top curve). Only the Coulomb mediated nonlinearities allow to observe strong oscillations, especially for negative time delays.

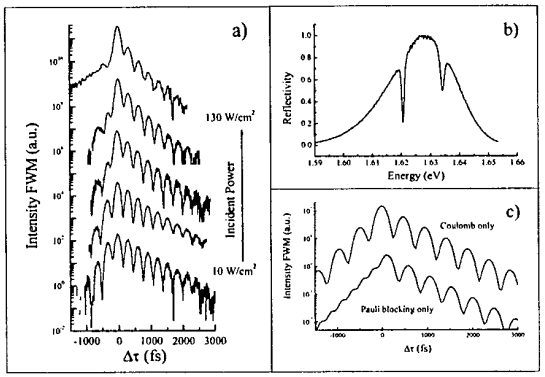

Fig. 1: (a) Time integrated four wave mixing v.s. delay for increasing incident power. (b) Reflectivity. (c) Numerical calculation of the TI-FWM.

A detailed analysis of the interference effects between polarization and electric field explains this different behavior. Comparison with the experiment allows us to evaluate quantitatively the relative contribution of the two nonlinearities as a function of the carrier density and detuning. Our results show that in this system, the phase space filling dominates more than one order of magnitude below the saturation density, for densities where this contribution is often neglected.

References

[1] Le Si Dang et al, Phys.Rev. Lett. 81, 3920 (1998) ; P. Senellart et al, Phys. Rev. Lett. 82, 1233 (1999) ; P.G. Savvidis et al, Phys. Rev. Lett. 84, 1547 (2000) ; C. Ciuti et al, Phys. Rev. B 62, R4825 (2000).
[2] R.M. Stevenson et al. Phys. Rev. Lett. 85, 3680 (2000).
[3] U. Neukirch et al, Phys. Rev. Lett. 84, 2215 (2000).

Corresponding author: Jerome Tignon, Laboratoire de Physique de la Matière Condensée, Ecole Normale Supérieure, 24, rue Lhomond, F-75005 Paris, France.
phone: + (33) 1 44 32 33 54, Fax: + (33) 1 44 32 38 40
email: Jerome.Tignon@lpmc.ens.fr

CQED experiments with InAs quantum dots

B. Gayral

Department of Electrical and Computer Engineering, University of California, Santa Barbara, California 93106

The quest to apply quantum optics and cavity quantum electrodynamics (CQED) concepts to semiconductor optoelectronics devices has been a major field of research in the last 10 years. In particular, control of the spontaneous emission dynamics, be it enhancement or inhibition, was seen as a key step to achieve. In this context, major issues were to find out if spontaneous emission control is possible in such semiconductor systems, if so under what experimental conditions this could be achieved, and finally if something "useful" (whatever that means) could stem out of such effects.

Self assembled Quantum Dots (QDs) proved to be excellent candidates to study spontaneous emission rate enhancement due to coupling to an optical cavity mode(also called Purcell effect). First of all, due to a large inhomogeneous broadening, the photoluminescence (PL) of an array of QDs can act as a broadband internal light-source to probe the modes of three-dimensional cavities. Thanks to a low absorption, the QD array does not degrade the optical properties of the cavities. This allowed to use InAs/GaAs QDs to probe the modal structures of micropillars, microdisks and photonic crystal microcavities.

The main property that makes QDs very desirable for CQED experiments is their discrete electronic structure, giving rise to very sharp emission lines for single QDs ($< 30\,\mu$eV for InAs/GaAs QDs at 8 K). This allows to take full advantage of the Purcell effect in high-Q cavities. Thus a QD (emitting at wavelength λ) coupled to a cavity mode with quality factor Q and volume V will undergo an enhancement of its spontaneous emission rate by the Purcell factor $F_p = \frac{3}{4\pi^2}\frac{Q(\frac{\lambda}{n})^3}{V}$, n being the refractive index of the cavity. This effect has been first clearly demonstrated for InAs/GaAs QDs coupled to a $F_p = 32$ mode of a GaAs/AlAs micropillar, with a global enhancement by a factor of 5 [1]. The global enhancement is smaller than the Purcell factor due to the fact that all QDs do not ideally overlap (both spectrally and spatially) with the considered mode, leading to an averaging of the Purcell effect.

More recently, the coupling of QDs to whispering gallery modes of GaAs microdisks was studied. Indeed, we showed [2,3] that a thorough processing of these structures could lead to very high Q values (12000) combined with low volumes ($\sim 5(\frac{\lambda}{n})^3$), allowing to achieve Purcell factors as high as 190. We could study by time-resolved photoluminescence the spontaneous emission dynamics of a collection of QDs coupled to such a high F_p mode (Fig. 1). We must note that as some QDs have a radiative lifetime that can be as short as 8 ps in these structures, a finite capture/relaxation time of the carriers of 20 ps has to be considered in order to account for the time-resolved experimental data [4].

We will also discuss recent experiments showing the Purcell effect for a single QD in a microdisk [5]. It is indeed possible to tune a QD in and out of resonance with a WGM by changing the sample temperature. The key results in these experiments are first that within a limited temperature range (4-60 K), the QD dynamics does not vary, which allows to safely use the temperature tuning technique over this range, and second that indeed the crossing with a WGM resonance induces a radiative lifetime shortening for the single QD.

Finally, we will discuss some possible prospects for QDs coupled to cavity modes, for instance for efficient single photon generation [2].

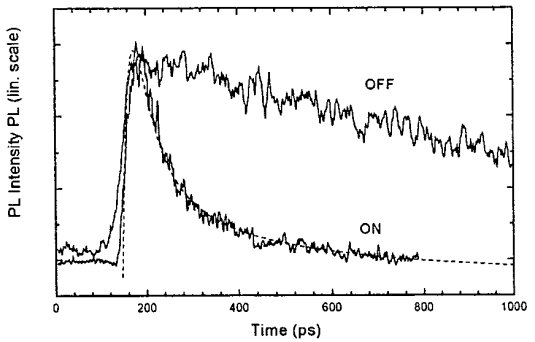

Figure 1: Time resolved PL for QDs inside a 2 μm microdisk with $Q = 10000$. For off-resonance QDs, the lifetime is 1.2 ns, whereas the decay is much shorter for on-resonance QDs. A model (dash line) taking into account a finite relaxation time (20 ps) of the carriers accounts well for the Purcell effect in this structure.

References

[1] J.-M. Gérard et al., Phys. Rev. Lett. **81**, 1110 (1998).
[2] J.-M. Gérard and B. Gayral, J. Lightwave Technol. **17**, 2089 (1999).
[3] B. Gayral et al., Appl. Phys. Lett. **75**, 1908 (1999).
[4] B. Gayral et al., Appl. Phys. Lett. *in press* (2001).
[5] A Kiraz et al., *submitted.*

Corresponding author: Bruno Gayral, ECE Department, University of California Santa Barbara, CA, 93106-9560 USA
phone: +1 (805) 893 8664, Fax: +1 (805) 893 3262,
email: bruno@ece.ucsb.edu

Carrier Dynamics and Device Characteristics of Quantum Dot Lasers and Microcavity Light Emitters

D.G. Deppe,[1] C. Cao,[1] O.B. Shchekin, [1] Z. Zou, [1] H. Chen, [1]
T.F. Boggess,[2] L. Zhang, [2] and K. Gundogdu[2]

[1]Microelectronics Research Center
Department of Electrical and Computer Engineering
The University of Texas at Austin, Austin, Texas 78712

[2]Optical Science and Technology Center
Department of Physics and Astronomy,
The University of Iowa, Iowa City, Iowa 52242

The carrier dynamics in self-organized III-V quantum dots (QDs) has emerged as an important area of research for their application to semiconductor lasers and other light emitters. Because the 3-dimensional confinement leads to discrete energy levels, the QD dynamic response is strongly influenced by its 0-dimensional energy levels. When these levels have energy spacings that correspond to an optical phonon energy the carrier relaxation is expected to be fast. However, when the energy level separation is significantly greater than the optical phonon energy, the relaxation is expected to be much slower. The electronic structure is furthermore unique in that the 0-dimensional energy levels are connected to a 2-dimensional density of levels associated with the QDs' wetting layer. Entropy effects can be important when electrons and holes relax from the wetting layer into the QDs' 0-dimensional levels, because of the large disparity in the effective density of states. The result of both entropy effects and slowed relaxation between the 0-dimensional energy levels is that the QDs' dynamic response can show strikingly different temperature dependencies [1], [2], becoming either faster or slower with increasing temperature, depending on which effect may dominate. These carrier dynamics set the device characteristics of QD lasers and microcavity light emitters. Because the QDs "sit on top of" the wetting layer, their 0-dimensional energy levels are coupled to the 2-dimensional density of states of the wetting layer. Excitons are believed to relax to their ground state energy in a cascade process mainly through emission of phonons. We have measured the rise time dependence on excitation level for both the ground and first excited radiative transitions, and compared these rise times with the relative intensity changes from the different levels for small InAs QDs and the large InGaAs QDs. Significant differences in their relaxation characteristics are found, with the larger QDs showing much faster relaxation. In addition, we have measured the relaxation times both to the ground and first excited states to uncover details of the cascade relaxation of the excitons and charge carriers.

Experimental data characterizing the cascade emission are shown in Fig. 1 [3]. Figure 1 (a) shows that the crossing between the intensity of the ground state and that of the first excited state for excitons with increasing excitation level. Figure 1 (b) shows the rise time (in picoseconds) for either the ground or excited state excitons. While the rise time of the ground state is approximately independent of the excitation level, the rise time of the first excited state is faster than that of the ground state for low excitation levels, but slower than the ground state for high excitation levels. Modeling the exciton relaxation with rate equations, we find that the cross-over behavior occurs because at low excitation level there still exists a small probability for obtaining light emission from the excited state even for a single exciton in the QD. As the exciton number increases to three, and saturates the doubly degenerate ground state, the rise time of the excited state becomes dominated by the highest energy exciton. Because the ground state must saturate first, there exists a delay prior to the occupation of the excited state. Although there still exists a probability for excitonic emission from the excited state prior to relaxation and filling of the ground state, the intensity from these excitons is now negligible for the higher excitation levels.

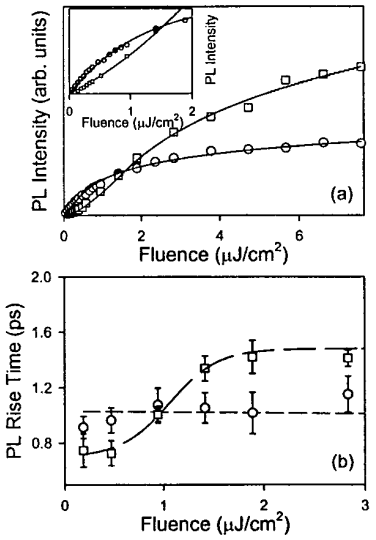

Fig. 1 Time-resolved photoluminescence intensity vs excitation fluence (a) for the 1st excited state (square) and the ground state (dot) 10ps after zero at 12K with the inset showing the same thing in low excitation regime. The solid lines in (a) are guided for view. In the inset, the solid line for the 1st excited state is quadratic fit, which indicates the 1st excited state emission arising mainly from the multiply excited dots. Fig. 1 (b) shows the photoluminescence rise time vs excitation fluence for the 1st excited state (square) and the ground state (dot) at 12K.

Understanding these excitonic and carrier-carrier dynamics is important for applying these QDs to both lasers and spontaneous light emitters. Thermal effects result in increased carrier diffusion and decreased radiative lifetimes. The low temperature measurements are useful in developing realistic relaxation models for excitons in QDs that can then be applied to room temperature operation as well. In this talk we will discuss the applications of these QDs to laser and microcavity light emitters.

This work has been supported by the National Science Foundation and the DARPA University of New Mexico OptoCenter.

References

[1] L. Zhang, T. Boggess, D.G. Deppe, D.L. Huffaker, O.B. Shchekin, and C. Cao, "Dynamic Response of 1.3 μm Wavelength InGaAs/GaAs Quantum Dots," Appl. Phys. Lett. 76, 1222-1224 (6 March, 2000).

[2] T.F. Boggess, L. Zhang, D.G. Deppe, D.L. Huffaker, and C. Cao, "Spectral Engineering of Carrier Dynamics in In(Ga)As Self-Assembled Quantum Dots," Appl. Phys. Lett. 78, 276-278 (15 January, 2001).

[3] L. Zhang, T.F. Boggess, K. Gundogdu, M.E. Flatte, D.G. Deppe, C. Cao, and O. Shchekin, "Excited state dynamics in 1.3 μm wavelength InGaAs/GaAs quantum dots," unpublished.

Mid-infrared surface-emitting PbSe/PbEuTe quantum dot lasers

G. Springholz,[1] T. Schwarzl,[1] W. Heiss,[1] M. Aigle,[2] H. Pascher,[2] T. Fromherz,[1] G. Bauer,[1]

[1]Institut für Halbleiter- und Festkörperphysik, Johannes Kepler Universität Linz, Altenbergerstraße 69, A-4040 Linz, Austria
[2] Experimentalphysik I, Universität Bayreuth, D-95447 Bayreuth, Germany

Semiconductor quantum dots have attracted tremendous interest due to their great potential for opto-electronic device applications. In particular, quantum dot lasers have been predicted to yield strongly increased material gain and differential gain, lower threshold currents, higher modulation band widths and better temperature stability as compared to quantum well lasers [1,2]. Up to now, quantum dot lasers have been made exclusively from III-V semiconductors with emission wavelengths in the visible or near infrared spectral region. Here, we report the first realization of mid-infrared quantum dot lasers based on self-organized PbSe quantum dots [3] grown by molecular beam epitaxy. The dot laser structure is based on our recently developed high finesse vertical microcavity structures (VCSEL) [4].

As shown in Fig. 1, the samples consist of two dielectric Bragg mirrors with a PbSe/$Pb_{1-x}Eu_xTe$ (x=5%) quantum dot superlattice inserted in between. The Bragg mirrors contain three EuTe/$Pb_{0.94}Eu_{0.06}Te$ $\lambda/4$ layer pairs, which yields mirror reflectivities exceeding 99 % due to the very high refractive index contrast [4]. For the active region, first a 3 μm thick $Pb_{1-x}Eu_xTe$ buffer layer was deposited on the top of the bottom mirror. Then, a 140 period dot superlattice of 5 monolayers PbSe alternating with 480 Å $Pb_{1-x}Eu_xTe$ was grown, followed by the deposition of the top mirror. Figure 1b) shows a cross sectional SEM micrograph of the complete VCSEL structure, and the PbSe dot arrangement in the superlattice is illustrated in Fig. 1c) by the TEM images of a reference sample grown under identical conditions.

Because of the large total cavity length a large number of cavity resonance modes are observed within the stop band region. The central $m = 28^{th}$ cavity mode is located at 290 meV (λ = 4.27 μm), corresponding to the low temperature onset of quantum dot absorption measured on PbSe/$Pb_{1-x}Eu_xTe$ reference samples. The stimulated emission spectra of the VCSEL structure induced by optical pumping with a pulsed Nd:YAG laser is shown in Fig. 2. At 1.5 K, simultaneous emission at the $m = 28$ and 29th order cavity modes at λ = 4.24 and 4.09 μm occurs, with a line width of only 700 μeV. This two-mode laser operation is a result of the inhomogeneous broadening of the quantum dot gain spectrum due to dot size fluctuations. The angular dependence of the emission shows a very rapid drop even for slight deviations of the emission angle off the surface normal direction. Measurements of the integrated output intensity as a function of pump power indicates an external threshold of P_{th} = 510 kW/cm^2, which is comparable to PbTe quantum well VCSELs [4]. As shown in Fig. 2, with increasing temperature, the intensity of the 29th mode increases whereas that of the central 28th mode decreases and eventually disappears at a temperature of 40 K. As the temperature is further increased, the 29th emission in turn decreases and at 60 K the next higher laser mode turns on. At 70 K, the 29th mode completely disappears, whereas the 30th mode emission persists up to 90 K. This successive switching of the laser emission is explained by the increase of the PbSe band gap with increasing temperature. The envelope of the emission lines is given by the inhomogenously broadened dot gain spectrum with a width of about 18 meV. Similar as in PbTe quantum well VCSELs, the upper limit of operation temperature is caused by the detuning between the gain spectrum and the central cavity modes at higher temperatures. This indicates that much higher operation temperatures can be achieved for the dot lasers by appropriate tuning of the optical cavity modes to the dot emission at higher temperatures.

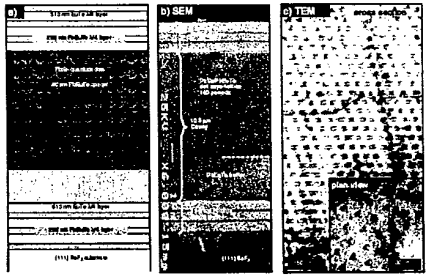

FIG. 1: Schematic representation (a) and cross sectional SEM micrograph (b) of the PbSe quantum dot VCSEL structure. (c) Cross sectional and plan-view TEM micrographs of a PbSe/$Pb_{1-x}Eu_xTe$ dot superlattice reference sample with 5 ML PbSe and 480 Å $Pb_{1-x}Eu_xTe$.

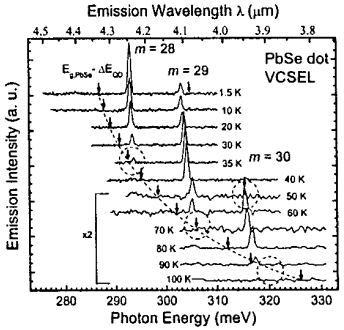

FIG. 2: VCSEL emission spectra at temperatures between 1.5 and 100 K showing the switching of the laser emission to higher cavity modes as the temperature increases. The arrows and dashed line indicate the low energy edge of the quantum dot gain spectrum.

References

[1] M. Asada, Y. Miyamoto, and Y. Seimitsu, IEEE J. Quantum Electron. **22**, 1915 (1986).
[2] Y. Arakawa and H. Sakaki, Appl. Phys. Lett. **40**, 939 (1982).
[3] G. Springholz, *et al.*, Phys. Rev. Lett. **84**, 4669 (2000).
[4] G. Springholz, *et al.*, Appl. Phys. Lett. **76**, 1807 (2000). W. Heiss, *et al.*, *ibid* **78** (2001).

Corresponding author: G. Springholz, Institut für Halbleiter- und Festkörperhysik, Johannes Kepler Universität Linz, Altenbergerstraße 69, A-4040 Linz, Austria.
phone: +43 732 2468 9602, Fax: +43 732 2468 8650
email: g.springholz@hlphys.uni-linz.ac.at

Optical emission in a V-groove Quantum Wire Laser diode under high magnetic fields

L. Sirigu[1], H. Weman[1-2], F. Karlsson[2], D. Y. Oberli[1], A. Rudra[1] and E. Kapon[1]

[1]Department of Physics, Swiss Federal Institute of Technology-EPFL, CH-1015 Lausanne, Switzerland
[2]Department of Physics, Linköping University, S-581 83 Linköping, Sweden

Semiconductor nanostructures like quantum wires (QWR) and quantum dots (QD) are expected to improve performances of lasers due to their peaked density of states profile and the reduced active volume [1]. Earlier attempts to study the impact of the reduced dimensionality on the performances of a semiconductor laser employed high magnetic fields to simulate quasi-1D and 0D carriers [2-3]. By applying a magnetic field perpendicular to the growth plane of a quantum well (QW) structure, a quantum dot-like system can be simulated if the magnetic confinement becomes sufficient. Despite the theoretical expectations, the threshold current of these devices was not reduced by the additional magnetic confinement even at very high field intensities. More recently, the lasing emission of QWR laser structures formed by cleaved-edge overgrowth was investigated in a magnetic field up to 12 T for both field orientations with respect to the QWR axis [4].

In this abstract we present a study of the behavior of the lasing and spontaneous emission of a V-groove QWR laser diode by applying very high magnetic fields (up to 27 T). The sample investigated is a p.i.n. GaAs/AlGaAs QWR laser diode grown by low pressure organometallic chemical vapor deposition (OMCVD) on V-grooved n-doped (001) GaAs substrates. The layer sequence consists of a 1μm thick n-doped $Al_{0.55}Ga_{0.45}As$ cladding layer, a 320 nm thick $Al_{0.2}Ga_{0.8}As$ core layer in which 5 GaAs QW active layers are embedded each 2.5 nm thick, a 1 μm thick p-doped $Al_{0.55}Ga_{0.45}As$ upper cladding layer and a 5 nm thick p-doped GaAs cap layer. In order to confine the injected current in the vicinity of the wires the structure was partially etched by wet etching to eliminate part of the QW active layers in the top (100) region and in the (111) side-walls of the groove. The etched surface was subsequently oxidized by anodic oxidation and the groove metallized with a 30 nm thick semitransparent Ti/Au p-contact layer which allows the observation of the surface emitted spontaneous emission. After metallization the sample was cleaved along the (110) crystallographic direction orthogonal to the wire axis in order to form an optical Fabry-Perot cavity. The mirror facets were left uncoated and the cavity was 1.3 mm long. The measurements were performed at liquid helium temperature (T = 4.2 K) under high magnetic fields.

The main purpose of our study is to gain insight on the nature of the laser emission in 1D. For this reason we have analyzed the magnetic field induced energy shift of both the spontaneous and lasing emission from the QWR and we have compared these energy shifts for two values of the injected current, $I_1 = 7$ mA and $I_2 = 3$ mA, above and below the threshold current $I_{th} = 5.2$ mA respectively. The energy shifts of the surface spontaneous emission peak with the magnetic field perpendicular to the wires in the growth direction for the two current values are shown in the figure below. An identical behavior is found as a function of the magnetic field intensity suggesting that the origin of the emitted light is the same. It is worth noting that in the low injection regime the characteristics of the spontaneous emission spectra demonstrate that the luminescence originates exclusively from the e_1-h_1 transition between the respective ground-state 1D-subbands of electrons and holes. In this case the dominance of excitonic recombination at low temperature was established in previous studies of similar QWR structures [5]. To further understand the nature of the lasing emission we also studied the magnetic field dependence of the light collected from one of the cleaved facets. The lasing systematically appears on the low energy side of the ground state spontaneous emission peak. Furthermore the edge emitted light displays a dependence on the magnetic field analogous to what is observed for the surface emission. From these results we infer that the lasing emission originates from recombination of localized excitons as suggested in a previous study on optically pumped V-groove QWR laser [6].

Other interesting effects observed are a pronounced decrease in the threshold current (from 5.2 mA at 0 T to 4 mA at 27 T) and an enhancement of the lasing emission intensity (by more than one order of magnitude) for a magnetic field larger than 10 T, indicating a magnetic field enhanced gain. These results will be discussed in light of the dependence of the exciton binding energy with magnetic field. The spectral evolution and the behavior of the optical emission with the magnetic field parallel to the QWR will also be presented and compared to the other configuration of the field.

The high magnetic field experiments performed in Grenoble, France, were supported by the "European Community Program" Access to Research Infrastructures Action of the Improving Human Potential.

References

[1] Y. Arakawa and H. Sakaki, Appl. Phys. Lett., **40**, 939 (1982)
[2] Y. Arakawa and A. Yariv, IEEE J. Quantum Electron. **QE-22**, 1915 (1986)
[3] T. T. J. M. Berendshot et al., Appl. Phys. Lett., **54**, 1827 (1989)
[4] W. Wegscheider et al., Solid State Electron., **40**, 1 (1996)
[5] F. Vouilloz et al., Phys. Rev. Lett., **78**, 1580 (1997)
[6] L. Sirigu et al., Phys. Rev. B, **61**, R10578 (2000)

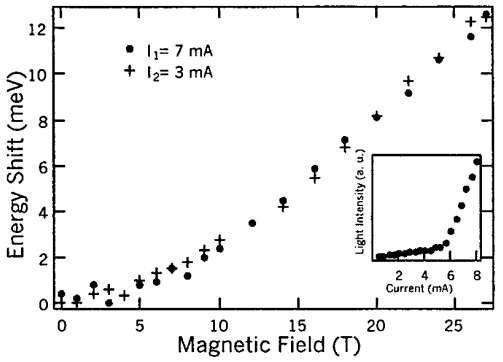

Fig. Magnetic field induced energy shift in the spontaneous emission peak from a QWR laser for two different injection currents $I_1 > I_{th}$ and $I_2 < I_{th}$. In the inset the output light vs. injected current characteristic of the laser diode.

Quantum dots for VCSEL applications at $\lambda = 1.3$ μm

N. Ledentsov[1,2], D. Bimberg[1], V.M. Ustinov[2], Zh.I. Alferov[2], and J.A. Lott[3]

[1]Technische Universitaet Berlin, Institut für Festkörperphysik,PN5-2, Hardenbergstrasse 36, D-10623 Berlin, Germany
[2]Abraham F. Ioffe Physical Technical Institute, Politekhnicheskaya 26, 194021, St.Petersburg
[2]Air Force Institute of Technology, 2950 P Street B640, Wright-Patterson AFB, OH 45433 USA

There is a strong interest in GaAs-based vertical cavity surface-emitting lasers (VCSELs) emitting at 1.3 μm [1]. Lasers using self-organized quantum dots (QDs) [2] are particularly advantageous for VCSELs, as nonequilibrium carriers are localized in the QDs and thus spreading of nonequilibrium carriers out of the injection region can be suppressed. This may results in ultralow threshold currents (<70 μA) at ultrasmall apertures [3]. We report studies of 1.3 μm-emitting GaAs-based VCSELs with QD active regions suitable for microcavity applications.

The epitaxial structures are prepared by solid-source molecular beam epitaxy on (001) (n^+) GaAs substrates as described in [1]. The self-organized QDs consist of planar sheets of initially small InAs pyramidal islands formed by a 2.5 monolayer InAs deposition covered by a 5 nm-thick $In_{0.15}Ga_{0.85}As$ layer. This process results in spinodal decomposition of the alloy layer, which is activated by the InAs stressors and results in significant increase of the volume of the QDs [4]. The QDs were followed by a 25 nm-thick GaAs barrier/separation layer. Three-fold stacked QDs were used. The dot density per stack was 5×10^{10} cm^{-2}.

The microcavity [8] was surrounded by (p) and (n) $Al_{0.98}Ga_{0.02}As$ layers (less than λ/4-thick) followed by 1λ-thick (p) and (n)GaAs current spreading/intracavity contact spacer layers doped to 10^{18} cm^{-3}. The spacer layers were followed by DBRs composed of alternating $Al_{0.98}Ga_{0.02}As$ and λ/4-thick GaAs layers. The $Al_{0.98}Ga_{0.02}As$ layers in the DBR, as well as those surrounding the optical cavity, were selectively oxidized to form Al(Ga)O. The QDs are centered in a 1λ-thick GaAs optical microcavity, whose edges are doped to 10^{17} cm^{-3}. The ends of the microcavity are composed of $Al_xGa_{1-x}As$ linearly graded from x = 0.02 up to 0.98.

The CW light power-current-voltage (L-I-V) characteristics of a QD VCSEL at 25°C are shown in Fig. 1, left. The threshold current is 1.2 mA and remains practically unchanged with temperature increase. The electroluminescence measurements from QD LED test structures, indicate that the lasing proceeds via the QD ground state transition. The maximum differential efficiency is 64%. The emission wavelength was near 1.3 μm (1.28-1.306 μm) depending on the particular position on the wafer. Variation in the threshold current across the wafer was ~10% (Fig. 1, right). During the lifetime test in excess of 700 hrs CW at 35°C no change of the performance of the devices was found.

We found that the threshold current demonstrates only weak dependence on the aperture size down to submicrometer cavities (Fig. 2a), while the photon confinement effect becomes increasingly important (Fig. 2b).

To conclude we fabricated GaAs-based VCSELs using InAs QDs emitting at 1.3 μm in a CW mode with differential quantum efficiency up to 64% and output power up to 0.65 mW at operating voltages below 2 V. Thus, 1.3 μm QDs are potentially advantageous for applications in VCSEL microcavities and phase-coupled VCSEL arrays.

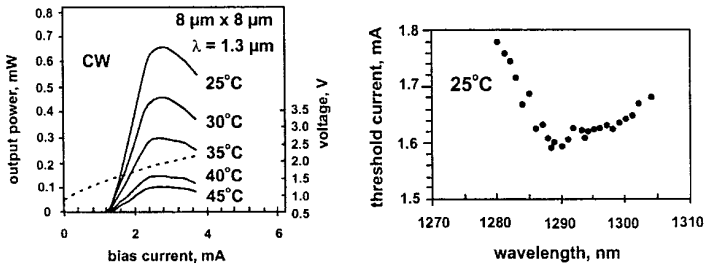

Fig. 1: L-I-V-curves of the 1.3 μm-emitting GaAs-based QD VCSEL (left) the threshold current and the lasing wavelength variation across the waver (right). Note very high (64%) maximum differential efficiency of the device at 25°C.

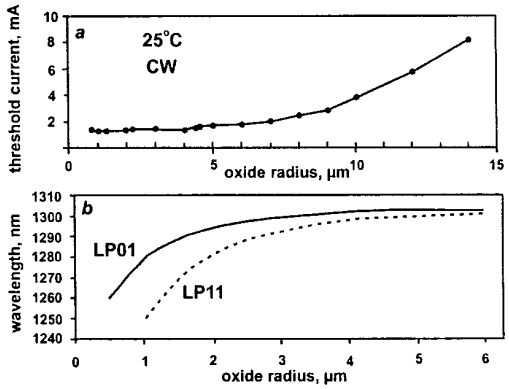

Fig. 2 The dependence (a) of the threshold current, and (b) of the confined photon modes on the oxide aperture size. Note low threshold currents at ultrasmall oxide apertures and significant energy splitting of the fundamental and the first cavity modes.

References

[1] J.A. Lott *et al., Electron. Lett.*, 2000, **36**, p. 1384
[2] N.N. Ledentsov *et al., Semiconductors,* 1994, **28**, p. 832
[3] N.N. Ledentsov *et al., Semicond. Sci. Technol.*, 1999, **13**, p. 99
[4] M.V. Maximov *et al., Phys. Rev. B*, 2000, **62**, p. 16671

Corresponding author: Prof. Nikolai N. Ledentsov, Technische Universitaet Berlin
Institut fuer Festkoerperphysik,PN5-2, Hardenbergstrasse 36, D-10623 Berlin, Germany.
phone:+49 30 314 22073, Fax: +49 30 314 22569
email: leden@sol.physik.TU-Berlin.DE

POSTER PRESENTATIONS

Phonons in self-assembled Ge/Si structures

A.G.Milekhin[1], A.I.Nikiforov[1], O.P. Pchelyakov[1], S.Schulze[2], D.R.T.Zahn[2]

[1]Institute of Semiconductor Physics, 630090 Novosibirsk, Russia
[2]Institut für Physik, Technische Universität Chemnitz, D-09107, Chemnitz, Germany

In this paper we present the results of an investigation of fundamental vibrations in self-organised Ge/Si structures with small-size Ge quantum dots (QDs) performed using macro- and micro-Raman spectroscopy under resonant and off-resonant conditions.
Samples under investigation were grown by molecular beam epitaxy utilising the Stranski-Krastanov growth mode on Si(001) substrates. The period of structures consisting of Ge and Si layers with a nominal thickness of 1.4nm and 37nm, respectively, was n=1-10. An average dot base size of Ge QDs obtained from transmission electron microscopy measurements was found to be approximately 15 nm with a QD height of 2 nm (Fig.1).
A number of periodic oscillations (up to 15th order) assigned to folded LA phonons in the Ge QD superlattices was observed in the low-frequency region of the Raman spectra taken in the z(xx)-z scattering geometry (Fig.2). These oscillations are superimposed with a broad continuous emission with a maximum at about 40 cm^{-1}. The measured phonon frequencies are in a good agreement with those calculated using the Rytov model. The origin of the continuous emission observed can be understood using a model based on interaction between bulk-like acoustic phonons and confined electronic states. The electronic confinement causes a breaking up of translational invariance and leads to Raman scattering by phonons originating from the whole acoustic dispersion branch [1].
The Raman spectra of the structure with a single Ge QD layer (Fig.3) reveal a series of peaks corresponding to localized LA phonons in the Si layer. Using the measured phonon frequencies and corresponding wavevectors the dispersion of the LA phonons in Si shown in Fig.3 was obtained. The longitudinal-acoustic wave velocity determined from the dispersion was 8365m/s that is in excellent agreement with that derived from a Brillouin study [2].
In the optical spectral range, the LO and TO phonons localized in Ge QDs are observed in the Raman spectra shown in Fig.1. Their frequency positions correspond to fully strained Ge QDs where the biaxial compressive strain of Ge bonds is 3.6%. The position of the LO Ge phonons shifts downwards with increasing excitation energy (from 2.5 to 2.7 eV) that indicates the presence of a QD size distribution in Ge dot superlattices. Raman scattering from smaller Ge QDs for which the E_1 exciton is at a higher energy, is size-selectively enhanced by the resonance of the exciting laser energy and the confined excitonic states. The size-confinement effect of optical phonons in Ge QDs which is stronger for the QDs with a small size, gives rise to a shift of optical phonons towards lower frequencies due to a negative dispersion of optical phonons in Ge.

References

[1] A.Mlayah, A.Sayari, R.Grac, et al., Phys. Rev. B 56, 1486 (1997).
[2] M.H.Kuok, S.C.Ng, Z.L.Rang, and D.C.Lockwood, Phys.Rev.B62, 12902, (2000).

Corresponding author: Alexander Milekhin, Institute of Semiconductor Physics, Russian Academy of Sciences, Lavrentjev av.13, 630090 Novosibirsk, Russia,
phone:++7-3832-343591, Fax:++7-3832-332771,
email:milekhin@thermo.isp.nsc.ru

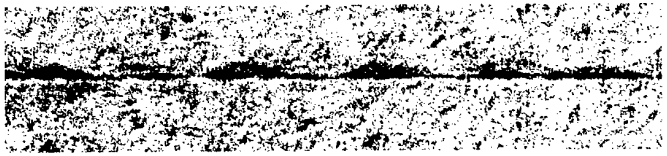

Fig.1 Cross-sectional high resolution transmission electron microscopy images of Ge QD superlattice with n=10. Dark regions are the Ge QD layers, light regions are the Si layers.

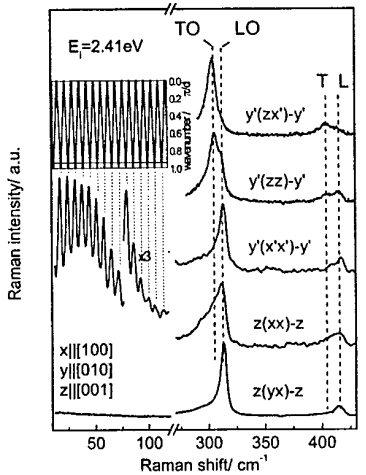

Fig.2 The experimental Raman spectra of the sample with n=10. Weak features labelled as L and T are attributed to the longitudinal and transverse Ge-Si vibrational modes, respectively. The inset shows the calculated dispersion of LA phonons for the planar Ge/Si superlattice.

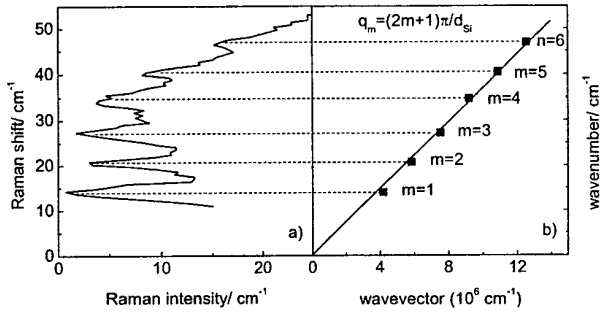

Fig.3 The experimental Raman spectrum of the sample with n=1 measured in z(xx)-z scattering geometry at E_l=2.41eV-a). The calculated dispersion of LA phonons in Si using wavevector for d_{Si}=37.3nm shown in the figure –b). Here m is the quantum number of localized acoustic modes. Solid line in Fig.3b is a guide for the eye.

Hole transport of $Si_{1-x}Ge_x$ channels on step-bunched vicinal Si surfaces

R. Neumann[1], K. Brunner, and G. Abstreiter

Walter Schottky Institut, Technische Universität München, Am Coulombwall, D-85748 Garching, Germany

A long-range attractive interaction between atomic steps on vicinal surfaces drives surface steps to assemble into bunches [1]. This bunching is enhanced by strain during SiGe heteroepitaxy. During growth and post-growth annealing step-bunching competes with debunching due to step flow kinetics. As a consequence, self-organized formation of regular arrays of uniform step bunches may take place when appropriate growth conditions are used.

Here we present recent results obtained from samples in which a modulation doped $Si_{1-x}Ge_x$ hole channel was grown on such an array of step bunches. We studied the influence of the current direction on resistivity, carrier density and mobility at low temperatures.

Fairly regular steps have been obtained by growing 100 nm Si and subsequent in-situ annealing at T = 1100°C on a vicinal (113)-Si substrate by molecular beam epitaxy, as shown by atomic force microscopy (AFM) in Fig. 1(a). The direction of the steps is perpendicular to the orientation of the substrate miscut. The regularity of the surface steps is restricted by varying terrace widths and bending of step bunches. Growth of a strained Si/SiGe multilayer on such an annealed Si buffer at appropriate growth conditions results in the self-organization of very uniform terraces with a mean terrace width of 240 nm and a mean step height of 4 nm (corresponding to ~25 monolayers), as shown in Fig. 1(b). Transmission electron microscopy (TEM) images show [2], that in such multilayers a considerable amount of SiGe material accumulates at the Si step edges forming wire-like structures.

At low temperatures, we find a strong resistivity anisotropy in samples in which a thin modulation doped $Si_{1-x}Ge_x$ hole channel was grown on such step-bunched surfaces on annealed Si buffer layers and on $Si_{1-x}Ge_x$/Si multilayers on (113)-Si (see Fig. 2). The resistivity is maximum for the current flow perpendicular to the step edges. The hole sheet densities, as determined from Hall measurements, are independent of Hall bar orientation within experimental accuracy. These results suggest that the hole gas is still two-dimensional but laterally modulated by the periodic thickness variations of the $Si_{1-x}Ge_x$ channel. Lowering the doping concentration, i. e. decreasing the effective carrier density in the hole channel, enhances the anisotropy up to $\rho_\perp/\rho_\parallel \approx 16$, as shown in Fig. 3. We attribute this to an increasing resistivity of depleted SiGe layer regions in between the wire-like structures when the Fermi energy gets comparable to the lateral potential barriers (see inset in Fig. 3).

In thick and highly doped $Si_{1-x}Ge_x$ channels on weakly stepped (113)-Si we find only a small anisotropy in the mobility with a maximum ratio of less than 1.5 between the $[33\bar{2}]$ and the perpendicular $[\bar{1}10]$ direction. This suggests that an "intrinsic" anisotropy of hole transport in (113)-$Si_{1-x}Ge_x$ quantum wells is weak. It might originate in an anisotropic effective in-plane hole mass and in anisotropic interface roughness scattering caused by intrinsic shear strain and interface steps in strained heterostructures on low-index surfaces like (113)-Si.

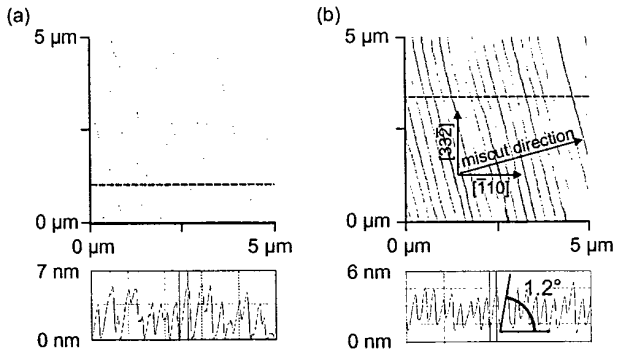

Fig. 1: AFM images of two samples containing (a) 100 nm Si annealed at T ≈ 1100°C and (b) overgrown with 18 double-layers of 2.5 nm $Si_{0.55}Ge_{0.45}$/10 nm Si and a 2.5 nm $Si_{0.55}Ge_{0.45}$ cap layer on (113)-Si substrate with a miscut angle of 1.0°. The direction of the steps, which are a result of strain induced step-bunching, is given by the direction of the substrate miscut.

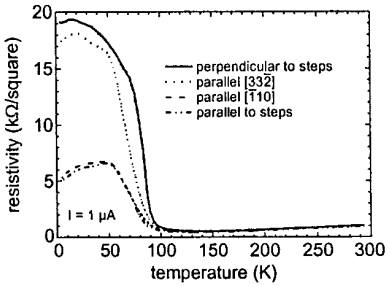

Fig. 2: Temperature dependent resistivity along different directions of a (113)-$Si_{0.65}Ge_{0.35}$ hole channel with step bunches towards a direction which is 30° off $[33\bar{2}]$ towards $[\bar{1}10]$.

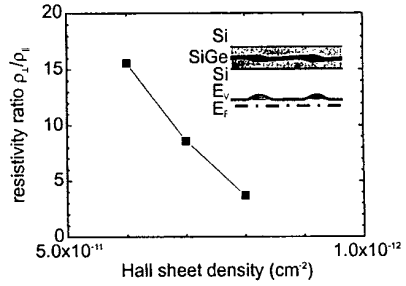

Fig. 3: Resistivity anisotropy $\rho_\perp/\rho_\parallel$ for the current flowing perpendicular and parallel to steps as a function of the sheet density of (113)-$Si_{0.65}Ge_{0.35}$ hole channels.

References

[1] J. Tersoff, Y. H. Phang, Z. Zhang, and M. G. Lagally, Phys. Rev. Lett. **76**, 1675 (1996).
[2] Jian-hong Zhu et al., Phys. Rev. **B 60**, 10935 (1999).

Corresponding author: Robert Neumann, Walter Schottky Institut, Technische Universität München, Am Coulombwall, D-85748 Garching, Germany.
phone: +49 89 289 12777, Fax: +49 89 3 20 66 20
email: neumann@wsi.tum.de

The surface morphology of single $Si_{1-x}Ge_x$ layers grown on vicinal Si (001): step bunching and strain-effects

C. Schelling, M. Mühlberger, G. Springholz and F. Schäffler

Institut für Halbleiter- und Festkörperphysik, Johannes Kepler Universität Linz, Altenbergerstraße 69, A-4040 Linz, Austria

For optimum performance of heterostructure devices, semiconductor heterointerfaces are required to be as smooth as possible in order to suppress interface roughness scattering or fluctuations in quantum confinement energies [1]. On the other hand, growth instabilities that lead to well-defined surface corrugations or growth of three-dimensional islands have gained widespread interest as a means to implement self-assembled one- and zero-dimensional nanostructures [2].

Recently, we found that under growth conditions far from thermodynamic equilibrium Si homoepitaxial layers on vicinal Si (001) surfaces exhibit a roughening transition, which is due to purely kinetic step bunching [3]. So far, such corrugated growth surfaces were commonly associated with built-in strain in lattice-mismatched heteroepitaxial layers [4][5]. Here, we present a study to discriminate between kinetic and strain-related effects on the surface morphology of single $Si_{1-x}Ge_x$ layers on Si (001).

Tuning the growth conditions it is possible to fabricate Si-buffers that are either atomically flat or provide a kinetically roughened template with adjustable amplitude and period. On this base we systematically studied the morphology of strained $Si_{1-x}Ge_x$ layers deposited either under kinetically limited, or under equilibrium growth conditions. By increasing the composition from x=0.05 to x=0.5 the compressive in-plane strain was varied between 0.2% and 2.1%.

With atomically flat buffers and for substrate miscuts between 0.05° and 4.3° we found no indications for strain-driven one-dimensional step bunching. Instead we observe elongated hut-clusters under kinetically limited growth conditions that evolve into square-based pyramids near thermal equilibrium.

Low-composition $Si_{1-x}Ge_x$ layers grown on corrugated Si-buffers basically replicate the buffer morphology. It is most likely this phenomenon that has led to the erroneous reports on strain induced one-dimensional step bunching of single $Si_{1-x}Ge_x$ layers in literature [6].

For higher Ge contents around 50% the formation of small mounds, which evolve into dots for equilibrium conditions, is observed. Again there is no indication for strain-induced step-bunching. The surface morphology is dominated by the more efficient mechanism of 3D island formation.

References

[1] M. A. Sadeghzadeh et al., Appl. Phys. Lett. **76,** 2568 (2000)
[2] D. Bimberg et al., Quantum Dot Heterostructures, John Wiley & Sons, Chichester 1999
[3] C. Schelling et al., Phys Rev. Lett. **83,** 995 (1999)
[4] J. Tersoff et al., Phys. Rev. Lett. **75,** 2730 (1995)
[5] A. J. Pidduck et al., Thin Solid Films **222,** 78 (1992)
[6] C. Teichert at al., in Surface Diffusion and Collective Processes, Ed. M. C. Tingides NATO-ASI Series, Plenum Press, New York 1997, 297 - 307

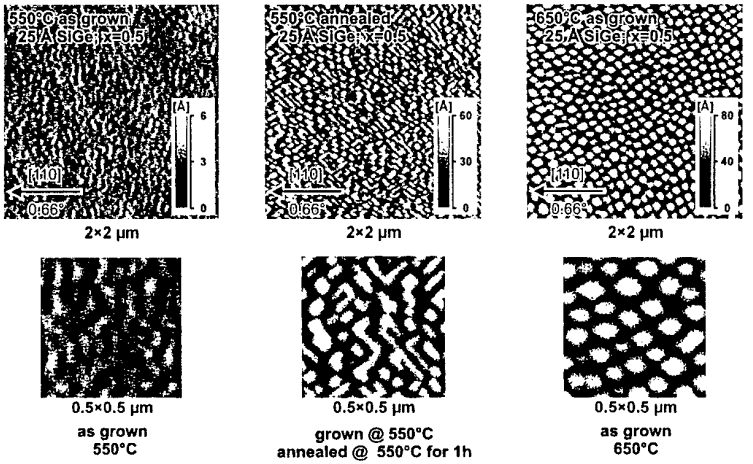

Figure 1 AFM images of single $Si_{1-x}Ge_x$ layers on a vicinal Si (001) substrate with a miscut of 0.66° along [110]. 25 Å thick $Si_{1-x}Ge_x$ layers with x=0.5 were deposited on a flat Si buffer at a growth temperature of 550°C (left picture) and 650°C (on the right). The sample in the middle was grown at 550°C and annealed after growth for 1 h at 550°C.

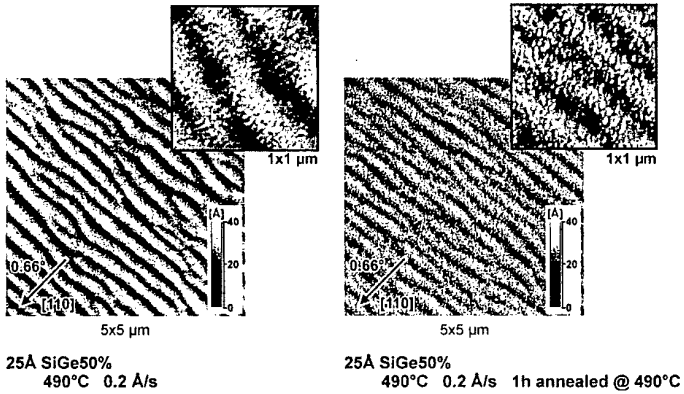

Figure 2 AFM images of single $Si_{1-x}Ge_x$-layers (x=0.5) on corrugated Si-buffers. The left picture shows the sample as grown, the right sample was left at the growth temperature of 490 °C for 1 hour directly after growth.

Corresponding author: Michael Mühlberger, Institut für Halbleiter- und Festkörperhysik, Johannes Kepler Universität Linz, Altenbergerstraße 69, A-4040 Linz, Austria.
phone: +43 732 2468 9607, Fax: +43 732 2468 8650
email: m.muehlberger@hlphys.uni-linz.ac.at

Chemically vapor deposited Si nanowires nucleated by self-assembled Ti islands on patterned and unpatterned Si substrates

T. I. Kamins[1], R. Stanley Williams[1], T. Hesjedal[2], and J. S. Harris[2]

[1] Quantum Science Research, Hewlett-Packard Laboratories, Palo Alto CA 94304-1126, USA
[2] Dept. of Electrical Engineering, Stanford University, Stanford CA 94305 USA

With the ever decreasing dimensions of integrated circuits, self-assembly techniques become attractive for forming fine features. Using self assembly may minimize the need for fine-scale lithography, while coarser lithography may possibly be used to position the features. Self-assembled nanoislands and nanowires are attractive elements for such an approach, especially if they can be integrated with more conventional CMOS ICs.

Of the materials that form nanoislands and nucleate nanowires, Ti is especially attractive because of its compatibility with Si integrated-circuit technology. Ti is already widely used in IC fabrication facilities to lower the resistance of source and drain regions of MOS transistors.

Self-assembled Ti-containing islands can be grown on Si substrates by chemical vapor deposition using the decomposition of $TiCl_4$. The amount of Ti deposited can be readily varied in the fractional monolayer range by changing the deposition temperature. After deposition, a large number of small islands are present. (10^3 - 10^4 atoms/island). The density of islands increases only slowly as the amount of Ti increases while the size of each island increases rapidly. After annealing above 800°C, the Ti coalesces into a smaller number of larger islands, although the amount of Ti on the surface does not change. The density of annealed islands increases rapidly as the amount of Ti increases while the size of each island increases only slowly with increasing amounts of Ti.

When the Ti-containing islands are exposed to a Si-containing gas, such as SiH_4 or SiH_2Cl_2, the metal catalyzes the decomposition of the Si precursor, and long Si nanowires can grow (Figures 1 and 2). The mechanism is analogous to the vapor-liquid-solid (VLS) mechanism, although the catalyzing Ti-containing nanoparticle probably remains in the solid state. As shown in Fig. 3, the steps in the overall process include (1) transport of the Si-containing gas to the nanoparticle; (2) enhanced decomposition of the Si-containing gas by the Ti-containing island; (3) diffusion of Si through or around the Ti-containing nanoparticle; (4) precipitation of the Si on the growing nanowire. The growth pushes the Ti-containing nanoparticle up so that it remains at the growing end of the nanowire, allowing wire growth to continue.

Self-assembled structures can be especially valuable if they can be integrated on a Si CMOS IC. For efficient integration, the nanowires should be grown at pre-determined locations on a partially oxide-covered Si wafer. Figure 4 shows Ti islands preferentially nucleated on exposed Si regions of an oxide-patterned Si substrate after growth and annealing. Figure 5 shows Si nanowires grown on the Ti islands. The Ti nanoislands and subsequently grown Si nanowires are preferentially positioned at the sloping edge facets of the Si regions, leaving the tops of the Si regions almost free of deposited Ti nanoislands and Si nanowires.

Figure 1: Transmission electron micrograph of defect-free Si nanowire with a Ti-containing particle at the growing end.

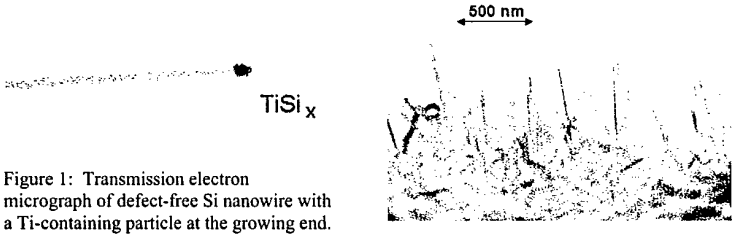

Figure 2: Shallow-angle scanning electron micrograph of dense nanowire array

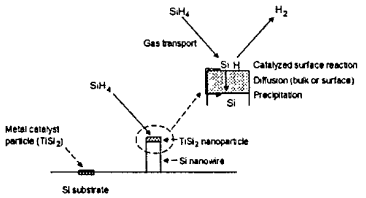

Figure 3: Mechanism of nanowire growth

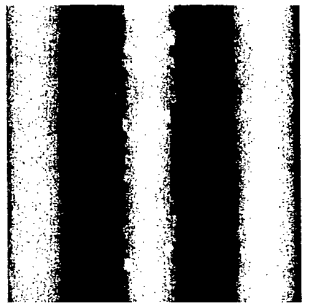

Figure 4: Ti-containing islands selectively grown on exposed Si region. (~1.5 μm image size)

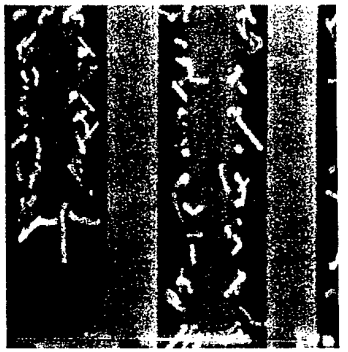

Figure 5: Si nanowires nucleated by the selective Ti-containing nanoisland.

Corresponding author: Ted Kamins, Principal Scientist, Quantum Science Research
Hewlett-Packard Labs, 1501 Page Mill Road, Palo Alto CA 94304-1126, USA
Telephone: 650-857-5470; FAX: 650-236-9885
e-mail: kamins@hpl.hp.com

LEPECVD – a novel process for high-speed heterostructure SiGe FET's

M. Kummer[1], C. Soltmann[1], E. Müller[1], C. Rosenblad[2], T. Hackbarth[3], M. Zeuner[3], G. Höck[4] and H. von Känel[1]

[1]Institut für Festkörperphysik, ETH Hönggerberg, CH-8093 Zürich, Switzerland
[2]Unaxis Semiconductors, FL-9496 Balzers, Liechtenstein
[3]DaimlerChrysler AG, Research and Technology, Wilhelm-Runge-Str. 11, D-89081 Ulm, Germany
[4]Siemens AG, Lise-Meitner-Str. 5, D-89081 Ulm, Germany

We present recent results on SiGe virtual substrates and their application for strained-layer SiGe heterostructures, fabricated with low energy plasma enhanced chemical vapor deposition (LEPECVD). We demonstrate the application of these heterostructures for different high-speed SiGe FET's.

LEPECVD is a growth process introduced recently, with its major advantages for semiconductor epitaxy being its exceptionally high growth rates (up to 7 nm/s have been demonstrated so far) and independence of the growth rate and film composition from the substrate temperature in the range interesting for strained-layer heterostructures [1].

The high growth rates of LEPECVD even at moderate substrate temperatures make it an ideal process for thick epitaxial layers like relaxed, compositionally graded buffer layers which are needed as the basis for 'virtual $Si_{1-x}Ge_x$ substrates' for thin strained Si or $Si_{1-x}Ge_x$ layers (for an example, see Fig. 1a).

We investigated the dependence of the surface morphology and defect density on the growth temperature, the steepness of the compositional grading, and the thickness of the constant-composition virtual substrate on top of the graded buffer layer. We show that by exploiting the capability of LEPECVD to economically grow very thick epitaxial layers, it is possible to optimize virtual SiGe substrates in terms of surface morphology and defect density, without paying the price of very long process times or additional process steps like chemo-mechanical polishing (CMP). The surface morphology has been studied with atomic force microscopy (AFM), the defect density has been investigated with defect etching and subsequent scanning electron microscopy (SEM) and AFM, and the structural quality with transmission electron microscopy (TEM, Fig. 2b) and high-resolution x-ray diffraction reciprocal space mapping (HRXRD-RSM, Fig. 1b).

To demonstrate the device-grade quality of these virtual substrates, we fabricated and characterized different field effect transistor (FET) devices. SiGe p-MOSFET's have been processed based on the layer sequence shown in Fig. 1a, which has been completely grown by LEPECVD [2]. N- and p-MODFET's have been fabricated by overgrowing with MBE a virtual substrate grown by LEPECVD, after transfer in air and applying a standard chemical cleaning procedure (RCA). All the devices show comparable or superior properties when compared with purely MBE-grown reference samples, and in all cases exhibit a better performance than the corresponding Si-based devices (Fig. 2).

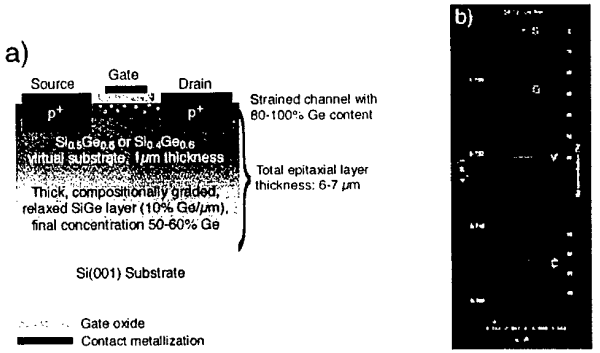

Fig. 1: a) Schematic of a strained-channel SiGe p-MOSFET based on a virtual SiGe substrate on a relaxed, graded SiGe buffer layer.
b) HRXRD reciprocal space map around the (004) Bragg reflection of a sample with the structure as shown in a). S: Si substrate peak, G: diffracted intensity from the graded $Si_{1-x}Ge_x$ buffer layer, V: diffraction peak from the virtual $Si_{0.4}Ge_{0.6}$ substrate, C: diffracted intensity from the thin (8 nm) strained $Si_{0.1}Ge_{0.9}$ channel

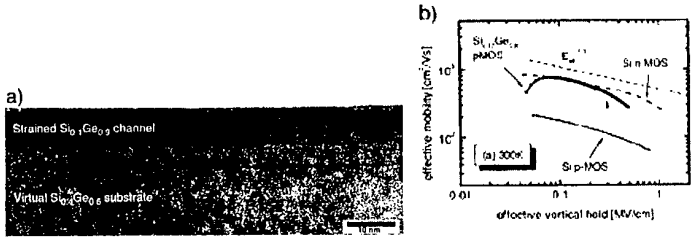

Fig. 2: a) Transmission electron micrograph of a strained, 8 nm thick $Si_{0.1}Ge_{0.9}$ channel on a relaxed $Si_{0.4}Ge_{0.6}$ virtual substrate for a high-mobility p-MOSFET. The complete heterostructure has been grown by LEPECVD
b) Effective carrier mobility in a $Si_{0.17}Ge_{0.83}$ channel p-MOSFET and in conventional Si n- and p-MOSFET's as a function of the vertical electric field at room temperature [2]

References

[1] C. Rosenblad, H. von Känel, M. Kummer, A. Dommann and E. Müller, Appl. Phys. Lett. 76, 427 (2000).
[2] G. Höck, E. Kohn, C. Rosenblad, H. von Känel, H.-J. Herzog and U. König, Appl. Phys. Lett. 76, 3920 (2000).

Corresponding author: Matthias Kummer, Institut für Festkörperhysik, ETH Hönggerberg, CH-8093 Zürich, Switzerland.
phone: +41 1 633 2258, Fax: +41 1 633 1072
email: kummer@phys.ethz.ch

Morphology of virtual SiGe substrates grown at very low temperatures

C. Teichert[1], C. Hofer[1], K. Lyutovich[2], M. Bauer[2], E. Kasper[2]

[1]Institut für Physik, Montanuniversität Leoben, Franz-Josef Str. 18, A-8700 Leoben, Austria
[2]Institut für Halbleitertechnik, Universität Stuttgart, Pfaffenwaldring 47, D-70569 Stuttgart, Germany

Virtual substrates play an important role for SiGe/Si heterostructures on Si(001) because they can adjust the strain of the active SiGe layers in the devices. In virtual substrates on the basis of thin relaxed buffer layers strain relaxation is provided by point defect injection using modified molecular beam epitaxy (MBE) techniques [1,2]. These techniques involve growth at significantly reduced substrate temperatures and/or simultaneous ion bombardment during growth.

Here we use *ex situ* atomic force microscopy (AFM) to characterize the morphology of 80 nm thick $Si_{0.7}Ge_{0.3}$ films that were grown by MBE on vicinal Si(001) substrates on which a 150 nm Si buffer layer was deposited at 600°C with a rate of 0.1nm/s. The alloy layer growth was performed by applying a two-temperature process. In the first stage, a 30 nm $Si_{0.7}Ge_{0.3}$ film is deposited at temperatures substantially reduced with respect to conventional growth conditions of SiGe. Hereafter, this stage will be referred to as low-temperature (LT) stage. The subsequent 50 nm alloy layer is grown after the sample temperature has been increased to 550°C. Growth rates are in both cases 0.1 nm/s. The LT stage has been performed in two different techniques: conventional MBE and ion assisted MBE (IAMBE), respectively. In IAMBE, the SiGe layer is grown under simultaneous bombardment with 1 keV Si^+ ions [2]. Further the influence of a Sb precoverage was studied.

The rms-roughness of the film, the dislocation density as well as the size and shape of three-dimensional islands were recorded as a function of both, LT growth technique and LT deposition temperature. These results are compared to quantitative data on the layer relaxation obtained by Raman spectroscopy and x-ray diffraction. We found that the temperature at which the cross-hatch pattern due to the dislocation network vanishes and the film becomes polycrystalline depends strongly on the growth procedure during LT growth (see Fig. 1). For an antimony precoverage of half a monolayer, this transition occurs between 220 and 210°C (Fig. 1a,b) whereas for conventional LT the dislocation network is visible down to 110°C, the lowest temperature studied (see Fig. 1c). In this case the intersections of the straight dislocation lines are decorated by {105} faceted pyramids. In Fig. 2 the results of an IAMBE grown film are shown where the increased dislocation density results in ordered array of uniform {105} facets [3].

[1] E. Kasper, K. Lyutovich, M. Bauer, M. Oehme, Thin Solid Films 336 (1998) 319.
[2] M. Bauer, M. Oehme, K. Lyutovich, E. Kasper, Thin Solid Films 336 (1998) 104.
[3] C. Teichert, C. Hofer, K. Lyutovich, M. Bauer, E. Kasper, Thin Solid Films, 380 (2000) 25-28.
[4] C. Schelling, G. Springholz, F. Schäffler, Phys. Rev. Lett. 83 (1999) 995.

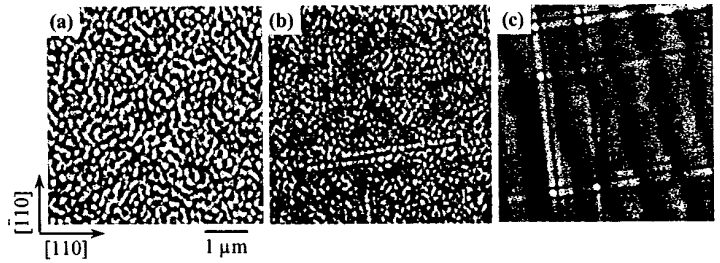

Fig. 1. AFM results of 80 nm $Si_{0.7}Ge_{0.3}$ films MBE grown in two-stage processes on vicinal Si(001). a,b) 0.5 monolayers Sb precoverage at LT of 210°C (a) and 220°C (b).
c) Conventional MBE growth at LT of 110°C. The underlying ripple pattern results from a kinetic instability during buffer layer growth [4]. Image sizes: 5 μm x 5 μm, gray-scale: 15 nm.

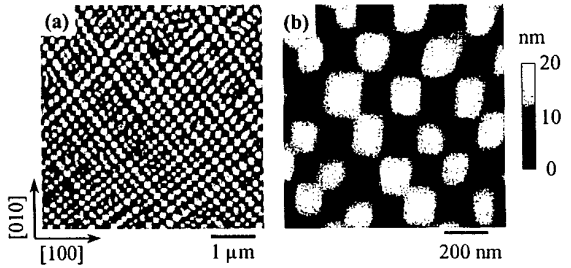

Fig. 2. Morphology of an 80 nm $Si_{0.7}Ge_{0.3}$ film, where the LT part was grown under simultaneous 1 keV Si^+ ion bombardment at 150°C. The dense dislocation network results in a checkerboard array of {105} faceted pyramids and pits. Image sizes: 5 μm x 5 μm (a) and 1 μm x 1 μm (b).

Corresponding author: Christian Teichert, Institut für Physik,
Montanuniversität Leoben, Franz Josef Str. 18, A-8700 Leoben, Austria
phone: +43-3842-302-763, Fax: +43-3842-302-760
email: teichert@unileoben.ac.at

Strain and composition profile of uncapped SiGe islands

J. Stangl, A. Daniel, V. Holý, T. Roch, G. Bauer, O.G. Schmidt†, K. Eberl†
Institut für Halbleiter-und Festkörperhysik, Universität Linz, A-4040 Linz
†Max-Planck-Institut für Festkörperforschung Stuttgart, Germany

The strain status and the composition of SiGe islands determine their optical and electronical properties. Even for pure Ge deposition on Si, there has been evidence for intermixing of Si and Ge already in uncapped islands, despite Ge segregation.

We have investigated the strain and composition distribution in uncapped SiGe islands on Si (001) by x-ray diffraction. In order to be sensitive to the dot layer at the sample surface, and at the same time being able to measure in-plane strain and strain in growth direction, we utilized a novel scattering geometry at grazing incidence angles, but with high exit angles. The measured intensity distribution is compared to simulations based on the strain distribution calculated by the finite element method (FEM). It turns out that, although pure Ge has been deposited during island growth by molecular beam epitaxy, indeed a Ge composition gradient within the islands exists.

Our investigations focus on a sample with uncapped SiGe islands grown by MBE on [001]-oriented Si. A layer of Ge islands at the surface was formed by the deposition of 6 ML of Ge at a growth temperature of 600° C. With atomic force microscopy the following island parameters have been found: density about 4×10^9 cm^{-2}, height and base diameter about 13 nm and 110 nm, respectively.

In order to distinguish between material composition and strain state, the previously developed technique for InAs dots [1] based on grazing incidence diffraction studies, comparing the intensity distributions for strong and weak reflections along a common azimuth is not applicable for diamond structures. Instead, we measure not only the in-plane lattice parameter, as in grazing incidence diffraction studies alone, but also the lattice parameter in growth direction. This can be achieved by measuring reciprocal space maps (RSMs) with the momentum transfer component along growth direction $Q_z > 0$. RSMs have been recorded around two {202} reciprocal lattice points (RLP) of Si, which are inaccessible in the conventional coplanar geometry at a wavelength of 1.55 Å, but can be accessed by rotating the scattering plane around the scattering vector **Q**, out of the plane of the RSM, as is shown in Fig. 1. With this setup, it is possible to keep the incidence angle α_i and hence the penetration depth constant at a value below the critical angle of external reflection α_c for the entire RSM, in order to be sensitive to the dot layer at the sample surface. For the determination of the Ge distribution within the islands, we use a fitting procedure: we start with an assumption on the Ge distribution and calculate the strain distribution using the FEM. With this result, the XRD pattern is calculated, and compared to the experimental result. Repeating the procedure while varying Ge distribution and island shape until a good correspondence between experiment and simulation is reached, we are able to establish the distributions of Ge content and strain within the islands.

Figure 2(a) shows the Ge profile giving the best correspondence to the experimental diffraction data, starting at a value of $x_{Ge,1} = 0.5$ at the wetting layer, and increasing up to $x_{Ge,2} = 1.0$ at the top of the islands. Fig 2(b) shows the corresponding strain distribution (in plane component ε_{xx}) within the islands. Due to the small aspect ratio of the islands, the in-plane relaxation reaches only about 50% at the top of the islands. An extension of these x-ray scattering investigations for Ge islands embedded in a Si matrix is in progress.

[1] I.Kegel, T.H.Metzger, A.Lorke, J.Peisl, J.Stangl, G.Bauer, J.M.Garcia, P.M.Petroff, Phys.Rev.Lett. **85**, 1694 (2000); I. Kegel et al. Phys.Rev. B **63**, 035318 (2001).

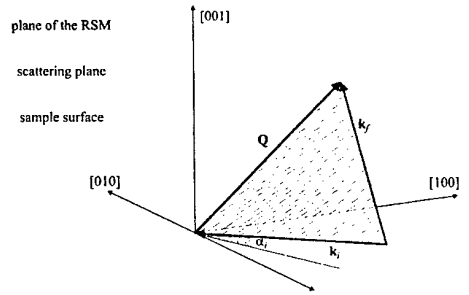

Fig. 1: Sketch of the grazing incidence high angle exit x-ray scattering geometry:

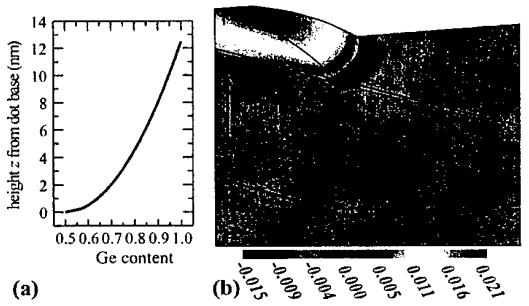

Fig. 2: (a) Ge profile along the height of the islands. (b) in-plane strain distribution within the islands, calculated by FEM, giving the best fit to the x-ray diffraction data.

Corresponding author: J. Stangl
Institut für Halbleiter- und Festkörperphysik
Johannes Kepler Universität Linz
Altenbergerstr. 69, A-4040 Linz
Fax +43 732 2468 8650
j.stangl@hlphys.uni-linz.ac.at

Shape evolution of Ge domes on Si(001) during first stages of Si capping

A. Rastelli[1], M. Kummer[2], H. von Känel[2],

[1]Dipartimento di Fisica A. Volta, Università di Pavia, Via Bassi 6, 27100 Pavia, Italy
[2]Laboratorium für Festkörperphysik, ETH Zürich, 8093 Zürich, Switzerland

Self assembled, coherently strained, 3D islands produced by epitaxially depositing a few monolayers of Ge on Si(001) received considerable attention in the last few years due to their potential applications as quantum dots in several devices.
In the system Ge/Si(001) various island shapes have been reported: {105} faceted clusters with rectangular or square base, named *hut clusters* and *pyramids,* respectivley, and larger multifaceted clusters, named *domes*.
For any kind of application those clusters have to be embedded in a matrix which will modify in general their shape as well as their eletronic and optical properties. For this reason, it is of great interest to study in detail the shape evolution of the islands taking place during the overgrowth with Si.
It has been shown that the embedding of {105} faceted clusters induces a flattening of their apex and the appearance of a (001) facet on top [1,2]. Most of the small hut clusters were even found to dissolve completely when buried. For domes, a significant reduction of their aspect ratio (defined as the ratio between height and base size) has been observed [1], but to our knowledge no detailed study exists about their shape change.
In this work we present the observation of a sudden morphology change of domes following the overgrowth with Si coverages as low as 2 monolayers.
Samples containing Ge domes and pyramids have been obtained by UHV magnetron sputtering epitaxy [3] at a substrate temperature of T_s=550 °C. In order to limit coarsening effects, the samples were immediately quenched to T_s=450 °C after growth and then covered with several monolayers of Si. The morphology changes induced by the capping were studied after growth by *in situ* room temperature STM microscopy.
The main feature observed already at very low Si coverages is the appearance of large {105} facets. Fig. 1 displays a typical Ge dome and a pyramid before the overgrowth. The various facets are clearly visible and indicated in the caption.
After capping with just 2 ML of Si (deposited at a rate of 0.1ML/s) some of the facets typical for the uncapped domes are still visible. However the four top {105} facets get larger and others of the same kind appear at the foot of the domes.
Such an abrupt transformation implies the diffusion of Ge away from the dome apex in quantities by far exceeding the amount of deposited Si.
With increasing coverages the new facet formation becomes more pronounced eventually leading to a complete transformation of domes into truncated pyramids.
Qualitatively similar results have been obtained with higher rates (0.9ML/s).

References

[1] M. Kummer, B. Vögeli, H. von Känel, Mat. Sci. & Eng. B**69-70**, 247 (2000)
[2] P. Sutter and M. G. Lagally, Phys. Rev. Lett. **81**(16), 3471 (1998)
[3] B. Vögeli, S. Zimmermann, H. von Känel, Thin Solid Films **318**, 29 (1998)
[4] F. M. Ross, R. M. Tromp, M. C. Reuter, Science **286**, 1931 (1999)

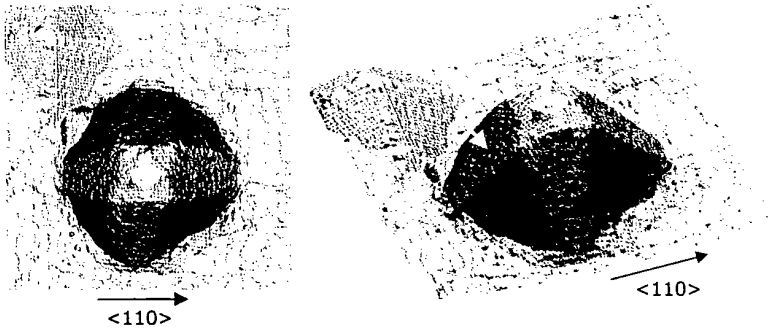

Fig. 1 Plain and perspective view of a 65 65nm^2 STM image of a typical uncapped dome. The gray-scale enhances the local slope of the surface (darker regions are steeper). The top of the dome is mainly composed by {105} facets. {105} facets are clearly visible also at the base of the dome.The body of the dome is delimited by 4 {113} facets (like the one pointed at by the white arrow) and 8 steeper facets (probably {15 3 23}, according to[4]). A {105} faceted pyramid is also present at the upper left corner.

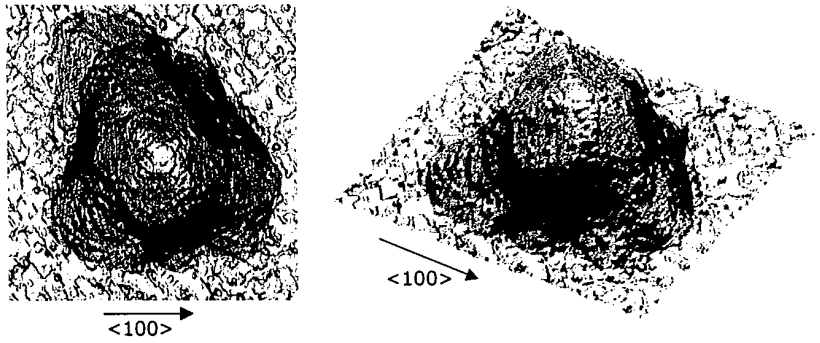

Fig. 2 Plain and perspective view of a 72 72nm^2 STM image of a dome after 2ML of Si capping. While facets typical for uncapped domes are still visible, large {105} facets appear.

Corresponding author: Armando Rastelli, ETH Zürich, Laboratorium für Festkörperphysik
ETH Hönggerberg (HPF F15), CH-8093 Zürich, phone: +41 1 6332258,
FAX: +41 1 6331072, e-mail: rastelli@solid.phys.ethz.ch

Photoluminescence of Si-based heterostructures and quantum dots

E. Ribeiro [1], E.F. da Silva Jr.[2], V.N. Freire[3], V. Lemos[3],
Y. Ikoma[4], F. Watanabe[4], and T. Motooka[4]

[1]Laboratorio Nacional de Luz Sincrotron- LNLS,
CEP 13088-902 Campinas, São Paulo, Brazil
[2]Departamento de Física, Universidade Federal de Pernambuco,
Cidade Universitária, CEP 50760-901 Recife, Pernambuco, Brazil
[3]Departamento de Física, Universidade Federal de Fortaleza,
Campus do Pici, Caixa Postal 6030 CEP 60455-760 Fortaleza, Ceará, Brazil
[4]Department of Materials Science and Engineering, Kyushu University,
Hakozaki, Fukuoka 812-8581, Japan

Silicon Carbide (SiC) is an important semiconductor material in the fabrication of high-power electronic devices, designed to work at elevated temperatures and pressures. The cubic silicon carbide, 3C-SiC, was found to be the only polytype which can be epitaxially grown on Si (001) substrate, to date. Several studies report on the growth of 3C-SiC on Si substrates but just a few have successfully achieved the reverse epitaxial growth of Si on 3C-SiC. This recent achievement makes it possible to fabricate Si-based quantum devices, such as tunneling diodes using very thin 3C-SiC films as electron barriers [1]. Also, by control of the growth parameters, it is possible to have a layer of Si quantum dots embedded into 3C-SiC, that could find application for the construction of light emitters and Si-based lasers. Despite the fact that silicon is extremely inefficient at emitting light, it was recently proven that light amplification is possible using silicon in the form of quantum dots [2]. Due to the lattice mismatch between 3C-SiC and Si, the epilayers may be under in-plane tensile strain that might cause problems in the further processing steps. It is convenient to have a conventional and fast method to measure the residual strain. Photoluminescence is useful for that purpose because of the electronic states depend on stress.

In this work, we measured low temperature photoluminescence, (PL), of thin films of 3C-SiC grown on Si (100) substrate, and capped with Si. The samples were grown by the pulsed supersonic free jets method that is described elsewhere [1]. The Si quantum dots sample was obtained using a similar procedure and resulted in a layer of dots in the shape of semi-spheres with 3-10 nm height and base of about 50 nm of diameter. The dots were covered with a ~3 nm 3C-SiC layer. Figure 1 (upper curve) shows the emission spectrum of sample I, a thin (~3 nm) 3C-SiC film, taken at 12 K using a half meter spectrograph with GaAs photomultiplier detector and the 488.0 nm line of an Ar ion laser as excitation. The sample holder contributed some structures which can be identified by comparison with its PL spectrum also given in Fig. 1 (lower curve). The peak at E = 2.114 eV observed in this figure, correspond to the heavy hole exciton line, displaced downward compared to the bulk 3C-SiC, due to tensile strain. The exciton bulk 3C-SiC energy gap was measured earlier as 2.39 eV at 6 K [3]. Using this value together with experimental values for the elastic constants and theoretical results for the deformation potentials reported recently [4], we determined the strain. The residual tensile strain in the 3C-SiC layer of sample I was found to be 2.7 %. Considering the 20 % lattice mismatch between 3C-SiC and Si, the strain was severely relaxed during growth, probably due to the effect of misfit dislocations. Figure 2 shows the PL spectrum of 3C-SiC existing as capping and under the Si dots of sample II. The sample holder spectrum is also plotted in this figure, for reference purposes. In the case of sample II, the PL peak is broader and located at 2.229 eV. This value is still below that for the exciton energy gap in bulk 3C-SiC, indicating the presence of tensile strain. To determine numerically the strain in this situation, it would be necessary to develop a model considering the shape of the 3C-SiC capping layer, and how the film under the dots respond to this effect.

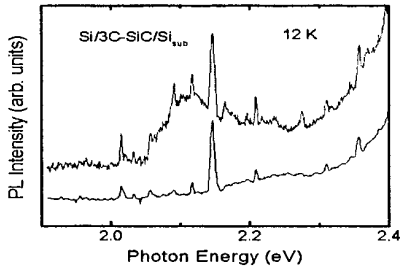

Fig. 1: Photoluminescence of a Si capped 3C-SiC thin epitaxial film grown on Si (100). Lower trace is PL from the sample holder.

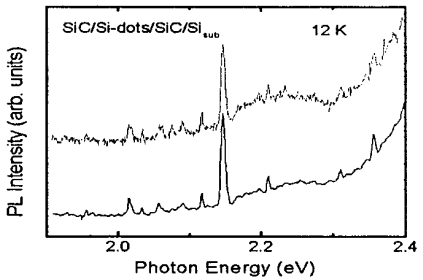

Fig. 2: Photoluminescence of 3C-SiC capping and film under Si quantum dots layer. Lower trace is PL from the sample holder.

[1] Y. Ikoma , T. Endo, F. Watanabe and T. Motooka, Appl. Phys. Lett. 75, 3977 (1999).
[2] L. Pavesi, L. Dal Negro, C. Mazzoleni, G. Franzo, and F. Priolo, Nature, 408, 440 (2000).
[3] W.J. Choyke. D.R. Hamilton, and L. Patrick, Phys. Rev. 133, A1163 (1964).
[4] W.R.L. Lambrecht, B. Segall, M. Methfessel, and M. van Schilfgaarde, Phys. Rev. B 44, 3685 (1991).

Corresponding author: Vólia Lemos, Departamento de Física, Universidade Federal de Fortaleza, Campus do Pici, Caixa Postal 6030 CEP 60455-760 Fortaleza, Ceará, Brazil
phone: 55 85 2889925, Fax: 2874138
email: volia@fisica.ufc.br

Unimodal dome-shaped islands of Ge-on-Si(001) by step-wise growth in UHV-CVD

Vilma Zela, Ines Pietzonka, Torsten Sass, Claes Thelander, and Werner Seifert
Solid State Physics, Lund University, Box 118, S-221 00 Lund/Sweden
Phone: -46 46 2227671, Fax: -46 46 2223637, e-mail: werner.seifert@ftf.lth.se

The size distribution of self-assembled heteroepitaxial islands is critical to their application as quantum dots in novel devices. In general a well defined size with little dispersion is desirable. However, under certain growth conditions the spontaneously formed 3-dimensional islands show bimodal size distributions. A well investigated heterosystem developing such bimodal size distributions is the system Ge/Si. Islands at small volume are pyramidal, exhibiting four {105} facets. These islands can form elongated "huts" as well as pyramids on a sqare base. At greater volume the islands have a dome shape exhibiting typically {113} and various other facets. For the origin of bimodal size distributions different explanations exist. One is that pyramids and domes correspond to two minimum-energy configurations of strained islands with an activated transition from pyramid to dome [1]. Another one is based on the idea that the chemical potential of an island undergoes an abrupt change as the equilibrium shape changes from pyramid to dome. This occurs at the well defined volume at which the dome energy becomes lower than the pyramid energy [2].

In detail this shape transition needs a nucleation step where steeper facets nucleate on the pyramid {105} facets. We show that this nucleation starts close to the most strain-relaxed top of the pyramid. We furthermore show that for a given surface density of Ge/Si islands with pyramids and domes almost all the pyramids can be converted into domes by a controlled supply of additional Ge. The additional Ge has to be provided in a second growth step under conditions of a reduced supersaturation in order to suppress new 3D island nucleation.

Growth experiments were done in an ultra-high vacuum CVD (UHV-CVD) equipment (EPIGRESS AB) using SiH_4 and GeH_4 as the source materials. Si(001) substrates were etched

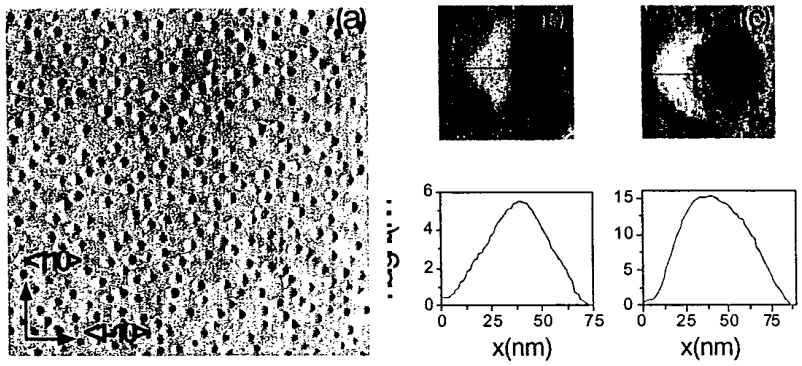

Figure 1: High-resolution AFM image of self-assembled Ge/Si islands, UHV-CVD, T=620°C
(a) 2x2 μm^2 image, showing the bimodal size distribution with pyramids and domes,
(b) and (c) show magnifications of a pyramid and a dome and the corresponding height profile

in H_2SO_4/H_2O_2 Piranha etch solution at 70 °C and surface-passivated by a treatment with diluted HF. The substrates were then inserted into the reactor at 450 °C and a 45 nm thick Si buffer layer was grown during ramping up to a temperature of 620 °C. After a growth interruption of 15 seconds the first germanium layer was deposited at 620 °C with varying GeH_4 pressures in the range between 1 and $7x10^{-4}$ mbar. This step in general results in a bimodal size distribution with pyramids and domes (Figure 1). The GeH_4 pressure and deposition time in this step determines in a first approximation the surface density of Ge dots. For longer deposition times a saturation density is observed which follows approximately the proportionality $\rho \propto R^{\frac{1}{2}} L^{\frac{1}{2}} D^{-\frac{1}{2}}(T)$, where R is the deposition rate (which is proportional to the GeH_4 pressure) and D(T) is the temperature dependent coefficient of surface diffusion [3]. After a growth interruption of one minute an additional amount of Ge was deposited. In this step a lower GeH_4 pressure was used in order to only supply the pyramids with material and to suppress creation of new nucleation sites. Under optimized conditions this procedure leads (best for not too high dot densities) to an almost uniform size distribution of dome shaped dots (Figure 2).

The TEM images of samples with pyramids and domes (Figure 3) suggest that the transition from pyramids to domes is initiated by nucleation of material onto the {105} facets close to the most strain-relaxed top-area of the pyramids. Note that a similar mechanism was proposed also for growth of InAs/GaAs islands [4].

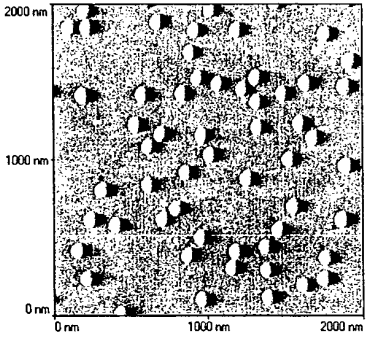

Figure 2: AFM image of Ge/Si domes grown in two steps at T_G = 620 °C.
Step 1: 57 sec, $pGeH_4 = 2.4x10^{-4}$ mbar
Step 2: 6 sec, $pGeH_4$ = 1.1x10-4 mbar
Growth interrupt was 70 sec

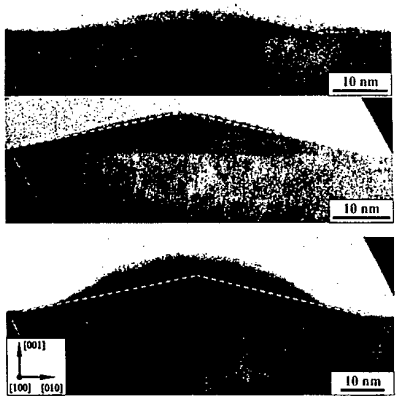

Figure 3: [100] cross-sectional TEM images of Ge dots on (001)Si. The transformation from pyramidal to dome shape is visible through the dotted lines indicating {105} planes.

References

[1] G. Medeiros-Ribeiro et al., Science **279**, 353 (1998)
[2] F. M. Ross et al., Phys. Rev. Lett. **80**, 984 (1998)
[3] J. Johansson et al., Physica **E 2**, 667 (1998)
[4] I. Mukhametzhanov et al., Appl. Phys. Lett. **75**, 85 (1999)

Ge quantum dots in Si: self-assembly, ordering and level spectroscopy

K. Brunner, D. Bougeard, C. Miesner, M. Herbst, C. Schramm, G. Abstreiter, A. Vörckel* and H. Kurz*

Walter Schottky Institute, TU Munich, Am Coulombwall, D-85748 Garching, Germany
* RWTH Aachen, Institut f. Halbleitertechnik II, Sommerfeldstr. 24, D-52074 Aachen

Ge quantum dots in Si were fabricated by MBE in the Stranski-Krastanow growth mode and investigated by photoluminescence (PL) and photocurrent (PC) spectroscopy as well as C-V and admittance spectroscopy. The effective valence band structure of Si/Ge quantum dots is consistently deduced from optical type-II inter-band transitions between electrons in the Si host and holes localized within the Ge dots at 0.8 eV, bound-to-continuum intra-valence band transitions of localized holes in the mid-infrared spectral range ($\Delta E_{VB} \approx 0.35$ eV), and admittance spectroscopy which reveals hole quantization energies of about 37 meV within dots of 20 nm lateral size. Possible optoelectronic applications of Si/Ge dot structures and novel properties of spatially self-ordered dots structures will be discussed.

The structural and electronic properties of Ge dots depend strongly on the parameters of MBE deposition in the Stranski-Krastanow growth mode, like temperature and orientation of the Si surface and the multi-layer sequence. Vertical ordering of dots in Si/Ge multi-layers and lateral ordering of Ge dots on self-ordered Si/SiGe wire structures formed by step-bunching on vicinal Si substrates is achieved by dot nucleation processes which are modified by the local strain fields of underlying nanostructures (see Fig. 1). [1] The effective band structure of spatially correlated nanostructures is modified by changes in structure size, local strain relaxation, Coulomb and quantum coupling of neighboring localized states. These may be beneficial for optoelectronic structures due to an enhanced oscillator strength, changes in effective band gap and level spacings, or modified life times of localized and excited carriers, as discussed later. A control of stacking of dots in Si/Ge multi-layers is also important for preventing relaxation of accumulating strain by dislocations. PC studies on closely packed Si/Ge dot structures in pin photodiodes will be presented.

In contrast to inter-band transitions, intra-valence band transitions are allowed in Si/Ge heterostructures. B-doped Si/Ge dot multi-layers embedded in pip-structures reveal a maximum in vertical PC at energies around 330 meV, as shown in Fig. 2. It corresponds to excitation of holes localized in the 20 nm-sized dots to the Si valence band edge. Mixing of hole states and their localization in 3 dimensions weaken the optical selection rules and similar spectra for TM and TE polarization are observed. Even though the responsivity is moderate so far due to a low total number of holes confined in the dots, a very small dark current of the Si/Ge dot structures results in a high detectivity of such vertical PC structures above 10^{10} cm $Hz^{1/2}/W$. [2] Studies of **lateral** conductivity demonstrate a novel concept of MIR detection based on the localization of holes within Ge dots and their excitation into wetting or doping layer states as illustrated in the inset of Fig. 2. The energy of maximum lateral PC is reduced compared to vertical PC (Fig. 2) indicating stronger contributions of vertically bound final states. At T<20K, the responsivity and detectivity are enhanced compared to vertical structures. Dot structures with neighboring SiGe quantum wells were grown which promise an enhanced life time of photoexcited holes and a further increased sensitivity.

The internal band structure of Ge dots is analysed by admittance measurements, which probe the localisation energy E_a of localised holes depending on the Fermi level varied by a Schottky gate bias. While large Ge islands of 70 nm diameter show a continuous shift of E_a with bias due to a low, quasi-continuous density of hole states, 20 nm-sized Ge dots reveal a step like increase of E_a with depleting the dots, as shown in Fig. 3. The observed level spacings of 15 and 37 meV of the 3 levels highest in energy are attributed to the Coulomb charging energy of ground state holes and mainly to the difference of s- and p-shell hole quantisation energy within the dots, respectively. They agree very well with values estimated from the dot size and the band offsets. [3] The admittance results imply a thermal escape time of ground state holes localised in Ge dots in the range of µs at room temperature. The impact of hole life times, for example, on pin photodiode and MIR photocurrent will be discussed.

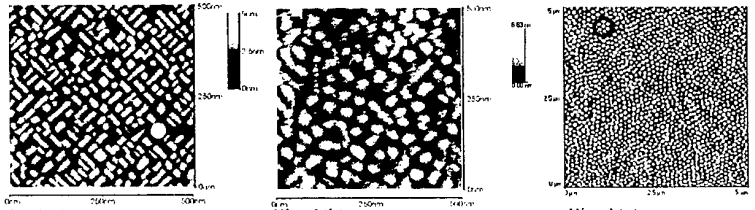

Fig. 1(a) Fig. 1(b) Fig. 1(c)

Fig. 1: AFM images of (a) Ge dots ("huts") formed from 8 ML Ge on (001)Si at T_S=510°C, (b) vertical stacks of dots developed from 8 ML Ge dots and 4x7 ML Ge separated by 6 nm Si spacers, and (c) 2-dimensionally self-ordered Ge dots (5 ML) on Si/SiGe wires formed by self-ordering on vicinal (001)Si.

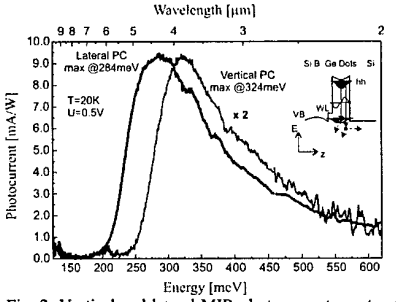

Fig. 2: Vertical and lateral MIR photocurrent spectra at normal incidence (TE-polarized) from B-doped 10-period Si/Ge dot MIR detector structures.

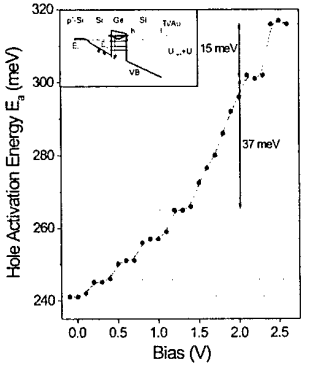

Fig. 3: Discrete hole localization energies deduced from admittance vs. biasing of a Si/Ti Schottky diode containing 20 nm-sized Ge dots.

References

[1] J. Zhu, K. Brunner, and G. Abstreiter, Appl. Phys. Lett. **73**, 620 (1998).
[2] C. Miesner, O. Röthig, K. Brunner, and G. Abstreiter, Appl. Phys. Lett. **76**, 1027 (2000).
[3] T. Asperger, C. Miesner, K. Brunner, and G. Abstreiter, Phys. Stat. Sol. (in press).

Corresponding author: Karl Brunner, Walter Schottky Institute, TU Munich, Am Coulombwall, D-85748 Garching, Germany. phone: ++49 89 289 12782, Fax: ++49 89 320 6620, email: brunner@wsi.tum.de

Optical properties of ordered Ge islands

L.Vescan1[1] and T. Stoica[2]
[1]ISG, Forschungszentrum Jülich, D-52425 Jülich, Germany
[2]Institutul National de Fizica Materialelor, R76900 Bucharest, Romania

In-plane ordering of islands in Stranski-Krastanow growth mode can be achieved on mesa edges [1-3], on vicinal surfaces with regular ripples [3] and along dislocations. We report new results on lateral ordering of Ge islands on {h10}facets of (001) Si mesas made by Low Pressure Chemical Vapor Deposition. The mesas are of lateral dimension of the order of the diffusion length of the adatoms, therefore the ordering of the islands and their optical properties will be influenced by the limited surface diffusion. The Si mesas were deposited at 800°C on Si(001) wafers with patterned thermally grown oxide. For mesas parallel to <100> directions the islands nucleate regularly spaced parallel to the mesa edges. Increasing the coverage the linear density of islands on facets remains the same, the arriving atoms diffuse on the (001) surface of the mesas until reaching the rows on the edges and attach there. This process, which increases the island size will slow down when the dimension of the islands reaches a value which becomes energetically unfavourable for additional incorporation (self-limiting behaviour).

The photoluminescence from ordered islands could be separated from the luminescence from islands on the (001) plane by varying the width of the mesa lines. Fig.1 shows spectral distributions of photoluminescence measured at 20 K on a sample with a capped Ge layer above the critical thickness for island formation. The specrum of the unpatterned sample is the response of islands and Ge wetting layer on a Si(001) surface. The spectra from the arrays contain beside the contribution from the (001) surface more and more (by decreasing the line width) contribution from the ordered islands. The features of the photoluminescence spectra from islands and wetting layer on the Si(001) plane and Si{h10} facets will be discussed in relation to the island size distribution. The influence of the buffer and the occurrence of a deep luminescence band will be analysed also.

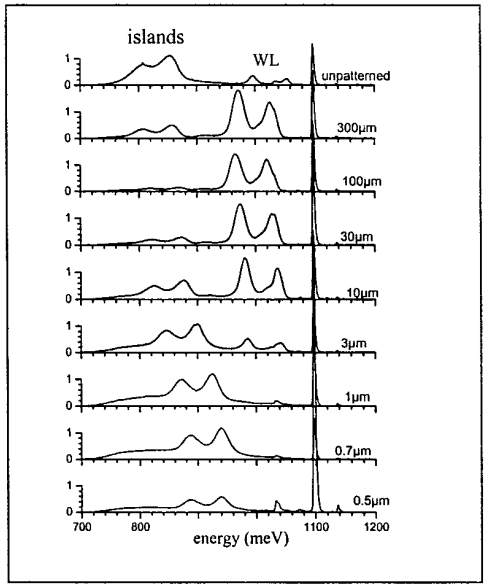

Fig.1. Spectral distribution of an unpatterned area and of arrays of long straight mesa lines parallel to the <100> directions.

References

[1] T.I. Kamins, R.S. Williams, Appl. Phys. Lett., **71**, 1201 (1997)
[2] L. Vescan, J. Cryst. Growth, **194**, 173 (1998)
[3] G. Jin, J.L. Liu, S.G. Thomas, Y.H. Luo, K.L. Wang, Appl. Phys. Lett. **75**, 2752 (1999)
[4] J. Zhu, K. Brunner, G. Abstreiter, Appl. Phys. Lett. **73**, 620 (1998)

Corresponding author: Lili Vescan, Institut für Schichten und Grenzflächen,
Forschungszentrum Jülich GmbH, D-52425 Jülich, Germany
phone: 0049 2461 612343, Fax: 0049 2461 612940
email: l.vescan@fz-juelich.de

Intersubband transitions in boron doped self-assembled Ge quantum dots

W. Mac[1], T. Fromherz[1], C. Miesner[2], K. Brunner[2], G. Bauer[1], G. Abstreiter[2]

[1]Institut für Halbleiter und Festkörperphysik, Johannes Kepler Universität Linz, Altenbergerstraße 69, A-4040 Linz, Austria
[2] Walter Schottky Institut, TU München, Am Coulombwall, D-85748 Garching, Germany

Self-assembled Ge quantum dots embedded in a Si matrix are a promising approach for the realization of infrared detectors in the Si system. The advantage of such a system in respect to a Si/SiGe superlattice is that a higher Ge content can be realized in the quantum dots shifting the absorption energy in the technologically interesting spectral region between 2 and 5 μm. Another benefit from quasi zero dimensional structure is a relaxation of polarization dependent selection rules that are responsible for relatively low absorption of radiation perpendicular to the surface of two dimensional quantum structures.

We report the first observation of electronic transitions between subbands confined in doped (p–type) Ge quantum dots in transmission experiments. The MBE grown Ge quantum dots have an average diameter and height of 30 nm and 3 nm, respectively (see Fig. 1 for a sketch of the sample structure). The transmission experiments were performed in a waveguide geometry for two linear light polarizations (p and s polarization parallel and perpendicular to the growth direction, respectively) in the temperature range from 10 K to room temperature. A metallic gold layer evaporated on top of the quantum dot layers enhances a coupling of the intersubband quantum dot transitions to the p-polarized infrared radiation. An absorption line centred at 260 meV with a FWHM of 60 meV is observed in the ratio of p and s polarized transmission spectra (see Fig. 2). We assign the line to a transition between the highest and a second hole subband confined in a quantum dot (denoted $E_{i,j,1}$ and $E_{i,j,2}$ in Fig1, respectively). The line is observed up to room temperature but its intensity decreases with increasing temperature. The different temperature spectra, divided by a room temperature spectrum, to remove strongly wavelength dependent background that is not related to the dots, are displayed in Fig 2. Remarkably, the width of the absorption line is only a factor of three larger than typical absorption line widths observed in p-type SiGe quantum wells (approx 20 meV), indicating a rather narrow distribution of the sizes of the individual quantum dots.

The *maximum* of the Ge dot absorption observed in the transmission experiments coincides with the *low energy onset* of photocurrent spectrum measured on the same samples recently. These experimental findings indicate that in the transmission spectrum transitions to weakly bound hole states (denoted $E_{i,j,2}$ in Fig.1) are observed. The final states contributing to the photocurrent spectrum are continuum state above the quantum dot barriers and, therefore, occur at higher transition energies. Due to the small matrix elements, the transitions to the continuum states are not observed in the transmission spectrum.

Corresponding author: W. Mac, Institut für Halbleiter- und Festkörperphysik, Johannes Kepler Universität Linz, Altenbergerstraße 69, A-4040 Linz, Austria
phone: +43 732 2468 9607,
Fax: +43 732 2468 8650
email: W.Mac@hlphys.uni-linz.ac.at

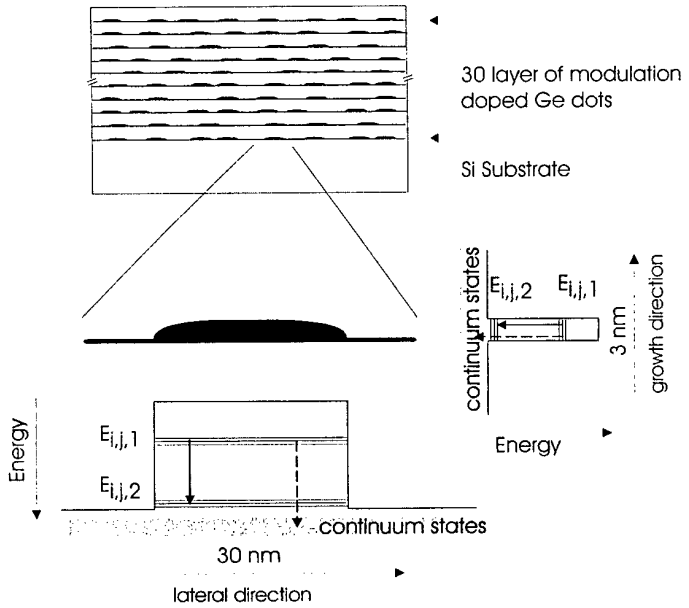

Fig 1.: Schematic sketch of the Ge dot sample. The occupied groundstates are denoted by $E_{i,j,1}$. In the absorption spectrum, the transitions to the confined states $E_{i,j,2}$ (indicated by the full arrow in the sketch) are observed. The transitions to the continuum states (indicated by the broken arrows in the sketch) are observed in the photocurrent spectrum

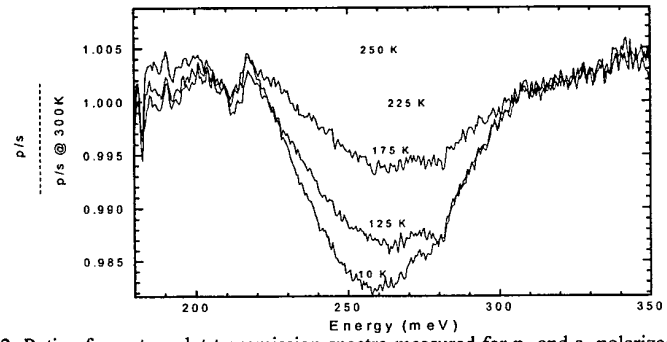

Fig.2: Ratio of quantum dot transmission spectra measured for p- and s- polarized radiation. For the various temperatures indicated in the plot, the ratio of the p and s polarized spectra is normalized to respective ratio measured at 300 K.

Many-particle effects in excitonic transitions in type-II Ge/Si quantum dots

A.I. Yakimov, N.P. Stepina, A.V. Dvurechenskii, A.I. Nikiforov, A.V. Nenashev

Institute of Semiconductor Physics, Novosibirsk 90, Russia

A fundamental feature of staggered QD's is the spatial separation of electrons and holes resulting in the formation of spatially inderect excitons, whose intriguing properties are still poorly understood. In particular, little is known about the influence of Coulomb interactions on the excitonic properties of charged QDs. Using electron-filling modulation absorption spectroscopy, we study the effect of quantum dot (QD) charging on the interband excitonic transitions in type-II Ge/Si heterostructures containing pyramidal Ge nanocrystals [1,2].

Ge dots are embedded into a n^+-p-p^+ Si diode, in which the number of holes in the QD's can be finely tuned by an external applied bias. Modulating the holes in and out of the state by applying an ac bias voltage induces corresponding changes in the infrared absorption. Thus, the absorption signal measured under different bias conditions directly reflects properties of excitons at charged quantum dots. The sample was grown by molecular beam epitaxy on a p-type Si(001) substrate. The Ge quantum dot layer with a nominal thickness of 10 ML was symmetrically embedded into a 1-μm thick p-Si region at 300 °C. A buried back contact is formed by 50-nm B-doped p^+-Si. The structure was finally capped with a 50 nm n^+-Si front contact. The area density of the dots estimated from STM-data is about 3×10^{11} cm^{-2}, the size of the dot base length about 15 nm, the height about 1.5 nm, and the dot uniformity approximately 20%. Infrared absorption measurements were performed in normal-incidence geometry on mesa diodes at room temperature.

The absorption signal measured at different values of the bias shown in Fig.1. Absorption maximum at energies $\sim$ 760–770 meV we interpreted as a spatially inderect excitonic transition between the hole ground state in the Ge dots and the electron ground state confined in Si near the heterojunction. When the dots are loaded with holes by charging the reverse bias, the ground-state transition in the absorption spectra shows a stepwise blueshift of about 11 meV accompanied by a decrease in intensity. Interband optical pumping at a fixed bias voltage leads to a shift of about 20 meV (Fig.2). The observed changes are explained by exciton-hole and exciton-exciton interactions. For a positively charged dot, we argue that this is the consequence of the dominance of the hole-hole interaction compared to the electron-hole interaction due to spatial separation of the electron and hole. The large oscillator strength (0.5) and the exciton binding energy (25 meV) are determined from the experimental data. The results are explained by effect of the electron and hole localization and by electron wave function leakage in the dots.

The electronic structure of spatially indirect excitons is calculated self-consistently in the effective-mass approximation for pyramidal-shaped Ge/Si quantum dots. The inhomogeneous strain distribution in the quantum dot layer has been taken into account through modification of the confining potential. The calculations show that the electron of a spatially indirect exciton resides in the Si near to the Ge pyramid apex due to maximum strain in this region, while the hole is confined close to the pyramid base. The electron-hole overlap is calculated to be 15%. When two excitons are excited in the dot, the electrons are found to be spatially separated and have different single-particle quantization energies. We argue that this is the reason why the biexciton absorption is blueshifted as compared to a single exciton. A satisfying agreement is found between theoretical and experimental data.

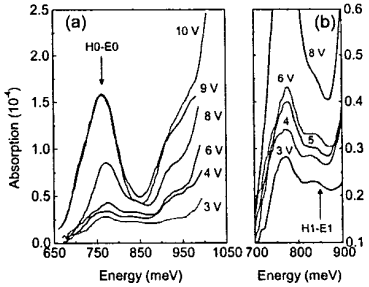

Figure 1: Room-temperature electron-filling absorption spectra at different reverse bias.

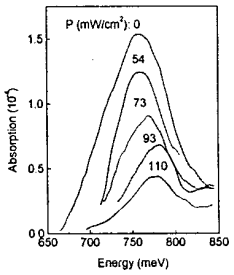

Figure 2: Effect of optical pumping on the EFA spectra at different pump intensities.

References

[1] A.I. Yakimov et al., Semicond. Sci. Technol. **15**, 1125 (2000).
[2] A.I. Yakimov et al., Phys. Rev. B **63**, 045312 (2001).

Corresponding author: Natalia Stepina, Institute of Semiconductor Physics, 630090 Novosibirsk, Russia.
phone: +7 3832 332624, Fax: +7 3832 332771,
email: stepina@isp.nsc.ru

Influence of the Si-Ge Interface on Phononless Radiative Recombination in Ge Hut-Clusters Grown on Si (001)

M.W. Dashiell, U. Denker, O.G. Schmidt and K. Eberl
Max-Planck-Institut für Festkörperforschung, Heisenbergstrasse 1, 70569 Stuttgart, Germany

An approach to enhancing the radiative-recombination efficiency of Si-based heterostructures is to spatially localize charge carriers within a reduced dimensionality. This effect has been investigated in both quantum dot structures[1,2], as well as strained $Si/Si_{1-x}Ge_x$ neighboring confinement structures (NCS) that exhibit enhanced no-phonon (NP) recombination due to in-plane carrier localization at the heterointerface[3].

We investigate carrier confinement in the vicinity of Ge *hut-clusters* grown by molecular beam epitaxy on Si (001) and the influence of the Si/Ge interface on phononless radiative recombination. Variation of growth temperature of the initial Si/Ge interface as well as post-growth annealing experiments, indicate that the NP photoluminescence (PL) from Ge hut-clusters is extremely sensitive to the atomic-scale arrangement at the Si-Ge interfaces.

The growth temperature of the initial 2.5 monolayers (ML) of the Ge wetting layer (WL) and its underlying 1nm of Si was varied from T_{WL} = 120 to 500°C. The final 2.5 ML Ge required for island formation was grown at 500°C. Ge huts, elongated in [001], and approximately 1.2 nm in height with base width of 20-30 nm were formed (see figure 1).

Figure 2 shows PL spectra of as-grown samples for several T_{WL} values. All spectra show a pronounced and intense hut-cluster related PL signal from the single layer of Ge huts. We suggest this intense PL originates from spatial-localization of both holes in the Ge huts, as well as electrons in the tensile strained Si below and above the Ge huts. This spatially indirect recombination was proposed for the intense NP-PL signal originating from C-induced Ge dots grown on Si (001)[1,2]. A simplified band diagram illustrating this recombination mechanism for our Ge huts is adapted from this model[1] (see inset). Decreasing T_{WL} from 500 to 320 °C results in a further enhancement of the hut-clusters' NP-PL intensity, while the emission energy and peak shape remain unchanged. We propose that the increased intensity results from further localization of electrons underneath the Ge hut at the abrupt Si-Ge interface, since the Si-Ge interface properties will be influenced by T_{WL}. For T_{WL} = 220 °C and below, the Ge hut PL as well as the Si reference peak decrease, presumably due to defects associated with the low growth temperature.

Figure 3 shows PL spectra of Ge huts grown with T_{WL}=320 °C before (dotted lines) and after selected 60s anneals (solid lines). We observe a decrease in the Ge hut-cluster PL intensity for annealing temperatures as low as 585 °C and a small blue shift in energy. The blue shift is attributed to slight Si-Ge intermixing at the interface. At higher anneal temperatures the intensity strongly decreased and the shape of the PL emission changes, eventually resembling the PL spectra commonly observed for thin, 2D Ge layers embedded in Si, i.e. NP emission and its phonon replica (spectra shown in top of figure). The PL intensity decrease is attributed to the loss of the NCS structure around the Ge huts.

Our results establish the strong sensitivity of Ge hut clusters' NP-PL to the atomic arrangement at the Si-Ge interfaces. For low annealing temperatures, NP intensity decreases, as even slight Si-Ge intermixing will decrease interface localization potentials[3]. At annealing temperatures above 700 °C, phonon-assisted recombination is observed, which indicates that the excitons are no longer three dimensionally localized within the strain fields of the Ge huts.

References

[1]O.G. Schmidt, C. Lange, K. Eberl, O. Kienzle, F. Ernst, Appl. Phys. Lett., **71**, 2340 (1997).
[2]O.G. Schmidt, K. Eberl, J. Auerswald, J. Luminescense, 80, 491 (1999)
[3] N. Usami, Y. Shiraki, S. Fukatsu, Semicond. Sci. Technol., 12, 1596 (1997).

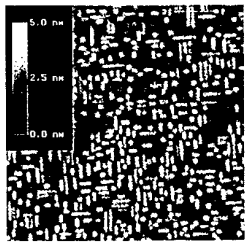

Figure 1

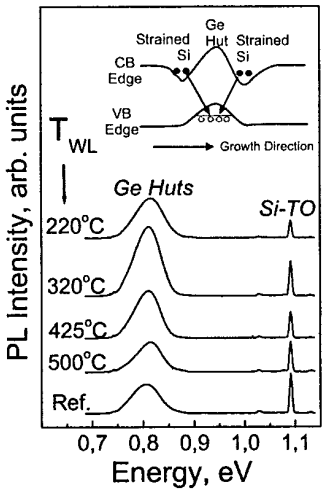

Figure 2

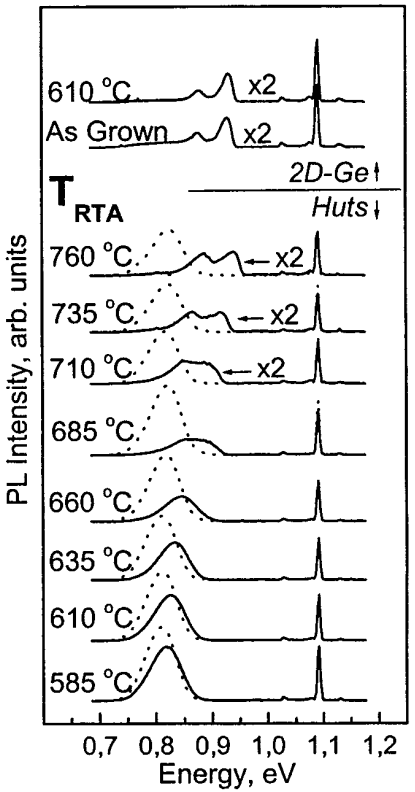

Figure 3

Figure 1) 1x1 μm^2 Atomic Force Microscopy image of 5 monolayer total Ge deposition with T_{WL}= 360 °C. The height scale, shown as an inset, is 5.0nm.

Figure 2) 8K PL spectra of 5 ML-total Ge deposition, grown for various values of T_{WL}. A reference Ge hut sample grown at 500 °C, which experienced no growth interruption required for temperature ramping, is included. The inset depicts a simplified band diagram of inhomogeneous-tensile strained Si above and below a compressively strained Ge hut.

Figure 3) 8K PL of Ge hut samples grown at T_{WL} = 320 °C before (dotted) and after (dashed) selected one minute anneals at T_{RTA}. The top two spectra show before and after spectra of the same sample structure grown with reduced total Ge thickness, so that Ge huts have not formed. The spectrum of this two-dimensional structure does not exhibit an observable difference after a 610 °C anneal.

Corresponding Author: *Michael W. Dashiell, Max-Planck-Institut für Festkörperforschung, Heisenbergstrasse 1, 70569 Stuttgart, Germany. . Phone +49 (0)711-1313, Fax +49(0)711-2931. Email: dashiell@servix.mpi-stuttgart.mpg.de*

Improvement in photoluminescence efficiency of $Si_{1-x}Ge_x$ alloy nanocrystals embedded in SiO_2 matrices by P doping

Kimiaki Toshikiyo[1], Masakazu Tokunaga[1], Shingi Takeoka[1], Minoru Fujii[2], and Shingi Hayashi[1,2]

[1] Graduate School of Science and Technology, Kobe University, Rokkodai, Nada, Kobe 657-8501, Japan

[2] Department of Electrical and Electronics Engineering, Faculty of Engineering, Kobe University, Rokkodai, Nada, Kobe 657-8501, Japan

Si nanocrystals (*nc*-Si) show efficient luminescence in near-infrared to visible regions due to the quantum confinement effects. However, even for *nc*-Si several nanometers in diameter, the indirect bandgap nature of bulk Si crystal is highly preserved. This results in a relatively long luminescence lifetime (small optical transition oscillator strength). This long lifetime is one of the obstacles to realizing Si-based light-emitting devices. $Si_{1-x}Ge_x$ alloy formation is one technique for enhancing the optical transition oscillator strength. In fact, the shortening of the radiative lifetime with increasing Ge concentration has been demonstrated for $Si_{1-x}Ge_x$ alloy nanocrystals (*nc*-$Si_{1-x}Ge_x$) in SiO_2 matrices [1] and porous $Si_{1-x}Ge_x$. However, the formation of *nc*-$Si_{1-x}Ge_x$ is often accompanied by the degradation of bandedge PL efficiency [2]. Electron spin resonance (ESR) studies revealed that the degradation is caused by the generation of Ge dangling bonds (Ge P_b centers)at the interfaces between *nc*-$Si_{1-x}Ge_x$ and SiO_2 matrices [3]

The purpose of this work is to propose a new method for eliminating the dangling-bond defects and improve the photoluminescence (PL) efficiency. The method is the electrical termination of dangling bonds by P doping. This method has been proved to be effective for the system containing *nc*-Si and SiO_2 matrices [4].

The samples studied are *nc*-$Si_{0.7}Ge_{0.3}$ in SiO_2 or phosphosilicate glass (PSG) matrices prepared by cosputtering and postannealing. During the growth of nanocrystals by postannealing, P atoms are incorporated into nanocrystals. The diameter of nanocrystals are fixed to at about 4 nm, and the P concentration [C_p (mol%)] was changed from 0 to 0.91 mol%. Figure 1(a) shows the room temperature PL spectra of *nc*-$Si_{0.7}Ge_{0.3}$ with various C_p. PL peaks are observed at around 1.44 eV, which corresponds to the exciton PL in *nc*-$Si_{0.7}Ge_{0.3}$. The integrated intensity of the PL is shown in Fig. 1(b). With increasing C_p, the PL intensity first increases and then decreases. The maximum PL intensity obtained at C_p=0.63 mol% is by a factor of 14 larger than the PL intensity of *nc*-$Si_{0.7}Ge_{0.3}$ in SiO_2 (without P doping). The intensity is nearly the same as that of *nc*-Si. Figure 1(c) shows the integrated intensities of the ESR signals for the Si and Ge P_b centers as a function of C_p. The intensities are derived by deconvoluting the ESR spectrum into two Lorentzian functions. The intensity of the signal from Ge P_b centers decreases rapidly with increasing C_p, while that from Si P_b centers is almost constant at low C_p range, and then decreases gradually with further increasing C_p.

Figure 1(c) clearly shows that both Si and Ge P_b centers are passivated by P doping. The passivation is considered to be made electrically, i.e., electrrons supplied by P doping are trapped by P_b centers and inactivate the centers. In Fig. 1(c), the quenching of the signal from Ge P_b centers is much faster than that from Si P_b centers. This result

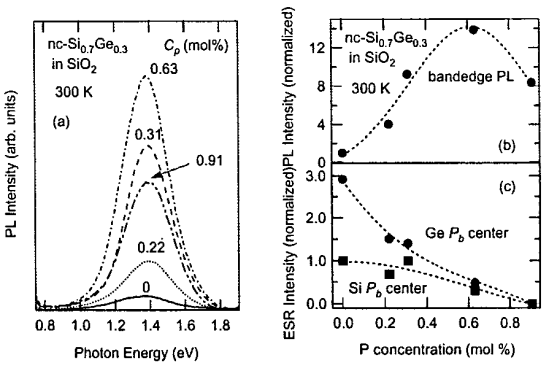

Figure 1: (a) PL spectra of *nc*-$Si_{0.7}Ge_{0.3}$ with various C_p (a) at room temperature. (b) PL intensities of the 1.44 eV peaks, and (c) the integrated intensities of the ESR signals from Si and Ge P_b centers as a function of C_p.

indicates that electrons supplied by P doping are preferentially captured by Ge P_b centers and inactivate the centers. After completing the passivation of Ge P_b centers, passivation of Si P_b centers starts. The decrease in the number of the P_b centers results in the drastic improvement in the PL efficiency.

By further increasing C_p, the PL intensity decreases. In this range, optical absorption due to the intravalley transitions of free electrons generated by P doping appears. The generation of free electrons and the resultant three-body Auger interaction between photogenerated excitons and electrons supplied by P doping is considered to be responsible for the observed PL quenching.

References

[1] M. Fujii, D. Kovalev, J. Diener, F. Koch, S. Takeoka, and S. Hayashi, J. Appl. Phys. **88**, 5772 (2000).

[2] S. Takeoka, K. Toshikiyo, M. Fujii, S. Hayashi, and K. Yamamoto, Phys. Rev. B **61**, 15988 (2000).

[3] K. Toshikiyo, M. Tokunaga, S. Takeoka, M. Fujii, and S. Hayashi, J. Appl. Phys. (in press).

[4] M. Fujii, A. Mimura, S. Hayashi, and K. Yamamoto, J. Appl. Phys. **75**, 184 (1999).

Corresponding author: Minoru Fujii, Department of Electrical and Electronics Engineering, Faculty of Eng., Kobe Univ., Rokkodai, Nada, Kobe 657-8501, Japan
phone & Fax: +81 78 803 6081, email: fujii@eedept.kobe-u.ac.jp

Excitation of Nd^{3+} and Tm^{3+} by the energy transfer from Si nanocrystals

K. Watanabe[1], H. Tamaoka[1], M. Fujii[2] and S. Hayashi[1,2]

[1] Graduate School of Science and Technology, Kobe University, Rokkodai, Nada, Kobe 657-8501, Japan

[2] Department of Electrical and Electronics Engineering, Faculty of Engineering, Kobe University, Rokkodai, Nada, Kobe 657-8501, Japan

It has recently been demonstrated that Si nanocrystals (nc-Si) can be used as a good sensitizer for rare-earth ions in glass material. In particular, the efficient energy transfer from nc-Si to Er^{3+} has been attracting much interest. Rare-earth ions have discrete electronic states. Furthermore, nc-Si has atomic-like discreate electronic states due to the zero-dimensional quantum size effects and the band-gap energy increases with decreasing the size. Therefore, the interactions between $4f$ shell electrons in rare-earth ions and nc-Si should depend on the size. However, only a few works have been done on the size dependence of the interactions. In this work, we have studied the interactions between Nd^{3+} (Tm^{3+}) and nc-Si with various average sizes. We will demonstrate that only nc-Si which are small than a threshold size can excite Nd^{3+} (Tm^{3+}).

The samples studied are SiO_2 films containing nc-Si and Nd (Tm) prepared by a cosputtering method. Figure 1(a) and 1(b) show the room temperature PL spectra of Nd and Tm doped SiO_2 films containing nc-Si, respectively. The insets show the energy diagrams of the $4f$ shell of Nd^{3+} and Tm^{3+}. The size of nc-Si (d_{Si}) is changed from 3.8 to 2.7 nm. Nd and Tm concentrations are fixed at 0.18 and 1.41 at.%, respectively.

First, we discuss PL properties of the Nd doped samples (Fig.1(a)). For the sample with d_{Si} = 3.8 nm, we can see a peak at around 1.25 eV. This peak corresponds to the recombination of excitons in nc-Si (nc-Si PL). Nd related peaks can not be detected. As the size decreases, the nc-Si PL peak is shifted toward higher energy. The high energy shift is accompanied by the appearance of new peaks at 0.87, 1.12 and 1.36 eV. These peaks correspond to the intra-$4f$ shell transitions of Nd^{3+} ($^4F_{3/2}$ to $^4I_{13/2}$, $^4F_{3/2}$ to $^4I_{11/2}$ and $^4F_{3/2}$ to $^4I_{9/2}$, respectively). The intensities of these peaks depend strongly on the size of nc-Si. These results imply that the band-gap widening of nc-Si arising from the quantum size effects make the excitation of Nd^{3+} to the forth excited state possible, resulting in the strong PL.

Very similar properties are observed for Tm doped samples (Fig.1(b)). For the sample with the largest nc-Si, Tm^{3+} peaks cannot be detected. As the size decreases, a new peak appears at 0.69 eV due to the intra-$4f$ shell transition of Tm^{3+} ($^3H_4$ to $^3H_6$). In particular, the decrease in the size from 3.1 to 2.7 nm, i.e., the high-energy shift of the nc-Si PL peak from 1.45 to 1.60 eV, causes a drastic increase in the 0.69 eV PL intensity (more than a factor of 10). The strong size dependence indicates that only excitons in nc-Si with the exciton energy of around larger than 1.60 eV can interact mainly with the 4f shell of Tm^{3+}. This energy is very close to the energy difference (1.57eV) between the third excited state ($^3F_4$) and the ground state ($^3H_6$) of Tm^{3+}. Therefore, Tm^{3+} is considered to be excited to the third excited state by the energy transfer from nc-Si. In fact, in the case of the sample with the smallest nc-Si, a week peak can be seen at 1.57 eV

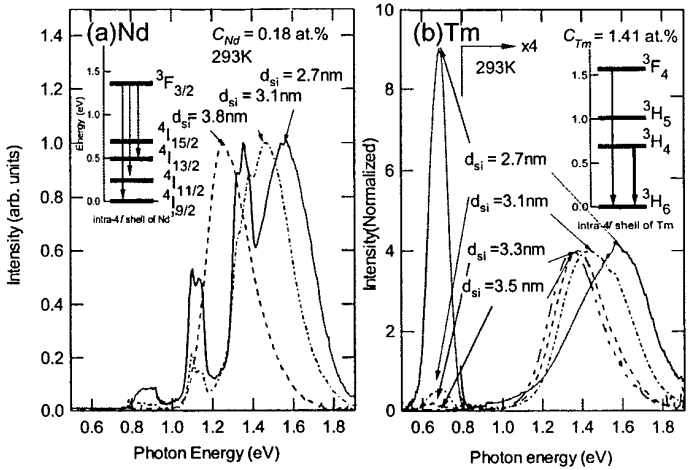

Figure 1: The room temperature PL spectra of Nd doped SiO_2 films containing nc-Si (a) and that of the Tm doped one (b). The insets show the energy diagrams of the $4f$ shell of Nd^{3+} and Tm^{3+}. The size of nc-Si (d_{Si}) was changed from 3.8 to 2.7 nm. Nd and Tm concentrations were fixed at 0.18 and 1.41 at.%, respectively.

due to the $^3F_4$ to $^3H_6$ transition. In the low temperature PL measurement, specroscopic evidence for the energy transfer from nc-Si to the third state of Tm^{3+} was obtained. The detail excitation mechanisms of Nd^{3+} and Tm^{3+} by the energy transfer from nc-Si are discussed.

References

[1] M. Fujii, M. Yoshida, S. Hayashi and K. Yamamoto, Appl. Phys. Lett. **71**, 1198 (1997).

[2] M. Fujii, M. Yoshida, S. Hayashi, and K. Yamamoto, J. Appl. Phys. **84**, 4525 (1998)

Corresponding author: Minoru Fujii, Department of Electrical and Electronics Engineering, Faculty of Eng., Kobe Univ., Rokkodai, Nada, Kobe 657-8501, Japan
phone & Fax: +81 78 803 6081, email: fujii@eedept.kobe-u.ac.jp

Gated wires and interferometers based on Si/SiGe heterostructures.

O.Estibals[1,4], Z.D.Kvon[1,2], J.C.Portal[1,3,4], A.Y.Plotnikov[2], J.L.Gauffier[4], N.J.Woods[5], J.Zhang[6], J.J.Harris[6]

[1]GHML, MPI-FKF/CNRS, BP 166, F-38042, Grenoble Cedex 9, France
[2]Institute of Semiconductor Physics, 630090 Novosibirsk, Russia
[3]Institut Universitaire de France, 103 Bd.St.Michel 75005 Paris
[4]INSA 135 Avenue de Rangueil 31077 Toulouse Cedex 4
[5]Imperial College of Science London SW7 2BW, UK
[6]University College London, WC15 75E, UK

We report the fabrication and study of the Si/SiGe gated quantum wires and interferometers. The initial samples were n-type modulation doped $Si/Si_{1-x}Ge_x$ heterostructures with two-dimensional electron gas (2DEG) situated in an 11 nm thick silicon quantum well. Mobility was $\mu = 5\cdot10^4 cm^2/V\cdot s$ at an electron density $N_s = 7.3\cdot10^{11} cm^{-2}$ After growth by means of MBE of this heterostructure and fabrication of Hall bars (with length 100 micron and width 50 micron) on its top, a 50 nm thick SiO_2 layer was evaporated. Then contacts to the 2DEG were made by means of ion implantation of phosphorous. Final contacts preparation was made by means of evaporation of Al on ion-implanted regions. Wires and interferometers were fabricated using electron beam lithography and anisotropic ion etching. The lithographic dimensions of the wire were the following: length L = 5 μm and width W = 0.5 μm. The inner diameter of the interferometer was d_{in} = 0.3 μm and the outer d_{out} = 0.8 μm. Finally a TiAu metallic gate was evaporated on the top of the structures. Negative magnetoresistance (NMR) or positive magnetoconductivity (PMC) connected with weak localization effects in the wires and Aharonov-Bohm oscillations in the ring were investigated in the temperature range 30 mK – 5 K. At zero gate voltage (V_g =0) the wire was closed and it opened at V_g = 50 mV. It means that there is a quite wide depletion layer of thickness d ≈ 0.1 μm - 0.2 μm in our structures. Figure 1 shows the typical results of NMR measurements. The rough estimation of the effective wire width from the wire resistance gives the values W = 0.1 – 0.2 μm. It is less than mean free path of the electrons l = 0.5 μm – 1 μm. Thus we have quasi-ballistic wires where l > W and l << L. The theory of weak localization PMC for such a situation has been developed in [1]. It gives for PMC the following expression in weak magnetic field (magnetic length $L_H^2 >> Wl$).

$$\Delta\sigma(B) = -(4e^2/h)\cdot(1/L)\cdot\left([1/L_\varphi^2 + 1/L_B^2]^{-1/2} - [1/L_\varphi^2 + 1/L_B^2 + 1/l^2]^{-1/2}\right) \quad (1)$$

where L_φ is the phase coherence length, $L_B = \sqrt{D\cdot\tau_B}$ (D is the diffusion constant, $\tau_B = (9.5L_H^4)/(W^3 v_F)$, v_F is the Fermi velocity). Figure 1 shows the typical results of PMC measurement in the wires that we studied. PMC calculated according to the above formula are presented in this figure too. This shows a quite a good agreement between the experiment and the theory. It is necessary to note that the fitting of expression (1) to experimental PMC curve gives access to the effective wire width W. In our case we have obtained W = 0.2 μm. This value is in a good agreement with the estimation made from wire resistance. It means that boundary scattering in our wires is specular. Thus one can conclude that the weak localization NMR in Si/SiGe wires is well described by the theory [1]. It gives the possibility to determine the phase coherence time in the wire. A very weak temperature dependence of τ_φ was found. Aharonov-Bohm oscillations measured in Si/SiGe ring are shown in figure 2 (they are clearly seen at B > 0.25 T). As seen from this figure the amplitude of these oscillations proved to be small in comparison with AlGaAs/GaAs rings even at T = 30 mK. It supposed that it is due to insufficiently large phase coherence time at low temperatures because of its very weak temperature dependence in Si/SiGe wires. The probable reasons of such their behavior are analyzed.

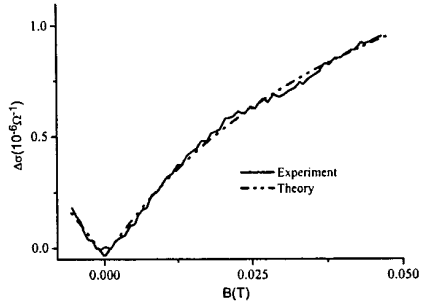

Figure 1: The example of the experimental and calculated PMC curves for Si/SiGe wire. The experimental curve was measured at T = 1 K, (V_g = 0.09 V). The fitting parameters for calculated curve were the following: W = 0.19 μm, $\tau_\varphi = 1.5\cdot10^{-11}$ c. The diffusion constant D, Fermi velocity v_F and mean free path l were found from the measurements of SdH oscillations.

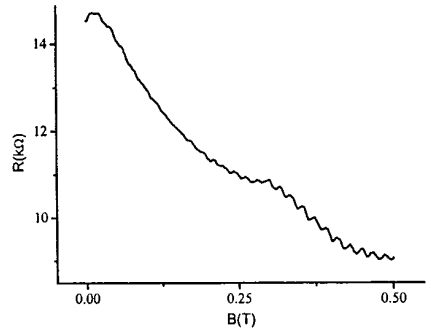

Figure 2: Magnetoresistance of Si/SiGe ring at 30 mK (V_g = 0.06 V).

References

[1]C.W.J.Beenakker and H. van Houten, Phys.Rev. **B 38**, 3232 (1988)

Corresponding author: Olivier Estibals, GHML, MPI-FKF/CNRS, BP 166, F-38042, Grenoble Cedex 9, France
Phone 33-4-7688-1057, Fax: 33-476855610
e-mail: estibals@labs.polycnrs-gre.fr

Fabrication of Si/SiGe quantum point contacts by electron-beam lithography and shallow wet-chemical etching

U. Wieser[1], U. Kunze[1], K. Ismail[2], J.O. Chu[2]

[1] Institut für Werkstoffe der Elektrotechnik, Ruhr-Universität Bochum, D-44780 Bochum, Germany
[2] IBM Thomas J. Watson Research Center, Yorktown Heights, New York 10598, USA

We present a low-damage processing technique for fabricating quantum point contacts (QPCs) in the two-dimensional electron gas (2DEG) of a strained Si/SiGe heterostructure. The result is a QPC conductance characteristic which at $T = 4.2$ K exhibits a series of smeared step-like features each of them contributing $4e^2/h$.

The QPCs were fabricated from a modulation doped $Si/Si_{0.7}Ge_{0.3}$ heterostructure consisting of an 8.5-nm-thick Si quantum well on a graded SiGe buffer, followed by a 14-nm-thick SiGe spacer, an 11-nm-thick SiGe supply layer, and a 4-nm-thick Si capping layer. At $T = 1.2$ K the electron density in the 2DEG is 5.4×10^{11} cm^{-2} and the mobility is 2.9×10^5 cm^{2}V^{-1}s^{-1}. A lateral confining potential is created by an etched groove with a break w of about 100 nm, which is positioned at the mesa center of a field-effect device. An evaporated Ni/Au layer covering the constriction and the surrounding 2DEG served as gate electrode. Unlike earlier split-gate devices [1] the present QPC benefits from a particular narrow confinement due to both the groove structure and the separation of only 29 nm from the surface to the 2DEG. The groove pattern was written by electron-beam lithography in PMMA resist. In order to obtain a low-damage pattern transfer we pursued wet-chemical etching instead of reactive ion etching. Even low-damage dry etching [2] is known to result in a combined lateral dead layer of at least 130 nm, which thus represents a lower bound for normally-on QPCs. Optimum masking capability of the resist and reliable pattern transfer is achieved by successively applied selective etching [3]. At first the PMMA pattern is transferred into a $1-2$ nm SiO_2 layer, subsequently into the Si, and finally into the SiGe layer, where the selectivity of the Si (SiGe) etching solution with respect to SiGe (Si) is about 20. Particular difficulties arise from dislocations and from the nearly isotropic etching characteristic of the SiGe etchant. While grooves transferred into bulk Si show smooth edges and a width equal to the mask dimensions the edges are rougher in the Si cap layer and the line width increases during SiGe etching (figure 1). Prolonged SiGe etching leads to large defects or even to surface roughening. A SiGe etch depth of 9 nm was chosen for fabricating the QPCs. In a device with a continuous line this depth proved to isolate the electron channel at $T = 4.2$ K up to gate voltages in excess of 0.8 V (figure 2). A QPC with 120 nm geometric SiGe width shows an abrupt threshold shifted by about 0.2 V compared with a device without constriction. The differential conductance of the QPC increases gradually with gate voltage imposed by a series of shoulders, each of them representing a step of $4e^2/h$ height. Additionally the lowest shoulder shows a step-like feature at about $2e^2/h$. These characteristics are reproducible from different samples and stable against cooling cycles.

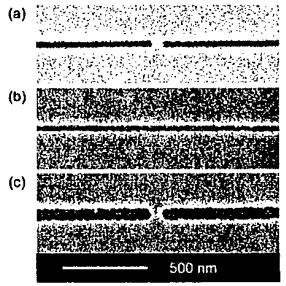

Figure 1: Top-view scanning electron micrographs of grooves transferred into (a) bulk Si, (b) the Si capping layer of a Si/SiGe heterostructure, and (c) the Si capping layer and SiGe supply layer of a Si/SiGe heterostructure. The break in (a) and (c) amounts to $w \approx 80$ nm.

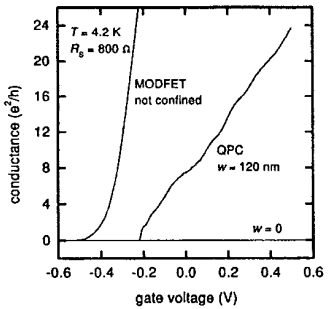

Figure 2: Differential conductance of a modulation doped field-effect transistor (MODFET), a QPC ($w \approx 120$ nm), and a device with a single barrier formed by a continuous line ($w = 0$) measured at $T = 4.2$ K. A series resistance of $R_S = 800\ \Omega$ has been subtracted.

References

[1] D. Többen et al., Semicond. Sci. Technol. **10**, 711 (1995).
[2] K.Y. Lee et al., Microelectron. Eng. **35**, 33 (1997).
[3] U. Wieser et al., Semicond. Sci. Technol. **15**, 862 (2000).

Corresponding author: Ulrich Wieser, Institut für Werkstoffe der Elektrotechnik, Ruhr-Universität Bochum, D-44780 Bochum, Germany.
phone: +49 234 32 26515, Fax: +43 234 32 14166,
email: uli@lwe.ruhr-uni-bochum.de

Si-based light emission from Ge-implanted SiO_2 layers: Electric and optoelectronic properties

L. Rebohle, T. Gebel, J. von Borany, W. Skorupa, M. Helm

Institut für Ionenstrahlphysik und Materialforschung, Forschungszentrum Rossendorf
01314 Dresden, Germany

Due to its indirect band gap, Si is known to be a notoriously bad light emitter. Since compound semiconductors, on the other hand, are hard to integrate with current Si technology, there is an intense quest for alternative, Si-based light emitting structures and devices. Here we present an efficient blue-light emitter, fabricated by Ge ion implantation into SiO_2, a process which is fully compatible with Si microelectronic technology.

SiO_2 films with a thickness between 130 and 500 nm were thermally grown at 1000°C on [100]-oriented, n-type Si substrates. The oxide films were implanted with Ge ions resulting in a Gaussian implant profile with a peak Ge concentration ranging between 0.3 and 3 %. After implantation, rapid thermal annealing (RTA) at 1000°C was performed with annealing times between 1 s and 30 s. Formation of Ge nanoclusters is observed under these conditions. Metal-oxide-semiconductor (MOS) device structures for electroluminescence (EL) studies were prepared using transparent, sputtered 80 nm thick layers of indium tin oxide (ITO) and Al as top and bottom electrodes, respectively.

Fig. 1a displays the normalized EL and photoluminescence (PL) spectrum of a 200 nm thick Ge-implanted SiO_2 layer containing 3 % Ge after RTA for 30 s, which were recorded using an external electric field of 7.15 $MVcm^{-1}$ and an excitation wavelength of 240 nm (5.17 eV), respectively. Both spectra are peaked in the violet spectral region at 3.18 eV (390 nm) and, apart from a marginally broader width of the EL peak, the spectra are almost identical. This implies that the PL and EL is caused by the same luminescence center and that the emission mechanism is identical. Fig. 1b shows the EL of the same device for different injection current densities on a logarithmic scale. Obviously the shape of the spectrum does not change at all with the injection current. Furthermore, the EL intensity exhibits a linear dependence on the injection current over 3 orders of magnitude. The best devices exhibit a power efficiency of up to 0.5 %, which is one of the best in the field of Si-based light emission.

In previous investigations [1,2] we found that the violet PL of Ge-implanted layers was caused by an oxygen deficiency center. The energy level scheme of such a center consists of a singlet ground state S_0, a singlet first excited state, S_1, and a triplet first excited state, T_1. The blue-violet PL is caused by optical excitation from S_0 to S_1, followed by intersystem crossing to T_1 and a radiative transition back to S_0. The radiative transition $T_1 \rightarrow S_0$ is also the origin of the observed EL. In the case of EL there are several possible mechanisms to populate the T_1 state, which will be discussed together with the corresponding results of the transport measurements.

Based on this blue light emitter, the first integrated Si-based optocoupler (Fig. 2) is demonstrated [3]. The emitter consists of a thin, Ge-implanted oxide layer on Si, which is galvanically separated by a thick oxide layer from the receiver. The receiver consists of a pin-diode made of amorphous silicon, which was deposited using a cluster tool for CVD processes. The receiver signal current exhibits a linear dependence on the emitter current over more than two orders of magnitude. The integrated optocoupler can be used as a sensor in microsystems or for integrated applications in biotechnology.

Presently our investigations are aimed at establishing whether optical gain [4] in the blue spectral region can be achieved with the present structures.

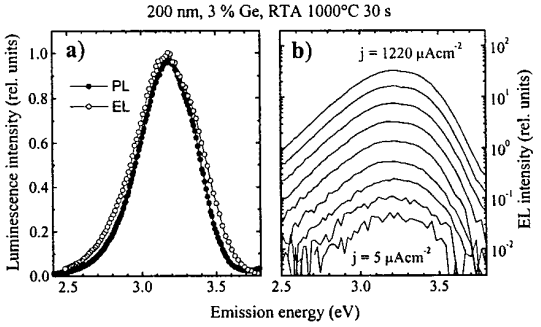

Fig. 1: The PL and EL spectrum of a 200 nm thick Ge-implanted oxide layer containing 3 % Ge in comparison (a). Whereas the shape of the EL spectrum does not change with the injection current density (b), the EL intensity shows a linear dependence on it.

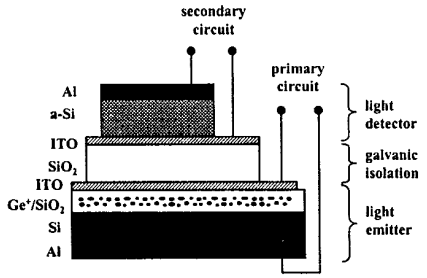

Fig. 2: Schematic structure of the integrated optocoupler consisting of a light emitter based on Ge-implanted SiO_2 layers and a light detector made of amorphous Si. Emitter and detector are galvanically isolated by a thick and transparent oxide layer.

References

[1] L. Rebohle, J. von Borany, H. Fröb, W. Skorupa, Appl. Phys. B **71**, 131 (2000).
[2] L. Rebohle, J. von Borany, W. Skorupa, H. Fröb, S. Niedermeier, Appl. Phys. Lett **77**, 969 (2000).
[3] T. Gebel, W. Skorupa, J. von Borany, L. Rebohle, D. Borchert, W. Fahrner, German Patent pending, reference number 100 11 258.7
[4] L. Pavesi, L. Dal Negro, C. Mazzoleni, G. Franzo, F. Priolo, Nature **408**, 440 (2000), and F. Priolo et al., this conference

Corresponding author: Lars Rebohle, Institut für Ionenstrahlphysik und Materialforschung, Forschungszentrum Rossendorf, Postfach 510119, 01314 Dresden, Germany
phone: +49 351 260 3674, fax: +49 351 260 3411
email: rebohle@fz-rossendorf.de

Fabrication of strain-balanced $Si_{0.73}Ge_{0.27}$/Si distributed Bragg reflectors on Si substrates for optical device applications

K. Kawaguchi[1], S. Koh[1], Y. Shiraki[1], and J. Zhang[2]

[1]Research Center for Advanced Science and Technology (RCAST), The University of Tokyo, 4-6-1, Komaba, Meguro-ku, Tokyo 153-8904, Japan

[2]Centre for Electronic Materials and Devices, Imperial College of Science, Technology and Medicine, Blackett Laboratory, Prince Consort Road, London SW7 2BW, UK

Strain-balanced $Si_{0.73}Ge_{0.27}$/Si distributed Bragg reflectors (DBRs) which were designed to overcome the limitation of the number of pairs originating from the strain accumulation were successfully fabricated, and their structural and optical properties were investigated.

The samples were grown on Si(001) substrates by gas-source molecular beam epitaxy. Relaxed $Si_{0.89}Ge_{0.11}$ virtual substrates with the thickness of about 2 μm were grown at 680 C by means of a standard graded buffer technique followed by an annealing at 800 C. On the virtual substrate, quarter-wavelength-thick Si and $Si_{0.73}Ge_{0.27}$ layers were grown alternatively. The 11 pair DBR was grown at 620 C, and the growth rate was about 1.3 Å/s and 2.7 Å/s for Si and $Si_{0.73}Ge_{0.27}$, respectively. For 25 pair DBR, the growth temperature was raised to 660 C in order to increase the growth rate, *i.e.* 3.3 Å/s and 4.2 Å/s for Si and $Si_{0.73}Ge_{0.27}$, respectively.

Figure 1 shows Raman spectra of the 11 and 25 pair DBRs. Two significant peaks that are assigned as Si-Si vibrations in Si and $Si_{0.73}Ge_{0.27}$ layers of DBR can be seen around 520 cm^{-1} in the spectrum of the 11 pair sample. As compared with Si-Si vibrations in (unstrained) Si substrate, Si-Si vibration peak of the Si layers of DBR is located 4 cm^{-1} lower due to the tensile strain. The Raman shift of Si-Si vibration in $Si_{0.73}Ge_{0.27}$ layers is seen at 511 cm^{-1} which is about 6 cm^{-1} higher than that of relaxed $Si_{0.73}Ge_{0.27}$, indicating that $Si_{0.73}Ge_{0.27}$ layers are compressively strained. These shifts are consistent with the values estimated from the strain of the layers in a pseudomorphic regime, which implies that the strain balance is realized. Moreover, the Raman spectrum of the 25 pair sample is seen to be almost the same as that of the 11 pair sample, and it can be said that the strain balance is maintained over 4 μm. X-ray diffraction spectra also showed that both of Si and SiGe layers were almost fully strained to match the virtual substrates.

Figure 2 shows reflectivity spectra of the 25 pair mirror sample. A record reflectivity of 80% was achieved at 1.44 μm. A large improvement of the reflectivity was realized compared with conventional SiGe/Si DBRs on Si substrates, and the reflectivity obtained here was almost the same as a calculated value. It should be noted here that the loss of reflectivity due to the deterioration of the crystalline quality coming from strain accumulation is hardly seen. These results indicate that this DBR can be applied to such optical devices as resonant cavity Ge photodetectors though the surface roughness of the 25 pair sample was increased to about 46 nm compared with 6.3 nm of the 11 pair sample.

In conclusion, the strain balance technique is a promising way to fabricate SiGe/Si DBRs with high reflectivity and develop novel opto-electronic devices on Si substrates. By optimizing the growth condition, the modulated luminescence from Si/SiGe quantum wells with strain-balanced DBRs was also observed, which will be demonstrated at the conference.

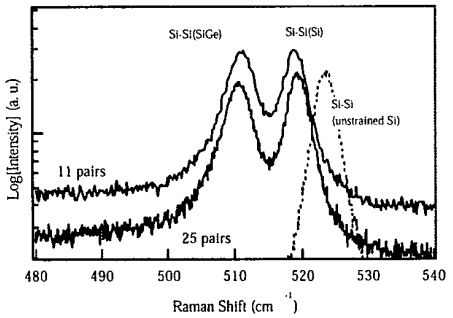

Fig. 1. Raman spectra of 11 and 25 pair $Si_{0.73}Ge_{0.27}$/Si DBR.

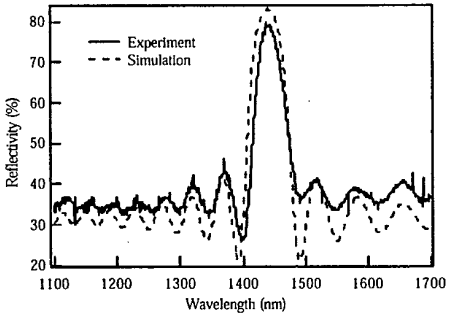

Fig. 2. Reflectivity spectrum of the strain-balanced SiGe/Si DBR with 25 pair mirrors.

Corresponding author: Kenichi Kawaguchi, Research Center for Advanced Science and Technology, The University of Tokyo, 4-6-1, Komaba, Meguro-ku, Tokyo 153-8904, Japan,
Phone: +81-3-5452-5096, Fax: +81-3-5452-5093,
email: kawaguti@photonics.rcast.u-tokyo.ac.jp

The advantages of p-type and design methodologies for $Si_{1-x}Ge_x$ far-infrared (Terahertz) quantum well infrared photodetectors (QWIPs)

M. A. Gadir[1], P. Harrison[1] and R. A. Soref[2]

[1]*IMP, School of Electronic and Electrical Engineering, The University of Leeds, LS2 9JT, U.K.*
[2]*Sensors Directorate, AFRL/SNHC, Air Force Research Laboratory, Hanscom Air Force Base, MA 01731, U.S.A.*

This work is motivated by the desire to extend the operating wavelength of contemporary quantum well infrared photodetectors (QWIPs)[1] from the mid- ($< 14\mu$m) to the far-infrared ($> 20\mu$m) or Terahertz region of the electromagnetic spectrum without recourse to liquid helium temperatures[2]. This apparently simple objective hides many challenges which stem from the parasitic current that flows even in the absence of any illumination—the so-called *dark current*.

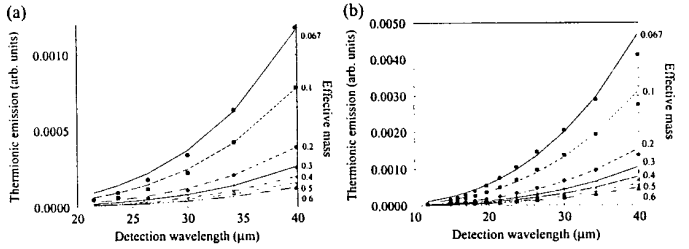

Figure 1: Calculations of the relative strength of the thermionic emission as a function of the detection wavelength (and for several different effective masses) for conventional bound-to-continuum $GaAs/Ga_{0.7}Al_{0.3}As$ QWIPs at (a) 100 K and (b) 300 K. The solid lines represent (a) λ^4 and (b) λ^2 fits to the data.

The dark current originates from three different carrier scattering processes[3]. Device designers have been able to effectively eliminate the contribution from sequential tunnelling of carriers from one quantum well into the next, and in addition, as field induced emission (ionisation) tends to be important only at fields higher than the typical operating conditions, then the major contributor to the dark current noise is from thermionic emission. The latter processes consists of thermal excitation of carriers out of the quantum well and increases with the temperature and as the bound state of the QWIP approaches the top of the barrier—as will need to occur if QWIPs are to work at longer wavelengths.

The calculated data in Fig 1 illustrates just how dramatic this increase in the thermionic emission is as a function of the detection wavelength λ of a device (varied by changing the quantum well width). In our model[3], the thermionic emission increases as λ^4 at 100 K, though interestingly this decreases to λ^2 at 300 K, see Figs. 1 (a) and (b) respectively. The λ^4 dependence at the common liquid nitrogen operating temperatures will be a major hindrance to the development of far-infrared (Terahertz) QWIPs.

One solution could be to increase the effective mass, m^*, of the charge carrier, which could mean considering p-type rather than the usual n-type material. The effect of increasing the effective mass, from the usual $0.067m_0$ for electrons in GaAs, is also shown in Fig. 1. This is summarised in Fig. 2(a)—for a fixed detection wavelength the thermionic emission contribution to the dark current varies as $1/m^*$.

Thus a move from n-type to p-type GaAs based devices could reduce the dark current by an order of magnitude—this would be one way to offset the increased noise as the detection wavelength of the devices is increased.

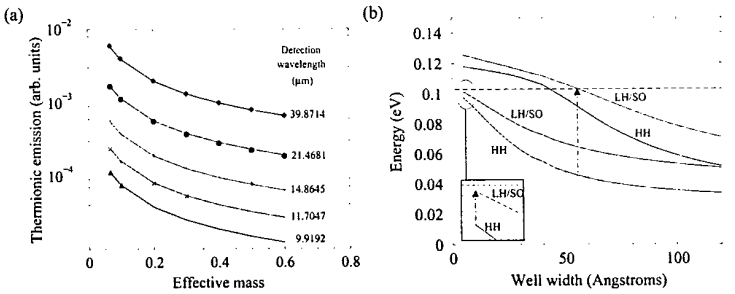

Figure 2: (a) Calculations of the relative strength of the thermionic emission as a function of the effective mass, for several different detection wavelengths, for $GaAs/Ga_{0.7}Al_{0.3}As$ quantum wells at 300 K. The solid lines are $1/m^*$ fits to the data and (b) 8-band **k.p** calculations of the subband structure of a strain-balanced $Si_{0.9}Ge_{0.1}$ quantum well surrounded by Si barriers, at 77 K. The letters (HH, LH and SO) indicate the character (heavy-hole, light-hole and split-off) of the subband at the zone centre.

A by-product of such a change in design philosophy would be the option of normal-incidence absorption, without the need for surface gratings, by employing a heavy- to light-hole interband absorption in a bound-to-quasibound configuration. Fig. 2(b) illustrates how this might be achieved in the $Si_{1-x}Ge_x/Si$ material system. The figure shows example results of an 8-band **k.p** calculation of a strain-balanced multi-quantum-well (grown on a relaxed $Si_{1-y}Ge_y$ buffer) with a 10% Ge content surrounded by Si barriers. The arrows on the figure indicate that, for this Ge content, there are just two quantum well widths that produce light-hole subbands which are sufficiently close to the top of the well (as indicated by the dashed horizontal line) to be used in a bound-to-quasi-bound device. Inspection of the figure shows that these widths are at 5 and 55 Å which give detection wavelengths of 310 and 21 μm respectively.

Acknowledgements—The authors would like to thank the USAF European Office of Aerospace Research and Development (EOARD), grant reference F61775-01-WE007, for financial support.

References

[1] B. F. Levine, A. Zussman, S. D. Gunapala, M. T. Asom, and J. M. Kuo ad W. S. Hobson. Photoexcited escape probability, optical gain, and noise in quantum well infrared photodetectors. *J. Appl. Phys.*, 72:4429, 1992.

[2] A. G. U. Perera, W. Z. Shen, S. G. Matsik, H. C. Liu, M. Buchanan, and W. J. Schaff. GaAs/AlGaAs quantum well photodetectors with a cutoff wavelength at 28 μm. *Appl. Phys. Lett.*, 72:1596, 1998.

[3] N. E. I. Etteh and P. Harrison. Carrier scattering approach to the origins of dark current in mid- and far-infrared (terahertz) quantum-well intersubband photodetectors (QWIPs). *IEEE J. Quan. Elec.*, 2001. accepted.

Corresponding author: Mazin Gadir,
IMP, School of Electronic and Electrical Engineering,
The University of Leeds, LS2 9JT, U.K.
Tel: +44-113 233 2000 Fax: +44-113 244 9451
email: eenmag@leeds.ac.uk

Light emission from erbium doped nanostructures embedded in silicon microcavities

N.T. Bagraev[1], A.D. Bouravleuv[1], W. Gehlhoff[2], L.E. Klyachkin[1], A.M. Malyarenko[1], M.M. Mezdrogina[1], V.V. Romanov[1] and A.P. Skvortsov[1]

[1]A. F. Ioffe Physico-Technical Institute, 194021, St.Petersburg, Russia
[2]Institut für Festkörperphysik, Technische Universität Berlin, D-10623 Berlin, Germany

We present the findings of high efficient Er^{3+}-related $^4I_{13/2} \rightarrow {}^4I_{15/2}$ photo and electroluminescence from self-assembled nanostructures embedded in silicon microcavities. The silicon (100) wafers of the n- and p-type were doped with erbium in the process of long-time diffusion using surface injection of vacancies. The working and back sides of the wafers were previously oxidized. Erbium doping was done on the working side of the wafers after covering the oxide overlayer with a mask and performing the subsequent photolithography. Then, short-time diffusion of boron and phosphorus was performed from gas phase into the n- and p- type Si (100) wafers respectively using controlled surface injection of both self-interstitials and vacancies. By varying the parameters of the surface oxide overlayer and diffusion temperature (800°C÷1100°C), it was possible to define the criteria leading to the ultra-shallow n^+-p and p^+-n junctions (5 nm÷30 nm), which were controlled using the SIMS and STM techniques. Besides, the self-assembled microdefects of the self-interstitials type that penetrate through the p^+- and n^+- diffusion profiles are found to be prepared by short time impurity diffusion (Fig.1). Scanning tunneling microscopy is used to demonstrate the self-organization of these microdefects in the microcavity system (Fig.2 a) that exhibits a distributed feedback identified by the FIR transmission spectra (Fig.2 b). The cyclotron resonance (CR) angular dependencies and current-voltage (CV) characteristics brought about the deflection of the bias voltage from the normal to the p-n junction plane show that the p^+- and n^+- diffusion profiles doped preliminary with erbium consist of both self-assembled longitudinal and lateral quantum wells (SQW) embedded in silicon microcavities which were controlled using the STM and FIR techniques.

The luminescence from the quantum well embedded in microcavity is shown to be enhanced in the Rabi splitting range (Fig.2 c). The built-in electric field induced by the quantum-size p^+-n junctions is found to give rise to the Stark effect that is revealed by the intracenter emission from a residual transition metal centre incorporated into self-assembled microcavity (Fig.2 c). The optically induced EPR of single point defects embedded in the silicon microcavity appears to be observable using the FIR transmission technique in earth magnetic fields.

The erbium doped microcavities obtained have been studied using the magnetic susceptibility and FIR photo and electroluminescence techniques. The erbium-related centres inside the SQW have been found to represent the molecular defects, in which the antiferromagnetic erbium pairs bound by the exchange interaction through the action of valence electrons from three oxygen atoms. The concentration ratios between the shallow donors and erbium molecular centres that give rise to an electric and recombined activity of magnetic centers and an increase of mobility in SQW. The electrically and optically induced intraband transitions induced by tunneling processes through SQW subsequence are observed to cause the Auger excitation of the $^4I_{13/2} \rightarrow {}^4I_{15/2}$ Er^{3+}-intracenter emission enhanced in microcavities that are revealed by the Rabi splitting in the PL and EL spectral dependencies (Fig.3). The built-in electric field induced by these n^+-p and p^+-n junctions is found to result in the Stark effect that perturbes strong *sp-f* mixing due to the electron-hole localization on the Er-related centres incorporated into nanostructures. This spatial confinement of the s-p states and the localized f-electron states as well as the e-h localization at the nanostructures is shown to cause ultrafast energy transfer to the erbium-related centres thereby enhancing Er^{3+}-intracenter emission Er^{3+}-intracenter emission and squeezing the lifetime of the $^4I_{13/2} \rightarrow {}^4I_{15/2}$ transitions.

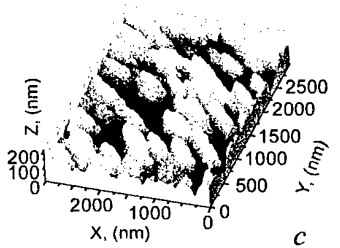

Fig. 1. STM images of the ultra-shallow boron diffusion profiles prepared at diffusion temperature of 800°C into the Si(100) wafer covered previously by thin oxide overlayer. X||[001], Y||[010], Z||[100].

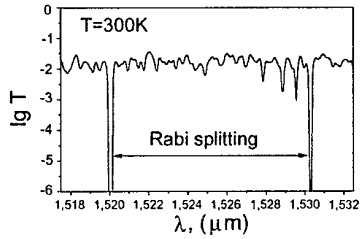

Fig. 3. Spectral dependence of the light transmission coefficient through the silicon microcavity containing the erbium-related centre.

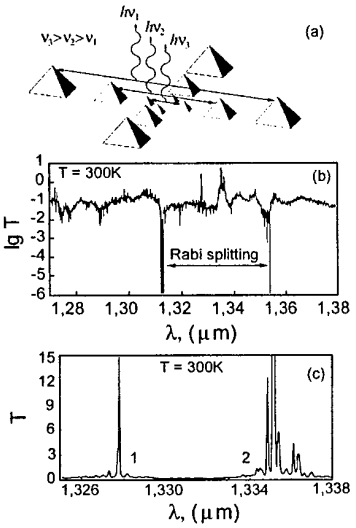

Fig. 2. The model of self-assembled microcavity systems (a) prepared on the Si (100) wafer and revealed by spectral dependence of the light transmission coefficient (b) that demonstrates the enhancement of the photoluminescence (c) from a self-assembled quantum well (1) and single residual transition metal centre (2).

corresponding author: Prof.Dr.N.T.Bagraev, A.F.Ioffe Physico-Technical Institute, 194021, St.Petersburg, Russia.
Phone 007 (812) 2479315, Fax 007 (812) 2471017
e-mail: impurity.dipole@pop.ioffe.rssi.ru

Reflection and transmission of light in the photonic-band-gap range of triangular lattice of Si nanopillars with the 500 nm period

Vladimir V. Poborchii[1], Tetsuya Tada[2] and Toshihiko Kanayama[2]

[1]Joint Research Center for Atom Technology - Angstrom Technology Partnership, 1-1-4 Higashi, Tsukuba, Ibaraki 305-0046, Japan
[2]Joint Research Center for Atom Technology - National Institute for Advanced Interdisciplinary Research, 1-1-4 Higashi, Tsukuba, Ibaraki 305-8562, Japan

Combination of the high refractive index (~ 3.5 in near infrared) and the existence of well-developed microfabrication methods make Si very promising for construction of photonic crystals (PC), in which photons can operate like electrons in semiconductors but at much higher speeds. In the last few years, significant progress in design of 2-dimensional PC made of Si took place. Most of these structures consist of periodically arranged parallel air cylinders in thin plate of bulk Si [1]. An alternative 2-dimensional PC is a lattice of parallel Si pillars surrounded by air [2,3]. Although this system is interesting for applications (for example in waveguides), it is not yet sufficiently investigated. As we show in this work theoretically and experimentally, Si-pillars-made PC has important advantages compared to other Si-made PCs.

Silicon is usually not considered as a practical material for submicrometer spectral range PCs because Si absorbs light with wavelengths shorter than ~ 1.1 μm (~ 1.1 eV). However, Si is an indirect-band-gap semiconductor with quite weak absorption in the submicrometer wavelength range (absorption coefficient $\alpha \sim 10^2$ cm^{-1} at 1.25 eV and $\alpha \sim 10^3$ cm^{-1} at 1.6 eV). Thus, absorption of light can be insignificant in PC with low volume fraction of Si f. As we show in the present paper, using Si nanopillars [2,3], one can construct 2-dimensional PC with certain small value of f, which is low enough for high transparency of PC in submicrometer range and high enough for opening quite large photonic band gap (PBG) for TM mode (light is polarized parallel to the pillars, **E//c**).

Triangular lattice of Si nanopillars (TRLN) with period of 500 nm and diameter of nanopillars ~ 85 nm studied in this work is shown in Fig. 1. The sample was prepared using the self-formed-etching-mask method combined with the electron beam lithography [2]. We have measured in-plane reflection spectra of TRLN using micro-optical technique [3]. We have also succeeded in measuring of transmission spectra of TRLN.

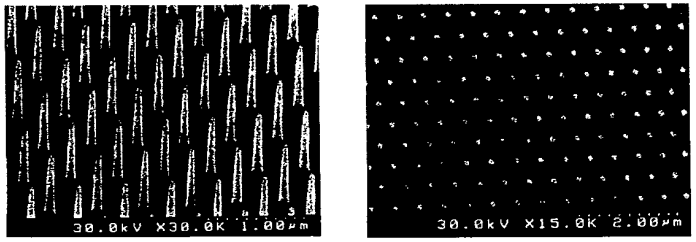

Fig.1: TRLN with period of 500 nm: view at the tilt angle of 40° (left) and top view (right).

Our calculations show that the omnidirectional photonic band gap (PBG) of TRLN with period 500 nm and pillars diameters 85 nm appears for TM mode in the submicrometer wavelength range, light losses in this range being insignificant. Our experimental data are in good correspondence with calculations. Reflection spectra for both TM and TE modes and for two different directions of the light propagation are shown in Fig. 2. In agreement with the existence of omnidirectional PBG for TM mode, the TM reflection band is observed for both Γ- X and Γ- J directions. The TE reflection band is observed only for Γ- X direction in accordance with the calculations showing that the TE mode displays PBG in the Γ- X direction and does not display PBG in the Γ - J direction (the Γ- X and Γ- J directions in the Brillouin zone of 2-dimensional triangular lattice corresponds to the vertical and horizontal directions, respectively in the top view of TRLN in Fig. 1.) Our transmission spectra data are also in agreement with the calculations and support idea about availability of Si-pillars-made PCs for the submicrometer wavelength range.

Available spectral range of Si-pillars-made PCs overlaps with the spectral range of operation of variety of light sources such as GaAs-based laser diodes, i.e. extension of the spectral range of Si PCs creates new technical opportunities for their applications.

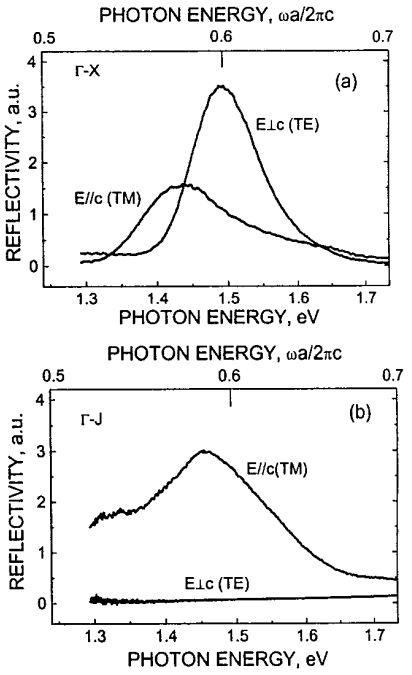

Fig.2: Reflection spectra of TRLN for two different polarizations of light and two different directions Γ- X (a) and Γ- J (b).

References

[1] U. Grüning, V. Lehmann, S. Ottow and K. Bush, Appl. Phys. Lett. 68, 747 (1996)
[2] T. Tada, V. Poborchii and T. Kanayama, Jpn. J. Appl. Phys., 38, 7253 (1999)
[3] V. Poborchii, T. Tada and T. Kanayama, Appl. Phys. Lett., 75, 3276 (1999)

Corresponding author: Vladimir V. Poborchii, JRCAT, 1-1-4 Higashi, Tsukuba, Ibaraki 305-0046, Japan
phone: +81 298 612627,
fax: +81 298 612576,
e-mail: vpob@jrcat.or.jp

Determination of the Rashba Field in modulation doped Si/SiGe Quantum Wells from Conduction Electron Spin Resonance

Z. Wilamowski[1] and W. Jantsch[2]

[1]Institute of Physics, Polish Academy of Sciences, P 02-668 Warsaw, Poland
[2]Institut für Halbleiter- und Festkörperphysik, Johannes Kepler Universität, A-4040 Linz, Austria

Some concepts for spintronics and quantum computers invoke the Rashba field, $\boldsymbol{H_R}$, [1] as a tool to manipulate the electron spin in a device by an external electric field [2]. In this contribution we show that a sizeable Rashba field appears in modulation doped Si quantum wells. We present two independent effects of $\boldsymbol{H_R}$: (i) an anisotropy of the spin resonance line width, and (ii) the anisotropy of the g-factor. In addition, both effects depend on the density of the two-dimensional electron gas (2DEG). We show that these effects can be explained consistently using a single value of α=1.1· 10^{-12} eV.cm for the Rashba parameter α.

The Rashba field is a consequence of broken mirror symmetry (axial symmetry + lack of inversion symmetry) which allows for a term $\propto \alpha.\boldsymbol{k}\cdot\ \sigma$ in the one-electron Hamiltonian [1]. Here $\boldsymbol{k}$ is the k-vector of the electron and σ its spin. The effect of this term can be described by a magnetic field $\boldsymbol{H_R}$ perpendicular to the k-vector of the electron and it lies in the 2D plane. In Si and cubic III-V compounds, this term appears only in heterostructures [3,4]. Mirror symmetry is broken in quantum wells in the presence of a perpendicular electric field, mostly because of the resulting triangular QW shape and the different penetration depth of the wave function of the 2D carriers into the barriers. This situation occurs for one-sided modulation doped quantum wells of Si embedded between $Si_{1-x}Ge_x$ barriers. On such structures the spin resonance of the 2DEG was recently identified and the extremely long spin life times found make them an attractive candidate for spin-based devices[5,6]. In this paper, we present properties of the 2DEG found in the conduction electron spin resonance (CESR) which can be explained consistently in terms of the Rashba field, $\boldsymbol{H_R}$.

Spin resonance was investigated in the X-band in a conventional spectrometer at a sample temperature of 1.9 K. One of the samples used showed strong persistent photo-conductivity which allowed us to vary the carrier concentration by step-wise increasing the illumination dose. The density of the 2DEG was determined *in-situ* from the cyclotron resonance seen in the same experiment. Fig. 1 shows the anisotropy of the CESR line width. For perpendicular field (Θ=0°), the line width is very small but it increases strongly with an in-plane magnetic field component. Line broadening is caused here by fluctuations of the static magnetic field. Such fluctuations can be caused by the Rashba field which is added to the externally applied magnetic field, $\boldsymbol{H_0}$. For perpendicular field, the Rashba field, which is always within the 2d plane, is perpendicular to $\boldsymbol{H_0}$ and thus its effect on the **magnitude** of the field, that determines the resonance frequency, is small. For in-plane field, however, $\boldsymbol{H_R}$, which is randomly oriented in-plane, has a component parallel to $\boldsymbol{H_0}$ and thus we expect much larger broadening as it is seen experimentally. Modelling the line width we took motional narrowing of the Rashba field by momentum scattering into account.

Since $\boldsymbol{H_R}$ depends also on $\boldsymbol{k}$ we expect also an increase of the CESR line width with increasing $\boldsymbol{k_F}$, and thus increasing carrier density, n_s. We observe an almost quadratic increase for low n_s and a saturation for n_s>3· 10^{11} cm^{-2}.

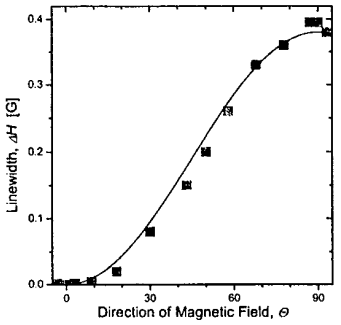

Fig. 1: Anisotropy of the CESR line width for an electron concentration of 3· 10^{11} cm^{-2} in a Si quantum well structure. (Θ=0° corresponds to perpendicular static magnetic field.

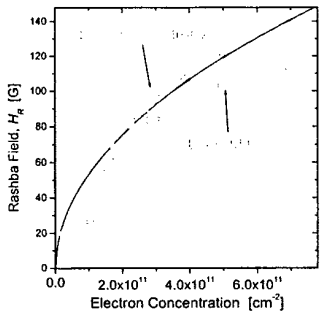

Fig. 2: Rashba field as evaluated by fitting data for the line width (squares) and the g-factor as a function of carrier density. The solid line shows the theoretically expected dependence.

The g-factor should be also affected by $\boldsymbol{H_R}$. Here we observe a small effect for Θ=0° and a decrease of g for $\Theta\rightarrow$90°. This decrease becomes bigger with increasing n_s. These effects can be modelled as follows. In the presence of $\boldsymbol{H_R}$ the g-factor is modified by a factor $|\langle \boldsymbol{H_0}+\boldsymbol{H_R}\rangle|/H_0$, where the average is taken for all $\boldsymbol{k_F}$. The result depends on k_F and Θ.

Modelling allows to evaluate the magnitude of α independently for the two quantities investigated: the anisotropy of the line width and the g-factor. The results of the two methods agree perfectly well as shown in Fig. 2 using a single value for the Rashba parameter of α=1.1· 10^{-12} eV.cm.

In summary, we found two independent methods to demonstrate the appearance of the Rashba effect in 2D quantum well structures. Modelling allows to evaluate the Rashba field and the result depends on the carrier density in the expected way.

Work supported by FWF and BM:WBK(Vienna).

References:

[1] Yu. A. Bychkov and E. I. Rashba, J. Phys. C**17**, 6039 (1984)
[2] S. Datta B. Das, Appl. Phys. Lett. **56**, 665 (1990)
[3] P. Pfeffer and W. Zawadzki, Phys.Rev.B**59**, R5312 (1999)
[4] J. Majewski and P. Vogl, *private communication*
[5] Z. Wilamowski, W. Jantsch, N .Sandersfeld, F. Schäffler, Physica B **284-288**, 1926-1927 (2000)
[6] W. Jantsch, Z. Wilamowski, N. Sandersfeld, and F. Schäffler,Physica E**6** 218-221 (2000), and:cond.matter/0010077 (2000)

Corresponding Author: Wolfgang Jantsch, Institut für Halbleiter- und Festkörperphysik, Johannes Kepler Universität, A-4040 Linz, Austria
phone: +43 732 2468 9641, fax: +43 732 2468 9696
e-mail:. wolfgang.jantsch@jk.uni-linz.ac.at

Influence of capping conditions on structural properties of CdSe/ZnSe quantum dot structures

T. Passow, K. Leonardi, H. Heinke, T. Schmidt, J. Falta, A. Stockmann, H. Selke, D. Hommel

Institut für Festkörperphysik, Universität Bremen, P.O. Box 330 440, 28334 Bremen, Germany

It is known for self-assembled CdSe/ZnSe quantum dot structures grown by molecular beam epitaxy (MBE) that a strong stacking fault formation occurs already near the critical thickness for growth mode transition obtained by reflection high energy electron diffraction. Stacking fault densities of $10^{10}\,cm^{-2}$ were observed above a CdSe deposition of about 3 monolayers (ML). Furthermore, a strong intermixing was found in CdSe/ZnSe quantum dot structures [1-3]. The origin of this intermixing is still under discussion [3,4]. It may be supposed that the growth conditions during overgrowth of the CdSe by ZnSe influence the stacking fault formation as well as the intermixing. Nevertheless there are no systematical investigations described in the literature up to now. Contrary to common beliefs we prove in our work that Cd surface segregation is the main cause for intermixing under typical growth conditions. Furthermore, we present parameters to reduce the stacking fault formation.

Several sample series were grown by MBE on GaAs(001) substrate with identical growth conditions except of the growth parameters for the capping layer on top of the CdSe quantum dot structures. Before the deposition of the II-VI layers, a GaAs buffer layer was grown for obtaining a high quality III/V-II/VI interface. The CdSe layers with a nominal thickness of 1 to 5 ML were embedded in a 50 nm thick ZnSe buffer and a 20 nm thick ZnSe cap layer. The substrate temperature during the growth of the ZnSe buffer layer and the CdSe was 280 °C for all samples. We systematically varied growth temperature, growth rate and VI/II flux ratio during the overgrowth of the CdSe. High resolution x-ray diffraction (HRXRD) has been used to determine the total amount of Cd in the samples [1] and the stacking fault densities [5]. The structural properties of the CdSe quantum dots *before* overgrowth by ZnSe were investigated by grazing incidence x-ray diffration (GIXRD). The Cd distribution has been studied by high resolution transmission electron microscopy (HRTEM).

A strong dependence of the incorporated amount of Cd on the VI/II flux ratio and the growth rate during the overgrowth has been observed by HRXRD. The determined amount of Cd differs by up to a factor of two at the same CdSe growth time. Since thermal CdSe desorption is negligibly weak at the used growth temperatures, the Cd must desorb during the overgrowth of the CdSe by ZnSe. The experimental results can be quantitatively explained by a segregation model taking into account a partial redesorption of segregating Cd atoms. The remaining amount of Cd will decrease by about 3.5 % if the temperature is increased by 10 K.

A minimum stacking fault density was detected at a growth temperature of 280 °C for a constant CdSe deposit before capping (see Fig. 1). This result must be interpreted in terms of the temperature dependence of the Cd redesorption process described above and an increased probability for stacking fault formation with increased growth temperature.

By HRTEM, we found a strong intermixing and a rather symmetrical depth profile of Cd concentration. To clarify the role of interdiffusion and surface segregation, a sample without cap layer was investigated by GIXRD. A partial intermixing is expected already before overgrowth in case of dominant interdiffusion because of the low CdSe growth rate. Figure 2 presents a reciprocal space map of the (202) reflection which allows the separation of strain and composition. It shows the signal of binary, partly relaxed CdSe. This result proves the importance of surface segregation. The rather symmetrical composition profiles obtained from HRTEM micrographs can be easily explained by the segregation model mentioned above.

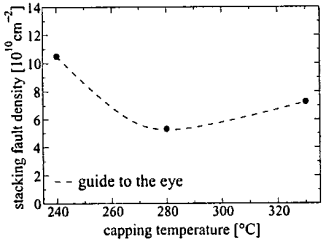

Figure 1: Stacking fault density vs. substrate temperature during overgrowth of the CdSe by ZnSe for samples with the same CdSe deposit before capping.

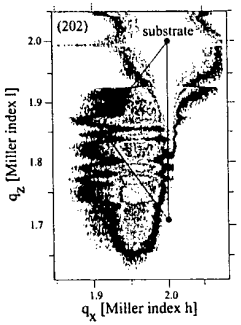

Figure 2: GIXRD reciprocal space map for the (202) reflection of uncapped 4.9 ML CdSe. The relaxation triangle of CdSe is given for comparison.

References

[1] T. Passow et al., J. Phys. D **32**, A42 (1999).
[2] R. N. Kyutt et al., Appl. Phys. Lett. **75**, 373 (1999).
[3] N. Peranio et al., Phys. Rev. B **61**, 16015 (2000).
[4] H. Heinke et al., J. Cryst. Growth **214/215**, 585 (2000).
[5] T. Passow et al., Appl. Phys. Lett. **77**, 3544 (2000).

Corresponding author: Thorsten Passow, Institut für Festkörperhysik, Universität Bremen, P.O. Box 330 440, 28334 Bremen, Germany.
phone: +49 421 218 3216, Fax: +49 421 218 4581,
email: tpassow@physik.uni-bremen.de

(GaMn) As: As incorporation in the host lattice depending on the substrate temperature and the Mn content

G.M.Schott, W. Faschinger,

Experimentelle Physik III, Universität Würzburg, Am Hubland, 97074 Würzburg.

GaMnAs is a metastable compound which can only be grown with low temperature (LT) MBE far from thermal equilibrium. GaAs grown at these low temperatures lead to a very high concentration of As antisites [1], which increase the lattice constant of LT-GaAs and can therefore be measured with HXRD. Experimental investigations indicate that As antisite concentration increases with the incorporation of Mn [2], so that even stronger effects of the growth conditions on the lattice constant can be expected for GaMnAs.

As a consequence, we perform a systematic HXRD investigation on GaMnAs layers as well as on GaMnAs/GaAs and GaAs/MnAs superlattices for samples grown by MBE at different conditions. Independent of the growth conditions, all samples are of high crystalline quality with rocking curve widths comparable to those of the GaAs substrate and show pronounced finite thickness fringes indicating flat interfaces and surfaces. All layers are fully pseudomorphic with respect to the GaAs substrate and all lattice constants given in the following are vertical lattice constants of tetragonally distorted layers.We grew two sets of samples, one at substrate temperature (T_{Sub}) 270 °C and Mn source temperature 640 °C - 670 °C and one at T_{Sub} = 220 °C and Mn source temperature 640 °C- 710 °C, both with As_4/Ga ratio 5. In order to measure the Mn content with an independent method, we grew a special calibration sample at T_{Sub} = 220 °C consisting of GaMnAs/GaAs superlattice (SL2) with thick GaMnAs and thin GaAs layers on top of an inverted superlattice (SL1).The HXRD spectrum is shown in Fig. 1. Under assumption that all fluxes were constant during growth and no phase separation occurs, the resulting Mn content is 6.0±0.5%.Consequently, the extrapolated vertical lattice constant of pure Zincblende MnAs is only 0.612±0.04nm compared to a value of 0.628 nm given bei ref [3]. This seems to indicate that the point defect incorporation is indeed influenced by Mn incorporation, substrate temperature and As flux. To make this more evident, in Fig. 2 the vertical lattice constant of both samples series is plotted as a function of their Mn content. Data points of T_{Sub} = 270 °C are included under the assumption that their total Mn content is identical to that of the corresponding 220 °C samples grown under identical flux conditions. It is evident that the lattice constant increase with Mn content x is very different for the two substrate temperatures used. To verify if the trend of the 270 °C series is continued for higher x, we grew a SL GaAs/MnAs at TSub = 270 °C under the source conditions used for the GaMnAs samples with a Mn content of 2%. Since the MnAs coverage can be calculated, the position of the peak of the HXRD spectrum only depends on the vertical MnAs lattice constant. The resulting MnAs lattice constant is 0.628±0.04nm, which corresponds to the value by Ohno et al. [3] and is indeed larger than the value at T_{Sub} = 220 °C. Two conclusions can be drawn from Fig. 2: First, since the growth conditions strongly influence the MnAs lattice constant, a determination of the Mn content based on literature calibration values can lead to significant errors. Second, the incorporation of As for a given As flux, which is the only factor that can produce a lattice constant increase, obviously depends on both substrate temperature and Mn content: While at low x the As antisites formation is suppressed at T_{Sub} = 270 °C, the situation at high Mn content is reversed. The simplest model to understand such a behavior is the assumption that at low substrate temperature the As antisites and the Mn ions are uncorrelated, while at high substrate temperatues the formation of a defect complex consisting of Mn and excess As becomes possible.

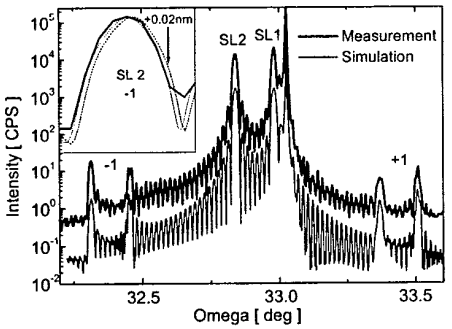

Fig.1: (004) high resolution X-ray diffraction pattern of a calibration sample consisting of two superlattices with thin GaMnAs layers (SL1) and thick GaMnAs layers (SL2).

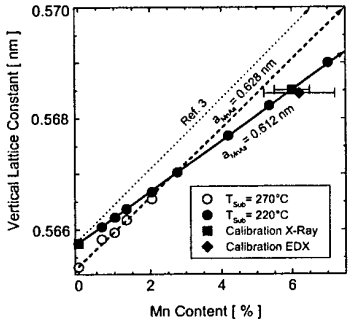

Fig.2: Vertical lattice constant of GaMnAs layers grown at different substrate temperatures as a function of the manganese content (circles). The solid line is linear extrapolation between two calibration points (solid squares), the dashed line a linear extrapolation between the GaAs bulk lattice constant and the MnAs lattice constant determined from a GaAs/MnAs superlattice. The dotted line is calculated from data given in ref. 3.

References:

1.M.Luysberg, H.Sohn, A.Prasad, P.Specht, H.Fujioka, R.Klockenbrink and E.R.Weber, Mat. Res. Soc. Symp. Proc. 442, 485 (1997)

2.Grandidier, J.P.Nys, C.Delerue, D.Stievenard, Y.Higo and M.Tanaka, Appl. Phys. Lett. 77, 4001 (2000)

3.H.Ohno, A.Shien, F.Matsukara, A.Oiwa, A.Endo, S.Katsumoto and Y.Iye, Appl. Phys. Lett. 69, 363 (1996)

Corresponding author: Gisela Schott, Experimentelle Physik III, Universität Würzburg, Am Hubland, D-97074 Würzburg,
phone: +49 888 5799, Fax: +49 888 5142,
email: schott@physik.uni-wuerzburg.de

Fabrication and characterization of III-V semiconductor superlattices with sinusoidal compositional modulation

X. Liu, Y. Sasaki, J. K. Furdyna
Department of Physics, University of Notre Dame, Notre Dame IN, 46556

P.M. Reimer
Turner Precision X-ray laboratory, Goshen College, Goshen IN, 46526

S. Lee
Department of Electronic Materials Engineering, Kwangwoon University, Seoul, 139-701, Korea

We have fabricated III-V-based "sinusoidal superlattices", i.e., periodic structures in which the chemical composition varies *sinusoidally* along one direction. This was accomplished by means of a novel MBE growth technique in which the periodic modulation is achieved by substrate rotation in the presence of non-uniform flux distributions of elemental sources, rather than by shutter openings and closings. We first focused on a specific alloy system, $GaAs_{1-x}Sb_x$, in which the concentrations of the two anions are sinusoidally modulate. The nonuniform flux distribution of anions incident on the substrate is obtained by appropriate placement of the As and Sb sources relative to the rotating stage. Rotation of the mounting block then makes the substrate pass regularly through different anion flux intensities, resulting in alternating As-rich and Sb-rich layers.

Superlattices fabricated by this technique indeed result in sinusoidal (or very nearly sinusoidal) compositional profiles, as inferred from the presence of *only a single* superlattice Fourier component in the X-ray diffraction spectra observed on these novel structures (see Fig. 1) – in sharp contrast with X-ray spectra of superlattices with abrupt interfaces, which are characterized by multiple satellite peaks. The quality of the superlattices is very high, as inferred from the fact that the satellite peaks are as narrow as the "parent" Bragg reflections. The modulation of chemical composition x is accompanied by a corresponding modulation of strain, owing to the differences in the Ga-As and the Ga-Sb bond lengths. By fitting the scans observed on the sinusoidal superlattices around specific Bragg reflections to a simple scattering theory, we have determined both the strain and the chemical modulation amplitudes in the $GaAs_{1-x}Sb_x$ modulated structures.

We have extended the growth of sinusoidal superlattice systems to other III-V materials such as $AlAs_{1-x}Sb_x$, and will compare the properties of these superlattices with their II-VI-based counterparts, e.g., $ZnSe_{1-x}Te_x$,[1] Furthermore, we will present results on the formation of sinusoidal superlattices in *two-cation* systems, such as $Ga_{1-x}In_xAs$ and $Ga_{1-x}Al_xAs$, which are known to have a type-I band alignment (in contrast with the systems which we have explored thus far). The sinusoidal modulation of composition in these systems leads to a sinusoidal energy band profile, which in turn is expected to result in new and unique electronic properties. We will discuss the band structure of such sinusoidal superlattices in terms of an adaptation of the nearly free electron model, originally developed for superlattices with small band offsets [2].

In addition to presenting the structural data and band structure for the novel superlattices grown by the technique described above, we will discuss the special advantages which this shutterless method holds in store -- particularly for fabricating ultra-short period structures, and for structures with compositional profiles other than sinusoidal. In the context of ultra-short-period systems, we will give special attention to the consequences of commensurability or non-commensurability of the superlattice period with the lattice parameter.

References

[1] Sinusoidally modulated $ZnSe_xTe_{1-x}$ superlattices: Fabrication and structural studies, P. M. Reimer, J. R. Buschert, S. Lee, and J. K. Furdyna, Phys. Rev. B **61**, 8388 (2000).
[2] Band structure and optical properties of sinusoidal superlattices: $ZnSe_xTe_{1-x}$, G. Yang, S. Lee, and J. K. Furdyna, Phys. Rev. B **61**, 10978 (2000).

FIGURE 1: An example of a θ/2θ scan obtained for a $GaAs_{1-x}Sb_x$ sinusoidally-modulated superlattice. The strongest and sharpest peak is from the [100]GaAs substrate; the peak just to the left represents the average "alloy" composition of modulated the $GaAs_{1-x}Sb_x$ system; and the two weaker peaks spaced evenly around the "alloy" peak are superlattice satellites, reflecting sinusoidal compositional modulation.

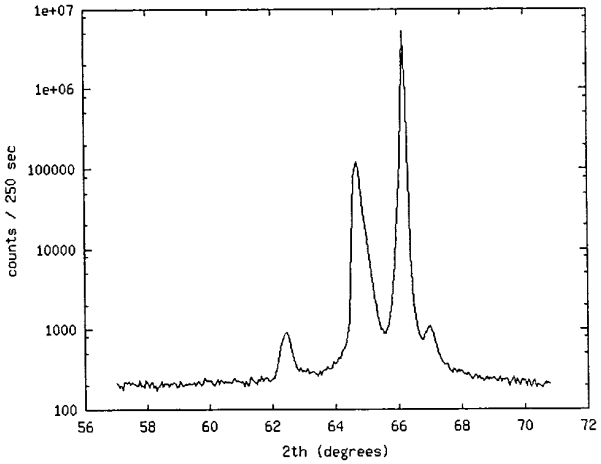

Corresponding author: Jacek K. Furdyna
Department of Physics, University of Notre Dame
225 Nieuwland Science Hall, Notre Dame, IN 46556, USA.
Phone: +1 219 631 6741, Fax: +1 219 631 5952
Email: Jacek.K.Furdyna.1@nd.edu

X-ray Scattering on InP/InGaP Quantum Dot Multilayers

M. Schmidbauer[1], F. Hatami[2], P. Schäfer[1], M. Hanke[1], T. Panzner[1], W.T. Masselink[2], and R. Köhler[1]

[1] AG Röntgenbeugung, Institut für Physik, Humboldt-Universität zu Berlin, Hausvogteiplatz 5-7, D-10117 Berlin, Germany
[2] AG Elementaranregungen, Institut für Physik, Humboldt-Universität zu Berlin, Invalidenstr.110, D-10115 Berlin, Germany

It is well known that structural properties such as size, shape, strains and strain distribution of semiconductor quantum dots (QD) have a large impact on the electronic properties [1]. However, during growth structural parameters are often interrelated: Strain is the dominant driving force for island formation, strongly influences size and shape and, may additionally lead to lateral and vertical correlation in QD multilayers. On the other hand, the elastic strain distribution in the surrounding host lattice is critically sensitive to the shape of the buried QDs. Detailed knowledge about these structural parameters is, therefore, essential.

We present results on the system InP/ $In_{0.48}Ga_{0.52}P$. The high lattice mismatch of 3.8% between both materials (InP: a = 5.87 Å; $In_{0.48}Ga_{0.52}P$: a = 5.65 Å) enables the formation of InP QDs, whereas the $In_{0.48}Ga_{0.52}P$ is latticed matched to GaAs. Results achieved on a single layer of free standing InP QDs will be compared to a 10 period multilayer consisting of nominally 1.5 nm thick InP layers and 5 nm thick $In_{0.48}Ga_{0.52}P$ spacer layers. The samples have been grown by gas source molecular beam epitaxy (GSMBE) on GaAs (001) substrates. Atomic force micrographs (AFM) (Figure 1) indicate a hemispherical dot shape, however, it is not clear as to what extent the measured shape is influenced by convolution effects introduced by the AFM tip. Statistical analysis yields a rather narrow size distribution with an average island base width of about w = 31 nm ± 4.4 nm and an average height of h = 5 nm. A high dot density of about 9×10^{10} cm^{-2} was achieved.

Due to the high coherence and intensity given by high brilliance synchrotron radiation sources, QD arrays can be investigated on an extensive range of length scales. This makes it possible to not only get information about strain but - simultaneously - also on shape, size, composition and spatial correlation [2,3,4]. Grazing incidence x-ray small angle scattering (GISAXS) and grazing incidence x-ray diffraction (GID) have been applied. Our data show both strong lateral ordering of the QDs along the <100> directions and vertical correlation of the dot positions through the entire multilayer stack. In addition, both GISAXS and GID show a distinct asymmetry of diffuse scattering with respect to the [110] and [1$\bar{1}$0] directions. As an example Figure 2 shows the in-plane x-ray diffuse scattering in the vicinity of the 220 and 2$\bar{2}$0 reciprocal lattice point. The observed asymmetry can be interpreted as elongated QDs along [110]. Our results will be compared to transmission electron microscopy and finite element calculations for the elastic strain field.

References

[1] See articles in MRS Bulletin **23**, 15 (1998).
[2] M. Schmidbauer, Th. Wiebach, H. Raidt, M. Hanke, R. Köhler, H. Wawra, Phys. Rev. B 58, 10523 (1998).
[3] Th. Wiebach, M. Schmidbauer, M. Hanke, H. Raidt, R. Köhler, H. Wawra, Phys. Rev. B 61, 5571 (2000).
[4] V. Holý, A.A. Darhuber, J. Stangl, S. Zerlauth, F. Schäffler, G. Bauer, N. Darowski, D. Lübbert, U. Pietsch, I. Vávra, Phys. Rev. B 58, 7934 (1998).

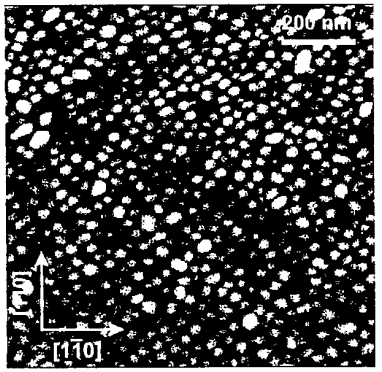

Fig. 1: AFM picture of InP quantum dots grown on $In_{0.48}Ga_{0.52}P$ /GaAs(001). The gray scale linearly varies from 0 nm (black) to 10 nm (white).

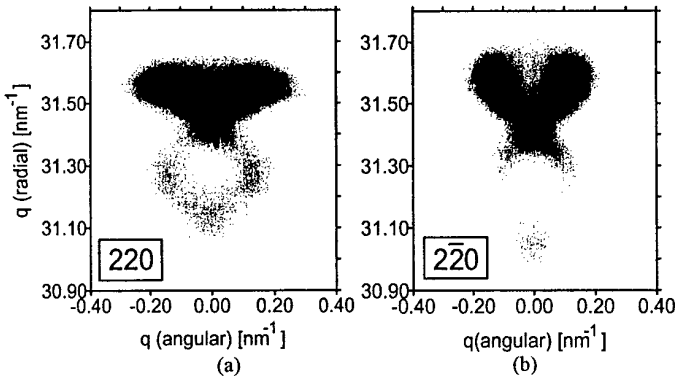

Fig. 2: In-plane GID map of InP quantum dot multilayer performed at the critical angle of total external reflection (a) around 220, and (b) around 2$\bar{2}$0. The radial direction is collinear with the scattering vector. The gray scale varies from white to black on a logarithmic scale.

Corresponding author: Martin Schmidbauer, AG Röntgenbeugung, Institut für Physik, Humboldt-Universität zu Berlin, Hausvogteiplatz 5-7, D-10117 Berlin, Germany
phone: +49-30-20246-719, Fax: +49-30-2044536
email: schmidbauer@physik.hu-berlin.de

Finite size effects in the vertical and lateral ordering of self-organized PbSe quantum dot superlattices

R. T. Lechner,[1] A. Raab,[1] G. Springholz,[1] M. Pinczolits,[1] V. Holy,[1] P. Mayer,[1] G. Bauer,[1] H. Kang,[2] and L. Salamanca-Riba[2]

[1]Institut für Halbleiter- und Festkörperphysik, Johannes Kepler Universität Linz, Altenbergerstraße 69, A-4040 Linz, Austria
[2] Dept. of Materials and Nuclear Engineering, University of Maryland, College Park, USA

Multilayering of self-assembled Stranski-Krastanow quantum dots often leads in the formation of vertical and lateral correlations within ensembles of quantum dots, driven by the elastic interactions between the dots on the surface and those buried within the previous layers. This can lead to improvements in size homogeneity, which is crucial for device applications. For most material systems, the dots are aligned along the superlattice growth directions, but the lateral ordering tendency is usually rather weak. However, in PbSe dot superlattices grown along the (111) directions dot correlations inclined to the growth direction are observed. This leads to a unique *fcc*-like *ABCABC*... dot stacking sequence with a nearly perfect ordering within the growth plane. As a result *trigonal* self-organized 3D lattices of dots are formed [1]. As shown by our previous work, this difference can be explained by modeling of the elastic interactions between the dots of the elastic anisotropy of the various materials systems is taken into account [2]. This anisotropy is particularly large in the case of the IV-VI compounds with their rock salt crystal structure.

In the present work, we have investigated how finite size effects affect the self-organization processes during PbSe superlattice growth. For this purpose we have fabricated a series of superlattice samples with large variations in the layer thicknesses and growth temperature. In contrast to our previous work (Ref. [3]), here we focus on the influence of the PbSe dot size and growth temperature on the self-organization process. From atomic force microscopy studies (see Fig. 1) we find that when the $Pb_{1-x}Eu_xTe$ spacer thickness is kept constant, an efficient lateral dot ordering takes place only for a certain range of PbSe dot sizes (dot layer thickness), and a similar effect is also observed for changes in substrate temperatures. Thus, ordering occurs only for a certain combination of spacer thicknesses and dot sizes. From cross sectional transmission electron microscopy and x-ray diffraction studies (see Fig. 2) we find that this effect is caused by abrupt changes in the type of vertical dot correlations formed at certain ratios of spacer thicknesses to dot base width. Whereas for thin spacers and/or large dot sizes, the dots are vertical aligned with a weak hexagonal ordering in the lateral direction, a well defined *fcc*-stacking with well ordered dots in the lateral direction are observed for intermediate spacer thicknesses and/or medium sized dots. For large spacer thicknesses and/or small dot sizes no dot correlations are formed. For the different 3D dot arrangements, also a qualitatively different scaling behavior of the lateral dot spacings versus spacer layer thickness is found. In addition, a different evolution of dot sizes and shapes as a function of the number of superlattice periods is observed for the differently correlated structures. From finite element calculations of the strain distribution around the buried dots within the matrix material it is shown that these different dot correlations are due to finite size effects, and the calculated transitions between the different dot phases are in good agreement with the experimental results.

Fig. 1. Atomic force microscopy images (1 x 1 μm^2) of PbSe quantum dots on the surface of $PbSe/Pb_{1-x}Eu_xTe$ quantum dot superlattices with constant $Pb_{1-x}Eu_xTe$ spacer layers thickness of 410 Å but varying PbSe dot layer thickness of 3, 5 and 8 monolayers for (a) to (c), respectively, indicating a completely different lateral ordering tendency for the different dot layer thicknesses.

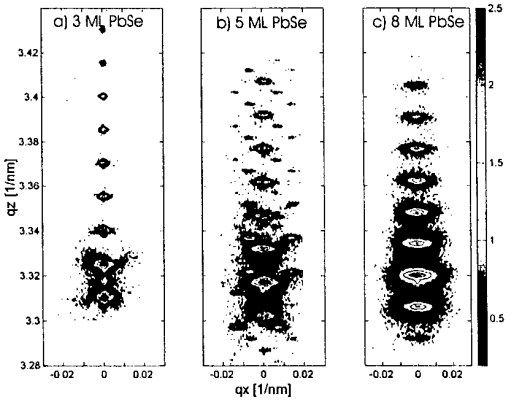

Fig. 2.: High resolution x-ray diffraction reciprocal space maps around the (222) Bragg reflection recorded along q_x = [-1-12] and q_z = [111] for PbSe dot superlattices with different PbSe dot layer thickness d_{PbSe} and constant 410 Å PbEuTe spacer thickness. For d_{PbSe} = 3 ML (a), no lateral satellite peaks appear, *i.e.*, the dots are not correlated laterally or vertically. For d_{PbSe} = 5 ML (b), the many lateral satellites indicate a well ordered trigonal dot arrangement with corresponding *fcc*-like vertical stacking. For d_{PbSe} = 8 ML (c) the strong diffuse broadening of the satellite peaks along q_x indicates that the dots are vertically aligned but are disordered in the lateral direction.

References

[1] G. Springholz, V. Holy, M. Pinczolits, and G. Bauer, Science **282,** 734 (1998).
[2] V. Holy, G. Springholz, M. Pinczolits and G. Bauer, Phys. Rev. Lett. **83**, 356 (1999).
[3] G. Springholz, *et al*, Phys. Rev. Lett. **84**, 4669 (2000).

Corresponding author: G. Springholz, Institut für Halbleiter- und Festkörperhysik, Johannes Kepler Universität Linz, Altenbergerstraße 69, A-4040 Linz, Austria.
phone: +43 732 2468 9602, Fax: +43 732 2468 8650
email: g.springholz@hlphys.uni-linz.ac.at

Atomistic Simulation of Strain Relaxation in $In_xGa_{1-x}As/GaAs$ Quantum Dots with Nonuniform Composition

M. A. Migliorato[1], A.G. Cullis[1], M. Fearn[2] and J. H. Jefferson[2]
[1]*Department of Electronic and Electrical Engineering, University of Sheffield, Sheffield S1 3JD, United Kingdom*
[2]*Defence Evaluation and Research Agency, Electronics Sector, St.Andrews Road, Malvern, Worcs. WR14 3PS, United Kingdom*

Atomistic simulations are a promising technique for modelling semiconductor nanostructures, requiring a minimal number of approximations in both the initial atomistic model of the structure and in the methodology employed to extract information such as local composition and strain. In this work we report the first atomistic simulation of $In_xGa_{1-x}As/GaAs$ Quantum Dots (QDs) with nonuniform composition, applied to the study of strain in capped QDs and strain relaxation of cleaved QDs. The structural studies realised in recent years have suggested that $In_xGa_{1-x}As/GaAs$ QDs can be either lens shaped [1-2] or truncated pyramids [3], and more recently non uniformities in composition have been investigated, revealing a higher concentration of In near the top of the pyramid compared to the bottom [1,4,5]. Following on from these observations we have built an atomistic model of a QD consisting of 400,000 atoms, introducing a graded 'trumpet shaped' composition in the truncated pyramid (Fig. 1a), and using carefully controlled bending of the (110) lattice planes to prevent the structure from forming dislocation lines extending into the capping layers in a non-physical manner. The Tersoff potential [6,7] is then used to model the atomic interactions of the inhomogeneous system of atoms and to obtain dynamic relaxation through energy minimisation. From the relaxed atomistic model, the bond deformations are analysed in order to predict the strain maps. Presented in Fig. (1b) is a map of the biaxial strain in a (101) plane passing through the centre of the QD, the darker regions representing larger positive biaxial strain. A higher strain is observed at the top of the pyramid and in the proximity of the side facets, outside the QD.

The same technique is also employed to model the strain relaxation of a cleaved QD, allowing us to study the loss of planarity of the cleavage surface and to compare this with experimental STM results. As expected the regions with higher strain relax along the direction [110], orthogonal to the cleavage plane, resulting in a strong loss of planarity of the cleaved surface. The results obtained are remarkably similar to the experimental ones obtained using the STM technique, presented in Fig. 1.b of Liu et al. [4], which was justified by proposing an inverted pyramid-like In distribution. The predicted distortion of the cleavage plane is ~0.35 nm, in close agreement with the ~0.3 nm distortion measured experimentally [4].

In conclusion, our work demonstrates the general validity of the model proposed by Liu et al. [4]. Further refinements to the model are possible, though our proposed 'trumpet-shaped' composition distribution results in the topographical map of a cleaved QD statistically similar to that presented in Liu et al. [4]. In general terms, we have demonstrated that atomistic simulations accurately reproduce the strain pattern of QDs, with minimal approximations, offering a valid and improved alternative to continuum elasticity theory and a useful tool with which to investigate reliably the consequences of compositional variations in semiconductor nanostructures.

[1] I. Kegel, T. H. Metzger, A. Lorke, J. Peisl, J. Stangl, G. Bauer, J. M. García and P. M. Petroff, Phys. Rev. Lett. **85**, 1694 (2000).
[2] J. Zou, X. Z. Liao, D. J. H. Cockayne and R. Leon, Phys. Rev. B **59**, 12 729 (1999).
[3] R. Heitz, M. Grundmann, N. N. Ledentsov, L. Heckey, M. Veit, D. Bimberg, V. M. Ustinov, A. Yu. Egorov, E. Zhuckov, P. S. Kop'ev and Zh. I. Alferov, Appl. Phys. Lett. **68**, 361 (1996).
[4] N. Liu, J. Tersoff, O. Baklenov, A. L. Holmes Jr. and C. K. Shih, Phys. Rev. Lett **84**, 334 (2000).
[5] T. Walther, A. G. Cullis, D. J. Norris and M. Hopkinson, Phys. Rev. Lett. **86**, (2001) *in press*.
[6] J. Tersoff, Phys. Rev. Lett. **56**, 632 (1986).
[7] J. Tersoff, Phys. Rev. B **39**, 5566 (1989).

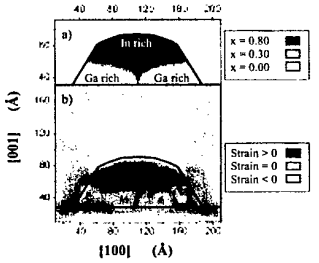

FIG. 1. a) Simulated [100] cross section of the QD showing a 'trumpet-shaped' In composition distribution. The darker regions are In rich, while the brighter are Ga rich.
b) Simulated [100] cross section of the QD biaxial strain map. The In rich regions are highly strained. Positive values of the biaxial strain are found outside the QD. Negative biaxial strain is found at the top of the pyramid and in the capping layer above it.

Contact details:
Mr M A Migliorato
Department of Electronic & Electrical Engineering
University of Sheffield
Mappin Street
Sheffield, S1 3JD
Tel: 0044 -114 -222 5848
Fax: 0044-114- 272 6391
Email: M.Migliorato@physics.org

Structure and ordering of GaN quantum dot multilayer investigated by x-ray grazing incidence techniques

V. Chamard[1] , T. H. Metzger[1], E. Bellet-Amalric[2], B. Daudin[2], C. Adelmann[2], H. Mariette[2,3], G. Mula[2,4]

[1]European Synchrotron Radiation Facility, ID01 Anomalous Scattering beamline, BP 220, 38043 Grenoble Cedex, France.
[2]CEA-CNRS group, "*Nanophysique et semiconducteurs*", Département de Recherche Fondamentale sur la Matière Condensée, CEA/Grenoble, 17 rue des Martyrs, 38054 Grenoble Cedex 9, France.
[3]Laboratoire de Spectrométrie Physique, Université J. Fourier Grenoble 1 - CNRS UMR 5588, BP 87, 38402 Saint-Martin d'Hères Cedex, France.
[4]INFM and Dipartemento di Fisica, Cittadella Universitaria, Strada Prov. le Monserrato-Setsu km 0.7, 09042 Monserrato, Cagliari, Italy.

The growth of GaN quantum dot multilayers embedded in an AlN matrix can be controlled using the Stranski-Krastanov mode [1]. For samples grown in the wurtzite structure, we present a non-destructive statistical investigation of the quantum dot size, correlation, in lateral and vertical direction, and strain, using depth resolved x-ray grazing incidence techniques.
In grazing incidence small angle x-ray scattering, we observe that the smaller quantum dots disappear with increasing numbers of deposited bi-layers and only dots with an average lateral size of 17 nm remain. The inter-dot lateral and vertical correlation is quantified using the method given by I. Kegel et al. [2].
With grazing incidence diffraction, the lateral strain in the superlattice is investigated as a function of depth. A diffraction maximum is observed at a position between the Bragg diffractions of bulk GaN and bulk AlN. It is attributed to the strain field in both, quantum dots and spacer layers along the dot columns. It is found that the strain relaxes elastically towards the bulk lattice parameter of GaN from the bottom to the top of the superlattice.

[1] B. Daudin, F. Widmann, G. Feuillet, Y. Samson, M. Arlery, and J.-L. Rouvière, Phys. Rev. B **56**, R7069 (1997).
[2] I. Kegel, T. H. Metzger, J. Peisl, J. Stangl, G. Bauer, and D. Smilgies, Phys. Rev. B **60**, 2516 (1999).

Corresponding author: Virginie Chamard, ESRF ID01 beamline, BP220, 38043 Grenoble Cedex, France.
Phone: 33 (0) 476 88 22 16, Fax: 33(0)476 88 23 25,
e-mail : chamard@esrf.fr

Two-wave X-ray optical diagnostics of Ge_xSi_{1-x}/Si modulation-doped heterostructures

A.G. Touryanski[a], I.V. Pirshin[a], M. M. Rzaev[a],
F. Schäffler[b], M. Mühlberger[b],

[a] P.N.Lebedev Phisical Institute, 53 Leninsky pr., 117924, Moscow, Russia
[b] Institut für Halbleiter- und Festkörperphysik, Johannes Kepler Universität Linz, Altenbergerstraße, A-4040 Linz, Austria

New X-ray optical methods – two-wave reflecto- and refractometry - have been used for the first time for determination of Ge_xSi_{1-x}/Si composition and exact measurements layer thickness in multilayer heterostructure. Both techniques are based on simultaneous measurements of two intense characteristic X-ray lines, separated from the polychromatic X-ray probe by semitransparent monochromators. Two-wave reflectometry study allows to realize unique opportunity to measure the ratio of reflected intensities for two X-ray lines providing almost complete elimination of the X-ray beam instability and geometrical errors at small grazing angles.

Samples used in this study were grown by molecular beam epitaxy in a Riber SIVA-45 system. After a standard RCA cleaning a modulation-doped heterostructure consisting of a HT(750°C) 100 nm undoped Si buffer, a LT (250°C) 50 nm $Si_{0,7}Ge_{0,3}$ buffer, a HT(500°C) 150 nm $Si_{0,7}Ge_{0,3}$ buffer, a 10 nm $Si_{0,3}Ge_{0,7}$ channel, a undoped 10 nm $Si_{0,7}Ge_{0,3}$ spacer, a 2 nm B-doped supply layer ($1\times10^{19}cm^{-3}$), a 50nm $Si_{0,7}Ge_{0,3}$ and 10 nm Si cap layers were grown on an 5" Si (001) n-type(3,5-40 Ω cm) substrate.

The ratio reflectogram with CuK_α and CuK_β lines for Ge_xSi_{1-x}/Si heterostructure is shown in Fig.1. The maximum thickness deviation of measured from a technologically predetermined value was 10% for thick 45-50 nm Ge_xSi_{1-x} layers.

The major advantage of newly developed refractometry metrology [1] lays in its insensitivity to high defect concentration and in the detector scan mode to mechanical strains in heterostructures. However, in the sample scan mode surface curvature and respectively non-relaxed strains may be easily identified. In this work we received for the first time clearly resolved refraction peaks from the Si substrate and the Ge_xSi_{1-x} layer under the Si cap-layer (Fig. 2). Composition calculations from of Ge_xSi_{1-x} refraction index for two characteristic lines gave x=0,32 as compared with technologically pre-assigned x=0.30 and x=0.29 from XRD measurements.

The work is partially supported by the RFBR grant ##00-02-16470 and 01-02-02007-BNTS_a.

References
[1].A.G. Touryanski at al. *Instrum. Experimental Techniques*. V. 42, 1 (1999) 827-34.

Corresponding author: Alexander G. Touryanski, P.N.Lebedev Phisical Institute, 53 Leninsky pr., 117924, Moscow, Russia, phone: (095)-132-62-68, Fax: 7(095)-135-10-59.
E-mail address: tour@mail1.lebedev.ru

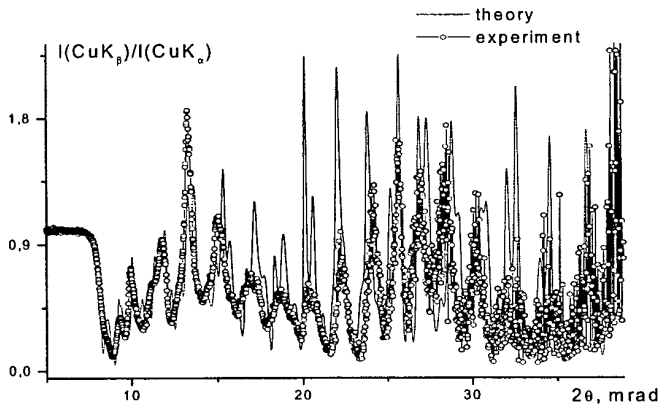

Fig.1. Ratio of reflected intensities $I(CuK_\alpha/I(CuK_\beta)$ from θ-2θ scan for Ge_xSi_{1-x}/Si heterostructure.

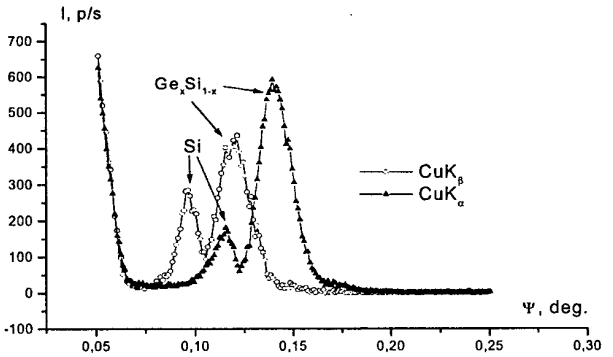

Fig. 2. Refracted intensity I versus deviation angle Ψ for Ge_xSi_{1-x}/Si heterostructure.

Fabrication of height-controlled InAs quantum dots on GaAs surfaces by in-situ $AsBr_3$ etching and molecular beam epitaxy

T. Yang, S. Kohmoto, H. Nakamura, and K. Asakawa

The Femtosecond Technology Research Association (FESTA)
5-5 Tokodai, Tsukuba 300-2635, Japan

InAs quantum dots (QDs) on GaAs surfaces in the Stranski-Krastanow (SK) growth mode are attractive for novel optical and electronic devices such as QD lasers [1]. However, a large photoluminescence (PL) linewidth from the QDs is a major problem in device applications, which results from large size fluctuations of self-organized QDs. Various efforts have been made to overcome the problem. Recent work has shown that it is more effective to suppress the fluctuation in height rather than in diameter of QDs to reduce the large PL linewidth [2].

Schuler *et al.* have recently found that *in-situ* $AsBr_3$ etching of a thin GaAs film covering InAs SK QDs in a molecular beam epitaxy (MBE) chamber can result in an array of small dips with the nanometer scale on the etched GaAs surface [3]. Furthermore, we have observed that the nanoholes on the GaAs surface can be completely filled up and a planar surface appears when the supply amount of InAs is ~ 1 monolayer (ML) during the growth of InAs QDs on the GaAs surface [4]. These results suggest that a structure of height-controlled InAs QDs on GaAs surface could be fabricated based on the *in-situ* $AsBr_3$ etching and MBE, which consists of a pair of closely stacked head to head InAs QD layers [3]. In this paper, we study the technique for controlling the height of InAs QDs on GaAs surfaces by the *in-situ* $AsBr_3$ etching and MBE.

We first study $AsBr_3$ etching of GaAs surfaces by *in-situ* reflection high-energy electron diffraction (RHEED) measurements to fabricate the structure. Figure 1 shows a typical trace of RHEED intensity during etching of the GaAs (001) surface. The clear RHEED intensity oscillations can be seen, indicating that the etching occurs via a layer-by-layer process. The period of the oscillation exactly corresponds to the time required to remove 1 ML of GaAs. Thus the use of the oscillatory effect in RHEED enables us to control the etching with ML precision. Next, we describe results for fabricating the structure of height-controlled InAs QDs on GaAs surfaces by combining the layer-by-layer *in-situ* etching and MBE.

Figure 2 shows AFM surface images (above) at different fabrication steps and schematic illustrations (below) of the sample structure corresponding to the steps for the height-controlled InAs QDs on the GaAs surface. Fig. 2 (a) shows the InAs SK QDs grown on the GaAs surface at a substrate temperature of 460 °C and an As pressure of 1 □ 10^{-5} Torr. Fig. 2(b) shows the nanoholes created by $AsBr_3$ etching, where a 2-nm-thick GaAs was removed after covering a 5-nm-thick GaAs on the InAs SK QDs at the same substrate temperature and As pressure as above. The $AsBr_3$ flow rate was 0.05 sccm. In addition, we have found that the size and density of the etched nanoholes strongly depend on the size and density of the underlying QDs. Fig. 2(c) shows the surface formed after supplying 1 ML InAs also at the same substrate temperature and As pressure as above. The InAs growth rate above was 0.1 ML/s. As shown in Fig. 2(c), the nanoholes were buried and a flat surface with a roughness of 0.2 nm was obtained, thus indicating that the total height of the closely stacked InAs QD pairs are precisely defined within ML precision. Since the closely stacked QD pairs can be viewed as single QDs [5], the height-controlled InAs ODs on the GaAs surface have been achieved.

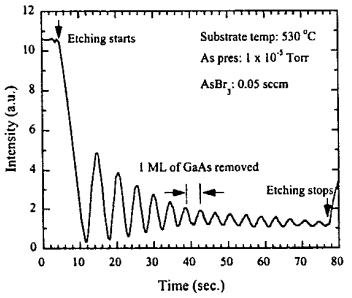

Fig. 1: A typical trace of RHEED intensity oscillation during etching of GaAs (001).

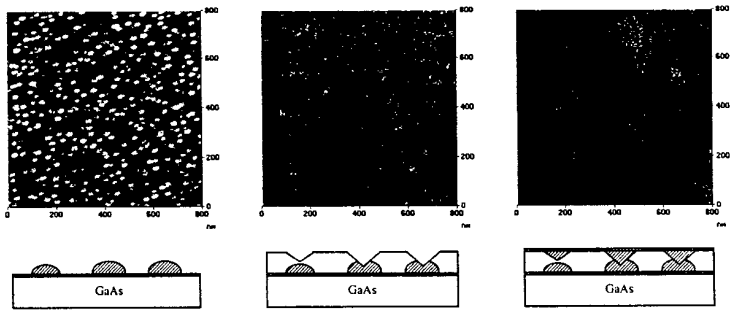

Fig. 2: AFM surface images (above) at different fabrication steps and schematic illustrations (below) of the sample structure corresponding to the steps for the height-controlled InAs QDs on the GaAs surface.

This work was supported by NEDO within the framework of the Femtosecond Technology Project.

References

[1] D. Bimberg *et al.*, *Quantum Dots Heterostructures* (Wiley, Chichester, 1999).
[2] A. Endoh *et al.*, Jpn. J. Appl. Phys. **38**, 1085(1999).
[3] H. Schuler, T. Kaneko, M. Lipinski, and K. Eberl, Semicond. Sci. Technol. **15**, 167(2000).
[4] H. Nakamura, S. Kohmoto, T. Ishikawa, and K. Asakawa, Physica E **7**, 331(2000).
[5] Q. Xie, A. Madhukar, P. Chen, and N-P. Kobayashi, Phys. Rev. Lett. **75**, 2542(1995).

Corresponding author: Tao Yang, The Femtosecond Technology Research Association (FESTA), 5-5 Tokodai, Tsukuba 300-2635, Japan,
phone: +81 298 47 5181, fax: +81 298 47 4417, email: yang@festa.or.jp

Direct fabrication of parallel quantum dots with an atomic force microscope

U. F. Keyser[1], M. Paesler[1], U. Zeitler[1], R. J. Haug[1], K. Eberl[2]

[1]Institut für Festkörperphysik, Universität Hannover, Appelstr. 2, D-30167 Hannover, Germany
[2]Max-Planck-Institut für Festkörperforschung, Heisenbergstr. 1, D-70569 Stuttgart, Germany

The atomic force microscope (AFM) is a powerful tool for the direct fabrication of lateral mesoscopic devices in GaAs/AlGaAs-heterostructures [1-3].
Here we present first experiments on laterally coupled double quantum dots with common leads. The system shows Coulomb-blockade oscillations with two different periods assigned to the two quantum dots (QD).
The device was fabricated in a stepwise manner. First the in-plane gates (IPG) for the devices are defined by controlled nanomachining [3]. By applying contact forces over 10 μN the silicon AFM-tip is used to scribe narrow trenches into the heterostructure depleting the 2DEG underneath. The trenches define a 2.5 μm wide channel between the IPGs. Subsequently we added two tunneling barriers into the channel with a lateral distance of 250 nm. For this the tip is negatively biased with respect to the sample leading to a local anodic oxidation of the sample. The oxidation current determines the electronic height of the tunneling barriers and can be tuned between a few meV and over 100 meV [4].
After the completition the device was characterized in a ^{3}He-cryostate. We observe the behaviour of a 2D-1D-2D resonant tunneling device (RTD) with a pronounced resonance in the IV-characteristic with the typical negative differential conductance. The peak-to-valley ratio (maximum 1.64) and the position of the resonance is controlled by the voltage on the two IPGs. This device resembles a tuneable resonant tunneling diode.
Subsequent to this first characterization step the RTD was removed from the cryostat and again mounted into the AFM. We cut the double-barrier structure into two parallel quantum dots (QD) by writing an additional oxide line. The oxidation current was chosen to form an approximately two times higher tunneling barrier compared to the tunneling barrier between the dots and the source-drain contacts. This leads to a lower tunneling coupling between the QDs than to the leads.
The low temperature characteristic of the double QDs show typical Coulomb-blockade oscillations of a 2D-0D-2D tunneling process with two different periods for the two quantum dots. Using the IPGs the electrochemical potential on both QDs can be tuned almost separately. By analyzing the Coulomb-blockade diamonds we can determine the total capacitance of QD1 C_1~500 aF and of QD2 C_2~100 aF. These results are in the same range as our previous measurements on single quantum dots [3,4]. Detailed measurements as function of backgate and IPG-voltage will be presented.

References

[1] M. Ishii, and Y. Matsumoto, Jpn. J. Appl. Phys. 34, 1329 (1995).
[2] R. Held et al., Appl. Phys. Lett. **73**, 262 (1998).
[3] H. W. Schumacher et al., Appl. Phys. Lett. **75**, 1107 (1999).
[4] U. F. Keyser et al., Appl. Phys. Lett. **76**, 457 (2000).

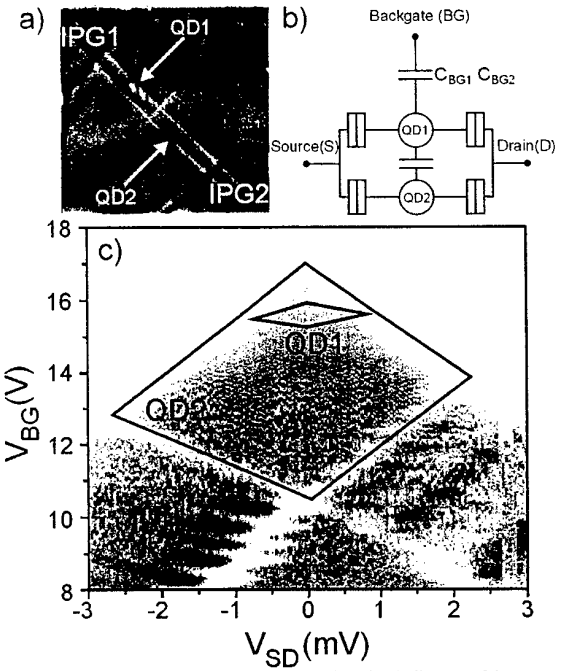

Fig. 1: a) AFM-micrograph of the parallel quantum dots (QD). b) Circuit diagram of the system. c) Differential conductance of the device. High differential conductance is diplayed in white. Coulomb-blockade diamonds of both QDs with diffrenet sizes are observed. From other measurements these are attributed to QD1 and QD2.

Corresponding author: Ulrich F. Keyser, Institut Festkörperhysik, Universität Hannover, Appelstr. 2, D-30167 Hannover, Germany.
phone: +49 511 762 19040, Fax: +49 511 762 2904
email: keyser@nano.uni-hannover.de

Quantitative determination of the charge on surface steps by high-resolution local scanning-tunneling spectroscopy

M. Kemerink[1], T.C.G. Reusch[2], D.M. Bruls[1], P.M. Koenraad[1], H.W.M Salemink[1], and J.H. Wolter[1]

[1]COBRA Inter-University Research Institute, Eindhoven University of Technology, P.O. Box 513, NL-5600 MB Eindhoven, The Netherlands
[2]IV. Physikalisches Institut, Universität Göttingen, Bunsenstrasse 13, D-37073 Göttingen, Germany

It is known that the tunneling current I_t in an STM experiment is determined by both electronic and topographic effects. On semiconducting samples, one furthermore has to deal with the effects of tip-induced band bending. All this makes it extremely hard to relate normal STM topographies to the local (energetic) position of the conduction and valence band, E_c and E_v. Such information gives, e.g., insight in the charging of surface defects or sub-surface dopants [1], but also on the potential distribution in laser diodes or p-n junctions. For determining the charge on a surface defect, the apparent topographic height of the region around the defect is usually taken as indication for the charge on the defect. From this type of measurement it is hard to extract the magnitude of the charge. This problem can be circumvented by AFM-based Kelvin probe techniques, which suffer from a limited spatial resolution [2]. Alternatively, Heinrich *et al.* [3] have estimated the charge on surface steps indirectly by the repulsive interaction with charged vacancies generated during thermal annealing which results in vacancy denuded zones along the steps. We present a novel method to quantitatively determine the charge on surface defects from I-V spectra taken with an extremely high spatial resolution. The method is applied to a p-n junction and a single and a double surface step, all on the (110) cleavage plane of GaAs.

The sample we used was MBE-grown on a n^+ GaAs substrate and contained a p-n junction with nominal doping concentrations of $N_{acc}=2*10^{16}$ cm^{-3} and $N_{don}=2*10^{18}$ cm^{-3}. The samples were cleaved under UHV conditions (<$3*10^{11}$ torr) and cross-sectional STM measurements were performed using tungsten tips. Atomically resolved topographic images were taken simultaneously with I-V spectra on a very fine grid. Typically between 64*64 and 256*256 I-V spectra were taken during one measurement.

The I-V spectra were analyzed using an extended version of the model proposed by Feenstra and Stroscio [4]. This allowed us to relate the *apparent* change in tunneling current onset bias to a *real* change in the position of E_c and E_v with respect to the Fermi level. To verify our model we followed the shift of E_c and E_v across the p-n junction, see Fig. 1. In this case we find that the real and apparent change in onset bias are identical. From the shift of the empty state tunneling current we extracted a hole doping concentration N_{acc} of $(2.1\pm0.5)*10^{16}$ cm^{-2}, in excellent agreement with the growth menu. Fig. 2. shows the same method applied to a double down surface step on the n-type GaAs. In this case the shift of the empty state onset is directly proportional to shift of E_c. The solid line is a fit to $E_c=a-b\cdot\ln(z-c)$, with z the position along the cut, which is the expected potential dependence of a line charge. From this we found that the charge at the step is (-0.8±0.1) q/nm, with q the positive elementary charge. In a similar measurement on a single up step on p-type GaAs we found a charge density of (+1.0±0.3) q/nm. In general, different charging of up and down step edges can either be due to amphoteric behavior of vacancies, or to the different termination of up and down steps on the (110) plane. The former situation is well known for the As vacancy on GaAs where, dependent on the position of the Fermi level, the resulting surface state can be either positively or negatively charged [1].

In summary, we have established a technique which allows one to quantitatively determine the charge on features on or near a semiconductor surface. This can be of great use to future studies on other surface defects such as vacancies, adatoms etc.

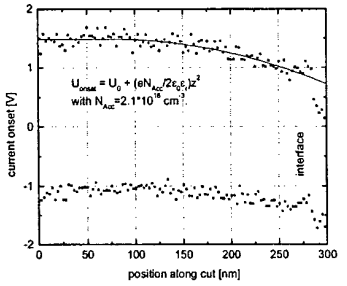

FIG. 1 Onset bias of I-V spectra as a function of postion. The cut is made over the p side (nominal doping concentration $N_{acc}=2*10^{16}$ cm^{-3}) of the p-n^+ junction. The solid line is a fit to the depletion formula, the dash-dotted line indicates the position of the p-n^+ interface. The tunneling setpoint is U_t=-2.5V, I_t=0.1nA.

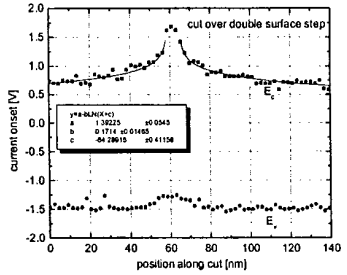

FIG. 2 Onset bias of I-V spectra as a function of position. The cut is made over a double surface step on n^+ GaAs. The tunneling setpoint is U_t=-1.8V, I_t=0.1nA.

References

[1] Ph. Ebert, Surf. Sci. Rep. **33**, 121 (1999).
[2] R. Shikler *et al*, Appl.Phys.Lett. **74**, 2972 (2000)
[3] M. Heinrich *et al.* Phys. Rev. B **53**, 10894(1996)
[4] R.M. Feenstra and J.A. Stroscio, J. Vac. Sci. Technol. B **5**, 923 (1987).

Corresponding author: Martijn Kemerink, Faculty of Applied Physics, Eindhoven University of Technology, P.O. Box 513, NL-5600 MB Eindhoven, The Netherlands
Phone +31-40-2474190, Fax. +31-40-2461339
email: m.kemerink@tue.nl

Characterization of GaAs Crystalline Nano-Rod grown by Molecular Beam Epitaxy(MBE)

H. G. Lee and T. W. Kang

Quantum-functional Semiconductor Research Center and Department of Physics, Dongguk University, 3-26, Pildong, Chunggu, Seoul 100-715, Korea.

Recently, nano-scale structures for the new functional devices are very attractive because of their possible application for next-generation electronic and photonic devices. Many works on nano-structures have been performed by many different groups[1-4]. In this report, we introduce the MBE grown GaAs nano-rod. In this experiment, semi-insulated GaAs(100) wafer are used for the substrate. On the growing procedure, the thin SiN film is used for the buffer layer on the GaAs(100). After loading the substrate, the typical growing method is performed for the rod-shape crystalline. The typical growth rate is approximately 1μm/hr with regular growth condition. While, the growth rate of nano-rod was found over 3 μm/hr with the same growth condition. The typical diameters of GaAs nano-rods are 70 ~ 85 nm(figure 1). This can be explained by migration of some portions of Ga atoms to the best stabilized points on the substrate surface. With the high resolution transmission electron microscopy (HRTEM) image and diffraction image of GaAs nano-rod(figure 2), the grown GaAs nano-rod is confirmed to be a defects free and cubic crystalline wire. On the constituent of the grown nano-rod, the contribution of Si atoms in the SiN film to the heavily Si self-doped GaAs is verified by energy dispersive X-ray fluorescence(EDX) measurement.(figure 3). During the growth of GaAs nano-rod at the temperature of 580 °C, the nitrogen near GaAs surface may react with Ga which lost the As by self annealing and the residual Si can contribute to GaAs nano-rod as a dopant. The cathode-luminescence(CL) of GaAs nano-rod(figure 4) proves this procedure. In this CL spectrum, three peaks are found due to GaAs substrate(1.42 eV), nano-rod(1.62 eV), and GaN(2.47 eV). With these results, the growth mechanism(does not include surfactant effect) of GaAs nano-rod which was reported already[5] can be confirmed again. In the conclusion, GaAs(self-Si doped) nano-rod, as a crystalline quantum wire for the one dimensional electron device which is attractive in the next generation, is grown first time by molecular beam epitaxy method. It is found that the grown GaAs nano-rod is cubic and heavily Si doped. The growth mechanism of GaAs nano-rod which has been suggested by one of authors is confirmed once again.

Acknowledgements

This work was supported by the Korea Science and Engineering Foundation through the Quantum-functional Semiconductor Research Center at Dongguk University.

Figure 1. Scanning electron microscopy image of GaAs nano-rods grown on the GaAs substrate with the 50 nm thick SiN buffer layers.

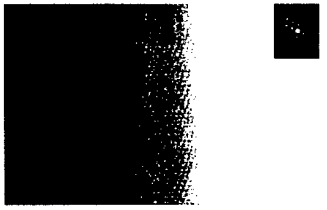

Figure 2. A high-resolution transmission electron microscopy image and a diffraction pattern of the GaAs nano-rods grown on the GaAs substrates

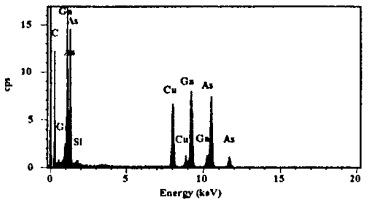

Figure 3. An energy dispersive X-ray fluorescence spectrum of the GaAs nano-rods grown on the GaAs substrates

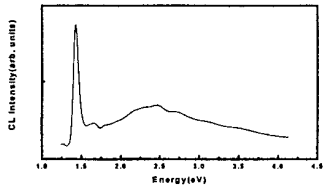

Figure 4. A Cathode-luminescence spectrum of the GaAs nano-rods grown on the GaAs substrates with the 50 nm thick SiN buffer layer

References

[1] Dai, H., Wong, E. W., Lu, Y. Z., Fan, S. & Lieber, C. M., Nature 375, 769(1995)
[2] Lu, Q. et. al. Appl. Phys. Lett. 75, 507(1999)
[3] Han, W. et. al. Science 277, 1287(1997)
[4] Ma, W. et. al. Appl. Phys. Lett. 75, 1836(1999)
[5] H. G. Lee, et. al. Appl. Phys. Lett. (in print, April. 02, 2001)

Corresponding Author: Hae Gwon Lee, Quantum-functional Semiconductor Research Center and Department of Physics, Dongguk University, 3-26, Pildong, Chunggu, Seoul 100-715, Korea. Phone: +82-2-2260-3951, E-mail: hglee2000@hanmail.net, or hglee2000@orgio.net
Web.: http://my.netian.net/~epifilm

In situ structuring during MBE regrowth with shadow masks

T.Schallenberg, C.Schumacher, W.Faschinger,

Institut für Experimentelle Physik III, Julius Maximilians Universität Würzburg,
Am Hubland, D-97074 Würzburg, Deutschland

We discuss the possibilities of MBE regrowth through shadow masks for semiconductor technology. Shadow masks developed from AlGaAs/GaAs layers on GaAs [001] substrates have first been used by Döhler to grow doping superlattices with selective contacts [1].
We proceed and explore the degrees of freedom which arise from a different chamber geometry. In our system up to five material sources are incident parallel with respect to a striped mask. The deposition area reflects the masks aperture which is defined by lithography. Manipulator tilting changes the angle of the incident molecular beams and therefore allows in situ lateral structuring in unabated structural quality.
As another growth mode we utilize an effect based on zero sticking of atoms which cannot reach their compound partner. This has first been investigated in our group and allows to further restrict the deposition area by nonparallel incidence of the compounds.
In small mask dimensions the sources halfshadows shrink and self ordering effects play a mayor role. Smooth [111] facets are observed in most cases, but dependent on material and mask orientation [114], vertical [110] or even not any facets form. ZnSe based compound semiconductors are well suited for nanostructuring as diffusion lengths along [1 –1 0] reveal to be very small. Therefore stripes oriented in [1 1 0] direction show steep edges, which may serve for secondary shadowing.
We demonstrate this technique with two sample structures. Figure 1 shows two stapled ZnSSe diodes as grown without interruption. After in situ metallization of the top n-type contact, the sample was reloaded into the II-VI chamber, and a p-ZnSe/ZnTe digital grating plus gold layer were deposited using secondary shadowing over the top diodes edge. In situ preparation of this contact structure is essential to obtain ohmic behaviour. In this way stapled three colour detectors with big filling factor, or contacts to imbedded 2DEGs can be realized with only one lithographic step. Furthermore, the 100nm offset between the gold and the grating layer is extremely homogeneous compared to the primary lithographic resolution (>100nm).
Sample 2 is a first attempt to produce wire structures of high crystalline quality with a contact structure of poor quality to be deposited before. In this case the inverted ZnSe/ZnTe p-contact was overgrown by two ZnSe layers. Due to its mismatch with the GaAs substrate the grating and all material deposited above it are fully relaxed (Figure 2 – reference). In the shadow mask experiment the edge of the grating structure plus first ZnSe layer was used for secondary shadowing of the second layer. In this way a pseudomorphic ZnSe wire was formed (Figure 2 – zs 2264 liftoff). A good III-V / II-VI interface is achieved by a special procedure during the growth of the grating structure.

References

[1] K.H.Gulden, X.Wu, J.S.Smith, P.Kiesel, A.Höfler, M.Kneissl, P.Riel and G.H.Döhler: *Novel shadow mask molecular beam epitaxial regrowth technique for selective doping.* Appl. Phys. Let. 62 (24), 3180 (1993)

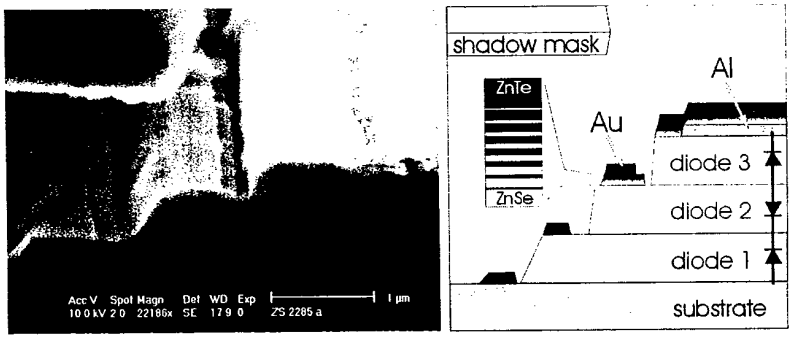

Fig. 1: In situ structured contact to an imbedded p-ZnSSe layer

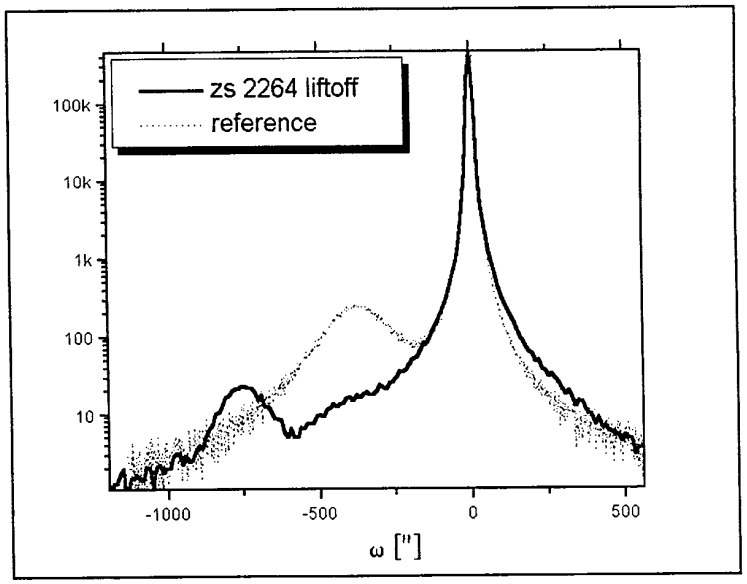

Fig. 2: HRXRD omega-2 theta scan around the [004] GaAs substrate peak

Corresponding author: Timo Schallenberg, Experimentelle Physik III, Universität Würzburg,
Am Hubland, D-97074 Würzburg, Germany,
phone: ++49 931 888 5124, fax: ++49 931 888 5142,
email: timo@physik.uni-wuerzburg.de

Carrier Confinement of a InGaAs QW Induced by a Periodical Stressor Layer

J. Grenzer[1], U. Zeimer[2], U. Pietsch[1], S. Gramlich[2], F. Bugge[2], V. Smirnitzki[2], Ch. Lienau[3], S. Grigorian[1], M. Weyers[2], and G. Tränkle[2]

[1]Institut für Physik, Universität Potsdam, Am Neuen Palais 10, D- 14415 Potsdam, Germany
[2]Ferdinand-Braun-Institut für Höchstfrequenztechnik, Albert-Einstein-Str. 11, D-12489 Berlin, Germany
[3]Max-Born-Institut, Rudower Chausee 6 D-12489 Berlin, Germany

We report on a strain induced lateral carrier confinement inside a GaAs-InGaAs-single quantum well structure (SQW) caused by etching of a lateral surface grating into the initially pseudomorphicly strained InGaP layer, while the SQW itself remains unaffected. We investigated the strain distribution using X-ray grazing incidence diffraction (GID) as well as the strain induced change of the photoluminescence (PL) spectrum. Compared to the pseudomorphic value we found an increase and a decrease of the strain in the SQW below the etched and nonetched stressor layer regions. This effect leads to a spatial and spectral shift of the PL line. This shift depends on the lattice mismatch as well as on the form of the lateral grating etched into the stressor layer.

In recent years many attempts were made to achieve a lateral carrier confinement either by self-organized growth of heavily strained islands [1], by lateral etching of a quantum well [2] or alternatively by patterning via lateral etching and regrowth, which is often accompanied by creation of nonradiative defects at the interfaces [3]. To avoid this Kash et al. [4] proposed the concept of a laterally patterned stressor layer on top of a SQW, which influences the optical properties of the underlying SQW by introducing a lateral inhomogeneous strain distribution.

In our study a lateral strain variation was realised by patterning of a initially pseudomorphically strained InGaP layer grown on top of a 10 nm thick $In_{0.16}Ga_{0.84}As$ SQW. The pseudomorphic strain of the InGaP stressor layer can easily be controlled by its In/Ga ratio, i.e. the layer can be strained either tensely or compressively. Lateral modulation of the electronic band gap within the SQW is achieved via strain relaxation of the etched ridges of the InGaP layer. The InGaAs-SQW remains unaffected by the etching process avoiding defect formation and subsequent nonradiative recombination of charge carriers. Due to the lateral strain modulation photoluminescence measurements (PL) at a temperature of 10 K show a splitting of the InGaAs-QW emission into two spatially separated lines.

Detailed knowledge of the 3D strain distribution within the sample is necessary to calculate the strain induced change of the band structure. Nondestructive X-ray diffraction in grazing-incidence geometry is capable to obtain in-plane strain information within a surface grating structure. Its particular depth sensitivity provides information about the in-plane strain distribution in depth [5]. The measured intensity profiles are discussed in terms of a strain distribution model, created by finite-element calculations using a linear elasticity theory approach. Using spatially resolved PL the strain-induced shift of the SQW electronic band levels was verified. The PL-results are compared to band structure calculations using a deformation potential ansatz.

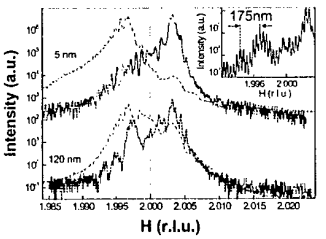

Fig.1: Strain sensitive x-ray patterns.

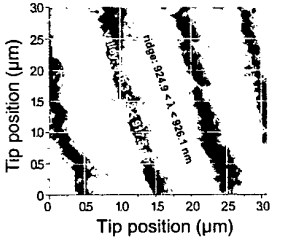

Fig.2: Spatial separation of the PL lines.

Fig.1 shows strain sensitive x-ray patterns (period 1 µm) for two penetration depths. For a tensily strained InGaP stressor layer (3000ppm, solid line) the highest intensity peak is observed at a higher H value compared to the GaAs substrate (H=2) indicating a smaller parallel lattice constant. This is attributed to the relaxed part of the patterned InGaP, where the total strain is compressive. Consequently other sample regions are tensely strained leading to additional features in the x-ray patterns (Fig.1 inset). The width of this tensely strained region can be estimated to be about 175 nm. A compressive strained InGaP layer leads to an opposite result. The partly relaxed InGaP layer (-3000ppm, dashed line) causes a tensile strain and therefore the region below the valley is now compressively strained. A clear depth dependence for QW structures can be observed. Therefore the location of the this region is in vicinity of the InGaAs-QW. Figure 2 shows a spatial resolved PL measurement for the compressively strained InGaP layer. Beneath the ridge the transition energy is smaller (~1.337 eV) compared to the initial value (~1.343 eV) whereas inside the valley it is increased (~1.355 eV).

We have shown, that a lateral patterning of an initially pseudomorphicly strained InGaP stressor layer results in a lateral periodic strain field. It extends through the underlying InGaAs-SQW and initiates a periodic band edge variation leading to a periodic charge carrier confinement without creation of nonradiative defects.

References

[1] D. Bimberg, M. Grundmann and N. N. Ledentsov "Quantum Dot Heterostructures" Wiley, Chicester (1998).
[2] B. P. Van der Gaag and A. Scherer, Appl. Phys. Lett. **56**, 481 (1990).
[3] A. Forchel, R. Steffen, T. Koch, M. Michel, M. Albrecht and T. L. Reinecke, Semicond Sci. And Technol. **11**, 1529 (1996).
[4] K. Kash, J. M. Worlock, M. D. Sturge, P. Grabbe, J. P. Harbinson, A. Scherer and P. S D. Lin, Appl. Phys. Lett. **53**, 782 (1988).
[5] U. Zeimer, J. Grenzer, U. Pietsch, S. Gramlich, F. Bugge, V. Smirnitzki, , M.Weyers and G. Tränkle, J. Phys. D: Appl. Phys. **34** 2001, in press.

Corresponding author: Joerg Grenzer, Universtät Potsdam, Institut für Physik, Strukturanalyse, Am neuen palais 10, D-14469 Potsdam, Germany
phone: + 49 331 977 1824, fax: +49 331 977 1133,
email: grenzer@rz.uni-potsdam.de

Highly efficient two-photon absorbing Material for application in three-dimensional Micro and Nanostructuring

C. Cagran[1], A. Hohenau[1], U. Scherf[2], G. Leising[3]

[1]Institut für Nanostrukturierte Materialien und Photonik, Joanneum Research Forschungsges.m.b.H., Franz Pichler Straße 30, A-8160 Weiz, Austria
[2]Intitute für Physikalische und Theoretische Chemie, Universität Potsdam, Germany
[3]AT&S Research & Techology AG, Fabriksgasse 13, A-8700 Leoben, Austria

Two-photon processes have been used to create a number of chemical and physical processes including optical data storage, fluorescent imaging, optical waveguiding and lithographic mircofabrication[1,2]. Recently, experimental progresses in lithographic microfabrication attracted a lot of attention as two-photon or higher order multiphoton processes show the promise of geometrically complex, 3D optical circuitry or photonic bandgap devices fabrication.
The fundamental idea behind using two-photon processes for 3-dimensional microstructuring is that - due to the nonlinear dependence on light-intensity – the absorption and the subsequent photochemical reaction is sharply localized in a small volume area around the focal point of a highly focused laser beam. The principle for this method is described.
The 3-dimensional microfabrication uses laser induced photopolymerization of a resin mixed with a polymer which acts as a two-photon absorbing polymerization initiator. The latest approach in two-photon absorbed microfabrication utilizes photoreduction of organic metal salts for producing 3-dimensional conducting structures in a host matrix [3].
For the practical use of any multi-photon process, the absolute value of the absorption crossection is of major relevance. Therefore, different efforts have been made to not only determine the two-photon absorption crossections for different organic materials but also to determine the physical origin of different crossections in varying materials[4].

We present two-photon absorption measurements, performed on a poly-phenylene like structure, which exhibits one of the highest known two-photon absorption crossection [5] and relate it to the special structural properties of the material. The narrow width of the absorption band, the well resolved vibronic structure and the small Stokes-shift are a consequence of the rigid backbone of the investigated material. We think that this rigid structure and its effect on the electronic structure is responsible for the observed effect.
The method for measuring the two-photon absorption crossection is presented. A cw Ti:Sapphire laser is focused on a 0.1mm cuevette containing a solution of the material under investigation. The value of two-photon absorption crossection is derived from the two-photon luminescence compared to single-photon luminescence, excited with a Ar^+-Ion laser at the wavelength of 360nm. Since the linear absorption of the sample can be measured at this wavelength with a commercial spectrophotometer, we are able to extract the two-photon absorption crossection from these measurements.

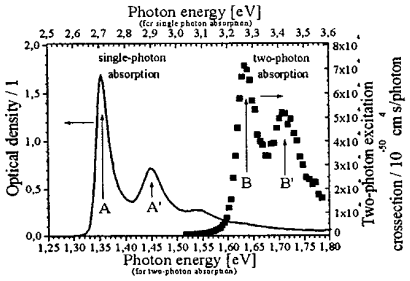

Fig. 1: Single and two-photon absorption spectra of the poly-para phenylene type material. A, A' and B, B' mark the single and two-photon absorption peaks and their vibronic replicas, respectively.

For 3D microstructuring, we introduced the phenylene-type polymer in a photoactive matrix, which is transparent to light at the two-photon absorption wavelength. The method for 3D structuring is analog to that one described above. We present AFM and SNOM pictures of the obtained structures and issue the achievable resolution.

References

[1] M. P. Joshi et.al., Appl. Phys. Lett, 74(2), 1999
[2] B.H. Cumpston et.al., NATURE, 398, 1999
[3] P.W. Wu et.al., Adv. Mat., 12(19) 2000
[4] T. Kogej et.al., Chem. Phys. Lett., 298,1998
[5] A. Hohenau et.al., submitted to Advanced Materials

Corresponding author: Andreas Hohenau, Institut für Nanostrukturierte Materialien und Photonik, Joanneum Research Forschungsges.m.b.H., Franz Pichlerstraße 30, A-8160 Weiz, Austria.
phone: +43 3172 44033 2704, Fax: +43 3172 603 2710
email: andreas.hohenau@joanneum.at

Nano-scale dislocation patterning in PbTe on PbSe (100) heteroepitaxy studied by UHV scanning tunneling microscopy

K. Wiesauer and G. Springholz

Institut für Halbleiter- und Festkörperphysik, Johannes Kepler Universität Linz, Altenbergerstraße 69, A-4040 Linz, Austria

Pattern formation during lattice-mismatched epitaxial growth of semiconductor heterostructures has recently evolved as a novel method for fabrication of low-dimensional nanostructures. Apart from the direct synthesis of self-assembled quantum dots via the Stranski-Krastanow growth mode, dislocation prepatterning has been demonstrated as a tool for spatial manipulation of the nucleation sites of self-assembled quantum dots [1]. It is based on the local perturbation of the total free energy of the growing surface due to the localized elastic strain fields of subsurface misfit dislocations, which provides preferential nucleation sites for subsequently deposited SK islands. In semiconductors, however, misfit dislocations are usually distributed in a highly irregular way within the layers. This is due to the fact that misfit dislocations are mostly formed within glide planes inclined to the layer/substrate interface. Thus, once formed, the mobility of dislocations within the interface is rather small.

In the present work, we have studied misfit dislocation patterning in the PbTe on PbSe (100) heteroepitaxial system using UHV scanning tunneling microscopy. From our experimental observations it is demonstrated that highly regular misfit dislocation arrays can be produced if certain conditions are fulfilled. These are: a) a strong mutual repulsive interaction between neighboring misfit dislocations, b) a high dislocation mobility within the interface, and c) a low threading dislocation density. As shown in this work, these conditions are fulfilled in the PbTe/PbSe system grown on (100) oriented substrates where in spite of the rather large 5.2 % lattice-mismatch a 2D growth mode prevails during deposition (see Fig. 1). From systematic STM studies of layers with varying PbTe thicknesses, strain relaxation is found to occur purely by misfit dislocation formation starting at a critical layer thickness of only 0.8 monolayers. The misfit dislocations are of pure edge character and they appear as dark lines along the fourfold <011> directions in large scale STM images (see Fig. 1 b)-d)).

Atomically resolved STM images of the threading ends of the dislocations (Fig. 1(f)) show that the Burgers vector is equal to 1/2<011> parallel to the heterointerface. As the heterointerface coincides with the (100) glide planes of the leadsalt materials system, the misfit dislocations are highly mobile within the interface. In addition, STM images of the very early relaxation stage show that dislocation half loops are injected homogenously from monolayer step edges on the surface. As the PbTe layer thickness increases, the dislocation density rapidly increases. Above around 5 ML PbTe a nearly perfect square array of misfit dislocations with lateral periods in the range 100 Å is formed. This is evidenced by the appearance of satellite peaks in the FFT power spectra of the STM images shown in Fig. 1 as inserts, as well as by the narrow width of the histograms of the dislocation spacing shown in Fig. 2. The regularity of this dislocation pattern is found to scale inversely with the misfit dislocation spacing that determines the strength of the elastic dislocation interactions. For the smallest dislocation separations a variation of ±12% in the dislocation spacing is achieved (Fig. 2d), which is less than the typical variations in size and spacing of self-assembled quantum dots formed by the Stranski-Krastanow growth mode. Thus, these structures can serve as template for the fabrication of self-organized ordered semiconductor nanostructures.

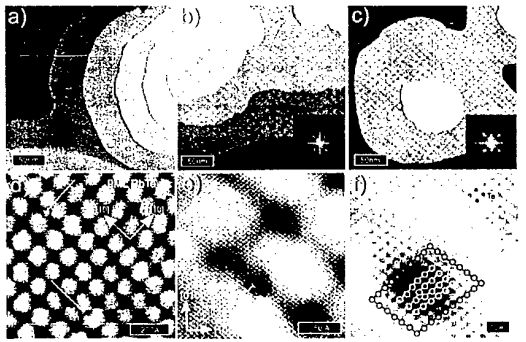

Figure 1: STM images of PbTe layers on PbSe (100) for different layer thicknesses of (a) 0.3, (b) 4.6 and (c) 9.2 monolayers (ML). Zoomed-in STM images at 9.2 ML coverage are shown in (d) to (f). As indicated in (d) a very regular quadratic dislocation array is formed along the fourfold <011> directions with an average dislocation spacing of about 10 nm. The atomically resolved STM lattice image of the end point of a misfit dislocation shown in (f) prooves that the burgers vector is equal to 1/2<011>, *i.e.*, the dislocations are of pure edge character and therefore have a very high mobility within the interface. Insert: FFT power spectra of the STM images with the appearance of strong satellite peaks indicating a well-defined periodicity of the dislocation array.

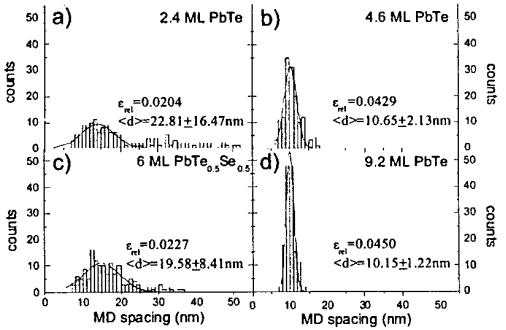

Figure 2: Histograms of the lateral misfit dislocation spacings for PbTe layers with increasing layer thickness of (a) 2.4 ML, (b) 4.6 and (d) 9.2 ML PbTe as well as (c) for a 6 ML $PbSe_{0.5}Te_{0.5}$ on PbSe (100), showing that the distributions narrow with decreasing average dislocation spacing due to the corresponding increase in the repulsive dislocation interaction.

References

[1] see, *e.g.*, S. Yu. Shiryaev, *et al.*, Phys. Rev. Lett. **78**, 503 (1997); and R. Leon, *et al.*, Appl. Phys. Lett. **74**, 2301 (1999).

Corresponding author: Karin Wiesauer, Institut für Halbleiter- und Festkörperhysik, Johannes Kepler Universität Linz, Altenbergerstraße 69, A-4040 Linz, Austria.
phone: +43 732 2468 9602, Fax: +43 732 2468 8650
email: k.wiesauer@hlphys.uni-linz.ac.at

Heteroepitaxial PbTe-on Si pn-junction IR-sensors: Correlations between material and device properties

Karim Alchalabi, Dmitri Zimin, Hans Zogg

Thin Film Physics Group, Swiss Federal Institute of Technology, Zurich, Switzerland

Epitaxial IV-VI narrow bandgap semiconductors can be grown on Si(111) substrates with high quality despite the large lattice and thermal expansion mismatch. A CaF_2 buffer layer is helpful for compatibility and an extended growth window. Dislocations are extremely mobile in narrow gap lead chalcogenides. When grown on Si(111), mechanical strain built up by the thermal mismatch relaxes easily on each temperature change due to dislocation glide, and the dislocation density even reduces by dislocation reactions [1].

Test arrays with photovoltaic n^+-p PbTe sensors (cut-off wavelength 5.5 µm at 80K) of different sizes were fabricated and analysed. The sensitivities are g-r-limited at temperatures T below 120K. The g-r carrier lifetimes in the depletion region are determined from the RoA-products (inverse noise current density) vs 1/T. The corresponding diffusion lengths are correlated with the material properties, namely low temperature saturation Hall mobilities and X-ray rocking curve line widths. All these parameters are determined by the density of the threading dislocations; good consistency is observed. The result is similar to that obtained for metal-semiconductor Pb/PbSnSe infrared sensors [2]: Each threading dislocation crossing the depletion region gives rise to a shunt resistance. However, narrow gap IV-VI materials are rather forgiving; even with dislocation densities up to the high 10^7 cm^{-2} range, useful devices still result.

Using Si substrates containing prefabricated CMOS read-out integrated circuits (ROIC) near each pixel, such PbTe layers were applied to fabricate a first heteroepitaxial, but monolithic two-dimensional infrared focal plane array (96 x 128 pixel) in a narrow gap semiconductor on an electrically active Si-substrate.

[1] P. Müller, H. Zogg, A. Fach, J. John, C. Paglino, A.N. Tiwari, M. Krejci, and G. Kostorz, Reduction of threading dislocation densities in heavily lattice mismatched PbSe on Si(111) by glide, Phys. Rev. Lett. 78, 1997, pp. 3007-3010.

[2] A. Fach, J. John, P. Müller, C. Paglino, and H. Zogg, Material properties of $Pb_{1-x}Sn_xSe$ epilayers on Si and their correlation with the performance of infrared photodiodes, Journal Electronic Materials 26, 1997, pp. 873-877.

Corresponding author:
H. Zogg, Thin Film Physics Group, ETH-Technopark, CH-8005 Zurich
phone +41 1 445 1480, fax +41 1 445 1499
zogg@phys.ethz.ch http://www.tfp.ethz.ch

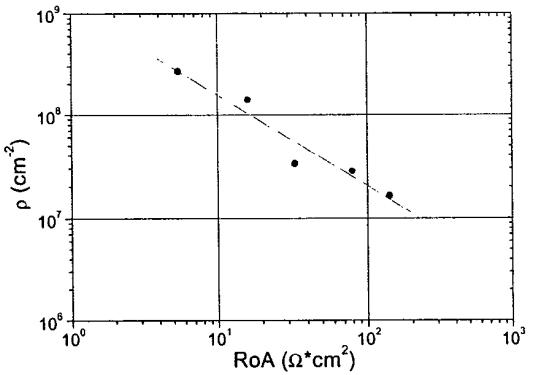

Fig. 1. Correlation of resistance-area products RoA (inverse noise currents) at 90K with dislocation densities ρ. The dislocation densities were independently determined from x-ray diffraction line widths and low temperature Hall-mobilities

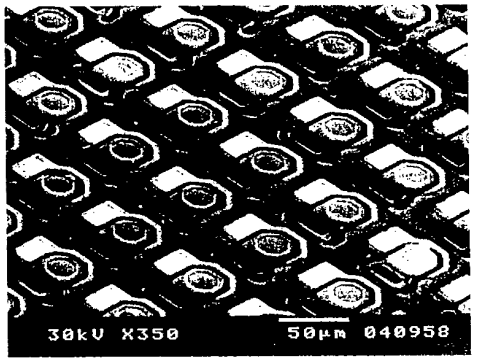

Fig. 2. Part of the first heteroepitaxial, but monolithic two-dimensional infrared focal plane array (96 x 128 pixel) fabricated in a narrow gap semiconductor on an electrically active Si-substrate containing the ROIC. The infrared sensors are photovoltaic Pb/p-PbTe for the 3-5 µm range.

Absorption and photoluminescence in PbTe/$Pb_{1-x}Eu_xTe$ quantum wells

E. Abramof [1], E. A. de Andrada e Silva [1], I.I. Zasavitskii [2], S.O. Ferreira [1*], P. Motisuke [1], P.H.O. Rappl [1], A.Y. Ueta [1]

[1] Laboratório Associado de Sensores e Materiais - LAS, Instituto Nacional de Pesquisas Espaciais - INPE, CP515, 12201-970 São José dos Campos - SP, Brazil
[2] P.N. Lebedev Physical Institute of RAS, Leninskii Pr. 53, 117924 Moscow, Russia

Due to the break of translation symmetry along the [111] growth direction, both strain and quantum size effects lift the four-fold valley degeneracy of the PbTe bulk material. The longitudinal valley (along the growth direction) is split from the other three equivalent ones, which are called oblique valleys. Therefore, the optical spectra of PbTe quantum wells (QW's) exhibit a complex structure with transitions involving the different types of valleys. The absorption due to the oblique transitions is stronger due to both the three-fold valley degeneracy and the higher two-dimensional density of states. However, due to the high mass-anisotropy in PbTe (~10), the absorption edge is in general the first longitudinal transition, and the energy separation between the longitudinal transitions is smaller than that for the oblique valleys.

Very recently, we have studied the absorption spectrum of PbTe quantum wells (QW's) as a function of well width and temperature [1]. For that purpose, a series of PbTe/$Pb_{1-x}Eu_xTe$ (x~0.05-0.07) MQW samples were grown on BaF_2(111) substrates by molecular beam epitaxy. The PbTe well width was varied from 2.3 to 20.6 nm, while the $Pb_{1-x}Eu_xTe$ barrier was kept thicker than 44 nm. Detailed high-resolution x-ray diffraction analysis allowed the determination of the structural parameters and the tensile parallel strain inside the PbTe wells with high accuracy, for each sample at room temperature [2]. From the absorption steps observed in the transmission spectra, measured at temperatures from 5 to 300 K, the interband optical transition energies between the confined states in the PbTe QW's were determined for all samples. Several transitions, involving both longitudinal and oblique valleys, were clearly observed. The electric-dipole transition energies were calculated analytically using a two-band **k.p** model and a perfect symmetric square well with Ben Daniel-Duke like boundary conditions. The strain effects were included in the calculations through different values of deformation potentials. Contrary to what is commonly believed, an overall good agreement (for the different transitions, well widths, and temperatures) was found between the calculations and the absorption data. However, a more accurate optical probe would be necessary for definite conclusions about the quantum effects in these QW's. Therefore, we have performed photoluminescence (PL) measurements on these MQW samples at 4.2 and 77 K, and present here the main data, comparing them with the absorption spectra. Figure 1 shows the photoluminescence signals at both temperatures for PbTe/$Pb_{1-x}Eu_xTe$ MQW samples with different well width L. The quantum size shift in these PbTe QW's is clearly observed. The narrow line width (1 - 4 meV) and the intensity of the PL curves demonstrated the high quality of the grown samples. Figure 2 shows the energy of the first absorption step corresponding to the first longitudinal transition together with the low energy edge of the photoluminescence signal as a function of PbTe well width. The solid and dashed curves correspond to the theoretical calculations with the lower (x = 0.05) and upper (x = 0.07) limit of Eu content of our series of samples. For these calculations, we used D_d=4.3eV and D_u=-2.8eV for the differences between conduction and valence-band deformation potentials, and a linear fit to the strain values obtained with room temperature x-ray measurements for the different samples. It is important to emphasize that, among the various values of deformation potentials found in the literature, the best fit to our absorption and PL experimental results point to this set of values. The remarkable agreement between the photoluminescence data and the simple square well model, with analytical solutions within the envelope function approximation, reinforces the validity of the proposed model to distinguish and predict quantum size and strain effects in PbTe. The difference between the PL edge and the first absorption step (Stokes shift) as well as the PL line width are found to increase for decreasing well width. The origins of the Stokes shift and of the PL line width in these QW's are discussed here together with the blueshift observed at low temperatures.

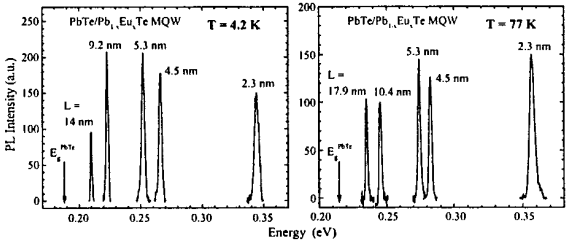

Fig. 1 - Photoluminescence signals at 4.2 and 77K of PbTe/$Pb_{1-x}Eu_xTe$ MQW samples with different PbTe well width L. The arrows indicate the energy gap of bulk PbTe.

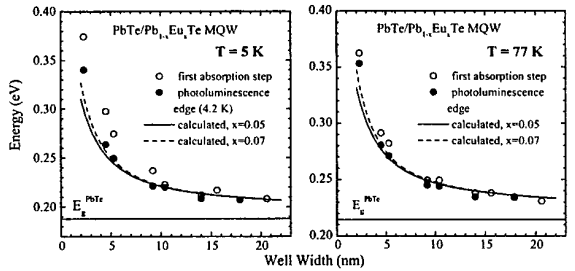

Fig. 2 - First absorption step and low energy photoluminescence edge as a function of PbTe well width. The solid (dashed) lines correspond to theoretical curves calculated with Eu content x=0.05 (x=0.07). The horizontal lines correspond to the energy gap of the bulk PbTe.

References

*Permanent address : Departamento de Física, Universidade Federal de Viçosa, 36751-000 Viçosa - MG, Brazil.
[1] E. Abramof, E.A. de Andrada e Silva, S.O. Ferreira, P. Motisuke, P.H.O. Rappl, A.Y. Ueta, Phys. Rev. B **63**, 85304 (2001).
[2] E. Abramof, P.H.O. Rappl, A.Y. Ueta, P. Motisuke, J. Appl. Phys. **88**, 725 (2000).

Corresponding author: Eduardo Abramof, Instituto Nacional de Pesquisas Espaciais / LAS, CP515, 12201-970 São José dos Campos - SP, Brazil.
phone: +55 12 345-6675, Fax: +55 12 345-6717, email: abramof@las.inpe.br

Nano-scale metallic and superconducting circuits in semiconducting superlattices

N.Ya.Fogel[1,2], E.A.Pashitskii[1,3], A.V.Danilov[1], Yu.V.Bomze [4], R.I.Shekhter[1], M.Jonson[1]

[1] Dept. Appl. Phys, Chalmers University of Technology, S-412 96, Göteborg, Sweden

[2] Solid State Institute, Technion, 32100 Haifa, Israel

[3] Institute of Physics, 46 Nauki Avenue, 01023, Kiev, Ukraine

[4] B.Verkin Institute for Low Temperature Physics and Engineering, 47 Lenin Avenue, 61164 Kharkov, Ukraine

Among a large variety of different superconducting superlattices (SL) the special place belongs to the semiconducting superconducting SLs consisting of semiconductors A^{IV}–B^{VI}. Two SLs of this type – PbTe/PbS and PbTe/SnTe – are known for a long time [1,2]. Recently the novel superconducting semiconducting SLs (PbTe/PbSe; PbS/PbSe; PbTe/YbS: PbTe/EuS) with the transition temperature T_c in the range 3-6 K have been discovered [3]. Appearance of superconductivity in all these SLs looks rather fascinating because it is inherent only to the multilayered compositions, while the individual materials constituting SLs are not superconductors (with only exception of SnTe having T_c=0.22 K). The single thin films (with thickness d =15-300 nm) of all chalcogenides do not reveal superconductivity too. The measurements of the critical magnetic fields revealed that typical for all layered superconductors 3D–2D dimensional crossover takes place when magnetic field is oriented along the layer planes. This is a clear indication that the system studied consists of the separate superconducting layers connected by weak Josephson coupling. Because the absence of the superconductivity in the single semiconducting films is the undoubtedly established fact, one arrives to the conclusion that superconducting layers should be confined to the interfaces between two semiconductors. All SLs which reveal superconductivity have metallic-type conductivity. The unique properties of the chalcogenide SLs described above usually appear at the sufficiently large thicknesses of the constituting SLs epitaxial films (d > 10 nm) when on the interfaces between two semiconductors the two-dimensional (2D) nanoscale superstructure of the edge misfit dislocations (EMD) forms [3]. Characteristic periods of the dislocation grids D_g=3÷25 nm. It is important to emphasize that metallic conductivity and superconductivity may be observed only in such SLs which contain as its component at least one narrow-gap semiconductor (PbS, PbTe, PbSe, SnTe) [3]. For these semiconductors anomalously strong dependence of the energy band gap on the pressure is reported, and the sign of this dependence is also anomalous ($dE_g/dP < 0$) [4].

Here we show that self-doping leading to the metallic-type conductivity and to the superconductivity in semiconducting heterostructures take place due to a spatially-inhomogeneous deformation of the crystal lattices created by the EMDs. Such a deformation gives rise to the essential energy bands bending of the material near the interfaces. Along with the contact potential difference such a deformation leads to the formation near the interfaces of the degenerated electron and hole layers consisting of the multi-connected

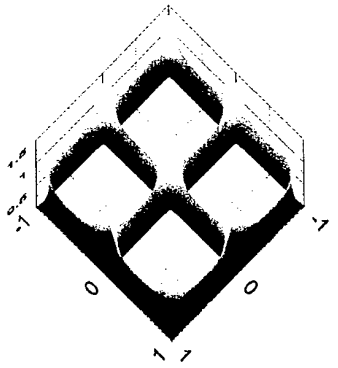

Figure 1

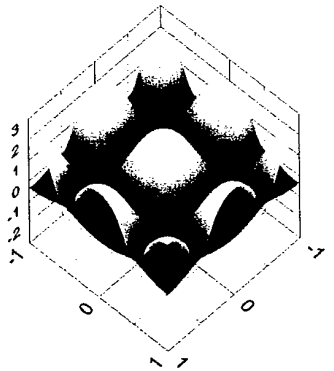

Figure 2

circuits of the conducting nanoscale channels. The structure of these layers reflects the periodic arrangement of the dislocation grids.

The calculations of the band structure in the vicinity of the interfaces where the influence of the non-uniform strain fields of the EMDs is the most essential was performed in a framework of continuum elastic theory of the crystals. This band structure differs significantly from one characteristic for the strain-free compounds, and depends essentially on the combination of the semiconductors chosen as well as on the contact potential difference. In Fig.1 the calculated form of the nanocircuit arising in a case of contact PbTe/PbS is shown. Multiconnected tubes in this figure show the spatial position of the surface where the band inversion in both materials takes place. If the common Fermi level is located around the points of the band inversion there are the charge carriers of the electron type above this surface. This situation corresponds to the metallic conductivity along the interface. When E_F is below of the band inversion points one obtains the hole-like "lakes" located inside the EMF grid elementary units instead of tubes, and metallic-type conductivity cannot be expected (see Fig.2).

If electron nanocircuits are present, the magnetoresistance (MR) should be an oscillating function of the perpendicular magnetic field with a period determined by an accomodation of magnetic flux quantum Φ_0 within a single unit of the nanocircuit. Estimates show, that for PbTe/PbS considered above the flux through the elementary unit will be equal to Φ_0 in a field ~80 T. In experiments the giant MR is observed in fields <5 T which is, maybe, a precursor of the oscillations predicted. For the SL SnTe/PbTe with Dg=23 nm the oscillations might be observed in the fields about 4 T. Such measurements are in process of preparation now.

References

[1] K. Murase et al., Surf. Sci. 170, 486 (1986)
[2] O.A.Mironov et al., JETP Letters 48, 106 (1988)
[3] N.Ya:Fogel et al., Phys. Rev. Lett. 86, (2001)
[4] G. Nimtz, B. Schlicht. Narrow-Gap Semiconductors, Springer-Verlag, 1983

Corresponding author: Nina Fogel, , Solid State Institute, Technion, 32100 Haifa, Israel
phone:+972 4 829 3916, Fax:+ 972 4 823 5107,
email: nfogel@techunix.technion.ac.il.

Fabrication and elastic properties of InAs freestanding structures based on InAs/GaAs(111)A heteroepitaxial systems

H. Yamaguchi[1], R. Dreyfus[1,2], S. Miyashita[3], and Y. Hirayama[1,4]

[1]NTT Basic Research Laboratories, Kanagawa 243-0198, Japan
[2]Ecole Superierure de Physique et de Chimie Industrielles de la ville de Paris, France
[3]NTT Advanced Technology, Kanagawa 243-0198, Japan
[4]Core Research for Evolutional Science & Technology (CREST), JST, Japan

The electrical and mechanical properties of micro- and nano-electromechanical systems (MEMS/NEMS) are of growing interest not only from technological standpoint but also from fundamental science, such as macroscopic quantum tunneling and quantized phonon transport [1]. The material systems so far used for fabricating MEMS/NEMS structures are mainly Si/SiO_2 and also semiconductor heterostructures. We have fabricated and characterized several number of freestanding InAs beams and cantilevers processed from InAs/GaAs heterostructures grown on GaAs (111)A surfaces, where the InAs thinfilm grows in layer by layer mode despite of the large lattice mismatch of 7 % [2]. Compared with other semiconductors, InAs-based structures have the advantage that the surface Fermi level pinning in the conduction band provides the possibility of fabricating much thinner conductive membranes without suffered from the problem of carrier depletion [3].

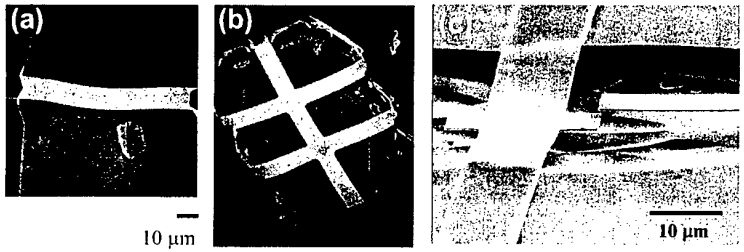

Fig. 1: SEM images of free standing InAs (a) beam, (b) Hall bar, and (c) cantilever. The InAs thickness is 100 nm ((a) and (b)) and 300 nm (c) with the width of 10 μm. Focused ion beam process was applied to fabricate the cantilever (c) with forming a 2μm vacuum gap.

Figure 1 shows the SEM images of typical freestanding InAs structures with the thickness and the width of 100-300 nm and 10μm, respectively. In the fabrication processes, the GaAs underlayer was selectively removed by alkaline etchant after defining the lateral dimension by conventional photolithographic technique. All the beams were deflected downward to relax the residual strain of about 0.5% in the InAs films. To fabricate cantilevers, focused ion beam was applied to cut the beams making a vacuum gap (Fig.1(c)). By applying the bias voltage across the gap, the mechanical motion of the cantilever was electrically activated. The Hall measurements proved that the freestanding InAs membranes show much higher electron concentration and mobility than as-grown heterostructures samples (i.e. InAs/GaAs). This is probably because the relaxation of residual strain in InAs layer reduces the deformation potential. As the results, the increased carrier concentration improves the electron mobility by screening effects. The removal of dislocation networks at the InAs/GaAs interfaces can also be responsible for the improvement in the mobility.

The SEM image and the mechanical resonance characteristics of a similarly fabricated 300 nm-thick coupled cantilever structure are shown in Fig.2. Applying an AC voltage, with a magnetic field perpendicular to the current thorough the coupling part of the cantilever, the induced Lorentz force actuates the oscillatory motion. This motion induces the resistive voltage to the current and the mechanical resonance can be electrically detected as the change in the AC resistance of the devices [1]. At about 24.8 kHz, we confirmed clear resonance, whose peak height was proportional to the square of magnetic field intensity. The quality factor has the range of 2000-3500 depending on the bias voltage and the magnetic fields. With strong magnetic fields and large applied voltages, we clearly observed a hysteresis. By applying a non-linear Duffing equation, this bi-stability can be explained by the non-linear elastic response of the InAs membrane, which becomes significant with large deflections of the coupled cantilever.

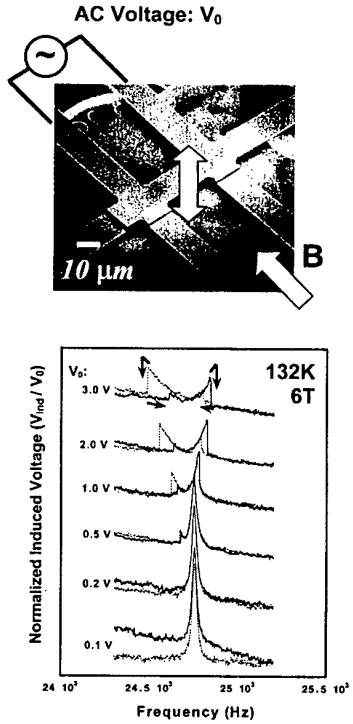

Fig.2 A SEM image and the induced voltage as a function of AC frequency at various applied voltages of a coupled InAs cantilever.

References

[1] A.N. Cleland and M.L. Roukes, in *Proc. of 24th Int. Conf. on Physics of Semiconductors*, ed. D. Gershoni, World Scientific, Singapore 1999, p261.
[2] H. Yamaguchi, Y. Homma, K. Kanisawa, and Y. Hirayama, Jpn. J. Appl. Phys. 38, 635 (1999).
[3] K. Yoh, A. Nishida, H. Kawahara, S. Izumiya, and M. Inoue, Semicond. Sci. Technol. 9, 961 (1994); H. Yamaguchi, R. Dreyfus, S. Miyashita, and Y. Hirayama, to be published in Appl. Phys. Lett.

Corresponding author: Hiroshi Yamaguchi, NTT Basic Research Laboratories, 3-1, Morinosato-Wakamiya, Atsugi-shi, Kanagawa, 243-0198 Japan.
phone: +81 46 240 3475, Fax: +81 46 240-4727
email: hiroshi@will.brl.ntt.co.jp

Etching temperature dependent mobilities up to 190.000 cm^2/Vs at chlorine etched and regrown interfaces

S. Beyer, S. Löhr, Ch. Heyn, D. Heitmann, W. Hansen

Institut für Angewandte Physik und Zentrum für Mikrostrukturforschung,
Universität Hamburg, Jungiusstrasse 11, D-20355 Hamburg, Germany

The combination of molecular beam epitaxie (MBE) with in-situ dry etching enables to design and prepare novel complex semiconductor-heterostructures. Concerning the electronic properties of such structures it is inevitable to establish etching techniques leaving contamination free, smooth surfaces. In this context, we examine chlorine etched GaAs surfaces, epitaxially overgrown with modulation doped AlGaAs. We have found a strong dependence of the electronic quality on etching temperature.

Our MBE system is equiped with an additional etching chamber allowing a combination of both, physical etching with a plasma ion source (not used here) and chemical etching via the injection of Cl_2. An UHV transfer module enables us to transfer samples between the two chambers without air exposure.

In this work we focus on the influence of the etching temperature on the etched/regrown interface, keeping the Cl_2 pressure and the etching time constant. As done by Kadoya et al.[1,2] we use a high-mobility two-dimensional electron gas (2DEG) to monitor the disturbances induced by the etching process. The structure was amended by a marker to control the etching depth via cross-sectional scanning electron microscopy (SEM). The etching depth after 60 seconds chlorine etching at 8×10^{-4} Torr was determined as 100 to 200 nm in all cases. The etched GaAs buffers were epitaxially overgrown with 15 nm undoped $Al_{0.3}Ga_{0.7}As$, 57 nm Si-doped $Al_{0.3}Ga_{0.7}As$, followed by a 5 nm GaAs cap layer. Thus the GaAs/AlGaAs interface, at which the 2DEG resides, is coincident with the etched inerface (fig.1).The carrier density N_s and mobility μ of the electron system at the interface were investigated via magneto-transport measurements at 4.2K (fig.2). We have found that for 450°C, at this specific Cl_2 pressure, the interface is almost damage free. At this temperature with μ = 190.000 cm^2/Vs the carrier mobility is only reduced by factor 2 in comparison to a reference structure grown without etching and no growth interruption. On either side of this minimum in damage the carrier mobility is diminished with etching temperature. Exept for the sample with the highest etching temperature, where no mobile electron system could be detected, the carrier density is not influenced by the etching temperature. This indicates that no electron trapping takes place. The mobility of the 2DEG is rather influenced by the surface reconstruction and compositions during etching according to Tanaka et al.[3] or by interface roughness.

Thus the process developed here is ideal for the fabrication of laterally structured quantum wells such as wires, dots or rings.

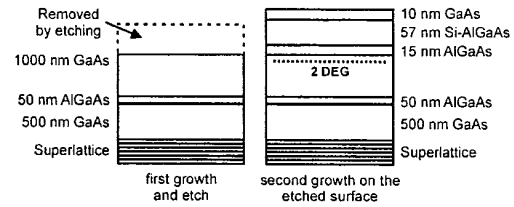

Fig. 1: Flow-chart of the etch regrowth process. The 2DEG is located directly at the etched regrown GaAs/AlGaAs interface.

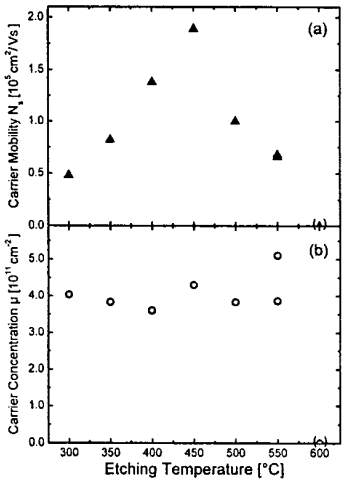

Fig. 2: (a) Measured carrier mobility μ and (b) carrier density N_s at 4.2K in dependence of the etching temperature. The etching was always performed at a Cl_2 pressure of 8×10^{-4} Torr in the chamber. The base pressure of the chamber prior to etching was 1×10^{-9} Torr. Two samples prepared at 600°C did not contain mobile electrons.

References

[1] Y. Kadoya et al., Appl. Phys. Lett. 61(14), pp.1658 (1992).
[2] Y. Kadoya et al., J. Cryst. Growth 127, pp.877 (1993).
[3] N. Tanaka et al., J. Vac. Sci. Technol. B 13(6), pp.2250 (1995).

Corresponding author: Sven Beyer,
Institut für Angewandte Physik und Zentrum für Mikrostrukturforschung,
Universität Hamburg, Jungiusstrasse 11, D-20355 Hamburg, Germany.
phone: +49 40 42838 6531, Fax: +49 40 42838 6332
email: sven.beyer@physnet.uni-hamburg.de

Much enhanced electron mobility in a pseudomorphic $In_{0.74}Ga_{0.26}As/In_{0.46}Al_{0.54}As$ QW-HEMT structure with (411)A super-flat interfaces grown by MBE

T. Kitada, T. Aoki, I. Watanabe, K. Kanzaki, S. Shimomura, S. Hiyamizu,

Graduate School of Engineering Science, Osaka University,
Toyonaka, Osaka 560-8531, Japan

InP-based InGaAs/InAlAs high electron mobility transistors (HEMTs) have been promising for millimeter-wave device applications. Recently, we have reported that effectively atomically flat interfaces over a wafer-size area ["(411)A super-flat interfaces"] can be formed in lattice-matched and pseudomorphic InGaAs/InAlAs QWs grown on (411)A oriented-InP substrates by molecular beam epitaxy (MBE).[1,2] Two-dimensional electron gas (2DEG) in a pseudomorphic $In_{0.74}Ga_{0.26}As/In_{0.52}Al_{0.48}As$ QW-HEMT structure with (411)A super-flat interfaces showed high mobility of 90,500 cm^2/Vs with sheet carrier concentration (N_s) of 3.1×10^{12} cm^{-2} at 77 K, which was 1.5 times larger than that the best value (μ = 61,000 cm^2/Vs at 77 K) of ever reported mobility with a similar N_s of 3.0×10^{12} cm^{-2}. [3] This suggests that the pseudomorphic InGaAs/InAlAs QW-HEMT with the (411)A super-flat interfaces has high potential for improvement of high-speed device performances. In this paper, we report that improved electron mobility of 105,000 cm^2/Vs ($N_s = 3.1 \times 10^{12}$ cm^{-2}) at 77 K was achieved in the (411)A QW-HEMT structure by using pseudomorphic $In_{0.46}Al_{0.54}As$ barriers instead of lattice-matched $In_{0.52}Al_{0.48}As$ barriers.

Pseudomorphic $In_{0.74}Ga_{0.26}As/In_{1-y}Al_yAs$ QW-HEMT structures with Al content y of 0.48, 0.52, 0.54, and 0.56 were grown on the (411)A InP substrates at T_s = 540°C under V/III [As_4/(Ga + In)] = 8 (in pressure) by MBE. The QW-HEMT structure consists of a 8-nm-thick $In_{0.74}Ga_{0.26}As$ QW channel layer separated from a Si-sheet doped $In_{1-y}Al_yAs$ layer ($N_D = 1 \times 10^{13}$ cm^{-2}) by a 9-nm-thick undoped $In_{1-y}Al_yAs$ spacer layer (see an inset of Fig. 1). The same QW-HEMT structure with y = 0.54 was grown on a conventional (100) InP substrate at T_s = 480°C under V/III = 15 for a reference sample. Transport properties of the samples were characterized by the van der Pauw method after removing the top Si-doped InGaAs contact layers. Figure 1 shows electron mobility and sheet electron concentration (77 K) of the (411)A QW-HEMT plotted as a function of Al content. Electron mobility of the (411)A sample increases from 90,500 cm^2/Vs to 105,000 cm^2/Vs with increasing Al content from y = 0.48 (lattice-matched case) to y = 0.54. The increase of electron mobility is considered to be due a better confinement of electron in the QW caused by higher barrier height and due to high crystalline quality of the (411)A QW-HEMT structure resulting from the strain compensation effect by the tensile strained $In_{1-y}Al_yAs$ barriers. Electron mobility and N_s slightly decreased for Al content of 0.56. This is probably due to degraded crystalline quality of the (411)A QW-HEMT structure, which was observed in high resolution x-ray diffraction (HRXRD) measurements of the (411)A samples. Figure 2 shows electron mobility at 77 K of the (411)A $In_{0.74}Ga_{0.26}As/In_{0.46}Al_{0.54}As$ QW-HEMT structure plotted as a function of sheet electron concentration. Electron mobilities (77 K) of the (100) reference sample (y = 0.54) of this study and (100) InGaAs/InAlAs QW-HEMT structures reported so far are also plotted in Fig. 2. A broken line in Fig. 2 is a guide for eyes. The (411)A QW-HEMT structure with y = 0.54 shows an outstanding electron mobility as high as 105,000 cm^2/Vs at $N_s = 3.0 \times 10^{12}$ cm^{-2} compared with those of (100) InGaAs/InAlAs QW-HEMT structures. It is, to our knowledge, the highest value of electron mobility (77 K) with $N_s \simeq 3.0 \times 10^{12}$ cm^{-2} for the InGaAs/InAlAs HEMT structure reported so far, which is mainly due to reduction of interface roughness scattering of 2DEG due to the (411)A super-flat interfaces.

References

[1] T. Kitada et al., J. Electron. Mater. **27**, 1043 (1998).
[2] T. Aoki et al., J. Vac. Sci. Technol. **B18**, 1598 (2000).
[3] T. Kitada et al., to be published in J. Cryst. Growth (2001).

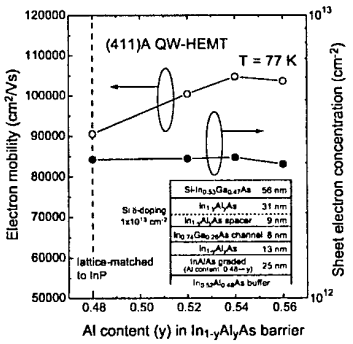

Figure 1: Electron mobility and sheet electron concentration measured at 77 K of the (411)A $In_{0.74}Ga_{0.26}As/In_{0.52}Al_{0.48}As$ QW-HEMT structure plotted as a function of Al content y.

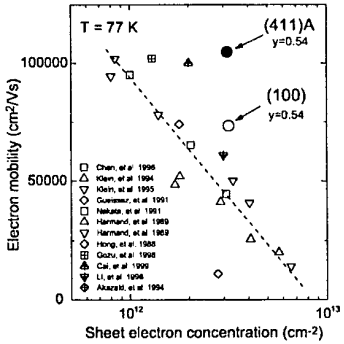

Figure 2: Electron mobilities at 77 K of the (411)A and (100) sample with Al content y of 0.46 plotted as a function of sheet electron concentration. Electron mobilities (77 K) of (100) InGaAs/InAlAs QW-HEMT structures reported so far are also plotted.

Corresponding author: Takahiro Kitada, Graduate School of Engineering Science,
Osaka University, Toyonaka, Osaka 560-8531, Japan.
phone: +81 6 6850 6456, Fax: +81 6 6845 4632,
email: kitada@d310.mp.es.osaka-u.ac.jp

Study of free GaAs surfaces using a back-gated undoped GaAs/AlGaAs heterostructure

A. Kawaharazuka[1,2], T. Saku[1], C. A. Kikuchi[1], Y. Horikoshi[2], and Y. Hirayama[1,3]

[1]NTT Basic Research Laboratories
3-1 Morinosato-Wakamiya, Atsugi-shi, Kanagawa 243-0198, Japan
[2]School of Science and Engineering, Waseda University
3-4-1 Okubo, Shinjuku-ku, Tokyo 169-0072, Japan
[3]CREST Core Research for Evolutional Science and Technology
4-1-8 Honmachi, Kawaguchi-shi, Saitama 331-0012, Japan

Recently, many types of low dimensional system have been fabricated based on GaAs/AlGaAs heterostructures by using surface Schottky gate and/or surface etching. They have a free semiconductor surface as well as a surface covered with metal. When modeling the electrostatics of these devices, the 'mid-gap pinning model' (MPM) [1] is widely used to determine the boundary condition for the surfaces and metal/(Al)GaAs interfaces. This model implicitly assumes that charges can be transferred to the surface and a system always maintains thermal equilibrium. However, it is not obvious if thermal equilibrium is also achieved for free GaAs surfaces at low temperatures where we usually operate these devices to enable us to see weak quantum mechanical effects. In this situation, the transfer of changes to the surface seems to be rather difficult. Therefore, it is very important to study the free surface of (Al)GaAs at low temperatures. An alternative surface model called the 'frozen surface model' (FSM) [2] has been proposed and investigated for the free surface of (Al)GaAs. This model assumes a constant surface charge density, namely surface electric field, for the free semiconductor surface. We study the surface state of free GaAs surface by using a back-gated undoped GaAs/AlGaAs heterostructure [3] shown in Fig.1. The whole device surface is a free GaAs surface since a two-dimensional electron gas (2DEG) is induced only by the back-gate. Therefore, the transport characteristics well reflect the condition of the free GaAs surface. We evaluate channel depth dependence of the transport characteristics by the Hall effect measurement. We analyze experimental results based on a simple capacitance model and assuming both the MPM and FSM for the free GaAs surface. Figure 2 shows the measured electron densities at various channel depths at 1.5 K as a function of the back-gate bias voltage. Note that the threshold voltages (V_{bth}) for deep channels (> 100 nm) are almost identical. For the sample with the 70-nm deep channel, the threshold voltage becomes higher. For the 54-nm deep channel, the threshold voltage increases when the back-gate bias scan is repeated during the experiment. Based on the MPM, the threshold voltage (V_{bth}) and the electron density (n) are expressed as

$$V_{bth} = \frac{d_2}{d_1}\frac{\varepsilon_1}{\varepsilon_2}\Phi_s \propto \frac{1}{d_1}, \quad n = \frac{\varepsilon_2}{d_2 e}V_b - \frac{\varepsilon_1}{d_1 e}\Phi_s, \quad \Phi_s : const. \qquad (1)$$

where Φ_s is the surface Fermi level. The threshold voltage calculated with this equation is plotted in Fig. 3 as a function of the channel depth (d_1) together with the measured data. We assume that the surface Fermi level is pinned at 0.96 eV below the conduction band-edge. When we compare the calculated results with the experimental data, the former depend strongly on the channel depth and much lager than the latter. To explain this discrepancy, we analyze the operation based on the FSM. We assume that the surface charge density is constant. Accordingly, the system is not at a state of thermal equilibrium when under an applied back-gate bias. The threshold voltage and the electron density are expressed as

$$V_{bth} = \frac{d_2}{\varepsilon_2}Q_s = \frac{d_2}{d_2 + (\varepsilon_2/\varepsilon_1)d_1}\Phi_{s0}, \quad n = \frac{\varepsilon_2}{d_2 e}\left(V_b - \frac{d_2}{(\varepsilon_2/\varepsilon_1)d_1 + d_2}\Phi_{s0}\right), \quad Q_s, \Phi_{s0} : const. \qquad (2)$$

where Q_s is the surface charge density and Φ_{s0} is the surface Fermi level in a state of equilibrium. We also plot the threshold voltage calculated this model in Fig. 3. The assumed Φ_{s0} is is the same as that used in the MPM. The threshold value depends on the channel depth even in the FSM. However, its dependence is much weaker than that in the MPM. The experimental results agree well with the calculated values for the deep channels (> 100 nm). Therefore, the appropriate model for the free GaAs surface is the FSM rather than the widely accepted the MPM. The increase in the threshold voltage observed in the shallow channels (70 nm, 54 nm), is explained by considering the charge transfer from the 2DEG to the surface since the system is substantially non-equilibrium in the FSM. When the cannel depth is less than 100 nm, charge transfer from the 2DEG to the surface due to the tunneling effect becomes significant. As expected Eq. (2), the threshold voltage increases as the surface charge density increase.

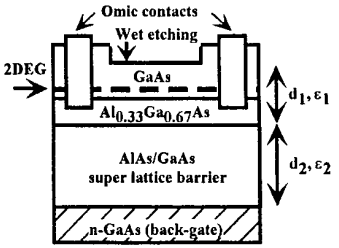

Fig 1. Schematic cross section of the back-gated undoped GaAs/AlGaAs heterostructure. To vary the channel depth, we wet chemically etched the central region

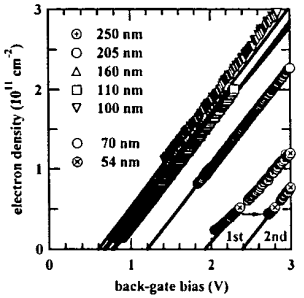

Fig 2. Electron densities as a function of the back-gate bias voltage for various channel depths.

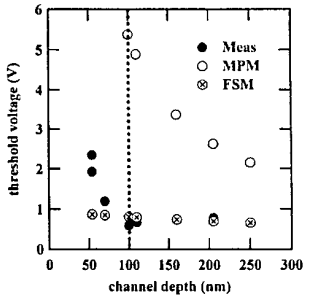

Fig 3. Estimated threshold voltage plotted as a function of the channel depth.

References

[1] W. E. Spicer *et al*, J. Vac. Sci. Technol. **16**, 1422 (1979).
[2] J. H. Davies, I. A. Larkin, and E. V. Sukhorukov, J. Appl. Phys. **77**, 4504 (1995).
[3] A. Kawaharazuka, T. Saku, Y. Hirayama, and Y. Horikoshi, J. Appl. Phys. **87**, 952 (2000).

Edge-channel transport through quantum wires with a magnetic quantum dot

H.-S. Sim[1], G. Ihm[2], N. Kim[3], S. J. Lee[3], and K. J. Chang[1]

[1] Department of Physics, Korea Advanced Institute of Science and Technology, Taejon 305-701, Korea
[2] Department of Physics, Chungnam National University, Taejon 305-764, Korea
[3] Quantum-functional Semiconductor Research Center, Dongguk University, Seoul 100-715, Korea

Transport properties of two-dimensional electron gas (2DEG) in spatially nonuniform magnetic fields have attracted much attention. In this theoretical work, we consider a quantum wire with a magnetic quantum dot [1]. Here, the wire is formed by applying an electrostatic confinement on 2DEG and the magnetic dot is formed at the center of the wire by nonuniform perpendicular magnetic fields; $\vec{B} = B^*\hat{z}$ within a circular disk with radius r_0, while $\vec{B} = B_0\hat{z}$ outside it. In this geometry, it is clear that classical trajectories of edge channels scattered by the dot with $\gamma\ [= B^*/B_0] < 0$ are very different from those for $\gamma > 0$. Such behavior is very contrast to the scattering of edge channels by local electrostatic modulations such as an antidot [2]. This indicates that the edge-channel scattering by local magnetic modulations can be quite different from that by electrostatic ones. However, to our knowledge, little attention has been paid to it.

We study the scattering of edge channels by a magnetic quantum dot in quantum wires. The two-terminal conductance (G) of the wires in zero-bias limit are found to exhibit distinct features between two cases of $\gamma > 0$ and $\gamma < 0$. For $\gamma > 0$, G is quantized and the dot behaves as a transmission barrier and a resonator. This feature results from the harmonic-potential-like magnetic confinements. On the other hand, for $\gamma < 0$, G is not quantized when incident channels are scattered by the dot. Moreover, for $\gamma < -1$, all incident channels can be completely reflected by the dot in some energy ranges, resulting in the plateaus of $G = 0$. These interesting features for $\gamma < 0$ are attributed to the double-well and merged-well magnetic confinements, which are caused by the field reversal at the dot boundary. We emphasize that the magnetic confinements can play an important role in electron states and transport in magnetic structures.

References

[1] H.-S. Sim *et al.*, Phys. Rev. Lett. **80**, 1501 (1998); J. Reijniers, F. M. Peeters, and A. Matulis, Phys. Rev. B **59**, 2817 (1999).
[2] J. K. Jain and S. A. Kivelson, Phys. Rev. Lett. **60**, 1542 (1988).

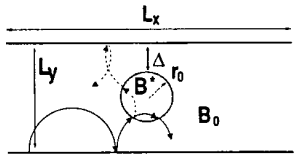

Figure 1: Schematic diagram of a quantum wire with a magnetic quantum dot. The solid (dashed) arrows represent classical electron trajectories for $B^*/B_0 > 0$ ($B^*/B_0 < 0$).

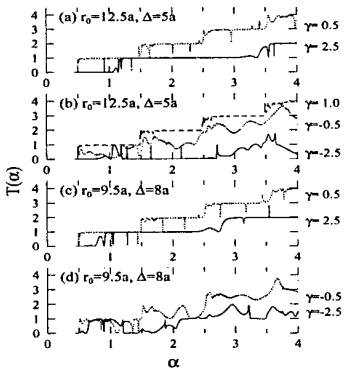

Figure 2: Dependence of the calculated transmission probability (T) through the wire in Fig. 1 on a dimensionless energy $\alpha\ [= E_F/(2E_0)]$ for some γ's and r_0's, where E_F is the energy of incident channels and $E_0 = \hbar eB_0/(2m^*)$. For all cases, L_y and $l_B(0)\ [= \sqrt{\hbar/(eB_0)}]$ are fixed as $35a$ and $5a$, where a is a length unit.

Corresponding author: Gukhyung Ihm, Department of Physics, Chungnam National University, Taejon 305-764, Korea.
phone: +82 42 821 6273, Fax: +82 42 822 8011,
email: ghihm@cnu.ac.kr

Transport in quantum dot-arrays

N. Mori , T. Ishida, Y. Takamura, and C. Hamaguchi

Department of Electronic Engineering, Osaka University
Suita City, Osaka 565-0871, Japan

We measured magnetoresistance through laterally coupled quantum dot-arrays fabricated on a GaAs/AlGaAs single heterostructure by using electron-beam lithography and wet chemical etching to study the effects of periodicity on the magnetoresistance characteristics. We also performed numerical simulation of magnetoconductance characteristics, and the results are compared with the experimental results.

Quantum dot-arrays were fabricated on a GaAs/$Al_xGa_{1-x}As$ single-heterostructure ($x = 0.265$). The elastic mean-free-path of electrons in the single-heterostructure was estimated to be 1.9 μm by a standard Hall measurement at $T = 77$ K. For measuring the magnetoresistance, 20μm-wide Hall-bars were fabricated by standard photolithgraphy and wet etching techniques. The dot-array patterns were defined on a 20 μm × 20 μm-area of the Hall-bars by using electron-beam lithography. In the present study, three types of samples were fabricated (see Fig. 1), which are two straight dot-arrays of different lateral sizes (SD1 and SD2), and zigzag-shaped dot-arrays (ZD). We also fabricated 760 nm-wide quantum wire for comparison.

Magnetoresistance of quantum dot-arrays was measured at 4.2 K and is shown in Fig. 2, where Shubnikov-de Haas oscillations dominate the magnetoresistance for $B \gtrsim 1$ T. Although the quantum wire shows weak magnetic field dependence for for $B \lesssim 1$ T, several pronounced peaks are observed for the straight and the zigzag-shaped dot-arrays in this region. For the sample SD1, a strong peak is found at 0.72 T and a weak shoulder peak is seen at 0.21 T.

Because the magnetoresistance was measured at 4.2 K, we expect that the observed structures for $B \lesssim 1$ T can be associated with classical magneto-size effects based on the billiard model [1]. We have confirmed that the billiard model predicts the magneto-size effects correctly (see Fig. 3). By performing Monte Carlo simulation of classical electrons within the billiard model [1] for several sample shapes, we find that a transmission peak of magnetoconductance at $B \approx 0.4$ T remains almost unchanged with increasing the number of dots in a dot-array (see Fig. 4). The transmission peak position is also found to agree with the experimental position (see Fig. 5). We therefore conclude that the resistance minima at $B \approx 0.4$ T observed in the sample SD1 is due to the stable transmission peak. The origin of the observed resistance peak and geometrical dependence of magnetoresistance characteristics are also discussed.

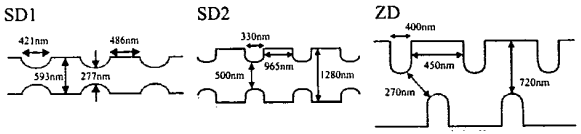

Figure 1: Fabricated dot-array patterns. Three types of samples were fabricated, which are two straight dot-arrays of different lateral sizes (SD1 and SD2), and zigzag-shaped dot-arrays (ZD).

[1] C.W.J. Beenakker and H. van Houten, Phys. Rev. Lett., **63**, 1857 (1989).

[2] T. Usuki, M. Saito, M. Takatsu, R.A. Kiehl, and N. Yokoyama, Phys. Rev. B, **52**, 8244 (1995).

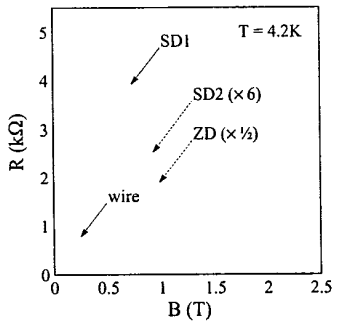

Figure 2: Measured magnetoresistances at $T = 4.2$ K for small straight dot-arrays (SD1), large straight dot-arrays (SD2) and zigzag-shaped dot-arrays (ZD). The magnetoresistances of a quantum wires is also plotted for comparison.

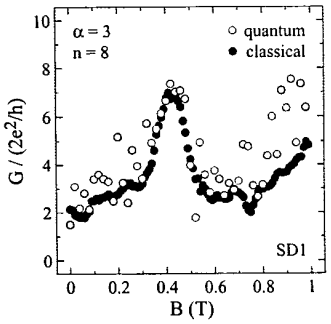

Figure 3: Calculated magnetoconductance of a small straight dot-array with 8-dots connected in series. Open circles are calculated with the numerically stabilized variant of the transfer matrix approach [2] and closed circles are calculated within the billiard model [1].

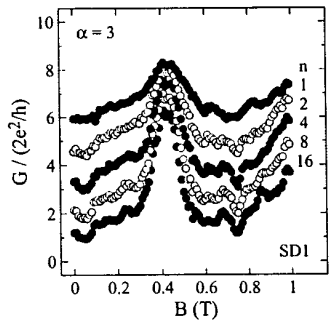

Figure 4: Calculated magnetoconductance of a small straight dot-array with n-dots connected in series for $n = 1$ (top), 2, 4, 8, and 16 (bottom).

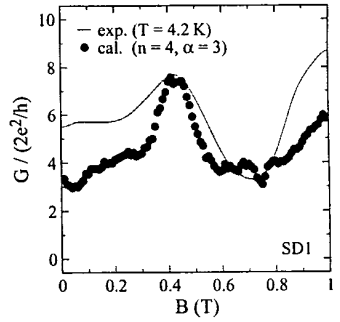

Figure 5: Comparison between measured (solid line) and calculated (closed circles) magnetoconductance. Note that the actual dot-arrays consist of ~20-dot-array in parallel and 20-dots are connected in series in each dot-array.

Corresponding author: Nobuya Mori, Department of Electronic Engineering
Osaka University, Suita City, Osaka 565-0871, Japan
phone: +81-6-6879-7766, Fax: +81-6-6879-7753, email: mori@ele.eng.osaka-u.ac.jp

Local 'spectroscopy' of mesoscopic systems with scanning probe techniques

T. Ihn[1], J. Rychen[1], T. Vančura, T. Cilento[1], R. Held[1], K. Ensslin[1], W. Wegscheider[2] and M. Bichler[3]

[1] Solid State Physics Laboratory, ETH Zürich, CH-8093 Zürich, Switzerland
[2] Department of Physics, Univ. of Regensburg, 93040 Regensburg, Germany
[3] Walter-Schottky Institut, 85748 Garching, Germany

Over the last two decades a great wealth of novel magnetotransport phenomena has been found in two-dimensional mesoscopic systems [1]. Famous examples are universal conductance fluctuations and conductance quantisation in a quantum point contact or in the quantum Hall effect. Typically, the conductance or resistance of systems was studied as a function of *global* parameters like magnetic field, carrier density or temperature. We report the realisation of a complementary approach to transport in mesoscopic systems. In our experiments we perturb the interior of a mesoscopic structure *locally* with the conducting tip of a scanning force microscope (SFM). This setup was successfully employed for two sets of experiments: first, the mesoscopic transport in a quantum wire was studied aiming at the observation of conductance fluctuations by moving a local potential perturbation through the system. The second experiment aimed at the realisation of local tunnelling spectroscopy between non-equilibrium edge states in the quantum Hall regime.

For these studies a home-built low-temperature SFM was operated at temperatures down to 2 K and in magnetic fields up to 8 T. Piezoelectric quartz tuning forks were employed for the force detection thereby avoiding the need for an involved optical cantilever deflection detection at low temperatures. A sharp metallic tip attached to one prong of the tuning fork induced the desired local potential perturbation in the structures [2].

For the quantum wire measurement a wire of 40 μm length and 400 nm width was fabricated by AFM-lithography [3] on a shallow heterostructure with the two-dimensional electron gas ($n_s = 4 \times 10^{15}$ m^{-2}, $\mu = 100$ m^2/Vs) 34 nm below the surface. In-plane gates allowed to tune the electron density in the wire. Theory predicts that in the diffusive transport regime moving only a single impurity over a distance of the Fermi-wavelength of the electrons will universally alter the resistance of samples on the scale of h/e^2 [4]. In a measurement of the sample resistance as a function of the position of the induced tip potential we observe the electrical image of the quantum wire in real space (see Fig. 1). As expected for an additional scattering potential, the resistance goes through a clear maximum when the tip is scanned across the wire. When the tip is scanned along the wire, the induced resistance fluctuates on two different length scales. We discuss our observations in terms of appropriate models.

An especially designed structure (based on a similar heterostructure as described above) has been used for the tunnelling spectroscopy in the quantum Hall regime which allows to study tunnelling between separately contacted non-equilibrium edge channels by using internal contacts. Scanning the tip-induced potential in the region where the filling factor $\nu = 2$ and $\nu = 4$ edge channels run in parallel we have been able to increase their tunnelling coupling locally and thereby increase the measured conductance. This leads to a spatial map of the edge channel coupling (see Fig. 2) which shows local structure in the best images. The imaging mechanism will be discussed applying the edge channel picture locally in the vicinity of the tip-induced perturbation.

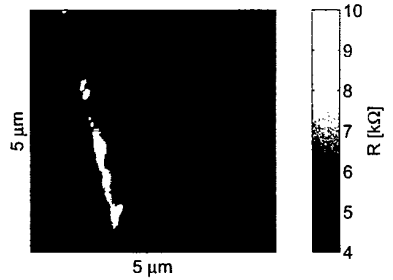

Figure 1: Resistance image of the quantum wire in real space

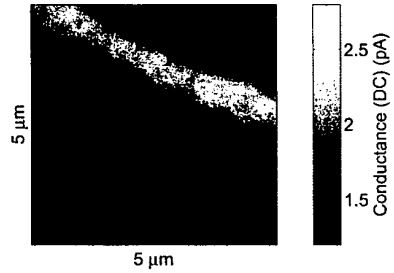

Figure 2: Spatial map of the ($\nu = 2$,$\nu = 4$) edge channel coupling.

References

[1] see e.g. S. Washburn and R.A. Webb, Rep. Prog. Phys. **55**, 1311 (1992).
[2] J. Rychen, T. Ihn, P. Studerus, A. Herrmann, K. Ensslin, Rev. Sci. Instrum. **70**, 2765 (1999).
[3] R. Held, S. Lüscher, T. Heinzel, K. Ensslin, and W. Wegscheider, Appl. Phys. Lett. **75**, 1134 (1999).
[4] B.L. Altshuler and B.Z. Spivak, JETP Lett. **42**, 447 (1985); S. Feng P.A. Lee and A.D. Stone, Phys. Rev. Lett. **56**, 1960 (1986).

Corresponding author: Thomas Ihn, Laboratorium für Festkörperphysik, ETH Hönggerberg, CH-8093 Zürich, Switzerland
phone: +41 1 63 32280, Fax: +41 1 63 31146,
email: ihn@solid.phys.ethz.ch

Spin-resolved transport in single electron tunneling

J. Könemann[1], P. König[1], R. J. Haug[1]

[1]Institut für Festkörperphysik, Universität Hannover, Appelstrasse 2, D-30167 Hannover, Germany

The effect of spin in electronic transport is attracting now a lot of interest both from an applied and a fundamental point of view. In this work we present spin-resolved measurements of single electron tunneling through impurity states in a resonant tunneling device. We found a clear anisotropy of the impurity g-factor. From a spin-reconstruction method we were able to probe the bulk g-factor of highly-doped GaAs on a mesoscopic scale.

The experiment was performed with a highly asymmetric double barrier resonant tunneling structure grown by molecular beam epitaxy on n^+-type GaAs substrate. The heterostructure consists of a 10 nm wide GaAs quantum well sandwiched between two $Al_{0.3}Ga_{0.7}As$-tunneling barriers of 5 and 8 nm. The contacts are formed with 300 nm thick GaAs layers highly doped with Si to $4 \cdot 10^{17}$ cm^{-3} and separated from the active region by 7 nm thin spacer layers of undoped GaAs. We performed DC measurements of the I-V-characteristics in a dilution refrigerator at 20 mK base temperature in high magnetic fields.

Single electron tunneling through donor-states in the quantum well leads to a step-like behaviour in the I-V-characteristics [1]. An applied magnetic field quantizes the electronic transport and leads to a diamagnetic shift of the step position due to stronger confinement. In our experimental setup we applied a magnetic field both parallel and perpendicular to the tunneling current. We noticed for B⊥I strong mesoscopic fluctuations of the peak position, which are superimposed on the oscillations of the Landau quantized emitter. In this configuration the tunneling current is strongly suppressed with increasing magnetic field. We observed Zeeman-splitting of the spin-degenerate impurity state. Whereas the Zeeman splitting in similar physical systems [2] has only been evaluated for one fixed magnetic field orientation, we compare now the g^*-value for both field orientations and find an anisotropic behaviour of the effective g-factor of the impurity state: $|g_\perp^*| = 0.17 > |g_\parallel^*| = 0.13$, see fig. 1.

On the current plateau we observe an oscillatory and temperature-insensitive fine structure, which we attribute to mesoscopic fluctuations of the local density of states (LDOS) in the emitter [3]. At higher magnetic field the irregular LDOS pattern in the I(V,B) plane changes to a stripe-like pattern. This allows us to probe the bulk g-factor of GaAs mesoscopically in the presence of disorder [4]. We determine for both field orientations bulk g-factors lower than that of GaAs g=-0.44 in agreement with theory [5]. We evaluated also a significantly smaller g-value of the bulk $g_\parallel$ =-0.30 compared to $g_\perp$=-0.35.

References

[1] M. W. Dellow , P. H. Beton, C. J . G. M. Langerak, T.J. Foster, P. Main, L. Eaves, M. Henini, S. P. Beaumont, C. D. W. Wilkison, Phys. Rev. Lett. 68, 1754 (1992).
[2] M. R. Deshpande, J. W. Sleight, M. A. Reed, R. G. Wheeler, R.J Matyi, Phys. Rev. Lett 76, 1328 (1996).
[3] T. Schmidt, P. König, E. McCann, V. I. Fal'ko, R. J. Haug, Phys. Rev. Lett. 86, 276 (2001).
[4] P. König, T. Schmidt, R. J. Haug, cond-mat/0004165.
[5] P. Pfeffer, W. Zawadzki, Phys. Rev. B 41, 1561 (1990).

Corresponding author: Jens Könemann, Institut für Festkörperhysik, Universität Hannover, Appelstr. 2, D-30167 Hannover, Germany.
phone: +49 511 762 19040, Fax: +49 511 762 2904
email: konemann@nano.uni-hannover.de

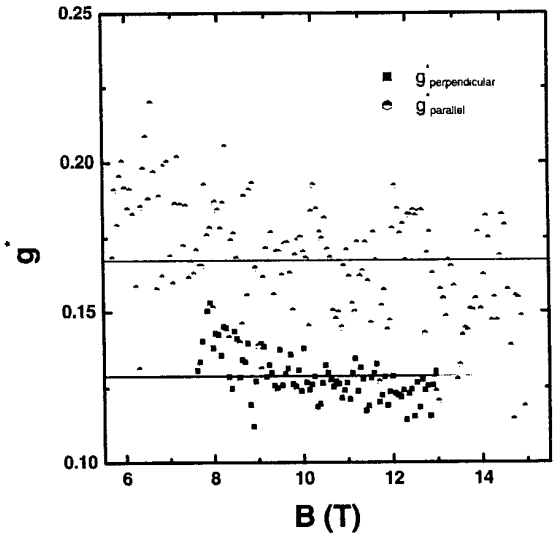

Fig. 1: Effective impurity g-factor for B ∥ I and B⊥I.

Intersubband scattering in serially connected quantum wires

B. Dwir[1], D. Kaufman[1], E. Kapon[1], A. Palevski[2]

[1] Physics department, Swiss Federal Institute of Technology Lausanne (EPFL), CH-1015 Lausanne, Switzerland
[2]School of Physics and Astronomy, Tel-Aviv University, Ramat-Aviv, Israel

Electron transport in quantum wires (QWRs) with a rigid confinement potential (CP), made by etching, cleaved-edge or V-groove regrowth [1,2], shows quantized conductance steps which are smaller than the quantized value $G_0 \equiv 2e^2/h$ observed in structures with adiabatic 2D/1D transitions. In an ideal QWR with rigid CP, and in the absence of scattering, the 1D states are very weakly coupled to the 2D states and through them to the external contacts, and therefore are impossible to contact. In rigid CP wires, one could thus only attempt to approach the ideal conductance values by searching a compromise between strong 1D/2D coupling and small backscattering. In this work we use a system of two serially connected V-groove QWRs [1], where we can vary independently the channel population in each QWR, to show that the transmission of the combined system can be explained only by invoking intersubband scattering over distances short compared to the 1D/2D contact length.

In order to demonstrate the weakness of 1D/2D coupling in QWRs with a strong CP, we first performed a series of measurements on QWRs with a dual gate configuration as shown in Fig.1a, varying the QWR thickness (t = 12, 26 nm) and gate distance Δ (0.4 - 6 μm). The resulting conductance of one of these devices, with Δ = 0.5 μm, is shown in Fig. 1b. As the fork gate FG cuts off the conductance of the QWR under it (the conductance in the sidewall 2DEG is never cut off), the conductance of the low-lying states under the straight gate SG vanishes, whereas the conductance of higher states remains finite. The conductance value of the first plateau, measured when the FG cuts off the QWR but not the 2DEG, is plotted in Fig.1c as function of the distance Δ. It is clear that for t = 12 nm the 1D/2D contact resistance for the low-lying states becomes enormous for $\Delta < 2$ μm, whereas for t = 26 nm (weaker CP) the same occurs at $\Delta < 1$ μm. The large contact resistance to the low-lying subbands is the evidence for the lack of scattering with large momentum exchange over small distances. The higher QWR subbands do not exhibit such resistance, showing that they are much better coupled to the 2DEG. These results are consistent with experiments in T-shaped QWRs [2].

We now look at samples with two straight gates (which we call RG and LG, see Fig.2a), each 0.25 μm wide and spaced 0.8 μm apart. A typical plot of conductance (in units of e^2/h) as function of a (single) gate voltage is shown in Fig.2b. When *both* gates are biased (Fig. 2c) we can easily identify the values of combined conductance which correspond to plateaus under both gates. Although the combined conductance of the system with one and two channels under each gate is much higher than it would be in the case of serial connection, it is lower than for a ballistic transmission through two barriers. This is the proof that electrons passing through the first two channels are scattered to higher subbands already in the short distance between the gates. For example, we know (from Fig.2b) that the transmission of the 1st channel under each gate is no less than $T_1 \approx T_2 \approx 0.9$, so the combined transmission of the system without subband scattering should be at least : $\frac{T_1 T_2}{1 - R_1 R_2} \approx 0.82$ (R ≡ 1-T and we suppose that phase relaxation rate is much higher than scattering rate). Therefore, the observed transmission of 0.7 when both gates allow a single channel population, is a clear indication of significant intersubband mixing.

Unfortunately, it is impossible to obtain quantitative evaluation of the scattering rates for each subband and their energy dependence. Yet, a simplified approach, neglecting multiple reflections between the gates, can give us bounds : $0.075 < T_{12} < 0.27$, where T_{12} = the fraction of electrons scattered between the 1st and 2nd subband of the QWR. This figure decreases significantly for scattering from the 1st to higher subbands. The origin of the observed intersubband scattering could be related to either static potentials (interface roughness, impurities), or to electron-electron interaction.

References

[1] D. Kaufman et al., Phys. Rev. B **59**, R10433 (1999), B. Dwir et al., Physica B **259**, 1025 (1999).
[2] A. Yacoby et al., Phys. Rev. Lett.. **77**, 4612 (1996), R. de Picciotto, et al., Physica E **6**, 514 (2000) and Phys. Rev. Lett. **85**, 1730 (2000).

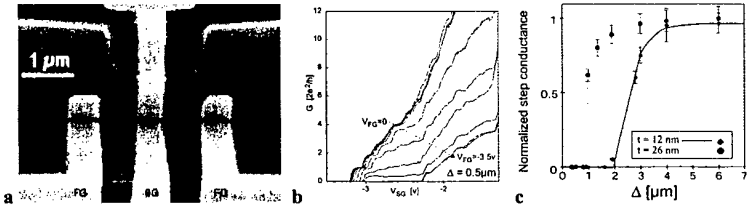

Fig. 1: a. Scanning electron micrograph of a device with a straight gate SG and a fork gate FG at a distance Δ. b. Conductance (in units of $2e^2/h$) of the device, as function of the V_{SG}, with V_{FG} as parameter. c. Conductance of many devices, all measured when SG allows only one channel to pass, and FG cuts off the QWR (normalized to the conductance when $V_{FG} = 0$), as function of Δ..

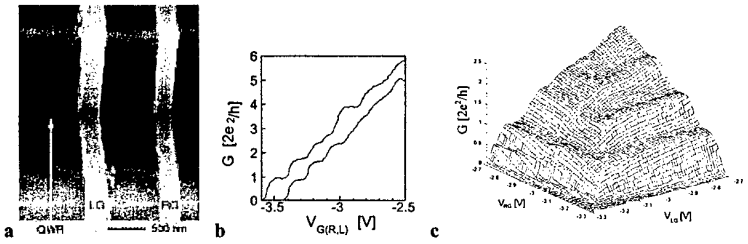

Fig. 2: a. Scanning electron micrograph of a device with two straight gates, RG (right) and LG (left). b. Conductance (in units of $2e^2/h$) of the device vs. voltage of each of the two gates, while the other gate is at 0V. c. Conductance (same units) of the device vs. voltage on both gates.

Corresponding author: Benjamin Dwir, IMO-DP, EPFL, CH-1015 Lausanne Switzerland
phone: +41 21 693 3755, Fax: +41 21 693 4525
email: benjamin.dwir@epfl.ch

Hund's Rule and Addition Energy Spectra of Cylindrical Quantum Dots

P. Matagne[1], J.P. Leburton[1,2], D.G Austing[3] and S. Tarucha[3,4]

[1] Beckman Institute for Advanced Science & Technology,
University of Illinois at Urbana-Champaign, 405 N. Mathews Avenue,
Urbana, Illinois 61801, USA
[2] Department of Electrical and Computer Engineering,
University of Illinois at Urbana-Champaign, 1406 W. Green Street,
Urbana, Illinois 61801, USA
[3] NTT Basic Research Laboratories, 3-1, Morinosoto Wakamiya
Atsugi-shi, Kawagana 243-0198, Japan
[4] Department of Physics, University of Tokyo, 7-3-1,
Hongo, Bunkyo-ku, Tokyo 113-033, Japan

In atomic physics, Hund's rules constitute a set of heuristic rules that determine the ground state of a N electron system if the electronic configuration is known [1]. Since in cylindrical quantum dots (CQD), the quantum states are characterized by spatial degeneracy that leads to shell structures in the electronic properties [2], an interesting question arises whether Hund's first rules can predict the ground state of a CQD. For this purpose, we have measured the addition energy spectrum, i.e., the second energy difference or the variation of the electro-chemical potential $\Delta_2(N) = \mu(N+1) - \mu(N)$ as a function of the number of electrons in the dot N of 14 high quality CQDs at 100mK directly from the Coulomb diamonds up to 12 electrons. We paid particular attention to the filling of the third shell. The experimental spectra are then compared to spectra generated from a three-dimensional (3D) quantum device modeling using density functional calculations. We show that i) Hund's first rule cannot predict the general shape of the addition energy spectra; ii) maximal spin does not guarantee a peak at half-shell filling; iii) a particular spin filling sequence doesn't result in a unique addition energy spectrum. These features are the consequence of a subtle interplay between many-body interactions and the exact shape of the confinement potential that contains 3D components of the nanostructure.

References

[1] M.A. Morrison, T.S. Estle and N.F. Lane, *Understanding More Quantum Physics* (Prentice Hall, 1991).

[2] S. Tarucha *et al.*, Physical Review Letters **77**, 3613 (1996).

Corresponding author: Philippe Matagne, Beckman Institute for Advanced Science & Technology, 405 N. Mathews Avenue, Urbana, Illinois 61801, USA.
phone: (217) 2446913, Fax: (217) 2444333,
email: matagne@ceg.uiuc.edu

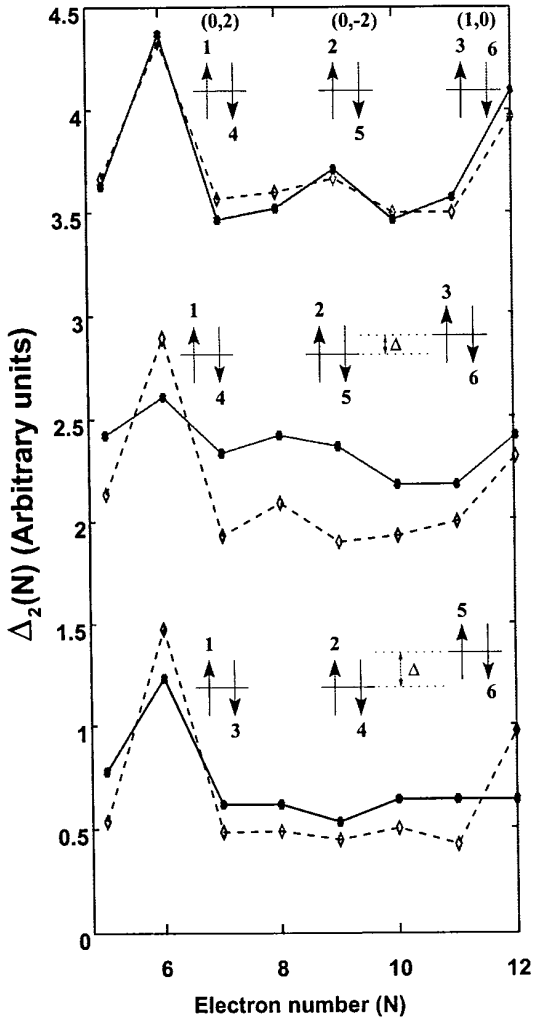

Figure 1: Addition energy spectra of three different CQDs showing different filling sequences for the third shell as a function of the energy separation Δ between the two d-states ($(n,l) = (0,\pm 2)$) and the s-state ($(n,l) = (1,0)$). Solid : experiment, dashed : theory. Top : $\Delta < 0.1meV$; middle : $0.1meV < \Delta < 0.5meV$; bottom : $\Delta > 0.5meV$

The Evolution of Fractal Patterns during a Classical-Quantum Transition

A.P. Micolich[1], R.P. Taylor[1], A.G. Davies[2], J.P. Bird[3], A. Ehlert[4], T.M. Fromhold[5], R. Newbury[4], L.D. Macks[2], W.R. Tribe[2], H. Linke[1,4], E.H. Linfield[2] and D.A. Ritchie[2]

1. Materials Science Institute, Physics Department, University of Oregon, Eugene OR 97403-1274, U.S.A.
2. Semiconductor Physics Group, Cavendish Laboratory, University of Cambridge, Cambridge CB3 0HE, U.K.
3. Center for Solid State Research, Arizona State University, Tempe AZ 85287-6206, U.S.A.
4. School of Physics, University of NSW, Sydney NSW 2052, Australia.
5. School of Physics and Astronomy, University of Nottingham, Nottingham NG7 2RD, U.K.

Billiards are defined electrostatically using a set of negatively-biased metal gates deposited on the surface of an epitaxially-grown AlGaAs/GaAs heterostructure [1]. A two-dimensional electron gas (2DEG) is formed at the AlGaAs/GaAs interface and depleted in the regions directly below the surface-gates to form a quantum dot (billiard) connected to two 2DEG reservoirs via a pair of quantum point contact (QPC) leads. The electrostatic depletion regions that penetrate the 2DEG produce a two-dimensional potential well that has a flat bottom and 'soft' walls with an approximately parabolic energy profile [2]. The mixed (stable/chaotic) phase-space found in 'soft-wall' semiconductor billiards has been predicted, through a semiclassical process, to generate fractal conductance fluctuations [3]. These have subsequently been the focus of significant theoretical [2-5] and experimental interest [6-9].

A fundamental question in this area of research is how fractals evolve into non-fractal behavior as the generating process is gradually suppressed. In experiments we suppress the semiclassical generation process by tuning various parameters of the billiard system to induce controlled transitions towards either fully classical or fully quantum-mechanical electron transport through the billiard. Investigating a range of billiards and parameters (including temperature, billiard area, width of the QPC leads and electron mean free path), we show that the FCF are surprisingly robust to the suppression process and that these transitions induce a smooth evolution rather than deterioration in the fractal scaling properties of the conductance fluctuations.

Furthermore, we will present a remarkable behavior where the fractal dimension of the FCF depends solely on an empirical parameter that we have called the 'quantumness' Q, which quantifies the average discreteness of the billiard energy levels. Fractal dimension values obtained for seven billiards with different geometries, as a function of the four billiard parameters mentioned earlier, condense onto a single 'universal' curve as a function of Q, as shown in Figure 1. This curve indicates a continuous evolution to non-fractal behavior in the limits of Q = 0 and Q>>1 with a peak fractal dimension occurring in the vicinity of Q = 1. At this stage, this novel behavior remains unexplained and presents a new challenge to both experimental and theoretical physicists in this field.

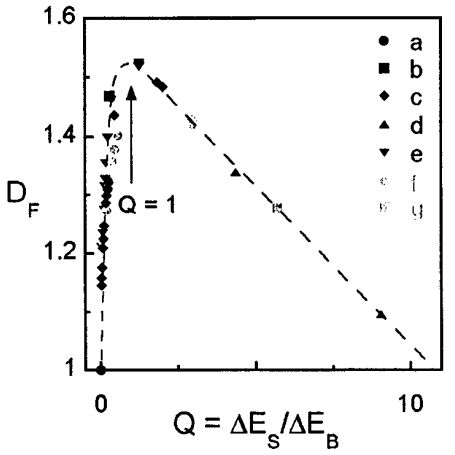

Figure 1: Plot of fractal dimension D_F as a function of the 'quantumness' Q that quantifies the average discreteness of the billiard energy levels. Data from seven different billiard samples condenses onto a single 'universal' curve (the dashed line serves as a guide to the eye).

References

[1] R.P. Taylor, *Nanotechnology* **5**, 183 (1994).
[2] T.M. Fromhold *et al.*, *Physica B* **249-251**, 334 (1998).
[3] R. Ketzmerick, *Phys. Rev. B* **54**, 10841 (1996).
[4] Y. Takagaki and K.H. Ploog, *Phys. Rev. B* **61**, 4457 (2000).
[5] E. Louis and J.A. Vergés, *Phys. Rev. B* **61**, 13014 (2000).
[6] A.P. Micolich *et al.*, *J. Phys.: Condens. Matter* **10**, 1339 (1998).
[7] Y. Ochiai *et al. Semicond. Sci. Technol.* **13**, A15 (1998).
[8] A.S. Sachrajda *et al.*, *Phys. Rev. Lett.* **80**, 1948 (1998).
[9] Y. Takagaki *et al.*, *Phys. Rev. B* **62**, 10255 (2000).

Corresponding Author: A.P. Micolich, Materials Science Institute, Physics Department, University of Oregon, Eugene OR 97403-1274, U.S.A.
Phone: +1-541-346-4771 Fax: +1-541-346-5861
e-mail: mico@darkwing.uoregon.edu

Low temperature transport in dual-gated SETs fabricated by selective area metalorganic vapor phase epitaxy

J. Motohisa[1], W.G. van der Wiel[2], J.M. Elzerman[2], S. De Franceschi[2], F. Nakajima[1], Y. Ogasawara[1], T. Fukui[1], and L. P. Kouwenhoven[2]

[1] Research Center for Interface Quantum Electronics, Hokkaido University, North 13, West 8, Sapporo 060-8628, Japan
[2] Department of Applied Physics, Delft University of Technology, PO Box 4046, 2000 GA Delft, The Netherlands

We describe transport measurements in a novel dual-gated single electron transistor (SET) based on a quantum dot (QD) fabricated by selective area (SA) growth of metalorganic vapor phase epitaxy (MOVPE). We observed, for the first time, clear Coulomb oscillations fabricated in combination with direct growth and lithographically defined metal gates and independent control of the QD potential and the tunneling barrier height.

Our quantum dot device is formed by SA-MOVPE on a specially designed masked substrate. This approach enables us to form extremely small QDs, going beyond the limit of current lithographic techniques. In addition, the dual-gated structure enables us to almost independently tune the electrostatic potential of the QDs and the height of the tunnel barriers, retaining strong lateral confinement. The nominal dot diameter is 150nm (Fig. 1), and is reduced by the application of a negative top gate voltage. The top gate is also used to form tunnel barriers between the QD and the leads formed by quantum wires. In contrast, the side gate mainly changes the potential of QD. The measurements were carried out in a dilution refrigerator with a base temperature of 15mK.

Without applying top gate voltage V_{TG}, the conductance through the QD hardly changes when sweeping the side gate voltage V_{SG}. However, by applying a voltage more negative than -250mV to V_{TG}, the conductance shows Coulomb oscillations as a function of V_{SG}, as shown in Fig. 2(a). Coulomb oscillations shift to the more negative side gate voltages when V_{TG} becomes more positive. Similar Coulomb oscillations for V_{SG} and their shift with respect to V_{TG} were also observed for $-265\text{mV} < V_{TG} < -285\text{mV}$, as shown in Fig. 2(b). For these top gate conditions, the valley conductance as well as the Coulomb peaks seem to be enhanced, as the tunneling resistance of the barrier is reduced as compared to the case of more negative V_{TG}. This clearly indicates that a QD is formed in our device by negative voltage to the top gate. We also note that in Fig.2(b) a plateau-like structure is observed, as indicated by the arrow. This plateau possibly originates from the Kondo effect, expected when the coupling between the leads and the QD is strong and the ground state is spin degenerate.

Measurements of the differential conductance, dI_{DS}/dV_{DS} as a function of both V_{DS} and V_{SG} show clear Coulomb diamonds when $V_{TG} = -299$mV. The Coulomb gap strongly depends on the side gate voltage V_{SG}. The magnetic field dependence of the Coulomb oscillations shows clear anti-crossing behavior.

References

[1] F. Nakajima *et al.*, Appl. Surf. Sci. **162–163** 650 (2000).
[2] M. Dilger *et al.*, Semicond. Sci. Technol. **11** 1493 (1996).

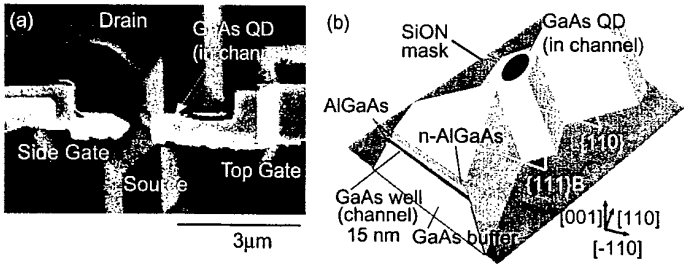

Figure 1: (a) SEM image of the device and (b) its schematic illustration.

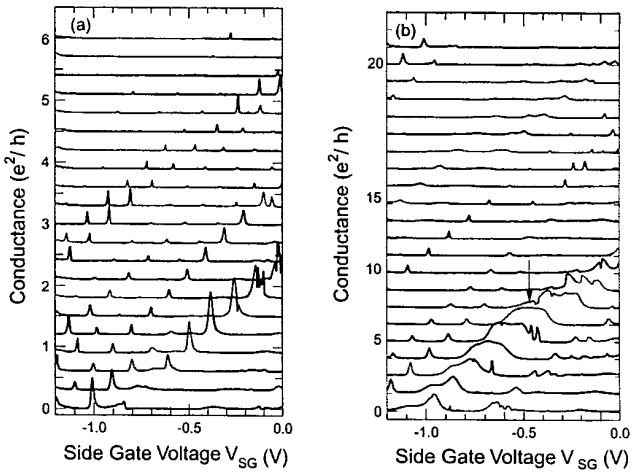

Figure 2: Linear conductance of the device measured at $\sim$ 15mK, plotted as a function of side gate voltage V_{SG} for fixed top gate voltage V_{TG} and source-drain voltage $V_{DS} = 10\mu$V. The top gate voltage V_{TG} is varied (a) from -305mV to -285mV, and (b) from -285mV to -265mV. The step for V_{TG} is 1mV for each figure. The curves are offset for clarity with $0.3e^2/h$ and e^2/h for (a) and (b), respectively.

Corresponding author: Junichi Motohisa, Research Center for Interface Quantum Electronics, Hokkaido University North 13, West 8, Sapporo 060-8628, Japan
phone: +81-11-706-6871, Fax: +81-11-716-6004,
email: motohisa@rciqe.hokudai.ac.jp

T - dependent Resistivity Anomaly in Doped AlAs/GaAs Lateral Superlattices: Evidence for Fermi-Liquid Behaviour

Petra Denk [1,2] and Jean - Luc Pelouard[1]

[1] Laboratoire de Photonique et de Nanostructures, 196 avenue Henri Ravera, BP 29, 92222 Bagneux, France
[2] Lehrstuhl für angewandte Physik, Amalienstraße 54, 80799 München, Germany

In low dimensional (organic) electron systems, the dimensionality crossover between 1 and 2D is currently raising strong interest, both theoretically and experimentally, because the system is changing from Luttinger liquid to Fermi liquid behavior. This was measured by T-dependent electrical resistivity along and perpendicular to the wires (1).
Performing the same kind of measurement in lateral superlattices made of III-V semiconductors, we observe a qualitatively similar behavior as Moser et al. (1) between 4-80K, although the anisotropy of resistivity is much smaller because of stronger wire coupling (2).

To explain our set of experimental data, we present an analysis which is solely based on Fermi liquid theory and is thus in contrast with the theories evoked for the 1D organic conductors. However, we do not find only qualitatively, but even quantitatively good agreement with the experimental data, demonstrating that the essence of the most important effects in the T – dependent resistivity of these structures has been captured. To find such good agreement, we consider with great care all effects arising from the anisotropic band structure (e.g. minigaps and –bands) on the scattering processes, e.g. how high order Fourier components of the lateral potential come into play and the importance of treating the T-dependence of the dielectric response function in a multi-subband description (3).

In Fig. 1 the to the lateral potential modulation perpendicular ($\rho_\perp$) and parallel ($\rho_{//}$) experimental measured resistivity (points) is shown as a function of temperature T together with different theoretical models. Taking only the first Fourier coefficient $V^{(1)}$ (dashed line), the absolute value at T = 4K is well reproduced. However, the strong increase of the experimental perpendicular resistivity, as one increases the temperature, is not reproduced. In contrast, including the second Fourier coefficient $V^{(2)}$ in the lateral potential modulation, leads to a good quantitative fit of the experimental data up to a temperature T=50 K. The reason for the initial rise of the perpendicular resistivity is found in the ionized impurity scattering (2), significantly exalted by $V^{(2)}$ in the upper part of the second miniband. As the temperature increases, the electrons begin to fill higher subbands. Accordingly, in the dielectric function higher subbands have to be taken into account (3). The dielectric function becomes a matrix which has to be inverted to obtain the screened potential involved in the scattering processes. Taking higher subbands in the dielectric function as well as the second Fourier component of the lateral potential modulation into account, we find good agreement (solid line) with the experimental values. This allows us to determine the size of the first minigap (=11 meV) of the lateral potential modulation by transport measurements.

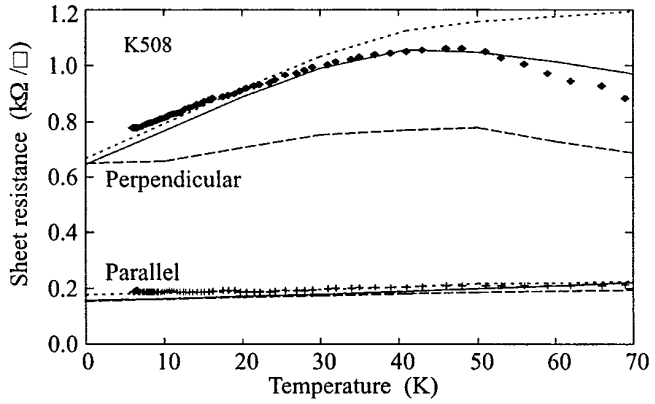

Fig.1: Diagonal resistivities $\rho_{//}$ and $\rho_\perp$ as a function of T: experimental data (points), only $V^{(1)}$ and five subbands in dielectric function (dashed line), $V^{(1)}$ and $V^{(2)}$, one subband in dielectric function (dotted line), $V^{(1)}$ and $V^{(2)}$ and five subbands in dielectric function (solid line).

References

(1) J. Moser, M. Gabay, P. Auban-Senzier, D. Jerome, K. Bechgaard, and J.M. Fabre, Eur. Phys. J. B1, 39 (1998).
(2) P. Denk and Jean – Luc Pelouard, Phys. Rev. B **3**, 041304 (R) (2001).
(3) P. Denk and Jean – Luc Pelouard, submitted to Phys. Rev. B.

Corresponding author:
Petra Denk, Lehrstuhl für angewandte Physik, Amalienstraße 54, 80799 München, Germany, phone:+49 89-2180-2306, Fax: :+49 89-2180-2050, email:petra.denk@physik.uni-muenchen.de

Exclusion of quantum coherence as the origin of the metallic state in Si-MOS structures

G. Brunthaler[1], A. Prinz[1], G. Bauer[1] and V.M. Pudalov[2]

[1]Institute for Semiconductor Physics, Johannes Kepler University, A-4040 Linz, Austria
[2]P. N. Lebedev Physics Institute of the Russian Academy of Sciences, Moscow 117924, Russia

The confirmation of the "metallic" behavior in several material systems, has raised the question whether it constitutes a new quantum mechanical ground state, or if the resistivity drop towards lower temperature is based on familiar effects.

We answer this question partly, by excluding quantum interference (QI) effects as the origin of the metallic state. This is achieved by determining the borders for QI and comparing it with the extension of the metallic state. From investigations of the weak localization, the phase coherence time τ_φ is deduce in a wide range of temperature and electron density. Only if τ_φ is larger than the momentum relaxation time τ, a coherent return of electrons to their origin is possible. The temperature where $\tau_\varphi = \tau$ thus defines the threshold temperature T_q for single-electron QI. In addition, the relation $k_BT = \hbar/\tau$ defines a temperature limit T_e for disorder induced electron-electron interaction effects.

The most characteristic feature of the metallic state is the decrease of the resistivity towards lower temperature. By comparing the threshold temperature T_q for single-electron QI and the threshold temperature T_e for electron-electron interaction with the regime of the metallic state in the resistivity versus temperature plane, we find that the border lines for QI effects do not coincide with the low resistivity regime. There is even an area at relative high density and temperature with strongly decreased resistivity, where QI is not present at all.

As the metallic state exists even without QI, we ask for the remaining possible explanations of the unexpected state. There is still the possibility that the metallic state originates from a quantum mechanical effect, i.e. screening. It has been shown that temperature dependent screening of impurity scattering is able to explain the large resistivity changes by up to a factor of 10 [1, 2]. Further models have been presented, which are of semi-classical nature. E.g. the temperature dependent scattering of trap states by Altshuler and Maslov [3] and the two-band model by Yaish et al. [4].

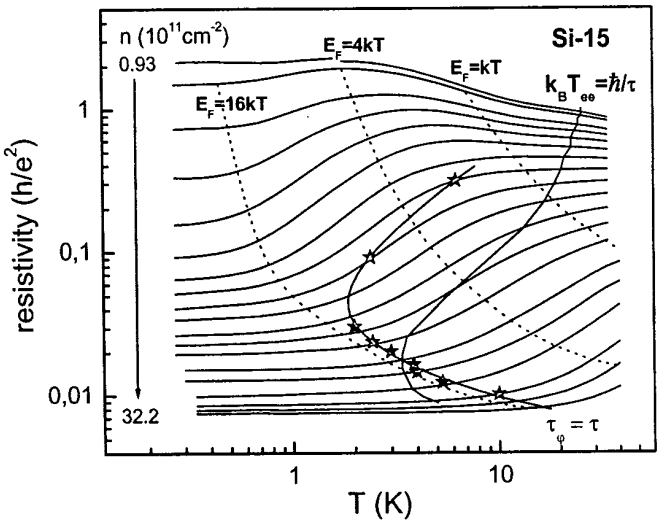

Fig. 1: Temperature thresholds in the resistivity versus temperature plane for sample Si-15. The asterisks mark the threshold T_q for single-electron quantum interference, and the $k_BT = \hbar/\tau$ line indicates the threshold for quantum interference effects due to e-e interaction. Dashed lines mark $E_F/i = k_BT$, with i = 1, 4, and 16. The experimental ρ vs. T curves are shown for n = 0.928, 0.970, 1.09, 1.18, 1.30, 1.45, 1.64, 1.89, 2.22, 2.64, 3.18, 3.88, 4.79, 6.30, 7.95, 10.2, 15.7, 21.2, and 32.2 x 10^{11} cm^{-2}.

References

[1] Das Sarma and Hwang, Phys. Rev. Lett. **83**, 164 (1999).
[2] Gold, JETP Lett. **72**, 401 (2000).
[3] Altshuler and Maslov, Phys. Rev. Lett. **82**, 145 (1999).
[4] Yaish et al., Phys. Rev. Lett. **84**, 4954 (2000).

Corresponding author: Gerhard Brunthaler, Institut für Halbleiter- und Festkörperhysik, Johannes Kepler Universität Linz, Altenbergerstraße 69, A-4040 Linz, Austria.
phone: +43 732 2468 9603, Fax: +43 732 2468 8650
email: G.Brunthaler@hlphys.uni-linz.ac.at

Random 1D structures as filters for electrical and optical signals

A. Krokhin[1], F. Izrailev[1], U. Kuhl[2], H.-J. Stöckmann[2], S. Ulloa[3]

[1]Instituto de Física, Universidad Autónoma de Puebla, Apdo.Post.J-48, Puebla, 72570, México
[2]Fachbereich Physik, Universität Marburg, D-35032 Marburg, Germany
[3]Department of Physics and Astronomy and Condensed Matter and Surface Science Program
Ohio University, Athens, Ohio 45701-2979

Conventional cutoff filters used in electronics and optoelectronics are based on periodic structures, which possess stop-bands i.e. gaps in the frequency spectrum. Depending on the frequency band, a typical filter is either a periodic superlattice or a waveguide with periodically arranged scatterers. Here we propose a different method of filtering of electromagnetic signals, which is based on selective transparency of disordered structures.

It has been known that disordered systems in 1D always exhibit Anderson localization, i.e. the average transmissivity of a disordered sample decays exponentially with a sample length L, $\langle t(L)\rangle \propto \exp(-L/4l)$, where l is the localization length. If the potential is uncorrelated (white noise) the localization length $l_0(E)$ is a smooth function of energy E, therefore it cannot be used as a basic element for a cutoff filter. The situation is changed for random potentials with correlations. Short-range correlations give rise for a discrete number of extended states [1]. Delocalized electron states have been observed in irregular superlattices with short-range correlations between layers ("random dimers") [2].

A general case of random potential with arbitrary correlations was analyzed in Refs. [3-5]. Here a relation between the pair correlator and the localization length has been derived. This relation shows that long-range correlations give rise to a continuum set of delocalized states, and thus to the mobility edge. The mobility edge can be very sharp and this property can be employed for design of the cutoff filters. The bandwidth of a filter can be made arbitrary wide or narrow depending on the statistics of the random potential. For example, Fig. 1 shows the dimensionless inverse localization length $\Lambda = l^{-1}/l_0^{-1}$ vs the electron momentum $q \propto \sqrt{E}$ for a chain of δ-peaks of equal amplitudes but random distance between peaks. This potential is an example of "structural" disorder in solids. An obvious realization of this model is a superlattice with fluctuating period. We consider a case of weak disorder, i.e. the chain is periodic on average, and the random displacements of the peaks are much less than the period. Solid line in Fig. 1 shows the analytical result for $\Lambda(q)$. The corresponding correlator decays slowly with the distance k between peaks, $\langle \Delta_n \Delta_{n+k}\rangle = \Delta_0^2 (5/2\pi k)[\sin(0.8\pi k) - \sin(0.4\pi k)]$. Here Δ_n is the displacement of the peak centered at site n (measured in units of the lattice period). Circles and crosses in Fig. 1 show the numerical results for two amplitudes of disorder, $\Delta_0 = 0.05$ and $\Delta_0 = 0.15$ respectively. One can see a good correspondence between analytical and numerical results. The random sequence, with the abovementioned correlator can serve as a basic element of a filter. In the interval of energies where $\Lambda = 0$ (i.e. $l = \infty$) the system is transparent, $T \approx 1$, while it exhibits low transmission in the regions where $\Lambda \neq 0$. The positions of the δ - peaks, which provide the desired transmission window are calculated using the algorithm proposed in Refs. [4,5]. The mobility edge does not appear if the correlator decays exponentially fast [3,5].

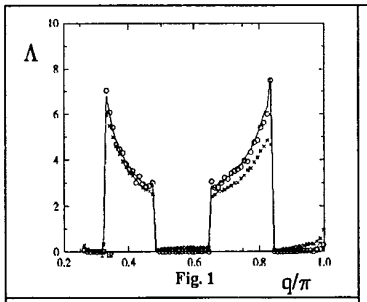

Fig. 1

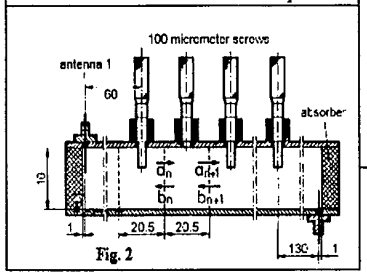

Fig. 2

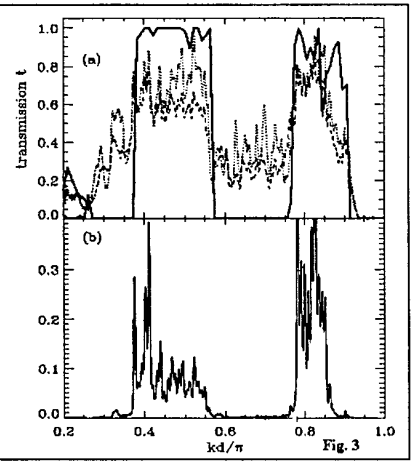

Fig. 3

The case of "compositional" disorder, i.e. equidistant δ-peaks with random amplitudes has been realized in experiment [4] with microwave transmission through an array of 100 screws inserted periodically into a metallic waveguide (Fig. 2). Solid curve in Fig. 3a shows the result of numerical simulation of transmission through an array of 10^4 random δ-scatterers with long-range correlations. The amplitude of the scatterers was mapped into screw lengths (the correlator of the screw lengths decays as $1/k$) and the measured transmission is shown in Fig. 3a by dotted line. The mobility edges are clearly seen exactly at the expected positions. The results for the array of 500 scatterers obtained by multiplicating the transfer matrices of 5 individual measurements demonstrate that the quality of a filter is much higher for the longer array, see Fig. 3b. There is a considerable technical potential in the correlated disorder, specially in connection with nanostructures and fiber optics, where the absorption is much lower. It allows us to compensate unwanted frequency dependencies in the transmission of digital and stochastic signals.

This work is supported by CONACYT, grant No. 28626 E.

References

[1] P. Phillips and H.-L. Wu, Science **252**, 1805 (1991).
[2] V. Bellani, E. Diez, R. Hey *et al.*, Phys. Rev. Lett. **82**, 2159 (1999).
[3] F.M. Izrailev, A.A. Krokhin, Phys. Rev. Lett. **82**, 4062 (1999).
[4] U. Kuhl, F.M. Izrailev, A.A. Krokhin, H.-J. Stöckmann, Appl. Phys. Lett. **77**, 633 (2000).
[5] F.M. Izrailev, A.A. Krokhin, S. Ulloa, Phys. Rev. B, **63**, 041102 (2001).

Corresponding author: Arkady Krokhin, IFUAP, Apdo. Post. J-48, Puebla, 72570, México,
phone: +(52-22) 45.76.45, fax: +(52-22) 44.89.47,
e-mail: arkady@sirio.ifuap.buap.mx

Electrical Rectification in Channelling by Magnetic Edge States

D.N.Lawton[1], A.Nogaret[1], M.V.Makarenko[2], O.V.Kibis[2], M.Henini[3]
[1]Department of Physics, University of Bath, Bath BA2 7AY, UK
[2]Department of Applied and Theoretical Physics, Novosibirsk State Technical University, 630092 Novosibirsk, Russia
[3]School of Physics and Astronomy, University of Nottingham, Nottingham NG7 2RD, UK

Hybrid semiconductor/ferromagnetic structures allow the realisation of microscopic magnetic potentials capable of channelling electrons in snake and cycloid states [1]. These systems have displayed robust giant magnetoresistance effects that promise novel magnetoelectronic devices. In this paper, we investigate the d.c. conductivity along the drift path of snake orbits and demonstrate rectification in the I-V characteristics when the lowest lying snake orbit modes remain populated. This non-linearity disappears when the magnetic modulation vanishes or when higher lying snake modes start to conduct. We interpret these findings in the light of the asymmetric energy dispersion of snake orbits. Because of this asymmetry, phonon emission is accompanied by a finite transfer of momentum to the electron system [2]. We propose a new theory to evaluate the electromotive force resulting from this phonon drag of electrons and compare it to the size of the non-linear behaviour.

Our hybrid structure, shown in Fig.1, consists of a ferromagnetic stripe fabricated at the surface of a shallow two-dimensional electron gas. The stripe is magnetised in the plane so that snake orbit channelling occurs at its centre.

Channelling is unidirectional: this is a direct consequence of the asymmetric dispersion curve of snake states, shown in Fig.2. In the presence of a heating current, electrons will relax by emitting phonons with momentum q along the direction of channelling. The rate of momentum transfer from the isotropic phonon distribution to electrons results in the electromotive force, ε_x:

$$\varepsilon_x \sim \left(\frac{\Xi m}{\pi}\right)^2 \frac{L_x l_H^3}{\rho v_l^5 e\hbar^7} (2k_B \Delta T)^5 \qquad (1)$$

Using the tabulated electron mass m, crystal density ρ, deformation potential Ξ, phonon velocity v_l in GaAs, a magnetic length l_H=25nm, a temperature difference $\Delta T \sim 1K$ between the electron and the lattice, and fundamental constants, we calculate the electromotive force to be $|\varepsilon_x/L_x| \sim 10^{-2}$V/cm.

Fig.3 shows the asymmetry in the non-local resistance measured when changing the sign of the current. This asymmetry vanishes at B=0, and has an amplitude of ~18Ω at saturation. We deduce the experimental e.m.f. to be $|\varepsilon_x/L_x| = 4.5\times10^{-2}$V.cm^{-1} in good agreement with the prediction of Eq.1.

References:

[1] A.Nogaret, S.J.Bending, M.Henini, Phys.Rev.Lett. **84**, 2231 (2000)
[2] O.V.Kibis, Phys.Lett.A 244, 432 (1998)

Coresponding author: Alain Nogaret, Department of Physics, University of Bath, Bath BA2 7AY, UK
Phone: +44 01225 826826 ext: 5609, Fax: +44 01225 826110
Email: A.R.Nogaret@bath.ac.uk

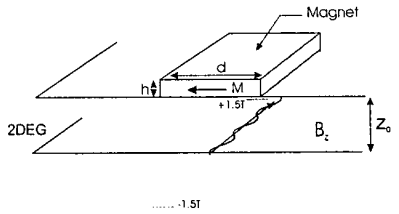

Fig.1: Magnetic field profile arising from a stripe magnetised in the plane of the 2DEG with magnetisation *M*. h=140nm, d=400nm, z_o=24nm. Snake orbits are guided by the line of zero magnetic field at the centre.

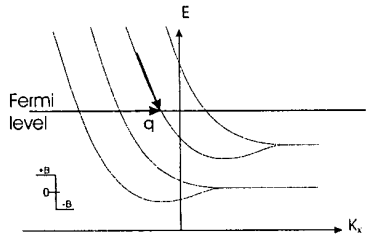

Fig 2: Energy dispersion curves for electrons confined in the step of magnetic field shown in the inset. Dispersive regions correspond to snake states and non dispersive regions to Landau levels. The electron distribution gains an average momentum by emitting phonons along the snake drift.

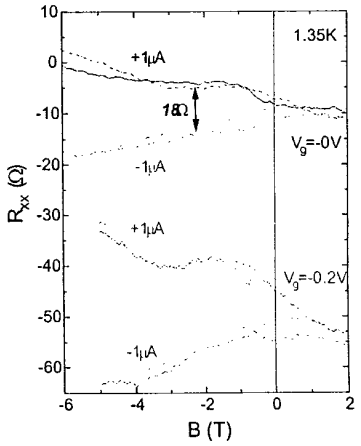

Fig.3: Non-local resistance for forward and reverse current and at two values of the gate voltage. Full (dashed) lines were measured while raising (decreasing) the applied magnetic field. Note the larger resistance splitting as more power is dissipated in the 2DEG.

The work is supported by INTAS under Grant #99-1661 and partially supported by Russian Foundation for Basic Research under Grants #00-02-18010 and #01-02-99305.

Two-way current switch using Coulomb blockade in GaAs quantum dots fabricated by selective area MOVPE

*F. Nakajima, Y. Ogasawara, J. Motohisa and T. Fukui
Research Center for Interface Quantum Electronics (RCIQE),
Hokkaido University, North 13 West 8, Sapporo 060-8628, Japan.
*e-mail: nfumito@rciqe.hokudai.ac.jp

We have been demonstrating the fabrication of single electron transistors (SETs) and single electron inverter circuits by selective area MOVPE (SA-MOVPE) [1]. Such single electron devices are very promising for future LSIs because of their potential for ultra-low power consumption and large scale integration. On the other hand, small gain and unilateral nature of the devices are the practical problems for the high-density integration. To overcome these shortcomings, an architecture based on binary decision diagram (BDD) is proposed for single electron logic system application [2], where a two-way current switch utilizing single electron tunneling phenomena is a key device as a unit element of the circuit. Here, we report on the fabrication and operation of a two-way current switch integrating two SETs fabricated by SA-MOVPE.

Figure 1(a) and (b) show an SEM image of our two-way current switch and its equivalent circuit, respectively. This circuit consists of two SETs which are made from width-modulated channel of two dimensional electron gas (see Fig.1(c)) grown by SA-MOVPE. The circuit also has the three gate electrodes (V_{G1}, V_{G2}, V_{GC}), to control single electron transport through quantum dots (QDs) of two SETs independently as shown in Fig.1(b). The side gates (V_{G1}, V_{G2}) are used to form QDs and to control the phase of Coulomb blockade oscillation. The center gate (corresponding to V_{GC}) is common for two SETs. A messenger electron enters from the entry branch V_S and goes through either of two exit branch V_{V1} and V_{V2}. The current can be switched from one exit branch to another by sweeping V_{GC}, if V_{G1} and V_{G2} are set to suitable values so that the conductance oscillations of two SETs are out of phase.

For the fabrication, GaAs/AlGaAs selectively doped double heterostructures were grown by SA-MOVPE at 700 ℃ on the masked substrate. The mask pattern was defined by EB lithography. Figure 1(c) shows a schematic illustration of one of SETs. The structure was composed of three facets, namely, (001) on the top surfaces, {110} and {111}B at the sidewalls. QD is formed in between two constrictions of the channel. The geometrical dot diameter estimated from SEM image was about 150 nm. After the growth, Ge/Au/Ni ohmic contacts at the source and drain were formed and three Al gate electrodes were also formed as shown in Fig.1(a).

Figure 2 shows a typical I_{DS}-$V_G$characteristics of the single wrap gate SET at 1.7 K. V_{DS} was set to 200 μV. Clear Coulomb oscillation was observed. From I_{DS}-V_{DS} characteristics, the Coulomb gap was about 3 mV. It correspond to 60 nm for dot diameter. Deviation from the geometrical size indicates that the depletion layers spread from the sidewall is an important factor for formation of the dot and tunneling barriers.

Figures 3(a),(b) and (c) show current through two SETs in a two-way switch at 1.8 K. Measurement parameters are shown in the figure. Solid (dotted) lines indicate the current for V_{G2}=-0.75V (-0.95V) in each figure. It is clear that I_{D1} was almost unchanged by the change of V_{G2} as shown in (a). On the other hand, peaks in I_{D2} was shifted to the positive direction (see (b)). At the same time, as shown in Fig.3(c), the peak near V_{GC}=-2V was shifted to the positive direction, which is in accordance with the shift of I_{D2}. These results indicate that it is possible to control the phase of conductance oscillation independently by the side gate and that the current through the entry branch is a simple sum of that through exit branch. Therefore, our circuit can be operated as a two-way current switch utilizing Coulomb blockade and SA-MOVPE is an effective technique to integrate SETs and to realize single electron BDD logic devices.

[1] F. Nakajima, K. Kumakura, J. Motohisa and T. Fukui: Jpn. J. Appl. Phys. 38 (1999) 415.
[2] N. Asahi and M. Akazawa and Y. Amemiya: IEEE Trans. ED 44 (1997) 1109.

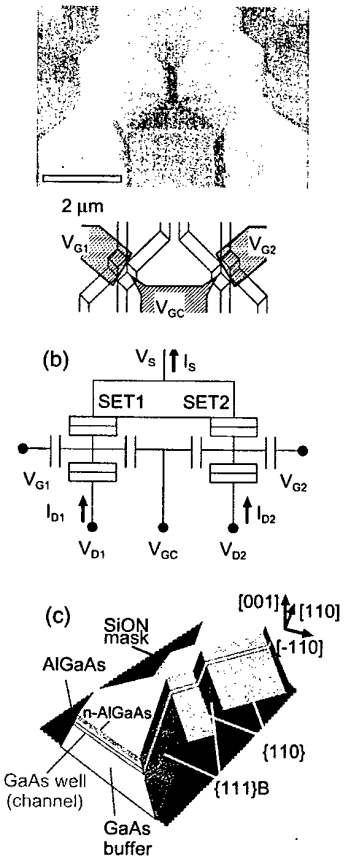

Fig.1 (a) SEM image of two-way current switch with two SETs and (b) its equivalent circuit. (c) One of the SET structures formed after selective area growth.

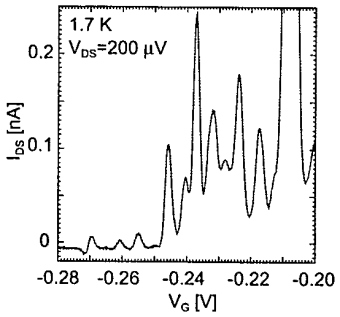

Fig.2 Typical Coulomb oscillation of a single SET controlled by a single gate

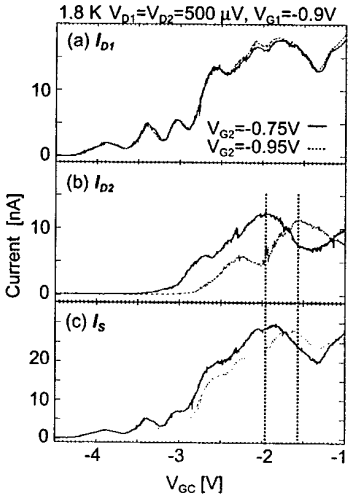

Fig.3 Conductance characteristics of each branch for main gate voltage.

Transient high-field transport and electro-optical properties of $Al_xGa_{1-x}As$-grading-structures

L. Robledo[1], A.Schwanhäußer[1], M.Eckardt[1], G.Döhler[1], H.Lutz[2], A.Seilmeier[2]

[1] Institut für Technische Physik 1, Universität Erlangen-Nürnberg, Erwin-Rommel-Str.1, 91058 Erlangen, Germany
[2]Physikalisches Institut, Universität Bayreuth, Universitätsstr.30, 95440 Bayreuth, Germany

The goal of this contribution is to extract the information on high-field non-equilibrium transport of photo-generated charge carriers in specially designed semiconductor structures which we have obtained by fs- pump and probe studies with a tunable two-color laser system [1]. Our approach is based on determining (1) the spatial and time evolution of the distribution of the photogenerated carriers propagating through the structure (2) deriving the local field changes and (3) determine the associated transient absorption change spectra. In order to obtain the most conclusive information, it is desirable that all the carriers are generated at about the same specific position within the structure. This has been achieved by a suitable design of our structures. For the study of electron transport the sample consists basically of a p-i-n-i-p doping structure with i-layer thicknesses typically in the range of 50 to 500 nm. (For hole transport n-i-p-i-n structures are used). This results in a V-shaped space charge induced potential well with a uniform built-in electric field. In order to vary the electric fields (up to >100 kV/cm) an external bias can be applied between ohmic contacts to the doped layers. The locally confined generation of electrons by the pump beam is achieved by suitable grading of the Al-content x of the two i-$Al_xGa_{1-x}As$ layers. The pump beam generates only carriers in the zone of lowest Al-content, which is chosen to be the region neighboring the p-layers. In this way the holes do not contribute to the transport, which allows us to study exclusively the electron transport. The grading also assures that the transport is not delayed by a tunneling barrier. After their generation the electrons are accelerated by the electric field (modified by the "pseudo-field" introduced by the grading). In the zone between the p-layer and the propagating electron distribution the field is screened by a fixed amount which depends on the sheet density of the electron distribution. The Franz-Keldysh absorption changes associated with these field changes (as well as absorption bleaching due to state filling) can be calculated if the propagation of the electron distribution as a function of time is known. Thus, calculated and experimentally observed transient transmission spectra agree, if the transport is calculated correctly (by realistic Monte Carlo simulations in our case). The quality of the simulation of the absorption change spectra can be tested by performing dc measurements as a function of applied voltage between the p- and n-layers. These transmission change spectra are reproduced by the spectra observed in pump and probe experiments after all the electrons have arrived (spatially and energetically) at the lower edge of the V-shaped potential. (Note that a given sheet electron density directly corresponds to a fixed voltage change). Fig. 2 shows, as an example, a calculated absorption change spectrum together with the corresponding experimental counterpart for the p-i-n-i-p structure depicted schematically in Fig. 1. The calculated transient absorption change spectra shown in Fig. 3, which reflect the transit of the electron distribution through the first grading zone, drastically differ from the "finalstate" spectra shown in Fig. 2. This corroborates the experimental finding that our sophisticated sample design, indeed, allows for very detailed information on the high-field transport.

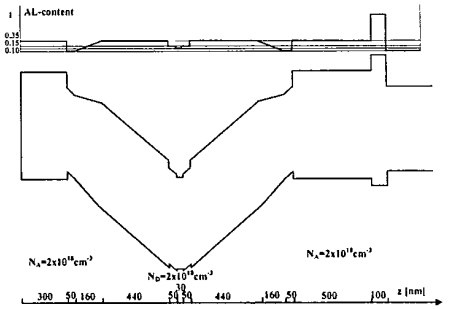

Fig. 1: Design of the AlGaAs p-i-n-i-p structure.

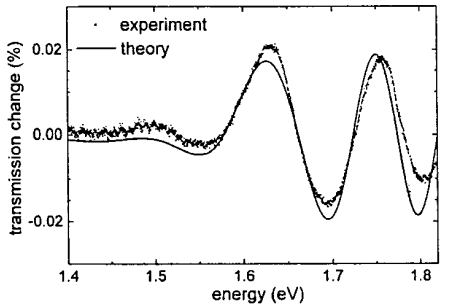

Fig. 2: Measured and calculated transmission change spectra for the structure.

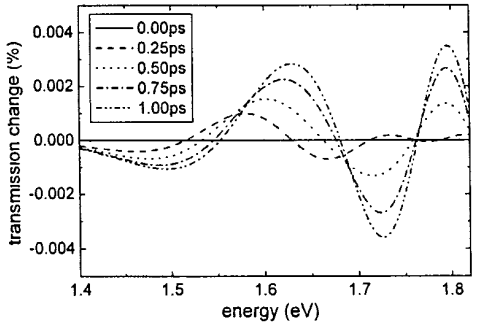

Fig. 3: Calculated transient transmission change spectra.

[1] H. Lutz et al., "High field electron transport in GaAs/$Al_xGa_{1-x}As$ p-i-n-i-p-structures investigated by ultra fast absorption changes", MSS10, Linz (2001)

Corresponding author: Martin Eckardt, Institut für Technische Physik 1, Friedrich-Alexander Universität Erlangen, Erwin-Rommel-Straße 1, D-91058 Erlangen, Germany.
phone: +49 9131 85 28319, Fax: +49 9131 85 27293
email: martin.eckardt@physik.uni-erlangen.de

Dynamical transport of photoexcited carriers between shallow and deep quantum wells embedded in a GaAs/AlAs superlattice

A. Satake[1], T. Ikemoto[1], K. Fujiwara[1], L. Schrottke[2], R. Hey[2], and H. T. Grahn[2]

[1]Department of Electrical Engineering, Kyushu Institute of Technology, Tobata, Kitakyushu, 804-8550, Japan
[2]Paul-Drude-Institut für Festkörperelektronik, Hausvogteiplatz 5-7, 10117 Berlin, Germany

Transport of photoexcited carriers along the growth direction (i.e., vertical transport) has recently received considerable interest. In a short-period superlattice (SL) with an enlarged single quantum well (SQW), photoexcited carriers are transported by Bloch conduction via extended states or by tunneling-assisted hopping conduction, being eventually trapped by the enlarged SQW. This phenomenon has been observed in steady-state and time-resolved photoluminescence (PL) experiments [1-3]. In this work, we investigate the vertical transport between several GaAs SQWs with different well widths, which are intentionally placed between short-period GaAs/AlAs SLs. We perform steady-state and time-resolved PL measurements as a function of lattice temperature (T). The vertical transport between these QWs and in the SL depends strongly on T. The dynamical, phonon-assisted transport of photoexcited carriers between the QWs of different thickness and the short-period GaAs/AlAs SL is studied.

The sample studied here is grown on a GaAs (100) substrate by molecular beam epitaxy. The heterostructure consists of two GaAs QWs with well widths of 7.8 nm (QW1) and 5.5 nm (QW2). The barriers are formed by 6 periods of a GaAs/AlAs (4.9 nm/1.0 nm) superlattice (SL1). The whole system is put between a pair of another GaAs/AlAs (2.3 nm/1.0 nm) superlattice (SL2). The steady-state and time-resolved PL measurements are performed between 20 and 280 K in a closed-cycle He cryostat. Steady-state PL spectra are recorded using a He-Ne laser for excitation and a conventional lock-in technique for detection. The time-resolved PL measurements are performed with a streak-scope system. A pulsed laser diode was used for excitation at 653 nm (1.90 eV).

Figure 1 shows a steady-state PL spectrum recorded at 20 K. PL peaks originating from the QW1 and QW2 as well as from SL1 and SL2 are identified. The PL transients at 20 and 60 K shown in Fig. 2 indicate decay times of the order of nanoseconds for QW1, QW2, and SL1. When T is increased to 60 K, the decay time of QW1 increases, while the ones of QW2 and SL1 decrease. Moreover, the PL intensity of QW1 increases with increasing T, while the ones of QW2 and SL1 gradually decrease. These observations indicate the following processes as shown in Fig. 3. The photoexcited carriers in QW2 (shallow QW) are thermally activated into the miniband of SL1, where they are transported by Bloch conduction via the extended miniband states, until they relax into QW1 (deep QW). Therefore, the PL decay time of QW2 decreases with increasing T, while the PL intensity of QW1 increases. At even higher T, the carriers in QW1 can also be thermally excited into the miniband of SL1. Therefore, at 140 K, the decay time as well as the PL intensity of SL1 suddenly increases, while the ratio I_{QW1}/I_{SL1} is strongly reduced for T above 140 K. We will present a detailed discussion of this unique temperature evolution of the vertical transport between shallow and deep QWs as evidenced by steady-state and time-resolved PL spectroscopy.

References

[1] A. Nakamura, K. Fujiwara, Y. Tokuda, T. Nakayama, and H. Hirai, Phys. Rev. B **34**, 9019 (1986).
[2] A. Chomette, B. Deveaud, A. Regreny, and G. Bastard, Phys. Rev. Lett. **57**, 1464 (1986).
[3] K. Fujiwara, N. Tsukada, T. Nakayama, and A. Nakamura, Phys. Rev. B **40**, 1906 (1989).

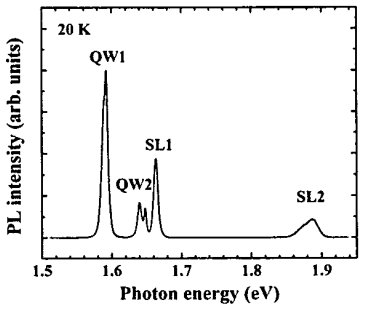

Fig. 1 Steady-state PL spectrum recorded at 20 K.

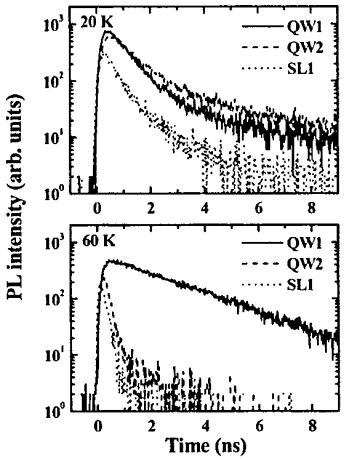

Fig. 2 PL transients of QW1, QW2 and SL1 at 20 (top) and 60 K (bottom).

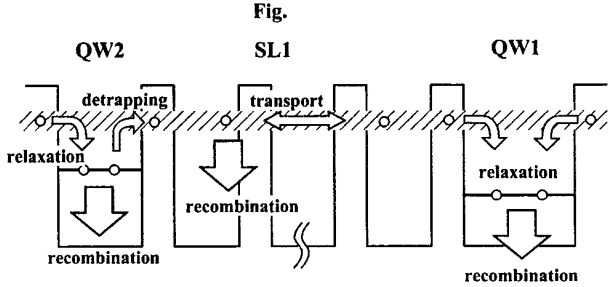

Fig. 3 Schematic diagram of vertical transport between shallow and deep QWs.

Corresponding author: Akihiro Satake, Department of Electrical Engineering, Kyushu Institute of Technology, 1-1 Sensui-cho, Tobata, Kitakyushu, 804-8550, Japan
phone: +81-93-884-3240, Fax: +81-93-884-3240,
email: satake@ele.kyutech.ac.jp

Hot-carrier dynamics in semiconductor-based quantum-cascade lasers: a Monte Carlo study

R. C. Iotti, F. Rossi

Istituto Nazionale per la Fisica della Materia (INFM) and Dipartimento di Fisica, Politecnico di Torino, Corso Duca degli Abruzzi 24, I-10129 Torino, Italy

Hot-electron relaxation processes play a crucial role in determining the operation efficiency of many semiconductor-based quantum devices like, e.g., quantum cascade lasers (QCLs) [1]. From the theoretical point of view, these unipolar coherent-light sources are usually described in terms of purely macroscopic multi-level models. This simplified picture, however, does not take into account the existence of transverse, or "in-plane", degrees of freedom, and can only operate as an a-posteriori fitting procedure [2]. In this contribution, we present a fully three-dimensional (3D) multi-subband analysis of hot-carrier dynamics governing intersubband light-emitting devices: a global Monte Carlo (MC) simulation scheme is proposed, which allows to directly access microscopic key-features of the carrier relaxation, without resorting to phenomenological parameters [3].

QCLs are complex structures, whose core is made up of repeated stages of active regions, sandwiched between electron injecting and collecting regions. As a starting point of our MC approach, we evaluate the set of 3D single-particle electron states, corresponding to the generic QCL stage λ (active region plus injector/collector), in the presence of a proper bias. To "close the circuit", we impose periodic boundary conditions limiting the inter-stage ($\lambda' \neq \lambda$) scattering to just nearest-neighbors coupling ($\lambda' = \lambda \pm 1$). In view of the translational symmetry, we are allowed to simulate carrier transport over the central stage only: whenever a carrier undergoes an inter-stage scattering process, it is properly re-injected into the simulated region and the corresponding electron charge contributes to the current through the device. To model charge transport along the growth direction, the relevant interaction mechanisms have been included at a kinetic level in our simulation, namely all various intra- as well as inter-subband carrier-optical phonon and carrier-carrier scattering processes.

The proposed simulation scheme has been applied to finite multiple quantum wells forming the active region of state-of-the-art QCLs. In particular, we have investigated the GaAs/(Al,Ga)As-based diagonal-configuration device of Ref. [4]. The time evolution of the carrier population of the various subbands has been studied in the presence and absence of inter-carrier interaction, in order to focus on the relative weight of the carrier-carrier and the carrier-phonon competing energy-relaxation channels. Our results [3] clearly show that, for typical operating conditions, carrier-carrier scattering is effective in setting up a heated Maxwellian distribution: electrons thermalise within each subband and temperatures corresponding to the diverse subbands vary in a quite narrow range.

Particle and energy redistribution within the various subbands, due to carrier-carrier interaction, is of fundamental importance in determining the device performances as well. Figure 1 reports the gain spectra corresponding to the lasing transition obtained from simulated experiments performed with (solid curve) and without (dashed curve) carrier-carrier interaction. The positive values of both gain spectra show that a regime of population inversion between the highest and intermediate level of the active region is eventually established in both cases. Inter-carrier scattering, however, does strongly increase the gain efficiency.

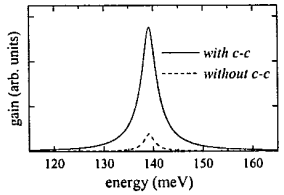

Fig. 1: Gain spectra at the lasing transition for the structure of Ref. [4]. Full line: with carrier-phonon as well as carrier-carrier interactions; dashed line: with carrier-phonon scattering only.

In the proposed MC scheme, the current-versus-voltage behavior can be obtained without resorting to any phenomenological external parameter. Our simulations show that while carrier-phonon relaxation well describes the electronic quantum cascade within the bare active region [2], carrier-carrier scattering plays an essential role in determining charge transport across the full core region. Figure 2 presents the simulated current-voltage characteristics for the structure of Ref. [4]. The current density increases with the applied field, due to the increased coupling between active-region and lower-energy injector states. The agreement between theoretical results and measured dependence [4] is extremely good and supports the incoherent nature of charge transport in such unipolar quantum devices.

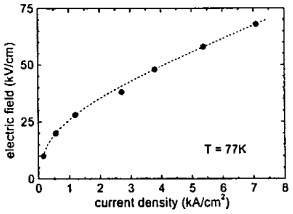

Fig. 2: Applied-field vs current-density characteristics for the structure of Ref. [4]. The dashed line is a guide to the eye.

References

[1] J. Faist et al., Science 264, 553 (1994); G. Scamarcio et al., Science 276, 773 (1997); C. Gmachl et al., Science 286, 749 (1999).
[2] R. C. Iotti and F. Rossi, Appl. Phys. Lett. 76, 2265 (2000).
[3] R. C. Iotti and F. Rossi, to be published in Appl. Phys. Lett.
[4] C. Sirtori et al., Appl. Phys. Lett. 73, 3846 (1998).

Corresponding author: Rita Claudia Iotti, Dipartimento di Fisica, Politecnico di Torino, Corso Duca degli Abruzzi 24, I-10129 Torino, Italy.
phone: +39 11 564 7335, fax: +39 11 564 7399
e-mail: iotti@athena.polito.it

Magnetotransport through AFM-defined Antidot Arrays

A. Dorn[1], A. Fuhrer[1], T. Heinzel[1], K. Ensslin[1], W. Wegscheider[2], and M. Bichler[3]

[1] Solid State Physics Laboratory, ETH Zurich, 8093Zurich, Switzerland
[2]Experimental and Applied Physics, University of Regensburg, 93040 Regensburg, Germany
[3]Walter Schottky Institute, TU München, 85748 Garching, Germany

Magnetotransport experiments on antidot lattices in two-dimensional electron gases (2DEGs) have been of considerable interest over the last 10 years. [1] More recent studies on arrays with smaller lattice constants have reported Aharanov-Bohm-type oscillations and indications of a Hofstadter-type bandsplitting [2,3]. Samples are fabricated from GaAs-AlGaAs heterojunctions containing high mobility 2DEGs close to the surface. The periodic potential modulation is usually introduced by employing e-beam lithography. In this cases the feature size is limited by electron backscattering from the GaAs surface and the resolution of the PMMA resist development process. Here we proceed by employing our newly developed atomic force microscope (AFM) based lithography which was successfully demonstrated for the fabrication of high-quality quantum wires [4] and quantum dots [5].

Our approach is to use an AFM with a conducting tip (boron doped Si or TiN) as a tool for local anodic oxidation [4, 5]. If the AFM tip acts as a cathode while the chip that is to be nanostructured is grounded, very local oxidation processes can be performed. A thin water film that naturally forms on the sample surface under ambient conditions serves as the electrolyte. The structures described here were written with tip voltages between -10V and -20V. The resulting oxide dots and lines have heights and widths between 10nm and 20 nm and 100nm and 200nm respectively. Previous investigations have shown that the oxide height correlates well with the imposed electronic depletion of the underlying 2DEG and lines become insulating at heights between 12nm and 15nm for 2DEGs ca. 34nm below the surface.

For AFM lithography the challenge is to have an extremely stable set-up where drift and creep of the piezo drivers are compensated. This is crucial in order to guarantee a perfect periodicity. Figure 1 shows a periodic lattice of oxide pillars fabricated on top of a GaAs heterostructure. The 20*20 array with a period of 300 nm is enclosed by 4 lines which isolate the antidot pattern from the surrounding.

A Ti/Au topgate was applied via shadow mask evaporation, that allows the electron sheet density to be tuned between 1 and $7*10^{11}$ cm^{-2}. The resistance of the antidot system is measured via the four point contact-like openings at the corners of the square. A typical magnetoresistance and Hall resistance trace is shown in Fig. 2 for a temperature of 1.7 K. All typical features of a high-quality antidot lattice [1], namely commensurability oscillations including the onset of quantum oscillations (at 1.7 K!), a quenching of the Hall effect close to B=0, plateau-like features in the Hall effect and weak localization around B=0 can be observed indicating the quality of our fabrication process,.

This demonstrates that AFM-nanolithography is well suited for the fabrication of electronically functional antidot arrays and we have indications that large improvements in resolution are still possible.

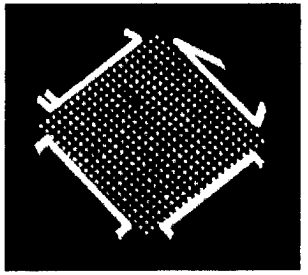

Fig. 1: Antidot lattice with a=300nm fabricated by AFM-Lithography. The 2DEG is 34nm below the surface, the height of the oxide is 10-20nm.

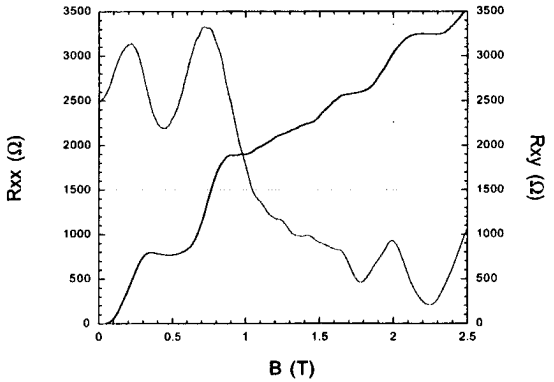

Fig. 1: Longitudinal and Hall resistance of the antidot lattice shown above at 1.6K

References

[1] for a review see R. Schuster and K. Ensslin, Festkörperprobleme **34**, 195 (1994).
[2] T. Schlösser, K. Ensslin, J. P. Kotthaus, and M. Holland, Europhys. Lett. **33**, 683 (1996)
[3] C. Albrecht, J. H. Smet, K. von Klitzing, D. Weiss, V. Umansky, and H. Schweizer, Phys. Rev. Lett. **86**, 147 (2001)
[4] T. Heinzel, G. Salis, S. Lüscher, R. Held, K. Ensslin, and W. Wegscheider, Phys. Rev. B **61**, R13353 (2000)
[5] S. Lüscher, T. Heinzel, K. Ensslin, W. Wegscheider, and M. Bichler, Phys. Rev. Lett. **86**, 2118 (2001)

Corresponding author: Klaus Ensslin, Solid State Physics Laboratory, ETH Zurich, 8093 Zurich, Switzerland
phone: +41-1-633 2209, Fax: +41-1-633 1146
email: ensslin@solid.phys.ethz.ch

Comparison of experimental and calculated resistance in p-SiGe over a wide temperature range

V. Senz[1], T. Ihn[1], T. Heinzel[1], K. Ensslin[1], G. Dehlinger[2], D. Grützmacher[2], U. Gennser[2], E.H. Hwang[3] and S. Das Sarma[3]

[1]Solid State Physics Laboratory, ETH Zürich, CH-8093 Zürich, Switzerland
[2]Paul Scherrer Institute, CH-5234 Villigen PSI, Switzerland
[3] Department of Physics, University of Maryland, Maryland 20742-4111, USA

The observation of what has become known as the 'metal-insulator transition in two dimensions at zero magnetic field' (MIT) has initiated a great variety of experimental and theoretical research in recent years [1]. To date the microscopic origin of the metallic behavior is still under discussion. We have recently analyzed the temperature dependence of the metallic phase in p-SiGe [2] in terms of temperature dependent screening [3,4]. At low temperatures, where weak localization corrections are clearly present the temperature dependence of the conductivity could be quantitatively described by three contributions, namely

$$\sigma(T) = \sigma_D(T) + \delta\sigma_{WL}(T) + \delta\sigma_I(T),$$

where $\sigma_D(T)$ is the Drude conductivity, $\delta\sigma_{WL}(T)$ and $\delta\sigma_I(T)$ are the WL and the interaction contributions, respectively.

In the present study we extend the experimental range of temperatures up to 70 K. Below 5K temperature dependent screening is the dominant contribution to the temperature dependence of the resisitvity. At higher temperatures the smearing of the Fermi function and phonon scattering produce a non-monotonic temperature dependence which we actually find in the experimental data.

In the model we consider various scattering mechanisms, such as ionized impurity scattering, interface roughness scattering, alloy disorder scattering, ionized background impurity scattering and acoustic phonon scattering. This way we are able to make a quantitative comparison of the experimental data (Fig. 1) in a wide range of temperatures ($1.7K \leq T \leq 20K$) and densities ($1.5 \times 10^{11}cm^{-2} \leq N_s \leq 5.1 \times 10^{11}cm^{-2}$) to the model (Fig. 2). The good agreement indicates that temperature dependent screening cannot only account for the metallic behavior close to the metal-insulator transition but is equally important in adjacent temperature and density regimes. This gives further confidence to the description of the temperature dependence of the resistivity in p-SiGe in terms of single-particle models.

The model fails in the insulating regime ($\rho \geq h/e^2$), probably because the sample becomes inhomogeneous and multiple scattering events have to be taken into account.

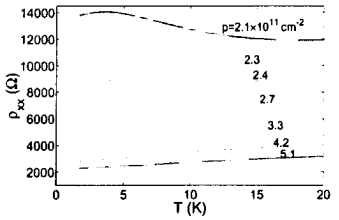

Fig. 1: Experiment: measured resistivities for the densites $p = 2.1 \ldots 5.1 \times 10^{11}cm^{-2}$ as a function of temperature.

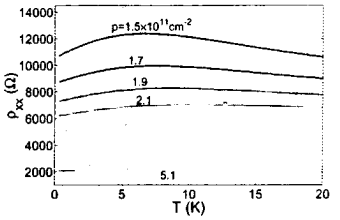

Fig. 2: Theory: Calculated resistivities according to our model for the densities $p = 1.5 \ldots 5.1 \times 10^{11}cm^{-2}$ (the corresponding experimental curve with the same density has equal color in Fig. 1).

References

[1] for recent reviews see E. Abrahams, S. V. Kravchenko, M. P. Sarachik cond-mat/0006055 and B. L. Altshuler, D. L. Maslov, V. M. Pudalov, cond-mat/0003032
[2] V. Senz *et al.*, Phys. Rev. Lett. **85**, 4357 (2000)
[3] A. Gold, V.T. Dolgopolov, Phys. Rev. B **33**, 1076 (1986)
[4] S. Das Sarma, E. H. Hwang, Phys. Rev. Lett. **83**, 164 (1999)

Corresponding author: Volkmar Senz, Solid State Physics Laboratory HPF E13, ETH Hönggerberg, CH - 8093 Zürich, Switzerland .
phone +41 1 633 2314, Fax: +41 1 633 1146,
email: senz@phys.ethz.ch

An Ultra-narrow Electron Injector for Ballistic Electron Spectroscopy

M. Kast, C. Pacher, M. Coquelin, G. Fasching, G. Strasser, E. Gornik

Institut für Festkörperelektronik, TU Wien
Floragasse 7, 1040 Wien, Austria

Ballistic electron spectroscopy is a suitable method to investigate both semiconductor bulk and heterostructure material systems[1,2,3]. The basic concept is a three terminal device where hot electrons are injected into a very thin highly doped GaAs layer via an AlGaAs tunneling barrier, and are collected after traversing an energy spectrometer as the collector current. The aim of this work is to reduce the width of the electron distribution by optimizing the layer structure of the electron injector. To measure the energetic width of the ballistic electron beam, a three terminal device[3] was designed using a triple barrier RTD as a narrow energy filter between base and collector. It consists of three $Al_{0.3}Ga_{0.7}As$ barriers and two GaAs wells. The two well widths are chosen to be 4.2 nm in order to get a first resonant state (for the isolated well) at 100 meV. To optimize the transmission properties of the analyzer we choose the center barrier (8 nm) twice as thick as the neighbouring barriers (4 nm). The complete conduction band structure of the three terminal device is shown in FIG. 1. An energy tunable electron beam is generated by the tunneling emitter barrier and reaches the triple barrier RTD after traversing a highly doped n-GaAs base layer and a slightly n-doped drift region. Electrons, which are transmitted through the analyzer are measured as the collector current. The static transfer ratio ($=I_c/I_e$) reflects the probability of an injected electron to be transmitted through the analyzer. The structures shown in FIG. 1 were grown by molecular beam epitaxy on semi-insulating GaAs substrates. The three terminal devices were fabricated by standard photolithographic and wet etching techniques in a 30 x 30 μm^2-MESA structure. The transfer ratio vs. emitter bias is shown in FIG. 2. Due to the transmission properties of the analyzer the first peak is proportional to the energy distribution of the injected electrons. The following peaks in the transfer ratio are due to electrons which are scattered by LO-phonons while traversing the drift region and which have lost 36 meV during the scattering processes. After deconvoluting the transfer ratio and considering the influence of the analyzer we derive a full width at half maximum of the injected electrons of 10 meV. Using this new spectroscopic source we observe for the first time in a direct current experiment the field dependence of Wannier-Stark-states[4] in the first miniband of a 5 period superlattice up to an electric field of 33 kV/cm (FIG. 3). The intensity dependence on electric field of the individual peaks directly reveals the transmission probability. The superlattice consists of 6 AlGaAs barriers of 3.5 nm and 5 GaAs wells of 3 nm. This parameters leads to a subband spacing of 10 meV in the first miniband according to the energetic width of the ballistic electrons generated by the new electron injector.

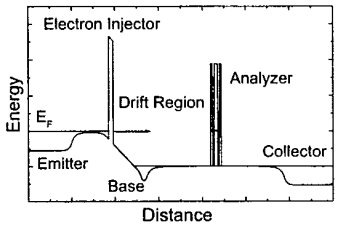

Figure 1: Calculated conduction band structure of a three terminal device along the growth direction. The analyzer acts as a narrow energy filter for the ballistic electrons generated by the new electron injector.

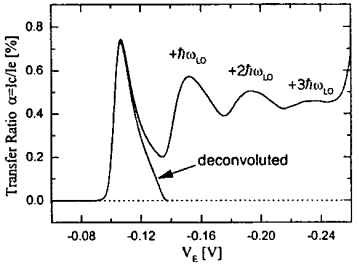

Figure 2: Transfer ratio vs. emitter bias of the triple barrier RTD. Deconvoluting the transfer ratio gives the true lineshape of the energy distribution of the ballistic electron beam.

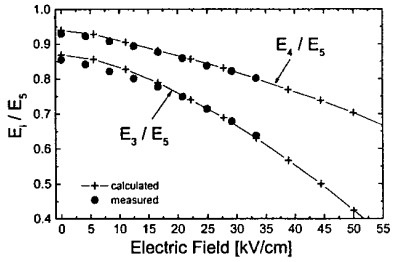

Figure 3: Electric field dependence of the normalized energetic subband positions E_i/E_5.

References

[1] J. R. Hayes et al., Phys.Rev.Lett. **54**, 1570 (1985).
[2] M. Heiblum et al., Phys.Rev.Lett. **55**, 2200 (1985).
[3] C. Rauch et al., Phys.Rev.Lett. **81**, 3495 (1998).
[4] E. E. Mendez et al., Phys.Rev.Lett. **60**, 2426 (1988).

Corresponding author: Michael Kast, Institut für Festkörperelektronik, TU Wien,
Floragasse 7, 1040 Wien, Austria
phone: +43 1 58801 36229, Fax: +43 1 58801 36299
email: michael.kast@tuwien.ac.at

Magnetoresistance of a modulated two-dimensional electron gas in parallel magnetic field

A. Nauen[1], U. Zeitler[1], A.G.M. Jansen[2], R. J. Haug[1], M. Dilger[3] and K. Eberl[3]

[1]Institut für Festkörperphysik, Universität Hannover, Appelstr. 2, D-30167 Hannover
[2]Grenoble High Magnetic Field Laboratory, MPIF-CNRS, Boîte Postale 166, F-38 042 Grenoble Cedex 09, France
[3]Max-Planck-Institut für Festkörperforschung, Heisenbergstr.1, D-70569 Stuttgart, Germany

While two-dimensional electron gases (2DEG) in a uniform magnetic field represent an area of great interest in modern semiconductor physics, the more complex situation of a 2DEG in a spatially varying field has attracted attention only recently [1-2].

We present magnetotransport experiments on a 2DEG with a pre-structured trench in parallel magnetic fields up to 28 T. We observe a dramatic step-like increase of the magnetoresistance which we attribute to selective transport of edge channels through the trench.

Our sample consists of a heterostructure grown on a pre-patterned GaAs-substrate where a trench was defined by electron-beam lithography in combination with 470 nm-deep wet-etching (see Fig.1). A second sample was grown on the same wafer without pre-patterning to serve as a reference.

The zero field resistance of the trench sample is slightly enhanced with respect to the reference what we attribute to an increased electron scattering in the trench. Both samples show a negative magnetoresistance at low parallel magnetic fields caused by phase coherence effects.

The most striking feature is a dramatic increase of the magnetoresistance in the trench sample around $B = 15\ T$ that is not present in the reference (see Fig. 2). This magnetic field corresponds to the situation where the Landau level filling in the trench walls changes from $N = 2$ to $N = 1$. As a consequence the number of channels transmitted from a trench wall to the opposite side is reduced by a factor of two and the resistance increases accordingly.

References

[1] M. L. Leadbeater *et al*, J. Phys.: Cond. Matter **7** L307 (1995)
[2] A. Nogaret, S.J. Bending, M. Henini, Phys. Rev. Lett. **84**, 2231 (2000)

Corresponding author: André Nauen, Institut für Festkörperhysik, Abt. Nanostrukturen
Universität Hannover, Appelstraße 2, D-30167 Hannover, Germany.
phone: +49 511 762 19017, Fax: +49 511 762 2904,
email: nauen@nano.uni-hannover.de

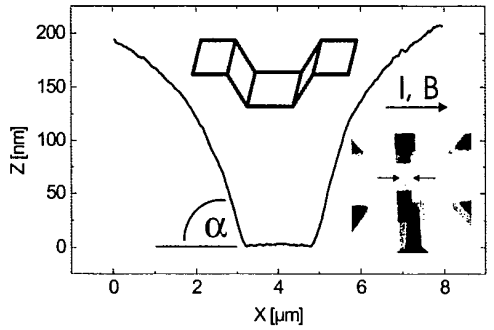

Figure 1: Profile of the structure measured with an AFM. Note the different axis scales — the maximum angle is $\alpha = 8°$. *Middle Inset*: Schematic view of the sample. *Right Inset*: topview of the sample. The trench is located between the arrows; the scanning area is $80 \times 80\ \mu$m. The direction of current I resp. parallel magnetic field B is indicated.

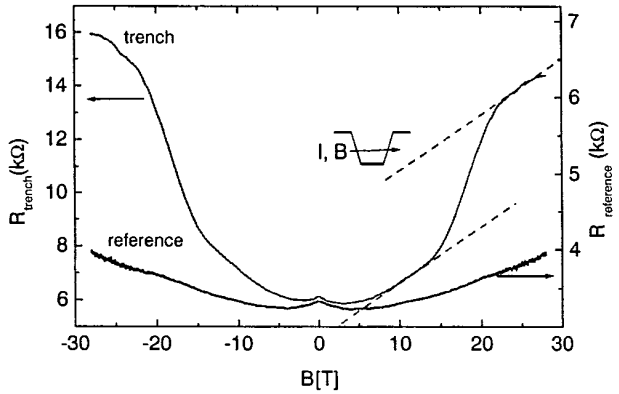

Figure 2: Resistance for both samples at 400 mK vs. parallel magnetic field. The dashed lines are guides to the eye.

Strain relaxation in high-mobility InAs inserted-channel heterostructures with metamorphic buffer.

S. Mendach, C. M. Hu, Ch. Heyn, S. Schnüll, H. P.Oepen, R. Anton and W. Hansen

Institut für Angewandte Physik, Universität Hamburg,
Jungiusstraße 11, D-20355 Hamburg, Germany

InAs based heterostructures provide significant advantages in comparison to conventional GaAs based devices. Very important is the absence of a Schottky-barrier between pure InAs and metals that enables to fabricate hybride systems e. g. in combination with ferromagnetic or superconducting metals.

In this work, we present high-mobility modulation doped InAs inserted-channel $In_{0.75}Al_{0.25}As$ / $In_{0.75}Ga_{0.25}As$ structures grown with molecular beam epitaxy (MBE) on GaAs substrates [1]. One key point crucially determining the device quality is the metamorphic buffer grown for lattice relaxation between the substrate and the active layers. Applying the focussed ion beam (FIB) technique, we prepare thin cross-sections for transmission electron microscopy (TEM) investigations. The FIB preparation allows TEM overviews of the complete 1.3 µm thick heterostructure as well as high resolution magnifications of interesting regimes. This enables us to observe the density and propagation of dislocations through the whole structure. An example is shown in Fig. 1 together with a scheme of the sample structure. Importantly, we find that the dislocation density in the step-graded metamorphic buffer decreases with the distance of the respective buffer step from the GaAs substrate. This is due to the optimised buffer design, where the relative lattice mismatch of each buffer step decreases as well. As result, the active layers of the heterostructure are nearly dislocation-free. Transport measurements of this heterostructure exhibit mobilities up to 400 000 cm^2 / Vs (see Fig. 2) which, to our knowledge, represent the highest value reported for such structures so far.

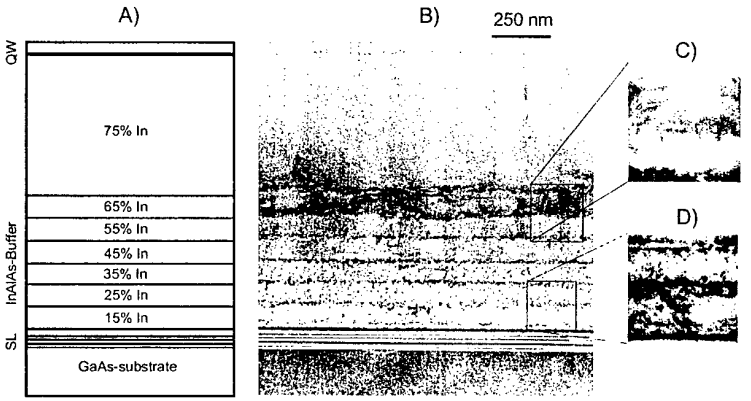

Fig.1: A) Scheme of InAs HEMT structure with step-graded metamorphic buffer on GaAs substrate. Starting with a GaAs/AlAs superlattice (SL), we increase the In content in the following InAlAs layers from 15 up to 75 percent in steps of 15% every 100 nm. After a 430 nm thick $In_{0.75}Al_{0.25}As$-layer, the active quantum well (QW) consists of: 7 nm Si-doped $In_{0.75}Al_{0.25}As$, 5 nm $In_{0.75}Al_{0.25}As$, 2.5 nm $In_{0.75}Ga_{0.25}As$, 4 nm InAs, 13.5 nm $In_{0.75}Ga_{0.25}As$ and 36 nm $In_{0.75}Al_{0.25}As$. .B) TEM cross-sectional overview of the complete sample structure. Importantly, very few threading dislocations propagate to the active region. C) and D) show magnified details.

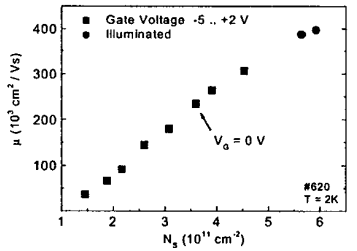

Fig. 2: Electron mobility µ vs. carrier density N_s of the sample described in Fig. 1. The data are taken with magneto transport measurements at 2 K in Hall-bar geometry. The carrier density was varied by both a gate voltage between an evaporated Al/Au layer and the InAs channel [1] as well as by illumination.

References

[1] A. Richter, M. Koch, T. Matsuyama, Ch. Heyn and U. Merkt, Appl. Phys. Lett. 77, 3227 (2000).

Corresponding author: Stefan Mendach, Institut für Angewandte Physik, Universität Hamburg, Jungiusstraße 11, D-20355 Hamburg, Germany.
phone: +49 40 42838 2040, Fax: +49 40 42838 6332
email: smendach@physnet.uni-hamburg.de

Magnetoresistance of vertical transport in InAs/GaSb Superlattices.

V.J. Hales, R.J. Nicholas, and N. J Mason

Clarendon Lab, Department of Physics, University of Oxford, Parks Road, Oxford, OX1 3PU, U.K.
Tel: +44 (0) 1865 272299; Fax: +44 (0) 1865 272400; Email: v.hales1@physics.ox.ac.uk

Keywords: magnetoresistance, InAs/GaSb, Superlattice, miniband.

We report a study of the vertical transport of short period InAs/GaSb superlattices. Applying a magnetic field parallel to the superlattice axis we find a remarkably large magnetoresistance and strongly non-linear I-V relations. In particular the I-V characteristics exhibit a bias and magnetic field dependent threshold for conduction at low biases. The conduction processes are found to be strongly influenced by the relative energy scales of the miniband width and cyclotron energy [1]. For low bias levels magnetoresistance of up to 1000X are observed in magnetic fields of 15T.

The superlattice band structure of InAs/GaSb structures is very different from that found in most semiconductors due to the broken gap alignment. As a result tunnelling between adjacent superlattice layers in dominated by interband coupling and hence is very strongly **k** dependent. When electrons move up in energy the tunnelling probability decreases rapidly and hence the miniband width decreases. This means that tunnelling is strongly suppressed in higher Landau levels and at high magnetic fields and forces any transport processes to be sequential.

In the experiment the I-V curves show a well-defined threshold for Ohmic conduction, which increases slowly when a magnetic field is applied (see fig. 1). Once the condition that the miniband width $\Delta > \hbar\omega_c$ is achieved then elastic interLandau level scattering becomes forbidden. We find that above this field there is a rapid rise in threshold voltage with field suggesting that the superlattice transport is changing very significantly in the high field regime (see fig. 2). Finally at much higher biases we find a series of Stark cyclotron resonances, where carriers tunnel directly between Landau levels in adjacent wells [2,3]. These are found to be considerably stronger than has been observed in GaAs based systems, which we attribute to the enforced sequential tunnelling process.

[1] L. Eaves et al., Physica B. **272**, 190 (1999).
[2] L. Canali et al., Phys. Rev. Lett. **3618**, 76 (1996).
[3] V. J. Hales et al., *proc. 25th Int. Conf. Phys. Semicond.*, Osaka, September 2000.

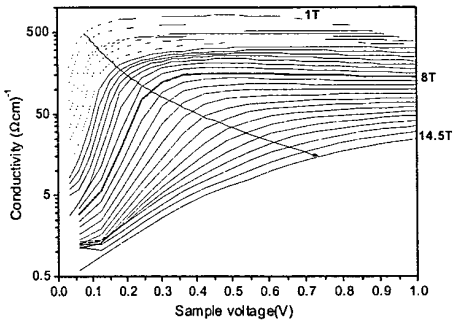

Figure1. dc magnetoconductivity at 4.2K.

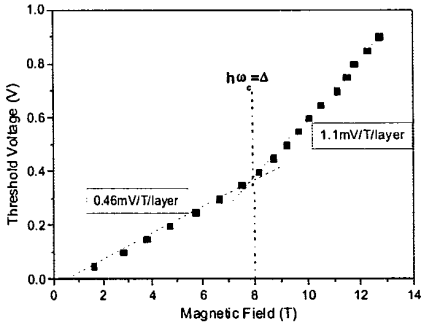

Figure 2. Threshold voltage against magnetic field at 4.2K.

Current modulated light reflectance spectroscopy with submicron spatial resolution in semiconductor heterostructures

O. A. Ryabushkin, E. I. Lonskaya

Institute of Radio Engineering and Electronics, Russian Academy of Sciences,
Vvedensky sq.1, Fryazino, Moscow District, 141120, Russia

We propose new method of the optical spectroscopy of semiconductor heterostructures for investigation of the hot electron transport due to electron temperature gradient. This technique is based on effect of electron heating on a dielectric function near fundamental absorption edge in layers of semiconductor structure. Electrons can be heated by passing electric current through ohmic contacts or in contactless manner by radio-frequency field. The latter way has been used in radio-frequency modulated reflectance (RMR) developed recently [1-3]. In spite of apparent advantages of RMR in comparison with traditional electroreflectance and photoreflectance (PR) [4] the RMR spectra are rather difficult for interpretation. This is due to contribution of all layers of heterostructure to RMR spectrum. Now we propose current modulated reflectance (CMR) technique using alternating electric current through ohmic contacts for carrier heating. This allows spectral features of conducting regions to be selectively extracted.

The two general mechanisms are responsible for CMR spectra. The electric current along heterostructure layers (at Y direction, fig.1) results in spatially inhomogeneous carrier heating in perpendicular direction (at Z axis). Due to inhomogeneous heating the hot electrons are redistributed and transverse thermoelectric fields arise. The built-in electric fields are changed because of thermoelectric fields. This results in modification of light reflectance of structure. Another mechanism is the modulation of exciton binding energy by hot electrons [2], with produces prominent features [5] in CMR spectra.

The selective doped heterostructure $Al_xGa_{1-x}As/GaAs$ (x~0.15) with two-dimensional electron gas (2DEG) was investigated at ambient temperature 77 K. The structure consisted of a 100 Å GaAs cap layer, a 650 Å n-doped AlGaAs, a 100 Å AlGaAs spacer layer, and a 0.5 μm GaAs buffer layer grown on 0.5 mm semi-insulating GaAs substrate (fig.1). AlGaAs/GaAs superlattice was in buffer layer on 225 Å distance from active interface. The sample measured 10 mm in length and 3 mm wide and had ohmic contacts. For CMR spectra measurement the ac amplitude of 10 mA, electric field inducing ac of 10 V/cm and 20 Hz – 20 kHz frequency range were used. The change of probe light reflectance intensity was measured on modulation frequency. Besides CMR photoreflectance was performed. The pump light source was He-Ne laser (λ=633 nm, incident power ~ 0.1 W/cm^2) with intensity modulated by a mechanical chopper with 2 kHz.

The CMR and PR spectra are compared in fig. 2. The bandgap energies of GaAs and AlGaAs are 1.51 eV and 1.67 eV respectively at 77 K. The PR spectrum is typical for such structures. The oscillations in the 1.52-1.54 eV energy range are attributed to Franz-Keldysh effect in 2DEG (region 4 in fig.1). The modulation of exciton states in quantum wells (region 5 in fig.1) gives rise to feature about 1.54 eV energy. The dramatic peak below GaAs bandgap energy (1.506 eV) is due to excitons existed in low field GaAs buffer (region 6 in fig.1). The GaAs cap layer (region 1 in fig.1) also contributes in PR spectrum, with results in appearance of broaden wide-period Franz-Keldysh oscillation in 1.48-1.60 eV energy range. The CMR spectrum seems to be different from PR one. The Franz-Keldysh oscillations in the 1.52-1.54 eV energy range are ascribed to modulation of electric field in 2DEG. The excitons in quantum wells display in CMR spectrum as well as in PR one. The excitons in buffer layer are shown in CMR spectrum at 1.507 eV energy. Cap layer doesn't appear to contribute in CMR spectrum. The mostly pronounced difference between spectra is in the AlGaAs bandgap energy region (fig. 3). Two kinds of Franz-Keldysh oscillations with different periods are clearly determined from CMR spectrum in comparison with PR spectrum. This allows the two pairs of built-in fields and thermoelectric fields on the edges of 75 nm thickness layer to be defined (2 and 3 regions in fig.1). Thus only regions with conducting carriers contribute in CMR spectrum. Modulation of exciton states is performed by transfer of hot electrons. The measured spectra are successfully described by the model [3]. The values of thermoelectric fields and internal fields are calculated in each layer.

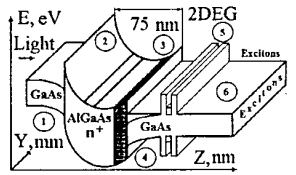

Fig.1: Band diagram of the active part of structure.

In conclusion, the proposed method enables the spectral features of conducting regions of selective doped heterostructure to be selectively extracted. This technique allows the internal thermoelectric fields induced electron temperature gradient to be measured in the each layer of structure. Diagnostics of different electric fields in rather narrow conducting layers is available.

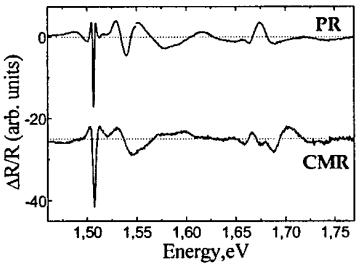

Fig.2: CMR and PR spectra. CMR spectrum is shifted down on 25 units. Current frequency is 2 kHz.

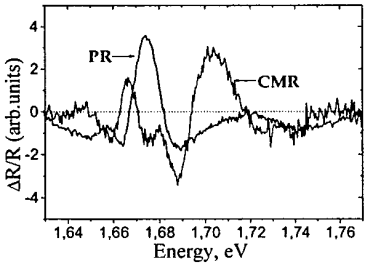

Fig.3: The same spectra near AlGaAs bandgap energy.

References

[1] O. A. Ryabushkin, V. A. Sablikov JETP Lett. **67**, 233 (1998).
[2] O. A. Ryabushkin in *Proc. Of Int. Simp. "Nanostructures: Physics and Technology"*, St. Peterburg 1997, p.270.
[3] O. A. Ryabushkin, V. A Sablikov Proc. of the SPIE **3732**, p.137 (1998).
[4] H. Shen, M. Dutta J.Appl.Phys. **78**, 2151 (1995).
[5] C. Tangye J. Appl. Phys. **80**, 4626 (1996)

Corresponding author: Ekaterina Lonskaya, Institute of Radio Engineering and Electronics, Russian Academy of Sciences, Vvedensky sq.1, Fryazino, Moscow District, 141120, Russia.
E-mail: roa228@ire216.msk.su.

Negative magnetoresistance of SiGe quantum wells doped with boron

R.Zobl[1], E.Gornik[1], I.V.Altukhov[2], N.G.Zhdanova[2], M.S.Kagan[2]

[1]Institute for Solid State Electronics, Technical University of Vienna,
Floragasse 7, A-4040 Vienna, Austria
[2]Institute of Radioengineering and Electronics, Russian Academy of Sciences,
Mokhovaya 11-7, GSP-9, 101999 Moscow K-9, Russia

Negative magnetoresistance (NMR) at hopping conductivity have been studied in many works (see, e.g., [1] and references within). The origin of NMR is the magnetic field destroying of constructive interference of electron wave functions on closed paths of hopes (coherent superposition of partial tunneling amplitudes). Another (incoherent) mechanism of NMR can be connected with a decrease of an impurity band width in magnetic field [2]. We will show that in our experimental situation, the NMR is caused by the interference.

The p-type Si/Ge_x Si_{1-x}/Si quantum-well (QW) structures MBE-grown pseudomorphically on the n-type Si substrate and selectively doped with boron were studied at liquid He temperature. The Ge content x in SiGe alloy was 0.15. The SiGe layer of 20 nm thickness was delta-doped with boron in the QW middle with the concentration of $6*10^{11}cm^{-2}$. It was sandwiched between undoped Si buffer (130nm wide) and cap (60nm) layers. Two boron delta-layers with B concentration of $4*10^{11}$ to $10^{12}cm^{-2}$ positioned within the buffer and cap layers on the distance of 30nm from each QW interface were aimed to diminish carrier outflow from QW into surface states (see [3]). The buffer delta-layer should also supply holes to form a p-n junction between the p-layers and the n-substrate. Ohmic contacts were deposited on the p-side of the structure so that the p-n junctions prevented from a current by-pass through the substrate. The distance between contacts was 0.6 cm. D.c. voltage up to 10 V and voltage pulses of 1 microsecond duration from 10 to 300 V were applied along the QW to the contacts. The pulsed voltage was used to avoid the sample heating. The structure is shown schematically in Fig. 1. The current I through the structure parallel to the interfaces was measured in dependence on magnetic field H up to 5 T directed perpendicular to the SiGe layer.

It has been shown in our previous studies [3] that the conductivity at the temperatures from 4.2 to 20 K is due to hopping. Magnetic field dependence of the current at low d.c. bias is presented in Fig. 2. The NMR is observed at $H < 2T$. Shown in the insert is the initial part of the magnetoresistance curve. At low H, the I(H) dependence obeys H^2 law showing the interference origin of the NMR. Additional evidence for this is given by the absence of NMR at H parallel to the interfaces (and perpendicular to the current).

Fig. 3 shows I(H) dependence at pulsed voltage of 300 V. At this voltage, boron acceptors in the QW are partially ionized. The magnetic field range where the NMR is observed is essentially less than for low voltages. It is evident from the figure that I(H) curve consists of three different regions: initial NMR region and two regions with positive magnetoresistance having different dependence on H. This indicates that there are two conductivity channels. One of them is the SiGe layer and another one can be one of δ-layers in the barriers which can be also partially filled at this voltage. The mobility estimated from the high magnetic field region is about 600 cm^2/Vs. The NMR observed at sufficiently high electric

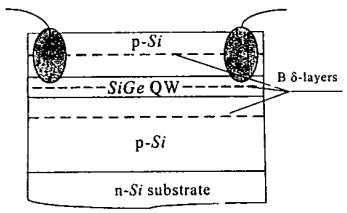

Fig. 1. Schematic view of structure.

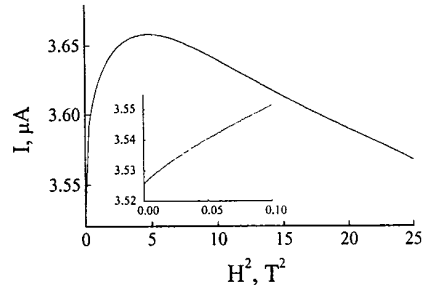

Fig. 2. Dependence I on H at low d.c. voltage.

field shows also that the ionization of acceptors in the well is due to Joule heating rather than due to direct ionization by electric field.

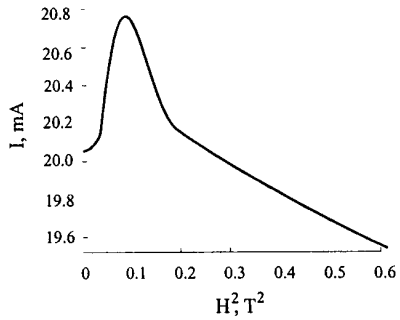

Fig. 3. I vs H at 300 V pulsed voltage.

In conclusion, the data obtained show that the negative magnetoresistance in boron doped SiGe QW is due to magnetic field suppression of quantum interference corrections to the two-dimensional hopping conductivity.

This work was supported in part by Grants 99-02-16169, 00-02-16093, and 00-02-16066 from Russian Foundation for Basic Research, 00-15-96663 from Russian Foundation for Leading Scientific Schools, and 97-10-55 from Russian Ministry of Science and Technology.

References

[1] M. E. Raikh et al., Phys. Rev. **B 45**, 6015 (1992).
[2] M.E.Raikh, Solid State Commun. **75**, 935 (1990).
[3] M.S.Kagan et al., Physica Status Solidi (b) **211**, 495 (1999).

Corresponding author: M.S. Kagan, Institute of Radioengineering and Electronics,
Russian Academy of Sciences,
Mokhovaya 11-7, GSP-9, 101999 Moscow K-9, Russia
phone: +7 095 2034812, FAX: +7 095 2038414
e-mail: kagan@mail.cplire.ru

Spin orientation of electrons by lateral electric field in 2D system without inversion symmetry

A.V. Chaplik, M.V. Entin and L.I. Magarill

Institute of Semiconductor Physics, Siberian Branch of Russian Academy of Sciences, 13, prospekt Lavrent'eva, Novosibirsk, 630090, Russia;
levm@isp.nsc.ru, tel.: +7-(383)2-333264, fax: +7-(383)2-332771

An electric field **E** parallel to a 2D system causes the spin orientation of electrons. This effect was theoretically studied in [1,2] within the framework of Rashba spin-orbit Hamiltonian $H_{so}^{(R)}$ [3,4], associated with the asymmetry of 2D quantum well. In this case the spin orientation can be described by the formula $\mathbf{S} = \gamma[\mathbf{E},\mathbf{n}]$, where $\boldsymbol{S}$ is the mean spin density of the system, $\mathbf{n}$ is the normal to the system plane.

In the general case the spin polarization $S_i = \gamma_{ij}E_j$ is caused by the inversion asymmetry of the system: crystal + quantum well, which may be initiated by the lack of inversion symmetry of cubic semiconductor crystal. The Dresselhaus Hamiltonian of the bulk electron spectrum near Γ point of a cubic crystal [5] has cubic in momentum spin splitting, which in a confined system converts to linear in momentum terms in the Hamiltonian $H_{so}^{(D)}$ [4].

In the present paper we study the spin orientation taking into account both mechanisms of spin-orbit interaction. 2D Hamiltonian has the form:

$$H = \frac{\mathbf{p}^2}{2m} + H_{so}^{(R)} + H_{so}^{(D)},$$

$$H_{so}^{(R)} = \alpha_R[\boldsymbol{\sigma},\mathbf{p}]\mathbf{n}, \quad H_{so}^{(D)} = \alpha_D(\varepsilon_{ilk}\lambda_{mjk} + \frac{1}{2}\varepsilon_{ijk}\lambda_{lmk})\sigma_i p_j n_l n_m$$

Here p_i are the spatial components of 2D electron momentum, ε_{ijk} is the absolutely antisymmetric tensor, $\boldsymbol{\sigma}$ are the Pauli matrices; the symmetric tensor λ_{ijk} characterises the anisotropy of the crystal (in the principal crystal axes it has the only non-zero component $\lambda_{123}=\lambda_{231}=\lambda_{321}=1$).

The axial tensor of spin admittance γ_{ij} determines linear response of the spin density to the external electric field and can be found by means of the Kubo-type formula. In the case when $H_{so}^{(R)}$ prevails,

$$\gamma_R = \frac{me\alpha_R\tau}{2\pi\hbar}.$$

If the spin splitting exceeds the collisional broadening of states, τ is the momentum relaxation time of electrons. The spins are polarized perpendicular both to the normal and to the direction of electric field.

In the general case the tensor γ_{ij} depends on the orientation of the surface:

$$\gamma_{ij} = \gamma_R\varepsilon_{ijk}n_k + \gamma_D(\varepsilon_{ilk}\lambda_{mjk} + \frac{1}{2}\varepsilon_{ijk}\lambda_{lmk})n_l n_m$$

Here γ_D is determined by the same equation as for γ_R with change α_R by α_D. In the specific case of (0,0,1) surface the spin density is

$$\boldsymbol{S} = \gamma_R(E_y, -E_x, 0) + \gamma_D(-E_x, E_y, 0).$$

For 2D system on (1,1,1) surface with the axis z along the direction [1,1,1] one can write

$$\boldsymbol{S} = (\gamma_R + (2/\sqrt{3})\gamma_D)(E_y, -E_x, 0).$$

In both cases the spin density has only planar components.

For (1,1,0) surface in coordinate system with $\boldsymbol{e}_x \| [1,-1,0]$, $\boldsymbol{e}_y \| [0,0,-1]$, $\boldsymbol{e}_z \| [1,1,0]$ we have

$$\boldsymbol{S} = \gamma_R(E_y, -E_x, 0) - (\gamma_D/2)(0, 0, E_x).$$

In this case the Dresselhaus mechanism leads to the normal component of the spin density.

Thus, we have shown that the allowing for the Dresselhaus term in the spin-orbit Hamiltonian results in various directions of the spin orientation for various crystal surfaces. Moreover, the spin-orbit constants α_R and α_D have different dependence on the confining potential. In particular, α_R vanishes for a symmetric quantum well. The ratio between α_R and α_D can be varied in a gated system. That means the spin orientation, induced by the lateral electric field, can be tuned (both in its direction and magnitude) by the gate voltage.

The possibilities of observation of electric-field-induced spin orientation are discussed.

[1] V.M. Edelstein, Sol.State.Comm., **73**, 233 (1990).
[2] L.I. Magarill and M.V. Entin, JETP Lett., **72**, 195 (2000).
[3]. Yu.A. Bychkov and E.I. Rashba, JETP Lett., **39**, 78 (1984);
[4] E.I. Rashba and V.I. Sheka, in *Landau Level Spectroscopy*, ed. By G.Landwehr and E.I. Rashba (Elsevier, 1991), p.178.
[5] G. Dresselhaus, Phys.Rev., **100**, 580 (1955).

In-plane magnetic field induced spin polarization and transition to insulating behavior in two-dimensional hole systems

E. Tutuc, E.P. De Poortere, S.J. Papadakis, and M. Shayegan

Department of Electrical Engineering, Princeton University, Princeton, NJ, 08544

A fundamental property of a two-dimensional (2D) carrier system is its response to a parallel magnetic field. Thanks to the Zeeman coupling, the parallel field induces a polarization of the carriers' spin and yields a system with two separate subbands. Using a novel technique, we perform direct measurements of the spin polarization, induced by a parallel magnetic field, in GaAs 2D hole systems. We demonstrate the role of spin polarization on the in-plane field magnetoresistance and, in particular, on the field induced metallic to insulating transition, whose origin is a hotly debated subject.

We study a Si-modulation doped quantum well grown on GaAs (311)A substrate. The experimental technique consists of applying a constant field (B) parallel to the 2D hole gas and then slowly rotating the sample in order to introduce a small $B_\perp$ (Fig. 1). We then analyze the Shubnikov de-Haas oscillations induced by $B_\perp$ and determine the two spin subband populations. Thanks to the high sample quality we are able to limit $B_\perp$ to sufficiently small values, so that $B_{||} \cong B$. As the parallel field is increased, the system gradually becomes spin polarized (Fig. 2). We have performed such measurements in the density range 3.4-6.8 $\times 10^{10}$ cm^{-2} and for different orientations of the parallel field relative to the crystal axes. The degree of polarization depends strongly on the orientation of the parallel field with respect to the crystal axes, revealing a strongly anisotropic in-plane g-factor.

We have also performed in-plane field magnetoresistance measurements in the same range of densities at different temperatures from 0.3K to 1.4K. The combination of spin-polarization and magnetoresistance measurements reveals that once the system is fully spin polarized the magnetoresistance follows a simple exponential behavior (Fig. 3). In the explored range of densities the 2D hole system has a metallic behavior at zero field, but the applied parallel field induces a transition to an insulating behavior. We demonstrate that the transition always happens *before* the system is fully spin polarized (Fig. 3). Remarkably, the minority spin subband at the transition is ~0.8 $\times 10^{10}$ cm^{-2}, independent of the total density or the orientation of the field with respect to the crystal axes. The data strongly suggest that two subbands are necessary to observe metallic behavior, and point to a temperature dependent inter-subband scattering mechanism being responsible for the observed metallic behavior in this 2D system.

References

[1] E. Tutuc *et al.*, cond-mat 0012128 (2000), to appear in Phys. Rev. Lett.

Corresponding author: Emanuel Tutuc, Department of Electrical Engineering,
Princeton University, Princeton, NJ, 08544, U.S.A.
phone: +1 609 258 5434, Fax: +1 609 258 1840
email: etutuc@ivy.princeton.edu

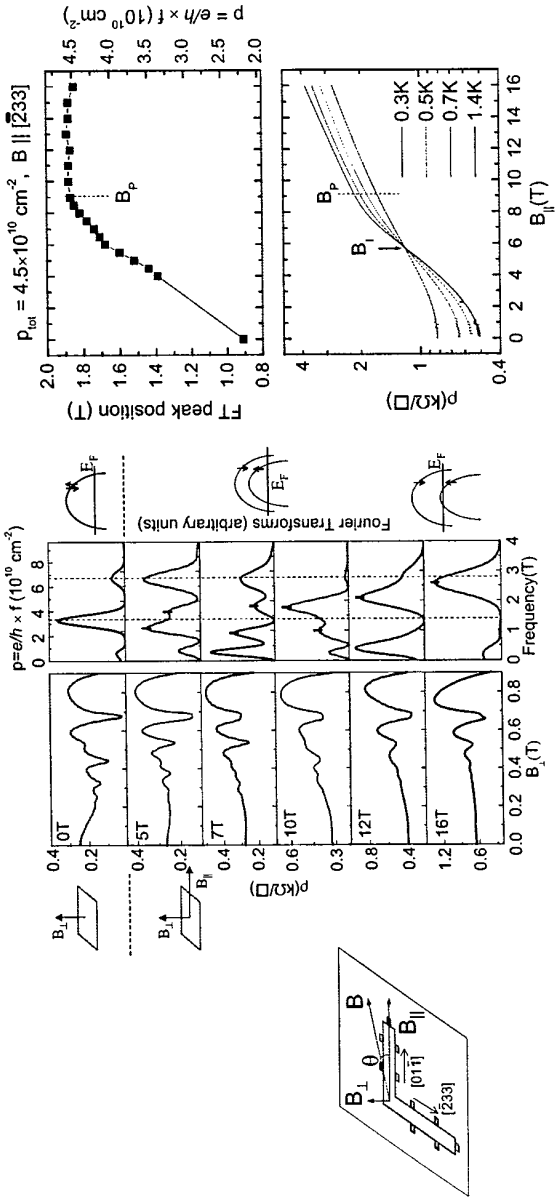

Fig. 1 L-shaped Hall bar used in the experiment. A strong constant magnetic field (B) is applied and the sample is rotated near θ=0° to induce a small perpendicular field component.

Fig. 2 Shubnikov de-Haas oscillations at the indicated parallel field applied along [01$\bar{1}$]. The total 2D hole density is 6.8×10^{10} cm^{-2}. The top trace was taken in a purely perpendicular field; the rest were taken by rotating the sample in a constant, nearly parallel field. The Fourier transforms shown on the right indicate the evolution of the 2D system from being spin degenerate at zero parallel field to becoming spin polarized at high parallel field. The top x-axis shows the conversion of the Fourier transform frequency (f) to 2D density. The sketches on the right illustrate the evolution of spin subbands with increasing parallel field.

Fig. 3 Top panel: Evolution of majority spin subband Fourier transform peak with parallel magnetic field. The saturation above the field marked B_P signals the full spin polarization.

Bottom panel: The magnetoresistance traces taken at different temperatures exhibit an exponential behavior once the system is fully spin polarized. The traces also clearly show that the transition to the insulating state occurs *before* the full spin polarization of the 2D hole gas.

Transport of a two-dimensional electrons in the lattice of diffusive and thermalizing scatterers.

Z.D.Kvon[1,2], O.Estibals[2,4], A.Y.Plotnikov[1], J.C.Portal[2,3,4], A.I.Toropov[1]

[1]Institute of Semiconductor Physics, 630090 Novosibirsk, Russia
[2]GHMFL, MPI-FKF/CNRS, BP 166, F-38042, Grenoble Cedex 9, France
[3]Institut Universitaire de France, 103 Bd.St.Michel 75005 Paris
[4]INSA 135 Avenue de Rangueil 31077 Toulouse Cedex 4

Transport of two-dimensional electrons in the lattice of artificial scatterers attracts a lot of attention within last ten years. All these studies are devoted mainly to the transport of two-dimensional electron gas in antidot lattice. In this case an electron moves ballistically between antidots and then scatters specularly on them. In this work we report the results of experimental study of a new kind of electron system with artificial scatterers – two-dimensional electron gas (2DEG) in the lattice of diffusive and thermalizing scatterers. This system was fabricated on the basis of high-mobility 2DEG in AlGaAs/GaAs heterostructure with the electron density Ns = $7 \cdot 10^{11} cm^{-2}$, the mobility $\mu = 4 \cdot 10^5 cm^2/V \cdot s$, and the corresponding mean free path l = 5 μm. The lattice was fabricated in the following way. First, the square lattice of holes was made by means of electron lithography in the electron resist PMMA. The period of the lattice was L = 0.7 μm, and the hole diameter was d = 0.2 μm. Second, GeAuNiAu alloy usually used for preparation of the contacts to 2DEG was evaporated on this structure. Then, the electron resist was removed, and the lattice of GeAuNiAu dots remained on the surface of the structure. Finally, ordinary annealing of the alloy was performed. Thus after all technological procedures we obtained 2DEG in the square lattice of dirty metallic (GeAuNiAu alloy) dots (see the insert of figure 1). Moving ballistically between these dots 2D electrons should undergo strong diffusive scattering as a result of collisions with the metallic dots. During the collisions an electron can also loose its initial energy because of inelastic scattering. Therefore we have quite unusual situation as compared with antidot lattices with specular electron scattering on antidots. On another hand the study of such lattice can give information about electron interaction with GeAuNiAu alloy which is very important in edge current transport problem in quantum Hall effect regime. Figure 1 shows the magnetoresistance ($\rho_{xx}(B)$) traces for 2DEG with the lattice of scatterers and for the unpatterned 2DEG at 1.5 K in magnetic fields up to 4 T. It is seen that at zero magnetic field the array sample has much larger (by a factor of 12) resistance. This means that the introduction of GeAuNiAu alloy dots leads to strong scattering of 2D electrons leading to mean free path comparable to the dot spacing. Also we can see that in magnetic field B = 0.32 T the commensurability peak corresponding the condition $2R_c = d$ is observed. At larger magnetic fields there is the large negative magnetoresistance. This behavior of the MR is similar to that observed in the antidot lattice. However careful analysis reveals important differences. In figures 2 a and b the detailed behavior of the $\rho_{xx}(B)$ and Hall resistance ($\rho_{xy}(B)$) is presented. The comparison of $\rho_{xx}(B)$ curve with the antidot magnetoresistance data shows three differences: 1) large positive magnetoresistance characteristic of the suppression of channeling electron trajectories between scatterers is not observed in weak magnetic fields, 2) the commensurability peak which corresponds to the condition $2R_c \approx 3d$ and observed in all antidot lattices with the same period and antidot sizes, is not observed here 3) the main commensurability peak is smaller than that observed in antidot lattice with the same period and antidot size; here this peak does not exceed the resistance of the array in zero magnetic field. It is suggested that these features can be connected with the possible inhomogeneous distribution of the electric field in the array because of very high conductivity of GeAuNiAu alloy dots. As figure 2b shows Hall resistance dependence $\rho_{xy}(B)$ has the weak anomalies corresponding minima in $\rho_{xx}(B)$ dependence and right side of the commensurability peak. Qualitatively these anomalies are similar to these observed in antidot lattice where they are much more pronounced. The explanation of Hall resistance features is based on the consideration of electron trajectories after specular scattering with antidots. Obviously, there is no the same scattering in our array. Thus, our experiments show that the Hall resistance anomalies can have another origin. Therefore these anomalies should be reexamined because it is necessary to take into account inhomogeneous distribution of the electric filed in 2DEG with artificial array of scatterers.

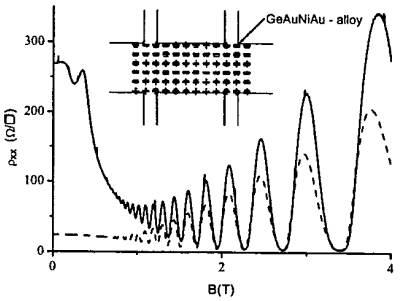

Figure 1: $\rho_{xx}(B)$ dependences of the 2DEG in lattice of GeAuNiAu dots (solid) and of the unpatterned 2DEG (dashed) at T = 1.5 K.

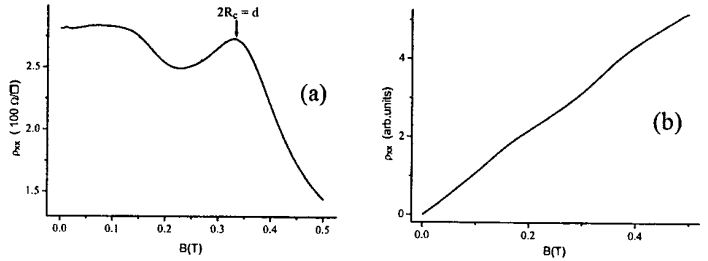

Figure 2: $\rho_{xx}(B)$ dependence (a) and $\rho_{xy}(B)$ dependence (b) of the 2DEG in lattice of the GeAuNiAu dots in magnetic fields range near the commensurability magnetoresistance peak at T = 1.5 K.

Corresponding author: Ze Don Kvon, Institute of Semiconductor Physics, Lavrentyev str.,13, 630090 Novosibirsk, Russia
Phone 7-3832-341733, fax: 7-3832-332771
e-mail: kvon@thermo.isp.nsc.ru

Magnetic field induced breakdown of the current-voltage characteristics in SiGe-heterostructures containing quantum dots

K.-M. Haendel[1], C. Lenz[1], U. Denker[2], O. G. Schmidt[2], K. Eberl[2], R. J. Haug[1]

[1]Institut für Festkörperphysik, Universität Hannover, Appelstraße 2, D-30167 Hannover, Germany
[2]Max-Planck-Institut für Festkörperforschung, Heisenbergstraße 1, D-70569 Stuttgart, Germany

Self-assembly of defect-free Ge islands on Si (001) have attracted large attention during the last years [1-3] and presents an easy method to fabricate low-dimensional nanostructures. Resonant tunneling of holes in Si/SiGe double-barrier resonant tunneling devices (DBRTD) has been studied so far using quantum wells [4] as well as self-assembled Ge islands [5]. Our experiments show a clear evidence that both heavy hole to heavy hole (hh → hh) as well as heavy hole to light hole (hh → hl) tunneling processes can be observed in our DBRTDs. At low temperatures and in high magnetic fields a striking instability is observed in the I(V) characteristics.

We have focused on samples with $Si/Si_{0.7}Ge_{0.3}$ quantum well structure with Germanium quantum dots in the well. The active region consists of 5.5 ML Ge dots confined by 5 nm Si barriers, sandwiched in turn by 10 nm thick $Si_{0.7}Ge_{0.3}$ emitter and collector reservoirs. Dots, barriers, and cladding layers are undoped. The processing involved the etching of a mesa of nominal 22 – 72 µm in diameter. Structural analysis of the Ge/Si heterostructure system rise to at least three different types of islands [1]: large multi-faceted 'domes', square-based 'pyramids', and elongated {105} faceted 'hut' clusters. 'Pyramids' and 'domes' usually form at high temperatures (> 600 °C) whereas the much smaller 'hut' clusters nucleate at lower temperatures (500 °C). Our samples were kept at 460 °C during the epitaxial growth. The formation of 'hut' cluster islands during growth of the 5.5 ML Ge layer was indicated by a clear changeover of the RHEED pattern from streaky to spotty pattern.

The data presented in this abstract were obtained using a 35 µm diameter diode. Diodes with different sizes showed the similar I(V) characteristics. We studied our samples by extensive magnetotunneling measurements in high magnetic fields (to 14 T) and low temperatures (down to 340 mK). We have investigated the influence of high magnetic fields of longitudinal (B ∥ I) and transverse (B ⊥ I) orientations to the current direction on the I(V) curves.

At zero magnetic field weak resonances corresponding to hh → hh and hh → lh transitions are observed. In high magnetic fields (B > 2 T) a magnetic field induced step in the I(V) characteristic is determined, see Fig. 1. Here the conductivity rises in a range of some 100 mV from a few µS to some mS. The dependence of V_{th} on B for both magnetic field orientations is exponentially. With rising temperature V_{th} shifts to lower voltages and the step smears out. Above 0.7 K no step in the I(V) curve can be observed. To the author's knowledge such an effect has not been reported till now.

Although the origin of this striking behaviour is not clear, one possible explanation of the feature is a strong shrinkage of the wavefunctions of hh and lh states that causes localisation which increases exponentially with magnetic field strength due to the overlapping of states at a critical voltage V_{th}.

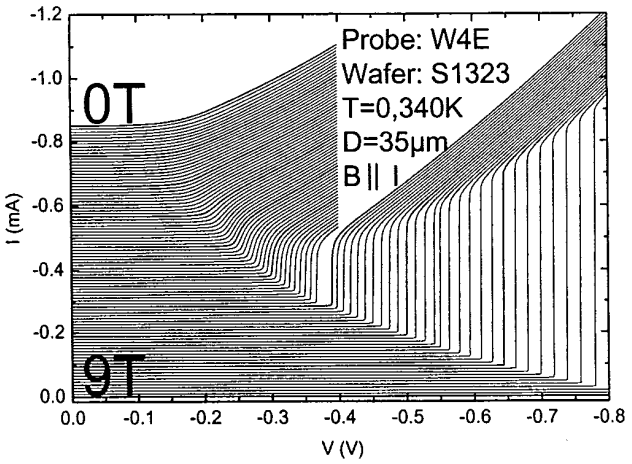

Fig. 1: Magnetic field induced step in the I(V) characteristics of a Si/SiGe-DBRTD

References

[1] O. G. Schmidt, C. Lange, and K. Eberl, Appl. Phys. Lett. **75**, 1905 (1999)
[2] D. J. Eaglesham and M. Cerullo, Phys. Rev. Lett. **64**, 1943 (1990);
[3] X. Deng, J. D. Weil, M. Krishnamuthy, Phys. Rev. Lett. **80**, 4721 (1998);
[4] H. C. Liu, D. Landher, M. Buchanan, and D. C. Houghton, Appl. Phys. Lett. **52**, 1809 (1988); G. Schuberth, G. Abstreiter, and E. Gornik, Phys. Rev. B **43**, 2280 (1991); C. D. Akyüz, A. Zaslavsky, L. B. Freund, D. A. Syphers, and T. O. Sedgwick, Appl. Phys. Lett. **72**, 1739 (1998)
[5] O. G. Schmidt et al. Appl. Phys. Lett. **77**, 4341 (2000)

Corresponding author: Kai-Martin Haendel, Institut für Festkörperhysik, Universität Hannover, Appelstraße 2, D-30167 Hannover, Germany.
phone: +49 511 762 5950, Fax: +49 511 762 2904
email: haendel@nano.uni-hannover.de

Random lasing from weakly scattering media; spectrum universality in DOO-PPV polymer films

M.E. Raikh, R.C. Polson, Z.V. Vardeny

Physics Department, University of Utah, Salt Lake City, Utah 84112, USA

It was recently demonstrated that when a disordered gain medium is optically excited above a certain intensity threshold, the emission spectrum acquires a multimode finely structured (with linewidth, $\delta\lambda \sim 0.1nm$) shape. This phenomenon that was dubbed "random lasing," was observed in various media ranging from ZnO polycrystalline films and powders[1] to organic dyes-doped gel films[2] and dye-infiltrated opal photonic crystals[3].

In the present work we demonstrate a remarkable *universality* in the *random* emission spectra from films of π-conjugated polymers (DOO-PPV). This universality was revealed upon applying the power Fourier transform analysis to the spectra. A typical spectrum measurerd from an excitation spot of $2mm \times 100\mu m$ is shown in Fig. 1a. The corresponding Fourier transform (Fig. 1b) shows several features. However, the structure of the spectra and the shape of the Fourier transforms vary when changing the position of the excitation spot. Our main observation is that when *averaging* the individual power Fourier transforms over different spots a series of *distinct* transform peaks appears. This is demonstrated in Fig. 2, in which the result of averaging of the Fourier transforms of 125 spectra obtained by shifting the excitation spot is shown. A regular structure in the *average* Fourier transform suggests that the underlying *random resonators*, which are responsible for lasing emission from the π-conjugated polymer film are almost *identical*. We argue that the reason for such an universality is the large size of a typical resonator $\sim 70\lambda$, where λ is the emission wavelength. We have determined this size from the peak to peak distance in Fig. 2. The large size of random resonators in DOO-PPV films contrasts previous observations of random lasing in powders[1], where the resonator size was of the order λ, which, in turn, was of the order of the light mean free path l^*. In our experiments l^* determined from the width of the coherent backscattering cone (Fig. 1b, inset) was $\simeq 10\lambda$. This suggests that the resonators are formed in the polymer film not as a result of localization but rather due to *classical* trapping of light by macroscopic ($\gg \lambda$) inhomogeneities. The origin of these inhomogeneities is most likely the fluctuations in the polymer film thickness. We develop a simple theory which explains the presence of the peaks in the average power Fourier transforms, $< I(d) >$ and predicts their shape. The theoretical dependence $< I(d) >$ is shown in Fig. 2 (solid curve). One of the theoretical predictions is that $< I(d) >$ depends on the ratio d/l^*. We have checked this scaling experimentally by adding TiO_2 particles that cause a reduction of l^* from $l^* = 9\mu m$ to $l^* = 7\mu m$. As in the polymer film seen in Fig. 2, the scaling agree very well with the experiments.

References

[1] H. Cao *et al.*, Phys. Rev. Lett. **82**, 2278 (1999); *ibid.* **84**, 5584 (2000).

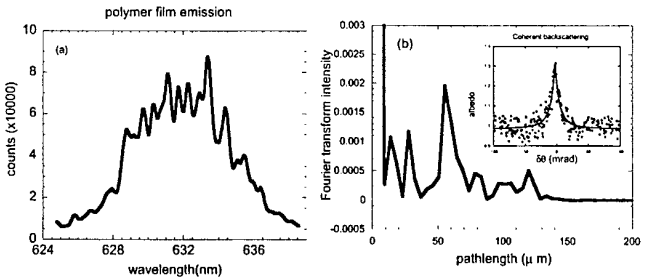

Figure 1: (a) random lasing spectrum from a DOO-PPV polymer film. (b) Fourier transform of (a); inset is the coherent backscattering cone from a bulk DOO-PPV sample.

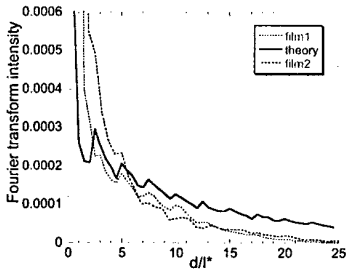

Figure 2: Average of 125 Fourier transforms of random laser emission spectra of two polymer films scaled by their mean light path l^*. Analytic expression superimposed on the resulting random background.

[2] S. V. Frolov,*et al.*, Phys. Rev. B **59**, R5284 (1999).

[3] S. V. Frolov,*et al.*, Opt. Commun. **162**, 241 (1999).

Corresponding author: Prof. Mikhail Raikh, Physics Department, University of Utah, Salt Lake City, UT 84112, USA.
phone: (801) 585-5017
email:raikh@physics.utah.edu

White light from blue: white emitting organic LEDs based on spin coated blends of blue emitting molecules.

M. Mazzeo[1], J. Thompson[1], R. I. R. Blyth[1], M. Anni[1], G. Gigli[1], R. Cingolani[1], G. Barbarella[2]

[1]Instituto Nazionale di Fisica della Materia, Dipartimento di Ingegneria dell'Innovazione, Universita' di Lecce, Via Arnesano, 73100 Lecce, Italy.
[2]ICoCEA, Area Ricerca CNR, Via Gobetti 101, 40129 Bologna, Italy

Light emitting diodes based on organic materials represent a potential cheap route to display technology, with the white LED the subject of a great deal of research effort. White light emission is generally achieved using combinations of different coloured organics in either a vacuum deposited evaporated multilayer structure [1], or via the spin coating of a blend [2]. The latter is clearly advantageous from the point of view of ease and cost of fabrication, but requires soluble molecules, which, in addition, do not interfere with each others' emission, e.g. by Foerster transfer. As an alternative route we show that blends of two blue emitting molecules will, in general emit white rather than blue light, and report on the fabrication of LEDs based on these blends. Four blue emitting molecules, from four different families of aromatic organics, were chosen: a diamine derivative, TPD, N,N'-bis(3-methylphenyl)-N,N'-diphenylbenzidine, an oxidiazole derivative, PBD, 2-(4-biphenylyl)-5-(4-tert-butylphenyl)-1,3,4-oxadiazole, a substituted thiophene dioxide, STO 2,5-bis(trimethylsilyl thiophene)-1,1-dioxide, and the poly-carbazole PVK, Poly(9-vinylcarbazole). All of the above are soluble in common organic solvents, and thus suitable for spin coating. STO was synthesised as described in Ref. [3], while the others, all materials familiar in organic LED research, are available commercially.

We show, via photoluminescence spectroscopy, that all possible binary combinations of the four molecules give, rather than the expected blue emission, a broadband emission in the visible range, with a peak energy significantly red shifted from the peaks of either of the individual components, as shown in fig. 1. UV / visible absorption spectroscopy indicates the absence of any new chemical species that might give rise to red-shifted emission, while photoluminescence excitation spectroscopy shows that the intensity of the broadband emission follows the absorption spectra of one of the component molecules. This behaviour is indicative of exciplex formation [4], i.e. the formation of a complex due to charge transfer from the excited state of one component to the ground state of the other. This can readily occur in blends of molecules with different electron affinities but similar HOMO-LUMO gaps, and we suggest is is likely to be a general phenomenon for blue emitting organics.

We show that exciplex formation does not occur in all relative concentrations of the two components, and we relate this to the morphology of the spin coated films, as measured using atomic force microscopy. We suggest that a limit to exciplex formation may be structural, i.e. where the structure and/or morphology of the solid state blend does not allow significant spacial overlap between the HOMO/LUMO of the two components.

A consequence of the broadband nature of exciplex emission centred in the visible is that that the emission of all the blends appears white, or near white, which we further quantify using CIE chromaticity co-ordinates. We note that the simple approximation for a solid state exciplex [5], assuming the same conditions as for exciplex formation in a non-polar solvent, significantly underestimates the red shift, and thus does not predict white emission. Given that white emission in fact occurs, it follows that LEDs based on a spin coated blend of two blue emitting molecules may give a potential route to a cheap white LED. We have fabricated LEDs using spin coated films of the TPD / STO blend, which gives the purest white emission of the blends in fig. 1.

We show that the electroluminescence is indeed white, showing the same double-peak structure as the spectrum of fig.1, with, under certain conditions, additional electroplex formation leading to almost equi-energetic, i.e. pure white, emission. We report on measurements aimed at optimising device performance, in terms of both luminance and quantum efficiency, using various hole transport layers and contact metals.

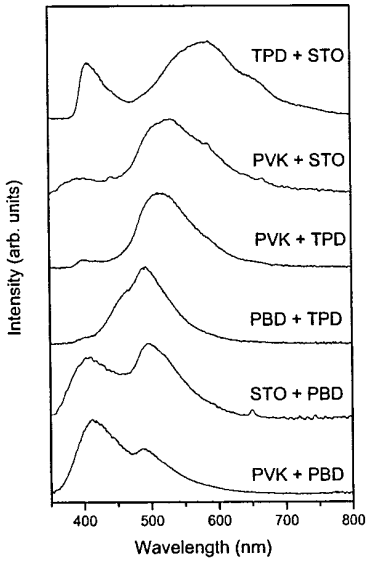

Fig. 1: Photoluminescence spectra of spin coated films of blended blue emitting molecules.

References

[1] e.g. L. Zugang and H. Nazare', Synth. Met. 111, 47 (2000)
[2] e.g. M. Anni et al., Appl. Phys. Lett. 77, 2458 (2000).
[3] G. Barbarella et al., J. Org. Chem. 63, 1742 (1998).
[4] A. Horvath and K. L. Stevenson, Coord. Chem. Rev. 153, 57 (1996).
[5] J. Rommens et al., J. Appl. Phys. 84, 4487 (1998)

Corresponding author: Guiseppe Gigli, Instituto Nazionale di Fisica della Materia, Dipartimento di Ingegneria dell'Innovazione, Universita' di Lecce, Via Arnesano, 73100 Lecce, Italy
phone: +39 (0)832 320 238, Fax: +39 (0)832 326 351
email: guiseppe.gigli @unile.it

Measuring the potential distribution inside soft organic semiconductors with a scanning-tunneling microscope

M. Kemerink[1], P. Offermans[1], J.K.J. van Duren[2], R.A.J. Janssen[2], P.M. Koenraad[1], H.W.M Salemink[1], and J.H. Wolter[1]

[1]COBRA Inter-University Research Institute, Eindhoven University of Technology, P.O. Box 513, NL-5600 MB Eindhoven, The Netherlands
[2]Laboratory of Macromolecular and Organic Chemistry, Eindhoven University of Technology, P.O. Box 513, NL-5600 MB Eindhoven, The Netherlands

In recent years the interest in the physical properties of organic semiconductors has strongly increased. An interesting result was reported by Alvarado *et al.* [1], who used the STM as an invasive probe to determine the single particle bandgap $E_{G,s}$. Up to now no attention has been paid to the functional form of the tip height vs. bias in these measurements. We present a model that takes both tunneling through the injection barrier and the subsequent transport through the polymer into account. This is then used to simultaneously fit current-voltage (I-U) and height-voltage (z-U) characteristics. The latter are taken with the feedback loop enabled, so the STM tip will penetrate the polymer layer with decreasing bias. We find that the gap observed in the z-U curves is not equal to $E_{G,s}$ but to the sum of the majority carrier injection barriers of both electrodes. Moreover, we find that z-U curves directly reflect the potential distribution *inside* the polymer at the moment of first tip-polymer contact.

Our samples consist of a glass substrate, on which a thin Ytterbium film is evaporated under vacuum conditions. On top of the Yb layer a MDMO-PPV layer is spin coated from hot (60 ^{0}C) o-xylene under ambient conditions. All STM experiments were performed in the dark, under an inert (He) atmosphere. Tips were etched from 0.15 mm Pt wire. Fig. 1 shows a typical result of a combined I-U and z-U measurement.

At this polarity the Pt tip acts as majority carrier (=hole) injector. Although Yb is known as an electron injector, the electron current is still small compared to the hole current [2], and will be ignored in the modeling. For the description of the tunneling through the injection barrier a WKB-model is used [3]. The transport through the rest of the PPV layer is described by a space-charge limited conduction (SCLC) model with a mobility that depends exponentially on the local field and an exponential trap distribution [2,4]. The two regions are matched by the normal continuity demands on current, field and potential. The lines in Figs. 1 and 2 are calculated with this model, using parameters that agree well with those found in literature [2]. The most interesting feature is the plateau in the z-U curve, right of point C in Fig. 1. It sets in as soon as the tip-sample distance equals the thickness of the tunneling barrier, which occurs when $U=\Psi_{h,Yb}$. The corresponding band alignment is schematically illustrated in the inset C in Fig. 2. From a similar argument it follows that the plateau at the other polarity yields $\Psi_{h,Pt}$. The observed gap therefore equals $\Psi_{h,Yb}+\Psi_{h,Pt}$, which is generally not equal to $E_{G,s}$.

Qualitatively, the observed z-U curves can be understood as follows. Since the tip is penetrating the polymer layer, no vacuum gap is present. Therefore, $\Psi_{h,Pt}$ stays constant during the z-U measurement. Therefore the tunneling barrier stays unaltered, since the (tunneling) current has to stay constant (feedback on). It is easy to show that for similar reasons the potential distribution directly behind this barrier remains unaffected. Although the potential distribution under the tip is constant during the z-U measurement, the distance over which it can extent, i.e. the layer thickness, is not constant. Therefore the voltage drop between tip and substrate is not constant, but depends on the thickness. In an actual measurement not the thickness but the bias is the independent variable, and the thickness is, via the tip height, regulated by the STM feedback system to match the current setpoint. Consequently, it turns out that the tip follows the potential distribution that is present at the moment the tip touches the polymer surface. This remarkable feature allows one to extract this potential distribution directly from a z-U curve, which is done in Fig. 2. As can be seen, the field distribution measured in this way agrees nicely with our model calculations.

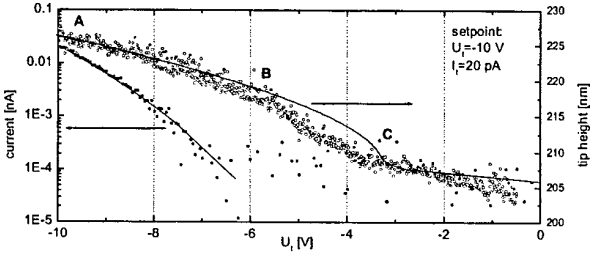

FIG. 1 I-U and z-U curves at forward bias. Between A and C the current flows through both the tunnel barrier and the SCLC region, for lower biases only a tunnel barrier is present in the current path. The solid lines are model calculations, points A, B and C refer to the illustrations in Fig. 2.

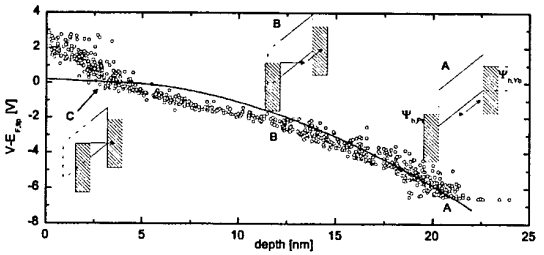

FIG. 2 Potential inside the polymer at U=-10 V. The experimental points are obtained by reversing the x and y axes of Fig. 1. The same model parameters have been used as in Fig. 1. The insets show schematic band diagrams at points A, B and C along V-z and z-U curves. The Pt tip is on the left.

References

[1] S.F. Alvarado *et al.*, Phys. Rev. Lett. 81, 1082 (1998).
[2] P.W.M. Blom *et al.* Phys. Rev. B **55**, 656 (1997)
[3] R.M. Feenstra and J.A. Stroscio, J. Vac. Sci. Technol. B **5**, 923 (1987).
[4] M.A. Lampert and P. Mark, *Current Injection in Solids* (Academic, New York, 1970).

Corresponding author: Martijn Kemerink, Faculty of Applied Physics, Eindhoven University of Technology, P.O. Box 513, NL-5600 MB Eindhoven, The Netherlands
Phone +31-40-2474190, Fax. +31-40-2461339
email: m.kemerink@tue.nl

Selfabsorption effects in a LEC with low Stokes shift

F.P. Wenzl[1], P.Pachler[1], D.Somitsch[2],P.Knoll[2] U. Scherf[3], C. Schmitt[3], R. Güntner[3]
G. Leising[4]

[1] Instiut für Festkörperphysik, TU Graz, Graz. Austria
[2] Inst. f. Experimentalphysik, Karl-Franzens Universität Graz, Austria
[3] Inst. f. physikalische und theoretische Chemie, Universtiät Potsdam, Germany
[4] Research & Technology AT&S AG, Leoben, Austria

Light emitting electrochemical cells (LECs) [1-4], first introduced in 1995 [1], are a new type of organic light-emitting devices that can be operated at low voltages and are therefore very promising for future applications in full color flat panel displays. In this study we compare the electroluminescence spectra of a LEC prepared from a methyl substituted ladder type polyparaphenylene (mLPPP) blended with a Li salt and a crown ether as ion coordinating and transporting compound. Due to the bridging of the phenylene rings, mLPPP has a planar structure what results in a redshift of the absorption and luminescence spectra compared with common PPP, the occurrence of a vibronic progression in the absorption band and a very low Stokes shift between the absorption and the photoluminescence spectra and therefore a strong overlap between the 0-0 absorption and the 0-0 photoluminescence peaks [5]. Electroluminescence from mLPPP based oLEDs therefore suffers from self-absorption effects, especially for devices with thicker active layers, the 0-0 transition, the dominant peak in the photoluminescence and the electroluminescence spectra of very thin devices becomes much smaller than its vibronic progression.

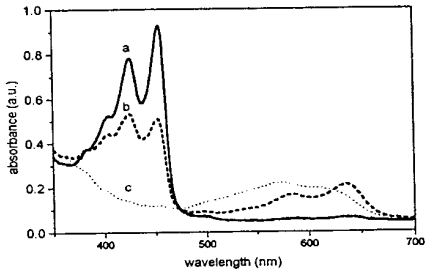

Figure1: Absorption spectra of chemically doped mLPPP. The degree of doping increases from a to c.

Figure 1 shows the absorption spectra of chemically doped mLPPP for three different degrees of doping. For mLPPP, two polaronic bands can be found, one at 1.9 eV with a vibronic progression at 2.1 eV and a second, much broader one, extending far into the infrared. Increasing the doping level, the absorption of pure mLPPP almost disappears and the new bands raise in intensity. At very high doping levels even the polaron band at 1.9 eV vanishes, with all the oscillator strength being shifted into the low energetic polaron band. As can be seen from figure 1, the 0-0 absorption peak that gives reason for the self-absorption effects in mLPPP based oLEDs is strongly influenced by doping and immediately decreases even for very low doping levels, much stronger than its vibronic progression, that starts to be effectively quenched a higher doping levels. Since the 0-0 absorption peak decreases and finally at higher doping levels is almost suppressed, one can expect the 0-0 peak of the electroluminescence spectra of LECs not to be influenced that strongly by self-absorption effects, since the recombination occurs in the undoped junction region and the electroluminescence spectrum therefore remains that of pristine mLPPP. However, while electroluminescence spectra in forward direction show blue light emission (CIE coordinates x=0.26, y=0.32), electroluminescence spectra in reverse direction still suffer from selfabsorption effects and show a greenish light emission (x=0.28, y=0.40), as shown in figure 2.

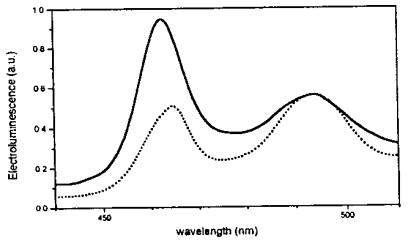

Figure 2: Comparison of the electroluminescence spectra in forward (solid line) and reverse direction (dottet line), normalized on the peak at 492 nm, on an expanded scale. The spectra were recorded at 4V and –4V after 20 s of operation, the current density was for both directions almost the same.

This behavior is discussed on different degrees of doping for the p-and n-type doped regions as found also in other LECs [6]. This effect can be applied to prepare two color light emitting devices that can be operated at low voltages by one simple spin coating process just by reversing the bias.

References

[1] Q. Pei, G. Yu , C. Zhang, Y. Yang, A.J. Heeger, Science 269, (1995), 1086
[2] Q. Pei, Y. Yang, G. Yu, C. Zhang, A.J. Heeger, J. Am. Chem. Soc. 118, (1996), 3922
[3] J. A. Manzanares, H. Reiss, A.J. Heeger, J.Phys Chem B 102, (1998), 4723
[4] S. Tasch, J. Gao, F.P. Wenzl, L. Holzer, U. Scherf, K. Müllen, A.J. Heeger, G. Leising, Electrochemical Solid State Lett. 2,(1999), 303
[5] S. Tasch, A. Niko, G. Leising, U. Scherf, Appl. Phys. Lett. 68, 1090, (1996)
[6] Y. Yang, Q. Pei, Appl. Phys. Lett. 68, 2708, (1996)

Corresponding author: Wenzl Franz-Peter, Institut für Festkörperphysik, TU-Graz,
Petersgasse 16, A 8010 Graz
phone: +43 316 873 8474, Fax: +43 316 873 8478
email: wenzl@sbox.tu-graz.ac.at

DEVICE CHARACTERIZATION OF CONJUGATED POLYMER/FULLERENE BULK HETERO-JUNCTION SOLAR CELLS

G. Matt[1], T. Munters[2], T. Fromherz[3] , D. Vanderzande[2], N. S.Sariciftci[1] and C. J. Brabec[1]

[1]Linz Institute for Organic Solar Cells (LIOS), Johannes Kepler University , 4040 Linz, Austria.

[2]Instituut voor Materiaal Onderzoek (IMO) , Limburgs Universitair Centrum (LUC), Wetenschapspark 1 , 3590 Diepenbeek, Belgium.

[3]Institute for Semiconductor and Solid State Physics , Johannes Kepler University, 4040 Linz, Austria.

We recently reported [1] a power conversion efficiency of about $\eta_e = 2.5$ (electrical power out/incident light power) for bulk heterojunction solar cells from poly(2-methoxy- 5-(3',7'-dimethyl-octyloxy))-p-phenylene vinylene, (MDMO-PPV), as an electron donor , and (6,6)-phenyl-C61-butyric-acid (PCBM) (a soluble C60 derivative) as electron acceptor . These efficiencies are the highest for this class of devices . The understanding of the device properties of bulk heterojunction solar cells formed between conjugated polymers and fullerenes is a key ingredient for further device optimization . We have measured the current-voltage (I-V) characteristics of solar cells with different thickness of the optical active bulk heterojunction layer in the range between 70 nm and 250 nm. Electrical contacts to the heterojunction layer were formed by an indium tin oxide (ITO) layer with a 100 nm poly(3,4-ethylene-dioxy-thiophene) (PEDOT) layer as the anode and a combination of lithium-fluoride and aluminum (LiF/Al) as the cathode. The dependence of the I-V characteristics of these devices on the temperature in the range between 15 K and 300 K is carefully analyzed (Figure1 & Figure 2). Typical sets of I-V curves measured in the dark and under illumination are shown in Figs. 1 and 2, respectively. In the back direction (negative bias voltage), the current is limited by a leakage current. In forward direction (positive bias voltages) the behavior appears to be dominated by a delicate interplay between carrier injection and transport efficiency. A model based on the simultaneous solution of the coupled transport equations for electrons and holes and Poisson's equation will be discussed. By comparing the experimental data with the results of these calculations, the influence of carrier mobility, carrier injection, life time, and device layout including the influence of the contact electrodes on the performance of the solar cells will be discussed. The parameters limiting the performance of the solar cells will be identified. Based on these results, strategies for further optimizing the solar cell performance will be outlined.

References

[1] S. E. Shaheen, C. J. Brabec, F. Padinger, T. Fromherz, J. C. Hummelen, N. S. Sariciftci, Appl. Phys. Lett. **78**: 841-843 (2001).

Corresponding author: G. Matt, Linz Institute for Organic Solar Cells (LIOS), Physical Chemistry, Johannes Kepler University Linz , Altenbergerstr. 69, 4040 Linz, Austria.
Phone: +43 732 2468 1767 Fax: +43 732 2468 8770
Email: gebhard.matt@jk.uni-linz.ac.at

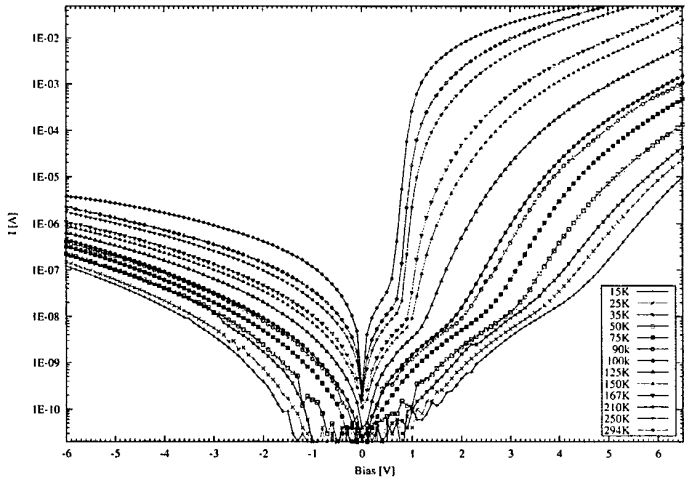

Figure 1: Temperature dependent dark I/V behavior of ITO/PEDOT/MDMO-PPV:PCBM/LiF/Al solar cell.

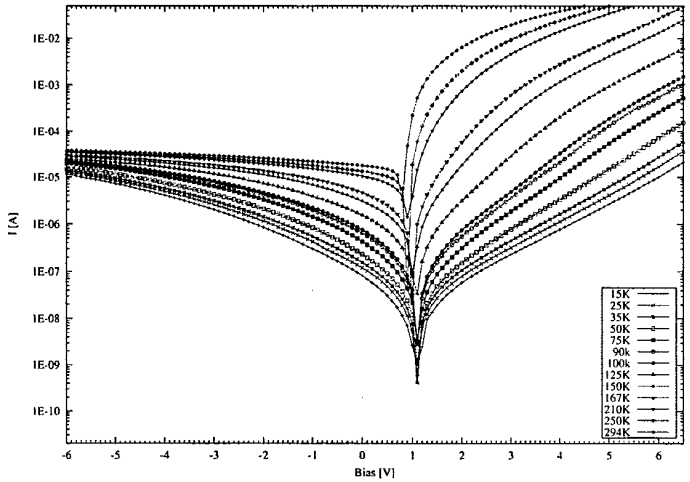

Figure 2: Temperature dependent illuminated I/V behavior of ITO/PEDOT /MDMO-PPV:PCBM/LiF/Al solar cell.

Superlattice model to describe inter-molecular wavefunction overlap in polydiacetylene crystalline films

H. Munekata and T. Kondo

Imaging Science and Engineering Laboratory, Tokyo Institute of Technology, 4259 Nagatsuda, Midori-ku, Yokohama 226-8503, Japan

Inter-molecular distance is one of the most important parameters that are responsible for macroscopic electronic and optical properties of crystalline organic semiconductors and functional polymers. This immediately lead us to the point that the change in crystalline quality can cause great impact on the physical properties, because the irregularities of the molecular orientation and spatial distance should vary the extent of the wavefunction overlap. In this letter, we discuss the blue shift in the optical absorption spectra in polydiacetylene (PDA) crystalline films in terms of the inter-molecular distance. In the crystalline films, each PDA unit can be regarded as a natural one-dimensional (1D) wire. We first show that both exciton absorption peak and the mobility edge shift monotonically toward higher energy when crystalline quality deteriorates. We then point out that the shifts can be explained by the reduction in the overlap of π-electron wavefunction among PDA polymer wires. Finally, this point is further discussed in terms of the Kronig-Penney (K-P) model in which π-conjugated main chains and the space in between are regarded as quantum wells and barriers, respectively.

Samples were prepared by molecular beam deposition technique on either a naked Corning C7059 glass substrate or a rubbed-PDA/C7059 substrate. The starting source material was (5,7-dodecadinye-1,12-diyl-bis-ethylurethane) (DA-4U2) monomer evaporated from a low-temperature effusion cell (70-80°C). During the deposition, substrates were continuously irradiated with the 365-nm UV light (~2mW/cm^2) to promote photo-polymerization. This procedure appeared to enhance the sticking coefficient of source molecules [1,2], yielding deposition rate of 0.03-0.07Å/sec at the substrate temperatures of T_s = 20-80 °C. All the samples examined in this study are in the *so called* low-temperature, blue phase. The effect of strain has been negligibly small, as evaluated by the Raman scattering.

Figure 1 shows optical absorption and photoconductivity spectra for two PDA films with different crystal quality. Plan view images obtained by atomic force microscope (AFM) are also shown together. Sample A shows atomically flat terraces with straight, abrupt steps (2nm), whereas the alignment of molecular steps becomes less irregular for the Sample B. The former sample has apparently higher crystal quality than the latter sample. Looking into the optical absorption spectra, the spectrum of the sample A resembles that of the bulk crystalline PDA of blue phase. On the other hand, a shift toward higher energies (ΔE_G = 40meV) is noticeable for the sample B, especially for the 1.8 – 2 eV excitonic region.

More importantly, the threshold photon energy for photoconductivity also shifts toward higher energies. Since the threshold energy corresponds to the effective band gap energy, it is reasonable to infer that the increased irregularity in molecular ordering leads to an increase in the band gap. This is one of the main behavior that can be expected qualitatively from the superlattice model (Fig.2). It is worth mentioning that the exciton binding energy, defined as a difference between exciton absorption peak and the threshold of photoconductivity, is estimated to be 0.52eV, being comparable to the reported values.

Using the K-P model as shown schematically in Fig.2, we have examined our superlattice model with experimental data [3]. Here, π-electrons in the PDA wires are expressed as electrons separated by thin barriers which are align periodically along the *c*-axis. The first excited state forms a narrow subband, and the energy separation from the ground state corresponds to the band gap energy. The averaged lattice spacing increases when the crystal quality degrades, which in turn reduces the width of the subband and thus an increase in the band gap. In the first step, the barrier height E_B = 4.7 eV was determined by solving the K-P model with the lattice parameter along the *c*-axis (l = 0.54 nm), the spread of the π-electron cloud (d~0.26 nm) of DA oligomers, the ionization energy E_I = 5.2 eV, and the band gap energy E_G = 2.4 eV. We then calculated a change in the band gap by increasing the width of the barrier, and the calculation has yielded an increase in the band gap energy of 40-50 meV when the barrier width is increased for about 0.1 Å, being close to the value obtained experimentally from symmetrical (100) and anti-symmetrical (302) θ-2θ x-ray diffraction measurements.

In summary, we have showed that the irregularity in molecular ordering can be analyzed quantitatively by using the superlattice model.

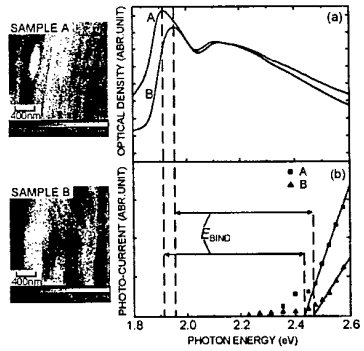

FIG.1 : (a) Optical absorption spectra and (b) photoconductivity spectra of sample A and B. AFM images of samples A and B are also shown. Film thicknesses are 40 and 65 nm for samples A and

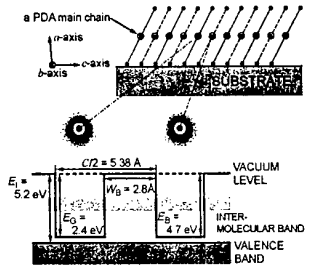

FIG. 2. : Schematic illustration showing the relation between PDA molecules and well/barrier regions in the Kronig-Penney model. A PDA main chain is a well for a π-electron whereas the inter-molecular region is as a barrier.

References

[1] T. Kondo, A. Ishii and H. Munekata, Physica E **2** 991 (1998).
[2] T. Kondo, A. Ishii, H. Munekata and K. Takeda, Jpn. J. Appl. Phys. **38** L764 (1999).
[3] T. Kondo, A. Ishii, H. Manabe, and H. Munekata, Appl. Phys. Lett. **78**, 1352 (2001).

Corresponding author *: H. Munekata, Imaging Science and Engineering Laboratory, Tokyo Institute of Technology, 4259 Nagatsuda, Midori-ku, Yokohama 226-8503, Japan,*
Phone : +81-45-924-5185, Fax : +81-45-924-5178, e-mail : hiro@isl.titech.ac.jp

Organic-template induced structural phase transition of GeS_2 and $GeSe_2$ in organic-inorganic hybrid superstructures

P.J. Klar[1], L. Chen[1], M. Güngerich[1], W. Heimbrodt[1], N. Oberender[2,3], D. Kempe[2] and M. Fröba[2,3]

[1]Department of Physics and Materials Science Center, Philipps-University of Marburg, Renthof 5, 35032 Marburg, Germany
[2]Institute of Inorganic and Applied Chemistry, University of Hamburg, Martin-Luther-King-Platz 6, 20146 Hamburg, Germany
[3]Institute of Inorganic and Analytical Chemistry, Justus-Liebig University of Gießen, Heinrich-Buff-Ring 58, 35392 Gießen, Germany

Highly-ordered, mesoporous structures with regular pores as well as lamellar superstructures with periodicities in the nanometer range can be synthesised as organic-inorganic hybrid structures. Under adequate conditions organic molecules self-assemble in solution to a regular template structure. In the spaces between the organic molecules inorganic compounds such as SiO_2, TiO_2, GeS_2 or $GeSe_2$ can be synthesised [1-3] using various precursors. This novel class of materials is of interest from chemical as well as physical points of view. For example, due to their large surface to volume ratio the mesoporous compounds can be used for catalytic applications [4]. Due to their regular pore structure they are also suitable host materials for the synthesis of highly-ordered semiconductor nanostructures or, in the case of the layered structures of GeS_2 and $GeSe_2$, represent semiconductor nanostructures themselves [5].

We have synthesised such layered organic-inorganic hybrid superstructures of GeX_2 (X = S, Se) and corresponding bulk inorganic reference samples using various precursors and different growth temperatures. X-ray as well as TEM studies confirm the high degree of order of the superstructure of the synthesised organic-inorganic hybrids. The period of the superstructure is about 3.5 nm with roughly equal thickness of the organic and inorganic layers. The organic-inorganic hybrids and reference bulk materials were studied by Raman spectroscopy. It is well known that several different bulk phases (e.g. amorphous, α– and β-crystalline phases) of GeX_2 exist and that various thiogermanates (e.g. GeX_4^{4-} or $Ge_4S_{10}^{4-}$) can be formed in aqueous solutions of different pH-values. All these compounds can be clearly distinguished by their Raman spectra. Therefore, a thorough analysis of the vibrational modes in the Raman spectra allows one to draw conclusions about the microscopic structure of the inorganic layers of the organic-inorganic hybrids. With increasing growth temperature the bulk GeX_2 reference samples exhibit an abrupt structural phase transition from the amorphous to the α-crystalline phase. In contrast, the GeX_2 layers of the hybrid superstructures transform rather continuously with increasing growth temperature from the amorphous network to a quasi-crystalline $Ge_4X_{6+4/2}$ network consisting of $Ge_4X_{10}^{4-}$ adamantane units i.e. the organic template induces constraints which lead to a structural phase diagram of the nanostructured GeX_2 other than for bulk GeX_2. By rescaling the Raman spectra of the new quasi-crystalline $Ge_4S_{6+4/2}$ and $Ge_4Se_{6+4/2}$ phases with the appropriate scaling factors for bond-bending and bond-stretching modes derived from the α– and β-crystalline GeX_2 phases, it can be shown that both $Ge_4X_{6+4/2}$ layers have the same microscopic structure. The microscopic origin for the formation of this new quasi-crystalline phase will be discussed in detail.

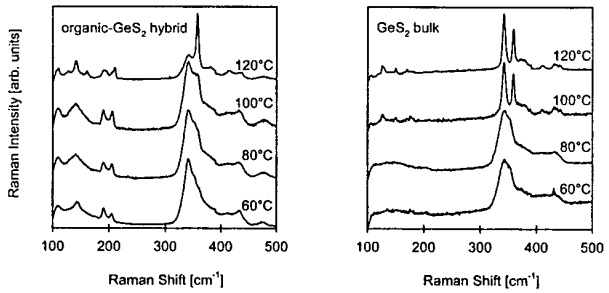

Fig. 1: *Raman spectra of (a)layered organic-GeS_2 hybrid superstructures and (b) GeS_2 bulk references synthesised at different temperatures*

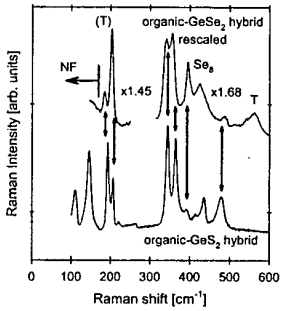

Fig. 2: *Raman spectra of layered organic-GeX_2 hybrid superstructures after rescaling*

References

[1] C.T. Kresge, M.E. Leonowicz, W.J. Roth, J.C. Vartulli and J.S. Beck, Nature **359**, 710 (1992).
[2] M. Fröba, O. Muth, A. Reller, Solid State Ionics **101-103**, 249 (1997).
[3] L. Chen, P.J. Klar, W. Heimbrodt, N. Oberender, D. Kempe and M. Fröba, Appl. Phys. Lett. **77**, 3965 (2000).
[4] J.Y. Ying, C.P. Mehnert and M.S. Wong, Angew. Chem. Int. Ed. (Engl.) **38**, 56 (1999).
[5] L. Chen, P.J. Klar, W. Heimbrodt, F. Brieler and M. Fröba, Appl. Phys. Lett. **76**, 3531 (2000).

Corresponding author: Dr. P.J. Klar, Department of Physics and Materials Science Center, Philipps University Marburg, Renthof 5, D-35032 Marburg, Germany
phone: ++49 6421 2821354, fax: ++49 6421 2821354, e-mail: klarp@mailer.uni-marburg.de

Epitaxial growth of para-sexiphenyl films on mica characterised with X-ray diffraction pole figure technique

[1]H. Plank, [1]R. Resel, [2,3]J. Keckes, [4]A. Andreev, [4]N. S. Sariciftci, [5]H. Sitter, [1]S. Purger, [6]A. Thierry, [6]B. Lotz,

[1]Institute of Solid State Physics, Graz University of Technology, Austria
[2] temp. address: Erich Schmid Inst. for Material Science, Austrian Academy of Science and Inst. of Metal Physics, University Leoben
[3] perm. address: Institute of Inorganic Chemistry, Slovak Academy of Sciences, SK-842 36 Bratislava, Slovak Repuplic
[4]Institute for Physical Chemistry University Linz, Austria
[5]Institute for Semiconductor- and Solid State Physics, University Linz, Austria
[6]Institute Charles Sadron, Strasbourg, France

Para-sexiphenyl (PSP) (C_6H_5 - (C_6H_4)4 - C_6H_5) is a promising *organic semiconductor* suitable for applications in optoelectronics to act in light-emitting devices as an emission layer with polarised emitting properties [1]. The preferred orientation of the PSP molecules within the active layers decisively influences spatial distribution of the emission intensity and thus its control is necessary for a successful application of this material [2]. In our previous studies it has been shown that the substrate temperature and the growth time are very important parameters to control the film morphology in terms of the long range order and the degree of anisotropy [3,4]. The present work focuses on the epitaxial growth of highly purified PSP on freshly cleaved (00l) mica substrates.

The films were prepared at high vacuum of about 6 x 10^{-6} mbar by Hot Wall Epitaxy (HWE) with a substrate temperature of 90°C and a deposition time of 60 min. X-ray diffraction (XRD) pole figure technique, atomic force microscopy (AFM) and transmission electron diffraction (TED) were used to characterise the thin films.

The films exhibit a needle-like morphology with a typical height, width and length of 130 nm, 800 nm and 100 µm, respectively (Fig.1.a.). Between the needles there are free areas of roughly 300-400 nm. Optical measurements revealed that the films are highly anisotropic in absorption and emission of light [3]. The crystallographic anisotropy of the films was confirmed by XRD pole figure measurements (and measurements using 2D detector) indicating a heteroepitaxial growth of PSP on mica (Fig.1.b.). Two distinct orientations of crystallites with (11-1) and (11-2) crystallographic planes of PSP (both of them cleavage planes) oriented parallel to the substrate surface were observed. Moreover, within each above orientation, the PSP crystallites were found to grow in two antiparallel directions constituting a twofold symmetry. For all crystal orientations, the long PSP molecule axes are tilted about 5° with respect to the mica surface and the planar phenyl rings are standing normal on the substrate. Therefore, only one phenyl ring per molecule is in a contact with the substrate surface. Hence, a two dimensional distribution of the contact points of the PSP on the mica surface can be generated. Computer simulations turned out that the distribution of contact points and the pseudo-hexagonal mica surface are incommensurate. Therefore the observed heteroepitaxial growth is referred to quasi-epitaxy [5]. Between the mica substrate and the organic layer there are the epitaxial relationships PSP(11-1) || mica(001) and PSP[1-2-1] || mica[-340] in case of the crystallographic (11-1) orientation and further PSP(11-2) || mica(001) and PSP[-20-1] || mica[-310] for the crystallographic (11-2) orientation of PSP. The unexpected two-fold symmetry of the PSP films can be explained by the distortion of the pseudo-hexagonal rings of mica as revealed by computer simulations [6]. This distortion provides a minimum potential energy for two equivalent orientations of PSP molecules what is in accordance with the observed two fold symmetry of the crystallites. Considering the comparable small mismatch of the contact points of PSP and the mica ring structure a strained-quasi-epitaxial growth is also conceivable which could be explain the needle like morphology of the PSP due to the different strains in different directions.

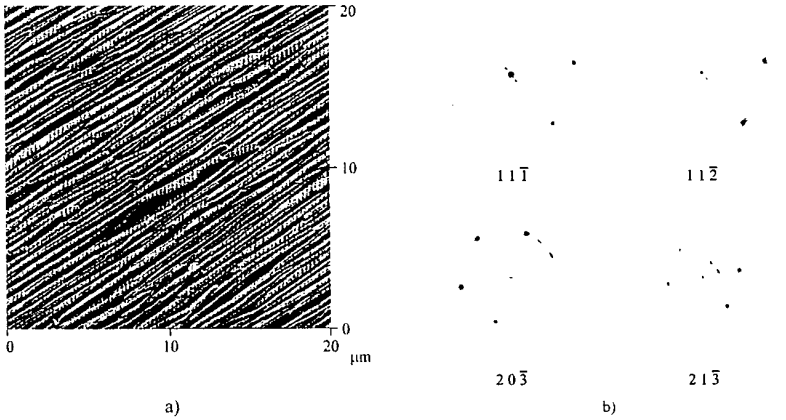

Fig.1: a) Atomic Force Microscopy (AFM) image of the PSP film grown on mica which revealed the needle like morphology. b) pole figure measurements of the four strongest PSP reflections. The darker the area the higher intensity.

References:

[1] M. Era, T. Tsutsui, S. Saito, Appl. Phys. Lett. 67, 2436 (1995).
[2] H. Yanagi, T. Moorikawa, Appl. Phys. Lett. 75, 187 (1999).
[3] A. Andreev, G. Matt, C. J. Brabec, H. Sitter, D. Badt, H. Seyringer, N. S. Sariciftci, Adv. Mater. 12, 629 (2000).
[4] A. Andreev, H. Sitter, C. J. Brabec, P. Hinterdorfer, G. Springholz, N. S. Sariciftci, Synth. Met. in print (2001).
[5] P. E. Burrows, Y. Zhang, E. I. Haskal, S. R. Forrest, Appl. Phys. Lett. 61, 2417 (1992).
[6] M. Odelius, M. Bernasconi, M.Parrinello, Physical Review Letters 78 (14), 2855 (1997)

Corresponding author: Roland Resel, Institute of Solid State Physics, Graz University of Technology, Petersgasse 16, A-8010 Graz, Austria
phone: +43 316 873 8469
mail: roland.resel@tugraz.at

Topology effects on local electronic properties and on the conductance of molecular structures

A. Latgé[1], D. C. Marcucci[1], and M. V. Tovar Costa[2]

[1]Instituto de Física, Univ. Federal Fluminense, Av. Litorânea sn, 24210-340-Niterói, RJ-Brazil
[2]Instituto de Física, Univ. do Estado do Rio de Janeiro, São Francisco Xavier 524, 205500-13 Rio de Janeiro, RJ-Brazil

The recent advances in scanning probes and self-assembly techniques play an important role in the progress of mesoscopic systems and molecular electronic research. Both techniques represent powerful tools of atomic-scale manipulation and allow the realization of distinct kinds of molecular complexes. Quasi-one dimensional structures (metallic and semiconducting) are being now extensively studied, mainly the carbon nanotubes (CNs) and related-mixed networks, as they are considered promising building blocks of molecular circuits. Also, a subject of particular interest in both fundamental and applied research is the nature of the metallic regime for highly doped polymers for which structural disorder plays a fundamental role. In particular it was shown [1] that the concentration of the interchain cross-links between wires are crucial for a correct understood of the metal-insulation transition. Otherwise, topological characteristics of comb-like structures, composed by infinite one dimension backbone with grafted finite chains, are directly reflected on their electronic properties [2]. In this work we present a detailed analysis of electronic and transport properties of different quasi-one-dimensional structures such as, comb-like structures, wire-like systems, polymeric structures and molecular complex modeled by CNs used as metallic leads. We are mainly motivated in establishing a close analogy between lattice topology and local electronic and transport properties. For all considered nanosystems we use a simple one-band tight-binding description, due to its simplicity, and adopt Green-function formalism. Local density of states and linear-response conductance, based on the Landauer theory are calculated following real-space renormalization group approaches [3] which have been successfully used in the theoretical description of more interacted systems, including nanotube heterojunctions [4]. As the presence of gaps, continuous or flat bands at the Fermi level is completely determined by the topology characteristics of the model-networks such theoretical study may be viewed as an essential route to engineering new devices based on low dimensional networks. Comb-like network are used here as a basic lattice to describe polymeric structures exhibiting loops of randomic lengths at randomic positions in a main chain. Based on a simple picture we address here the effects of disorder on the conductance. The dependence of the local density of states (LDOS) at the center of the electronic band, on the size L of the grafted chains for comb-like structures modeled by unit cells of N+L atomic sites is shown in figure 1. Similar oscillations of the LDOS are obtained for the case of polymeric-like systems modeled by L-order loops spaced by chains of N sites. A clear relation between the parity of the parameters N and L with the main features of the LDOS is presented. Results for the conductance of two different based-nanotube systems are shown in figure 2 as a function of the energy. The left panel corresponds to a finite wire connected to metallic CNs (zigzag configuration) of different diameters whereas in the right one a CN quantum-dot is modeled by attaching three CNs. The conductances of the isolated constituents are also depicted. We analyze the dependence of the conductance on the length of the spacer for both examples. For the quantum-dot based CN, exponential decay and oscillatory behaviors of the conductance are analytically predicted by investigating the corresponding electronic structure of the semiconductor-space CN.

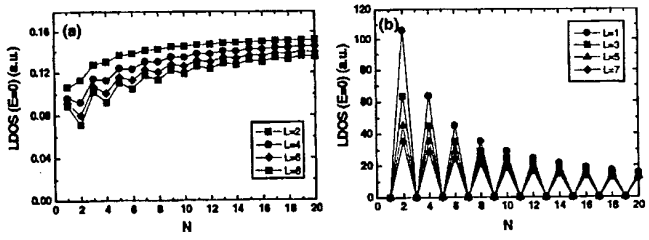

Fig.1: LDOS at the center of the band for comb-like structures .

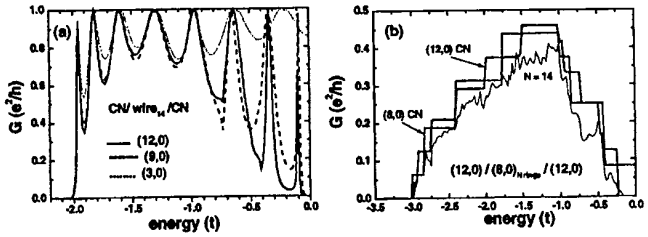

Fig.2: Conductance as a function of the energy (written in units of the hopping energy) for structures modeled by metallic nanotube leads connected to (a) a single wire and (b) a semiconductor CN (8,0).

References
[1] Shi-Jie Xiong and S. N. Evangelou, Phys. Rev. B **52**, R13079 (1995).
[2] J. O. Vasseur et al, J. Phys.: Cond. Matt. **10**, 8973 (1998).
[3] D. C. Marcucci, A. Latgé, E. V. Anda, M. Matos, and J. C. Fernandes, Phys. Rev. B **56**, 3672 (1997).
[4] M. S. Ferreira, T. Dargam, R. B. Muniz, and A. Latgé, Phys. Rev. B **62**, 16040 (2000).

Corresponding author: Andrea Latgé, Instituto de Física, Universidade Federal Fluminense, Av. Litorânea sn, 24210-340 Niteróii-RJ, Brazil.
phone: +55 21 620 6735, Fax: +55 21 620 3881,
email: latge@if.uff.br

Characterization of intrinsic and doped GaN layers and nanocolumns

J. Sánchez-Páramo[1], J.M. Calleja[1], E. Calleja[2], M.A. Sánchez-García[2] and U. Jahn[3]
[1]Dpt. Física de Materiales, Universidad Autónoma, Cantoblanco 28049 Madrid, Spain
[2]Dpt. Ing. Electrónica, ETSI Telecomunicación, Univ. Politécnica, 28040 Madrid, Spain
[3]Paul Drude Institut für Festkörperelektronic, Hausvogteiplatz 5-7, D-10117 Berlin, Germany

GaN films grown by plasma-assisted Molecular Beam Epitaxy develop a columnar structure or form a compact layer depending on the growth conditions, in particular, the III/V ratio. In this work, GaN layers and columnar samples have been grown on Si(111) and c-sapphire substrates. The effect of doping on the strain conditions of the films and their defect distribution have been studied by different optical techniques

At stoichiometry, or under Ga-rich conditions, the GaN layer becomes compact. Half micron thick epitaxial layers of hexagonal GaN were grown by MBE on AlN buffered p-type Si(111) substrates. Five samples were prepared with different Si doping in the range from 10^{17} cm^{-3} to 10^{19} cm^{-3}. Also an undoped sample was prepared for comparison[1]. The effect of Si doping in the strain state of the samples has been studied using Raman scattering, low temperature photoluminescence and X-ray diffraction. The strain appears as a consequence of the different thermal expansion coefficients of GaN and Si during the sample cooling after growth[2].

With this purpose, both the bound-exciton emission at 3.455 eV, which is dominant in the photoluminescence (PL) spectra, and the E_2 high frequency phonon of the layers have been measured as a function of the Si concentration. As the Si concentration increases a progressive decrease is observed both in the exciton energy (measured in PL) and the phonon frequency (measured by inelastic light scattering). Both effects are observed up to a Si concentration of around $5x10^{18}$ cm^{-3}. They indicate an enhancement of the biaxial tensile strain for increasing doping level, which is confirmed by x-ray diffraction measurements (Fig 1). The linear dependences of both trends, shown in Fig 1 as a function of the in-plane strain, correspond to values of the deformation potentials already reported for GaN[3]. At higher Si concentration, both the phonon frequency and the exciton emission energy increase again. This change is attributed to a partial strain relaxation due to a change in the growth mode.

For epitaxial growth under N-rich conditions the GaN films develop a columnar structure, with the hexagonal nanocolumns orientated with the c-axis parallel to the growth direction. In this work, nanocolumns with controlled diameter, length and density, were grown either on Si(111) with or without AlN buffer, or on sapphire substrates[4]. The morphology, homogeneity and optical properties of the columns have been studied by PL, scanning electron microscope (SEM) and cathodoluminescence (CL). The crystal quality of the columns is very good. The SEM images show (fig 2) hexagonal, homogeneous, straight columns whose average diameter can vary from 100 nm to 600 nm depending on the growth conditions. The narrowness of the excitonic emission (FWMH less than 2 meV) confirms the optical quality of the columns. Their Raman spectra indicate that they are strain-free, as expected. Besides the free excitonic emission, the PL spectra of the columns show a band centred at 3.41 eV. This emission was previously attributed[3] to defects formed at the bottom interface of the columns, whose exact nature is not known.

We have performed CL measurements on lateral cleaved surfaces of the sample. While the free excitonic emission is observed along the whole length of the columns, the new emission at 3.41eV is observed at the interface of the columns with the substrate, thus confirming unambiguously the previous assignment[3].

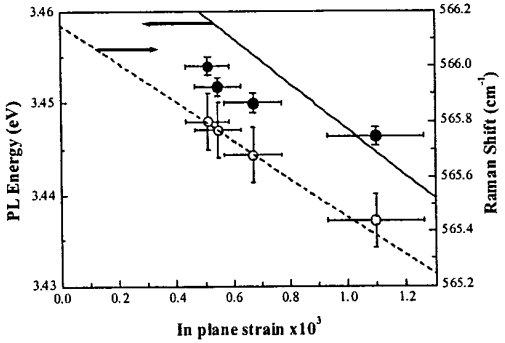

Figure 1 PL energies (full dots) and E_2 Raman frequencies (open dots) as a function of the in-plane strain. The full and dotted lines stand for theoretical trends, based on the parameters given in ref 3.

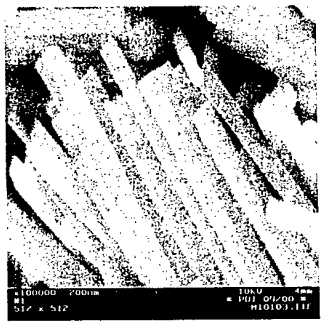

Figure 2 SEM image of some "broken" columns in one of the columnar GaN samples

References

[1] M.A. Sánchez-García, E.Calleja, E. Monroy, F.J. Sánchez, F. Calle, E. Muñoz and R. Beresford. J. Crys. Growth, **183**, 23 (1998)
[2] H. Heinke, V. Kirchner, S. Einfeld, U. Birkle and D. Hommel. J. Crys Growth, **189**, 375 (1998).
[3] V.Yu Davydov, N.S. Averkiev, I.N. Goncharuk, D.K. Nelson, I.P. Nikitina, A.S. Polkovnikov, A.N. Smirnov, A.N. Smirnov, M.A. Jacobson and O.K. Semchinova, J. Appl. Phys., **82**, 5097 (1997)
[4] E. Calleja, M.A. Sánchez-García, F.J. Sánchez, F. Calle, F.B. Naranjo, E. Muñoz, U.Jahn and K. Ploog. Phys. Rev. B. **62**, 16840 (2000)

Evidence for type I band alignment in GaNAs/GaAs quantum structures from optical spectroscopies

A. Buyanova[1], G. Pozina[1], P. N. Hai[1], W. M. Chen[1], H. P. Xin[2] and C. W. Tu[2]

[1]Department of Physics and Measurement Technology
Linköping University, SWEDEN
[2]Department of Electrical and Computer Engineering
University of California, La Jolla, USA

The N-containing III-V-V' alloys and related quantum structures have been extensively investigated over recent years owing to their unique physical properties and technological importance for optoelectronics and photonics. One of the remaining debating issues involves the valence band (VB) lineup in the GaNAs/GaAs quantum structures. It is clear that alloy forms a well for electrons, due to the giant bowing in the CB edge induced by incorporation of nitrogen. It is also commonly accepted that the VB offset is rather small. However, the conclusions regarding the VB lineup are rather controversial [1-4].

Reliable information on the band alignment in the quantum structures can be obtained by analyzing oscillator strength and polarization properties of the corresponding optical transitions, as well as spatial location of photo-excited holes in the structure. Thus the following independent experiments are employed to determine the band lineup.
(i) Time-resolved measurements. Decay time of the near-band-edge photoluminescence (PL) should be comparable in the single epilayers and the type I QW structures, whereas significant slowing of the radiative decay is expected for the spatially indirect transitions of the type II QWs. The identical radiative lifetime of the GaNAs near band edge emission in the GaNAs/GaAs multiple quantum wells (MQW) and GaNAs epilayers (Fig.1) provides the first piece of evidence for the type I band alignment.
(ii) Polarization measurements. Biaxial tensile strain present in the thin GaNAs layers, due to the lattice mismatch between GaAs and GaNAs, lifts the degeneracy of the VB states. If the strain effect dominates, the topmost VB states in both thin GaNAs epilayers and GaNAs QWs are light-hole (lh) like. On the other hand, in the strain-free GaAs barriers, the lh and heavy hole (hh) states in VB either remain degenerate for the type I structure or can be largely hh-like for the type II band line up. Thus an analysis of the PL polarization can provide information about the band alignment. According to the performed polarization measurements, the topmost VB states in the MQW structures are lh-like in support of the type I model.
(iii) Optically Detected Cyclotron Resonance (ODCR) measurements. The spatial location (GaNAs in the case of type-I or GaAs for the type-II structures) of the holes participating in the radiative recombination can be directly determined via measuring hole effective mass from, e.g. the ODCR studies. From Fig.2, the CR peaks arising from the free electrons and free holes in GaAs disappear under resonant excitation of the GaNAs MQWs. Thus, the photoexcited holes are spatially confined within the GaNAs layers under resonant excitation of the GaNAs MQW. This is only possible in the type I structure, where the resonant light absorption in the GaNAs MQW does not create free holes in GaAs.

Thus our results obtained by using three different experimental techniques, namely time-resolved photoluminescence spectroscopy, PL polarization measurements and optically-detected cyclotron resonance studies, provide unambiguous evidence for the type I band alignment in the GaN_xAs_{1-x}/GaAs heterostructures with x 3.3 %.

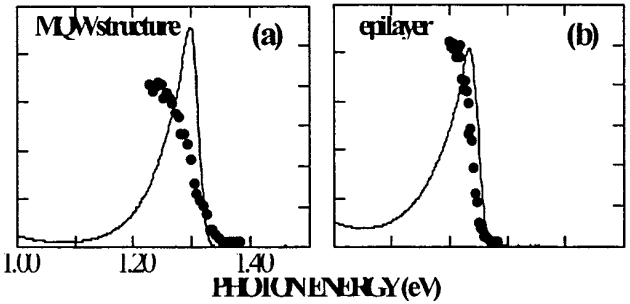

Figure 1. The PL spectra detected at 2K from the $GaN_{0.011}As_{0.989}$/GaAs MQW (a) and the single $GaN_{0.012}As_{0.988}$ epilayer (b). Spectral dependence of the PL decay time from the same structures is shown by dots.

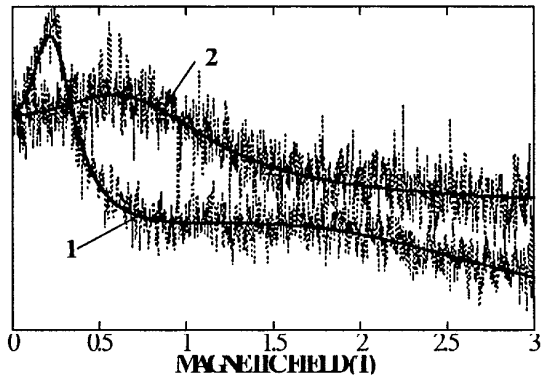

Figure 2. The ODCR spectra arising from the GaAsN/GaAs MQW with 2% of N when the excitation energy was above (1) and below (2) the GaAs bandgap, respectively. The dashed lines represent experimental data. The solid lines are the fit curves with m_e=0.66 m_0 and m_h=0.47 m_0 (curve 1) for the electron and hole in GaAs, respectively and m_e=0.19 m_0 (curve 2) for the electron in GaAs.

References

[1] S. Sakai, Y. Ueta, and Y. Terauchi, Jpn. J. Appl. Phys. 1 **32** (1993) 4413.
[2] L. Bellaiche, S.-H- Wei, and A. Zunger, Phys. Rev. **B 56** 10 233 (1997).
[3] Kitani et al, Jpn. J. Appl. Phys. **38** (1999) 5003.
[4] P. Krispin, S. G. Spruytte, J. S. Harris, K. H. Ploog, J. Appl. Phys. **88** (2000) 4153.

Corresponding author: Irina Buyanova, Department of Physics and Measurement Technology, Linköping University, S-581 83 Linköping, Sweden,
Phone: +46.13.28 17 45, Fax, +46-13-14 23 37, e-mail: irb@ifm.liu.se

N incorporation in GaInNAs materials grown by MBE

Wei Li, Markus Pessa, Jari Likonen, Juha Riikonen, Juha Toivonen, and Harri Lipsanen

Optoelectronics Reaserch Center, Tampere university of Technology,
P.O.Box 692, FIN-33101 Tampere, Finland
Tel:+358 3 365 2914; Fax: +358 3 365 3400

Ga(In)AsN alloy has attracted considerable attention in recent years both because of a practical and a fundamental point of view. For the determination of the nitrogen content of Ga(In)NAs epilayers on GaAs x-ray diffraction (XRD) technique is often used. However, by XRD the lattice spacings are determined, and not directly the N contents of the Ga(In)N_xAs_{1-x} alloys. Thus the calculation of these values requires assumptions on the variation of the lattice parameters and of the elastic constants with x. A linear interpolation (Vegard's law) between the values of GaAs and cubic type GaN has been commonly assumed to be justified. We have measured the N content in a series of GaN_xAs_{1-x} ($0 < x < 3$ %) samples by secondary ion mass spectroscopy (SIMS) and the lattice constant in the epilayers by XRD rocking scans. A significant deviation of the lattice parameter variation in GaN_xAs_{1-x} from Vegard's law between GaAs and cubic GaN was observed, which leads to overestimation of the nitrogen content by up to 30 % for x 2.5 % (Fig. 1). The physical origin of this negative deviation is discussed.

Secondly, Si- and Be-doped $Ga_{1-3x}In_{3x}N_xAs_{1-x}$ ($0 \le x \le 3\%$) lattice-matched layers are grown on GaAs substrates by gas-source molecular beam epitaxy with a nitrogen radical beam source. The carrier concentration and mobility are observed to decrease substantially with increasing nitrogen content in both p- and n-type GaInNAs films. After rapid thermal annealing at 750 °C, the Be dopants are almost fully activated in p-type material; yet only a small fraction of the Si dopants are activated in n-type films (Fig. 2a and 2b). A broad photoluminescence band around 1.041 eV is observed (Fig. 3), probably related to N-related defects acting as acceptors in n-type GaInNAs material.

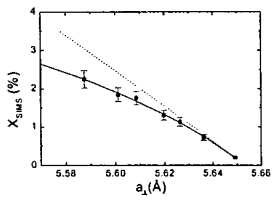

Figure 1. Dependence of the lattice constant in growth direction ($a_\perp$) of pseudomorphically strained GaN_xAs_{1-x} epilayers with N content. Dashed line: calculated lattice parameters according to the Vegard's law between GaAs and cubic phase GaN; solid line: polynomial fit of our experimental results; Black squares represent our experimental results.

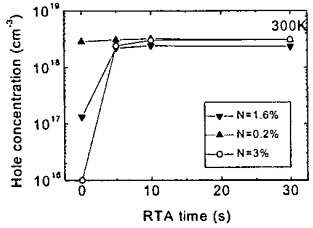

Figure 2a . Hole concentrations as a function of RTA time for as-grown and annealed GaInNAs samples doped with Be (3×10^{18} cm^{-3}).

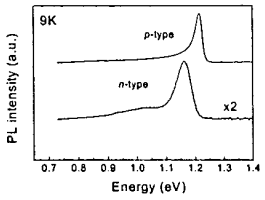

Figure 3. Low temperature PL spectra of Si- and Be-doped GaInNAs (N ~ 1.6%) annealed at 750 °C for 10 sec.

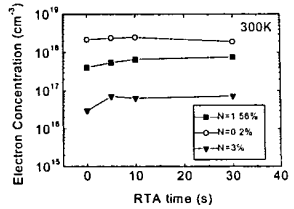

Figure 2b. Electron concentrations as a function of RTA time for as-grown and annealed GaInNAs samples doped with Si (2×10^{18} cm^{-3}).

The effective mass and conduction band states of GaAsN/GaAs quantum wells.

C. Skierbiszewski[1], S. P. Łepkowski[1], P. Perlin[1], T. Suski[1], W. Jantsch[2]

[1]High Pressure Research Center Unipress, Sokołowska 29/37, 01-142 Warszawa, Poland
[2]Institut für Halbleiterphysik, Johannes-Kepler-Universität, A-4040 Linz, Austria

$In_yGa_{1-y}As_{1-x}N_x$ alloys have attracted substantial attention during the last few years due to their technological potential for device applications like lasers and detectors operating in 1.3-1.5 μm wavelength region. These alloys exhibit interesting properties which can not be explained within the framework of the virtual crystal approximation. We mention only a strong decrease of the energy gap with increasing nitrogen content [1], a high degree of conduction band (CB) non-parabolicity and unusual behavior of the effective mass m* [2]. In bulk material we observe a large increase of m* with increasing electron concentration (s. Fig. 1). However, in a 1%N sample for a electron Fermi wavevector k≈0 we found that m* does not exceed 0.1 m_0. A recent study of the photo-reflectivity of $GaAs/GaAs_{1-x}N_x/GaAs$ QW's performed by Zhang *et. al.* [3] shows that m* at the bottom of the CB is as large as 0.5 m_0 for 1%N. In order to determine m* from experimentally measured optical transition energies the authors of Ref. 3 assumed a parabolic CB and treated m* as a fitting parameter.

In this work we clarify this discrepancy. In particular, we prove that the parabolic band approximation is not valid for the case of the InGaAsN alloys. Moreover, we show that by taking into account the strong non-parabolicity of the CB in $GaAs_{1-x}N_x$ the energy band structure of $GaAs_{1-x}N_x/GaAs$ QW's is obtained correctly. We derive values of effective mass in line with those measured for 3D crystal. At the beginning we determine experimentally the degree of the nonparabolicity of the CB of InGaAsN by measuring the effective mass in infrared reflectivity experiments for bulk samples with different densities of electrons (see Fig. 1). In this alloy, indium reduces the strain caused by nitrogen and decreases the energy gap without changing the shape of the CB dispersion relation. The solid line in Fig. 2. shows E(k) for InGaAsN containing 1% of N. The way to determine E(k) from $m^*(n_e)$ is described in Ref. 4. For comparison we present also E(k) for GaAs obtained by the same technique. Fig. 2 shows large non-parabolicity of the CB of InGaAsN crystals in comparison with GaAs. We analyse experimental results for InGaAsN within a recently proposed simple model which correctly describes and predicts a variety of new effects in GaAsN [5]. This model is based on the assumption of band anti-crossing (BAC) interaction between GaAs (or InGaAs) CB states and N-related states. The results for bulk InGaAsN are well described by the BAC model (see dotted line in Fig. 2). This enables us to use the BAC model also to calculate the conduction band states in QW's [6]. First we check the validity of such an approach by comparing the fundamental electron – heavy hole transition energies calculated by us (for a 70Å QW *vs.* the N content in the QW region) with experimental results taken from Ref. 3 – see Fig. 3. Since the agreement is reasonably good, the BAC model is taken as appropriate tool to determine m* in QW's. The squares in Fig. 4 show data for m^* at the bottom of the CB in $GaAs_{1-x}N_x$ as a function of x as obtained from our modelling. For comparison we also plot here (by dots) the results obtained for the parabolic band model proposed in Ref. 3. In contrast to the strong decrease of m* obtained within the parabolic model we get an increase of m* with increasing N content.

In conclusion, we show that by taking into account the strong non-parabolicity of the CB we are able to describe successfully the positions of the electronic subbands in $GaAs_{1-x}N_x$ QW's as well as to derive the alloy dependence of the effective mass. It turned out that: (i) the values obtained for m* are much smaller than those given in Ref. 3; and (ii) the increase of m* is accompanied by an increase of the N content – which is in contrast to the findings based on the parabolic CB model given in Ref. 3. Both results (i) and (ii) agree qualitatively with findings in InGaAsN bulk material [2,4].

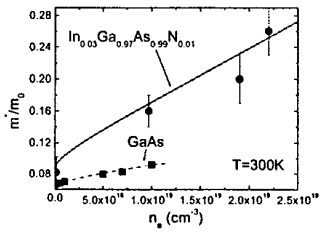

Fig. 1. Experimental data for the electron effective mass m vs. electron density, n_e, for MOCVD grown $In_{0.03}Ga_{0.97}As_{0.99}N_{0.01}$ (dots) and GaAs (squares) samples. The solid line shows predictions of the BAC model. The dashed line represents the much smaller enhancement predicted for GaAs due to nonparabolicity of its conduction band.*

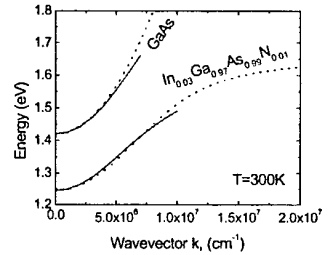

Fig. 2. Experimentally determined E(k) for GaAs and InGaAsN bulk crystals (solid lines). The dotted lines correspond to the parabolic approximation for GaAs and the BAC model for InGaAsN.

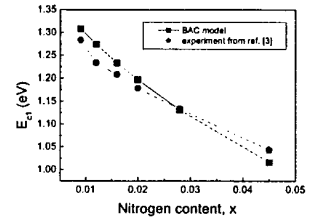

Fig. 3. Fundamental electron – heavy hole transition energy in 70Å $GaAs_{1-x}N_x$ /GaAs QW. Dots – experimental results from Ref. 3. Squares – this work, the BAC model

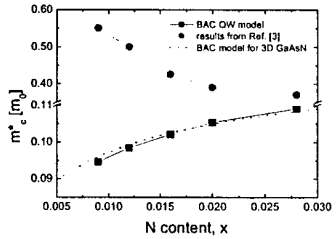

Fig. 4. Conduction band edge effective mass, m^* in $GaAs_{1-x}N_x$ obtained in Ref. 3 (dots) and from the BAC model (squares - this work). Dotted line – predictions of the BAC model for m at k=0 in bulk material.*

References.

1. M. Kondow, T. Kitatani, M. C. Larson, K. Nakahara, K. Uomi, and H.Inoue, J. Cryst. Growth **188**, 255 1998

2. C. Skierbiszewski, P. Perlin, P. Wiśniewski, W. Knap, T. Suski, W. Walukiewicz, W. Shan, J.W. Ager, E.E. Haller, J.F. Geisz, D.J. Friedman, J.M. Olson, and S.R. Kurtz, Appl. Phys. Lett. **76**, 2409, (2000).

3. Yong Zhang, A. Mascarenhas, H.P. Xin and C.W. Tu, Phys. Rev. B **61**, 7479 (2000)

4. C. Skierbiszewski, P. Perlin, P. Wisniewski, T. Suski, J. Geisz, K. Hingerl, W. Jantsch, D.Mars, W. Walukiewicz, in press in PRB

5. W. Shan, W. Walukiewicz, J.W. Ager III, E.E. Haller, J.F. Geisz, D.J. Friedman, J.M. Olson, and S.R. Kurz, Phys. Rev. Lett. **82**, 1221 (1999).

6. J. Hader, S. W. Koch, J. V. Moloney, E. P. O'Reilly, Appl. Phys. Lett. **76**, 3685, (2000)

Corresponding author: Czesław Skierbiszewski, High Pressure Research Center, Unipress,
Sokolowska 29/37, 01-142 Warszawa, Poland
tel. (+4822) 6323628, fax. (+4822) 6324218, email: czeslaw@unipress.waw.pl

Effect of hydrogen on the electronic properties of $In_xGa_{1-x}As_{1-y}N_y$

M. Bissiri[1], V. Gaspari[1], A. Polimeni[1], G. Baldassarri H. v. H.[1], F. Ranalli[1], A. Nucara[1], M. Capizzi[1], M. Geddo[2], M. Fischer[3], M. Reinhardt[3], and A. Forchel[3]

[1]INFM, Dip. di Fisica, Univ. di Roma "La Sapienza", I-00185 Roma, Italy
[2]INFM, Dip. di Fisica, Univ. di Parma, I-43010 Fontanini (Parma), Italy
[3]Universität Würzburg, Technische Physik, 97074 Würzburg, Germany

We have investigated the effect of hydrogen on the electronic properties of $In_xGa_{1-x}As_{1-y}N_y$/GaAs heterostructures for x=0-0.41 and/or y=0-0.05. Hydrogen irradiation at 300 °C was obtained by a low-energy Kaufman source (hydrogen doses, d_H=10^{14}-10^{19} ions/cm^2). A post-hydrogenation thermal annealing was performed at 10^{-6} torr at temperatures ranging between 220 °C and 600 °C.

H irradiation strikingly affects the optical properties of the N-containing samples. In the impurity limit (y<0.001), we observe a full quenching of N-related recombination lines (vertical dashed lines in Fig. 1(a)) as well as a passivation of the broad background associated with N localization centers [1]; see Fig. 1(a). In the alloy limit (y~0.01), we find that the material band gap blue-shifts with increasing d_H until it reaches the value it has in a corresponding N-free sample; see Fig. 1(b). The broadening of the spectrum lineshape in hydrogenated samples suggests an increase of microscopic disorder. These effects can be accounted for by the formation of one (or more) "molecular orbital" between hydrogen and nitrogen. Indeed, the large electronegativity mismatch between N and its atomic neighbors in the lattice favors the formation of N^--H^+ complexes [2]. This neutralizes the N electrical activity with an ensuing disappearance of the N-related radiative recombination lines in the impurity limit and an increase of the band gap in the alloy limit. Therefore, the N associated wavefunctions seem to maintain a localized "impurity like" character even at nitrogen concentrations so high to strongly perturb the conduction band edge of the (InGa)As host lattice [3].

The effects of hydrogen irradiation can be reversed by thermal annealing. In the impurity limit, luminescence lines recover intensity at different rates with annealing time, as shown in Fig. 2(a) by vertical dashed lines. This suggests that the whole set of lines can be classified into subsets related to different N complexes or clusters. In the alloy limit, annealing recovers the band gaps and photoluminescence line widths the samples had before hydrogenation (see, e.g., Fig. 2(b) for a $In_{0.41}Ga_{0.59}As_{0.98}N_{0.02}$ quantum well). The activation energy for this process is 2.3 eV.

Therefore, (*i*) hydrogen is a powerful tool for investigating and tuning the optical gap of (InGa)(AsN) materials; (*ii*) the neat effects H exerts on the optical properties of (InGa)(AsN)/GaAs heterostructures may serve as a test bed for theoretical models aimed to explain the role played by N in (InGa)As-based materials.

References

[1] A. Polimeni *et al.*, *Appl. Phys. Lett.* 77, 2870 (2000).
[2] J. Neugebauer and C. G. Van de Walle, *Phys. Rev. Lett.* 75, 4452 (1995).
[3] W. Shan *et al.*, *Phys. Rev. Lett.* 82, 1221 (1999).

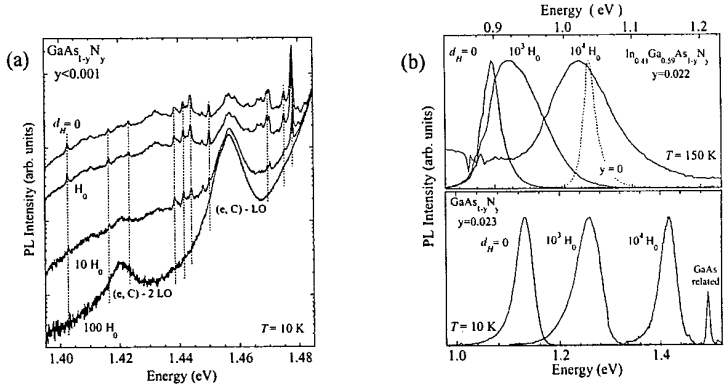

Fig. 1: (a) Photoluminescence, PL, spectra of Ga(AsN) epilayers with low N content irradiated at different hydrogen doses, d_H. (e,C)-nLO indicate phonon replica of a carbon to acceptor band transition. Vertical dashed lines are a guide to the eye. (b) PL spectra of (InGa)(AsN) (upper panel, continuous lines) and Ga(AsN) (lower panel) quantum wells for different hydrogen doses. Dashed line in the upper panel indicates the PL spectrum of a reference N-free quantum well. H_0=7×10^{13} ions/cm^2.

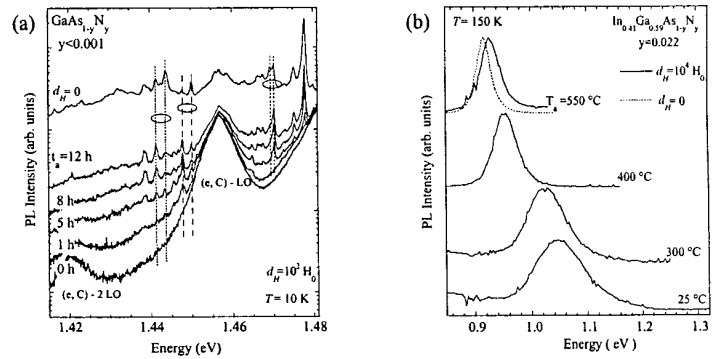

Fig. 2: (a) Photoluminescence, PL, spectra of Ga(AsN) epilayers with low N content. The upper line refers to an untreated sample. Lower spectra have been recorded on a hydrogenated sample annealed at 300 °C for different times, t_a. (e,C)-nLO indicate phonon replica of a carbon to acceptor band transition. (b) PL spectra of an hydrogenated (InGa)(AsN) quantum well (continuous lines) annealed at different temperatures, T_a. The dashed line indicates the PL spectrum of the non-hydrogenated sample. Both the PL peak energy and lineshape are recovered after annealing at the highest temperature. H_0=7×10^{13} ions/cm^2.

Corresponding author: Antonio Polimeni, Dipartimento di Fisica
Universita' di Roma ''La Sapienza'' Piazzale Aldo Moro 2, I-00185 Roma, Italy.
phone: +39-06-49914770, Fax: +39-06-4957697
email: polimeni@roma1.infn.it

Phase separation and gap bowing in zinc-blende InGaN, InAlN, BGaN, and BAlN alloy layers

L.M.R. Scolfaro[1], J.R. Leite[1], L.K. Teles[1], J. Furthmüller[2], F. Bechstedt[2], T. Frey[3], D.J. As[3], and K. Lischka[3]

[1]Instituto de Física, Universidade de São Paulo, CP 66318, 05315-970 São Paulo, SP, Brazil
[2] Institut für Festkörpertheorie und Theoretische Optik, Friedrich-Schiller-Universität, D-07743, Jena, Germany
[3]Universität Paderborn, FB-6 Physik, D-33095 Paderborn, Germany

Alloying among the group-III nitride binary compounds is expected to lead a wide range of energy for band-gap engineering since one may change the band gap from 1.9 eV (InN) to 6.0 eV (AlN or BN). However, recent experiments have shown that contrary to the alloys formed with other III-Vs, nitride alloys derived from large mismatched binaries display significant gap bowing and undergo phase separation giving rise to large miscibility gaps. Such properties of InGaN, for example, play an important role on the radiative emission process taking place in the nitride-based commercial optoelectronic devices. Therefore, a deep understanding of these properties of InGaN and of other nitride alloys is highly desirable due to their importance for the modern electronic and optoelectronic device technology.

In this work we study the thermodynamic and electronic properties of the *zinc-blende* ternary alloys $In_xGa_{1-x}N$ and $In_xAl_{1-x}N$, as well as the boron-related $B_xGa_{1-x}N$ and $B_xAl_{1-x}N$ alloys. The mixing free energies, ΔF, and phase diagrams, T versus x were calculated by combining the cluster expansion method within the framework of the generalized quasi-chemical approximation (GQCA) and *ab initio* plane-wave pseudopotential total energy calculations [1]. Biaxial strain induced by the coherent growth of the layers on rigid buffer layers is taken into account in the calculations. The effects of strain on phase diagrams and gap bowing of the alloys are discussed. We also study the fundamental gaps versus composition. According to composition fluctuations in the considered chemically disordered systems we suggest the definition of different gaps, e.g. an averaged one and a minimum gap. They are measured in different experiments and exhibit different bowing parameters. Fig.1 shows the calculated phase diagram for $In_xGa_{1-x}N$ together with experimental data for the In-rich phase compositions as obtained from X-ray diffraction and resonant Raman spectroscopy measurements on cubic 300nm layers grown on GaAs(001) substrates by molecular beam epitaxy with x=0.07, 0.19, and 0.33. The agreement between theory and experiment is very good. In-rich phase with $x \approx 0.8$ is observed in the three samples as obtained from the calculated phase diagram. In Fig.2 the mixing free energy of $In_xGa_{1-x}N$ alloys is depicted for unstrained (a) and considering an inhomogeneous biaxial strain induced by a thick GaN buffer (b). A suppression of the phase separation due to strain is clearly seen. The band-gap bowing also shows a remarkable decrease. A large miscibility gap is observed for both BAlN and BGaN (see Fig.3) with a very high value for the critical temperature, ~ 9000 K. This result may explain the experimental findings which show successful growth of these boron-related alloys only for very small B content, x<0.02, for the growth temperatures T~1300 K. We also predict phase separation for InAlN alloys with a miscibility gap in the range $0.1 < x < 0.8$ for typical growth temperatures (Fig.4).

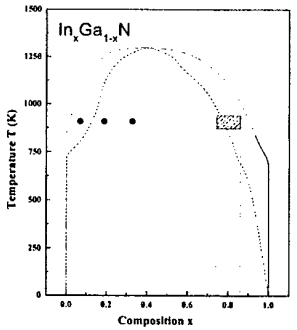

Fig. 1: Comparison between the measured values for the $In_xGa_{1-x}N$ alloy compositions and the calculated phase diagram. The horizontal dashed lines give the range of the growth temperatures. The circles denote the compositions of the samples, x=0.07, 0.19, and 0.33. The dashed rectangle denotes the observed In-rich phase.

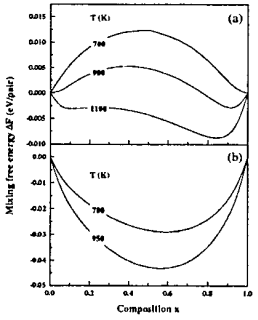

Fig. 2: Mixing free energy $\Delta F(x,T)$ of $In_xGa_{1-x}N$ alloys versus composition. (a) without strain; (b) with an inhomogeneous biaxial strain.

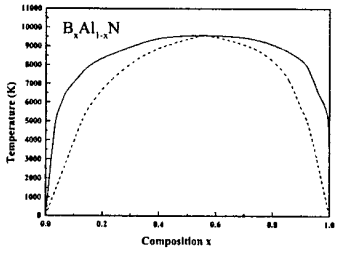

Fig. 3: T-x phase diagram of $B_xAl_{1-x}N$. Solid and dashed lines as in Fig.2.

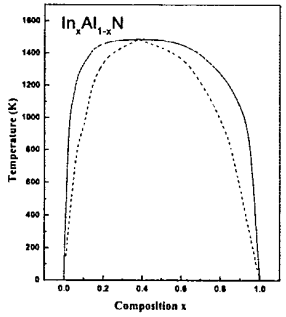

Fig. 4: T-x phase diagram of $In_xAl_{1-x}N$. Solid and dashed lines as in Fig.2.

References

[1] L.K. Teles, J. Furthmüller, L.M.R. Scolfaro, J.R. Leite, and F. Bechstedt, Phys. Rev. B 62, 2475 (2000); Phys. Rev. B 63, 5204 (2001).

Corresponding author: L.M.R. Scolfaro
Instituto de Física da USP, CP 66318, 05315-970 São Paulo, SP, Brazil
Phone: 55-11-38186997- Fax: 55-11-38186831
e-mail: scolfaro@macbeth.if.usp.br

Quantum dot photoluminescence from cubic GaN/InGaN/GaN heterostructures

K. Lischka[1], O. Husberg[1], A. Khartchenko[1], D.J. As[1], O. C. Noriega[2], A. Tabata[2], L. M. R. Scolfaro[2], J.R. Leite[2]

[1]*University of Paderborn, 33095 Paderborn, Germany*
[2]*Instituto de Fisica, Universidade de Sao Paulo, Sao Paulo-SP, Brazil*

Quantum wells (QW) containing InGaN form the active zone of light emitting devices based on wurtzite (hexagonal) group III-nitrides. Although these devices are produced commercially the mechanism of light generation is still subject of an ongoing discussion. The controversy is due to the fact that the luminescence from h-InGaN QWs is observed at energies significantly lower than the alloy band gap which is measured by absorption. The luminescence red shift has been explained to be due to excitons localized in Indium-rich regions [1]. A quite different approach [2] proposed that the photoluminescence (PL) red shift in strained InGaN QWs originate from band tail states which are induced by piezoelectric and spontaneous polarization fields. One of the distinguished physical properties of the cubic nitrides is the absence of electric fields due to spontaneous polarisation or piezoelectric effects in heterostructures. In InGaN with cubic crystal structure (c-InGaN) spontaneous polarization does not exist due to the higher crystal symmetry, and due to the (001) growth direction, strain-induced piezo electric fields are negligible. Therefore it has been suggested recently that investigations of cubic InGaN quantum wells which allow to eliminate the modulation due to the spontaneous and strain-induced electric fields are mandatory to understand the precise mechanism of light generation in InGaN quantum wells.[3] In this paper, we report a systematic investigation of the PL from c-GaN/InGaN/GaN double heterostructures with an In-content between x = 0.09 and x = 0.33. Our results demonstrate the importance of highly localized QD-like structures for the generation of luminescence light. The spectra in fig.1 show that the PL energy of the c-GaN/InGaN/GaN DH structures is almost independent of the In content of the InGaN layers. We find that the emission peak energy at room temperature is about 2.3 – 2.4 eV. HRXD measurements reveal that the InGaN layers (x = 0.09 – 0.33) contain a second In rich phase with x = 0.56 ± 0.02. Typical results are shown in fig.2. Since micro Raman experiments revealed clear evidence that these inclusions form nm sized QD like structures [4] we assume that the PL from our DH structures is due to the recombination of excitons localized at In rich QD like structures which are embedded in the InGaN layers. We are able to explain the PL peak energy and its shift with varying In content of the InGaN layers by assuming that the QD structures have an average size of about 15 nm. Our experiments reveal that the density of the dots is in the order of 10^{11} cm^{-2}. We can only speculate about the formation process of these QD like structures. However, since these structures have been observed in InGaN layers as well as in DH structures and thermal annealing of our samples did not affect the luminescence energy, we suppose that they may be formed in a phase separation process which is driven by the large difference between the lattice parameters of GaN and InN.[5,6]

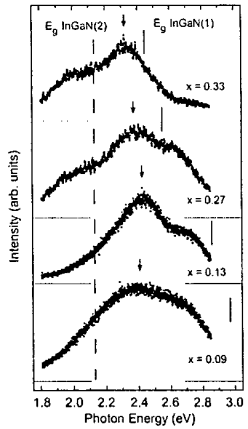

Fig.1: Room temperature photoluminescence spectra from four c-GaN/InGaN/GaN DH structures. The arrows mark the position of the maximum emission. The In-content and the gap energy of the InGaN(1) layers are indicated in the figure by vertical lines. The gap energy which corresponds to the strained In-rich phase, InGaN(2), is also shown.

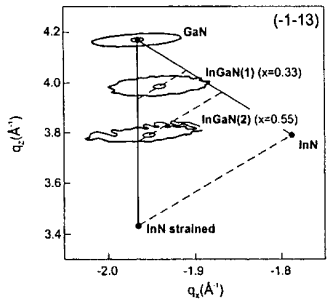

Fig. 2: The distribution of the scattered x-ray intensity in reciprocal space (reciprocal space map) of the asymmetric (-1-1 3) Bragg reflex of a c-GaN/InGaN/GaN DH structure. The curves show isointensity-contours of the maximum intensity and the half maximum intensity, respectively. The dots show the calculated positions of the GaN Bragg reflex and the Bragg reflex of fully relaxed and pseudomorphic InN. The dashed lines are the relaxation lines of InGaN layers of a given composition.

References

[1] S. F. Chichibu, K. Wada, J. Müllhäuser, O. Brandt, K. H. Ploog, T. Mizutani, A. Setoguchi, R. Naki, M. Sugiyama, H. Nakanishi, K. Korii, T. Deguchi, T. Sota, and S. Nakamura, Appl. Phys Lett. **76,** 1671 (2000).

[2] C. Wetzel, T. Takeuchi, H. Amano, and I. Akasaki, J. Appl. Phys. **85,** 3786 (1999).

[3] S. F. Chichibu, A. C. Abare, M. P. Mack, M. S. Minsky, T. Deguchi, D. Cohen, P. Kozodoy, S. B. Fleischer, S. Keller, J. S. Speck, E. Hu, U. K. Mishra, L. A. Coldren, S. P. DenBaars, K. Wada, T. Sota, and S. Nakamura, Mat. Science and Engineering **B59,** 298 (1999).

[4] V. Lemos, E. Silveira, J. R. Leite, A. Tabata, R. Trentin, L. M. R. Scolfaro, T. Frey, D. J. As, D. Schikora, and K. Lischka, Phys. Rev. Lett. **84,** 3666 (2000).

[5] I.-h. Ho and G. B. Stringfellow, Appl. Phys. Lett. 69, 2701-2703 (1996).

[6] L. K. Teles, J. Furthmüller, L. M. R. Scolfaro, J. R. Leite, and F. Bechstedt, Phys. Rev. B62, 2475 (2000); Phys. Rev. B63, March, (2001).

Corresponding author: Klaus Lischka, University of Paderborn, 33095 Paderborn, Germany.
phone: +49 5251 60 3565, Fax: +49 5251 60 3490
email: Lischka@uni-paderborn.de

The effects of adjacent dislocations on the electronic and optical properties of GaN/AlN quantum dots

A. D. Andreev [1,3], J. R. Downes[2] and E. P. O'Reilly [3]

[1] A. F. Ioffe Institute, St.-Petersburg 194021, Russia, email: a.andreev@surrey.ac.uk
[2] Queen Mary, University of London, London, E1 4NS, UK
[3] Department of Physics, University of Surrey, Guildford, GU2 7XH, UK

The wide band gap semiconductors, which form the basis of the blue laser, are increasingly important device materials. Stranski-Krastanow GaN quantum dots grown on AlN are now being studied [1]. Aside from their wide band gap, the nitrides have several unusual characteristics compared to more common III-V semiconductors; these differences affect the properties of the dots. Device-quality GaN has a very high density of threading dislocations, typically as high as ~10^8 – 10^{11} cm^{-2} [2]. The wurtzite (hexagonal) crystal structure of III-N alloys means that they not only exhibit piezoelectricity but also spontaneous polarization effects. Photoluminescence experiments on a range of differently sized GaN dots has shown that the PL maximum of large dots is red shifted ~ 0.5 eV below the bulk GaN band gap [1]. Such a large red shift may arise from built-in piezoelectric and spontaneous polarization effects. Transmission electron microscopy studies of the dots have shown that each dot tends to nucleate adjacent to a threading dislocation [2]. This is probably because the distorted lattice around the dislocation provides a favorable template for the growth of the lattice-mismatched GaN inclusions. It is clearly important to include both these effects in any analysis of the electronic and optical properties of the dots.

In this paper, we present a theory of the electronic energy levels and wavefunctions within GaN dots, including the effect of the strain field of the nearby dislocation and a full treatment of the built-in electrostatic potential. The QD carrier spectra and wavefunctions are calculated using a plane-wave expansion method within an 8-band **k.p** model. The method is very efficient, because the strain and built-in electric fields can be included through their discrete Fourier transforms [3]. The QD structures considered have been previously analysed experimentally [1,2]. The GaN QDs are truncated hexagonal pyramids on a wetting layer with an edge dislocation adjacent to each dot (see Fig.1). The built-in piezoelectric potential strongly influences the localisation of the carrier wavefunctions. The potential pushes the electrons to the top of the dot, the holes to the bottom and, additionally, causes strong lateral confinement of the carriers near the dot center. The strong lateral confinement of the carriers, means that the effect of the strain field due to the dislocation is relatively small. Figure 2 shows the electron and hole wavefunctions in the GaN/AlN QDs. Results are presented for the confined state energies and optical matrix elements for a range of different sized dots with and without dislocations. The size of the dot influences the energies and overlaps, but the presence of the dislocation has minimal effect. The dependence of the ground state optical transition energy on the size of the dot is in good agreement with experimental data.

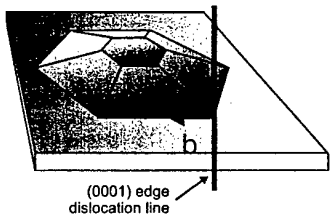

Fig. 1: Schematic view of a GaN quantum dot in an AlN matrix with an adjacent dislocation. The dislocation line points in the (0001) direction and the Burger vector is along one of the dot edges.

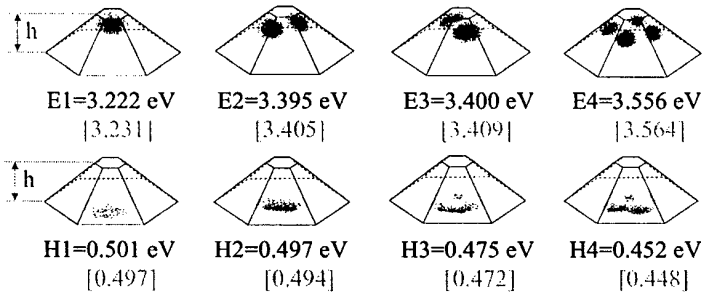

Fig. 2: Energies and contours of constant probability density for electron and hole states in a quantum dot with an adjacent dislocation. The dot height is h=3.6 nm. The energies of a dot without an adjacent dislocation are shown in square brackets. The probability density distributions for a dot without a dislocation would be indistinguishable from those shown here.

References

[1] F. Widmann, J. Simon, D. Daudin, G. Feuillet, J. L. Rouviere, N. T. Pelekanos, G. Fishman, Phys. Rev. B., **58**, 15989 (1998)
[2] J. L. Rouviere, J. Simon, N. Pelekanos, B. Daudin, and G. Feuillet, Appl. Phys. Lett., **75**, 2632 (1999)
[3] A. D. Andreev and E. P. O'Reilly, Phys.Rev. B, **62**, 15851 (2000)

Corresponding author: Aleksey ANDREEV, Physics Department, University of Surrey, Guildford, GU2 7XH, United Kingdom.
phone: +44 1483 879402, Fax: +44 1483 876781
email: a.andreev@surrey.ac.uk

AlN/GaN Short-Period Superlattices with Monolayer AlN for Optical-Device Applications

A.Ishida, M.Kitano, T.Ose, H.Nagasawa, K.Ishino, Y.Inoue, and H.Fujiyasu
Faculty of Engineering, Shizuoka University, 3-5-1 Johoku, Hamamatsu 432, Japan
Tel:+81-53-478-1104, Fax:+81-53-478-1005, E-Mail:tdaishi@ipc.shizuoka.ac.jp
H. Kan
Central Research Lab., HPK, Hirakuchi 5000, Hamakita 434-8601, Japan
H.Makino and T.Yao
Institute for Materials Research, Tohoku University, Sendai 980-8577, Japan

AlN/GaN short-period superlattices with atomic layer AlN have large subband broadening in the conduction band and relatively small piezoelectric effect owing to the short superlattice period and small strain in the GaN wells. They have great potential for applications to optical devices such as light emitting devices in the ultraviolet and mid-infrared regions via interband and intersubband electron transitions, respectively. The applications to optical modulators in the optical fiber communication region are also expected, where the intersubband optical transition at $k=\pi/L$ (L:superlattice period of $(AlN)_1/(GaN)_n(n\cong10)$) corresponds to the mid infrared region, while the optical transition at k=0 corresponds to the optical fiber communication region (Fig.2).

A series of AlN/GaN short-period superlattices with monolayer AlN were prepared by hot-wall epitaxy (HWE). The superlattice structure was confirmed by x-ray diffraction through a comparison between the measured diffraction curves and simulated ones (Fig.1), which indicates good controllability of the HWE technique. Interband photoluminescence (PL) and photoluminescence excitation (PLE) spectra were measured (Fig. 3). Relatively strong PL emissions compared with conventional AlGaN/GaN superlattices were observed, which can be attributed to the small piezoelectric effect. A small Stokes shift should be noted, which may suggest small interface fluctuation in consistence with the XRD observation. The energy shifts of the band edge emission with the GaN well thickness agree well with the calculated results within the envelope wave-function framework at least for the well thickness above 2 nm (Fig.4).

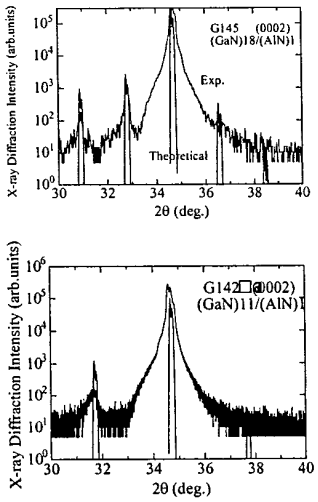

Fig.1. Experimental and theoretical x-ray diffraction patterns of $(AlN)_1/(GaN)_n$ superlattices.

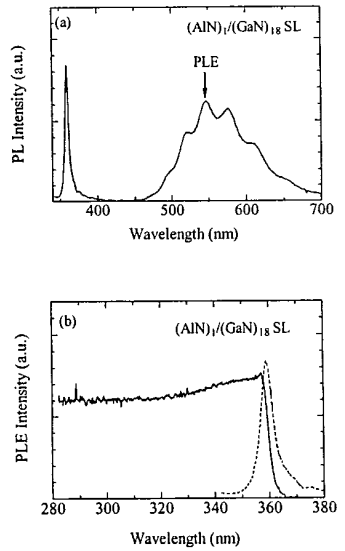

Fig.3. PL and PLE spectra of the $(AlN)_1/(GaN)_{18}$ superlattice.

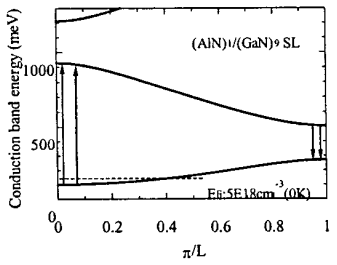

Fig.2. Conduction subband structure of the $(AlN)_1/(GaN)_9$ superlattice. Optical absorption of fiber communication region is expected at k=0, and mid-infrared optical emission is expected at $k=\pi/L$.

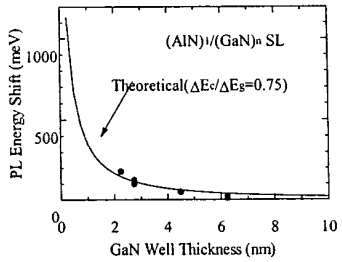

Fig.4. Dependence of band-edge PL energy shift of $(AlN)_1/(GaN)_n$ super-lattices on GaN well thickness.

Gain Characteristics of Ideal Dilute Nitride Quantum Well Lasers

S. Tomić and E.P. O'Reilly

Department of Physics, University of Surrey, Guildford, Surrey GU2 7XH,United Kingdom

Recently, dilute nitride GaNAs and InGaNAs compounds have been proposed as new semiconductor materials for the realisation of semiconductor quantum well (QW)laser diodes emitting in the 1.3 μm optical window. Because these compounds can be grown as quantum wells on a GaAs substrate, they can be incorporated into vertical cavity surface emitting laser (VCSEL) structures, using AlGaAs/GaAs Bragg mirrors with high refractive index contrast to acheive electrically pumped monolithic VCSELs at telecommunication wavelengths [1]. In addition, the inclusion of a small amount of nitrogen in the InGaNAs layers increases the conduction band offset, leading to improved electron confinement and decreased electron spill out at room temperature and above when compared with conventional InGaAsP/InP 1.3 μm lasers. We present here a detailed theoretical analysis of the gain as a function of carrier density and radiative current density in ideal GaNAs/GaAs and InGaNAs/GaAs quantum well structures, highlighting how the changes in band structure modify the gain characteristics compared to conventional laser structures.

The energy gap initially decreases rapidly when a small fraction of arsenic atoms are replaced by nitrogen to form GaN_xAs_{1-x} and $In_yGa_{1-y}N_xAs_{1-x}$. This reduction (of about 0.1 eV per % of N for $x <\sim 0.03$) occurs because of an anti-crossing interaction between the conduction band edge and a higher-lying nitrogen resonant band [2]. We have shown that it is necessary to introduce a modified 10-band $\mathbf{k}\cdot\mathbf{P}$ Hamiltonian to describe the band dispersion in these compounds, adding two spin-degenerate nitrogen states to the conventional 8-band $\mathbf{k}\cdot\mathbf{P}$ Hamiltonian to account for the band-gap reduction and modified conduction band dispersion [3]. The model gives excellent agreement with photomodulated reflectance measurements of the ground and excited state transition energies in GaNAs/GaAs quantum well (QW) structures [4]. We apply the modified Hamiltonian here to analyse the absorption and gain characteristics of GaNAs and InGaNAs bulk and QW structures. The coupling between the N level and the conduction band edge reduces the interband transition matrix elements compared to a conventional III-V alloy; with coupling between the N levels and valence band edge reducing the matrix elements by about a further 10% in the case of GaNAs. The nitrogen-conduction and nitrogen-valence coupling leads to an increased conduction band effective mass and band nonparabolicity. As a consequence the peak gain decreases at a fixed carrier density when compared to an equivalent conventional QW structure. However because of the reduced interband matrix element, there is far less variation in gain as a function of radiative current density between the different structures considered, and the gain saturates at a similar level in the N-based and equivalent conventional QW structures considered. The conduction band non-parabolicity increases the temperature dependence of the transparency carrier density in dilute nitride QWs compared to equivalent conventional QWs. Nevertheless, the gain characteristics of ideal dilute nitride QWs are comparable to those of conventional structures, confirming their potential for optoelectronic devices based on GaAs at the technologically important wavelengths of 1.3 and 1.55 μm.

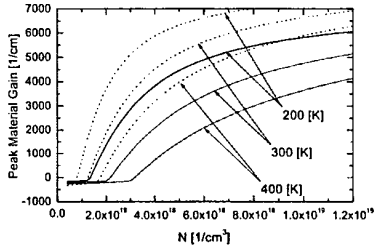

Figure 1: The temperature dependence of the peak material TE gain in a 6 nm $In_{0.3}Ga_{0.7}N_{0.02}As_{0.98}$ QW as a function of carrier density (solid line). Dotted lines are the same dependence but for an equivalent nitrogen-free structure.

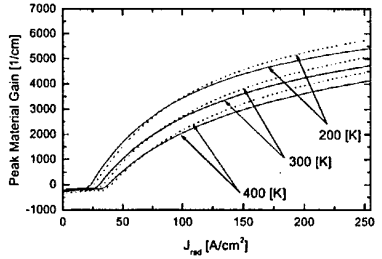

Figure 2: The temperature dependence of the peak material TE gain as a function of radiative current density. Solid lines represent 2% nitrogen and dotted lines nitrogen-free structure.

References

[1] G. Steinle, H. Riechert and A. Yu. Egorov, Electron. Lett. **37**, 93 (2001)
[2] W. Shan *et al.*, Phys. Rev. Lett. **82**, 1221 (1999).
[3] E.P. O'Reilly and A. Lindsay, phys. stat. sol. (b) **216**, 131 (1999).
[4] P.J. Klar *et al.*, phys. stat. sol. (b) **223**, 163 (2001).

Corresponding author: Stanko Tomić, Department of Physics, University of Surrey, Guildford, Surrey GU2 7XH,United Kingdom.
phone: +44 1483 879402, Fax: +44 1483 876781,
email: s.tomic@surrey.ac.uk

Strong graded interface related piezoelectric polarization weakening effects on exciton confinement in single $In_xGa_{1-x}N/GaN$ quantum wells

Ewerton Wagner Santos Caetano, Valder Nogueira Freire, Gil de Aquino Farias

Departamento de Física, Universidade Federal do Ceará,
Caixa Postal 6030, Campus do Pici, 60455-760, Fortaleza, Ceará, Brazil

The fabrication of III-V nitrides (InN, GaN, AlN) based optoelectronic devices emitting in the green-blue-violet range of spectrum caused strong impact on the semiconductor research community [1]. Various hypotheses were raised to explain the optical properties of these materials and their heterostructures, but there is no consensus nowadays about which is the correct one. For $In_xGa_{1-x}N/GaN$ wurtzite quantum wells, the more accepted explanations are [2]: (i) the compositional fluctuation picture – low miscibility of InN in GaN creates dot-like structures in which the carriers recombinate; (ii) the piezoelectric polarization picture – intense electric fields (MV/cm) are generated by the piezoelectric polarization, causing a very strong quantum confined Stark effect (QCSE).

Recently, Lakner *et al.* [3] investigated the In molar fraction profile in InGaN/GaN quantum wells using scanning tunneling electron microscopy (STEM). They verified the existence of asymmetrical gradual interfaces in these structures, with thickness starting at 1 nm. Wang *et al.*[4] showed that the existence of graded interfaces in single GaN/AlGaN quantum wells can blue shift very strongly the energy of the confined carriers and of their associated excitons. These results point to the need to consider how the existence of graded interfaces can change the carriers and exciton confinement in wurtzite $In_xGa_{1-x}N/GaN$ single quantum wells.

In this work, we present results on how the existence of graded interfaces acts by decreasing the piezoelectric polarization (weakening the internal electric field) and consequently changing the carriers and exciton confinement energies in wurtzite $In_{0.2}Ga_{0.8}N/GaN$ single quantum wells. The redshift of the exciton energy is remarkable, and it is caused by the intense internal electric field. When the existence of graded interfaces is considered, the redshift of the exciton energy is strongly attenuated, which is due to the graded interface related weakening of the polarization field. Our results strongly suggest that the role of the graded interfaces on the confinement properties of single $In_xGa_{1-x}N/GaN$ quantum wells are more important than the uncertainty of some important parameters like the carriers effective mass and the band offset. As a matter of fact, a thin graded interface of only 1 nm can blue shift the exciton energy in wurtzite $In_{0.2}Ga_{0.8}N/GaN$ single quantum wells by as much as 400 meV.

References

[1] S. Nakamura and G. Fasol, The Blue Laser Diode, Springer-Verlag, Heidelberg, 1997.
[2] J. A. Davidson, P. Dawson, T. Wang, T. Sugahara, J. W. Orton, and S. Sakai, Semicond. Sci. Technol. **15**, 497-505 (2000).
[3] H. Lakner, G. Brockt, C. Mendorf, A. Radefeld, F. Scholz, V. Harle, J. Off, and A. Sohmer, Journal of Electronic Materials **26**, 1103 (1997).
[4] H. Wang, G. A. Farias, V. N. Freire, Phys. Rev. B **60**, 5705 (1999).

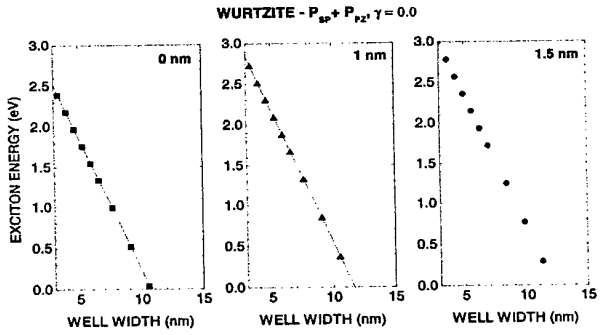

Fig 1. Confined exciton energy in wurtzite $In_{0.2}Ga_{0.8}N/GaN$ single quantum wells with graded interface thickness of 0, 1, and 1.5 nm. The interface related reduction of the strain was not considered.

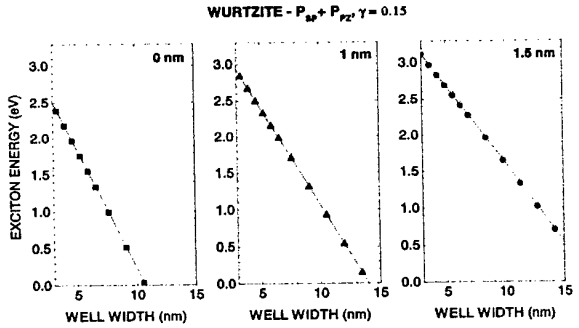

Fig 2. Confined exciton energy in wurtzite $In_{0.2}Ga_{0.8}N/GaN$ single quantum wells with graded interface thickness of 0, 1, and 1.5 nm. The interface related reduction of the strain was considered.

Corresponding author: Valder Nogueira Freire, Departamento de Física, Universidade Federal do Ceará, Caixa Postal 6030, Campus do Pici, 60455-760, Fortaleza, Ceará, Brazil.
phone: +55 85 288 9937, Fax: +55 85 288 9903
email: valder@fisica.ufc.br

Gate voltage dependence of subband structure in a two-dimensional electron gas in AlGaN/GaN heterostructures

K. Tsubaki, N. Maeda, T. Saitoh, T. Nishida, and N. Kobayashi
NTT Basic Research Laboratories
3-1 Morinosato-Wakamiya, Atsugi-shi, Kanagawa 243-0198, Japan

AlGaN/GaN heterostructure devices have recently been attracting much attention because of their potential for high-voltage, high-power, and high-temperature microwave applications. [1-3] Therefore, the electronic properties of a two-dimensional electron gas (2DEG) in AlGaN/GaN heterostructures have recently been discussed. [4-7] In this paper we describe for the first time measurements of the gate-voltage dependence of the 2DEG's magnetoresistance and discuss the detailed subband structure of the 2DEG.

The AlGaN/GaN heterostructures are grown by low-pressure metal-organic chemical vapour phase epitaxy on (0001) SiC substrate using AlN buffers. The epitaxial layers consist of non-doped GaN (1000nm), non-doped $Al_{0.15}Ga_{0.85}N$ (2nm) and Si-doped $Al_{0.15}Ga_{0.85}N$ (28nm). The electron concentration and the mobility obtained from Hall measurements at 4.2 K are $6.8\times10^{12}cm^{-2}$, and 9300 cm^2/Vs, respectively. After Hall-bar-structures are defined by photolithography and subsequent dry etching, Al/Au current contacts and voltage probes are formed by vacuum evaporation. The backgate electrode (Ti/Au) is then deposited on the substrate. The backgate voltage (V_B) can control the current (I) as shown in Fig.1. Magnetoresistance is measured at a temperature of 0.3K up to a magnetic filed of 8T using a small AC current by applying a backgate voltage from 0V to –20V.

From the magnetoresistance as a function of inverse magnetic filed shown in Fig. 2, observed two kinds of periodic oscillations suggest the existence of 0th and 1st subbands. The Fourier transformation of the magnetoresistance for V_B =-20, -10, 0V is shown in Fig. 3. While the position of main peak is independent of V_B, the position of the side peak depends on V_B. The peak-position dependence on V_B is shown in Fig.4. Since the main peak corresponds to electrons occupying the 0th subband, the electron concentration in the 0th subband (N_o) is independent of V_B. Due to the negative slope of the position of the side peak, we deduce that the side peak corresponds to the difference in electron concentration between N_o and N_1 (the electron concentration of the 1st subband). N_1 is proportional to gate voltage. Similar behaviour is well established for 2DEG in AlGaAs/GaAs heterostructures. [8]

References. [1] N. Maeda *et al.*, Jpn. J. Appl. Phys. **38**, L987 (1999). [2] N. Maeda *et al.*, Jpn. J. Appl. Phys. **38**, L799 (1999). [3] N. Maeda *et al.*, Appl. Phys. Lett. **76**, 3118 (2000). [4] T. Wang *et al.*, Appl. Phys. Lett. **74**, 3531 (1999). [5] I.P. Smorchkova *et al.* J. Appl. Phys. 86, 4520 (1999). [6] Z. W. Zheng *et al.*, Phys. Rev. B **62**, R7739 (2000). [7] K. Tsubaki *et al.*, *Int. Conf. Phys. Semiconductors*, Osaka, 2000, H248. [8] H. L. Störmer *et al.*, Solid State Comm. **41**, 707, (1982).

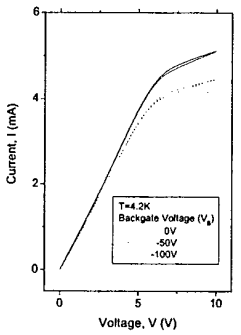

Fig.1. I-V characteristics of the sample. The backgate voltage can control the current.

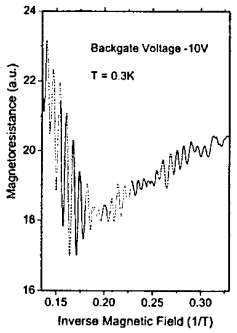

Fig.2. Magnetoresistance plot with the background extracted as a function of inverse magnetic field. Observed two kinds of periodic oscillations indicate the existence of 0th and 1st subbands.

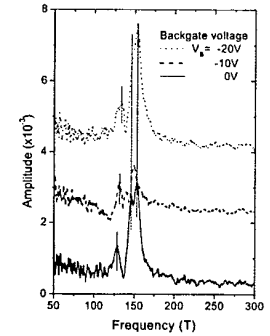

Fig. 3. Fourier transformation of magnetoresistance for various values of V_B. While the position of the main peak is independent of V_B, the position of the side peak depends on V_B.

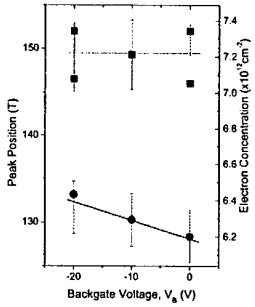

Fig. 4. The position of the main and side peak vs. V_B. Right hand-side vertical axis shows electron concentration. The main peak and side peak correspond to $N_o=7.2\times10^{12}cm^{-2}$, and N_o - N_1, respectively.

Corresponding author: Kotaro Tsubaki, NTT Basic Research Laboratories,
3-1 Morinosato-Wakamiya Atsugi-shi Kanagawa, 243-0198 Japan,
tel: +81-46-240-3418, fax: +81-46-240-4723
E-mail: tsubaki@will.brl.ntt.co.jp

Quantum gates using tunneling electron spins of a quantum-dot-chain

S. Muto, H. Sasakura, S. Adachi, Y. Kajiwara and K. Shiramine
Department of Applied Physics,
Hokkaido University, N13 W8 Kitaku, Sapporo 060-8628, Japan

Quantum computation using tunneling qubits: tunneling of electrons whose spins work as qubits is described by the Hamiltonian using both electron spins and pseudospins representing the photon-assisted tunneling. The phase factor during the controlled-NOT operation is also discussed.

An electron spin of semiconductor quantum dot (QD) is a good candidate for the qubit and quantum gates based on its exchange interaction have already been proposed. In contrast, we have proposed another way of using electron spins of QDs which uses the photon-assisted tunneling and its Coulomb blockade to realize the controlled-NOT (CNOT) operation [1]. Although the model can be extended to arbitrary number of qubits in a quantum dot chain, the elementary unit can be described by triply-coupled quantum dots in series. Due to the size dependence of quantization energy and Zeeman energy of quantum dot, the energy separations of 6 states of triple quantum dots under static magnetic field can be all different if the size of 3 dots are different (Fig. 1). The spins of 2 electrons: one in the dot "1" and the other in the dot "3", act as the qubits. By the difference of the Zeeman energy of individual dot, we can selectively rotate the electron spins by using the oscillatory magnetic field resonant to the Zeeman splitting (1-bit rotation) as in the electron spin resonance experiments. Also, by applying terahertz optical π-pulse whose electric field is in the direction of QD chain, an electron can tunnel through the barrier from both sides to the dot "2" without changing the spin state (C_1-C_3). We can select a path of the photon-assisted tunneling by the difference of the transition energy. Since this tunneling is the Rabi oscillation of intersubband transition under the resonant optical field, it can be described by a pseudo-spin whose equation of motion is described by the optical Bloch equation. In this way, the Hamiltonian of the system of Fig. 1 is given by

$$H = H_M + H_E + H_C.$$

Here, H_M indicates isolated spins under static and oscillatory magnetic field and is given by,

$$H_M = E_1(\sigma^{(1)})(1-\sigma_z^{(12)})/2 + E_2(\sigma^{(1)})(1+\sigma_z^{(12)})/2 + E_2(\sigma^{(3)})(1+\sigma_z^{(23)})/2 + E_3(\sigma^{(3)})(1-\sigma_z^{(23)})/2.$$

Here, $\sigma^{(12)}$ ($\sigma^{(23)}$) denotes the Pauli matrix of a pseudo-spin describing the tunneling between 1-2 (3-2) dots, $\sigma^{(1)}$($\sigma^{(3)}$) denotes Pauli spin matrix of electron which is localized at the dot "1" ("3"), and E_i (i=1,2 and 3) denotes the energy of electron spin localized at the i-th dot, and is given by,

$$E_i(\sigma) = E_i(0) + \sigma_z\mu_B g_i B/2 + \sigma_x\mu_B g_i B_r\cos\omega t.$$

H_E indicates the effect of teraherz radiation under the electric dipole approximation, and is given by

$$H_E = \sigma_x^{(12)}\mu_{12}E_z\cos\omega_p t + \sigma_x^{(32)}\mu_{32}E_z\cos\omega_p t.$$

H_C represents the Coulomb blockade of 2 electrons within the dot "2", and is given by

$$H_C = U(1 + \sigma_z^{(12)})(1 + \sigma_z^{(23)})/4.$$

The CNOT gate in which the spin $\sigma^{(1)}$ acts as the control bit and the $\sigma^{(3)}$ as the target bit, is realized by the unitary operation $C_1C_2C_3R_TC_3C_2C_1$ in Fig. 1. Figure 2 shows the flow of states created by the operation. Note that only a single (optical or magnetic) π-pulse is applied at one time. Therefore, the flow consists of flipping of either electron spin or pseudo-spin. The net result is that the $\sigma^{(3)}$ is inverted only when the spin $\sigma^{(1)}$ is in the state $|1>$, namely the CNOT operation. The areas in Fig. 2 also illustrate the phase factor during the gate operation. A (not necessary but) sufficient condition to cancel these phases is to make all 4 shaded areas 0 (mod 2π), which is possible by adjusting the 4 time intervals, t_1-t_3, and t_R.

Extension to a QD chain with many qubits is straight forward, and it is shown that it can be extended to a QD chain with more than 100 QDs (50 qubits) using the energy selectivity.

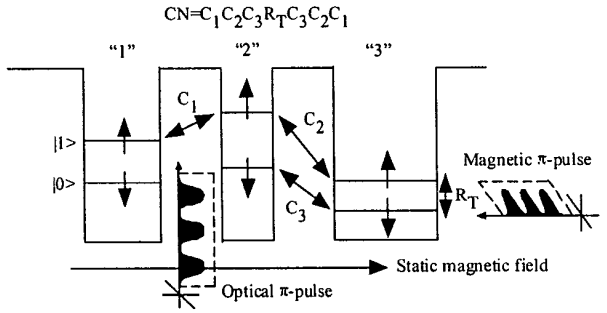

Fig. 1: Optical transitions (photon-assisted tunneling), C_1-C_3, and spin inversion, R_T, used to realize the controlled-NOT with 6 levels of electrons confined in three quantum dots.

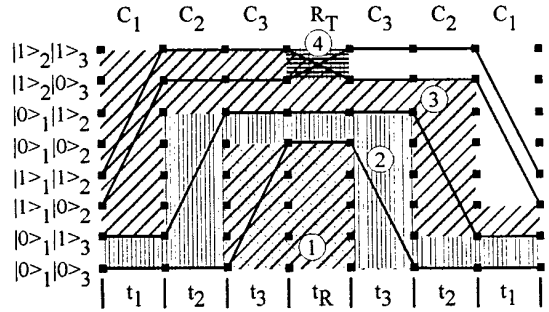

Fig. 2: Two-electron spin-states realized during the controlled-NOT operation. The longitudinal represents the energy of states for the phase change.

Reference

[1] H. Sasakura and S. Muto: Los Alamos preprint archive (quant-ph/9910100).

Corresponding author: Shunichi Muto, Department of Applied Physics,
Hokkaido University, N13 W8 Kitaku, Sapporo 060-8628, Japan
phone: +81 11 706 7129, Fax: +81 11 706 7129, Email: GFD01102@nifty.ne.jp

Quantum Information Processing with Semiconductor Macroatoms

Irene D'Amico[1], Eliana Biolatti[2], Ehoud Pazy[1], Paolo Zanardi[1], and Fausto Rossi[1,2]

[1] Institute for Scientific Interchange (ISI),
Villa Gualino, Viale Settimio Severo 65, I-10133 Torino, Italy
[2] Dipartimento di Fisica, Politecnico di Torino, C.so Duca degli Abruzzi 24,
I-10129 Torino, Italy

Any physical implementation of quantum-computation schemes taking actual advantage from the additional power provided by quantum theory [1] is known to be extremely demanding; One should be able to perform, on a system with a well-defined state space, long coherent quantum manipulations (*gating*), precise quantum-state synthesis and detection as well. Ever since the very beginning it has been recognized that the major obstacle arises from the unavoidable open character of any realistic quantum system. The coupling to external (i.e., non computational) degrees of freedom spoils the unitary structure of quantum evolution, which is the crucial ingredient in quantum computation (QC). This is the well-known decoherence problem. Mostly due to the need of low decoherence rates, the up-to-date proposals for experimental realizations of quantum processors are based on quantum optics as well as atomic and molecular systems. It is however generally believed that future applications of quantum information may hardly be realized in terms of such systems, which do not permit the large-scale integration of existing microelectronics technology. In contrast, in spite of the serious difficulties related to the "fast" decoherence times, a solid-state implementation of QC seems to be the only way to benefit synergistically from the recent progress in ultrafast optoelectronics as well as in nanostructure fabrication and characterization [2].

Following this spirit, in this contribution we present a recent proposal [3] for the implementation of quantum computation/information with semiconductor quantum dots. As for the case of the semiconductor-based implementation of noiseless quantum codes recently proposed in [4], the quantum hardware considered is an array of Coulomb-coupled quantum dots. Here, we choose as computational degrees of freedom interband optical excitations connecting the lowest electron and hole states of each quantum dot, i.e., the ground-state excitons. Single- as well as two-qubit operations are performed by means of properly tailored multi-color trains of ultrafast laser pulses (see figure) exploiting inter-dot energy-renormalisation effects due to exciton-exciton coupling. The density-matrix formalism used in our simulated experiments allows to properly describe the interplay between coherent evolution and dephasing, i.e., phase-breaking, processes, thus identifying the typical operation time-scales.

Finally, we shall discuss a potential scheme for the measurement of the computational state, based on a quantum-dot "storage qubit".

[1] See, e.g., D.P. DiVincenzo and C. Bennet, Nature **404**, 247 (2000).
[2] N.H. Bonadeo *et al.*, Science **282**, 1473 (1998).
[3] E. Biolatti, R.C. Iotti, P. Zanardi, and F. Rossi, Phys. Rev. Lett. **85**, 5647 (2000).
[4] P. Zanardi and F. Rossi, Phys. Rev. Lett. **81**, 4752 (1998).

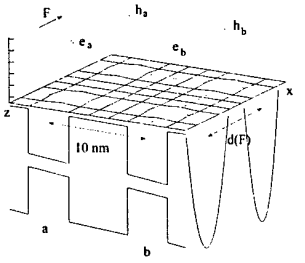

Schematic representation of the square-like potential profile for electrons and holes along the growth direction and of the parabolic in-plane potential. The square-well profile is tailored in such a way to allow for an energy selective creation/destruction of excitons in dots a and b. Moreover, the inter-dot barrier is such to prevent single-particle tunnelling and at the same time to allow for significant inter-dot Coulomb coupling. The three-dimensional scheme of the spatial charge distributions of electrons (e_a and e_b) and holes (h_a and h_b) corresponds to the biexcitonic ground state. The charge separation induced by the electric field F increases the average distance between electrons and holes, thus decreasing their attractive interaction. On the other hand, the repulsive terms are basically field independent. This is the origin of the positive energy difference $\Delta\mathcal{E}$.

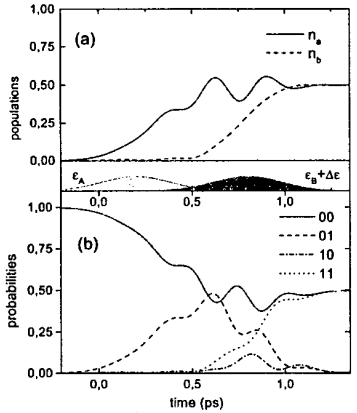

Time-dependent simulation of single (unconditional) plus two-qubit (conditional) operations. Initially the system is in the state $|0,0\rangle \equiv |0\rangle_a \otimes |0\rangle_b$. The first laser pulse (at $t = 0.2$ ps) is tailored in such a way to induce a $\frac{\pi}{2}$ rotation of the qubit a: $|0,0\rangle \rightarrow (|0,0\rangle + |1,0\rangle)/\sqrt{2}$. At time $t = 0.8$ ps a second pulse induces a conditional π-rotation of the qubit b: $|0,0\rangle + |1,0\rangle \rightarrow |0,0\rangle + |1,1\rangle$. This last operation plays a central role in any quantum information processing, since it transforms a factorized state $((|0\rangle + |1\rangle) \otimes |0\rangle)$ into an entangled state. The scenario described so far is confirmed by the time evolution of the exciton occupation numbers n_a and n_b reported in (a) as well as of the diagonal elements of the density matrix (in our four-dimensional computational basis) reported in (b). The two-color laser pulse sequence is also sketched schematically.

Intrinsic dipole-dipole excitonic coupling in GaN quantum dots: application to quantum information processing

S.De Rinaldis[1)], R.Rinaldi, R.Cingolani

INFM-Unita' di Lecce-Dipartimento di Ingegneria dell'Innovazione, Universita' di Lecce,via Arnesano,73100 Lecce,Italy

1)also with ISUFI-Istituto superiore universitario per la formazione interdisciplinare,via Arnesano,73100 Lecce, Italy

I.D'Amico

Institute for Scientific Interchange (ISI), Villa Gualino, I-10133 Torino, Italy

E. Biolatti and F. Rossi

INFM and Dipartimento di Fisica, Politecnico di Torino, I-10129 Torino, Italy

In this contribution we propose to use GaN coupled quantum dots as prototypical hardware for the experimental realization of the fully-optical semiconductor-based implementation of quantum information processing described in [1].

In the proposed implementation the prototypical quantum bit is based on optically created excitons in GaN quantum dots. In GaN quantum dots a giant built-in electric field is formed due to spontaneous polarization, arising from the ionic nature of the crystal, and piezoelectric effects, due to strain and vicinal high index surfaces delimiting the dots. Fields as high as 1 MV/cm can routinely be achieved in these nanostructures. The two level quantum system for performing computation exploits the following charge degrees of freedom: $|1\rangle$ is a state with one ground level exciton in a dot, whereas $|0\rangle$ corresponds to an empty dot.

Coulomb interactions between excitons of first neighbour vertically-coupled quantum dots is the essential mechanism creating entangled states. The Coulomb interaction in GaN dots is strongly enhanced by the intrinsic dipole moment along the growth direction. In order to explain the proposal it is enough to examine a model with two vertically coupled GaN quantum dots.

The distance between the dots is tailored to preserve their electronic structure as individual quantum dots and tunneling of charge from one dot to the other dot is not allowed. Quantum operations are then achieved by modern ultra-fast coherent carrier control methods. This idea is scalable to an array of dots and it does not employ any external (electric or magnetic) field, but only the peculiar properties of nitride materials.

The physical mechanism at the base of this model is that the presence of an electron-hole pair in one dot shifts the absorption line of the ground level exciton in the other dot by means of Coulomb interaction. The generation of an e-h pair in a GaN dot having an height of 4 nm are the base of our theoretical calculation. This shift is enough to resonantly excite only one level at time with a 100fs pulse laser. The strong shift is due to the giant internal electric fields[2] of about 5.5MV/cm that localize the electron(hole) wavefunction on the top(bottom)of the dot.

To create maximally entangled $|00\rangle+|11\rangle$ states a sequence of two laser pulses is needed: the first resonant to the ground state energy of one dot, the second to the absorption line of the ground state of the neighbour dot in presence of an exciton in the first dot.

1-E.Biolatti,R.C.Iotti,P.Zanardi,F.Rossi,Phys.Rev.Lett.,85,pp.5647-5650(2000)

2-F.Widmann,J.Simon,B.Daudin,G.Feuillet,J.L.Rouviere,N.T.Pelekanos,G.Fishman, Phys.Rev.B,58,pp.15989-15992(1998)

3-A.D.Andreev,E.P.O'Really,Phys.Rev.B,62,pp.15851-15869(2000)

Designing heterostructures with predefined value of light-hole g factor for coherent solid-state quantum receiver

Andrey A. Kiselev[1], Ki Wook Kim[1], and Eli Yablonovitch[2],

[1] Department of Electrical and Computer Engineering, North Carolina State University, Raleigh, North Carolina 27695-7911, USA

[2] Department of Electrical Engineering, University of California, Los Angeles, Los Angeles, California 90024, USA

In the context of a proposed design of a solid-state receiver for quantum communications [1], we consider the Zeeman splitting of the light-hole (LH) states in strained cubic heterostructures with an in-plane external magnetic field. The choice of interband optical transitions that allows coherent transfer of photon polarization to electron spin suggests that the magnitude of corresponding g factor component will be a critically important quantity for the success of such devices.

No work has been done for the light-hole (LH) states to the best of the authors knowledge. That is due, in part, to the fact that the much smaller effective mass and resulting higher quantization energies (compared to those for HHs) make it difficult even to detect LH states in typical heterostructures. Applied or lattice-mismatch-induced intrinsic strain can reverse this situation making LH the ground hole state in the structure with a QW. In this paper, we give a consistent theoretical analysis of the in-plane Zeeman effect for quantum-confined LH holes and evaluate possibilities to design structures with desired property of large g factor for these valence states.

Our approach allows a straightforward calculation of this parameter in the framework of the sophisticated 8×8 **kp** model and incorporates the quantum confinement, heterolayers composition, and strain effects on the g factor. We specifically analyze InGaAs/InP both lattice-matched and strained heterosystems suitable for 1.3 and 1.55 μm optoelectronic applications. Our calculation gives g factor dependencies that are steep at small layer thicknesses, but asymptotically approach their respective "bulk" values in wide QWs. At narrow well widths the in-plane LH g factor crosses zero for our InGaAs/InP heterosystem choice. In this case, there will be no Zeeman splitting of the spin-up and spin-down LH states. For the purposes of the quantum receiver, one should avoid this region of well widths. At the same time, we have shown that it is feasible to keep the g factor at a reasonably large value for a broad range of structure widths.

Acknowledgements — This work has been supported, in part, by the Defense Advanced Research Projects Agency and the Office of Naval Research.

References

[1] R. Vrijen and E. Yablonovitch, quant-ph/0004078 (2000).

Corresponding author: Andrey A. Kiselev, Department of Electrical and Computer Engineering, North Carolina State University, Box 7911, Raleigh, NC 27695-7911, USA.
phone: +1-919-515-5080, fax: +1-919-515-3027,
email: kiselev@eos.ncsu.edu

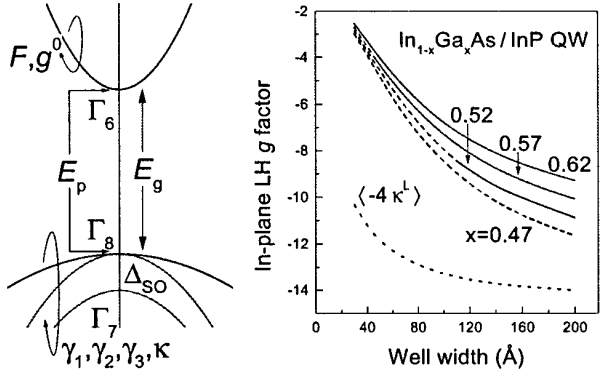

Figure 1: Left: Band diagram of a typical III-V semiconductor; Right: The in-plane LH g factor in $In_{1-x}Ga_xAs/InP$ QW as a function of the well layer width. Solid and dashed lines present results of the calculation. Depending on the QW width and intrinsic strain defined by the InGaAs layer composition x, either HH or LH subband acts as a ground hole state in the QW, this information is delivered by the line type: dashed and solid respectively. Dotted line visualizes *naive* approach based on the averaging of the material-dependent Luttinger parameter $\kappa^L(E)$ ("bulk" in-plane LH g factor) with probabilities to find the hole in the well and barrier layers.

COLLOIDALLY SYNTHESIZED PHOTONIC CRYSTALS IMPREGNATED WITH SEMICONDUCTOR NANOCRYSTALS

Nikolai Gaponik[1,2], Andrei Susha[1], Alexander Eychmüller[2], and Andrey Rogach[1,2]

[1]Physico-Chemical Research Institute, Belarussian State University, Leningradskaya Str. 14, 220050 Minsk, Belarus
[2]Institute of Physical Chemistry, University of Hamburg, Bundesstrasse 45, 20146 Hamburg, Germany

From the moment of the introduction of the photonic bandgap concept in 1987 by Jablonovitch and John [1], materials possessing a three-dimensional periodicity of the dielectric constant have attracted increasing attention [2]. Monodisperse silica and latex spheres are the most widely used species for the fabrication of colloidal photonic crystals (artificial opals) [3]. Photonic crystals are potentially interesting in a variety of applications, including the inhibition of the spontaneous emission of luminescing species embedded therein in a selected range of wavelengths resulting in the redistribution of the emission energy. This may lead to novel effects like low threshold nonlinear response [4]. 3D colloidal photonic crystals have been filled with organic dyes, luminescing semiconductor nanocrystals, and rare-earth ions [5] although the preparation routes and the overall quality of these systems are still to be optimized.

In the present work composite 3D colloidal photonic crystals have been fabricated using monodisperse silica or polystyrene latex spheres and highly luminescing CdTe nanocrystals, and their structural and optical properties have been studied by scanning electron microscopy, high resolution transmission electron microscopy and spectroscopic (UV-VIS absorption, transmission, reflection, luminescence) methods. Gravity sedimentation and electrophoretic deposition have been chosen as fabrication techniques. The latter method provides a convenient way to a rapid and controllable formation of photonic bandgap structures on optically transparent conducting indium-tin oxide (ITO) supports (Figure 1a,b) [6].

Highly luminescing CdTe nanocrystals stabilized with different thiols were synthesized in aqueous colloidal solutions and used for the impregnation of 3D colloidal photonic crystals. A number of impregnation techniques were developed including adsorption of CdTe nanoparticles in the voids of pre-formed opals [5], subsequent electrophoretic deposition of latex spheres and CdTe nanocrystals onto the ITO-electrode [6], and layer-by-layer formation of CdTe shells on the surface of individual latex spheres followed by their self-organisation into colloidal crystals during slow gravity sedimentation [7]. The optical properties of CdTe nanocrystals are strongly size-dependent, and the position of the photonic bandgap of the opals depends on the size of the colloidal silica or latex spheres. By this, the optical properties of composite 3D colloidal crystals are tuned (Figure 1c).

This work was supported by the research grant INTAS-Belarus 97-0250. The cooperation and fruitful discussions with Dr. S. V. Gaponenko (Minsk, Belarus), Dr. N. A. Kotov (Stillwater, OK, USA) and Dr. F. Caruso (Potsdam, Germany) are greatfully acknowledged.

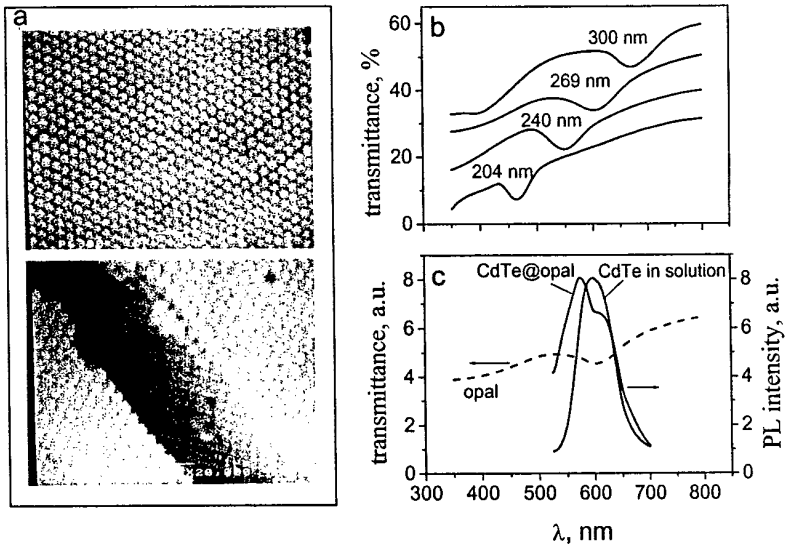

Figure 1. (a) SEM image and (b) a set of normal incidence transmission spectra of colloidal photonic crystals made from latex spheres of different sizes by electrophoretic deposition. (c) Modification of the spontaneous emission of CdTe nanocrystals electrophoretically deposited into the voids of a colloidal crystal made of latex spheres.

References

1. E. Yablonovitch. *Phys. Rev. Lett.* 1987, **58**, 2059; S. John. *ibid.* 2486.
2. J.D. Joannopoulos, P.R. Villeneuve, S. Fan. *Nature* 1997, **386**, 143.
3. Y. Xia, B. Gates, Y. Yin, Y. Lu. *Adv. Mater.* 2000, **12**, 693.
4. S. John, K. Busch. *IEEE J. Lightwave Techn.* 1999, **17**, 1931.
5. S.V. Gaponenko, V.N. Bogomolov, E.P. Petrov, A.M. Kapitonov, D.A: Yarotsky, I.I. Kalosha, A. Eychmüller, A.L. Rogach, J. McGilp, U. Woggon, F. Gindele. *IEEE J. Lightwave Techn.* 1999, **17**, 2128.
6. A.L. Rogach, N.A. Kotov, D.S. Koktysh, J.W. Ostrander, G.A. Ragoisha. *Chem. Mater.* 2000, **12**, 2721.
7. A.L. Rogach, A.S. Susha, F. Caruso, G.B. Sukhorukov, A. Kornowski, S. Kershaw, H. Möhwald, A. Eychmüller, H. Weller. *Adv. Mater.* 2000, **12**, 333.

Above-room-temperature operation of IV-VI microcavity lasers

T. Schwarzl[1], W. Heiß[1], G. Springholz[1], K. Biermann[2], K. Reimann[2]

[1]Institut für Halbleiter- und Festkörperphysik, Johannes Kepler Universität Linz, Altenbergerstraße 69, A-4040 Linz, Austria
[2]Max-Born-Institut für Nichtlineare Optik und Kurzzeitspektroskopie, D-12489 Berlin, Germany

Mid-infrared semiconductor lasers are important tools for high resolution chemical gas analysis and atmospheric pollution monitoring. Currently, in most applications, edge-emitting IV-VI (lead salt) semiconductor diode lasers are used because they allow to access the longest emission wavelength of 30 μm and the highest cw operation temperature of 223 K. Apart from the conventional edge-emitting lasers, recently, surface-emitting lead-salt mid-infrared microcavity lasers were demonstrated for the first time [1, 2]. These vertical-cavity surface-emitting lasers (VCSELs) offer several advantages like small beam divergence, single mode operation, or simplified monolithic integration. However, up to now, all vertical emitting IV-VI lasers have the disadvantage that they only work at temperatures below room temperature.

In this work, we present a IV-VI microcavity for which pulsed laser emission from PbTe quantum wells (QWs) is demonstrated for temperatures as high as 65 °C. In contrast to our previous work [1, 3], the microcavities were designed for room temperature laser operation, i. e., the microcavity resonances are shifted to shorter wavelengths of about 3 μm in order to match the transition energy of the PbTe QWs at room temperature. The samples consist of two highly efficient PbEuTe/EuTe Bragg mirrors and a 2λ cavity with nine PbTe QWs at the antinode positions of the cavity standing wave. Two microcavity samples were grown by molecular beam epitaxy for different target wavelengths of the central cavity mode of $\lambda = 3.1$ μm for sample 1 and of $\lambda = 3.6$ μm for sample 2. The room temperature FTIR reflectivity spectrum of sample 1 is depicted in Fig. 1. It shows a wide Bragg mirror stop band with high reflectivity with three microcavity resonance dips of orders m = 3, 4, and 5. In contrast to the strong and narrow resonance with m = 3, the higher m = 4 and 5 modes are less pronounced and broader exhibiting a strong damping due to absorption in the PbTe QWs with an effective band gap of 2600 cm^{-1} (3.8 μm).

The VCSEL devices were optically pumped with 100-fs laser pulses at a wavelength of 1.97 μm leading to a blue shift and a broadening of the microcavity resonances due to dynamic band filling. The intensity of the laser emission and the laser threshold depend on the energy difference between the cavity resonance and the band gap. The dependence of the emission spectra of both samples on operation temperature is depicted in Fig. 2. For sample 2 (Fig. 2a), the stimulated emission at 3.5 μm strongly decreases when the sample temperature is increased from room temperature to 30 °C, and it completely quenches at 35 °C. This quenching is due to the increase of the QW transition energy with increasing temperature shifting the QW gain spectrum out of the cavity resonance mode. For sample 1, this intrinsic process is expected at much higher temperatures due to the higher resonance energy. Indeed this laser sample shows emission at 3.1 μm up to temperatures as high as 65 °C (Fig. 2b), above which nonradiative processes quench the lasing. The laser operation above room temperature at mid-infrared wavelengths is very promising for the future development of electrically pumped surface emitting IV-VI microcavity lasers, which benefit from the negligible temperature drift of the emission wavelength.

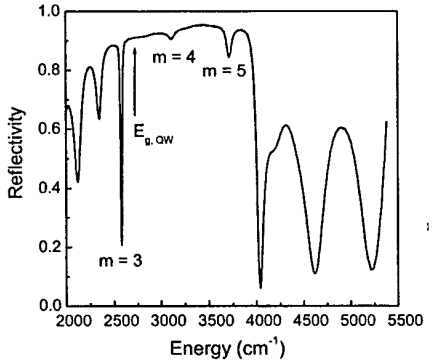

Fig 1: FTIR reflectivity spectrum of sample 1. The arrow indicates the absorption edge of the 20 nm wide PbTe quantum wells.

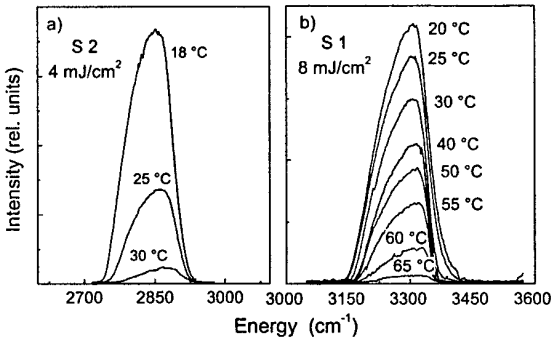

Fig 2: Emission spectra for various temperatures showing laser operation of (a) sample 2 up to 30 °C and (b) of sample 1 up to 65 °C.

References

[1] T. Schwarzl et al., Electron. Lett., **36**, 322 (2000).
[2] W. W. Bewley et al., Electron. Lett. **36**, 539 (2000)
[3] G. Springholz et al., Appl. Phys. Lett., **76**, 1807 (2000)

Corresponding author: Thomas Schwarzl, Institut für Halbleiter- und Festkörperphysik, Johannes Kepler Universität Linz, Altenbergerstraße 69, A-4040 Linz, Austria.
phone: +43 732 2468 9644, Fax: +43 732 2468 9696
email: thomas.schwarzl@jk.uni-linz.ac.at

Branching ratio of an incident light at the multi-branch region of photonic bands

T. Minami and K. Cho

Graduate School of Engineering Science, Osaka University,
1-3 Machikaneyama, Toyonaka, Osaka, 560-8531, Japan

Light dispersion in a photonic crystal has a band structure similar to that for an electron in a crystal [1]. This energy dispersion modifies the refractive indices of constituent dielectrics, and can lead to a drastic change in the light propagation behavior, such as a super-prism effect [2] and localiaztion at a defect level in the photonic gap [3], which are the subjects of active applicational research.

Except for the lowest frequency region, photonic bands have multi-branch structure, where an incident light of a given frequency splits into different modes in the crystal. The purpose of this paper is to make a theory to determine the branching ratio of this splitting into modes. We consider a semi-infinite photonic crystal, and calculate the reflection (R) and transmission (T) coefficients for an incident plane wave.

Boundary conditions between vacuum and the photonic crystal must be satisfied at every point on the surface or, equivalently, for all the reciprocal lattice vector components of the surface. Because of the two-dimensional periodicity, both reflected and transmitted waves are specified by the surface parallel wave vector $\mathbf{k}_{//}+\mathbf{g}_{//}$, where $\mathbf{k}_{//}$ is the common wave vector to incident, refelected and transmitted waves, and $\mathbf{g}_{//}$ is the 2D receiprocal lattice vector of the surface. In practice, the boundary condition is required for N components of $\mathbf{g}_{//}$. The reflected wave is taken as a superposition of $2N$ plane waves which include evanescent ones, and the transmitted wave is described as the superposition of $2N$ eigen-modes of the photonic crystal. Since there are $4N$ boundary conditions to be required for electric and magnetic fields, we can uniquely determine the reflected and transmitted amplitudes, and hence the branching ratio to individual modes. Eigen-moeds of a photonic crystal are calculated with the transfer matrix method [4] for each given frequency and $\mathbf{k}_{//}$, which gives all the Bloch modes as well as evanescent modes. R(ω) and T(ω) are calculated for the Poynting vector of each mode.

The numerical calculation is made for the intersecting square rods model (ε=13 and filling factor 0.18) [5] with N=100. We take an oblique incidence with $\mathbf{k}_{//}$=(0, 0.1). Fig. 1 shows the band structure and T(ω) for s- and p-polarized incident lights. The characteristic dependence of T(ω) for each band on the polarization and ω should be noted. In a photonic crystral, there are different ways to prepare, e.g., a (100) surface. Fig. 2 shows R(ω) for 3 different (100) surfaces, which gives a first demonstration of the very sensitive dependence of R(ω) on the choice of the surface.

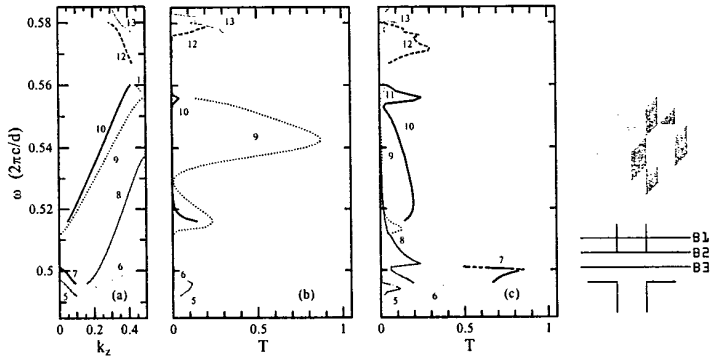

Fig. 1: (a) Band structure for $\mathbf{k}_{//}$=(0, 0.1), (b) T(ω) for s-polarized light, and (c) T(ω) for p-polarized light. (b) and (c) are for the surface B1.

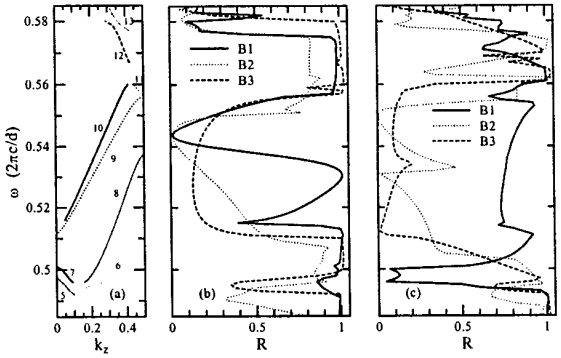

Fig. 2: R(ω) for the surfaces B1, B2, and B3. (a) band structure for $\mathbf{k}_{//}$=(0, 0.1), (b) s-polarized light, and (c) p-polarized light.

References

[1] E. Yablonovitch, Phys. Rev. Lett. 58, 2059 (1987)
[2] H. Kosaka *et al.*, Appl. Phys. Lett. 58, 10096 (1998)
[3] S. Noda, A. Chutinan and M. Imada, Nature 407, 608 (2000)
[4] J.B. Pendry, J. Mod. Opt. 41, 209 (1994)
[5] H.S. Sözüer and J.W. Haus, J. Opt. Soc. Am. B 10, 296 (1993)

Corresponding author: Kikuo Cho, Graduate School of Engineering Science, Osaka University, 1-3 Machikaneyama, Toyonaka, Osaka, 560-8531, Japan
phone: +81 6 6850 6400, Fax: +81 6 6850 6400
email: cho@mp.es.osaka-u.ac.jp

Finite size effects on superlattice phonons studied by coupled microcavity enhanced Raman scattering

M. Trigo[1], R. G. Pregliasco[2], A. Fainstein[1,2], B. Jusserand[3], and V. Thierry-Mieg[3]

[1]Centro Atómico Bariloche & Instituto Balseiro, CNEA, 8400 S. C. de Bariloche, Argentina
[2] Centro Atómico Bariloche, CONICET, 8400 S. C. de Bariloche, Argentina
[3]LPN/CNRS, B. P. 107, 92225 Bagneux Cedex, France

We report four orders of magnitude double optical resonant (DOR) enhancement of Raman scattering in a new two-mode microcavity geometry. The design allows backscattering geometries, providing easy access to the excitations in-plane dispersion. In adition, k~0 excitations are detected due to the photon confinement induced forward scattering component. The microcavity is used to study the optical and acoustical phonon spectra of a finite GaAs/AlAs superlattice (SL). A new type of "standing optical vibration" is demonstrated involving the GaAs confined phonons with a standing wave envelope determined by the SL thickness. A giant dispersion of the first order standing wave mode is observed, as well as its anticrossing with higher order confined modes of the same symmetry. The acoustic phonon spectra in the folded phonon region displays a complex series of peaks reflecting interference effects on the Raman scattering due to the superlattice finite size.

A two-mode microcavity [1] consists of two identical $\lambda/2$ spacers enclosed by top and bottom distributed Bragg reflectors (DBR's), and separated by a lower reflectivity mirror. Two degenerate cavity optical modes exist which are split by the mutual coupling. This splitting can be tuned with an excitation of the active material (e.g., vibrations of nanostructures) by selecting appropriately the middle DBR [2]. In this way the structure can be used for DOR Raman scattering [3] in a backscattering geometry by tuning the incidence and scattered photons with the upper and lower cavity modes, respectively. The cavity described here has two $\lambda/2$ spacers made by 10.5 period GaAs(8.5nm)/AlAs(4.4nm) SL's, with 20 DBR $Ga_{0.8}Al_{0.2}As$/AlAs pairs on the bottom, 16 on top, and 7.5 in between. The four orders of magnitude enhancement of the Raman efficiency [3] together with the backscattering geometry enables the study of the $k_{||}$ dispersion of the finite SL phonon spectra by simply turning the sample respect to the incidence angle.

The optical phonon Raman spectra for varying $k_{||}$ are displayed in Fig.1. A series of peaks displaying a complex dispersion and anticrossing behavior are observed in the GaAs-like spectral region. We have assigned the main peaks (labeled N=1,3 in Fig.1) to standing optical phonons (SOP), vibrations characterized by a standing wave envelope of uniform displacements on the GaAs regions of the finite SL's [4]. With increasing $k_{||}$ the SOP mode N=1 softens strongly and anticrosses with the high-order confined vibration (m=7,9,11). Their energies, derived using the corresponding effective wavevector k_m, are shown with dashed lines in Fig.1 and nicely reproduce the spectral position of the smaller Raman peaks. The SOP dispersion, on the other hand, can be well described using a matrix-method based continuum dielectric model [5].

In Fig.2 we show the measured folded acoustic phonons (Exp.), together with calculations of the Raman spectra performed using a photoelastic model and a linear dispersion which is valid away from the edges where gaps occur [6]. In fact, for the SL studied the calculated first zone-center gap is ~0.7 cm^{-1}, below our experimental resolution (>1 cm^{-1}). Three calculated curves are shown, corresponding to an "infinite" 40 period SL excited with a photon plane wave (SL_{40}), a finite 10 period SL in a cavity (SL^{C}_{10}) where also forward scattering (FS) is present, and two 10 period SL's in a double cavity (SL^{DC}_{10}). In the later interference effects due to the two SL's are predicted which, however, cannot be observed with our experimental set-up. Three main peaks are observed in the experiment, together with smaller oscillation towards lower Raman shifts. Based on the calculations the former can be understood as the backward and forward components of the folded phonon spectra. The later, on the other hand, stem from k non-conservation due to the SL finite size.

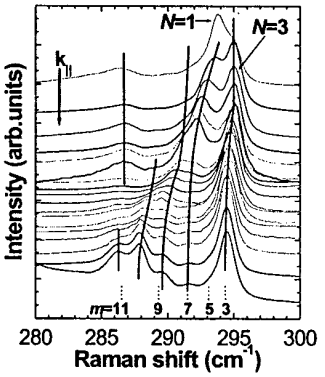

Fig. 1: Finite SL GaAs-like optical phonon spectra for varying $k_{||}$. The solid lines are guides to the eye. N labels the order of the SOP. m=3 to 11 indicate the calculated confined phonon energies

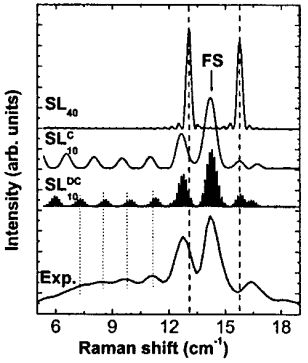

Fig. 1: Folded acoustic phonon Raman spectra of the finite SL (Exp.). The three top curves correspond to the Raman spectra calculated for a 40 period SL and incident photon plane wave (SL_{40}), a 10 period SL in a cavity (SL^{C}_{10}), and two 10 period SL's in a double microcavity (SL^{DC}_{10}), respectively.

References

[1] P. Pellandini et al., Appl. Phys. Lett. 71, 864 (1997).
[2] B.Jusserand et al., Physica E 7 , 646 (2000)
[3] A. Fainstein et al., Phys. Rev. Lett. 75, 3764 (1995).
[4] A. Fainstein et al., Phys. Rev. Lett., in press.
[5] A. Fainstein et al., Phys. Rev. B 54, 11505 (1996).
[6] M. Giehler et al., Phys. Rev. B 55, 7124 (1997).

Corresponding author: Alex Fainstein, Centro Atómico Bariloche, 8400 S. C. de Bariloche, Argentina.
phone: +54 2944 445100, Fax: +54 2944 445299
email: afains@cab.cnea.gov.ar

Modified spontaneous emission properties of CdS quantum dots embedded in novel three-dimensional microcavities

H. Kumano, A. Ueta and I. Suemune

Research Institute for Electronic Science (RIES), Hokkaido University
Kita-12, Nishi-6, Kita-ku Sapporo 060-0812 Japan

Spatial confinement of photon modes enables us to control spontaneous emission rate artificially and will introduce a new degree of freedom in electron-photon interactions [1]. A number of attempts to give the efficient confinement of radiation field have been made from a viewpoint of practical devices with attractive functions as well as basic physics. Up to now, most studies are based on planar microcavities with distributed Bragg reflectors (DBR). In these structures, the photonic confinement is only one-dimensional normal to the DBRs, thus the predicted enhancement factor of spontaneous emission rate is limited below 3. In order to realize further enhancement of this value, fabrication of three-dimensional (3-D.) optical microcavity structures is an essential issue. Recently, we have demonstrated that self-organized semiconductor pyramidal structures which function as 3-D. microcavities [2], where the resonance peaks corresponding to the photon mode inside the pyramidal structures showed up clearly. In this paper, active layers are embedded inside the microcavity structures towards the fabrication of light-emitting devices and luminescence properties were investigated. Modified spontaneous emission properties in the presence of 3-D. confined radiation field will be discussed, which becomes possible by the achievement of present low-loss 3-D. microcavities with small volume comparable to the light wavelength λ.

ZnS pyramidal structures were grown selectively with metalorganic molecular-beam epitaxy at the substrate temperature of 350°C. Prior to the growth, carbonaceous masks with square-shaped openings were deposited of which edges are aligned along the [100] directions on ZnSe/MgS-SL DBR surfaces [3]. ZnS is selectively grown in the opening area, and pyramidal structures whose sidewalls were completed with four smooth {034} crystal facets were fabricated as shown in Fig. 1. CdS QDs were embedded as active layers within the ZnS pyramidal structures. Optical characterizations were carried out with μ-photoluminescence (PL) and μ-reflection spectroscopies. To probe the signal from a single pyramidal microcavity, the optical image was expanded by an objective lens and a part of the expanded image was selected by a pinhole. All the measurements were performed at room temperature. Figure 2 shows the PL spectrum of 3-D. microcavity and the spectrum of non-patterned area for comparison. Distinguished modification of spontaneous emisson at around 539 nm was unambiguously observed from the microcavity area in contrast to the non-patterned area where the only broad luminescence from underlying DBR layer was dominated. To elucidate the origin of this modification, PL spectrum was compared with photon resonance modes revealed by the μ-reflection measurements and is shown in Fig. 3. In μ-reflection spectrum, high Q values as large as 1000 were shown. Furthermore, Purcell factors calculated from the obtained Q values reach ~9, which is inaccessible in the planar microcavities with only one-dimensional photon confinement. It should be noted that PL peak wavelength was almost perfectly coincided with the resonance modes inside the microcavity. These results indicate that the spontaneous emission rate is effectively alterd in the presence of three-demensionally confined photonic modes. Time-resolved PL measurements of present pyramidal microcavity structures are now under way to reveal decay time modulation as a direct proof of modified electron-photon interactions.

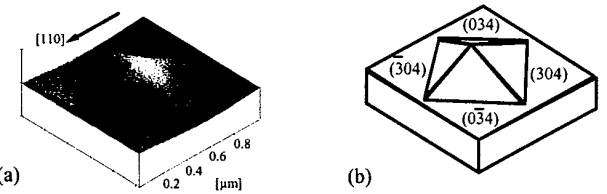

Fig. 1: (a) Atomic force microscope image of a selectively grown ZnS pyramidal-shaped 3-D. microcavity structure. (b) The schematic drawing of (a). Selective growth was clearly observed on 700-nm square opening of carbonaceous mask. Four pyramidal sidewalls are composed of atomically flat {034} facets. In this paper, optical characterizations are performed of the samples with CdS active layers within this structure by replacing the intermediate ZnS layers by CdS QDs layers.

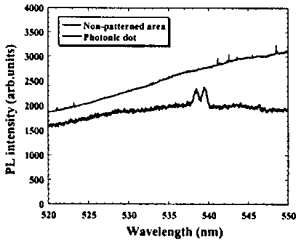

Fig. 2: μ-PL spectra of both 3-D. microcavity area (thick curve) and non-patterned area (thin curve) measured at room temperature. Clear resonant structure at around 539 nm is observed by proving 3-D. microcavity area. On the other hand, only featureless luminescence from underlying DBR layer was observed from non-patterned area.

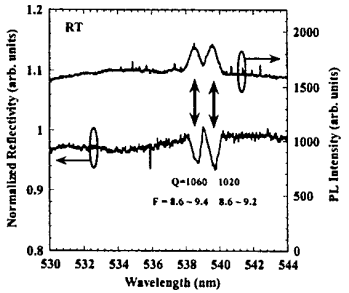

Fig. 3: μ-PL (upper curve) and μ-reflectance (lower curve) spectra obtained from 3-D. microcavity area. PL peak positions are well coincident with photon resonant modes with high Q values ~1000. Calculated Purcell factor F reaches ~9, which indicates the effective coupling between electronic system and 3-D. confined radiation field.

References

[1] E. M. Purcell, Phys. Rev. 69, 681 (1946).
[2] I. Suemune et al., Appl. Phys. Lett. 74, 1963 (1999).
[3] T. Tawara et al., J. Cryst. Growth 221, 699 (2000).

Corresponding author: Hidekazu Kumano, Research Institute for Electronic Science (RIES), Hokkaido University, Kita-12, Nishi-6, Kita-ku Sapporo 060-0812 Japan
phone: +81 11 706 2898, Fax: +81 11 706 4973
e-mail: kumano@es.hokudai.ac.jp

Dressing the electronic states of quantum dots in pillar microcavities

G. Panzarini[1], L.C. Andreani[2], U. Hohenester[1,3], and E. Molinari[1]
[1] Istituto Nazionale per la Fisica della Materia (INFM) and Dipartimento di Fisica, Universita' di Modena e Reggio Emilia, via Campi 213/A, I-41100 Modena
[2] Istituto Nazionale per la Fisica della Materia (INFM) and Dipartimento di Fisica "A. Volta", Universita' di Pavia, via A. Bassi 6, I-27100 Pavia
[3] Institut für Theoretische Physik, Karl-Franzens-Universität Graz, Universitätsplatz 5, 8010 Graz, Austria

Continuous progress of epitaxial growth and nanolithographic techniques has now made possible the fabrication of laterally patterned semiconductor microcavities (MC's) with complete three-dimensional confinement of the optical modes: this is achieved by combining vertical optical confinement by the distributed Bragg reflectors with the lateral optical confinement provided by the large refractive index discontinuity at the etched sidewalls.
When a resonant medium is placed inside a MC, optical excitations become strongly modified by the enhanced radiation-matter interaction produced by the confinement of the photon modes. Indeed, effects such as reduction of the radiative lifetime for quantum dots (QD's) and vacuum-field Rabi splitting for quantum-well excitons inside pillar MC's have been demonstrated experimentally[1,2]. It can be envisioned that complete control over the electronic and optical degrees of freedom would have strong impact on future quantum-information-processing devices.
In this contribution we present a theoretical study of the interaction between the three-dimensionally confined states of a QD with the fully confined modes of a pillar MC, and propose a system where both exciton and biexciton states can be in strong coupling regime with the cavity modes.
The coherent radiation-matter interaction couples the QD-field states with both degenerate circularly polarized lowest energy radiation modes with opposite helicity sustained by the pillar MC. We consider the case of a QD initially prepared in the ground biexciton state (i.e.in a state formed by two Coulomb correlated excitons with opposite spin orientations) interacting with the vacuum field. The coherent interaction couples the QD-field state $|b,0,0\rangle$ with $|x_\uparrow,0,1\rangle$, $|x_\downarrow,1,0\rangle$, and the states $|x_\uparrow,0,1\rangle$, $|x_\downarrow,1,0\rangle$ with $|g,1,1\rangle$ [here the first position in the kets indicates the QD state, with $|g\rangle$, $|x_\uparrow\rangle$, $|x_\downarrow\rangle$, $|b\rangle$ denoting the groundstate, the spin-up and spin-down excitons, and the fundamental biexciton states respectively, and the second (third) position represents the number of photons in the cavity mode with positive (negative) helicity].
The composite QD/cavity-mode system radiates via two distinct channels: coupling of the QD to free space modes, and losses through the cavity mirrors. These relaxation channels, in turn, bring the composite system towards the lower energy states $|x_\uparrow,0,0\rangle$, $|x_\downarrow,0,0\rangle$, $|g,1,0\rangle$, $|g,0,1\rangle$. Coherent radiation-matter interaction takes then place between $|x_\uparrow,0,0\rangle$ and $|g,1,0\rangle$, and between $|x_\downarrow,0,0\rangle$ and $|g,0,1\rangle$, until the finite lifetimes of the dot levels and of the cavity modes cause the final decay of the system towards the lowest energy state $|g,0,0\rangle$.
By solving the Liouville master equation for the QD-field density operator in the presence of relaxation processes, we calculate the spontaneous emission spectrum as a function of the cavity mode frequency and of the coupling constants for the QD-cavity interactions.
For a single self-assembled InAs QD inside state-of-the-art pillar MC's (with radius a=0.5 micrometers) the oscillator strengths are a factor of ten too small for strong coupling. On the other hand our calculations predict the occurrence of vacuum field Rabi splitting for the confined states localized to monolayer fluctuations in quantum wells.

Fig.1 shows the calculated luminescence spectrum for this latter system as a function of the frequency. Using realistic parameters for the electronic states[5] and for the cavity[1], a clear fingerprint of the formation of dressed biexciton states (evidenced by the vertical arrows in the plot) is revealed. The lines arising in the luminescence spectrum are interpreted in terms of transitions between dressed states.
We finally consider the coherent driving of a cavity containing a single QD by an external field. Starting with the QD interacting with the vacuum field of the cavity, we gradually increase the intensity of the laser beam and show that the luminescence spectrum transforms from the single-peaked structure characteristic of the weak coupling regime to the three-peaked "
structure when the external field is sufficiently intense.

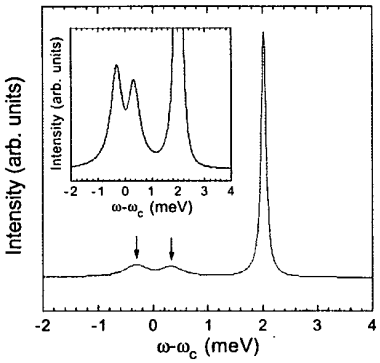

Fig.1 Calculated luminescence spectrum for the states bound to interface defects in narrow quantum wells when the biexciton to exciton transition is at resonance with the cavity mode (of frequency ω_c). Parameters: biexciton binding energy=2 meV; linewidths of the exciton- and of the biexciton transitions=0.1 meV; linewidth of the cavity mode=0.5 meV. Inset: same plot on an expanded vertical scale, showing the formation of dressed biexciton states.

[1] See e.g. J.M. Gerard *et al*, Phys. Rev. Lett.**81**, 1110 (1998).
[2] J. Bloch *et al*, Physica E**2**, 915 (1998).
[3] G. Panzarini and L.C. Andreani, Phys. Rev. B**60**, 16799 (1999).
[4] L.C. Andreani, G. Panzarini and J.M. Gerard, Phys. Rev. B**60**, 13276 (1999).
[5] K. Brunner *et al.*, Phys. Rev. Lett.**73**, 1138 (1994).

Corresponding author: Giovanna Panzarini. Dipartimento di Fisica, Universita' di Modena e Reggio Emilia, via Campi 213/A, I-41100 Modena.
Phone: +39-59-2055300 ; Fax: +39-59-367488 ; e-mail: panzarini@unimo.it
Oral presentation preferred

Formation of air-bridge type two-dimensional photonic crystals having air hole array grown by selective area metal-organic vapor phase epitaxy

M. Akabori, J. Motohisa, T. Fukui

RCIQE, Hokkaido University, North 13, West 8, Kita-ku, Sapporo 060-8628, Japan

Fabrication and characterization of photonic crystals (PCs), which have periodically modulated dielectric structures with periods near light wavelengths, have been receiving much attention lately, because PC's ability to control spontaneous emission should lead to new optical devices [1]. In fact, new optical devices using air-bridge or thin-slab type two-dimensional (2D) PCs have been already reported [2, 3]. However, most of the structures have been formed by using dry etching processes, in which process-induced damages is one of the critical problems, particularly for active devices like lasers. We have proposed a new approach to form periodic dielectric structures by using selective area metal-organic vapor phase epitaxy (SA-MOVPE) [4], which can be applied to form 2D PCs having air hole array. In this paper, we report on a formation of air-bridge type two-dimensional PC structures using SA-MOVPE regrowth and selective wet-chemical etching.

Figure 1 shows a schematic illustration of the fabrication sequence of air-bridge type 2D PCs using SA-MOVPE. First, thick $Al_{0.5}Ga_{0.5}As$ layer was grown on GaAs (111)B substrates to form an undercut region after the selective wet-chemical etching. After the first growth, thin SiO_2 film was deposited, and then triangular lattice array of hexagonal masks for SA-MOVPE was defined by electron-beam lithography and wet-chemical etching. Next, SA-MOVPE regrowth of GaAs on $Al_{0.5}Ga_{0.5}As$ surfaces is carried out to form PC structures having hexagonal air hole array. Finally, SiO_2 masks and underlying $Al_{0.5}Ga_{0.5}As$ are removed by selective wet-chemical etching to obtain air-bridge type 2D PCs.

The growth was carried out by a horizontal low pressure MOVPE system with trimethylgallium (TMGa), trimethylaluminum (TMAl) and arsine (AsH_3) as source materials. The growth temperature was fixed to 850°C, and the AsH_3 partial pressure was 5.0×10^{-5} atm. For the growth of $Al_{0.5}Ga_{0.5}As$ layer, the partial pressures of TMGa and TMAl were 3.7×10^{-6} atm and 1.2×10^{-6} atm, respectively. For SA-MOVPE regrowth of GaAs, TMGa partial pressure was reduced to 7.3×10^{-7} atm in order to obtain uniform structures [4]. We used HF solution for selective etching of both SiO_2 and $Al_{0.5}Ga_{0.5}As$.

Figures 2 shows a scanning electron microscope (SEM) image of a GaAs 2D PC. The period or lattice constant a is 1 μm. Uniform hexagonal network structures according to mask pattern were obtained. We also have succeeded in obtaining network structures for $a = 0.4$ μm. The calculated photonic bands of the GaAs 2D PC are shown in Fig. 3 with the insets which indicate the lattice array and the Brillouin zone. There are clear photonic band gaps in H-polarization, therefore optical modulation effects are expected in the PC. However, the band gap structure cannot be clearly observed in E-polarization.

Figure 4 shows a SEM image of a PC structure after selective wet-chemical etching. As can be seen, an air-bridge type 2D PC having the GaAs hexagonal network structure is successively realized. The result suggests that it is possible to realize air-bridge type PCs by the combination of SA-MOVPE and selective wet-chemical etching without any dry etching processes.

References

[1] E. Yablonovitch, *Phys. Rev. Lett.* **58**, 2059 (1987).

[2] O. Painter *et al.*, *Science*, **284**, 1819 (1999).

[3] M. Boroditsky *et al.*, *Appl. Phys. Lett.* **75**, 1036 (1999).

[4] M. Akabori *et al.*, *IEEE Conf. Proc. 27th Int. Symp. Compound Semiconductors* (2000).

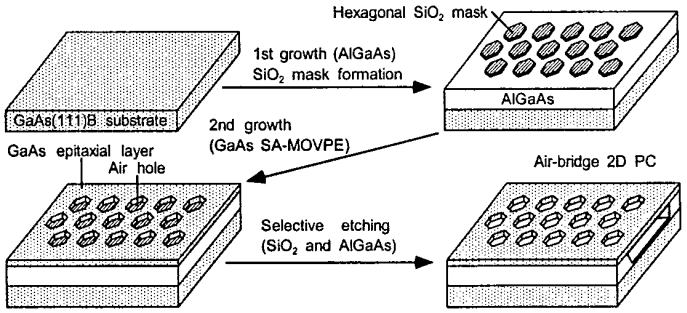

Fig. 1. Fabrication sequence of air-bridge-type 2D PC formation.

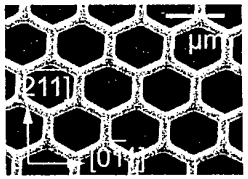

Fig. 2. GaAs 2D PC structure after SA-MOVPE.

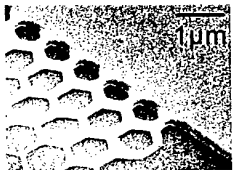

Fig. 4. GaAs air-bridge type 2D PC obtained after selective etching.

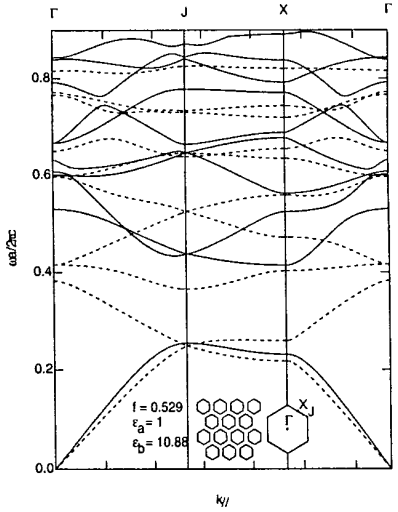

Fig. 3. Calculated photonic bands. Solid and broken lines indicate H- and E-polarization, respectively.

Corresponding author: Masashi Akabori

RCIQE, Hokkaido University, North 13, West 8, Kita-ku, Sapporo 060-8628, Japan

Phone: +81-11-706-7176, Fax: +81-11-716-6004, E-mail: akabori@rciqe.hokudai.ac.jp

Photoreflectance and photoluminescence characterisation of InGaAs/AlAsSb quantum wells grown by molecular beam epitaxy

T. Mozume and N. Georgiev

FESTA Laboratories, Femtosecond Technology Research Association
5-5 Tokodai, Tsukuba 300-2635, Japan

Ultrafast relaxation times and large optical nonlinearities of the intersubband transitions in doped quantum wells (QWs) are attractive for advanced photonic devices applicable to current optical communication system such as high speed photonic switches, modulators, and lasers. In future optical communication systems operating beyond 1 Tb/s, ultrafast multiwavelength all-optical switching devices will become crucial. $In_{0.53}Ga_{0.47}As/AlAs_{0.56}Sb_{0.44}$ system lattice-matched to InP is one of the most suitable systems for this purpose because of its large conduction band offset of 1.6 eV[1]. We have reported the near-infrared intersubband transitions[2, 3] and the ultra-fast absorption response of 685 fs[4] at 1.55 μm from this materials system, and shown that this materials system is suited for the ultra high-speed optical devices used in the optical communication network. However, in spite of the potential applications of these novel quantum structures, very few studies have been reported on AlAsSb systems because of the difficulties involved in growing the AlAsSb material as it includes two group-V elements and has a large miscibility gap.

We have already reported that the interface termination procedure has a profound influence on the QW property of InGaAs/AlAsSb. The PL spectra of Sb-terminated InGaAs/AlAsSb SQWs are broadened and red-shifted than that of the equivalent As-terminated version[5, 6]. This paper reports the detailed study of the effects of interface termination on the optical properties of InGaAs/AlAsSb QWs using photoreflectance (PR) and the photoluminescence (PL).

The InGaAs/AlAsSb quantum-wells (QWs) were grown on Fe-doped (001) InP substrate by solid source MBE. Elemental Ga, In, and Al were used for the group III growth species, and Sb_2 and As_2 were used for the group V growth species. As_2 was supplied using a valved cracker cell. Photoluminescence measurements were carried out at 77 K and room temperature using an argon-ion laser emitting at 514.5 nm as an excitation source. PR spectra were taken using an InGaAs photodiode and a conventional lock-in detection system.

Figure 1 shows the 77 K and room temperature photoluminescence spectra of Sb- and As-terminated InGaAs/AlAsSb MQWs with 10-nm well width. As-terminated QW shows sharp PL peaks at around 0.85 eV and 0.78 eV at 77 K and room temperature, respectively, corresponding well with the calculated energies. While PL spectra of Sb-terminated QW shows strong broadening, especially at 77 K. At low excitation power regime, the peak around 0.78 eV dominates. As the excitation power increases, the peak around 0.85 eV becomes dominant.

Room temperature and 77 K PR spectra of these samples are shown in Fig. 2. Features of the interband transitions in the quantum wells are clearly observed. PL peak energy of As-teminated QW and PR critical point energies of As-terminated and Sb-terminated QWs correspond well with the interband transition energies between confined energy levels in InGaAs calculated based on the envelope function approximation and taking into account the nonparabolicity of the conduction bands.

Although the origin of the PL peak observed in the Sb-terminated QW at low excitation regime has not been fully clarified, the defects caused by the Sb incorporation in InGaAs would be the key to explain the unique excitation power dependence of the PL spectra.

New Energy and Industrial Technology Development Organization (NEDO) in the frame of Femtosecond Technology Project supported this work.

1) N. Georgiev and T. Mozume, J. Appl. Phys. **89**, 1064 (2001).
2) T. Mozume, H. Yoshida, A. Neogi, and M. Kudo, Jpn. J. Appl. Phys. **38**, 1286 (1999).
3) T. Mozume, H.Yoshida, A. Neogi, N.Georgiev, K. Asakawa, and M. Kudo, Inst. Phys. Conf. Ser. **162**, 131 (1999).
4) T. Akiyama, N. Georgiev, T. Mozume, H. Yoshida, A. V. Gopal, and O. Wada, to be published in Electronics Lett.
5) T. Mozume and N. Georgiev, Thin Solid Films,380 (2000) 249.
6) N. Georgiev and T. Mozume, J. Appl. Phys. 89 (2001) 1064.

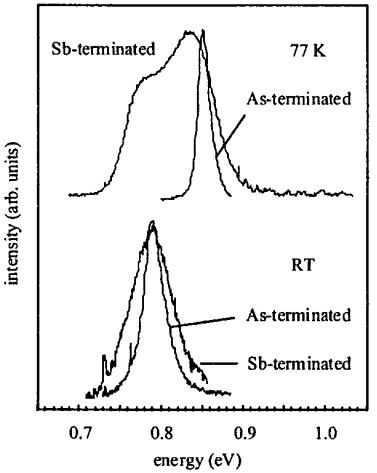

Fig. 1 77 K and room temperature PL spectra of InGaAs/AlAsSb SQW. InGaAs well width is 10 nm . InGaAs to AlAsSb interfaces are terminated either by Sb or As.

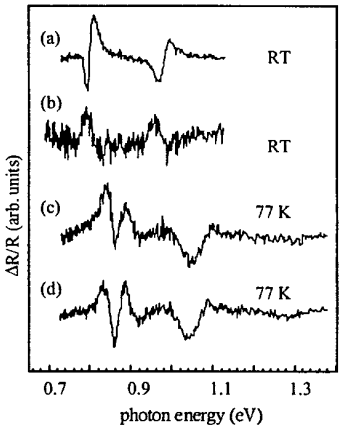

Fig. 2 Room temperature and 77K photoreflectance spectra of As- and Sb-terminated 10 nm InGaAs/AlAsSbquantum wells. (a) and (c) are for As-terminated sample; (b) and (d) are for Sb-terminated sample.

Corresponding author : Teruo Mozume, FESTA Laboratories, Femtosecond Technology Research Association, 5-5 Tokodai, Tsukuba 300-2635, Japan
Phone: +81-298-47-5181, Fax: +81-298-47-4417
e-mail: mozume@festa.or.jp

Corresponding author : Teruo Mozume, FESTA Laboratories, Femtosecond Technology Research Association, 5-5 Tokodai, Tsukuba 300-2635, Japan
Phone: +81-298-47-5181, Fax: +81-298-47-4417
e-mail: mozume@festa.or.jp

Room temperature lasing of quantum wire VCSELs by optical pumping grown on the (775)B GaAs substrates by MBE

Y. Ohno, H. Kanamori, S. Shimomura, S. Hiyamizu

Graduate School of Engineering Science, Osaka University, Toyonaka, Osaka 560-8531, Japan

Quantum wires (QWRs) can be one of the strongest candidates to solve polarization instability of conventional vertical cavity surface emitting lasers (VCSELs) because of polarization anisotropy of the luminescence from QWRs. Recently, we have reported highly uniform GaAs and InGaAs QWRs can be fabricated on the (775)B-oriented GaAs substrates and room temperature (RT) oscillation of (775)B QWR lasers [1, 2]. In this paper, we report the fabrication of a VCSEL including an active region with self-organized $In_{0.1}Ga_{0.9}As$ QWRs on the (775)B GaAs substrates and their RT lasing by optical pumping, for the first time.

The (775)B InGaAs/AlAs quantum well (QW) has a regularly corrugated upper interface and a flat lower interface. Figure 1 shows a surface AFM image of an $In_{0.1}Ga_{0.9}As$ layer grown on the (775)B GaAs substrates by MBE. Regular surface corrugation with average lateral period of 40 nm and vertical amplitude of 1 nm can be seen. Thus, QWRs was naturally formed in the thin QW grown on the (775)B GaAs substrates by MBE. The VCSEL structure as shown in Fig. 2 was grown on a Si-doped (775)B GaAs substrate by MBE. The bottom n-type distributed Bragg reflector (DBR) consists of 28 pairs of Si-doped $AlAs/Al_{0.15}Ga_{0.85}As$ and the top DBR consists of 24 pairs of Be-doped $AlAs/Al_{0.15}Ga_{0.85}As$, and 2 pairs p-DBR sample was also fabricated to study the reflectivity and photoluminescence (PL). The active region consists of five 30Å $In_{0.1}Ga_{0.9}As/(GaAs)_6(AlAs)_1$ QWR layers surrounded by an $Al_{0.15}Ga_{0.85}As$ clad layer. Figure 3 shows the reflectivity of the sample and their polarized PL spectra at 24°C. The reflectivity of the (775)B DBR was above 98%, and its PL peak agreed with the etalon wavelength. The PL was polarized in the wire direction and its polarization degree $[P \equiv (I_{\parallel} - I_{\perp})/(I_{\parallel} + I_{\perp})]$ was 0.13, indicating the formation of the (775)B QWRs. In order to study the lasing properties, we optically pump the (775)B VCSEL with titanium-doped sapphire laser (λ=777 nm). The emission spectra with various pump power (P=2.2, 7.6 and 440 nW/μm^2) at 24°C was shown in Fig. 4. Clear lasing spectra could be seen with pump powers above 7.6 nW/μm^2, and their lasing wavelength was 845.6 nm. This is the first RT oscillation of VCSELs containing self-organized QWRs, to our knowledge.

References

[1] M. Higashiwaki et al., Appl. Phys. Lett. **74**, 780 (1999).
[2] Y. Ohno et al., J. Vac. Sci. Technol. B **18**, 1672 (2000).

Corresponding author: Yasuhide Ohno, Department of Physics,
Graduate School of Engineering Science, Osaka University, 1-3 Machikaneyama,
Toyonaka, Osaka 560-8531, Japan.
phone: +81 6 6850 6457, Fax: +81 6 6845 4632,
email: y_ohno@d310.mp.es.osaka-u.ac.jp

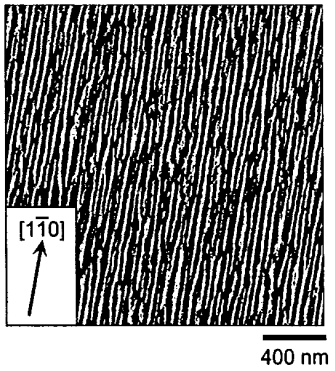

Figure 1: Surface AFM image of an $In_{0.1}Ga_{0.9}As$ layer grown on the (775)B GaAs substrates at T_s of 630±C by MBE.

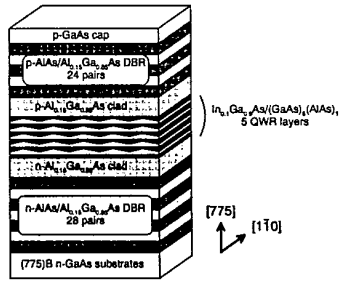

Figure 2: Schematic illustration of QWR VCSEL grown on the (775)B GaAs substrates by MBE.

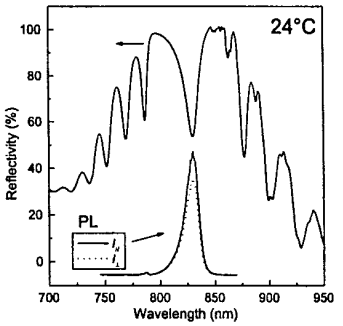

Figure 3: Re°ectivity of the (775)B QWR VCSEL structure with 2 pairs top p-DBR and their polarized PL spectra.

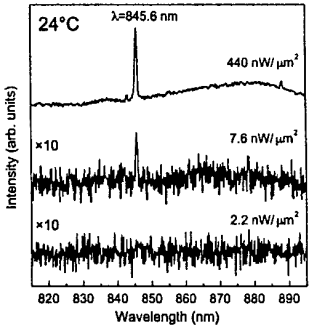

Figure 4: Emission spectra at 24±C from (775)B QWR VCSEL with various pump power.

Organic μ-cavities based on thermally evaporated TeO_x-LiF Dielectric Mirrors

M. Anni[1], G. Gigli[1], S. Patanè[2],A. Arena[2], M. Allegrini[3], and R. Cingolani[1]

[1] Istituto Nazionale Fisica per Materia (INFM), Dip. Ingegneria dell'Innovazione, Università di Lecce, Via per Arnesano, 73100 Lecce, ITALY
[2] Istituto Nazionale Fisica per Materia (INFM), Dip. Fisica della Materia e Tecnologie Fisiche Avanzate, Università di Messina, Salita Sperone 31, 98166 Sant'Agata-Messina, ITALY.

[3]Istituto Nazionale di Fisica per la Materia, Dip. di Fisica, Università di Pisa, Via F. Buonarroti n. 2 Pisa, ITALY

Organic semiconductors have recently attracted much attention for application in electroluminescent devices such as Light Emitting Diodes (LEDs) and displays. In this frame several works on organic microcavity structures demonstrated their utility to obtain a full control of the emission energy, linewidth, intensity and directionality for LED as well as to obtain the optical feedback in laser resonators. The commonly studied organic microcavities are realized by cladding the active material between a Distributed Bragg Reflector (DBR) and an evaporated metallic mirror, or by high temperature mechanical pressing of two half DBR cavities. Moreover, in order to have a single μ-cavity resonance, the cavity needs DBR having a stopping band wider than luminescence of the organic (typically hundreds of nanometers). To satisfy such requirement DBR consisting of materials with an high refractive index difference must be used. To date, many different techniques and many different materials have been used for wide bandwidth DBR deposition, such as SiO_2-Si_xN_y by Plasma Enhanced Chemical Vapor Deposition (PECVD), CF-CF(Au) by sputtering and MgF_2-ZrO_2 by laser induced vapor deposition [18]. These techniques cannot be used in the presence of the organic active material, thus requiring a complicated multi-step process for the realization of the cavity.

In this work we report on the realization of DBR dielectric mirrors entirely based on low cost thermal evaporation of Lithium Fluoride (LiF) as the low refractive index material and Tellurium Oxide (TeO_x) as the high refractive index material. This approach allows us to realize highly reproducible and ultra low cost mirrors. The high difference in the refractive index of the two materials allows us to obtain reflectivity higher then 98% with a small number of periods, and to obtain a wide stopping band with a Full Width at Half Maximum (FWHM) of about 200 nm. Moreover, this permits to grow fully evaporated microcavities in a single step process.

As demonstrators, we have realized three different λ quantum-microcavities with Pyrromethene 580 as active material, an 8 periods bottom mirror and with 6, 7 or 8 periods output coupler. We obtained a FWHM of the mode as low as 1.9 nm and a cavity Q-value of about 300 by using the 8 periods output coupler. Angular dependent reflectivity is measured to probe the cavity mode for different longitudinal wavenumbers. The mode energy shows a blue shift as the incidence angle increases, consistent with the theoretical photon-like dispersion inside the cavity. The cavity uniformity, probed by mapping the reflectivity in different position across the sample surface, is very good, despite the large sample dimension (about 25 mm^2) and the absence of a rotating sample holder in the evaporation chamber.

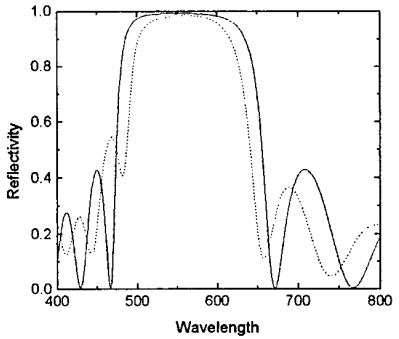

Fig.1: reflectivity of a 8 periods LiF/TeO_x DBR calculated by the Transfer Matrix Model (solid line) and experimental data from a real structure designed with the same parameters of the simulation. The peak reflectivity is 98.5% while the stopping band is 160 nm wide.

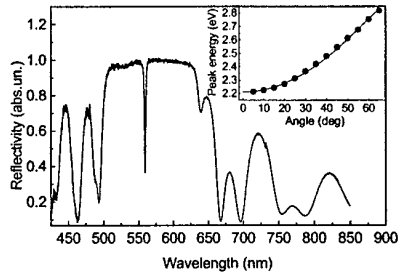

Fig.2: reflectivity spectrum of the 8 periods top mirror cavity for normal incidence. The stopping band FWHM is about 160 nm. Inset: mode energy as a function of the angle of incidence. The continuos line is the best fit curve with a photon-like dispersion curve obtained for a cavity energy at normal incidence E_0=2.212 ± 0.001 eV and a cavity effective refractive index n=1.451 ± 0.002.

Corresponding author: Marco Anni, Istituto Nazionale di Fisica della Materia, Univarsità degli Studi di Lecce,Dipartimento di Ingegneria dell'Innovazione. Via per Arnesano 73100 Lecce, Italy.
phone: +390832320231, Fax: +390832326351
email: marco.anni@unile.it

Parametric polariton oscillation: Temperature dependence and Non-linear polarization properties

A. I. Tartakovskii[2,1], D. N. Krizhanovskii[1], V. D. Kulakovskii[1], M. S. Skolnick[2], J. S. Roberts[3]

[1]*Institute of Solid State Physics, Chernogolovka, Russia*
[2]*Department of Physics & Astronomy, University of Sheffield, Sheffield, UK*
[3]*Department of Electronic and Electrical Engineering, University of Sheffield, Sheffield, UK*

Recent experiments on semiconductor microcavities (MCs) demonstrated a series of pronounced non-linear effects related to the parametric scattering of lower branch polaritons (LP) resonantly generated by laser excitation incident at a particular angle satisfying energy and k-vector conservation laws [1-3]. Here we present the detailed study of the renormalization of the energy of the LP states occurring due to polariton-polariton interaction in the regime of parametric scattering and also report the non-linear polarization properties of the process. The renormalization of the LP dispersion has been measured in two types of cw experiments: we study the temperature dependence of the process and also the modification of the whole emission pattern due to the tuning of the energy of the laser excitation (while keeping the angle of excitation and sample spot unchanged). The polarization properties of the parametric scattering have been studied using circularly and elliptically polarized resonant laser excitation leading respectively to generation of LPs with defined orientation of spin, or to a mixed population of both spin orientations.

Parametric oscillation is observed when resonant laser excitation generates high population of a particular LP state with energy E_o and wavevector k_o leading to LP-LP scattering which can be described by two conservation equations $2E_o=E_1+E_2$, $2k_o=k_1+k_2$ ($E_{1,2}$ and $k_{1,2}$ are the energies and wavevectors of two final LP states). In the case where k_1 equals 0 emission at two final LP states exhibit a threshold-like non-linear behaviour on excitation power due to stimulation by the high population of final state. In the case of circular σ^+ polarized excitation the parametric process is clearly observed only in σ^+ polarisation: two strong sharp peaks are observed at $k_1=0$ and $k_2=2k_o$ (the one at k=0 is referred to as "signal" below). Surprisingly, the threshold power, P_{th}, strongly depends on the polarization degree of the excitation, ρ. This leads to a strong increase of the "signal" emission with decreasing ρ in a range of powers close to P_{th} (Fig.1a). The effect can be explained in terms of a resonant two-photon scattering via biexciton state in analogy to the phenomenon observed in hyper-Raman scattering in bulk semiconductors [4]. The process becomes more efficient with increasing depolarization of the laser excitation since the biexciton state is a spin singlet. Due to stimulated character of the scattering the $k_1=0$ emission remains highly circularly polarised even when the sample is excited with strongly depolarized light (Fig.1b).

A notable feature of the parametric process is the blue shifting of the polariton dispersion curve due to polariton-polariton interaction. As predicted by theory [5] the blue-shifting of the "signal" relative to the energy of the LP emission at low laser power, E_{LP}, is determined by the linewidth of the LP state characterised by its dephasing rate. Our measurements show that in a wide range of excitation powers the energy of the σ^- polarised LP emission remains unchanged (equal to E_{LP}) thus leading to the appearance of an energy gap, *G*, between the "signal" and the σ^- line (Fig.1e). At higher temperature the laser has to be tuned to higher energy to maintain resonance and as a result *G* grows notably with T changing from 0.2 to 1.4 meV in the range of 5.9 -23 K (Fig.1c, d). A strong variation of *G* is also found when the laser is tuned to higher energy by up to 1.1 meV (at constant T) and the parametric scattering proceeds to a new pair of renormalized LP final states fulfilling energy and momentum conservation. In both experiments the increase of G is accompanied by the growth of P_{th}. In good agreement with the theory [5] in both cases the blue-shift is accompanied by a notable increase of the σ^- emission linewidth (which is roughly equal to the blue-shift) which, for example, grows with T from 0.2 to 1 meV in the range of 5.9 K<T<23 K (Fig.1d). The latter can be explained by the fast dephasing of LPs due to a large population of high energy exciton states which increases notably with T. It also increases when the laser energy is tuned close to the uncoupled exciton energy where the light absorption is much higher. Finally, we note that the renormalization of the LP states has been detected in a large range of both positive and negative k-vectors (Fig.1e).

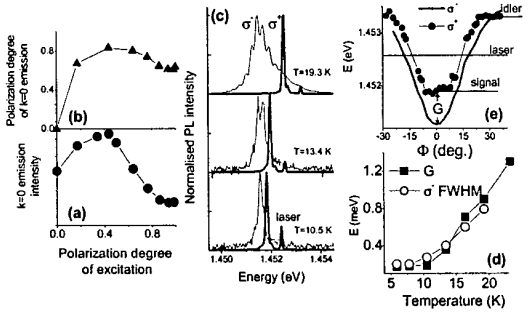

Fig.1. (a) k=0 emission intensity and (b) dependence of degree of circular polarization on circular polarization of the laser for excitation density 540 W/cm^2. (c) σ^+ (thick lines) and σ^- (thin lines) polarised emission spectra recorded at Φ=0 at different T. (d) Temperature dependence of the energy shift *G* (solid symbols) and σ^- polarised emission FWHM (open symbols). (e) Dispersion of σ^+ (symbols) and σ^- (line) polarised polariton states at T=13 K.

References

[1] P. G. Savvidis *et al.*, Phys. Rev. Lett. **84**, 1547 (2000)
[2] R. M. Stevenson *et al.*, Phys. Rev. Lett. **85**, 3680 (2000)
[3] A. I. Tartakovskii, D. N. Krizhanovskii, V. D. Kulakovskii, Phys. Rev. **B 62**, R13298 (2000)
[4] J. B. Grun, B. Honerlage, and R. Levy in *Excitons*, edited by E. I. Rashba and M. D. Sturge (North-Holland, Amsterdam, 1982), p. 459; E. S. Koteles, *ibid.*, pp. 95-102.
[5] C. Ciuti *et al.*, Phys. Rev. **B 62**, R4825 (2000)

Corresponding author: Dr. Alexander I. Tartakovskii, Department of Physics and Astronomy, University of Sheffield, Hicks Building, Hounsfield Road, Sheffield, S3 7RH, UK
Tel: +44 (0)114 2223522, Fax: +44 (0)114 2728079, e-mail:A.Tartakovskii@sheffield.ac.uk

Impact of exciton localisation on cavity polaritons

V. D. Kulakovskii[1], A. I. Tartakovskii[2,1], D. N. Krizhanovskii[1], M. S. Skolnick[2], J. S. Roberts[3]

[1]*Institute of Solid State Physics, Chernogolovka, Russia*

[2]*Department of Physics & Astronomy, University of Sheffield, Sheffield, UK*

[3]*Department of Electronic and Electrical Engineering, University of Sheffield, Sheffield, UK*

The high density of the photon field in semiconductor microcavities (MCs) with embedded quantum wells (QWs) leads to occurrence of new types of light-matter interaction effects [1-5]. In most studies of these phenomena, however, the impact of exciton localisation was practically neglected. In many cases this approach is justified because relatively weak fluctuations of the confinement potential of QWs neither change the dispersion nor cause additional broadening of the polariton states because of the large coherence size of the latter (of order of a few microns) [6]. However, since the localised exciton states are in resonance with the extended polariton states they may be expected to influence strongly the decay and energy relaxation of the excited polariton system. The greatest effect of the localised states should appear in the range of the polariton bottleneck [7,8]. Indeed, in this range phonon-assisted relaxation becomes ineffective since its characteristic time is comparable to the LP lifetime [7]. At the same time the effective density of localised states although decreasing exponentially with increasing energy separation from free exciton energy, E_X, is still very high in this energy range.

To study the impact of exciton localisation on cavity polaritons we have investigated polariton emission from a GaAs based MC under various excitation conditions, namely, with the predominant photocreation of (i) hot free carriers and excitons (excitation with a HeNe laser above band gap, Eg), (ii) lower branch polaritons and localised excitons (resonant excitation with a Ti-sapphire laser below E_X), and (iii) a mixed system (with simultaneous excitation by the two lasers).

Our studies have shown that the polariton energy distribution and emission intensity as well as their modification with temperature depend strongly not only on the density of photoexcited particles but also on their initial energy and momentum distribution, i.e. on the excitation conditions. In particular, it has been found that at low temperature T<15 K the relaxation into the LP states with high photon fraction situated 2-6 meV below E_X is much more efficient under the high energy non-resonant excitation in comparison to that in the case of resonant excitation below E_X. As a result, the difference in the polariton emission intensity for similar density of excited particles in the two cases can markedly exceed one order of magnitude. The more efficient relaxation also leads to a markedly different polariton population distribution in the two cases (see Fig.1). Furthermore, it has been found that a very weak additional illumination by a HeNe laser of MC resonantly excited with a Ti-sapphire laser into the LP branch below E_X, can result in very large changes (up to more than one order of magnitude) of the emission intensity from the LP branch. In such conditions a large emission enhancement is observed for the LP states several meV below E_X while the effect has opposite sign for the states with large exciton fraction located close to E_X.

A detailed study of the above mentioned effects have shown that the dynamics of the polariton system in the MCs excited below E_X is highly influenced by the exciton localisation at the QW potential fluctuations. The reservoir of the long (about 100 ps) lived localised exciton states is effectively filled by the Ti-sapphire laser excitation at the energy several kT below E_X. These states weakly contribute to the polariton emission at the energies other than that of the Ti-sapphire laser until collisions with hot carriers, mobile excitons, and phonons generated with an additional illumination of the sample with a HeNe laser excite them into the free exciton states. It has been demonstrated that the most effective energy relaxation to the LP branch bottom occurs via the capture of mobile excitons by deep potential fluctuations with following elastic or one phonon assisted scattering into the polariton states or via the direct exciton-exciton scattering from high energy states into the deep LP states.

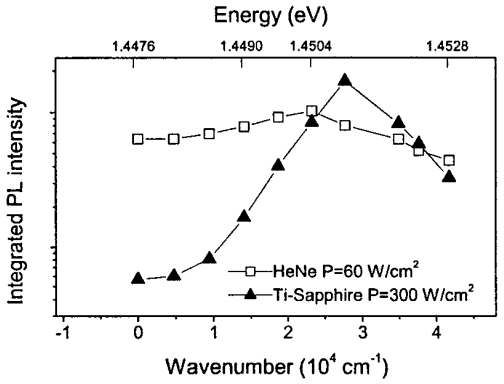

FIG.1. Polariton population distribution at temperature 6 K for 60 W/cm^2 non-resonant excitation (open symbols) and 300 W/cm^2 resonant excitation into the LP branch at 1.4508 eV (solid symbols).

References

[1] Le Si Dang *et al.*, Phys. Rev. Lett. **81**, 3920 (1998).
[2] P. Senellart, J. Bloch, Phys. Rev. Lett. **82**, 1233 (1998).
[3] P. N. Savvidis *et al.*, Phys. Rev. Lett. **84**, 1547 (2000); Phys. Rev. B, **62**, R13278 (2000).
[4] C. Ciuti *et al.*, Phys. Rev. B **62**, R4825 (2000).
[5] A. I. Tartakovskii *et al.*, Phys. Rev. B **60**, R11293 (1999).
[6] D. M. Whittaker et al., Phys. Rev. Lett. **77**, 4792 (1997).
[7] F. Tassone *et al.*, Phys. Rev. B **56**, 7554 (1997).
[8] A. I. Tartakovskii *et al.*, Phys. Rev. B **62**, R2283 (2000).

Corresponding author: Prof. Vladimir D. Kulakovskii, Institute of Solid State Physics, Chernogolovka, 142432 Moscow reg., Russia, Tel: ++7 095 7204959 ext. 2691, Fax: ++7 096-576-4111, e-mail: kulakovs@issp.ac.ru

Manifestations of quantum chaos in spectra of 2D photonic crystals

L.N. Gumen[1], J. Arriaga[2], A. Krokhin[2]

[1]Universidad Popular Autónoma del Estado de Puebla, 21 Sur, 1103, Puebla, 72160, Mexico

[2]Instituto de Física, Universidad Autónoma de Puebla, Apdo.Post.J-48, Puebla, 72570, Mexico

Photonic crystals (PC's) are novel periodic composites, which have found numerous applications in optics, optoelectronics, and radiophysics. PC's may posses a photonic band-gap - the optical analogue of the energy gap in the electronic spectra of semiconductors. For any fixed Bloch vector $\vec{k}$ within the Brillouin zone, the allowed photon frequencies form a discrete sequence $\omega_n(\vec{k})$, where $n = 1,2,3,\ldots$ is a band index. If considered as an array, the numbers $\omega_n(\vec{k})$ exhibit definite statistical properties, which are connected with the measure of chaos in the underlying classical system [1]. Highly chaotic spectra of quantum systems, e.g. nuclei, mesoscopic billiards, as well as frequency spectra of classical chaotic cavities, reveal statistical similarities and universalities, which are well-studied [1]. Statistical properties of the energy bands of natural crystals also exhibit signatures of quantum chaos, however they received much less attention [2]. We are not aware of any study related to statistical analysis of the spectra of artificial photonic crystals. Band-structure calculations for PC's are usually limited to the calculation of the first few bands (see review [3]) that is not enough at all for statistical analysis.

We consider a PC consisting of a set of infinitely long dielectric rods with constants ε_a arranged in a square lattice in air. This structure supports propagation of E and H-polarized modes. In the Γ point the Bloch vector $\vec{k} = 0$. That is in this point one can consider the Maxwell's equations in the long-wavelength limit. Applying the analytical method developed in Ref. [5], we obtain the following exact equation to calculate $\omega_n(0)$ for the E -mode,

$$\det\left[\frac{\omega^2}{c^2}\delta_{\vec{G},\vec{G}'} - GG'\eta(\vec{G}-\vec{G}')\right] = 0, \qquad \vec{G},\vec{G}' \neq 0. \qquad (1)$$

Here $\vec{G}$, $\vec{G}'$ are the reciprocal lattice vectors and $\eta(\vec{G})$ is the Fourier transform of the inverse dielectric constant, $\eta(\vec{r}) = 1/\varepsilon(\vec{r})$. For the H -mode the product GG' is replaced by $\vec{G}\cdot\vec{G}'$.

Eq. (1) is a polynomial equation with respect to ω^2; its roots are $\omega_n^2(0)$. This polynomial is of infinite order giving an infinite sequence of $\omega_n(0)$. In numerical calculations we truncate the number of $\vec{G}$ values to 1340. Due to the high-symmetry of the unit cell the bands at the Γ point are usually degenerated. In order to see the clean features of chaos we consider a unit cell which contains two "atoms" and thus it does not possess any discrete symmetry, see insert in Fig. 1. The Hermitian matrix $GG'\eta(\vec{G}-\vec{G}')$ in eq. (1) is positively defined, $\omega_n^2 > 0$. It belongs to the so-called Gaussian Orthogonal Ensemble (GOE) [1]. The level-spacing distribution for the GOE is given by a Wigner function, $p_W(s) = (\pi s/2)\exp(-\pi s^2/4)$. Here $p(s)$ is the probability density to find two neighbouring levels separated by an interval s. The dimensionless variable s is energy (frequency) normalized to the mean-level-spacing. In integrable systems the level spacing distribution is described by a Poisson function, $p_P(s) = \exp(-s)$. Any real system usually is neither integrable nor completely chaotic but is somewhere between Poisson and Wigner-like behavior [1].

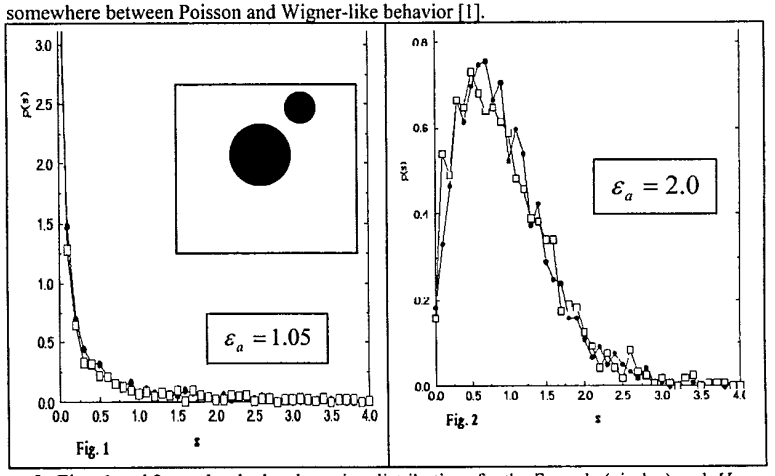

Fig. 1

Fig. 2

In Figs. 1 and 2 we plot the level spacing distributions for the E-mode (circles) and H-mode (squares) for two values of the dielectric constant, $\varepsilon_a = 1.05$ and $\varepsilon_a = 2.0$ respectively. In Fig. 1 the distribution is Poisson-like, i.e. the underlying dynamics is almost regular. Due to the low dielectric contrast between constituents the scattering at the rods is weak. The wave propagates like in a free space and the frequency spectrum is quasi-regular. On the contrary the spectrum in Fig. 2 is Wigner-like, i.e. the dynamics in this case of higher contrast is almost chaotic. For e/m waves the classical limit corresponds to the limit of geometrical optics. If the rods are unpenetrable, i.e. $\varepsilon_b = \infty$ the rays propagate like particles in the periodic array of hard cylinders. The latter system is known as *Lorenz gas* and it is completely chaotic. The tendency to the chaotization of the spectrum when the dielectric contrast increases is clearly seen in Figs. 1,2. Transport properties of a PC are directly related to the correlation functions of its frequency spectrum. Parametric correlations can be calculated using eq. (1). This will be done elsewhere.

This work is supported by CONACyT, grants No. 28626-E and 33808-E.

References

[1] H.-J. Stöckmann, *Quantum Chaos - An Introduction*, Cambridge University Press, 1999.
[2] E. Mucciolo, R. Capaz, B. Altshuler, and J. Joannopoulos, Phys. Rev. B **50**, 8245 (1999).
[3] J. Joannopoulos et al, *Photonic Crystals*, Princeton University Press, 1995.
[4] P. Halevi, A. Krokhin, J. Arriaga, Phys. Rev. Lett. **82**, 719 (1999); Appl. Phys. Lett.**75**, 2725 (2000).

Corresponding author: Ludmila Gumen, Departamento de Matemáticas, Universidad Popular Autónoma del Estado de Puebla, 21 Sur, 1103, Puebla, 72160, Mexico
phone: +(52-22)29.94.00 ext. 530 , fax: +(52-22)32.52.51 ,
e-mail: lgumen@sun1.pue.upaep.mx

Radiative Width of a collective mode in a resonant Bragg reflector: the Validity Limit of Super-Radiant mode

T. Ikawa and K. Cho
Department of Material Physics, Graduate School of Engineering Science
Osaka University,1-3 Machikaneyama, Toyonaka, Osaka, 560-8531 Japan

We investigate the radiation-matter interaction in a Bragg reflector consisting of N quantum wells (QW's) with a regular spacing d=0.5λ_0 (λ_0 = resonant wavelength), which satisfies Bragg condition. Based on the earlier works [1, 2] on the radiative width of QW exicitons, Ivchenko *et al.*[3] derived a super-radiant (SR) mode in a N layered QW's which has a radiative width of N times that of a single QW Γ_0. The reflection amplitude is shown to be $r_N(\omega) = -iN\Gamma_0/[\hbar\omega_0 - \hbar\omega - i(\Gamma + N\Gamma_0)]$, where Γ is a nonradiative damping. Theoretical study has been further extended by other groups [4, 5]. There are also experimental studies with multiple (N) QW's that back up the theoretical result by showing the enhanced decay rate of superradiance by the factor of N in time domain [6, 7] or the N-linear broadening of reflectance spectrum in frequency domain [8, 9].

The above result of $r_N(\omega)$ is obviously unphysical for large N, because the N-linear enhancement goes without limit. There has been no reasonable argument about the fate of this SR mode as we increase N. Focusing on this problem, we have considered how this SR mode evolves with increasing N by using microscopic nonlocal theory [10]. This theory describes the radiative correction (i.e., shift and width) of a given quantum level from the first principles as the interaction energy between induced current densities via transverse light field. For the present problem, it turns out essential to consider the dependence of this interaction energy on the frequency (ω) of the mediating light. By taking into account the ω-dependence properly, we obtain a reasonable evolution of the reflectance curve with N. Namely, for smaller N, the reflectance spectram has a Lorentzian shape whose HWHM is the radiative width, and for larger N, the spectrum evolves into a silk-hat shape, which is typical for a photonic gap [11, 12]. The result of this limiting case (N$\rightarrow\infty$) agrees with the position of the photonic band gap studied by Deych*et al.*[13].

Since the resonant levels on QW's are electronically isolated, this spectral evolution is entirely caused by the (ω, N)-dependence of radiative correction, which becomes more and more important as N gets larger. The idea of SR mode is valid as long as the ω-dependence of radiative width is small, because otherwise there is no unique way to connect the imaginary part of radiative correction with the spectral width of the mode. Thus, the concept of SR mode is lost, when its spectral shape starts to be distorted from a Lorentzian shape. The experimental proof of the SR mode mentioned above does not mean the validity of the concept for arbitrarily large N. Its vaidity limit should be observable in both time and frequency domains as a silk-hat shaped spectrum or as a non-exponential decay.

We have also studied the temporal response of the system for a Gaussian shaped incident pulse to the N layer Bragg reflector made of atomic planes. Fig.1 shows the time-resolved reflection dynamics for several different N's. For smaller N the super-radiant behavior of the system is reconfirmed. For larger N (N$\geq$40), the reflected signal shows a decay with oscillations and the average decay rate decreases with increasing N. The oscillation period

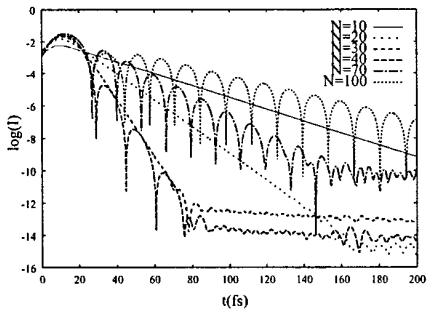

Figure 1: Time-resolved reflection dynamics for a Gaussian pulse of light on the periodic structures containing N=10,20,30,40,70 and 100 atomic layers.

reflects the width of silk-hat in the reflectance spectrum. This result also indicates the vanishing of the super-radiant mode for larger N. The theoretical scheme allows us also to calculate the N- and ω-dependent internal field $\vec{E}(\vec{r})$. Its detailed structure also confirms the arguments mentioned above.

We conclude that, for N larger than a critical value, the ω-dependence of radiative width becomes important, invalidating the concept of SR mode, and leading to the disappearance of the Lorentzian spectrum and the exponential decay signal.

[1] L. Andreani, Solid State Commun.**77**(1991)641
[2] D. S. Citrin, Solid State Commun.**84**(1992)281
[3] E. L. Ivchenko *et al.*, Phys. Solid State **36** (1994) 1156
[4] L. C. Andreani *et al.*, Phys. Rev. Lett.**B57** (1998) 4670
[5] S. Haas *et al.*, Phys. Rev.**B57** (1998) 14860
[6] M. Hübner *et al.*, Phys. Rev. Lett.**76**(1996)4199
[7] M. Hübner *et al.*, Solid State Commun.**105**(1998)105
[8] Y. Merle d'Aubigné *et al.*, Phys. Rev.**B54**(1996)14003
[9] M. Hübner *et.al.*, Phys. Rev. Lett.**83** (1999) 2841
[10] K. Cho, Prog. Theor. Phys. Suppl.**106** (1991) 225
[11] T. Ikawa and K. Cho, Jounal of luminescence **87-89** (2000) 305
[12] T. Ikawa and K. Cho, Proc. 25th Int. Conf. on Physics of Semiconductors (Osaka,Japan,2000/9/17-22)(to be publised)
[13] L.I. Deych and A.A. Lisyansky, Phys. Rev. **B62** (2000) 4242

Corresponding author: Tomoe Ikawa, Department of Material Physics, Graduate School of Engineering Science, Osaka University, Toyonaka, 560-8531, Japan
phone: +81-6-6850-6402, Fax: +81-6-6850-6401
email: ikawa@aria.mp.es.osaka-u.ac.jp

Coupling of GaAs/AlGaAs quantum well photoluminescence to metal surface plasmons excited by grating couplers

N. Sawaki, T. Ohashi, M. Yamaguchi
Nagoya University, Dept. of Electronics, Chikusa-ku, Nagoya 464-8603, Japan

The surface plasmons excited at the interface between a metal and a semiconductor can propagate along the surface and have a finite electromagnetic field which is maximum at the interface and penetrates into the semiconductor. If we have a quantum well/dot near the surface, the excitons in the well/dot would couple to the electromagnetic field. The manipulation of the excitonic states by the surface plasmons might open a new possibility of the quantum wells/dots as electronic as well as photonic devices, since the excitation of the plasmons is achieved by various means[1].

The surface plasmons can be excited by a laser light using the attenuated total reflection (ATR) or a metal film with non-uniform thickness[2]. The deposition of metal island films has been found to enhance the optical absorption efficiency of the semiconductors[3]. But a grating coupler is more convenient to the systematic study of the phenomena. Moreover, the modification of the semiconductor surface by a periodic structure will open further possibilities in the field of electro-optics. In this paper, we will demonstrate that the excitation of the surface plasmons actually enhances the band-to-band transition in a quantum well under the surface.

A 6 nm wide GaAs quantum well was grown by molecular beam epitaxy between AlGaAs cladding layers. The quantum well is at 35 nm from the surface. On the surface of the quantum well sample, a 12 nm thick gold film was deposited. The grating coupler was made with electron beam lithography on the gold film by depositing another 12 nm thick gold layer. The period of the grating was L=400 nm or 500 nm. The schematic structure of the sample is illustrated in Fig.1. The thickness of the gold metal film is modulated to ensure the excitation of the surface plasmons[2]. This is the main difference from the former reports where the grating couplers were made by metal stripes[4,5]. The uniform contact of the metal film with the semiconductor surface might help the propagation of the surface plasmons and hence the life time of the plasmons would be enhanced. As a result, we should observe clearer evidence of the plasmon modes. The reflection/photoluminescence was measured at 77 K using 632.8 nm line of a He-Ne laser.

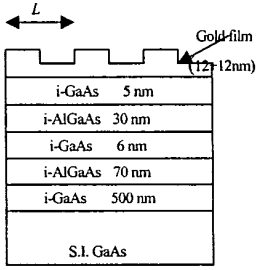

Fig.1. Schematic sample structure

By a laser beam of a frequency ⊔ incident at an angle ⊔ from the surface normal, we can excite a plasmon with a wave vector $k = (⊔/c)\sin ⊔ \pm j(2\pi/L)$, where j is an integer[4]. The dispersion of the surface plasmon-polariton mode between the gold film and GaAs is, on the other hand, determined by the dielectric constants of the materials[2]. In order to exclude the ambiguity, the dielectric constant of a 12 nm thick gold film on GaAs for 632.8 nm light was determined by reflection analyses; (⊔= -15.2 + i1.0). Using this value and the dielectric constant for GaAs, we estimated the incident angle that we could ever excite the surface plasmons; ⊔=39.9°for L=400 nm and ⊔=17.9°for L=500 nm.

Figure 2 shows the variation of the first order diffraction signal intensity from the grating, the minimum of which shows the resonant excitation of the surface plasmons. It is at 40.3°for a sample with L=400 nm. For a sample with L=500 nm, the minimum was obtained at 19.3°. These values are in good agreement with the prediction given above, which suggesting we are exciting plasmons at these angles. The slight deviation is attributed to that we have assumed a constant dielectric constant for GaAs and AlGaAs.

The photoluminescence spectra at 77 K, excited by the 632.8 nm beam, exhibited a main peak at 787 nm which is due to the band-to-band transition in the quantum well, in addition to a peak at 820 nm which is from the bulk GaAs. The 787 nm peak intensity was measured as a function of the angle of the incident laser beam. A typical result is shown in Fig.3, which shows that the quantum well luminescence is enhanced at⊔=40.1°, where the surface plasmons are excited. The enhancement is on the order of a few percent.

The electromagnetic field due to the plasmons penetrates into the semiconductor, and the penetration length is estimated using the dielectric constants of gold film and GaAs. Assuming uniform dielectric constant in the semiconductor, the penetration length for the present sample was estimated to be 36 nm, which is comparable to the distance of the quantum well from the surface. This proves the coupling of the plasmons to the quantum well luminescence.

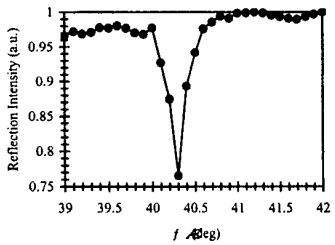

Fig.2. First order diffraction intensity of L=400 nm grating

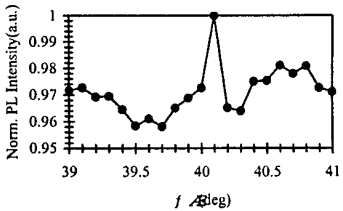

Fig.3. PL intensity from the quantum well

References

[1] A. Koeck, W. Beistingel, K. Berthold, and E. Gornik, Appl. Phys. Lett. **52**(1988) 1164.
[2] U. Schroeter and D. Heitmann, Phys. Rev. **B60** (1999) 4992.
[3] H.R. Stuart and D.G. Hall, Appl. Phys. Lett. **69**(1996) 2327.
[4] N. E. Hecker, R.A. Hoepfel, N. Sawaki, T. Maier, and G. Strasser, Appl. Phys. Lett. **75**(1999) 1577.
[5] L.Wendler and T. Kraft; Physica **B 271**(1999) 33.

Corresponding author: Nobuhiko Sawaki,
Nagoya University, Dept. of Electronics, Chikusa-ku, Nagoya 464-8603, Japan
Phone: +81-52-789-3321, Fax: +81-52-789-3157
E-mail: sawaki@nuee.nagoya-u.ac.jp

Time-resolved imaging by using μ-PL measurement and sum frequency mixing

Y. Nagamune[1,2] and M. Ogura[1,2]

[1]Electrotechnical Laboratory, 1-1-4 Umezono, Tsukuba-shi, Ibaraki, 305-8568, Japan
[2]Core Research for Evolutional Science and Technology, Japan Science and Technology Corporation, Kawaguchi Center Building,
4-1-8 Honcho, Kawaguchi-shi, Saitama 332-0012, Japan

Time-resolved measurements are very important for the investigation of various electronic effects in physics and for the characterization of devices using quantum nanostructures[1]. We have so far reported on the time-resolved imaging of carrier drag effect in GaAs/AlGaAs nanostructures in the time resolution of 90 ps[2]. These investigations provide novel observation approaches for visualization of electron flow and understanding of the nature of exciton-electron scattering or exciton-phonon in quantum nanostructures. In the present work, we report on the ultrafast time-resolved imaging in the time-resolution of 200 fs by the combination of micro-photoluminescence (μ-PL) measurement[3] and sum frequency mixing (SFM), namely up-conversion technique[4]. We demonstrate time-resolved measurements as for the emission from vertical cavity surface emitting lasers (VCSELs) as an example. Here, it is known that VCSELs indicate very short pulse generation less than 8 ps[4].

A schematic illustration of the setup is shown in Fig. 1. A laser beam from a mode-locked Ti: Sapphire laser was divided into two by a beam splitter in a Michelson interferometer, and one was used for sample excitation and another reference beam for the non-collinear cross-correlation at the nonlinear crystal BBO. The excitation beam was focused on a sample surface by an objective lens. The emission from the sample was collected by the same objective lens and focused in the BBO. An image of the reference beam in the BBO was defocused by a pair lens for imaging of the emission from the sample. Images of the excitation laser on the sample surface and the emission were monitored by a charge coupled device (CCD) camera. A white light illumination was used for observing the sample structure. The CCD camera was also used for monitoring the virtual images in the BBO. The SFM beam generated in the BBO was focused on an intensified CCD (ICCD) camera through an aperture and a spectrometer. Minimum spatial resolution was about 1 μm and time resolution was about 200 fs, which was estimated from the auto-correlation between the reference beam and the reflection from the sample. For observing two-dimensional time-resolved images, 0th order dispersion of the grating in the spectrometer and a band-pass filter were used.

Figure 2 shows time-, spatial-, and spectral-resolved images taken by the present measurement system at the delay time of zero. Here, an image indicated by an arrow in the lower photograph is the SMF of the VCSEL with a wavelength 818 nm and the Ti: Sapphire laser 775 nm. In order to achieve optical pumping, the VCSEL was biased so as to be set at the lasing threshold. When the bias current was switched off, no optical pumping was achieved, therefore, no SMF was observed as shown in the upper photograph. An image around 388 nm is the second harmonic generation (SHG) of the Ti: Sapphire laser which was generated by the imperfection of the BBO.

In conclusion, we first developed ultrafast time-resolved imaging by using μ-PL and SFM techniques, and demonstrated time-resolved photographs of VSCELs.

References

1) H. Watabe, Y. Nagamune, F. Sogawa, and Y. Arakawa, Solid-State Electronics **40** (1996) 537.
2) Y. Nagamune, in *Proceedings of the Society of Photo-Optical Instrumentation Engineers (SPIE), Physics and Simulation of Optoelectric Devices VIII*, San Jose, 2000, edited by R. H. Binder, P. Blood, and M. Osinski (SPIE, Washington, 2000) vol. **3944**, p. 480.
3) S. Haacke, R. A. Taylor, I. Bar-Joseph, M. J. S. P. Brasil, and M. Hartig, and B. Deveaud, J. Opt. Soc. Am. B**15** (1998) 1410.
4) F. Sogawa, A. Hangleiter, H. Watabe, Y. Nagamune, M. Nishioka, and Y. Arakawa, in *Abstracts of the International Workshop on Femtosecond Technology*, Tsukuba, 1996 (Femtosecond Technology Research Association, Tsukuba, 1996) p.115.

Corresponding author: Yasushi Nagamune, Electrotechnical Laboratory, National Institute of Advanced Industrial Science and Technology,
1-1-4 Umezono, Tsukuba-shi, Ibaraki, 305-8568, Japan
Phone: +81-298-61-5619, Fax: +81-298-61-3349, Email: nagamune@etl.go.jp

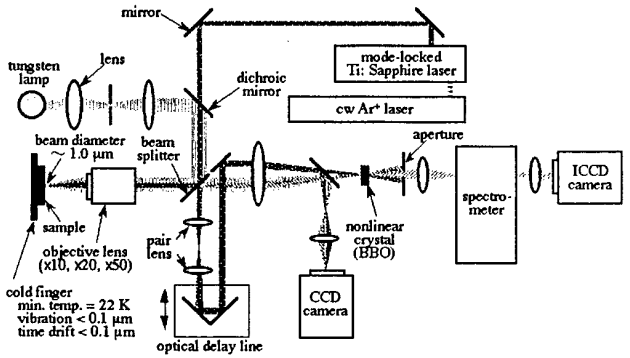

Fig. 1 Schematic illustration of the measurement setup.

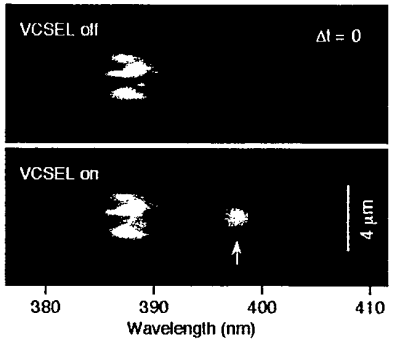

Fig. 2 Time-, spatial-, and spectral-resolved photographs.

Intersubband plasmon polaritions in MQW structures and their manifestation in TIR spectra

M. Załużny, W. Ziętkowski

Institute of Physics, M. Curie Skłodowska University,
pl. M. Curie Skłodowskiej 1, 20-031 Lublin, Poland

Properties of the intersubband transitions (plasmons) in single quantum well (SQW) and multiple quantum well (MQW) structures have been discussed recently in the review article by Helm [1]. The surface intersubband plasmon polaritons (SIPPs) and radiative intersubband plasmon polaritons (RIPPs) in SQW structures have been studied by Chen *et al.* [2] in the framework of the so-called local slab model and by Wendler *et al.* [3,4] employing the fully nonlocal approach based on the vector random-phase approximation and the Green's function formalism. In this paper we consider RIPPs in MQW structure with large number of QWs ($N_{QW} \gg 1$). We also discuss the manifestation of the intersubband polaritons in total internal reflection (TIR) spectra. The above configuration is formed by a semi-infinite isotropic dielectric (medium of incidence), MQW structure, a thin caplayer and air.

Following Ref. [5], we assume that MQW structure can be modeled by an effective uniaxial local medium. (The usefulness of the local susceptibility model for description of the optical properties of MQW structures in the range of intersubband transitions was recently demonstrated by Dupont *et al.* [6].) The dispersion relations are derived employing approach similar to the one developed by Kliewer *et al.* [7,8] for the case of radiative phonon polaritons. However, in contrast to these papers we take into account a very strong anisotropy of the effective medium.

In the standard virtual-mode treatment the frequency of a mode (ω_n) should be treated as a complex number. The results obtained indicate that intersubband radiative (virtual) modes can be divided into two groups: low frequency (L) modes with $Re(\omega_n) < \tilde{\omega}_{21}$ and high frequency (H) modes with $Re(\omega_n) > \tilde{\omega}_{21}$ where $\tilde{\omega}_{21}$ denotes the depolarization shifted intersubband frequency. (We work in the two-parabolic-subband model.) The low-frequency modes with large n are all tightly packed into region very near $\tilde{\omega}_{21}$ while high-frequency modes with large n occur at very high frequency. The structures in the absorption spectrum can be associated with virtual modes [8]. The absorption due to an individual mode is a resonance peak centered at $Im(\omega_n)$ with total width $\gamma_n = 2|Im(\omega_n)|$. Numerical value of γ_n is determined by the radiative width due to the flow of energy out of MQW and the presence of the damping in MQW structure.

Figure 1 shows the absorption (A) of GaAs/GaAlAs multiple quantum well structure (similar to the one discussed in Ref. [5]) as a function of the normalized frequency $* \rightarrow \omega/\tilde{\omega}_{21}$. The bars above peaks are labeled by the type and the number of the mode with which it is associated. They illustrate the center frequency of the virtual mode and its total width γ_n. It is easily noticeable that mode 0H is responsible for the maximum at $* \rightarrow 1.2$. When $0.8 < * < 1.1$, the spacing between modes is smaller than their width, and the absorption peaks merge.

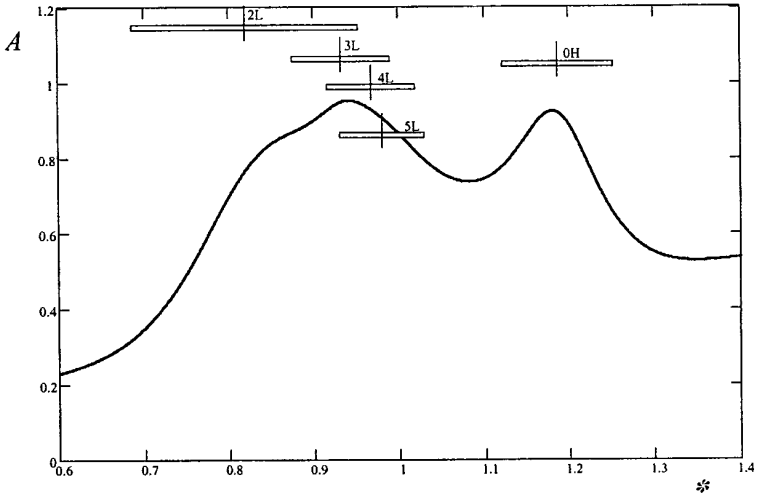

Fig. 1 Absorption as a function of * for the system GaAs–MQW–air; an angle of incidence θ = 65 and $N_{QW} = 200$.

References

[1] M. Helm, in "Intersubband transitions in quantum wells: physics and devices applications" Semiconductors and Semimetals, **62**, eds H.C. Liu and F. Capasso (Academic Press, San Diego, 2000)
[2] W.P. Chen, Y.J. Chen, and E. Burstein, Surf. Sci. **58** (1976) 263.
[3] L. Wendler and E. Knadler, Phys. Status Solidi B **177** (1993) 9.
[4] L. Wendler and T. Kraft, Phys. Rev. B **60** (1999) 16 603.
[5] M. Załużny and C. Nalewajko, Phys. Rev. B **59** (1999) 13 043.
[6] E. Dupont, M. Gao, H.C. Liu, Z.R. Wasilewski, A. Shen, M. Załużny, S.R. Schmidt, and A. Seimeier, Phys. Rev. B **61** (2000) 13 050.
[7] K.I. Kliewer, R. Fuchs, Phys. Rev. **150** (1966) 573.
[8] K.I. Kliewer, R. Fuchs and W.J. Pardee, Phys. Rev. **150** (1966) 589.

Corresponding author: Mirosław Załużny, Instituite of Physics, M. Curie Skłodowska University, pl. M. Curie Skłodowskiej 1, 20-031 Lublin, Poland
phone:,Fax: (48-81) 537-61-91
e-mail: zaluzny@tytan.umcs.lublin.pl

Miniband magneto-transport in GaAs-AlAs island superlattices

A. Patanè[1], A. Ignatov[1,2], E. Schomburg[2], L. Eaves[1], A. Levin[1], R. Scheuerer[2], P.C. Main[1]
K. F. Renk[2], V.M.Ustinov[3], A.E.Zhukov[3], A.R.Kovsh[3]

[1]*School of Physics and Astronomy, University of Nottingham, Nottingham NG7 2RD, UK*
[2]*Institut fur Angewandte und Experimentelle Physik, Universitat Regensburg, Germany*
[3]*A.F.Ioffe-Physico-Technical Institute, St.Petersburg, Russia*

We study miniband magneto-transport in a GaAs/AlAs superlattice (SL) with AlAs barriers each of half a monolayer thickness. The novel concept is the replacement of the conventional two-dimensional AlAs barrier by an in-plane distribution of two-dimensional AlAs islands [1]. The thin effective AlAs barrier results into a wide miniband (Δ= 105 meV) (see Fig.1), which is of interest for the development of microwave oscillators operating at THz frequencies.
We investigate magneto-transport for different directions of magnetic fields, B: parallel and perpendicular to the SL growth axis, z.
For $B \perp z$, electrons are deflected from the SL axis due to the action of the Lorentz force and acquire a momentum in the growth plane x-y (see Fig. 2) [2]. In turn this affects the miniband current, I, to an extent that depends on magnetic field and the in-plane elastic scattering rate along the deflection direction of the electron. The scattering is caused in part by the AlAs island barriers. By rotating the magnetic field in the growth plane and measuring $I(B)$ for each rotational angle, ϕ, we probe the anisotropy of the scattering associated with AlAs islands. The islands are elongated along a preferential crystallographic direction, which generate anisotropic scattering of the electron in the growth plane. We use a semiclassical transport model [3] including the Lorentz force for explaining the dependence of current on the rotational angle of B and for probing the rate of elastic scattering.
For $B//z$, the magnetic field suppresses the lateral motion of the electron and induces a quasi-one-dimensional motion along the SL axis. The electronic motion is quantized by B and additional Landau-quantized minigaps and minibands are formed. We observe a relative small quenching of current with increasing B that we interpret as due to partial suppression of inelastic scattering [3] when the Landau minibands form. We compare the extent of current quenching with that observed in narrower miniband SLs (Δ~ 10 meV) [4], examining the mechanisms responsible for current conduction in the quasi-1d SL induced by B.

References

[1] E. Schomburg et al., Phys. Lett.A 262, 396 (1999)
[2] F. Aristone et al., Appl. Phys. Lett. 67, 2916 (1995)
[3] A. A. Ignatov et al., Mod. Phys. Lett. B 5, 1087 (1991)
[4] L. Eaves et al., Physica B 272, 190 (1999)

Corresponding author: Amalia Patanè
School of Physics and Astronomy, University of Nottingham, NG7 2RD, UK
phone: +44-115-9515151-8334 fax: +44-115-9515180
e-mail: Amalia.Patane@nottingham.ac.uk

Fig. 1: Continuous line: current-voltage characteristics at 300 K of a GaAs/AlAs SL with sub-monolayer AlAs barriers [1]. The dotted line is the theoretical curve calculated by a semiclassical model [3]. The inset sketches the conduction band diagram of the SL.

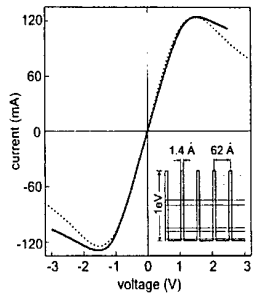

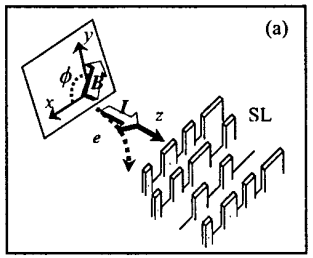

Fig. 2 (a): Geometry of our magneto-tunnelling experiment: the magnetic field, B, is perpendicular to the growth axis, z, of the GaAs/AlAs island superlattice, SL.

Fig. 2 (b): Dependence of the miniband current, I, on the angle of rotation, ϕ, of B in the SL plane (V=0.3 V). ΔI is the maximum angular variation of I and I_{min} is the minimum current value.

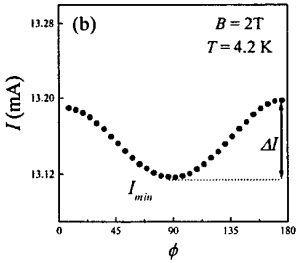

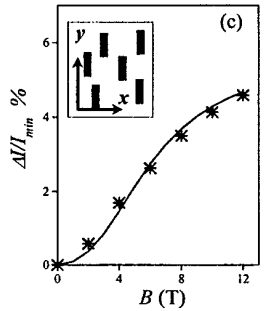

Fig. 2 (c): Dependence of $\Delta I/I_{min}$ on B. The stars are the experimental data and the continuous line is the theoretical curve derived from a semiclassical transport model with anisotropic in-plane scattering. The rate of elastic scattering along x and y is 2×10^{13} s^{-1} and 2.1×10^{13} s^{-1}, respectively. The inset sketches the anisotropy of the SL interface.

Ultra Fast Decay of Enhanced Degenerate Four Wave Mixing of Multiple GaAs Thin Layers

Hajime Ishihara
Department of Physical Science, Graduate School of Engineering Science,
Osaka University, Machikaneyama 1-3, Toyonaka, Osaka 560 - 8531, Japan

Realization of the large nonlinear effect combined with the ultra fast response is a challenging subject because the resonant effect for the large nonlinearity usually induces a long decay time of excited carriers, which makes it difficult to realize ultra fast optical devices. Recently, a enhanced degenerate four wave mixing (DFWM) signal has been observed for a particular thickness of GaAs thin layer[1], which establishes former proposed large nonlinearity by "nonlocality-induced double resonance in energy and size (NIDORES)"[2]. And further, it has been shown that this type of nonlinear response exhibits a ultra fast decay time of a few ps[3]. The purpose of this contribution is to elucidate theoretically why the nonlinear response by NIDORES shows such a very short response time for this material, and to show the possibility of further speed up by using a periodically stacked GaAs thin layers.

First, we calculate DFWM of a GaAs single layer with the self-consistent transient response theory[4] where we consider the microscopic position dependence of the field and induced polarization. As a model system, we assume a thin film with thickness d confining the center-of-mass (CM) motion of excitons. If we suppose simplified boundary conditions, the eigenfunction of confined CM motion is $\Phi_{EX,n}(Z) = \sqrt{2/d}\sin(K_n Z)$, where Z is the coordinate of the surface normal direction, and K_n satisfies the quantization condition $K_n d = n\pi$ (n = 1,2,3...). Figure 1 shows the time profile of the DFWM signal from the front surface for the several different thicknesses. The signal intensity is largely enhanced around d = 120 nm, and at the same time, the decay time becomes very short at this thickness. The large DFWM signal with a very short decay time is attributed to the second quantized state with n = 2 whose wavefunction has one node in the surface normal direction. Actually, if we calculate the same quantity with the contribution of n = 1 exciton alone, such an enhancement never appear, and the decay time becomes much longer (Fig. 1(b)). As explained in Ref.[5], such a large contribution of n = 2 exciton is due to the resonant enhancement of the internal field with a non-dipole type spatial pattern which is induced by the nonlocal effect.

To understand the short response time seen in Fig 1(a), we evaluate the radiative width of each excitonic level, which can be calculated as the imaginary part of complex eigenmodes of the exciton-radiation coupled system[6]. Figure 2 shows the thickness dependence of the radiative width in the case of (a) single, (b) double, and (c) triple layer structure. For (b) and (c), we assume the 5-nm-thick barrier layers between the GaAs layers. In (a), we can see the increase of the radiative width of the lowest level in the very thin region, which corresponds to the size linear enhancement of the oscillator strength in the long wavelength approximation (LWA) regime[7]. This, however, turns to decrease with the further increase of thickness, and then, the width of the second level is enhanced and takes maximum value around d = 120 nm. This means that LWA is no longer valid in this size region, and the radiation couples strongly with the non-dipole type excitonic state rather than the lowest excitonic state. Interestingly, for this material, this optimum thickness almost coincides with the thickness where DFWM is strongly enhanced by NIDORES. Thus, we understand that the very fast decay of the large DFWM reported in Ref.[2] is due to a non-dipole type transition, which is in a striking contrast to the optical effects described within the macroscopic framework.

Figure 2 (b) and (c) show further speed up of the response time. Namely, in (b) and (c), almost two and three times enhancement occur, respectively, at the thickness where a single layer exhibits a maximum width. In the case of the multiple layers, the excitonic modes that are confined in individual layers couple with each other via radiation, and one coupled mode almost monopolizes the radiative width if the Bragg condition is satisfied. Such radiative width increases in proportion to the number of the layers, and a response time of several 100 fs would be realized if we use triple layer structure, for example. This phenomenon has similar aspects to the recently discussed large coupling between the radiation and multiple-quantum-well Bragg structure[8]. The different point is that the large radiation-exciton coupling, in the present effect, is obtained by making good use of the spatial structures of both the excited state and radiation field within a single layer. And more importantly, the thickness of each layer is almost optimized for the enhancement of the nonlinear signal due to NIDORES, which is favorable for the simultaneous realization of the large nonlinearity and ultra first response.

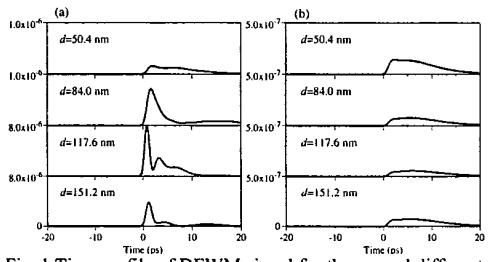

Fig. 1 Time profile of DFWM signal for the several different thicknesses. (a): Up to n=4 excitonic state are included in the calculation. (b): Only n=1 excitonic state is considered.

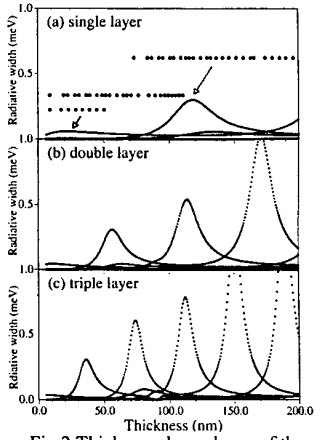

Fig.2 Thickness dependence of the radiative width of coupled modes.

[1] K. Akiyama, N. Tomita, Y. Nomura and T. Isu, Appl. Phys. Lett. **75**, 475 (1999).
[2] H. Ishihara and K. Cho, Phys. Rev. B**53**, 15823 (1996).
[3] K. Akiyama, N. Tomita, T. Nishimura, Y. Nomura and T. Isu, in Abstracts of The 7th International Workshop on Femtosecond Technology (FST2000, Tsukuba).
[4] H. Ishihara, J. Luminescence Vol.87-89 905 (2000).
[5] H. Ishihara, K. Cho, K. Akiyama N. Tomita, Y. Nomura and T. Isu, Proc. 25th Int. Conference on the Physics of Semiconductors (Osaka 2000) to be published.
[6] K. Cho: Prog. Theor. Phys. Suppl. No.106 225 (1991).
[7] E. Hanamura: Phys. Rev. B37 1273 (1988).
[8] M Hübner, J. Kuhl, T. Stroucken, A. Knorr, S.W. Koch, R. Hey and K. Ploog, Phys. Rev. Lett. **76**, 4199 (1996).

Corresponding author: Hajime Ishihara, Department of hysical Science, Graduate School of Engineering Science, Osaka University, Machikaneyama, Toyonaka, Osaka 560 - 8531, Japan
Phone: +81 6 6850 6401, Fax +81 6 6850 6401,
e-mail: ishi@mp.es.osaka-u.ac.jp

Investigation of intersubband relaxation dynamics by pump-probe spectroscopy and application to ultrafast all-optical modulation scheme

T. Asano, S. Yoshizawa, and S. Noda

Department of Electronic Science and Engineering, Kyoto University
Yoshida-Honmachi, Sakyo-ku, 606-8501, Japan

Introduction: We have previously proposed an ultrafast all-optical modulation scheme based on intersubband transition (ISB-T) in an n-doped quantum wells (QWs) [1]. Figure 1-(a) shows the schematic diagram. An intense ISB-resonant (CB1-CB2) light pulse (=control light) can decrease electron population in CB1 to modulate the absorption of HH1-CB1 interband (IB) resonant light (=signal light). The modulation speed is determined by the population relaxation time of the ISB-T. We have demonstrated the modulation by using GaAs/AlGaAs QWs, and observed an ultrafast response time of ~ 1ps (FWHM) [2]. However, the modulation also contains a slowly tailing component (3~5 ps), which restricts the repetition rate of the modulation.

The understanding of the population relaxation process of the ISB-T is a key to improve the modulation scheme. The ISB relaxation path is generally considered to consist from two serial processes: (A) ISB scattering from CB2 to CB1 via electron-longitudinal optical (LO) phonon scattering, and (B) intrasubband relaxation within CB1 via electron-electron and electron-phonon scatterings. The process (A) has been clarified well (~1ps in GaAs/AlGaAs QWs) while (B) has not been clarified, yet. Therefore, we considered that the slow component is due to the process (B), and proposed an improved scheme where the signal light is tuned to HH2-CB2 transition (see Fig. 1-(b)). In this scheme, the process (B) can be avoided since the population relaxation dynamics in CB2 determines the modulation speed.

In this report, we investigate the previous and new modulation scheme simultaneously. The electron relaxation mechanism is precisely investigated by the quantitative method.

Experimental: The sample investigated was multiple QWs that consist of 150 periods of GaAs (59Å) / $Al_{0.35}Ga_{0.65}As$ (150 Å). Only the barrier layers were doped with Si (~$1.5\times10^{18}cm^{-3}$). The energy separations between subbands are shown in the inset of Fig. 2-(b). In the modulation experiments, the sample was pumped by an ISB-resonant light pulse (0.17 eV, ~ 120 fs) and was probed by a white-light continuum that ranges from 1.45~1.9 eV. All the measurements were carried out at room temperature.

Results and Discussions: Figure 2-(a) shows the obtained pump-probe profile (T/T_0). The modulation in a photon energy range of 1.50~1.7eV corresponds to HH1-CB1 transition and reflects the change in the electron occupation in CB1. The modulation in a photon energy range of 1.7~1.9 eV corresponds to HH2-CB2 transition and reflects the change in the electron occupation in CB2. The former and the latter correspond to the previous and new modulation schemes, respectively.

Figure 2-(b) shows the cross section of the modulation profile at representative photon energy. The cross section at 1.75 eV (near the bottom of HH2-CB2 transition) shows single exponential relaxation, and the relaxation time is about ~ 0.4 ps. The cross section at 1.55 eV (near the bottom of HH1-CB1 transition) shows double exponential relaxation, and the fast and slow components of the relaxation times are about 2.5 ps and 6 ps, respectively. The overall response time of the new scheme was faster than that of the previous scheme by a factor of almost 10. This is considered to be partly due to the avoidance of the intrasubband relaxation process, as we expected. However, the observed relaxation time (~ 0.4 ps) is much shorter than that expected from the electron-LO phonon scattering (~ 1 ps).

In order to make the point clear, we tried to extract the electron relaxation dynamics that exists behind the modulation profile. The pump-probe profile was converted into the time-profile of the total electron population within each subband (N_{CB1}, N_{CB2}, and $N_{total} = N_{CB1} + N_{CB2}$) by quantitative method. The obtained profile is shown in Fig. 3, where we can recognize that the increase of N_{CB2} is distinctly smaller than the decrease of N_{CB1}. About 1.3×10^{16} electrons/m^2 (almost half of the doped electrons) are removed from CB1 at the peak, but only 30% of them are injected into CB2. It is clear that a large part (~70%) of the electrons excited to CB2 instantly transferred to unknown trapping level(s) where electron population does not influence the transmittance of the probe light. The trapped electrons relax to CB1 with much slower relaxation time than the transfer time from CB2 to trapping level(s). Relaxation process other than the intersubband electron-LO phonon scattering should be considered.

We tried to identify such relaxation process, and found strong evidences that the intervalley scattering between Γ and L valleys [3] takes a dominant role. The calculated scattering time from CB2 to the 1st L valley subband (denoted as L1) was about 0.3 ps, which agrees well with the ultrafast relaxation time of N_{CB2}. The scattering time from L1 to CB1 is slower than that of CB2 to L1 by a factor of more than 10 due to the difference in the density of states of the final states. The asymmetric characteristic of the scattering time also agrees well with the experimental results.

Conclusion: We have proposed and investigated an improvement of the modulation scheme. Ultrafast modulation response time of 0.4 ps has been demonstrated using GaAs/AlGaAs QWs. In contrary to our assumption, such ultrafast response time has been mainly attributed to the existence of the intervalley scattering process between Γ and L valleys.

References

[1] S. Noda, T. Uemura, T. Yamashita, and A. Sasaki, *J. Appl. Phys.* 68 (1990) 6529.

[2] T. Asano, S. Noda, and K. Tomoda: *Appl. Phys. Lett.* 74 (1999) 1418.

[3] M. A. Littlejohn, J. R. Hauser, and T. H. Glisson: *J. Appl. Phys.* 48 (1977) 4587.

Corresponding Auther: Takashi Asano, Dept. of Electron. Sci. and Eng., Kyoto Univ., Kyoto 606-8501 Japan, *TEL: +81-75-753-5298, FAX: +81-75-751-1576, email: tasano@kuee.kyoto-u.ac.jp*

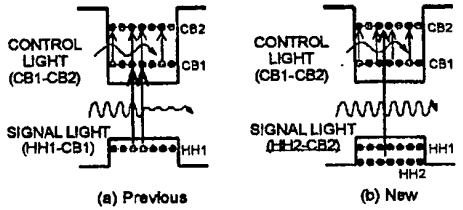

Fig. 1: Schematic diagrams of all-optical modulation using intersubband transition in n-doped quantum wells, where the 1st and 2nd conduction subbands (CB1 and CB2), and the 1st and 2nd heavy hole subbands (HH1 and HH2) are utilized: (a) Previously proposed scheme, which utilizes the population dynamics in CB1. (b) Newly proposed scheme, which utilizes the population dynamics in CB2.

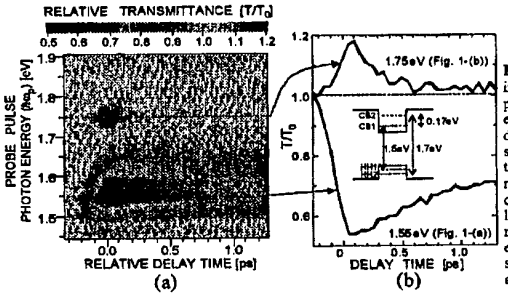

Fig. 2: An example of intersubband-pump and interband-probe (white-light) modulation experiments: **(a)** Three-dimensional view. **(b)** A cross-section at 1.55 eV (lower line) that corresponds to the previous modulation scheme, and a cross-section at 1.75eV (upper line) that corresponds to the new modulation scheme. **Inset:** the energy separations between subbands measured by ordinary absorption measurements.

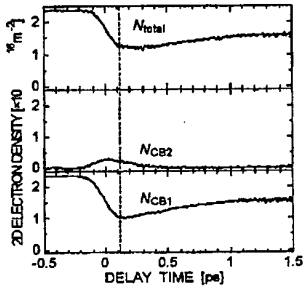

Fig. 3: The time-profile of the total electron population within each subband (N_{CB1} and N_{CB2}) and sum of them (N_{total}) obtained from the data shown in Fig. 2-(a). The dashed line is a guideline indicating the time when the intersubband excitation is finished.

Temperature-induced breakdown of stationary electric field domains in superlattices

David Sánchez[1], Luis L. Bonilla[2,3], Gloria Platero[1],

[1] Instituto de Ciencia de Materiales de Madrid (CSIC), Cantoblanco, 28049 Madrid, Spain
[2] Departamento de Matemáticas, Escuela Politécnica Superior, Universidad Carlos III de Madrid, Avenida de la Universidad 30, 28911 Leganés, Spain
[3]Also: Unidad Asociada al Instituto de Ciencia de Materiales (CSIC)

Manifestations of vertical transport in weakly coupled semiconductor doped superlattices (SLs) include electric field domain formation, multistability, and self-sustained current oscillations [1]. Stationary electric field domains appear in voltage biased SLs if the doping is large enough. When the carrier density is below a critical value, self-sustained oscillations of the current may appear. At high contact doping, they are due to the dynamics of the domain wall (which is a charge monopole accumulation layer or, briefly, a *monopole*) separating the electric field domains. This domain wall moves through the structure and is periodically recycled [2]. The frequencies of the corresponding oscillation depend on the applied bias and range from the kHz to the GHz regime. Self-oscillations persist even at room temperature, which makes these devices promising candidates for microwave generation. Since doping is not a feasible control parameter, other quantities affecting carrier density should be used to observe these behaviors.

Despite its practical and theoretical interest, the effect of temperature on electric field domains and current self-oscillations is still poorly understood. Detailed experimental studies dealing with the influence of temperature on self-oscillations which have appeared recently [3] show that raising the temperature is similar to lowering the SL doping. At low temperature a multiplicity of purely static states (corresponding to coexistence of low and high field domains in the SL) was observed. As the temperature increased, voltage windows corresponding to self-oscillations appeared and widened in the SL I–V characteristics. By using our previous work on this subject [4] we examine how the current–voltage characteristics of a doped GaAs/AlAs SL depends on temperature [5]. The drift velocity of a discrete drift-diffusion model of sequential tunneling is calculated as a function of temperature (ranging from 0 to 175 K). Our results show that increasing temperature facilitates current self-oscillations in the second plateau of the I–V curve.

In these systems the macroscopic time scale of the self-sustained oscillations is larger than the tunneling time. In turn, this latter time is supposed to be much larger than the scattering time. At each well the distribution is thus in local equilibrium with well-defined Fermi energies. The tunneling current density across each barrier in the SL is calculated by means of the Transfer Hamiltonian method. From the continuity equation we are able to derive a kind of Ampère's law establishing that the total current density is sum of displacement and tunneling currents. The latter consists of a drift term and a diffusion term. Furthermore, as typical lateral dimensions are much larger than the vertical structure, electron-electron interaction may be accounted for within a Hartree approximation. These are the main components of our model. The resulting system of equations must be solved self-consistently. The only adjustable parameter is the half-width of the spectral functions related to scattering amplitudes, γ. A critical well doping was analitically estimated [2] above which there are stable static electric field domain branches: $N_{Dc}^{w} = \varepsilon v_m \frac{F_m - F_M}{e(v_M - v_m)}$, where F_M (F_m) is the maximum (minimum) field at which the maximum (minimum) velocity, v_M (v_m), occurs. We observe that N_{Dc}^{w} increases with temperature, indicating that the voltage range for which self-oscillations exist increases as temperature does.

Results of our simulations show that $I - V$ curves present intervals in which the average current increases with voltage, followed by intervals in which the average current decreases. At lower temperatures the intervals of increasing current are wider whereas the opposite occurs at higher temperatures. Likewise, the calculation of the frequency of the self-oscillations as a function of voltage for certain values of the temperature leads us to conclude that stable solutions change from stationary field profiles with two coexisting electric field domains at low temperature to recycling moving monopoles giving rise to current self-oscillations at higher temperature. In other words, *dynamic* voltage windows in the I–V diagram appear and widen as temperature increases. Likewise, it turns out that the frequency increases with voltage, while the average current decreases with voltage, thereby reproducing the behaviour observed in the experiment [3]. In summary, our numerical results agree with the available experimental data and explain them qualitatively as well as quantitatively for the first time. Our analysis shows that temperature is a critical effect in the dynamical behaviour of a weakly coupled SL.

References

[1] A.P. Jauho, A. Wacker, and A. A. Ignatov in *Statistical and Dynamical Aspects of Mesoscopic Systems*, eds. D. Reguero, G. Platero, L.L. Bonilla, and J.M. Rubí, Spinger-Verlag, Berlin (2000); H.T. Grahn, *ibid.* and refereces cited therein.
[2] A. Wacker, M. Moscoso, M. Kindelan and L. L. Bonilla, Phys. Rev. B **55**, 2466 (1997).
[3] J.N. Wang, B.Q. Sun, X.R. Wang, Y. Wang, W. Ge and H. Wang, Appl. Phys. Lett. **75**, 2620 (1999); X.R. Wang, J.N. Wang, B.Q. Sun and D.S. Jiang, Phys. Rev. B **61**, 7261 (2000).
[4] L. L. Bonilla, G. Platero and D. Sánchez, Phys. Rev. B **62**, 2786 (2000).
[5] D. Sánchez, L. L. Bonilla and G. Platero (preprint).

Corresponding author: David Sánchez, Instituto de Ciencia de Materiales de Madrid (CSIC), Cantoblanco, 28049 Madrid, Spain.
Phone: +34 913349000 no. 168, fax: +34 913720623,
email: dsanchez@icmm.csic.es

High field electron transport in GaAs/$Al_xGa_{1-x}As$ p-i-n-i-p-structures investigated by ultrafast absorption changes

H.Lutz[1], A.Schwanhäußer[2], M.Eckardt[2], G.Döhler[2], L.Robledo[2], A.Seilmeier[1],

[1]Physikalisches Institut, Universität Bayreuth, Universitätsstr.30, 95440 Bayreuth, Germany
[2] Institut für Technische Physik 1, Universität Erlangen-Nürnberg, Erwin-Rommel-Str.1, 91058 Erlangen, Germany

N-i-p-i-structures are well known for their exceptionally high nonlinearity, which is based on a spatial separation of electrons and holes. The switch-on time depends on the transport of charge carriers which is investigated in this paper. The drift of electrons and holes is studied by specially designed samples in which only one type of charge carriers takes part in the transport process. In this way we are able to investigate the drift of either electrons by using a p-i-n-i-p-structure or holes by using a n-i-p-i-n-structure in an optical experiment.

The design of such a GaAs/$Al_xGa_{1-x}As$ p-i-n-i-p-structure is depicted in Fig.1. The structure has two p-doped layers and a central n-doped layer, which allow to apply an electric field to the 600 nm long intrinsic $Al_{0,35}Ga_{0,65}As$ "acceleration section" ranging from 20 kV/cm to 300 kV/cm according to a reverse bias between 0V and 20V. Due to the sophisticated Al-content profile (see Fig. 1) a selective excitation of electron-hole-pairs close to the p-contacts and a spatially selective monitoring of the arrival of electrons close to the n-contact is possible.

With a 150fs-pump pulse at hν = 1.48 eV pairs of electrons and holes are injected within the GaAs layer close to the p-contacts. The electrons pass the transport section of 600 nm length with the freely adjustable electric field. They can be detected in the central quantum well by a weak time delayed probe pulse at hν = 1.65 eV via changes of the absorption due to the Franz-Keldysh-effect and at hν = 1,59eV due to band filling. The holes, however, are captured by the p-doped contact region and do not contribute to the transport signal. The same experiment performed in a corresponding n-i-p-i-n- structure allows to study the transport of holes.

A typical result of a time resolved experiment performed on a reverse biased p-i-n-i-p-structure (U_{pn}=11V) at room temperature is presented in Fig. 2. The most important feature is the pronounced signal change about 10 ps after optical carrier injection. Curve (a) represents the arrival of the electrons in the n-doped quantum well. In curve (b) band filling in the $Al_{0,1}Ga_{0,9}As$ layer is observed which is delayed by the time necessary for carrier cooling. The arrival time turned out to be almost independent of the applied electric field between 60kV/cm and 180kV/cm. In such high electric fields the electrons exceed the maximum of the drift velocity. Electrons are rapidly scattered to both the L- and the X-valley where the mobility is reduced due to the higher effective mass resulting in the relatively long transit times [1].Details of the time dependence of the signal around t_D=10ps gives information on the distribution of the arrival times.

Besides the time resolved experiments transient absorption spectra were taken between 1.4eV and 1.7eV at various delay times. In that way, we obtain detailed information on changes of the internal electric field and screening in various regions of the structure due to the Franz-Keldysh-effect [2]. The field begins to change immediately after excitation as shown at short delay times in Fig.2 (curve (b)).

The experimental findings are in good agreement with the results of Monte-Carlo-simulations, which were performed for different values of the applied voltage and of the

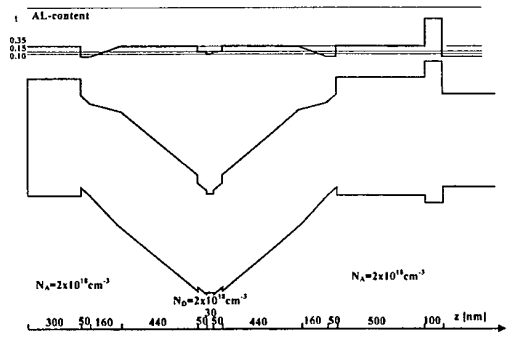

Fig. 1: Design of the GaAs/$Al_xGa_{1-x}As$ p-i-n-i-p-structure

temperature. The calculations show that the electrons are scattered from the Γ-valley to both the L-valleys and the X-valleys within the first few hundred femtoseconds after their generation. The average electron velocity amounts to ~$7*10^6$cm/s and is nearly constant in the investigated range of electric fields. Quite interesting is the distribution of the arrival times of the electrons at the n-doped region, which is deduced from the experimental data and the Monte-Carlo-calculations.

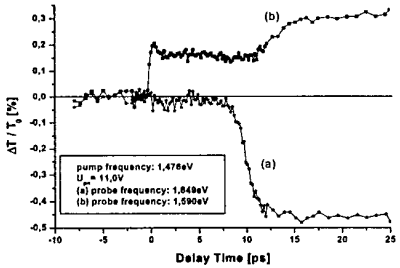

Fig. 2: Time resolved measurements at two different probe energies

The technique discussed here allows to investigate not only carrier transport but also emerging space charge fields and carrier relaxation processes and gives a complete picture of the dynamics of the nonlinearity in n-i-p-i-structures.

References:

[1] A. Leitenstorfer et al., Phys. Rev. Lett. 82, 5140 (1999).
[2] H. Heesel et al., Phys. Rev. B 47, 16000 (1993).

Corresponding author: Holger Lutz, Physikalisches Institut, Experimentalphysik 3, Universität Bayreuth, Universitätsstraße.30, D-95447 Bayreuth, Germany,
phone: +49 921 55-3161, Fax: +49 921 55-3172
email: holger.lutz@uni-bayreuth.de

Intensity-independent, highly polarization- or wavelength sensitive opto-electronic switches

P. Kiesel, M. Müller, T. Kippenberg, J. Spieler, S. Malzer, and G.H. Döhler

[1]Institut für Technische Physik 1, Universität Erlangen-Nürnberg, Erwin-Rommel-Str. 1, D-91058 Erlangen, Germany

Control and detection of the polarization state or the wavelength of the incident light is of fundamental importance in many optical applications. Currently, this is achieved by a hybrid combination of standard active devices with polarization or wavelength selective passive elements (sheet polarizer, micro-optical gratings, etc.). Potential disadvantages of such a hybrid system are the relatively large size that limits the packaging density, as well as the necessity of an accurate alignment and the usage of mechanical elements.

In this paper we report on monolithically integrated opto-electronic detectors and switching devices with high photoconductive gain. The most interesting aspect of this device is the fact that the switching behavior depends only on the polarization angle or wavelength, but not on the intensity of the incoming light.

Our device structure basically consists of two stacked double hetero p-i-n structures connect in series to a reverse bias. Its operation principle is based on the absorption difference in both diodes. For the wavelength sensitive switch the intrinsic layers of the stacked diodes consist of different material compositions as shown in Fig. 1 (AlGaAs for the FET diode and GaAs for the reference diode). The whole structure is illuminated from the top with monochromatic light. Due to the different absorption spectra of GaAs and AlGaAs the ratio of the photo currents generated in the two diodes changes when changing the wavelength of the incident light. Depending on the wavelength the applied reverse voltage either drops over the reference or the FET diode depleting or not depleting the top n-layer of the structure. Using interdigitated contacts on top of that layer the "on" and "off" state can be detected with a high opto-electronic gain. Thus the FET diode basically represents a pin diode and a field effect transistor integrated into a single device.

The switching behavior with respect to the polarization can be achieved by using the polarization dependence of the absorption in spontaneous ordered semiconductor crystals (e.g. GaInP or InGaAs). By using ordered GaInP instead of AlGaAs in the intrinsic region FET diode (Fig. 1) the absorption and therefore the photocurrent in this diode depends on the state of polarization. Thus, we can demonstrated an integrated switch highly sensible to the direction of polarization of the incident light.

As an increase of the optical power affects both diodes in the same way, both concepts provide an intensity independent switching point. In Fig. 2 the intensity independent polarization and wavelength switching is shown. The electrical output signal can be switched "on" and "off" by shifting the wavelength of the input light by less than 1 nm or turning the polarization angle by less than 1°.

By choosing a special design and taking advantage of the special behavior of the electroabsorption slightly above the band gap in both cases a bistable switching behavior with respect to polarization or wavelength can be achieved.

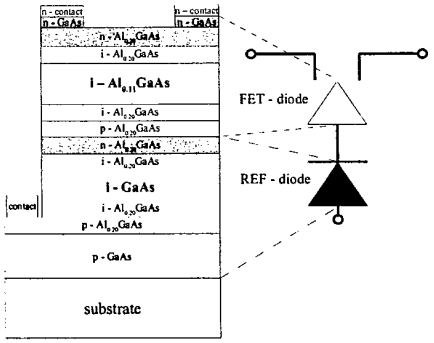

Fig.1: Schematic layer structure of the wavelength switch

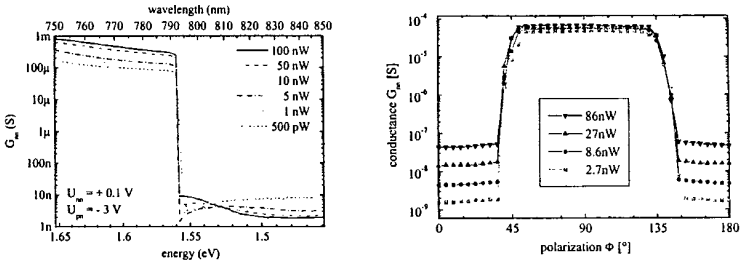

Fig.2: Switching behavior of the n-channel conductance as a function of the wavelength (left) and polarization angle (right) of the incident light.

Corresponding author: Peter Kiesel, Institut für Technische Physik 1, Universität Erlangen-Nürnberg, Erwin-Rommel-Str. 1, D-91058 Erlangen, Germany
phone: +49 9131 85 27254, Fax: +49 9131 85 27293
email: kiesel@physik.uni-erlangen.de

Resonant-tunneling effect in a periodically modulated electrical field.

S.A.Vitusevich[1], A.Förster[1], A.E.Belyaev[2], D.I.Sheka[3], H.Lüth[1], N.Klein[1], S.V.Danylyuk[2] and R.V.Konakova[2].

[1]Institut für Schichten und Grenzflächen (ISG), Forschungszentrum Jülich, D-52425 Jülich, Germany
[2]Institute of Semiconductor Physics, National Academy of Sciences of Ukraine, 03028 Kiev, Ukraine
[3] Radiophysics Faculty, National Taras Shevchenko University of Kiev, 03127 Kiev, Ukraine

There has been a great deal of interest in the study of transport phenomena in one and zero-dimensional systems. Usually for decreasing the dimensionality of a two-dimensional system represented by layered heterostructure are used split gate[1] or ring gate[2] configurations. These configurations allow decreasing the effective lateral dimension resulting in a formation of a semiconductor dot. One or zero dimensional density of states and single electron phenomena can be observed but those structures are not suitable for optical and power device application because of a too small active area. To control the lateral confinement at a large surface a system of interdigitated gates was employed on top of a heterostructure and one dimensional electron wires formation was verified with capacitance measurement technique[3].

In this communication we present results of theoretical and experimental investigations of novel resonant tunneling structure (RTS) laterally confined by a periodically modulated electrical field created by a system of interlocked finger contacts. It is shown that the confinement in the system and the resonant conditions are determined by changes in the spatial potential distribution at a certain finger voltage.

The measured heterostructure is grown by molecular-beam epitaxy. An active double barrier structure with 2 nm AlAs barriers and 4 nm GaAs quantum well was embedded in a depletion region of an Schottky finger contact (Fig1a). One of two interlocked fingers with 20μm length and a variable widths (b =0.5, 0.7, 1 μm) is used for the creation of the dimension of the confinement at a certain gate voltage U_g. The potential profile of the heterostructure with a=b=0.53 μm , h=0.148 μm , y_0=0.108 μm was derived from the solution of the Laplace equation taking into account the boundary condition at different gate and source voltages. The calculated surface potential for different distances from the top electrodes demonstrate the formation of a space distributed superlattice, which can be tuned with the gate voltages. The shape and the magnitude of the periodic potential distribution determine the condition for a resonant tunnelling process through the structure. A lateral confinement at a certain gate voltage renormalizes the effective confinement potential transforming a two-dimensional quantum well into a one dimensional wire array resulting in changes the resonant voltage V_{sr}. In Fig. 1b the cross-section of the calculated surface for different distances from the top electrodes at V_g= 5V and source voltage V_s = -2V is shown.

Current-voltage characteristics (drain current dependence on source drain voltage at different gate voltages) of the resonant tunnelling structure were measured at room temperature in a transistor mode with common-drain configuration with an HP 4145B Parameter Analyser. The resonance voltage obtained from the experiment (circles in Fig.2) is in good agreement with the theoretically predicted values. The resonant tunnelling effect is very sensitive to a splitting between the upper electrodes and can find application in new kind electronic and optoelectronic switchers.

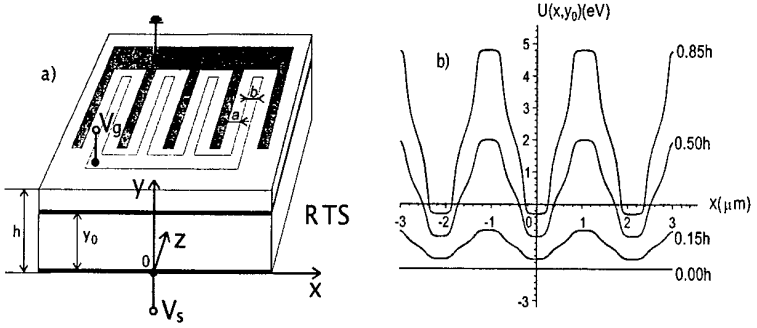

Fig. 1: a) resonant tunneling structure with an interlocked finger contacts; b) cross-section of the calculated surface for different distances from the bottom electrode.

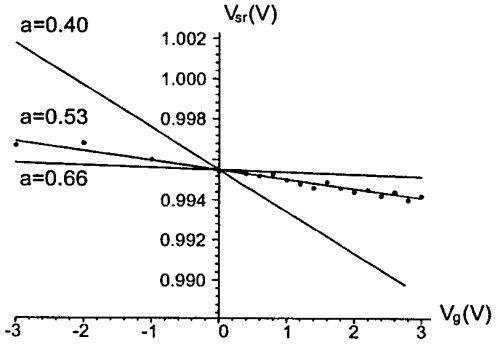

Fig. 2:Dependencies of the resonant voltages V_{sr} versus V_g calculated for different spacing a between gates. Circles represent experimental data.

References

[1] T.J. Thornton et al. Phys. Rev. Lett. 56, 1198 (1986).
[2] M.W. Dellow et al. Phys. Rev. Lett. 68, 1754 (1992).
[3] W. Hansen et al. Semicond. Sci. Technol. 9, 1946 (1994).

Corresponding author: S.Vitusevich, Institut für Schichten und Grenzflächen (ISG), Forschungszentrum Jülich, D-52425 Jülich, Germany.
phone:+49-2461-2345, Fax:+49-2461-2940
e.mail: s.vitusevich@fz-juelich.de

Spontaneous Spin Splitting Observed in Resonant Tunneling Diode with a Narrow Band Gap Asymmetric Quantum Well

T. Kikutani, S. Gozu, Y. Sato and S. Yamada*

Center for New Materials, Japan Advanced Institute of Science and Technology (JAIST)

1-1 Asahidai, Tatsunokuchi, Ishikawa 923-1292, Japan

*Corresponding author: e-mail; shooji@jaist.ac.jp

Spontaneous spin splitting (SSS) of the electron subbands in narrow-gap semiconductor heterojunction is believed to be caused by the lack of structure inversion symmetry and it has so far been analyzed mainly by measuring Shubnikov-de Haas (SdH) oscillations [1-4]. In order to estimate the genuine SSS, however, the measurements under the finite magnetic fields are essentially unfavorable, since the effect of Zeeman splitting is more or less included in the SdH oscillation[5]. In this work, we propose a new estimation method of SSS without a magnetic field, which utilizes resonant tunneling diode (RTD) structure with a narrow band gap materials $In_xGa_{1-x}As$ ($x > 0.5$) as a well. If an SSS of electron subbands could be induced by designing an appropriate quantum well, we might observe current peak splittings in negative differential resistance (NDR) regions. The key concepts are a built-in potential asymmetry and a non-zero $k_{//}$ of 2-dimensional electrons in the well. It is also noted that such an RTD device discussed here seems promising as a new class of spin-filter.

Schematic layer structure of our RTD is shown in Fig. 1, which was grown by molecular beam epitaxy (MBE). The asymmetric quantum well is made by stacking 5 nm undoped $In_xGa_{1-x}As$ layer ($x = 0.75$) on 5 nm undoped $In_xGa_{1-x}As$ layer ($x = 0.66$), both of which are confirmed to reveal the SSS of about 10meV [6]. A Ti/Ni/Au (possibly spin-injective) emitter electrode and a mesa of RTD have typically a size of 10 μm × 20 μm. Ti/Au collector electrodes were fabricated on Si doped $In_{0.5}Ga_{0.5}As$ collector layer ($n = 1 \times 10^{19}$ cm^{-3}).

Temperature dependence of I -V characteristics under zero magnetic field is shown in Fig. 2, where the vicinity of the first current peak is enelarged. As seen in the derivative trace, *dI/dV*, splitted peaks (P_{1-1} and P_{1-2}) were clearly confirmed at 1.55 K in both the injection directions. The spacing between P_{1-1} and P_{1-2} was ~29 mV and ~32 mV for the cases of the emitter and collector injections, respectively. Splitting energies of ~14.5 meV and ~16.0 meV can be estimated from those values. On the other hands, splitting peaks were not detected at 147.3 K. This result seems very consistent, since generally spin splitting becomes unclear with increasing temperature. Next, we have investigated the dependences of the peak strength upon the low magnetic field applied parallel to the easy axis of the emitter and compared the result with that of M-H curve of the electrode. It is found that, in the emitter injection region, the strength of P_{1-1} increases with magnetic field, while that of P_{1-2} rather decreases (Fig. 3). In contrast, for the peaks in the collector injection region, the peak strengths almost did not vary against the field. Since the effects of possible LO phonos at the interface (AlAs-like: 50meV, GaAs like: 36 meVand InAs like: 30 meV) can be excluded from the origin of the peak-splitting, we thus conclude that the splitting appeared in the current peak at the lower voltage is mostly due to the SSS in the well, although the splitting energies are some extent larger than the value obtained in the SdH measurement.

References

1) J. Luo et al., Phys. Rev. B 38, 10142, (1988). 2) B. Das et al., Phys. Rev. B 39, 1411, (1989). 3) G. Engels e al, Phys. Rev. B 55, R1958, (1997). 4) Th. Schapers et al, J. Appl. Phys., 83, 4324, (1998). 5) T. Kita et al., Proc. Semimag-2000, Sep. 2000, Matsue, Japan. 6) Y. Sato, T. Kita, S. Gozu and S. Yamada, J. Appl. Phys. in press.

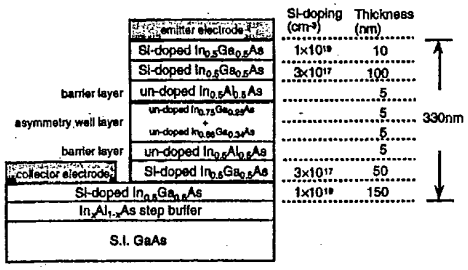

Fig. 1. Schematic layer structure of our RTD.

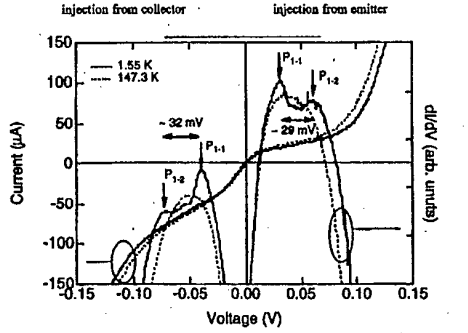

Fig. 2. Temperature dependence of I -V characteristics without magnetic field and those differential conductance.

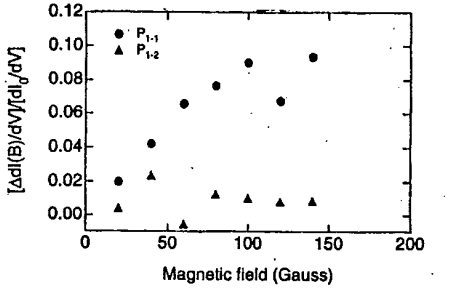

Fig. 3 Field dependences of the splitted peaks observed in the emitter injection region.

Nano-scale Schottky contacts: Ultrafast drift-diffusion dynamics studied in the optical near-field

M. Achermann[1], U. Siegner[2], L.-E. Wernersson[3], and U. Keller[1]

[1]Institute of Quantum Electronics, Swiss Federal Institute of Technology, ETH Honggerberg, CH-8093 Zurich, Switzerland
[2]Physikalisch-Technische Bundesanstalt, Bundesallee 100, D-38116 Braunschweig, Germany
[3]Solid State Physics/Nanometer Structure Consortium Lund University, Box 118 S-221 00 Lund, Sweden

We present the first direct measurements of ultrafast carrier dynamics around buried nano-scale Schottky contacts with < 250 nm spatial and 250 fs temporal resolution. The experiments have been performed with a recently developed femtosecond near-field (NF) optical microscope [1]. It is shown that high optically excited carrier densities screen the built-in field around a Schottky contact and allow for efficient transport of electrons towards the contact, followed by trapping of electrons into the metal. Good agreement is found between the experimental data and calculations of the drift-diffusion dynamics.

The investigated structure consists of tungsten (W) discs with ~80 nm diameter and a thickness of 20 nm. The discs are embedded in weakly n-doped GaAs in a rectangular pattern with 2 µm disc spacing. In such samples, Schottky contacts are formed at the W/GaAs interface [2]. Degenerate NF pump-probe measurements are performed at room temperature with 100 fs pulses, centered at a photon energy of 1.46 eV. The sample is globally excited and the pump-induced transmission changes are locally detected with a probe pulse, which is sent through the NF tip and the sample [1]. We note that electrons yield the major contribution to the pump-probe traces for detection close to the band edge [3].

Figure 1 shows a two-dimensional image of the amplitude of the pump-probe signal at a time delay of 15 ps and a high optically excited carrier density of 6.7×10^{16} cm^{-3}. The disc pattern is clearly visible. Moreover, the electron density is substantially reduced in a wide region around the discs (for comparison the white disc in the lower left corner marks the size of a W disc). We conclude that electrons have diffused towards the discs where they have been trapped. Efficient electron transport towards the discs is only possible if the built-in field is screened. Otherwise electron drift away from the discs counteracts diffusion towards them, suppressing net electron transport. Thus, Fig.1 demonstrates strong field screening. The screening is due to the partial neutralization of the initially negatively charged discs by holes that have drifted and diffused towards the discs and have been trapped into them.

The details of the spatiotemporal carrier dynamics can be inferred from direct measurements of the pump-probe signal versus distance across a single W disc for fixed time delays Δt. These data are shown in Fig. 2(a). At zero time delay, the electron density is mainly reduced in the close vicinity of the W disc. With time, the shape of the traces changes and a reduction of the electron density is also observed farther away from the disc. Figure 2(b) shows how the full width at half maximum (FWHM) of the dip increases with time. At very late times (Δt=40 ps), the carrier density is so much reduced that the built-in field is restored, slowing down electron transport and trapping [4]. The experimental data are in good agreement with numerical simulations of the carrier density based on Poisson's and the drift-diffusion equation (Figs. 2(a) and (b)).

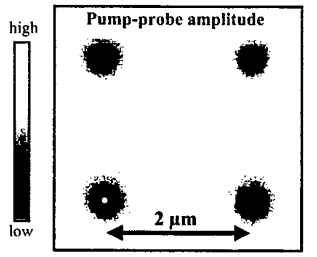

Fig.1: Two-dimensional image of the pump-probe amplitude at time delay Δt=15 ps and an optically excited carrier density of 6.7×10^{16} cm^{-3} (high-density regime). For comparison the white disc in the lower left corner marks the size of a W disc.

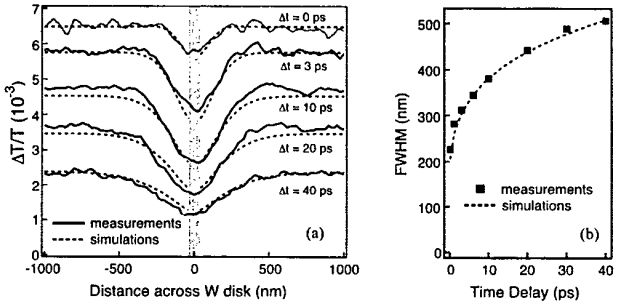

Fig.2(a) Line scans across a tungsten disc for different time delays taken in the high density regime. The gray bar marks the extension of the tungsten disc. (b) Full width at half maximum (FWHM) of gaussian fits to the measured curves (squares) and FWHM of gaussian fits to calculated traces (dashed line).

References

[1] B.A. Nechay, U. Siegner, M. Achermann, H. Bielefeldt, U. Keller, "Femtosecond pump-probe near-field optical microscopy," Rev. Sci. Instr. **70**, 2758 (1999).
[2] L.-E. Wernersson, A. Litwin, L. Samuelson, W. Seifert, "Controlled carrier depletion around nano-scale metal discs embedded in GaAs," Jpn. J. Appl. Phys. **36**, L 1628 (1997).
[3] R. Tommasi, P. Langot, F. Vallee, "Femtosecond hole thermalisation in bulk GaAs," Appl. Phys. Lett. **66**, 1361-1363 (1995).
[4] M. Achermann, U. Siegner, L.-E. Wernersson, U. Keller, "Ultrafast carrier dynamics around nano-scale Schottky contacts studied by femtosecond far- and near-field optics," Appl. Phys. Lett. **77**, 3370 (2000).

Corresponding author: Marc Achermann, Institute of Quantum Electronics, Swiss Federal Institute of Technology, ETH Honggerberg, CH-8093 Zurich, Switzerland
phone: +41 1 633 2529, fax: +41 1 633 1059, email: acherman@iqe.phys.ethz.ch

Two modes of Ga diffusion into InAs self-assembled quantum dots suggested by ion channeling

N. Matsumura[1*], T. Haga[1], S. Muto[1], Y.Nakata[2] and N.Yokoyama[2]
[1]Department of Applied Physics, Hokkaido University, Sapporo 060-8628, Japan
[2]Fujitsu Laboratories, Ltd., Morinosato-Wakamiya, Atsugi 243-0197, Japan

InAs Self-Assembled Quantum Dots (SAQDs) on GaAs (100) have been challenged to be used for a potential optoelectronic devices. Growth process of InAs SAQDs is of vital importance for device fabrication reproducibility. In our previous report, an accurate value of InAs coverage was determined and diffusion of Ga atoms into InAs QDs was observed by using Rutherford backscattering for uncapped samples with 60 s growth interruption [1]. Moreover, our study revealed that the amount of diffused Ga strongly depended on the InAs coverage [2]. However, it remains an unsettled question whether Ga diffusion occurs during InAs deposition or during growth interruption. The diffusion is important to describe a conclusive picture of the self-assembled growth process. In this study, InAs SAQDs is structurally studied as a function of the growth interruption time, $\tau_{interrupt}$, by ion channeling observed by particle-induced x-ray emission (PIXE).

All samples, grown by molecular beam epitaxy (MBE), contained a single InAs layer whose nominal coverage was 1.8 monolayer (ML) estimated by the growth rate of the order of 0.1 ML/s. After the InAs deposition, the growth was interrupted between 0 and 60 s before capping layer was grown. In order to evaluate lattice deformation, we introduced the normalized minimum yield, χ_{min}, which is defined as a ratio of aligned yields to random yields. In general, the larger χ_{min} suggests the higher lattice deformation which was defined as a lateral displacement from a GaAs host lattice.

Figure 1 shows correlation between χ_{min}'s (In, Ga) and photoluminescence (PL) peak wavelength as a function of the growth interruption time. Lattice deformation of In increased with the growth interruption time. In particular, the deformation drastically increased from 0 to 15 s. Also, a strong correlation between the deformation and PL redshift was found. This suggests that the size of the dots increased during the growth interruption.

Deformation of Ga decreased when growth interruption time was changed from 0 (non-interruption) to 30 s, and increased from 30 to 60 s. Since Ga deformation resulted from the Ga diffusion to form InGaAs dots [2], this result indicates that two different mechanisms of Ga diffusion into QDs exist. If the diffusion occurred before or during growth interruption, the diffusion cannot decrease with increased $\tau_{interrupt}$. Therefore, we attributed the decrease from 0 to 30 s to the Ga diffusion after the growth interruption. Previously, in the coverage-dependence of Ga diffusion [2], we observed that the Ga diffusion was suppressed for larger dots probably because lattice constant of upper part of InAs QDs becomes closer to that of bulk InAs. The decreased Ga diffusion from 0 to 30 s can be attributed to this size dependence.

The diffusion from 30 to 60 s, slightly increased and thus is considered to have occurred during the growth interruption. Although the size of the QDs was not fully saturated from 30 to 60 s, Ga diffusion increased during this period. The size effect was supposed to be not so large as that for 0-30 s.

In summary, we investigated the Ga diffusion into InAs SAQDs as a function of the growth interruption time by using PIXE/ion channeling. A strong correlation between the deformation of In and redshft of PL peak was found indicating increased size of dots during growth interruption. The deformation of Ga of the sample was reduced when growth interruption time was changed from 0 to 30 s, and increased from 30 to 60 s, which is explained by the Ga diffusion into QDs. The Ga diffusion from 0 to 30 s was concluded to have occurred after the growth interruption, and was interpreted as the size dependent diffusion.

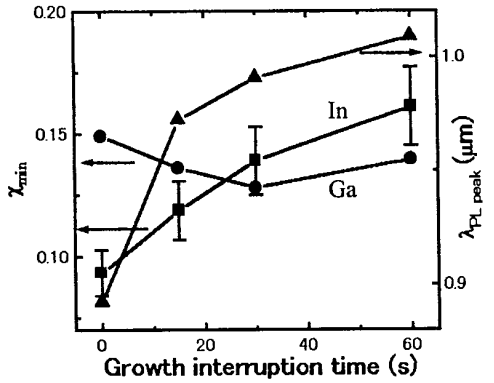

Fig.1 The lattice deformation (χ_{min}'s) and PL peak as a function of the growth interruption time

References

[1] T. Haga, M. Kataoka, N. Matsumura, S. Muto, Y. Nakata, and N. Yokoyama, Jpn. J. Appl. Phys., Part 2 **36**, L1113 (1997)

[2] N. Matsumura, T. Haga, S. Muto, Y. Nakata, and N. Yokoyama, J. Appl. Phys. **89**, 160 (2001)

Corresponding author. Shunichi Muto, Department of Applied Phyiscs, Hokkaido university, N13 W8 Kita-ku, Sapporo 060-8628, Japan, phone: +81-11-706-7129, fax: +81-11-706-7129, email: gfd01102@nifty.ne.jp

Monte Carlo Simulation of Self-organized Quantum Dot Structures: crossover from kinetics to thermodynamics

R. Kunert[1], M. Meixner[1], E. Schöll[1],V. A. Shchukin[2], D. Bimberg[2]

[1] Institut für Theoretische Physik, Technische Universität Berlin, Hardenbergstraße 36, D-10623 Berlin , Germany

[2] Institut für Festkörperphysik, Technische Universität Berlin, Hardenbergstraße 36, D-10623 Berlin , Germany

The growth of high density, dislocation free quantum dot layers for applications in modern semiconductor devices is a major challenge for process engineering. A promising way to obtain highly efficient dot layers is the use of self-organisation effects present in the Stransky-Krastanov or Vollmer-Weber growth mode [1].

We simulate the heteroepitaxial growth of quantum dots by means of a continuous time kinetic Monte Carlo (MC) scheme [2]. This technique allows us to simulate the nucleation and growth of sub-monolayer islands far from equilibrium as well as to analyse the processes relevant during equilibration. The basis of our simulations is a model of activated diffusion incorporating self-consistently the local elastic strain field. The hopping probability of an adatom onto a nearest neighbor site is given by the Arrhenius law

$$p = \nu_0 \exp\left(-\frac{E_s + nE_b + E_d - E_{str}(x,y)}{k_b T}\right)$$

where ν_0 is the attempt frequency, E_s and E_b are the binding energies to the surface and to the n nearest neighbor atoms, respectively. E_d accounts for anisotropic diffusion, and $E_{str}(x,y)$ is the energy correction due to the local strain field generated by the growing islands.

By varying experimentally accessible growth parameters like temperature, flux and coverage we are able to identify optimal growth conditions where narrow size distributions and good spatial ordering can be achieved (Fig.1a,1b). The effect of anisotropic surface diffusion is also discussed. As a general trend we predict that growth interruptions enhance the spatial ordering, which is mediated by weak, long-range island-island interactions.

The equilibration process during longer simulation times affects the size distribution of the islands and leads to a marked crossover effect. Right after deposition we observe that the islands become larger with increasing temperature. This is an effect contradictory to thermodynamic predictions, and indicates that initially the size distribution is kinetically controlled. If the system is allowed to equilibrate for sufficiently long times, the average island size shifts towards larger islands. In our kinetic MC simulations we observe a crossover of average island sizes for systems of different temperatures (Fig.2a). Asymptotically, the thermodynamic equilibrium size distribution is reached, where larger islands can be found at lower temperature (Fig.2b). Thus we are able to resolve the apparent discrepancies between kinetic and thermodynamic approaches to the growth of self-assembled quantum dots within a single MC simulation. Furthermore, we present first results for quantum dot stacks, where correlation and anticorrelation effects are known to occur in dependence on the buffer layer thickness [3].

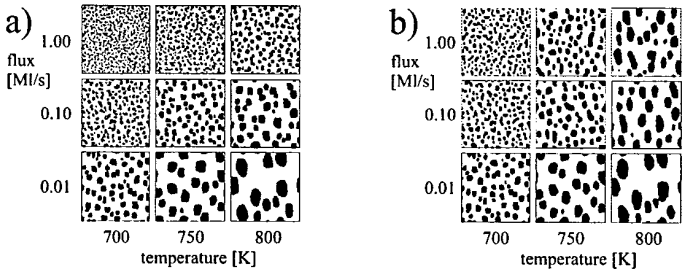

Figure 1: a) Monte Carlo simulation of quantum dots for different temperatures and flux rates for a coverage of $c = 0.3$ ML above the wetting layer after the end of deposition. b) Same as a) after 50s simulation time.

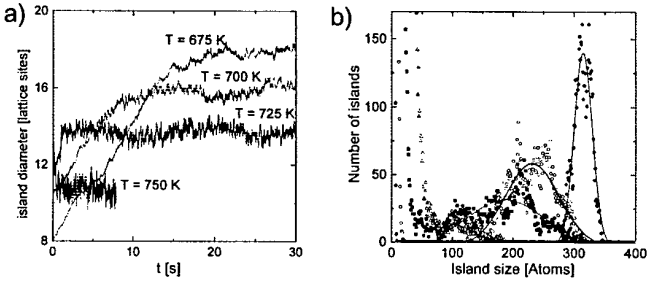

Figure 2: a) Kinetic Monte Carlo simulation of the temporal evolution of average island sizes for different temperatures. Coverage $c = 0.04$, flux rate 1 ML/s.
b) Equilibrium size distribution for different temperatures, extracted from the kinetic MC simulation at $t = 35s$. The solid lines are fits to the MC data.

References

[1] D. Bimberg, M. Grundmann, and N. N. Ledentsov, *Quantum Dot Heterostructures*, Wiley, Chichester (1998).

[2] E. Schöll, and S. Bose, Sol. State Electron. **1587**, (1997) .

[3] V. Holy, G. Springholz, M. Pinczolits, and G. Bauer, Phys. Rev. Lett. **83**, (1999).

Corresponding author: Roland Kunert, Institut für Theoretische Physik, Technische Universität Berlin, Hardenbergstraße 36, D-10623 Berlin, Germany.
phone: +49 (0)30 314 22 0 87, Fax: +49 (0)30 314 21 1 30,
email: kunert@physik.tu-berlin.de

Density and size control of self-assembled InAs quantum dots

I. Kamiya[1], Ichiro Tanaka[2,3], H. Sakaki[2]

[1]Research Center for Advanced Science and Technology, University of Tokyo,
4-6-1 Komaba, Meguro-ku, Tokyo 153-8904, JAPAN
[2]Institute of Industrial Science, University of Tokyo,
7-22-1 Roppongi, Minato-ku, Tokyo 106-8558, JAPAN
[3]Department of Materials Science and Chemistry, Wakayama University,
930 Sakaedani, Wakayama 640-8510, JAPAN

The unique electronic properties of quantum dots (QDs) have attracted much attention of both those in basic science and optoelectronic engineering [1]. Self-assembled (SA) QDs, in particular, have been intensively studied for the last decade because nano scale QDs are easily obtained by molecular beam epitaxy (MBE) or organometallic vapor phase epitaxy (OMVPE) [2]. Recently, scanning probe measurements have been performed in order to reveal the unique properties of single SA InAs QDs to avoid the size, density and distribution of the SA QDs are rather random [3]. However, these measurements are still technically difficult or requires sophisticated processing. Here we show that through precise control of growth conditions, density and size of SA InAs QDs can be well controlled, and that SA QDs at a density low enough to enable us to perform measurements on single QD devices with minimum processing or possibly none can be obtained.

SA QDs were prepared by depositing InAs onto (001)GaAs by solid source MBE. The oxide desorption and (2x4) to c(4x4) transition were checked to occur at 590±5°C and 510± 5°C, respectively, by reflection high energy electron diffraction (RHEED), which confirmed the high reproducibility and reliability of our temperature reading. Also the amount of InAs deposited was estimated by observing the RHEED transition into 3D chevron pattern which is known to occur at a coverage of 1.7 monolayer (ML) at 450°C, and is accurate within ±10%. After removal from the MBE system, the surface morphology of the sample was investigated by atomic force microscopy (AFM) operated in cyclic contact mode in air.

The results are summarized in the arrays of AFM images in Fig. 1, where SA QDs formed by deposition of 2.7, 2.3, 2.0, 1.8 ML (±10%) of InAs at 530, 502, 455, and 410 (±5) °C followed by immediate quenching are shown (1μm x 1μm area for all images). In general, larger QDs with lower density are formed as the temperature is raised. Here, InAs desorbing off from the surface is negligible within the accuracy of the present experiment. It is shown that the dot size and density can be well controlled in the range of 20~60 nm and $2x10^{11}$~ $6x10^{9}$ cm^{-2}, respectively

We also find that by post annealing of samples after deposition of InAs slightly less than the critical thickness (θ_c), dot density of 10^{9} cm^{-2} or lower can be achieved by enhancing migration of InAs islands on the surface. Figures 2 (a) and (b) show how InAs islands formed below θ_c evolve into low density QDs. Annealing at 500°C after deposition of ~1.5 ML (just below θ_c) of InAs results in QDs of ~$1x10^{8}$ cm^{-2}. Dots prepared in this manner are well isolated, and hence suitable for single QD measurements and device applications.

Detailed morphological evolution in the early stage of dot growth and the effect of post annealing will be discussed.

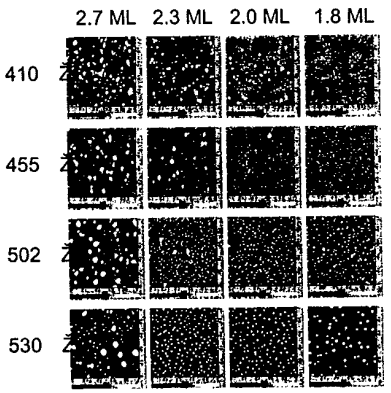

Fig. 1: AFM images of SA QDs on (001) GaAs grown by MBE at 410, 455, 502, and 530°C after deposition of 1.8, 2.0, 2.3 and 2.7 ML of InAs.

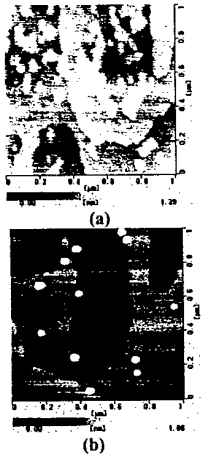

Fig. 2: AFM images following the evolution of InAs islands into very low density QDs by post annealing.

References

[1] H. Sakaki, Surface Sci. **267**, 623 (1992); Solid State Commun. **92**, 119 (1994).
[2] For example, D. Leonard, M. Krishnamurthy, C. M. Reaves, S. P. DenBaars, P. M. Petroff, Appl. Phys. Lett. **63**, 3203 (1993).
[3] M. E. Rubin, G. Medeiros-Ribeiro, J. J. O'Shea, M. A. Chin, E. Y. Lee, P. M. Petroff, V. Narayanamurti, Phys. Rev. Lett. **77**, 5268 (1996); I.Tanaka, I. Kamiya, H. Sakaki, N. Qureshi, S. J. Allen, P. M. Petroff, Appl. Phys. Lett. **74**, 844 (1999); H. Yamamoto, T. Takahashi, I. Kamiya, Appl. Phys. Lett. **77**, 1994 (2000).
[4] I. Kamiya, I. Tanaka, H. Sakaki, J. Cryst. Growth **201/202**, 1146 (1999).

Corresponding author (Present address): Itaru Kamiya,
Non-Equilibrium Laboratory, Mitsubishi Chemical Corporation,
1000 Kamoshida-cho, Aoba-ku, Yokohama 227-8502, JAPAN,
Phone:+81-45-963-4365, Fax:+81-45-963-4366,
e-mail: ikamiya@rc.m-kagaku.co.jp

InGaAs islands formed on shallow patterned GaAs (100) substrates by molecular-beam epitaxy

Q. Gong[1], R. Nötzel[1], H.-P. Schönherr[2], K. H. Ploog[2]

[1] COBRA Inter-University Research Institute, Eindhoven University of Technology, 5600 MB Eindhoven, The Netherlands
[2] Paul-Drude-Institut für Festköperelektronik, Hausvogteiplatz 5-7, D-10117 Berlin, Germany

Patterned growth on shallow (several ten nanometers deep) patterned substrates has been demonstrated to fabricate low-dimensional structures [1]. Moreover, the relatively stable nonplanar surface formed after the growth of a buffer layer can be used as a novel template for further materials growth [2]. In this paper we investigate the molecular-beam epitaxy of InGaAs islands on the nonplanar surface formed on shallow patterned GaAs (100) substrates. For comparison, the growth of InGaAs islands on vicinal GaAs (100) substrates (2° off towards (111)A) was also studied.

The GaAs (100) substrates were patterned by optical lithography and wet chemical etching. Periodic mesa gratings with 20 nm height and 2 μm width were patterned along the [011], [010] and [0$\bar{1}$1] direction, respectively. InGaAs islands were formed during growth of a 1.8nm-thick $In_{0.34}Ga_{0.66}As$ layer at 500 °C, following a 400nm-thick GaAs buffer grown at 580 °C. Atomic force microscopy was performed after growth to view the surface morphology of the samples, as shown in Figure 1. The morphology of the nonplanar surfaces is extremely sensitive to the pattern direction. On mesa gratings along the [0$\bar{1}$1] direction, the surface consists of ridges and relative flat bottoms. The ridge is formed on the mesa top and is slowly expanding during the growth. On the contrary, wave-like structures are formed on the mesa gratings along the [011] direction as the sidewalls of the mesas develop and advance very fast, consuming the mesa bottoms. The different evolution of growth front between the [0$\bar{1}$1] and the [011]-aligned mesas is related to the anisotropic properties of the GaAs (100) surface, muck likely caused by the different properties of the type-A and type-B steps for the (2×4) surface reconstruction. The surface formed on the mesa gratings along the [010] direction appears as the combination of these two different trends mentioned above.

The distribution of InGaAs islands on the nonplanar surface formed on [011]-aligned mesa gratings indicates that the influence of this nonplanar surface structure on island formation is very weak. On the contrary, on the [0$\bar{1}$1]-aligned mesas InGaAs islands tend to align along the [0$\bar{1}$1] direction. The ordering degree depends on the tilt angle of the slope. It is easy to find a string of InGaAs islands at the conjuction corner between the ridge and the flat mesa bottom, as shown in Figure 2(a), where the tilt angle reaches the maximum value. Since the tilt angles of the slopes on all nonplanar surfaces are around 1°, it is reasonable to consider these nonplanar surfaces as a complex structure composed of surface steps and (100) terraces. Therefore, only type-A ([0$\bar{1}$1]-aligned) surface steps are identified to induce the ordering and alignment of the InGaAs islands. This conclusion is further confirmed by the distribution of InGaAs islands formed on the vicinal GaAs (100) substrate (2° off towards (111)A), as shown in Figure 2(b).

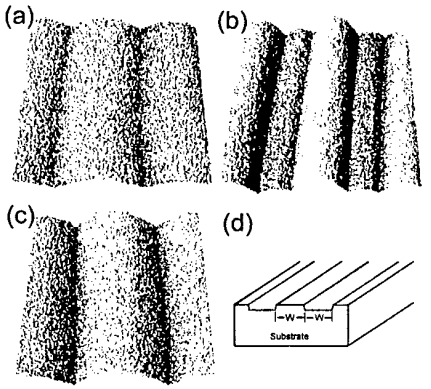

Figure 1: AFM images of the surface morphology of samples with mesa gratings along the (a) [011], (b) [0$\bar{1}$1], and (c) [010] direction. The scan size is 10μm×10μm. (d) Schematic of the substrate pattern. W represents the mesa width.

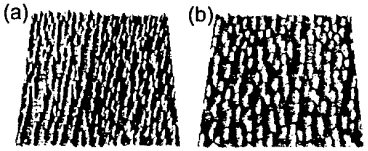

Figure 2: AFM images of the InGaAs islands formed on (a) the nonplanar surface for [0$\bar{1}$1]-aligned mesas and (b) the vicinal GaAs (100) substrate (2° off towards (111)A). The scan size is 1μm×1μm. The left part in (a) is the lower slope of the ridge while the right part is the flat bottom.

References

[1] R. Nötzel et al., Nature **392**, 56 (1998).
[2] Q. Gong, R. Nötzel, H.-P. Schönherr and K. H. Ploog, Appl. Phys. Lett. **77**, 3538 (2000).

Work performed while at Paul-Drude-Institut für Festköperelektronik, berlin.

Corresponding author: R. Nötzel, COBRA Inter-Univeristy Research Institute, Eindhoven University of Technology, 5600 MB Eindhoven, The Netherlands
phone: +31 40 247 2047, Fax: +31 40 245 2277,
email: r.noetzel@tue.nl

Formation of GaSb/GaAs Quantum Dots in MOCVD growth

L. Müller-Kirsch[1], R. Heitz[1], U. W. Pohl[1], I. Häusler[2], H. Kirmse[2], W. Neumann[2], D. Bimberg[1]

[1]Institut für Festkörperphysik, Technische Universität Berlin, Hardenbergstr. 36, D-10623 Berlin, Germany
[2]Institut für Kristallzucht, Humboldt Universität zu Berlin, Invalidenstr. 110, D-10115 Berlin, Germany

GaSb quantum dots (QDs) in GaAs are of special interest due to their type II band alignment. The QDs provide localization energies up to 400 meV for holes[1] whereas the electrons are only weakly confined in the surrounding barrier by the Coulomb interaction with the localized holes. The large hole confinement energy makes GaSb/GaAs QDs particulary interesting for storage devices [2] requiring room temperature localization. On the other hand, the type II character of the excitonic transition leads to peculiar optical properties which have been suggested already for the case of simple heterostructures to be advantageous for device applications [3].

The self-organized formation of GaSb/GaAs QDs in the Stranski-Krastanow growth mode was reported previously for molecular beam epitaxy [4]. The work concentrated mainly on the optical properties of the system. The understanding of the details of the 2D/3D morphology transition, being a precondition for the control of the structural properties, is still poor.

Here we report for the first time on the growth of GaSb/GaAs QDs using MOCVD. The GaSb films were capped after a growth interruption with GaAs and structurally characterized by means of transmission electron microscopy and by photoluminescence measurements.

Growth interruption after GaSb film deposition provides time for the evolution of the growth surface. The interplay between the formation of coherent QDs and Ostwald ripening indicates the character of thermodynamic and kinetic contributions to the QD formation [5]. Fig.1 shows the size distributions obtained for different growth interruptions under the constraint of fixed coverage determined from plane-view transmission electron microscopy images. With prolonged growth interruption the lateral size of the QDs first increases and then saturates. This suggests a mass transfer from the two-dimensional wetting layer in the QDs until a quasi-equilibrium state is reached for the wetting layer and the QDs. Apparently the size distributions are not Gaussian but show a bimodal behaviour during the formation of the QDs, which we attribute to a shape transition depending on the QD volume. The QD density being constant for all growth interruptions and the bimodal behaviour being present in the final distribution hints to a local equilibrium rather than to a total equilibrium for the description of the QD formation using the present growth parameters. The optical properties of the sample series support well the structural results and reveal the behaviour of the wetting layer thickness. Finally dislocation-free coherent GaSb islands with a density of 3×10^{10} cm^{-2} are obtained for a GaSb deposition of 4.5 ML.

With increasing photoluminescence excitation density both the wetting layer and the QD peak maxima shift to higher energies, which we attribute to hole-hole interactions in the many particle regime. Although preliminary self-consistent calculations of the electronic states suggest the localization energy of the electrons to be small, photoluminescence of such QDs is observed up to room temperature supporting the notion of holes being responsible for the observed PL properties.

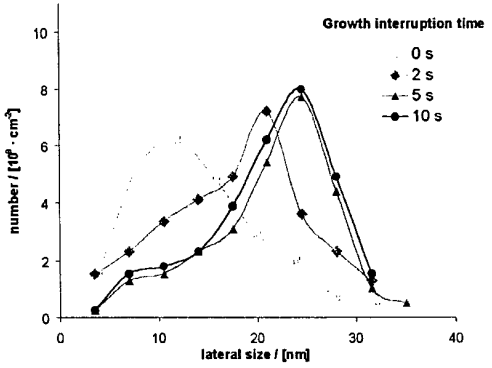

Fig.1: Size distributions of the GaSb QDs for different growth interruptions after the GaSb film deposition studied by plane view TEM.

References

1 R. Magno, B. R. Bennett E. R. Glaser, J. Appl. Phys. 88, 5843 (2000).
2 Y. Sugiyama, Y. Nakata, S. Muto, T. Futasugi, N. Yokoyama, J. Selec. Top. in Quant. Electr. 4, 880 (1998).
3 H. Kroemer, G. Griffiths, IEEE Electron Device Lett. EDL-4, 20 (1983).
4 D. Bimberg, M. Grundmann, N. N. Ledentsov, Quantum Dot Heterostructures (John Wiley &Sons, Sussex,, 1999). B. R. Bennett, R. Magno, B. V. Shanabrook, Appl. Phys, Lett. 68, 505 (1996).
5 V. A. Shchukin, D. Bimberg, Rev. Mod. Phys. 71, 1125 (1998).

Corresponding author: Lutz Müller-Kirsch, Institut für Festkörperhysik, Technische Universität Berlin, Hardenbergstrasse 36, D-10623 Berlin, Germany.
phone: +49 30 314 22061, Fax: +49 30 314 22569
email: igel@physik.tu-berlin.de

Photoconductive response of InAs/GaAs quantum dot stacks

S. Hofer, H. Hirner, R. Bratschitsch, G. Strasser, K. Unterrainer

Institut für Festkörperelektronik, Technische Universität Wien,
Floragasse 7, A-1040 Wien, Austria

Using electrical and optical techniques we investigate the energy levels of InAs quantum dots embedded in GaAs used for normal incidence photodetectors in the midinfrared.

Two sampels are used for the investigations. Both structures are grown on semi-insulating GaAs(001) substrate by molecular beam epitaxy. The dots arise from the Stranski-Krastanov growth mechanism by which 30 dot layers are stacked in sample A and 20 layers in sample B between two highly Si-doped contact layers. The dot layers of both samples are embedded into a GaAs Matrix of 10 nm width which -for sample B- is Si-doped so that each dot is filled with about one electron. Sample B is provided additionally with thin AlAs layers of 1 nm thickness, 1 nm spaced from the dots to restrict the vertical current. From the relatively small distance between the dots we assume that the states in the dots must couple vertically[1]. The work is done within the future goal to obtain emission from interdot transitions in the THz region from quantum dots[2] and from quantum dot cascade emitters[3].

To measure the dark current-voltage characteristic of the samples mesa diodes of 30x30 μm^2 were processed. The measurements show a nonlinear asymmetric behaviour with turn-on-voltages of 0.5 V and –0.14 V for sample A and 0.66 V and -2.5 V for sample B. The dark current is of the order of mA. Sample B shows a smaller dark current than sample A due to the AlAs barriers.

The 300K photoluminescence data show for both samples sharp peaks at 994 meV and at 1021 meV with a FWHM of 57 meV and 54 meV whereas the intensity for sample B is 7 times higher than for sample A. The frequency shift gives evidence that the dots of sample A are larger. There is no higher transition visible than the ground state recombination which we attribute to the relatively low laser intensity of 0.5 W/cm^2. The TEM pictures of the samples show that the dots do not consist of aggregated InAs islands but of strained areas in the InAs layers.

Photocurrent measurements are done in the same way as by K.W. Berryman et al.[4]and by L.Chu et al.[5] for uncoupled dots. We process the samples into mesas by standard photolithography and wet chemical etching with thermally alloyed Ni/Ge/Au contacts consisting of a rectangular contact and 32 or 8 fingers each 1 mm long, 25 µm wide and with a 25 µm spacing. The samples are mounted on the cold finger of a He flow cryostat system with ZnSe or polyethylene windows. The spectral dependence of the photoresponse of the detector structure is measured using a standard FTIR spectrometer with a glow-bar infrared source. The samples are measured in a normal incidence geometry. In figure 1 the measured transition from the ground state of the quantum dots to the continuum of sample B is depicted. We expect a higher transition energy for sample B compared to sample A since the electrons have to be excited into the higher lying lowest miniband of the AlAs-GaAs superlattice. In fact, there is a energy difference of 27 meV between the peaks of the two samples. Sample B shows also a large signal at zero bias which we ascribe to the built in field between the ionized donors next to the dots and the electrons in the dots. The GaAs matrix of sample A is not doped. Therefore there is no photoresponse signal at the unbiased state.

Measurements in a lower frequency range show a broad peak with several features around 55 meV which we interpret as interdot transitions (see also D. Pan et al.[6]). The strong normal incidence response supports the interpretation that the observed peaks are from optical transitions in the quantum dots rather than from the two dimensional wetting layer. Sample A does not show this peak which we attribute to the larger dark current in this sample.

In conclusion, we were able to see interdot transitions as well as bound states-continuum transitions for the same sample which allows to develop a photodetector with two response peaks at 55 meV and 253 meV. The very good spectral response of the stacked dots shows that cascaded quantum dot emitters are feasible.

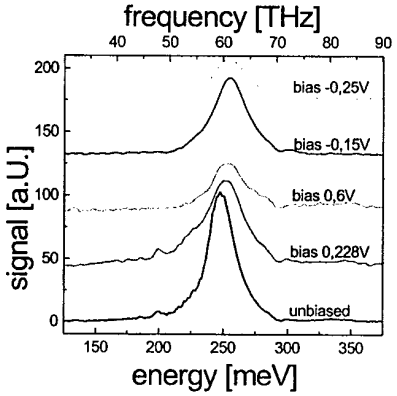

Fig. 1 Photoresponse signal of sample B due to ground state-continuum transitions in the quantum dots at different bias voltages. T=10K

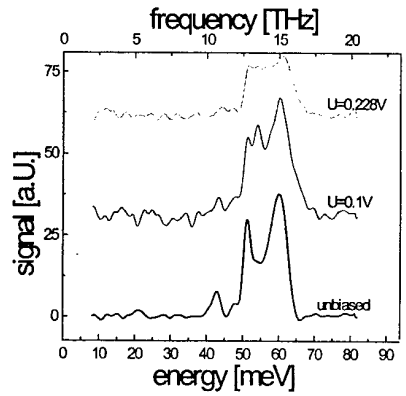

Fig. 2 Photoresponse signal of sample B due to interdot transitions in the quantum dots at different bias voltages. T=10K

References

[1] M. Bayer, P.Hawrylak, *Science* **291**, 451 (2001)
[2] M. Grundmann, A. Weber, *Appl. Phys. Lett.* **77**, 4 (2000)
[3] N.S. Wingreen, C.A. Stafford, *J. of Quantum Electronics*, **33**, 1170 (1997)
[4] K.W. Berryman, S.A. Lyon, *Appl. Phys. Lett.* **70**, 1861 (1997)
[5] L. Chu, A. Zrenner, *Appl. Phys. Lett.* **75**, 3599 (1999)
[6] D. Pan, E. Towe, *Appl. Phys. Lett.* **73**, 1937 (1998)

Corresponding author: Stefan Hofer, Institut für Festkörperelektronik, Technische Universität Wien, Floragasse 7, A-1040 Wien
phone: +43/1/5880136238, Fax: +43/1/5880136299
Email: Stefan.Hofer@tuwien.ac.at

Piezoelectric effects in ultrahigh quality AlGaAs/GaAs single quantum wire

X.-Q. Liu[a,b], X.-L. Wang[a,b], M. Ogura[a,b], T. Guillet[c], V. Voliotis[c,d], R. Grousson[c]

[a]Electrotechnical Laboratory, 1-1-4 Umezono, Tsukuba 305-8568, Japan
[b]CREST, Japan Science and Technology Corporation (JST)
[c]Groupe de Physique des Solides, CNRS, Univserités Paris 6 et Paris 7, 2 place Jussieu, F-75251 Paris Cedex 05, France
[d]Université Evry-val d'Essonne, boulevard Francois Mitterand, 91025 Evry, France

Strain induced piezoelectric effects have been shown to strongly affect the optical properties of quantum structures in strained III-V heterostructures[1-3]. However, up to now, investigations are mainly concentrated on material systems with large lattice mismatch, such as the InGaAs/GaAs structures, and the AlGaAs/GaAs system is generally considered not to exhibit important piezoelectric effects due to the very small lattice mismatch. Here we demonstrate for the first time the strong modification of optical properties by the tiny lattice mismatch induced piezoelectric field along the wire in ultrahigh quality AlGaAs/GaAs V-grooved quantum wire (QWR) structure.

A 5nm thick $Al_{0.425}Ga_{0.575}As$/GaAs single QWR was grown using flow rate modulation epitaxy[4]. To improve the interface quality, a short period superlattice buffer layer [AlGaAs(2.8nm)/GaAs(1.4nm)x150] was grown before the growth of the AlGaAs barrier and the QWR structure[5]. QWRs grown by this technique is proved to be of extremely high interface quality [6], which is composed of QWR sections defined by monlayer (ML) steps with length of at least several 100 nm for one section. Figure1 demonstrates the temperature-dependent photoluminescence (PL) and photoluminescence excitation (PLE) spectra. One striking feature in Fig.1 is that the PLE intensity of the ground state (e_1-hh_1) transition is almost zero at low temperature. With increasing temperature, the e_1-hh_1 transition appears gradually. Clear e_1-hh_1 transition peaks can be observed when temperature is higher than 100K. The zero PLE intensity strongly suggests complete spatial separation of electron and hole wavefunctions. Figure 2 shows laser power density dependence of PL peak energy and line width (FWHM). Obvious blue shifts of the order of 4 meV and decrease then increase of FWHM were observed with increasing power density. These results are characteristic of those observed in structures with strong piezoelectric effects [3]. To confirm the existence of piezoelectric field effects, we used the He-Ne laser to pump the sample when accomplishing PLE measurements at 90K. As can be seen from Fig.3, the PLE intensity of the e_1-hh_1 transition is obviously enhanced with pumping. This is probably due to the partial screening of the piezoelectric field by the photo-generated carriers. The piezoelectric effects induced polarization around the QWR has two components: one is perpendicular to the {113}A facets, the other is parallel with the wire [2], with the polarization about $1.77x10^{-4}$ Cm^{-2}, and $1.59x10^{-4}Cm^{-2}$, respectively. Fig. 4 shows the schematic diagram of the geometric directions. The electric field perpendicular to the {113}A facets will only slightly modify the lateral confinement potential. Concerning the polarization parallel with the wire, the situation is quite interesting: the polarizations inside the (113)A and the (11-3)A are in the opposite directions. Therefore, if the interface fluctuations on the two sides are exactly the same, the influence of the polarization induced electric field at interface steps on e_1-hh_1 wavefunctions will be cancelled out with each other. However, the interface on the two sides will fluctuate randomly, and hence e_1-hh_1 wavefunctions can experience some net potential change due to incomplete cancellation within one QWR section. It is worthwhile to notice that a very small net electric field can produce very large potential change due to the extremely long QWR section (at least several hundreds nm)[6]. This net potential change is responsible for the separation of the electron and hole wavefunctions in one QWR section. When the temperature is higher than 100K(8.6meV), the 1ML fluctuation induced potential step (about 9meV) will be overcome and the electron and hole are completely free. Thus the electric field effects will disappear with increasing temperature.

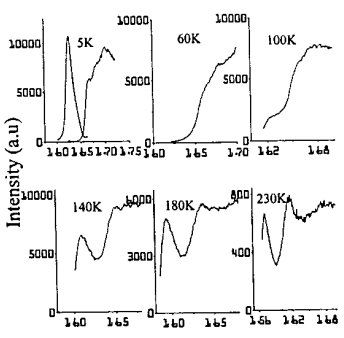

Fig.1 Temperature dependent PLE spectra.

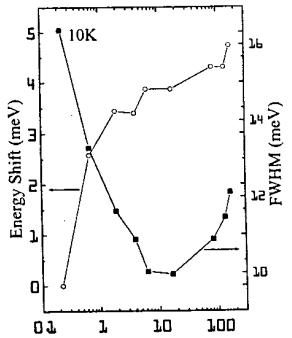

Fig.2 Laser power density-dependent peak energy shift and peak FWHM. Excitation laser is Ar^+514.5nm line.

Fig.3 PL and PLE spectra at 90K. The dash line is the PLE spectrum pumped by He-Ne laser during PLE measurement

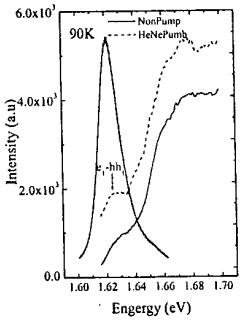

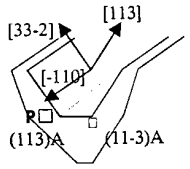

Fig.4 Schematic diagram of axis.

Reference:
[1] D. L. Smith and C. Mailhiot, Phys. Rev. Lett., 58, 1264(1987).
[2] L. D. Caro and L. Tapfer, Phys. Rev. B, 48, 2298(1993).
[3] M. Ilg, K. H. Ploog, and A. Trampert, Phys. Rev. B, 50, 17111(1994).
[4] X.-L Wang, M. Ogura, H. Matsuhara, Appl. Phys. Lett., 66, 1506(1995).
[5] X.-L. Wang, V. Voliotis, R. Grousson, and M. Ogura, J. Crystal Growth, 213, 19(2000).
[6] A. Crottiui, J.-L. Stachli, D. Deveaud, X.-L. Wang, M. Ogura, Phys. Rev. B, Mar. 15(2001)

Corresponding Author: Xing-Quan Liu: Electron Devices Division, Electrotechnical Laboratory, 1-1-4 Umezono, Tsukuba 305-8568, Japan.
Tel: 81-298-615299, Fax: 81-298-61-3357, email: xqliu@etl.go.jp

Raman study of self-assembled InAs quantum dots embedded in AlAs: influence of growth temperature

D. A. Tenne[1], A. K. Bakarov[1], A. I. Toropov[1], D. R. T. Zahn[2]

[1]Institute of Semiconductor Physics, pr. Lavrenteva 13, 630090 Novosibirsk, Russia
[1]Institut für Physik, Technische Universität Chemnitz, D-09107 Chemnitz, Germany

Self-assembled semiconductor quantum dots (QD's) have attracted much research interest during recent years [1]. Despite the large amount of research dealing with self-assembled QD's, many aspects are still not well investigated, especially for InAs QD's embedded in AlAs, which are much less studied than (In,Ga)As QD's in a GaAs matrix. In particular, little attention has been paid to the vibrational spectra of QD structures. Recently we reported the observation of phonon Raman scattering in InAs QD's in an AlAs matrix [2]. In the present paper we apply Raman spectroscopy to study the effect of growth temperature on the vibrational spectra of InAs QD's embedded in AlAs.

A series of InAs QD's was grown by molecular beam epitaxy on GaAs (001)-oriented substrates at the following substrate temperatures during the QD formation: 420, 440, 480, 520 and 550°C (samples A–E, respectively). The samples consist of five layers of self-assembled InAs QD's separated by 12 nm AlAs spacers. The growth monitoring by reflection high-energy electron diffraction showed that the transition from a two-dimensional to a three-dimensional growth mode for all the samples occurs after the deposition of 1.8 monolayers of InAs. After the deposition of the nominal amount of InAs (2 monolayers for all samples), the growth was interrupted for 100 s allowing self-assembled islands to reach equilibrium sizes. Raman spectra were recorded at 80 and 300 K in a backscattering geometry using a Dilor *XY* triple spectrometer equipped with a multichannel CCD detector. Several lines of Ar^+ and Kr^+ lasers (514.5, 568.2, 647.1, 676.4, and 752.5 nm) were used for excitation.

Figure 1 shows the Raman spectra of sample C measured with different laser lines. The asymmetry of InAs QD phonon lines and its dependence on the excitation energy are caused by QD size distribution. At lower excitation energies the observed LO phonon frequencies of InAs QD's (259 cm^{-1} for sample C) agree well with theoretical calculations of optical phonon energies taking into account strain distribution in large QD's where phonon confinement effect is negligible [3] and experimental values for InAs QD's in GaAs matrix obtained by resonant photoluminescence [4] and by Raman spectroscopy [5]. The frequencies of QD phonons are significantly higher compared to the bulk InAs values due to compressive strain. The downward shift of the maximum of the phonon line with increasing excitation energy is due to the presence of smaller-size dots in which the phonon confinement effect becomes more significant and leads to a noticeable decrease of the phonon frequencies. The large dots have lower energies of electronic transitions (about 1.65 – 1.7 eV for InAs QD's embedded in AlAs). The contribution of these QD's in the Raman spectra is stronger for laser lines in the red spectral range, which are close to the resonance with electronic transitions. The smaller QD's have higher energies of electronic and hole ground states. Therefore, the relative contribution of small dots to the Raman spectra increases at higher excitation energies, leading to downward shift of the optical phonon features.

Phonon lines of a wetting layer (WL) at 232 and 244 cm^{-1} have been identified by measuring the Raman spectra of a superlattice $(AlAs)_{30}(InAs)_{1.5}$ (see Fig.1) with thin InAs layers (below the critical thickness of island formation). The relative contribution of the WL phonons to the Raman spectra also increases with excitation energy as the latter becomes closer to resonance with the bandgap energy of WL, which is higher compared to QD's.

Similar behaviour (asymmetric line which is downward shifted with increasing excitation energy) was observed in the spectra Raman spectra of samples A and B. However, the position of QD phonon line maximum decreases and the linewidth increases for the samples grown at lower substrate temperatures (See Fig. 1a showing the normalized spectra of samples A–C in the InAs region). This indicates that the phonon confinement effect becomes larger for these samples, i.e. the QD's grown at lower substrate temperature have smaller sizes. Sample D grown at 520°C, is characterized by weak broad Raman feature with maximum close to the bulk InAs LO phonon frequency. Therefore, we assume QD's in this sample to become so large, that strain is mainly relaxed. In the last sample E grown at the highest temperature (550°C) the features of InAs phonons almost disappear, probably, because of partial evaporation of InAs at such a high substrate temperature.

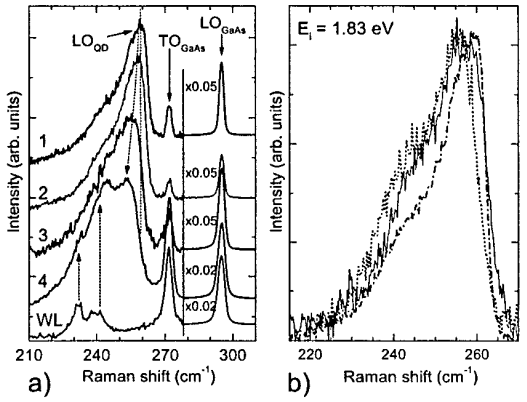

T = 80 K, $z(x,y)\bar{z}$

Fig. 1: a) Raman spectra of sample C measured with different laser lines: 1.83, 1.92, 2.18, and 2.41 eV (1–4, respectively), and the spectrum of $(AlAs)_{30}(InAs)_{1.5}$ superlattice (WL). The dotted lines are guides to the eye. b) Raman spectra of samples A, B, and C (dotted, solid, and dashed-dotted lines, respectively).

References

[1] D. Bimberg, M. Grundmann, and N. N. Ledentsov, *Quantum Dot Heterostructures* (Wiley, New York, 1999).
[2] D. A. Tenne et al., Phys. Stat. Sol. (b) 224, 25 (2001).
[3] M. Grundmann, O. Stier, and D. Bimberg, Phys.Rev.B 52, 11969 (1995).
[4] R. Heitz et al., Appl. Phys. Lett. 68, 361 (1996).
[5] Yu. A. Pusep et al., Phys. Rev. B 58, R1770 (1998).

Corresponding author: Dmitri Tenne,
Institute of Semiconductor Physics, pr. Lavrenteva 13, 630090 Novosibirsk, Russia
phone: +7 3832 341945, Fax: +7 3832 332771
email: tenne@thermo.isp.nsc.ru

Transition from spatially indirect to direct recombination in stacked layers of self-assembled InP quantum dots

J. Maes[1], M. Hayne[1], Y.M. Manz[2], O.G. Schmidt[2], K. Eberl[2] and V.V. Moshchalkov[1]

[1]Laboratorium voor Vaste-Stoffysica en Magnetisme, Katholieke Universiteit Leuven, Celestijnenlaan 200D, B-3001 Leuven, Belgium
[2]Max-Planck-Institut für Festkörperforschung, Heisenbergstr. 1, 70569 Stuttgart, Germany

We observe a 20-fold increase in the relative photoluminescence (PL) intensity associated with the uppermost dot in a triple stack of self-assembled InP quantum dots as its separation from the other two closely stacked layers is reduced. Magneto-PL measurements confirm that this is the result of a transition from spatially indirect to direct recombination between an electron confined to the uppermost dot and a hole confined to the two closely stacked layers.

Three samples with triply-stacked layers of InP self-assembled quantum dots in a GaInP matrix were grown by solid-source molecular beam epitaxy. In each two vertically-aligned dot layers were grown with 4 nm separation. The distance of the third stacked layer was then varied from 30 nm to 15 nm to 4 nm in samples A, B and C respectively. For clarity we label the dots in the stack from top to bottom as 'upper', 'middle' and 'lower'. Thus the experiment may be viewed as measuring what happens when upper is lowered on to the other two dots. The amount of InP deposited in each dot layer was nominally 3.8±0.1 ML. Details of the experimental set-up may be found elsewhere [1,2].

Fig. 1 shows that the zero-field PL spectra of the three samples has a single high-energy peak at ~1.95 eV from the GaInP, with the PL from the dots at 200 meV lower energy. In sample A this is seen as a broad peak with a long low-energy tail comprised of two gaussians associated with different dots in the stack. In sample B the intensity of the lower dot-peak has increased, and it has moved to higher energy, whilst the position of the upper peak remains the same. In sample C the PL spectrum looks strikingly different: there is a single symmetric dot peak at slightly lower energy than the dominant peak in samples A and B. Of special note is the remarkable difference in relative intensities of the dot and GaInP peaks in sample C compared to samples A and B. The interpretation of these data is as follows. Sample A can be considered as a single dot (upper) and two stacked dots (middle and lower). Measurements on a double dot system nominally identical to middle plus lower have shown that strain localises the hole [3] across the double stack [2], with the electron occupying the top dot [2]. Thus we believe that the hole is localised across middle and lower, and that the electron occupies either upper or middle (Fig. 1). We therefore attribute the strong high-energy peak in sample A to recombination between a hole in the double stack and an electron in middle, and the weak low-energy peak to the same hole and an electron in upper. The latter recombination is spatially indirect. Note that we expect each stack to have only one electron-hole pair, so the hole is always localised across lower and middle, but the electron is either in upper or middle. Exactly the same interpretation may be applied to Sample B, though the low-energy peak has moved to higher energy and is much more intense, consistent with the closer proximity between the electron in upper and the hole localised across lower and middle. The high energy dot peak is associated entirely with lower and middle and so its position does not change.

Confirmation of these assignments comes from the PL data with a magnetic field applied in the growth direction (not shown). We concentrate on sample B, where the intensity of the low-energy dot peak is sufficient to allow detailed analysis of the field-dependent energy shift of both peaks. For InP dots such an analysis reveals the effective mass and radii of the holes [1,2]. Furthermore, a hole mass of ~0.23 m_e indicates a hole localised entirely in the GaInP matrix, as is the case for an isolated dot [3], whereas a mass of ~0.16 m_e shows that the hole is localised across a stack, *i.e.* in both GaInP and InP [1,2]. Here we find effective masses of 0.186 m_e and 0.154 m_e for the lower and higher energy peaks respectively, consistent with the holes being localised across the stack formed by lower and middle for both recombinations. Finally, we turn to sample C. A single dot peak is observed, due to an electron in upper and a hole localised across the stack. The high-energy dot peak has disappeared because the dots are sufficiently close that the electrons can always tunnel to upper. The previously spatially indirect transition which gave the weak low energy tail in Sample A is now a strong spatially direct transition, resulting in a 20-fold increase in its intensity relative to the GaInP peak.

Acknowledgments - This work was supported by the FWO-Vlaanderen, the Flemish GOA and Belgian IUAP programmes, the Flemish IWT, the VIS programme of the KU Leuven and Philips Optical Storage.

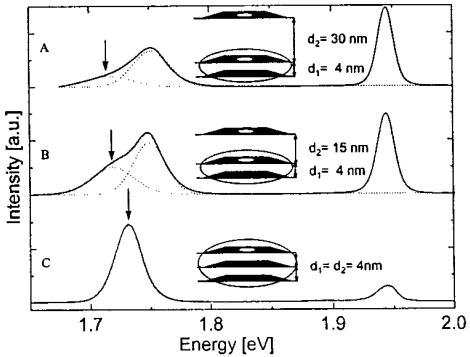

Fig. 1: PL spectra and schematic drawings of InP quantum dot structures (dark). For samples A and B, the hole (grey) is localised across middle and lower and the electron (white) is in either upper or middle resulting in a double peak at around 1.75 eV. For sample C the electron is in upper. The previously indirect recombination from upper in A and B (indicated by the arrow) becomes a direct recombination, resulting in a strong increase in intensity.

References

[1] M. Hayne *et al.*, Phys. Rev. B **62**, 10324 (2000).
[2] M. Hayne *et al.*, submitted to Appl. Phys. Lett.
[3] C. Prior, M.-E. Pistol and L. Samuelson, Phys. Rev. B **56**, 10404 (1997).

Corresponding author: Manus Hayne, Laboratorium voor Vaste-Stoffysica en Magnetisme, Katholieke Universiteit Leuven, Celestijnenlaan 200D, B-3001 Leuven, Belgium.
phone: +32 (0)16 327202, Fax: +32 (0)16 327983
email: manus.hayne@fys.kuleuven.ac.be

Electronic structure of Self-Assembled InAs Quantum Dots

C. Bock[1], K.H. Schmidt[1], U. Kunze[1], V. V. Khorenko[2], S. Malzer[2], G. Döhler[2]

[1] Lehrstuhl für Werkstoffe der Elektrotechnik, Ruhr-Universität Bochum, D-44780 Bochum, Germany
[2] Institut für Technische Physik I, Universität Erlangen-Nürnberg, Erwin-Rommel-Str. 1, D-91058 Erlangen, Germany

Electroluminescence (EL) is always related to carrier transport (i.e. current flow) into an active region. We used both signals to study in detail the electronic structure in InAs QDs embedded in the intrinsic GaAs region of a double hetero p-i-n diode. According to the position of the dot layer with respect to the n- and p-doped region we investigated the QD levels of electrons and holes independently.

The inset of Fig. 1a shows the band diagram of such a diode. When the dot layer is in the center of the intrinsic GaAs region electrons as well as holes simultaneously tunnel into the ground state of the dots at a forward voltage of $U_1 = 1.1$ V. Consequently, there is no structure in the capacitive signal for $U < 1.1$ V and the onset of the ohmic current signal coincides with the onset of the electroluminescence. In the low voltage regime ($U < 1.12$ V) the EL signal can nicely be fitted by a single Gaussian which reflects the size inhomogeneity of the investigated islands. At $U_2 = 1.144$ V holes tunnel into the p-shell of the dots resulting in another pronounced feature in the curvature of the ohmic signal (Fig. 1a). At the same voltage the line shape of the EL signal becomes asymmetric on the high energy side and two Gaussians are necessary to fit the EL spectrum (Fig. 1b). We attribute the second Gaussian to a weak transition between the electrons of the ground state and the holes of the first excited level. The centers of the fit functions are seperated by $\Delta E_h = 20$ meV which is in excellent agreement with our transport data and reflects the energy splitting between the ground and the first excited QD level of the hole system. The structure labeled U_3 results from the Coulomb blocked electron transport into the QD s-shell in the conduction-band. The shoulder at $U_4 = 1.26$ V in der $I - U$ trace of Fig. 1a reflects the tunneling process of electrons into the first excited QD level. The recombination process between p-electrons and p-holes seems to be very efficient since a pronounced transition appears in the EL spectra at an energy of $\Delta E = 1.14$ eV for $U > 1.26$ V. An energetic distance of $\Delta E_e \approx 40$ meV for electrons in the QD s- and p-shell can be extracted from the optical as well as from the electrical data.

When the dot layer is positioned near the p-doped layer the QDs are loaded with holes before electrons are able to tunnel into the dots giving rise to a EL as well as to an ohmic current signal. From the capacitive signal (Fig. 2a) a Coulomb blockade energy $\Delta E_{Ch} \approx 23$ meV of holes in the s-shell is determined. For higher voltages the structure in the ohmic signal reflects the energy spacing of the electron system. Five levels can be detected (arrows in Fig. 2b). Their level distance is approximately constant and amounts in average $\Delta E_e \approx 45$ meV. This value agrees reasonably well with the one determined from Fig. 1a.

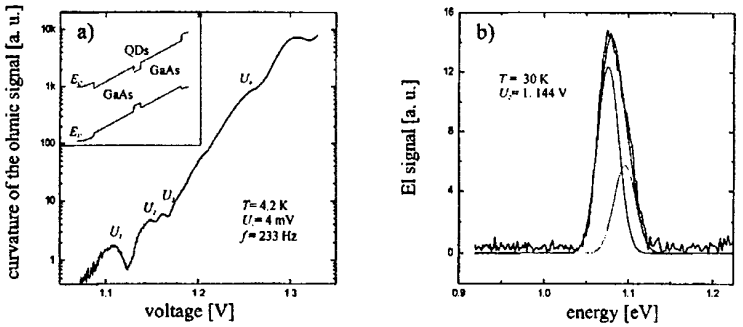

Figure 1: (a) Second derivative of the current with respect to the voltage for a sample with the dot layer in the center of the intrinsic GaAs region (see inset). (b) Corresponding EL spectra at an applied gate voltage of $U_2 = 1.144$ V. The line shape becomes asymmetric at $U = 1.144$ V and two Gaussians are necessary to fit the measured data.

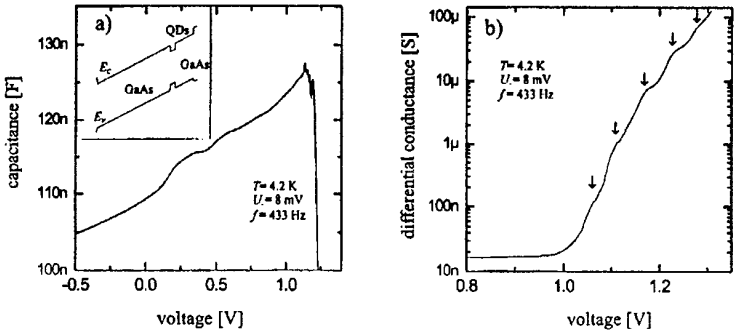

Figure 2: (a) Loading of the QDs with holes at low voltages ($U < 1$ V). For higher voltages electrons tunnel into the dots and clear shoulders appear in the differential conductance of Fig. 2b. Each feature is correlated with the onset of a new transition in the EL spectra. The band diagram of the asymmetric structure is shown in the inset of Fig 2a.

Corresponding author: Claudia Bock, Lehrstuhl für Werkstoffe der Elektrotechnik, Ruhr-Universität-Bochum, D-44780 Bochum, Germany.
phone: +49 234 322 3084, Fax: +49 234 321 4166,
email: bock@lwe.ruhr-uni-bochum.de

Photoluminescence of quasi-zero-dimensional InGaAsP quantum dots

Kazunari OZASA and Yoshinobu AOYAGI,

The Institute of Physical and Chemical Research (RIKEN),
2-1 Hirosawa, Wako, Saitama 351-0198, Japan

We present the photoluminescence (PL) of InGaAs(P) dots with quasi zero-dimensional (0D) confinement, studied from the viewpoint of dot composition/shape, energetic/spatial confinement, and 0D/2D transition. In the series of near-field PL spectrum for the structures with various degrees of 0D/2D, measured by using a scanning near-field optical microscope (SNOM), the coexistence of 0D and 2D confinement in the same layer was observed. We believe that quasi-0D structures are useful for applications such as nanosensors, where excitons in 0D-confinements are emitted by an external perturbation (surface adsorption of chemicals for example) into a 2D conducting layer and detected electrically.

Quasi-0D confinement structures, which we defined as the intermediate structures between QD and QW, were prepared by the conventional self-assembly of InGaAs dots on GaAs and their *in situ* phosphidation, performed in chemical beam epitaxy (CBE) chamber [1]. The exposure of InGaAs dots to phosphorus flux at growth temperature (480oC) brings the replacement of arsenic in InGaAs QDs by phosphorus. The composition and shape of the dots were modified by the phosphidation (Fig.1), and intermediate quasi-0D structures between InGaAs dots (0D) and an InGaAsP flat layer (2D) resulted depending on the phosphidation time [2]. We chose several degrees of phosphidation for characterization, which are indicated in Fig.1 with phosphidation time, phosphorus-fraction of the dots, and the estimated height of the dots. Each structure was capped by subsequent GaAs growth (50nm).

Figure 2 shows the PL spectra obtained from the near-field PL measurements at 10K for various quasi-0D structures. The spectra were taken by a SNOM apparatus, which is equipped with an Au-coated fiber probe and operated with collection-mode (532nm excitation). The distributed fine peaks of 0D confinement converge into one peak as phosphidation proceeds, showing that QDs were fused into a QW (Fig.2). For the dots with 8s- and 10s-phosphidation, most of the dots still have 0D confinement, although a finite diamagnetic shift was observed for 10s-phosphidated dots (approx. 40ueV/T2 at 4.2K, by macroscopic measurements not shown here). It suggests that the extension of electron wave function proceeds with keeping the discreteness of energy levels.

The spectrum of 20s-phosphidated dots in Fig.2 shows the coexistence of 0D and 2D confinement by the fine peaks superimposed on the 2D (QW) peak (a rather broad peak at the base of fine peaks). The coalescence of fine peaks corresponds to the saturation in the change of dot composition at 20s phosphidation (Fig.1). No obvious deviation between 0D fine peaks and the 2D peak in the photon energies of spectrum implies that the dot-to-dot electron interaction is weak in this quasi-0D system, since a red shift of the merged 2D peak from the 0D fine peaks should be observed if there is a strong interaction between the electrons in the neighboring dots during the dot coupling.

We have performed macroscopic PL measurement as well for phosphidation-time dependence, temperature dependence, and diamagnetic shift. The results showed that the energetic confinement (dot composition) rather than spatial confinement (dot shape) dominates the low-temperature optical properties of quasi-0D confinements in InGaAs(P) half-flattened dots, and that nonradiative recombination centers are not newly created by the phosphidation.

The coexistence of 0D and 2D confinement in the same layer is expected to be useful for various applications including nanosensors, where an external perturbation causes immobile excitons in 0D to be mobile carriers in a 2D conducting layer.

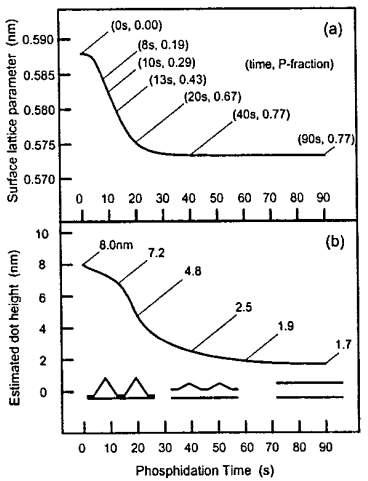

Fig.1: Temporal change (*in situ* RHEED observation) of surface lattice parameter (a) and dot height (b), caused by the phosphidation of InGaAs dots.

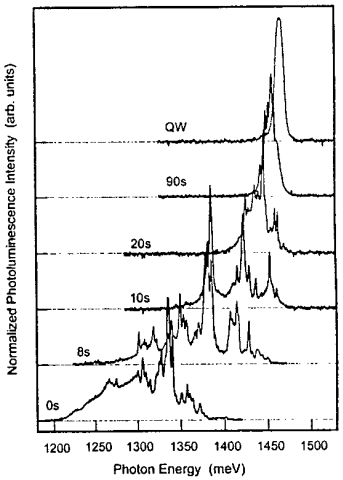

Fig.2: Near-field PL spectrum of dots with various degrees of phosphidation. Spectrum of strained InGaAs QW is also presented for comparison.

References

[1] K.Ozasa, Y.Aoyagi, Y.J.Park, and L.Samuelson, Appl.Phys.Lett. **71** (1997) 797.
[2] K.Ozasa and Y.Aoyagi, J.Cryst.Growth, **188** (1998) 370.

Corresponding author: Kazunari OZASA,
The Institute of Physical and Chemical Research (RIKEN),
2-1 Hirosawa, Wako, Saitama 351-0198, Japan,
phone: +81 48 462 1111, Fax: +81 48 462 4659,
email: ozasa@postman.riken.go.jp

Band offset of InAs Self-assembled Dots on GaAs

D. Rakoczy[1], G. Strasser[1], J.Smoliner[1]

[1] Institut für Festkörperelektronik, TU-Wien, Floragasse 7, A-1040 Wien, Austria

The expectation of significant improvements both of electronic and optoelectronic behaviour together with the prospect for completely new aspects of physics have led to a flourishing in the production and characterisation of self-assembled quantum dots (SAQDs) during the last few years. Among the various methods which are employed in the investigation of SAQDs, scanning tunneling microscopy (STM) and ballistic electron emission microscopy (BEEM) are valuable tools, because they offer the possibility to probe single dots instead of just averaging over a large ensemble of dots.

In this work, we used BEEM to investigate how 3-dimensional InAs dots on the one hand and a 2-dimensional InAs wetting layer between the dots on the other hand influence the barrier height of an InAs/GaAs interface, which was covered with a gold film to provide the electric contact necessary for STM/BEEM [1]. It is well known, that the contact between Au and InAs is ohmic, therefore the measured barrier height for regions with a thick InAs layer can be seen as the effective band offset between the InAs and the GaAs [2]. In contrast, regions without any InAs wetting layer should exhibit an onset determined by the GaAs/Au Schottky contact. Studies were carried out on samples with a native InAs wetting layer as well as on samples were the wetting layer was removed using diluted hydrochloric acid. High contrast BEEM images of dots are only possible for samples without a wetting layer (see Fig. 1). Systematic studies of the local barrier height variations of the InAs wetting layer were performed on samples with intact wetting layers.

From the onset of the BEEM spectra we can directly determine the band offset. Fig. 2 shows two typical BEEM curves, one measured on a dot and the other one on the sample surface between the dots. Measurements at 300 K on various dots showed that the barrier height varies between 0.63 eV and 0.74 eV for the 'on-dot' position. On etched samples the barrier height between the dots is 0.82 eV–0.9 eV, indicating that the wetting layer has been removed to a large extent.

On samples with an intact wetting layer, the band offset at 300 K varies from 0.70 eV to 0.83 eV with a mean value of 0.78 eV (see Fig. 3). The broadness of this distribution is only partly caused by the measurement conditions; a significant contribution is due to the inhomogeneity of the wetting layer itself. Cooling the sample down to 185 K shifts the mean band offset to 0.86 eV and narrows the distribution (supressing fluctuations due to the measurement conditions). The standard deviation of the distribution is 19 meV at 185 K (compared to 35 meV at 300 K).

Comparison of our data with band offsets measured on plain, strained InAs Layers [2] suggest that the thickness of the wetting layer varies with position between 1 and 3 monolayers, while the dots are about 33 monolayers high (the later was also confirmed by AFM measurements on our samples).

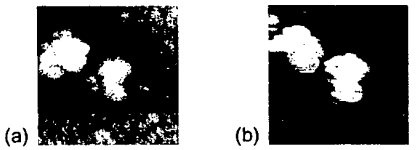

Figure 1: Image of two large InAs dot clusters on a sample with a removed wetting layer. Scan range 200 nm × 200 nm. (a) Topographic STM image, (b) corresponding BEEM image.

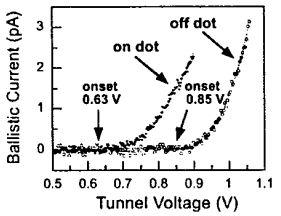

Figure 2: BEEM onset voltage on an InAs quantum dot and between the dots respectively, for a sample with a (largely) removed wetting layer. T=300 K.

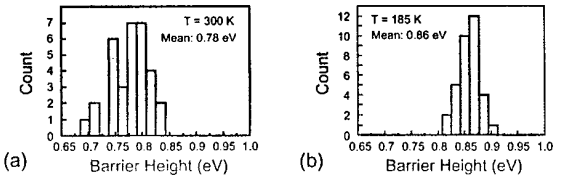

Figure 3: Distribution of the band offset measured at different positions on the wetting layer. (a) T=300 K, (b) T=185 K

References

[1] D. Rakoczy, G. Strasser, J. Smoliner, submitted to J. Vac. Sci. Technol. B
[2] Mao-Iong Ke et al., J. Vac. Sci. Technol. B **14**(4), 2786 (1996)

Corresponding author: D. Rakoczy, Institut für Festkörperelektronik, TU-Wien, Floragasse 7, A-1040 Wien, Austria
phone: +43 1 58801 362-314, Fax: ++43 1 58801 362-99,
email: doris.rakoczy@tuwien.ac.at

Tailoring and controlling electron-hole states in single and coupled semiconductor quantum dots

Ulrich Hohenester[1,2], Filippo Troiani[1], and Elisa Molinari[1]

[1] Istituto Nazionale per la Fisica della Materia (INFM) and Dipartimento di Fisica, Universita' di Modena e Reggio E. Via Campi 213/A, I–41100, Italy
[2] Institut für Theoretische Physik, Karl–Franzens–Universität Graz, Universitätsplatz 5, 8010 Graz, Austria

Semiconductor quantum dots (QDs), often referred to as "artificial atoms", are solid state heterostructures which allow the confinement of carriers in all directions of space within dimensions smaller than their de Broglie wavelength. Such confinement results in a characteristic discrete energy spectrum and a δ-like density of states. Part of the attention that QDs currently receive is due to the possibility to explore, through tailoring the characteristical physical parameters, regimes inaccessible to conventional atomic physics; on the other hand, their electrical and optical properties are starting to yield QD based devices, e.g., QD infrared detectors, QD lasers, or QD memory devices. In addition, these structures allow to partially decouple a few degrees of freedom of the solid-state structure from all the others, thus enabling in principle their coherent and controlled manipulation, as requested for example by current quantum-information-processing strategies.

In this contribution we present a theoretical analysis of electron-hole states in single and coupled semiconductor QDs, and propose an all-optical implementation of quantum-information processing in such dot structures. A full configuration-interaction description is employed for the calculation of few-particle electron-hole states in realistic single and coupled QD structures. Our approach accounts for intra- and inter-dot few-body interactions in a first principles manner. We show that because of the strong quantum confinement Coulomb correlations between electrons and holes are strongly enhanced, and that each electron-hole configuration leads to its characteristic fingerprint in the optical spectra (both in single-dot spectroscopy of multi-excitons [1] and multi-charged excitons [2,3]). We discuss that the optical peak positions provide a sensitive measure of strongly confined carrier wavefunctions in QDs. For vertically coupled quantum dots, the multi-exciton groundstate configuration is shown to undergo non-trivial quantum transitions as a function of the interdot distance d, resulting in unexpected spatial correlations among carriers. For instance, while at small interdot distances d a system of two electron-hole pairs is distributed over both dots, at larger distances the most favorable quantum state becomes the one with all four particles localized within the same dot (see Figure 1).

Finally, we discuss how electron-hole states in semiconductor QDs could be exploited for quantum-information processing [4] and novel coherent-carrier-control techniques [5]. Within our quantum computation scheme the excitonic states serve as the qubits, and the conditional and unconditional qubit operations which are required for quantum-information processing are performed by means of femtosecond spectroscopy. We discuss how quantum transitions in coupled QDs may be used to tailor the Hilbert space structure and the qubit identification in quantum dot arrays.

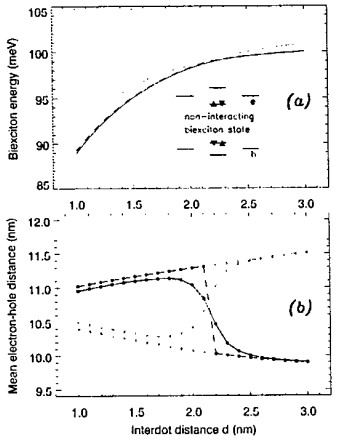

Figure 1: (a) Biexciton energies in a vertically coupled QD structure as a function of interdot distance d for the four biexciton states of lowest energy; the inset sketches the formation of bonding and antibonding states and the occupation with two electron-hole pairs with opposite spin orientations. (b) Mean electron-hole distance. At a critical distance of approximately 2 nm the biexciton groundstate changes from a configuration where both electron-hole pairs are distributed over the whole structure to a configuration where all carriers are localized in one of the two dots.

References

[1] For a review see, e.g., A. Zrenner, J. Chem. Phys. **112**. 7790 (2000).
[2] A. Hartmann, Y. Ducommun, E. Kapon, U. Hohenester, and E. Molinari, Phys. Rev. Lett. **84**, 5648 (2000).
[3] F. Findeis, M. Baier, A. Zrenner, M. Bichler, G. Abstreiter, U. Hohenester, and E. Molinari, Phys. Rev. B. **63**, 121309(R) (2001).
[4] F. Troiani, U. Hohenester, and E. Molinari, Phys. Rev. B **62**, R2263 (2000).
[5] U. Hohenester, F. Troiani, E. Molinari, G. Panzarini, and C. Machiavello, Appl. Phys. Lett. **77**, 1864 (2000).

Corresponding author: Ulrich Hohenester, Institut für Theoretische Physik, Karl–Franzens–Universität Graz, Universitätsplatz 5, 8010 Graz, Austria
phone: +43 316 380 5227, Fax: +43 316 380 9820,
email: ulrich.hohenester@uni-graz.at

Exchange coupling and polarization relaxation in self-assembled quantum dots

R. Ferreira

Laboratoire de Physique de la Matière Condensée ENS
24 rue Lhomond F75005 Paris (France)

The existence of a discrete sequence of narrow transition lines involving the bound levels of a single quantum dot is nowadays well established. Furthermore, a few high accuracy experiments were able to resolve the fine structure of the inter-band lines. In particular, c.w. experiments show the existence of an energy splitting between two lines linearly polarized along the directions [-1,1,0] and [1,1,0] (see for instance [1-2]). This polarization anisotropy has also been observed on far-infrared (intra-band) magnetoabsorption experiments performed on an ensemble of dots and interpreted using the former mechanism [3]. Also, time resolved experiments performed in the strict resonant excitation and detection situation show that the linear polarizations of the ground dot transitions are conserved at low temperature [4]. The existence of two particular (orthogonal) directions for the light polarization has been attributed to either a geometric anisotropy of the dot confining potential or to internal strain fields. The states with Px and Py polarizations are the exchange-splitted linear combinations of the two bright, circularly polarized /±1> levels [5-7].

A few experimental results show, however, that in certain cases a ground inter-band luminescence that is circularly polarized can be observed after a non-resonant excitation. This is in contradiction with the image of linearly polarized stationary states for the dots, as originated by the concomitant actions of the long-range exchange coupling and of the geometry-induced anisotropy of the confining potential (for an ensemble of dots we assume, as corroborated by the intra-band experiments, that the anisotropy directions are the same for the different dots [3]).

We report initially on calculations of the exchange couplings for an electron-hole pair confined in self-assembled quantum wells. We obtain different energy couplings for the different pairs of electron-hole states. For instance, we obtain that the splitting associated to the ground transition (electron and the hole in their respective ground levels) is generally much smaller (by roughly an order of magnitude) than the one related to an excited pair state involving an excited electron (and/or hole) level. This means in particular that the existence of a preferential orientation for the polarization of the dot luminescence is not very robust but rather sensitive to any additional external perturbation which breaks the cylindrical symmetry of the dot.

We propose correspondingly a mechanism for the polarization relaxation of an electron-hole pair confined in the dot. It is based on a "motional" inhibition of the geometry-induced coupling of the /±1> states, induced by a statistical fluctuation of the dot environment. The physical picture is as follows. For a given dot occupied by a single electron-hole pair the (long-range) exchange coupling mix the twofold degenerate circularly polarized /±1> bright levels and leads to the formation of the new radiative Px and Py states. The polarization axes are imposed by the geometry of the dot confining potential. However, it is well known that, very often, the dot environment is far from being perfect but presents defect levels that act as traps for the electrons and holes. After illumination, electrons and holes are captured by the dots but also by these trap levels. The occupancy of the shallow levels will evolve in time (for instance, they can be populated from the wetting-layer and subsequently thermally depopulated) in the scale of the radiative lifetime of the pair confined in the dot. A trap level populated by, say, an electron, should add (via the electrostatic interaction) an anisotropic contribution to the potential felt by the bound pair and thus affect their exchange coupling. Because of the random nature of the spatial localization of the defects and of their populations, on the average there would be no net principal axis along which a Px and Py polarizations could be defined. This finally leads to : (i) a suppression of the coherent (as due to an anisotropic static) exchange coupling between the /±1> states and (ii) an irreversible evolution (a relaxation) for the circular polarization. This mechanism recalls the "motional narrowing" one for mobile carriers and excitons in disordered bulk and quantum well samples. Here, however, the electron/hole pair is strongly confined in the dot and it is the environment that fluctuates in a random way nearby the dot.

We propose a model to describe this statistical evolution and evaluate the corresponding depolarization relaxation rate for the ground dot radiative transition. We show in particular that the depolarization rate decreases with increasing mean potential fluctuation due to the charging and decharging of the defect levels around the dot.

References

[1]. M. Bayer *et al*, Phys. Rev. Lett 82, 1748 (1999)
[2] D. Gammon *et al*, Phys. Rev. Lett 76, 3005 (1996)
[3] S. Hameau *et al*, Phys. Rev. Lett 83, 4152 (1999)
[4] M. Paillard et al, Phys. Rev. Lett. (to appear)
[5] S. V. Gupalov *et al*, JETP Lett 86, 388 (1998)
[6] D. Larousserie *et al*, Phys. Rev. B60, 1892 (1999)
[7] T. Takagahara, Phys. Rev. B62, 16840 (2000)

Corresponding author: R. Ferreira, Laboratoire de Physique de la Matière Condensée ENS
24 rue Lhomond F75005 Paris (France)
phone: +33 1 44323373, Fax: +33 1 44323840
email: Robson.Ferreira@lpmc.ens.fr

Spatial and dynamic effects on the capacitance of self-organized semiconductor quantum dot structures

R. Wetzler[1], A. Rack[1], A. Wacker[1], E. Schöll [1],C.M.A. Kapteyn [2], R. Heitz [2],D. Bimberg [2],

[1] Institut für Theoretische Physik, Technische Universität Berlin, Hardenbergstraße 36, D-10623 Berlin, Germany
[2] Institut für Festkörperphysik, Technische Universität Berlin, Hardenbergstraße 36, D-10623 Berlin, Germany

From low-frequency capacitance spectroscopy of quantum dots (QDs) embedded in a *pn* structure the energy levels of the QDs and their inhomogeneous broadening can be obtained [1]. To this end capacitance-voltage (C-V) characteristics, obtained by solving self-consistently the non-linear one-dimensional Poisson equation and current equations, are fitted to experimental data. Information about the states originating from the wetting layer, the influence of impurities in the vicinity of the dots and other growth dependent effects can also be achieved. We apply this method to various InAs and SiGe QD structures to characterise both electon and hole states. It turns out that fully three-dimensional calculations are necessary to simulate realistic QDs correctly.

The limitation of the simple one-dimensional approach is that the self-consistent electric potential varies only in the growth direction. Because QD electrons are confined in all three directions, the spatial charge distribution in a QD array depends on the lateral position, and therefore the lateral potential distribution is not invariant. This effect is particularly pronounced if the Debye length in the structure (typically 100nm) is comparable to the distance between the QDs, so that screening may vanish.

In contrast to a quantum well, electrons captured in QDs cannot easily rearrange themselves to form a laterally homogeneous charge distribution. Electrons, once captured into the QDs, have to overcome large barriers. Since carrier capture is a random process [2], the charge stored in the QDs varies spatially, and leads to a potential distribution which strongly depends on the coordinates perpendicular to growth direction.

In this work we solve the three-dimensional Poisson equation to determine the electrochemical potential in the QDs. The statistics of an ensemble of inhomogeneously charged quantum dots is compared with one-dimensional calculations. We map the size distribution of QDs on the QD energy level distribution, making use of the QD size versus energy relation for single dots as determined in Ref. [3]. We find that the average energy level of an esemble of QDs determined by a full three dimensional simulation differs from the energies obtained by a one-dimensional calculation.

For higher measurement frequencies (typically 1 MHz), there are deviations between experiment and theory which must be accounted for by a fully dynamic simulation incorporating the capture of carriers from the bulk through the wetting layer and the generation-recombination kinetics of the quatum dots.

An example shows the need for a three dimensional calculation. We simulated an array of 25 spherical shaped QDs with a sheet density of $10^{14}m^{-2}$ and a diameter of 20 nm. We assume that these dots have two localized states at 200 meV and 100 meV below the conduction band of the GaAs matrix. The QDs can be populated in two ways. In case A the dots were filled statistically with up to 8 electrons per dot. In case B the lowest lying states were occupied sequentially with electrons. In Fig. 1 the mean energy is plotted versus the mean occupation. One can observe that if less than every second dot is filled, Coulomb charging plays a minor role, and the potential is the sum of Coulomb potentials of single electrons. As the occupation rises, the energy rises linearly with occupation, and the potential becomes similar to a potential as we know, e.g., from a quantum well.

In Fig. 2 we plotted the energy distribiution for the average occupation n=0, 3, 6. One observes that Coulomb charging leads to a broadening of the energy levels in both cases. This shows that theoretical calculations have to account for the three-dimensional nature of QDs for, e.g.. a detailed analysis of C-V measurements on QDs.

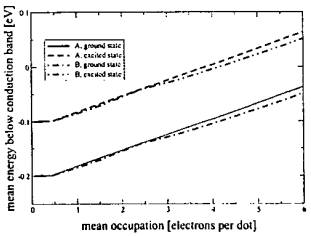

Figure 1: The mean energy of the QD levels as a function of the mean occupation for case A and B (see text)

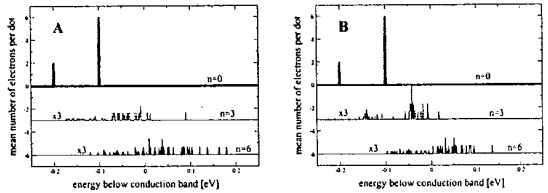

Figure 2: Energy distribution for different average occupation n for case A and B (see text). Curves for n=3, 9 are offset by 3 and 6 and vertically rescaled.

References

[1] R. Wetzler, A. Wacker, E. Schöll, C.M.A. Kapteyn, R. Heitz, and D. Bimberg, Appl. Phys. Lett. **77**, 1671-1673 (2000).
[2] M. Grundmann, and D. Bimberg, Phys. Rev. B **55**, 9740-9745 (1997).
[3] O. Stier, M. Grundmann, and D. Bimberg, Phys. Rev. B **59**, 5688 (1999).

Corresponding author: Reinhard Wetzler, Institut für Theoretische Physik, Technische Universität Berlin, Hardenbergstraße 36, D-10623 Berlin, Germany.
phone: +49 314 27658, Fax: +49 314 21130,
email: wetzler@physik.tu-berlin.de

Polarization of the interband optical dipole in InAs/GaAs self-organized quantum dots

S. Cortez[1], O. Krebs[1], P. Voisin[1], J-M. Gérard[2]

[1]Laboratoire de Physique de la Matière Condensée de l'Ecole Normale Supérieure, 24 rue Lhomond, 75005 Paris, France

[2]Laboratoire de Photonique et Nanostructures, 196 Av. H. Ravera, 92220 Bagneux, France

Self-assembled InAs quantum dots (QD's) have been extensively studied this last decade, in particular by using photoluminescence (PL) and photoluminescence excitation (PLE) in order to determine their electronic structure. Although quantum dots are often referred to as artificial atoms, their lens shape symmetry is characterized by a much stronger confinement in the [001] growth direction than in the layer plane, yielding highly anisotropic optical transitions. Formally, if the symmetry of the dots is perfectly cylindrical, the electronic states are characterized by their momentum quantum numbers J^2, and J_z. Experimentally, one can distinguish between the heavy-hole ($Jz = \pm 3/2$) to conduction state transitions and the light-hole ($Jz = \pm 1/2$) to conduction state transitions, by studying their optical properties with light propagating in the plane and polarized along [110] (or transverse electric (TE) mode) and [001] (or. transverse magnetic (TM) mode). The "heavy-hole" transitions are forbidden in TM mode and the "light-hole" transitions are expected to be four times larger in TM mode than in TE mode. Although many authors have measured in-plane anisotropy of quantum dots [1], these guided wave polarization properties have not been carefully analyzed, and their study remains a challenge due to the complex interpretation of usual spectroscopic methods. Conversely, when light propagates along the growth axis, all observed transitions should be isotropic with respect to the in-plane polarization direction. Deviations from these simple selection rules evidence a symmetry reduction, due to interfaces and/or shape anisotropy, that mainly results in valence band mixings which are crucial for the understanding of QD emission properties [2] as well as of the spin dynamics.

In order to analyze these properties, we report on the study of a InAs/GaAs self-organized QD sample containing 40 QD layers by measuring for the first time to our knowledge, the optical transmission in a guided-wave configuration. The latter method offers several advantages over indirect techniques like PL, PLE and photocurrent, especially for the observation of the excited states. Thanks to the low excitation density, no thermalization mechanisms affect the absorption properties, and in contrast to the photocurrent measurements no spurious effects associated to the complex tunneling process limit the analysis [3]. On the other side, absorption measurements with light propagating along the growth axis can only be achieved using bleaching modulation techniques because of the weak absorption ($<2.10^{-4}$) of each QD layer. A 20 µm thick, 6-mm long multimode planar waveguide was obtained by mechanical polishing of the substrate. Two broad absorption regions appear around 1230meV and 1300meV for the TE and TM polarizations respectively, while the onset of the wetting layer is situated at 1380 meV. The relative oscillator strength and polarization of four interband optical transitions have been determined within an estimated accuracy of 10%. Figure 1 shows the absorption of TE and TM modes, with a gaussian fit of optical transitions labeled Ti (i =1,...,4) assuming a common inhomogeneous linewidth of 45 meV (FWHM). The low energy TE absorption region is composed of two heavy hole-like transitions (T1 and T2), that involve the same conduction band level. This interpretation is supported by the PL power dependence that shows a shoulder developing when the excitation power is increased. The TM spectrum shown in Fig. 1(b) presents mainly a broad absorption region up to the wetting layer gap. It clearly involves a light hole-like transition T3 that gives rise to a strong TM absorption and a weak TE absorption. The TE and TM absorption spectra show also a high energy peak T4 that can possibly be attributed to a single transition characterized by a strong heavy-light hole mixing. We discuss in more details these results completed by a polarization analysis of the photoluminescence emitted along the growth axis and in the layer plane. In conclusion, we show that the first valence states in these flat, lens shaped, self-assembled dots are "nearly pure" heavy or light hole states, as expected from their dominant two-dimensional character.

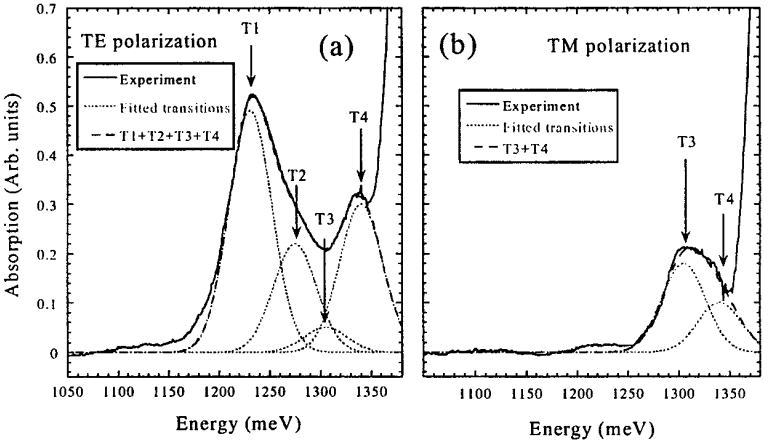

Fig. 1 Room temperature polarization resolved absorption spectra obtained by transmission measurement through a 6 mm-long, 20 µm-thick multimode waveguide containing 40 planes of InAs quantum dots. The T1, T2 fitted transitions involve "nearly pure" heavy holes, while T3 corresponds to a light hole transition with an oscillator strength four times smaller in TE than TM.

References

[1] Lin-Wang Wang, J. Kim and A. Zunger, Phys. Rev. B **59**, 5678 (1999)
[3] J-M. Gérard et al, Phys. Rev. Lett. **81**, 1110 (1998)
[2] Ivan V. Ignatiev, et al., Phys. Rev. B **61**, 15633 (2000)

Corresponding author: Krebs Olivier, LPMC-ENS, 24 rue Lhomond
75005 Paris , France
phone: +33 1 44 32 33 81, Fax: +33 1 44 32 38 40
e-mail: Olivier.Krebs@lpmc.ens.fr

Photoconductive spectra in InAs/InAlAs/InP quantum dot structures

S.E. Schacham[2], G. Bahir[1], E. Finkman[1], W. Sheng[3] and J.P. Leburton[3]
[1]Dept. of Electrical Engineering, Technion, Haifa, Israel 32000
[2]Dept. of Electrical and Electronic Engineering, College of Judea and Samaria, Ariel, Israel 44837
[3]Dept. of Electrical and Computer Engineering and Beckman Institute for Advanced Science and Technology, University of Illinois at Urbana-Champaign, Urbana, Illinois 61801

Photoconductive spectra of InAs quantum dots embedded in InAlAs barrier lattice matched to InP substrate show several peaks in the range of 100-400 meV [1]. These peaks are partly polarized and depend on illumination configuration. These results are in drastic contrast to absorption measurements, which show a single polarized peak around 100 meV.

The electrons in the quantum dots are confined due to conduction band discontinuity between the InAs and InAlAs. The InAlAs layer is lattice matched to the InP substrate, i.e. with 52 % In. InAs is a narrow bandgap material, with E_g = 0.413 eV at T=77 K, while the bandgap of the InAlAs barrier is 1.456 eV. The conduction band offset is 0.80 eV without strain. Taking into account the strain between the two materials results in an effective conduction band offset of 0.61 eV.

The confined energy levels in the dot, and the allowed transitions were calculated using a 8-band strain dependent **k.p** Hamiltonian to account for the electron-hole state mixing in the conduction band. The calculations are based on an InAs dot in a shape of ellipsoid. The dimensions of the dot are taken as 50 nm long, defined as the y direction, 30 nm wide, in the x direction, and 2 nm high, in the z direction. The ground state is found to be at 253 meV above the conduction band edge in the dot, so that the barrier height is up to 357 meV. There are hundreds of confined energy levels, the separation between levels is 12 meV or less. Still, the number of allowed transitions is limited. We assume that the three bottom-most levels are occupied. Figure 1 shows the oscillator strength for the three polarizations in a logarithmic scale. In the range of 100-270 meV there are some four peaks. In the x polarization there is a dominant peak at 100 meV. This is the only peak observed in absorption measurements, there, too, it is polarized purely in the x direction. One can see a large number of peaks at around 170 meV and a broader peak around 260 meV. The peak at 260 meV is present in all polarizations, mainly in the Z polarization. This is the first transition between the $n_z = 0$ and the $n_z = 1$ quantum numbers. Since the excited level is less than 100 meV below the barrier, it is likely that this transition is very pronounced in PC measurements. All these peaks are present in the experimental data, as shown in Fig. 2.

The simulation is performed under flat band conditions, while the presence of space charge due to ionized donors in the barrier definitely cause band bending and may increase the tunneling probability out of the dot. Also diffusion of AlAs into the QD would lower the barrier. Fluctuations in dot dimensions produce energy shifts and results in wider peaks. The multi-peak shape of the spectrum in Fig. 2b is attributed to fluctuations in the Z dimension.

References

[1] E. Finkman, S. Maimon, V. Immer, G. Bahir, S. E. Schacham, F. Fossard, F. H. Julien, J. Brault and M. Gendry, "Polarized front-illumination response in intraband quantum dot infrared photodetectors at 77 K", Phys. Rev. **B 63**, 045323 (2001).

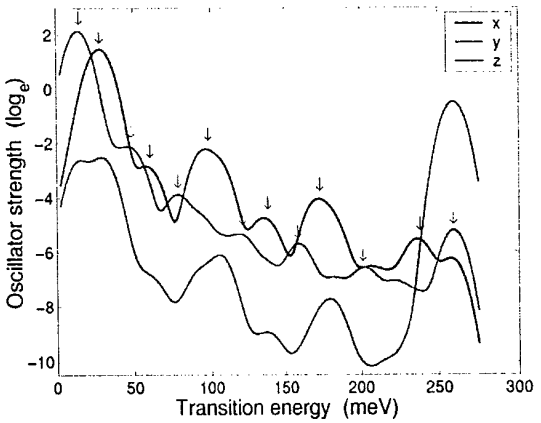

Fig. 1: Calculated oscillator strengths for the InAs/InAlAs dots.

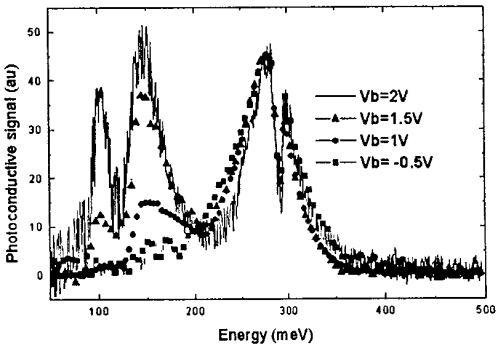

Fig. 2: Measured photoconductive spectra for the InAs/InAlAs dots, T=77K, wedge illumination, x+z polarization.

Corresponding author: S.E. Schacham, Department of Electrical Engineering, The Technion, Haifa 32000, Israel,
Phone: 972 4 829 4642, Fax: 972 4 832 3041,
e-mail: schacham@ee.technion.ac.il

Manipulating single quantum dot states in a lateral electric field

J. Seufert[1], M. Obert[1], M. Rambach[1], G. Bacher[1], N. A. Gippius[2], A. Forchel[1], T. Passow[3], K. Leonardi[3], and D. Hommel[3]

[1]Technische Physik, Universität Würzburg, Am Hubland, 97074 Würzburg, Germany
[2]General Physics Institute, Russian Academy of Sciences, 117942 Moscow, Russia
[3]Institut für Festkörperphysik, Universität Bremen, 28359 Bremen, Germany

Manipulating the eigenstates in single semiconductor quantum dots (SQDs) is on one hand required for visionary device prospects based on the control of single particles [1] and, on the other hand, will give access to both the spin and the charge distribution of carriers in SQDs. For example, the spin part of the zero-dimensional excitonic wavefunction can be tuned in an external magnetic field [2], whereas the orbital part is sensitive to electrical fields due to the charges of electron and hole.

Here we present a new experimental approach towards the goal to expose a self-assembled CdSe/ZnSe SQD to a well-defined lateral electric field. We use a micrometer-scale capacitor geometry, i. e. the SQD of interest is placed between two electrodes located in the same plane. This allows a direct correlation between applied voltage and lateral electric field in the SQD and therefore a quantitative extraction of the permanent dipole moment and the polarizability of a single electron-hole pair, in contrast to earlier approaches [3, 4].

The sample consists of a 50 nm ZnSe buffer layer, 2.5 ML CdSe, deposited by migration enhanced epitaxy, and a 25 nm thick ZnSe capping layer, all grown on a GaAs substrate. To provide experimental access to single quantum dots, we used nanomesas with lateral extensions down to 40 x 40 nm^2 which were defined by electron-beam lithography and wet chemical etching. In a subsequent lithography step pairs of parallel gold pads with distances ranging from 2 to 8 μm were defined on top of the sample, such that the etched mesas are centered in the channel between the pads (see Fig. 1). The sample was mounted on the cold finger of a He-cryostat and kept at a temperature of T=2K. Photoluminescence (PL) spectroscopy on SQDs was carried out using an Argon-ion laser operating at λ=350...364 nm for excitation. The PL-emission was dispersed by a 0.32 m double monochromator system, and detected using a nitrogen cooled charged coupled device camera. The experimental setup provides a spectral resolution of 100 μeV.

The inset of Fig. 2 shows the PL-spectrum of a SQD from a 200 nm mesa structure placed in the center of a 2 μm channel capacitor. The ultranarrow emission line reflects the three-dimensional confinement of the corresponding exciton in the SQD under investigation. The behavior of this line was monitored as a function of the applied voltage between the adjacent electrodes giving rise to a lateral electric field. A pronounced redshift of the luminescence energy due to the Quantum Confined Stark effect is observed which amounts to about 1 meV for an applied electrical field of 15 kV/cm. The reduction of the emission intensity observed can be explained by a field-induced spatial separation of the electron- and the hole-wavefunction in the SQD and/or a decrease of the carrier capture efficiency into the SQD, as the excitation energy was above the energy of the ZnSe barrier bandgap.

Most interesting, however, is the fact, that the Stark shift depends purely quadratic on the electric field, which can be explained in terms of an induced dipole formation within the dot. Within our experimental resolution, no indication for a permanent dipole moment in lateral direction is found. From the analysis of the redshift we extract the single exciton polarization to be $4.9 \cdot 10^{-3}$ meVcmkV^{-1}. The experimental results fit quite well to calculations of the ground state polarizability of a zero-dimensional exciton, assuming a cylindrical shape of the SQD according to what is obtained in TEM measurements.

The manipulation of the zero-dimensional excitonic wavefunction is most prominently reflected in the angular distribution of the emission : for increasing electric field the single dot luminescence becomes increasingly polarized perpendicular to the applied field.

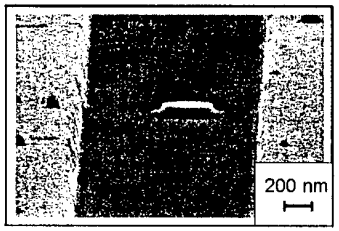

Fig. 1: Scanning electron micrograph of a mesa structure centered in the gap between two electrodes.

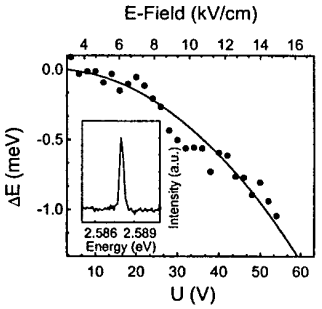

Fig. 2: Energy shift of a SQD transition in an electric field; Inset: PL-Spectrum of the SQD

References

[1] D. Loss and D. DiVincenzo, Phys. Rev A **57**, 120 (1998)
[2] V. D. Kulakovskii, G. Bacher, R. Weigand, T. Kümmell, A. Forchel, E. Borovitskaya, K. Leonardi, and D. Hommel, Phys. Rev. Lett. **82**, 1780 (1999)
[3] W. Heller, U. Bockelmann, and G. Abstreiter, Phys. Rev. B **57**, 6270 (1998)
[4] H. Gotoh, H. Kamada, H. Ando, and J. Temmyo, Appl. Phys. Lett **76**, 867 (2000)

Corresponding author: Jochen Seufert, Technische Physik, Universtät Würzburg, Am Hubland, D-97074 Würzburg, Germany,
phone: +49-931-888-5116, fax: +49-931-888-5143,
email: jnseufer@cip.physik.uni-wuerzburg.de

Photoluminescence linewidth narrowing of InAs/GaAs self-assembled quantum dots

S. Kiravittaya, Y. Nakamura, and O. G. Schmidt
Max-Planck-Institut für Festkörperforschung, Heisenbergstrasse 1, 70569 Stuttgart, Germany

In order to achieve high uniformity in quantum dots (QDs) size and shape, special growth techniques are required. In this work, we report the narrowing of photoluminescence (PL) linewidth of InAs/GaAs self-assembled QDs by introducing a growth interruption (GI) after the deposition of QDs layer. We attribute the linewidth narrowing to the improvement of the uniformity of QDs during the GI.

The samples, which are single InAs QD layer embedded in GaAs, were grown by molecular beam epitaxy at 500°C using low indium deposition rate (0.010 ML/s). A GI after and in-between deposition of InAs was applied. After capping the QD layer with GaAs, a second QDs layer was grown on the surface with the same growth conditions for characterization by atomic force microscope (AFM). The PL measurement was performed at room temperature.

The 2×2 μm^2 AFM images of the samples with different GIs are shown in Fig. 1. In Fig. 1(a) and (b), the sample is grown without GI and 30s GI, respectively. The disappearance of small dots and the increase in dot diameter are clearly observed when a 30s GI is introduced. The phenomenon can be explained by the desorption and diffusion of the small unstable dots at the first stage. After no small dots are left over on the surface, indium atoms in large dots begin to desorb, resulting in a non-uniform size distribution again (see Fig. 1(c)). The PL spectra of the corresponding samples in Fig. 1 are shown in Fig. 2. The narrowest PL linewidth (32 meV) is observed for the sample with 30s GI compared to the sample without GI (38 meV). The PL result corresponds well with the AFM images. The full width at half maximum (FWHM) dependence of the GI (t_{int}) is summarized in the inset of Fig. 2. It shows a pronounced minimum of the FWHM at GI a time between 15 and 30s. Due to the diffusion and desorption of indium atoms, the PL peak energies of both QDs and wetting layer (WL) are explicitly changed when the GI is varied as shown in Fig. 3. From this result, we believe that the origin of the narrowing of the PL linewidth comes from the improvement of the uniformity of the QDs.

A PL spectrum and an AFM image of a sample, which was overgrown with InAs, is shown in Fig. 4. After deposition of 1.8 ML InAs, 0.06 ML InAs is desobed and again regrown. It is noticeable that the FWHM stays narrower (31 meV) than the FWHM of the original 1.8 ML InAs. We therefore suggest to use a repetitive growth and desorption procedure to approach a thermodynamically homogeneous and stable QD ensemble.

Corresponding author: Suwit Kiravittaya, Max-Planck-Institut für Festkörperforschung,
Heisenbergstrasse 1, 70569 Stuttgart, Germany,
phone: +49 711 689 1315; fax: +49 711 689 1010,
email: kira@servix.mpi-stuttgart.mpg.de

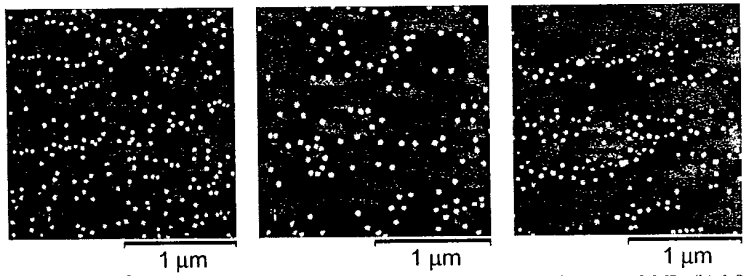

Fig. 1. 2×2 μm^2 AFM images of InAs QDs on GaAs. Indium deposition: (a) 1.8 ML, (b) 1.8 ML/30s GI, (c) 1.8 ML/240s GI.

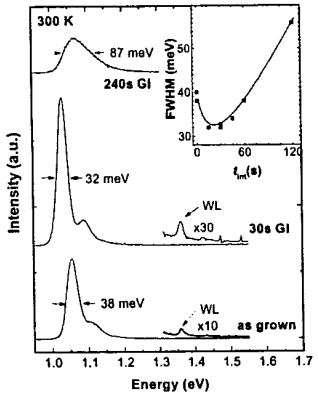

Fig. 2. Room temperature PL of InAs/GaAs QDs for as grown, 30s, 240s GI. The FWHM of the spectra with different GI time (t_{int}) is shown in the inset.

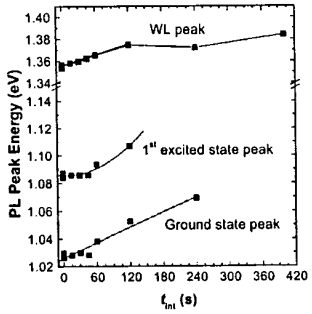

Fig. 3. PL peak energy dependence on GI time.

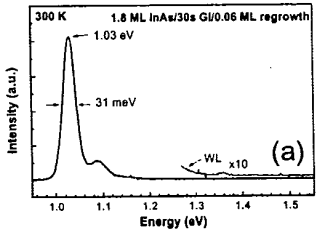

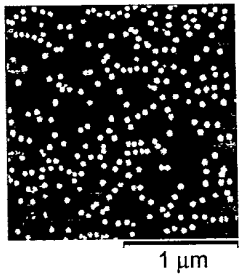

Fig. 4. PL spectrum (a) and AFM image (b) of the 30s GI/0.06 ML regrowth sample.

Polarization anisotropy of photoluminescence from multilayer InAs/GaAs quantum dots

J. Humlíček[1], D. Munzar[1], K. Navrátil[1], M. Lorenc[1], J. Oswald[2], J. Pangrác[2], E. Hulicius[2]

[1]Institute of Condensed Matter Physics, Masaryk University Brno, Kotlářská 2, CZ-61137 Brno, Czech Republic
[2]Institute of Physics, Academy of Sciences of the Czech Republic, Cukrovarnická 10 CZ-162 53 Praha

Self-assembled In(Ga)As/GaAs quantum dots (QD's) exhibit very efficient luminescence related to their zero-dimensional nature [1,2]. Polarization properties of the emitted light have not been investigated very frequently; reported results include cathodoluminescence [3], photoluminescence (PL) [4,5], and photoluminescence excitation [4] techniques.

In this work, we report results of PL experiments on multilayer InAs/GaAs QD structures grown by metal organic vapor phase epitaxy (MOVPE). The growth conditions have been optimized for maximum PL efficiency as described elsewhere [6]. In particular, the thickness of the GaAs spacer between consecutive InAs layers has been found to be a critical parameter [6]. The typical height of these QD's ranges from about 3 to 6 nm depending on the sample, the in-plane dimensions are larger, typically a few tens nm.

We have obtained the most intense PL from a triple InAs/GaAs structure with the density of InAs QD's of about 25 μm^{-2}. The room-temperature PL band is located at 0.93 eV, its full width at half maximum is about 35 meV. Using the excitation with the near-infrared wavelength of 1.06 μm, the PL signal remains easily detectable for temperatures above 400 K. Another optimized sample of 7-times repeated InAs/GaAs structure exhibited slightly smaller dot density and larger dispersion of their sizes (i.e., broader PL bands).

All of the studied samples were grown on (001) oriented GaAs substrates. Atomic force microscopy reveals elongated bases of the QD's. We have observed pronounced anisotropy of the PL signal using different linear polarization of the exciting light (related to the azimuth of polarizer, P), and polarization-sensitive detection (defined by the azimuth of analyzer, A). The PL signal measured with P along (110) and (1$\bar{1}$0) cleavage directions (i.e., with the usual configuration of the laser beam parallel to the growth direction) has been found to be polarized. The relative PL intensity with A oriented along (110) and (1$\bar{1}$0) varied across the sample surface; an example of the results is shown in Fig. 1. We have taken a slight polarization sensitivity of our detection system into account. We discuss the relation of this preferential polarization to the elongated shapes of the QD's.

The high luminescent efficiency allowed us to use the excitation directed to the edges of the samples and detect the PL signal emitted from them. The electric vector of the laser light illuminating the cleavage edges has been polarized along either (110) or (001) directions, and the emitted light has been detected with different settings of A. Typical results are shown in Fig. 2. The polarization plane defined by the azimuth A=0 is parallel to (001), which is the direction of the most severe confinement of excited states in the QD's. We discuss the observed anisotropy in terms of the underlying electronic structure, in particular, the mixing of heavy and light hole states.

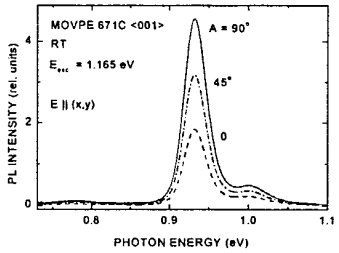

Fig. 1: PL spectra of InAs/GaAs QD's at room temperature, excited and detected along (001) direction.

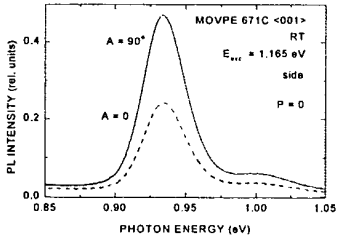

Fig. 2: PL spectra of InAs/GaAs QD's at room temperature, excited and detected perpendicularly to the (001) direction.

Our results demonstrate the possibility of growing dense quantum dot structures by MOVPE, with fairly narrow size distribution and the emission in a favorable spectral range. Moreover, resulting shapes of the dots lead to well defined polarization properties of the luminescent light.

References

[1] D. Bimberg, M. Grundmann, and N. N. Ledentsov, *Quantum Dot Heterostructures* (Wiley, Chichester, 1999).
[2] *Self-Assembled InGaAs/GaAs Quantum Dots*, ed.: M. Sugawara, in Semiconductors and Semimetals Vol. **60** (Academic Press, 1999).
[3] Y. Tang, D. H. Rich, I. Mukhametzhanov, P. Chen, and A. Madhukar, J. Appl. Phys. **84**, 3342 (1998).
[4] S. Noda, T. Abe, and M. Tamura, Phys. Rev. B **58**, 7181 (1998).
[5] P. Yu, W. Langbein, K. Leosson, J.M. Hvam, N. N. Ledentsov, D. Bimberg, V. M. Ustinov, A. Yu. Egorov, A. E. Zhukov, A. F. Tsatsul'nikov, and Yu. G. Musikhin, Phys. Rev. B **60**, 16680 (1999).
[6] J. Pangrác, J. Oswald, E. Hulicius, K. Melichar, V. Vorlíček, I. Drbohlav, T. Šimeček, Thin Solid Films **380,** 101 (2000).

Corresponding author: Dominik Munzar, Institute of Condensed Matter Physics, Masaryk University Brno, Kotlářská 2, CZ-61137 Brno, Czech Republic
phone: +420 5 41129 448, Fax: +420 5 41211 214
email: munzar@physics.muni.cz

Tuned exciton kinetics in self-organized InGaAs/GaAs quantum dots

H. Born, R. Heitz, A. Hoffmann, D. Bimberg

Institut für Festkörperphysik, Technische Universität Berlin, Hardenbergstraße 36, D-10623 Berlin, Germany

Within the last decade quantum dots (QDs) attracted continuously increasing interest due to their unique optical properties. The defect-free and coherent nature of self-organized QDs suppresses the interaction with surface and defect states otherwise often dominating the intrinsic zero-dimensional properties. [1] Nevertheless, in self-organized structures relaxation and recombination processes are a still controversial. The dynamics of carriers/excitons is of basic physical and technological interest as emphasized, e.g. by the recent development of GaAs-based lasers for telecommunications operating at 1.3μm. [2] The desired high-speed operation demands insight into and tuning of the carrier/exciton dynamics in these QDs.

QDs formed in the In(Ga)As/GaAs system provide strong quantum confinement, i.e. the size of the QDs (typically 20 nm base by 5 to 20 nm height) is sufficiently small for confinement energies to exceed Coulomb energies. For such QD structures a variety of time-resolved photoluminescence (PL) measurements are reported. [3,4] The observed variation of the decay times ranging from some hundred ps up to several ns are not yet understood. Up to now, quantitative descriptions of the dynamics are limited to idealized dots, assuming a complete overlap of the electron and hole wave functions within the structure. [5] The exciton life time is expected to scale reciprocal to the QD volume $V/(\pi a_B^3)$. The effect of the asymmetry of electron and hole wave functions in low-symmetry, strained QDs and, thus, the structural properties, is not understood yet.

In this paper we present resonantly excited TRPL experiments on a series of annealed, self-organized InGaAs/GaAs QDs providing systematically changing structural properties. The investigated samples were derived from a single sample by ex-situ annealing as described in detail in Ref. [6]. The original ('as-grown') dots were fabricated by MOCVD on a GaAs (001) substrate depositing five monolayers of $In_{0.5}Ga_{0.5}As$ and capping them with GaAs at 485 °C. Transmission electron microscope images revealed ~10^9 QDs/cm^2 with an average base length and height of 14-19 nm and 6-8 nm, respectively. Different parts of the sample were annealed at 580, 610, 640, and 700 °C. The sharp potential steps especially in the growth direction are smoothed by the thermal treatment and the localization decreases for electron and hole. In conclusion an increasing penetration of the barrier by the carrier wave functions, scaling with the reciprocal effective masses, is expected. (see insets in Fig. 1 (b))

PL and PL excitation (PLE) spectra reveal ground (I0) and excited state transitions (I1, I2). Contrary to common expectation suppressed relaxation and hot exciton luminescence are observed as published in [4]. The time constants shown in Fig. 1 (a) were derived from transients excited resonantly in I1 while detecting at I0 and I1, respectively. We find decay of I1 to mirror the rise of I0 in all samples indicating an excitonic relaxation. The observed lifetime of I0 rises with annealing and is followed by that of I1 for samples annealed at temperatures lower than 640 °C. At higher annealing temperatures the decay of I1 accelerates becoming finally twice as fast as that of I0. Interestingly, the radiative lifetime increases with an increasing effective QD size, whereas commonly the opposite trend is expected. The bright exciton lifetime in the strong confinement limit it is proportional to $1/(E\ P_{cv}^2\ I)$ [5] where E is the transition energy, P_{cv} the optical interband matrix element representing the Bloch-functions and I the overlap integral of electron and hole envelope functions. As shown in Fig. 1 (b) the product $A \sim (P_{cv}^2\ I)$ drastically decreases upon annealing. The decrease in electron and hole overlap with annealing allows to tune the exciton dynamics in the self-organized QDs.

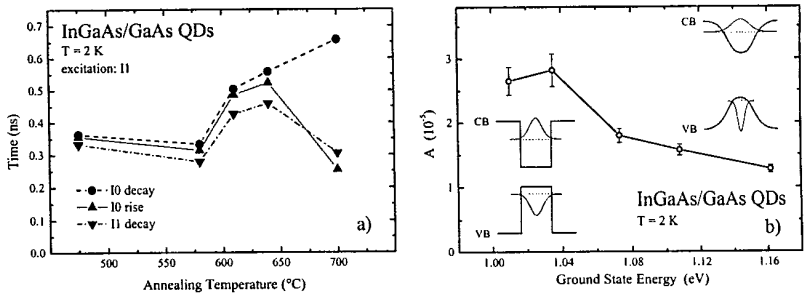

Fig. 1: a) Time constants derived from transients taken at I1 and I0 while exciting resonant to I1.
b) Scaled product $A \sim (P_{cv}^2\ I)$ derived from the life time of I0 and corrected for transition energy.

In conclusion, a significant influence of the electron-hole overlap integral on the exciton dynamics in self-organized InGaAs/GaAs QDs was demonstrated. Ex-situ annealing slows down radiative recombination and accelerates relaxation in qualitative agreement with the expected change of the electron-hole overlap caused by In/Ga interdiffusion. The results unambiguously evidence the effect of the complex confining potential of strained self-organized QDs on the exciton dynamics, pointing out possible pathways to optimize such QDs for device applications.

References

[1] D. Bimberg, M. Grundmann, and N. N. Ledentsov, *Quantum Dot Heterostructures*, J. Wiley & Sons, London 1999

[2] M.V. Maximov et al., Microelectronic Engineering **51-52**, 61 (2000) / G.T. Liu et al., Proc. of the SPIE **3944**, 814 (2000)

[3] G. Wang et al., Appl. Phys. Lett. **64**, 2815 (1994) / M. Paillard et al., phys. stat. sol. (a) **178**, 349 (2000) / B. Ohnesorge et al., Phys. Rev. B **54**, 11532 (1996). / R. Heitz et al., Appl. Phys. Lett. **77**, 3746 (2000)

[4] R. Heitz et al., phys. stat. sol. (b) **221**, 65 (2000)

[5] D. S. Citrin, Superlattices Microstruct. **13**, 303 (1993) / M. Sugawara, Phys. Rev. B **51**, 10743 (1995)

[6] F. Heinrichsdorff et al., J. Cryst. Growth **195**, 540 (1998)

Corresponding author: Harald Born, Institut für Festkörperhysik, Technische Universität Berlin, Hardenbergstraße 36, D-10623 Berlin, Germany.
phone: +49 30 314 22083, Fax: +49 30 314 22064
email: harald@physik.tu-berlin.de

Electronic Properties of InAs/GaAs quantum dot stacks

A. Schliwa [1], O. Stier, R. Heitz, M. Grundmann, D. Bimberg

Institut für Festkörperphysik, Technische Universität Berlin,
Sekr. PN 5-2, Hardenbergstraße 36, D-10623 Berlin, Germany

Vertical alignment of self-organized Stranski-Krastanow islands by stacking is one of the most promising approaches to control the electronic properties of such quantum dots (QDs) [1, 2, 3]. Stacking of QDs leads to an experimentally observed low energy shift [3]. which cannot be understood only in terms of electronic coupling: It is necessary to consider also the strainfield interaction in this context. Fluctuations in the growingprocess prevent the formation of structurally identical QDs, and the question arises how this affects the coupling behaviour of electron and hole states. Early works on idealized QDs [4] adressed the influence of interdot tunneling, lateral confinement, and intradot correlation on the charge transfer. Other previous studies concerning the coupling of electrons in vertical pairs of pyramid shaped QDs [5] gave first insight into the characteristic inhomogeneous strain distribution and the, generally, non-resonant electronic coupling.

We investigate the electronic and optical properties of both pairs and triple stacks of both identical or nonidentical QDs dependent on the spacer thickness and the shape in the framework of eight-band $\mathbf{k}\cdot\mathbf{p}$ theory following our previous work [6, 7, 8]. Even in stacks of nominally identical QDs, the inhomogeneous strain distribution affects the individual QDs in a very different manner, rendering them electronically inequivalent. We concentrate on a detailed analysis of the various strain contributions (hydrostatic- and shear strains) in order to trace back the evolution of electron states and understand the complex behaviour of hole states. The QDs are assumed to be full or truncated InAs pyramids with {101} facets, separated by spacer layers of varying thickness.

The figure shows the probability densities and energies of electron and hole states in stacks of two (left) and three (right) geometrically identical InAs pyramids dependent on the dot separation. Electrons show coupling in the whole investigated spacer thickness range, with the groundstate located predominantly in the upper QD, whereas the hole groundstate shows no coupling at all and always occupies first grown QD. This reflects the asymmetry of the coupled strain field and suggests a spatially indirect exciton groundstate with small oscillator strength. Additionally, the energy levels are modified when considering stacks of unequally large QDs. The general preconditions for electronic coupling are discussed with emphasis on the intricate effects of strain interaction.

References

[1] S. Solomon, J. A. Trezza, A. F. Marshall, J. S. Harris Phys. Rev. Lett. **76**, 952 (1996).
[2] N. N. Ledentsov et al. Phys. Rev. B **54**, 8743 (1996).
[3] R. Heitz, A. Kalburge, Q. Xie, M. Grundmann, P. Chen, A. Hoffmann, A. Madhukar, D. Bimberg, Phys. Rev. B **57**, 9050 (1998).
[4] G. W. Bryant, Phys. Rev. B **48**, 8024 (1993).
[5] L. R. C. Fonseca, J. L. Jimenez, J. P. Leburton Phys. Rev. B **58**, 9955 (1998).
[6] O. Stier, M. Grundmann, D. Bimberg, Phys. Rev. B **59**, 5688 (1999).
[7] A. Schliwa, O. Stier, R. Heitz, M. Grundmann, D. Bimberg, phys. stat. sol. (b) **224**, 2232 (2001).
[8] O. Stier, Electronic and Optical Properties of Quantum Dots and Wires (Wissenschaft und Technik, Berlin, 2000).

[1]email: andrei@sol.physik.tu-berlin.de

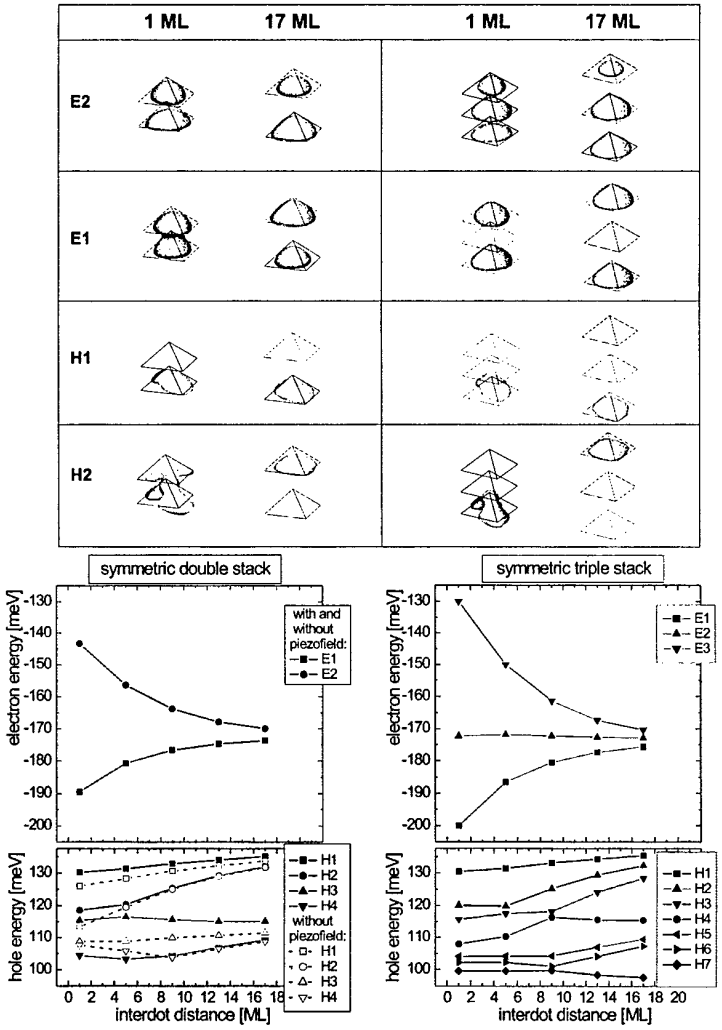

Fig. 1: Electron and hole levels in vertical QD pairs (left) and triple stacks (left) for varying spacer thicknesses with respect to the GaAs matrix band edges. Probability density isosurfaces for $p = 65\%$.

Electron and hole localization in coupled InP/InGaP self-assembled quantum dots

M. Tadic,† F. M. Peeters, B. Partoens, and K. Janssens

Departement Natuurkunde, Universiteit Antwerpen (UIA)
Universiteitsplein 1, B-2610 Antwerpen, Belgium

In order to improve the laser characteristics of self-assembled quantum dots (SAQD's), multi-layers are grown on top of each other. Such growth of one SAQD on top of another is efficiently established by strain fields in thin spacer layers [1], and stacks of both type I and type II systems were successfully demonstrated [1,2,3]. It was found that the photoluminescence energy decreases when either the number of layers increases or the separation between the dots decreases [3], which is the result of the coupling between the dots. In order to explain the magnetophotoluminiscence experimental results, a heuristic model of hole localization in the InGaP spacers was proposed recently [3].

In this paper, the theoretical results for systems explored experimentally in Ref. [3] are presented. The 6×6 multiband effective-mass theory and the extensive valence force field model are applied to InP/InGaP quantum dots of 2 nm height and 8 nm radius in the configuration of one, two, and three coupled layers. Since the dots have cylindrical shape, the axial approximation is employed. The states are classified according to the value of the total orbital momentum L_z. The exciton diamagnetic shift [4] is then computed from the free electron and hole states.

Without strain InP/InGaP system is a type II system with electrons inside the dot and the holes outside the dot region. We found that the effective potential, resulting from the band offset and the strain confines electrons and heavy holes in the dots, while the light holes are located above and below the stack. Due to the band mixing, the heavy hole contribution to the $L_z = 1/2$ state in the single quantum dot cannot be neglected. These states are located near the radial periphery of the dots in a ring configuration, as shown in Fig. 1(a). If extra layers are added, the heavy holes are expelled from the dots, and the light holes dominate in the mixed hole $L_z = 1/2$ state, see Fig. 1(b). The hole ground state wavefunction of the two and three layer system is localized above and below the stack of dots as in the single quantum dot case, but now it is almost pure light-hole like. However, there is a difference between the two-layer and the three-layer case. The calculations show that in the two vertically coupled SAQD's case the barrier between the dots shifts the electron ground state upwards and the hole ground state downwards, thus increasing the transition energy in the flat quantum dots. Experimentally the opposite behavior is found which can be explained by allowing a non-abrupt compositional variation of the Ga content between the dot and the spacer material. $L_z = 1/2$ holes are localized within a few meV of the valence band top, while the electrons are confined by 100 meV. The exciton binding energies are calculated and the resulting total energies are compared with the experimental transition energies.

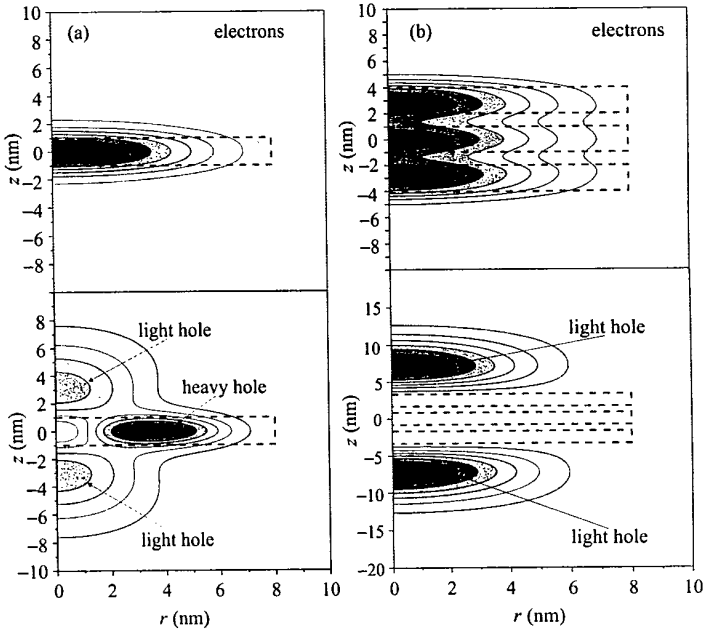

Figure 1: The hole and electron ground state wavefunctions modulus squared for $L_z = 1/2$ in the system of: (a) the single and (b) three coupled quantum dots separated by 1nm. Darker regions denote higher values. Electron and hole clouds are indicated in the figure. The dashed lines indicate the positions of the dots.

References

[1] M. K. Zundel et al., Appl. Phys. Lett. **71**, 2972 (1997).
[2] N. N. Ledentsov et al., Phys. Rev. B **54**, 8743 (1996).
[3] M. Hayne et al., Phys. Rev. B **62**, 10324 (2000).
[4] K. L. Janssens, F. M. Peeters, and V. A. Schweigert, Phys. Rev. B **63** (2001).

Corresponding author: Milan Tadic, Department of Physics,
University of Antwerp (UIA), Universiteitsplein 1,
B-2610 Antwerpen, Belgium,
phone: +32-3-820-24-68, fax: +32-3-820-22-45,
email: tadic@uia.ua.ac.be

Coherent propagation in multistacked layers of quantum dots

Giovanna Panzarini[1], Ulrich Hohenester[1,2], and Elisa Molinari[1]

[1] Istituto Nazionale per la Fisica della Materia (INFM) and Dipartimento di Fisica, Universita' di Modena e Reggio E. Via Campi 213/A, I-41100, Italy
[2] Institut für Theoretische Physik, Karl-Franzens-Universität Graz, Universitätsplatz 5, 8010 Graz, Austria

Among the most striking examples of coherent radiation-matter interaction is the highly non linear cooperative phenomenon of self-induced transparency (SIT) [1]. This effect predicts that a short coherent light pulse with a given width above a critical power threshold propagates with anomalously low energy loss while at resonance with a two-level system of absorbers. The process takes place in media with a very large inhomogeneous broadening when the input pulse with power above the critical value has a time duration shorter than all relaxation rates in the system. It differs from other coherent interactions such as Rabi oscillations in that it is a cooperative effect; it also differs from phenomena like photon-echo since the modification of the field produced by the emission of the material system can by no means be neglected.

While for atoms and molecules SIT was detected a long time ago [1], its observation in solids is more difficult owing to the complex level structure and to the much shorter decoherence times. In this contribution we propose a solid-state implementation of SIT in an ensemble of quantum dots (QDs). It is shown that the long decoherence times of electron-hole states and the large inhomogeneous size dispersion render samples of multiple stacked QDs [2] as ideal candidates for the observation of self-induced transparency.

A proper description of the mutual interaction between radiation and matter requires the simultaneous solution of Maxwell wave equation together with an equation describing the evolution of the material system under the action of the electric field E. We evaluate the evolution of E within the slowly varying envelope approximation, and calculate the macroscopic polarization in terms of the microscopic properties of the medium. The inhomogeneous broadening of the resonance frequencies is modeled with a Gaussian distribution centered at the laser frequency, and the Liouville master equation for the density operator is solved as a function of frequency, time and position including relaxation terms. A generic description model for the QD electron-hole states, consisting of ground, exciton, and biexciton states is used.

Figure 1 shows typical results of our simulations: Below a given threshold, Fig. 1(a), the pulse propagates through the medium and looses intensity because of excitations of QD excitons; however, above a given threshold the pulse reaches a stable form and propagates without significant losses to the electronic system, Fig. 1(b). This occurs when the pulse area becomes an integer multiple m of 2π; under such circumstances each QD in the ensemble undergoes m coherent transitions from the ground to the exciton state, and then back to the ground state, so that no attenuation for the incoming pulse takes place. In this paper we identify the pertinent parameters for the laser pulses and quantum dots, and we show that SIT should be observable with state-of-the-art QD samples and laser sources. We finally discuss possible effects due to the presence of higher-excitonic states.

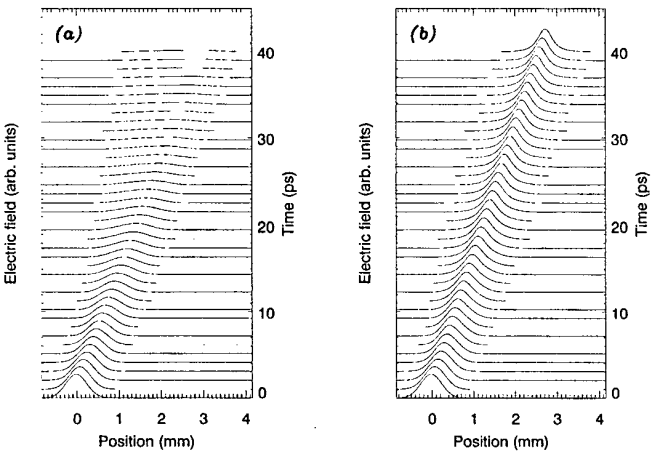

Figure 1: Propagation of a laser pulse through a medium of inhomogeneously broadened QDs. Below a given threshold, Fig. 1(a), the pulse is damped because of excitations of the QDs. Above a given threshold, Fig. 1(b), the pulse reaches a stable form and propagates without significant losses (i.e., *self-induced transparency*).

References

[1] S. L. McCall and E. L. Hahn, Phys. Rev. Lett. **18**, 908 (1967); R. E. Slusher and H. M. Gibbs, Phys.Rev.A **5**, 1634 (1972).
[2] See, e.g., P. Yu *et al.*, Phys. Rev. B **60**, 16 680 (1999); M. Colocci et al., Appl. Phys. Lett. **74**, 564 (1999).

Corresponding author: Giovanna Panzarini, Dipartimento di Fisica, Universita' di Modena e Reggio Emilia, via Campi 213/A, I-41100 Modena,
Phone: +39-059-2055300, Fax: +39-059-367488, e-mail: panzarini@unimo.it

Tunable Mid-IR Emission using a Novel Quantum Dot-Quantum Well Coupled System

R.A.Child, R. J. Nicholas, N. J. Mason and E. Alphandery
Physics Dept., Oxford University, Clarendon Laboratory, Parks Rd, Oxford, OX1 3PU, UK.

We report the first study of quantum dot photoluminescence (PL) where the emission energy can be tuned by adding a strongly coupled narrow quantum well. Inserting an almost lattice matched InAs layer below the self organized InSb/GaSb Quantum Dots allows us to extend the emission wavelength from 1.8μm out to beyond 3μm. Large enhancement of the PL has also been observed, compared to that from a single dot layer.

The system studied here consists of a single InAs well coupled to a single layer of InSb dots, which are grown in a GaSb matrix. The InAs/GaSb system has type II alignment, which generates an extremely deep electron well. The InAs layer therefore shifts the dot emission to lower energies, potentially providing a more flexible, versatile system with a variety of tunable parameters. For example, by adding a 2ML InAs well the emission shifts from 1.8μm to 2.21μm with dots whereas the well alone emits at 2.06μm. The potential range of energies that could be produced varies between 1.8 and 3.8μm, a typical wavelength observed for InSb dots grown directly on InAs.

We have studied the effects of varying the InAs well widths and the well-dot layer separation, with dots grown using identical growth conditions. Control samples are used to provide evidence for coupling while highlighting any advantages this system has over type II broken gap InAs/GaSb. Magneto photoluminescence allows us to probe and understand the extent of the coupling between the dots and well.

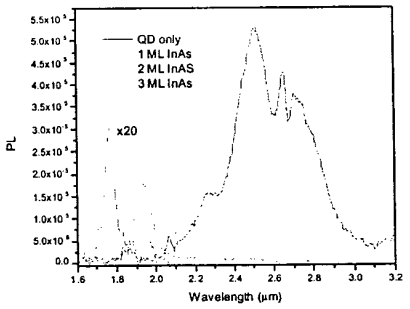

Fig 1: Tuning of the PL as a function of InAs well width, for constant dot-well spacing.

Pauli-blocking absorption experiments on self-assembled quantum dots

F. Bickel[1], D. Haft[1], R. J. Warburton[1,2], K. Karrai[1], W. Schoenfeld[3], J. M. Garcia[3,4], P. M. Petroff[3]

[1]Center for NanoScience and Sektion Physik, Ludwig-Maximilians-Universität München, Geschwister-Scholl-Platz 1, D-80539 München, Germany
[2]Department of Physics, Heriot-Watt University, Edinburgh EH14 4AS, UK
[3]Materials Department and QUEST, University of California, Santa Barbara, California 93106, USA
[4]Instituto de Microelectrónica de Madrid, Isaac Newton 8, 28760 Tres Cantos, Madrid, Spain

Self-assembled semiconductor quantum dots (SAQDs) have been the focus of intensive research in the past few years. Although observing the emission of single quantum dots and rings [1] by photoluminescence spectroscopy is nowadays a common experimental setup, the direct absorption of an isolated InAs dot has not yet been observed. Nevertheless this is a major aim because absorption represents a direct measurement of fundamental properties such as line width and line shifts due to many particle effects, which cannot be resolved in inhomogeneous broadened ensemble measurements. Therefore it is an outstanding challenge to measure the absorption spectrum of a single quantum dot.

Because of the weak absorption signal of a single quantum dot one of the major problems with these experiments is the signal to noise ratio. Laser instabilities and detector noise are just two reasons for failure of observation. Laser chopping techniques can of course only be a solution if the tunable light source is very stable during a scan of the wavelength. There is therefore the need for a steady and easy to use modulation mechanism of the absorption signal, in the best case from the sample itself.

Self-assembled InAs-QDs can well be described by a 2D-oscillator model as the quantisation in the growth direction is usually much larger than in the lateral direction. According to Pauli's rule this allows two electrons of opposite spin to be accommodated in the first quantum level, four in the second and so on. By applying a voltage between an embedded back contact and a surface gate electrode, the band structure can be tilted making it possible to control the number of electrons in the dots. It was shown by capacitance spectroscopy that up to six electrons can be bound in these artificial atoms. If the observed dot is fully occupied by tuning the voltage to a level above the six-electron point no more electrons can be optically exited to the first or second energy level. As a result the absorption lines of the corresponding transitions are turned off. This "Pauli-blocking" effect can be used to improve the signal to noise ratio in optical absorption measurements. Switching the dots between absorbing and non-absorbing state of a special transition the transmission signal can be intrinsically modulated with a known frequency and phase. Common lock-in techniques can consequently demodulate and measure the detected signal to high accuracy.

We are using a low temperature near field scanning optical microscope (NSOM) for the measurements rather than a far field setup on a low dot density sample. This is because calculations based on the absorption cross section of a single dot derived from the ensemble measurements [2] together with an expected line width below 100 μeV show that the absorption amplitude increases quadratically with the radius of the illuminating spot. Currently our setup is capable of resolving amplitudes of 10^{-5} of the incident power. The sample itself consists of a layer of self-organized InAs quantum dots embedded in GaAs. The absorption energies for the first and second quantum level are around 1.10 eV and 1.18 eV, respectively [2]. With the use of a tunable external cavity diode laser emitting between 1.16 eV and 1.19 eV it was possible to see the second level absorption of a few hundred dots with statistically significant fluctuations in the spectrum. The results of these measurements on the way to the single dot absorption will be discussed.

The Pauli-Blocking modulation technique can of course also be used for studying many particle effects in SAQDs. By changing the electric field across the dots the electron occupation in the artificial atom can be altered. As a consequence the Coulomb and exchange interaction energies for the bound exciton are modified thus changing the absorption wavelength. If the voltage is switched between a common dark state (fully occupied dot) and a tuned emitting state these shifts can be observed.

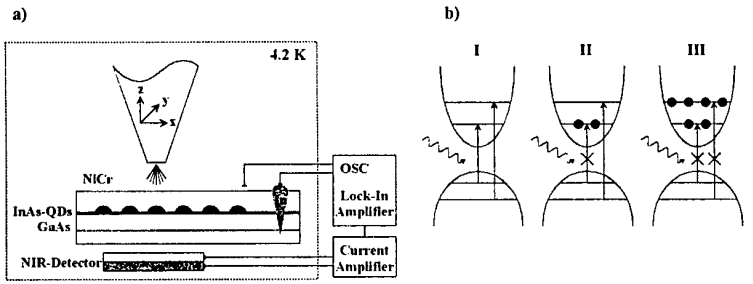

Fig. 1: a) The Setup of single dot Pauli-blocking measurements: An oscillating voltage across the SAQDs is used to change the electron filling in the dots. The modulated absorption signal can be measured to high accuracy with common lock-in techniques. The near field tip yields high spatial resolution. b) Level filling with increasing gate voltage: (I) empty dot, both transitions can be excited; (II) first level filled, the corresponding transition is blocked; (III) both levels filled, both transitions are blocked.

References

[1] R. J. Warburton, C. Schäflein, D. Haft, F. Bickel, A. Lorke, K. Karrai, J. M. Garcia, W. Schoenfeld & P. M. Petroff, *Optical emission from a charge-tunable quantum ring*, Nature **405**, 926 (2000)

[2] R. J. Warburton, C. S. Dürr, K. Karrai, J. P. Kotthaus, G. Medeiros-Ribeiro, and P. M. Petroff, *Charged Excitons in Self-Assembled Semiconductor Quantum Dots*, Phys. Rev. Lett. **79**, 5282 (1997)

Corresponding author: Florian Bickel, Center for NanoScience and Sektion Physik, Ludwig-Maximilians-Universität München, Geschwister-Scholl-Platz 1, D-80539 München, Germany.
phone: +49 89 2180 3586, fax: +49 89 2180 3182
email: florian.bickel@physik.uni-muenchen.de

Photocurrent spectroscopy of modulation doped InAs self-assembled quantum dots

P. Hawrylak, M.Korkusinski, J. Kyriakidis, H.C.Liu, R. Dudek, S. Fafard and Z. Wasilewski

Institute for Microstructural Sciences, National Research Council of Canada,

Ottawa, K1A OR6, Canada

We present results of calculations and experiments on photocurrent spectroscopy of modulation doped InAs self-assembled quantum dots. The quantum dots have been grown using the In-flush technique[1] which allows the fabrication of InAs disks with high uniformity and well resolved quantized single particle levels. The single particle levels are populated with carriers via modulation doping in the GaAs barrier region. An absorption of infrared photons results in transitions from populated bound states in the quantum dot to scattering states in the GaAs barrier region[2]. The absorption process depends on the energy and polarization of the incident light, and on the number of carriers in the dot. In this paper, we derive an expression for the transition probability describing the dependence of the photocurrent on the parameters of the dot, the number of carriers, and the polarization and energy of incident photons. The electronic states in InAs self-assembled quantum disks are calculated using the effective mass and adiabatic approximation. The effective confining potential is determined from the calculation of the shift of the conduction band minima in the InAs and GaAs due to strain. The effective mass is treated as an adjustable parameter, with values close to the ones obtained from k*p calculations. The calculations of dipole allowed transition involves bound to continuum transitions for different angular momenta, depending on the polarization of light. For light polarized in the growth direction, transition from bound to continuum states proceeds without change of angular momentum, while light polarized in the plane requires a change of angular momentum by one. The transition into continuum leaves a vacancy (a hole) in the ground state of the N electron system. We calculate both the ground state and the spectral function of the hole as a function of the filling of quantum dot levels using exact diagonalization techniques[3]. The dipole matrix elements, the ground state, and the spectral functions are used as an input to the calculation of the photocurrent spectrum. The results of calculations are compared with experiments, which clearly show the dependence on photon energy and polarization. Implications of this work for quantum dot infrared detectors are discussed.

References

[1] Z.R.Wasilewski, S. Fafard, and J.P. McCaffrey, J.Cryst.Growth,**201**,1131(2001).
[2] H.C.Liu,M.Gao,J.McCaffrey,Z.R.Wasilewski, and S. Fafard, Appl.Phys.Lett.**78**, 79(2001)
[3] A. Wojs and P. Hawrylak, Phys. Rev. B53, 10841 (1996).

Corresponding author: Pawel Hawrylak, Institute for Microstructural Sciences, National Research Council of Canada, Ottawa, K1A OR6, Canada

phone: +001 613 993 9389, Fax: +001 613 993 9389

email: pawel.hawrylak@nrc.ca

Time-resolved photoluminescence near Fermi level in a field-induced quantum dot lattice

K. Hammura[1], S. Nomura[2], Y. Aoyagi[3,1]

[1]RIKEN, 2-1 Hirosawa, Wako-shi, Saitama 351-0198, Japan
[2]Institute of Physics, University of Tsukuba, 1-1-1 Tennodai, Tsukuba-shi, Ibaraki 305-8571, Japan
[3]Interdisciplinary Graduate School of Science and Engineering, Tokyo Institute of Technology, 4259 Ngatsuda-cho, Midori-ku, Yokohama-shi, Kanagawa 226-8502, Japan

Since Mahan's novel suggestion of the Fermi-edge singularity (FES) that the correlation between a photo-excited hole and Fermi-sea electrons should induce a resonance with a non-Lorenzian lineshape[1], the FES in optical response of doped semiconductors have been investigated both theoretically[2] and experimentally[3-6].

Among the experiments above, Nomura *et al.*'s results at low temperature[3] has received a growing interest because of giving spatial modulation of the potential contributing to a photoluminescence (PL) peak originating from the FES (a FES-peak, in the following). The peak was due to recombination of two-dimensional electron system (2DES) with a hole. The peak disappeared in the cases of either no periodic potential or no 2DES with a Fermi-sea. By the latter, the peak was considered to be due to the FES.

The purpose of the present paper is to investigate the dynamics of an optically created hole in a periodic potential. We measured time-resolved PL spectra near the Fermi level in a lattice of quantum dots. The sample preparation was described in Ref.[3]. A lattice of quantum dots was prepared by applying bias voltage on a two-dimensional square mesh Ti/Au gate structure on a modulation-doped GaAs/$Ga_{1-x}Al_xAs$ quantum well structure. By biasing negative voltage, a periodic potential is formed. The electron density is considered to be higher in the area away from the gate structure, i.e., the center of the quantum dots, while the potential minimum of a hole is located below the gate structure. The recombination of a hole with electrons occurs before the hole relaxes to the potential minimum. Thus, understanding of the dynamics of holes is a key to identify the FES-peak. With the characteristic lifetime of a hole, we discuss the time dependence of the probability of existence of holes on the periodic potential.

We measured the time-resolved PL under those conditions as, bias voltage (V_B) between -0.4 V and +0.3 V, at magnetic fields (B) 0 T and 3 T, at temperatures (T) between 4.2 K and 30 K. The main results are as follows: (1) The lifetime of the FES-peak increased with increasing temperatures, (2) and decreased with increasing negative bias voltage, while the lifetime time of the peak originating from bulk increased. (3) In the wavelength region where the FES-peak was observed at 0 T, several peaks of Landau levels (LL) were observed and the LL peak with shorter wavelength had shorter lifetime than that with longer wavelength, in magnetic fields.

Those experimental results indicate (1) the increase of the phonon scattering due to increasing temperatures induces the shrink of the overlap of the wavefunctions of electrons and holes because of the increasing of incoherency, (2) the overlap of the wavefunctions of 2DES and a hole increases with increasing confinement energy, and (3) the holes with higher energy and momentum have shorter lifetime component indicative of spatially indirect transition was not observed.

References

[1] G. D. Mahan, Phys. Rev. **153**, 882 (1967).
[2] G. E. Bauer, Phys. Rev. **B45**, 9153 (1992).
[3] S. Nomura et al., Solid State Commun. **106**, 815 (1998).
[4] M. S. Skolnick et al., Phys. Rev. Lett. **58**, 2130 (1987).
[5] H. Wang et al., Phys. Rev. **B52**, R17013 (1995).
[6] J. X. Shen et al., Phys. Rev. **B59**, 8093 (1999).

Corresponding author: Kiyotaka Hammura, RIKEN, 2-1 Hirosawa, Wako-shi, Saitama 351-0198, Japan.
phone: +81 48 462 1111, Fax: +81 48 467 4659
email: hammura@postman.riken.go.jp

Interdot Energy Transfer in a System of Coupled InAs/GaAs Quantum Dots

Yu. I. Mazur[1], J. W. Tomm[1], G.G. Tarasov[2], H. Kissel[3], C. Walther[2], Z. Ya. Zhuchenko[2], and W.T. Masselink[2]

[1]Max-Born-Institut für Nichtlineare Optik und Kurzzeitspektroskopie, Max-Born-Str. 2A, D-12489, Berlin, Germany
[2]Department of Physics, Humboldt-Universität zu Berlin, Invalidenstraße 110, D-10115 Berlin, Germany
[3]Ferdinand-Braun-Institut für Höchstfrequenztechnik, Albert-Einstein-Str. 11, D-12489 Berlin, Germany

Quantum dot (QD)-based heterostructures provide a broad field for applications. Many of these applications, however, require the use of high-density QD-systems, for example, to get sufficiently high optical gains in laser structures. In this case, the inter-dot coupling becomes of principal importance due to the strong influence on recombination, tunneling, carrier injection, and lasing properties. The situation becomes even more complicated if the QD size distribution exhibits several peaks, distinguishing various 'quasi' independent QD families that possess different relaxation properties within and among them. A complete picture of the energy and carrier transfer in such multi-family and high-density systems is still far of clarity.
On the other hand, this complicated system promises advantages for applications due to the possibility to suppress the size fluctuation effect dynamically through the energy and carrier transfer towards the lowest potential minimum. The effective size distribution is expected to become substantially narrower leading to a stabilization of the optical properties of QDs belonging to an intentionally selected family. For these new structures, however, there is a rather large scattering in the reported PL data even for QD-systems with the same nominal layer architecture and data are interpreted either in terms of excited states of mono- or as multi-modal behavior of the QD size distribution.
For increasing the understanding of such systems, it is important to separate the effects caused by the different parameters. We report here on the development of a very effective technique to perform such a separation. It is based on comparison of time-resolved and steady-state PL data from multi-family high-density InAs/GaAs QD systems. A strong correlation between the spectral behavior of the PL decay time and the shape of the PL spectrum for steady-state excitation is found. The 'PL decay time versus photon energy relation' appears staircase-like and the energetic positions of the steps as well as the shape can be correlated to the shape of the steady-state PL emission through a rate-equation theory. This provides an independent tool for separating QD families. These results show how transient PL can be used to investigate the dynamics of carrier transfer in quantum dot systems.
Fig. 1 shows the correlated behavior of low temperature steady state PL for a sample with d_{InAs} = 1.79 ML and the 'PL-decay time constants' (τ) determined from a least-square fit from the PL transients measured at almost constant excitation flux below 10^{11} photons/(pulse·cm^2). It is easily seen that the steps in the spectral dependence of τ are unequivocally related to the positions of the spectral bands obtained from a decomposition of the steady state PL spectrum. The correspondence observed has a profound physical explanation and is described in terms of carrier transfer within and among QD families. This process has a cascade-like nature. The probability to escape from the ground state of small QDs is determined by the number of available states with lower energies supplied by the larger sized QDs. Thus, this probability will be determined by the integral over the Gaussian distribution up to the photon energy of the PL emission. The theory developed for the case explains precisely the spectral shape of the τ dependence.

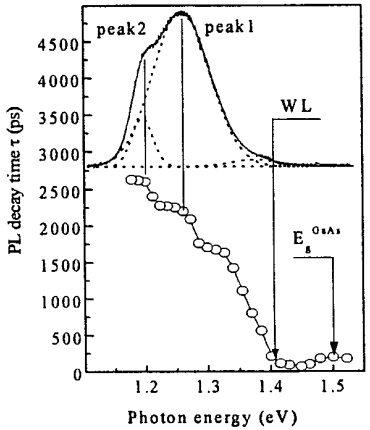

Fig. 1: PL spectrum (line) and decay time (τ, circles) for high-density InAs/GaAs QDs at T = 10 K. Sample parameters are d_{InAs} = 1.79 ML and growth temperature T_G = 505°C. A de-convolution into 3 lines is shown as dotted lines. Spectral positions of the QD PL bands, wetting layer PL and GaAs PL are marked by arrows. Excitation density is $2 \cdot 10^{10}$ photons/(pulse·cm^2).

A novel effect is observed in conjunction with the saturation of the interdot relaxation channel. In this case, the shape of PL transients becomes strongly dependent on the excitation flux, transforming from a non-exponential to an exponential shape for extremely low excitation. Intra- and inter-dot relaxation is responsible for this behavior.
In summary, we report for the first time a two-step-like spectral behavior of the time constants of ground-state related PL transients in high-density self-assembled InAs/GaAs quantum dots appearing in a two-family QD distribution. This characteristic spectral dependence is well pronounced even in the case of strongly overlapping PL bands that are practically not resolved in the steady-state PL spectrum. Thus, we show that monitoring the spectral behavior of time constants of ground-state related PL offers a new and independent tool for distinguishing between PL contributions from different dot size families.

Corresponding author: G.G. Tarasov, Department of Physics, Humboldt-Universität zu Berlin, Invalidenstraße 110, D-10115 Berlin, Germany,
Phone: +49-30-2093-7663, Fax: +49-30-2093-7659
Email: tarasov@physik.hu-berlin.de

Size-Selective Optically Excited Capacitance Transient Spectroscopy of InAs/GaAs Quantum Dots

C. M. A. Kapteyn[1], J. Ehehalt[1], R. Heitz[1], and D. Bimberg[1],
G. E. Cirlin[2], V. M. Ustinov[2], and N. N. Ledentsov[2]

[1]Institut für Festkörperphysik, Technische Universität Berlin, Hardenbergerstr. 36, 10623 Berlin, Germany
[2]A. F. Ioffe Phisico-Technical Institute, Polytechnicheskaya 26, 194021 St-Petersburg, Russia

Capacitance transient spectroscopy (CTS) has been proven to be a powerful tool for the investigation and distinction of the carrier dynamics of electrons and holes in self-organized quantum dots (QDs) [1-3]. CTS is therefore ideally suited to investigate details of the electronic structure of QDs. Here, we demonstrate the extension of this technique to optically induced charging, which adds with the choice of the excitation wavelength an important degree of freedom and hence combines the strength of optical techniques with the power of CTS. Resonantly generated carriers allow to study *energy-resolved* and hence *size-selective* properties of sub-ensembles of QDs.

In our contribution, we present the first CTS experiments of carrier emission from InAs/GaAs QDs with optical excitation, Figure 1. The investigations employ standard data evaluation methods known from deep level transient spectroscopy. For the present experiments, we make use of the previously investigated differences in the emission mechanisms for electrons and holes in InAs/GaAs QDs [2]. The differing emission rates allow very elegantly to build up a net hole charge in the QDs. This is due to the fact, that the electrons of electron-hole pairs generated by optical excitation are removed from the QDs with a much higher probability.

From a standard Arrhenius plot evaluation of the CTS peak position, Figure 1(a), an activation energy of 210 meV, Figure 1(b), is determined for the given excitation wavelength. This activation energy corresponds to the hole ground state energy in the QDs. The negative sign of the CTS signal clearly indicates minority carrier emission due to hole escape from the QD ground states. From the reverse bias dependence of the optically induced CTS signal and by comparison with reference samples without QDs, the QD layer is verified as the source of the observed CTS signal.

The use of monochromatic light for the charging pulse allows for the first time to study the emission process of sub-ensembles of QDs of equal size. This can be done by simply tuning the excitation wavelength. The activation energy is found to change by up to several 10 meV, reflecting the selection of sub-ensembles of QDs with increasing size by increasing the excitation wavelength.

Our results clearly demonstrate resonant size-selective carrier generation in the QD ground and excited states. Optically excited CTS hence allows to investigate the fundamental physical ingredients of the carrier dynamics for future experiments on spectral-hole burning and optical memory structures based on wavelength-domain multiplexing techniques.

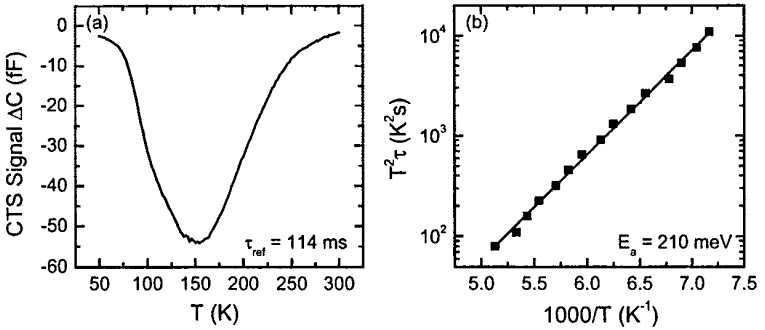

Fig. 1: CTS signal with optical excitation for a reference time constant of 114 ms, panel (a). A negative peak at 150 K due to hole emission from the QDs is apparent. The p^+n diode sample was illuminated with pulses of monochromatic light with an energy of 1 eV (at 300 K) for each transient. From a standard Arrhenius plot evaluation of the peak position as function of reference time constant, panel (b), an activation energy of 210 meV was obtained.

References

[1] C. M. A. Kapteyn, F. Heinrichsdorff, O. Stier, R. Heitz, M. Grundmann, N. D. Zakharov, D. Bimberg, P. Werner, Phys. Rev. B **60**, 14265 (1999).
[2] C. M. A. Kapteyn, M. Lion, R. Heitz, D. Bimberg, P. Brunkov, B. V. Volovik, S. G. Konnikov, A. R. Kovsh, V. M. Ustinov, Appl. Phys. Lett. **76**, 1573 (2000).
[3] C. M. A. Kapteyn, M. Lion, R. Heitz, D. Bimberg, C. Miesner, T. Asperger, K. Brunner, G. Abstreiter, Appl. Phys. Lett. **77**, 4169 (2000).

Corresponding author: Christian Kapteyn, Institut für Festkörperphysik, Technische Universität Berlin, PN 5-2, Hardenbergstr. 36, 10623 Berlin, Germany.
phone: +49 30 314-21977, Fax: +49 30 314-22569
email: kaptey@physik.tu-berlin.de

Observation of dip structures in PLE spectra of a highly excited single self-assembled quantum dot

S. Kako[1], T. Sugimoto[1], Y. Toda[2], S. Ishida[1], M. Nishioka[1], Y. Arakawa[1]

[1] Research Center for Advanced Science and Technology, University of Tokyo, 4-6-1 Komaba, Meguro-ku, Tokyo 153-8904, Japan
[2] Department of Applied Physics, Hokkaido University, Kita 13, Nishi 8, Kita-ku, Sapporo 060-8628, Japan

Recent developments of spatially resolved techniques have enabled us to investigate the electronic states of individual quantum dots. We have found that in PLE spectra of single quantum dot there exists continuum states that play an important role in efficient carrier relaxation.[1] Recently, we performed excitation power dependence of PLE spectrum, and confirmed that the continuum states can work as large carrier bath.[2] In this contribution, we report the first observation of dip structures in PLE spectrum of a highly excited single quantum dot.

The sample studied here is self-assembled InGaAs quantum dots grown by MOCVD. Spatially resolved single dot spectroscopy was performed using a low-temperature μ-PL with an island-etched sample. As an excitation source we used a tunable CW Ti:Sapphire laser. Figure 1 shows the PLE spectra from the excitonic ground state at different excitation powers. The PL energy of the excitonic ground state is 1282.8meV. At the low excitation power (P_0), we can see some peaks and gradually increasing continuum states.

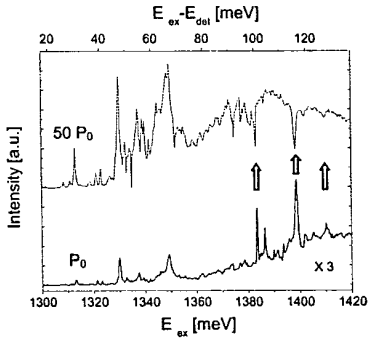

Figure 1: PLE spectra of the exctonic ground state at the different excitation powers. $P_0 = 4\mu W$ which corresponds to 400 W/cm^{-2}. The peaks lying continuum states turn into the dips. (see arrows.)

With increasing excitation power most of the peaks and continuum states grow almost lineally. However at highly excitation power (50 P_0) the peaks lying continuum states turn into the dips. In addition to this experiments, we also performed two-color PLE measurements using the Ti:Sapphire laser and a He-Ne laser. When the power of He-Ne laser was set appropriately, most of peaks in all PLE spectral range turned into the dip structure.

In order to explain this evolution, we noticed a biexciton luminescence. Figure 2 shows the PLE spectra from excitonic ground state (X) and its biexciton state (XX) at the excitation energy of 50 P_0. The PL energy of biexciton state is 1278.4meV. The binding energy of biexciton is about 4.4 meV. This value is almost consistent with that of previous reports.[3,4] We also confirmed the biexciton luminescence from excitation power dependence of the PL intensity. Most remarkable feature is that the biexciton PLE emerges as a peak at the excitation energy at which the exciton PLE shows the dip structure. Therefore we attribute such dip structures to energy transfer from exciton luminescence to the biexciton luminescence.

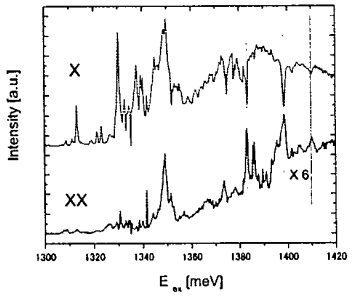

Figure 2: PLE spectra of exciton and biexciton luminescence at the power of 200μW.

References

[1] Y. Toda et al., Phys. Rev. Lett. **82**, 4114 (1999).
[2] T. Sugimoto et al., Technical Digest of Int. Conf. on Quantum Electronics and Laser Science, San Francisco, California, QTuD3(2000).
[3] K. Brunner et al., Phys. Rev. Lett. **73**, 1138(1994).
[4] H. Kamada et al., Phys. Rev. B. **58**, 16243(1998).

Corresponding author: Satoshi Kako, Research Center for Advanced Science and Technology, University of Tokyo, 4-6-1 Komaba, Meguro-ku, Tokyo 153-8904, Japan
phone: +81 3 5452 6247, Fax: +81 3 5452 6246,
email: kako@iis.u-tokyo.ac.jp

Very large subband separation in GaAs/AlGaAs V-groove quantum wires

T. Otterburg[1], F. Lelarge[1], D.Y. Oberli[1], A. Rudra[1], and E. Kapon[1]

[1]Department of Physics, Swiss Federal Institute of Technology Lausanne
CH-1015 Lausanne EPFL, Switzerland

Strong lateral confinement has always been one of the most important objectives in the field of low-dimensional heterostructures. It is important both for observing well-resolved lateral quantum size effects in electronic and optical spectra as well as for device applications utilizing these effects. This objective is even more challenging considering that at the same time small inhomogeneous broadening effects are required. The strength of the lateral confinement in low-dimensional semiconductor heterostructures is reflected in their optical properties as the energy separation ΔE between optical transitions related to adjacent subbands in quantum wires (QWRs) or fully confined states in quantum dots (QDs). The inhomogeneous broadening effects can be characterized by the energy width δE (δE_{PL}) of the corresponding optical absorption (photoluminescence) lines observed for wires of a certain length or dot arrays of a given size. Therefore, the ratio $\rho=\Delta E/\delta E$ ($\rho_{PL}=\Delta E/\delta E_{PL}$) is a useful figure of merit to evaluate a sample's optical quality.

In this work we have investigated how and to what extent the subband separation of V-groove GaAs/$Al_xGa_{1-x}As$ QWRs can be tuned in a controlled way without compromising the wire uniformity and interface quality. Our quantum wires were grown by low-pressure (20 mbar) Organometallic Chemical Vapor Deposition (OMCVD) on a patterned (100)-GaAs substrate. The tuning of the subband separation is done by varying one of the OMCVD growth parameters at a time, namely the growth temperature T_G, the aluminium content x in the wire barrier or the wire thickness . The subband separation and the inhomogeneous broadening were obtained from low-temperature photoluminescence excitation (PLE) and photoluminescence (PL) measurements, respectively.

Our results demonstrate that the 2D confinement is tunable in a controlled way and over a wide range, making it possible to fabricate QWRs with predetermined lateral confinement. The figure of merit $\rho=\Delta E/\delta E$ ($\rho_{PL}=\Delta E/\delta E_{PL}$) for our V-groove QWRs can be as large as 5 (7). These values of $\rho_{(PL)}$ are equal to or even better than values found in other high quality quantum wires [1,2,3] or quantum dots [4,5]. Our investigations enabled us to implement growth parameters for fabricating V-groove QWR samples with a subband separation of about $3k_BT_{room}$ (ΔE = 80meV), which is comparable to values found for Stranski-Krastanow grown quantum dots [4,5]. Moreover, we show that the characteristic 1D features such as subband separation and polarization anisotropy are maintained in the PLE spectra up to room temperature.

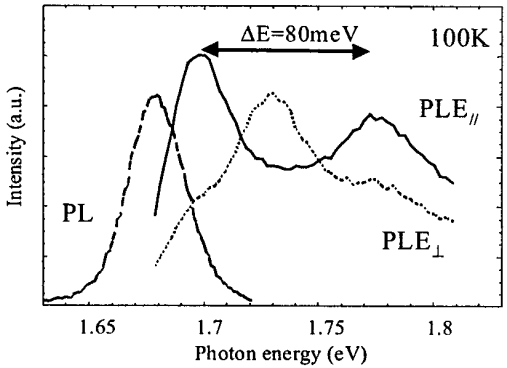

Fig. 1: PL and PLE of a quantum wire sample showing a 1D subband separation of 80meV. Also visible is the polarization anisotropy of the PLE spectrum when exciting with laser light linearly polarized parallel or perpendicular to the wire axis.

References

[1] X.-L. Wang et al., *J. Crystal Growth 221*, p.556 (2000)
[2] W. Langbein, H. Gislason, and J.M. Hvam, *Phys. Rev. B 54*, p. 14595 (1996)
[3] H. Akiyama, T. Someya, and H. Sakaki, *Phys. Rev. B 53*, p. R4229 (1996)
[4] P. Hawrylak et al, *Phys. Rev. Lett. 85*, p. 389 (2000)
[5] K. Nishi et al., *Appl. Phys. Lett. 74*, p. 1111 (1999)

Corresponding author: Tim Otterburg, Department of Physics,
Swiss Federal Institute of Technology Lausanne,
CH-1015 Lausanne EPFL, Switzerland.
phone: +41 21 693 3387, Fax: +41 21 693 5480
email: tim.otterburg@epfl.ch

Growth of InGaAs Ridge Quantum Wires and Dots for Quantum LSIs by Atomic Hydrogen-Assisted Selective MBE Growth on InP Substrates

Tsutomu Muranaka, Seiya Kasai, Chao Jiang and Hideki Hasegawa

Research Center for Interface Quantum Electronics & Graduate School of Electronics and Information Engineering, Hokkaido University, Sapporo 060-8628, Japan
Phone: +81-11-706-7174, Fax: +81-11-716-6004, e-mail: muranaka@rciqe.hokudai.ac.jp

Quantum wire transistors (QWRTrs) and single electron transistors (SETs) are promising candidates for next generation quantum (Q-) LSIs. However, previous works on quantum devices have been carried out mainly on discrete device levels without seriously looking into the capability for high-density integration. For realization of room temperature operating Q-LSIs, formation of high-density arrays of high-quality and highly uniform quantum wires (QWRs) and quantum dots (QDs) with sub-10 nm sizes is required. Among various material combinations and growth/processing alternatives, growth of compound semiconductor nanostructures by selective molecular beam epitaxy (MBE) growth seems to be most promising.

The purpose of this paper is to establish the optimum conditions to grow high-density and highly uniform InGaAs QWR and QD arrays suitable for Q-LSI applications by an atomic hydrogen-assisted selective MBE growth on patterned InP substrates.

The following growth procedure [1, 2] was used. (001) InP substrates were patterned by EB lithography and wet chemical etching. The patterns used for growth of QWR arrays and coupled QWR-QD arrays are shown in **Fig. 1(a)** and **(b)**, respectively. Low-temperature atomic hydrogen (H*) cleaning of the InP surface was applied in the MBE chamber prior to growth. Then, InGaAs was deposited first by MBE, followed by MBE growth of InAlAs/InGaAs/InAlAs layers, leading to formation of QWR/QD structures. In this study, various growth and processing conditions including H* cleaning were optimized with respect to density, uniformity and feature size, using SEM, AFM, XPS, PL and CL techniques. In order to test the feasibility for device applications, QWRTr and SET test structures were fabricated and characterized.

Examples of QWR/QD structures grown in this study are shown in **Fig. 2**. It has been found that integrity of the ridge structure obtained after first InGaAs growth has the greatest impact on the available density, uniformity and feature size, and that the optimum H* cleaning substantially improves the ridge integrity. For example, PL spectra of InGaAs QWRs obtained by the previous As_4 thermal cleaning and by the present H* cleaning are compared in **Fig. 3(a)** and **(b)**. H* cleaning suppressed peaks from parasitic side facet QWs, and sharpened the peak very much. Measured PL peak positions agreed well with theory as shown in **Fig. 4**. Wire arrays with wire widths below 10 nm and a sub micron wire pitch of 900 nm have been realized.

Fabricated QWTr and SET test structures having the Schottky wrap gates (WPGs) [3] are shown in **Fig.5**. In a gated magneto transport measurement on the QWRTr test structure, clear Shubnikov-de Haas (SdH) oscillations were seen, and Landau plots shown in **Fig. 6(a)** were obtained. Using the theory based on the harmonic potential approximation (HPA), large subband spacing values of 13-15 meV and tight gate control characteristics shown in **Fig. 6(b)** were obtained. The QWRTr structure showed clear conductance quantization up to 70 K. The SET test structure showed clear conductance oscillation peaks at 4.2 K due to lateral resonant tunneling of single electrons.

References

[1] T. Muranaka, H. Fujikura and H. Hasegawa: Inst. Phys. Conf. Ser. **166** (2000) 187.
[2] T. Muranaka, C. Jiang, A. Ito and H. Hasegawa: Thin Solid Films **380** (2000) 189.
[3] S. Kasai and H. Hasegawa, Jpn. J. Appl. Phys. **40** (2001) in press.

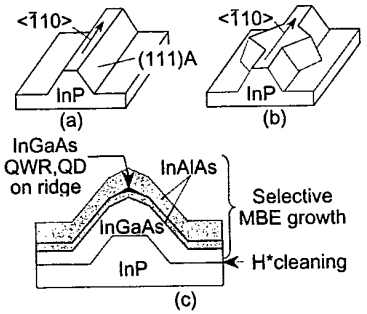

Fig.1 (a), (b) Schematic views of InP patterned substrates and (b) selective MBE procedure.

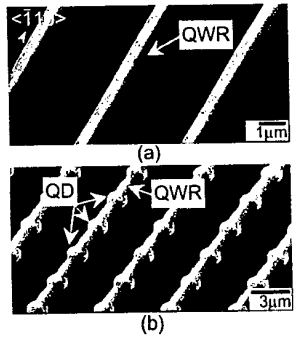

Fig.2 SEM images of (a) QWRs and (b) coupled QWR-QD structure arrays.

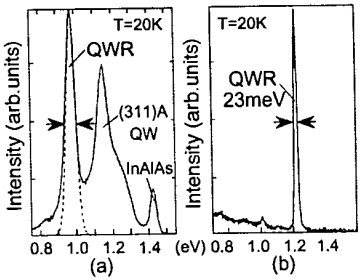

Fig.3 PL spectra of QWRs subjected to (a) As_4 thermal cleaning and (b) H* cleaning.

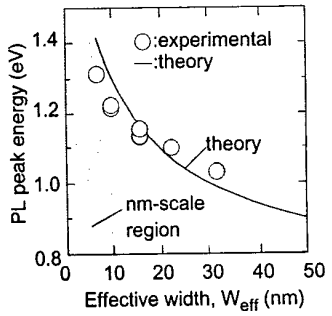

Fig.4 PL peak energies vs. effective wire widths of QWRs, W_{eff}.

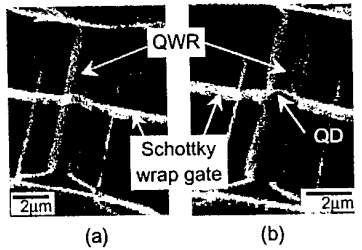

Fig.5 SEM images of InGaAs ridge (a) QWRTr and (b) SET.

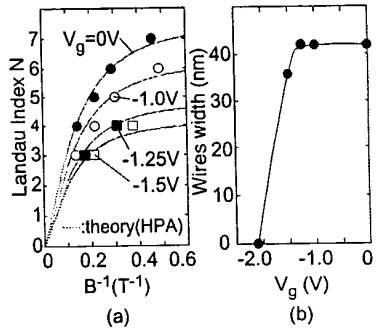

Fig.6 (a) Landau plots from SdH oscillations as a function of gate voltage and (b) wire widths vs. gate voltages.

Carrier Recombination Processes in Disordered Quantum Wire Superlattice

A.Sasaki[1], R.Okanishi[1], X.Q.Liu[2], X-L.Wang,[3] and M.Ogura[3]
[1]Dpt. of Electronics and [2]Academic Frontier Promotion Ctr., Osaka Electro-Communication Univ.
Neyagawa 572-8530, Japan, Tele.+81-72-824-1131, Fax.+81-72-824-0014, email sasaki@isc.osakac.ac.jp
[3]Electrotechnical Laboratory, Tsukuba 305-8568, Japan

A disordered crystalline semiconductor has been proposed to enhance luminescence capability.[1] Atomic arrangements in that semiconductor are randomly disordered to some extent but ordered enough to form a crystalline structure. An example is the disordered superlattice in which individual layer thicknesses of wells and barriers are grown randomly disordered. In experiments, the AlAs/GaAs disordered superlattice exhibited the luminescence intensity enhanced at least 500 times stronger[2] than the AlAs/GaAs ordered superlattice, i.e., the conventional superlattice (SL). The luminescence from the AlP/GaP disordered superlattice also was enhanced.[3] The luminescence capability enhanced by disordering in atomic arrangement has been theoretically derived.[4]

In this study, carrier recombination processes in the $Al_{0.425}Ga_{0.575}As$/GaAs disordered quantum wire superlattice (d-QWRSL) are investigated experimentally comparing with those in the $Al_{0.425}Ga_{0.575}As$ / GaAs ordered quantum wire superlattice (o-QWRSL). Hereafter the composition rates are not written for simplicity. We observed the enhanced luminescence intensity from the disordered quantum wires (QWRs).

The samples were grown on the V-grooved GaAs substrate by the flow rate modulation epitaxy.[5] The layer structure of the o-QWRSL consists of 32 periods of $(AlGaAs)_{12}/(GaAs)_6$, indicating 12 and 6 monolayers (MLs) of all barrier and wire layers, respectively. The d-QWRSL consists of 32 periods of $(AlGaAs)_m(GaAs)_n$ where m denotes 7, 12, or 17 and n 3, 6, or 9 MLs. They appear randomly with an equal probability and thus total numbers of atoms in the o- and the d-QWRSLs are equal. The (001) flat layers and the part of the (111)A side wall were selectively removed by a self-aligned wet chemical etching.[6] Their cross sectional images by TEM are shown in Fig.1, where the QWRs are seen at the V-grooved bottoms and the SLs on the side walls of the V-groove.

Figure 2 shows photoluminescence (PL) spectra measured in the temperature range from 16 to 240K and excited by an Ar-laser. Two PL spectra are dominantly observed in the low temperature region: the peak at the low energy side is the luminescence from the QWRs and the peak at the high energy side from the SLs. The luminescence of the d-QWRSL exhibits a red-shift relative to that of the o-QWRSL. It was experimentally observed in the d-SL[2,3] and theoretically verified.[4]

Variations of the PL integrated intensity with increasing measurement temperature are shown in Fig.3. The PL integrated intensity of the SL decreases monotonically with the temperature, whereas that of the QWR increases first and then decreases. It is understood that the carriers excited by the Ar-laser to the SL are transferred to the QWR with increasing the measurement temperature. The PL intensity increases up to 50K for the o-QWR and 80K for the d-QWR, and the former increases steeply and the latter gently. The luminescence of the d-QWR was observed to the temperature higher than that of the o-QWR, as ~240 and ~180K to each QWR. The carrier transfer from the d-SL to the d-QWR occurs gradually up to a higher temperature. These are interpreted in terms of the localization effects caused by disordering the atomic arrangement in a SL.[2,4]

The QWR PL integrated intensities are not much different at low temperature region, but the intensity of the d-QWR becomes stronger than that of the o-QWR in the high temperature region beyond 100K, as shown in Fig.3 (a log-linear scale). The QWR PL spectra at 160K are shown in Fig.4 where the d-QWR PL is about 7.5 times greater than the o-QWR PL. These are luminescence enhancement caused by disordered atomic arrangement. In the temperature region beyond 100K where the localization effects of the SL would not affect to the carrier recombination processes in the QWR. The carrier localization phenomena of the d-QWR have been verified also by the carrier recombination relaxation times.[7] Then, it is the first time to observe the carrier localization effects and the luminescence enhancement for the disordered quantum wires. The localization effects become greater with the larger band offset between the barriers and wells (or wires), as AlAs and GaAs, and AlP and GaP. They can be made further stronger by the interactions of the carrier wave functions along the lateral direction among wires.

In summary, the enhanced luminescence capability of the disordered quantum wires has been experimentally observed. They can be interpreted in terms of the localization effects caused by disordering atomic arrangement. This work is supported in part with the grant-in-aid #10450128 of the Ministry of Education, Science, Culture, and Sport of Japan and with the CREST of Japan Science and Technology Corporation of Japan.

Fig.1(a) TEM image of o-QWRSL

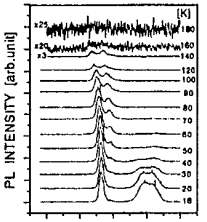

Fig.2(a) PL of o-QWRSL

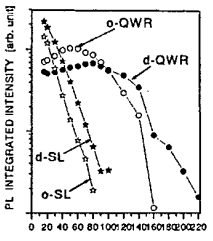

Fig.3 Temp. characteristcs. of PL

Fig.1(b) TEM image of d-QWRSL

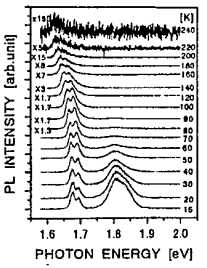

Fig.2(b) PL of d-QWRSL

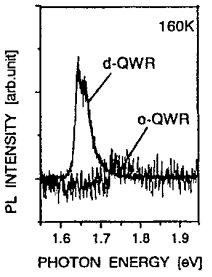

Fig.4 PL intensities of QWRs

References: [1]A.Sasaki, M.Kasu, T.Yamamoto, and S.Noda, *Jpn.J.Appl.Phys.*28, L1249 (1989). [2]K.Uno, S.Noda, and A.Sasaki, *J.Appl.Phys.*77,4693(1995). [3]A.Sasaki, X-L.Wang, and A.Wakahara, *Appl.Phys.Lett.*64, 2016 (1994). [4]K.A. Mäder, L.W.Wang, and A.Zunger, *Phys.Rev.Lett.*74, 2555(1995). [5]X-L.Wang, M.Ogura, and H.Matsuhata, *J.Cryst.Growth*, 171, 341(1997). [6]X-L.Wang, M.Ogura, and H.Matsuhata, *Appl.Phys.Lett.*66, 1506(1995). [7]X.Q.Liu, A.Sasaki, N.Ohno, X-L.Wang, and M.Ogura, *Phys.Rev.B*, (submitted).

High peak-to-valley ratio in resonant tunnelling through stacked InAs quantum dots

T. Bryllert, M. Borgstrom, T. Sass, B. Gustafson, L-E. Wernersson, W. Seifert, L. Samuelson
Solid state Physics, University of Lund, Box 118, S-221 00, Sweden

Resonant tunnelling diodes (RTD's) with an active structure consisting of stacks of self-assembled quantum dots have been fabricated. Exceptional I-V characteristics, where tunnelling through individual stack can be clearly resolved, have been measured. Peak-to-valley ratios as high as 85 were recorded at 4K.

Triple barrier systems based on quantum wells have been fabricated and investigated for quite some time, and in 1989 Reed et al [1] presented the first report on a structure with quasi zero-dimensional resonant states. This device was formed by etching a quantum well structure. Only recently the first results on RTD's based on stacked self-assembled quantum dots were reported [2,3]. Resonant tunnelling through zero-dimensional states is expected to have several advantages compared to ordinary RTD's, including: a sharp onset of current, small size and good high-temperature stability due to large energy difference between states. These features provide great potential for future applications both in electronics and photonics.

Our structure (fig 1) was grown by low pressure (50mbar) MOVPE. The active part consists of two layers of self-assembled InAs quantum dots embedded in InP that act as barrier material. Starting from the substrate side the growth was as follows: 5nm InP barrier, InAs QD's (on average 30nm in diameter 5nm in height), 15nm InP barrier, a second layer of QD's (on average 40nm in diameter 6nm in height), 12 nm inP barrier. The active region is surrounded by an undoped InGaAs buffer layer. The structure was characterized by transmission electron microscope (TEM). Details of the growth can be found elsewhere [2]. By taking advantage of the chemical reactions at the InP/InAs surface when forming the InAs dots, samples with a very low density of self-assembled dots could be produced. The low density, where only ~150 stacks are covered by a macroscopic contact, is vital to resolve tunnelling through individual stacks.

For resonant transfer of electrons to occur through the structure, the two zero-dimensional dot-states have to be aligned at the same time as electrons are available at the emitter-side of the active region. Due to the asymmetry of the device (the upper dot is slightly larger) this can be accomplished if a negative bias is applied to the top of the sample. Since the top barrier is much thinner than the middle, an electron will easily enter the upper dot, which will effectively act as a zero-dimensional emitter. This will further improve the properties of the device.
The I-V characteristics (fig 2) show the sharp resonance peak corresponding to tunnelling through a single stack of quantum dots. The narrow peak (FWHM 7mV) reflects the sharpness of the zero-dimensional emitter state and the resonant dot-state. An estimate of the voltage-to-energy conversion factor based on geometrical arguments and supported by photo luminescence measurements, suggests a width of the energy levels of ~1meV. The inset in the figure shows the I-V characteristics over a wide range of bias. Due to fluctuations in size of the quantum dots the resonant contribution to the current will occur at slightly different biases for different stacks. The main feature centred at a bias of 0.45V is the superposition of all these contributions, and can be thought of as the "energy equivalent" of the statistical size-distribution of the dots. When the bias is applied in the opposite direction, i.e. when the substrate side is negatively biased, the features are much less pronounced. This is an effect of the asymmetry of the structure. With the bias applied in this direction tunnelling through the ground states of the dots is not possible. The steps and peaks seen here are instead attributed to a combination of tunnelling through excited states and charging effects.

The temperature dependence of the I-V characteristics has been investigated (fig 3). The narrow peaks attributed to single stack tunnelling are smeared out with increasing temperature, however, the main feature associated with the statistical distribution is not effected seriously at a temperature of 50K, and a clear negative differential resistance is visible up to above 100K.

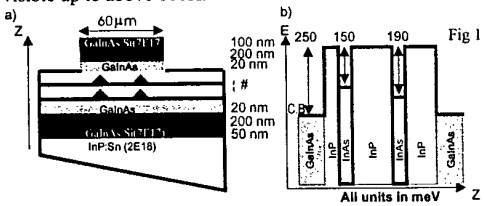

Fig 1 Schematic illustrations
a) The epitaxially grown structure after mesa etch: #5nm InP, 0,3ML InAs, 15nm InP, 0,3Ml InAs, 12nm InP
b) Corresponding ideal banddiagram

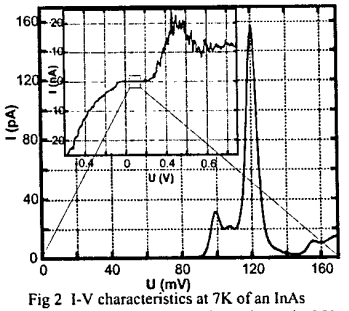

Fig 2 I-V characteristics at 7K of an InAs double dot stack, the inset shows the I-V characteristics for a wider range of bias

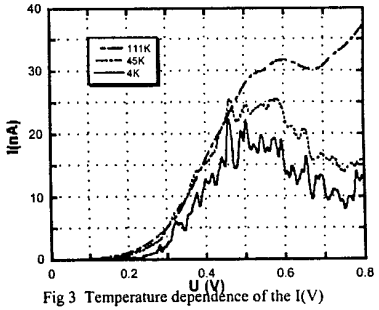

Fig 3 Temperature dependence of the I(V)

[1] M. A. Reed, J. N. Randall, J. H. Luscombe, W. R. Frensley, R. J. Aggarwal, R. J. Matyi, T. M. Moore, and A. E. Wetsel, Adv. Solid State Phys. **29**, 267 (1989).
[2] M. Borgstrom, T. Bryllert T. Sass, B. Gustafson, L-E. Wernersson, W. Seifert, L. Samuelson, submitted
[3] O. G. Schmidt, U. Denker, K. Eberl, O. Kienzle, F. Ernst, R. J. Haug, Appl. Phys. Lett. **77**, 4341 (2000)

Corresponding author: Tomas Bryllert, Solid State Physics, University of Lund, Box 118, S-221 00, Sweden Phone: +46 2228063, fax: +46 2223637, e-mail: Tomas.Bryllert@ftf.lth.se

Influence of the size of self-assembled InAs/AlAs quantum dots on photoluminescence and resonant tunneling

K. Pierz[1], Z. Ma[1], I. Hapke-Wurst[2], U. F. Keyser[2], U. Zeitler[2], R. J. Haug[2]

[1]Physikalisch-Technische Bundesanstalt, Bundesallee 100, 38116 Braunschweig, Germany
[2]Institut für Festkörperphysik, Universität Hannover, Appelstraße 2, 30167 Hannover, Germany

Self-assembled InAs quantum dots (QDs) embedded in an AlAs matrix are of increasing interest [1,2,3]. The smaller size and stronger confinement within the high band gap material AlAs instead of GaAs shift the photoluminescence (PL) energy of the QDs into the visible range and open up some potential for opto-electronic applications [4]. Compared to InAs/GaAs little is known about the growth, the properties and the electronic structure of the InAs/AlAs QD system. But nevertheless, this material system has been used for several years in nin-structures for investigations of resonant tunneling through zero-dimensional QD states [5-8]. In this study we have performed resonant tunneling experiments and PL spectroscopy on InAs/AlAs QD samples and we correlate the results with structural data of the QDs obtained by atomic force microscopy (AFM). We show that the onset voltage of single-electron tunneling as well as the PL energy can be tuned by the amount of deposited InAs and from the data an energy diagram for the InAs/AlAs QD system is derived.

InAs QDs were embedded in three different sample structures, all fabricated with molecular beam epitaxy. For AFM investigations the QDs were grown on 20 nm AlAs and for PL spectroscopy the QDs were cladded in 2×20 nm AlAs. The InAs QDs were grown under similar conditions (substrate temperature of 500°C, InAs rate of 0.05 ML/s) without substrate rotation in order to vary the InAs coverage across the wafer. The change of the RHEED pattern indicated the formation of QDs at 1.6 ML InAs. For vertical transport experiments the QDs were embedded symmetrically in a 10 nm AlAs barrier, 15 nm GaAs pre-wells and 1 μm n^+GaAs emitter and collector, respectively. The wet-chemically etched tunnel diodes of 40×40 μm^2 base length are equipped with standard AuGe contacts.

The AFM images show a high QD density of about 7×10^{11} cm^{-2} which is nearly constant for all InAs coverage. With an increasing supply of InAs the size of the QDs increases and the size distribution is getting smaller in agreement with ref. 2. For a coverage of 2.0 ML InAs the majority of the QDs reach their maximum size with a diameter of about 14 nm, before they coalesce and inelastically relax.

This increase of the QD size goes along with a continuous shift of the QD related emission peak from about 1.95 eV (wetting-layer) to 1.6 eV in the PL samples, see Fig.1. The PL spectra are measured at $T = 6$ K under cw-excitation (λ = 514 nm, P = 10 $mWcm^{-2}$) of an Ar^+ laser. This red shift is explained by a lower ground state energy in the larger QDs. The smallest linewidth (FWHM≈100 meV) and the highest quantum efficiency is obtained for the sample with large coherently strained QDs at high InAs coverage.

The *I-V* characteristics of the resonant tunnel diodes are plotted in Fig. 2 and we observe a shift of the curves to lower bias voltages for the diodes with large InAs coverage. At positive bias voltages (electron tunneling into the base of the QDs) steps in the *I-V* characteristics appear above a certain onset voltage U_{on} which we attribute to single-electron tunneling from the 3-d emitter into 0-d-states of the QDs [8,9]. Since with increasing voltage the Fermi level in the emitter shifts upwards it is reasonable to assume that the first steps are due to tunneling into the energetically lowest states of the large QDs. The onset voltage U_{on} is a function of the InAs coverage and we observe a gradual shift from about U_{on} = 0.3 V to nearly 0 V for the samples with 1.76 ML to 2.0 ML InAs, see inset of Fig. 2. This result is in good agreement with the AFM and PL data, that with increasing QD size the ground state energy is lowered and the difference to the Fermi energy in the emitter is reduced so that tunneling occur at lower bias voltage. Using an appropriate value for the lever arm we can estimate the electron levels of the QDs and the wetting-layer. Together with the PL results an energy diagram for the InAs/AlAs system is obtained.

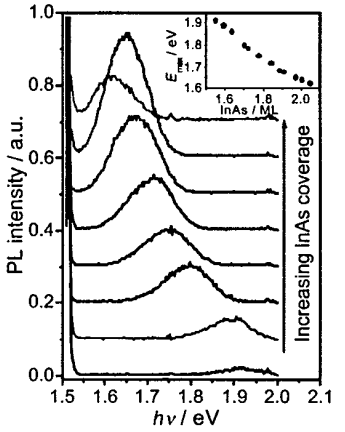

Fig. 1: PL spectra of InAs/AlAs QDs measured at T = 6 K for samples with different InAs coverage. The spectra have been shifted for clarity. The inset shows the dependence of the PL peak maximum E_{max} on the InAs coverage.

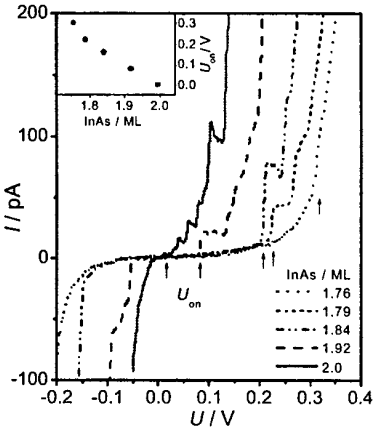

Fig. 2: *I-V* characteristics at T = 4.2 K of resonant tunnel diodes with InAs QDs grown with different InAs coverage. The arrows mark the onset of single-electron tunneling at U_{on}. The inset shows the dependence of U_{on} on the InAs coverage.

References

[1] U. H. Lee et al., Appl. Phys. Lett. 74, 1597 (1999).
[2] P. Ballet et al., Appl. Phys. Lett. 75, 337 (1999).
[3] K. Pierz et al., phys. stat. sol. B 224, (2001).
[4] K. Hinzer et al., Journ. of Appl. Phys. 87, 1496 (2000).
[5] I. E. Itskevich et al., Phys. Rev. B 54, 16401 (1996).
[6] T. Suzuki et al., Jpn. J. Appl. Phys. 36, 1917 (1997).
[7] M. Narihiro et al., Appl. Phys. Lett. 70, 105(1997).
[8] I. Hapke-Wurst et al., Semicond. Sci. Techn. 14, L41 (1999).
[9] I. Hapke-Wurst et al., Phys. Rev. B 62, 12621 (2000).

Corresponding author: Klaus Pierz, Physikalisch-Technische Bundesanstalt, Postfach 3345, 38023 Braunschweig, Germany.
phone: +49 531 592 2412, Fax: +49 531 592 2405
email: klaus.pierz@ptb.de

Resonant tunneling through a single self-assembled InAs quantum dots in a micro-RTD structure

I. Kamiya[1], Ichiro Tanaka[2,3], K. Tanaka[1], H. Sakaki[2]

[1]Research Center for Advanced Science and Technology, University of Tokyo,
4-6-1 Komaba, Meguro-ku, Tokyo 153-8904, JAPAN
[2]Institute of Industrial Science, University of Tokyo,
7-22-1 Roppongi, Minato-ku, Tokyo 106-8558, JAPAN
[3]Department of Materials Science and Chemistry, Wakayama University,
930 Sakaedani, Wakayama 640-8510, JAPAN

Self-assembled (SA) quantum dots (QDs) have been one of the interesting research targets because nano-scale dots are easily formed by growth of lattice mismatched epitaxy [1]. In particular, the electronic and optical properties of InAs SA QDs grown on the (001)GaAs substrates have been intensively studied during the last decade. Recently, scanning probe techneques have been applied to the investigation of individual InAs SA QDs in order to reveal the unique properties of the QDs [2].

Here, we performed transport study on single QDs embedded in a thin undoped GaAs layer by atomic force microscopy (AFM) with a conductive tip. We have already reported that the size and density of InAs SA QDs on (001)GaAs prepared by molecular beam epitaxy (MBE) can be controlled in a wide range through precise adjustment of the growth conditions [3], and we have established a recipe to routinely prepare InAs SA QDs whose density is in the low $10^8/cm^2$. With this recipe, we fabricated micron-size resonant tunneling diode (μ-RTD) structures where the low density QDs are sandwiched between thin GaAs barriers. As shown in Fig. 1, an n^+-GaAs buffer layer, a 20 nm undoped GaAs layer, low density InAs SA QDs, and a 10 nm undoped GaAs cap layer were succesively grown on an n^+-(001)GaAs substrate. After coating with a NiCr/Au film, it was patterned into microstructures of 0.5, 1, or 2 μm square by electron-beam lithography and wet chemical etching. These μ-RTD structures were then placed into a vacuum chamber where current-voltage (I-V) measurements were performed by conductive AFM at ~130 K.

The effective number of the QDs in the μ-RTDs was estimated in the following way. Since the off-resonant thermal current should be proportional to the active area of the device, by comparing the thermal currents from μ-RTDs of different sizes, we estimated that the area within 0.17 μm from the side-wall is depleted. Hence, the effective area of the 0.5 μm square device becomes 0.16 μm square, i.e., 0.03 μm^2. The density of QDs has been measured to be 4 μm^{-2}, therefore, the average number of the dots contained in the area is about 0.12, i.e., we expect either one or no dot in each 0.5 μm square μ-RTD.

The I-V curves obtained from the 0.5 μm square μ-RTD are shown in Fig. 2. The four I-V curves, which are averages of ten voltage sweeps, are obtained by bringing the conductive tip in contact with four different points on the micro electrode. Here, applying a negative sample bias voltage corresponds to a forward bias condition. In Fig. 2, the resonant tunneling currents superimposed on the thermal currents exhibit a peak between Vs = - 0.49 V, and Vs = -0.54 V. We attribute this rather broad peak to two main factors which affect the resonant tunneling current: i.e., (1) high temperature, and (2) lowering of the barrier height with increasing bias voltage. The measurements in this study were performed at about 130 K, which implies 10-20 meV energy distribution at the Fermi level of the emitter electrode. The lowered barrier height increases the tunneling probability, which results in broadening of the tunneling current peak.

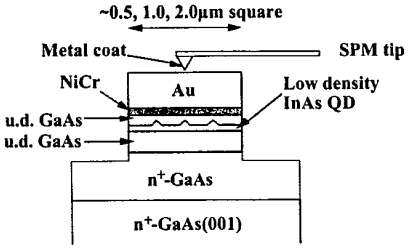

Fig. 1: A schematic diagram of the μ-RTD structure and the experimental setup.

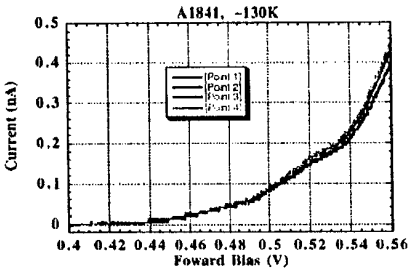

Fig. 2: I-V curves of the μ-RTD obtained at ~130 K.

References

[1] D. Leonard, M. Krishnamurthy, C. M. Reaves, S. P. DenBaars, and P. M. Petroff, Appl. Phys. Lett. **63**, 3203 (1993).

[2] M. E. Rubin, G. Medeiros-Ribeiro, J. J. O'Shea, M. A. Chin, E. Y. Lee, P. M. Petroff, and V. Narayanamurti, Phys. Rev. Lett. **77**, 5268 (1996); I.Tanaka, I. Kamiya, H. Sakaki, N. Qureshi, S. J. Allen, and P. M. Petoff, Appl. Phys. Lett. **74**, 844 (1999)

[3] I. Kamiya, I. Tanaka, and H. Sakaki, J. Cryst. Growth **201/202**, 1146 (1999).

Corresponding author (Present address): Itaru Kamiya,
Non-Equilibrium Laboratory, Mitsubishi Chemical Corporation,
1000 Kamoshida-cho, Aoba-ku, Yokohama 227-8502, JAPAN,
Phone:+81-45-963-4365, Fax:+81-45-963-4366,
e-mail: ikamiya@rc.m-kagaku.co.jp

Anomalous diamagnetic shift of excitons in II-VI quantum dots and in indirect short period superlattices

N. Miura[1], T. Yasuhira[1], K. Uchida[1], E. Kurtz[2], C. Klingshirn[2], H. Nakashima[3], F. Issiki[4], Y. Shiraki[4]

[1] Institute for Solid State Physics, University of Tokyo, Kashiwanoha, Kashiwa, Chiba, Japan
[2] Institut fuer Angewandte Physik, Universitaet Karlsruhe, D-76128 Karlsruhe, Germany
[3]Institute of Scientific and Industrial Research, Osaka University, Ibaraki, Osaka, Japan
[4]Research Center for Advanced Science and Technology (RCAST), University of Tokyo, Komaba, Meguroku, Tokyo, Japan

We have observed anomalous diamagnetic shift of excitons in the photoluminescence from CdSe/ZnSe quantum dots; the diamagnetic shift is towards the lower energy (red shift) and the luminescence intensity decreases with increasing field for relatively small dot diameter of about 5nm. This is completely opposite to the magnetic field effect on excitons in usual cases as for III-V quantum dots [1]. Since the anomalous effect was observed in different samples from both Karlsruhe and Osaka, it is considered to be a general property of small quantum dots of CdSe/ZnSe. For larger quantum dots of about 10nm in diameter, the diamagnetic shift is a blue shift as in the normal case. However, the wave-function extension estimated from the shift is not so much different from that in bulk CdSe. The anomalous behavior of excitons in magnetic fields is similar to the case for excitons in GaP/AlP short period superlattices where the exciton peak shows a prominent decrease in intensity when the field is applied perpendicular to the layers [2]. Both of these effects are explained by a model assuming shrinkage of exciton wave function consisting of spatially separated electrons and holes. Namely, in CdSe quantum dots, as there are many dots with different sizes, exciton energy is distributed in a wide range of spectrum, and the excitons would relax to low energy sites. While electrons are well confined inside the dots, the hole confinement is relatively weak since the valence band offset is small in II-VI quantum interfaces. The large strain effect in the vicinity of the dots would cause localization of holes in the area around the dots off the center. If the electrons and holes composing the excitons are spatially separated, the shrinkage of the wave-function extension of electrons and holes by magnetic field would cause a decrease in their overlap, and thus it would result in the decrease of the intensity and the prolongation of the recombination time that leads to the red shift. A very similar model can be applied to GaP/AlP short period superlattices. The localized nature of the excitons is the reason of the intense photoemission from the indirect gap superlattices.

References

[1] R. K. Hayden, K. Uchida, N. Miura, A. Polimeni, S. T. Stoddart, M. Henini, L. Eaves and P. C. Main, Physica B **246-247**, 93 (1998).
[2] K. Uchida, N. Miura, T. Sugita, F. Issiki, N. Usami and Y. Shiraki, Physica B **249-251**, 909 (1998).

Corresponding author: Noboru Miura,
Institute for Solid State Physics, University of Tokyo
5-1-5 Kashiwanoha, Kashiwa, Chiba 277-8581, Japan
phone: +81 471 36 3341, Fax.: +81 471 36 3335
e-mail: miura@issp.u-tokyo.ac.jp phone:

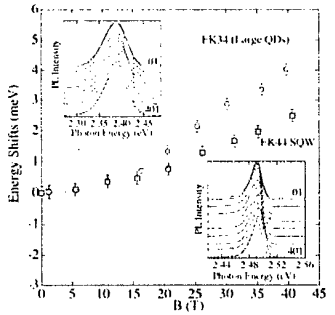

Fig. 1 Magneto-photoluminescence spectra (insets) and the diamagnetic shift of excitons in CdSe/ZnSe quantum dots of large size (EK34, 10nm) and a single quantum well (EK44). (The Faraday configuration.)

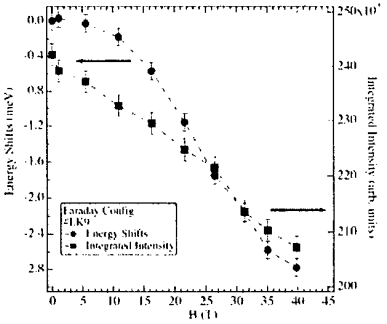

Fig. 2 Energy shift and the intensity of the exciton peak for small quantum dots (EK9, 5nm) as a function of magnetic field. The magnetic field effects are opposite to the usual case. (The Faraday configuration.)

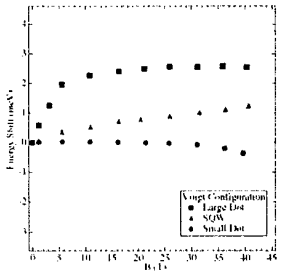

Fig. 3 Energy shift of the exciton peak as function of magnetic field for the large dots (EK9), the small dots (EK34) and the single quantum well (EK44) for the Voigt configuration.

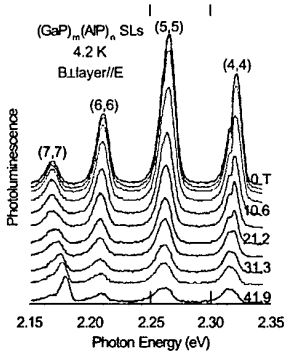

Fig. 4 Magneto-photoluminescence spectra of excitons in $(GaP)_m/(AlP)_n$ short period superlattices ((m,n) = (7,7), (6,6), (5,5), (4,4)). As the field is increased both the energy and the intensity are decreased.

Interplay of surface charges and excitons localized in CdSe/ZnSe quantum dots

V. Türck, S. Rodt, R. Heitz, O. Stier, M. Straßburg, U. W. Pohl, D. Bimberg

Institut für Festkörperphysik, Technische Universität Berlin, Hardenbergstraße 36, D-10623 Berlin, Germany

In recent years single-dot spectroscopy has evolved as an important tool in the investigation of semiconductor quantum dots (QDs). The study of epitaxially grown CdSe/ZnSe QDs revealed e. g. the fine-structure of the QD-exciton [1] as well as many particle QD-states [2]. In colloidal CdSe QDs [3] as well as in epitaxially grown CdSe QDs in ZnSe matrix [4] spectral diffusion is a commonly observed effect. It is attributed to a quantum-confined Stark-effect (QCSE) induced by random fluctuations of local electric fields.

Although spectral diffusion can prevent the determination of the homogeneous linewith of individual emission lines it allows the unambiguous identification of the emission spectrum of a single QD. Figure 1 shows the emission spectrum of a single CdSe QD embedded in ZnSe matrix, measured using cathodoluminescence (CL). The emission of the radiative decay of various excitonic and multi-excitonic states such as the exciton (X) and biexciton (XX) as well as the negatively charged trion (X^-) and biexciton (XX^-) are observed. Both, the exciton and the biexciton emission exhibit a doublet structure which is caused by the splitting of the bright exciton state. The temporal evolution of the QD emission spectrum (Fig. 1, lower panel) shows the variation of the emission wavelength due to spectral diffusion. All emission lines of a single QD exhibit *exactly the same* temporal evolution.

We have investigated a series of CdSe/ZnSe QD structures grown by metalorganic chemical vapour phase epitaxy. The samples have nominally identical QD layers and differ only by the thickness of the cap layer covering the QDs. CL measurements of these samples show that the strength of the spectral diffusion is determined by the thickness of the cap layer. While samples with 20 nm cap thickness show a well pronounced spectral diffusion a clear decrease of the diffusion is observed in samples having 50 nm cap thickness. Samples covered with 80 nm cap material exhibit almost no spectral diffusion.

A statistical evaluation of the variation of the emission energies shows that the underlying QCSE is a linear effect. The observation of identical spectral diffusion patterns shows that the excitonic and multi-excitonic states of a single QD exhibit a permanent electric dipole moment. The fluctuating electric field that induces the spectral diffusion must be oriented parallel to the electric dipole moment. This is the case only if the electric field is generated by charges located at the surface of the sample. Thus the strength of spectral diffusion depends strongly on the thickness of the cap layer on top of the QDs. The experimental results clearly demonstrate that the commonly assumed connection between spectral diffusion and a local density of randomly distributed traps is incorrect and that the interaction between excitons and surface charges is by means of a linear QCSE.

Oriented electric dipole moments which are necessary for such type of QCSE have previously been observed in III-V In(Ga)As QDs [5]. In this particular case the existence of an electric dipole moment is the consequence of the pyramidal shape of the QDs. In the CdSe/ZnSe QDs investigated in the present study the observation of a permanent electric dipole moment has an implication for the geometrical shape of the QDs.

We compare the experimental observations with the results of extensive numerical calculations of the electronic structure of the investigated CdSe/ZnSe QDs. The calculations are based on the 8-band **k·p**-method. The interplay of the geometrical shape and the electronic properties of the investigated CdSe/ZnSe QDs is discussed.

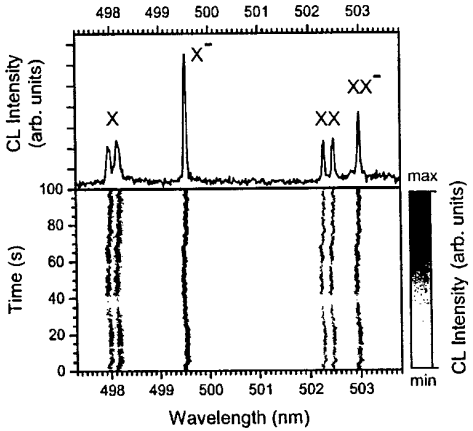

Fig. 1: Upper panel: emission spectrum of a single CdSe quantum dot, the emission lines from the radiative decay of the exciton, negative trion, biexciton and negatively charged biexciton are denoted as X, X^-, XX and XX^-, respectively. Lower panel: temporal evolution of the same emission spectrum over a time of 100 seconds. The variation of the wavelengths of the emission lines shows the influence of spectral diffusion.

References

[1] V. D. Kulakovskii et al., Phys. Rev. Lett. **82**, 1780 (1999).
[2] V. Türck et al., phys. stat. sol. (b) **224**, 217 (2001).
[3] S. A.Empedocles et al., Phys. Rev. Lett. **77**, 3873 (1996).
[4] V. Türck et al., J. Lumin. **87 - 89**, 337 (2000).
[5] P. W. Fry et al., Phys. Rev. Lett. **84**, 733 (2000).

Corresponding author: Volker Türck, Institut für Festkörperhysik, Technische Universität Berlin, Hardenbergstraße 36, D-10623 Berlin, Germany.
phone: +49 30 - 314 22 184, Fax: +49 30 - 314 22 569
email: tuerck@physik.tu-berlin.de

Excitons, biexcitons and charged excitons in CdTe single quantum dots

L. Besombes[1], K. Kheng[1], L. Marsal[2], H. Mariette[2]

[1] Département de Recherche Fondamentale sur la Matière Condensée / SP2M, CEA Grenoble, 17 avenue des Martyrs, 38054 Grenoble cedex 9, France.
[2] Laboratoire de Spectrométrie Physique, Université J.Fourier , B.P. 87, 38402 Saint Martin d'Hères Cedex, France

Spatially resolved spectroscopy is a powerful technique for studying the optical properties of a single quantum dot. By reducing the probed area of the sample, just a few quantum dots can be probed and a small number of sharp lines are observed in the emission spectra. However much care is needed to assign lines to the same dot.

By mean of micro-photoluminescence spectroscopy, we have studied CdTe zero-dimensional structures formed in ZnTe matrix. The exciton, biexciton and charged exciton in a single dot are identified in the emission spectra. We report the study of the binding energy of the biexciton and of the charged exciton in a single quantum dot as a function of an external electric field.

The investigated samples consist of 6 monolayers of CdTe grown by atomic layer epitaxy on ZnTe barriers and ZnTe substrates. Compositional analysis of Transmission Electron Microscopy images shows the presence of CdTe rich regions that can confine excitonic complexes. Charged dots are obtained by doping the barriers (modulation doping) with aluminum donor impurities. At low temperature (4K), the donors are ionized and their electrons are transferred to the dots. The single dots are investigated through sub-micron apertures in an opaque 100 nm thick Al film deposited onto the samples.

The biexciton emission line X_2 appears a few meV below the exciton line when the excitation density is increased. Its emission intensity increases quadratically at low excitation power. A distribution of the biexciton binding energy is found (9-14 meV) with a maximum of the distribution around 13 meV. In asymmetric quantum dots, the electron-hole exchange interaction splits the heavy-hole exciton line X into a doublet structure linearly polarized at zero-magnetic field and circularly polarized at high magnetic field. As a consequence of the existence of a unique biexciton state, the biexciton transition reproduces the exciton fine structure in a reverse order [1].

In modulation doped samples, a third line is observed between the exciton and the biexciton line (Fig. 1). Moreover the lines position fluctuates with time. The time-scale of the fluctuation can be as low as 0.5 s (our integration time) and periods of 60-70s can be found where the lines position is stable.

We attribute this effect to the presence of photo-generated charges trapped in the vicinity of the dot. These fluctuating charges create an electric field that caused a random Stark shift of each sharp emission line [2]. We found that, although the line shift is random, the shift of the three line is totally correlated (Fig. 2). This allows us to attribute the new line to the charged exciton X^- confined in the same dot. Moreover the emission intensity of line X^- decreases when that of line X increases and *vice versa*. This is accounted for by the fact that during the integration time, the dot has a certain probability to be charged or to be neutral.

The amplitude of the Stark shift is about two time smaller for the biexciton than for the exciton. The analysis of the line separation shows that (i) the binding energy of the exciton and that of the charged exciton both decrease with the electric field intensity (ii) the charged exciton binding energy decreases twice as fast as than that of the biexciton.

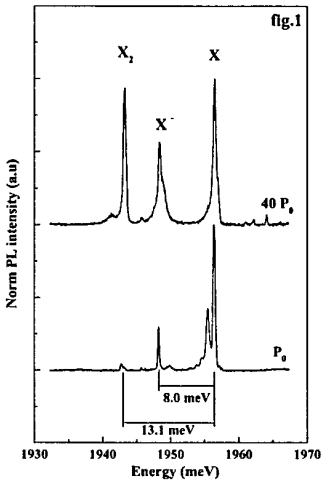

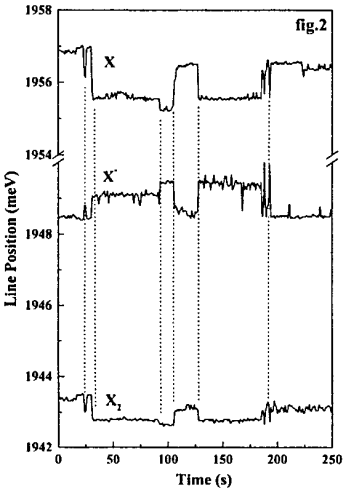

Fig. 1: Emission spectra of a single CdTe quantum dot for two different excitation densities (P_0 is about 5 $W.cm^{-2}$). The biexciton line X_2 appears 13.1 meV below the heavy-hole exciton line X when the excitation density is increased. The CdTe/ZnTe structure is doped in the barriers with aluminum donor impurities. The charged exciton line X^- is observed between these two lines.

Fig. 2: Emission energy of the exciton X, the charged exciton X^- and the biexciton X_2 as a function of time. The integration time is 0.5 s. Though the three emission lines shift randomly with time, their shifts are totally correlated.

References

[1] L.Besombes, K.Kheng, D. Martrou, Phys. Rev. Lett. 85, 425 (2000)
[2] H. D. Robinson and B. B. Goldberg, Phys. Rev. B 61, R5086 (2000)

Corresponding author: Kuntheak Kheng, Département de Recherche Fondamentale sur la Matière Condensée / SP2M, CEA Grenoble, 17 avenue des Martyrs, 38054 Grenoble cedex 9, France.
phone: +33 476 88 47 01, Fax: +33 476 88 51 97
email: kkheng@cea.fr

Growth simulation of GaAs/AlGaAs quantum dot grown in tetrahedral-shaped recesses on GaAs (111)B substrate

Tomoko Tsujikawa-Yutani[1], Mutsuo Ogura[2] and Hiroyuki Yaguchi[3]
[1]Osaka National Research Institute, AIST
3-8-1 Midorigaoka, Ikeda, Osaka 563-8577, JAPAN
Phone : +81-727-51-9655, Fax : +81-727-51-9637
E-mail : yutani@onri.go.jp
[2]Electrotechnical Laboratory, AIST, JAPAN
[3]Department of Electrical and Electronic Systems, Saitama University, JAPAN

Fabrication of semiconductor quantum dots has been intensively studied both for studies of low-dimensional physics and applications to novel devices.

We have studied the growth features of GaAs/AlGaAs quantum dot structures grown on tetrahedral-shaped recesses (TSRs) on GaAs (111)B substrates.[1,2] By μ-PL spectroscopy and cathodoluminescence observation, we confirmed that the quantum dot was formed at the bottom of the TSR only if the trench-like AlGaAs region was formed at the bottom of the TSR before the growth of GaAs well layer. [3] For the growth of AlGaAs layer, the differences in growth rates at each facet and the surface migration length between Ga and Al adatoms are very important because they determine the shapes of facets and the Al composition at each facet which may cause to self-limiting effect of the size of quantum structures or spontaneous vertical quantum well.[4] However, the mechanism of the trench-like AlGaAs formation is not clearly understood.

In this study we calculated the growth profile of GaAs/AlGaAs layer in the TSR by iterative method with Ohtsuka's model. [5,6] Ohtsuka's model takes into account the kinetic processes of adatoms : (i) incorporation, (ii) desorption and (iii) surface migration. The actual growth rate modulated by the flow of surface migration from adjacent facets at any positions were simulated by giving the desorption time of adatoms, the growth rate and the surface migration length and on each planer plane. The growth rate of $Al_xGa_{1-x}As$ layer R_{AlGaAs} was given by the growth rate of GaAs R_{GaAs} and that of AlAs R_{AlGaAs} as $R_{AlGaAs} = (1-x)R_{GaAs} + xR_{AlAs}$. We used the experimental data of the Al composition and the growth rates at each plane given in ref. 4.

Figure 1 shows the SEM images of the GaAs/AlGaAs multilayers grown in the TSR. The GaAs layer formed at the bottom (111) region was thicker than those formed at the {111} sidewall, {001} edge regions. The {112} and {11$\bar{2}$} vertical regions were thinner than either sidewall or edge region. Figure 2 shows the calculated profile of the GaAs/AlGaAs layers. As the growth proceeds, trench-like region was formed on the bottom of the TSR. For GaAs layer, the bottom region is thicker than surrounded regions and vertical region were thinner than either sidewall or edge regions. The experimental result is well reproduced in the simulation. The formation of trench-like region of AlGaAs layer is explained as follows: the growth rate of (111)B plane is faster than vertical {112} and {11$\bar{2}$} planes for GaAs growth, whereas that of (111)B plane is slower than vertical {112} and {11$\bar{2}$} planes for AlAs growth. The profile of GaAs/AlGaAs quantum wires grown in the V-groove will be presented based on this model as well as GaAs/AlGaAs quantum dots in the TSR.

References

[1]T. Tsujikawa, K. Momma, H. Yaguchi, K. Onabe, Y. Shiraki, and R. Ito, Jpn. J. Appl. Phys. **37,** 1493 (1998)
[2]T. Tsujikawa, T. Irisawa, H. Yaguchi, K. Onabe, Y. Shiraki, and R. Ito, Jpn. J. Appl. Phys. **38,** 469 (1999)
[3]T. Tsujikawa, S. Mori, H. Watanabe, M. Yoshita, H. Akiyama, R. van Dalen, K. Onabe, H. Yaguchi, Y. Shiraki, and R. Ito, Physica E **7,** 308 (2000)
[4]G. Biasiol, F. Reinhardt, A. Gustafsson, and E. Kapon, Appl. Phys. Lett. **71,** 1831 (1997)
[5]M. Ohtsuka and A. Suzuki, J. Cryst. Growth **95,** 55 (1989)
[6]M. Ohtsuka and S. Miyazawa, J. Appl. Phys. **64,** 3522 (1988)

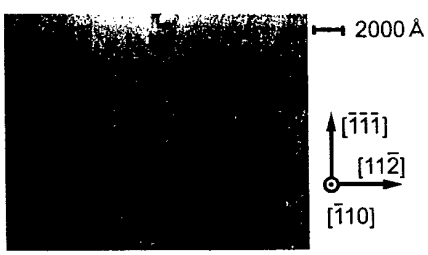

Fig.1 SEM image of the GaAs/AlGaAs multilayers grown in the TSR.

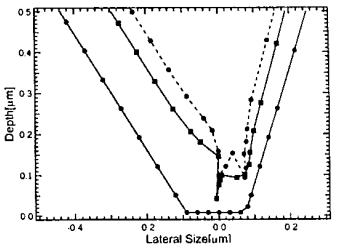

Fig. 2 Growth profile of the GaAs/AlGaAs layers in the TSR. Circle and solid line is the TSR, circle and dotted line is the profile of GaAs layer, and square and solid line is the profile of AlGaAs layer.

State-filling and renormalization in charged InGaAs/GaAs quantum dots

R. Heitz, F. Guffarth, C. M. A. Kapteyn, F. Heinrichsdorff, D. Bimberg

Institut für Festkörperphysik, TU-Berlin, Sekr. PN 5-2, Hardenbergstr. 36, D-10623 Berlin, Germany

The electronic properties of self-organized quantum dots (QDs) are affected by the presence of spectator electrons due to many-particle interactions. Such charging might be provided intentionally by doping, e.g., for inter-sublevel detectors or in a tunable space-charge region of a memory structure, as well as randomly under electrical or optical excitation. Coulomb charging of QDs has been investigated by capacitance spectroscopy [1], whereas the renormalization of interband transitions in charged QDs has been studied in transmission [2] and single-dot experiments [3]. The presence of spectator charges leads to a saturation of transitions and renormalizes transition energies. The transmission experiments are limited by the inhomogeneous broadening, masking the details of the excited state transition spectrum of self-organized QDs [4,5], and the single-dot experiments are limited to the ground-state transition yet.

Here we report on a size-selective study of excited state transitions in charged InGaAs/GaAs by photoluminescence excitation spectroscopy (PLE), providing insight into the complex effects of state-filling and renormalization on the exciton fine structure and the excitation processes in the presence of spectator electrons. The InGaAs/GaAs QDs were grown by metalorganic chemical vapor deposition on semi-insulating GaAs(001). The QDs were embedded in a low (~10^{16}cm^{-3}) n-doped region near the space-charge region of a pn-diode-structure with two front-side contacts. Capacitance spectroscopy shows that the charge state of the QDs can be tuned applying a reverse bias: Below ~-6.5 V the QDs are neutral and start to charge reducing the reverse bias. The number of spectator electrons is limited by Coulomb charging to ~10.

Though the charge state of the QDs has only limited effect on the low-temperature PL centered at 1.024eV with a full width at half maximum of ~50meV, the excitation behavior is strongly affected. The spectator electrons quench excitation channels due to state filling and renormalize transition energies. Figure 1 shows a typical contour plot of the PL intensity as a function of the applied bias (i.e. the charge state) and the excitation energy at a sample temperature of 77K. As shown in Figure 2 the evolution of the intensity and energy of the excitation resonances is rather complex and characteristic for each excited exciton transition. The most pronounced effects occur when the ground state is populated with spectator electrons (-6.5V<V_{bias}<-5.5V). Phonon-assisted ground state absorption at ~35meV vanishes and the excited state transitions show a strong low energy shift by up to 16meV. Further charging of the QDs bleaches the components of the first excited state transition, whereas those of the second one remain some intensity even when the QDs are outside of the space-charge region. Bend-bending due to Coulomb charging prevents complete saturation of the QDs. Furthermore, investigations of the temperature dependence of the PLE and, in particular, of the PL spectra provide information on field dependent carrier capture and escape in the space charge region, the thermal hole distribution in the QDs and 'forbidden' exciton transitions.

The results are discussed in view of the complex electronic properties of low-symmetry and strained self-organized QDs, [4,5] allowing for the identification of excited state transitions and providing insight into the many-particle effects, leading to a complex renormalization pattern.

References

[1] B. T. Miller, W. Hansen, S. Manus, R. J. Luyken, A. Lorke, and J. P. Kotthaus, Phys. Rev. B **56**, 6764 (1997).
[2] R. J. Warburton, C. S. Dürr, K. Karrai, J. P. Kotthaus, G. Medeiros-Ribeiro, and P. M. Petroff, Phys. Rev. Lett. **79**, 5282 (1997).
[3] R. J. Warburton, C. Schäflein, D. Haft, F. Bickel, A. Lorke, K. Karrai, J. M. Garcia, W. Schoenfeld, and P. M. Petroff, Nature 405, 926 (2000).
[4] O. Stier, M. Grundmann, and D. Bimberg, Phys. Rev. B **59**, 5688 (1999).
[5] R. Heitz, O. Stier, I. Mukhametzhanov, A. Madhukar, and D. Bimberg, Phys. Rev. B **62**, 11017 (2000).

Corresponding author: Florian Guffarth, Institut für Festkörperhysik, TU Berlin, Hardenbergstr. 36, D-10623 Berlin, Germany.
phone: +49 30 314 22074, Fax: +49 30 314 22569
email: florian@sol.physik.tu-berlin.de

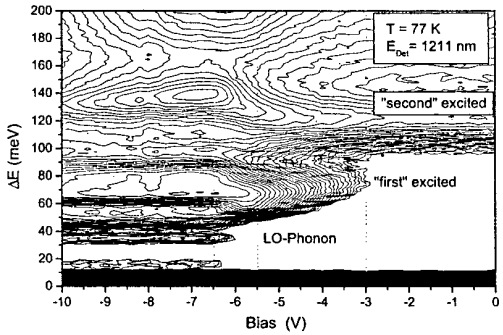

Fig. 1: Contour-plot of the PL intensity as a function of the applied bias voltage and the excitation energy. ΔE, the excess energy, is the difference between the excitation energy and the detection energy. The intensity is plotted on a logarithmic scale.

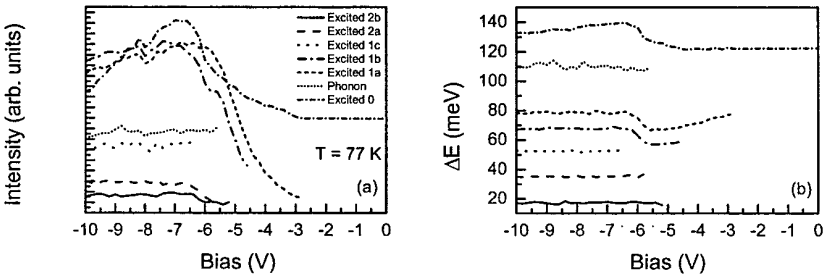

Fig. 2: (a) Intensity and (b) energy dependence of the various excitation resonances shown in Fig. 1.

A combined investigation of lateral and vertical Stark effect in InAs self-assembled quantum dots in waveguide structures

O. Wolst, M. Schardt, S. Malzer, and G. H. Döhler,

Institut für Technische Physik I , Friedrich-Alexander Universität Erlangen,
Erwin-Rommel-Str. 1, D-91058 Erlangen, Germany

Gaining detailed knowledge of the confining potential in self-assembled InAs quantum dots (SADs) is a tedious task, as the geometrical form, the strain distribution, and the intermixing of In and Ga have strong influence on the electronic structure. At present most of our information on the electronic structure of SADs stems from photoluminescence (PL) and capacitance spectroscopy. Both, in PL and CV experiments many-body effects significantly influence the energies deduced from these studies. On the other side, direct absorption experiments on SADs, which should reflect the single exciton absorption spectra, are difficult to perform due to the relatively weak absorption. This difficulty has been overcome recently in an elegant way by using photo-current spectroscopy [1]. In this contribution, we report on a different approach, which, in addition, provides much new information, particularly on the confining potential. We are using GaAs/AlGaAs waveguide structures with a SAD layer at its center. This way we can (1) compensate for the low absorption coefficient by having a long interaction length (in the range of mm). (2) we can measure directly the absorption spectra without being limited by the requirement that the photo-generated carriers have to escape from the dots. (3) we can study not only absorption of light with in-plane polarization (TE) but also with polarization in growth direction (TM; thus probing light-hole states). (4) we are able to perform electro-absorption measurements not only with an electric field in growth direction („vertical Stark effect" [1]), but also with in-plane electric field („lateral Stark effect"). In the latter case we have a new and very powerful tool to test not only the energetic Stark shift, but also the effect of the field-induced real-space in-plane shift of the electron and hole states against each other, resulting in drastic changes of the selection rules and the corresponding oscillator strengths. For the investigation of the vertical Stark effect we have used p-i-n waveguide structures (Fig. 1(a)). To apply strong in-plane electric fields, narrow (undoped) waveguide structures were fabricated (Fig. 2(a)). To achieve a homogeneous field distribution in the waveguide, a bottom and top semi-insulating low-temperature-grown AlGaAs („LT-AlGaAs") layer was included in the structure. Thus, due to midgap Fermi level pinning the potential drop between the left and right Schottky contacts becomes linear. Both kinds of devices show excellent electrical behavior with low dark currents. A thorough investigation of the PL, EL, photo-current, and transmission spectra as a function of electric field and light polarization has been performed. Fig.s 1 and 2 (b)-(d) demonstrate the rich information evolving from these experiments. In Fig. 1(b) the zero bias TE- and TM-transmission spectra of the sample with dots and a reference sample without dots are compared. TE- and TM-electro-absorption spectra for this sample are depicted in Fig. 1(d) and (c). The drastically different effect of a lateral electric field becomes apparent in Fig. 2 (b) (with increasing lateral field transmission at energies corresponding to (1,1)-, ..., (4,4)- transitions *increases* due to decreasing oscillator strength, e.g.) and Fig. 2 (c) - (d) (electromodulation signal strongly decreases at high fields as (v,v)- selection rule breaks down, e.g.).

Fig. 1

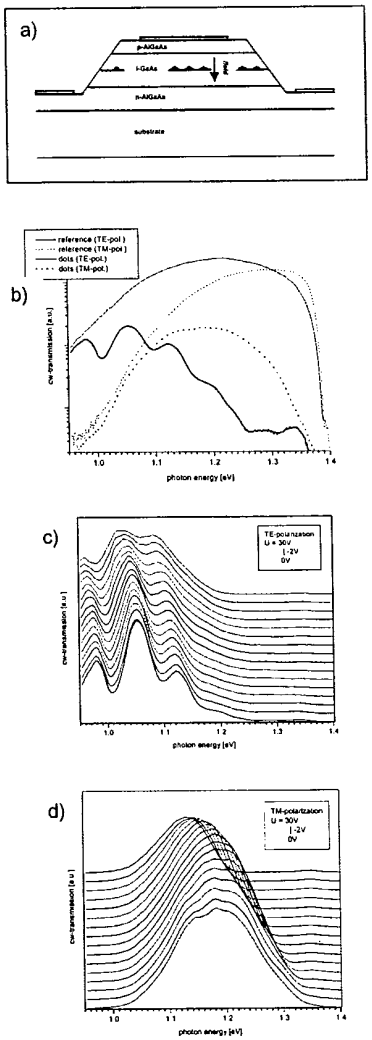

Fig. 2

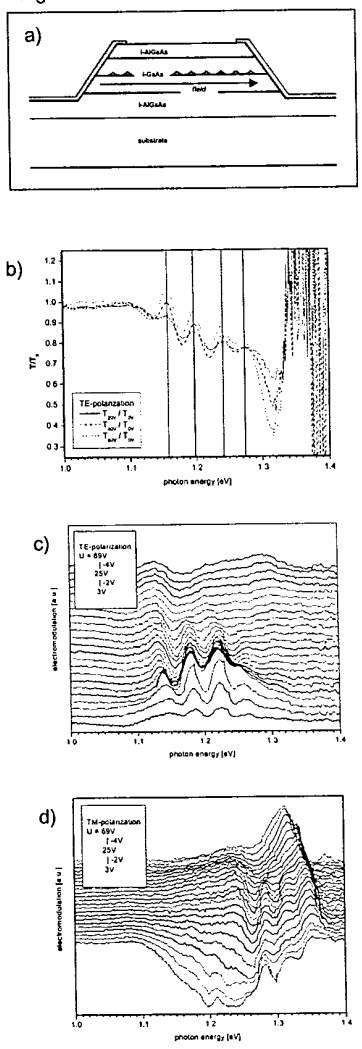

References:

[1] P.W.Fry et al., PRB62(24),16784-16791 (2000)

Corresponding author: Oliver Wolst, Institut für Technische Physik, Friedrich-Alexander-Universität Erlangen, Erwin-Rommel-Str. 1, D-91058 Erlangen, Germany.
phone: +49 9131 85 27254, Fax: +49 9131 85 7293
email: oliver@wolst.de,

Optical properties of wetting layers in stacked InAs/GaAs quantum dot structures: strain effects and electronic coupling

A.T. Winzer[1], R. Goldhahn[1], G. Gobsch[1], H. Heidemeyer[2], O.G. Schmidt[2], K. Eberl[2]

[1]Institut für Physik, Technische Universität Ilmenau, PF 100565, 98684 Ilmenau, Germany
[2]Max-Planck-Institut für Festkörperforschung, Heisenbergstraße 1, 70569 Stuttgart, Germany

The structural and therefore electronic and optical properties of self-assembled quantum dot (QD) multilayer structures are strongly influenced by strain fields during deposition. The strain fields of underlying islands create a strain energy modulation at the spacer surface, and induce stacks of vertically aligned QDs. Moreover, strain induced material intermixing was observed for stacks of Ge QDs in Si [1] and InAs QDs in GaAs [2]. Applying transmission electron microscopy (TEM) to the Ge/Si system it was demonstrated that the strain field of the initial Ge island layer causes a reduction of the wetting layer (WL) thickness of the upper layers resulting in an energy shift of the WL related optical transitions [3]. To our knowledge, no similar observations have been made for III-V self-assembling systems so far.

We present for the first time a systematic study of optical properties of WLs for two-fold stacked InAs QDs as a function of GaAs spacer thickness d_{Sp}. WL transition energies are deduced from photoluminescence (PL), PL excitation (PLE), and photoreflectance (PR) spectroscopy. In combination with anodic oxidation for well controlled layer removal unambiguous assignment of the optical transitions to the lower and upper WL becomes possible. We will prove that strain field interaction does not only induce QD material intermixing [2] but also WL thickness reduction in the upper layers. Samples with spacer layers thin enough show strong electronic coupling between the WLs in addition.

The samples were fabricated using solid source molecular beam epitaxy. Each stacked sample consists of two WLs (WL1 and WL2 from bottom to top) and the accompanying dot layers (QD1 and QD2). They were formed by depositing 2 monolayers (ML) of InAs with a growth rate of 0.01ML/s at a substrate temperature of 500 °C. WL1 and WL2 are separated by GaAs spacers of d_{Sp}=20, 15, 10, and 3 nm thickness, respectively. The stacks are covered by a 100 nm thick capping layer. A reference sample containing only a single dot layer was grown under identical conditions. TEM studies of all two-fold stacked samples revealed vertical alignment of QD1 and QD2 which clearly proves the existence of strain field modulation at the surface when the upper 2MLs of InAs were grown.

The formation of an InAs WL in a GaAs matrix produces a confining potential on the length scale of about 1ML, which introduces bound electron (e), heavy-hole (hh), and light-hole (lh) states in the GaAs band gap giving rise to the formation of e-hh and e-lh excitons. Light absorption due to these states generates excess carriers which can move along the confining potential of the WL and are captured very efficiently by the deeper QD potentials. Therefore, monitoring QD emission intensity as a function of WL excitation energy in PLE allows the determination of WL states. If PLE is detected at the QD1 emission, one obtains spectra displayed in Fig. 1. For the reference sample, both e-hh and e-lh excitonic transitions are clearly resolved. Brübach et al. [4] calculated the transition energies for a single InAs layer in a GaAs matrix by applying a δ-potential model. A comparison with their results yields an average WL thickness of 1.3 ML for the single layer. In the PLE spectra of the stacked samples the following peculiarities should be noticed:

(i) For spacer thicknesses of d_{Sp}=20 nm and d_{Sp}=15 nm, the e-hh transition shows a high energetic shoulder separated from the main absorption line by ΔE_{WL}=9 meV and ΔE_{WL}=10 meV, respectively. The splitting is confirmed by independent PR studies as the example in Fig. 2 (a) demonstrates. If PLE is detected at the energetic different QD2 emission line (not shown here) the shoulder becomes dominant. Finally, after removing the upper dot and wetting layer the shoulder disappears which is depicted in Fig. 2 (b) and (c). It suggests that the shoulder is induced by the e-hh excitonic absorption in the upper WL.
(ii) When ML size InAs layers of equal thickness are separated by a thin GaAs barrier the electron and light-hole states are split into symmetric (+) and antisymmetric states (-), and the e_+-hh_+ transition energy decreases with spacer thickness [4]. These distinguishing features are clearly observed in the PLE spectra for the d_{Sp}=10 nm and 3 nm samples in Fig. 1. However, the observed splitting is larger than predicted for InAs layers of equal size.
(iii) We can exclude coupling as the origin of the shoulder for the two other samples because then the e-hh transition should be shifted to higher energies after layer removal. This is unambiguously no the case. Therefore, it can be concluded that the upper WL is thinner than the lower one which emphasizes the influence of strain field modulation on WL properties.

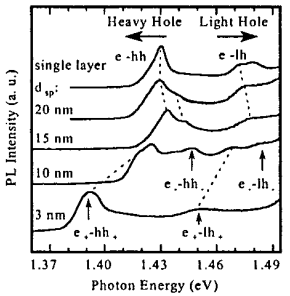

Fig. 1: PLE spectra measured at 79.5 K. The detection energy was set on the luminescence of the QD's in the lower lying layer. The transitions are denoted according to Ref. 4.

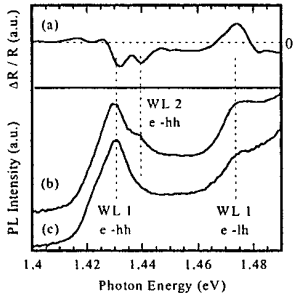

Fig. 2: PR (a) and PLE (b,c) spectra of the 20 nm spacer width sample at 79.5 K. The detection energy in PLE was set to QD1. (a,b) and (c) were recorded before and after removal of the upper QD layer and its WL, respectively.

References

[1] O.G. Schmidt et al., Phys. Rev. B 61, 13721 (2000).
[2] M.O. Lipinski et al., Appl. Phys. Lett. 77, 1789 (2000).
[3] O.G. Schmidt et al., Appl. Phys. Lett. 74, 1905 (1999).
[4] J. Brübach et al., Phys. Rev. B 59, 10315 (1999).

Corresponding author: R. Goldhahn, Institut für Physik, Technische Universität Ilmenau, PF 100565, 98684 Ilmenau, Germany
phone: +49 3677 69 3650, Fax: +49 3677 69 3173, email: goldhahn@physik.tu-ilmenau.de

Level bleaching in a single quantum dot observed by photocurrent-spectroscopy

Evelin Beham, Artur Zrenner, Frank Findeis, Martin Baier, Max Bichler, and Gerhard Abstreiter

Walter Schottky Institut, Technische Universität München, Am Coulombwall, D-85748 Garching, Germany

In recent years, optical and electrical experiments on single quantum dots became possible. This allows to explore the specific properties of single quantum systems. In the current contribution we report about level bleaching in a single quantum dot under the condition of resonant excitation in the ground state of the dot. This is a characteristic property of a fully quantized few particle system. The level bleaching is observed as saturation of the photocurrent in single quantum dot photodiodes.

The investigated sample was grown by molecular beam epitaxy on a n^+-GaAs substrate. The $In_{0.5}Ga_{0.5}As$ quantum dots are embedded in a 180 nm thick intrinsic layer, 20 nm above the n-doped GaAs back contact. The samples are processed as photodiodes combined with near field shadow masks. Electron beam lithography and a dry chemical etch process are used to define aluminum shadow masks with apertures ranging from 150 nm to 500 nm. As a top Schottky contact we use a 5 nm thick semitransparent Titan layer to achieve a homogeneous electric field in the region of the investigated QD. Due to the typically high surface density of self assembled QDs ($>1\times10^{10}$ cm^{-2}) a spatial resolution in the range of 100 nm is needed to isolate a single QD. Our shadow mask technique allows the selection of single quantum dots for optical experiments.

The band profile of our sample under negative bias condition is shown schematically in the inset of fig. 1. A tunable Ti:sapphire laser is used for resonant excitation of the quantum dot. In a regime of sufficiently high electric field the optically generated carriers are able to tunnel out of the quantum dot. Thus the cw excitation leads to a dc photocurrent. By tuning the excitation energy the photocurrent signal exhibits sharp spectral resonances revealing the discrete density of states of a single quantum dot.

In the case of low excitation the quantum dot can absorb at its resonance energy. With increasing excitation power we observe a saturation of the photocurrent peak amplitude (see fig. 1). When the quantum dot is occupied its energy levels undergo a spectral shift due to a renormalization caused by few particle interactions. Thus no second absorption process can take place at the same excitation energy as long as the quantum dot is occupied. In other words the quantum dot level is bleached. After a tunneling time the quantum dot is empty again and the next absorption process can occur. The interplay between resonant occupation and tunneling results in a saturation of the photocurrent.

Furthermore the saturation level of the photocurrent amplitude shows a pronounced dependence on the bias voltage. At higher electric fields F the tunneling time is reduced and the quantum dot gets faster in its initial empty state. Therefore more absorption processes per time are possible leading to a higher saturated photocurrent. The saturation of the quantum dot photocurrent with increasing excitation power is put down to a fundamental rate equation model. The steady state solutions are in good agreement with the experimentally observed photocurrent amplitudes (see fig. 1).

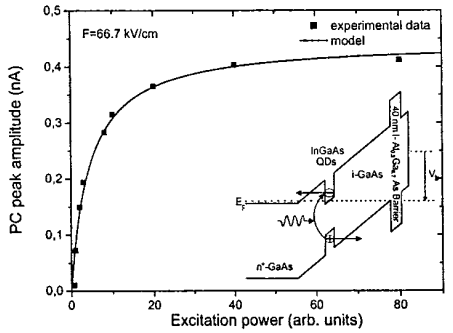

Fig. 1: Photocurrent peak amplitude as a function of excitation power. The inset shows a schematic band diagram of our sample under negative bias condition.

Corresponding author: Evelin Beham, Walter Schottky Institut, Technische Universität München, Am Coulombwall, D-85748 Garching, Germany.
phone: +49 89 28912784, Fax: +49 89 3206620
email: evelin.beham@wsi.tu-muenchen.de

Determination of Binding Energies of Electron and Hole Bound States in Self-Assembled InAs Quantum Dots

S. Fujimoto[1], S. -W. Lee[1,2], K. Hirotani[1], and K. Hirakawa[1,2]
[1]*Institute of Industrial Science, University of Tokyo*
4-6-1 Komaba, Meguro-ku, Tokyo 153-8505, Japan
[2]*CREST, Japan Science and Technology Corporation*

Interband sublevel separation in self-assembled InAs quantum dots (QDs) embedded in GaAs matrix can be easily determined by photoluminescence (PL). However, concerning the energy positions of the bound states in the QDs with respect to the conduction/valence band edges of GaAs, which are quite important parameters in designing various type of devices, only few works have been done [1].

In this work, we have investigated the binding energies of s-bound states confined in InAs QDs by measuring photoionization thresholds of QDs in n- and p-type quantum dot infrared photodetectors. It is found that for the case of relatively small QDs (diameter~20 nm; PL peak energy~1.28 eV) the binding energies of electron and hole s-bound states in the QDs are both ~120 meV.

The samples used in this experiment were recently developed high-sensitivity modulation-doped quantum dot infrared photodetectors (MD-QDIPs) [2]. We grew Si-doped n-type and Be-doped p-type MD-QDIPs on (001) semi-insulating GaAs substrates by molecular beam epitaxy. The growth conditions and structural parameters for n- and p-type devices were set to be identical. 10 InAs QD layers were grown at 470 °C. The typical diameter of the QDs observed by atomic force microscope was ~18 nm. The density of the dots was approximately 8×10^{10} cm^{-2}. Each QD layer was embedded in the middle of 120 nm-wide GaAs quantum wells. Since the 30 nm-thick AlGaAs barriers were δ-doped with Si or Be up to 1×10^{11} cm^{-2}, electrons or holes occupy only s-bound states in the QDs.

Fig. 1 show the PL spectra measured on n- and p-type MD-QDIP samples. Although the PL linewidths are rather broad, both samples have PL peaks around 1.28 eV. This energy corresponds to the interband energy distance between electron and hole s-states.

Figs. 2(a) and (b) show the photocurrent spectra measured on n-type and p-type MD-QDIPs at T = 50 K, respectively. (The broad photocurrent peaks observed above 600 meV for both types of samples are due to deep levels in the substrates and not relevant here.) As seen in the figures, the n- and p-type MD-QDIPs have almost the same photoionization thresholds of about 120 meV. Therefore, we can conclude that the binding energies of electron and hole s-bound states in relatively small InAs QDs are 120 meV. Fig. 3 schematically summarizes the energy band scheme of the QD embedded in GaAs matrix.

Incidentally, we always observed much larger photocurrent in p-type MD-QDIPs, suggesting that p-type QDIPs may be more promising than n-type devices.

References: [1] G. Medeiros-Ribeiro, et al., Appl. Phys. Lett. **66**, 1767 (1995). [2] S. –W. Lee, K. Hirakawa, and Y. Shimada, Appl. Phys. Lett. **75**, 1428 (1999).

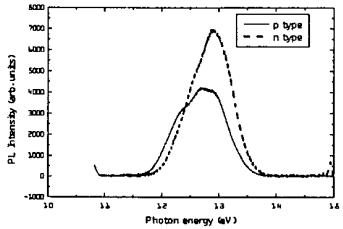

Fig. 1 Photoluminescence spectra for n- and p-type MD-QDIPs.

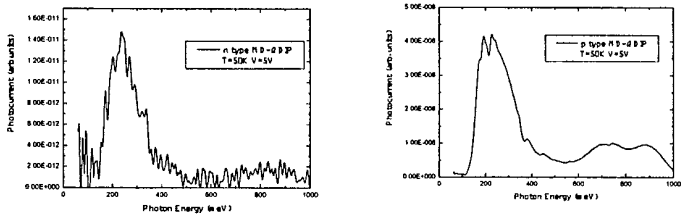

(a) (b)

Fig. 2 Photocurrent spectra measured for n-type MD-QDIP (a) and p-type MD-QDIP (b) at T=50K.

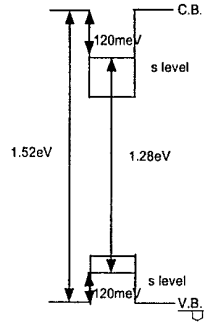

Fig.3 Energy band diagram in InAs small quantum dot embedded in GaAs matrix.

Corresponding author: Institute of Industrial Science, University of Tokyo
4-6-1 Komaba, Meguro-ku, Tokyo 153-8505, Japan
Phone: +81-3-5452-6001-57641, Fax: +81-3-5452-6261
Email: fujimoto@nano.iis.u-tokyo.ac.jp

Electronic structure of quantum-dot molecules and solids

Garnett W. Bryant[1], W. Jaskolski[2]

[1]Atomic Physics Division, National Institute of Standards and Technology, Gaithersburg, MD, 20899-8423, USA
[2]Instytut Fizyki, UMK, Grudziadzka 5, Torun, Poland

Nanocrystals and quantum dots have been intensely studied for their potential as tailorable, man-made, artificial atoms. Artificial molecules and solids fabricated from nanocrystals and quantum dots offer intriguing new possibilities, not possible in natural molecules and solids, because quantum-dot molecules and solids are not limited by the rules of chemical binding that determine natural molecules and solids. Nanocrystal nanosystems require nanocrystals with precisely determined geometry, nanocrystals tailored with internal structure for enhanced functionality, and arrays of close-packed nanocrystals (quantum-dot molecules and solids). To provide an understanding of these nanosystems, models of nanocrystals must describe variations in composition on the monolayer scale, realistic shapes and faceting, coupling between closely spaced nanocrystals, and ordered arrays of nanocrystals. A theory on the atomic scale is needed. We present an empirical tight-binding theory of nanocrystal nanosystems. We use the theory to model the individual nanocrystals that serve as the building blocks for nanocrystal architectures to determine how the electronic structure of these nanocrystals can be tailored by shape and internal structure. Small clusters of nanocrystals are studied to determine the extent of the electronic coupling between nanocrystals and the degree of hybridization in the electronic states in coupled nanocrystal clusters. The results are used to determine the electronic structure of ordered nanocrystal arrays and to explore the possibilities for novel electronic properties in these artificial molecules and solids.

Recently, several groups have shown that nanostructures with internal structure can be fabricated [1,2]. These quantum-dot quantum-well (QDQW) heteronanostructures are multishell nanocrystallites. Fabrication of a QDQW, for example a ZnS/CdS QDQW with a ZnS core, a CdS shell and a ZnS cladding shell [1], produces a barrier/well/barrier nanocrystal that has a radial band-profile with an internal quantum well (the CdS shell) inside the (ZnS) quantum dot. We have calculated the electronic structure and optical spectra of ZnS/CdS/ZnS [1] and CdS/HgS/CdS [3] QDQWs. A comparison with observed level structure for CdS/HgS/CdS and ZnS/CdS/ZnS nanocrystal heteronanostructures [1,2] shows that the tight-binding approach provides a good description of nanosystems with monolayer variations in composition. Calculations confirm that the internal shell acts as an electron and hole trap. Calculations predict an optically weak ground state transition coupling the lowest (1S-like) electron and lowest ($1P_0$-like) hole state. The first optically active state involves the 1S-like electron state and an excited ($1S_1$-like) hole state. The measured Stokes shift between absorption and emission corresponds closely to the calculated splitting between ground and excited hole states. Higher calculated absorption peaks agree with observed structure.

Well/barrier and well/barrier/well nanocrystal heteronanostructures could also be used to tailor states and energy levels in nanocrystals. As examples, we consider CdS/ZnS and CdS/ZnS/CdS nanocrystals [3]. CdS/ZnS is typical of nanocrystals grown with a high-barrier capping material to passivate the surface of the core dot. The capping layer is not just a passivant but can significantly alter the states in the nanocrystal. For a bare CdS dot, the hole ground state is P-like, just as in a QDQW, and the ground state transition is optically dark. As the cap thickness increases, the level ordering of the first two hole states switches, the S-like odd state becomes the ground state and the ground state becomes optically active. Well/barrier/well structures could be used, in analogy with coupled 2D quantum wells, to tailor states by exploiting interwell tunneling to modify the states trapped in the core and cladding wells. Our results show that resonant coupling between electron states in the core and clad wells occurs between states with the same spatial angular momentum. The resonant coupling between hole states is more complicated due to the mixed symmetry of the hole states.

Experiments on quantum-dot solids provide evidence for both dipole-dipole interdot coupling [4] and for electronic interdot coupling [5]. To understand electronic states in quantum-dot solids, the coupling between nanocrystals and the hybridization of states in coupled structures must be determined. We have considered coupled double-dot structures. Results for epitaxial connections, with the dots lattice-matched across the interdot interface, show significant coupling when the connection is through more than a few atoms. The coupling strength depends on the spatial distribution of the states involved, just as in molecular hybridization. States that lie along the axis joining two dots couple strongly to form σ bonds. States perpendicular to the axis couple to form π bonds. Degenerate states in the individual nanocrystals are split by the hybridization. Coupled dots with disordered, nonepitaxial connections between the dots will be modeled to estimate the importance of epitaxial order for interdot coupling. The effects of nanocrystal shape and orientation on coupling will also be addressed.

Finally, ordered, periodic arrays of nanocrystals will be modeled. The electronic structure of quantum-dot solids can be engineered by separately optimizing the electronic properties of the nanocrystal building blocks and the lattice geometry. The electronic structure of arrays with different lattice geometries will be determined. The effect of nanocrystal size, shape, and internal structure on the electronic structure of quantum-dot solids will be determined and used to understand the recent experimental results on energy transfer in quantum-dot solids.

References

[1] R. B. Little, M. A. El-Sayed, G. W. Bryant, S. Burke, J. Chem. Phys. 114, 1813 (2001).
[2] A. Mews, A. V. Kadavanich, U. Banin, A. P. Alivisatos, Phys. Rev. B 53, R13242 (1996) and related references therein.
[3] G. W. Bryant, W. Jaskolski, Physica E (accepted).
[4] C. R. Kagan, C. B. Murray, M. Nirmal, M. G. Bawendi, Phys. Rev. Lett. 76, 1517 (1996).
[5] M. V. Artemyev, A. I. Bibik, L. I. Gurinovich, S. V. Gaponenko, U. Woggon, Phys. Rev. B 60, 1504 (1999).

Corresponding author: Garnett W. Bryant, National Institute of Standards and Technology, 100 Bureau Dr., Stop 8423, Gaithersburg, MD, 20899-8423, USA.
phone: +1 301 975 2595, Fax: +1 301 990 1350
email: garnett.bryant@nist.gov

Binding energies of excitonic complexes in square and T-shaped quantum wires

Takuma Tsuchiya

Japan Advanced Institute of Science and Technology (JAIST)
1-1 Asahidai, Tatsunokuchi, Ishikawa 923-1292, Japan

Binding energies for excitons, charged excitons, and biexcitons in rectangular and T-shaped quantum wires have been calculated exactly by the diffusion Monte Carlo method. The resulting binding energies for biexcitons are about one fourth of variational results [1,2] and are in accordance with experimental ones. [3,4]

Excitonic complexes, or biexcitons and charged excitons in quantum wells and quantum dots have been investigated quite actively, because they are important for nonlinear optical devices. Those in quantum wires, however, have not been observed until recently. [3,4] Further, the discrepancy between the observed [3,4] and the variational biexcitonic binding energies [1,2] is serious. It is known that simple variational wavefunctions for biexcitons underestimate binding energies in the bulk. [5] In quantum structures, it becomes difficult to know wavefunctions and energies even for excitons. In this study, we have employed the diffusion Monte Carlo method to calculate the ground state energies for excitons and excitonic complexes in quantum wires. In this method, variational wavefunctions are not necessary, and we can obtain exact ground state energies within a small statistical error.

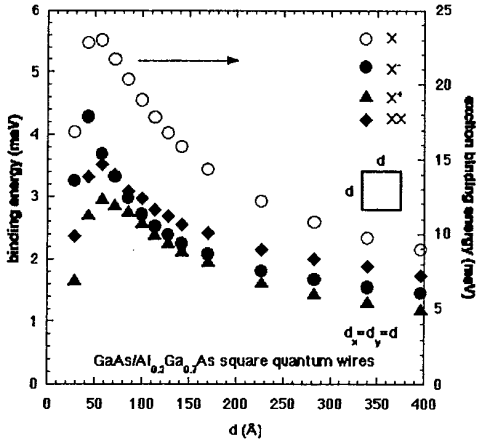

Fig. 1: Calculated binding energies for excitons (X), negatively (X^-) and positively (X^+) charged excitons, and biexcitons (XX) in GaAs/AlGaAs square quantum wires.

In Figure 1, we show calculated binding energies in GaAs/AlGaAs square quantum wires. The present binding energies for excitons are larger, and those for biexcitons are much smaller than the variational ones. [1,2] The resulting biexcitonic binding energy is comparable to experimental one. [3]

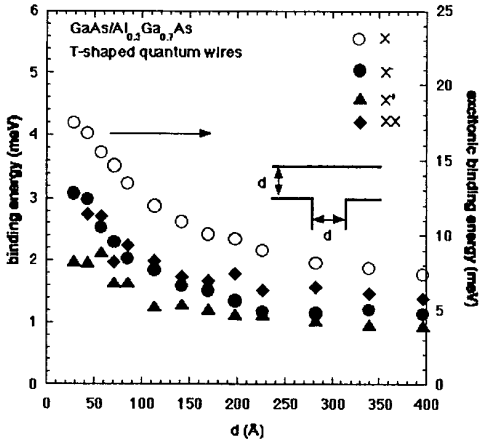

Fig. 2: Binding energies for excitons (X), negatively (X^-) and positively (X^+) charged excitons, and biexcitons (XX) in GaAs/AlGaAs T-shaped quantum wires.

Figure 2 shows the results for excitons and excitonic complexes in GaAs/AlGaAs T-shaped quantum wires. Because the structure is complicated, the statistical errors are rather large. The binding energies are smaller than those in square quantum wires but are larger than those in quantum wells. [6] The biexcitonic binding energies are also comparable to experimental results for similar structures. [4]

It is quite interesting that the binding energies for negatively charged excitons are comparable to or exceed those of biexcitons for narrower wires both T-shaped and square. This phenomenon is due to the different quantum confinement between electrons and holes and does not take place in the bulk GaAs and $GaAs/Al_{0.3}Ga_{0.7}As$ quantum wells.

References

[1] F. L. Madarasz, F. Szmulowicz, and F. K. Hopkins, Phys. Rev. B 52, 8964 (1995).
[2] R. O. Klepfer, F. L. Madarasz, and F. Szmulowicz, Phys. Rev. B 51, 4633 (1995).
[3] T. Baars, W. Braun, M. Bayer, and A. Forchel, Phys. Rev. B 58, R1750 (1998).
[4] W. Langbein, H. Gislason, and J. M. Hvam, Phys. Rev. B 60, 16667 (1999).
[5] M. A. Lee, P. Vashishta, and R. K. Kalia, Phys. Rev. Lett. 51, 2422 (1983).
[6] T. Tsuchiya, in *Proceedings of the 24th International Conference on the Physics of Semiconductors* (CD-ROM), (World Scientific, Singapore, 1999)

Corresponding author: Takuma Tsuchiya, Japan Advanced Institute of Science and Technology (JAIST), 1-1 Asahidai, Tatsunokuchi, Ishikawa 923-1292, Japan
phone: +81 761 51 1512, Fax: +81 761 51 1515
email: tsuchiya@jaist.ac.jp

Excitons in quantum ring structures in a magnetic field: Persistent currents

A. O. Govorov[1], A. V. Kalameitsev[1], R. J. Warburton[2] and K. Karrai[3],

[1] Institute of Semiconductor Physics, Russian Academy of Sciences, Siberian Branch, 630090 Novosibirsk, Russia
[2]Department of Physics, Heriot-Watt University, Edinburgh, UK
[3]Center for NanoScience, LMU, Geschwister-Scholl-Platz 1, 80539 München, Germany

The growth of ring-shaped semiconductor quantum dots with nanometre-sized radii has triggered much interest in the theoretical and experimental investigation of their electronic and optical properties [1,2]. We present in this theoretical work the effect of static high magnetic fields on the optical spectra of excitons confined in semiconductor quantum rings. The joint action of the Coulomb forces and the shape of the nano-structure potential on electrons and holes makes this problem interesting and challenging. At high enough magnetic fields, we found that the ground state of a neutral magneto-exciton confined in a finite width quantum ring possesses a non-zero angular momentum. This effect is accompanied by a suppression of the photoluminescence (PL) in well defined windows of the magnetic field. Recent predictions show that the binding energy of a neutral exciton oscillates with increasing magnetic field [3]. This Aharonov-Bohm (AB) effect for a neutral exciton occurs due to electron to hole tunneling around the ring [3]. However, the amplitude of the predicted AB oscillations in the exciton binding energy is very sensitive to a finite width of a quantum ring [4]. In this work, we consider a different manifestation of the AB effect, which relates to the exciton persistent current in a quantum ring with a finite width.

The confining potentials in ring-shaped semiconductor quantum dots are different for electrons and holes [2]. As a result of this, the potential can polarize a quantum ring exciton in the radial direction. Using a simple model, we show that an exciton possessing a finite radial electric dipole changes its angular momentum with increasing magnetic fields. The appearance of the persistent current in the ground state of the neutral exciton has a strong effect on its optical spectrum. In particular, an exciton with a non-zero angular momentum cannot emit a photon. We calculated indeed that the photoluminescence intensity is suppressed in the regions of the magnetic field where the persistent current occurs.

In order to demonstrate the effect of the persistent current of a neutral exciton we present two models. The first model relates to a type-II quantum dot embedded into a two-dimensional quantum well [5]. In such a system the potential of a quantum dot localizes a hole near the center whereas an electron moves in a quantum ring potential due to the joint action of the Coulomb force and the quantum dot potential. This type-II potential would correspond to that of GaSb/GaAs quantum dots [6]. The second model describes the exciton spectrum in the InAs self-organized quantum rings [1,2]. First, we calculate the single electron spectrum and the wave functions of electron and holes for the potentials $U_{e(h)} = m_{e(h)}\Omega_{e(h)}{}^2(\rho - R)^2/2$ [1,7], where $m_{e(h)}$ and $\Omega_{e(h)}$ are the effective masses and the characteristic radial oscillation frequencies, respectively; ρ is the distance to the center of a ring and R is the ring radius. The exciton has a non-zero dipole moment in the radial direction since the wave functions of electrons and holes peak at different radii. We calculate that the ground state of an exciton changes its momentum from $L_{exc} = 0$ to -1 in a finite range of magnetic field. In the next step, we calculate the PL spectrum at low temperature. The appearance of the persistent current is accompanied with a reduction of the PL emission intensity in a window of magnetic field. In both models the persistent current in the ground state originates from the finite radial electric dipole (Fig.1). Qualitatively, the persistent current occurs when the magnetic flux through the area between the electron and hole trajectories exceeds the flux quantum. This condition is $\Phi = \pi (R_h^2 - R_e^2)B > \Phi_0 = h/e$, where B is the magnetic field applied perpendicular to the ring, and R_e and R_h are the averaged distances of electrons and holes to the ring center, respectively. Using realistic range of material parameters for self-organized InAs nano-rings [1] we calculate that persistent current occurs up to 10 T and the windows in which the corresponding exciton PL vanishes is about 1 to 2 T wide.

In addition, we analyze the spectrum and the optical properties of charged excitons in a one-dimensional quantum ring. By introducing the Coulomb interaction as a perturbation we show that the spectra of charged and neutral excitons are qualitatively different. In the case of the neutral exciton, the ground state has always zero angular momentum and the energy level as a function of B anticrosses with that of the first excited state. In contrast the energy spectrum for the charged exciton shows level crossing. This is due to the fact that the angular momentum in the ground state of a charged complex becomes non-zero at level crossing [8]. However, even in the presence of the persistent current, the charged exciton in its ground state can contribute to the PL at any magnetic field.

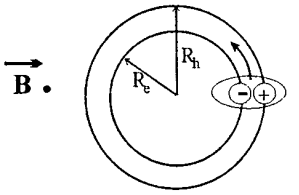

Fig. 1

References

[1] A. Lorke, R. J. Luyken, A. O. Govorov, J. P. Kotthaus, J. M. Garcia, and P. M. Petroff, Phys. Phys. Lett. **84**, 2223 (2000).
[2] R. J. Warburton, C. Schäflein, D. Haft, F. Bickel, A. Lorke, K. Karrai, J. M. Garcia, W. Schoenfeld, and P. M. Petroff, Nature **405**, 926 (2000).
[3] A. Chaplik, JETP Lett. **62**, 900 (1995); R. A. Römer and M. E. Raikh, Phys. Rev. B **62**, 7045 (2000).
[4] J. Song and S. E. Ulloa, Phys. Rev. B **63**, 125302 (2001).
[5] A. V. Kalameitsev, A. O. Govorov, and V. Kovalev, JETP Lett. **68**, 669 (1998).
[6] F. Hatami, M. Grundmann, N. N. Ledentsov, F. Heinrichsdorff, R. Heitz, J. Böhrer, D. Bimberg , S. S. Ruvimov , P. Werner, V. M. Ustinov, P. S. Kop'ev, and Zh. I. Alferov, Phys. Rev. B **57**, 4635 (1998).
[7] V. Halonen, P. Pietiläinen, and T. Chakraborty, Europhys. Lett. **33**, 377 (1996).
[8] A. O. Govorov and A. V. Chaplik, JETP Lett. **66**, 455 (1997).

Corresponding author: Alexander Govorov, Institute of Semiconductor Physics, Russian Academy of Sciences, Siberian Branch, 630090 Novosibirsk, Russia;
e-mail: govor@isp.nsc.ru; phone: ++7-3832-333264; Fax: ++7-3832-332-771

STM-induced luminescence of individual InGaAs quantum dots: evidence for charged excitons

T. K. Johal[1], G. Pagliara[2], R. Rinaldi[1], M. Lomascolo[3], A. Passaseo[1] and R. Cingolani[1]

[1] INFM- Unita di Lecce, Dip. Ingegneria, Dell'Innovazione,73100 Via Per Arnesano, Lecce
[2] Department of Physics, University of Lecce, Lecce
[3] Istituto per lo studio di nuovi Materiali per l'Elettronica IME-CNR, University of Lecce,73100 - LECCE (Italy)

Semiconductor quantum dots are nanostructures formed of a smaller band gap material in a matrix of a wider gap material [1]. Their dimensions are comparable to the effective Bohr radius of the host semiconductor material, and so result in three dimensional carrier confinement, energy quantization and shell structures typical of atoms. Whereas atomic phenomena is on the scale of a few angstroms, the quantum dot is usually of a few hundreds of angstroms. Interest in these systems has been both intense and broadly based. The main motivations lie in technological applications such as high efficiency lasers [2] and ultra-small memories [3] as well as basic research into their fundamental electronic properties [4].

From a fundamental point of view the optical properties of quantum dots are strongly modified by Coulomb interactions and correlation effects. The tendency to form charged multi-particle complexes, due to the strong Coulomb interaction of carriers in the confining potential of the dot, have been predicted [5] and observed [6]. It is expected that the participation of multi-particle complexes, in the radiative processes of the quantum dot, becomes increasingly important under electrical injection [5]. To investigate these processes it is

desirable to study the luminescence spectra collected, under single dot injection conditions.

In this abstract, we present results of STM-induced luminescence of single InGaAs quantum dots in a GaAs matrix formed by strain driven self-assembly by MOCVD. The non-uniformity in the dot size(usually approximately 10%), shape and composition (usually approximately 1%) of these systems necessitate single dot spectroscopy techniques since spatially averaging techniques are susceptible to inhomogeneous broadening (usually >30meV) which obscure many effects. Spatial resolution is afforded by the use of a scanning tunneling microscope tip to inject carriers, either electrons or hole, into capped quantum dots. A combination of temperature dependent (over a range of temperature from 20K to 100K), tunneling current (0.5 to 50nA) and area dependent measurements of the luminescence signal have been carried out. In contrast to the inhomogeneously broadened photoluminescence, the STM induced luminescence shows sharp lines of both neutral and charged excitons. The luminescence spectra shall be explained in terms of the Coulomb interaction between excitons and carriers and carrier-carrier correlations.

[1] A. Zrenner, J. of Chem. Phys. **112**, 7790 (2000)
[2] A. Passaseo et al., Appl. Phys. Lett., **78**, 1382 (2001)
[3] T. Lundstrom et al., Science, **286**, 2312 (1999)
[4] M. Rotani et al., Phys. Rev. B **59**, 10165 (1999)
[5] A. Barenco and M.A. Dupertuis, Phys. Rev. B **52**, 2766 (1995)
[6] A. Hartmann et al. Phys. Rev. Lett. **84**, p5648 (2000)

corresponding author: Dr T.K. Johal, INFM- Unita di Lecce,Dip. Ingegneria Dell'Innovazione,73100 Via Per Arnesano, Lecce, Italy I-73100, johal@axpmat.unile.it

A quantum dot infrared photodetector with lateral carrier transport

L. Chu, A. Zrenner, D. Bougeard, M. Bichler, G. Abstreiter

Walter Schottky Institut, Technische Universität München, Am Coulombwall, D-85748 Garching, Germany

It has been shown that intersubband bound-to-continuum transitions in the self-assembled In(Ga)As/GaAs quantum dots (QDs) are nearly independent of the polarization of radiation [1, 2]. In a lateral electric field, intersubband transition between the first excited states and the wetting layer (WL) subband can be observed, where carrier transport mainly takes place in the WL subband. Based on the principle of lateral intersubband photocurrent, it is possible to reach a high infrared photoresponse if carrier transport is shifted to a neighboring channel with high electron mobility. The first demonstration of such an effect has been reported by Lee et al. [3].

In this contribution, we demonstrate an infrared photodetector structure using self-assembled In(Ga)As/GaAs QDs as active material, and an InGaAs quantum well (QW) next to QD layers as transport medium. The QDs are doped with Si. Delta-doping has been introduced to a nominal donor sheet concentration of 8×10^{10} cm^{-2}, which results in a population of about 6 electrons in each QD. The doping layers are located 2 nm below each QD layer. An InGaAs QW is grown 20 nm above the topmost QD layer. The structure is capped with 160 nm intrinsic GaAs containing a Si δ-doping layer, which leads to a small electric field along the growth direction between the QD-layers and the QW. This facilitates electron transfer from the WL to the QW. Standard photolithography techniques have been used to define an interdigital contact structure on the sample surface. The contact fingers are 20 μm broad with 40 μm spacing in between.

Intersubband photocurrent measurements are performed with a calibrated glow-bar infrared light source in front of a grating spectrometer. The sample is mounted on the cold finger of a He flow cryostat system equipped with a temperature controller. Photocurrent data have been recorded using standard Lock-In techniques. The intrinsic spectral dependence of the experimental setup has been eliminated.

The photoresponse spectra of the detector structure at different temperatures are depicted in Fig. 1. The bias voltage is 0.6 V. Photoresponse of the order of A/W can be obtained for temperatures up to T=60 K. The spectra are peaked at E=186 meV (λ=6.5 μm) with a small shoulder on the high energy side. The response maximum is attributed to the transition between the first excited states and the WL-subband. The shoulder arises from the transition between the QD ground states and the wetting layer subband. The photoresponse increases slightly with increasing temperature for T<33 K. This is probably due to the thermally activated electron transfer between the WL-subband and the parallel InGaAs channel. For higher temperatures, the electrons are thermally excited out of the quantum dots, which reduces the intersubband absorption in the quantum dots and results in a decrease of the detector signal. The observed photoresponse is about 60 mA/W at T=77 K.

The photoconductance gain is strongly affected by the modulation frequency f. The dynamics of the detector structure has been investigated by frequency dependent studies of the detector signals. The detector signal decreases strongly with increasing chopper frequency. The maximum peak response obtained at f=11 Hz drops by an order of magnitude when f is increased to 650 Hz. The frequency dependence of the detector structure is most probably due to the back-transfer of electrons from the InGaAs channel to the QDs, which is expected to be rather slow due to the real space transfer of the electrons. At low chopper frequency, i. e. f=11 Hz, most electrons in the transport channel are expected to be recaptured by the quantum dots during the dark period. Thus, large photoresponse is obtained for low frequencies. The intrinsic response time is determined to be 800 μs. It can be shown that the frequency dependence of the detector response is strongly reduced for higher temperature, showing thermally enhanced real space electron transfer.

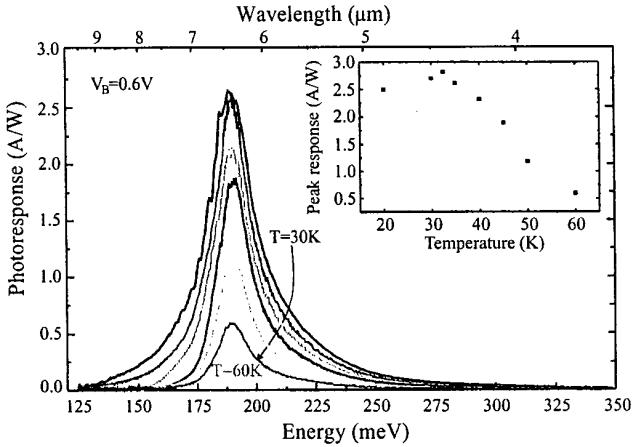

Fig. 1: Temperature dependent photoresponse spectra of the QDIP. Photoresponse of several A/W can be obtained. The peak response as a function of temperature is shown in the inset.

References

[1] L. Chu et al., Appl. Phys. Lett. 75, 3599 (1999).
[2] L. Chu et al., Appl. Phys. Lett. 76, 1944 (2000).
[3] S. -W. Lee et al., Appl. Phys. Lett. 75, 1428 (1999).

Corresponding author: Dominique Bougeard, Walter Schottky Institut, Technische Universität München, Am Coulombwall, D-85748 Garching, Germany
phone: +49 89 289 12777, Fax: +49 89 3206 620
email: dominique.Bougeard@wsi.tu-muenchen.de

Quantum dot micro-LEDs for the study of single-dot electro-luminescence, fabricated by focused ion beam.

M. Vitzethum[1], R. Schmidt[1], P. Kiesel[1], P. Schafmeister[2], D. Reuter[2], J. Koch[2], A.D. Wieck[2] and G.H. Döhler[1]

[1]Institut für Technische Physik 1, Universität Erlangen-Nürnberg, Erwin-Rommel-Str. 1, D-91058 Erlangen, Germany
[2]Institut für Angewandte Festkörperphysik, Ruhr-Universität Bochum, Universitätsstr. 150, D-44801 Bochum, Germany

In contrast to the large number of photo luminescence investigations which have been performed on self-assembled quantum dots (SADs), there are hardly any reports on fundamental electromluminescence studies (except for those on quantum dot lasers). This is even more true for single quantum dot investigations, probably due to the difficulties of contacting single dots. To our best knowledge there is no report at all on single dot electro-luminescence (EL), except for the work on luminescence by STM injection by Zrenner and coworkers [1]. The small number of reports on EL is surprising, as EL– in particular when performed at low temperatures and in p-i-n diodes with thin i-layers – should provide a lot of detailed information on the energetic position of electron and hole energy levels and on many-body effects related to the number of occupied electron and hole levels. Depending on the relative position of the dots within the i-layer (i.e. closer to the n- or to the p-layer) the voltage-dependent alignment of electron and hole quasi Fermi levels will result in very different populations of electron and hole levels of the dots due to tunneling injection (See Fig.1) [2]. In this contribution we report on a new approach for the fabrication of SAD-LEDs. Our goal is, on the device side, an addressable N x N array of micro-LEDs. On the physics side, it is the single-dot-LED, possibly working as a turnstile for sequential single photon emission. The LEDs are fabricated by first writing narrow, highly p-conducting stripes into the otherwise intrinsic GaAs bottom layer by focused ion beam (FIB) implantation of Be. Subsequently, the first i-layer, the InAs dot-layer, the second i- and the highly n-doped top doped layer are grown by MBE (schematic Fig. 2(a)). Finally, the n-layer is structured by conventional (by now) or e-beam lithography (in the future) and etching to define narrow n-conducting stripes, oriented perpendicular to the p-doped stripes in the bottom layer. After deposition of ohmic n- and p-contacts the micro-LEDs (schematic Fig. 2(b)) can be tested. Fig. 2(c) demonstrates the (room temperature) operation of our first micro-LED with a (relatively large) cross sectional area of the n- and p-stripe of 10 x 10μm^2. For forward bias $U_{pn} < 2$ V the luminescence remains strictly confined to the cross sectional area. The luminescence starts at 1.0 V, i.e. at $eU_{pn} < E_g^{GaAs}$ and attains about 10% of its maximum value already at 1.4 V. For $U_{pn} < 3$ V only dot-luminescence and no GaAs or wetting layer luminescence is observed. These results indicate that small-area devices can be fabricated by this method. Even more impressive results are expected from our forthcoming low temperature experiments. While the present LED structure still contains about 10^4 dots (assuming a dot density of 10^{10} cm^{-2}) we expect to be able to study single dot electro-luminescence spectra for doping stripe widths of about 1 µm or less. Due to the strongly 3-dimensional character of the space charge potential of the crossed n- and p-stripe the number of dots close to its saddle point should be in the order of one.

References
[1] A. Zrenner et.al., Journal of Luminescence 87-89 (2000), 35-39
[2] V. Khorenko, et. al., phys. stat. sol. (b) 2001, Vol. 224, No. 1, 129-132

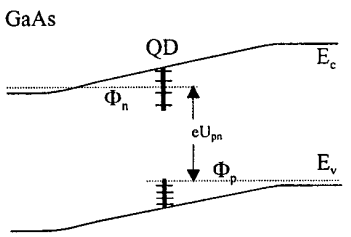

Fig. 1: Schematic band diagram of a dot-LED under forward bias.

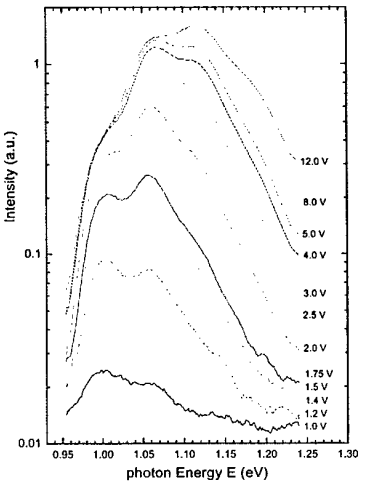

Fig. 3: EL spectra obtained from the crossing area of the n- and p-doped stripes of the device depicted in Fig. 2 (c).

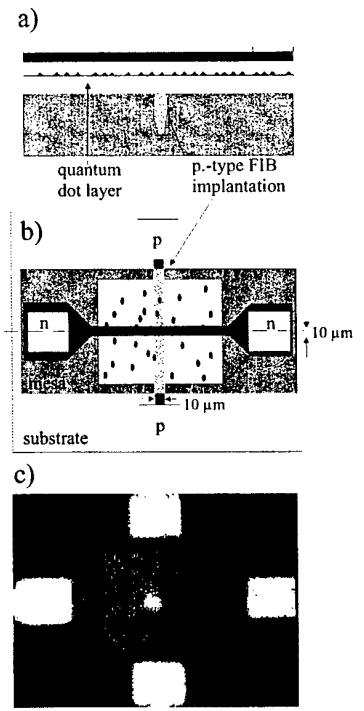

Fig. 2: The cross-section (a) of the dot-LED, showing the FIB- implanted buried p-stripe and the i-, dot- and n-layers obtained by subsequent regrowth. Additionally, the n-contacts are depicted. (b) Plan view of the device, showing the arrangement of the p- and n-doped stripes and the mesa. (c) Plan view, as seen with a CCD camera, showing dot-luminescence from the cross-section of the n-stripe and the buried p-stripe.

Corresponding author: Markus Vitzethum, Institut für Technische Physik 1, Universität Erlangen-Nürnberg, Erwin-Rommel-Str. 1, D-91058 Erlangen, Germany
phone: +49 9131 85 27251, Fax: +49 9131 85 27293
email: Markus.Vitzethum@physik.uni-erlangen.de

Lifetime of Photoexcited Carriers in Modulation-Doped Quantum Dot Infrared Photodetectors

S. -W. Lee and K. Hirakawa
Institute of Industrial Science, University of Tokyo,
4-6-1 Komaba, Meguro-ku, Tokyo 153-8505, Japan
CREST, Japan Science and Technology Corporation

Quantum dot infrared photodetectors (QDIPs) using InAs self-assembled quantum dots (QDs) have been proposed and successful operation in the mid-infrared range has been demonstrated [1]. We have proposed and fabricated a new type of quantum dot infrared photodetector (modulation-doped quantum dot infrared photodetectors; MD-QDIP), which utilizes lateral transport of photoexcited carriers in the high mobility modulation-doped two-dimensional channels [2]. In this structure high photoconductive gains are achieved due to long lifetime of photoexcited carriers as well as high electron mobility in the conduction channels.

In this report, we have systematically investigated the relationship between the lifetime of photoexcited carries, τ, and the distance from heterointerface to the QD layer, d. τ as long as 85 μs was observed when d=60 nm at T=77 K. This very long τ enables high sensitivity operation and demonstrates superiority of MD-QDIPs. Furthermore, it is found that τ increases exponentially with increasing d.

The samples were grown on (001) semi-insulating GaAs substrates by molecular beam epitaxy. 10 InAs QD layers were grown at 470 °C. Each QD layer was embedded in the middle of GaAs quantum wells with width of 2d. The density of the QDs was approximately 5×10^{10} cm^{-2}. The 30 nm-thick AlGaAs barriers were δ-doped with Si up to 1×10^{11} cm^{-2}. d was systematically varied from 20 to 100 nm in different samples. A high modulation-speed InGaP LED with λ=630 nm was used to create photoexcited carriers. Fig. 1 shows the schematic illustration for the photocurrent measurements. When the LED is on, electrons and holes are generated in the conduction and valence band of QWs. The photoexcited electrons relax to the heterointerface and holes to the QDs. Then, photoexcited holes recombine with electrons in the QDs. When the LED is turned off, the electrons at the heterointerfaces are slowly captured into the bound state of the QDs due to phonon scattering. This process is expected to be strongly dependent on the distance between the QDs and the heterointerface and much longer than other processes (radiative recombination time, etc.). Therefore, we can measure the lifetime of the photoexcited carriers in this simple measurement setup.

Fig. 2 shows the temporal waveform of the photocurrent of the MD-QDIP samples with various d measured at T=77 K. The determined lifetimes dramatically increased with increasing d and were about 85 μs, 360 μs, and 2.92 ms for 60, 80, and 100 nm samples at T = 77 K, respectively. The lifetime of photoexcited carriers are controlled by the overlapping of the wavefunctions of the bound states in the QDs and 2DEG at the heterointerfaces. The determined lifetimes are plotted for various d in the inset of Fig. 2. As seen in the figure, τ increases almost exponentially with increasing d. In photoconductive detectors, τ is quite essential in determining the detector performance such as photoconductive gains and responsivities. Very high sensitivity infrared photodetectors can, thus, be realized by long lifetimes of photoexcited carriers in the proposed MD-QDIP structures.

References

[1] For example, S.J. Xu et al, Appl Phys. Lett, **73**, 3153 (1998). [2] S.-W. Lee e al, Appl. Phys. Lett. **75**, 1428 (1999).

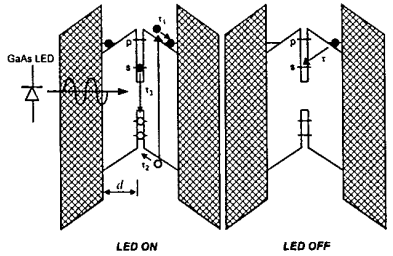

Fig. 1 The excitation and relaxation processes of photoexcited carriers.

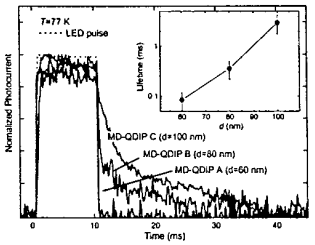

Fig. 2 Temporal waveform of the photocurrent measured at 77 K for MD-QDIPs with d = 60, 80 and 100 nm. In the inset, the lifetime is plotted with various d.

Corresponding author: Seung-Woong Lee, Institute of Industrial Science, University of Tokyo,
4-6-1 Komaba, Meguro-ku, Tokyo 158-8505, Japan
Phone & Fax: +81-3-5452-6261
Email: swlee@nano.iis.u-tokyo.ac.jp

Theoretical analysis of electron transport in quantum dot structures

V. Ryzhii[1], I. Khmyrova[1], M. Willander[2], and V. Mitin[3],

[1] Computer Solid State Physics Laboratory,
University of Aizu, Aizu-Wakamatsu 965-8580, Japan

[2] Department of Microelectronics and Nanoscience,
Chalmers University of Technology and Gothenburg University,
Gothenburg S -412 96, Sweden

[3] Department of Electrical and Computer Engineering,
Wayne State University, Detroit 48202, USA

The advancement of the concept of the three-dimensional carrier confinement in semiconductor quantum dots (QDs) has resulted in the successful realization of various electronic and optoelectronic heterostructure devices. As shown theoretically by one of the authors [1], infrared photodetectors utilizing the electron (hole) photoexcitation from QD arrays, can exhibit substantial advantages over quantum well infrared photodetectors (QWIPs). The structure of a QD infrared photodetector (QDIP) consists of a two-dimensional array (or a stack of several arrays) of QDs buried in a layer of a material with relatively wide energy gap. This layer is sandwiched between doped emitter and collector contact layers. Various InAs/GaAs, InGaAs/GaAs, InGaAs/InGaP, and SiGe/Si QDIPs of this type have been recently fabricated and experimentally studied by several groups (see, for example, Refs. [2,3,4]). However, most of the fabricated and experimentally investigated QD photodetectors are inferior to QWIPs so the potential advantages of QDIPs predicted using an idealized model [1] have not been realized yet. The operation of QDIPs based on realistic QD structures is fairly complex. Many interdependent factors are involved in their operation [5,6].

In this communication, we present a physical model for QD structures similar to those used in QDIPs (see Fig. 1). The model includes the effect of the space charge formed by electrons captured in QDs and donors, the self-consistent electric potential, the activation character of the electron capture and its limitation by the Pauli principle, the thermionic electron emission from QDs and thermionic injection from the emitter contact, and the existence of the punctures between QDs. Using this model, we calculated the dark current and photocurrent in QD structures as functions of their parameters and the applied voltage, demonstrated in Figs. 2 - 4. The following parameters of InAs/GaAs QD structures at $T = 40$ K were chosen: number of QD arrays $K = 10$, spacing between them $L = 100$ nm, and lateral size of QDs $a_{QD} = 15$ nm. In particular, it is shown that both the dark current-voltage and photocurrent-voltage characteristics exhibit an exponential rise. This result is in agreement with the experimental data [3,4]. Our model clarifies also the origin of the effect of negative differential infrared photoconductivity observed experimentally at low temperatures [2].

References

[1] V. Ryzhii, Semicond. Sci. Technol. **11**, 759 (1996).
[2] S. J. Xu, S. J. Chua, T. Mei, X. C. Wang, X. H. Zhang, H. G. Karunasiri, W. J. Fan, C. H. Wang, J. Jiang, S. Wang, and X. G. Xie, Appl. Phys. Lett. **73**, 3153 (1998).
[3] J. Phillips, P. Bhattacharya, S. W. Kennerly, D. W. Beekman, and M. Dutta, IEEE J. Quantum Electron. **35**, 936 (1999).
[4] E. Towe and D. Pan, IEEE J. Sel. Topics Quant. Electron. **6**, 408 (2000).
[5] V. Ryzhii, V. Pipa, I. Khmyrova, V. Mitin, and M. Willander, Jpn. J. Appl. Phys. **39**, L1283 (2000).
[6] V. Ryzhii, Jpn. J. Appl. Phys. **40**, L148 (2001).

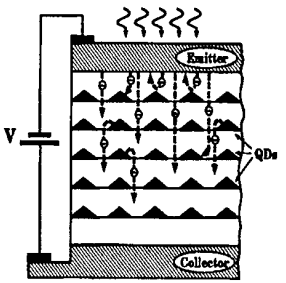

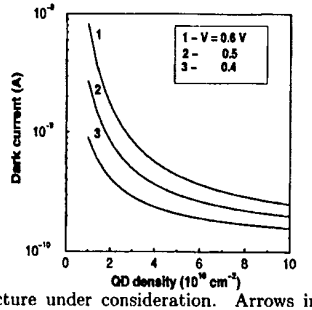

Figure 1: Schematic view of the QD structure under consideration. Arrows indicate electron trajectories.

Figure 2: Dark current as a function of QD sheet density at different applied bias voltages.

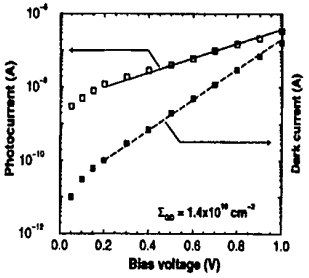

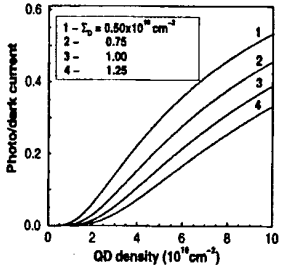

Figure 3: Theoretical (dashed and solid lines) and experimental (squares) [3] dark current-voltage and photocurrent-voltage characteristics.

Figure 4: Photocurrent-to-dark current ratio versus QD density for structures with different doping levels.

Corresponding author: Prof. Victor Ryzhii, Computer Solid State Physics Laboratory, University of Aizu, Aizu-Wakamatsu 965-8580, Japan,
Phone: +81-242-372563, Fax: +81-242-372596, E-mail: v-ryzhii@u-aizu.ac.jp

Spin-Dependent Single-Hole Tunneling in Self-Assembled Silicon Quantum Rings

N.T.Bagraev[1], A.D.Bouravleuv[1], W.Gehlhoff[2], V.K.Ivanov[3], L.E.Klyachkin[1], A.M.Malyarenko[1], S.A.Rykov[3], I.A.Shelykh[3]

[1]A.F. Ioffe Physico-Technical Institute, 194021, St.Petersburg, Russia
[2]Institut für Festkörperphysik, Technische Universität Berlin, Germany
[3]St.Petersburg State Technical University, 195251, St.Petersburg, Russia

We present the first findings of the quantum conductance and NMR techniques which reveal the spin-dependent confinement and quantization phenomena in the Aharonov-Bohm (AB) rings prepared inside self-assembled silicon quantum wells (SQW). The quantum wells of this art are naturally formed inside ultra-shallow silicon p^+-n junctions obtained by non-equilibrium diffusion of boron.

Short-time diffusion of boron was performed from gas phase into n- type Si (100) wafer using surface injection of self-interstitials and vacancies. By varying the parameters of the surface oxide layer and diffusion temperature (800°C-1100°C) it was possible to define the criteria leading to the ultra-shallow p^+ -n junction (10 nm), which was controlled using SIMS and STM techniques. The cyclotron resonance (CR) angular dependencies show that the p^+-diffusion profile contains a longitudinal SQW. The STM images exhibit self-assembled one-dimensional rings that are caused by the antidots which consist of self-interstitials and penetrate through the SQW plane.

The AB double-path interferometer that contains the quantum point contact (QPC) embedded into one of the self-assembled AB ring's arms obtained inside silicon SQW was used to study the coherence of the single-hole transport. The quantum staircase $G(E)=2(e^2/h)nT(E)$ revealed by the quantum conductance (QC) measurements is shown to identify the principal role of heavy holes tunneling through this QPC (Fig.1a). Meanwhile, the logarithmic temperature dependence of the resistance points out the weak localization regime of the heavy holes inside the AB ring, which is confirmed by the measurements of the negative magnetic resistance (Figs.1d and 3). By varying an external weak magnetic field, the QC periodic oscillations that exhibit the magnitude and phase of the transmission coefficient through QPC prove the coherence of the single-hole transport and negative magnetic resistance effect (Figs.2 and 1d). Besides, a phase change of π is found to correspond to a full occupied heavy hole subband, which is complementary attributable of a weak localization regime (Fig.1b). The antilocalization due to the spin-orbit coupling induced by the p^+n junction electric field was measured as a positive magnetic resistance in the weakest magnetic fields (Fig.3). The oscillations of the magnetic resistance as a function of the electric field value are observed, for the first time, at a zero magnetic field. Finally, the effect of the hyperfine interaction between the ^{29}Si nuclei and spin-polarized holes on the antilocalization processes was studied by the electrically-detected nuclear magnetic resonance that demonstrates the positive/negative transformation of the magnetoresistance in weak magnetic fields (Fig.3). The electrically-detected NMR of the ^{29}Si nuclei allowed to verify the nuclear spin polarization by the corresponding shift of the resonance frequency because of the Overhauser effect.

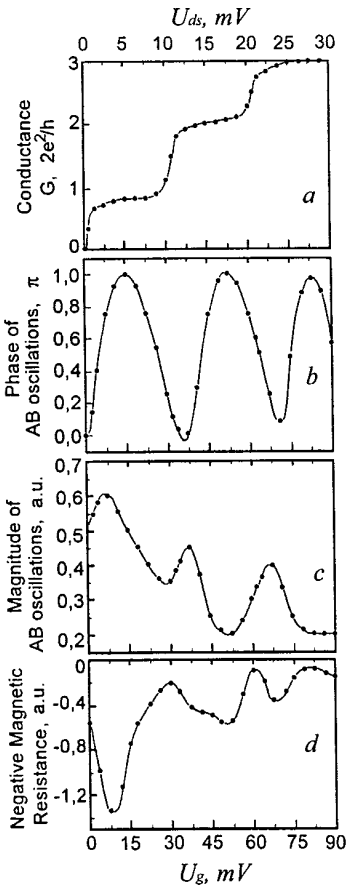

Fig. 1: The quantum staircase (a), the phase (b) and magnitude (c) of the AB oscillations as well as the negative magnetic resistance (d), which are obtained from QC oscillations taken at the marked points in the staircase

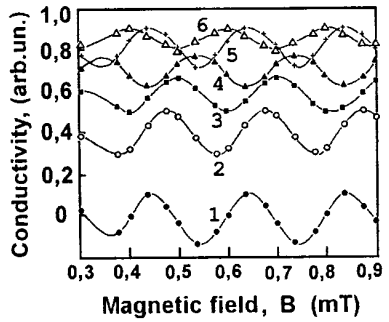

Fig. 2: A series of AB oscillations taken at specified positions on the quantum staircase revealed by a quantum wire; U_{ds}(V): 1-0.01; 2-0.02; 3-0.03; 4-0.04; 5-0.05; 6-0.06.

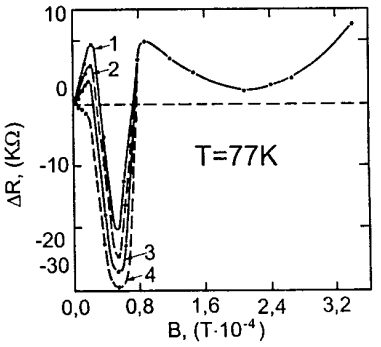

Fig. 3: The variations of the resistance with an magnetic field under different NMR saturation conditions of the ^{29}Si nuclei: U_g= 15 mV, B_0= 0.02 mT; f_0 = 545Hz; H_1: 1 – 0, 2 - $0.4\cdot10^{-5}$mT, 3 – $1.0\cdot10^{-5}$mT, 4 – $5.0\cdot10^{-5}$mT

Corresponding author: Prof.Dr.N.T.Bagraev, A.F.Ioffe Physico-Technical Institute, 194021, St.Petersburg, Russia.
Phone: +007 (812) 2479315, Fax +007 (812) 2471017
e-mail: impurity.dipole@pop.ioffe.rssi.ru

Surface morphology evolution of 1.3 μm wavelength $In_{0.5}Ga_{0.5}As/GaAs$ island structures grown by molecular beam epitaxy

Z.C. Niu, X.D. Wang, Z.H. Miao, S.L. Feng
National Laboratory for Superlattices and Microstructures, Institute of Semiconductors, Chinese Academy of Sciences, Beijing 100083, P. R. China

Surface morphology evolution and photoluminescence (PL) characteristics of 1.3 μm wavelength $In_{0.5}Ga_{0.5}As/GaAs$ islands structures grown by molecular beam epitaxy (MBE) are investigated, comparatively characterizing the dependence on the growth parameters using cycled sub-monolayer, monolayer, and super-monolayer deposition approaches. Atomic force microscopy (AFM) images show that after deposition of 16 monolayers (ML) of $In_{0.5}Ga_{0.5}As$, islands obviously elongated along the $[1\bar{1}0]$ direction are formed when using sub-monolayer depositions, while quite uniform large size InGaAs mounds or islands are formed when using monolayer or super-monolayer depositions. In contrast to the optical nonlinearity of the PL from the InGaAs islands of $n < 1.0$, the InGaAs mounds or islands of $n \geq 1.0$ do not show optical nonlinearity, indicating that strain relaxation can be achieved through the evolution of surface morphology. Additionally, enhanced photoluminescence efficiency is obtained from the islands formed by the monolayer and super-monolayer depositions.

References:

[1] X.D. Wang, Z.C. Niu, S.L. Feng, Z.H., Miao, J. Cryst. Growth 220 (2000) 16.
[2] X.D. Wang, Z.C. Niu, S.L. Feng, Jpn. J. Appl. Phys. 39 (2000) 5076.

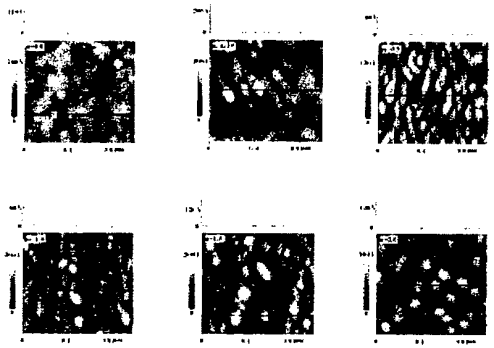

Fig. 1. Typical *ex-situ* AFM images of the surface morphologies of the $In_{0.5}Ga_{0.5}As$ islands corresponding to the monolayer number n from 0.0 to 2.0.

Corresponding author: Zhichuan Niu, Institute of Semiconductors, Chinese Academy of Sciences, P.O. Box 912, Beijing 100083, P.R. China. Phone: +86-10-82304268. Fax. +86-10-82305056, Email: zcniu@red.semi.ac.cn

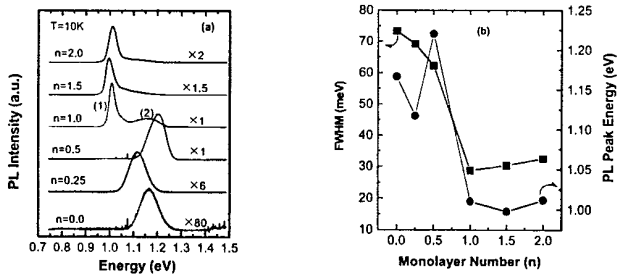

Fig. 2 (a) PL spectra taken at 10K under excitation power of 0.3 mW for all the cycled $(InAs)_n/(GaAs)_n$ ($n = 0.0 \sim 2.0$) grown island samples. The separated higher energy peak of $n = 1.0$ curve (marked as peak (2)) is positioned at about 1.17eV. (b) PL peak energy and the full width of half maximum (FWHM) of spectra with different monolayer number n.

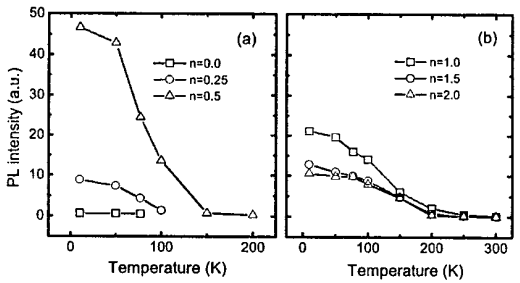

Fig. 3 Comparison of the temperature dependent spectra of PL integrated intensity measured under the constant excitation power of 0.3 mW. **(a)** No detectable PL emissions from the n = 0.0, 0.25, 0.5 samples if the temperature is increased above 77K, 100K and 200K, respectively; **(b)** strong PL signals from samples n = 1.0, 1.5 and 2.0 can be detected until the measured temperature about 300K.

Polaron couplings in quantum dot molecules

O. Verzelen, R. Ferreira, G. Bastard,

Laboratoire de Physique de la Matière Condensée ENS,
24 rue Lhomond F75005 Paris (France)

Recent theoretical and experimental works have evidenced the existence of a strong coupling between longitudinal optical phonons and electrons tightly bound in single quantum dots [1,2]. Here, we report on energy level calculations of polaron states in double dot structures. We have considered both cases of vertically or laterally coupled dots. The dots have a small size, as realized in the self organized InAs/GaAs quantum dots. Their shape is approximated by truncated cones floating on a one monolayer thick InAs wetting layer. Hence, the envelope functions of a single dot retain a cylindrical symmetry. Dots typical dimensions are 10 nm for the basal radius R and $1-2$ nm for the height h. With an effective mass close to that of GaAs, a single dot binds 3 bound states with S and $P\pm$ symmetry respectively. It is known that dots grow vertically on top of each others, and the double dot structures retain the same cylindrical symmetry as the single dots.

Polaron eigenstates in vertically coupled dots have been calculated for fixed dot separation versus the size of one dot keeping the other dot fixed ($R_l = 10$ nm, $h_l = 1.3$ nm), as well as the aspect ratio h/R ($= 0.13$). We have numerically diagonalized the Fröhlich hamiltonian in a basis spanned by the six double dot electron states with zero or one LO phonon (the LO phonons are taken dispersionless and bulk – like). Several anticrossings results from the simultaneous diagonalization of the tunnel and Fröhlich couplings. Many of them are ascribed to intra – dot polaron effects weakly modified by tunnel coupling. There also exist situations where a pronounced delocalization of the polaron states over the whole dot molecule shows up. For instance, when the bonding polaron state of the upper dot and the antibonding polaron state of the lower dot are lined up, the tunnel coupling leads to delocalized mixed eigenstates between electron and LO phonons. These effects should clearly show up in the far infrared absorption spectra of dot molecules containing one electron, which we predict to display two (main) lines in the non resonant case, basically associated with intra - dot polarons but will display a triplet pattern when the polaron delocalizes over the dot molecule.

Similar calculations were performed for laterally coupled dots. New effects are associated with the breaking of the cylindrical symmetry of the system but, overall, the anticrossing effects are smaller because the lateral coupling between dots is weaker than the vertical ones as a result of the tighter in - plane localization of the single dot eigenstates compared to the vertical one.

Figs(1,2) show the calculated absorption spectrum of vertically coupled double dot structures in the case of a small tunnel coupling: $R_l = 10$ nm, $h_l = 1.3$ nm, a distance between wetting layers $d = 10$ nm and $R_u = 10.4$ nm in case of fig.(1) (resonant coupling) while $R_u = 11$ nm in case of fig.(2) (non resonant coupling).

References

[1] S. Hameau et al., Phys. Rev. Lett. 83, 4152 (1999),
[2] O. Verzelen et al., Jpn. J. Appl. Phys. (march/2001).

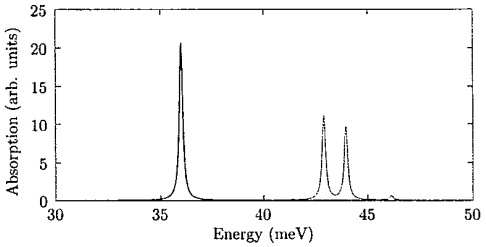

Figure 1: Absorption spectrum, $R_u = 10.4$ nm.

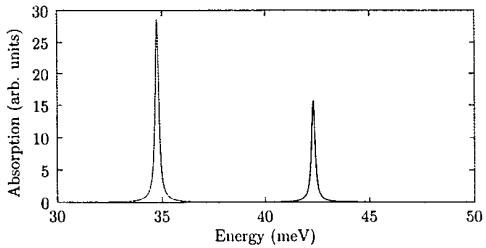

Figure 2: Absorption spectrum, □ $_u$ = 11□ nm.

Corresponding author: Olivier Verzelen, Laboratoire de Physique de la Matière Condensée ENS, 24, rue Lhomond F75005 Paris (France).
phone: +33 1 44 32 33 73, Fax: +33 1 44 32 38 40,
email: olivier.verzelen@ens.fr

On the spin injection in ZnMnSe/ZnCdSe heterostructures

I.A. Buyanova[1], W.M. Chen[1], B. Monemar[1], A.A. Toropov[2], Y. Terent'ev[2], S.V. Sorokin[2], A.V. Lebedev[2], S.V. Ivanov[2] and P.S. Kop'ev[2]

[1]Department of Physics and Measurement Technology, Linköping University, S-581 83 Linköping, SWEDEN

[2]A.F. Ioffe Physico-Technical Institute, Russian Academy of Sciences Polytechnicheskaya 26, St. Petersburg, 194021, RUSSIA

With the limits of microelectronic miniaturization in sight there has been an enormous drive to introduce radically new technologies. As an alternative to electronic charge, the storage and transport of electronic spin in "spintronics" have attracted great attention. Very recent discoveries about the generation and transport of coherent spins in semiconductors [1-3] opens the door to a new generation of semiconductor spintronic devices. New device concepts have already started to emerge, such as spin-based transistors, opto-electronic spin devices, spin memory, or even spin quantum computers. The success of spintronics relies on the ability to create, control, maintain and manipulate spin coherence over practical time and length scale. One of the focal points in the research field of spintronics at the moment is the efficiency of spin polarization and spin injection.

In this work, we carry out a detailed study of spin polarization and spin injection in II-VI semiconductor heterostructures consisting of diluted magnetic semiconductor (DMS) barriers and a non-magnetic quantum well (QW). The DMS barriers serve as spin polarizers as a result of the giant Zeeman effect in the presence of an external magnetic field, whereas the non-magnetic ZnCdSe QW is employed as a detector of spin polarization via its spin-dependent excitonic recombination. Two types of DMS barriers were designed and their properties were examined, one is a ZnMnSe layer and the other is a 10-period ZnMnSe/CdSe superlattice. The composition of Mn in the structures is up to 4 %. Between the DMS barriers and the non-magnetic quantum well, a non-magnetic ZnSe spacer is inserted to avoid direct overlap of electron and hole wave functions between the barriers and the QW and thus to ensure a predominant role of the spin injection as the source of spin polarization. By varying the spacer thickness, information on spin diffusion length can be obtained. Polarized magnetooptical experiments were employed. The photon energy of the optical excitation and the bandgap of the barriers can be varied in the experiments such that optical excitation either above or below the bandgap of the DMS barriers can be realized.

It is shown that the spin population and polarization in the QW is largely determined by the spin injection from the DMS barriers leading to a reverse in sign of the circular polarization of the QW exciton emission. Similarly, up to 30 % spin polarization can be achieved at 5T in structures with two different semimagnetic barriers. With an increasing thickness of the non-magnetic spacer up to 8-10 nm, on the other hand, the efficiency of the spin injection starts to deviate between the two structures. It declines noticeably (down to 8 %) in the structures with the ZnMnSe barriers, whereas no significant change was found in the structures with the ZnMnSe/CdSe superlattice barrier. By magnetically fine tuning the bandgap of the DMS barriers, it was also possible to investigate the spin injection near the resonance excitation condition. The physical mechanism responsible for the observations will be discussed in terms of various spin transfer and scattering processes.

References

[1] Y. Ohno, D.K. Young, B. Beschoten, F. Matsukura, H. Ohno and D.D. Awschalom, Nature 402, 490 (1999).
[2] R. Fiederling, M. Keim, G. Reuscher, W. Ossau, G. Schmidt, A. Waag and L.W. Molenkamp, Nature 402, 787 (1999).
[3] J.M. Kikkawa and D.D. Awschalom, Nature 397, 139 (1999).

Corresponding author: Weimin M. Chen, Department of Physics and Measurement Technology, Linköping University, S-581 83 Linköping, SWEDEN,
Phone: +46-13-281795, Fax: +46-13-142337,
e-mail: wmc@ifm.liu.se

Rashba spin-splitting energies probed by anti-weak-localization analyses in symmetric and asymmetric InAlAs/InGaAs/InAlAs quantum wells

Takaaki Koga, Junsaku Nitta, Tatsushi Akazaki and Hideaki Takayanagi,

NTT Basic Research Laboratories, 3-1 Morinosato-Wakamiya, Atsugi-city, Kanagawa, 243-0198, Japan

Future spin devices, such as the spin-polarized FET that is proposed by Datta and Das in 1990 [1], utilize the properties of electron spin besides the properties of the electron charge on which any conventional semiconductor device is based. In order to realize such future spin devices, it is essential to understand the details of the spin motion of the conduction electrons in a semiconductor solid. It is especially important to clarify experimentally that the electron spin actually precesses in an asymmetric quantum well due to the Rashba spin splitting so that the proposed spin devices may be designed in a predictable manner.

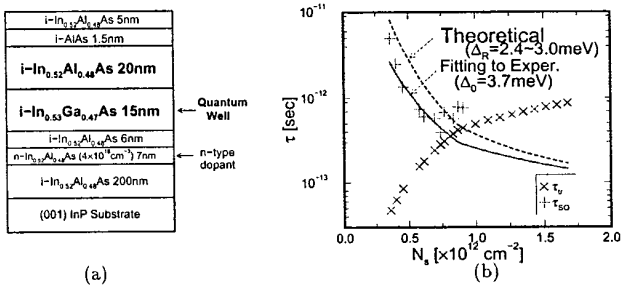

Figure 1: (a) A typical sample structure of the asymmetric quantum wells used in the present study. (b) The spin-orbit relaxation time (τ_{SO}) and the elastic scattering time (τ_{tr}) of the asymmetric quantum well shown in (a) deduced from the anti-weak-localization analyses.

In the present study, the value of Rashba spin-splitting energy is determined through the analyses of the anti-weak-localization measurements of the InAlAs/InGaAs/InAlAs asymmetric quantum well [see Fig. 1(a)]. An example of such analysis is shown in Fig. 1(b). We can clearly see that the spin-orbit relaxation time (τ_{SO}) deduced from the anti-weak-localization analysis is inversely proportional to the elastic scattering time (τ_{tr}). Therefore, we conclude that τ_{SO} in this system is governed by the D'yakonov-Perel mechanism [2], and the spin splitting energy Δ_0 in this system is deduced to be 3.7 meV [see Fig. 1(b)]. This value of Δ_0 is found to be consistent with those of Rashba spin splitting energy Δ_R in this system calculated using the Poisson-Schrödinger self-consistent simulation [3] ($\Delta_R = 2.4 \sim 3.0$ meV are obtained in the theoretical calculation).

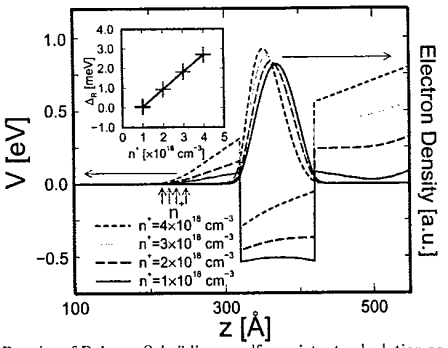

Figure 2: Results of Poisson-Schrödinger self-consistent calculation as a function of quantum well asymmetry in $In_{0.52}Al_{0.48}As/In_{0.53}Ga_{0.47}As/In_{0.52}Al_{0.48}As$ quantum wells. It is noted that the impurity concentration in the carrier supplying layer (indicated by the four arrows and n^+) underneath the quantum well (the right hand side of the figure corresponds to the surface side of the sample) is varied between 1×10^{18} cm^{-3} and 4×10^{18} cm^{-3} and the sheet-density of the carriers in the quantum well is chosen to be 1.2×10^{12} cm^{-2}. It is also noted that there is an additional carrier supplying layer in the surface side of the quantum wells so that the total numbers of the impurities in the samples are the same among the four different structures considered here. The inset figure shows the calculated values for the Rashba spin splitting energy Δ_R as a function of the impurity concentration n^+ underneath the quantum well.

As an ongoing project, we study the values of Δ_0 as a function of the quantum well asymmetry. It is predicted, using the Poisson-Schrödinger self-consistent simulation, that the value of the Rashba spin splitting energy Δ_R decreases with decreasing the degree of the quantum well asymmetry (see Fig. 2). We will experimentally confirm this theoretical result using both the beating pattern of the Shubnikov de Haas oscillation [4] and the anti-weak-localization analyses.

References

[1] S. Datta and B. Das, Appl. Phys. Lett. **56**, 665 (1990).
[2] G. L. Chen, J. Han, T. T. Huang, S. Datta and D. B. Janes, Phys. Rev. B **47**, 4084 (1993); P. D. Dresselhaus, C. M. A. Papavassiliou and R. G. Wheeler, Phys. Rev. Lett. **68**, 106 (1992).
[3] Th. Schäpers, G. Engles, J. Lange, Th. Klocke, M. Hollfelder and H. Lüth, J. Appl. Phys. **83**, 4324 (1998).
[4] J. Nitta, T. Akazaki, H. Takayanagi and T. Enoki, Phy. Rev. Lett. **78**, 1335 (1997).

Corresponding author: Takaaki Koga, NTT Basic Research Laboratories,
3-1 Morinosato-Wakamiya, Atsugi-city, Kanagawa, 243-0198, Japan.
phone: +81 46 240 3325, Fax: +81 46 240 4722,
email: koga@will.brl.ntt.co.jp

Correlation between exciton-decay and localization in digital magnetic heterostructures

W. Heiss[1], G. Prechtl[1], S. Mackowski[2], E. Janik[2]

[1]Institut für Halbleiter- und Festkörperphysik, Johannes Kepler Universität Linz, Altenbergerstraße 69, A-4040 Linz, Austria
[2]Institute of Physics, Polish Academy of Sciences, 02-668 Warsaw, Poland

In two-dimensional systems, the exciton recombination-time is directly related to the homogeneous line-width of the excitonic transition [1]. For excitons localized in potential fluctuations such a correlation between these two quantities is not expected, due to the variation of the exciton radius in the potential minima leading to an inhomogeneous broadening of the exciton transitions. Recently, for an *inhomogeneously* broadened system, namely for excitons in self-organized InAs quantum dots, a direct proportionality of the photoluminescence (PL*) line-width* to the *Stokes-shift* of the PL transitions was presented [2]. In this work, we demonstrate for a different inhomogeniously broadened system a further direct correlation between two experimental paramaters: We show a direct proportionality between the *exciton decay-time* and the PL *Stokes-shift*.

We investigate semiconductor quantum-wells containing several thin magnetic layers. In such digital magnetic heterostructures the excitons are localized not only by potential fluctuations due to the variations of the well-width or of the alloy composition, but they get trapped also by the formation of magnetic polarons which are eventually formed due to exchange interactions between the excitons and the localized magnetic moments present within the magnetic layers. In particular, we used three sets of $CdTe/Cd_{1-x}Mg_xTe$ quantum well samples containing narrow MnTe barriers. In the first set of samples, containing 4 MnTe layers with equidistant spacing, the overall Mn concentration is varied. In the second set, the position of a single MnTe within the quantum well is varied whereas the structure of the third set of samples deviates from the first two by the well width and by the Mg concentration x of the barriers. The exciton decay-time we deduced from transient PL experiments and it is found to be in the range between 100 and 1000 ps, strongly dependent on the details of the individual sample. The PL-Stokes shift also varies strongly from sample to sample, the ratio between decay time and PL-Stokes shift $\tau/\Delta E$, however, gives for all samples almost the same value of 26 ps/meV. Furthermore, we find that annealing the samples or applying an external magnetic field to the samples influences the exciton decay-time, but it does not change the ration $\tau/\Delta E$.

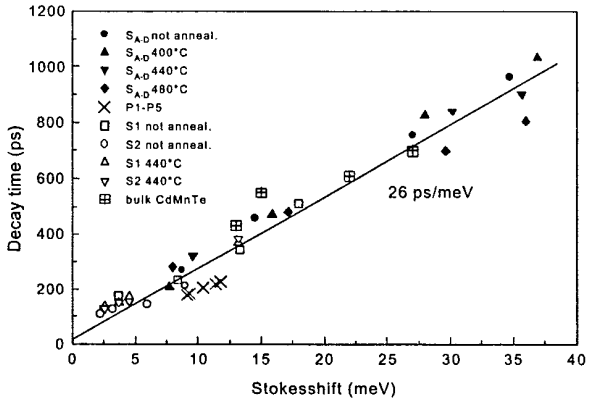

Fig. 1: Exciton decay-time as function of Stokes-shift for various digital magnetic heterostructure samples.

References

[1] J. Feldmann, G. Peter, E. O. Göbel, P. Dawson, K. Moore, C. Foxon, R. J. Elliott, Phys. Rev. Lett. **59**, 2337 (1987)
[2] A. Polimeni, A. Patane, M. Henini, L. Eaves, P. C. Main, Phys. Rev. **B59**, 5064 (1999)

Corresponding author: Wolfgang Heiss, Institut für Halbleiter- und Festkörperhysik, Johannes Kepler Universität Linz, Altenbergerstraße 69, A-4040 Linz, Austria,
phone: +43 732 2468 9643, Fax: +43 732 2468 9696,
email: wolfgang.heiss@hlphys.uni-linz.ac.at

μ-Luminescence study of hybrid ferromagnet/diluted magnetic semiconductor quantum structures

G. Cywiński, M. Czeczott, J. Wróbel, K. Fronc, S. Maćkowski, T. Wojtowicz and J. Kossut

Institute of Physics Polish Academy of Science, Al. Lotników 32/46, PL 02-668 Warsaw, Poland

The influence of external magnetic fields on diluted magnetic semiconductor (DMS) quantum structures has been a subject of very intensive research over the past years. However, almost all experimental and theoretical studies were concentrated on cases with the magnetic field uniform over the area of examined objects. On the other hand, interesting effects are expected to occur in DMS structures subject to a highly inhomogeneous, local in nature, magnetic fields. Such local magnetic fields can be produced in a quantum structure, as calculated and shown experimentally [1], by deposition of thin ferromagnetic layers on a structure surface. These overlayers are to be magnetized in the plane of structure and, thus, act through their fringing fields as micromagnets.

We have fabricated ferromagnetic/semiconductor hybrid device based on MBE-grown semiconductor structure containing 61ML-wide $Cd_{0.96}Mn_{0.04}Te$ DMS quantum well (QW) embedded in $Cd_{0.91}Mg_{0.09}Te$ barriers 300 Å bellow the surface. Matrices of ~ 0.2 μm thick rectangular Fe stripes with lateral dimensions 6x10 micrometers were deposited on the surface of semiconductor structure. The pattern had been first defined be an e-beam writer in the electron sensitive resist and, then, by use of the low temperature sputtering of Fe, and of the lift-off technique, the small Fe rectangles were obtained. Hybrid structures, produced in this way, were examined first by atomic and magnetic force microscopy.

We measured spatially resolved micro magneto-photoluminescence (μ-PL) excited by the 476 nm line of the Argon laser. The laser beam was focused on the hybrid sample surface into the spot of ~2 μm in diameter by an optical microscope. The emitted light was collected by the same microscope and dispersed by a 1 m double monochromator. A constant magnetic field, of approximately 1.2 T, applied in the plane of the structure (Voigt configuration), was produced in the narrow slit between pole shoes attached to the permanent neodymium-iron-boron.

By placing the hybrid sample inside the magnet slit and by magnetizing the ferromagnetic stripes along their longer axis we have expected to produce sub-micron regions with locally strong fringe magnetic fields having nonvanishing component also along to the growth axis of QW. This local magnetic field component should induce, in turn, a local giant splitting of the band edges in the buried DMS QW and, thus, it should result in a local energy minimum for some excitonic states. We could expect, then, to observe in spatially resolved PL experiments an appearance of additional low energy line(s) originating from magnetically induced objects of lower dimensionality. These objects could be, e. g., of the nature of quantum wires, if the corresponding μ-PL lines would appear near the shorter edges of an Fe rectangle. Our low temperature, spatially resolved μ-PL experiments in fact revealed the presence of an additional low energy peak (see Fig. 1) in the spectra provided that the measurements were carried out in the close vicinity of the Fe stripe edge. No additional signal was seen when the exciting laser was focused away from the stripe. We have performed also temperature dependent studies of this additional feature in. The observed dependence is at small variance to that of PL from a normal DMS QW temperature behavior. We can not decisively prove at present that the additional peak is related to the fringing fields or rather they are due to the thermal strain exerted by the iron mesa. However, the temperature dependence exerted in the latter case is predicted to be much smaller indicating that the former is more probable.

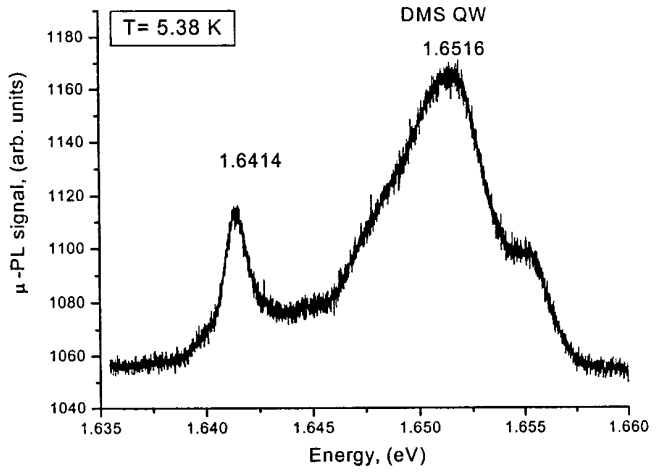

Fig. 1: μ-Luminescence of hybrid ferromagnet/diluted magnetic semiconductor quantum structures near the ferromagnetic overlayer.

References

[1] see, e. g., Reijniers J, Peeters FM. *Appl. Phys. Lett.*, **73**, 357, (1998)

Corresponding author: Grzegorz Cywiński, Institute of Physics Polish Academy of Science, al. Lotników 32/46 PL 02-668 Warsaw, Poland,
Phone/Fax : +48 22 843 13 31
e-mail: cywin@ifpan.edu.pl

Model for ballistic spin-transport in ferromagnet/2-dimensional electron gas/ferromagnet structures

Th. Schäpers[1], J. Nitta[2], H. B. Heersche[3], H. Takayanagi[2]

[1]Institut für Schichten und Grenzflächen, Forschungszentrum Jülich, 52425 Jülich, Germany
[2]NTT Basic Research Laboratories, 3-1, Morinosato, Wakamiya, Atsugi, Kanagawa 243-0198, Japan
[3]Department of Applied Physics and Materials Science Centre, University of Groningen, Nijenborgh 4, 9747 AG Groningen, The Netherlands

In structures where ferromagnets are combined with a two-dimensional electron gas (2DEG) in a semiconductor heterostructure interesting effects and novel applications are predicted. Compared to normal metals as non-magnetic interlayers, a long elastic mean free path and a large Fermi wave length are obtained in two-dimensional electron gases so that novel quantum effects can be expected. A prominent example is the spin-transistor based on the Rashba effect, as proposed by Datta and Das [1]. Nevertheless, the experimental realization of spin-polarized transport in a 2DEG remains problematic. One possible reason might be the large conductivity mismatch between both materials, as pointed out by Schmidt et al. [2]. However, for a diffusive system Rashba [3] recently calculated, that this problem might be solvable by introducing a barrier between the ferromagnet and the semiconductor.

By using a ballistic model we studied the spin-polarized transport in a structure with a 2DEG sandwiched between two ferromagnetic (FM) electrodes. An interface barrier between both materials is approximated by a δ-shaped potential. In accordance to the results obtained in a the diffusive system [3], we found the spin-polarization of the current injected into the 2DEG is improved by inserting an interface barrier. Consequently, the relative resistance change $\Delta R/R_p$ of a FM/2DEG/FM structure increases considerably for increasing barrier heights as shown in Fig 1. Here, ΔR is the difference of the resistance in parallel and anti–parallel magnetization and R_p is the resistance for parallel magnetization. In the limit of large barrier heights, $\Delta R/R_p$ saturates to a value solely determined by the ratio of the Fermi velocities of the majority and minority carriers of the ferromagnets. For small barrier heights a reversal of the polarization direction is predicted, if the carrier concentration in the 2DEG is decreased below a certain threshold value. The latter is defined by the ratio of the Fermi velocities between the 2DEG and the ferromagnet.

For a transistor structure, as depicted in Fig. 2 (inset), the relative conductance change $\Delta G/G_{ave}$ was theoretically investigated by using a transfer matrix method [4]. Pronounced oscillations in $\Delta G/G_{ave}$ due to interference effects are found if the electron concentration n_{2D} in the 2DEG is varied by applying a gate voltage (Fig. 2). In case of no or small barriers at the interface and large exchange energies Δ_h the ratio $\Delta G/G_{ave}$ can even change sign with increasing carrier concentration in the 2DEG. By introducing a sufficiently large interface barrier the ratio $\Delta G/G_{ave}$ is improved on average while the width of the minima in $\Delta G/G_{ave}$ decreases at same time (Fig. 2, inset). Our results clearly demonstrate, that the spin-signal in a FM/2DEG/FM structure is improved considerably by injecting carriers through an interface barrier and by employing interference effects.

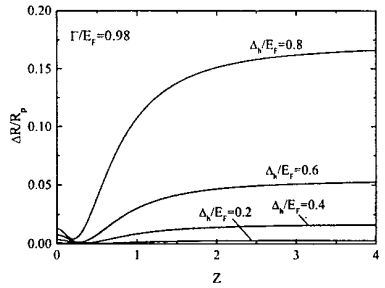

Fig. 1: Relative resistance change $\Delta R/R_p$ of a FM/2DEG/FM structure as a function of the interface barrier height. The latter is expressed by the dimensionless Z-factor. Γ/E_F is the difference between the bottom of the conductance band of the majority band of the ferromagnet and the 2DEG normalized to the Fermi energy E_F of the majority band. The normalized exchange energy Δ_h/E_F is varied as a parameter. Interference effects are neglected.

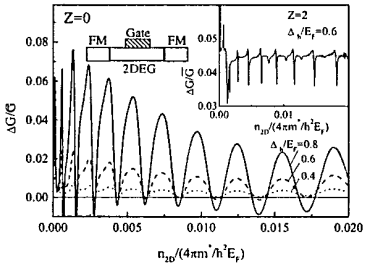

Fig. 2: Relative conductance change $\Delta G/G_{ave}$ of a FM/2DEG/FM transistor structure (inset) as a function of normalized electron concentration underneath the gate electrode for various exchange energies Δ_h/E_F . The inset shows $\Delta G/G_{ave}$ for a finite interface barrier height (Z=2). The oscillations are due to interference effects since the separation of the FM electrodes (300nm, gate length 100nm) is in the order of Fermi wavelength of the 2DEG.

References

[1] S. Datta and B. Das, Appl. Phys. Lett., 56, 665 (1990).
[2] G. Schmidt et al., Phys. Rev. B, 62, 4790 (2000).
[3] E. I .Rashba, Phys. Rev. B. 62, 16267 (2000).
[4] Y. Ando and T. Itoh, J. Appl. Phys., 61, 1487 (1987).

This work is supported by NEDO International Joint Research Grant Program

Corresponding author: Th. Schäpers, Institut für Schichten und Grenzflächen, Forschungszentrum Jülich, 52425 Jülich.
phone: +49 2461 61 2668, Fax: +49 2461 61 2940

Exchange interactions in CdMnTe/CdMgTe quantum wells under high magnetic fields and high pressure

T. Yasuhira[1], K. Uchida[1], Y. H. Matsuda[1], N. Miura[1], S. Kuroda[2], and K. Takita[2]

[1] Institute for Solid State Physics, University of Tokyo,
Kashiwanoha, Kashiwa, Chiba, 277-8581, Japan
[2] Institute of Material Science, University of Tsukuba,
Tsukuba, Ibaraki 305-8573, Japan

Magneto-photoluminescence spectra of excitons were measured in CdMnTe/CdMgTe quantum wells at pulsed high magnetic fields up to 45T and high hydrostatic pressure up to 1.6 GPa to study the effect of the dimensionality on the exchange interactions in magnetic quantum wells. We found a number of new features of the sp-d exchange $J_{sp\text{-}d}$ interaction and the J_{NN} between the nearest neighbor Mn ions. The samples were grown on GaAs substrates by the MBE. Eight samples were prepared with different Mn concentrations (0-8%). The Mg concentration was set at 24-37%. In each sample, 3 quantum wells with different layer widths (2.4-14 nm) were fabricated, so that the well-width dependence of the magnetic and pressure effect was observed in a single run of the measurement under the same condition. The magnitude of the sp-d exchange interaction $J_{sp\text{-}d}$ estimated from the observed Zeeman splitting was found to decrease as the quantum well width decreased. The decrease is partly due to the penetration of the wavefunction into the nonmagnetic CdMgTe barrier layers, whose effect is larger for thinner well width. After subtracting the interface effect, we found that $J_{sp\text{-}d}$ still decreases with decreasing well width due to the *k*-dependence of the interaction. However, the extent of the decrease is much larger than the theoretical prediction [1]. On application of hydrostatic pressure, it was found that the $J_{sp\text{-}d}$ increases with increasing pressure, and the extent of the increase was enhanced as the well width was decreased. We found that that the pressure effect is mainly due to the relaxation of the strain effect at the interface. All the features mentioned above are well explained by a model assuming the existence of a region at the interfaces in the quantum well, where the interaction is different from the interior of the well. As such a region has a finite thickness (~0.35nm), it increases its importance in thinner quantum wells. A quantitatively good agreement was obtained between the experimental result and the calculation based on this model and by employing the data of Merkulov et al. [2] for the interior region in the well. J_{NN} estimated from the steps in the photoluminescence showed no dependence on the well width. Both $J_{sp\text{-}d}$ and J_{NN} are represented by the same parameters, the p-d transfer energy, the on-site Coulomb energy, the energies of p and d levels, *etc.*, the experimental results showed the different character between the exchange interactions J_{NN} and $J_{sp\text{-}d}$.

References

[1] A. K. Battacharjee, Phys. Rev. B, **58**, 15660 (1998).
[2] I. A. Merkulov et al. Phys. Rev. Lett. **83**, 1431 (1999).

Corresponding author: Noboru Miura,
Institute for Solid State Physics, University of Tokyo
5-1-5 Kashiwanoha, Kashiwa, Chiba 277-8581, Japan
phone: +81 471 36 3341, Fax.: +81 471 36 3335
e-mail: miura@issp.u-tokyo.ac.jp phone:

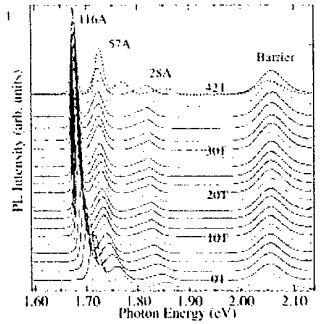

Fig. 1 Magneto-photoluminescence spectra in three $Cd_{1-x}Mn_xTe/Cd_{1-y}Mg_yTe$ ($x = 0.067$, $y = 0.243$) quantum wells with different thicknesses.

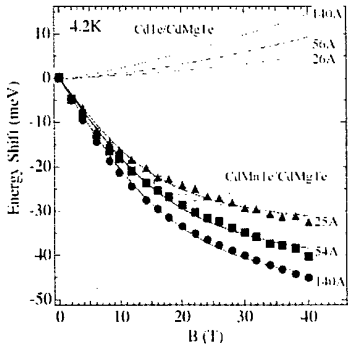

Fig. 2 Energy shift of the exciton peak for three different quantum wells. Open data points are the raw data, and the closed points are the points representing the difference from CdTe wells with the same thickness. $x = 0.049$, $\nu = 0.37$.

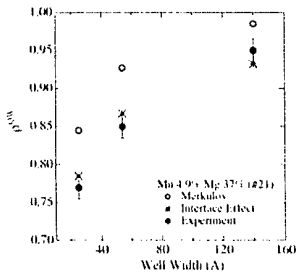

Fig. 3 Comparison of the present results with the data of ref. [2] and the calculated result taking account of the interface effect. A good agreement between the experiment and the calculation was obtained.

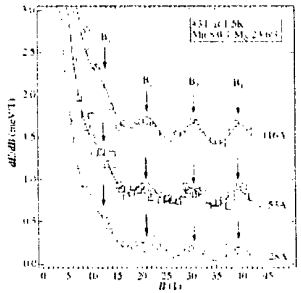

Fig. 4 Magnetization steps observed in the photon energy of the photoluminescence peak of excitons in CdMnTe/CdMgTe quantum wells with different well widths. Temperature is 1.6K. We can see that the peak positions are independent of the well width.

Effective spin diffusion across hugely lattice mismatched heterointerfaces

M. Ghali[1], J. Kossut[1], E. Janik[1], K. Regiński[2], Ł. Kłopotowski[3], S. Maćkowski[1], G. Cywiński[1], and P. Dłużewski[1]

[1]Institute of Physics, Polish Academy of Sciences, Al. Lotików 32/46, 02-668 Warsaw, Poland,
[2]Institute of Electon Technology, Al. Lotników 32/46, 02-668 Warsaw, Poland
[3]Institute of Experimental Physics, Warsaw University, ul. Hoża 69, Warsaw, Poland

An ability to control the electron spin rather than its charge represents the basic requirement of an emerging field of spintronics. A major progress has been made recently by demonstrating an effective spin injection across a semiconductor interface without substantial loss of its quantum coherence. This process has been achieved in non-magnetic semiconductors heterogeneous systems [1]. Yet another important progress was made by incorporating magnetic semiconductors as spin aligners with spin injection has been achieved either optically [2] or electrically [3] across diluted-magnetic/normal semiconductor or ferromagnetic semiconductor/non-magnetic semiconductors heterointerfaces. In all cases, an extreme care was taken to assure a good lattice matching of the constituent layers of the entire structure. A natural question arises concerning the role of lattice matching as a factor limiting the effectiveness of the spin transport across different semiconductor interfaces.
In this work we study a very large (~7.8%) lattice-mismatched materials where the hetero-interface includes a large amount of misfit dislocations as evidenced in TEM images. Our structure consists of 1.1μm thick $Zn_{0.97}Mn_{0.03}Te$ layer, playing the role of the spin aligner, grown on top of $Ga_{0.8}In_{0.2}As/GaAs$ quantum well burried 200 below the heterointerface. The later structure serves as a spin polarization detector. The growth process has been carried out in separated steps using two different MBE machines. Nevertheless, the high-resolution TEM images show a good crystalline character of the interface itself with an array of dislocations being present in the spin aligner. Magneto luminescence experiments have been carried out in a magnetic field range from 0-5T at 1.8K. Circular polarized excitation (σ^+ and σ^-) above and below the ZnMnTe band gap (~ 2.403eV) was used in the Faraday geometry. The degree of the circular polarization (ρ) detected of the GaInAs QW luminescence (~1.34eV) was measured.

Our PL measurements exhibit in the case of the excitation above the ZnMnTe band gap at 4T ρ ~15% under σ^+ circularly polarized light while a lower value ρ ~ 2%, under σ^- excitation. Moreover, the degree of the circular polarization has been measured as a function of the magnetic field for the both circular polarization excitations and for various excitation energies. The effect is absent in the below the ZnMnTe band gap excitation. A significant difference in ρ in the former case is then observed, which can be interpreted as being due to electrons with spin down orientation diffusing from the diluted magnetic layer ($g > 0$) to the non-magnetic ($g < 0$) QW although a dense array of misfit dislocations is present at the heterointerface. In the case of σ^+ excitation the large value of ρ ~15% indicates that the injected spin-down electrons were in the same spin-down state as those excited ***intrinsically*** in the non-magnetic regions. On the other hand, in the case of σ^- excitation the injected spin-down electrons mix with those generated intrinsically in the nonmagnetic regions, which have opposite polarization, thus diminishing the net ρ.

References

1- I. Malajovich, J.M Kikawa, D.D Awschalom, J.J.Berry and N.Samarth, Phys. Rev. Lettr. **84**, 1015(2000).
2- M.Oestreich, J. Hubner, D. Haggle, P.J. Klar, W.Heimbrodt, W.W.Ruhle, D.E.Ashenford, and B. Lunn, Appl. Phys. Lettr., **74**, 1251 (1999).
3- R.Fiederling, M.Keim, G.Reuscher, W.Ossau, G.Schmidt, A.Waag and L.M.Molenkamp, Nature **402**, 787 (1999).

Corresponding auther: Mohsen Ghali, Institute of Physics, Polish Academy of Sciences, Al.Lotików 32/46, 02-668 Warsaw, Poland
Phone: (+48)(+22) 843 13 31 ; Fax: (+48) (+22) 843 13 31
e-mail : Mohsen@ifpan.edu.pl

Correlation of magnetism and doping in the magnetic semiconductor (Ga,Mn)As with Mn(Ga)As clusters

Th. Hartmann[1], M. Lampalzer[1], P. J. Klar[1], K.Volz[1], W.Stolz[1], W. Heimbrodt[1], H.-A. Krug von Nidda[2], A. Loidl[2]

[1] Department of Physics and Material Sciences Center, Philipps-University Marburg, Renthof 5, D-35032 Marburg
[2]Department of Physics, University of Augsburg, Universitätsstraße 2, D-86135 Augsburg

Magneto-electronics, spin-electronics and spin optoelectronics are widely regarded as key technologies of the future [1]. Break-throughs are expected for semiconductor electronics when spin-transistors and spin optoelectronic devices can be realised. Several obstacles need to be overcome: (i) spin-injection into the semiconductor, (ii) spin transport over distances comparable to the device lengths and (iii) conversion of spins into polarised light in the active region of spin-optoelectronic devices. Whereas the latter two problems are fairly easy to solve, the spin-injection still poses a major challenge. A promising candidate which may serve as spin aligner and spin injector is ferromagnetic (Ga,Mn)As. Ferromagnetism at room-temperature occurs in this material only when ferromagnetic Mn(Ga)As clusters are formed within a paramagnetic host. We studied in detail the correlation between magnetism of the (Ga,Mn)As host as well as the Mn(Ga)As clusters and the doping of the host material.

We have grown successfully (Ga,Mn)As layers on (001) GaAs substrates with a thin undoped GaAs buffer by metal-organic vapour phase epitaxy (MOVPE) in a horizontal reactor system at substrate temperatures in the range of 400^{0}C to 550^{0}C. We have obtained (Ga,Mn)As samples with and without Mn(Ga)As clusters [2,3]. We used magneto-optical spectroscopy (PL, PLE), spin-flip Raman spectroscopy (SFR), magneto-transport as well as angle resolved ferromagnetic resonance (FR) measurements using X-band frequencies.

Independent of the type of majority carriers in the (Ga,Mn)As host material the Mn(Ga)As clusters exhibit ferromagnetic behaviour with a phase transition into the paramagnetic state above room-temperature ($T_C \approx 320$ K). The temperature-dependent FR signal shows a clear indication of this phase transition. This magnetic phase transition is probably related to a structural transition. Bulk MnAs has hexagonal NiAs-type below and orthorhombic MnP-type above 318 K [4]. An additional abrupt change of the FR signal is observed at about 290 K possibly indicating another phase transition which is not known for bulk MnAs. Analysing the angle dependence of the FR signals at 200 K for various crystallographic orientations of the (Ga,Mn)As matrix with respect to the magnetic field direction, we deduced that the Mn(Ga)As [0001] axis (which is the hard magnetic axis of the clusters) is approximately parallel to the [111] directions of the host. The easy axis of magnetisation is perpendicular to Mn(Ga)As [0001].

The s,p-d exchange interaction in the (Ga,Mn)As host between the band states and the magnetic moments of the Mn-ions has been studied by combining PLE and SFR results. A strong correlation of the sign of the p-d exchange integral $N_0\beta$ of the valence band with the type of the majority carriers has been found. A positive $N_0\beta$ (ferromagnetic coupling) is observed for p-type conductivity and a negative $N_0\beta$ (antiferromagnetic coupling) is observed for n-type conductivity. This will be discussed and explained on the basis of a microscopic model of the local electronic structure of Mn on Ga sites.

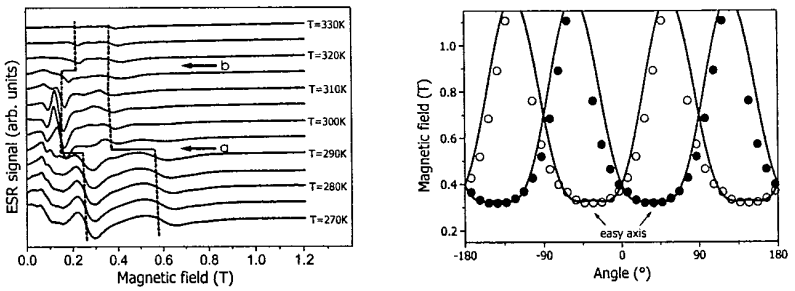

Fig. 1: *(a) Temperature dependence of FR signal, magnetic field direction parallel to the easy axis of magnetisation; (b) Peak positions of the angle-dependent FR signals rotating the sample about the [110] direction of the host and the magnetic field perpendicular to the rotation axis.*

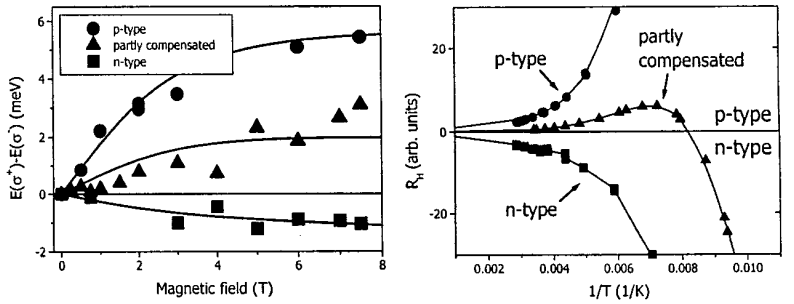

Fig. 2: *(a) Giant Zeeman splitting of the heavy-hole exciton states and (b) corresponding Hall coefficients for a p-type, partly compensated and a n-type sample*

References

[1] G. Prinz, Science **282**, 1660 (1998).
[2] Th. Hartmann, M. Lampalzer, W. Stolz, K. Megges, J. Lorberth, P.J. Klar, W. Heimbrodt, Thin Solid Films **364**, 209 (2000).
[3] W. Heimbrodt, Th. Hartmann, P.J. Klar, M. Lampalzer, W. Stolz, K. Volz, A. Schaper, W. Treutmann, H.-A. Krug von Nidda, A. Loidl, T. Ruf, V.F. Sapega Physica E, (2001) in print.
[4] C.P. Bean and D.S. Rodbell, Phys. Rev. **126**, 104 (1962).

Corresponding author: Th. Hartmann, Department of Physics and Materials Science Center, Philipps University Marburg, Renthof 5, D-35032 Marburg, Germany
phone: ++49 6421 2822118, fax: ++49 6421 2827036,
e-mail: thorsten.hartmann@physik.uni-marburg.de

Spin interference and Fabry-Pérot resonances in ferromagnet-semiconductor-ferromagnet devices

T. Matsuyama, C.-M. Hu, D. Grundler, G. Meier, D. Heitmann, and U. Merkt

Institut für Angewandte Physik und Zentrum für Mikrostrukturforschung,
Universität Hamburg, Jungiusstraße 11, D-20355 Hamburg, Germany

In this contribution we present the carrier-density dependence of transmission coefficients, conductances and spin-injection rates across a FM/InAs(2DES) single interface as well as a FM/InAs(2DES)/FM double junction. The results are applicable for, both, spin-valve [1] and spin-transistor devices [2] in the ballistic limit. We employ a transfer-matrix formalism taking into account the spin-orbit interaction due to the confinement potential inside an inversion layer on p-type InAs [3]. In samples of finite channel width, we study the influence of oblique modes in the 2DES. The band-structure parameters for different ferromagnets (Fe, Permalloy, Co) are explicitely included. We consider distinct magnetization configurations of the FM electrodes assuming an isotropic exchange interaction in the ferromagnet and a Rashba spin-orbit interaction [2] in the 2DES, both, in the effective mass approximation. We neglect any spin-flips due to spin-spin scattering of magnetic impurities at the interfaces or inside the channel. However, we introduce a delta-potential barrier at the FM/InAs interfaces, whose strength is characterized by a dimensionless Z parameter [4]. The conductance of the junction is determined by the number of modes in the 2DES. Using the appropriate spin-dependent boundary condition and realistic material parameters, we obtain a magneto-conductance ratio $\Delta G/G$ of up to 5% for a double-junction device. The transmission probability T_{ij} at an interface is determined by the Fermi-velocity mismatch as well as by the overlap of the spin eigenstates i = 1,2 and j = 1,2 in the FM and the 2DES, respectively. Accordingly, the spin-filtering effect is caused by the difference in the particular conditions that apply for the two injected spin subbands. Oblique modes [Fig. 1 (a)-(d)] decrease the injection rate. In case of a magnetization and concomitant spin alignment perpendicular to the interface [2], the spin-precession performance is strongly favored by normal incidence. This becomes clear from Fig. 1 (c,d). In addition, we find that spin filtering can be enhanced by increasing the Z parameter. The double junctions show Fabry-Pérot type interferences. The period of the resonance positions is independent of the band structure of the ferromagnetic as well as of the semiconductor material as can be seen in Fig. 2 (a,b). It depends on the channel length between the two FM electrodes. The main finding is that in case of the spin-valve configuration the resonances are due to particle interference, whereas in case of the spin-transistor configuration [Fig. 2 (c)-(f)] the spin is involved in the interference process.

We thank the Deutsche Forschungsgemeinschaft via SFB 508 'Quantenmaterialien' and the NEDO International Joint Research Program for financial support.

References

[1] C.-M. Hu, J. Nitta, A. Jensen, J. B. Hansen, and H. Takayanagi, Phys. Rev. B **63**, March 15 (2001).
[2] S. Datta and B. Das, Appl. Phys. Lett. **56**, 665 (1990).
[3] T. Matsuyama, R. Kürsten, C. Meißner, and U. Merkt, Phys. Rev. B **61**, 15 588 (2000).
[4] D. Grundler, Phys. Rev. Lett. **86**, 1058 (2001); Phys. Rev. B, April 15 (2001).

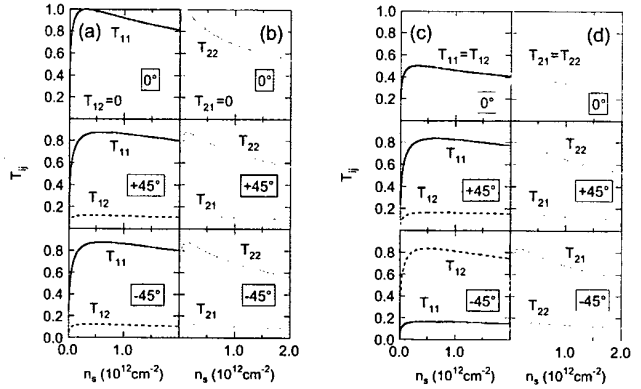

Fig. 1: Density dependence of the single-mode transmission coefficients for a Fe/InAs(2DES) junction for three angles between the normal of the interface and the k-direction inside the semiconductor without elastic interface scattering (Z=0). Panels (a,b) are for the spin-valve and (c,d) for the spin-transistor configuration.

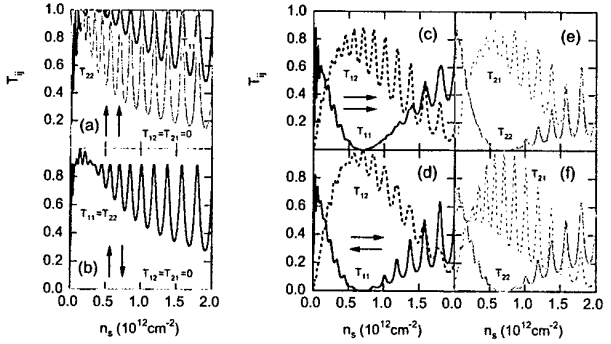

Fig. 2: Density dependence of the single-mode transmission coefficients for a ballistic Fe/InAs(2DES)/Fe device in the spin-valve (a,b) and the spin-transistor configuration (c-f) without elastic scattering potential (Z=0). For both configurations the upper and the lower panels are for parallel and antiparallel magnetizations in the electrodes, respectively.

Corresponding author: Toru Matsuyama, Institut für Angewandte Physik,
Universität Hamburg, Jungiusstraße 11, D-20355 Hamburg, Germany
Phone: +49 40 42838 2917, Fax: +49 40 42838 4368,
email: matsuyama@PHYSnet.uni-hamburg.de

Molecular beam epitaxy of CdMnSe on InAs: a new material system for spin injection

G. Richter, P. Grabs, R. Fiederling, P. Bach, G. Schmidt, L. W. Molenkamp
Experimentelle Physik III, Universität Würzburg, Am Hubland, 97074 Würzburg, Germany

W. Weigand, Th. Gleim, C. Heske, E. Umbach
Experimentelle Physik II, Universität Würzburg, Am Hubland, 97074 Würzburg, Germany

Heterostructures containing CdMnSe on InAs are promising candidates for spintronic devices. Using InAs as a substrate material should eventually provide the opportunity to fabricate transport structures, containing a spin injector in combination with a high mobility two dimensional electron gas. For a manganese concentration of about 12% the dilute magnetic semiconductor is lattice matched to InAs and therefore can be grown without strain.
MBE-growth of the samples was performed in a RIBER 2300 system with III/V and II/VI growth chambers and an analysis chamber for in-situ SPA-LEED (Spot Profile Analysis – Low Energy Electron Diffraction) examinations which are connected via an UHV-module.
Clear RHEED oscillations taken during the growth of a ZnTe buffer and the CdMnSe layer indicate a good layer-by-layer growth mode for both InAs as well as CdMnSe.
Additional characterization was done by SPA-LEED and X Ray diffraction (XRD). The SPA-LEED measurements were done during different stages of the growth process showing a clear (2x1) surface reconstruction. With XRD a good structural quality could be observed for small Mn concentrations. The influence of the growth conditions especially the use of a ZnTe-buffer prior to the growth of the CdMnSe layer on its quality will be discussed.
Photoluminescence measurements show a giant Zeeman splitting which depends on the Mn concentration as is typical for dilute magnetic semiconductors.
Electrical measurements reveal an ohmic behaviour at the CdMnSe-InAs interface which substantially adds to our confidence of the suitability of the material system for lateral spin injection devices. From preliminary magnetoresistance measurements we conclude that spin injection actually does occur across this interface.

corresponding author:
Georg Richter
Experimentalphysik 3
Physikalisches Institut
Universität Würzburg
Am Hubland
97074 Würzburg
georg.mueller@physik.uni-wuerzburg.de
tel. (++49) 0931 – 888 – 5106
fax: (++49) 0941 – 888 – 5142

Growth characteristics and magnetic properties of MnAs/AlAs/MnAs trilayer heterostructures grown on vicinal GaAs(111)B substrates

Satoshi Sugahara and Masaaki Tanaka

Department of Electronic Engineering, The University of Tokyo
7-3-1 Hongo, Bunkyo-ku, Tokyo 113-8656, Japan
Phone: +81-3-5841-6773, Fax: +81-3-5803-3975, Email: sugahara@cryst.t.u-tokyo.ac.jp

Magnetic tunnel junctions (MTJs), consisting of ferromagnet (FM) / insulater (I) / FM trilayers, are extensively studied for applications to magnetic field sensors and magnetic random access memory (MRAM). While most of MTJs studied so far were made of polycrystalline (FM) electrodes and amorphous (I) tunneling barrier, atomically controlled all-epitaxial MTJs are highly desirable, since one can have a lot more freedom in the design of materials and device structures [1]. MnAs/III-V/MnAs heterostructures are expected to be promising for all-epitaxial MTJs, since 1) MnAs is a ferromagnetic metal at room temperature, 2) high quality MnAs films can be grown epitaxially on GaAs and Si substrates using molecular beam epitaxy (MBE) [2], and 3) the heterostructures can be monolithically intrgrated with semiconductor devices. Although the growth of MnAs/GaAs/MnAs heterostructures has been already established [2], MnAs/AlAs/MnAs heterostructures are more attractive since the AlAs layer acts as the larger barrier height for MTJs in which the dependence of tunneling magneto-resistance (TMR) on the barrier thickness is predicted to be weak [3]. In this paper, we investigate the epitaxial growth characteristics and magnetic properties of MnAs/AlAs/MnAs trilayer heterostructures, aiming at the all-epitaxial MTJ application.

Although MnAs/III-V/MnAs heterostructures can be grown epitaxially on the exact GaAs(111)B surface by MBE, we found that the pyramidal facets on the GaAs buffer layer deteriorate the interface morphology. To avoid the formation of the pyramidal facets on the GaAs buffer layer, vicinal GaAs(111)B substrates (misoriented 2° toward the [-1-12] direction) were used here. When 20-nm-thick MnAs films were grown at 250°C on the atomic-stepped vicinal GaAs buffer layer, the surface was quasi-flat, having largely spread terraces (with 70 nm in width) and very smooth macrostep facets (with 2 nm in height) with gentle slopes with respect to the terraces [4]. This MnAs layer was used as the bottom layer of all MnAs/AlAs/MnAs trilayer samples.

AlAs films on the MnAs/GaAs(111)B surface were grown in the Stranski-Krastanov (SK)-like mode. The SK islands appeared on the AlAs overlayer when a 10-nm-thick AlAs film was grown at 250°C. When the film thickness of the AlAs layer was reduced to 2 nm (which is appropriate as the insulating tunnel barrier for the MTJ application), the surface morphology was dramatically improved, that is, the islands were not formed at all and the surface became very smooth. It was also found that the RHEED pattern was streaky for the 2-nm-thick AlAs film grown at 200°C, although the RHEED pattern showed rings for the 10-nm-thick AlAs film grown at 200°C. This indicates that the temperature window for epitaxial growth is widened to lower temperature by reducing the film thickness. A possible origin of this phenomenon is "limiting thickness" for epitaxial growth reported by Eaglesham *et al* [5].

Figure 1(a) shows a RHEED pattern from the 2-nm-thick AlAs film grown on the MnAs/GaAs(111)B surface at 250°C. It was clearly seen that the diffraction pattern of MnAs was superimposed on that of AlAs, as shown by arrows in the figure. This means that there exists surface segregation of Mn atoms during the AlAs growth. By decreasing the substrate temperature to 200°C, surface segregation of Mn atoms was not detected, as shown in Fig. 1(b).

The Volmer-Weber (VW) mode of growth occurred for a 20-nm-thick MnAs film grown at 250°C on the AlAs/MnAs/GaAs(111)B surface, i.e., the top MnAs layer formed plateau islands and the height of these islands was close to the grown MnAs film thickness. The surface morphology was changed from the VW islands to the relatively conformal film by increasing the film thickness from 20 nm to 40 nm or by decreasing the substrate temperature from 250°C to 200°C, although the surface morphology was roughened for both cases. For the MTJ application, the interface morphology of the tunnel barrier is much more important than the surface morphology of the top layer. Since the bottom MnAs surface and the AlAs surface exhibited very smooth morphology in the present MnAs/AlAs/MnAs heterostructures, the rough surface of the top MnAs layer is not a serious problem.

Figure 2 shows magnetization (*M-H*) loops measured at room temperature for the MnAs/AlAs(2nm)/MnAs(20nm) trilayers. For both samples, the bottom MnAs was grown at 250°C, and the AlAs and top MnAs layers were grown at (a) 250°C and (b) 200°C. The film thickness of top MnAs layer was 40 nm for the sample (a) and 20 nm for the sample (b). Two-step structures were observed in both *M-H* loops, that are caused by the large coercivity of the top MnAs layer due to its relatively poor crystallinity. Two steps are more pronounced in the sample (b) grown at 200°C. In the sample (a) grown at 250°C, the coercivity of the bottom MnAs layer increased to ~300 Oe, compared with 35 Oe of the single 20-nm-thick MnAs layer grown on GaAs. This is attributed to the ferromagnetic interlayer coupling between the bottom and top MnAs layers, that was induced by the incorporation of Mn atoms in the AlAs layer due to the surface segregation of Mn atoms during the AlAs growth. In the sample (b), however, no Mn segregation was detected in RHEED during the growth of the AlAs layer. Two-step structures were clearly observed in the *M-H* loop of the sample (b) and the coercivity of the bottom MnAs layer was as small as 35 Oe, indicating no interlayer coupling. This clear two-stepped *M-H* characteristics is essential for MTJs.

In summary, the low-temperature growth of the MnAs/AlAs/MnAs trilayers at 200°C was found to be very effective to establish fairly smooth interface morphology and to suppress surface segregation of Mn atoms. These topological and metallurgical features are very attractive for all-epitaxial MnAs/AlAs/MnAs MTJs. Transport properties including TMR will be also reported in the conference.

References: [1] Recently, we have fabricated all-epitaxial MTJs using GaMnAs/AlAs/GaMnAs ferromagnetic semiconductor heterostructures, and observed very large TMR ratios (>70%), see Y. Higo, H. Shimizu and M. Tanaka, presented at PASPS-2000, Sendai, Sept. 2000, to be published in Physica E. [2] M. Tanaka, K. Saito and T. Nishinaga, Appl. Phys. Lett. 74, 64 (1999). [3] J. Mathon, Phys Rev. B56, 11810 (1997). [4] S. Sugahara and M. Tanaka, to be published in J. Appl. Phys. [5] D.J. Eaglesham, H.-J. Gossman and M. Cerullo, Phys. Rev. Lett. 65, 1227 (1990).

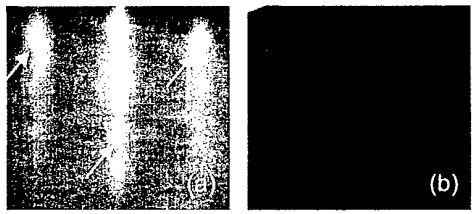

Fig.1 RHEED patterns from 2nm-thick AlAs films grown at (a) 250°C and (b) 200°C. While MnAs spots indicating the segregation of Mn atoms were obserbed in (a), no such segregation was observed in (b).

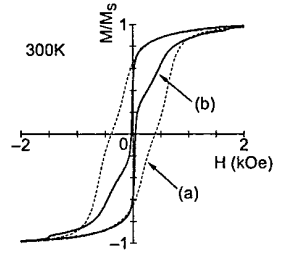

Fig.2 M-H loops for MnAs/AlAs/ MnAs trilayers measured at room temperature. The magnetic field was applied in-plane at 30° with respect to <-1-12> direction of the GaAs substrate. The AlAs layer and the successive top MnAs layer were grown at (a) 250°C and (b) 200°C.

Micro-Raman scattering study of $Ga_{1-x}Mn_xAs$

W. Limmer, M. Glunk, W. Schoch, A. Köder, R. Kling, R. Sauer, A. Waag

Abteilung Halbleiterphysik, Universität Ulm, Albert-Einstein-Allee 45, D-89081 Ulm, Germany

The III-V semimagnetic semiconductor $Ga_{1-x}Mn_xAs$ is considered one of the promising materials for the development of novel spin-electronic devices. Its magnetic properties arise from the magnetic moment of the Mn atoms which act as acceptors on the Ga lattice site and probably as donors in sixfold coordinated Mn^{6As} centers [1,2]. Carrier type and density are important parameters for the ferromagnetic Mn-Mn-interaction. In non-magnetic materials the carrier densities are usually determined by Hall measurements. However, in $Ga_{1-x}Mn_xAs$ the ordinary Hall effect is superimposed by an anomalous Hall effect which is proportional to the magnetization M. Therefore, the hole concentration can only be derived from the Hall resistance under high magnetic fields above 20 T where M saturates.

As an alternative method for the determination of carrier type and density in $Ga_{1-x}Mn_xAs$ we have used micro-Raman scattering by coupled plasmon-LO-phonon (PLP) modes. It is well known that in n-type GaAs two coupled PLP modes L_- and L_+ can be observed in the Raman spectrum, whereas in p-type GaAs only one coupled mode L_S is observed because of the strong damping of the hole plasmon. Its frequency shifts from the LO-phonon position to the TO-phonon position with increasing hole concentration p. For 10^{18} $cm^{-3} \leq p \leq 10^{19}$ cm^{-3} the mode is plasmon-like and appears as a broad band between the TO and LO positions. Beyond these limits it is phonon-like and its linewidth approaches that of the LO phonon with decreasing or increasing carrier density, respectively.

The $Ga_{1-x}Mn_xAs$ layers under investigation were grown by low temperature MBE on GaAs(100) substrates at 250 °C using elemental Mn and an ECR nitrogen plasma source. Mn concentrations up to 5% were incorporated in the 0.4 μm thick layers as deduced from HRXRD. The micro-Raman measurements were performed in backscattering configuration at room temperature using the 514 nm line of an Ar^+ laser as an excitation source. The laser beam was focused by a microscope lens system yielding a spot diameter of 0.7 μm. Further experimental details can be found in [3].

In Fig. 1 the Raman spectra of two $Ga_{1-x}Mn_xAs$ layers and of the GaAs substrate, recorded from the (001) surface, are shown for comparison. From the Raman spectra it follows that all $Ga_{1-x}Mn_xAs$ samples are p-type. The solid line represents a lineshape analysis yielding a hole concentration of $p \geq 5 \times 10^{19}$ cm^{-3}. The lineshape of the PLP mode was modeled within the linear response formalism using a Lindhard-Mermin expression for the dielectric constant [4]. The PLP mode becomes LO-phonon-like for high hole concentrations and thus knowledge of the LO-phonon linewidth in the $Ga_{1-x}Mn_xAs$ sample plays a crucial role in the lineshape analysis. Since the pure LO phonon could not be observed in our samples because of the plasmon-LO-phonon coupling we approximated the value for the LO-phonon linewidth in the model calculations with that of the TO phonon. According to the Raman selection rules scattering by TO phonons is forbidden for backscattering at the (001) surface and allowed for backscattering at the (110) surface. Although the $Ga_{1-x}Mn_xAs$ layers were only 0.4 μm thick we were able to measure the TO-phonon line in the layer on a cleaved (110) surface using the lateral resolution of our equipment. Figure 2 exhibits a Raman line scan on the cleaved (110) surface along the [001] direction. A TO-phonon linewidth of 15 cm^{-1} is determined in the $Ga_{1-x}Mn_xAs$ layer in comparison with 3 cm^{-1} in the GaAs substrate. It should be emphasized that the lineshape analysis strongly underestimates the hole concentration if the small phonon linewidth from the substrate is used in the calculations.

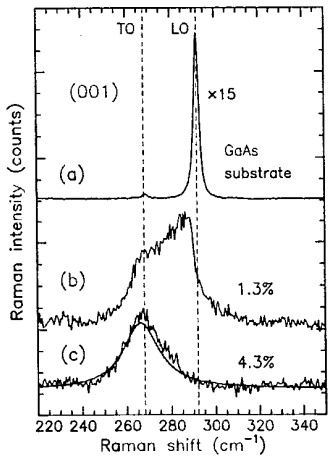

Figure 1: Raman spectra recorded from the GaAs(001) substrate (a) and from two $Ga_{1-x}Mn_xAs$ layers with 1.3% (b) and 4.3% (c) Mn concentration. The solid line represents a model calculation of the PLP lineshape.

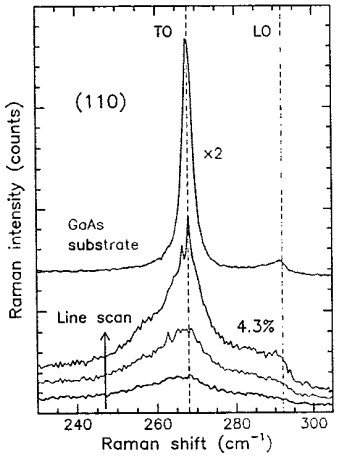

Figure 2: Raman line scan on the (110) surface along the [001] direction. The sample position between subsequent measurements was shifted by 0.4 μm. A Raman spectrum recorded from the GaAs substrate is shown for comparison.

References

[1] H. Ohno, Science **281**, 951 (1998).
[2] A. Van Esch et al., Phys. Rev. B **56**, 13103 (1997).
[3] W. Limmer et al., J. Crystal Growth **188**, 225 (1998).
[4] G. Irmer et al., Phys. Rev. B **56**, 9524 (1997).

Corresponding author: Wolfgang Limmer, Abteilung Halbleiterphysik, Universität Ulm, Albert-Einstein-Allee 45, D-89081 Ulm, Germany.
phone: +49 731 50 26130, Fax: +49 731 50 26108,
email: wolfgang.limmer@physik.uni-ulm.de

Abstract category G : Spin electronics, magnetic hetero- and nanostructures

Epitaxy and characterization of GaMn(N)As for spin electronics

A.Waag, A.Köder, R.Kling, W.Schoch, W.Limmer, R.Sauer
Abteilung Halbleiterphysik, Universität Ulm, Ulm, Germany

GaMnAs is a material which shows ferromagnetic coupling between the Mn ions at high p-type doping, and Curie temperatures up to 110K have been reported [1]. Recently, Dietl et al. [2] gave a theoretical description of that behavior and calculated the Curie temperatures of various semimagnetic semiconductors. According to this work, larger effective masses and higher p-type doping levels should increase the Curie temperatures. For ZnMnO and GaMnN, Curie temperatures above room temperature have been calculated, assuming that a high p-type doping level above 1E20 cm^{-3} is possible.

This was our motivation to start into investigating novel nitrogen containing III-V based semimagnetic material. Here we focus on GaMn(N)As. It is well known from GaNAs that – with nitrogen incorporation - the electron masses increase drastically (up to a factor 3), and that the band gap decreases, which should influence the dopability of the material and hence the Curie temperature. Hole masses as a function of nitrogen incoporation in GaNAs, which would be relevant for the ferromagnetic coupling, are unknown so far. A high-T_C ferromagnetic material, which can be pseudomorphically grown on GaAs, would be very interesting for spintronic devices operating at room temperature.

GaMnAs and GaMnNAs layers have been grown in a conventional MBE system, using elemental Mn and an ECR nitrogen plasma source. Low temperature (LT) growth at a substrate temperature of 250°C has been employed. 2D RHEED patterns can be seen even at such a low growth temperature. The thin films have been analyzed by HRXRD, and magnetotransport as well as Raman spectroscopy.

HRXRD scans are shown in fig.1 for a LT-GaMnAs, a LT-GaNAs and a LT-GaMnNAs layer. Whereas Mn incorporation increases the lattice constant, N incorporation decreases it. Hence, the GaMn(N)As quatnerary can be grown completely lattice matched on GaAs. Mn concentrations up to 5% and N concentrations up to 1% have been realised up to now. The Hall resistance of GaMnAs layers shows a remanence value below the Curie-temperature. The remanent Hall effect vs. temperature is plotted in fig.2 for one particular sample with 4.25% Mn, being an alternative and efficient way to determine Curie temperatures of these materials. Above T_C, the remanent Hall resistance becomes zero. Fig. 3 shows the Curie temperatures determined by the method described above, as a function of Mn content of the layers. For GaMnAs, we achieved Curie temperatures up to 90K. Positive and negative contributions to the magneto-resistance have been separated and analyzed as a function of temperature. The positive contribution to the magneto-resistance $(\Delta R/R)_P$ behaves Brillouin-function-like vs. magnetic field. $(\Delta R/R)_P$ increases below the paramagnetic-ferromagnetic phase transition, also indicating the Curie-temperature. In addition the specific resistance at B=0T shows a maximum at T_C, which is usually taken as a signature of the phase transition. The analysis of the magnetotransport data of the nitrogen containing GaMnNAs layers is under way.

[1] *F.Matsukura, H.Ohno, A.Shen, Y.Sugawa, Phys.Rev.B 57(1998)R2037.*
[2] *T.Dietl, H.Ohno, F.Matsukury, J.Cibert, D.Ferrand, Science 287(2000)1019.*

corresponding author: Andreas Waag, Abteilung Halbleiterphysik, Albert Einstein Allee 45, 89081 Ulm
phone xx49-731-50-26102, fax –50-26108, andreas.waag@physik.uni-ulm.de

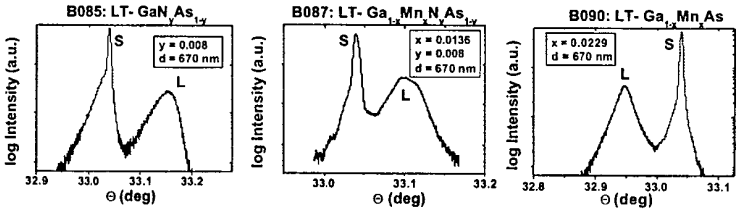

Fig.1: HRXRD of the 004 reflection of a GaNAs, GaMnAs and GaMnNAs thin films grown on GaAs substrate. Layer (L) and substrate peak (S) are indicated. Thicknesses d and composition are given in the inset.

Fig.2: Remanent Hall resistance as a function of temperature for a sample with a Mn concentration of 4,25%. The derived Curie temperature is indicated.

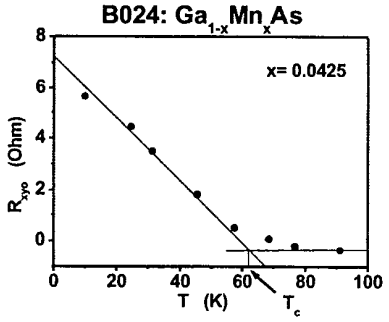

Fig.3: Curie temperatures as a function of Mn concentration for GaMnAs thin films.

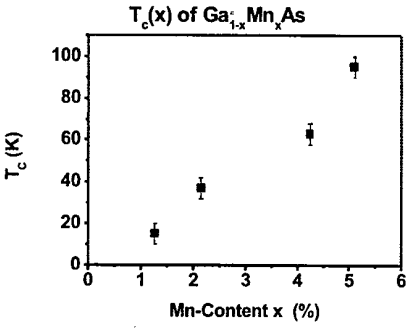

Scaling of ferromagnet/semiconductor contacts for the study of spin-dependent collection

A. Bournel, P. Dollfus, P. Hesto

Institut d'Electronique Fondamentale, CNRS UMR 8622, Université Paris Sud, Bât. 220, F-91405 Orsay cedex, France

The spintronics is an emerging research topic in the field of semiconductor structures. The key point for the viability of some proposed devices is the spin selectivity of ferromagnet (FM)/semiconductor SC contacts. This subject has been very debated. The spin-dependent collection at the interface between a FM contact and a semiconductor can be experimentally investigated by photogenerating spin polarized electrons in a GaAs-like SC. However, the spin polarization measured in such experiments is about 1% which is of the same order of magnitude than effects related to FM circular dichroism [1]. Significant spin injection effects have been obtained by using magnetic SCs, but until now at low temperatures or for spin-polarized holes only [2]. Otherwise, it was recently concluded that the conductivity mismatch between a FM metal and a SC is a fundamental obstacle for spin injection in the diffusive regime [3]. However, this difficulty could be circumvented by using tunnel contacts [4] or by optimizing the crystallographic properties of the heterointerface [5].

This paper deals with the scaling of a FM/SC contact usable to investigate the spin-dependent collection of electrons in a FM/SC contact at room temperature. In fact, the spin filtering effect can be strongly reduced in such contacts because of the different timescales of the phenomena driving the transport of the spin-polarized electrons photogenerated in the SC. To maintain the electric neutrality in SC and preserve a spin filtering effect, the electrons with a spin opposite to that preferentially collected have to recombine before loosing their spin coherence. At 300 K, the nanosecond electron lifetime is high compared to the spin relaxation time and to the picosecond collection time. These differences may explain the weak spin collection effects usually observed.

This difficulty may be overcome by reducing the electron lifetime in the SC, by increasing the collection time with a tunnel barrier, or by using two interdigitated contacts: a magnetic contact and a non magnetic contact to regulate the photogenerated electron population. Moreover, the use of a heterostructure, such as InGaAs/InP, instead of a bulk SC could make easier the scaling of a suitable structure. We investigate theoretically these solutions.

We have qualitatively evaluated the interest of a tunnel barrier by simple calculations based on drift-diffusion equation. As expected from the previously developed considerations, the spin asymmetry of the collected photocurrent appears to be on the same order of magnitude than the circular dicroism effect (about 0.5%) for high values of transmission coefficient T of the barrier. If T decreases ($T < 0.1$), the spin asymmetry increases but remains low, *i.e.* less than 1.5%, due to the spin relaxation in the SC. The use of a tunnel barrier is thus not sufficient to preserve a spin filtering effect.

We have studied a structure with double interdigitated contacts by using a particle Monte Carlo transport model. In Fig. 1, we compare the time variation of the spin asymmetry obtained in such a structure (continuous line) and in a single FM contact (dashed line) resulting from a 100 fs-pulse of photogeneration. The intrinsic spin polarization P_{FM} of the FM contact is 50%, that is we consider that the transmission probability at FM/SC interface is 75% for spin up electrons and 25% for spin down electrons. The non collected electrons are specularly reflected. In a single FM contact, the spin asymmetry vanishes while it is higher than 5% with the double contacts. Further studies are necessary to optimize such a promising structure configuration: we may consider the use of a tunnel barrier and of a heterostructure to enhance the spin asymmetry.

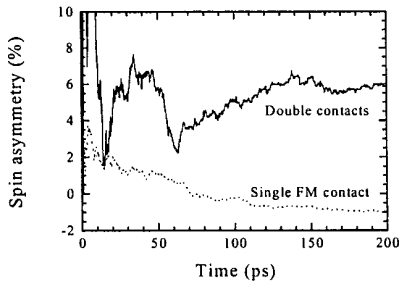

Fig. 1. Time variation of the spin asymmetry of the photocurrent collected in a single FM/GaAs Schottky contact (dashed line) and in a structure with interdigitated double Schottky contacts on GaAs (continuous line): a large non magnetic contact and a narrow FM contact, with intrinsic spin polarization P_{FM} = 50%. The spin-polarized electrons are generated by a 100 fs pulse.

References

[1] M.W.J. Prins *et al.*, J. Magn. Magn. Mater. **121**, 152 (1993).
[2] R. Fiederling *et al.*, Nature **402**, 787 (1999) ; Y. Ohno *et al.*, Nature **402**, 790 (1999).
[3] G. Schmidt *et al.*, Phys. Rev. B **62**, 4790 (2000).
[4] E.I. Rashba, Phys. Rev. B **62**, 16267 (2000).
[5] G. Kirczenow, Phys. Rev. B **63**, 054422 (2001).

Corresponding author: Arnaud Bournel, Institut d'Electronique Fondamentale, CNRS UMR 8622, Université Paris Sud, Bât. 220, F-91405 Orsay cedex, France
Phone: +33 1 69 15 40 25, Fax: +33 1 69 15 40 20, email: bournel@ief.u-psud.fr

Magneto-Optical Properties of GaAs Based Semiconductor Magneto Photonic Crystals

H. Shimizu[1,2], M. Tanaka[1,2]

[1]Department of Electronic Engineering, The University of Tokyo,
7-3-1 Hongo, Bunkyo-ku, Tokyo, 113-8656, Japan
[2]CREST, Japan Science and Technology Corporation

Realizing III-V semiconductor-based magneto-optical devices such as optical isolators, has been considered impossible due to incompatibility between III-V semiconductors and magnetic materials. For this purpose and their integration with III-V optoelectronic devices, large magneto-optical effect has to be obtained in a thin film at room temperature. Recently, we have investigated magneto-optical properties of III-V semiconductor / magnetic hybrid structure thin films and have demonstrated remarkable enhancement of magneto-optical intensity in MBE grown thin films consisting of GaAs/AlAs distributed Bragg reflector (DBR) / magneto-optical material / GaAs/AlAs DBR, which we call "semiconductor-based magneto-photonic crystal"[1]. As a magneto-optical material, we used MnAs nanoscale clusters embedded in a GaAs matrix (hereafter GaAs:MnAs), which are obtained by annealing low-temperature grown GaMnAs and show superparamagnetic properties at room temperature[2].

By multiple reflection of light, in other words, optical confinement into the central magnetic layer GaAs:MnAs, we have successfully enhanced the magneto-optical Faraday effect (up to 0.6 deg. corresponding to 4 deg./μm) in a GaAs/AlAs-DBR / GaAs:MnAs / GaAs/AlAs-DBR multilayer structure at room temperature under relatively low magnetic field of 0.1-0.2T. This value is much higher than those of conventional magneto-optical materials such as oxide garnet and II-VI based diluted magnetic semiconductor CdMnTe. The operation wavelength was set at 0.98μm for optical isolators for pumping laser diodes in Er doped fiber amplifiers [1]. We also theoretically analyzed optical transmission and magneto-optical properties of the multilayer structures and reproduced experimental spectra. For realizing higher magneto-optical performance, suppressing the optical loss in GaAs:MnAs is one of the most important issues. For solving the optical loss problem in GaAs:MnAs, we have found that operating at longer wavelength of ~1.55μm is effective. Also, magneto-optical properties of this multilayer system at 1.55μm are attractive for application in the fiber-optic telecommunication system.

As shown in Fig. 1, we fabricated a multilayer sample with the operation wavelength set at 1.55μm, whose structure is as follows; 5 pairs of bottom DBR composed of GaAs (115nm) and AlAs (134nm) / GaAs:MnAs (230nm) / 5 pairs of top DBR of GaAs and AlAs whose thicknesses are the same as those of the bottom DBR. The fabrication process consisted of three steps; (1) growth of the bottom DBR at the substrate temperature (T_s) of 580 on an AlGaAs etch-stop layer on a (001) GaAs substrate, (2) growth of $(Ga_{1-x}Mn_x)As$ at T_s = 250 , where the Mn concentration x was set at 0.065, (3) growth of the top DBR at T_s =580 . During the third step, where the substrate temperature was raised again up to 580 GaMnAs turned to MnAs nanoclusters embedded in a GaAs matrix by phase separation. Fig. 2 shows (a) optical transmission(T), (b) Faraday ellipticity(η_f) and (c) Faraday rotation(θ_f) spectra of this sample at room temperature. Faraday ellipticity and rotation spectra were measured at 1T applied perpendicular to the film plane. A local maximum (T=20%) was observed at 1.54μm at the center of the optical stop band in the optical transmission spectrum, and around this wavelength, the Faraday intensity was successfully enhanced. (η_f = 0.52 deg. and θ_f = 0.21deg. were obtained.) The enhancement factor of the Faraday effect per magnetic layer thickness was 4.8 compared with GaAs:MnAs without DBR. Figure of merit (FOM) of η_f is 0.32deg./dB at 1.54μm, which is twice as FOM of 0.16deg./dB at 0.98μm. This is because optical loss of GaAs:MnAs is lower at 1.54μm than that at 0.98μm and effective enhancement of the Faraday effect was realized. We can conclude that our new result of magneto-optical properties with operational wavelength of 1.54μm is improved, compared with our previous results at 0.98μm. The present semiconductor-based magneto-optical crystal is also attractive in longer wavelength of 1.55μm for optical isolator applications.

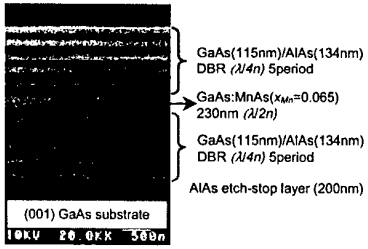

Fig. 1: Cross sectional image of GaAs based magneto-photonic crystal taken by scanning electron microscopy.

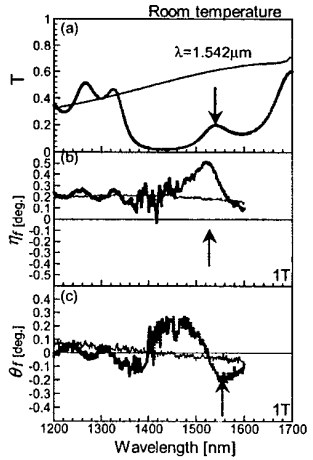

Fig. 2: (right) (a) Optical transmission(T), (b) Faraday ellipticity(η_f), and (c) Faraday rotation(θ_f) spectra of 5 DBR / GaAs:MnAs / 5 DBR multilayer sample (bold lines). Spectra of a GaAs:MnAs single layer (200nm) were also plotted as references (solid lines). Mn concentration of GaAs:MnAs is 6.5%. All the measurements were done at room temperature, and Faraday effect (η_f and θ_f) spectra were measured under the magnetic field of 1T applied perpendicular to the samples.

References
[1] H. Shimizu et al., J.Vac. Sci. Tech. B**18**, 2063 (2000), H. Shimizu et al., Appl. Phys. Lett., **78**, 1523, (2001), M. Tanaka et al., J. Cryst. Growth, in press
[2] J. De Boeck et al., Appl. Phys. Lett., **68**, 2744, (1996)

Corresponding author: Hiromasa Shimizu, M. Tanaka Lab. Department of Electronic Engineering, The University of Tokyo, 7-3-1 Hongo, Bunkyo-ku, Tokyo, 113-8656, Japan.
Phone: +81 3 5841 6729, Fax: +81 3 5803 3975
Email: shmz@cryst.t.u-tokyo.ac.jp

T-shaped ballistic structure with adjustable spin-orbit effect: Spin filtering and directional multiplexing

Andrey A. Kiselev and Ki Wook Kim

Department of Electrical and Computer Engineering, North Carolina State University, Raleigh, North Carolina 27695-7911, USA

The exciting possibility of developing the new paradigm of spin electronics [1] recently attracted intent scientific and engineering interest. Proposals range from spin analogs of conventional electronic devices and the utilization of the giant magnetoresistivity, to the quantum computers and secure quantum communications. The most straightforward way to influence carrier spin is by means of an external magnetic field. However, this requires extensive additional circuitry or composite systems with permanent micromagnets. As a simpler alternative, it is possible to utilize an *intrinsic effect* provided by the spin-orbit (SO) interaction that is readily present in crystals and structures with relatively low symmetry [2].

We propose a semiconductor structure that can filter electron spin without using external magnetic fields. The structure consists of a T-shaped quasi-one dimensional channel and an electrode (or electrodes) placed near the channel intersection. It was recently shown [3] that the SO splitting in the 2DEG can be effectively manipulated by the gate voltage; moreover, a pair of back and front gates with properly adjusted potentials can be used to control splitting even *without charging* the quantum well. Our calculations demonstrate that the proposed device can redirect electrons with opposite spins from unpolarized source to left and right output leads, respectively, and, thus, serve as a spin filter. When the incident electron energy is in resonance with the quasi-localized zero-dimensional states at the intersection, polarization of the transmitted fluxes approaches 100%. The same device will operate as effective directional multiplexer when applied to the spin-polarized electrons. For the fixed incident energy, the device functionality can be easily modified, slightly adjusting potentials at control gates. Thus, a whole variety of prospective devices including spin-polarization-based directional multiplexers, filters and polarizers can be designed based on the relatively simple ballistic devices with control electrodes modulating the SO interaction.

Acknowledgements — This work has been supported, in part, by the Defense Advanced Research Projects Agency and the Office of Naval Research.

References

[1] G. A. Prinz, Physics Today **48(4)**, 58 (1995); Science **282**, 1660 (1998).
[2] S. Datta and B. Das, Appl. Phys. Lett. **56**, 665 (1990); E. N. Bulgakov, K. N. Pichugin, A. F. Sadreev, P. Středa, and P. Šeba, Phys. Rev. Lett. **83**, 376 (1999).
[3] D. Grundler, Phys. Rev. Lett. **84**, 6074 (2000).

Corresponding author: Andrey A. Kiselev, Department of Electrical and Computer Engineering, North Carolina State University, Box 7911, Raleigh, NC 27695-7911, USA.
phone: +1-919-515-5080, fax: +1-919-515-3027,
email: kiselev@eos.ncsu.edu

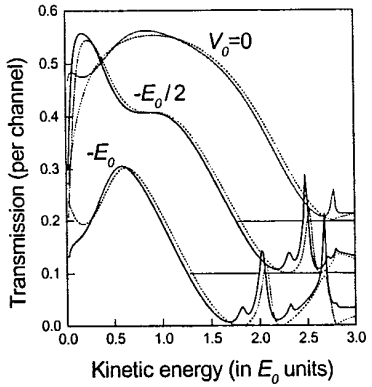

Figure 1: Transmission of incident electron flux into output channel of the symmetric T-shape structure as a function of electron kinetic energy taking into account SO term (solid lines) and neglecting it (dotted). Front/back electrode potentials are varied, so as $V_0 = 0, -E_0/2$, and $-E_0$.

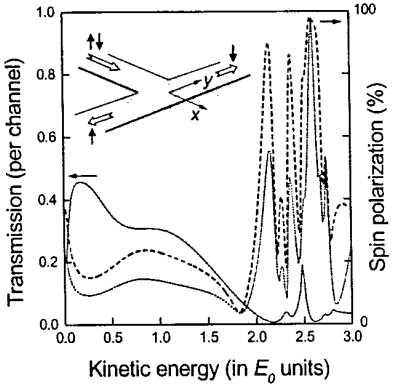

Figure 2: Energy dependence of the polarization of the transmitted flux. Dashed and dotted lines show total polarization $|\mathbf{P}|$ and the difference $(P_x^2+P_z^2)^{1/2}$ between flux polarization in the $+y$ and $-y$ channels, respectively. Both reach high values in the vicinity of the resonance with quasi-localized 0D electron state at the intersection. Total transmission dependence for $V = -E_0/2$ is reproduced from Fig. 1 as the solid line. Inset: schematic drawing of the T-shaped structure.

Conversion of spin into directed electric current in quantum wells.

S.D. Ganichev[1,2], E.L. Ivchenko[2], S.N. Danilov[1], W. Wegscheider[1], D. Weiss[1], J. Eroms[1], and W. Prettl[1]

[1]Institut für Exp. und Angew. Physik, Universität Regensburg, 93040 Regensburg, Germany
[2]A.F. Ioffe Physico-Technical Institute, 194021 St. Petersburg, Russia

A nonequilibrium population of spin-up and spin-down states in quantum well structures has been achieved applying circularly polarized radiation. The spin polarization results in a directed motion of free carriers in the plane of the quantum wells perpendicularly to the direction of light propagation. Due to spin selection rules the direction of the current is determined by the helicity of the light and can be reversed by switching the helicity from right- to left- handed. The conversion of the photon angular momentum into the linear motion of an electron, occurs in gyrotropic media and is an electron analog of a rotating wheel on a hard surface. A microscopic model is presented which describes the origin of the photon helicity driven current.

The experiments were carried out on heterostructures belonging to two different classes of symmetry. Higher symmetric structures of the point group D_{2d} were (001)-molecular-beam-epitaxy (MBE) grown *n*- InAs/AlGaSb QWs with a 15 nm single InAs channel and (001)- MBE grown *n*- GaAs/AlGaAs single heterojunctions. Structures of the lower symmetry C_s were (113)A- MBE grown *p*-GaAs/AlGaAs single QWs and multiple QWs containing 20 wells of 15 nm width. For optical excitation we used a high power far infrared pulsed NH_3 laser optically pumped by a TEA-CO_2 laser which yields strong linearly polarized emission in the wavelengths range from λ= 35 to 280 μm. The helicity P_{circ} of the incident light varied from -1 (left handed circular, σ_-) to +1 (right handed circular, σ_+) according to $P_{circ} = \sin 2\varphi$ were φ is the angle between the initial polarization plane and the optical axis of the $\lambda/4$ plate. The radiation induces indirect (Drude like) optical transitions in the lowest conduction subband of our *n*-type samples and direct optical transitions between valence subbands (heavy hole - light hole) in the *p*-type samples.

Phenomenologically, the connection between the photocurrent sensitive to the helicity of light, j, and the incoming light is given by the second-rank pseudotensor γ as $j = \gamma e E^2 P_{circ}$ where E is the amplitude of the electric field of the light and e is the unit vector pointing in the direction of the light propagation. The pseudotensor γ has nonzero components which depends on the symmetry of the system. Microscopically a conversion of photon helicity into a spin photocurrent arises due to k-linear terms in the effective Hamiltonian $H^{(1)} = \beta_{lm}\sigma_l k_m$ where k is the electron wavevector, σ_l are the Pauli spin matrices and β_{lm} are real coefficients. The coefficients β_{lm} form a pseudotensor subjected to the same symmetry restriction as the pseudotensor γ. The coupling between σ_l and the wavevector of the charged carriers k_m as well as spin controlled selection rules yield a net current dependent upon circularly polarized optical excitation. The effect, being sensitive to the degree of spin orientation, provides an easy access to spin dynamics in semiconductor structures.

Corresponding author: Sergey D. Ganichev, Institut für Experimentelle und Angewandte Physik, Universität Regensburg, 93040 Regensburg, Germany,
phone: +49-941-9432050, Fax:+49-941-9432177,
e-mail: sergey.ganichev@physik.uni-regensburg.de

Spin-orbit interaction in an InAlAs/InAs heterostructure

Kanji Yoh[1] , S.Abe[2], T. Doi[1], Y. Katano[1], H. Ohno[2], K. Sueoka[2] and K. Mukasa[2,]

[1]Research Center for Integrated Quantum Electronics, Hokkaido University, Japan
[2]Graduate School of Engineering, Hokkaido University, Japan

Spin-orbit interaction of electrons in surface inversion layers is known to be pronounced in mid-narrow gap semiconductors such as InAs or InSb. However, investigation of those materials suffer from substrate leakage current due to interband tunneling because of their narrow bandgap. Here we report the successful transport measurement of InAlAs/InAs haterostructures grown on p-type InAs substrate[1)] by solving the leakage current problem and report a large spin-orbit coupling in pure InAs/InAlAs heterostructure grown on InAs.

The heterointerface of arsenic-based material system was achieved by growing strained thin InAlAs barrier on top of undoped InAs channel layer as shown in Figs 1 and 2. The molecular beam epitaxially grown heterostructure is composed of p^+-InAs substrate, 1μm of p-InAs buffer layer, 500Å of InAs and 80Å of InAlAs. The surface electrode of Ti/Au was deposited on top of the surface so that the ohmic contact to the surface inversion layer was taken through the tunneling barrier. Shubunikov de Haas oscillation of the InAs surface inversion layer was successfully measured by improved heterointerface quality and reduced interband tunneling current. As a result, spin-orbit interaction was estimated through Rashba oscillations.

The overall current voltage characteristics with wide voltage range revealed that 2DEG saturation current characteristics dominates at relatively low bias (-1V to +1V) , while

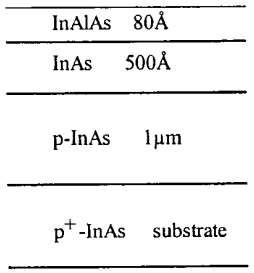

Fig.1 Heterostructure of the device

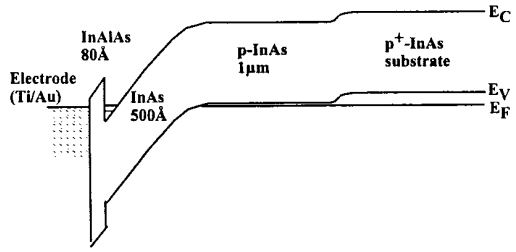

Fig.2 Schematic energyband diagram

the substrate leakage current due to interband tunneling dominates at higher bias voltages (>1.5V). In the low bias region, the Shubunikov de Haas oscillation was successfully obtained at 4K without any leakage problem especially at high magnetic fields. The carrier concentration at the inversion layer was estimated to be $6.9x10^{11}cm^{-2}$. The spin-orbit coupling constant was estimated from the beating characteristics of the oscillations[3)] and FFT analysys to be α_{zero} 30.3 ($x10^{-12}$eVm). This number corresponds to 13meV in spin split energy. These values were estimated assuming bulk effective mass of InAs. So that the estimation decreases accordingly if higher values were used taking into account of the non-parabolicity of the energy band. However, the direct measurement of the spin split energy[4)] of the same sample in a the separate experiment exhibited a band split energy of 18meV which is close enough to the above estimation by Rashba oscillation if we take into account the uncertainty of the effective mass. The present spin-orbit result is comparable to the large spin-orbit coupling value obtained in the strain relaxed $In_{0.75}Ga_{0.25}As/In_{0.75}Al_{0.25}As$ heterostructure[5)]. Unusually large coupling constants obtained in both structures suggest that the large spin-orbit coupling constant value arise not residual strain effects but from energyband structure of InAs (or $In_{0.75}Al_{0.25}As$) itself under asymmetric potential shape.

References

(1)D.C.Tsui, Phys.Rev.B 4, 4438 (1971),
(2)Th.Schaepers et al, J.Appl.Phys. 83, 4324 (1998)
(3)E.A.de Andrada e Silva et al, Phys. Rev.B, 50, 8523 (1994)
(4) To be published elsewhere.
(5)S.Yamada et al, 4th International Workshop on Quantum Functional Devices (Kanazawa, 2000)

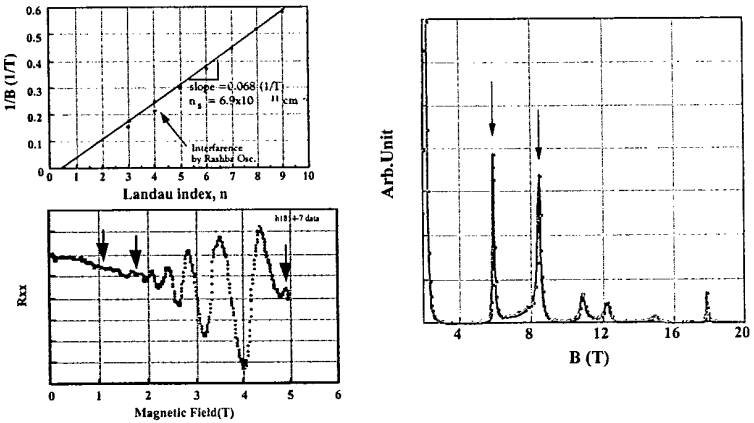

Fig.3 Shubunikov de Haas oscillation and Landau plot

Fig. 4 FFT (MEM) result of Shubunikov oscillation

Microstructure and electronic characterization of self-assembled ErAs nanoparticles in InGaAs

M. Hanson, D.C. Driscoll, C. Gallinat, A.C. Gossard

Materials Department, University of California, Santa Barbara, CA, USA 93106-5050

We report the growth by molecular beam epitaxy of a composite epitaxial material consisting of semimetallic ErAs particles embedded in an $In_{0.53}Ga_{0.47}As$ matrix. Previous materials composed of ErAs particles in GaAs possessed sufficiently high dark resistance, breakdown voltage, and short enough carrier lifetimes to be useful for photomixers and ultrafast photodiodes [1]. We extend this embedded ErAs particle approach to InGaAs in order to achieve a fast photoconductive material with strong absorption at the 1.55 μm wavelength. The new material consists of multiple layers of ErAs capped with 2.5 nm of InAlAs and separated by 37.5 nm of InGaAs grown on an InP substrate (see Fig. 1). ErAs depositions of ~0.04 nm to ~1.2 nm per layer (~0.12 to ~4 monolayers (ML) per layer) have been epitaxially overgrown with InGaAs. For these amounts of ErAs, the ErAs forms disconnected islands, which are on the order of a few nanometers in diameter. For ErAs depositions beyond ~4.5 to ~5 ML, the ErAs islands inter-connect, degrading the dark resistance of the structure and the structural quality of the overgrowth material. Initial transport measurements showed that the electrical properties of the material were strongly dependent on the amount of ErAs deposited per layer [2]. While an undoped InGaAs reference sample is nearly intrinsic, continuously Er-doped InGaAs up to $5x10^{19}$ cm^{-3} is conductive and n-type [3]. We found that for depositions of ErAs on InGaAs less than ~0.5 ML, n-type metallic conduction was observed. However, for larger depositions (between ~1 and ~4 ML) the carriers freeze out exponentially with temperature as shown in Fig. 2. Furthermore, the rate of carrier freeze out increases with increasing amounts of ErAs per layer indicating that the activation energy of the carriers is also increasing. The activation energy for ErAs depositions between ~3 and ~4 ML approaches the midgap of InGaAs. This suggests that InGaAs:ErAs may be a suitable candidate for a fast photoconductive material if the ErAs nanoparticles can act as recombination centers. We correlate these changes in electronic structure with the physical microstructure of the material determined by transmission electron microscopy. The size and distribution of the ErAs nanoparticles strongly influence the electronic properties of the material. Therefore, these properties can be readily engineered by altering superlattice spacing, amount of ErAs deposited per layer, and growth temperature. Since the ErAs nanocomposites can be grown at relatively ideal temperatures for semiconductor epitaxy, they possess major advantages of quality, robustness, and design flexibility compared to low temperature grown GaAs photoconductive materials [4].

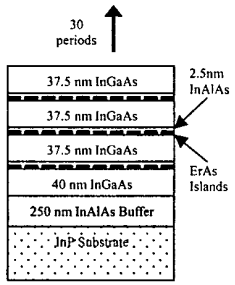

Fig. 1. Sample Structure

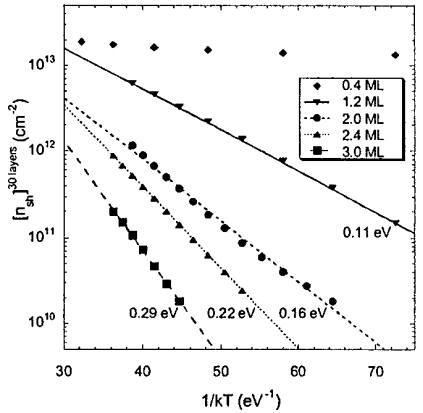

Fig. 2. Two-dimensional sheet charge density per 30 ErAs layers vs. 1/kT. The activation energy (E_a) increases with increasing ErAs deposition.

References

[1] C. Kadow, S. B. Fleischer, J.P. Ibbetson, J. E. Bowers, A. C. Gossard, J. W. Dong, and C. J. Palmstrom, Appl. Phys. Lett. 75, 3548 (2000).
[2] D. C. Driscoll, M. Hanson, C. Kadow, and A. C. Gossard, Appl. Phys. Lett. (accepted)
[3] S. Sethi and P. K. Bhattacharya, J. Electron. Mater. 25, 467 (1996)
[4] E.R. Brown, K.A. McIntosh, F.W. Smith, M.J. Manfra, and C.L. Dennis, Appl. Phys. Lett. 62, 1206 (1993)

Corresponding Author: Micah Hanson, Materials Department, University of California, Santa Barbara, CA, USA 93106-5050
phone: 01-805-893-8154
email: micah@engineering.ucsb.edu

Spin polarization spectra of strained superlattices

A. D. Andreev[1], A. V. Subashiev[2]

[1]Ioffe Physical Technical Institute, Polytechnicheskaya 26, 194021,
St. Petersburg, Russia,
[2]St. Petersburg State Technical University, Polytechnicheskaya 29, 195251,
St. Petersburg, Russia.

Optical spin polarization in semiconductor heterostructures is widely used to study spin relaxation and spin transport effects as well as to design novel spin-controlled electronic devices [1]. In addition, high electronic polarization have made strained GaAs-based superlattices very promising as photoemitters of highly polarized electrons [2]. They have proven to provide reproducibly the emitted electron polarization as high as 86 % with sufficiently high quantum efficiency at the polarization maximum [3].

We present the first calculation of the optical absorption and optical spin orientation spectra of strained InGaAs-AlGaAs and GaAs-AlInGaAs superlattices using the envelope-function approximation, in the framework of the Kane model including the conduction band states Γ_6, the states of light and heavy holes of the valence band Γ_8 and the states of the spin-orbit splitted band Γ_7.

In quantum well and superlattice (SL) structures the splitting of the 4-fold degenerate valence band into only 2-fold spin-degenerate states of the heavy-hole and the light hole minibands results in the electron spin polarization close to P=1 (P=-1) when an electron is excited by a circularly polarized light at the absorption edge from the heavy-hole (light hole) miniband. The splitting is enlarged in case of a compressive layer strain. At the energies above the absorption edge several hole minibands contribute to the absorption, and the resulting spin polarization of the excited electrons for a given excitation energy can be calculated as

$$P = \sum_i (K_{i+} - K_{i-}) / \sum_i (K_{i+} + K_{i-})$$

Here K_{i+} (K_{i-}) is the partial absorption coefficient for the spin up final electronic states when excited by the right-hand (left hand) circularly polarized light in the transitions from the hole miniband *i*. The dependence of the polarization and absorption spectra on the excitation energy follows the sequence of the miniband transitions. Partial contributions to the electron spin orientation are strongly controlled by the symmetry and mixing of the valence band states, while the absorption is determined by the inter-miniband density of states and the envelope function matrix elements.

Fig. 1 shows the miniband spectrum of GaAs-$Al_{0.18}In_{0.16}Ga_{0.66}As$ strained superalttice with the barrier and well width $d_w = d_b = 4$nm, grown along (100) direction, and the polarization spectrum of the excited electrons for the circularly polarized excitation. Strongly pronounced features in the spin-polarization dependence on the excitation energy are associated with Van-Hove singularities in absorption spectra and remain even for fairly small barriers for the electrons. The polarization value in the first maximum (hh1 → e1 transition) and its position is found to be very sensitive to the smearing of the absorption edge by the hole scattering processes, as well as the band edge fluctuations. While the first minimum in the polarization spectra is definitely associated with lh1 → e1 transition, the second maximum in the polarization spectra is found to be due to the hh2 → e2 transitions at the edge of the SL Brilluin zone $k_z = \pi/d$, $d = d_w + d_b$. For both considered SLs it corresponds to electronic states with the energy above the barriers in the conduction band. In case of GaAs-AlInGaAs the conduction band offset is of the order of 20 meV, the polarization in the second peak being dependent on the barrier height value. In line with the experiment [2,3], for both GaAs-AlInGaAs and AlGaAs-InGaAs SLs the maximum polarization value in this peak can exceed 50 % in case of a high confinement of the hole states which leads to the suppression of the hh1 → e1 absorbtion in this energy region. Taking into account the electron spin relaxation, the calculated spectra are in very good agreement with the observed excitation spectra of polarized electron photoemission both for AlGaAs-InGaAs and GaAs-AlInGaAs strained superlattices.

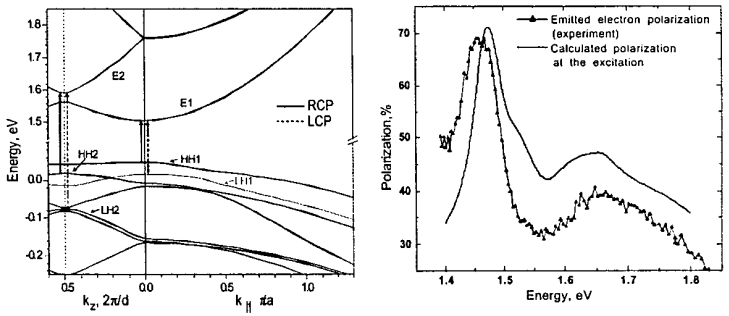

Fig. 1 (a) Miniband spectrum of GaAs-$Al_{0.18}In_{0.16}Ga_{0.66}As$ superalttice and the major optical transitions (shown by vertical arrows) contributing to the absorption spectrum; (b) polarization of the excited electrons (solid line) for the circularly polarized excitation together with the experimentally observed spectra of polarized electron photoemission (shown by triangles, from Ref. [3]), T = 300 K.

Calculated polarization spectra are sensitive to the band offsets which can be used for the band offset evaluation and fine tailoring of the band structure.

This work was supported by the Russian State Program "Physics of Solid State Nano-srtuctures" under grant 97-1091, Russian Fond for Basic Research under grant 00-02-16775, and INTAS grant 99-00125.

References

[1] H. Ohno, Science. 281, 951 (1998).
[2] A.V. Subashiev, et al., Phys. Low-Dim. Struct. 1/2, 1 (1999).
[3] A.V. Subashiev et al., in *Proc. of 24-th Int.Conf. on Phys. of Semicond.*, ed. D. Gershoni, World Scientific, Singapore 1999, (also SLAC-Pub-7922, 1998).

Corresponding author: Arsen V. Subashiev, Experimental Physics. Dept., St.Petersburg State Technical University, Politekhnicheskaya 29, 195251, St. Petersburg, Russia.
phone: +7 (812) 552 67 06, Fax: +7 (812) 552 67 06
email: arsen@subashiev.hop.stu.neva.ru

The performance of hybrid-molecular devices with current CMOS technology as a reference point

R. Stadler, M. Forshaw
Department of Physics and Astronomy, University College London,
Gower Street, WC1E 6BT London, United Kingdom

Due to the remarkable trend for miniaturisation in semiconductor technology within the last decades, the size of electronic circuits will soon approach the scale of single atoms. At this stage several new challenges in device fabrication will arise as well as operational difficulties. Molecular electronics is being considered as an alternative to conventional CMOS technology, because the structure of organic molecules can be designed on an atom-by-atom scale by means of chemical synthesis, which cannot be achieved for doped Si-heterostructures.

The rapidly growing field of molecular electronics can be divided into hybrid-molecular approaches, where molecules are used as active transistor elements interconnected by metallic wires, and mono-molecular (self-contained) approaches, where the wiring is integrated into the molecular circuits. A recent review of the state of the art in both fields can be found in Ref. [1].

There have been many proposals for two- or three-electrode transistors based on molecules on the device level, but not much attention has been focused on the circuit design or architecture level so far. In a recent work by S. Ami et al. [2] a electromechanical C_{60} transistor was used to construct 1-bit memory cells and simple logic gates such as NOT- and NOR-gates. In Ref. [3] these concepts were transferred to larger architectures, where 1-bit full adders and D-latches were designed and these elements were then put together in a simplified memory/adder model (Fig. 1). The architecture corresponding to that model contained 486 single C_{60} transistors and all stages of signal transmission have been simulated using the electrical circuit software SPICE.

The aim of the current work is to critically access the performance of C_{60} hybrid-molecular transistors as compared to current CMOS technology in terms of speed and size. Issues of fabricational and operational accuracy needed by these devices to perform reliable computations are also addressed. Another important feature of molecular transistors, namely the generally quite small ratio of the voltages corresponding to a logical 'ON' and 'OFF' state and its consequences for the usefulness of these devices, are also discussed. Finally, the results for the C_{60} hybrid-transistors are compared to available data on other hybrid-molecular devices in order to distinguish between properties specific to its particular design and those that apply to hybrid-molecular architectures in general.

References

[1] C. Joachim, J. K. Gimzewski and A. Aviram, 'Electronics using hybrid-molecular and mono-molecular devices', Nature **408**, 541 (2000).

[2] S. Ami and C. Joachim, 'Logic gates and memory cells based on single C_{60} electromechanical transistors', Nanotechnology **12**, in press (March 2001).

[3] R. Stadler, S. Ami, M. Forshaw and C. Joachim, 'A memory/adder model based on C_{60} transistors', to be published.

a)

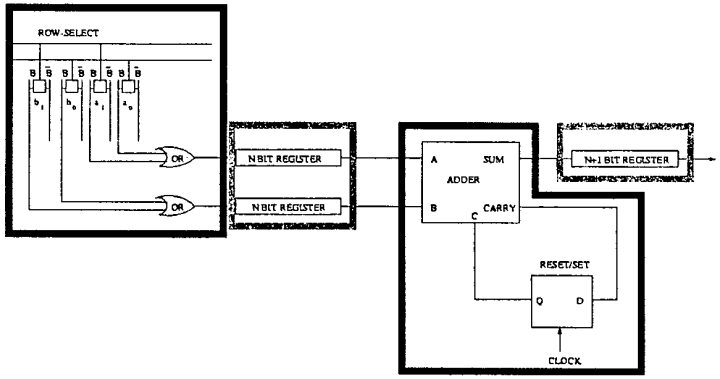

b)

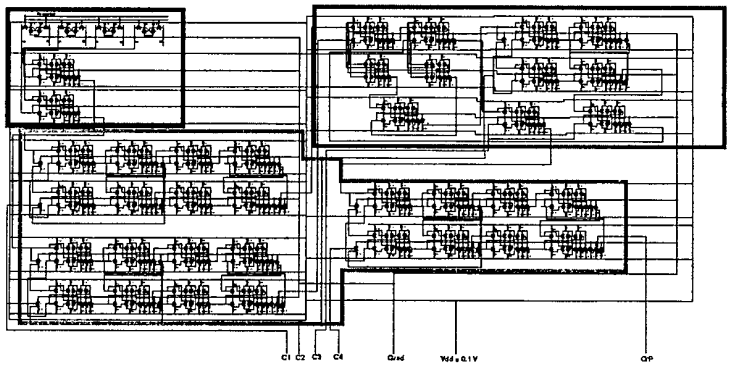

Fig. 1: Schematic layout (a) and detailed circuit diagram (b) of the simplified memory/adder model used to study the performance of the C_{60} electromechanical transistors. Two 2-bit words are read from four 1-bit memory cells activated by two different word-lines. The signals are passed through OR-gates and D-latches to a serial adder, where the addition is performed and the output can be passed through another register to be written on another part of the memory.

Corresponding author: Robert Stadler, Department of Physics and Astronomy, University College London, Gower Street, WC1E 6BT London, UK,
Phone:+44 020 7679 6583, Fax:+44 020 7679 6580,
Email:r.stadler@ucl.ac.uk

High Thermoelectric Figure of Merit ZT in PbTe and Bi_2Te_3 Based Superlattice Structures by Reducing the Thermal Conductivity

H. Beyer[1], J. Nurnus[1], H. Böttner[1], A. Lambrecht[1], E. Wagner[1], G. Bauer[2]

[1]Fraunhofer Institut Physikalische Messtechnik, D-79110 Freiburg, Germany
[2]Institut für Halbleiter- und Festkörperphysik, Universität Linz, A-4040 Linz, Austria

A significant enhancement of the thermoelectric figure of merit $ZT = \sigma S^2 T/\lambda$ (σ: electrical conductivity, S: thermopower, λ: thermal conductivity), which is directly related to the efficiency of thermoelectric devices, has been predicted for low dimensional structures such as multiple quantum wells (MQW) or superlattices (SL) [1]. A ZT-rise due to quantum confinement was actually observed which is mainly related to the two-dimensional density of states for sufficiently small well-widths, which results in an increase of the thermopower [2]. However, multiquantum well (MQW) structures are not useful for technical applications, because the barrier materials of the MQW's usually exhibit poor thermoelectric properties. A different concept to achieve an increase of ZT is based on the reduction of the thermal conductivity. A strong reduction of the thermal conductivity has been predicted to occur in superlattices (SL's), both parallel [3] and perpendicular [4] to the plane of the layers. The reason for this λ-reduction is the fact, that the interfaces in periodic multilayers strongly alter the phonon dispersion and also the phonon propagation, resulting in enhanced phonon scattering.

In this work we will give experimental evidence for the reduction of the thermal conductivity parallel to layer planes resulting in a ZT-enhancement. We investigated the thermoelectric properties of $Bi_2Te_3/Bi_2(Se_xTe_{1-x})_3$-SL's, PbTe-based doping superlattice structures, PbTe/$Pb_{1-x}Sr_xTe$- and PbTe/$PbSe_{0.2}Te_{0.8}$-SL's. The number of SL periods was typically between 100 and 500 depending on the period, which was between 4 and 20 nm. Typical doping concentrations were in the upper 10^{18} cm^{-3}-range in PbTe-based SL's and in the 10^{19} cm^{-3}-range in Bi_2Te_3-SL's. It turns out that the PbTe-based SL's are indeed the ones with the highest figure of merit reported so far for temperatures $T \approx 500$ to 600 K.

A reduction of the thermal conductivity was found compared to bulk Bi_2Te_3 and bulk PbTe (Fig. 1). Furthermore in the SL's the thermal conductivity is reduced to values below the λ-values of the corresponding ternary compounds having the same average content x of the ternary component. In addition, a reduced thermal conductivity with decreasing period or increasing x-values was found.

Despite of a small drop of the power factor σS^2 in the SL's we find an enhancement of the dimensionless figure of merit compared to corresponding values of the bulk materials. The range of achievable ZT enhancement in these structures is shown in Fig. 2 by the blue area for the Bi_2Te_3-based SL's and by the red areas for PbTe-based structures compared optimum ZT-values of the corresponding bulk material system. The red points denote experimentally determined data. We found that compared to the highest values for ZT reported so far for lead salts at T = 700 K, our SL's exhibit ZT-enhancement up to about 40 %. Bi_2Te_3-based SL's so far reach values comparable to optimum bulk values but with prospects for higher figure of merits after optimizing the SL growth. For the PbTe -based SL's the optimum temperature range is between 400 K and 600 K, for which so far no suitable bulk thermoelectric material has been known.

References

[1] L.D. Hicks, M.S. Dresselhaus, Phys. Rev. B 47(19), 1993, pp. 12727-12731
[2] T.C. Harman, D.L. Spears, M.J. Manfra, J. Electr. Mater. 25 (7), 1996, pp. 1121-1127
[3] A. Balandin, K.L. Wang, J. Appl. Phys. 84 (11), 1998, pp. 6149-6153
[4] R. Venkatasubramanian, Phys. Rev. B 61 (4), 2000, pp. 3091-3097

Corresponding author: Dr. Armin Lambrecht, Fraunhofer Institut Physikalische Messtechnik, Heidenhofstr. 8, D-79110 Freiburg i. Br., Germany
phone: ++49/(0)7 61/88 57-122, fax: ++49/(0)7 61/88 57-224
email: armin.lambrecht@ipm.fhg.de

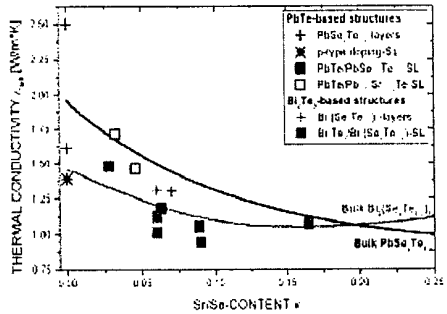

Fig. 1: Lattice thermal conductivity at T = 300 K of PbTe- and Bi_2Te_3-based superlattice structures compared with homogeneous PbTe- and Bi_2Te_3-layers and with literature data for corresponding bulk ternary alloys.

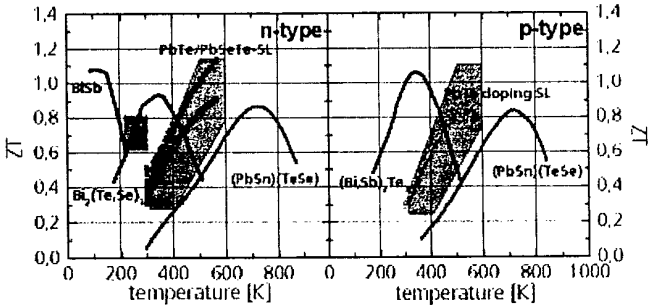

Fig. 2: Achievable figures of merit of PbTe- (red area) and Bi_2Te_3-based (blue area) superlattice structures compared with classical bulk IV-VI (red line) and V-VI (black/blue line) materials. The red points denote ZT-values determined from experimental data of PbTe-based structures. A ZT-rise up to ~40 % is achievable with these structures. Bi_2Te_3-based SL's reach bulk data in the temperature range between 200 K and 300 K. Here an optimization of growth parameters may result in higher ZT-values.

Electron-phonon coupling in n^{++}SOI film probed using Si-Al NIS junctions

M. Prunnila[1], J. Ahopelto[1], A. Savin[2], P. Kivinen[2], J. Pekola[2], and A. Manninen[3]

[1] VTT Microelectronics Centre, P.O.B. 1101, FIN-02044 VTT, Finland
[2]Department of Physics, University of Jyväskylä, P.O.B. 35, FIN-40351 Jyväskylä, Finland
[3]Nokia Research Centre, P.O. Box 407, FIN-00045 Nokia Group, Finland

In semiconductors the electronic temperature at low temperatures can be probed for example via SdH oscillations [1]. Normal metal-insulator-superconductor (NIS) junctions provide a straight forward method to determine the electronic temperature in the normal metal [2]. Here we use Al-n++Si NIS junctions to determine electronic temperature in a thin heavily doped silicon-on-insulator (SOI) film. In these junctions Schottky barrier acts as a tunneling barrier. We determine the strenght of the electron phonon coupling. We also observe anomalous drop in the electronic temperature at low bias. This effect is possibly related to the Peltier cooling effect observed in single NIS [3] and double NIS (SINIS) junctions [2].

The samples were fabricated on bonded SOI wafer with 200 nm-thick SOI film and 400 nm-thick buried oxide layer. Active n-type carrier concentration of ~$7*10^{19}$ cm^{-3} was produced by phosporous implantation and subsequent dry oxidation. This concentration is enough to make the SOI film a metallic conductor. After stripping the sacrificial oxide, a second oxidation step was performed and Al contacts were evaporated. The final thicness of the SOI film was 53 nm. The area of the SOI mesa used in the experiments was 750*100 μm^2.

Figure 1 shows IV-curves of a Al-Si junction below and above of the critical temperature of Al. The junction behaves more or less like an ideal NIS junction. These junctions are very sensitive to temperature and can be used as a thermometers by current biasing.

At low temperature the electron-phonon coupling is weak and the electron phonon system can be driven away from their mutual thermal equilibrium by heating the electron system by applying electric current through the film. In most cases the temperature of the phonons, T_{ph}, and the electrons, T_{el}, follow the 'universal' relation [1,4]

$$P = \Sigma V(T_{el}^5 - T_{ph}^5), \qquad (1)$$

where P is the heat flow from electrons to the phonons, V is the volume of the film and Σ is a material (and dimensionality) dependent constant that describes the strength of electron phonon coupling.

The sample geometry and biasing in the experiment are schematically shown in Fig. 2(a). In the experiment the electron temperature was measured using current biased Al-n^{++}Si NIS junctions. The electron temperature as a function of the heating power is shown in Fig. 2(b) at substrate temperature of 177 mK. The fitting with Eq.(1) gives Σ = $1.5*10^8$ W/K^5m^3. This is an order of magnitude smaller value than found in metals. At low power the electrons in the SOI film are cooled rather than heated [inset in Fig. 2(a)]. We believe that this is the SINIS cooling effect [2]. The effect is quite small but the sample geometry is far from optimal. Anyhow, the result suggests that Al-Si junctions can be used in low temperature micro-cooler applications.

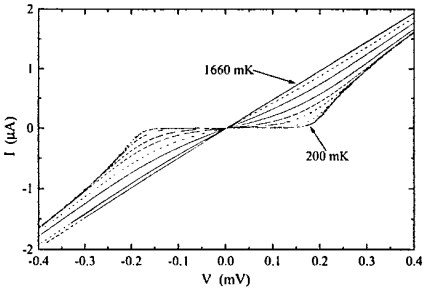

Fig. 1: IV-curves measured from a 10x10 μm^2 Al-n++Si junction at different temperatures. Starting from the highest temperature the temperatures for the curves are 1660 mK, 1350 mK, 1160 mK ,920 mK, 720 mK, 530 mK, 390 mK, 300 mK and 200 mK.

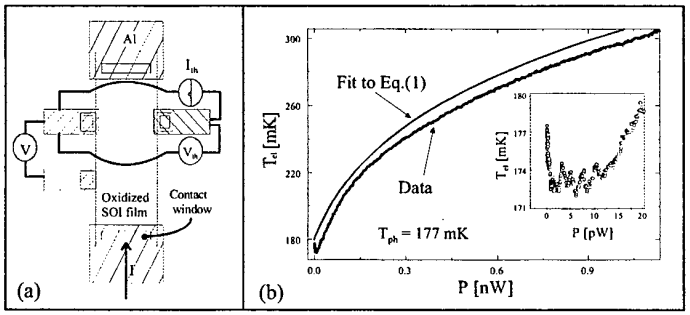

Fig. 2: (a) Schematic sample geometry and biasing in the experiment. I is the heating current. Electron temperature T_{el} is determined with I_{th} and V_{th}. (b) Electron temperature T_{el} as a function of applied power P = UI. Fit to Eq. (1) is off-set for the sake of clarity. The inset shows the low power regime.

References

[1] R. J. Zieve, D. E. Prober, and R. G. Wheeler, Phys. Rev. B 21, 2443 (1998).
[2] M.M. Leivo, J.P. Pekola, and D.V. Averin, Appl. Phys. Lett. 68, 1996 (1996).
[3] M. Nahum, T. M. Eiles, and J. M. Martinis, Appl. Phys. Lett. 65, 3123 (1994).
[4] F. C. Wellstood, C. Urbina, and J. Clarke, Phys. Rev. B 49, 5942 (1994)

Corresponding author: Mika Prunnila, VTT Microelectronics Centre, P.O.B. 1101, FIN-02044 VTT, Finland
phone: +358 (0)9 456 6668 , Fax: +358 (0)9 456 7012
email: mika.prunnila@vtt.fi

Investigation of Self-Aligned p^{++}-GaAs/n-InGaP Hetero-Junction Field-Effect Transistors

W.-S. Lour[1], M.-K. Tsai[2], K.-C. Chen[1], S.-W. Tan[1], Y.-W. Wu[1] and Y.-J. Yang[2]

[1]Department of Electrical Engineering, National Taiwan-Ocean Univ., No. 2, Peining Road, Keelung, Taiwan, Republic of China.

[2]Department of Electrical Engineering, National Taiwan University, No.1, Sec. 4, Roosevelt Road, Taipei, Taiwan, Republic of China.

InGaP/GaAs material system has recently become a promising material system for optoelectronic device [1] and high-speed electronic devices such as heterojunction bipolar transistor [2] (HBT) and many kinds of field-effect transistors [3-4] (high electron mobility transistors and metal-insulator-semiconductor like). To date, there is little experimental result related to InGaP/GaAs junction FET (JFET) that is a possible alternative to both HEMT's and MESFET-like devices [5]. In this letter, we report another type of InGaP/GaAs JFET with a p^{++}-GaAs hetero-gate and a wide-gap InGaP channel. The key features in this hetero-JFET are that all electrodes are ohmic types that suit for self-align process and highly carbon doped GaAs is available for very low gate resistance.

As shown in Fig. 1(a) and 1(b), a self-aligned T-shaped gate HJFET exhibits a gate of 0.6 μm in length by depositing gate metal of 1.0 μm. Fig. 2 shows the typical I-V curve of a p^{++}-GaAs/n-InGaP hetero-diode with a very low gate resistance (0.14 Ω·mm). It reveals that 1) a high turn-on voltage of ~ 2.0 V at 1 mA/mm, 2) a low reverse leakage current and a high breakdown voltage up to 30 V at 1mA/mm. As shown in Fig. 3(a) and 3(b), the available maximum transconductances are 160 and 230 mS/mm for non self-aligned and self-aligned HJFET's, respectively. With a self-aligned processing structure, the transconductance and f_{max} were improved to 230 mS/mm and 35 GHz, respectively, as shown in Fig. 4. The estimated electron velocity is of $6.3\sim7.2\times10^6$ cm/s.

The authors will further report detailed reliability investigation of this novel self-aligned T-shaped gate HJFET that uses InGaP and GaAs as a channel and a gate, respectively.

References

[1] Q. Liu et al., J. App. Phys. **77**, 1154 (1995).
[2] W. S. Lour, IEEE Trans. Electron Devices **ED-44**, 346 (1997).
[3] W. S. Lour et al., Appl. Phys. Lett. **74**, 2155 (1999).
[4] W. S. Lour, W. L. Chang, S. T. Young, and W. C. Liu, Electron. Lett. **34**, 814 (1998).
[5] M. M. Hashemi et al., IEEE Electron Device Lett. **14**, 60 (1993).

Corresponding author: Wen-Shiung Lour,
Department of Electrical Engineering,
National Taiwan-Ocean Univ., No. 2, Peining Road, Keelung, Taiwan, Republic of China,
Phone: 886-2-24622192, Fax: 886-2-24635408,
email:wslo@mail.ntou.edu.tw

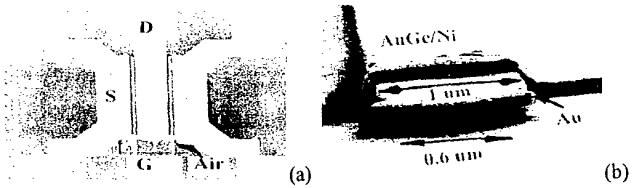

Fig. 1(a): the top view of a non self-aligned HJFET, and Fig. 1(b): the SEM picture of a self-aligned T-gate with a reduced length.

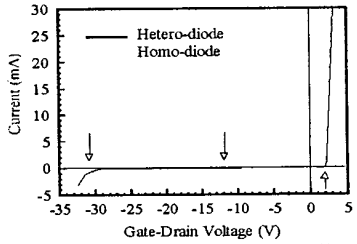

Fig. 2: the I-V curves for a p^{++}-GaAs/n-GaAs homo-diode and a p^{++}-GaAs/n-InGaP hetero-diode.

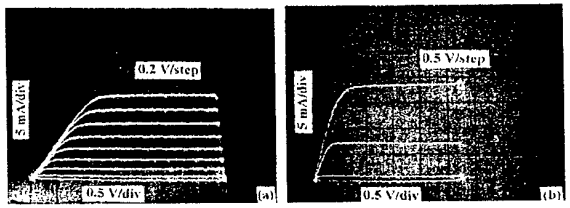

Fig. 3: the common-source characteristics for (a) a non self-aligned and (b) a self-aligned HJFET's.

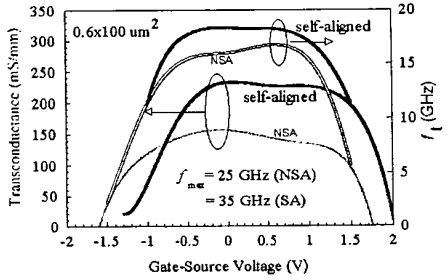

Fig. 4: the measured transconductance and f_t as a function of gate-source voltage.

Fabrication of two dimensional in-plane gate transistors by active focussed ion beam doping

D. Reuter, C. Meier, A. Seekamp, and A. D. Wieck

Lehrstuhl für Angewandte Festkörperphysik, Ruhr-Universität Bochum,
Universitätsstraße 150, D-44780 Bochum, Germany

The first two dimensional field effect transistor with source, drain, and gate in the same plane (see Fig. 1 for a schematic sketch) was realized by Wieck and Ploog [1]. It was fabricated by writing insulating lines into an $Al_xGa_{1-x}As/GaAs$ heterostructure containing a two dimensional electron gas (2DEG) using focussed ion beam (FIB) implantation. This negative mode pattern definition (insulation writing) resulted in transistors with good depletion characteristics but rather poor enhancement behavior. This is due to the fact that for positive gate voltages electrons are driven closer to the FIB-lines resulting in electron transport through areas with increased lattice damage caused by implanted ions. Because of the high resistance of these areas the overall channel conductance is not significantly increased allowing current flow through this areas. The basic idea present in this contribution to overcome the poor enhancement behavior of an IPG-transistor is to fabricate it by positive mode pattern definition, i. e. realizing electron transport through FIB-doped areas.

We are able to fabricate laterally structured 2DEG by FIB implantation of Si atoms into $Al_xGa_{1-x}As/GaAs$ heterostructures using optimized implantation parameters (implantation energy: 60 keV, dose: 4×10^{12} cm^{-2}). For these implantation parameters the electron density of the 2DEG is approximately 5×10^{11} cm^{-2} at room temperature with an electron mobility around 5500 cm^2/Vs. The two dimensionality of the carrier system was checked for unstructured implantation by magnetotransport measurements at low temperature. With this optimized implantation parameters an IPG geometry as shown schematically in Fig. 1 was realized.

In Fig. 2 the source-drain current I_{SD} is shown as a function of the source-drain voltage V_{SD} for different gate voltages V_G for a device with the following geometry: $w_{geo} = 1$ µm, $l_{ch} = 3.0$ µm, $d_{g\text{-}ch} = 1.5$ µm. It can be seen that for small values of V_{SD}, I_{SD} increases proportional to V_{SD} whereas for high source-drain voltages I_{SD} saturates due to the limited drift mobility of the electrons in the channel. This is the same behavior as observed for IPG transistors defined by negative mode writing. Figure 2 also shows that the channel conductance can be controlled well by an applied gate voltage. As for negatively written IPG transistors the channel can be totally pinched off by a negative gate voltage. By applying a positive gate voltage the source drain conductance can be enhanced approximately by a factor of two (see Fig. 2). This is in contrast to the case of negative pattern definition where the channel conductance can be enhanced only by about 20 % by applying a positive gate voltage. This is a major advantage of the positive mode written IPG transistor.

We think the reason for the better enhancement mode characteristics of the positive mode defined IPG transistor is the following: By applying a positive gate voltage the channel width is increased. This results in additional current flow at the boarders of the channel. For the negative mode written case this means that current is flowing through heavily implantation damaged areas with high resistance. Therefore, the overall channel conductance is only slightly increased. This is different for positive mode written channels: First of all, the implantation damage in the plane of the 2DEG is low as can be concluded from the good electrical properties of the formed 2DEG. Second, the implantation damage done is mainly concentrated to the main channel area where the highest dose was implanted. Therefore, the channel conductance can be significantly enhanced by applying a positive gate voltage. This represents a major improvement over negatively written IPG transistors.

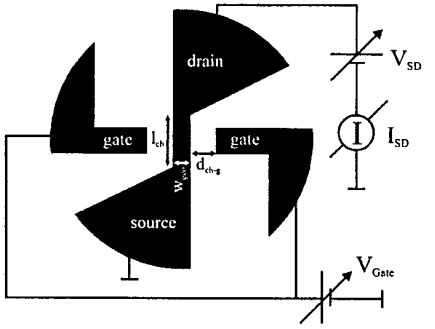

Fig. 1: Schematic sketch of an in-plane gate (IPG) transistor. The black areas represent the conducting 2DEG areas. The important dimensions of the device are indicated as well as the measurement configuration used for electrical characterization of the transistor.

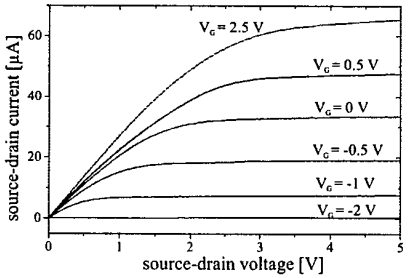

Fig. 2: The source-drain current I_{SD} as a function of the source-drain voltage V_{SD} for different gate voltages V_G is shown for an in-plane gate transistor with the following dimensions: $w_{geo} = 1$ µm, $l_{ch} = 3.0$ µm and $d_{ch\text{-}g} = 1.5$ µm. See Fig. 1 for a definition of the dimensions. Good transistor operation can be clearly seen and the channel conductance can be enhanced by a factor of two by applying a positive gate voltage.

References

[1] A. D. Wieck and K. Ploog, Appl. Phys. Lett. **56**, 928 (1990).

Corresponding author: Dirk Reuter, Lehrstuhl für Angewandte Festkörperphysik, Ruhr-Universität Bochum, Universitätsstraße 150, D-44780 Bochum, Germany.
phone: +49 234 3225864, Fax: +49 234 3214380
email: dirk.reuter@ruhr-uni-bochum.de

Novel Electrical Properties of Three-Terminal Ballistic Junctions and Demonstration of Their Applications in Nanoelectronics

H. Q. Xu, I. Shorubalko, I. Maximov, D. Nilsson, W. Seifert, P. Omling and L. Samuelson

Solid State Physics, Lund University, P.O. Box 118, SE-221 00 Lund, Sweden

We report on the results of our recent theoretical and experimental investigations of novel electrical properties [1] of three-terminal ballistic junctions (TBJs), with an emphasis on their applications in future nanoelectronics. For a symmetric TBJ device, it was shown [1] that when finite voltages V_L and V_R are applied in push-pull fashion, with $V_L = V$ and $V_R = -V$, to the left and right branches, the voltage output V_C from the central branch will always be negative, which is in strong contrast to the prediction from Ohm's law. This novel characteristic appears even when the device symmetry is broken, provided that $|V|$ is greater than a threshold. It was also shown [1] that the TBJ devices show a good parabolic behavior for V_C vs V in a large range of voltages V. These properties, which have several potential applications in nanoelectronics, have been verified experimentally.

The results of experiments reported here were obtained based on devices made from high-quality InGaAs quantum well materials, but the properties of the devices were also observed in experiments with silicon and AlGaAs/GaAs materials. Using electron beam lithography and wet chemical etching [2], three-terminal ballistic junctions are defined in high-mobility GaInAs/InP quantum well material [3]. The scanning electron micrograph of the central part of a TBJ device (in this case a T-branch) is shown in the right-lower corner inset of Fig. 1. As it can be seen, the dimension of the active area of the device is approximately 200 nm. The elastic electron mean free path for this material varies from a few microns at 4.2 K to $\sim$ 150 nm at room temperature, as extracted from Hall measurements. Thus, the electron transport in our devices is expected to be ballistic or quasi-ballistic up to room temperature. We have investigated correlation between the electron transmissions of the devices measured in the linear response regime as a function of top gate voltage (shown in the main part of Fig. 1) and the characteristics of the output voltage V_C measured as a function of V (shown in the left-upper corner inset of Fig. 1) with $V_L = V$ and $V_R = -V$. Obtained results are compared with the prediction of Ref. [1] and a good agreement is found. Also, we show that changing the waveguides in the Y-branch devices to quantum point contacts and changing the angle between left and right branches up to 180° do not affect these novel electrical properties of TBJs. This is also in agreement with the prediction of Ref. [1]. We have also demonstrated room temperature operation of the devices at high frequency up to 10 GHz.

Several potential applications of these devices in nanoelectronics have been proposed based on these novel electrical properties, and have been demonstrated experimentally. In this report, we will show examples such as rectification, frequency doubling, and logic AND and logic OR gate functions. We emphasize that all these interesting applications are based on extremely compact components – TBJ devices – with dimensions in the order of 100 nm or much less, and work at room temperature.

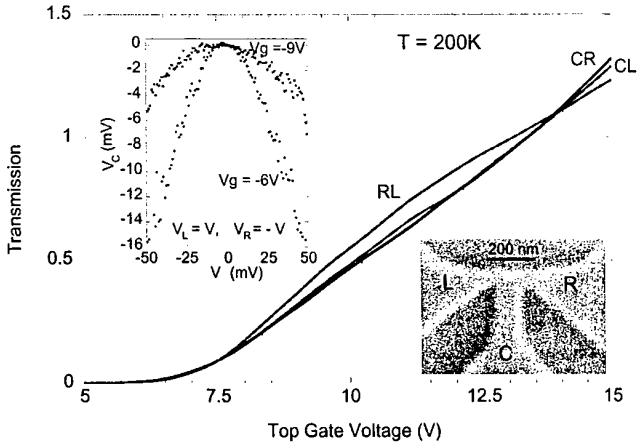

Figure 1: Right-lower corner inset shows the scanning electron micrograph of the central part of one device similar to the TBJ devices measured for this report. The conduction of the devices was controlled by top gate covering all the active area of the devices (not shown in this micrograph). Main figure shows various transmissions between three terminals of a TBJ device measured in the linear-response regime as a function of the top-gate voltage. Measured transmission between the central and left branches and that between the center and right branches are very similar, indicating that the device is highly symmetric with respect to the central branch. Left-upper corner inset shows measured output voltage V_C from the central branch of the device vs the voltage applied on the left branch $V_L = V$ (with the voltage applied to the right branch $V_R = -V$) at two top-gate voltages. It shows that the output voltage V_C from the central branch is always negative.

References

[1] H. Q. Xu, *Electrical properties of three-terminal ballistic junctions*, Appl. Phys. Lett. (2001), in press.

[2] I. Maximov et al., Proc. of 11th Internat. Conf. on InP and Related Materials (Switzerland 1999) p.237.

[3] P. Ramvall, et al., Appl. Phys. Lett. 68, 1111 (1996).

Corresponding author: Hongqi Xu, Solid State Physics, Lund University, P.O. Box 118, SE-221 00 Lund, Sweden
Phone: + 46 46 222 0338; Fax: + 46 46 222 3637
Email: Hongqi.Xu@ftf.lth.se

Double-dot-like charge transport through a small size silicon single electron transistor

B. H. Choi[1,2], Y. S. Yu[1,2], S. H. Son[1], S. W. Hwang[1,2], D. Ahn[2], D. H. Kim[3], B. G. Park[3]
[1]School of Electrical Engineering, Korea University
[2]Institute of Quantum Information Processing and Systems, University of Seoul
[3]School of Electrical Engineering, Seoul National University

Multiple oscillation periods in the transport of semiconductor single electron transistors (SETs) have been widely investigated. Recently, high temperature (T) operations have been successfully realized in many types of silicon single electron transistors (SETs) [1], but transport study on such multiple periodicities in silicon SETs has been rare [2]. We present transport study on an ultra-small silicon SET exhibiting double period oscillations at low temperatures (Ts).

Figure 1 shows a cross-sectional SEM image of the fabricated Si SET. A quantum wire with the width of 30 nm has been formed using side-wall definition technique [3], so that the fluctuation of the wire width is suppressed within 2 nm. Two side gates (not shown in Fig. 1) with the separation of 88 nm have been made on the wire for the definition of the quantum dot. Subsequently, a thick layer of SiO_2 and a poly silicon control gate have been formed. Figure 2 shows the drain current (I_{DS}) oscillations as a function of the control gate voltage (V_{CG}) at 4 K. A clear beating with double periodicities is observed, which suggests double dot transport. It is observed that the oscillation with the periodicity of 430 mV persists up to T > 100 K while the oscillation with the periodicity of 24 mV appears only when T < 10 K. Figure 3 shows simulated current oscillations assuming double dot geometry (inset). The best fitting parameters of the gate capacitance between the control gate and the dot1 (C_{G1}), the gate capacitance between the control gate and the dot2 (C_{G2}), the coupling capacitance between the dot1 and the dot2 (C_C), the drain capacitance (C_D), and the source capacitance (C_S) are 0.377, 6.78, 1.0, 2.37, and 5.37 aF, respectively. The Coulomb energies of the dot1 and the dot2 calculated from these capacitances are 806 and 12 meV, respectively. The larger Coulomb energy is consistent with the size of the quantum dot defined by the side gates. More detailed analysis of the data and several possible origins of the small period oscillations will be presented.

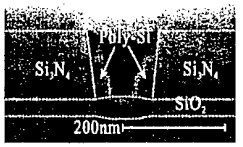

Fig. 1 : Cross-sectional SEM image of the fabricated Si SET.

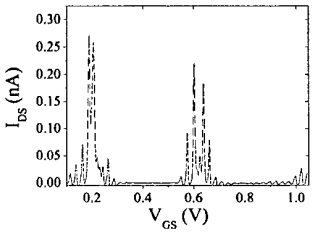

Fig. 2 : I_{DS}-V_{CG} characteristics measured at 4 K.

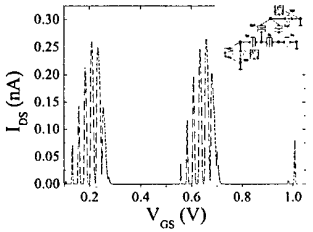

Fig. 3 : Simulation result of I_{DS}-V_{CG} characteristics at 4 K.

References

[1] See for examples, IEDM *Tech. Dig.* 1996~2000
[2] L. Rokhinson, L. Guo, S. Chou and D. Tsui., Appl. Phys. Lett. **76**, 1591 (2000).
[3] D. H. Kim *et al.*, Appl. Phys. Lett. (submitted)

Corresponding author: Sung Woo Hwang
School of Electical Engineering, Korea University, Anamdong, Sungbukku,
Seoul 136-701, Korea
phone: +82-02-3290-3241, Fax: +82-02-927-6114
e-mail: swhwang@mail.korea.ac.kr

The Fully Quantized Transistor

Boel Gustafson[1], Dan Csontos[1], Lars Erik Wernersson[1],
Michihiko Suhara[2], Hongqi Xu[1], and Lars Samuelson[1]

[1] Division of Solid State Physics, Lund University, Box 118, SE-221 00 Lund, Sweden
[2]Department of Electrical Engineering, Tokyo Metropolitan University,
1-1 Minami-ohsawa, Hachioji, Tokyo 192-0397, Japan

Today's devices and circuits still operate predominantly as classical devices. Visions of quantum-based electronics predict extremely compact, fast and power-conservative performance [1], with coherent or incoherent operation via discrete quantum states. Here, we demonstrate the fully quantized transistor, which is a potential building block for future Quantum Integrated Circuits (QICs).

Electron transport through quantum dots and quantum-dot like structures has been extensively studied with regard to detecting and making use of the discrete energy levels of the dots [2-4]. In most cases, however, the quantum dots have been investigated as isolated quantum systems coupled to non-quantized contact regions. We have instead considered the coherent transport through a gate-controlled quantum dot system including a quasi-one-dimensional (1D) emitter and collector. In such a system, all active regions are quantized and the gate can be used to control the mode coupling between quantum states in the different regions. The fully quantized transistor (FQT) is realized, where appropriate gate tuning enables selection of individual electron quantum states. In this way, the quantum nature, e.g., energy and parity, can be varied, providing gate-controlled, high-functionality, current-voltage characteristics.

In the fully quantized transistor, quantum states in the emitter, dot and collector are intercommunicating, resulting in very rich transport data. In simple terms, a current will flow when there are: (1) emitter electrons available, (2) a dot state, and (3) empty collector states, all of the same energy and parity. The current through the dot is thus dependent on the gate-controlled matching of dot states to both emitter and collector states.

Transport data from an asymmetric 1D-0D-1D structure are calculated using a scattering matrix approach [5] (Fig. 1). The gate-dependent trends found in the graph are intimately connected to a quantum system with individual lateral potential in emitter, dot and collector. The data can be interpreted as gate-dependent coupling between lateral modes in the three quantized regions, with fast (slow) moving peaks reflecting the gate-dependence of collector (dot) modes positioned close to (far away from) the gate.

Current-voltage measurements have been performed on gated quantum dot structures fabricated using selective growth over a metal gate [6]. Qualitative agreement is found between experimental data and the theoretical prediction, and the experiments may thus be the first step towards wave-function control in a fully quantized transistor.

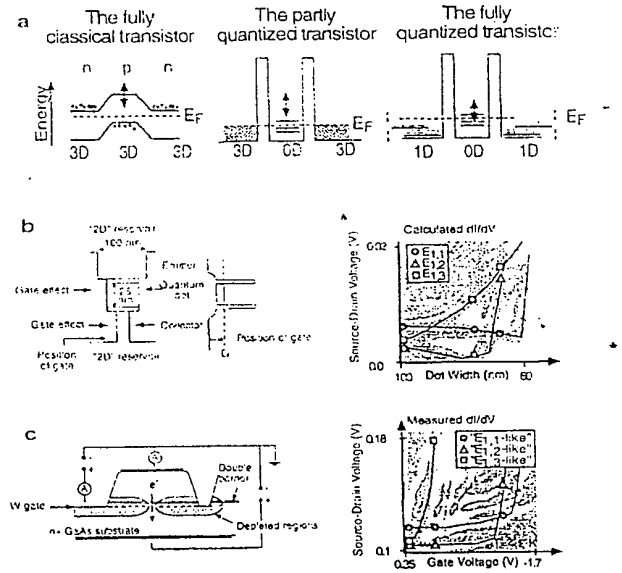

Figure 1: (a) Comparison of the classical, the partly quantized, and the fully quantized transistors. (b) Schematics and differential conductance, dI/dV_d, of the theoretical 1D-0D-1D structure, and (c) corresponding for the experimental structure.

References

[1] Amlani, I. *et al.*, Science 284, 289 (1999).
[2] Reed, M. A. *et al.*, Phys. Rev. Lett. 60, 535 (1988).
[3] Dellow, M.W. *et al.*, Phys. Rev. Lett. 68, 1754 (1992).
[4] Tarucha, S. *et al.*, Phys. Rev. Lett. 77, 3613 (1997).
[5] Xu, H. Q. Phys. Rev B 50, 8469 (1994).
[6] Wernersson, L.-E. *et al.*, Appl. Phys. Lett. 74, 311 (1999).

Corresponding author: Boel Gustafson, Div. of Solid State Physics, Lund University, Box 118, SE-221 00 Lund, Sweden.
Phone: +46 46 2220337, Fax: +46 46 2223637
E-mail: boel.gustafson@ftf.lth.se

Switching characteristics and demonstration of logic functions in modulation doped GaAs/AlGaAs nanoelectronic devices

L. Worschech, S. Reitzenstein, F. Fischer, M. Keßelring, A. Forchel

Technische Physik, Universität Würzburg, 97074 Würzburg, Germany

Since the first demonstration of hot electrons passing without loss of energy a thin GaAs layer [1], several attempts were made to utilize the fast motion of ballistic electrons. Devices composed by divers quantum point contacts have attracted considerable attention to study switching characteristics of electrons. Compared to field effect based switching, ballistic switching is expected to permit very low power and intrinsically very fast operation. The electron Y-branch switch is of particular interest for nanoelectronic applications, as it is based on the smallest possible ballistic transport zone in a three terminal device. We have fabricated and investigated electron Y-branch switches from GaAs/AlGaAs modulation doped heterostructures. The Y branch consists of a 1D source which is split into two 1D drains. In addition to a source drain voltage external fields can be applied via gates along the left and right drains. The length of the branching section in which the switching occurs is about 70 nm in our devices, of course small compared to the mean free path of the electrons in the unconstrained 2DEG. For the unprocessed wafer, the carrier density and the mobility determined at 4.2 K are about 3.7×10^{11} cm^{-2} and 2×10^{6} cm^2/Vs, respectively.

We report on a novel electrical property of ballistic Y-branch switching devices in the nonlinear response regime, demonstrating robust ballistic motion of hot electrons through the branching section. The hot electron transport is investigated through the two different drains as a function of the source-drain voltages and different gate voltages. We demonstrate selfgating of electrons when one mode of the Y-branch switch is occupied and voltage differences between the two drains smaller than the Fermi energy. The drain connected to the electron reservoir with lower potential possess the lower resistance [2]. In contrast for voltage differences of the two drains larger than the Fermi energy the resistance of the drain connected to the reservoir with the higher potential shows the lower resistance. Finite voltages V_l and V_r applied to the left and right branch reservoirs of a symmetric, ballistic Y-branch switch in push-pull fashion (i.e., V_l=-V_r) lead to a negative output voltage V_s of the floating, central stem reservoir located between the two branches. This bias voltage induced giant asymmetry persists up to room temperature indicating hot ballistic transport through nanoelectronic devices [3]. Thus the Y-branch switch operates as an extremely compact logic AND gate device, or as a logic OR gate depending on the voltage level definition. By cascading two back-to-back coupled Y-branch switches we observe side gate induced switching and inversion.

The bias voltage induced asymmetry is investigated for high frequencies at room temperature. The second harmonic of a microwave injected into the right branch is observed at the stem up to 10 GHz.

[1] M.Heiblum, M.I.Nathan, D.C.Thomas, C.M.Knoedler, Phys. Rev. Lett. **55**, 2200 (1985)

[2] J.O.W. Wesström, Phys. Rev. Lett. **82**, 2564 (1999).

[3] U.Sivan, M.Heiblum, and C.P.Umbach, Phys. Rev. Lett. **63**, 992 (1989).

The Transient Signal Response of Deep Submicron $Si/Si_{0.77}Ge_{0.23}$ MODFETs

A. Yangthaisong, G.C. Crow, R.A. Abram

Department of Physics, University of Durham, South Road, Durham DH1 3LE. UK.

Modulation doped Si/SiGe heterostructures grown on relaxed SiGe virtual substrates have been shown to produce high mobility two-dimensional electron gases, and have great potential for the development of fast Si-based MODFETs. Optimum transistor design is ultimately based on a full understanding and accurate modelling of charge-carrier transport in the device. We have studied electron transport in n-channel $Si/Si_{0.77}Ge_{0.23}$ MODFETs using 2D Monte Carlo simulation. The simulation provides information on the microscopic details of the carrier behavior, including carrier velocity, kinetic energy and carrier density, as a function of position in the device. Monte Carlo simulations have also been carried out to investigate the high frequency performance of the devices. Three enhancement mode devices with gate length down to 0.07 μm, as illustrated in Figure 1a, have been studied and are similar to those being investigated experimentally by several groups (for example, Daimler-Chrysler[1],IBM[2]). The effects of varying the gate length L_G and the source-gate distance L_{SG} are studied. Detailed time-dependent voltage signal analysis has been carried out to test the device response and derive the frequency bandwidth, as illustrated in Figure 1b. A sinc voltage pulse is applied to the gate and the resulting drain and gate currents used to calculate the current gain as a function of frequency. Figure 1c shows that the highest intrinsic current gain cut-off frequency f_T^i of 60 $\pm$ 10 GHz is obtained for a gate length of 0.07 μm.

References

[1] M. Glück, T. Hackbath,A. Haas, E. Khon and U. König, Physica E. ,**2**, 763, 1998.
[2] S.J. Koester, J.O. Chu, and R.A. Groves, Electronics Letters **35(1)**, 86, 1999.

Corresponding author: Mr Anucha Yangthaisong, Department of Physics,
University of Durham, South Road, Durham DH1 3LE, UK
phone: +44 +191 374 2000 ext 4029 Fax: +44 +191 374 3848,
email: anucha.yangthaisong@dur.ac.uk

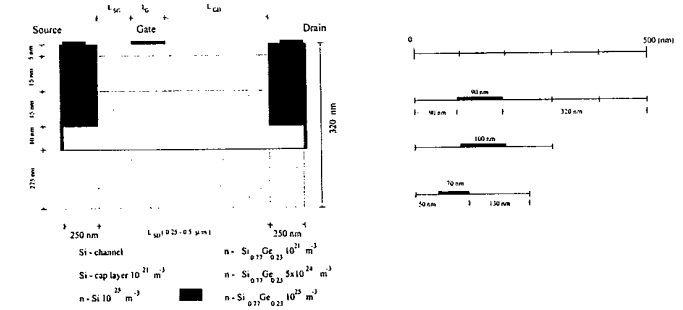

(a) simulated structures

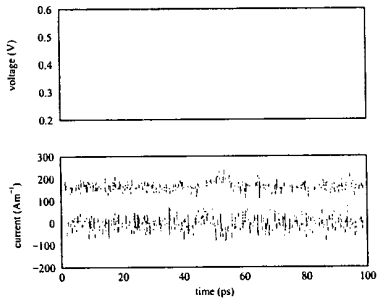

(b) frequency response

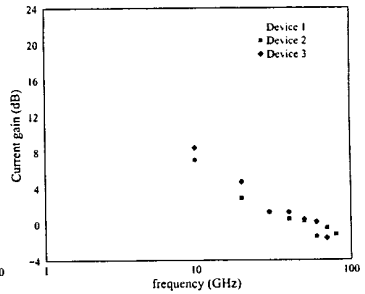

(c) current gain cut-off frequency

Figure 1: (a-left) The simulated device structure. A 10 nm tensile strained Si quantum well is grown on a relaxed $Si_{0.77}Ge_{0.23}$ virtual substrate, and is modulation doped via the top supply layer (15 nm, $5x10^{24}$ m^{-3}). The confined electron gas is separated from the supply layer by a 15 nm spacer (background doping density 10^{21} m^{-3}). The source and drain implants are taken to be $1x10^{25}$ m^{-3}. The gate is deposited on the top of a Si-cap layer (5 nm) and a Schottky barrier height of 0.8 eV has been used to represent the contact potential at the gate electrode. **(a-right)** From top to bottom, devices 1-3 with the varying gate length L_G and source-gate distance L_{SG}. **(b)** The simulated frequency response of a Si/SiGe n-MODFET with 0.09 μm gate length to a sinc gate voltage pulse. From top to bottom, this figure shows the gate voltage (V_{gate}) as a function of time for a truncated pulse of duration 100 ps, the drain current response (I_{drain}) and the gate current (I_{gate}), which is electric displacement. **(c)** Logarithmic plot showing the maximum intrinsic current gain calculated for n-MODFETs with various gate lengths. The intrinsic current gain cut-off frequencies f_T^i for devices 1-3 are 40 $\pm$ 10, 50 $\pm$ 10 and 60 $\pm$ 10 GHz, respectively.

First principles calculations of the dark current in QWIPs

N.E.I. Etteh and P. Harrison

IMP, School of Electronic and Electrical Engineering,
The University of Leeds, LS2 9JT, U.K.

This work demonstrates the calculation of the dark current in quantum well infrared photodetectors (QWIPs) entirely from a quantum mechanical viewpoint. The appropriate electron-electron (e-e) and electron-LO (e-LO) phonon absorption and emission scattering rates were evaluated for all three components of the dark current (see Figure 1): the Thermionic Emission (TE), Field Induced Emission (Thermally Assisted Tunnelling) (FIE), and Ground State Sequential Tunnelling (ST).

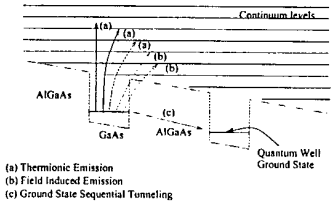

Figure 1: The three components of the dark current in QWIPs

This was achieved by solving the one-dimensional Schrödinger equation numerically using a shooting method to obtain both the energy eigenvalues, E, and the wave functions, $\psi(z)$. The resulting wave functions were used to calculate the e-LO and e-e scattering rates using an approach based on Fermi's Golden Rule (see Harrison [1] for full derivation and computer sourcecode).

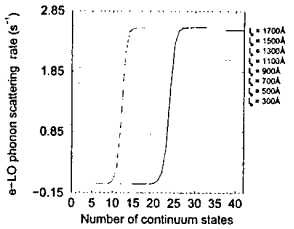

Figure 2: Total e-LO phonon absorption scattering rate as a function of the number of continuum states included in the summation at 77K

The main problem that had to be tackled in order to obtain a good numerical representation of the dark current was the representation of the thermionic field emission and field induced emission components. This was achieved by discretising the continuum (as shown in Figure 1). Scattering from the well to the continuum represents both thermionic emission (TE) and field induced emission (FIE), and this was evaluated by summing over continuum states of increasing energy, until convergence was achieved, (see Figure 2). The summation was controlled by increasing the barrier width (the distance from the well to the limits of the spatial domain), as illustrated. The fact that the summations converge to the same value, independently of how the continuum is discretised, is important evidence to validate this approach. The e-e scattering rates show a similar dependency.

Figures 3(a) and 3(b) show the results of this procedure for the QWIP of Walther *et al* [2] (44Å GaAs quantum well separated by 470Å $Ga_{0.63}Al_{0.27}As$ barriers). It can be seen from Figure 3(a) that the contribution to the dark current deduced from the thermionic emission, I^{TE}, and field induced emission, I^{FIE}, is similar to that usually measured - it increases with bias and temperatures. However, the results from the calculations of the sequential tunnelling contribution, I^{ST}, are not consistent with experimental measurements. In particular, no local maximum is ever observed at experimental low biases (this arises from resonant LO phonon emission).

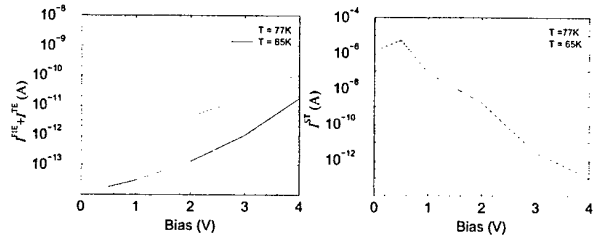

Figure 3: (a) Total FIE and TE components of the dark current with respect to bias at 77K and 65K and (b) ST component of the dark current with respect to bias at 77K and 65

We believe the reason stems from the assumption, within the scattering rate calculations, of perfectly uniform quantum wells and coherence of the wave function in the plane of the quantum wells. Real quantum wells have interface disorder and alloy fluctuations in the barrier material which are sufficient to produce localisation in the plane and reduce interwell scattering. We believe this is why sequential tunnelling is thought not to contribute to the dark current [3].

References

[1] P. Harrison, *Quantum wells, Wires and Dots: Theoretical and Computational Physics*, John Wiley and Sons, Chichester, 1999.

[2] M. Walther, F. Fuchs, H. Schneider, J. Fleißner, C. Schönbein, W. Pletschen, K. Schwarz, R. Rehm, G. Bihlmann, J. Braunstein, P. Koidl, J. Zeigler and G. Becker, "Electrical and Optical properties of 8-12 μm GaAs/AlGaAs Quantum well Infrared Photodetectors in 256 × 256 Focal Plane Arrays" in *Intersubband Transitions in Quantum Wells: Physics and Devices*, Sheng S. Li and Yan-Kuin Su, Rds., Kluwer Academic Publishers, Boston, U.S.A., 1998.

[3] S. Gunapala, G. Sarusi, J. Park, T. Lin, B. Levine, "Infrared detectors reach new lengths", *Physics World*, **7**, 35, 1994.

Corresponding author: Nkaepe Etteh,
IMP, School of Electronic and Electrical Engineering,
The University of Leeds, LS2 9JT, U.K.
Tel: +44-113 233 2060 Fax: +44-113 244 9451
email: eenneie@electeng.leeds.ac.uk

Effect of doping profile on the potential performance of buried channel SiGeC/Si heterostructure MOS devices

E. Cassan, P. Dollfus and S. Galdin
Institut d'Electronique Fondamentale, UMR CNRS 8622, Université Paris Sud, Bât. 220
91405 Orsay cedex, France, E-mail: eric.cassan@ief.u-psud.fr

Despite the technological difficulties encountered, the introduction of SiGeC alloys into Si VLSI technology has considerably progressed for several years. This tendency is due to both the bandgap engineering flexibility and the strain-induced enhancement of transport properties that can be obtained [1,2]. It has already led to significant improvements in bipolar device technology [3] and is currently in the research field regarding N and P-channel FETs for CMOS applications. In this context, this work is focussed on the potential of SiGeC/Si heterostructure for ultra-short N-MOSFET. The conduction band offset required to design a N-FET may be obtained from a heterostructure with tensile strain, which is achieved either by growing a Si layer on a $Si_{1-x}Ge_x$ virtual substrate, or by the growth of $Si_{1-y}C_y$ ($y<3\%$) on Si substrate [4-6]. It has been shown that with this such a buried-channel configuration, electrons may benefit from strain-induced mobility enhancement in strained Si [1,2,7] and may take advantage of reduced roughness scattering at semiconductor/SiO_2 interface due to the insertion of a wide-bandgap spacer layer. Nevertheless, this only holds true provided that the electron population is effectively confined in the buried strained quantum well (QW).

In this paper, we use a self-consistent one-dimensional Schrödinger-Poisson solver for MOS capacitors [8] to investigate the effect of the channel doping profile on the charge control. It has been shown indeed that wave-mechanical effects cannot be neglected for the description of such devices [9]. We also study in this work the reduction of gate leakage current that can be obtained by burying the channel of N-MOS devices having ultra-thin gate oxide. The strain-induced splitting of conduction and valence bands is accounted for in the model. The direct tunneling gate current is calculated by estimating the carrier lifetimes of the quasi-bound states in the quantum well structure. All details about the model and the numerical procedure can be found in Ref. [8]. The main technological parameters influencing the device operation are the oxide thickness t_{OX}, the spacer thickness t_S, the QW thickness t_{QW}, the conduction band offset ΔE_C, and the bulk doping profile $N_A(x)$, x being the spatial coordinate. We have investigated the influence of these five parameters on the proportion r_{QW} of the electron population confined in the strained QW, that should benefit effectively from enhancement of transport properties in the transistor configuration.

We have first studied uniformly doped devices. Figure 1 is a plot of r_{QW} of 1nm-thick gate oxide capacitors as a function of N_A for two conduction band offsets (0.1eV and 0.2 eV) and two spacer thicknesses (1 nm and 2 nm). The gate biases are chosen to induce the same total electron density in all cases ($n_S = 5\times10^{12}$ cm^{-2}). This figure shows that if the spacer thickness is chosen too thick, high bulk doping values (likely to be used in deep sub-0.1µm MOSFET to limit short channel effects) can yield a dramatic reduction of r_{QW} to a few percent, which should be highly detrimental to the transistor performance. This is due to the strong band bending near the oxide/semiconductor interface induced by high doping. This result is clearly illustrated in Fig. 2 which is a comparison of the electron concentration profiles obtained for $N_A = 10^{17}$ cm^{-3} and for $N_A = 10^{19}$ cm^{-3} (t_S =2 nm, $\Delta E_C = 0.1$ eV). By using retrograde doping profile $N_A(x)$ to relax the more as possible the band bending near the interface, the proportion of electrons confined in the strained-QW increases by about 10-20% depending on the MOS structure.

In Fig. 3 is plotted the direct tunneling gate current through 1nm-thick gate oxide for conventional and heterojunction capacitors as a function of uniform doping concentration. At low doping the confinement of electrons in the buried layers yields a strong reduction of gate leakage compared with conventional structure. At high doping, the degradation of confinement suppresses the advantage of the heterostructure. The increase of surface electric field tends to reduce the quasi-bound states lifetimes, which enhances the gate leakage.

A full investigation of the influence of technological and material parameters (t_{OX}, t_S, $N_A(x)$, ΔE_C) regarding both electron confinement and tunneling leakage will be presented.

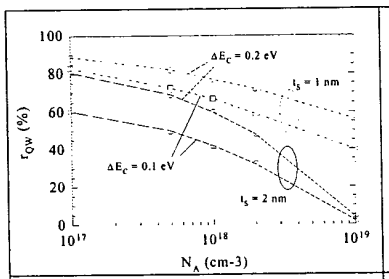

Fig.1. Proportion of the electron population confined in the strained QW of heterostruc-ture MOS capacitors as a function of bulk doping concentration (t_{OX} = 1 nm).

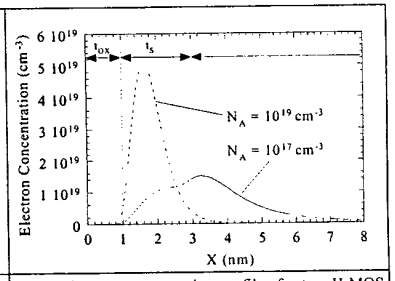

Fig.2. Electron concentration profiles for two H-MOS capacitors with $N_A = 10^{17}$ cm^{-3} and $N_A = 10^{19}$ cm^{-3}, respectively (t_S = 2 nm, ΔE_C = 0.1 eV, t_{OX} = 1 nm).

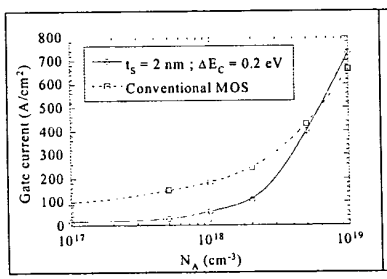

Fig.3. Gate current leakage in conventional and heterojunction MOS capacitors for t_{OX} = 1 nm and $n_S = 5\times10^{12}$ cm^{-2}.

References

[1] T. Hackbarth et al., J. Crystal Growth., vol. 201/202, p. 734, 1999.
[2] K. Ismail et al., Appl. Phys. Lett., vol. 63, p. 660, 1993.
[3] J.D. Cressler, IEEE Trans. on Microw. Theory and Techn., vol. 46, p. 572, 1998.
[4] K. Brunner et al., Phys. Rev. Lett., vol. 76, p. 303, 1996.
[5] D.V. Singh et al., J. Appl. Phys., vol. 85, p. 978, 1999.
[6] H.J. Osten et al., Appl. Phys. Lett. vol. 76, p. 200, 2000.
[7] P. Dollfus, J. Appl. Phys., vol. 82, p. 3911, 2000.
[8] E. Cassan, J. Appl. Phys., vol. 87, p. 7931, 2000.
[9] E. Cassan et al., IEEE Trans. on Electron. Devices, to be published (April 2001).

Corresponding author : Philippe Dollfus, IEF, CNRS UMR8622, Université Paris-Sud, Bâtiment 220, 91405 Orsay cedex, France
Phone: +33 1 69 15 72 83, Fax: +33 1 69 15 40 20, email: dollfus@ief.u-psud.fr

Multilevel logic element based on the long period GaAs/AlGaAs superlattice.

Yu.A.Mityagin, Yu.A.Efimov , V.N.Murzin, A.A.Pishchulin

P.N.Lebedev Physical Institute, 117924, Leninsky prosp., 53, Moscow, Russia

Recently a very large current hysteresis was found in vertical transport I-V characteristics of the long period GaAs/AlGaAs superlattices[1,2] (the plateau current values differed more than 2 times for sweep-up and sweep-down I-V curves). A set of multiple stable current branches, arising from different locations of the domain boundary along the superlattice [2-4], was observed inside each of hysteresis region, thus resulting in multistability effect - the existence of several stable current states for a given value of bias voltage. The idea of switching between this current states by applying short voltage pulses was proposed [4] and some preliminary results were reported [4,5].

Here we present the results of experimental studies of switching process between multistable current branches in long period (well width 250 Å, barrier width 100 A, doping density $N_d \sim 2.4 \cdot 10^{10}$ cm^{-2}) MBE-grown GaAs/AlGaAs superlatices and propose this structure as a multilevel logic device. A well-defined hysteresis and a set of current branches were observed in I-V curves of the samples (Fig.1), and 7 stable current states existed for the bias voltage in the plateau regions.

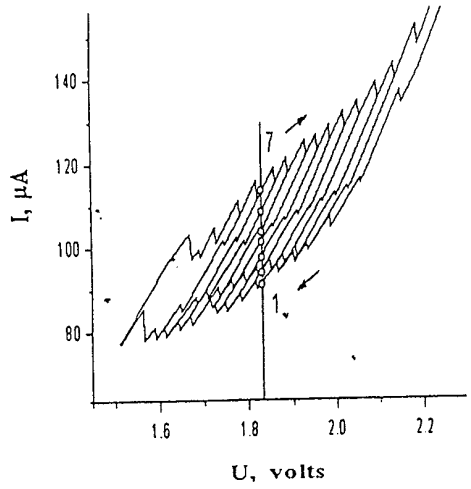

Fig.1. Fragment of experimental I-V curves corresponding to 1→5 electric field domain formation for GaAs/AlGaAs superlattice (well width 350Å, barrier width 120Å, T=4.2K).

The switching was carried out by applying to the sample the triangular pulses of voltage of various amplitude and duration.(5 μs – 1 ms).

The typical switching characteristics is shown in Fig. 2. The initial state is the point labeled by 7 in Fig.1. The pulses of positive polarity switch the system to lower current states, while negative ones switch it to higher current states As seen, in this range of pulse duration the switching is reproducible and reliable It was shown that it is possible to switch between any selected current states applying the pulses of certain polarity and of amplitude within certain voltage interval

The theoretical modeling of the switching processes was made on the basis of discrete drift model of the vertical transport in superlattices [1,2]. It was shown that the assumption of slow voltage variation during the triangular switching pulse for the superlattice parameters used in experiment is valid forl pulse duration longer than 1-3 μs. Only in this regime the switchidg is pbssible without missing any current state. This limiting values for switching times are

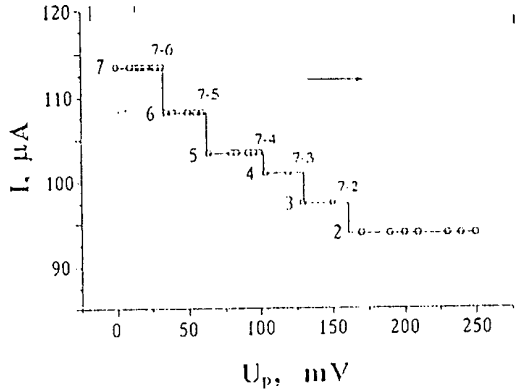

Fig.2. The switching characteristics (the dependence of current in the final state on the amplitude of the switching pulse) for positive polarity of pulses. Circles – experimental points, full curve - developed from I-V characteristics of Fig 1 supposing slow switching voltage sweeping up and down. Bias voltage - 1.83V, pulse duration - 5 μs, T=4.2K.

determined by characteristic times of resonant tunneling and electric field domain boundary space charge redistribution in the superlattice. According to the numerical simulation results the most direct way to improve switching characteristics of the proposed device is to use superlattices with lower barrier width

Finally, we proposed a multilevel logic device with several stable current states with the possibility of switching between any selected states by voltage pulses of appropriate amplitude and polarity.

The work was supported by Russian Basic Research Foundation (project No. 00-02-16709).

References:

[1]. Yu.A.Mityagin, V.N.Murzin JETP Lett., 64, 155 (1996)
[2] Yu.A.Mityagin, Appl.Phys. Lett., 70(22), 3008 (1997)

[3] J.Kastrup, H.T.Grahn, K.Ploog, F.Prengel, A.Wacker, E.Scholl, Appl.Phys.Lett., 65, 1808 (1994)

[4] Murzin V.N., Mityagin Y.A., Rasulova G.K., Stoklitsky S.A., Perestoronin A.V., Proc. Int. Symposium "Nanostractures: Physics and Technology", St. Petersburg, Russia. 1995, p.151-154.

[5] G.K Rasulova, Yu.A Efimov, V.N.,Murzin. J.Appl.Phys, 82(7), 3381, (1997).

Corresponding author: Yury A. Mityagin, P.N.Lebedev Physical Institute.
117924, Leninsky prosp., 53, Moscow, Russia.
phone: +7 095 1326952, Fax: +7 095 1357880
email: mityagin@mail1.lebedev.ru

Photoluminescence study of GaAs/AlGaAs micro-tube with uniaxially strained quantum wells

K. Kubota, P. Vaccaro, N. Ohtani, Y. Hirose*, M. Hosoda*, T. Aida
ATR Adaptive Communications Research Labs,
2-2-2 Hikaridai,Seika-cho, Soraku-gun, Kyoto 619-0288, Japan
*Department of Applied Physics, Osaka City University,
3-3-138, Sugimoto, Sumiyoshi-Ku, Osaka, 558-8585, Japan

It is well known that strained III-V compound semiconductor superlattices have their electronic band structure modified by the mismatch in the lattice parameter of the different layers.[1] These superlattices have biaxial strain in the plane of the epitaxial layers. It will be interesting if we can control the internal stress and strain by different approach. Recently, Prinz et al. demonstrated that multilayer structures including strained layers are useful to form micro-tubes. They fabricated these structures by using lattice-mismatched epitaxial layers that rolled up when freed from the substrate due to the built-in strain.[2]

In this study, a micro-tube including several GaAs/AlGaAs quantum wells located at positions with different strain was fabricated and its optical properties were investigated by photoluminescence spectroscopy. The quantum wells in the micro-tube have uniaxial strain in the plane of the epitaxial layers.

The multilayer structure was grown by MBE on a GaAs (100)-oriented substarate. Starting from the substrate, the structure consists of an $Al_{0.5}Ga_{0.5}As$/AlAs digital alloy (0.4 nm /0.4 nm x50 periods=39 nm) sacrificial layer, an $In_{0.15}Ga_{0.85}As$ (10 nm) strain layer, an $Al_{0.5}Ga_{0.5}As$ bottom barrier (15 nm), a GaAs quantum well (QW2) (3 nm), an $Al_{0.5}Ga_{0.5}As$ central barrier(40 nm), a GaAs quantum well (QW1) (2 nm), an $Al_{0.5}Ga_{0.5}As$ top barrier (15 nm) and a GaAs cap layer (10 nm). The sacrificial layer was partially removed by selective wet etching. After release of the film from the substrate, the pair of equal and opposite forces due to lattice mismatch at the interface between the InGaAs strained layer and AlGaAs generates a bending moment that forms the micro-tube. Figure 1 shows a photograph of micro-tube.

The micro-tube's curvature and stress can be calculated theoretically assuming balance of force and moment across the film. A schematic diagram of internal stress across the film is shown in Fig. 2. In this study, the position of QW1 and QW2 are such that they are under compressive and tensile strain, respectively, after release and curl.

Figure 3 shows the photoluminescence spectra of the light emitted from a micron-size spot on the micro-tube observed before and after release from the substrate. After release from the substrate, the photoluminescence peak of QW2 shifted towards longer wavelength. This is due to the tensile strain on the quantum well, and it agrees with the value calculated by k-p perturbation theory.[3] The photoluminescence peak of QW1 showed a shift towards longer wavelength after release but shifted towards shorter wavelength after curl because it is placed in a plane of the epilayer where strain is changed in an opposite direction to that of QW2.

In conclusion, a new type of structure that allows control of the uniaxial strain on quantum wells was fabricated and it was shown that optical properties of the films can be modified by the change of built-in strain.

Fig. 1. Photograph of the fabricated micro-tube

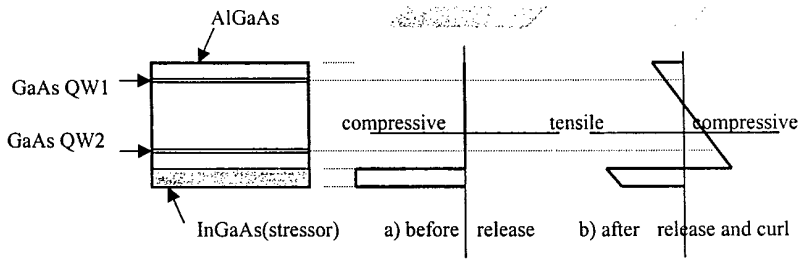

Quantum-confined impurities as single-electron quantum dots: Free-electron laser studies and application to Terahertz emitters

M. P. Halsall[1], P. Harrison[2], J.-P. R. Wells[3] and I. V. Bradley[3]

[1]*Department of Physics, UMIST, Manchester, M60 1QD, U.K.*
[2]*IMP, School of Electronic and Electrical Engineering, The University of Leeds, LS2 9JT, U.K.*
FOM-instituut voor Plasmafysica, 3430 BE Niewegeibn, The Netherlands

This work will demonstrate that impurities within semiconductor crystals can be thought of as the ultimate in quantum dots, with the three-dimensional confining potential being provided by individual atoms which are each capable of localising single electrons or holes. A heterostructure confining potential provides a means to tune the energy levels of the impurities, as illustrated in Fig. 1. Just as importantly, quantum well systems with these embedded quantum dots can be fabricated to very high qualities with contemporary molecular beam epitaxy growth techniques.

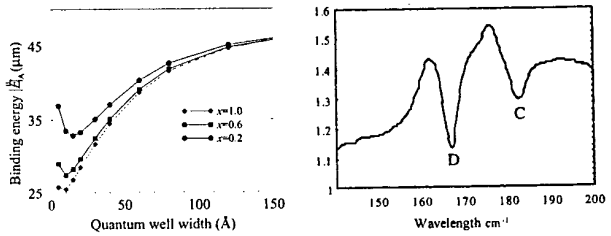

Figure 1: (a) Calculated[1] binding energy of a Be acceptor in a GaAs quantum well surrounded by $Ga_{1-x}Al_xAs$ barriers and (b) low temperature FTIR absorption spectra of Be-doped GaAs

The desire to produce a coherent source of far-infrared ($> 30\mu$m) or Terahertz (1-10 THz) radiation pointed towards Be acceptors in GaAs/$Ga_{1-x}Al_xAs$ heterostructures for two reasons. Firstly, the results of initial theoretical studies (see Fig. 1(a)) demonstrated that the binding energy of a Be acceptor could be engineered to lie between 26 and 50 meV (25–45 μm) merely by altering the width of the quantum well. The second reason for this choice is the availability of high quality epitaxially grown material.

Fig. 1(b) shows the results of Fourier Transform InfraRed (FTIR) absorption measurements on Be-doped bulk GaAs. This spectra was taken in *normal incidence* thus illustrating the three-dimensional nature of the confinement and shows two features corresponding to the C and D components of the 1s–2p transition at 184 and 167 cm^{-1} respectively (corresponding to 54 and 59 μm).

One of the main problems to be tackled in order to extend the operating wavelength of quantum cascade lasers will be the decreasing non-radiative intersubband lifetime. Any potential benefits of moving beneath the longitudianl-optical phonon energy are offset by increases in carrier–carrier scattering, thus making sustainable population inversions more difficult to attain. Fig. 2 shows the results of time-resolved pump-probe experiments at the Dutch free-electron laser (FELIX). Both curves show a decay rate of around 400 ps, which is almost two orders of magnitude longer than the equivalent intersubband lifetime. Furthermore, measurements upto 60 K showed that this lifetime was quite insensitive to temperature[2]. Both qualities offer great potential for a population inversion of the 2p level over the 1s level and hence show the promise of a solid-state source of terahertz radiation.

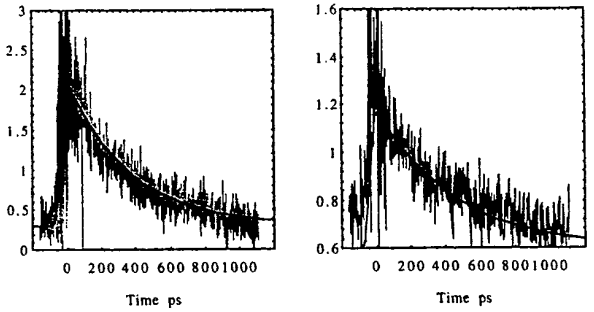

Figure 2: The pump probe signal for the C (left) and D (right) lines in the 1s–2p intra-acceptor transitions of Be-doped GaAs.

Recent measurements have extended this work to consider the manipulation of the impurity levels with a quantum well potential. GaAs/AlAs multiple quantum wells doped with Be were grown and the structural tunability of the impurity levels was demonstrated by a 10% increase in the 1s–2p absorption energy. The effect on the wave functions of the impurity states was demonstrated by the reduction in the lifetime of the 2p level, from 400 ps (as in the bulk) to just 100 ps[3].

In addition to reporting these results this work will discuss moves towards incorporating internal acceptor transitions in eventual Terahertz emitters and lasers; and will present preliminary designs of such devices.

References

[1] P. Harrison. *Quantum Wells, Wires and Dots: Theoretical and computational physics.* John Wiley and Sons, Ltd, Chichester, United Kingdom, 1999. 456 pages, ISBN 0 471 98495 7.

[2] M. P. Halsall, P. Harrison, H. Pellemans, and C. R. Pidgeon. Free-electron laser studies of intra-acceptor transitions in gaas: a potential far-infrared emission system. In P. Harrison and E. Schomburg, editors, *Terahertz spectroscopy and applications*, volume 3617, pages 171–176. SPIE, 1999.

[3] M. P. Halsall, P. Harrison, J.-P. R. Wells, and I. V. Bradley. Picosecond far-infrared studies of intra-acceptor dynamics in bulk gaas and δ-doped alas/gaas quantum wells. *Phys. Rev. B*, 2001. accepted.

Corresponding author: Paul Harrison,
IMP, School of Electronic and Electrical Engineering,
The University of Leeds, LS2 9JT, U.K.
Tel: +44-113 233 2043 Fax: +44-113 244 9451
email: p.harrison@physics.org

Theoretical Analysis of THz Photon-Assisted Tunneling and Optical Gain in Resonant Tunneling Diodes

M. Asada and N.Sashinaka

Interdisciplinary Graduate School of Science & Engineering, Tokyo Institute of Technology, 2-12-1 O-okayama, Meguro-Ku, Tokyo 152-8552, Japan

Photon-assisted tunneling current under THz irradiation in resonant tunneling diodes (RTDs) was analyzed with density-matrix theory. Very good agreement with measured results was obtained. The analysis was extended to THz gain due to inter-quantum well transition for intersubband THz lasers.

Interaction of nanostructures with THz electromagnetic waves has received considerable attention. THz photon-assisted tunneling phenomenon [1][2] is one of such interactions. THz emission and oscillation by intersubband transition, which are closely related to the photon-assisted tunneling, have also been studied extensively [3]-[5]. In this paper, we applied the density-matrix method to the photon-assisted tunneling in triple-barrier RTDs, and extended it to the THz optical gain due to inter-well intersubband transitions.

Figure 1 shows the band diagram of a triple-barrier RTD with dc and THz voltages used for the density-matrix analysis. Photon-assisted tunneling at the central barrier dominantly causes the current change under the THz irradiation. The current changes at the left and right barriers are small due to wide energy distribution in the electrodes at room temperature.

Figure 2 shows a comparison between the theoretical calculations and measured results [2] of THz-irradiated current-voltage (*I-V*) curves of a GaInAs/InAlAs triple-barrier RTD. The Fermi level and quantized levels were estimated initially from the doping concentration and structure, and the broadening of the levels was determined by fitting the peak width of the *I-V* curve without THz irradiation to the measurement.

As seen in Fig.2, fairly good agreement was obtained including the change of the peak heights. Fig.3 shows theoretical *I-V* curves of a THz-irradiated RTD with narrow energy broadening. Multiple peaks are generated due to the photon-assisted tunneling. These curves also agree well with the measurement[1].

Since the theoretical analysis explains measurements quite well, we extended it to the THz gain due to electron transition between adjacent wells in a RTD. The generated THz power was calculated at first by the product between the applied THz voltage and the THz component of the photon-assisted tunneling current, and then, the gain coefficient was obtained. Fig.4 shows the calculated gain coefficients for various frequencies. The gain is positive in the negative differential resistance region. These shapes are similar to those with a simple estimation from the measured *I-V* curves[6]. The peak current density of the RTD was assumed 50kA/cm^2 in the calculation, which value was around the estimated laser threshold.

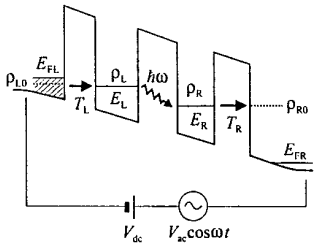

Fig.1: Triple-barrier RTD structure for density-matrix analysis of photon-assisted tunneling.

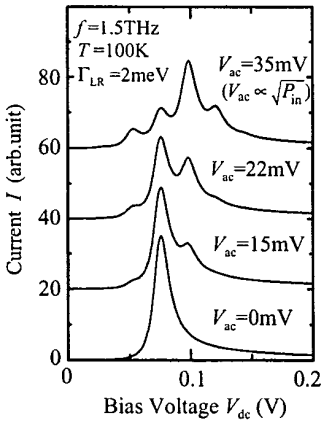

Fig.3: Theoretical *I-V* curves of a RTD with photon-assisted tunneling in narrow energy broadening case.

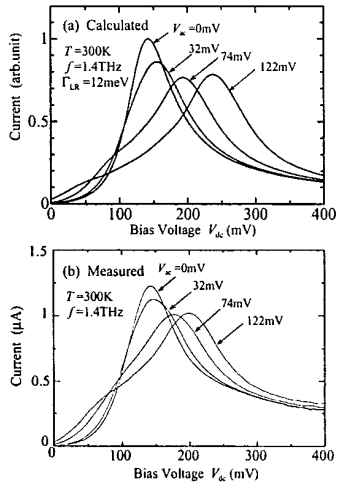

Fig.2: Comparison between theoretical and measured [2] *I-V* curves of a THz-irradiated triple-barrier RTD.

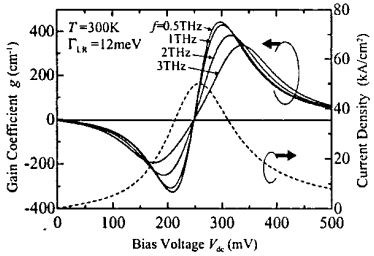

Fig.4: Theoretical inter-well THz gain coefficients for various frequencies.

References

[1] H.Drexler, J.S.Scott, S.J.Allen, K.L.Campman, and A.C.Gossard, Appl.Phys.Lett, 67 (1995) 2816.
[2] N.Sashinak, Y.Oguma, and M.Asada, Japan.J.Appl.Phys, 39 (2000) 4899.
[3] M.Helm, P.England, E.Colas, F.DeRosa, and S.J.Allen, Phys.Rev.Lett, 63 (1989) 74.
[4] M.Rochat, J.Faist, M.Beck, U.Oesterle, and M.Ilegems, Appl.Phys.Lett, 73 (1998) 3724.
[5] J.Ulrich, R.Zobl, K.Unterrainer, G.Strasser, E.Gornik, K.D.Maranowski, and A.C.Gossard, Appl.Phys.Lett, 74 (1999) 3158.
[6] M.Asada, Y.Oguma, and N.Sashinaka, Appl.Phys.Lett, 77 (2000) 618.

Corresponding author: Masahiro Asada, Dept. Electrical & Electronic Eng., Tokyo Institute of Technology, 2-12-1 O-okayama, Meguro-Ku, Tokyo 152-8552, Japan,
Phone: +81-3-5734-2564, Fax:+81-3-5734-2907, e-mail:asada@pe.titech.ac.jp

Intersubband relaxation dynamics in semiconductor quantum structures

R. Bratschitsch, T. Müller, G. Strasser, and K. Unterrainer

Institute for Solid State Electronics, Technical University of Vienna, Floragasse 7, A-1040 Vienna, Austria

The ability to generate intense ultrashort pulses in the mid-infrared (MIR) using a tabletop laser system [1] has stimulated the field of ultrafast MIR experiments [2]. One now has the possibility to *directly* probe the dynamics of carriers in quantized states of semiconductor structures [3]. A detailed knowledge of the various relaxation processes is very important for the improvement of quantum cascade lasers and new quantum devices.

We have studied the time-resolved photoinduced intersubband absorption in an undoped double quantum well (QW) by performing a visible pump/mid-infrared probe experiment. We deduce a relaxation time of 100 ps for the transition between the two lowest levels 2 and 1 which have an energy separation smaller than the LO phonon energy and a recombination time of 400 ps from the ground level.

Our sample is an undoped GaAs/AlGaAs double quantum well (80x) with 90 Å and 80 Å wells separated by a 30 Å barrier. There are four energy levels in the double well potential with energy separations in the far- and mid-infrared (inset of Fig 1). We performed a visible pump/MIR probe experiment to study the different relaxation processes inside the quantum well: a visible pump pulse is used to generate carriers in the sample and the MIR transmission spectrum which probes the quantum well transitions is recorded at different time delays. The MIR pulses are generated by phase-matched difference frequency mixing of spectral components within the ultrabroadband spectrum of a 12 fs Ti:sapphire laser [1]. The spectrum of the transmitted MIR radiation is recorded by performing an autocorrelation measurement and using a HgCdTe detector. The experiment is done in a waveguide geometry which provides a time resolution of about 2 ps. The sample is cooled in a cryostat to about T = 5 K.

Figure 1 shows the intersubband absorption at four different time delays. Two prominent peaks are visible that can be associated with the different transitions inside the QW. The low frequency peak which is distorted by the HgCdTe detector cutoff around 21.5 THz corresponds to the transitions 1-3 and 2-3. The high frequency peak time corresponds to the transitions 1-4 and 2-4. It shows a clear blue shift over time. Fitting two Gaussian peaks with a fixed separation of 1.7 THz - the transition energy between levels 1 and 2 has been measured in a quantum beat experiment - reveals the different relaxation processes inside the QW (Fig. 2). While the relaxation from level 2 to 1 shows an exponential decay with a time constant T_{21} of 100 ps, the recombination from the ground level shows a more complex behavior. An analysis based on a rate equation model (lines in fig. 2) gives an explanation for the physical processes involved. Since levels 3 and 4 are depopulated very quickly (< 2 ps) by optical phonon scattering (E_{13}, E_{14}, E_{23}, E_{24} >> E_{LO}) only levels 1 and 2 have to be considered in the model. The carriers relaxing down from level 2 to 1 add to the population in the ground level which explains the rise of the absorption signal until 70 ps after the excitation. Subsequently, the carriers of level 1 recombine with a time constant τ_{rec} of 400 ps.

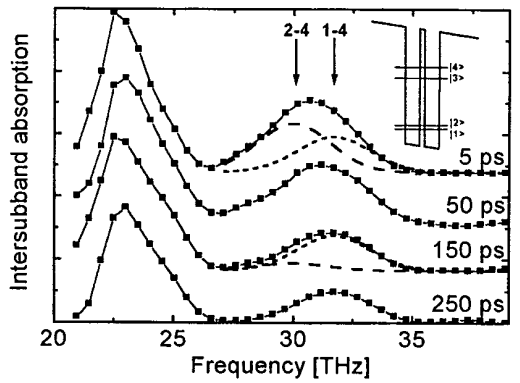

Fig. 1: Intersubband absorption at four different time delays (points) with two Gaussian fits for the transitions 2-4 (dashed line) and 1-4 (dotted line); inset: double quantum well potential

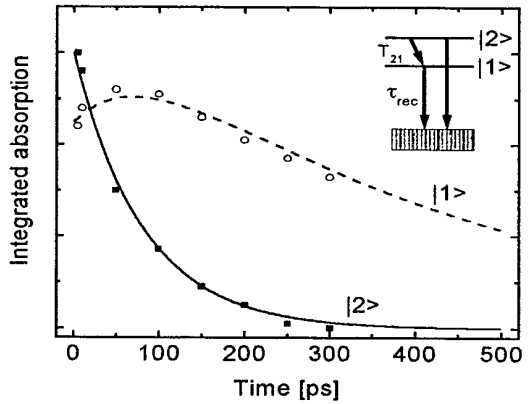

Fig. 2: Measured (squares and circles) and calculated (lines) integrated absorption of subbands 1 and 2; inset: level diagram with relaxation time T_{21} and recombination time τ_{rec}.

References

[1] R. A. Kaindl et al., Opt. Lett. 23, 861 (1998).
[2] R. A. Kaindl et al., Science 287, 470 (2000).
[3] J. N. Heyman et al., Appl. Phys. Lett. 72, 644 (1998).

Corresponding author: Rudolf Bratschitsch, Institute for Solid State Electronics, Technical University of Vienna, Floragasse 7, A-1040 Wien, Austria.
phone: +43 1 58801 36228, Fax: +43 1 58801 36299
email: Rudolf.Bratschitsch@tuwien.ac.at

LOCALIZED AND RESONANT ACCEPTOR STATES IN STRAINED Ge/Ge$_{1-x}$Si$_x$ MULTIPLE-QUANTUM WELL HETEROSTRUCTURES

V.Ya.Aleshkin, I.V.Erofeeva, V.I.Gavrilenko, D.V.Kozlov, and O.A.Kuznetsov

Institute for Physics of Microstructures of Russian Academy of Sciences
GSP-105, Nizhny Novgorod, 603600, Russia, E-mail: dvkoz@ipm.sci-nnov.ru

Energy spectra of shallow impurities in quantum well (QW) heterostructures are known to depend on both the QW width and the impurity ion position in the well (see, for example, [1]). This gives a possibility to reconstruct the impurity spectra changing the heterostructure parameters and the position of the impurity. This fact makes strained QW heterostructures to be an excellent material for photodetectors of far infrared (FIR) radiation, which operate the photoexcitation of shallow acceptor centers. From another hand the resonant states of shallow acceptors are known to be responsible for the stimulated FIR emission observed in uniaxially stressed p-Ge excited by electric field [2]. At large enough stress the impurity levels pertaining to the upper split-off subband found themselves in the energy continuum of the lower subband, i.e. become resonant. A similar situation can be easily realized in QW heterostructures. The paper is devoted to the theoretical and experimental study of both the localized and the resonant acceptor states in strained Ge/GeSi(111) multiple-quantum-well (MQW) heterostructures.

Spectra of shallow acceptors in Ge/GeSi QW heterostructures were calculated using the developed nonvariational technique [3]. The acceptor envelope function was expanded in the basis of free hole envelope functions in the QW (which are eigenstates of the Hamiltonian not containing the Coulomb potential). This method allowed to calculate both the localized (pertained to the lowest subband) and the resonant (pertained to the upper subbands) impurity states.

The measured (solid lines) and the calculated acceptor photoconductivity spectra in FIR range of two undoped Ge/Ge$_{1-x}$Si$_x$ samples are given in Fig.1: a: #306 (x=0.12, N_{QW} = 162, d_{Ge} = 200A, d_{GeSi}=260A, biaxial elastic deformation ε_{Ge}=2.1·10^{-3}); b: #308 (x=0.09, N_{QW} = 162, d_{Ge} = 350A, d_{GeSi}=200A, ε_{Ge}=0.34·10^{-3}). The residual shallow acceptor concentration is estimated to be about 10^{14} cm^{-3}. In the given spectral range the photoconductivity results from the optical transitions from the acceptor ground state to the continuum (to the first subband of size quantization) and to the excited localized states (and subsequent thermoionization) [3]. At the calculations the impurity level halfwidth was taken of 0.25 meV [3]. Arrows 1a,b,c in the Fig.1a,b correspond to the ionization energies of acceptors at QW center, heterointerface (on-edge) and barrier center correspondingly. The dotted line in Fig.1a shows the calculated spectrum for the uniform acceptor distribution over the structure. Two broadened peaks in this spectrum results from the density-of-state maximums at the centers of QW and the barrier and roughly

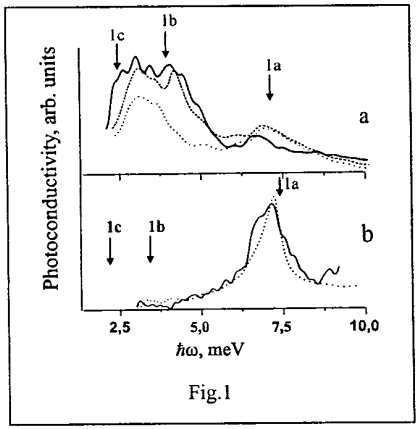

Fig.1

corresponds to the arrows 1a and 1c. However the best fitting of the calculated spectrum to the measured one can be obtained if to assume that there are some additional acceptors (namely ¼ of the total amount) concentrated at heterointerfaces[1]: see the dashed curve in Fig.1a. The binding energy of on-edge acceptors (arrow 1b) just corresponds to the high-energy end of the broad photoconductivity band in between 2.5-5 meV in Fig.1a. For the sample #308 with wide QWs the spectrum can be described very well by the uniform acceptor distribution over QW (see dotted line in Fig.1b). In such broad wells the binding energies of about 75% acceptors are nearly the same as of QW-center impurities.

Calculated energy diagram of hole states in Ge/Ge$_{0.88}$Si$_{0.12}$ QW heterostructure #306 is given in Fig.2. Solid lines correspond to heavy (hh1- hh4) and light (lh1) hole subbands. The lowest dashed curve shows the dependence of the acceptor ground state (J_z =±3/2, J_z being

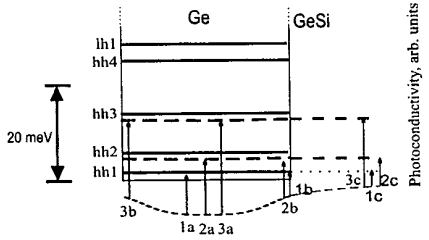

Fig.2

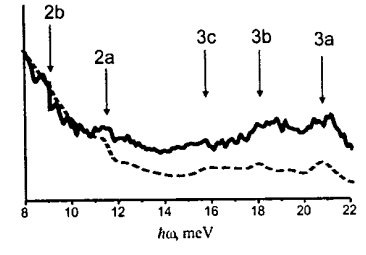

Fig.3

the projection of the total angular momentum on the heterostructure axis) energy on the impurity position both in QW and in the barrier. The upper dashed lines correspond to the resonant states (J_z = ±1/2, ±5/2) pertaining to the upper hole subbands hh2 and hh3. Fig.2 represents the impurity photoconductivity spectra of the sample #306 in the energy range corresponding to the transitions between ground state and resonant states. The measured spectrum is given by the solid curve. Dashed curve represents the calculated spectrum, the acceptor distribution over the heterostructure being assumed to the combination of uniform one and δ-doping (1/4 of the total amount) at each heterointerface (on-edge acceptors). Arrows 2 and 3 in Fig.1,2 indicate the allowed intracenter optical transitions from ground (localized) state to resonant states for QW-center (a), on-edge (b) and barrier-center (c) impurities. There are no doubts that the triplet 3a-3c really presents in the measured spectra in Fig.3. Moreover there are noticeable spectral features in between 9-12 meV in the measured spectrum that can be attributed to the transitions 2a-2b. To the authors knowledge this is the first observation of the resonant acceptor states in QWs.

The research was supported by RFBR (Grants #00-02-16568, #00-02-81022, #01-02-16106), NATO CLG 975592, Russian Scientific Programs "Physics of Solid State Nanostructures" (project #97-1069), "Physics of Microwaves" (project #4.5)", "Fundamental Spectroscopy" (project #8/02.08), "Leading Scientific Schools" (#01-15-96618), "Universities of Russia" (project #015.01.01.94) and "Integration" (projects ##540,541).

[1] J.-M. Mercy, N. C. Jarosik, B. D. McCombe, *et al. Semicond. Sci. Tchnol.* **4,** 1011 (1986).
[2] Altukhov I.V., Kagan M.S., Korolev K.A. *et al. JETP* **88,** 51 (1999).
[3] Aleshkin V.Ya., Andreev B.A., Gavrilenko V.I. *et al. Semiconductors* **34,** 582 (2000).

[1] A heterointerface is known to be a better of point defects and some of observed residual acceptors are likely to be connected with vacancies rather than with the chemical impurities.

Stimulated Emission of Teraherz Acoustic Phonons as a Result of Action of Nonequilibrium Phonon Flux Upon the Localized Exciton Ensemble

E. E. Onishchenko, V. S. Bagaev, and V. V. Zaitsev

P.N. Lebedev Physical Institute RAS, Leninskii pr. 53, 119991, Moscow, Russia

Last few years, the possibility of development of teraherz acoustic phonon generators (and "phonon lasers") based on semiconductor heterostructures is actively discussed [1,2]. There is a great number of theoretical studies but lack of experimental works. We present here likely the first experimental observation of stimulated emission of teraherz acoustic phonons induced by the nonequilibrium phonon flux effect on the localized exciton ensemble. The other intriguing feature is a quasi-two-dimensional propagation mode of teraherz acoustic phonons and their ability to propagate at the distances up to 1 cm by such a way.

An ultrathin CdTe/ZnTe quantum well (QW) (the nominal thickness of CdTe layer ~ 1.3 nm) was grown onto the (100) GaAs substrate by MBE [3]. The high-resolution TEM studies have shown that the ultrathin CdTe QW represents a CdTe layer of the varying local thickness. The fluctuations of the QW thickness result in the appearance of a various extent of lateral exciton localization in the QW at low temperatures. The main mechanism of exciton lateral migration in QWs in this case is the tunnel transition between localized exciton states with emission (absorption) of acoustic phonons.

The geometry of experiment is shown in Fig. 1. The QW photoluminescence (PL) was quasi-resonantly excited by a He-Ne laser (region A). Generation of nonequilibrium phonons was carried out by the Ar laser beam (region B) at a distance (from 1.5 up to 7 mm) to the A region. The measurements were performed at temperatures 4.2 and 1.8 K. The QW PL spectra under the He-Ne laser quasi-resonant excitation are shown in Fig. 2 in the absence (bold line) and in the presence of the nonequilibrium phonon flux - phonon wind (solid line and dots). The features marked by dashed lines are associated with the fact that in the relaxation process of excitons produced by He-Ne laser quantum the interface ($h\nu_1$ = 19 meV) and confined ($h\nu_2$ = 25 meV) optical phonons are participating [4]. It is seen that under the action of the phonon wind, a noticeable weakening of the features induced by the exciton relaxation with participation of confined and interface phonons is observed and the integral PL intensity increases. The influence of the phonon wind reveals already for the Ar laser power 0.4 mW (!) and at the distance between A and B regions of about 7 mm. The magnitude of the effect stops to depend on the distance between the A and B regions for the pumping power more than 10 mW. One should note that an opposite behavior is observed with the temperature increase (see the insert in Fig.2).

Due to the fact that the emission of optical phonons $h\nu_1$ and $h\nu_2$ serves as the main channel of a primary energy relaxation of photoexcited excitons, the predominant population of localized exciton states positioned in energy from the He-Ne laser quantum by $h\nu_1$ and $h\nu_2$ occurs. As the further exciton relaxation in energy can occur only via a considerably slower process (the transition with participation of acoustic phonon), the "excess" population of localized exciton states is realized in this energy range that is clearly pronounced in the PL spectrum (Fig.2). In a situation when such a nonequilibrium population of localized exciton states is present, the phonon flux with the energies comparable with the energy difference between the states closely placed (typically several meV) has to induce the tunnel exciton transition between these states, which is accompanied by the stimulated phonon emission. As a result, the population of the states with smaller energy will increase and the population of high-energy states will decrease that is observed experimentally.

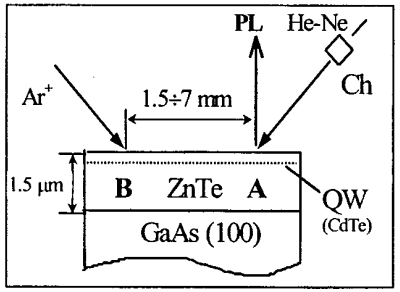

Fig.1. Experimental geometry. Quasi-resonant PL excitation by He-Ne laser (a spot diameter ~ 0.1 mm, power - 1 mW), nonequilibrium phonons were produced in the B region by Ar laser beam (the excitation power was varied in the range 0.4 ÷ 150 mW). He-Ne laser radiation was modulated by a chopper Ch.

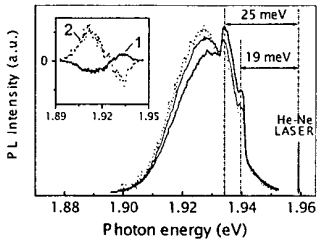

Fig.2. Bold line – QW PL spectrum in the absence of phonon wind. Solid line – QW PL spectrum for Ar laser power 1 mW, dots – QW PL spectrum for Ar laser power 150 mW. In both cases, the distance between A and B regions was 7 mm. In the insert: the change of PL signal with the temperature increase up to 10 K (1) and under the action of phonon wind (2).

In the case of uniform bulk material, for the nearly isotrope (due to a strong scattering [5]) propagation of phonons, only an insignificant fraction of the phonons can reach the region A. Consequently, one should suggest that the phonon propagation occurs in a quasi-two-dimensional mode along the CdTe layers. There is a fact, which can testify this conclusion: when the sample was immersed in a superfluid helium, the decrease of the phonon-wind effect was not observed. Under these conditions, the phonons reaching the sample boundaries usually escape into a liquid helium [6]. Therefore, in the case of three-dimensional quasi-diffusive propagation mode, one would expect a decrease of phonon-wind influence by the sample immersion in a liquid helium.

References.

1. Yu.E.Lozovik, I.V.Ovchinnikov. e-Print cond-mat/0007162.
2. I. Camps, S. S. Makler, H.M. Pastawski et al. e-Print cond-mat/0101043.
3. V.V.Zaitsev, V.S.Bagaev, and E.E.Onishchenko. Phys. Solid State **41**, 647 (1999).
4. J.Mendez, A.Pinczuk, J.P.Valladares et al. Appl.Phys.Lett. **50**, 1101 (1987).
5. A.I.Sharkov, A.Yu.Klokov, T.I.Galkina et al. J. Russ. Laser Reaserch. **21**, 478 (2000).
6. E.S.Sabisky and C.H.Anderson. Solid State Commun. **17**, 1095 (1975).

Corresponding author: Evgeny E.Onishchenko, P.N.Lebedev Physical Institute RAS,
Leninskii pr. 53, 119991, Moscow, Russia,
phone: +007-095-135-7941, Fax: +007-095-938-2251, e-mail: evgeny@lebedev.ru

Physics and Application of Terahertz Phase Modulation

R. Kersting[1], R. Bratschitsch[2], G. Strasser[2], and K. Unterrainer[2]

[1]Department of Physics, Rensselaer Polytechnic Institute, Troy, NY 12180, USA
[2]Institute for Solid State Electronics, Technical University of Vienna, Floragasse 7, A-1040 Vienna, Austria

Modulation-doped intersubband structures offer novel opportunities to control ultrafast electromagnetic signals. Terahertz intersubband transitions can be tailored for specific frequencies, the transitions exhibit giant dipole moments and the oscillator strengths can be controlled electronically. In this contribution we report on THz experiments, which have been performed on intersubband systems with a time resolution shorter than the intersubband oscillation time [1]. The experimental results give insight into the underlying quantum dynamics and allow the demonstration of a THz phase modulator [2].

The investigated GaAs/AlGaAs heterostructures are modulation-doped parabolic quantum wells (PQWs). The 1200Å and a 1400 Å wide PQWs have intersubband resonances at 3.0 THz and 1.6 THz, respectively. Due to the modulation doping we achieve electron sheet densities of $2.7*10^{11}cm^{-2}$ and $2.7*10^{11}cm^{-2}$ with mobilities of about 80.000 $Vscm^{-2}$. Semi-transparent Schottky gratings with a periodicity of 16 µm were fabricated on top of the structures to couple the THz pulses to the intersubband transitions.

We performed THz time-domain spectroscopy exciting the structures with ultrafast THz pulses and recording the transmission signal (see. figure 1) [3]. Modulation spectroscopy is performed by switching electronically the charge density within the PQWs. The achieved modulation signals show directly the polarization dynamics of the quantum system and illustrate the motion of the electrons when driven by an ultrafast THz signal. In case of a nonresonant excitation as shown in figure 1, the electrons follow the driving THz field although this frequeny doesn't fit the PQW's optical transition frequency. When the driving field decays, the electrons perform a phase jump and oscillate at their eigenfrequency. Calculations of the optical Bloch equations

$$i\hbar\frac{d}{dt}\rho = [H_0,\rho] + [H_{int},\rho] + i\hbar\left.\frac{\partial}{\partial t}\rho\right|_{relax}$$

agree with the experimental data and allow us to deduce parameters such as the dephasing times ($T_2 \approx 2$ ps) as well as the excited state population ($\rho_{22} \approx 10^{-6}$).

We applied the observed intersubband dynamics for the demonstration of a THz phase modulator. Transmitted THz pulses can be phase-shifted by switching electronically the electron density within the device. The phase shifts were measured in dependence of the applied voltage (see figure 2). A 2% modulation depth was achieved which is peaked at the intersubband transition frequency at 3.0 THz. The modulation frequency of our device is given by the 50 Ohms sheet resistivity and the 100 nF capacitance of the Schottky grating. An increase of up to 8 GHz may be reached by reducing the device dimensions to the diffraction limit. A maximum operation temperature of 150 K was deduced.

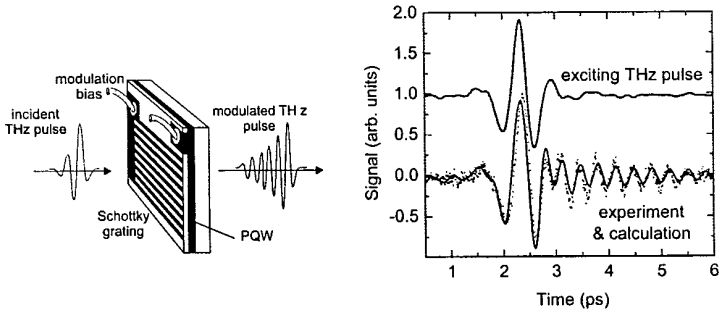

Fig. 1: Schematic of the Schottky grating device fabricated on a modulation doped PQW structure (left side). Right side: Transients of exciting THz pulse and modulation signal (dots), which shows the transient polarization. The excitation is nonresonant. The driving THz pulse has a center frequency of 1.6 THz while the optical quantum transition of the PQW is at 3.0 THz.

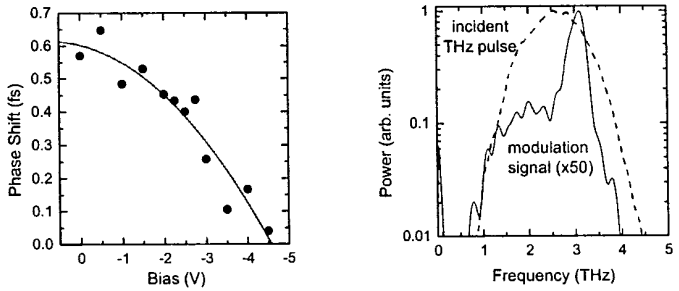

Fig. 2: Phase shift of THz signals transmitted through the phase modulator device (left side). Right side: Power spectra of the modulation signal and the incident terahertz pulse.

References

[1] R. Kersting, R. Bratschitsch, G. Strasser, and K. Unterrainer, Opt. Lett. 25, 272 (2000).
[2] R. Kersting, G. Strasser, and K. Unterrainer. Electr. Lett. 36, 1156 (2000).
[3] J.N. Heyman, R. Kersting, and K. Unterrainer. Appl. Phys. Lett. 72, 664 (1998).

Corresponding author: Roland Kersting, Department of Physics,
Rensselaer Polytechnic Institute, 110 8th Street, Troy, NY 12180, USA.
phone: +1 518 276 3092, Fax: +1 518 276 6680
email: kerstr@rpi.edu

InGaAs/InAlAs superlattice detector for THz radiation

E.Schomburg[1], M.Krätschmer[1], A.Vollnhals[1], F.Klappenberger[1], R.Scheuerer[1], K.F.Renk[1], V.Ustinov[2], A.Zhukov[2], and A.Kovsh[2]

[1] Institut für Angewandte Physik, Universität Regensburg, 93040 Regensburg, Germany

[2] A.F.Ioffe-Physico-Technical Institute, Russian Academy of Science, St.Petersburg, Russia

We report on the use of a InGaAs/InAlAs superlattice for detection of THz radiation pulses. The detector showed a response corresponding to a reduction of the direct current through the superlattice. The current reduction is attributed to the THz-field induced modulation of Bloch oscillations performed by miniband electrons. The detector response was measured in a frequency range between 4 THz and 12 THz and showed strong minima at the frequencies of infrared active transversal optical phonons. The experiment has been performed by use of the Free-Electron-Laser (FELIX) in Nieuwegein, The Netherlands.

We used a n-doped wide-miniband InGaAs/InAlAs superlattice grown by molecular beam epitaxy lattice matched on an InP substrate. The superlattice was structured to superlattice mesas with a typical diameter of 5 μm. The detector consisted of a single superlattice mesa contacted by a wire antenna in a corner cube reflector. The current-voltage characteristic showed a non-linear behaviour, with an ohmic part for small voltages, a current maximum, and a region of negative differential conductance. We operated the superlattice detector at a voltage slightly below the current maximum. Irradiation of the detector with a THz radiation pulse (duration about 10 ps) resulted in a reduction of the direct current leading to a short electrical signal. The electrical signal had a full width at half maximum of about 40 ps; this value was mainly determined by the time resolution of the electronic circuit. The intrinsic response time of the superlattice to a THz field is below 1 ps. We found that the responsivity, i.e. the ratio of the current change to the power of THz radiation, decreased with increasing frequency and showed strong minima at the frequencies of the infrared active transversal optical (TO) phonons of the superlattice material. We found that the detector was robust against intense THz radiation pulses up to a power of about 10 kW.

In comparison to a GaAs/AlAs superlattice detector [1], the InGaAs/InAlAs superlattice detector has a higher responsivity by an order of magnitude. The higher responsivity is caused by an higher current density due to a larger miniband of the InGaAs/InAlAs superlattice.

We present an analysis of the frequency dependence of the detector responsivity taking into account a THz-current circuit with an antenna impedance and the superlattice impedance for electron and dielectric currents. The incident THz radiation produces in the antenna a THz current, which mainly flows as dielectric current through the superlattice leading to a THz voltage across the superlattice. The THz voltage causes a modulation of the Bloch oscillations performed by miniband electrons; the modulation results in a reduction of the direct current through the superlattice. Infrared active TO phonons of the superlattice material were considered by the dielectric function of the superlattice. Our analysis indicates that the THz voltage has minima at frequencies of infrared active TO phonons. The minima in the THz voltage cause the minima in the detector responsivity observed in the experiment.

In conclusion, we demonstrated an InGaAs/InAlAs superlattice detector, which is suitable for detection of short THz radiation pulses in a wide frequency range.

[1] F.Klappenberger et al., in press in Appl. Phys. Lett. (2001).

Corresponding author: Ekkehard Schomburg, Institut für Angewandte Physik, Universität Regensburg, Universitätsstr.31, D-93040 Regensburg, Germany
Phone: +49 941 943 2074, Fax: +49 941 943 4223
email: ekkehard.schomburg@physik.uni-regensburg.de

Stable and Unstable homoepitaxy of GaAs at low substrate temperatures

G.Apostolopoulos[1], J. Herfort[2], N.Boukos[1], A. Travlos[1], K.H. Ploog[2]

[1]Institute of Materials Science, National Centre for Scientific Research "Demokritos", 153 10 Ag. Paraskevi Attikis, Greece
[2]Paul-Drude-Institut fuer Festkörperelektronik, Hausvogteiplatz 5-7, D-10117, Berlin, Germany

Epitaxial growth of semiconductors at low substrate temperatures has recently attracted considerable interest, in coping with a number of problems like dopant segregation and interface interdiffussion [1]. The growth of GaAs at low substrate temperatures (LT-GaAs) is most interesting due to the unique properties acquired by the material, such as ultra-short carrier lifetimes, which make it ideal for fast optoelectronic applications [2]. A recent report has shown that low temperature epitaxy of GaAs on GaAs(001) substrates is unstable [3]. This means that surface undulations of a GaAs film have the tendency to increase during growth, leading gradually to the formation of large 3-dimensional structures called mounds. Consequently, these films exhibit considerable surface roughness, which is detrimental to the applications of LT-GaAs. In this contribution we will present a method to overcome this problem.

As shown in ref. [3], unstable growth in LT-GaAs is mainly due to two effects: (a) the increase of adatom diffusivity on the surface, which was attributed to an As self-surfactant effect, and (b) the presence of Ehrlich-Schwoebel (ES) diffusion barriers which inhibit the downward movement of adatoms at step-edges. The first effect is very difficult to avoid, since it is essential for LT-GaAs to be grown under As-rich conditions, in order to retain its particular electronic properties as, for instance, the ultra-short lifetime. Thus, the only possibility is to try to reduce the effect of the ES barriers, for which we propose the use of vicinal substrates. If the conditions could be achieved, where an adatom landing on a terrace of a vicinal substrate is quickly attached to the nearby step-edge, before having the chance to interact with other adatoms to form islands, then mound formation would be suppressed, i.e., the growth mode will be stable. A number of parameters are involved in this process: growth temperature, growth rate and miscut angle of the vicinal substrate. To test the feasibility of this idea and to find the proper combination of parameters, we performed kinetic Monte-Carlo simulations of the epitaxial growth, based on the models of ref. [3]. Results of the simulations are depicted in figure 1. One can see that the surface undulations appearing in the simulation of a layer grown on a singular substrate become gradually smoother as we pass to vicinal substrates with high misorientation angles. At an angle of 8 °, epitaxial growth is found to be stable. The growth parameters for the simulation were: substrate temperature of 200 °C, growth rate of 1 μm/h, and layer thickness of 1 μm.

We have performed first experiments on LT-GaAs layers grown on vicinal GaAs(001) substrates 4 ° → (111)A, which show indeed that the surface of films grown on a vicinal substrate is significantly smoother than those grown on singular substrates under the same conditions. Furthermore, the use of vicinal substrates has another important consequence: it delays the breakdown of epitaxial growth of LT-GaAs, which is another important issue for this material. Layers of LT-GaAs grown on singular substrates may not exceed a thickness of about 1 μm (depending on the substrate temperature), due to the nucleation of defects which gradually pushes the material to polycrystallinity [4]. We have found, that this thickness limit may be extended by the use of vicinal substrates. We assume that this is due to the reduction of the surface roughness.

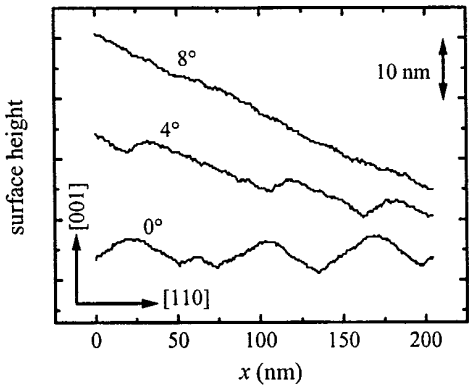

Fig. 1: Surface profiles obtained from numerical simulations of low temperature epitaxial growth of GaAs on singular and vicinal GaAs(001) substrates. The respective misorientation angle of the substrate towards (111)A is given on each curve. Curves are shifted vertically for clarity.

References

[1] D.J. Eaglesham, J. Appl. Phys. **77**, 3597 (1995).
[2] M.R. Melloch, N. Otsuka, J.M. Woodall, A.C. Warren, and J.L. Freeouf, Appl. Phys. Lett. **57**, 1531 (1990).
[3] G. Apostolopoulos, J. Herfort, L. Däweritz, K. H. Ploog, and M. Luysberg, Phys. Rev. Lett. **84**, 3358 (2000).
[4] Z. Liliental-Weber, W. Swider, K.M. Yu, and J. Kortright, Appl. Phys. Lett. **58**, 2153 (1991).

Corresponding author: Jens Herfort, Paul-Drude-Institut fuer Festkörperelektronik, Hausvogteiplatz 5-7, D-10117, Berlin, Germany
phone: +49-30-20377344, Fax: +49-30-20377201
email: herfort@pdi-berlin.de

Segregation effects on the optical properties of (InAs)/(GaSb) superlattices

Rita Magri[1], Alex Zunger[2]

[1]Dipartimento di Fisica, Università di Modena e Reggio Emilia and INFM, Via Campi 213/A, I-41100 Modena, Italy
[2]National Renewable Energy Laboratory, Golden, CO, 80401, USA

The differences in surface energies of various materials necessarily lead to a structural and chemical asymmetry of composition profiles of quantum wells and superlattices. The segregation induced structural asymmetry affects the electronic and optical properties. We investigate here segregation effects in a system where both anion and cation segregation occurs: the infrared laser and detector material GaSb/InAs grown along the [001] direction. Since the binary components do not share a common element, the two interfaces of an ideal quantum well have chemically distinct bonds that do not appear in the respective end-point materials: the growth of GaSb-on-InAs (normal interface) has interfacial Ga-As bonds whereas the growth of InAs-on-GaSb (inverted interface) has interfacial In-Sb bonds. Segregation profiles which are different at the two interfaces modify this bond configuration, thus, the optical properties of these systems are particularly susceptible to segregation. In this work we study (1) the segregation profiles at the normal and inverted interfaces and (2) how the structural disorder at the interfaces due to atomic segregation affects the optical properties of (InAs)/(GaSb) superlattices.

To generate composition profiles we used a kinetic model for MBE growth[1] that we have extended to treat simoultaneously segregation of both group III and group V species. The model of segregation considers a layer by layer growth. Atomic exchanges involve the barrier energies $E^1_{In/Ga}$ ($E^1_{As/Sb}$) associated with the process in which a subsurface In (As) atom undergoes an exchange with a Ga (Sb) atom originally at the surface. The inverse process requires energies $E^2_{In/Ga}$ ($E^2_{In/Ga}$). The rate of these processes are $P_i = \nu \exp(-E^1_{In(As)/Ga(Sb)}/kT_G)$, where ν is a characteristic frequency, k is the Boltzmann constant, and T_G is the growth temperature. For the cation segregation energies we have used the values proposed in previous papers[1] $E^1 = 1.8$ eV and $E^2 = 2.0$ eV, whereas for anions we have adjusted the atomic segregation energies of Sb and As so as to fit the detailed segregation profile measured by cross-sectional STM for GaInSb/InAs[2]. We obtained $E^1 = 1.750$ eV and $E^2 = 1.680$ eV. We find an excellent fit to the X-STM profile.

The determined segregation energies indicate that Sb segregates into InAs and In segregates into GaSb in agreement with the experimental observations. Since the segregation energies of anions are both smaller than those of cations, at very low temperatures (< 375°C) only anion (Sb) segregation takes place, whereas In segregation starts at higher temperatures (> 375°C). Fig. 1 shows the anion and cation segregation profiles obtained for a $(InAs)_8/(GaSb)_{16}$ superlattice at high growth temperature compared with the abrupt profile.

Having determined the composition profiles along the growth direction we model the atomistic structure of the superlattices assuming random arrangements in the (001) planes consistent with the planar composition profiles dictated by the growth model. Local atomic relaxations are calculated using a valence force field approach. Finally, we apply to these atomistic models of superlattices the empirical pseudopotential electronic structure calculation method, finding the energy levels, wavefunctions, transition probabilities, thus directly establishing the effect of segregation on the electronic properties.

We find that: (i) Sb segregates primarily at the normal interface, whereas In segregates primarily at the inverted interface. In segregation becomes significant at higher growth temperatures (> 400°C). Depending on growth temperature some minority segregation occurs too: As segregates somewhat at the inverted interface but Ga does not segregate at the normal interface. (ii) Segregation reduces significantly the amplitude of the hh1 hole wavefunction at the inverted interface, hence diminishing significantly the dissimilarity with the normal interface where hh1 always has a small amplitude. Thus, the transition hh1 to e1 is the one most influenced by segregation. A consequence of the reduced dissimilarity between the interfaces is the diminishing of the in-plane polarization anisotropy which is maximum in the abrupt geometry. (iii) At growth temperatures > 400°C, driven by In and As segregation the potential of GaSb at the inverted interface shifts into the InAs well region, reducing effectively the InAs electron well and widening the GaSb hole well by ≈ 1 ML. The effect is larger on the electron energies so the net effect is a blue shift of all interband transitions by as much as 40-50 meV.

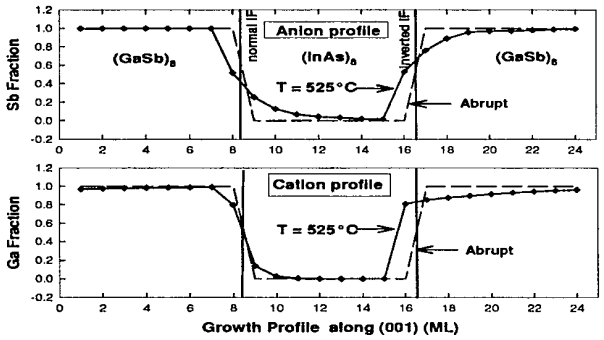

Fig. 1: Calculated Sb and Ga composition profiles along the superlattice [001] growth direction obtained by the kinetic growth model at $T_G = 525°$ C for the $(InAs)_8/(GaSb)_{16}$ superlattice. The segregated profile (diamond plus continous line) is compared with the profile corresponding to abrupt interfaces (dashed line).

References

[1] O. Dehaese et al., Appl. Phys. Lett. 66, 52 (1995).
[2] J. Steinshnider et al., Phys. Rev. Lett. 85, 4562 (2000).

Corresponding author: Rita Magri, Dipartimento di Fisica- Università di Modena e Reggio Emilia, Via Campi 213/a, I-41100 Modena, Italy.
phone: +39 059 205 5285, Fax: +39 059 367488
email: magri@unimo.it

Two-dimensional electron gas at $Ga_{0.5}In_{0.5}P$/GaAs heterointerface spontaneously induced by atomic ordering

[1]K. Yamashita, [1]T. Kita, [2]Y. Wang, [2]K. Murase,
[3]C. Geng, [3]F. Scholz, and [3]H. Schweizer

[1]*Department of Electrical and Electronics Engineering, Faculty of Engineering, Kobe University, Rokkodai 1-1, Nada, Kobe 657-8501, Japan*
[2]*Department of Physics, Graduate School of Science, Osaka University, Machikaneyama 1-1, Toyonaka 560-0043, Japan*
[3]*4. Physikalisches Institut, Universität Stuttgart, D-70550 Stuttgart, Germany*

We found spontaneously generated two-dimensional electron gas (2DEG) at $Ga_{0.5}In_{0.5}P$ and GaAs heterointerface by atomic ordering using Raman-scattering and photoluminescence (PL) measurements. The PL spectra reveal the interband recombination of dense 2DEG, and the Raman-scattering spectra show plasmon-phonon coupled modes.

Epitaxial $Ga_{0.5}In_{0.5}P$ alloys grown by metalorganic vapor-phase epitaxy (MOVPE) on GaAs(001) spontaneously form long-range sublattice ordering along $[\bar{1}11]$ or $[1\bar{1}1]$ direction. The space group of the ordered $Ga_{0.5}In_{0.5}P$ is $R3m$. The crystal filed induces piezoelectric field along the ordering direction [1], which causes unique properties of electronic structure near the heterointerface. Samples investigated in this study are single heterostructures of undoped $Ga_{0.5}In_{0.5}P$ grown on undoped GaAs(001) by MOVPE. Order parameters ηs of $Ga_{0.5}In_{0.5}P$ are 0.0 and 0.30 for the samples grown at 810 and 660 °C, respectively.

Figure 1 shows GaAs-PL spectra from the disordered (η = 0.0) and ordered (η = 0.30) $Ga_{0.5}In_{0.5}P$/GaAs heterointerfaces. The disordered sample shows transitions of the free and bound excitons. On the other hand, the ordered sample shows two broad peaks at 1.519 and 1.524 eV. These peaks are located at the higher energy side of the free-exciton transition. The PL intensity for the ordered sample is plotted in Fig. 2 as functions of excitation and detection energies. The Franz-Keldysh oscillation (FKO) due to an internal electric field was clearly observed. The electric field is estimated from the FKO to be 136.0 kV/cm. Furthermore, the absorption edge was observed at ~1.54 eV, which is higher than the GaAs-band gap. As shown in Fig. 3, we found plasmon-phonon coupled modes in the Raman-scattering measurements for the ordered sample, while the spectrum of the disordered sample shows a typical spectrum of a bulk GaAs. This indicates that an electron accumulation at the ordered $Ga_{0.5}In_{0.5}P$/GaAs heterointerface. The estimated density of the accumulated electrons is ~4.0×10^{18} cm^{-3}. The broad PL and the blue shift of the absorption edge well agree with optical properties of 2DEG systems. Detailed PL properties under magnetic field will be discussed.

Reference

[1] S. Froyen, A. Zunger, and A. Mascarenhas, Appl. Phys. Lett. **68,** 2852 (1996).

Abstract category: (A)

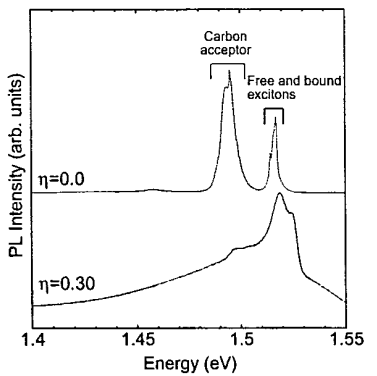

Fig. 1 GaAs-PL spectra from disordered and ordered $Ga_{0.5}In_{0.5}P$/GaAs heterointerfaces.

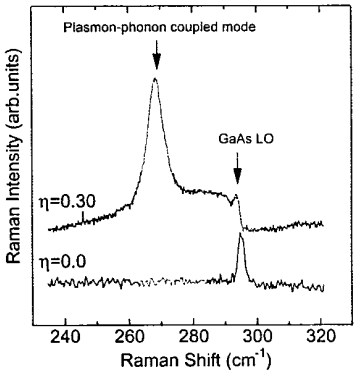

Fig. 3 Raman spectra of disordered and ordered samples.

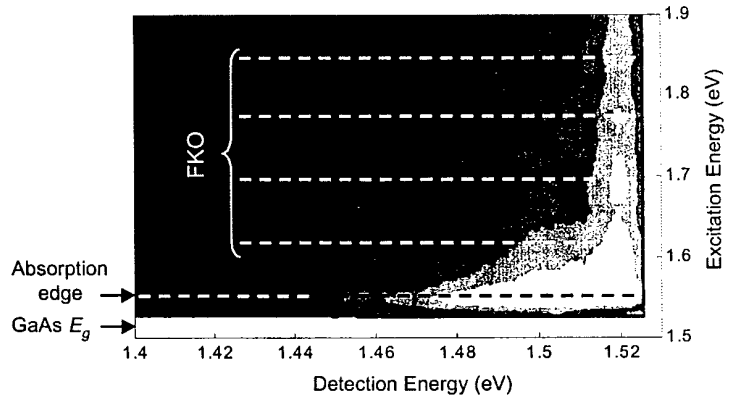

Fig. 2 Counter plot of PL intensity for the ordered sample as functions of detection and excitation energies.

Corresponding author: Kenichi Yamashita, Department of Electrical and Electronics Engineering, Faculty of Engineering, Kobe University, Rokkodai 1-1, Nada, Kobe 657-8501, Japan,
phone & Fax: +81-78-803-6072
email: biwa@kobe-u.ac.jp

Electron transport and optical properties of InGaAs QWs with quasi-periodic (Λ~30nm) interface corrugation grown on vicinal (111)B GaAs

T. Noda [1], Y. Nagamune [2], Y. Nakamura [1], and H. Sakaki [1]

1 Institute of Industrial Science, Univ. of Tokyo, 4-6-1 Komaba, Meguro-ku, Tokyo 153-8505, Japan
2 National Institute of Advanced Industrial Science and Technology, 1-1-4 Umezono, Tsukuba-shi, 305-8568, Japan

When the heterointerface of a 2 dimensional (2D) electron system is spatially modulated, in-plane potential V(x,y) will be modulated and influence both its transport and optical properties. For example, the rough interface scatters 2D electrons in thin QWs and reduces their mobilities [1]. When regularly spaced multiatomic steps are introduced at the interface of n-AlGaAs/GaAs heterojunctions, a large anisotropy in their electron transport appears because of quasi-periodic potential modulations [2), 3)]. As an attempt to enhance influences of such a corrugation, we have grown InGaAs QWs with on corrugated interface and investigated their transport and optical properties.

All the samples were grown by molecular beam epitaxy on a vicinal (111)B GaAs with misorientation angle of 8.5 degrees toward the <-10-1>. Reference QWs were grown simultaneously on flat (100) substrates. Figure 1 shows an atomic force microscope image of the surface on a 0.6 μm thick GaAs grown at 580 degree C. The growth rate was 0.27 μm/hr and As_4/Ga ratio was ~20. Note that multiatomic steps of about 30 nm in period and 2 nm in height lie along the <10-1> direction.

In order to study the influence of such corrugation on 2D electrons and excitons, we grew pseudo-morphic single InGaAs QWs with the In content of 11 % both on corrugated (111)B GaAs and a flat (100) GaAs. Figure 2 shows photoluminescence (PL) spectra of 11 nm thick InGaAs QWs. Unlike the sharp (Δhν~3 meV) PL peak from QW on (100), a broadened PL with the width of 8 meV was observed in corrugated QW on (111)B, suggesting that steps have some irregularities. Electron mobilities μ were also studied in an 8 nm thick modulation-doped AlGaAs/InGaAs/GaAs QW structure as functions of electron concentration Ns at 77 K. Circles and triangles in Fig. 3 indicate μ of such QWs on (111)B and (100), respectively. μ of (100) QW is roughly proportional to $Ns^{0.6}$ and has a small anisotropy. In contrast, μ of (111)B QW is substantially lower than that on (100), even for electrons moving parallel to the steps. More notably, electron mobilities perpendicular to the steps are 3 to 4 times as small as that parallel to steps. These features are quite different from those in corrugated n-AlGaAs/GaAs heterojunction system. By comparing the data with the theory [4], we have extracted the geometrical parameters of interface corrugation and characterized both periodic and random scattering components.

In summary, InGaAs QWs with corrugated interfaces were formed and μ across the steps was found to be drastically reduced. The results were analyzed to estimate periodic and random components of interface corrugation.

References

1) H. Sakaki, T. Noda, K. Hirakawa, M. Tanaka, and T. Matsusue, Appl. Phys. Lett., 51 (1987) 1934.
2) Y. Nakamura, and H. Sakaki, Physica B, 256-258 (1998) 273.
3) Y. Nakamura, T. Noda, and H. Sakaki, Proc. of the 24th of Int. Conf. on Physics of Semiconductors (1999) 1190.
4) J. Motohisa, Phd thesis (1993).

Corresponding author: Takeshi Noda, Institute of Industrial Science, University of Tokyo, 4-6-1 Komaba, Meguro-ku, 153-8505, Tokyo, Japan
Phone:+81-3-5452-6235, Fax:+81-3-5452-6235, Email: noda@iis.u-tokyo.ac.jp

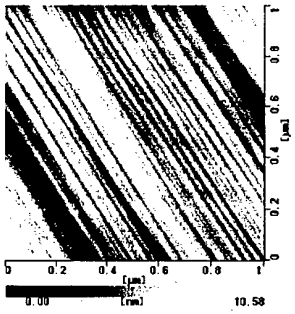

Fig. 1 AFM image of a corrugated GaAs surface grown on a vicinal (111)B GaAs substrate.

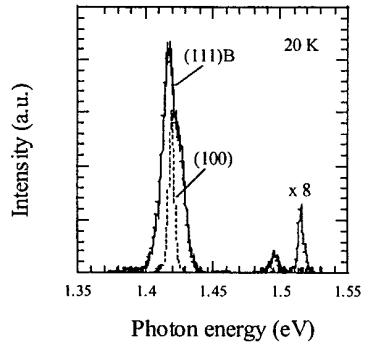

Fig. 2 PL spectra of 11 nm thick InGaAs QWs grown on (111)B (solid line) and (100) (broken line) GaAs measured at 20K with the excitation power of 95 μW.

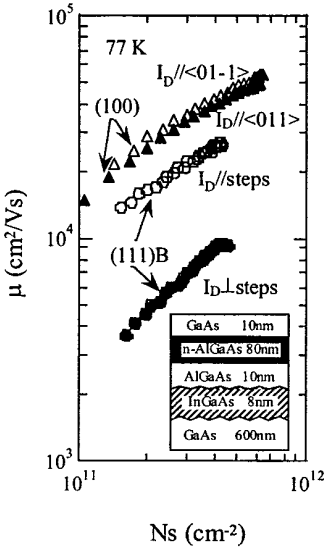

Fig. 3 Electron mobilities of 8 nm thick InGaAs QWs measured at 77 K as functions of electron concentration Ns for two samples grown on (111)B (circles) and (100) (triangles) GaAs. The inset shows the sample structure.

Extremely flat growth-interrupted InAlAs surface grown on (411)A-oriented InP substrate by MBE

I. Watanabe[1], T. Kitada[1], K. Kanzaki[1], D. Kawaura[1], M. Yamamoto[1], S. Shimomura[1], S. Hiyamizu[1]

[1]Graduate School of Engineering Science, Osaka University,
1-3 Machikaneyama, Toyonaka, Osaka 560-8531, Japan

InGaAs/InAlAs pseudomorphic high electron mobility transistors (pHEMTs) are the most important high-speed electronic devices. We have reported that an $In_{0.7}Ga_{0.3}As/In_{0.52}Al_{0.48}As$ pHEMT structure grown on a (411)A-oriented InP substrate by molecular beam epitaxy (MBE) shows 2.5 times higher electron mobility [52,200 cm^2/Vs] at 15K than the same pHEMT structure grown on the (100) InP substrate. The both pHEMT structures with a 3-nm-thick spacer layer and a 12-nm-thick channel layer have the almost same carrier concentration [4.4-4.8×10^{12} cm^{-2}] [1]. The enhanced electron mobility for the (411)A pHEMT structure is attributed to large suppression of the remote impurity scattering because of the thin spacer layer and rather thick channel layer [2]. Under the same Si sheet doping, the spacer layer thickness and the distribution of sheet doped Si impurities strongly affect the remote impurity scattering. Hence, the flatness of the spacer layer surface is very important which is growth-interrupted during Si sheet doping. In this study, we investigated the flatness of the (411)A and (100) growth-interrupted InGaAs/InAlAs interfaces using quantum wells (QWs) and found that growth-interruption does not degrade the (411)A interface roughness, while the (100) interface flatness becomes worse.

Figure 1 shows a schematic illustration of the (a) growth-interrupted InGaAs/InAlAs QWs and (b) reference ones grown on (411)A and (100) InP substrates. Growth-interruption was introduced on the bottom InAlAs barrier layer for 76.5 seconds when was equal to the time of a Si planer doping of the pHEMT structures, while growth-interruption was not introduced anywhere in the reference samples. The (411)A QWs was grown at a growth temperature (*Ts*) of 540 °C under a V/III [As_4/(Ga+In)] pressure ratio of 8, while the (100) QWs was grown at *Ts* = 480 °C under V/III = 14. These growth conditions were optimized ones for each (411)A and (100) InGaAs/InAlAs QWs. Figure 2 shows full widths at half maximum (FWHMs) of photoluminescence (PL) peaks at 12K from the growth-interrupted and reference QWs with well widths (*Lw*) of 0.6-12 nm grown on (411)A and (100) InP substrates plotted as a function of peak wavelengths. In all samples, there exists only one peak from each QW. In the (411)A QWs, the FWHMs of the growth-interrupted QWs are almost the same as those of the reference QWs. But in the (100) QWs, the FWHMs of the growth-interrupted QWs are 13-80% larger than those of the reference QWs. This result shows that the flatness of growth-interrupted InAlAs surface is the same as that of InAlAs surface without growth-interruption in the (411)A QWs, while the flatness of growth-interrupted InAlAs surface is much rougher than that of reference QWs in the (100) QWs. Linewidths of both of the (411)A QWs are also smaller than that of the (100) reference QWs, which indicates that the growth-interrupted InAlAs surface keeps extremely flat in the (411)A QWs compared with the conventional (100) QWs.

Fig. 1. Schematic illustrations of the (a) growth-interrupted and (b) reference InGaAs/InAlAs QW structure grown on (411)A-oriented and (100) InP substrate (*Lw* = 0.6–12 nm).

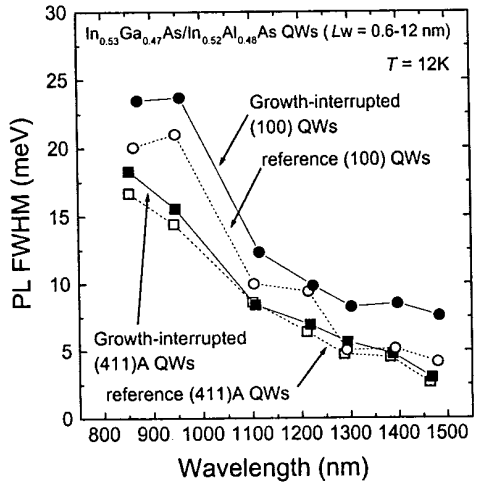

Fig. 2: FWHMs of PL (12K) peaks form the (411)A and (100) growth-interrupted InGaAs/InAlAs QWs [(□) and (□), respectively] and reference QWs [(□) and (□), respectively] plotted as a function of peak wavelengths.

References

[1] S. Hiyamizu, T. Kitada, T. Aoki, M. Higashiwaki, and S. Shimomura, *Postdeadline Paper Proc. 11th Int. Conf. Indium Phosphide and Related Materials*, Davos, Switzerland, 1999, pp. 24.

[2] I. Watanabe, K. Kanzaki, T. Aoki, T. Kitada, S. Shimomura, and S. Hiyamizu, *to be published in J. Vac. Sci. & Technol. B, 2001.*

Corresponding author: Issei Watanabe, Graduate School of Engineering Science,
Osaka University, 1-3 Machikaneyama, Toyonaka, Osaka 560-8531, Japan
phone: +81-6-6850-6456, Fax: +81-6-6845-4632
email: watanabe@d310.mp.es.osaka-u.ac.jp

Direct experimental verification of the q-dependence of the electron-LO-phonon interaction

D. S. Kainth, M. N. Khalid and H. P. Hughes
Cavendish Laboratory,
Madingley Road,
Cambridge CB3 0E, U.K.

The hot electron luminescence from p-doped semiconductors and quantum wells is partly polarized because of the optical selection rules involved. For linearly polarized excitation, the photoelectrons have an angularly anisotropic distribution in $\boldsymbol{k}$-space which determines the degree of linear polarization of the resulting luminescence. Following electron-LO-phonon scattering, the excess hot electron energy is reduced and the initial structure in the angular distribution in $\boldsymbol{k}$-space is degraded, and this is directly reflected in a reduced degree of polarization of the hot electron luminescence. Measurements of this depolarization for electrons excited in specific $\boldsymbol{k}$-directions are compared with calculations of that expected for various q-dependences of the electron-LO-phonon interaction, and for several models for the quantum well phonon confinement. The comparison directly demonstrates experimentally the validity of the generally accepted Fröhlich q^{-2} interaction, and shows that the partial confinement of the bulk GaAs phonon modes in the quantum well must be correctly taken into account.

Wavevector dispersion of excitations of the two-dimensional electron gas from light scattering using a grating coupler

C. Kristukat[1], A.R. Goñi[1], P. Grambow[2], K. Eberl[2], and C. Thomsen[1]

[1]Institut für Festkörperphysik, Technische Universität Berlin, Hardenbergstr. 36, D-10623 Berlin, Germany
[2]Max-Planck-Institut für Festkörperforschung, Heisenbergstr. 1, D-70569 Stuttgart, Germany

The wavevector dispersion of elementary excitations of the two-dimensional electron gas (2DEG) like plasmons and intersubband excitations of the charge (CDE) and spin density (SDE) has been determined by inelastic light scattering using a grating coupler. For that purpose an array of metallic stripes with 650 nm period has been produced on top of a modulation-doped single quantum well of 25 nm thickness. In this way, even in backscattering geometry light can couple to elementary excitations of the 2DEG with finite wavevector in the range between $1x10^4$ to $1x10^6$ cm^{-1} [1].

In resonant inelastic light scattering spectra, up to six peaks are observed at energies below 20 meV, which are associated to plasmon excitations of the 2DEG with wavevectors corresponding to different multiples of the wavevector determined by the inverse of the grating period. Figure 1 shows representative light scattering spectra for parallel and crossed linear polarizations of the incident and scattered beam, as obtained with the grating coupler in resonance with an optical transition between excited confined states of the single quantum well. The energy positions of the peaks observed in spectra with both polarizations are plotted in Fig. 2 as a function of wavevector. Solid and open symbols represent the excitations of the charge and the spin density detected with parallel and crossed polarization, respectively. The intersubband single-particle continuum of electron-hole pair excitations is centered for q=0 at the subband spacing energy E_{01}.

The 2D plasmon dispersion is very well described by a square-root function in excellent agreement with the prediction within the random-phase approximation (RPA). The solid curve through the data points represents the result of a least-squares fit using only the electron density in the quantum well as an adjustable parameter. A value of $n_{2D} = 5.2x10^{11}$ cm^{-2} is obtained, which agrees within 10% with the one determined from photoluminescence measurements. Intersubband excitations, in turn, exhibit a much flatter but noticeable wavevector dispersion. The spin-density excitation, for instance, which in the long wavelength limit is shifted down in energy with respect to the intersubband spacing E_{01} due to exchange-correlation vertex corrections, displays a negative dispersion with a slope of $9.3x10^{-6}$ meV.cm.

References

[1] S.J. Allen *et al.*, Phys. Rev. Lett. **38**, 980 (1977).

Corresponding author: Alejandro R. Goñi, Institut für Festkörperphysik, Technische Universität Berlin, PN 5-4, Hardenbergstraße 36, D-10623 Berlin, Germany.
phone: +49 30 314 24442, Fax: +49 30 314 27705
email: goni@physik.tu-berlin.de

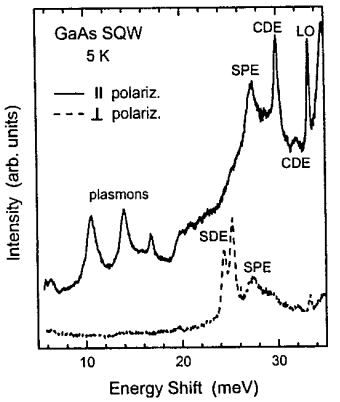

Fig.1: Polarized and depolarized inelastic light scattering spectra of the single quantum well (SQW) measured at 5 K with the grating coupler. The assignment of the peaks to plasmons, charge-density (CDE), spin-density (SDE), single-particle excitations (SPE) and the LO phonon is indicated.

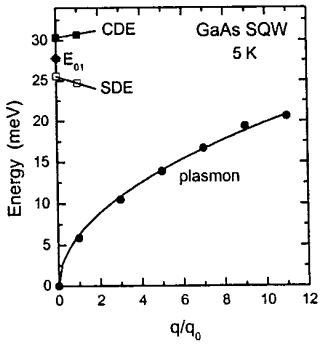

Fig.2: Wavevector dispersion of elementary excitations of the 2DEG observed in light scattering spectra using a grating coupler. The fundamental wavevector of the grating is $q_0=0.96x10^5$ cm^{-1}. E_{01} denotes the subband spacing and CDE (SDE) stands for the intersubband charge (spin) density excitation.

Effect of an electric field on electronic excitations in double quantum well systems

U. Haboeck[1], A.R. Goñi[1], K. Eberl[2], and C. Thomsen[1]

[1]Institut für Festkörperphysik, Technische Universität Berlin, Hardenbergstr. 36, D-10623 Berlin, Germany
[2]Max-Planck-Institut für Festkörperforschung, Heisenbergstr. 1, D-70569 Stuttgart, Germany

High-mobility two-dimensional electron gases (2DEG) fabricated in semiconductor quantum well structures are particularly suitable for studies of electronic correlations in reduced dimensions. Coulomb interaction effects are apparent in the spectrum of elementary excitations of the 2DEG, which can be probed by inelastic light scattering. Electron-electron interactions give rise to collective excitations of the charge (CDE) and spin density (SDE), which are shifted in energy with respect to single-particle excitations (SPE) centered at the intersubband spacings. In double quantum wells (DQW), interlayer correlations play a fundamental role in the many-body behavior of the electronic system leading, for example, to spin phases with different magnetic order [1]. Many-body effects manifest themselves also in the renormalization of 2D subband energies, when there is a finite occupation with electrons of the corresponding states [2]. In this work we have investigated the influence of an electric field on the excitations of double-layer electron gases in modulation-doped DQWs by means of photoluminescence (PL) and inelastic light scattering measurements. The electron density as well as the subband spacings have been changed by applying a gate voltage between two contacts at the top and the back surface of the samples. We have studied two different DQW structures, a symmetric and an asymmetric one.

Figure 1 shows representative PL spectra of the symmetric DQW measured at different voltages in the situation for which the applied bias leads to an increase in electron density in the structure. The whole spectra are depicted in the inset, where E_0, E_1 denotes peaks corresponding to the ground state emission of each quantum well. The peaks at higher energy are assigned to optical transitions from both first excited states of the wells. As the Fermi energy increases with bias the excited subband labeled "2" becomes populated with electrons causing the redshift of the E_2 transition by about 3 meV. This energy renormalization is a purely many-body effect arising from exchange-correlation terms of the Coulomb interaction between electrons in the excited subband. Furthermore, the appearance of the E_3 peak with bias is a consequence of the breaking of the optical selection rule, as the symmetry of the DQW potential is lifted by the external electric field. Inelastic light scattering spectra display a rich structure corresponding to excitations associated with different intersubband transitions between electronic states confined to each well. Representative polarized spectra of the symmetric DQW for different voltages are shown in Fig. 2. The effect of the applied bias is to reduce the coupling between layers by shifting the intersubband SPE energies in each quantum well in different directions. The external field tilts the bands in such a way that in one well all excitations become blueshifted with bias, whereas for the other one only a slight redshift takes place.

References

[1] F.A. Reboredo and C.R. Proetto, Phys. Rev. B **58**, 7450 (1998).
[2] S. Das Sarma, R. Jalabert, and S.-R.E. Yang, Phys. Rev. B **41**, 8288 (1990).

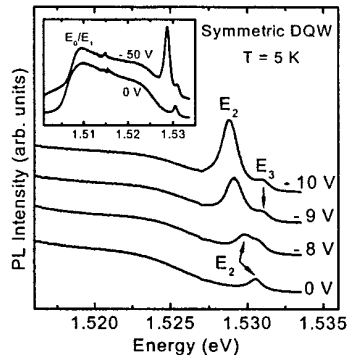

Fig.1: Photoluminescence (PL) spectra of a symmetric double quantum well (DQW) for different gate bias. Peaks labeled as E_0/E_1 correspond to the ground state emission of both wells, whereas the E_2 and E_3 peaks are assigned to optical transitions between the first excited states of each well.

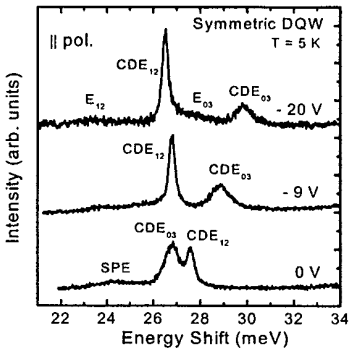

Fig.2: Polarized inelastic light scattering spectra of the symmetric DQW measured at 5 K for different voltages. The assignment of the peaks to charge-density (CDE), spin-density (SDE) and single-particle excitations (SPE) is indicated.

Corresponding author: Alejandro R. Goñi, Institut für Festkörperphysik, Technische Universität Berlin, PN 5-4, Hardenbergstraße 36, D-10623 Berlin, Germany.
phone: +49 30 314 24442, Fax: +49 30 314 27705
email: goni@physik.tu-berlin.de

Linewidth broadening of excitonic luminescence from quantum wells in pulsed magnetic fields

A. Polimeni[1], A. Patanè[1], R. K. Hayden[2], L. Eaves[1]
M. Henini[1], P.C. Main[1], K. Uchida[2], N. Miura[2], D. Sherwood[1], M. Fromhold[1]

[(1)]*School of Physics and Astronomy, University of Nottingham, Nottingham NG7 2RD, UK*
[(2)]*Institute for Solid State Physics, University of Tokyo, Roppongi, Minato-ku, Tokyo, Japan*

We have studied the magnetic field dependence of the exciton size in narrow (0.5-1.0 nm) strained $In_{0.5}Ga_{0.5}As/GaAs$ single quantum wells (QWs) using photoluminescence spectroscopy in pulsed magnetic fields ranging from B=0 T to B=42 T, applied parallel or perpendicular to the QW plane. We find that the full-width at half-maximum, W, of the excitonic recombination spectrum increases significantly at these high fields and that the degree of increase in the linewidth depends on the direction of B (see Fig. 1(b)).
The increase of W with magnetic field is due to the squeezing of the exciton size induced by B, which, in turns, leads to a reduction in the spatial averaging of the potential energy fluctuations of the quantum well due to the finite exciton size. In these narrow QWs significant broadening at zero field is expected due to fluctuations of the well width. For B perpendicular to the QW plane, we model the magnetic field dependence of the excitonic recombination line shape by using a statistical model for the QW interface disorder [1]. We show that $W(B)$ is proportional to $1/\rho_{exc}(B)$, where ρ_{exc} is the in-plane exciton size, and hence we determine the variation of ρ_{exc} with B (see Fig. 2 (a), full dots).
The magnetic field dependence of W depends on the field orientation (see Fig. 1(b)) and is weaker when B is parallel to the QW plane. This is consistent with the fact that the in-plane exciton size is not strongly changed for this configuration of B and the weak increase of the linewidth may indicate that at high fields the electron wave function is compressed in all directions (see Fig. 2 (b)) [2].
We compare numerical and approximate analytical models (Fig. 2 (a), continuous line) for the squeezing of the exciton wave function induced by magnetic field. We also discuss the similarities with hydrogenic systems close to highly magnetized astrophysical objects, such as white dwarfs, neutron stars, and black holes.

References

[1] A. Patanè, A. Polimeni, M. Capizzi, and F. Martelli, *Phys. Rev.* B **52**, 2784 (1995).
[2] I. P. Roche, G. P. Whittington, P. C. Main, L. Eaves, F. W. Sheard, G. Wunner, and K. E. Singer, *J. Phys.* C **2**, 4439 (1990).

Corresponding author: Dr Antonio Polimeni
University of Rome "La Sapienza", Department of Physics, P.le A. Moro 2 00185 Roma, Italy
phone: +39-06-49914770, fax: +39-06-4957697
e-mail: polimeni@roma1.infn.it

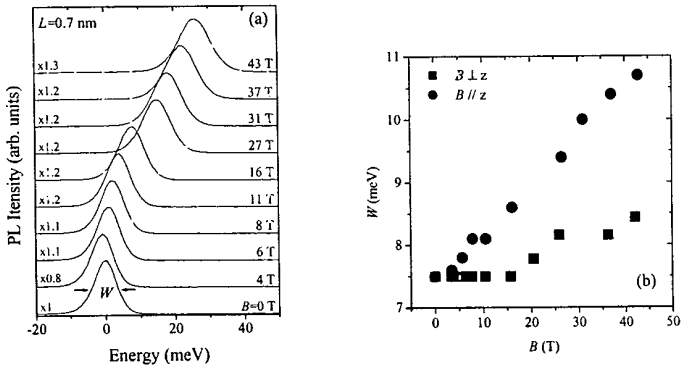

Fig. 1: (a): Peak-normalized photoluminescence (PL) spectra at 4.2 K of a 0.7 nm thick $In_{0.5}Ga_{0.5}As$ single quantum well at different magnetic field intensities. Normalization factors are given for each spectrum. (b): Dependence of the photoluminescence linewidth on magnetic field for B applied along and perpendicular to the growth axis z for a quantum well with well thickness of 0.7 nm.

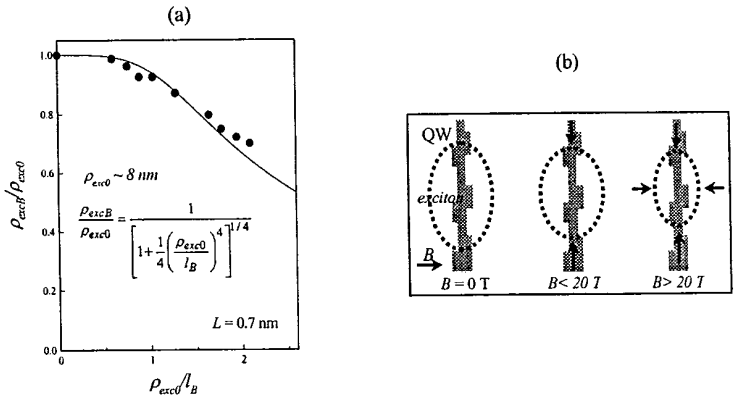

Fig. 2: (a) In-plane exciton radius at different B's (ρ_{excB}) normalized to the exciton radius at B=0 T ($\rho_{exc0} \sim 8nm$) as a function of (ρ_{exc0}/l_B) where l_B is the magnetic length $(=\hbar/eB)^{1/2}$. The continuous line is the theoretical curve calculated using an approximate analytical model for the squeezing of the exciton wave function induced by B. (b) Sketch of the squeezing of the exciton wave function induced by B.

Excitonic Instabilities in Semiconductor Superlattices

D. C. Marinescu[1] and J. J. Quinn[2],

[1] Department of Physics, Clemson University, Clemson, SC 29634
[2] Department of Physics, University of Tennessee, Knoxville, TN 37996

The resurgence of the interest in the classical problem of spin instabilities in a two dimensional (2D) electron layer in the presence of a magnetic field [1] has been triggered recently by the realization of multi-layer semiconductor structures that can serve as experimental support for testing the theoretical predictions. In a single 2D electron layer, at $\nu = 2$, a sharp paramagnetic to ferromagnetic phase change occurs, prompted by electron transitions from $|0\uparrow>$ to $|1\downarrow>$. Within the Hartree-Fock approximation, this situation is realized even for positive values of the difference $\epsilon = \hbar(\omega_c - \omega_s)$ (ω_c and ω_s are the cyclotron and Zeeman frequency respectively)when the electron-hole correlation energy (also referred to as the vertex correction) overcomes the exchange energy loss. Experimental evidence of this transition has been found recently [2-3]. In a natural extension of this study to the case of an infinite sequence of attractive quantum wells, between which weak tunneling is allowed, we found that a collective spin instability appears for values of the tunneling probability leading to a bandwidth larger than a critical value, Δ_c [4]. As a result,the system evolves from a paramagnetic or ferromagnetic occupancy to a spin density wave state [5] of wavevector π/a, where a is the superlattice constant. In this work we investigate the existence of magnetic phase transitions in the case of a semiconductor superlattice of identical double quantum wells. In the unit cell, the two quantum wells, for simplicity taken to be attractive delta functions, are separated by a distance b, while the constant of the superlattice is a. If $a \gg b$, there are two essentially flat minibands with energies E_S and E_{AS}, and $\Delta_{SAS} = E_S - E_{AS}$. When weak tunneling is allowed, these energy levels broaden into minibands of width proportional to the tunneling probability. We inspect this system for possible spin instabilities realized for small values of $\Delta_{SAS} - 2\hbar\omega_s$ when low-frequency spin-flip transitions $|S\uparrow> \rightarrow |A\downarrow>$ can occur. This situation is of experimental interest because the $E_S(k_z)$ and $E_{AS}(k_z)$ bands can be fixed in growing the superlattice structure. Then $\nu = 2$ is set by fixing the value of B_z, while $\hbar\omega_s$ is determined by $B = (B_\perp^2 + B_z^2)^{1/2}$. Thus $\hbar\omega_s$ can be controlled experimentally in a single sample. Results obtained within the Hartree-Fock approximation are discussed.

References

[1] G. F. Giuliani and J. J. Quinn, Solid State Commun. **54**, 1013 (1984); and Phys. Rev. B **31**, 6228 (1985).
[2] A. J. Daneshvar, C. J. B. Ford, M. Y. Simmons, A. V. Khaetskii, A. R. Hamilton, M. Pepper and D. A. Ritchie, Phys. Rev. Lett. **79**, 4449 (1997).
[3] V. Piazza, V. Pellegrini, F. Beltram, W. Wegscheider, T. Jungwirth, A. H. McDonald, Nature, **402** 638 (1999).
[4] D. C. Marinescu, G. F. Giuliani, and J. J. Quinn, Phys. Rev. B, **61**, 7245 (2000).
[5] A. W. Overhauser, Phys. Rev. Lett. **4**, 462 (1960); Phys. Rev. **128**, 1437 (1962).

Corresponding author: D. C. Marinescu, Department of Physics, 118 Kinard Laboratory, Clemson University, Clemson SC 29634, USA,
phone: 864 656 5315, Fax: 864 656 0805, email: dcm@clemson.edu

The influence of intrersubband transitions on the resonant and extended electronic states in GaAs/AlGaAs asymmetric quantum wells

R. Beserman[(1)], M. Levy[(1)], D. Krapf[(2)], A. Sa'ar[(2)], V. Thierry-Mieg[(3)], R. Planel[(3)]

[(1)] Solid State Institute and Physics Department, Technion, Israel Institute of Technology, Haifa 32000, Israel.
[(2)] Department of Applied Physics, The Fredi and Nadine Hermann School of Applied Science, The Hebrew University of Jerusalem, Jerusalem 91904, Israel.
[(3)] Laboratoire de Microstructures et Microelectronique - CNRS, 196 Avenue H. Ravera, BP107, 92225 Bagneux, France.

The continuum states with energy higher than the barrier height in quantum well (QW) structures have attracted a lot of interest in recent years due to their physical properties and their potential application for IR photo detectors. The confinement of resonant states above the QW, is accompanied with a change of their quasi three-dimensional behavior into a quasi two-dimensional one. In addition the increase of localization of these states manifests itself in their behavior under dc local electric fields.

We found that these above the barrier resonant states shift to lower energies when a local electric field is applied, as expected for real bound states, and the shift depends linearly on the increasing field up to 35 kV/cm. Furthermore, higher degree of localization of these states is accompanied with the appearance of a step like peak in the photoluminescence excitation spectrum (PLE), and an asymmetry between the incoming and outgoing resonances in the Resonant Raman spectrum (RRS) of the QW phonons.

Experimentally, localization of these states was studied by using two asymmetric QW structures, each characterized by a different localization of the above the barrier states. Our Bragg sample (fig. 1), which is characterized by a modified localization of the above the barrier states, consist of an asymmetric QW (AQW) sandwiched between two Bragg mirrors. The maximum localization of above the barrier states in the AQW region is achieved by using additional thin "delta" AlAs barriers grown on both sides of the AQW (fig. 2).

The modulated local dc electric field across the QWs is generated using infrared (IR) intersubband optical excitation (with a tunable CO_2 laser) of carriers from the wide QW into the narrow QW. The excitation process generates local electric dipoles in the AQW that vanish outside this region. Hence, The local electric field gives rise to a Stark shift which modifies of the continuum resonant states that are localized in the AQW.

When the modulation scheme is applied to the Bragg mirror sample, a group of highly bound resonant states were resolved. These states probed either by modulated RRS or PLE spectroscopies showed large red shifts at IR excitation powers of 10 kW/cm^2 (fig. 3). We studied the confinement of the resonant states and their behavior under optically induced local electric fields and we present a model based on the Stark effect to explain quantitatively the shifts of the different levels in the Bragg confining structure. In addition we studied their confinement by considering the asymmetry between the incoming and outgoing resonances intensities of the RRS spectrum (fig. 4). For the electronic transition which is localized in the AQW region the incoming resonance intensity is the strongest on the other hand when the electronic transition is localized in the Bragg mirror region the outgoing resonance is the strongest.

The sample with the delta like AlAs was processed and fabricated into an IR photovoltaic detector. The detection mechanism is based on the transfer of charge by the IR light from the wide QW into the narrow one thus generating a dc electric field. A preliminary results of the performance of this device will be presented.

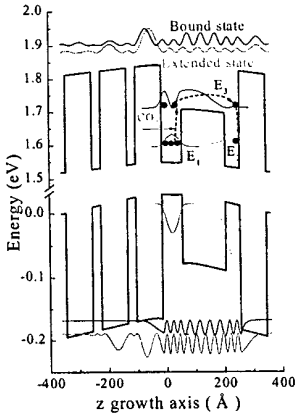

Fig. 1: Bragg confined structure, truly confined continuum states in the AQW.

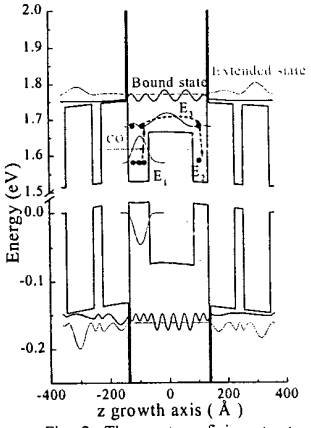

Fig. 2: The most confining structure, Bragg mirrors plus delta AlAs barriers.

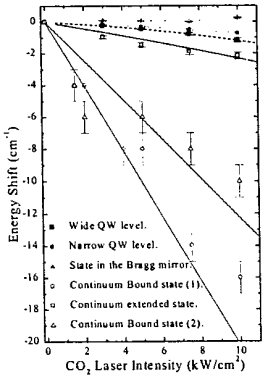

Fig. 3: The Bragg sample. Energy shifts of bound states inside the well and of the bound states in the continuum.

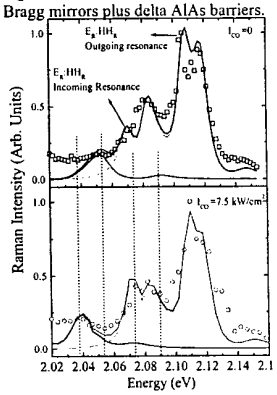

Fig. 4: RRS spectrum of the Bragg sample. The asymmetry between the incoming and outgoing resonance is presented.

References

[1] M. Levy, R. Beserman, et al., Phys. Rev. B 63, 075132 (2001).

Corresponding author: Robert Beserman, Solid State Institute and Physics Department, Technion, Israel Institute of Technology, Haifa 32000, Israel.
phone: 942 4 8293985, Fax: 972 4 8235107
email: ssrobert@tx.technion.ac.il

Intersubband terahertz electro-luminescence from GaAs–AlGaAs quantum cascade structures

S. S. Dhillon,[1] D. D. Arnone,[2] A. G. Davies,[1] E. H. Linfield,[1] R. Harrell,[1] D. A. Ritchie[1]

[1]Cavendish Laboratory, Madingley Road, Cambridge CB3 0HE, UK
[2]Toshiba Research Europe Limited, Cambridge Science Park, Cambridge CB4 OWE, UK

Following the successful demonstration of the mid-infrared unipolar quantum cascade laser [1], there is interest in extending this concept to the far-infrared (terahertz) region of the spectrum where the lack of convenient sources remains acute. Quantum cascade devices are fabricated from multi-quantum-well semiconductor heterostructures in which an appropriate engineering of the thickness and composition of the semiconductor layers adjusts the intersubband electron transitions. By stacking together successive active regions, each injected electron cascades through the device generating a number of photons. Far-infrared electro-luminescence has already been observed in quantum cascade structures [2–4] and the development of lasers from these devices is the next challenge.

We have performed a comprehensive study of a series of GaAs–$Al_{0.15}Ga_{0.85}As$ quantum cascade electro-luminescence devices designed to emit in the far-infrared. The electro-luminescence was investigated as a function of injector doping density, number of periods, and the widths of the quantum wells and barriers. The devices were fabricated by molecular beam epitaxy and were processed into 360μm x 360μm mesas with surface metal gratings to couple out the radiation. The devices were characterized in a continuous flow cryostat at 10K by I–V measurements and Fourier transform infrared spectroscopy, the latter employing a step-scan infrared spectrometer and a helium-cooled silicon bolometer.

Figure 1 shows the spectra obtained for a range of injector doping densities. The injector doping density needs to be optimised to achieve a uniform electric field across the device and is a key factor in the design of quantum cascade structures. The spectra show clear, narrow spectral lines (FWHM ~ 0.21THz) around 4.1THz, at biases where electrons are resonantly tunnelling through the structure, as confirmed by the I–V characteristics. We observe a systematic increase in THz emission with doping density. The spectral features at lower frequencies are attributed to the detector, the overall spectral envelope to thermal emission.

Figure 2 shows spectra obtained from a set of devices, each designed to emit at a different, specific frequency. The expected intersubband transition was calculated using a self-consistent Poisson–Schrödinger program. The measured emission frequency is shown in bold and is in good agreement with the calculated value shown in italics. This tuning provides clear evidence that the emission is of intersubband origin. These results correlate well with the I–V measurements which demonstrate that maximum peak intensity and a line narrowing are observed at biases just prior to the onset of the negative differential resistance region.

We will present detailed results on these devices and discuss the origins of the other features present in the spectra.

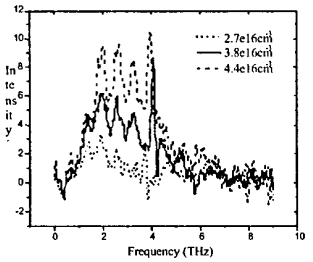

Fig. 1 Emission spectra as a function of injector doping density.

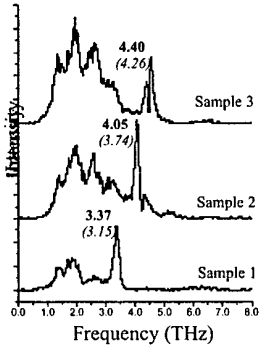

Fig. 2 Spectra illustrating tuning of the intersubband emission. Measured and calculated values of emission frequency (THz) are shown in bold and italics, respectively.

References

[1] J. Faist *et al.*, Science **264**, 553–556 (1994).
[2] S. Blaser *et al.*, Phys. Rev. B **61**, 8369–8374 (2000).
[3] J. Ulrich *et al.*, Appl. Phys. Lett. **77**, 1928–1930 (2000).
[4] M. Rochat *et al.*, Appl. Phys. Lett. **73**, 3724–3726 (1998).

Corresponding author: A. G. Davies, Semiconductor Physics Group, Cavendish Laboratory, Madingley Road, Cambridge CB3 0HE, UK.
Phone: +44 1223 337387, Fax: +44 1223 337271, Email: agd11@cam.ac.uk

RESONANT STATES AND THz LASING IN SiGe QUANTUM WELL STRUCTURES δ - DOPED WITH BORON.

M.S. Kagan[1] and I.N.Yassievich[2]

[1]*Institute of Radioengineering and Electronics of RAS, Mokhovaya 11-7, 101999 Moscow K-9, Russia*
[2]*Ioffe Physico-Technical Institute, Politekhnicheskaya 26, 198 024 St.Petersburg, Russia,*

Recently, the activity towards the quantum cascade THz laser on the basis of SiGe/Si heterostructure has started [1]. Silicon-germanium alloy is very attractive due to its good thermal properties, low absorption in the THz range, relatively cheap technology, as well as possible integration with Si-based electronics. Here we discuss the possibility to create an alternative type of THz laser sources which could utilize a much simpler quantum well (QW) structures, i.e. a resonant-state laser (RSL). We report on observation of an intense terahertz emission of stimulated character from Boron-δ -doped $Si/Si_{1-x}Ge_x/Si$ quantum well structures. Theoretical consideration of the possibility to form resonant impurity states and intra-impurity population inversion is presented, too.

Recently, the pressure-tunable pulsed and continuous-wave operating THz Ge RSLs were demonstrated [2, 3]. Population inversion in the RSL is realized for the states of a shallow acceptor split under external stress. If the strain is high enough (above ~3 kbar for Ge), the split-off acceptor state enters the light-hole branch of the valence band and creates a resonant state [4]. Electric field applied provides depopulating the local impurity states due to an impact ionization. In the post-breakdown regime, practically all carriers occur in the valence band. Free holes are accelerated by electric field and can be captured into the resonant states induced by impurities. A population inversion of resonant states with respect to the impurity states in the gap is then formed [5] and THz lasing occurs.

Since thin layers of binary alloys $Si_{1-x}Ge_x$ are strained internally due to the lattice mismatch, it seems attractive to use them for an RSL without external stress. Note, that such a suggestion was presented first at MSS-7 [6]. The p-type $Si_{1-x}Ge_x$ QW structures MBE-grown pseudomorphically on n-type Si substrate have been used. The design of the structures is presented in Fig. 1. The $Si_{1-x}Ge_x$ .layer of 20 nm thick was sandwiched between undoped Si buffer (130 nm wide) and cap Si (60 nm) layers. The Ge content in the alloy was 0.15. The δ-layer of Boron with concentration of $6\cdot10^{11}$ cm^{-2} was grown in the QW middle. Two Boron-doped δ-layers with B concentration from $4\cdot10^{11}$ to 10^{12} cm^{-2} were positioned within the buffer and cap layers at the distance of 30 nm from QW interfaces, which were aimed to diminish carrier outflow from QW into surface states and to form the suitable built-in transverse electric field in the QW layer. The pulsed ($0.3\mu sec$) electric field was applied along the SiGe layer, to the ohmic contacts, parallel to the interfaces. The measurements were performed at liquid He temperature. Radiation in the THz range was registered with a cooled Ge:Ga photodetector. Luminescence measurements were performed for samples with and without optical resonator, which was obtained by high-accuracy polishing of lateral facets. For samples without the optical resonator, THz emission intensity increased smoothly with bias

voltage. For samples with optical resonator, we have observed a step-like increase in emission intensity by two

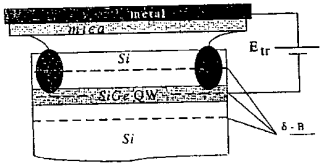

Fig. 1. SiGe QW structure.

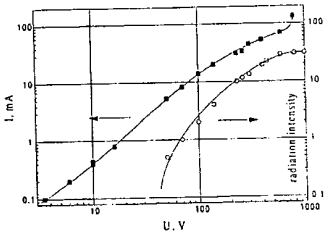

Fig. 2. Radiation intensity and the structure current parallel to interfaces vs pulsed voltage.

orders of magnitude at high enough bias voltage (Fig. 2). The frequency range of 3-6 THz for the intense emission was determined by using a set of microwave high-pass and infrared low-pass filters. We believe that high-intensity emission observed corresponds to the regime of lasing in the $Si/Si_{1-x}Ge_x/Si$ QW, which is proved by the jump in the emission intensity at a threshold field, by the narrow spectral range where emission occurs, and by the necessity of the resonator. We suppose also that population inversion in the QW is due to the resonant states of Boron. A built-in transverse electric field of $\sim10^4$ V/cm controls the position of space-quantization levels and improves conditions for the formation of the resonant state E_{1s} (see Fig.3). Calculated energy distance between E_{1s} and the top of 2D continuum is about 8 meV. The main emission line should correspond to the transition from E_{1s} to the first excited p-type state E_p. Thus, we expect the main emission line to be ~120 μm (10 meV).

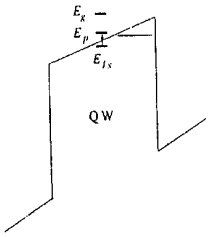

Fig. 3. Scheme of energy levels.

References

1. G.Dehlinger, et al, *Science* **290**, 2297 (2000)
2. I.V.Altukhov, et al, *JETP* **88**, 51 (1999).
3. Yu.P.Gousev, et al, *Appl. Phys. Lett.* **75**, 757 (1999)
4. M.A.Odnoblyudov, et al, *Phys.Rev.* B **62**, 2486 (2000)
5. M.A.Odnoblyudov, et al, *Phys.Rev.* B **62**, 15291 (2000)
6. I.N.Yassievich, et al, *Solid State Electr.*, **40**, 97 (1996)

Corresponding author: Irina Yassievich, Ioffe Physico-Technical Institute, Politekhnicheskaya 26, 194 021 St.Petersburg, Russia, phone +7-812-247-9974, Fax: +7-812-247-1017, e.mail:Irina.Yassievich@pop.ioffe.rssi.ru

Mid infrared range injection laser, based on intersubband carrier transitions and resonant Auger processes in type II quantum wells.

L.E. Vorobjev[1], V.L. Zerova[1], D.A. Firsov[1], G.G. Zegrya[2].

[1]St. Petersburg State Technical University, Politechnicheskaya str., 29, St. Petersburg 195251, Russia
[2]A.F.Ioffe Physico-technical Institute of Russian Academy of Sciences, Politechnicheskaya str., 26, St. Petersburg 194021, Russia

In usual injection lasers interband Auger recombination does not allow to obtain mid infrared range (MIR, $\lambda > 4$ μm) stimulated emission. Quantum cascade laser (QCL) based on tunneling and interband (intersubband) transitions of electrons in type I quantum wells (QW) [1] is one of the decisions of the problem. Recently the promising interband cascade laser (ICL) based on type II QW was suggested [2-4] and fabricated [5-7]. Threshold current of these lasers is lower than one of QCL.

In this report we propose another type of MIR laser based on type II funnel shape QWs. Mechanism of intraband population inversion (PI) is illustrated in fig.1. QW having the shape of asymmetrical funnel can be embedded in intrinsic region sandwiched between graded AlGaAsSb layers forming the MIR waveguide. Under the current (when p-i-n diode is used) or optical injection of electrons are mainly captured by the upper electron level e_3. Then the electrons get the levels e_2 and e_1 after emission of optical phonon $\hbar\omega_0$ ($E_{e2} - E_{e1}$, $E_{e3} - E_{e2} > \hbar\omega_0$). The electron lifetime τ_3 on level e_3 is much more than lifetime on level e_2 because of weak overlap of electron wave functions of e_3 and e_2, e_1 levels. The overlap of wave functions of levels e_2 and e_1 is strong and lifetime τ_2 is significantly less than τ_3. So, the PI can appear between levels e_3 and e_2. The additional pumping of level e_3 is realized due to resonant Auger recombination (see Fig. 1). So, Auger recombination plays the positive role. Under high pumping current or high level of optical pumping the PI between levels e_3 and e_2 can be destroyed due to Auger-like processes [8] (Fig. 2) if the concentrations of electrons and holes are large. Resonant Auger processes stabilize the electron and hole concentrations and prevent the increase of concentration at high current.

In this work the probabilities of intersubband transitions, resonant Auger processes, Auger-like e-e and e-h collisions are calculated using 4-band Kane model. We determined the PI as a function of temperature, pumping current and intensity of optical pumping. The optical gain and density of threshold current were also calculated.

The preliminary structure with funnel shape QW was grown. The PL spectrum of this structure is presented in Fig. 3. Analysis of this spectrum shows that electron lifetime τ_3 on level e_3 is at least one order of value larger, than lifetime on level e_2.

References

[1] J. Faist, F. Capasso, D.L. Sivco, C. Sirtori, A.L. Hutchinson, A.Y. Cho, Science **264** 553 (1994) .
[2] R.Q. Yang. Superlattices Microstruct. **17**, 77 (1995).
[3] J.F. Meyer, I. Vurgaftman, R.Q. Yang, L.R. Ram-Mohan. Electron. Letters, **32**, 45, 1996.
[4] I. Vurgaftman, J.F. Meyer, R.Q. Yang, L.R. Ram-Mohan. IEEE Photonics Technology Letters, **9**, 170 (1997).
[5] R.Q. Yang, B.H. Yang, D. Zhang et al., Appl. Phys. Lett. **71**, 2409 (1997).
[6] C.L. Felix, W.W. Bewley, I. Vurgaftman, J.F. Meyer, D. Zhang, C.-H. Lin, R.Q. Yang, S.S Pei. IEEE Photonics Technology Letters, **9**, 1433 (1997).
[7] C.L. Felix, W.W. Bewley, E.H. Aifer, I. Vurgaftman, J.F. Meyer, C.-H. Lin, D. Zhang, S.J. Murry, R.Q. Yang, S.S Pei. Journals of Electron. Materials, **27**, 77 (1998).
[8] P. Kinsler, P. Harrison, R.W. Kelsall, Phys.Rev.B **58**, 4771 (1998).

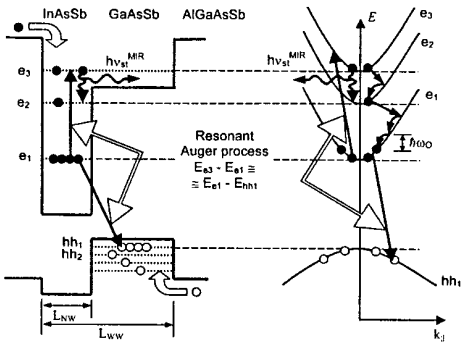

Fig. 1: Schematic of electron transitions (in both coordinate and momentum space) in a asymmetric funnel-shaped QW laser structure/

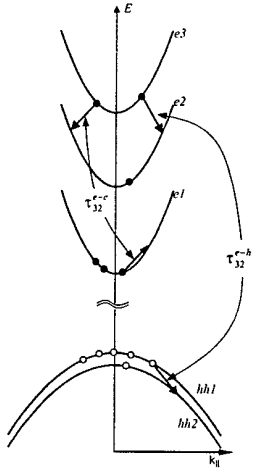

Fig. 2: Diagram showing destructive e-e and e-h collisions.

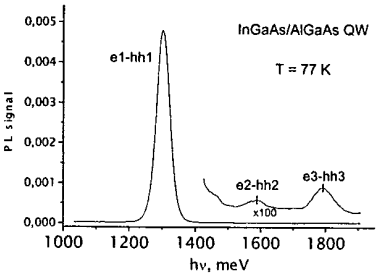

Fig. 3: PL spectrum of funnel-shaped InGaAs/AlGaAs QW

Corresponding author: German Zegrya, A.F.Ioffe Physico-technical Institute of Russian Academy of Sciences, Politechnicheskaya str., 26, St. Petersburg 194021, Russia
phone: +7 812 247-9367; Fax: +7 812 247-1017; email: zegrya@theory.ioffe.rssi.ru

Quantum transport calculations for quantum cascade laser structures

S.-C. Lee and A. Wacker

Institut für Theoretische Physik, Technische Universität Berlin, Hardenbergstr. 36, 10623 Berlin, Germany

The operation of a quantum cascade laser (QCL) is dominated by the interplay of electron transmission through funnel injectors, and relaxation due to scattering in the active region. Complementary to existing approaches, which model the (semiclassical) scattering processes in the active region in detail, we focus on the quantum transport through the whole structure.

The modelling is done within the quantum transport theory of nonequilibrium Green's functions [1]. We extend this method, which was successfully applied to semiconductor superlattices [2], to QCL structures. The quantum kinetic equations are solved self-consistently using self-energies for impurity and phonon scattering processes within the self-consistent Born approximation. In this way, we obtain the current density J and the average electronic distribution $f(E) = -i \sum_k G^<(k,E) / \sum_k A(k,E)$, which gives the average occupation of the levels at a given energy E. [$G^<(k,E)$ is the lesser Green's function and $A(k,E)$ is the spectral function.]

As a test case for the calculations, we consider the GaAs/Al_xGa_{1-x}As QCL structure described by Sirtori *et al.* in Ref. [3]. Fig. 1 shows the I-V curve calculated in the theory. Taking into account a residual series resistance in the experiment, there is very good agreement with the experimental measurements [3]. Fig. 2 shows the calculated distribution of electrons as a function of energy in the QCL structure. For vanishing field, $f(E)$ becomes the Fermi function with the lattice temperature 77 K, while the population of higher states increases if an electric field causes transitions to higher bands. At a voltage of 7 V we find inversion, i.e., the occupation of states at an energy of 0.2 eV is larger than the occupation of states in the energy range 0 to 0.2 eV. This agrees well with the experimental observation of lasing in this range of currents and fields.

References

[1] H. Haug and A.-P. Jauho, 'Quantum Kinetics in Transport and Optics of Semiconductors', Springer-Verlag, Berlin 1996.

[2] A. Wacker *et al.*, Phys. Rev. Lett. **83** 836 (1999).

[3] C. Sirtori *et al.*, App. Phys. Lett. **73** 3486 (1998).

Corresponding author: S.-C. Lee, Institut für Theoretische Physik, Technische Universität Berlin, Hardenbergstr. 36, 10623 Berlin, Germany. Tel: +49 30 314-24858, Fax: +49 30 314-21130, email: lee@physik.tu-berlin.de

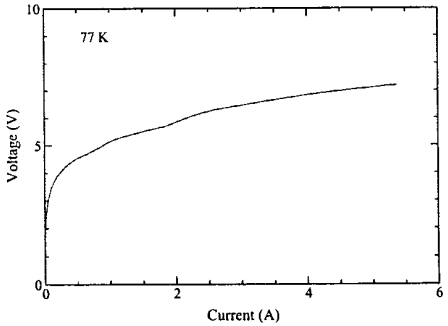

Figure 1: Calculated I-V characteristic for the GaAs/Al_xGa_{1-x}As QCL structure reported in [3].

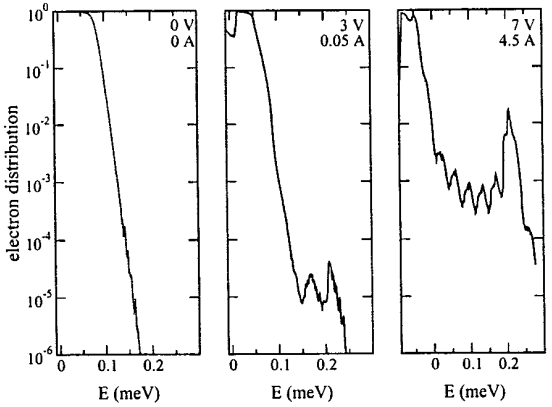

Figure 2: Distribution function of electrons. The current and applied bias are shown with each curve. The corresponding electric fields are 0, 22, and 53 kV/cm.

Gain Optimization in Optically Pumped Unipolar Quantum Well Lasers

S. Tomić[1], V. Milanović[2], Z. Ikonić[3]

[1] Department of Physics, University of Surrey, Guildford, Surrey GU2 7XH,United Kingdom

[2] Faculty of Electrical Engineering, University of Belgrade, P.O. Box 3554, 11120 Belgrade, Yugoslavia

[3] School of Electronic and Electrical Engineering, University of Leeds, Leeds LS2 9JT, United Kingdom

In this abstract we discuss a systematic procedure for the QW profile optimization in respect to maximizing the gain, where the gain depends not only on the dipole matrix elements, but also on the levels relaxation rates: $g \sim \Xi = (1 - \tau_{21}/\tau_{32})\tau_3 z_{13}^2 z_{23}^2$. The procedure relies on the supersymmetric quantum mechanics (SUSYQM) [1]. This technique enables one to manipulate the states of a quantum system (deletion and/or insertion of a state, while leaving others intact) by changing the potential, and at the same time it introduces one or more free parameters via which the potential shape may be further varied isospectrally. Variation of the potential does affect the wave functions, however, in contrast to energies, and therefore the values of matrix elements involving these states, and eventually the physical property of interest. It remains therefore to scan the value of the target function in the space of free parameter(s) and spot the value(s) giving the optimal potential. The resulting optimized potential we derive is realizable by continuous grading of $Al_xGa_{1-x}As$ alloy, with the possiblility of discretizing it subsequently, to make the structure realization easier. The spacing between the lowest two states ΔE_{21} (these will be the lower and upper laser states, while the ground state of the system is generated by the supersymmetric optimization procedure itself), is in this work set to 80 meV, corresponding to the laser wave length of $\lambda \approx 15.5$ μm, so that $\Delta E_{21} + \hbar\omega_{LO} = 116$ meV equals the CO_2 pump laser photon energy. After performing this search we find that the maximal value of $\Xi = 99000$ psÅ^4. This optimized Ξ exceeds by about 50% the value obtained in asymmetric coupled QW system [2]. The truely smooth optimal potential cannot be realized, however, so we have discretized it, choosing the step size of three crystalline monolayers (3 × 2.83 Å in AlGaAs). This discretization slightly changes the parameters obtained within the smooth-potential model, and next we give both sets (the values in brackets corresponding to the discretized case). Thus, the dipole matrix elements amount to $z_{\epsilon 2} = 11.4(10.8)$ Å and $z_{21} = 27.8(27.9)$ Å. Carriers relaxation times were calculated using the expressions for bulk-like polar optical and acustical phonon scattering, within the parabolic approximation [3], and amount to: $\tau_{1\epsilon} = 0.44(0.44)$ ps, $\tau_{2\epsilon} = 3.19(3.07)$ ps, $\tau_{21} = 2.03(1.96)$ ps, and $\tau_2 = 1.24(1.20)$ ps. Certainly, since the SUSYQM procedure was used the interlevel spacings are exactly as required, i.e., $\Delta E_{2\epsilon} = 116$ meV and $\Delta E_{1\epsilon} = 36$ meV, with the energies of the three states individually being E_ϵ =-121.76 (-121.57) meV, E_1 =-85.76 (-85.14) meV, and E_2 =-5.76 (-5.99) meV. The laser gain which could be obtained in such an optimized structure at $T = 77$ K exceeds $g = 980$ cm^{-1} for pump power ≥ 500 kWcm^{-2}. An even coarser discretization may be employed, which will make it even more readily realizable. Here we have taken into account the position dependent effective mass, and the self-consistent potential. The latter is calculated by iteratively solving the Schrödinger and Poisson equations. Thus we have designed a 5-layer structure: $Al_{0.17}Ga_{0.83}As$ (17 Å) – $Al_{0.06}Ga_{0.94}As$ (45 Å) – $Al_{0.17}Ga_{0.83}As$ (44 Å) – GaAs (51 Å) – $Al_{0.17}Ga_{0.83}As$ (30 Å), embedded in $Al_{0.28}Ga_{0.72}As$ outer barrier bulk, Fig. 1. The modulation doping to $n_s = 3 \times 10^{11}$ cm^{-1} is assumed, the doped region being 50 Å wide, and 60 Å away from the QW boundary. The energy spacings in this structure (at $k_{||} = 0$) amount to $\Delta E_{21} = 36.25$ meV and $\Delta E_{32} = 80.26$ meV, and the Fermi level E_f is 9.1 meV above the ground state. At $T = 77$ K the ratio of carrier densities on the ground and the lower laser state is $n_1/n_2 \approx 10^2$. The dipole matrix elements in this structure are calculated to be $z_{13} = 14.9$ Å, and $z_{23} = 24.9$ Å, the relaxation times are $\tau_{21} = 0.63$ ps, $\tau_{31} = 1.71$ ps, $\tau_{32} = 1.96$ ps, and $\tau_3 = 0.91$ ps, and the gain parameter is $\Xi = 86000$ psÅ^4. The gain would thus exceed $g = 800$ cm^{-1} at the pump intensity ≥ 500 kWcm^{-2} and $T = 77$ K. The gain saturation starts at pump intensities ≥ 10 MWcm^{-2}, the saturated gain being $g \simeq 1500$ cm^{-1}. As a final note, because of low operating temperatures we have here used the values corresponding to $k_{||} = 0$ for the electron scattering rates in gain calculations. At higher temperatures or larger doping densities a considerable portion of the total carrier density will reside in states with larger $k_{||}$, and then it may be necessary to use the appropriate averages of the scattering rates. It is then that the fully self-consistent optimization, specific to the chosen carrier density, should be performed.

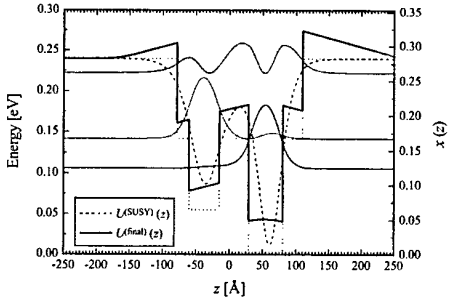

Figure 1: The final coarse-discretized and the self-consistent potential. The dashed line is the Al mole fraction (grading) profile in the $Al_xGa_{1-x}As$ alloy, to be read on the right vertical axis.

References

[1] S. Tomić, V. Milanovic and Z. Ikonić, Phys. Rev. B **62**, 16681 (2000).

[2] O. Gauthier-Lafaye et al, Appl. Phys. Lett. **74**, 1537 (1999).

[3] G. Sun and J. Khurgin, IEEE J. Quantum Electron. **29**, 1104 (1993).

Corresponding author: Stanko Tomić, Department of Physics, University of Surrey, Guildford, Surrey GU2 7XH,United Kingdom.
phone: +44 1483 879402, Fax: +44 1483 876781,
email: s.tomic@surrey.ac.uk

Optical and electrical investigation of population properties for quantum cascade structures

L. Schrottke, R. Hey, H.-Y. Hao, H. T. Grahn,

Paul Drude Institute for Solid State Electronics, Hausvogteiplatz 5-7, 10117 Berlin, Germany

We have investigated the electric-field-dependent electronic subband population and carrier dynamics in double-quantum-well superlattices (DQW-SLs) as well as quantum cascade structures (QCSs) in the GaAs/(Al,Ga)As material system by (interband) photoluminescence (PL) spectroscopy and current-voltage (I-V) characteristics. PL spectroscopy, which is a bipolar method as both the electron *and* hole concentrations determine the intensity, has proven to be a powerful tool for the investigation of unipolar systems, if only one hole subband is involved in the interband transitions [1,2]. In more complex structures such as QCSs, the electron distribution has only been determined qualitatively through various optical methods [3]. For a precise quantitative discussion of the electric-field-dependent electronic subband population, the dynamics of electrons *and* holes has to be considered.

Previously, we have analyzed the electronic subband population produced by current injection into a DQW-SL, which serves as a model system for QCSs, using continuous-wave spectroscopy [4]. One period of a DQW-SL consists of two quantum wells and two barriers, which all have different thicknesses. While the variation of barrier thicknesses results in different transfer rates, which are expected to lead to an occupation inhomogeneity between the electronic ground states of the adjacent wells, the difference in the well widths allows to identify the QWs following the thin or thick barrier (with respect to the direction of the electric field) through their PL energies. In order to determine the population of the electronic subbands from the intensities of the respective PL lines, two conditions have to be fulfilled: First, the density of the optically excited carriers must be low compared to the electrically injected one (condition of weak excitation) and, second, the distribution of the holes in the respective hole subbands has to be homogeneous or well known. In Ref. [4], the experimental determination of the limit of weak excitation was discussed.

Generally, the hole distribution is inhomogeneous due to their dynamical properties. However, if the excitation is carried out with ultra-short pulses and the intensity is measured immediately after the excitation, a homogenous hole distribution can be assumed. For DQW-SLs, it is possible to determine even the absolute values of the electronic subband population and the transfer rates of the holes from the time-dependent PL spectroscopy.

Figure 1 shows the electronic occupation of the two quantum wells n_1 and n_2 of a DQW-SL and the total occupation $n = n_1 + n_2$ derived from time-resolved PL spectroscopy. While the population of the well (n_2) following the thicker barrier increases approximately linearly with increasing voltage, the well (n_1) following the thinner barrier exhibits a distinct maximum. The total occupation follows approximately the occupation of the latter. For higher voltages, the population of both quantum wells coincides. This is an indication for a transport mechanism, for which the thicknesses of the barriers do not play any role. We believe that the transport in this voltage range is determined by carrier escape into continuum states and recapture. The exponential I-V characteristic suggests an increasing current contribution, which originates from transport into quasi-continuum states rather than from inter-well tunneling processes through the barriers. Furthermore, for higher carrier densities, the electron-electron scattering rate increases, which may lead to an additional depopulation of the subbands. For QCSs, the determination of the absolute values of the subband population is more difficult. However, relative values for the population of the various subbands can be derived from time-resolved PL spectra, which allow a detailed discussion of the relation between the current and the subband population in the active regions.

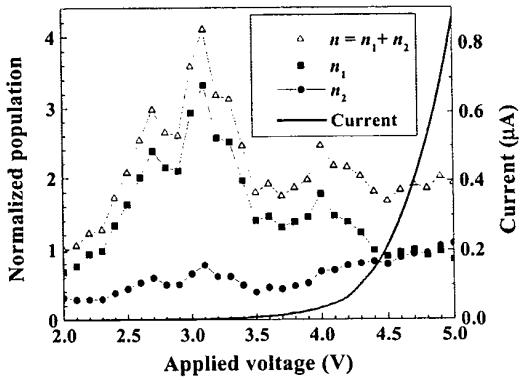

Figure 1: Electron population n_1 and n_2 of the subbands of the wells following the thinner and thicker barrier, respectively, and total population $n = n_1 + n_2$ versus applied voltage. The values have been normalized to n at 2 V. For comparison, the current-voltage characteristic is also shown (solid line).

References

[1] H. T. Grahn, H. Schneider, W. W. Rühle, K. v. Klitzing, and K. Ploog, Phys. Rev. Lett. **64**, 2426 (1990).

[2] Y. B. Li, J. W. Cockburn, J. P. Duck, M. J. Birkett, M. S. Skolnick, I. A. Larkin, M. Hopkinson, R. Grey, and G. Hill, Phys. Rev. B **57**, 6290 (1998).

[3] L. R. Wilson, P. T. Keighley, J. W. Cockburn, J. P. Duck, M. S. Skolnick, J. C. Clark, G. Hill, M. Moran, and R. Grey, Appl. Phys. Lett. **75**, 2079 (1999).

[4] L. Schrottke, R. Hey, and H. T. Grahn, Phys. Rev. B **60**, 16635 (1999).

Corresponding author: Lutz Schrottke, Paul-Drude-Institut für Festkörperelektronik, Hausvogteiplatz 5-7, 10117 Berlin, Germany.
phone: +49 30 20377 339, Fax: +49 30 20377 515,
email: lutz@pdi-berlin.de

Capture and confinement of light and carriers in graded index quantum well laser structures

G. Aichmayr, H. P. van der Meulen, L. Viña, and J. M. Calleja
Departamento de Física de Materiales, Universidad Autonoma Madrid, 28049 Madrid, Spain
F. Schäfer, J. P. Reithmaier, and A. Forchel
Technische Physik, Universität Würzburg, Am Hubland, 97074 Würzburg, Germany

Carrier-capture, -escape and light mode guiding, are responsible for the modulation response of laser devices in optoelectronic applications. We investigated graded index separate confinement heterostructure (GRINSCH) lasers and compared their performance with a conventional quantum well laser. We found that grading the index of the waveguide improves considerably both, the carrier and light trapping and reduces carrier escape from the active region.

Three laser structures were studied, each containing a 9 nm single GaInAs quantum well (SQW) as active layer but different barrier designs, which serve for carrier confinement and light guiding. While in laser #1 the SQW was embedded in a simple GaAs waveguide, lasers #2 and #3 had a graded waveguide, which was obtained incorporating short period superlattices (SPSLs) made of $Al_xGa_{1-x}As$ layers with the Al content increasing from the centre towards the cladding layer. In laser #3 the Al content was basically twice that of #2, yielding a higher confinement potential. Time resolved photoluminescence (trPL) measurements were done with the up-conversion technique providing a time resolution of 2 ps. Raman spectra were collected in the back-scattering geometry at different incidence angles, from 0° to 60° to the sample normal, and different polarisation conditions.

The carrier capture time obtained from the rise of the trPL emission was measured as a function of excitation energy (Fig. 1a). This allowed selective carrier injection into specific layers of the structure, due to the different band gap of the different layers. The carrier escape from the SQW was probed by applying an electric field perpendicularly to the SQW plane. The electric-field-induced tunnelling gives direct insight into the laser structures capability of carrier confinement to the active layer: the rise and decay time of the PL are strongly reduced when tunnelling occurs (Fig. 1b). Apart from the carrier confinement, to avoid photon leakage, optical mode guiding is essential for optimum device performance. We guided a probe beam through the structures and analysed its Raman spectrum, which gave information on the spatial confinement of the light mode (Fig. 2).

The GRINSCH laser structures (#2 and #3) show superior carrier (Fig. 1a) and light trapping properties (Fig.2b) as compared to those of lasers with simple GaAlAs barriers (#1). The PL rise in #3 is an order of magnitude shorter than in #1 and unaffected by the excitation energy. Lasers #1 and #2, however, show a markedly increase in rise time when the carriers are injected into the waveguide rather than into the active layer (Fig. 1a). Confinement of the lasing light mode is improved in #2, and increased by almost a factor 2 in #3 compared to #1 as observed in the angle dependent Raman spectra (Fig. 2). The decay times of the carriers in lasers #1 and #2 increase considerably with increasing electric field (Fig. 1b), indicating high tunnelling rates. In contrast, the field dependence of the PL decay time in the #3 GRINSCH demonstrates the strong reduction of the carrier escape, thus proving the superiority of the SPSL with higher Al content for efficient carrier confinement.

Corresponding author: Luis Viña, Departamento Física de Materiales, UAM, E-28049 Madrid
Tel.: +34 91 397 4782 Fax: +34 91 397 8579 email: luis.vina@uam.es

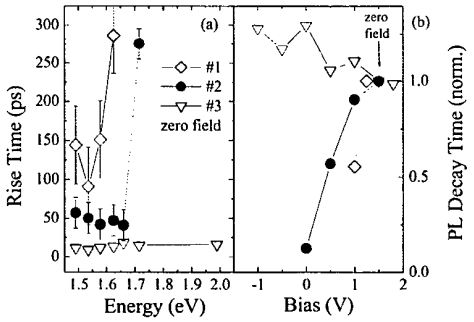

Fig.1 (a) Carrier capture times as a function of injection energy at zero electric field. The lowest energy corresponds to the direct injection into the GaInAs SQW. Above a certain energy, both lasers, #1 and #2, have considerably increased rise times reflecting the influence of the barrier structures in the capture process. Only laser #3 maintains a fast capture even at high injection energies, which approximately correspond to the case of electrical injection. (b) Change of the normalized decay time of the PL as a function of electric field, for an injection energy of 1.49 eV. As the field increases (bias decreases) tunnelling of carriers reduces the density in the SQW, and thereby the PL intensity, leading to a shorter decay time. Only in #3 the decay time slightly increases with field, indicating reduced tunnelling.

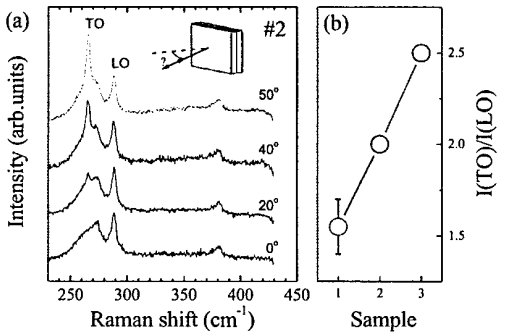

Fig.2 (a) Raman spectra of laser #2 at different angles of incidence. At normal incidence, where light polarisation is parallel to the SQW plane, the TO mode is forbidden. When the beam is efficiently guided through the SQW, the intensity of the TO peak, for p-polarised excitation, is enhanced with increasing incidence angle. The intensity of the LO mode is practically angle independent, therefore the ratio between the TO and LO intensities serves as a measure of light guiding efficiency in the SQW, which is shown in (b) for the three laser structures.

LIST OF AUTHORS

LIST OF AUTHORS

Abe, S	THP37	Arnone, D D	TUA8	Bennett, B.R.	TUA7
Abram, I.	FRM9	Arriaga, J.	TUP30	Berer, T.	MOP59
Abram, I.	TUA10	As, D. J.	TUP6	Berry, J.J.	THE1
Abram, R.A.	THP49	As, D.J.	TUP7	Beserman, R.	THP72
Abramof, E.	MOP44	Asada, M	THP56	Besombes, L.	TUP85
Abstreiter, G.	MOM1	Asakawa, K.	MOP35	Beyer, H.	THP41
Abstreiter, G.	MOP12	Asakawa, K.	THA4	Beyer, S.	MOP47
Abstreiter, G.	MOP14	Asano, Takashi	TUP37	Bichler, M.	MOM1
Abstreiter, G.	MOP2	Ashmore, A. D.	MOM2	Bichler, M.	MOP52
Abstreiter, G.	THA6	Ashmore, A.D	TUM11	Bichler, M.	MOP66
Abstreiter, G.	THM8	Asperger, T.	THM9	Bichler, M.	THM9
Abstreiter, G.	THM9	Austind, D.G.	MOP55	Bichler, M.	THP11
Abstreiter, G.	THP11	Austing, D G	MOM7	Bichler, Max	THM4
Abstreiter, Gerhard	THM4	Awschalom, D.D.	THE1	Bichler, Max	THP5
Abstreiter, Gerhard	THP5	Bach, P.	THP29	Bickel, F.	TUP70
Achermann, M.	TUP44	Bacher, G.	FRM4	Biermann, K.	TUP19
Adachi, S.	TUP13	Bacher, G.	TUP62	Bimberg, D.	FRA4
Adelmann, C.	MOP33	Bader, A.	MOP28	Bimberg, D.	THP2
Agulló-Rueda, F.	TUM4	Bagaev, V. S.	THP59	Bimberg, D.	TUP46
Ahn, D.	THP46	Bagraev, N.T.	MOP24	Bimberg, D.	TUP49
Ahopelto, J.	THP42	Bagraev, N.T.	THM12	Bimberg, D.	TUP59
Aichmayr, G.	THP79	Bagraev, N.T.	THP15	Bimberg, D.	TUP65
Aida, T.	THP54	Bahir, G.	TUP61	Bimberg, D.	TUP66
Aigle, M.	FRA2	Baier, M.	MOM1	Bimberg, D.	TUP74
Airey, R	THM2	Baier, Martin	THP5	Bimberg, D.	TUP84
Akabori, M.	TUP24	Bakarov, A. K.	TUP52	Biolatti, E	TUP15
Akazaki, T.	THP20	Baldassarri, H. G.	TUP5	Biolatti, Eliana	TUP14
Alchalabi, K.	MOP43	Barbarella, G	WEM7	Bird, J.P.	MOP56
Aleshkin, V.Ya	THP58	Barbarella, G.	MOP79	Bissiri, M.	TUP5
Alferov, Zh.I.	FRA4	Bastard, G.	THP17	Bjork, M.	THA3
Allegrini, M.	TUP27	Bastard, G.	TUA1	Blaser, S	MOA5
Allerman, A. A.	TUM4	Batlogg, B.	MoE2	Blaser, Stéphane	THM6
Alphandery, E.	TUP69	Bauer, G.	FRA2	Blick, R.H.	MOA2
Alsina, F.	MOA1	Bauer, G.	MOM12	Blick, R.H.	MOM6
Altukhov, I. V.	MOP73	Bauer, G.	MOP14	Bloch, J.	TUM2
Amand, T	FRM3	Bauer, G.	MOP31	Blyth, R. I. R.	MOP79
Amann, M.-Ch.	THM4	Bauer, G.	MOP59	Bock, C.	TUP54
André, R.	FRM10	Bauer, G.	MOP8	Boggess, T.F.	FRA1
Andreani, L.C.	TUP23	Bauer, G.	THP41	Bohm, G.	MOA6
Andreev, A. D.	THP39	Bauer, M.	MOP7	Bomze, Yu	MOP45
Andreev, A.D.	TUP8	Baumberg, J. J.	TUM1	Bonilla, Luis L.	TUP39
Andreev, Andrei	MOP85	Bayer, M.	TUA11	Borany, J. von	MOP21
Anni, M.	MOP79	Bayer, M.	TUM10	Borgstrom, M.	TUP79
Anton, R.	MOP70	Bayer, M.	TUM3	Born, H.	TUP65
Aoki, T.	MOP48	Becher, C.	FRM8	Böttner, H.	THP41
AOYAGI, Y	TUP55	Bechstedt, F.	TUP6	Bouchiat, V.	MOP5
Aoyagi, Y.	TUP72	Beck, M	MOA5	Bougeard, D.	MOP12
Aoyagi, Y.	WEM5	Beck, Mattias	THM6	Bougeard, D.	THP11
Apostolopoulos, G.	THP62	Beham, Evelin	THP5	Boukos, N.	THP62
Arakawa, Y.	TUP75	Beil, F. W.	MOA2	Bouravleuv, A.D.	MOP24
Arata, I	FRM6	Bellet-Amalric, E.	MOP33	Bouravleuv, A.D.	THM12
Arena, A.	TUP27	Belyaev, A.E	TUP42	Bouravleuv, A.D.	THP15
Arnone, D D	THP73	Bending, S.J.	MOP61	Bournel, A.	THP33

Brabec, C. J.	MOP82	Cingolani, R.	THP10	Downes, J.R.	TUP8
Bradley, I. V.	THP55	Cingolani, R.	TUP27	Dremin, A.A.	TUM3
Bratschitsch, R.	THP57	Cirlin, G. E.	TUP74	Dreyfus, R.	MOP46
Bratschitsch, R.	THP60	Clement, N.	MOP5	Driscoll, D.C.	THP38
Bratschitsch, R.	TUP50	Cockburn, J.W	THM2	Dubrovskii, Yu. V.	TUA2
Bruls, D.M.	MOP37	Colombelli, R.	THM5	Ducommun, Y.	MOM5
Brunner, K	THA6	Comanescu, G.	TUA7	Dudek, R.	TUP71
Brunner, K.	MOP12	Coquelin, M.	MOP68	Duren, J.K.J. van	MOP80
Brunner, K.	MOP14	Corchia, A	TUA8	Dvurechenskii, A.V.	MOP15
Brunner, K.	MOP2	Cortez, S.	FRM3	Dwir, B.	MOP54
Brunner, K.	THM8	Cortez, S.	TUP60	Dwir, B.	THA2
Brunthaler, G.	MOP59	Costa, M. V. Tovar	MOP87	E. P. O'Reilly	TUP8
Bryant, Garnett W.	THP7	Crow, G.C.	THP49	E. Ribeiro	MOP10
Bryllert, T.	TUP79	Csontos, D.	THP47	Eaves, L	MOM7
Buckle, P. D.	TUM11	Cullis, A. G.	MOP32	Eaves, L.	THP70
Bugge, F.	MOP40	Cywinski, G.	THP22	Eaves, L.	TUA2
Bürkle, L.	MOA4	Cywinski, G.	THP25	Eaves, L.	TUP35
Bussi, G.	MOP86	Czeczott, M.	THP22	Eberl, K.	MOM6
Buyanova, I.A	TUP2	da Silva Jr., E.F.	MOP10	Eberl, K.	MOP16
Buyanova, I.A.	THP19	Dallaporta, H.	MOP5	Eberl, K.	MOP36
Cade, N.I.	TUA4	D'Amico, I	TUP15	Eberl, K.	MOP69
Caetano, E. W. S.	TUP11	D'Amico, Irene	TUP14	Eberl, K.	MOP77
Cagran, C.	MOP41	Dang, D. Le Si	FRM10	Eberl, K.	MOP8
Caldas, M. J.	MOP86	Daniel, A.	MOP8	Eberl, K.	THP4
Calleja, E.	TUP1	Danilov, A.V.	MOP45	Eberl, K.	THP68
Calleja, J. M.	THP79	Danilov, S. N.	THP36	Eberl, K.	THP69
Calleja, J.M.	TUP1	Danylyuk, S.V	TUP42	Eberl, K.	TUP53
Calzolari, A.	WEM8	Dasbach, G.	TUM3	Eckardt, M.	MOP63
Cantarero, A.	MOA1	Dashiell, M.W.	MOP16	Eckardt, M.	TUP40
Canzler, T.W.	WEM6	Daudin, B.	MOP33	Efimov, Yu.A	THP52
Cao, C.	FRA1	Davies, A G	THP73	Ehehalt, J.	TUP74
Capasso, F.	THM5	Davies, A G	TUA8	Ehlert, A	MOP56
Capasso, F.	THM1	Davies, A.G.	MOP56	Ehrenfreund, E.	TUM8
Capizzi, M.	TUP5	Dehlinger, G.	MOP67	Eickemeyer, F.	MOA3
Carder, D.A	THM2	Dehlinger, G.	THM7	Elsaesser, T.	MOA3
Cassabois, G.	MOM4	Delalande, C.	FRM10	Elsaesser, T.	THM8
Cassan, E.	THP51	Delalande, C.	MOM4	Elsaesser, T.	TUA5
Chamard, V.	MOP33	Deleporte, E.	TUA1	Elsholz, F.	MOM13
Chang, K. J.	MOP50	Denk, P.	MOP58	Elzerman, J.M.	MOP57
Chaplik, A. V.	MOP74	Denker, U.	MOP16	Emiliani, V.	TUA5
Chen, H.	FRA1	Denker, U.	MOP77	Endler, D.	TUM6
Chen, K.-C.	THP43	Deppe, D.G.	FRA1	Ensslin, K.	MOM9
Chen, L.	MOP84	Deutschmann, R. A.	THM9	Ensslin, K.	MOP52
Chen, W.M	TUP2	Dhillon, S S	THP73	Ensslin, K.	MOP66
Chen, W.M.	THP19	Dickerson, J. H.	TUM4	Ensslin, K.	MOP67
Chia, C.K	THM2	Diehl, L.	THM7	Ensslin, K.	THM7
Child, R. A.	TUP69	Dietl, T.	MOM12	Entin, M. V.	MOP74
Cho, A. Y.	THM1	Dietl, T.	THE2	Erofeeva, I.V	THP58
Cho, A. Y.	THM5	Dilger, M.	MOP69	Eroms, J.	THP36
Cho, K	TUP31	Dluzewski, P.	THP25	Ertl, F.	THM9
Cho, K.	TUP20	Dobrowolska, M.	FRM4	Estibals, O	MOP19
Choi, B. H.	THP46	Döhler, G. H.	THP3	Estibals, O	MOP76
Chou, S. Y.	MOM8	Döhler, G.	MOP63	Etteh, N. E. I.	THP50
Chu, J. O.	MOP20	Döhler, G.	TUP40	Eychmüller, Alexander	TUP18
Chu, L.	THP11	Döhler, G.	TUP54	Fafard, S.	TUA11
Chye, Y.	THA7	Döhler, G.H	MOA5	Fafard, S.	TUM10
Cibert, J.	THE2	Döhler, G.H.	THP12	Fafard, S.	TUP71
Cilento, T.	MOP52	Döhler, G.H.	TUP41	Fainstein, A.	TUP21
Cingolani, R	TUP15	Doi, T.	THP37	Faist, J	MOA5
Cingolani, R	WEM7	Dollfus, P.	THP33	Faist, J.	THM7
Cingolani, R.	MOE3	Dollfus, P.	THP51	Faist, Jérôme	THM6
Cingolani, R.	MOP79	Dorn, A.	MOP66	Falta, J.	MOP27

Farias, Gil de Aquino TUP11
Fasching, G. MOP68
Faschinger, W. MOP28
Faschinger, W. MOP39
Favaretto, L. WEM7
Fearn, M. MOP32
Felice, R. Di WEM8
Feng, S.L. THP16
Ferrand, D. THE2
Ferreira, R. FRM3
Ferreira, R. THP17
Ferreira, R. TUA1
Ferreira, R. TUP58
Ferreira, S.O. MOP44
Fiederling, R. THP29
Findeis, F. MOM1
Findeis, Frank THP5
Finkman, E. TUP61
Finley, J. J. MOM2
Finley, J.J TUM11
Firsov, D.A. THP75
Fischer, F. THP48
Fischer, M. TUP5
Flissikowski, T. TUM7
Forchel, A. FRM4
Forchel, A. THP48
Forchel, A. THP79
Forchel, A. TUA11
Forchel, A. TUM10
Forchel, A. TUM3
Forchel, A. TUP62
Forshaw, M. THP40
Förster, A TUP42
Fraboulet, D. MOP5
Franceschi, S. De MOP57
Frank, W. R. THM11
Franzò, G. WEM3
Freire, V.N. MOP10
Freire, Valder Nogueira TUP11
Frey, T. TUP6
Friedland, K.- J. MOM10
Friend, R. MoE1
Fröba, M. MOP84
Frolov, S. V. THM1
Fromherz, T. FRA2
Fromherz, T. MOP14
Fromherz, T. MOP82
Fromhold, M. THP70
Fromhold, T.M. MOP56
Fronc, K. THP22
Fry, P.W TUM11
Fuchs, F. MOA4
Fuhrer, A. MOP66
Fujii, M. MOP17
Fujii, M. MOP18
Fujimoto, S. THP6
Fujimoto, S. TUA3
Fujiwara, K. MOP64
Fujiwara, K. TUA6
Fujiyasu, H. TUP9
Fukui, T. MOP57
Fukui, T. MOP62
Fukui, T. TUP24
Furdyna, J. K. MOP29
Furdyna, J.K. FRM4
Furthmüller, J. TUP6
Gadermaier, C. WEM7
Gadir, M. A. MOP23
Galdin, S. THP51
Gallinat, C. THP38
Ganichev, S. D. THP36
Gaponik, Nikolai TUP18
Garbesi, A. WEM8
Garcia, J. M. TUM12
Garcia, J. M. TUM13
Garcia, J. M. TUP70
García-Cristóbal, A. MOA1
Gaspari, V. TUP5
Gauffier, J.L MOP19
Gautier, J. MOP5
Gavrilenko, V.I THP58
Gayral, B. FRM12
Gebel, T. MOP21
Geddo, M. TUP5
Gefen, Yuval THP18
Gehlhoff, W. MOP24
Gehlhoff, W. THP15
Geng, C. THP64
Gennser, U. MOP67
Gennser, U. THM7
Georgiev, N. TUP25
Gerard, J. M. MOM4
Gérard, J.M. FRM9
Gérard, J.M. TUA1
Gérard, J.M. TUA10
Gérard, J-M. FRM3
Gérard, J-M. TUP60
Gerardot, Brian D. TUM9
Gershoni, D TUM8
Ghali, M. THP25
Gigli, G WEM7
Gigli, G. MOP79
Gigli, G. TUP27
Gippius, N. A. TUP62
Gippius, N.A. TUM3
Gleim, T. THP29
Glunk, M. THP31
Gmachl, C. THM1
Gmachl, C. THM5
Gobsch, G. THP4
Goldhahn, R. THP4
Goldoni, G. MOP86
Goldoni, G. TUP17
Gong, Q. TUP48
Goñi, A.R. THP68
Goñi, A.R. THP69
Gornik, E. MOM13
Gornik, E. MOP68
Gornik, E. MOP73
Gornik, E. THM3
Gossard, A. C. MOM9
Gossard, A.C. THP38
Gould, C. FRM2
Govorov, A. O. THM11
Govorov, A. O. THP9
Govorov, A. O. TUM13
Gozu, S. TUP43
Grabecki, G. MOM12
Grabs, P. FRM2
Grabs, P. THP29
Grahn, H. T. THP78
Grahn, T. MOP64
Grambow, P. THP68
Gramlich, S. MOP40
Grenzer, J. MOP40
Grigorian, S. MOP40
Grousson, R. TUP51
Gruetzmacher, D. MOP67
Grundler, D. THP28
Grundmann, M. TUP66
Grützmacher, D. THM7
Guffarth, F. THP2
Guillet, T. TUP51
Guldner, Y. TUA1
Gumen, L. TUP30
Gundogdu, K. FRA1
Güngerich, M. MOP84
Güntner, R MOP81
Guo, L. J. MOM8
Gustafson, B MOM7
Gustafson, B. THP47
Gustafson, B. TUP79
Haboeck, U. THP69
Hackbarth, T. MOP6
Haendel, K.-M. MOP77
Haft, D. TUM12
Haft, D. TUM13
Haft, D. TUP70
Haga, T. TUP45
Hai, P.N TUP2
Hales, V. J. MOP71
Halsall, M. P. THP55
Hamaguchi, C. MOA6
Hamaguchi, C. MOP51
Hameau, S. TUA1
Hammura, K. TUP72
Hanke, M. MOP30
Hansen, W. MOP47
Hansen, W. MOP70
Hanson, M. THP38
Hao, H.-Y. THP78
Hapke-Wurst, I. TUP80
Harrell, R THP73
Harris, J. S. MOP4
Harris, J.J MOP19
Harrison, P. MOP23
Harrison, P. THP50
Harrison, P. THP55
Hartmann, A. MOM5
Hartmann, Th. THP27
Hasche, T. WEM6
Hasegawa, H. THM10
Hasegawa, Hideki TUP77
Hatami, F. MOP30
Hauert, M TUA4
Haug, R. J. MOP36
Haug, R. J. MOP53
Haug, R. J. MOP69
Haug, R. J. MOP77
Haug, R. J. TUP80
Häusler, I. TUP49
Hawrylak, P. TUA11
Hawrylak, P. TUM10
Hawrylak, P. TUP71
Hayashi, S. MOP17
Hayashi, S. MOP18
Hayden, R. K. THP70
Hayne, M. TUP53
Heersche, H. B. THP23
Heidemeyer, H. THP4
Heimbrodt, W. MOP84
Heimbrodt, W. THP27
Heinke, H. MOP27
Heinrichsdorff, F. THP2
Heinzel, T. MOM9
Heinzel, T. MOP66
Heinzel, T. MOP67
Heis, W. FRA2
Heiss, W. THP21
Heiss, W. TUP19
Heitmann, D. MOP47
Heitmann, D. THP28
Heitmann, D. TUM6
Heitz, R. THP2
Heitz, R. TUP49
Heitz, R. TUP59
Heitz, R. TUP65
Heitz, R. TUP66
Heitz, R. TUP74
Heitz, R. TUP84
Held, R. MOP52
Helm, M. MOP21
Henini, M MOM7
Henini, M. MOP61
Henini, M. THP70
Henini, M. TUA2
Henneberger, F. TUM7
Herbst, M. MOP12
Herfort, J. THP62
Hesjedal, T. MOP4
Heske, C. THP29
Hesto, P. THP33
Hey, R. MOA1
Hey, R. MOA3
Hey, R. MOP64
Hey, R. THP78
Heyn, Ch. MOP47
Heyn, Ch. MOP70
Heyn, Ch. TUM6
Hill, G THM2
Hill, R J A MOM7
Hirakawa, K. THP13
Hirakawa, K. THP6
Hirakawa, K. TUA3
Hirayama, Y. MOM10
Hirayama, Y. MOP46
Hirayama, Y. MOP49
Hirner, H. TUP50
Hirose, Y. THP54
Hirotani, K. THP6
Hirotani, K. TUA3
Hiyamizu, S. MOP48
Hiyamizu, S. THP66
Hiyamizu, S. TUP26
Höck, G. MOP6
Hofer, C. MOP7
Hofer, S. TUP50
Hoffmann, A. TUP65
Hofstetter, D MOA5
Hohenau, A. MOP41
Hohenester, U. MOM1
Hohenester, U. MOP86
Hohenester, U. TUP23
Hohenester, Ulrich TUP57
Hohenester, Ulrich TUP68
Holtz, P. O. MOM3
Holy, V. MOP31
Holy, V. MOP8
Hommel, D. MOP27
Hommel, D. TUP62
Hopkinson, M THM2
Hopkinson, M. MOM2
Hopkinson, M. TUM11
Horikoshi, Y. MOP49
Hörner, A. MOA2
Hosoda, M. THP54
Hu, C. M. MOP70
Hu, C.-M. THP28
Hu, E. FRM8
Huard, V. THA7
Hughes, H. P. THP67
Hulicius, E. TUP64
Humlicek, J. TUP64
Hundt, A. TUM7
Husberg, O. TUP7
Hutchinson, A. L. THM5
Huynh, A. FRM10
Hvam, J.M. TUA6
Hwang, E.H. MOP67
Hwang, H. Y. THM1
Hwang, S. W. THP46
Iacona, F. WEM3
Ida, T. WEM5
Ignatov, A. TUP35
Ihm, G. MOP50
Ihn, T. MOP52
Ihn, T. MOP67
Ikawa, T TUP31
Ikemoto, T. MOP64
Ikoma, Y. MOP10
Ikonic, Z. THP77
Imai, T. MOA6
Imamoglu, A. FRM8
Inoue, Y. TUP9
Intonti, F. TUA5
Iotti, R. C. MOP65
Irrera, A. WEM3
Isaia, J.N. TUA1
Ishibashi, K. WEM5
Ishida, A. TUP9
Ishida, S. TUP75
Ishida, T. MOP51
Ishihara, H. TUP36
Ishino, K. TUP9
Ismail, K. MOP20
Issiki, F. TUP83
Ivanov, S.V. THP19
Ivanov, V.K. THP15
Ivchenko, E. L. THP36
Izrailev, F. MOP60
Jacquot, C. TUM2
Jahn, U. TUP1
Janik, E. THP21
Janik, E. THP25
Jansen, A. G. M. MOP69
Janssen, R.A.J. MOP80
Janssens, K. TUP67
Jantsch, W. FRM1
Jantsch, W. MOP26
Jantsch, W. TUP4
Jaskolski, W. THP7
Jbeli, A FRM3
Jefferson, J. H. MOP32
Jensen, J.R. TUA6
Jiang, Chao TUP77
Johal, T. K. THP10
Johnston, M B TUA8
Johnston-Halperin, E. THE1
Jonson, M. MOP45
Jungwirth, Tomas THP26
Jusserand, B. TUP21
Kaenel, H. von MOP9
Kagan, M. S. MOP73
Kagan, M.S. THP74
Kaindl, R. A. MOA3
Kaindl, R. A. THM8
Kainth, D. S. THP67
Kajiwara, Y. TUP13
Kako, S. TUP75
Kalameitsev, A. V. THP9
Kamins, T. I. MOP4
Kamins, T. I. THA5
Kaminska, E. MOM12
Kamiya, I. TUP47
Kamiya, I. TUP81
Kammerer, C. MOM4
Kanamori, H. TUP26
Kanayama, Toshihiko MOP25
Känel, H. von MOP6
Kang, H. MOP31
Kang, T. W. MOP38
Kanzaki, K. MOP48
Kanzaki, K. THP66
Kapon, E. FRA3
Kapon, E. MOM5
Kapon, E. MOP54
Kapon, E. THA2
Kapon, E. TUP76
Kapteyn, C. M. A. THP2
Kapteyn, C. M. A. TUP74
Kapteyn, C.M.A. TUP59
Karlsson, F. FRA3

Karlsson, K. F.	MOM3	Klopotowski, L.	THP25	Kyriakidis, J.	TUP71
Karrai, K.	THM11	Klyachkin, L.E.	MOP24	L. Rebohle	MOP21
Karrai, K.	THP9	Klyachkin, L.E.	THM12	Lambrecht, A.	THP41
Karrai, K.	TUM12	Klyachkin, L.E.	THP15	Lampalzer, M.	THP27
Karrai, K.	TUM13	Knoll, P	MOP81	Lanzani, G.	WEM7
Karrai, K.	TUP70	Kobayashi, N	TUP12	Larionov, A.	TUA11
Kasai, S.	THM10	Koch, J.	THP12	Latge, A.	MOP87
Kasai, Seiya	TUP77	Köder, A.	THP31	Lawton, D. N.	MOP61
Kasper, E.	MOP7	Köder, A.	THP32	Lebedev, A.V.	THP19
Kast, M.	MOP68	Koehler, K	MOA7	Leburton, J.P	MOP55
Katano, Y.	THP37	Koenraad, P.M.	MOP37	Leburton, J.P.	TUP61
Kaufman, D.	MOP54	Koenraad, P.M.	MOP80	Lechner, R.	MOP31
Kawaguchi, K.	MOP22	Koga, T.	THP20	Ledentsov, N. N.	TUP74
Kawaharazuka, A.	MOP49	Koh, S.	MOP22	Ledentsov, N.N.	FRA4
Kawakami, R.L.	THE1	Kohmoto, S.	MOP35	Lee, H. G.	MOP38
Kawasaki, M.	WEM1	Kohmoto, S.	THA4	Lee, S. J.	MOP50
Kawaura, D.	THP66	Konakova, R.V	TUP42	Lee, S. -W.	THP13
Keckes, Jozef	MOP85	Kondo, T.	MOP83	Lee, S. -W.	THP6
Keller, U.	TUP44	Könemann, J.	MOP53	Lee, S. -W.	TUA3
Kemerink, M.	MOP37	König, Jürgen	THP18	Lee, S.	FRM4
Kemerink, M.	MOP80	König, Jürgen	THP26	Lee, S.	MOP29
Kempe, D.	MOP84	König, P.	MOP53	Lee, S.-C.	THP76
Kersting, R.	THP60	Kop'ev, P.S.	THP19	Leifer, K.	THA2
Keßelring, M.	THP48	Korkusinski, M.	TUA11	Leising, G	MOP81
Keyser, U. F.	MOP36	Korkusinski, M.	TUP71	Leising, G.	MOP41
Keyser, U. F.	TUP80	Kossacki, P.	THE2	Leite, J. R.	TUP6
Khalid, M. N.	THP67	Kossut, J.	THP22	Leite, J.R.	TUP7
Khanin, Yu. N.	TUA2	Kossut, J.	THP25	Lelarge, F.	TUP76
Khartchenko, A.	TUP7	Kostial, H.	MOM10	Lelong, Ph.	TUA3
Kheng, K.	TUP85	Kotthaus, J. P.	THM11	Lemaitre, A.	MOM2
Khmyrova, I.	THP14	Kouwenhoven, L.P.	MOP57	Lemaitre, A.	TUM11
Khorenko, V. V.	TUP54	Kovsh, A	THP61	Lemos, V.	MOP10
Kibis, O. V.	MOP61	Kozlov, D.V	THP58	Lenz, C.	MOP77
Kiesel, P.	THP12	Krapf, D.	THP72	Leo, K	MOA7
Kiesel, P.	TUP41	Krätschmer, M	THP61	Leo, K	WEM6
Kießlich, G.	MOM13	Krauss, T. F.	MOM2	Leonardi, K.	MOP27
Kikuchi, C. A.	MOP49	Krebs, O.	FRM3	Leonardi, K.	TUP62
Kikutani, T.	TUP43	Krebs, O.	TUP60	Lepkowski, S. P.	TUP4
Kim, D. H.	THP46	Kristukat, C.	THP68	Levin, A.	TUA2
Kim, K. W.	THP35	Krizhanovskii, D. N.	TUP29	Levin, A.	TUP35
Kim, K. W.	TUP16	Krizhanovskii, D. N.	TUP28	Levy, M.	THP72
Kim, N.	MOP50	Krokhin, A.	MOP60	Li, W.	TUP3
Kipp, T.	TUM6	Krokhin, A.	TUP30	Lienau, C.	TUA5
Kippenberg, T.	TUP41	Kubota, K.	THP54	Lienau, Ch.	MOP40
Kiravittaya, S.	TUP63	Kuhl, U.	MOP60	Likonen, J.	TUP3
Kiraz, A.	FRM8	Kulakovskii, V. D.	TUP28	Limmer, W.	THP31
Kirmse, H.	TUP49	Kulakovskii, V. D.	TUM3	Limmer, W.	THP32
Kiselev, A. A.	THP35	Kulakovskii, V. D.	TUP29	Lindemann, S.	MOM9
Kiselev, A. A.	TUP16	Kulakovskii, V.D.	FRM4	Linfield, E H	THP73
Kissel, H.	TUP73	Kumano, H.	TUM5	Linfield, E H	TUA8
Kita, T.	THP64	Kumano, H.	TUP22	Linke, H.	MOP56
Kitada, T.	MOP48	Kummer, M.	MOP6	Lipsanen, H.	TUP3
KItada, T.	THP66	Kummer, M.	MOP9	Lischka, K.	TUP6
Kitano, M.	TUP9	Kunert, R.	TUP46	Lischka, K.	TUP7
Kivinen, P.	THP42	Kunze, U.	MOP20	Liu, H. C.	THM1
Klappenberger, F	THP61	Kunze, U.	TUP54	Liu, H.C.	TUP71
Klar, P.J.	MOP84	Kuroda, S.	THP24	Liu, X. Q.	TUP78
Klar, P.J.	THP27	Kurtz, E.	TUP83	Liu, X.	MOP29
Klein, N	TUP42	Kurz, H.	MOP12	Liu, X-Q	TUP51
Kling, R.	THP31	Kuznetsov, O.A	THP58	Loeser, F	MOA7
Kling, R.	THP32	Kvon, Z.D	MOP19	Löhr, S.	MOP47
Klingshirn, C.	TUP83	Kvon, Z.D	MOP76	Loidl, A.	THP27

Lomascolo, M.	THP10	Matagne, P.	MOP55	Motohisa, J.	MOP62
Lonskaya, E. I.	MOP72	Matsuda, Y. H.	THP24	Motohisa, J.	TUP24
Lorenc, M.	TUP64	Matsumura, N.	TUP45	Motooka, T.	MOP10
Loss, D.	TUA12	Matsuo, M.	TUA6	Mowbray, D. J.	MOM2
Lott, J.A.	FRA4	Matsuyama, T.	THP28	Mowbray, D. J.	TUM11
Lotz, Bernard	MOP85	Matt, G.	MOP82	Mozume, T.	TUP25
Lour, W.-S.	THP43	Maude, D.K.	MOP61	Mühlberger, M	FRM1
Luth, H	TUA4	Maximov, I.	THP45	Mühlberger, M.	MOP3
Lüth, H	TUP42	Mayer, P.	MOP31	Mukasa, K.	THP37
Lutz, H.	MOP63	Mazur, Yu. I.	TUP73	Mula, G.	MOP33
Lutz, H.	TUP40	Mazzeo, M.	MOP79	Müller, E.	MOP6
Lyssenko, V.G	MOA7	McCombe, B.D.	TUA7	Müller, E.	THM7
Lyutovich, K.	MOP7	McLaughlin, R	TUA8	Müller, M.	TUP41
M. Anni	TUP27	Medeiros-Ribeiro, G.	THA5	Müller, T.	THP57
M. M. Rzaev	MOP34	M.Meduna	MOP8	Müller-Kirsch, L.	TUP49
M. Muhlberger	MOP34	Meier, C.	THP44	Munekata, H.	MOP83
M.Anni	WEM7	Meier, G.	THP28	Munekata, H.	FRM5
Ma, Z.	TUP80	Meinhold, D.	MOA7	Munzar, D.	TUP64
Mac, W.	MOP14	Meixner, M.	TUP46	Muranaka, Tsutomu	TUP77
MacDonald, A. H.	FRM7	Mendach, S.	MOP70	Murase, K.	THP64
MacDonald, Allan H.	THP26	Mendez, E. E.	TUM4	Murzin, V.N	THP52
Machida, S.	TUA6	Merkt, U.	THP28	Muters, T.	MOP82
Maciel, A..C	TUA4	Metzger, T. H.	MOP33	Muto, S.	TUP13
Mackowski, S.	THP21	Metzner, Claus	TUM9	Muto, S.	TUP45
Mackowski, S.	THP22	Meulen, H. P. van der	THP79	N.Ya. Fogel	MOP45
Mackowski, S.	THP25	Mezdrogina, M.M.	MOP24	Nagamune, Y.	THP65
Macks, L.D.	MOP56	Miao, Z.H.	THP16	Nagamune, Y.	TUP33
Maeda, N	TUP12	Michler, P.	FRM8	Nagasawa, H.	TUP9
Maes, J.	TUP53	Micolich, A.P.	MOP56	Nakajima, F.	MOP57
Magarill, L. I.	MOP74	Miesner, C.	MOP12	Nakajima, F.	MOP62
Magnusson, M. H.	THA3	Miesner, C.	MOP14	Nakamura, H.	MOP35
Magri, R.	THP63	Miesner, C.	THM8	Nakamura, H.	THA4
Main, P C	MOM7	Migliorato, M. A.	MOP32	Nakamura, Y.	THP65
Main, P. C.	THP70	Milanovic, V.	THP77	Nakamura, Y.	TUP63
Main, P. C.	TUA2	Milekhin, A.G	MOP1	Nakashima, H.	TUP83
Main, P.C.	TUP35	Minami, T.	TUP20	Nakata, Y.	TUP45
Makarenko, M. V.	MOP61	Mishra, U.K.	WEM2	Nauen, A.	MOP69
Maksym, P. A.	TUM11	Mitin, V.	THP14	Navratil, K.	TUP64
Malajovich, I.	THE1	Mityagin, Yu.A	THP52	Nenashev, A.V.	MOP15
Malyarenko, A.M.	MOP24	Miura, N.	THP24	Neumann, R.	MOP2
Malyarenko, A.M.	THM12	Miura, N.	THP70	Neumann, W.	TUP49
Malyarenko, A.M.	THP15	Miura, N.	TUP83	Newbury, R.	MOP56
Malzer, S.	THP3	Miyashita, S.	MOP46	Ng, H. M.	THM1
Malzer, S.	TUP41	Molenkamp, L. W.	THP29	Nicholas, R. J.	MOP71
Malzer, S.	TUP54	Molenkamp, L.W.	FRM2	Nicholas, R. J.	TUP69
Manin, L.	FRM9	Molinari, E.	MOM1	Nidda, H.-A. Krug von	THP27
Manninen, A.	THP42	Molinari, E.	MOP86	Nikiforov, A.I.	MOP15
Manotas, S.	TUM4	Molinari, E.	TUP23	Nilsson, D.	THP45
Manz, Y. M.	TUP53	Molinari, E.	WEM8	Nishida, T	TUP12
Maranowski, K.	MOM9	Molinari, Elisa	TUP57	Nishikawa, S.	THA4
Marcucci, D. C.	MOP87	Molinari, Elisa	TUP68	Nishioka, M.	TUP75
Marie, X	FRM3	Monemar, B.	MOM3	Nitta, J.	THP20
Mariette, H.	MOP33	Monemar, B.	THP19	Nitta, J.	THP23
Mariette, H.	TUP85	Moreau, E.	FRM9	Niu, Z.C.	THP16
Marinescu, D. C.	THP71	Moreau, E.	TUA10	Noda, Susumu	TUP37
Markmann, M.	THA6	Moreira, E. Ceretta	WEM3	Noda, T.	THP65
Marsal, L.	TUP85	Mori, N.	MOP51	Noetzel, R.	TUP48
Martini, R.	THM1	Morifuji, M.	MOA6	Nogaret, A.	MOP61
Mason, N. J.	MOP71	Moshchalkov, V. V.	TUP53	Nomura, S.	TUP72
Mason, N. J.	TUP69	Moskalenko, E. S.	MOM3	Noriega, O.C.	TUP7
Masselink, W. T.	TUP73	Motisuke, P.	MOP44	Nötzel, R.	TUA5
Masselink, W.T.	MOP30	Motohisa, J.	MOP57	Nucara, N.	TUP5

Nurnus, J. THP41
Oberender, N. MOP84
Oberli, D. Y. FRA3
Oberli, D.Y. TUP76
Obert, M. TUP62
Oepen, H. P. MOP70
Offermans, P. MOP80
Ogasawara, Y. MOP57
Ogasawara, Y. MOP62
Ogura, M THP1
Ogura, M. TUP33
Ogura, M. TUP51
Ogura, M. TUP78
Ohashi, T. TUP32
Ohlberg, D. A. A. THA5
Ohlsson, B. J. THA3
Ohno, H FRM6
Ohno, H. THP37
Ohno, Y FRM6
Ohno, Y. TUP26
Ohtani, N. THP54
Oiwa, A. FRM5
Okanishi, R. TUP78
Omling, P. THP45
Onishchenko, E. E. THP59
O'Reilly, E.P. TUP10
Ortiz, V. THM3
Ortner, G. TUA11
Ortner, G. TUM10
Ose, T. TUP9
Oswald, J. TUP64
Otterburg, T. TUP76
Oulton, R. TUM11
Ozasa, K TUP55
P.M. Petroff TUM8
Pacher, C. MOM13
Pacher, C. MOP68
Pachler, P MOP81
Pacifici, D. WEM3
Paesler, M. MOP36
Page, H. THM3
Pagliara, G. THP10
Paiella, R. THM1
Palevski, A. MOP54
Pangrac, J. TUP64
Panzarini, G. TUP23
Panzarini, Giovanna TUP68
Panzner, T. MOP30
Papadakis, S. J. MOM11
Papadakis, S.J. MOP75
Papis, E. MOM12
Park, B. G. THP46
Partoens, B. TUP67
Pascher, H. FRA2
Pashitskii, E.A. MOP45
Passaseo, A. THP10
Passow, T. MOP27
Passow, T. TUP62
Patanè, A MOM7
Patanè, A. THP70
Patanè, A. TUA2
Patanè, A. TUP35
Patanè, S. TUP27
Pazy, Ehoud TUP14
Pecharromán, C. TUM4
Peeters, F. M. TUP67
Pekola, J. THP42
Pelouard, J. - L. MOP58
Pepper, M TUA8
Perlin, P. TUP4
Persson, A. THA3
Pessa, M. TUP3
Petroff, P. M. TUM12
Petroff, P. M. TUM13
Petroff, P. M. TUP70
Petroff, P. THA7
Petroff, P.M. FRM8
Petroff, Pierre M. TUM9
Pierz, K. TUP80
Pietsch, U. MOP40
Pietzonka, Ines MOP11
Pillwein, G. MOP59
Pinczolits, M. MOP31
Piotrowska, A. MOM12
Pirshin, I.V. MOP34
Pishchulin, A.A THP52
Planel, R. THP72
Plank, Harald MOP85
Platero, Gloria FRM7
Platero, Gloria TUP39
Pletschen, W. MOA4
Ploog, K. H. MOM10
Ploog, K. H. THP62
Ploog, K. H. TUA5
Ploog, K. H. TUP48
Ploog, K. MOA3
Plotnikov, A.Y MOP19
Plotnikov, A.Y MOP76
Poborchii, Vladimir V. MOP25
Pohl, U. W. TUP49
Pohl, U. W. TUP84
Polimeni, A. THP70
Polimeni, A. TUP5
Polson, R.C. MOP78
Poortere, E. P. De MOM11
Poortere, E.P. De MOP75
Portal, J.C MOP19
Portal, J.C MOP61
Portal, J.C MOP76
Pozina, G TUP2
Prechtl, G. THP21
Pregliasco, R. G. TUP21
Prettl, W. THP36
Prinz, A. MOP59
Priolo, F. WEM3
Prunnila, M. THP42
Pudalov, V.M. MOP59
Purger, Sabine MOP85
Qin, H. MOM6
Quinn, J. J. THP71
R. Hey, MOM10
R. Köhler MOP30
Raab, A. MOP31
Rack, A. TUP59
Raikh, M.E. MOP78
Rakoczy, D. TUP56
Rambach, M. TUP62
Ranalli, F. TUP5
Rappl, P.H.O. MOP44
Rastelli, A. MOP9
Regelman, D.V. TUM8
Reginski, K. THP25
Reimann, K. MOA3
Reimann, K. THM8
Reimann, K. TUP19
Reimer, P.M. MOP29
Reinhardt, M. TUP5
Reithmaier, J. P. THP79
Reitzenstein, S. THP48
Renk, K. F. TUP35
Renk, K.F THP61
Resel, Roland MOP85
Reusch, T.C.G. MOP37
Reuter, D. THP12
Reuter, D. THP44
Richter, G. FRM2
Richter, G. THP29
Riikonen, J. TUP3
Rinaldi, R TUP15
Rinaldi, R. THP10
Rinaldis, S.De TUP15
Ritchie, D A THP73
Robert, I. FRM9
Robert, I. TUA10
Roberts, J. S. TUP28
Roberts, J. S. TUP29
Robledo, L. MOP63
Robledo, L. TUP40
Roch, T. MOP8
Rochat, Michel THM6
Rodt, S. TUP84
Rogach, Andrey TUP18
Rokhinson, L. P. MOM8
Rolf, L. TUM6
Romanov, V.V. MOP24
Romestain, R. FRM10
Rosam, B MOA7
Rosenblad, C. MOP6
Roshan, R. TUA4
Rossi, F MOA7
Rossi, F TUP15
Rossi, F. MOP65
Rossi, F. MOP86
Rossi, F. TUP17
Rossi, Fausto TUP14
Roussignol, Ph. FRM10
Roussignol, Ph. MOM4
Rudra, A. FRA3
Rudra, A. TUP76
Ruini, A. MOP86
Runge, E. TUA5
Ryabushkin, O. A. MOP72
Ryan, J.F TUA4
Rychen, J. MOP52
Rykov, S.A. THM12
Rykov, S.A. THP15
Ryzhii, V. THP14
Sa'ar, A. THP72
Safarov, V.I. MOP5
Saitoh, T. TUP12
Sakaki, H. THP65
Sakaki, H. TUA3
Sakaki, H. TUP47
Sakaki, H. TUP81
Saku, T. MOP49
Salamanca-Riba, L. MOP31
Salemink, H.W.M. MOP37
Salemink, H.W.M. MOP80
Samarth, N. THE1
Samuelson, L. THA3
Samuelson, L. THP45
Samuelson, L. THP47
Samuelson, L. TUP79
Sanchez, David FRM7
Sanchez, David TUP39
Sánchez-García, M.A. TUP1
Sánchez-Páramo, J. TUP1
Sandersfeld, N. FRM1
Santos, P.V. MOA1
Saricifci, N. S. MOP82
Sarma, S. das MOP67
Sasaki, A. TUP78
Sasaki, Y. MOP29
Sasakura, H. TUP13
Sashinaka, N THP56
Sass, T. TUP79
Sass, Torsten MOP11
Satake, A. MOP64
Sato, Y. TUP43
Sauer, R. THP31
Sauer, R. THP32
Savin, A. THP42
Savona, V. TUA5
Sawaki, N. TUP32
Scarpa, Giuseppe THM4
Schacham, S.E. TUP61
Schaefer, F. THP79
Schäfer, P. MOP30
Schäffler, F. MOP34
Schäffler, F. FRM1
Schäffler, F. MOP3
Schafmeister, P. THP12
Schallenberg, T. MOP39
Schapers, T TUA4
Schäpers, Th. THP23
Schardt, M. THP3
Schelling, C. MOP3
Scherf, U MOP81
Scherf, U. MOP41
Scheuerer, R THP61
Scheuerer, R. TUP35
Schliemann, John THP26
Schliwa, A. TUP66
Schmidbauer, M. MOP30
Schmidt, G. FRM2
Schmidt, G. THP29
Schmidt, K. H. TUP54
Schmidt, O. G. MOP77
Schmidt, O. G. TUP53
Schmidt, O. G. TUP63
Schmidt, O. G. WEM4
Schmidt, O.G. MOP16
Schmidt, O.G. MOP8
Schmidt, O.G. THP4
Schmidt, R. THP12
Schmidt, T. MOP27
Schmitt, C MOP81
Schmitz, J. MOA4
Schnüll, S. MOP70
Schoch, W. THP31
Schoch, W. THP32
Schoenfeld, W. V. FRM8
Schoenfeld, W. V. MOM3
Schoenfeld, W. TUM12
Schoenfeld, W. TUM13
Schoenfeld, W. TUP70
Schoenfeld, W.V. TUM8
Schoenfeld, Winston V. TUM9
Schoenherr, H.-P. TUP48
Schöll, E. MOM13
Schöll, E. TUP46
Schöll, E. TUP59
Scholz, F. THP64
Scholz, R. WEM6
Schomburg, E THP61
Schomburg, E. TUP35
Schömig, H. FRM4
Schott, G.M. MOP28
Schramm, C. MOP12
Schrenk, W. THM3
Schrenk, W. TUA9
Schrottke, L. MOP64
Schrottke, L. THP78
Schuh, Dieter THM4
Schuhmacher, C. MOP28
Schulhauser, C. TUM12
Schulhauser, C. TUM13
Schüller, C. TUM6
Schumacher, C. MOP39
Schwanhäußer, A. MOP63
Schwanhäußer, A. TUP40
Schwarz, A TUA4
Schwarzl, T. FRA2
Schwarzl, T. TUP19
Schweizer, H. THP64
Scolfaro, L. M. R. TUP6
Scolfaro, L.M.R. TUP7
Seekamp, A. THP44
Seifert, W. THP45
Seifert, W. TUP79
Seifert, Werner MOP11
Seilmeier, A. MOP63
Seilmeier, A. TUP40
Selke, H. MOP27
Senellart, P. TUM2
Senz, V. MOP67
Sergent, A. M. THM5
Sermage, B. TUM2
Seufert, J. TUP62
Shanabrook, B.V. TUA7
Shayegan, M. MOM11
Shayegan, M. MOP75
Shchekin, O.B. FRA1
Shchukin, V. A. TUP46
Sheka, D.I TUP42
Shekhter, R.I. MOP45
Shelykh, I.A. THP15
Sheng, W. TUP61
Sherwood, D. THP70
Shimizu, H. THP34
Shimomura, S. MOP48
Shimomura, S. THP66
Shimomura, S. TUP26
Shiraki, Y. MOP22
Shiraki, Y. TUP83
Shiramine, K. TUP13
Shkolnikov, Y. MOM11
Shorubalko, I. THP45
Shtrichman, Itay TUM9
Siegner, U. TUP44
Sigg, H. THM7
Sigl, Alfred THM4
Silva, E.A. de Andrada MOP44
Sim, H.-S. MOP50
Simserides, C. MOP86
Singh, S.K. TUA7
Sirigu, L. FRA3
Sirtori, C. THM3
Sitter, Helmut MOP85
Sivco, D. L. THM1
Sivco, D. L. THM5
Skierbiszewski, C. TUP4
Skolnick, M. S. MOM2
Skolnick, M. S. TUM11
Skolnick, M. S. TUP28
Skolnick, M. S. TUP29
Skorupa, W. MOP21
Skvortsov, A.P. MOP24
Slupinski, T. FRM5
Smirnitzki, V. MOP40
Smoliner, J. TUP56
Soltmann, C. MOP6
Somitsch, D MOP81
Son, S. H. THP46
Soref, R. A. MOP23
Sorokin, S.V. THP19
Spieler, J. TUP41
Springholz, G. FRA2
Springholz, G. MOM12
Springholz, G. MOP3
Springholz, G. MOP31
Springholz, G. MOP42
Springholz, G. TUP19
Stadler, R. THP40
Stangl, J. MOP8
Steer, M.J THM2
Stepina, N.P. MOP15
Sticht, A. THA6
Stier, O. TUP66
Stier, O. TUP84
Stockmann, A. MOP27

Stöckmann, H.-J.	MOP60	Tischler, J.G.	TUA7	Voliotis, V.	TUP51	Winzer, A.T.	THP4
Stoica, T.	MOP13	Toda, Y.	TUP75	Vollnhals, A	THP61	Wixforth, A.	MOA2
Stolz, W.	THP27	Toivonen, J.	TUP3	Volz, K.	THP27	Woerner, M.	MOA3
Straßburg, M.	TUP84	Tokunaga, M.	MOP17	Vörckel, A.	MOP12	Woerner, M.	THM8
Strasser, G.	MOM13	Tomic, S.	THP77	Vorobjev, L.E.	THP75	Wojtowicz, T.	THP22
Strasser, G.	MOP68	Tomic, S.	TUP10	Waag, A.	THP31	Wolst, O.	THP3
Strasser, G.	THM3	Tomm, J. W.	TUP73	Waag, A.	THP32	Wolter, J.H.	MOP37
Strasser, G.	THP57	Tonneau, D.	MOP5	Wacker, A.	MOM13	Wolter, J.H.	MOP80
Strasser, G.	THP60	Toropov, A. I.	TUP52	Wacker, A.	THP76	Woods, N.J	MOP19
Strasser, G.	TUA9	Toropov, A.A.	THP19	Wacker, A.	TUP59	Worschech, L.	THP48
Strasser, G.	TUP50	Toropov, A.I	MOP76	Wagner, E.	THP41	Wróbel, J.	MOM12
Strasser, G.	TUP56	Toshikiyo, K.	MOP17	Wagner, R.J.	TUA7	Wrobel, J.	THP22
Subashiev, A. V.	THP39	Touryanski, A.G.	MOP34	Wallenberg, L. R.	THA3	Wu, Y.-W.	THP43
Suemune, I.	TUM5	Trampert, A.	THA1	Walther, C.	TUP73	Wurm, M.	THM8
Suemune, I.	TUP22	Trankle, G.	MOA6	Wang, X. L.	TUP78	Xin, H.P	TUP2
Sueoka, K.	THP37	Tränkle, G.	MOP40	Wang, X.D.	THP16	Xu, H. Q.	THP45
Sugahara, S.	THP30	Travlos, A.	THP62	Wang, X.-L	TUP51	Xu, H.Q.	THP47
Sugimoto, T.	TUP75	Tredicucci, A.	THM5	Wang, Y.	THP64	Yablonovitch, E.	TUP16
Suhara, M.	THP47	Tribe, W.R.	MOP56	Wanke, M. C.	THM5	Yaguchi, H	THP1
Susha, Andrei	TUP18	Trigo, M.	TUP21	Warburton, R. J.	THP9	Yakimov, A.I.	MOP15
Suski, T.	TUP4	Troiani, Filippo	TUP57	Warburton, R. J.	TUM12	Yamada, S.	TUP43
Suzuki, M.	WEM5	Tsai, M.-K.	THP43	Warburton, R. J.	TUM13	Yamaguchi, H.	MOP46
Tabata, A.	TUP7	Tsubaki, K	TUP12	Warburton, R. J.	TUP70	Yamaguchi, M.	TUP32
Tada, Tetsuya	MOP25	Tsuchiya, Takuma	THP8	Wasiela, A.	THE2	Yamamoto, M.	THP66
Tadic, M.	TUP67	Tsui, D. C.	MOM8	Wasilewski, Z.	TUA11	Yamashita, K.	THP64
Takamura, Y.	MOP51	Tsujikawa, T	THP1	Wasilewski, Z.	TUP71		
Takayanagi, H.	THP20	Tu, C.W	TUP2	Watanabe, F.	MOP10		
Takayanagi, H.	THP23	Türck, V.	TUP84	Watanabe, I.	MOP48		
Takeoka, S.	MOP17	Tutuc, E.	MOM11	Watanabe, I.	THP66		
Takita, K.	THP24	Tutuc, E.	MOP75	Watanabe, K.	MOP18		
Tamaoka, H.	MOP18	Uchida, K.	THP24	Wees, B.J. van	THE4		
Tan, S.-W.	THP43	Uchida, K.	THP70	Wegscheider, W.	MOP52		
Tanaka, I.	TUP81	Uchida, K.	TUP83	Wegscheider, W.	MOP66		
Tanaka, Ichiro	TUP47	Ueta, A.	TUP22	Wegscheider, W.	THM11		
Tanaka, K.	TUP81	Ueta, A.Y.	MOP44	Wegscheider, W.	THP36		
Tanaka, M.	THE3	Ulbrich, Nicolaus	THM4	Weide, D.W. van der	MOM6		
Tanaka, M.	THP30	Ulloa, S.	MOP60	Weigand, W.	THP29		
Tanaka, M.	THP34	Ulrich, J.	TUA9	Weimann, G.	MOA6		
Tarasov, G. G.	TUP73	Umbach, E.	THP29	Weinstein, B.A.	TUA7		
Tartakovskii, A. I.	TUP29	Unterrainer, K.	THP57	Weiss, D.	THP36		
Tartakovskii, A. I.	TUP28	Unterrainer, K.	THP60	Wells, J.-P. R.	THP55		
Tarucha, S	MOM7	Unterrainer, K.	TUA9	Welsch, M.K.	FRM4		
Tarucha, S.	MOP55	Unterrainer, K.	TUP50	Weman, H.	FRA3		
Tatarenko, S.	THE2	Ustinov, V	THP61	Wenzl, F.P.	MOP81		
Tavares, Marcos R.S.	TUP38	Ustinov, V. M.	TUP35	Wernersson, L.-E.	THP47		
Tawara, T.	TUM5	Ustinov, V. M.	TUP74	Wernersson, L.-E.	TUP44		
Taylor, R.P.	MOP56	Ustinov, V.M.	FRA4	Wernersson, L-E.	TUP79		
Teichert, C.	MOP7	Vaccaro, P.	THP54	Wetzler, R.	TUP59		
Teles, L. K.	TUP6	Vancura, T.	MOP52	Weyers, M.	MOP40		
Tenne, D. A.	TUP52	Vanderzande, D.	MOP82	White, M.	THA7		
Terent'ev, Y.	THP19	Vardeny, Z.V.	MOP78	Wieck, A. D.	THP44		
Thelander, Claes	MOP11	Vdovin, E.E.	TUA2	Wieck, A.D.	THP12		
Thierry, Annette	MOP85	Verzelen, O.	THP17	Wiel, W.G. wan der	MOP57		
Thierry-Mieg, V.	FRM9	Verzelen, O.	TUA1	Wiesauer, K.	MOP42		
Thierry-Mieg, V.	THP72	Vescan, L	MOP13	Wieser, U.	MOP20		
Thierry-Mieg, V.	TUM2	Vina, L.	THP79	Wilamowski, Z.	FRM1		
Thierry-Mieg, V.	TUP21	Vitusevich, S.A	TUP42	Wilamowski, Z.	MOP26		
Thompson, J.	MOP79	Vitzethum, M	THP12	Willander, M.	THP14		
Thomsen, C.	THP68	Vogl, P.	MOA6	Willenberg, H	MOA5		
Thomsen, C.	THP69	Voisin, C.	MOM4	Williams, R. Stanley	MOP4		
Tignon, J.	FRM10	Voisin, P.	FRM3	Williams, R. Stanley	THA5		
Timofeev, V. B.	TUA11	Voisin, P.	TUP60	Wilson, L.R	THM2		

Yang, T.	MOP35	Zerova, V.L.	THP75		
Yang, Y.-J.	THP43	Zeuner, M.	MOP6		
Yangthaisong, A.	THP49	Zhang, J	MOA7		
Yassievich, I.N	THP74	Zhang, J	MOP19		
Yasuhira, T.	THP24	Zhang, J.	MOP22		
Yasuhira, T.	TUP83	Zhang, L.	FRA1		
Yoh, Kanji	THP37	Zhang, L.	FRM8		
Yokoyama, N.	TUP45	Zhang, S.K.	MOA1		
Yoshizawa, Shin	TUP37	Zhdanova, N. G.	MOP73		
Yu, Y. S.	THP46	Zhuchenko, Z. Ya.	TUP73		
Zahn, D. R. T.	TUP52	Zhukov, A	THP61		
Zaitsev, S.	FRM4	Zhukov, A. E.	TUP35		
Zaitsev, V. V.	THP59	Zietkowski, W.	TUP34		
Zaluzny, M.	TUP34	Zimin, D.	MOP43		
Zanardi, Paolo	TUP14	Zimmermann, R.	TUA5		
Zandler, G.	THA6	Zobl, R.	MOP73		
Zasavitskii, I.I.	MOP44	Zobl, R.	TUA9		
Zavelani-Rossi, M.	WEM7	Zogg, H.	MOP43		
Zegrya, G.G.	THP75	Zou, Z.	FRA1		
Zeimer, U.	MOP40	Zrenner, A.	MOM1		
Zeitler, U.	MOP36	Zrenner, A.	THP11		
Zeitler, U.	MOP69	Zrenner, Artur	THP5		
Zeitler, U.	TUP80	Zunger, A.	THP63		
Zela, Vilma	MOP11				
Zeman, J.	TUA1				

SPONSORS AND EXHIBITORS

LIST OF SPONSORS

Institutions

- Johannes Kepler University, Linz
- Federal Ministry of Education, Science and Culture, Vienna
- Government of the Province of Upper Austria
- City of Linz
- European Research Office of the US Army, UK
- Office of Naval Research, Washington D.C.
- Gesellschaft für Mikroelektronik, Vienna
- Linzer Hochschulfonds
- Österreichische Physikalische Gesellschaft
  Fachausschuß Festkörperphysik

Companies

- Aixtron AG www.aixtron.com
- Applied Epi Europe www.applied-epi.com
- Atos www.atos-online.de
- Austria Mikro Systeme International www.amsint.at
- Austrian Airlines www.aua.at
- Bruker Optik GmbH http://www.bruker.de/wwwir
- Bruker AXS GmbH www.bruker-axs.de
- Daimler-Chrysler AG www.daimlerchrysler.com
- Dr. Eberl MBE-Komponenten www.mbe-komponenten.de
- Linz AG www.linzag.de
- Hueck Folien www.hueck-folien.at
- Infineon Technologies Austria AG www.infineo.com
- ISA Jobin Yvon GmbH www.isagmbh.com
- ISEG Spezialelektronik GmbH http://iseg-hv.com
- Johnson Matthey GmbH www.alfa-chemcat.com
- Klaus Schaefer AG www.-schaefer-tec.com
- Linde Gas AG www.linde.de
- National Instruments www.ni.com
- Oxford Instruments GmbH www.oxford.de
- Pfeiffer Vacuum Austria GmbH www.pfeiffer-vacuum.at
- Philips Analytical www.analytical.philips.com
- Physicon www.physicon.com
- Phystech GmbH www.PhysTech.de
- Piezosystems Jena www.piezojena.de
- Pink GmbH Vakuumtechnik www.pink.de
- Riber GmbH www.riber.de
- Scutum AnalysenTechnik GmbH scutum@t-online.de
- SENTECH Instruments GmbH www.sentech.de
- Spectra Physics GmbH www.spectra-physics.com
- Varian Deutschland GmbH www.varian.de
- Vishay Telefunken Austria www.vishay.com
- VTS - Createc & Co GmbH www.vts-createc.com

LIST OF EXHIBITORS

Aixtron AG
www.aixtron.com
Kackerstr. 15-17
D - 52072 Aachen

Applied Epi
www.applied-epi.com
147 Chorley New Road Horwich
Bolton BL6 5QE, England

ATOS GmbH
www.atos-online.de
Robert-Bosch-Straße 14
D-64319 Pfungstadt

Bruker Advanced X-Ray Solutions GmbH
www.bruker-axs.de
Oestliche Rheinbrueckenstr. 50
D-76187 Karlsruhe, Germany

ISA Jobin Yvon GmbH
www.isagmbh.com
Kackerstr. 15-17
D - 52072 Aachen, Germany

iseg Spezialelektronik GmbH
http://iseg-hv.com
Bautzner Landstraße 23
D-01454 Rossendorf

Linde Gas AG
www.linde.de
Waschenbergerstraße 13
A-4651 Stadl-Paura, Austria

Oxford Instruments GmbH
www.oxford.de
Otto-von-Guericke-Ring 10
D-65205 Wiesbaden, Germany

Pfeiffer Vaccum Austria GmbH
www.pfeiffer-vacuum.at
Diefenbachgasse 35
A-1150 Wien, Austria

Philips Analytical
www.analytical.philips.com
Lelyweg 1
NL- 7602 EA Almelo, The Netherlands

Phystech GmbH
www.PhysTech.de
Egilbertstr. 2
D - 85368 Moosburg, Germany

Piezosystems Jena
www.piezojena.de
Prüssingstrasse 27
D - 07745 Jena, Germany

Riber GmbH
www.riber.de
Hohenzollernstr. 102
D-80796 München, Germany

Scutum AnalysenTechnik GmbH
scutum@t-online.de
Vogelsbergstr. 45 b
D-55129 Mainz, Germany

SENTECH Instruments GmbH
www.sentech.de
Carl-Scheele-Straße 16
D-12489 Berlin, Germany

Varian Deutschland GmbH
www.varian.de
Im Grün 21
D-79219 Staufen, Germany

VTS-Createc & Co GmbH
www.vts-createc.com
Hindenburgstraße 12
D-76332 Bad-Herrenalb

Alfa Aesar®

Johnson Matthey

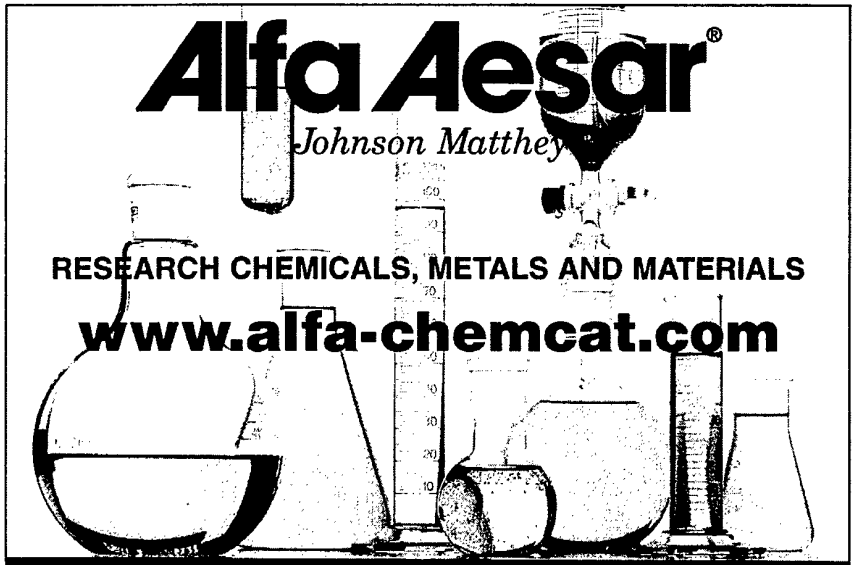

RESEARCH CHEMICALS, METALS AND MATERIALS

www.alfa-chemcat.com

PHONE: 00800 4566 4566 FAX: 00800 4577 4577 Email: gcat@matthey.com

Alfa Aesar is a leading international manufacturer and supplier of research chemicals, metals and materials. With more than 15,000 products in the current Alfa Aesar Catalogue. Alfa Aesar is a comprehensive source for chemicals, metals and laboratory materials from sizes for research to semi-bulk and bulk quantities. The Alfa Aesar Catalogue carries high purity inorganics, pure metals, alloys, elements, precious metal compounds and catalysts, rare earths, analytical fluxes, ceramics, labware, AA/ICP standards and more.

The product descriptions have detailed technical information and many of the product descriptions have physical property data and application notes. Several hundred cross references make it easier for customers to find the exact product they need. All this will of course also be found on the website **www.alfa-chemcat.com** for easy and up-to-date access of product data for the enduser. Efficient customer service and technical advise to help the customers form a rounded service package for customers in industrial and academic laboratories.

For products of the highest quality and purity Alfa Aesar offers a variety of brand lines:

Puratronic®
Alfa Aesar's higher purity inorganic compounds and metal powders make up the Puratronic® brand line. Puratronic® product purities are typically 99.995 % to 99.9999 %.

Specpure®
Specpure® is the trade name for Alfa Aesar's analytical standard solutions.

REacton®
Under the REacton®-name, Alfa Aesar offers a broad range of high purity earth compounds.

Premion™
Premion™ is the trademark for high purity precious metal compounds and pure elements. The minimum purity for pure elements is 99.99 % and for compounds 99.95 % (metals basis).

All trademark-products come with a batch-specific Certificate of Analysis.

Johnson Matthey GmbH, Zeppelinstraße 7, D-76185 Karlsruhe

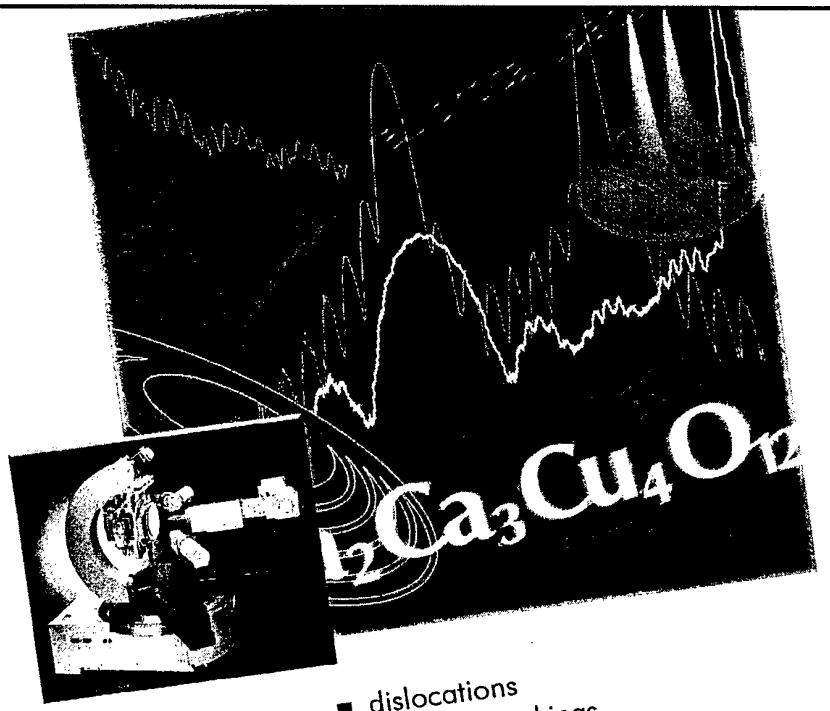

- surface roughness
- layer thickness
- lattice mismatch
- chemical composition
- layer density
- dislocations
- periodic stackings
- stacking faults
- surface topography
- lattice topography

Germany:
Tel. (+49) (7 21) 595-2888
Fax (+49) (7 21) 595-4587
http://www.bruker-axs.de
E-mail: info@bruker-axs.de

USA:
Tel. (+1) (608) 276-3000
Fax (+1) (608) 276-3006
http://www.bruker-axs.com
E-mail: info@bruker-axs.com

THE SOLUTION:
D8 DISCOVER FOR
THIN FILM ANALYSIS!

find out what's inside

BRUKER AXS

BRUKER ADVANCED X-RAY SOLUTIONS

HUECK FOLIEN

Technische Folien

Hueck Folien Gesellschaft m.b.H.
A-4342 Baumgartenberg, Gewerbepark 30
Österreich

Das Baumgartenberger Unternehmen beschäftigt 230 Mitarbeiter und veredelt Kunststoff-Folien, Papier, Gewebestoffe und Metallfolien zu anspruchsvollen Materialien für technische Einsatzgebiete.
Umfangreiche Forschungs- und Entwicklungsarbeiten legen die Basis für eine weltweit führende Rolle in vielen Marktsegmenten.
Mit einem Schwerpunkt im EU-Bereich beliefert das Unternehmen weltweit seine Partner mit maßgeschneiderten Produkten.

SCHAEFER

SURFACE SCIENCE PRODUCTS

The biggest choice in SPM

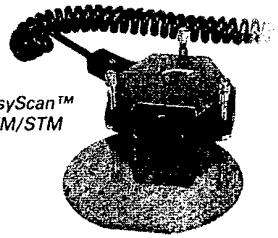

easyScan™
AFM/STM

nanoSurf

Q-Scope™
multi mode
AFM

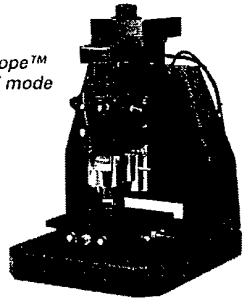

Quesant
VISUALIZES THE NANOWORLD

SPM Control electronics

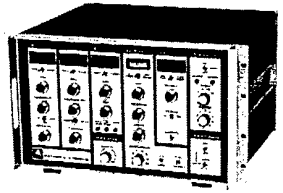

RHK TECHNOLOGY

For AFM in liquids:
RHK Control electronics +
Molecular Imaging

UHV STM
UHV AFM

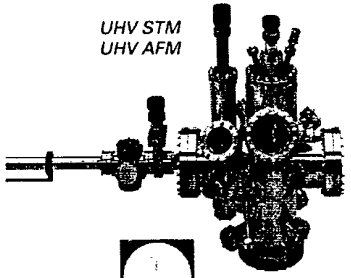

RHK TECHNOLOGY

For complete UHV surface
analysis systems:
RHK UHV STM + VG Microtech

For more information please contact the sales office in your region

D, Benelux, Scandinavia, Eastern Europe
Schaefer Technologie GmbH
D-63225 Langen
Tel. + 49 6103 790 85
e-mail: info@schaefer-tec.com
www.schaefer-tec.com

CH, A, I
Schaefer AG
CH-3178 Bösingen
Tel. + 41 31 747 64 64
e-mail: ch@schaefer-tec.com
www.schaefer-tec.com

F, E, P
Schaefer-Techniques sarl
F-91620 Nozay
Tel. + 33 1 64 49 63 50
e-mail: info@schaefer-tech.com
www.schaefer-tech.com

PHYSICON ion source Model 310 for collimated ion beams from Be and B to In, Sb and heavier masses.

Ion sources, raytraced systems and accessories for accelerator upgrades and new beam line setups for R&D and pilot production.

PHYSICON Reg. TM

Physicon Corporation
12 Kendrick Road #15 Industrial Park
Wareham Massachusetts 02571 USA
508 295 9262 (P) Fax: 508 295 4372
email: physicon@aol.com; website: www.physicon.com

The **iseg Spezialelektronik GmbH** company specialises in the development and production of High Voltage Power Supplies for Industry and Research.

This is based on 20 years of experience in the development and use of technologies of modern High Voltage generation.

Competence in all concerns referred to High Voltage

in development
manufacturing
in quality control
the final test
in service and last but not least in
customer support is
the essence of our company philosophy.

Through the development of a new generation of High Voltage Power Supplies in modern, patented resonance mode technique it is possible to offer our customers very efficient HV units with small dimensions and excellent electrical parameters.
This new generation besides using modern circuit technique is also directed to modern component and manufacturing technologies, in order to arrive at cost effective production and high quality.
All units are available as standard version or optionally with digital interfaces.
Therefore integration into computer based systems is guaranteed.

This present product family does not only represent a new generation of Standard units. It also hopefully shows almost unlimited opportu nities, how - with help of mechanical changes, with help of combination of components of different families or through the modification of electronics - customer requirements could be fulfilled on time and cost effective.

Our team of development engineers , physicists, designers, quality specialist and engineers for technology is ready to support you for the solution of specific High Voltage questions.

iseg Spezialelektronik GmbH
Bautzner Landstraße 23
D - 01454 Rossendorf

Tel.: ++ 49 (0) 351 / 26 99 6 0
Fax: ++ 49 (0) 351 / 26 99 6 21
Email: sales@iseg-hv.de , http://iseg-hv.com

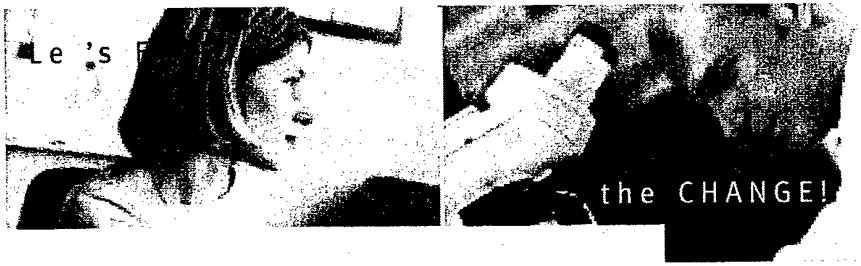

Infineon Technologies Villach

Design Center Villach

Design Center Graz

Design Center Wien

DICE Linz

IT'S GETTING FASTER. I's getting better. I's getting bigger. Or smaller, much smaller. Our 32,000 experts worldwide know how. They specialize in semiconductor applications for cordless and wired communication, for automobile and industry electronics, for security systems and chip cards as well as memory products. In the financial year 2000 we achieved a turnover of more than seven billion Euros with our innovative solutions. Encouraging enough to keep on implementing new ideas and keep on thinking ahead.

Infineon Technologies in Austria

INFINEON TECHNOLOGIES AUSTRIA AG with almost 2,400 employees in Villach is the competence center for power semiconductors. Highly qualified personnel and a consistent quality safeguard (the location has ISO and CECC certification) guarantee the highest level of customer satisfaction. Among other areas, the products from Villach are used in communication, automobile, and motive power engineering technology.

INFINEON TECHNOLOGIES Microelectronic Design Centres Austria GmbH is the largest development unit for microelectronics in Austria and with nearly 500 employees in Villach, Graz, Vienna, and Linz has at its disposal one of the most significant research and development potentials for the planning and implementation of integrated circuits.

CONTACT US! We would be very pleased to make your acquaintance. Tomorrow?

Infineon Technologies Austria AG
Infineon Technologies Microelectronic Design Centers Austria GmbH
Human Resources, Siemensstraße 2, A-9500 Villach
E-mail: austria.jobs@infineon.com

www.infineon.com

Infineon technologies

Never stop thinking.

VISHAY PRODUCT LINES

Passive Components:

Bulk Metal Foil Resistors
Metal Film Resistors & Networks
Thick Film Resistors & Networks
Thin Film Resistors & Networks
Current Sensing Resistors
Wirewound Discrete Resistors
Thick Film R/C Networks
Tantalum (Solid) Capacitors
Tantalum (Wet) Capacitors
MLCCs
Ceramic Capacitors
Film Capacitors
Aluminum Capacitors
Trimming Potentiometers
Panel Controls
Custom Magnetics
Inductors
Fuses
Thermistors

Semiconductors:

Optoelectronic Components
Small Signal Transistors
Power Integrated Circuits
Diodes
Power MOSFETs
RFI Suppressors
Analog Switches & Multiplexers

VISHAY INTERTECHNOLOGY

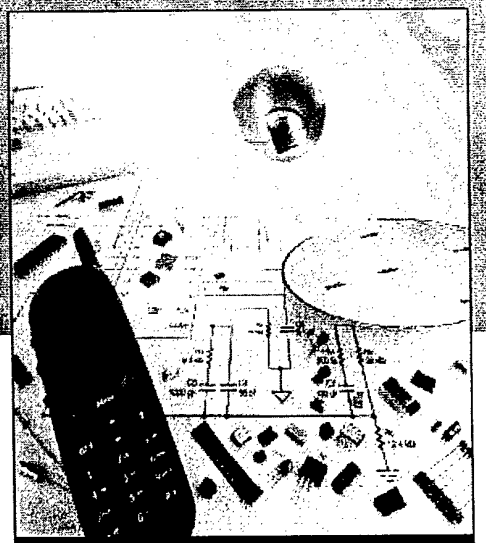

TECHNOLOGY LEADER

Access the latest technology, across the board, from the manufacturer of the broadest line of passive components and discrete semiconductors. Get the resistors, capacitors, inductors; the power MOSFETs, transistors, optoelectronic components, and diodes you need to complete your design.

VISHAY

MANUFACTURER OF THE WORLD'S BROADEST LINE OF DISCRETE ELECTRONIC COMPONENTS

www.vishay.com

tyrolean AUSTRIAN AIRLINES Lauda

AIXTRON

Dr. Eberl
MBE-Komponenten GmbH

Dr. Eberl MBE-Komponenten GmbH
Gutenbergstr. 8
71263 Weil der Stadt (Germany)

Tel.: +49 (0)7033 6937-0
Fax: +49 (0) 7033 6937-20

email: info@mbe-komponenten.de
http://www.mbe-komponenten.de

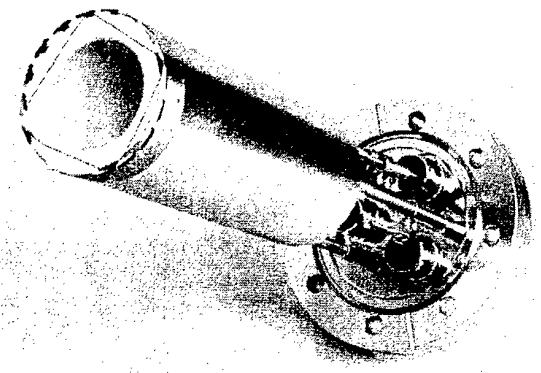

Production Effusion Cell PEZ 63-60 with 60ccm conical crucible on flange DN63CF (O.D.4.5")

Standard product range :

- Standard Effusion Cells
- Sublimation Sources (Si and C)
- Doping Sources
- High Temperature Effusion Cells
- Low Temperature Effusion Cells
- Custom designed Cluster Sources
- Cooling Shrouds
- Substrate Manipulators up to 1250℃
- Additional Equipment for MBE-Systems

We are specialized in individually designed MBE-components and in modified standard MBE-components.

Do not hesitate to ask for your special solution.

JOHANNES KEPLER UNIVERSITY LINZ

CAMPUS

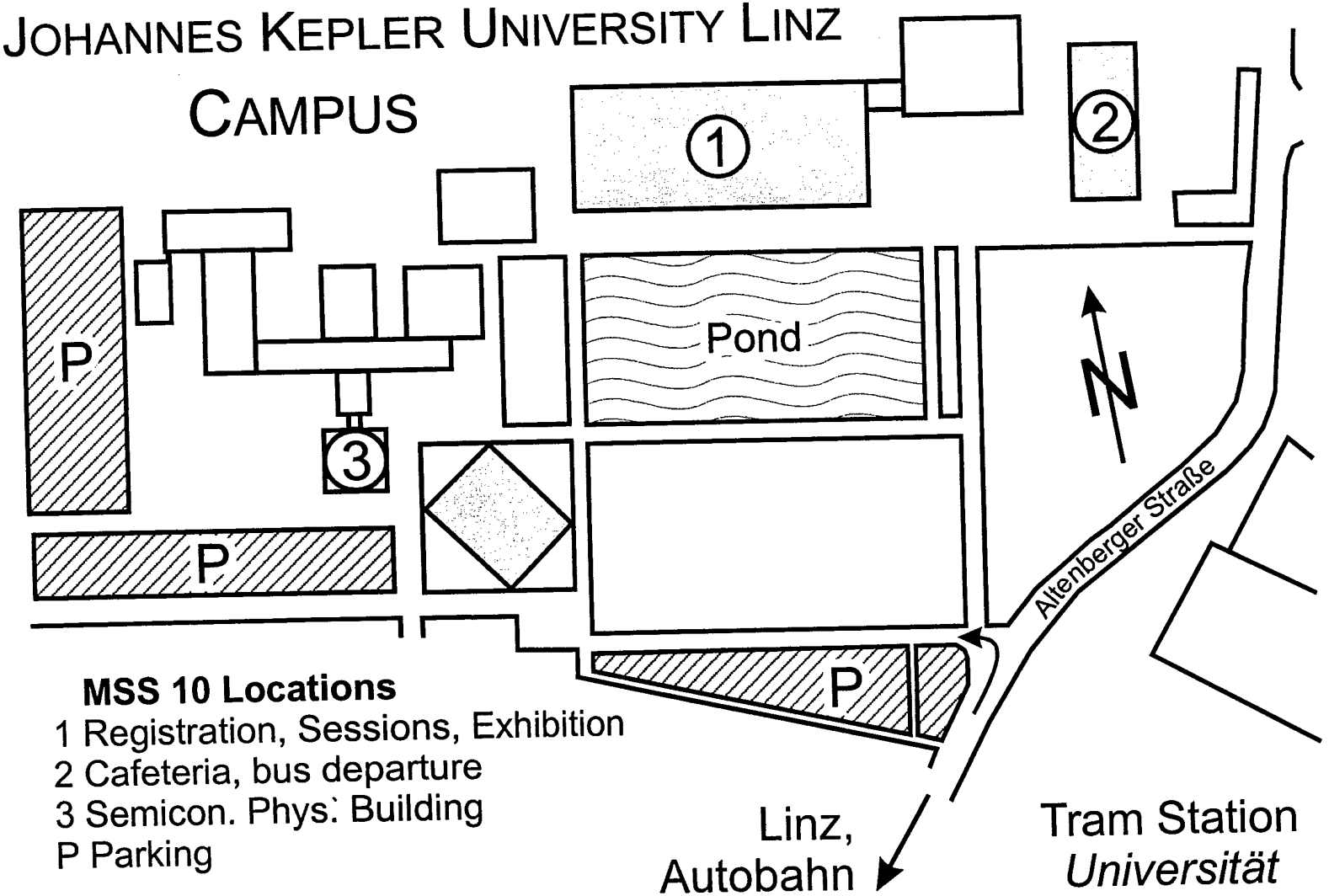

MSS 10 Locations

1 Registration, Sessions, Exhibition
2 Cafeteria, bus departure
3 Semicon. Phys. Building
P Parking

If you can dream it. You can do it.

Hans Jörg Kaltenbrunner
Vorstandsvorsitzender

Wolfgang Pribyl,
Mitglied des Vorstandes

austriamicrosystems AG erforscht, entwickelt und produziert Halbleiteranwendungen. Wir sind in den Bereichen Automobil, Kommunikation und Industrie führend. Unser Ziel: für die nächsten Generationen neue Lösungen zu entwickeln und zu fertigen, die unseren Alltag sicherer, angenehmer und einfacher machen. Mit 850 Mitarbeitern sind wir im Jahr 2000 um rund 40% gewachsen und haben 122 Mio. Euro Umsatz erzielt. Im Jänner 2002 startet unsere neue 200 mm Wafer Fabrik in Unterpremstätten bei Graz – mit 305 Mio. Euro das grösste Technologieinvestment Österreichs. Die globale Dynamik unseres Konzerns erfordert vor allem auch eine massive Expansion unseres Teams. Dafür wollen wir Sie gewinnen!
If you can dream it. You can do it.

www.*austria**micro**systems*.com/career

austriamicrosystems AG, Mag. Evelyn Poms, 8141 Schloss Premstätten, Austria
Tel.: 03136/500-5963, Fax: 03136/500-5678, E-mail: evelyn.poms@amsint.com

Tunable Ultrafast Pulses _for the Scientists

MaiTai–

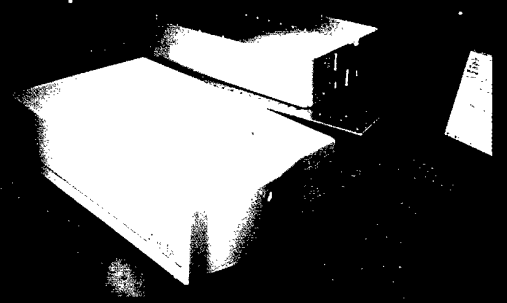

Spectra-Physics

Guerickeweg 7 • D-64291 Darmstadt
Telefon (0 61 51) 708 240 • Telefax (0 61 51) 708 217
E-mail: vertrieb@splasers.de • http://www.spectra-physics.com

NSS10

Johannes Kepler University Linz, July 23 - 27, 2001

Sunday 22.07.01	Monday 23.07.01	Tuesday 24.07.01	Wednesday 25.07.01	Thursday 26.07.01	Friday 27.07.01
MSS10	Morning Session 8:30 - 12:35 **Opening** **Single Dot Spectroscopy I** **Transport**	Morning Session 8:30 - 12:25 **Microcavities and Photonics** **Single Dot Spectroscopy II;** **Optical Properties of Nanostructures I**	Morning Session 8:30 - 12:00 **Novel Materials** **Novel Modulated Structures**	Morning Session 8:30 - 12:15 **Quantum Cascade Structures I** **Quantum Cascade Structures II** **Devices**	Morning Session 8:30 - 12:00 **Spin Electronics and Magnetic Heterostructures** **Cavities and Single Photon Sources**
	Lunch 12:35 - 13:50	Lunch 12:25 - 13:40	**Conference Excursion** 12:15 - 19:30	Lunch 12:15 - 13:15	Lunch 12:00 - 13:30
	Afternoon Session 13:50 - 15:50 **Fast and Ultrafast Carrier Dynamics**	Afternoon Session 13:40 - 17:15 **Optical Properties of Nanostructures II** **THz Emission** **Toward Quantum Communication**		Afternoon Session 13:15 - 15:15 **Nanostructure Growth and Fabrication**	Afternoon Session 13:30 - 15:00 **Quantum Dot and Wire Lasers** **Closing**
Registration 15:00 - 19:00	Break 15:50 - 16:10	Break 17:15 - 17:30		Break 15:15 - 16:00	LINZ 2001
	Poster Session I 16:10 - 18:00	**Poster Session II** 17:30 - 19:30		**Poster Session III** 16:00 - 18:00	
Reception of the Mayor of Linz 18:00 and 19:30	Break 18:00 - 19:00			Break 18:00 - 19:00	
	Rump Session I **Molecular Electronics** 19:00 - 20:30		**Conference Banquet** 19:30 -22:00	*Rump Session II* **Spintronics** 19:00 - 21:00	

9207-EE-02
N68171-01-M-5939

AD NUMBER	DATE	DTIC ACCESSION NOTICE
1. REPORT IDENTIFYING INFORMATION		REQU
A. ORIGINATING AGENCY Johannes Kepler Univ. Linz, Austria		1. Put y on re 2. Comp
B. REPORT TITLE AND/OR NUMBER 10th Internat. Conf. on Modulated Semiconductor Structures		3. Attac mail
C. MONITOR REPORT NUMBER R&D 9207-EE-02		4. Use u infor
D. PREPARED UNDER CONTRACT NUMBER N68171-01-M-5939		5. Do no for 6
2. DISTRIBUTION STATEMENT APPROVED FOR PUBLIC DISTRIBUTION DISTRIBUTION UNLIMITED PROCEEDINGS		DTIC: 1. Assig 2. Retu

20010827061

DTIC OCT 95 ITIONS ARE OBSOLETE